INTRODUCTION TO EARTH SCIENCE

SECOND EDITION

ADAPTED BY

LAURA NESER

Introduction to Earth Science, Second Edition is an open textbook designed to provide a comprehensive introduction to Earth Science that can be freely accessed online, read offline, printed, or purchased as a print-on-demand book. It is intended for a typical 1000-level university introductory course in the Geosciences, although its contents could be applied to many other related courses.

This text includes various important features designed to enhance the student learning experience in introductory Earth Science courses. These include a multitude of high-quality figures and images within each chapter that help to clarify key concepts. Self-test assessment questions are embedded in each online chapter that help students focus their learning. QR codes are provided for each assessment to allow students using print or PDF versions to easily access the quiz from an internet-capable device of their choice.

The sequence of the book differs from mainstream commercial texts. It has been arranged to present elementary or foundational knowledge regarding rocks and minerals prior to discussion of more complex topics in Earth Science. Similar to the layout of the first edition, this book dedicates one chapter to each of the three major rock types, the processes of mass wasting, geological time, Earth history, and the origin of the universe and our Solar System. Additionally, the second edition includes a new chapter on meteorology, and combines the previously separate chapters on deserts and glaciers into a single, comprehensive chapter that explores these extreme environments.

COLLEGE OF SCIENCE GEOSCIENCES VIRGINIA TECH

VIRGINIA TECH PUBLISHING

Licensed with a Creative Commons Attribution NonCommercial-ShareAlike 4.0 license

DOI: https://doi.org/10.21061/Introearthscience2e
ISBN: 978-1-962841-24-5

Introduction to Earth Science, Second Edition

INTRODUCTION TO EARTH SCIENCE

SECOND EDITION

ADAPTED BY
LAURA NESER

PDF AND EPUB FREE ONLINE AT: HTTPS://DOI.ORG/10.21061/INTROEARTHSCIENCE2E

VIRGINIA TECH DEPARTMENT OF GEOSCIENCES IN ASSOCIATION WITH THE OPEN EDUCATION INITIATIVE AND VIRGINIA TECH PUBLISHING
BLACKSBURG, VA

© Laura Neser, 2025. *Introduction to Earth Science, Second Edition* by Laura Neser is licensed under a Creative Commons Attribution-NonCommercial-ShareAlike 4.0 International License, except where otherwise noted.

You are free to copy, share, adapt, remix, transform, and build on the material for any primarily noncommercial purpose as long as you follow the terms of the license: https://creativecommons.org/licenses/by-nc-sa/4.0.

You must:

- Attribute—You must give appropriate credit, provide a link to the license, and indicate if changes were made. You may do so in any reasonable manner, but not in any way that suggests the licensor endorses you or your use.
- ShareAlike—If you remix, transform, or build on the material, you must distribute your contributions under the same license as the original.

You may not:

- NonCommercial—You may not use the work for primarily commercial use.
- Additional restrictions—You may not add any legal terms or technological measures that legally restrict others from doing anything the license permits.

Attributions: This work includes content from multiple sources reproduced under the terms of Creative Commons licenses, Public Domain, and Fair Use. Specifically: Most chapters in this textbook match the organization of *An Introduction to Geology* (CC BY-NC-SA) with the exception of Chapter 14 and Chapter 17. Chapter 14 was adapted from parts of Chapter 9 of *Physical Geography and Natural Disasters* (CC BY-NC-SA) and Chapter 11 of *Dynamic Planet: Exploring Geological Disasters and Environmental Change* (CC BY-NC-SA), as well as parts of Chapter 15 of *Principles of Earth Science* (CC BY-NC-SA). Chapter 17 was adapted from parts of Chapter 22 of *Physical Geology*, 2nd edition (CC BY), and parts of Chapter 7 of OpenStax *Astronomy*, 2nd edition (CC BY). Parts of Chapters 15 and 16 were adapted from *Introduction to Environmental Science*, 2nd edition (CC BY-NC-SA). Parts of Chapter 16 were also adapted from *Introduction to Environmental Sciences and Sustainability* (CC BY).

Suggested citation: Neser, Laura (2025). Introduction to Earth Science. Second Edition, Blacksburg: Virginia Tech Department of Geosciences. https://doi.org/10.21061/introearthscience2e. Licensed with CC BY-NC-SA 4.0. https://creativecommons.org/licenses/by-nc-sa/4.0.

Publisher: This work is published by the Virginia Tech Department of Geosciences in association with the Open Education Initiative and Virginia Tech Publishing.

Virginia Tech Department of Geosciences
4044 Derring Hall
926 West Campus Drive, Blacksburg, VA 24061
https://geos.vt.edu

Open Education Initiative,
University Libraries at Virginia Tech
560 Drillfield Drive Blacksburg, VA 24061 USA
openeducation@vt.edu

Virginia Tech Publishing,
University Libraries at Virginia Tech
560 Drillfield Drive Blacksburg, VA 24061 USA
https://publishing.vt.edu | publishing@vt.edu

Accessibility statement: Virginia Tech is committed to making its publications accessible in accordance with the Americans with Disabilities Act of 1990. The text, images, and links in the PDF version of this text are tagged structurally and include alternative text, which allows for machine readability. We are continuously working to improve accessibility and welcome any feedback from readers.

Publication cataloging information:
Neser, Laura, author
Introduction to Earth Science, Second Edition / Laura Neser
Pages cm
ISBN 978-1-962841-24-5 (PDF)
ISBN 978-1-962841-23-8 (ePub)
ISBN 978-1-962841-25-2 (Pressbooks) https://pressbooks.lib.vt.edu/introearthscience2e
ISBN 978-1-962841-22-1 (Print)
URI (Universal Resource Identifier): https://hdl.handle.net/10919/124132
DOI https://doi.org/10.21061/introearthscience2e
Earth sciences—Textbooks.
QE26.3 .N47 2025

Disclaimer: This work may contain components (e.g., illustrations, or quotations) not covered by the license. Every effort has been made to clearly identify these components but ultimately it is your responsibility to independently evaluate the copyright status of any work or component part of a work you use, in light of your intended use. Please check the references at the end of each chapter before redistributing.

Cover image: Jesse Bowser via Unsplash, Unsplash license
Cover design: Kindred Grey

CONTENTS

ACKNOWLEDGMENTS

Funding for this edition was provided in part by a grant from the University Libraries at Virginia Tech through its Open Education Initiative which provides development assistance and financial support to Virginia Tech faculty who wish to use, create, or adapt openly licensed teaching materials to support student learning.

Virginia Tech Publishing provided typesetting, layout, and design support for this edition.

Anita Walz, Project Manager

Anita Walz is an associate professor and the Assistant Director of Open Education and Scholarly Communication Librarian in the University Libraries at Virginia Tech. She received her MS in Library and Information Science from the University of Illinois at Urbana-Champaign and has worked in university, government, school, and international libraries for over 20 years. She is the founder of the Open Education Initiative at Virginia Tech and the managing editor of over twenty open textbooks adapted or created at Virginia Tech, many of which may be found here: https://vtechworks.lib.vt.edu/handle/10919/70959. She has provided overall planning, project coordination, coaching, problem-solving, and oversight for this adapted version.

INTRODUCTION

Introduction to Earth Science, Second Edition is designed to provide a comprehensive introduction to Earth Science that can be freely accessed online, read offline, printed, or purchased as a print-on-demand book. It is intended for typical 1000-level university introductory courses in the Geosciences, although its contents could be applied to many other related courses. The first edition of this textbook was an amalgamation of existing open-source textbooks (*An Introduction to Geology* from Salt Lake Community College, *Physical Geology* from BCcampus, and *Astronomy* by OpenStax), and this second edition includes additional material from existing open-source textbooks (*Physical Geography and Natural Disasters* from Salt Lake Community College, *Dynamic Planet: Exploring Geological Disasters and Environmental Change* from Maricopa Community College, and *Principles of Earth Science* from Open Oregon Educational Resources). It has been customized to match the Pathways General Education Curriculum at Virginia Tech with a focus on Student Learning Outcomes (SLOs) from Pathways' Concept 4: Reasoning in the Natural Sciences.

The sequence of chapters in this book may differ from a typical commercial publisher's introductory Earth Science textbook. Selected concepts in the book have been reorganized to summarize elementary or foundation topics prior to discussion of more complex topics. Although a foundational knowledge of minerals and rocks is essential in an introductory Earth Science course, all three rock classifications are often bundled into a single "Rocks" chapter; since the classifications vary extensively in the way they form and their overall features, this textbook gives the three major rock types their own dedicated chapters. A similar issue occurs with mass wasting, which is usually included as a small section within an overall "Water" chapter, but in the geosciences, mass wasting is an important surficial process that moves material across the surface of Earth. Therefore, mass wasting has received its own full chapter. Geologic time is commonly paired with Earth history, but both topics are uniquely important parts of a foundational knowledge of Earth, and as such, each topic has its own chapter.

This textbook includes a chapter dedicated to the origin of the universe and our Solar System. Many existing introductory Earth Science books lack a chapter dedicated to astronomy and the Solar System. Understanding our Solar System is important for a variety of reasons: it contains the only known example of a habitable planet, the only star that is observable close-up, and the only planets we can visit with modern technology such as satellites, probes, and landers. Knowledge of Earth's place within the Solar System is essential to understanding the origin of planets, along with the conditions that allow life to exist on Earth.

This second edition of the textbook features several additions to enhance its scope and relevance. Chapter 12, previously titled "Coastlines," has been renamed "Earth's Coastlines and Oceans" and now has a new dedicated section on ocean water properties, exploring salinity, density, and ocean layering, along with a section focused on the ocean floor, including mapping techniques and the classification of oceanic provinces. Chapter 16 ("Energy and Mineral Resources") now includes a comprehensive discussion on renewable energy resources, covering solar, wind, hydroelectric, geothermal, and biomass energy. Chapter 17 ("Origin of the Universe and Our Solar System") has been expanded to address the search for life beyond Earth, delving into topics such as Mars exploration, the outer Solar System, exoplanets, and interstellar communication. Updates to Chapter 15 ("Global Climate Change") incorporate the latest climate change data and provide information on key climate organizations and international treaties. To streamline the content, the former Chapters 13 and 14 ("Deserts" and "Glaciers," respectively), have been combined into a single chapter titled "Deserts and Glaciers." Lastly, a brand new chapter dedicated to meteorology and severe weather has been added (Chapter 14: "Meteorology"), offering in-depth coverage of these critical topics. The Version Notes at the end of this textbook provide more detailed information on the changes made between the first and second editions.

This open-source textbook includes various important features designed to enhance the student learning experience in introductory Earth Science courses. These include a multitude of high-quality figures and images within each chapter that help to clarify key concepts and are optimized for viewing online. Self-test assessment questions are embedded in each online chapter that help students focus their learning. QR codes are provided for each assessment to allow students using print or PDF versions to easily access the quiz from an internet-capable device of their choice. Selected graphics and tables have been replaced or updated to enhance quality and clarity.

ABOUT THE AUTHOR

Adapted by

Laura Neser, PhD, is an instructor in the Department of Geosciences at Virginia Tech. Dr. Neser earned her BS in Geosciences at Virginia Tech in the spring of 2008 and completed her PhD in Geological Sciences at the University of North Carolina at Chapel Hill (UNC) in 2014. Her doctoral research focused on the structural geology, sedimentology, and stratigraphy of formations that were deposited along the flanks of the Beartooth Mountains as they rose during the late Paleocene-Eocene time period. Since earning her PhD, Dr. Neser has worked as an athletic tutor and online instructor at the University of North Carolina at Chapel Hill, held temporary positions as an adjunct instructor at Chowan University (Murfreesboro, NC) and as a full-time lecturer at Indiana State University (Terre Haute, IN), and worked as a professor at Seminole State College (Sanford, FL) before joining Virginia Tech as an instructor in the fall of 2021.

Although she is currently focused on teaching sections of Introduction to Earth Science, Earth Resources, Society and the Environment, and Climate History, her teaching background is significantly broader and includes Sedimentology-Stratigraphy, Environmental Science, Astronomy, Environmental Ethics, Earth History, Structural Geology, and Field Geology.

Incorporating Original Works by

Chris Johnson, Matthew D. Affolter, Paul Inkenbrandt, and Cam Mosher (2017). *An Introduction to Geology,* (CC BY-NC-SA 4.0) Salt Lake City Community College. Retrieved from https://slcc.pressbooks.pub/introgeology.

An Introduction to Geology (2017) was edited and reviewed by

- Johnathan Barnes, Salt Lake Community College
- Jack Bloom, Rio Tinto Kennecott Copper (retired)
- Deanna Brandau, Utah Museum of Natural History
- Gereld Bryant, Dixie State University
- Gregg Beukelman, Utah Geological Survey
- Peter Davis, Pacific Lutheran University
- Renee Faatz, Snow College
- Gabriel Filippelli, Indiana University-Purdue University Indianapolis
- Michelle Cooper Fleck, Utah State University
- Colby Ford, Dixie State University
- Michael Hylland, Utah Geological Survey
- J. Lucy Jordan, Utah Geological Survey
- Mike Kass, Salt Lake Community College
- Ben Laabs, North Dakota State University
- Tom Lachmar, Utah State University
- Johnny MacLean, Southern Utah University
- Erich Peterson, University of Utah
- Tiffany Rivera, Westminster College
- Leif Tapanila, Idaho State University

With special thanks to:

- Jason Pickavance, Salt Lake Community College, Director of Educational Initiatives
- R. Adam Dastrup, Salt Lake Community College, Geoscience Dept. Chair, Director of Opengeography.org

R. Adam Dastrup, MA, GISP (2020). *Physical Geography and Natural Disasters*. (CC BY-NC-SA). Salt Lake Community College. Retrieved from https://slcc.pressbooks.pub/physicalgeography.

Physical Geography and Natural Disasters (2020) was developed by

- R. Adam Dastrup

Charlene Estrada, Carolina Londono Michel, Merry Wilson, Jeff Simpson, Mike Santoro, and Katherine J. Megivern (2021). *Dynamic Planet: Exploring Geological Disasters and Environmental Change*. (CC BY-NC-SA). Maricopa Community Colleges. Retrieved from https://open.maricopa.edu/hazards.

Dynamic Planet: Exploring Geological Disasters and Environmental Change (2021) was developed in collaboration between

- Dr. Charlene Estrada, South Mountain Community College
- Dr. Carolina Michel, Chandler-Gilbert Community College
- Dr. Merry Wilson, Scottsdale Community College
- Jeff Simpson, Chandler-Gilbert Community College

Katharine Solada and K. Sean Daniels (2021). *Principles of Earth Science*. (CC BY-NC-SA). Open Oregon Educational Resources. Retrieved from https://openoregon.pressbooks.pub/earthscience.

Principles of Earth Science (2021) was developed for students taking the course Earth Science at Linn Benton Community College in collaboration between

- Katharine Solada, formerly Linn Benton Community College; currently Yakima Valley College
- K. Sean Daniels, Linn Benton Community College

Karla Panchuk (2019) "Starting with a Big Bang" in Steven Earle, ed., *Physical Geology*, 2nd edition. (CC BY 4.0) BC Campus. Retrieved from https://opentextbc.ca/physicalgeology2ed/chapter/22-1-starting-with-a-big-bang.

"Climate Change" in Steven Earle (2019). *Physical Geology*, 2nd edition. (CC BY 4.0). BC Campus. Retrieved from https://opentextbc.ca/physicalgeology2ed/part/chapter-19-climate-change.

Andrew Fraknoi, David Morrison, and Sidney C. Wolff (2016). *Astronomy*. (CC BY 4.0). OpenStax. Retrieved from https://openstax.org/details/books/astronomy.

Contributing authors to Astronomy (2016) included

- John Beck, Stanford University
- Susan D. Benecchi, Planetary Science Institute
- John Bochanski, Rider University
- Howard Bond, Pennsylvania State University, Emeritus, Space Telescope Science Institute
- Jennifer Carson, Occidental College
- Bryan Dunne, University of Illinois at Urbana-Champaign
- Martin Elvis, Harvard-Smithsonian Center for Astrophysics
- Debra Fischer, Yale University
- Heidi Hammel, Association of Universities for Research in Astronomy
- Tori Hoehler, NASA Ames Research Center
- Douglas Ingram, Texas Christian University
- Steven Kawaler, Iowa State University
- Lloyd Knox, University of California, Davis
- Todd Young, Wayne State College
- Mark Krumholz, Australian National University
- James Lowenthal, Smith College
- Siobahn Morgan, University of Northern Iowa
- Daniel Perley, California Institute of Technology
- Claire Raftery, National Solar Observatory
- Deborah Scherrer, retired, Stanford University
- Phillip Scherrer, Stanford University
- Sanjoy Som, Blue Marble Space Institute of Science, NASA Ames Research Center
- Wes Tobin, Indiana University East
- William H. Waller, retired, Tufts University, Rockport (MA) Public Schools

Caralyn Zehnder, Kalina Manoylov, Samuel Mutiti, Christine Mutiti, Allison VandeVoort, and Donna Bennett (2018). *Introduction to Environmental Science: 2nd edition*. (CC BY-NC-SA). University System of Georgia. Retrieved from https://alg.manifoldapp.org/projects/introduction-to-environmental-science.

Introduction to Environmental Science: 2nd Edition (2018) was developed for students taking the course Introduction to Environmental Science in collaboration between

- Caralyn Zehnder, formerly Georgia College and State University; currently University of Massachusetts Amherst
- Kalina Manoylov, Georgia College and State University
- Samuel Mutiti, Georgia College and State University
- Christine Mutiti, Georgia College and State University
- Allison VandeVoort, Georgia College and State University
- Donna Bennett, Georgia College and State University

Emily P. Harris (2023). *Introduction to Environmental Sciences and Sustainability*. (CC BY). University of West Florida. Retrieved from https://pressbooks.uwf.edu/envrioscience. Book is a cloned version of *Environmental Biology* by Matthew R. Fisher, published using Pressbooks by Open Oregon Educational Resources under a CC BY (Attribution) license (may differ from the original).

Introduction to Environmental Sciences and Sustainability (2023) was edited and co-authored by

- Emily P. Harris
- The Department of Earth and Environmental Sciences at the University of West Florida

Features of This Book

- Example-rich narrative
- Graphic elements that illustrate and reinforce concepts
- Linked online glossary (glossary appears at the end for PDF)
- Embedded navigation and image alt-text for screen readers
- Online interactive self-test quiz questions
- Available free online and in PDF, and in-print at vendor cost of production
- Open license, Creative Commons BY NC-SA 4.0 permits customization and sharing
- Instructor community portal for sharing ancillary resources
- Interest form allows instructors to opt in to receiving book updates
- Errata and report-an-error/share-a-suggestion forms promote currentness

INSTRUCTOR RESOURCES

Available formats and helpful links

Navigate to the book's main landing page to access:

- Links to multiple electronic versions of the textbook (PDF, EPUB, HTML)
- A link to Amazon for ordering a print copy
- A link to the errata document
- A link to report errors

If you are interested in making your own version of this book, check out the book's license and information on recommended practices for attribution.

Instructors reviewing, adopting, or adapting this textbook are encouraged to register their interest and check out the public-facing instructor sharing portal. This assists the Open Education Initiative at Virginia Tech in assessing the impact of the book and allows us to more easily alert instructors of additional resources, features and opportunities.

About open educational resources (OER)

OER are free teaching and learning materials that are licensed to allow for revision and reuse. They can be fully self-contained textbooks, videos, quizzes, learning modules, and more. OER are distinct from free online resources in that they permit others to use, copy, distribute, modify, or reuse the content. The legal permission to modify and customize OER to meet the specific learning objectives of a particular course make them a useful pedagogical tool.

About this book

Introduction to Earth Science, second edition is an open book. You are welcome to freely use, adapt, and share this book with attribution according to the CC BY-NC-SA 4.0 license. This license allows sharing and adaptation as long as (1) attribution is provided, (2) the new work is licensed the same as the original, and (3) the material is not used in ways that are primarily commercial.

URLs

License: https://creativecommons.org/licenses/by-nc-sa/4.0/deed.en

Instructor interest form: https://bit.ly/interest_intro_earth_science

Public-facing instructor sharing portal: https://www.oercommons.org/groups/introduction-to-earth-science-instructor-group/12785

Book's main landing page: https://doi.org/10.21061/introearthscience2e

View known errata: https://bit.ly/errata_intro_earth_science_2e

Report an error: https://bit.ly/report_error_intro_earth_science

Recommended practices for attribution: https://wiki.creativecommons.org/wiki/Recommended_practices_for_attribution

1. UNDERSTANDING SCIENCE

Learning Objectives

By the end of this chapter, students should be able to:

- Contrast objective and subjective observations, as well as quantitative and qualitative observations.
- Identify a pseudoscience based on its lack of falsifiability.
- Contrast the methods used by Aristotle and Galileo to describe the natural environment.
- Explain the scientific method, and apply it to a problem or question.
- Describe the foundations of modern geology, such as the principle of uniformitarianism.
- Contrast uniformitarianism with catastrophism.
- Explain why studying geology is important.
- Identify how Earth materials are transformed by rock cycle processes.
- Describe the steps involved in a reputable scientific study.
- Explain rhetorical arguments used by science deniers.

1.1 What Is Science?

Scientists seek to understand the fundamental principles that explain natural patterns and processes. Science is more than just a body of knowledge; science provides a means to evaluate and create new knowledge without bias. Scientists use objective evidence over subjective evidence to reach sound and logical conclusions.

An **objective observation** is made without personal bias and will be the same for all individuals. Humans are biased by nature, so they cannot be completely objective; the goal is to be as unbiased as possible. A **subjective** observation is based on a person's feelings and beliefs and is unique to that individual.

Another way scientists avoid bias is by using quantitative over qualitative measurements whenever possible. A **quantitative** measurement is expressed with a specific numerical value. **Qualitative** observations are general or relative descriptions. For example, describing a rock as red or heavy is a qualitative observation. Determining a rock's color by measuring wavelengths of reflected light or the proportions of minerals it contains is quantitative. Numerical values are more precise than general descriptions, and they can be analyzed using statistical calculations. This is why quantitative measurements are much more useful to scientists than qualitative observations.

Figure 1.1: This is Cascade Falls in Pembroke, Virginia. An objective statement about this would be: "The picture is of a waterfall." A subjective statement would be: "The setting is beautiful," or "The waterfall is there because of erosion." Figure description available at the end of the chapter.

Establishing truth in science is difficult because all scientific claims are **falsifiable**, which means any initial hypothesis may be tested and proven false. A hypothesis can only become regarded as a reliable scientific **theory** after exhaustively eliminating false results, competing ideas, and possible variations. This meticulous scrutiny reveals weaknesses or flaws in a hypothesis and is the source of the strength that supports all scientific ideas and procedures. In fact, proving current ideas are wrong has been the driving force behind many scientific careers.

Figure 1.2: Canyons like this, carved in the deposit left by the May 18th, 1980, eruption of Mount St. Helens, are sometimes used by purveyors of pseudoscience as evidence for the Earth being very young. In reality, the unconsolidated and unlithified volcanic deposit is carved much more easily than other canyons like the Grand Canyon. Figure description available at the end of the chapter.

Figure 1.3: Geologists share information by publishing, attending conferences, and even going on field trips, such as this trip to the Lake Owyhee Volcanic Field in Oregon by the Bureau of Land Management in 2019. Figure description available at the end of the chapter.

Falsifiability separates science from pseudoscience. Scientists are wary of explanations of natural phenomena that discourage or avoid falsifiability. An explanation that cannot be tested or does not meet scientific standards is not considered science, but pseudoscience. **Pseudoscience** is a collection of ideas that may appear scientific but does not use the scientific method. Astrology is an example of pseudoscience. It is a belief system that attributes human behaviors to the movement of celestial bodies. Astrologers rely on celestial observations, but their conclusions are not based on experimental evidence and their statements are not falsifiable. Astrology should not be confused with **astronomy**, which is the scientific study of celestial bodies and the cosmos.

Science is also a social process. Scientists share their ideas with peers at conferences, seeking guidance and feedback. Research papers and data submitted for publication are rigorously reviewed by qualified peers, scientists who are experts in the same field. The scientific review process aims to weed out misinformation, invalid research results, and wild speculation. Thus, the process is slow, cautious, and conservative. Scientists tend to wait until a hypothesis is supported by an overwhelming amount of evidence from many independent researchers before accepting it as scientific theory.

Take this quiz to check your comprehension of this section.

Access the quiz for Section 1.1 by scanning the QR code.

1.2 The Scientific Method

Modern science is based on the **scientific method**, a procedure that follows these steps:

- Formulate a question or observe a problem.
- Apply objective experimentation and observation.
- Analyze collected data and interpret results.
- Devise an evidence-based theory.
- Submit findings to peer review and/or publication.

This process has a long history in human thought but was first fully formed by Ibn al-Haytham over 1,000 years ago. At the forefront of the scientific method are conclusions based on objective evidence, not opinion or hearsay.

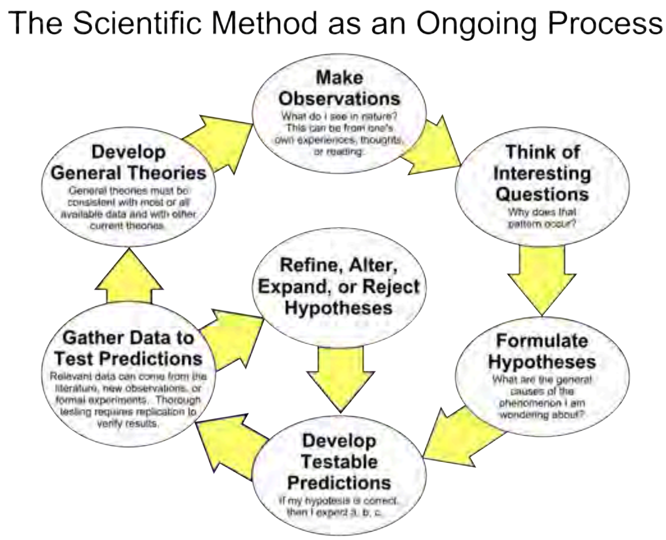

Figure 1.4: Diagram of the cyclical nature of the scientific method. [Figure description available at the end of the chapter.]

Step One: Observation, Problem, or Research Question

The procedure begins with identifying a problem or research question about, for instance, a geological phenomenon that is not well explained in the scientific community's collective knowledge. This step usually involves reviewing the scientific literature to understand previous studies that may be related to the question.

Step Two: Hypothesis

Figure 1.5: A famous hypothesis. Leland Stanford wanted to know if a horse lifted all four legs off the ground during a gallop, since the legs are too fast for the human eye to perceive. This series of photographs by Eadweard Muybridge proved the horse does, in fact, lift all four legs off the ground during the gallop. [Figure description available at the end of the chapter.]

Once the problem or question is well defined, the scientist proposes a possible answer, a **hypothesis**, before conducting an **experiment** or field work. This **hypothesis** must be specific and falsifiable, and should be based on other scientific work. Geologists often develop multiple working hypotheses because they usually cannot impose strict experimental controls or have limited opportunities to visit a field location.

Step Three: Experiment and Hypothesis Revision

The next step is developing an **experiment** that either supports or refutes the hypothesis. Many people mistakenly think experiments are only done in labs; however, an experiment can simply involve observing natural processes in the field. Regardless of what form an experiment takes, it always includes the systematic gathering of objective data. This data is interpreted to determine whether it contradicts or supports the hypothesis, which may be revised and tested again. When a hypothesis holds up under experimentation, it is ready to be shared with other experts in the field.

Step Four: Peer Review, Publication, and Replication

Scientists share the results of their research by publishing articles in scientific journals, such as *Science* and *Nature*. Reputable journals and publishing houses will not publish an experimental study until they have determined its methods are scientifically rigorous and the conclusions are supported by evidence. Before an article is published, it undergoes a rigorous **peer review** by scientific experts who scrutinize the methods, results, and discussion. Once an article is published, other scientists may attempt to replicate the results. This replication is necessary to confirm the reliability of the study's reported results. A hypothesis that seemed compelling in one study might be proven false in studies conducted by other scientists. New technology can be applied to published studies, which can aid in confirming or rejecting once-accepted ideas and/or hypotheses.

Figure 1.6: An experiment at the University of Queensland has been ongoing since 1927. A petroleum product called pitch, which is highly viscous, drips out of a funnel about once per decade. [Figure description available at the end of the chapter.]

Step Five: Theory Development

In casual conversation, the word *theory* implies guesswork or speculation. In the language of science, an explanation or conclusion made in a **theory** carries much more weight because it is supported by experimental verification and widely accepted by the scientific community. After a hypothesis has been repeatedly tested for falsifiability through documented and independent studies, it eventually becomes accepted as a scientific **theory**.

Figure 1.7: Wegener later in his life, ca. 1924-1930. Figure description available at the end of the chapter.

While a hypothesis provides a tentative explanation *before* an experiment, a theory is the best explanation *after* confirmation from multiple independent experiments. Confirmation of a theory may take years or even longer. For example, the continental drift hypothesis first proposed by Alfred Wegener in 1912 was initially dismissed; after decades of additional evidence collection by other scientists using more advanced technology, Wegener's hypothesis was accepted and revised as the theory of plate tectonics.

The theory of evolution by natural selection is another example. Originating from the work of Charles Darwin in the mid-nineteenth century, the theory of evolution has withstood generations of scientific testing for falsifiability. While it has been updated and revised to accommodate knowledge gained by using modern technologies, the theory of evolution continues to be supported by the latest evidence.

Take this quiz to check your comprehension of this section.

Access the quiz for Section 1.2 by scanning the QR code.

1.3 Early Scientific Thought

Figure 1.8: Fresco by Raphael of Plato (left) and Aristotle (right). Figure description available at the end of the chapter.

Western scientific thought began in the ancient city of Athens, Greece. Athens was governed as a democracy, which encouraged individuals to think independently at a time when most civilizations were ruled by monarchies or military conquerors. Foremost among the early philosopher-scientists to use empirical thinking was Aristotle, born in 384 BCE. Empiricism emphasizes the value of evidence gained from experimentation and observation. Aristotle studied under Plato and tutored Alexander the Great. Alexander would later conquer the Persian Empire and, in the process, spread Greek culture as far east as India.

Aristotle applied an empirical method of analysis called **deductive reasoning**, which applies known principles of thought to establish new ideas or predict new outcomes. Deductive reasoning starts with generalized principles and logically extends them to new ideas or specific conclusions. If the initial principle is valid, then it is highly likely the conclusion is also valid. An example of deductive reasoning is "if A = B and B = C, then A = C". Another example is "if all birds have feathers and a sparrow is a bird, then a sparrow must also have feathers." The problem with deductive reasoning is, if the initial principle is flawed, the conclusion will inherit that flaw. Here is an example of a flawed initial principle leading to the wrong conclusion: if all animals that fly are birds and bats also fly, then bats must also be birds.

This type of empirical thinking contrasts with **inductive reasoning**, which begins from new observations and attempts to discern underlying generalized principles. A conclusion made through inductive reasoning comes from analyzing measurable evidence rather making a logical connection. For example, to determine whether bats are birds, a scientist might list various characteristics observed in birds (i.e., the presence of feathers, a toothless beak, hollow bones, lack of forelegs, and externally laid eggs); next, the scientist would check whether bats share the same characteristics and, if they do not, draw the conclusion that bats are not birds.

Both types of reasoning are important in science because they emphasize the two most important aspects of science: observation and inference. Scientists test existing principles to see if they accurately infer or predict their observations. They also analyze new observations to determine if the inferred underlying principles still support them.

Greek culture was spread by Alexander and then absorbed by the Romans, who further extended Greek knowledge into Europe through their vast infrastructure of roads, bridges, and aqueducts. After the fall of the Roman Empire in 476 CE, scientific progress in Europe stalled. Scientific thinkers of the medieval period that followed had such high regard for Aristotle's wisdom and knowledge that they faithfully followed his logical approach to understanding nature for centuries. By contrast, science in the Middle East progressed and flourished between 800 and 1450 CE, along with culture and the arts.

Figure 1.9: Drawing of Avicenna (Ibn Sina). He is among the first to link mountains to earthquakes and erosion. Figure description available at the end of the chapter.

Near the end of the medieval period, empirical experimentation became more common in Europe. During the Renaissance, which lasted from the fourteenth through seventeenth centuries, artistic and scientific thought experienced a great awakening. European scholars began to criticize the traditional Aristotelian approach, and by the end of the Renaissance period, empiricism was poised to become a key component of the Scientific Revolution that would arise in the seventeenth century.

Figure 1.10: Geocentric drawing by Bartolomeu Velho in 1568. Figure description available at the end of the chapter.

An early example of how Renaissance scientists began to apply a modern empirical approach is their study of the **Solar System**. In the second century, the Greek astronomer Claudius Ptolemy observed the Sun, Moon, and stars moving across the sky. Applying Aristotelian logic to his astronomical calculations, he deductively reasoned all celestial bodies orbited around the Earth, which was thought to be located at the center of the universe. Ptolemy was a highly regarded mathematician, and his mathematical calculations were widely accepted by the scientific community. The view of the cosmos with Earth at its center is called the geocentric model. This geocentric model persisted until the Renaissance period, when some revolutionary thinkers challenged the centuries-old hypothesis.

RECENS HABITAE. 23

dentalis proxima min. 2. ab hac vero elongabatur occidentalior altera min: 10. erant præcisè in eadem recta, & magnitudinis æqualis.

Die quarta hora secunda circa Iouem quatuor stabant Stellæ, orientales duæ, ac duæ occidentales in eadem ad vnguem recta linea dispositæ, vt in proxima figura. Orientalior distabat à sequenti min. 3. hæc verò à Ioue aberat min. 0. sec. 40. Iuppiter à proxima occidentali min 4. hæc ab occidentaliori min. 6. magnitudine erant ferè æquales, proximior Ioui reliquis paulo minor apparebat. Hora autem septima orientales Stellæ distabant tantum min. 0. sec. 30. Iuppiter ab orientali viciniori aberat min. 2. ab occidentali verò sequente min. 4. hæc verò ab occidentaliori distabat min. 3. erantque æquales omnes, & in eadem recta secundum Eclypticam extensa.

Die quinta Cœlum fuit nubilosum.

Die sexta duæ solummodo apparuerunt Stellæ me-

Ori. Occ.

dium

Figure 1.11: Galileo's first mention of Jupiter's moons. Figure description available at the end of the chapter.

By contrast, early Renaissance scholars such as astronomer Nicolaus Copernicus (1473-1543) proposed an alternative explanation for the perceived movement of the Sun, Moon, and stars. Sometime between 1507 and 1515, he provided credible mathematical proof for a radically new model of the cosmos, one in which the Earth and other planets orbited around a centrally located Sun. After the invention of the telescope in 1608, scientists used their enhanced astronomical observations to support this heliocentric, Sun-centered model.

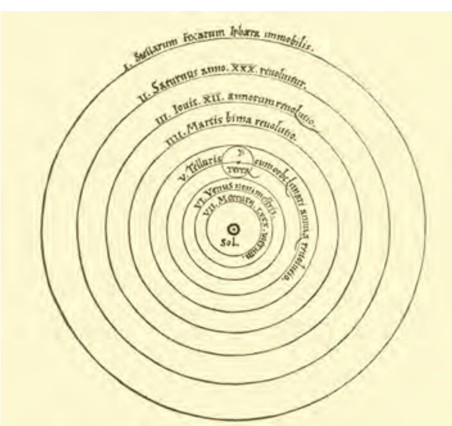

Figure 1.12: Copernicus's heliocentric model. Figure description available at the end of the chapter.

Two scientists, Johannes Kepler and Galileo Galilei, are credited with jump-starting the scientific revolution. They accomplished this by building on Copernicus's work and challenging long-established ideas about nature and science.

Johannes Kepler (1571–1630) was a German mathematician and astronomer who expanded on the heliocentric model, improving Copernicus's original calculations and describing planetary motion as elliptical paths. Galileo Galilei (1564–1642) was an Italian astronomer who used the newly developed telescope to observe the four largest moons of Jupiter. This was the first piece of direct evidence to contradict the geocentric model, since moons orbiting Jupiter could not also be orbiting Earth.

Galileo strongly supported the heliocentric model and attacked the geocentric model, arguing for a more scientific approach to determine the credibility of ideas. Because of this, he found himself at odds with prevailing scientific views and the Catholic Church. In 1633, he was found guilty of heresy and placed under house arrest, where he would remain until his death in 1642.

Galileo is regarded as the first modern scientist because he conducted experiments that would prove or disprove falsifiable ideas and based his conclusions on mathematical analysis of quantifiable evidence—a radical departure from the deductive thinking of Greek philosophers such as Aristotle. His methods marked the beginning of a major shift in how scientists studied the natural world, with an increasing number relying on evidence and experimentation to form their hypotheses. It was during this revolutionary time that geologists such as James Hutton and Nicolas Steno also made great advances in their scientific fields of study.

Take this quiz to check your comprehension of this section.

Access the quiz for Section 1.3 by scanning the QR code.

1.4 Foundations of Modern Geology

As part of the Scientific Revolution in Europe, modern geologic principles developed in the 17th and 18th centuries. One major contributor was Nicolaus Steno (1638–1686), a Danish priest who studied anatomy and geology. Steno was the first to propose that Earth's surface could change over time. He suggested sedimentary rocks, such as **sandstone** and **shale**, originally formed in horizontal layers with the oldest on the bottom and progressively younger layers on top.

Figure 1.13: Illustration by Steno showing a comparison between fossils and modern shark teeth. Figure description available at the end of the chapter.

In the eighteenth century, Scottish naturalist James Hutton (1726–1797) studied **rivers** and coastlines and compared the sediments they left behind to exposed sedimentary rock strata. He hypothesized the ancient rocks must have been formed by processes like those producing the features in oceans and **streams**. Hutton also proposed the Earth was much older than previously thought. Modern geologic processes operate slowly; Hutton realized that, if these processes formed rocks, then the Earth must be very old, possibly hundreds of millions of years old.

Hutton's idea is called the **principle of uniformitarianism** and states that natural processes operate the same now as in the past, i.e., the laws of nature are uniform across space and time. Geologist often state "the present is the key to the past," meaning they can understand ancient rocks by studying modern geologic processes.

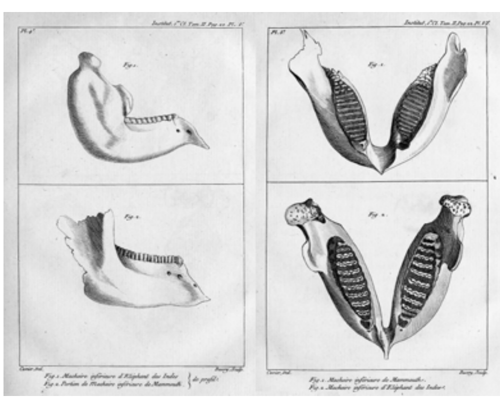

Figure 1.14: Cuvier's comparison of modern elephant and mammoth jaw bones. Figure description available at the end of the chapter.

Prior to the acceptance of uniformitarianism, scientists such as German geologist Abraham Gottlob Werner (1750–1817) and French anatomist Georges Cuvier (1769–1832) thought rocks and landforms were formed by great catastrophic events. Cuvier championed this view, known as **catastrophism**, and stated, "The thread of operation is broken; nature has changed course, and none of the agents she employs today would have been sufficient to produce her former works." He meant processes that operate today did not operate in the past. Known as the father of **vertebrate** paleontology, Cuvier made significant contributions to the study of ancient life and taught at Paris's Museum of Natural History. Based on his study of large vertebrate fossils, he was the first to suggest species could go **extinct**. However, he thought new species were introduced by special creation after catastrophic floods.

Hutton's ideas about uniformitarianism and Earth's age were not well received by the scientific community of his time. His ideas were falling into obscurity when Charles Lyell, a British lawyer and geologist (1797–1875), wrote *Principles of Geology* in the early 1830s and later, *Elements of Geology*. Lyell's books promoted Hutton's principle of uniformitarianism, his studies of rocks and the processes that formed them, and the idea that Earth was possibly over 300 million years old. Lyell and his three-volume *Principles of Geology* had a lasting influence on the geologic community and public at large, who eventually accepted uniformitarianism and Earth being millions of years old. The principle of uniformitarianism became so widely accepted that geologists regarded catastrophic change as heresy. This made it harder for ideas like the sudden demise of the dinosaurs by asteroid impact to gain traction.

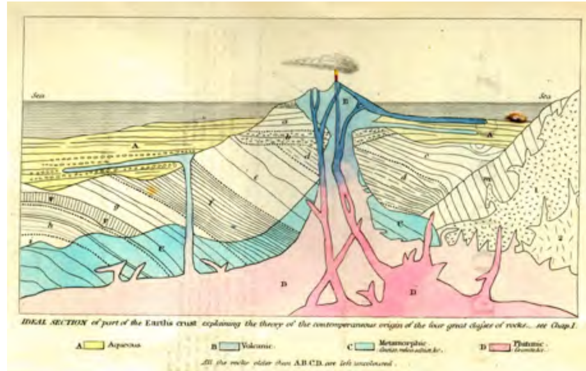

Figure 1.15: Inside cover of Lyell's *Elements of Geology*. Figure description available at the end of the chapter.

A contemporary of Lyell, Charles Darwin (1809–1882) took *Principles of Geology* on his five-year trip on the HMS Beagle. Darwin used uniformitarianism and deep geologic time to develop his initial ideas about evolution. Lyell was one of the first to publish a reference to Darwin's idea of evolution.

The next big advancement, and perhaps the largest in the history of geology, is the theory of plate tectonics and continental drift. Dogmatic acceptance of uniformitarianism inhibited the progress of this idea, mainly because of the permanency placed on the continents and their positions. Ironically, slow and steady movement of **plates** would fit well into a uniformitarianist model. However, much time passed and a great deal of scientific resistance had to be overcome before the idea took hold. This delay happened for several reasons. Firstly, the movement was so slow, it was overlooked. Secondly, the best evidence was hidden under the ocean. Finally, the accepted theories were anchored by a large amount of inertia. Instead of being bias-free, scientists resisted and ridiculed the emerging idea of plate tectonics. This example of dogmatic thinking remains, to this day, a tarnish on the geoscience community.

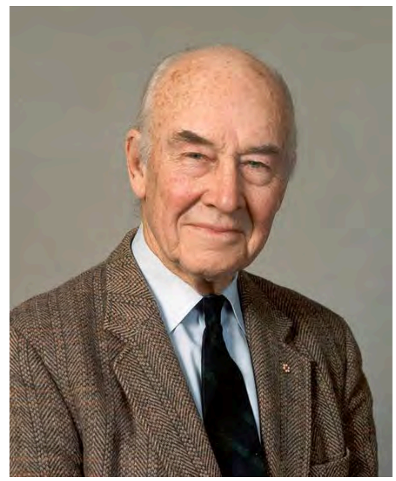

Figure 1.16: J. Tuzo Wilson. Figure description available at the end of the chapter.

Plate tectonics is most commonly attributed to Alfred Wegener, the first scientist to compile a large data set supporting the idea of continents shifting places over time. He was mostly ignored and ridiculed for his ideas, but later contributors like Marie Tharp, Bruce Heezen, Harry Hess, Laurence Morley, Frederick Vine, Drummond Matthews, Kiyoo Wadati, Hugo Benioff, Robert Coats, and J. Tuzo Wilson benefited from advances in subsea technologies. They discovered, described, and analyzed new features like the **mid-ocean ridge**, alignment of earthquakes, and **magnetic striping**. Gradually, these scientists introduced a paradigm shift that revolutionized geology into the science we know today.

Take this quiz to check your comprehension of this section.

Access the quiz for Section 1.4 by scanning the QR code.

1.5 The Study of Geology

Geologists apply the scientific method to learn about Earth's materials and processes. Geology plays an important role in society, as its principles are essential to locating, extracting, and managing natural resources; evaluating environmental impacts of using or extracting these resources; as well as understanding and mitigating the effects of natural hazards.

Geology often applies information from physics and chemistry to understand parts of the natural world, like the physical forces in a **landslide** or the chemical interaction between water and rocks. The term comes from the Greek word *geo*, meaning Earth, and *logos*, meaning to think or reckon with.

Figure 1.17: Girls into Geoscience inaugural Irish fieldtrip. Figure description available at the end of the chapter.

1.5.1 Why Study Geology?

Figure 1.18: Glen Canyon Dam in the Southwestern United States forms Lake Powell, a reservoir on the Colorado River in Utah and Arizona. The dam also provides hydroelectric energy. Figure description available at the end of the chapter.

Geology plays a key role in how we use **natural resources**—any naturally occurring material that can be extracted from the Earth for economic gain. Our developed modern society, like all societies before it, is dependent on geologic resources. Geologists are involved in extracting **fossil fuels**, such as **coal** and **petroleum**; **metals**, such as copper, aluminum, and iron; and water resources in streams and underground reservoirs inside soil and rocks. They can help conserve our planet's finite supply of **nonrenewable resources**, like petroleum, which are fixed in quantity and depleted by consumption. Geologists can also help manage **renewable resources** that can be replaced or regenerated, such as solar energy, wind energy, and timber.

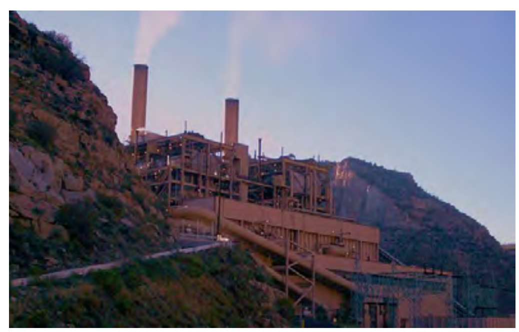

Figure 1.19: Coal power plant in Helper, Utah. Figure description available at the end of the chapter.

Resource extraction and usage impacts our environment, which can negatively affect human health. For example, burning fossil fuels releases chemicals into the air that are unhealthy for humans, especially children. Mining activities can release toxic heavy metals, such as lead and mercury, into the soil and waterways. Our choices will have an effect on Earth's environment for the foreseeable future. Understanding the remaining quantity, extractability, and renewability of geologic resources will help us manage those resources more sustainably.

Figure 1.20: Buildings toppled from liquefaction during a 7.5 magnitude earthquake in Japan. Figure description available at the end of the chapter.

Geologists also study natural hazards created by geologic processes. **Natural hazards** are phenomena that are potentially dangerous to human life or property. No place on Earth is completely free of natural hazards, so one of the best ways people can protect themselves is by understanding geology. Geology can teach people about the natural hazards in an area and how to prepare for them. Geologic hazards include landslides, earthquakes, tsunamis, floods, volcanic eruptions, and sea-level rise.

Figure 1.21: Oregon's Crater Lake was formed about 7,700 years ago after the eruption of Mount Mazama. Figure description available at the end of the chapter.

Finally, geology is where other scientific disciplines intersect in the concept known as Earth system science. In science, a **system** is a group of interactive objects and processes. **Earth system science** views the entire planet as a combination of systems that interact with each other via complex relationships. This geology textbook provides an introduction to science in general and will often reference other scientific disciplines.

Earth system science includes five basic systems (or spheres): the **geosphere** (the solid body of the Earth), the **atmosphere** (the gas envelope surrounding the Earth), the **hydrosphere** (water in all its forms at and near the surface of the Earth), the **cryosphere** (the frozen water part of Earth), and the **biosphere** (life on Earth in all its forms and interactions, including humankind).

Rather than viewing geology as an isolated system, Earth system scientists study how geologic processes shape not only the world but all the spheres it contains. They study how these multidisciplinary spheres relate, interact, and change in response to natural cycles and human-driven forces. They use elements from physics, chemistry, biology, meteorology, environmental science, zoology, hydrology, and many other sciences.

1.5.2 Rock Cycle

The most fundamental view of Earth materials is the **rock cycle**, which describes the major materials that comprise the Earth, the processes that form them, and how they relate to each other. It usually begins with hot molten liquid rock called magma or lava. **Magma** forms under the Earth's surface in the crust or mantle. **Lava** is molten rock that erupts onto the Earth's surface. When magma or lava cools, it solidifies by a process called **crystallization** in which minerals grow within the magma or lava. The resulting rocks are **igneous** rocks (*ignis* is Latin for "fire").

Igneous rocks, as well as other types of rocks, on Earth's surface are exposed to weathering and erosion, which produce sediments. **Weathering** is the physical and chemical breakdown of rocks into smaller fragments. **Erosion** is the removal of those fragments from their original location. The broken-down and transported fragments and grains are considered **sediments**, which include gravel, sand, silt, and clay. These sediments may be transported by streams and rivers, ocean currents, glaciers, and wind.

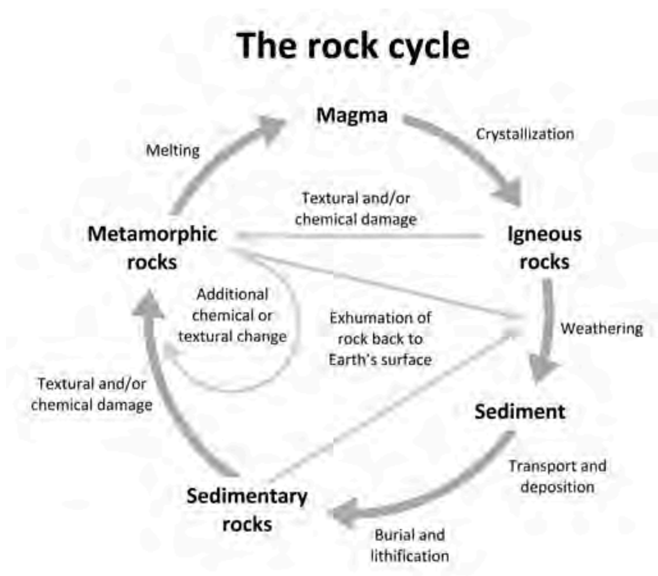

Figure 1.22: Rock cycle showing the five materials (such as igneous rocks and sediment) and the processes by which one changes into another (such as weathering). Figure description available at the end of the chapter.

Figure 1.23: Jurassic-aged sandstone makes up the walls of Antelope Canyon in the American Southwest. The slot canyon itself is estimated to have been naturally carved out over the last 5–6 million years. Figure description available at the end of the chapter.

Sediments come to rest in a process known as **deposition**. As the deposited sediments accumulate—often under water, such as in a shallow **marine environment**—the older sediments get buried by the new deposits. The deposits are compacted by the weight of the overlying sediments, and individual grains are cemented together by minerals in **groundwater**. These processes of **compaction** and **cementation** are called **lithification**. Lithified sediments are considered a **sedimentary rock**, such as sandstone and shale. Other sedimentary rocks are made by direct chemical precipitation of minerals rather than eroded sediments and are known as **chemical** sedimentary rocks.

Figure 1.24: Metamorphic rock in Georgian Bay, Ontario. Figure description available at the end of the chapter.

Preexisting rocks may be transformed into **metamorphic** rocks (*meta-* means "change" and *-morphos* means "form" or "shape"). When rocks are subjected to extreme increases in temperature or pressure, the mineral crystals are enlarged or altered into entirely new minerals with similar chemical makeups. High temperatures and pressures occur in rocks that are buried deep within the Earth's crust or that come into contact with hot magma or lava. If the temperature and pressure conditions melt the rocks to create magma and lava, the rock cycle begins anew with the creation of new rocks.

1.5.3 Plate Tectonics and Layers of Earth

Figure 1.25: Map of the major plates and their motions along boundaries. Figure description available at the end of the chapter.

The theory of **plate tectonics** is the fundamental unifying principle of geology and the rock cycle. Plate tectonics describes how Earth's layers move relative to each other, focusing on the **tectonic** or lithospheric plates of the outer layer. Tectonic plates float, collide, slide past each other, and split apart on an underlying mobile layer called the **asthenosphere**. Major landforms are created at the plate boundaries, and rocks within the tectonic plates move through the rock cycle. Plate tectonics is discussed in more detail in Chapter 2.

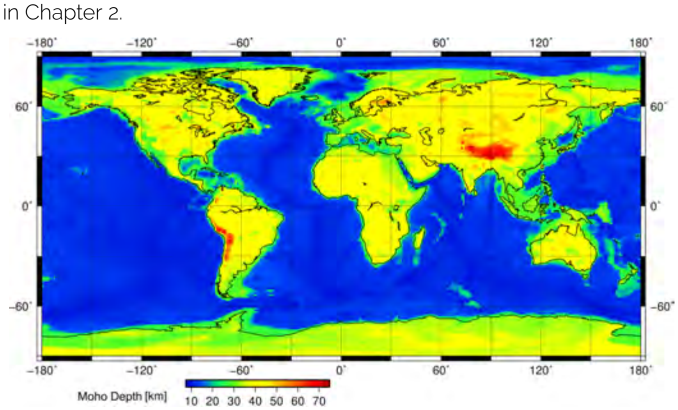

Figure 1.26: The global map of the depth of the boundary between the crust and mantle. Figure description available at the end of the chapter.

Earth's three main geological layers can be categorized by chemical **composition** or the chemical makeup: crust, mantle, and core. The **crust** is the outermost layer and is composed of mostly silicon, oxygen, aluminum, iron, and magnesium. There are two types, continental crust and oceanic crust. **Continental crust** is about 50 km (30 mi) thick and is composed of low-density igneous and sedimentary rocks. **Oceanic crust** is approximately 10 km (6 mi) thick and made of high-density igneous **basalt**-type rocks. Oceanic crust makes up most of the ocean floor, covering about 70% of the planet. Tectonic plates are made of crust and a portion the upper mantle, forming a rigid physical layer called the **lithosphere**.

The **mantle**, the largest chemical layer by volume, lies below the crust and extends down to about 2,900 km (1,800 mi) below the Earth's surface. The mostly solid mantle is made of **peridotite**, a high-density rock composed of silica, iron, and magnesium. The upper part of mantel is very hot and flexible, which allows the overlying tectonic plates to float and move about on it. Under the mantle is the Earth's **core**, which is 3,500 km (2,200 mi) thick and made of iron and nickel. The core consists of two parts, a liquid **outer core** and solid **inner core**. Rotations within the solid and liquid metallic core generate Earth's magnetic field (see Figure 1.27).

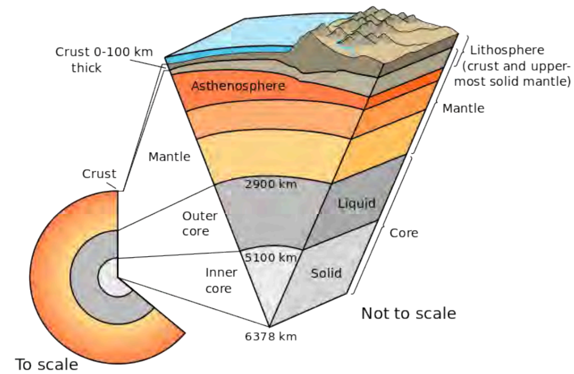

Figure 1.27: The layers of the Earth. Physical layers include lithosphere and asthenosphere; chemical layers are crust, mantle, and core. Figure description available at the end of the chapter.

1.5.4 Geologic (Deep) Time

> "The result, therefore, of our present enquiry is that we find no vestige of a beginning, no prospect of an end." (James Hutton, 1788)

One of the early pioneers of geology, James Hutton, wrote this about the age of the Earth after many years of geological study. Although he wasn't exactly correct—there is a beginning and will be an end to planet Earth—Hutton was expressing the difficulty humans have in perceiving the vastness of geological time. Hutton did not assign an age to the Earth, although he was the first to suggest the planet was very old.

Today, we know Earth is approximately 4.54 ± 0.05 billion years old. This age was first calculated by Caltech professor Clair Patterson in 1956, who measured the half-lives of lead isotopes to radiometrically date a meteorite recovered in Arizona. Studying geologic time, also known as deep time, can help us move past a limited perspective of Earth based on our short lifetimes. Compared to the geologic scale, the human lifespan is very short, resulting in our struggle to comprehend the depth of geologic time and slowness of geologic processes. For example, the study of earthquakes only goes back about 100 years; however, there is geologic evidence of large earthquakes occurring thousands of years ago, with scientific evidence indicating that earthquakes will continue for many centuries into the future.

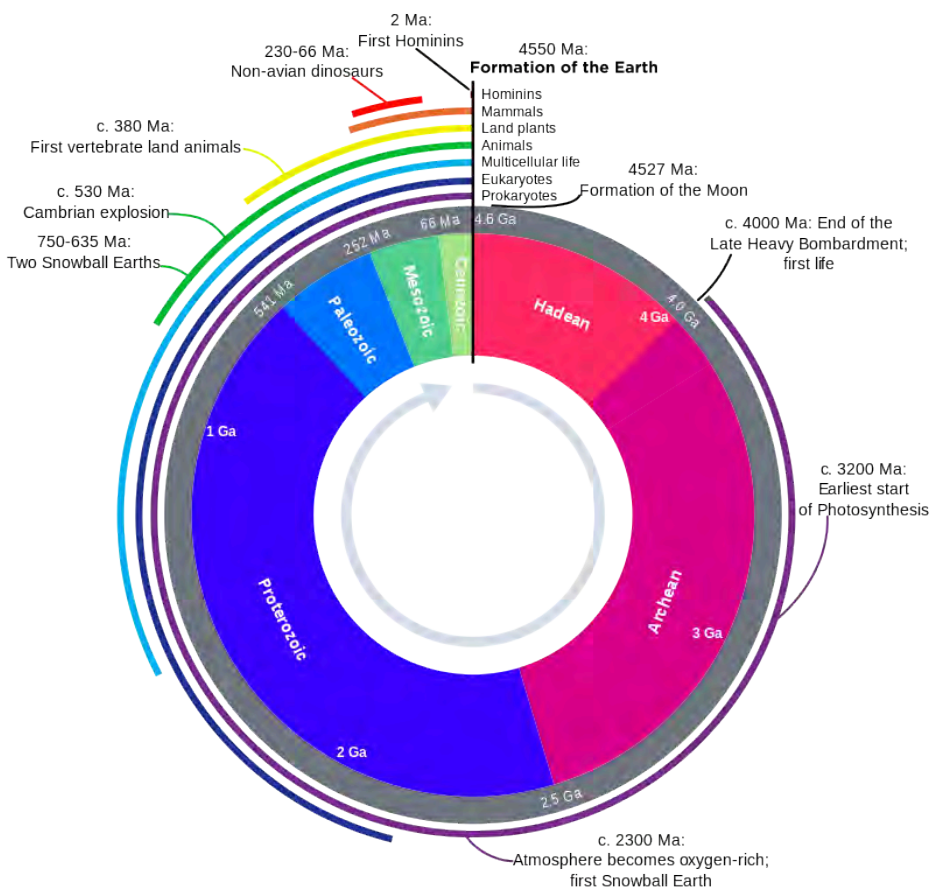

Figure 1.28: Geologic time on Earth, represented circularly, showing the individual time divisions and important events. Ga = billion years ago, Ma = million years ago. Figure description available at the end of the chapter.

Eons are the largest divisions of time and are named, from oldest to youngest, Hadean, Archean, Proterozoic, and Phanerozoic. The three oldest eons are sometimes collectively referred to as **Precambrian** time.

Life first appeared more than 3,800 million years ago (Ma). From 3,500 Ma to 542 Ma, or 88% of geologic time, the predominant life forms were single-celled organisms such as bacteria. More complex organisms appeared only more recently during the current **Phanerozoic** Eon, which includes the last 542 million years, or 12% of geologic time.

The name Phanerozoic comes from *phaneros*, which means "visible," and *zoic*, meaning "life." This eon marks the proliferation of multicellular animals with hard body parts, such as shells, which are preserved in the geological record as **fossils**. Land-dwelling animals have existed for 360 million years, or 8% of geologic time. The demise of the dinosaurs and subsequent rise of mammals occurred around 65 Ma, spanning 1.5% of geologic time. Our human ancestors belonging to the genus *Homo* have existed for approximately 2.2 million years—0.05% of geological time, or just 1/2,000th the total age of Earth.

The Phanerozoic Eon is divided into three **eras**: Paleozoic, Mesozoic, and Cenozoic. **Paleozoic** means "ancient life," and organisms of this era include invertebrate animals, fish, amphibians, and reptiles. The **Mesozoic** ("middle life") is popularly known as the Age of Reptiles and is characterized by the abundance of dinosaurs, many of which evolved into birds. The **mass extinction** of the dinosaurs and other apex predator reptiles marked the end of the Mesozoic and beginning of the Cenozoic. **Cenozoic** means "new life" and is also called the Age of Mammals, during which mammals evolved to become the predominant land-dwelling animals. Fossils of early humans, or hominids, appear in the rock record only during the last few million years of the Cenozoic. The geologic timescale, geologic time, and geologic history are discussed in more detail in Chapters 7 and 8.

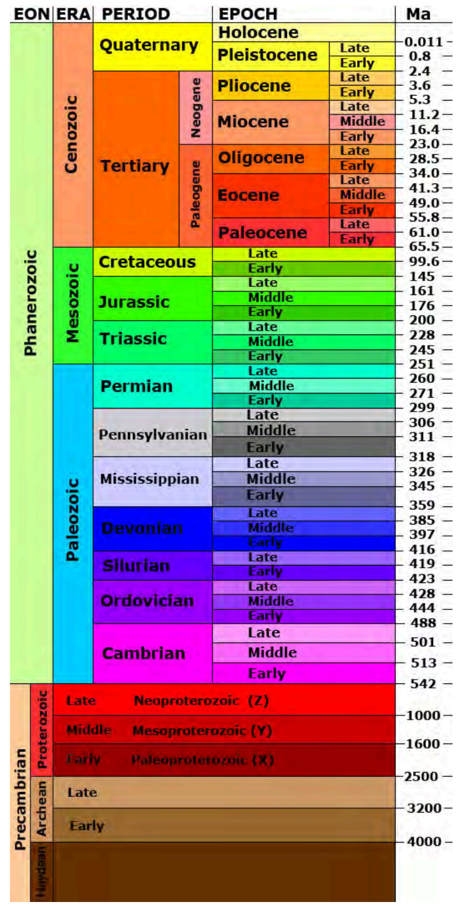

Figure 1.29: Geologic timescale showing time period names and ages. Figure description available at the end of the chapter.

1.5.5 The Geologist's Tools

A geologist's tool can be as simple as a rock hammer used for sampling a fresh surface of a rock. A basic toolset for fieldwork might also include:

- Magnifying lens for looking at mineralogical details
- Compass for measuring the orientation of geologic features
- Map for documenting the local distribution of rocks and minerals
- Magnet for identifying magnetic minerals like magnetite
- Dilute solution of hydrochloric acid to identify carbonate-containing minerals like calcite or limestone.

In the laboratory, geologists use optical microscopes to closely examine rocks and soil for mineral composition and **grain size**. Laser and mass spectrometers precisely measure the chemical composition and geological age of minerals. **Seismographs** record and locate earthquake activity or, when used in conjunction with ground penetrating **radar**, locate objects buried beneath the surface of the earth. Scientists apply computer simulations to turn their collected data into testable, theoretical models. Hydrogeologists drill wells to sample and analyze underground water quality and availability. Geochemists use scanning electron microscopes to analyze minerals at the atomic level via x-rays. Other geologists use gas chromatography to analyze liquids and gases trapped in **glacial** ice or rocks.

Technology provides new tools for scientific observation, which leads to new evidence that helps scientists revise and even refute old ideas. Because the ultimate technology will never be discovered, the ultimate observation will never be made. And this is the beauty of science—it is always advancing through new discoveries.

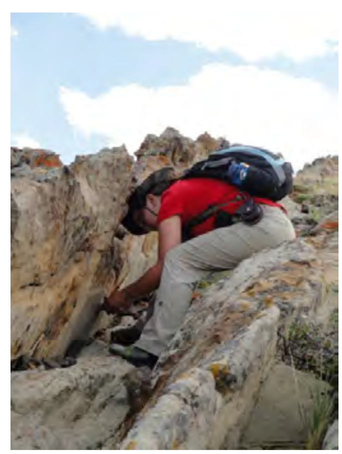

Figure 1.30: Dr. Laura Neser using a Brunton compass to measure the orientation of tilted sedimentary rocks in northwestern Wyoming. Figure description available at the end of the chapter.

Take this quiz to check your comprehension of this section.

Access the quiz for Section 1.5 by scanning the QR code.

1.6 Science Denial and Evaluating Sources

Video 1.1: Science in America

Access this YouTube video by scanning the QR code. ["Science in America – Neil deGrasse Tyson" by StarTalk | https://www.youtube.com/watch?v=8MqTOEospfo]

Introductory science courses usually deal with accepted scientific theory and do not include opposing ideas, even though these alternate ideas may be credible. This makes it easier for students to understand the complex material. Advanced students will encounter more controversies as they continue to study their discipline.

Various groups argue that some established scientific theories are wrong—an assertion that is not based on their scientific merit but rather on the ideology of the group. This section focuses on how to identify evidence based information and differentiate it from pseudoscience.

Figure 1.31: Anti-evolution league at the infamous Tennessee v. Scopes trial. Figure description available at the end of the chapter.

1.6.1 Science Denial

Figure 1.32: 2017 March for Science in Washington, DC. This and other similar marches were in response to funding cuts and anti-science rhetoric. Figure description available at the end of the chapter.

Science denial involves arguing that established scientific theories are wrong based on subjective ideology—such as social, political, or economic reasons. Organizations and people use science denial as a rhetorical argument against issues or ideas they oppose. Three examples of science denial can be seen in controversies surrounding: 1) teaching evolution in public schools, 2) linking tobacco smoke to cancer, and 3) linking human activity to climate change. Among these, denial of climate change is strongly connected with geology. A climate denier specifically denies or doubts the objective conclusions of geologists and climate scientists.

Science denial generally uses three false arguments. The first argument tries to undermine the credibility of a scientific conclusion by claiming the research methods are flawed or the theory is not universally accepted—the science is unsettled. The notion that scientific ideas are not absolute creates doubt for nonscientists; however, a lack of universal truths should not be confused with scientific uncertainty. Since science is based on falsifiability, scientists avoid claiming universal truths and use language that conveys uncertainty. This allows scientific ideas to change and evolve as more evidence is uncovered.

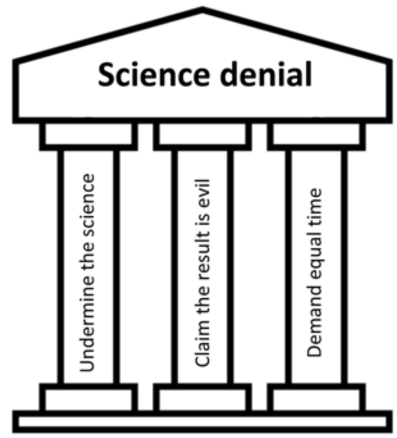

Figure 1.33: Three false rhetorical arguments of science denial. Figure description available at the end of the chapter.

The second argument claims the researchers are not objective and are motivated by an ideology or economic agenda. This is an ad hominem argument in which a person's character is attacked instead of the merit of their argument. They claim results have been manipulated so researchers can justify asking for more funding. They claim that, because the researchers are funded by federal grants, they are using their results to lobby for expanded government regulation.

The third argument is to demand a balanced view, with equal time in media coverage and educational curricula, to engender the false illusion of two equally valid arguments. Science deniers frequently demand equal coverage of their proposals, even when there is little scientific evidence supporting their ideology. For example, science deniers might demand that religious explanations be taught as an alternative to the well-established theory of evolution or that all possible causes of climate change be discussed as equally probable, regardless of the body of evidence. Conclusions derived using the scientific method should not be confused with those based on ideologies.

Furthermore, conclusions about nature derived from ideologies have no place in science research and education. For example, it would be inappropriate to teach the flat Earth model in a modern geology course because this idea has been disproved by the scientific method. The formation of new conclusions based on the scientific method is the only way to change scientific conclusions. The fact that scientists avoid universal truths and change their ideas as more evidence is uncovered shouldn't be seen as an indication that the science is unsettled. Unfortunately, widespread scientific illiteracy allows these arguments to be used to suppress scientific knowledge and spread misinformation.

In a classic case of science denial, beginning in the 1960s and for the next three decades, the tobacco industry and their scientists used rhetorical arguments to deny a connection between tobacco usage and cancer. Once it became clear that scientific studies overwhelmingly found that using tobacco dramatically increased a person's likelihood of getting cancer, their next strategy was to create a sense of doubt around the science. The tobacco industry suggested the results were not yet fully understood and more study was needed. They used this doubt to lobby for delaying legislative action that would warn consumers of the potential health hazards. This same tactic is currently being employed by those who deny the significance of human involvement in climate change.

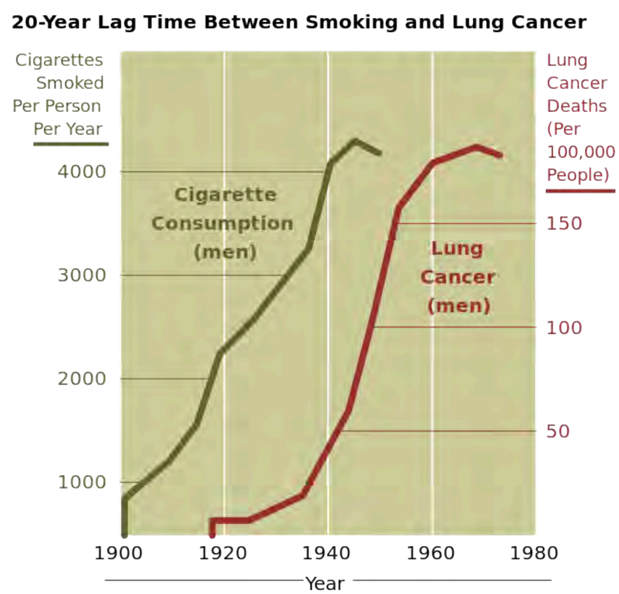

Figure 1.34: The lag time between cancer after smoking, plus the ethics of running human trials, delayed the government in taking action against tobacco. Figure description available at the end of the chapter.

1.6.2 Evaluating Sources of Information

In the age of the internet, information is plentiful. Geologists, scientists, or anyone exploring scientific inquiry must discern valid sources of information from pseudoscience and misinformation. This evaluation is especially important in scientific research because scientific knowledge is respected for its reliability. Textbooks such as this one can aid in this complex and crucial task. At its roots, quality information comes from the scientific method, beginning with the empirical thinking of Aristotle. The application of the scientific method helps produce unbiased results. A valid inference or interpretation is based on objective evidence or data. Credible data and inferences are clearly labeled, separated, and differentiated. Anyone looking over the data can understand how the author's conclusion was derived or can come to an alternative conclusion. Scientific procedures are clearly defined to ensure that the investigation can be replicated to confirm the original results or expanded further to produce new results. These measures make a scientific inquiry valid and its use as a source reputable. Of course, substandard work occasionally slips through and retractions are published from time to time. An infamous article linking the MMR vaccine to autism appeared in the highly reputable journal *Lancet* in 1998. Journalists discovered the author had multiple conflicts of interest and fabricated data, and the article was retracted in 2010.

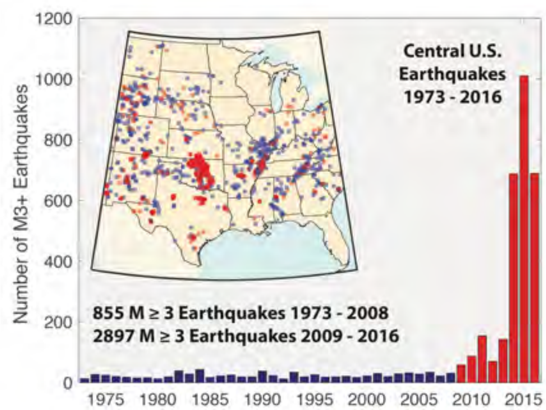

Figure 1.35: This graph shows earthquake data. To call this data induced due to fracking would be an interpretation. Figure description available at the end of the chapter.

In addition to methodology, data, and results, the authors of a study should be investigated when looking into any research. An author's credibility is based on multiple factors, such as having a degree in a relevant topic or being funded by an unbiased source.

The same rigor should be applied to evaluating the publisher, ensuring that the results reported come from an unbiased process. The publisher should be easy to discover. Good publishers will include the latest papers in the journal and make their contact information and identification clear. Reputable journals show their peer review style. Some journals are predatory, requiring unexplained and unnecessary fees to submit and access journals. Reputable journals also have recognizable editorial boards. Often, a reliable journal will associate with a trade, association, or recognized open source initiative.

THE GEOLOGICAL SOCIETY OF AMERICA®

Figure 1.36: Logo for the Geological Society of America, one of the leading geoscience organizations. They also publish *GSA Bulletin*, a reputable geology journal. Figure description available at the end of the chapter.

One of the hallmarks of scientific research is peer review. Research should be transparent to peer review. This allows the scientific community to reproduce experimental results, correct and retract errors, and validate theories.

Citation is not just important because it avoids plagiarism; it also allows readers to investigate an author's line of thought and conclusions. When reading scientific works, it is important to confirm the citations are from reputable scientific research. Most often, scientific citations are used to reference instances of paraphrasing rather than direct quotes. The number of times a work is cited is said to be a measure of the influence an investigation has within the scientific community, although this technique is inherently biased.

Take this quiz to check your comprehension of this section.

Access the quiz for Section 1.6 by scanning the QR code.

Summary

Science is a process with no beginning and no end. Science is never finished because a full truth can never be known. However, science and the scientific method are the best way to understand the universe in which we live. Scientists draw conclusions based on objective evidence; they then consolidate these conclusions into unifying models. Geologists likewise understand that studying the Earth is an ongoing process, beginning with James Hutton who declared the Earth has "no vestige of a beginning, no prospect of an end." Geologists explore the 4.5 billion-year history of Earth, its resources, and its many hazards. From a larger viewpoint, geology can teach people how to develop credible conclusions, as well as identify and stop misinformation.

Take this quiz to check your comprehension of this chapter.

Access the quiz for Chapter 1 by scanning the QR code.

Text References

1. Adams, F.D. (1954). *The birth and development of the geological sciences.*
2. Alfè, D., Gillan, M.J., and Price, G.D. (2002). Composition and temperature of the Earth's core constrained by combining ab initio calculations and seismic data. *Earth Planet. Sci. Lett., 195*(1), 91–98.
3. Alkin, M.C. (Ed.) (2004). *Evaluation roots: Tracing theorists' views and influences:* SAGE.
4. Beckwith, C. (2013). *How western Europe developed a full scientific method:* Berfrois.
5. Birch, F. (1952). Elasticity and constitution of the Earth's interior. *J. Geophys. Res., 57*(2), 227–286. doi: 10.1029/JZ057i002p00227.
6. Bocking, S. (2004). *Nature's experts: Science, politics, and the environment:* Rutgers University Press.
7. Chamberlin, T.C. (1890). The method of multiple working hypotheses. *Science, 15*(366), 92–96.
8. Cohen, H.F. (2010). *How modern science came into the world: Four civilizations, one 17th-century breakthrough:* Amsterdam University Press.
9. Darwin, C. (1846). *Geological observations on South America: Being the third part of the geology of the voyage of the Beagle, under the command of Capt. Fitzroy, R.N., during the years 1832 to 1836:* Smith, Elder and Company.
10. Drake, S. (1990) *Galileo: Pioneer Scientist:* University of Toronto Press.
11. Engdahl, E.R., Flynn, E.A., and Masse, R.P. (1974), Differential PkiKP travel times and the radius of the core. *Geophysical J. Royal Astro. Soc., 40*, 457–463.
12. Everitt, A. (2016). *The rise of Athens: The story of the world's greatest civilization:* Random House.
13. Goldstein, B.R. (2002). Copernicus and the origin of his heliocentric system. *Journal for the History of Astronomy, 33*, 219–235.
14. Goldsworthy, A.K. (2011). *The complete Roman army:* Thames & Hudson.
15. Hans Wedepohl, K. (1995). The composition of the continental crust. *Geochim. Cosmochim. Acta, 59*(7), 1217–1232.
16. Heilbron, J.L. (2012) *Galileo:* Oxford University Press.
17. Hogendijk, J.P., and Sabra, A.I. (2003) *The enterprise of science in Islam: New perspectives:* MIT Press.
18. Jakosky, B.M., Grebowsky, J.M., Luhmann, J.G., Connerney, J., Eparvier, F., Ergun, R., Halekas, J., Larson, D., Mahaffy, P., McFadden, J., Mitchell, D.F., Schneider, N., Zurek, R., Bougher, S., et al. (2015). MAVEN observations of the response of Mars to an interplanetary coronal mass ejection. *Science, 350*(6261), aad0210.
19. Kerferd, G.B. (1959). The biography of Aristotle – Ingemar Düring: Aristotle in the ancient biographical tradition. (Studia Graeca et Latina Gothoburgensia v.) Pp. 490; 1 plate. Gothenburg: Institute of Classical Studies, 1957. Paper, Kr. 32: *Classical Rev., 9*(2), 128–130.
20. Kolbert, E. (2014). *The sixth extinction: An unnatural history:* Henry Holt and Co.
21. Krimsky, S. (2013). Do financial conflicts of interest bias research? An inquiry into the "funding effect" hypothesis. *Sci. Technol. Human Values, 38*(4), 566–587.
22. Lehmann, I. (1936). P', *Bur. Centr. Seism. Internat. A*(14), 87–115.
23. Marshall, J. (2010). *A short history of Greek philosophy:* Andrews UK Limited.
24. Martin, C. (2014). *Subverting Aristotle: Religion, history, and philosophy in early modern science:* Johns Hopkins University Press.
25. Mayr, E. (1942). *Systematics and the origin of species, from the viewpoint of a zoologist:* Harvard University Press.
26. Montgomery, K. (2003). Siccar Point and teaching the history of geology. *J. Geosci. Educ.*
27. Mooney, W.D., Laske, G., and Masters, T.G. (1998). CRUST 5.1: A global crustal model. *J. Geophys. Res. [Solid Earth], 103*(B1), 727–747.
28. Moustafa, K. (2016) Aberration of the citation. *Account. Res., 23*(4), 230–244.
29. National Center for Science Education (2016). Climate change denial. Online, https://ncse.ngo/climate-change-denial, accessed April 2016.
30. Oreskes, N., Conway, E., and Cain, S. (2010). *Merchants of doubt: How a handful of scientists obscured the truth on issues from tobacco smoke to global warming:* Bloomsbury Press.
31. Paradowski, R.J. (2012). Nicolas Steno: Danish anatomist and geologist, in *Great lives from history: Scientists & science,* 830–832.
32. Patterson, C. (1956). Age of meteorites and the earth. *Geochim. Cosmochim. Acta,* 10(4), 230–237.
33. Popper, K. (2002). *Conjectures and refutations: The Growth of scientific knowledge:* Routledge.
34. Porter, R. (1976). Charles Lyell and the principles of the history of geology. *Br. J. Hist. Sci., 9*(2), 91–103.
35. Railsback, B.L. (1990). T. C. Chamberlin's "method of multiple working hypotheses": An encapsulation for modern students. Online, http://www.gly.uga.edu/railsback/railsback_chamberlin.html, accessed December 2016.
36. Railsback, B.L. (2004). T. C. Chamberlin's "method of multiple working hypotheses": An encapsulation for modern students. *Houston Geological Society Bulletin, 47*(2), 68–69.

37. Rappaport, R. (1994). James Hutton and the history of geology. Dennis R. Dean. *Isis, 85*(3), 524–525.
38. Repcheck, J. (2007). *Copernicus' secret: How the scientific revolution began:* Simon and Schuster.
39. Repcheck, J. (2009). *The man who found time: James Hutton and the discovery of the Earth's antiquity:* Basic Books.
40. Sabra, A.I. et al. (1989). *The optics of Ibn al-Haytham: Books I-III: On direct vision:* Warburg Institute, University of London.
41. Saliba, G. (2007). *Islamic science and the making of the European renaissance:* MIT Press.
42. Shermer, M. (2011). What Is Pseudoscience? *Scientific American.*
43. Snow, C.E. (Ed.). (2016). *Science literacy: Concepts, contexts, and consequences:* National Academies Press (US).
44. Spier, R. (2002). The history of the peer-review process. *Trends Biotechnol., 20*(8), 357–358.
45. Van Reybrouck, D. (2012). *From primitives to primates: A history of ethnographic and primatological analogies in the study of prehistory:* Sidestone Press.
46. Waters, C.N., Zalasiewicz, J., Summerhayes, C., Barnosky, A.D., Poirier, C., Galuszka, A., Cearreta, A., Edgeworth, M., Ellis, E.C., Ellis, M., Jeandel, C., Leinfelder, R., McNeill, J.R., Richter, D.D., et al. (2016). The Anthropocene is functionally and stratigraphically distinct from the Holocene. *Science, 351*(6269), aad2622.
47. de Wijs, G.A., Kresse, G., Vočadlo, L., Dobson, D., Alfè, D., Gillan, M.J., and Price, G.D. (1998). The viscosity of liquid iron at the physical conditions of the Earth's core. *Nature, 392*(6678), 805–807., doi: 10.1038/33905.
48. Wyhe, J.V. (2008). *Darwin:* Andre Deutsch.
49. Wyllie, P.J. (1970). Ultramafic rocks and the upper mantle, *in* Morgan, B.A. (ed.), *Fiftieth anniversary symposia: Mineralogy and petrology of the Upper Mantle; Sulfides; Mineralogy and geochemistry of non-marine evaporites:* Mineralogical Society of America, 3–32.
50. Zalasiewicz, J., Williams, M., Smith, A., Barry, T.L., Coe, A.L., Bown, P.R., Brenchley, P., Cantrill, D., Gale, A., Gibbard, P., et al. (2008). Are we now living in the Anthropocene? *GSA Today, 18*(2), 4.

Figure References

Figure 1.1: This is Cascade Falls in Pembroke, Virginia. Laura Neser. September 8, 2021. CC BY-NC.

Figure 1.2: Canyons like this, carved in the deposit left by the May 18th, 1980, eruption of Mount St. Helens, are sometimes used by purveyors of pseudoscience as evidence for the Earth being very young. Richard Droker. 2011. CC BY-NC-ND 2.0. https://flic.kr/p/2cNFV8D

Figure 1.3: Geologists share information by publishing, attending conferences, and even going on field trips, such as this trip to the Lake Owyhee Volcanic Field in Oregon by the Bureau of Land Management in 2019. Bureau of Land Management Oregon and Washington. 2019. CC BY 2.0. https://flic.kr/p/RCtkjX

Figure 1.4: Diagram of the cyclical nature of the scientific method. ArchonMagnus. 2015. CC BY-SA 4.0. https://commons.wikimedia.org/wiki/File:The_Scientific_Method_as_an_Ongoing_Process.svg

Figure 1.5: A famous hypothesis. Eadweard Muybridge. 1878. Public domain. https://commons.wikimedia.org/wiki/File:Eadweard_Muybridge-Sallie_Gardner_1878.jpg

Figure 1.6: An experiment at the University of Queensland has been ongoing since 1927. John Mainstone; adapted by Amada44. 2012. CC BY-SA 3.0. https://commons.wikimedia.org/wiki/File:University_of_Queensland_Pitch_drop_experiment-white_bg.jpg

Figure 1.7: Wegener later in his life, ca. 1924–1930. Author unknown. ca.1924–1930. Public domain. https://commons.wikimedia.org/wiki/File:Alfred_Wegener_ca.1924-30.jpg

Figure 1.8: Fresco by Raphael of Plato (left) and Aristotle (right). Raphael. 1509. Public domain. https://commons.wikimedia.org/wiki/File:Sanzio_01_Plato_Aristotle.jpg

Figure 1.9: Drawing of Avicenna (Ibn Sina). Unknown artist. Unknown date. Public domain. https://commons.wikimedia.org/wiki/File:Avicenna-miniatur.jpg

Figure 1.10: Geocentric drawing by Bartolomeu Velho in 1568. Bartolomeu Velho. Original work, 1568. Photo taken in 2008. Public domain. https://en.wikipedia.org/wiki/File:Bartolomeu_Velho_1568.jpg

Figure 1.11: Galileo's first mention of moons of Jupiter. Galileo Galilei. 1610. Public domain. https://commons.wikimedia.org/wiki/File:Sidereus_Nuncius_Medicean_Stars.jpg

Figure 1.12: Copernicus' heliocentric model. Copernicus; adapted by Professor marginalia. 1543; 2010. Public domain. https://commons.wikimedia.org/wiki/File:Copernican_heliocentrism_diagram-2.jpg

Figure 1.13: Illustration by Steno showing a comparison between fossils and modern shark teeth. Niels Steensen. 1669 AD. Public domain. https://commons.wikimedia.org/wiki/File:Steensen_-_Elementorum_myologiae_specimen,_1669_-_4715289.tif

Figure 1.14: Cuvier's comparison of modern elephant and mammoth jaw bones. Georges Cuvier. 1796. Public domain. https://commons.wikimedia.org/wiki/File:Cuvier_elephant_jaw.jpg

Figure 1.15: Inside cover of Lyell's Elements of Geology. Charles Lyell. 1857. Public domain. https://commons.wikimedia.org/wiki/File:Lyell_Principles_frontispiece.jpg

Figure 1.16: J. Tuzo Wilson. Stephen Morris. 1992. CC BY-SA 3.0. https://commons.wikimedia.org/wiki/File:John_Tuzo_Wilson_in_1992.jpg

Figure 1.17: Girls into Geoscience inaugural Irish Fieldtrip. Aileen Doran. 2019. CC BY 4.0. https://commons.wikimedia.org/wiki/File:Exceptional_folds_during_the_Girls_into_Geoscience_inaugural_Irish_Fieldtrip.jpg

Figure 1.18: Glen Canyon Dam in the southwestern United States forms Lake Powell, a reservoir on the Colorado River in Utah and Arizona. Laura Neser. March 9, 2022. CC BY-NC.

Figure 1.19: Coal power plant in Helper, Utah. David Jolley. 2007. CC BY-SA 3.0. https://commons.wikimedia.org/wiki/File:Castle_Gate_Power_Plant,_Utah_2007.jpg

Figure 1.20: Buildings toppled from liquefaction during a 7.5 magnitude earthquake in Japan. Ungtss. 1964. Public domain. https://commons.wikimedia.org/wiki/File:Liquefaction_at_Niigata.JPG

Figure 1.21: Oregon's Crater Lake was formed about 7,700 years ago after the eruption of Mount Mazama. Zainubrazvi. 2006. CC BY-SA 3.0. https://en.wikipedia.org/wiki/File:Crater_lake_oregon.jpg

Figure 1.22: Rock cycle showing the five materials (such as igneous rocks and sediment) and the processes by which one changes into another (such as weathering). Kindred Grey. 2022. CC BY 4.0.

Figure 1.23: Jurassic-aged sandstone makes up the walls of Antelope Canyon in the American Southwest. Laura Neser. September 8, 2021. CC BY-NC.

Figure 1.24: Metamorphic rock in Georgian Bay, Ontario. P199. 2013. CC BY-SA 4.0. https://commons.wikimedia.org/wiki/File:Metamorphic_rock_Georgian_Bay.jpg

Figure 1.25: Map of the major plates and their motions along boundaries. Scott Nash via United States Geological Survey (USGS). 1996. Public domain. https://commons.wikimedia.org/wiki/File:Plates_tect2_en.svg

Figure 1.26: The global map of the depth of the boundary between the crust and mantle. AllenMcC. 2013. CC BY-SA 3.0. https://commons.wikimedia.org/wiki/File:Mohomap.png

Figure 1.27: The layers of the Earth. Drlauraguertin. 2015. CC BY-SA 3.0. https://wiki.seg.org/wiki/File:Earthlayers.png#file

Figure 1.28: Geologic time on Earth, represented circularly, showing the individual time divisions and important events. Woudloper; adapted by Hardwigg. 2010. Public domain. https://commons.wikimedia.org/wiki/File:Geologic_Clock_with_events_and_periods.svg

Figure 1.29: Geologic timescale showing time period names and ages. USGS. 2009. Public domain. https://commons.wikimedia.org/wiki/File:Geologic_time_scale.jpg

Figure 1.30: Dr. Laura Neser using a Brunton compass to measure the orientation of tilted sedimentary rocks in northwestern Wyoming. Laura Neser. 2011. CC BY-NC.

Figure 1.31: Anti-evolution league at the infamous Tennessee v. Scopes trial. Mike Licht. 1925. CC BY 2.0. https://commons.wikimedia.org/wiki/File:Anti-EvolutionLeague.jpg

Figure 1.32: 2017 March for Science in Washington, DC. Becker1999. 2017. CC BY 2.0. https://commons.wikimedia.org/wiki/File:March_for_Science,_Washington,_DC_(34168985286).jpg

Figure 1.33: Three false rhetorical arguments of science denial. Kindred Grey. 2022. CC BY 4.0. Includes columns by Med MB from Noun Project (Noun Project license).

Figure 1.34: The lag time between cancer after smoking, plus the ethics of running human trials, delayed the government in taking action against tobacco. Sakurambo. 2007. Public domain. https://commons.wikimedia.org/wiki/File:Cancer_smoking_lung_cancer_correlation_from_NIH.svg

Figure 1.35: This graph shows earthquake data. USGS. 2019. Public domain. https://en.wikipedia.org/wiki/File:Cumulative_induced_seismicity.png

Figure 1.36: Logo for the Geological Society of America, one of the leading geoscience organizations. GSA. Retrieved 2022. https://www.geosociety.org/GSA/About/Who_We_Are/Society_Documents/GSA/About/logo_usage.aspx

Figure Descriptions

Figure 1.1: A waterfall flowing into a pool of water. There are green trees on either side of the falls and tan to brown flat rocks in the foreground.

Figure 1.2: Aerial view of modern canyons carved through dark gray unconsolidated volcanic deposits with sparse vegetation in the area.

Figure 1.3: 15 people at a field trip looking at large rock outcrops in the distance.

Figure 1.4: Diagram showing the steps of the scientific method in a circular pattern that repeats itself. Clockwise starting from the top. Make observations (What do I see in nature? This can be from one's own experiences, thoughts, or reading.). Think of interesting questions (Why does that pattern occur?). Formulate hypotheses (What are the general causes of the phenomenon I am wondering about?). Develop testable predictions (If my hypothesis is correct, then I expect a, b, c…). Gather data to test predictions (Relevant data can come from the literature, new observations, or formal experiments. Thorough testing requires replication to verify results.). Refine, alter, expand, or reject hypotheses. Develop general theories (General theories must be consistent with most or all available data and with other current theories.).

Figure 1.5: A grid of 12 images showing a horse throughout stages of galloping, some of which show that the horse lifted all 4 legs off the ground during the gallop.

Figure 1.6: A highly viscous black petroleum fluid that drips out of a funnel into a beaker extremely slowly, about once a decade.

Figure 1.7: Headshot of Alfred Wegener, a white man, in a suit.

Figure 1.8: Mural painting of Plato and Aristotle walking together while dressed in Greek robes.

Figure 1.9: Modern depiction of a man. He is wearing a turban, dressed in robes, writing a letter, sitting on the ground.

Figure 1.10: Illustration of the Ptolemaic geocentric conception of the Universe. The left-hand side of the diagram shows the distances of the bodies to the center of the Earth and the right-hand side shows each body's time of revolution, in years. The text is in Portuguese.

Figure 1.11: Page with Italian text that includes four drawings of Jupiter with multiple moons on either side of it which change position in each drawing.

Figure 1.12: Series of concentric circles representing each planet's orbit from Mercury to Saturn (the only known planets at the time) with the Sun in the center.

Figure 1.13: Black and white illustration of a shark head with a close-up view of a fossil shark tooth and a modern shark tooth at the bottom of the page.

Figure 1.14: Black and white drawings of the jaw of an Indian elephant and the fossil jaw of a mammoth. Side views of each jaw are on the left and front views of each jaw are on the right.

Figure 1.15: Idealized cross section of part of the Earth's crust with a volcano and its magma chambers in the center.

Figure 1.16: Headshot of an older man wearing a suit and tie.

Figure 1.17: A group of women look at geological folds on a rock in Ireland.

Figure 1.18: A large tan concrete dam. The water level is much higher behind the dam than in front of it.

Figure 1.19: A power plant with steam coming out, surrounded by rocky hills on either side.

Figure 1.20: Three rows of rectangular-shaped buildings with the second and third rows of buildings having fallen over.

Figure 1.21: A large hole in the top of a mountain that is filled with a lake. There is also an island in the lake.

Figure 1.22: The rock cycle (clockwise). Magma turns to Igneous rock through crystallization. Igneous rocks turn to sediment through weathering. Sediment turns to sedimentary rocks through transport and deposition and burial and lithification. Sedimentary rocks turn to metamorphic rocks through textural and or chemical damage. Metamorphic rocks turn to magma through melting. Igneous rocks turn to metamorphic rocks through textural and/or chemical damage. metamorphic and sedimentary rocks endure weathering by exhumation of rock back to Earth's surface.

Figure 1.23: This grey rock has round circles left by raindrops. There is a 3-centimeter scale bar on the upper right of the rock.

Figure 1.24: Grey-and-orange rock with wavy texture.

Figure 1.25: World map with the largest tectonic plates outlined and filled in with a different color for each plate: the Eurasian Plate is col-

ored green, the North American Plate is gray, the Australian Plate is orange, the Filipino Plate is red, the Pacific Plate is yellow, the Juan de Fuca and Cocos Plates are blueish purple, the Nazca Plate is light blue, the Antarctic Plate is dark blue, the Scotia Plate is medium blue, the Caribbean plate is pinkish orange, the South American Plate is purple, the African Plate is dark orange, the Arabian Plate is yellow, and the Indian Plate is dark red.

Figure 1.26: World map with the Moho depth color coded on the map: red is the deepest while blue is the shallowest. The Moho is deepest under central Asia and western South America, and the Moho is shallowest under the world ocean basins.

Figure 1.27: From core to surface: Inner core (solid), outer core (liquid), mantle (including asthenosphere), crust (including lithosphere)

Figure 1.28: From oldest to newest time divisions: Hadean, archean, proterozoic, paleozoic, mesozoic, cenozoic. 4550 Ma: formation of the earth. 4527 Ma: formation of the moon.4000 Ma: end of the late heavy bombardment; first life. 3200 Ma: earliest start of photosynthesis. 2300 Ma: atmosphere becomes oxygen-rich; first snowball earth. 750-635 Ma: two snowball earths. 530 Ma: cambrian explosion. 380 Ma: first vertebrate land animals. 230-66 Ma: Non-avian dinosaurs. 2 Ma: first hominins.

Figure 1.29: Precambrian eon is made up of haydean, archean, and proterozoic eons. Phanerozoic eon is made up of paleozoic (permian, pennsylvanian, mississippian, devonian, silurian, ordovician, cambrian periods), mesozoic (cretaceous, jurassic, triassic periods), and cenozoic eras (quaternary and tertiary periods).

Figure 1.30: Woman wearing a red tee shirt and tan pants sitting on a steeply tilted tan rock bed while leaning forward and holding a compass against the face of another steeply tilted tan rock bed in front of her.

Figure 1.31: A group of 12 people stand below a banner that says "T.T. Martin Headquarters Anti-Evolution League 'The Conflict' – "Hell & The High School'

Figure 1.32: Huge crowd of people marching on the street holding a banner that says "March for Science"

Figure 1.33: Shows three pillars labeled "Undermine the Science", "Claim the Result is Evil", and "Demand Equal Time".

Figure 1.34: Cigarettes smoked per person per year and lung cancer deaths per 100,000 people shown on the same timeline. cigarette consumption (men) and lung cancer (men) have the same increasing slope, only lung cancer is 20 years delayed.

Figure 1.35: A bar graph: the y-axis is "Number of M3+ Earthquakes" with a scale of 0 to 1200, and the x-axis is the year in question with a scale of 1970 to 2020. The bars spike sharply up after the year 2009, with the highest bar peak in 2015. There is also an inset map of the central United States that has dots of locations of earthquakes during this period, color-coded by magnitude. The densest cluster is in Oklahoma.

Figure 1.36: The geological society of America logo

2. PLATE TECTONICS

Learning Objectives

By the end of this chapter, students should be able to:

- Describe how the ideas behind plate tectonics started with Alfred Wegener's hypothesis of continental drift.
- Describe the physical and chemical layers of the Earth and how they affect plate movement.
- Explain how movement at the three types of plate boundaries causes earthquakes, volcanoes, and mountain building.
- Identify convergent boundaries, including subduction and collisions, as places where plates come together.
- Identify divergent boundaries, including rifts and mid-ocean ridges, as places where plates separate.
- Explain transform boundaries as places where adjacent plates shear past each other.
- Describe the Wilson cycle, from continental rifting, ocean basin creation, and plate subduction to ocean basin closure.
- Explain how the tracks of hotspots, places that have continually rising magma, are used to calculate plate motion.

Figure 2.1: Detailed map of all known plates, their boundaries, and movements. Figure description available at the end of the chapter.

Revolution is a word usually reserved for significant political or social changes. Several revolutionary ideas forced scientists to re-examine their entire fields, triggering a paradigm shift that shook up their conventionally held knowledge. Charles Darwin's book on evolution, *On the Origin of Species*, published in 1859; Gregor Mendel's discovery of the genetic principles of inheritance in 1866; and James Watson, Francis Crick, and Rosalind Franklin's model for the structure of DNA in 1953 did that for **biology**. Albert Einstein's concepts of relativity and quantum mechanics in the early twentieth century did the same for Newtonian physics.

The concept of **plate tectonics** was just as revolutionary for geology. The theory of plate tectonics attributes the movement of massive sections of the Earth's outer layers with creating earthquakes, **mountains**, and **volcanoes**. Many Earth processes make more sense when viewed through the lens of plate tectonics. Because it is so important in understanding how the world works, plate tectonics is the first topic of discussion in this textbook.

2.1 Alfred Wegener's Continental Drift Hypothesis

Alfred Wegener (1880–1930) was a German scientist who specialized in meteorology and climatology. His knack for questioning accepted ideas started in 1910, when he disagreed with the explanation that the Bering Land Bridge was formed by **isostasy** and that similar land bridges once connected the continents. After reviewing the scientific literature, he published a hypothesis stating the continents were originally connected and then drifted apart. While he did not have the precise mechanism worked out, his hypothesis was backed up by a long list of evidence.

Figure 2.2: Wegener later in his life, ca. 1924–1930. Figure description available at the end of the chapter.

2.1.1 Early Evidence for Continental Drift Hypothesis

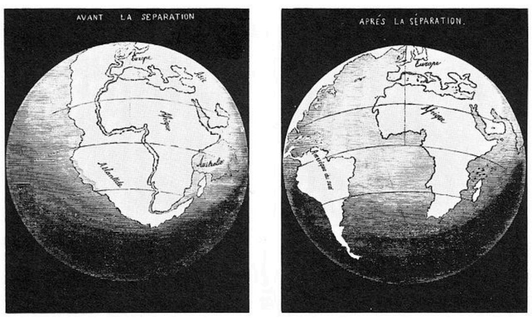

Figure 2.3: Snider-Pellegrini's map showing the continental fit and separation, 1858. Figure description available at the end of the chapter.

Wegener's first piece of evidence was that the coastlines of some continents fit together like pieces of a jigsaw puzzle. People noticed the similarities in the coastlines of South America and Africa on the first world maps, and some suggested the continents had been ripped apart. Antonio Snider-Pellegrini did preliminary work on continental separation and matching fossils in 1858.

What Wegener did differently was synthesize a large amount of data in one place. He used the true edges of the continents, based on the shapes of the continental shelves. This resulted in a better fit than previous efforts that traced the existing coastlines.

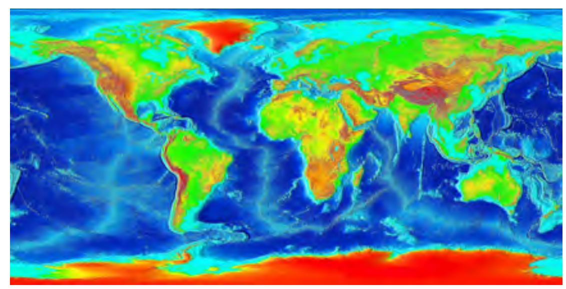

Figure 2.4: Map of world elevations. Note the light blue areas, which are continental shelves flooded by shallow ocean water. These show the true shapes of the continents. Figure description available at the end of the chapter.

Wegener also compiled evidence by comparing similar rocks, mountains, fossils, and glacial formations across oceans. For example, the fossils of the primitive aquatic reptile *Mesosaurus* were found on the coastlines of both Africa and South America. Fossils of another reptile, *Lystrosaurus,* were found on Africa, India, and Antarctica. He pointed out these were land-dwelling creatures could not have swum across an entire ocean.

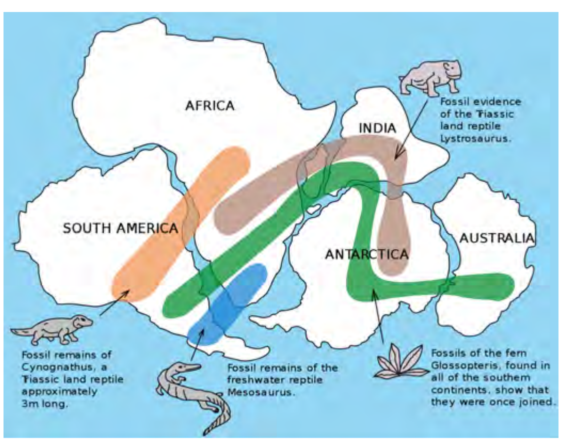

Figure 2.5: Image showing fossils that connect the continents of Gondwana (the southern continents of Pangea). Figure description available at the end of the chapter.

Opponents of continental drift insisted transoceanic land bridges allowed animals and plants to move between continents. The land bridges eventually eroded away, leaving the continents permanently separated. The problem with this hypothesis is the improbability of a land bridge being tall and long enough to stretch across a broad, deep ocean.

More support for continental drift came from the puzzling evidence that glaciers once existed in normally very warm areas in southern Africa, India, Australia, and Arabia. These climate anomalies could not be explained by land bridges. Wegener found similar evidence when he discovered tropical plant fossils in the frozen region of the Arctic Circle. As Wegener collected more data, he realized the explanation that best fit all the climate, rock, and fossil observations involved moving continents.

2.1.2 Proposed Mechanism for Continental Drift

Wegener's work was considered a fringe science theory for his entire life. One of the biggest flaws in his hypothesis was an inability to provide a mechanism for how the continents moved. Obviously, the continents did not appear to move, so changing the conservative minds of the scientific community would require exceptional evidence that supported a credible mechanism. Other followers of continental drift used expansion, contraction, or even the Moon's origin to explain how the continents moved. Wegener used centrifugal forces and precession, but this model was proven wrong. He also speculated about seafloor spreading, with hints of **convection**, but could not substantiate these proposals. As it turns out, current scientific knowledge reveals convection is one the major forces in driving plate movements, along with gravity and density.

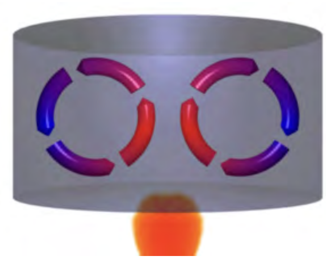

Figure 2.6: Animation of the basic idea of convection: an uneven heat source in a fluid causes rising material next to the heat and sinking material far from the heat. Figure description available at the end of the chapter.

2.1.3 Development of Plate Tectonic Theory

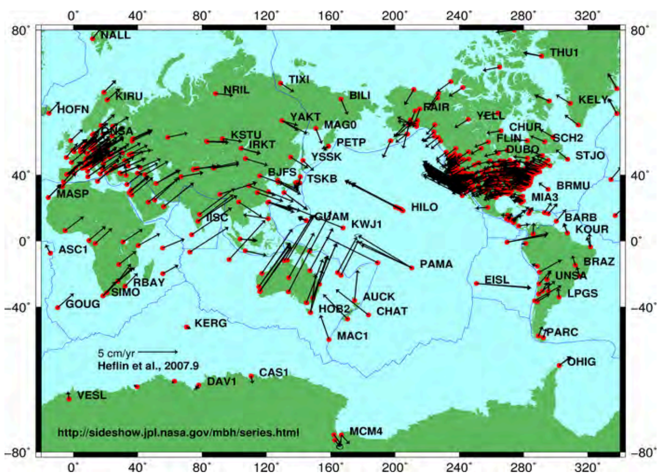

Figure 2.7: GPS measurements of plate motions. Figure description available at the end of the chapter.

Wegener died in 1930 on an expedition in Greenland. Poorly respected in his lifetime, Wegener and his ideas about moving continents seemed destined to be lost in history as fringe science. However, in the 1950s, evidence started to trickle in that made continental drift a more viable idea. By the 1960s, scientists had amassed enough evidence to support the missing mechanism—namely, sea-floor spreading—for Wegener's hypothesis of continental drift to be accepted as the theory of plate tectonics. Ongoing GPS and earthquake data analyses continue to support this theory. The next section provides the pieces of evidence that helped transform one man's wild notion into a scientific theory.

Mapping of the Ocean Floors

In 1947, researchers started using an adaptation of sonar to map a region in the middle of the Atlantic Ocean with poorly understood topographic and thermal properties. Using this information, Bruce Heezen and Marie Tharp created the first detailed map of the ocean floor to reveal the Mid-Atlantic Ridge, a basaltic mountain range that spanned the length of the Atlantic Ocean, with rock chemistry and dimensions unlike the mountains found on the continents. Initially, scientists thought the ridge was part of a mechanism that explained the expanding Earth or ocean-basin growth hypotheses. In 1959, Harry Hess proposed the hypothesis of seafloor spreading, which suggested that the mid-ocean ridges represented tectonic plate factories, where new oceanic plate was issuing from these long volcanic ridges. Scientists later included transform **faults** perpendicular to the ridges to better account for varying rates of movement between the newly formed plates. When earthquake epicenters were discovered along the ridges, the idea that earthquakes were linked to plate movement took hold.

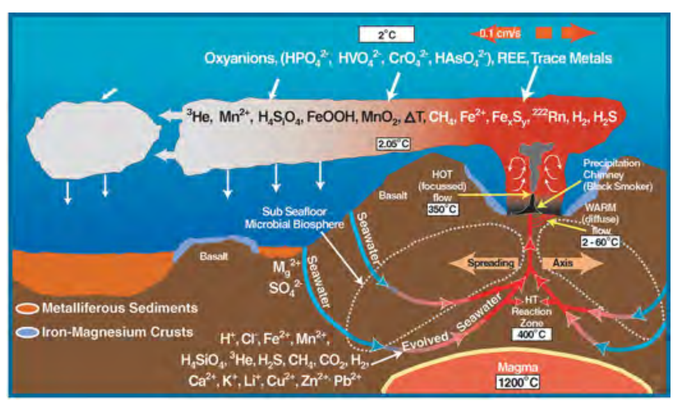

Figure 2.8: The complex chemistry around mid-ocean ridges. Figure description available at the end of the chapter.

Video 2.1: Uncovering the secrets of the ocean floor

Access this YouTube video by scanning the QR code. ["Marie Tharp: Uncovering the Secrets of the Ocean Floor – with Helen Czerski" by The Royal Institution | https://www.youtube.com/watch?v=TgfYjS0OTWw]

Seafloor **sediment**, measured by dredging and drilling, provided another clue. Scientists once believed sediment accumulated on the ocean floors over a very long time in a static environment. When some studies showed less sediment than expected, these results were initially used to argue against continental movement. With more time, researchers discovered these thinner sediment layers were located close to mid-ocean ridges, indicating the ridges were younger than the surrounding ocean floor. This finding supported the idea that the seafloor was not fixed in one place.

Paleomagnetism

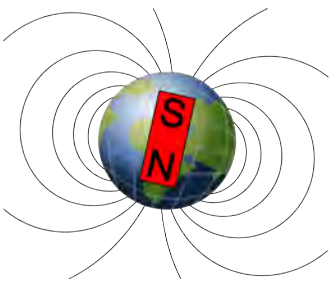

Figure 2.9: The magnetic field of Earth, simplified as a bar magnet. Figure description available at the end of the chapter.

The seafloor was also mapped magnetically. Scientists had long known of strange magnetic anomalies that formed a striped pattern of symmetrical rows on both sides of mid-oceanic ridges. What made these features unusual was that the north and south magnetic poles within each stripe were reversed in alternating rows. By 1963, Harry Hess and other scientists used these magnetic reversal patterns to support their model for seafloor spreading (see also Lawrence W. Morley).

Paleomagnetism is the study of magnetic fields frozen within rocks—basically a fossilized compass. In fact, the first hard evidence to support plate motion came from paleomagnetism.

Igneous rocks containing magnetic minerals like magnetite typically provide the most useful data. In their liquid state as magma or lava, the magnetic poles of the minerals align themselves with the Earth's magnetic field. When the rock cools and solidifies, this alignment is frozen into place, creating a permanent paleomagnetic record that includes magnetic inclination related to global **latitude** and declination related to magnetic north.

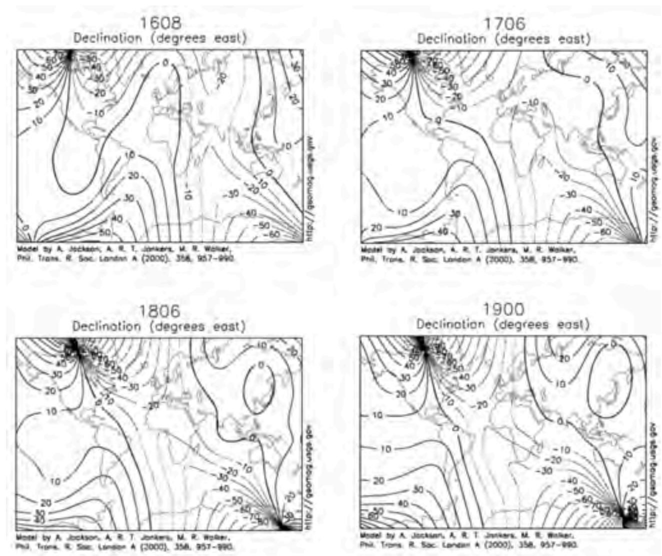

Figure 2.10: This animation shows how the magnetic poles have moved over 400 years. Figure description available at the end of the chapter.

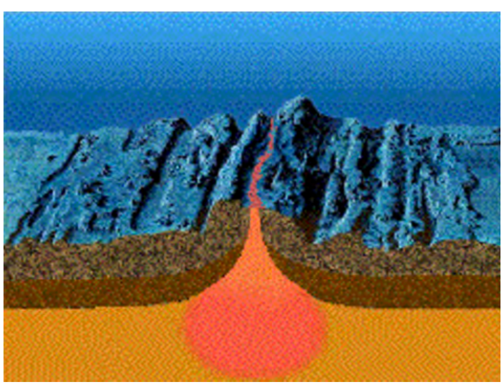

Figure 2.11: The iron in the solidifying rock preserves the current magnetic polarity as new oceanic plates form at mid-ocean ridges. Figure description available at the end of the chapter.

Scientists had noticed for some time the alignment of magnetic north in many rocks was nowhere close to the Earth's current magnetic north. Some explained this away are part of the normal movement of Earth's magnetic north pole. Eventually, scientists realized adding the idea of continental movement explained the data better than pole movement alone.

Wadati–Benioff Zones

Around the same time mid-ocean ridges were being investigated, other scientists linked the creation of ocean trenches and island arcs to seismic activity and tectonic plate movement. Several independent research groups recognized that earthquake epicenters traced the shapes of oceanic plates sinking into the mantle. These deep earthquake zones congregated in planes that started near the surface around ocean trenches and angled beneath the continents and island arcs. Today, these earthquake zones called **Wadati-Benioff zones**.

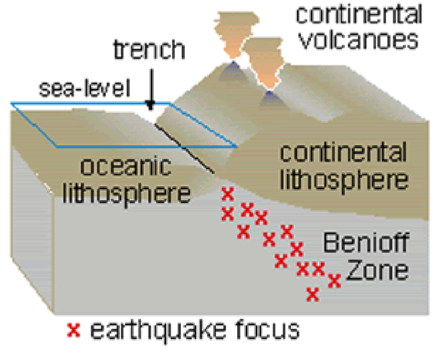

Figure 2.12: The Wadati-Benioff zone, showing earthquakes following the subducting slab down. [Figure description available at the end of the chapter](#).

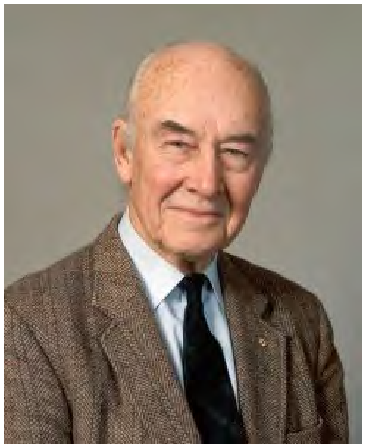

Figure 2.13: J. Tuzo Wilson. [Figure description available at the end of the chapter](#).

Based on the mounting evidence, the theory of plate tectonics continued to take shape. J. Tuzo Wilson was the first scientist to put the entire picture together by proposing the opening and closing of the ocean basins. Before long, scientists proposed other models showing plates moving with respect to each other, with clear boundaries between them. Others started piecing together complicated histories of tectonic plate movement. The Plate Tectonics Revolution had taken hold.

Complete this interactive activity to check your understanding.

Access this interactive activity by scanning the QR code.

Take this quiz to check your comprehension of this section.

Access the quiz for Section 2.1 by scanning the QR code.

2.2 Layers of the Earth

In order to understand the details of plate tectonics, it is essential to first understand the layers of the Earth. Firsthand information about what is below the surface is very limited; most of what we know is pieced together from hypothetical models and analysis of **seismic wave** data and **meteorite** materials. In general, the Earth can be divided into layers based on chemical composition and physical characteristics.

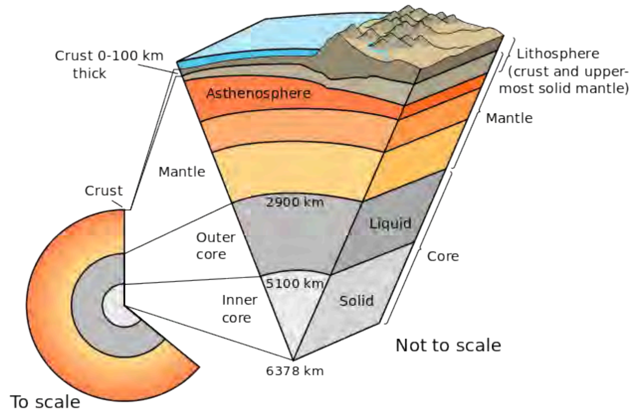

Figure 2.14: The layers of the Earth. Physical layers include lithosphere and asthenosphere; chemical layers are crust, mantle, and core. Figure description available at the end of the chapter.

2.2.1 Chemical Layers

The Earth is composed of a countless combination of elements. Regardless of what elements are involved, two major factors—**temperature** and **pressure**—are responsible for creating three distinct chemical layers.

Crust

The outermost chemical layer, and the one on which we currently reside, is the crust. There are two types of crust. Continental crust has a relatively low density and composition similar to granite. Oceanic crust has a relatively high density, especially when cold and old, and its composition is similar to basalt. The surface levels of crust are relatively brittle. The deeper parts of the crust are subjected to higher temperatures and pressure, which makes them more ductile. **Ductile** materials are like soft plastics or putty, moving under force. **Brittle** materials are like solid glass or pottery; they break under force, especially when it is applied quickly. Earthquakes generally occur in the upper crust and are caused by the rapid movement of relatively brittle materials.

The base of the crust is characterized by a large increase in seismic velocity, which measures how fast earthquake waves travel through solid matter. Called the Mohorovičić discontinuity, or **Moho** for short, this zone was discovered by Andrija Mohorovičić (pronounced mo-ho-ro-vee-cheech; audio pronunciation) in 1909 after studying earthquake wave paths in his native Croatia. The change in wave direction and speed is caused by dramatic chemical differences of the crust and mantle. Underneath the oceans, the Moho is found roughly 5 km below the ocean floor; under the continents, it is located about 30–40 km below the surface. Near some large mountain-building events known as orogenies, the continental Moho depth is doubled.

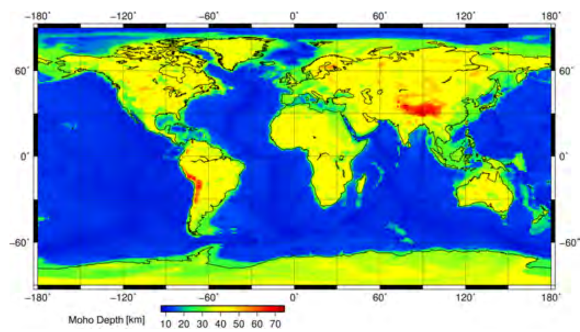

Figure 2.15: The global map of the depth of the Moho. Figure description available at the end of the chapter.

Mantle

Figure 2.16: This mantle xenolith containing olivine (green) is chemically weathering by hydrolysis and oxidation into the pseudomineral iddingsite, which is a complex of water, clay, and iron oxides. The more altered side of the rock has been exposed to the environment longer. Figure description available at the end of the chapter.

The mantle sits below the crust and above the core. It is the largest chemical layer by volume, extending from the base of the crust to a depth of about 2,900 km. Most of what we know about the mantle comes from seismic wave analysis, though information is gathered by studying ophiolites and xenoliths. **Ophiolites** are pieces of mantle that have risen through the crust until they are exposed as part of the ocean floor. **Xenoliths** are carried within magma and brought to the Earth's surface by volcanic eruptions. Most xenoliths are made of peridotite, an ultramafic class of igneous rock (see Section 4.2 for explanation). Because of this, scientists hypothesize most of the mantle is made of peridotite.

Core

The core of the Earth, which has both liquid and solid layers, consists mostly of iron, nickel, and possibly some oxygen. Scientists looking at seismic data first discovered this innermost chemical layer in 1906. Through a union of hypothetical modeling, astronomical insight, and hard seismic data, they concluded the core is mostly **metallic** iron. Scientists studying **meteorites**, which typically contain more iron than surface rocks, have proposed the Earth was formed from meteoric material. They believe the liquid component of the core was created as the iron and nickel sank into the center of the planet, where it was liquefied by intense pressure.

Figure 2.17: A polished fragment of iron-rich Toluca meteorite with octahedral Widmanstätten pattern. Figure description available at the end of the chapter.

2.2.2 Physical Layers

The Earth can also be broken down into five distinct physical layers based on how each layer responds to stress. While there is some overlap in the chemical and physical designations of layers, specifically the core-mantle boundary, there are significant differences between the two systems.

Lithosphere

The **lithosphere** (from *Lithos,* Greek for stone) is the outermost physical layer of the Earth. It is grouped into two types: oceanic and continental. Oceanic lithosphere is thin and relatively rigid. It ranges in thickness from nearly zero in new plates found around mid-ocean ridges to an average of 140 km in most other locations. Continental lithosphere is generally thicker and considerably more plastic, especially at the deeper levels. Its thickness ranges from 40 to 280 km. The lithosphere is not continuous. It is broken into segments called plates. A **plate boundary** is where two plates meet and move relative to each other. Plate boundaries are where we see plate tectonics in action—building mountains, triggering earthquakes, and generating volcanic activity.

Figure 2.18: Map of the major plates and their motions along boundaries. Figure description available at the end of the chapter.

Asthenosphere

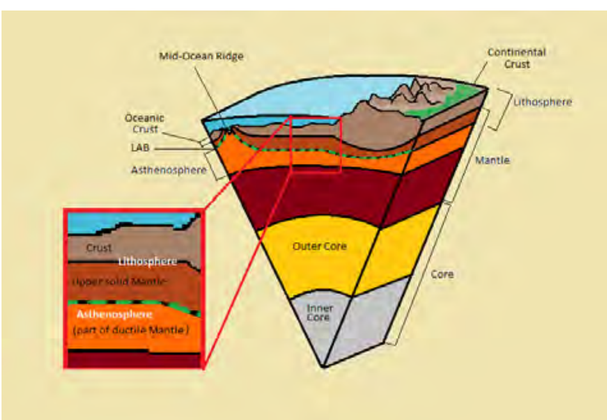

Figure 2.19: The lithosphere-asthenosphere boundary changes with certain tectonic situations. Figure description available at the end of the chapter.

The **asthenosphere** is the layer below the lithosphere. *Astheno-* means lacking strength, and the most distinctive property of the asthenosphere is movement. Because it is mechanically weak, this layer moves and flows due to convection currents created by heat coming from the Earth's core. Unlike the lithosphere, which consists of multiple plates, the asthenosphere is relatively unbroken. Scientists have determined this by analyzing seismic waves that pass through the layer. The depth at which the asthenosphere is found is temperature-dependent. It tends to lie closer to the Earth's surface around mid-ocean ridges and much deeper underneath mountains and the centers of lithospheric plates.

Mesosphere

The **mesosphere**, sometimes known as the lower mantle, is more rigid and immobile than the asthenosphere. Located at a depth of approximately 410 to 660 km below the Earth's surface, the mesosphere is subjected to very high pressures and temperatures. These extreme conditions create a transition zone in the upper mesosphere where minerals continuously change into various forms, or pseudomorphs. Scientists identify this zone by changes in seismic velocity and sometimes by physical barriers to movement. Below this transitional zone, the mesosphere is relatively uniform until it reaches the core.

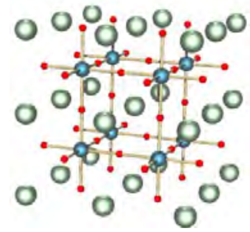

Figure 2.20: General perovskite structure. Perovskite silicates (i.e., bridgmenite, (Mg,Fe)SiO_3) are thought to be the main component of the lower mantle, making it the most common mineral in or on Earth. Figure description available at the end of the chapter.

Inner and Outer Core

Figure 2.21: Lehmann in 1932. Figure description available at the end of the chapter.

The **outer core** is the only entirely liquid layer within the Earth. It starts at a depth of 2,890 km and extends to 5,150 km, making it about 2,300 km thick. In 1936, the Danish geophysicist Inge Lehmann analyzed seismic data and was the first to prove a solid **inner core** existed within a liquid outer core. The solid inner core is about 1,220 km thick, and the outer core is about 2,300 km thick.

It seems like a contradiction that the hottest part of the Earth is solid, as the minerals making up the core should be liquified or vaporized at this temperature. Immense pressure keeps the minerals of the inner core in a solid phase. The inner core grows slowly from the lower outer core, solidifying as heat escapes the interior of the Earth and is dispersed to the outer layers.

The Earth's liquid outer core is critically important in maintaining a breathable atmosphere and other environmental conditions favorable for life. Scientists believe the Earth's magnetic field is generated by the circulation of molten iron and nickel within the outer core. If the outer core were to stop circulating or become solid, the loss of the magnetic field would result in Earth being stripped of life-supporting gases and water. This is what happened, and continues to happen, on Mars.

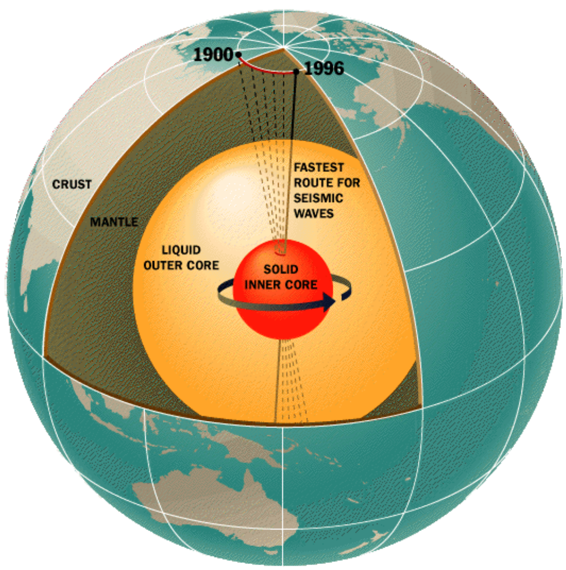

Figure 2.22: The outer core's spin causes our protective magnetic field. Figure description available at the end of the chapter.

Complete this interactive activity to check your understanding.

Access this interactive activity by scanning the QR code.

2.2.3 Plate Tectonic Boundaries

At **passive margins**, the plates don't move; the continental lithosphere transitions into oceanic lithosphere and forms plates made of both types. A tectonic plate may be made of both oceanic and continental lithosphere connected by a passive margin. North and South America's eastern coastlines are examples of passive margins. Active margins are places where the oceanic and continental lithospheric tectonic plates meet and move relative to each other, such as the western coasts of North and South America. This movement is caused by **frictional** drag created between the plates and differences in plate densities. The majority of mountain-building events, earthquake activity, and active volcanism on the Earth's surface can be attributed to tectonic plate movement at active margins.

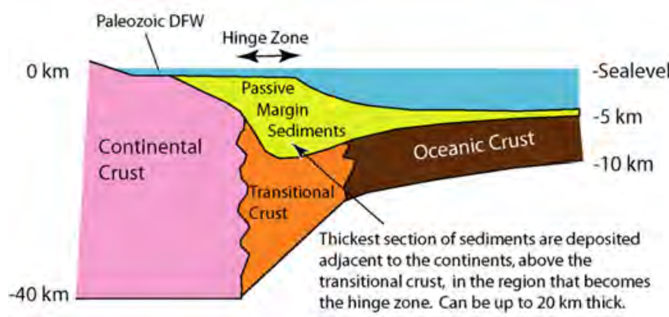

Figure 2.23: Passive margin. [Figure description available at the end of the chapter](#).

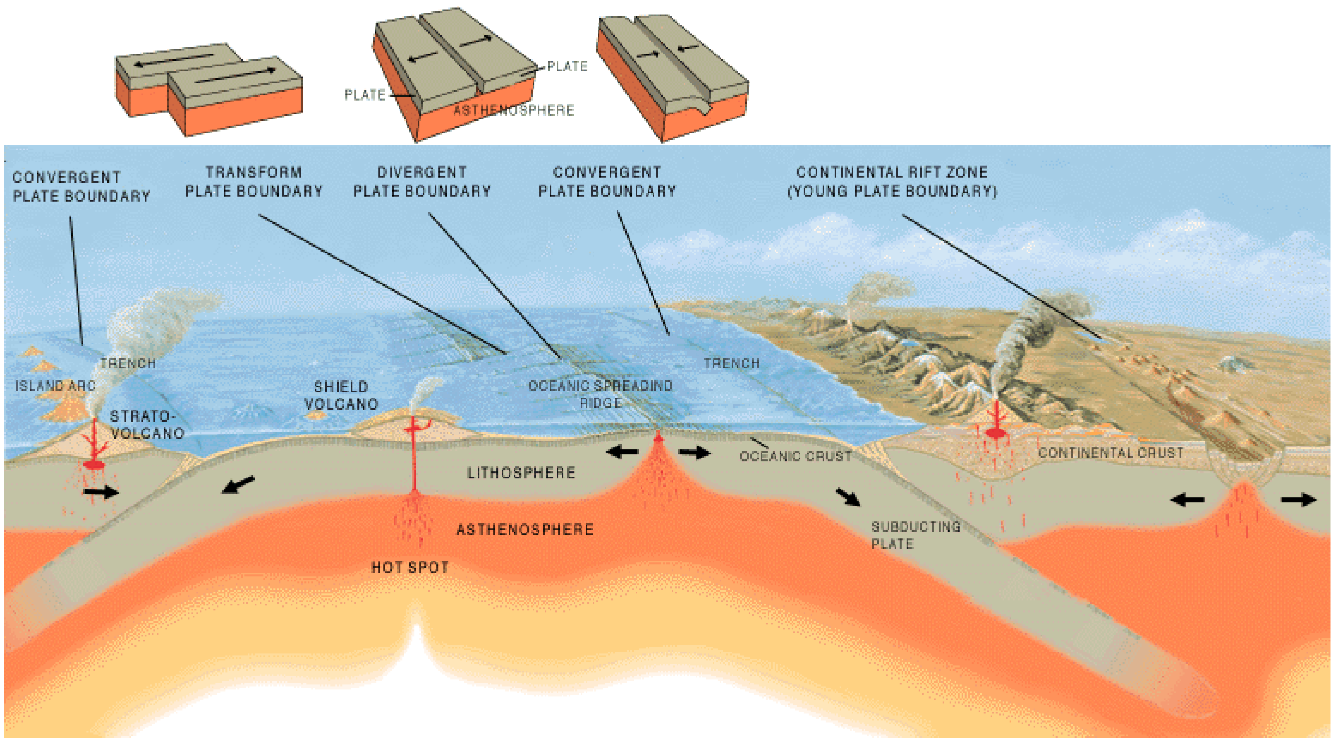

Figure 2.24: Schematic of plate boundary types. [Figure description available at the end of the chapter](#).

In a simplified model, there are three categories of tectonic plate boundaries. **Convergent** boundaries are places where plates move toward each other. At **divergent** boundaries, the plates move apart. At **transform** boundaries, the plates slide past each other.

Take this quiz to check your comprehension of this section.

Access the [quiz for Section 2.2](#) by scanning the QR code.

2.3 Convergent Boundaries

Convergent boundaries, also called destructive boundaries, are places where two or more plates move toward each other. Convergent boundary movement is divided into two types, **subduction** and **collision**, depending on the density of the involved plates. Continental lithosphere is of lower density and thus more buoyant than the underlying asthenosphere. Oceanic lithosphere is more dense than continental lithosphere, and, when old and cold, may even be more dense than asthenosphere.

When plates of different densities converge, the higher-density plate is pushed beneath the more buoyant plate in a process called subduction. When continental plates converge without subduction occurring, this process is called collision.

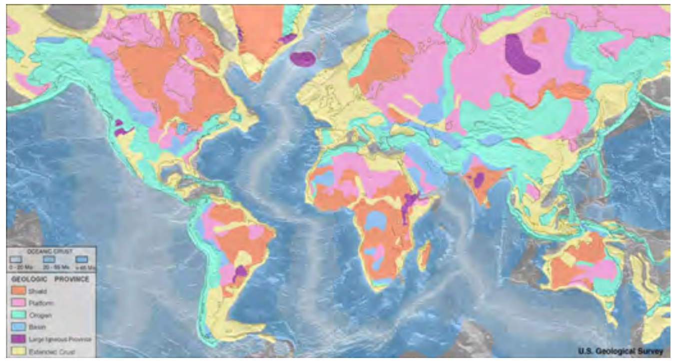

Figure 2.25: Geologic provinces, with the shield (orange) and platform (pink) comprising the craton, the stable interior of continents. Figure description available at the end of the chapter.

2.3.1. Subduction

Subduction occurs when a dense oceanic plate meets a more buoyant plate, like a continental plate or a warmer/younger oceanic plate, and descends into the mantle. The worldwide average rate of oceanic plate subduction is 25 miles per million years—about a half-inch per year. As an oceanic plate descends, it pulls the ocean floor down into a **trench**. These trenches can be more than twice as deep as the average depth of the adjacent ocean **basin**, which is usually 3–4 km. The Mariana Trench, for example, approaches a staggering 11 km.

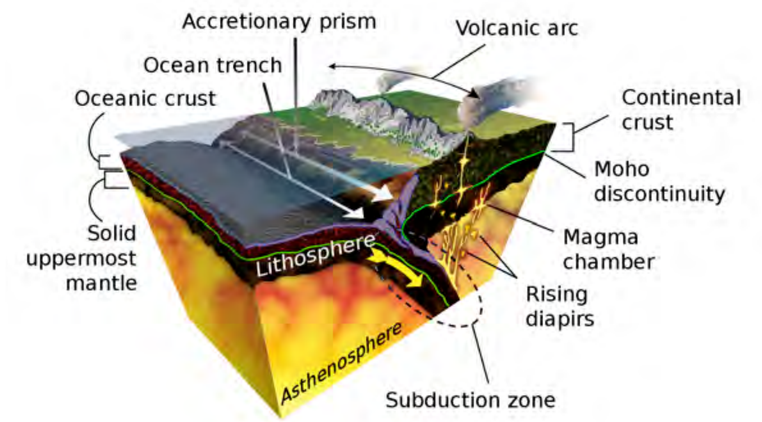

Figure 2.26: Diagram of ocean-continent subduction. Figure description available at the end of the chapter.

Within the trench, ocean-floor sediments are scraped together and compressed between the subducting and overriding plates. This feature is called the **accretionary wedge**, mélange, or accretionary prism. Fragments of continental material, including microcontinents, riding atop the subducting plate may become sutured to the accretionary wedge and accumulate into a large area of land called a **terrane**. Vast portions of California are comprised of accreted terranes.

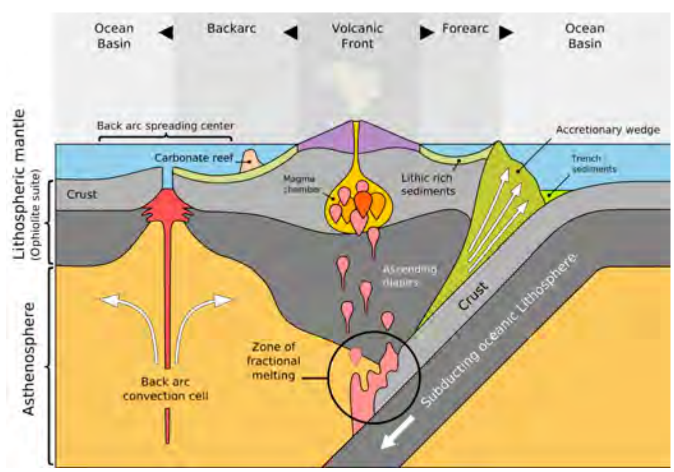

Figure 2.27: Microcontinents can become part of the accretionary prism of a subduction zone. Figure description available at the end of the chapter.

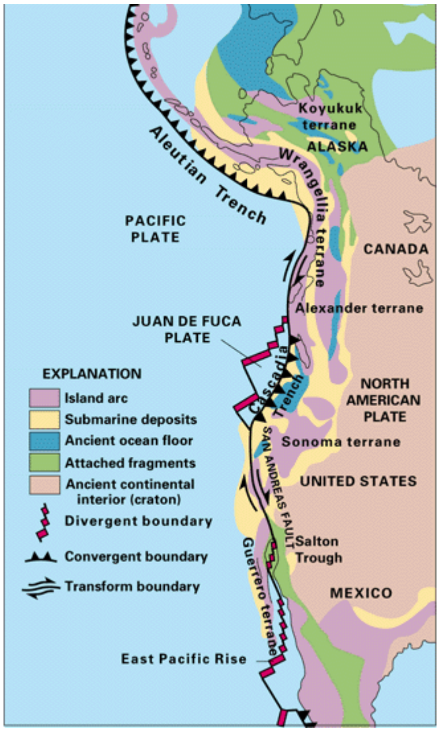

Figure 2.28: Accreted terranes of Western North America. Everything that is not the "ancient continental interior (craton)" has been smeared onto the side of the continent by accretion from subduction. Figure description available at the end of the chapter.

When the subducting oceanic plate, or **slab**, sinks into the mantle, the immense heat and pressure pushes volatile materials like water and carbon dioxide into an area below the continental plate and above the descending plate called the **mantle wedge**. The **volatiles** are released mostly by hydrated minerals that revert to nonhydrated minerals in these higher temperature and pressure conditions. When mixed with asthenospheric material above the plate, the volatile lower the melting point of the mantle wedge, and through a process called **flux melting**, it becomes liquid magma. The molten magma is more buoyant than the lithospheric plate above it, migrating to the Earth's surface, where it emerges as volcanism. The resulting **volcanoes** frequently appear as curved mountain chains (known as **volcanic arcs**) due to the curvature of the Earth. Both oceanic and continental plates can contain volcanic arcs.

How subduction is initiated is still a matter of scientific debate. It is generally accepted that subduction zones start as passive margins, where oceanic and continental plates come together, and then gravity initiates subduction and converts to margin from passive to active. One hypothesis is that gravity pulls the denser oceanic plate down or that the plate can start to flow with ductility at a low angle. Scientists seeking to answer this question have collected evidence that suggests a new subduction zone is forming off the coast of Portugal. Some scientists have proposed that large earthquakes like the 1755 Lisbon earthquake may even have something to do with this process of creating a subduction zone, although the evidence is not definitive. Another hypothesis proposes that subduction happens at transform boundaries involving plates of different densities.

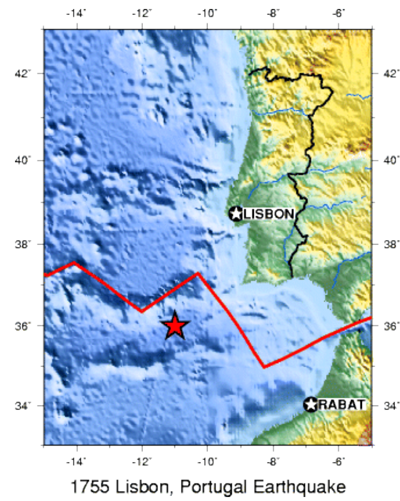

Figure 2.29: Location of the large (Mw 8.5–9.0) 1755 Lisbon earthquake. Figure description available at the end of the chapter.

Some plate boundaries look like they should be active but show no evidence of subduction. For example, the oceanic lithospheric plates on either side of the Atlantic Ocean are denser than the underlying asthenosphere and are not subducting beneath the continental plates. One hypothesis is that the bond holding the oceanic and continental plates together is stronger than the downward force created by the difference in plate densities.

Subduction zones are known for having the largest earthquakes and tsunamis; they are the only places with fault surfaces large enough to create magnitude 9 earthquakes. These subduction-zone earthquakes are not only very large but are also very deep. When a subducting slab becomes stuck and cannot descend, a massive amount of energy builds up between the stuck plates. If this energy is not gradually dispersed, it may force the plates to suddenly release along several hundred kilometers of the subduction zone. Because subduction-zone faults are located on the ocean floor, this massive amount of movement can generate giant **tsunamis** such as those that followed the 2004 Indian Ocean earthquake and 2011 Tōhoku earthquake in Japan.

All subduction zones have a **forearc basin**, a feature of the overriding plate found between the volcanic arc and oceanic trench. The forearc basin experiences a lot of faulting and **deformation** activity, particularly within the accretionary wedge.

In some subduction zones, tensional forces working on the continental plate create a **backarc basin** on the interior side of the volcanic **arc**. Some scientists have proposed a subduction mechanism called oceanic slab rollback, which creates extension faults in the overriding plates. In this model, the descending oceanic slab does not slide directly under the overriding plate but instead rolls back, pulling the overlying plate seaward. The continental plate behind the volcanic arc gets stretched like pizza dough until the surface cracks and collapses to form a backarc basin. If the extension activity is extensive and deep enough, a backarc basin can develop into a continental rifting zone. These continental divergent boundaries may be less symmetrical than their mid-ocean ridge counterparts.

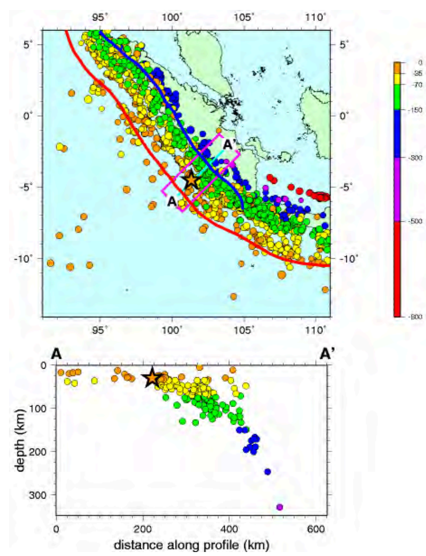

Figure 2.30: Earthquakes along the Sunda megathrust subduction zone along the island of Sumatra, showing the 2006 Mw 9.1-9.3 Indian Ocean earthquake as a star. Figure description available at the end of the chapter.

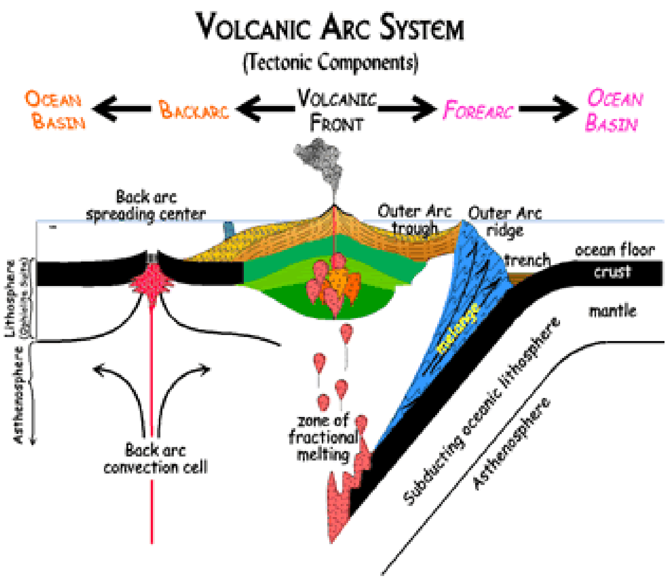

Figure 2.31: Various parts of a subduction zone. This subduction zone is ocean-ocean subduction, though the same features can apply to continent-ocean subduction. Figure description available at the end of the chapter.

In places where numerous young buoyant oceanic plates converge and subduct at a relatively high velocity, they may force the overlying continental plate to buckle and crack. This is called **back-arc** faulting. Extensional back-arc faults pull rocks and chunks of plates apart. Compressional back-arc faults, also known as **thrust faults**, push them together.

The dual spines of the Andes mountain range include a example of compressional thrust faulting. The western spine is part of a volcanic arc. Thrust faults have deformed the nonvolcanic eastern spine, pushing rocks and pieces of continental plate on top of each other.

There are two styles of thrust fault deformation: **thin-skinned** faults that occur in superficial rocks lying on top of the continental plate and **thick-skinned** faults that reach deeper into the crust. The Sevier **orogeny** in the Western US is a notable thin-skinned type of deformation created during the Cretaceous Period. The Laramide orogeny, a thick-skinned type of deformation, occurred near the end of and slightly after the Sevier orogeny in the same region.

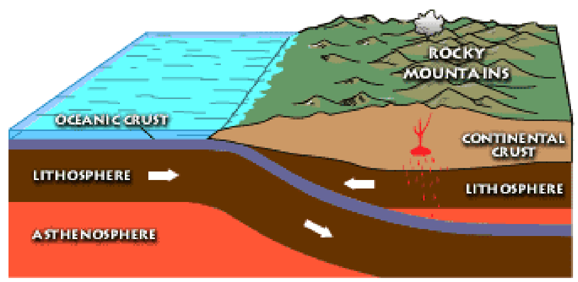

Figure 2.32: Shallow subduction during the Laramide orogeny. Figure description available at the end of the chapter.

Flat-slab, or shallow, subduction caused the Laramide orogeny. When the descending slab subducts at a low angle, there is more contact between the slab and the overlying continental plate than in a typical subduction zone. The shallowly subducting slab pushes against the overriding plate and creates an area of deformation on the overriding plate many kilometers away from the subduction zone.

Oceanic-Continental Subduction

Oceanic-continental subduction occurs when an oceanic plate dives below a continental plate. This convergent boundary has a trench, mantle wedge, and frequently, a volcanic arc. Well-known examples of continental volcanic arcs are the Cascade Mountains in the Pacific Northwest and the western Andes Mountains in South America.

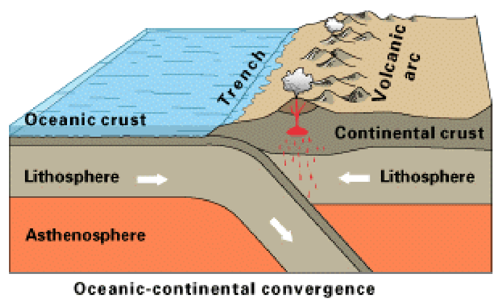

Figure 2.33: Subduction of an oceanic plate beneath a continental plate, forming a trench and volcanic arc. Figure description available at the end of the chapter.

Oceanic-Oceanic Subduction

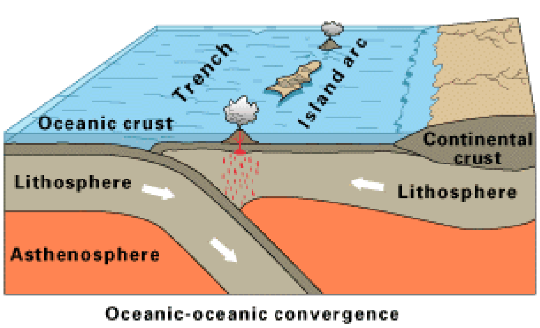

Figure 2.34: Subduction of an oceanic plate beneath another oceanic plate, forming a trench and an island arc. Figure description available at the end of the chapter.

The boundaries of **oceanic-oceanic subduction** zones show very different activity from those involving oceanic-continental plates. Since both oceanic lithosphere, it is usually the older plate that subducts because it is colder and denser. The volcanism on the overlying oceanic plate may remain hidden underwater. If the volcanoes rise high enough to reach the ocean surface, the chain of volcanism forms an **island arc**. Examples of these island arcs include the Aleutian Islands in the northern Pacific Ocean, the Lesser Antilles in the Caribbean Sea, and numerous island chains scattered throughout the western Pacific Ocean.

2.3.2. Collisions

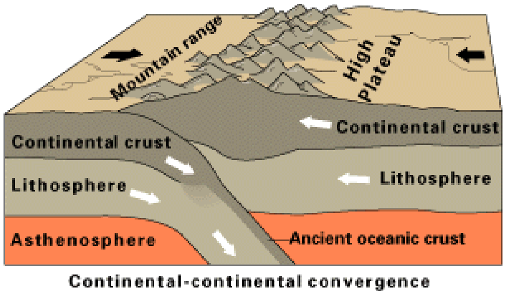

Figure 2.35: Two continental plates colliding. Figure description available at the end of the chapter.

When continental plates converge—for example, during the closing of an ocean basin—subduction is not possible between the equally buoyant plates. Instead of one plate descending beneath another, the two masses of continental lithosphere slam together in a process known as **collision**. Without subduction, there is no magma formation and no volcanism. Collision zones are characterized by tall, non-volcanic mountains; broad zones of frequent, large earthquakes; and very little volcanism.

When oceanic crust connected by a passive margin to continental crust completely subducts beneath a continent, an ocean basin closes and continental collision begins. Eventually, as ocean basins close, continents join together to form a massive accumulation of continents called a **supercontinent**, a process that takes place in ~500-million-year cycles over Earth's history.

The process of collision created **Pangea**, the supercontinent envisioned by Wegener as the key component of his continental drift hypothesis. Geologists now have evidence that continental plates have been continuously converging into supercontinents and splitting into smaller basin-separated continents throughout Earth's existence in a process known as the supercontinent cycle, which takes approximately 500 million years. For example, Pangea is estimated to have begun separating 200 million years ago. Pangea was preceded by an earlier supercontinents, including Rodinia, which existed 1.1 billion years ago and started breaking apart 800 million to 600 million years ago.

Figure 2.36: A reconstruction of Pangea, showing approximate positions of modern continents. Figure description available at the end of the chapter.

A foreland basin is a feature that develops near mountain belts, as the combined mass of the mountains forms a depression in the lithospheric plate. While foreland basins may occur at subduction zones, they are most commonly found at collision boundaries. The Persian Gulf is possibly the best modern example, created entirely by the weight of the nearby Zagros Mountains.

If continental and oceanic lithosphere are fused on the same plate, it can partially subduct, but its buoyancy prevents it from fully descending. In very rare cases, part of a continental plate may become trapped beneath a descending oceanic plate in a process called **obduction**. When a portion of the continental crust is driven down into the subduction zone, it returns to the surface relatively quickly due to its buoyancy.

Figure 2.37: The tectonics of the Zagros Mountains. Note the Persian Gulf foreland basin. Figure description available at the end of the chapter.

As pieces of the continental lithosphere break loose and migrate upward through the obduction zone, they bring along bits of the mantle and ocean floor to the top of the continental plate. Rocks composed of this mantle and ocean-floor material are called ophiolites, and they provide valuable information about the composition of the mantle.

Figure 2.38: Pillow lavas, which only form under water, from an ophiolite in the Apennine Mountains of Central Italy. Figure description available at the end of the chapter.

The area of collision-zone deformation and seismic activity usually covers a broader area because continental lithosphere is plastic and malleable. Unlike subduction-zone earthquakes, which tend to be located along a narrow swath near the convergent boundary, collision-zone earthquakes may occur hundreds of kilometers from the boundary between the plates.

The Eurasian continent has many examples of collision-zone deformations covering vast areas. The Pyrenees Mountains begin in the Iberian Peninsula and cross into France. Additionally, the Alps stretch from Italy to Central Europe; the Zagros Mountains from Arabia to Iran; and the Himalayas from the Indian subcontinent to Central Asia.

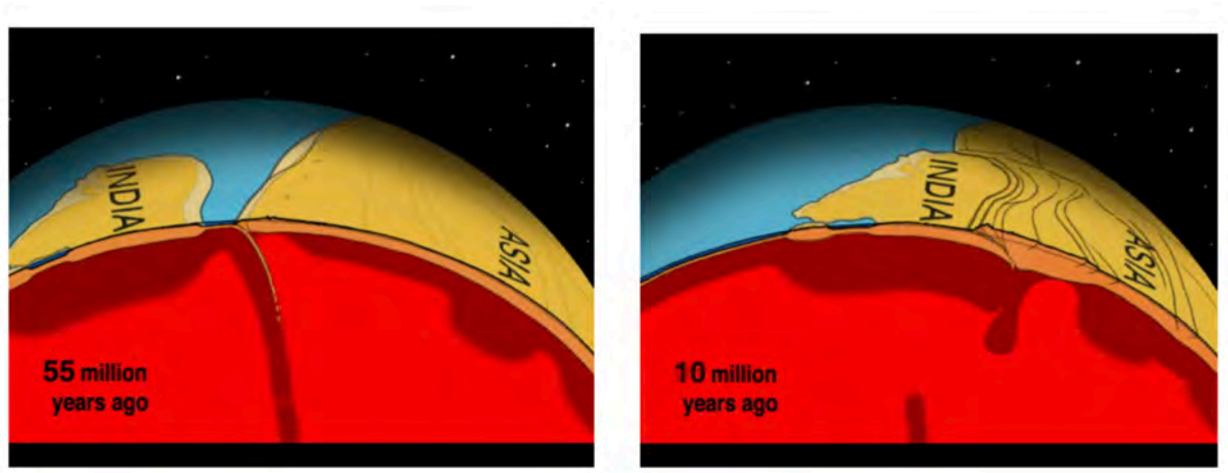

Figure 2.39: Animation of India crashing into Asia. Figure description available at the end of the chapter.

Take this quiz to check your comprehension of this section.

Access the quiz for Section 2.3 by scanning the QR code.

2.4 Divergent Boundaries

At **divergent** boundaries, sometimes called constructive boundaries, lithospheric plates move away from each other. There are two types of divergent boundaries, categorized by where they occur: continental **rift** zones and mid-ocean ridges. Continental rift zones occur in weak spots in the continental lithospheric plate. A **mid-ocean ridge** usually originates in a continental plate as a rift zone that expands to the point of splitting the plate apart, with seawater filling the gap. The separate pieces continue to drift apart and become individual continents. This process is known as rift-to-drift.

2.4.1. Continental Rifting

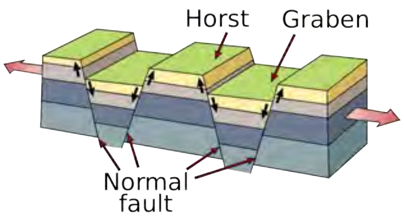

Figure 2.40: Faulting that occurs in divergent boundaries. Figure description available at the end of the chapter.

In places where the continental plates are very thick, they reflect so much heat back into the mantle that it develops strong convection currents that push super-heated mantle material up against the overlying plate, softening it. Tensional forces created by this convective upwelling begin to pull the weakened plate apart. As it stretches, it becomes thinner and develops deep cracks called extension faults, or normal faults. Eventually plate sections located between large faults drop into deep depressions known as rift valleys, which often contain keystone-shaped blocks of down-dropped crust known as **grabens**. The shoulders of these grabens are called **horsts**. If only one side of a section drops, it is called a half-graben. Depending on the conditions, rifts can grow into very large lakes and even oceans.

Figure 2.41: The Afar Triangle (center) has the Red Sea ridge (center to upper left), Gulf of Aden ridge (center to right), and East African Rift (center to lower left) form a triple junction that are about 120° apart. Figure description available at the end of the chapter.

While seemingly occurring at random, rifting is dictated by two factors. Rifting does not occur in continents with older and more stable interiors, known as **cratons**. When continental rifting does occur, the break-up pattern is called a truncated icosahedron, which resembles the seams of a soccer ball. This is the most common surface-fracture pattern to develop on an evenly expanding sphere because it uses the least amount of energy.

Using the soccer ball model, rifting tends to lengthen and expand along a particular seam while fizzling out in the other directions. These seams with little or no tectonic activity are called failed rift arms. A **failed rift arm** is still a weak spot in the continental plate; even without the presence of active extension faults, it may develop into what is known as an **aulacogen**. One example of a failed rift arm is the Mississippi Valley embayment, a depression through which the upper end of the Mississippi River flows. Occasionally, connected rift arms do develop concurrently, creating multiple boundaries of active rifting. In places where the rift arms do not fail, for example the Afar Triangle, three divergent boundaries can develop near each other, forming a **triple junction**.

Figure 2.42: NASA image of the Basin and Range horsts and grabens across central Nevada. Figure description available at the end of the chapter.

Rifts come in two types: narrow and broad. Narrow rifts are characterized by a high density of highly active divergent boundaries. The East African rift zone, where the Horn of Africa is pulling away from the mainland, is an excellent example of an active narrow rift. Lake Baikal in Russia is another. Broad rifts also have numerous fault zones, but they are distributed over wide areas of deformation. The **Basin and Range** region located in the Western United States is a type of broad rift. The Wasatch fault, which also created the Wasatch mountain range in the state of Utah, forms the eastern divergent boundary of this broad rift (Animation 1 and Animation 2).

Rifts have earthquakes, although not of the magnitude and frequency of other boundaries. They may also exhibit volcanism. Unlike the flux-melted magma found in subduction zones, rift-zone magma is created by decompression melting. As the continental plates are pulled apart, they create a region of low pressure that melts the lithosphere and draws it upwards. When this molten magma reaches the weakened and fault-riddled rift zone, it migrates to the surface by breaking through the plate or escaping via an open fault. Examples of young rift volcanoes are scattered throughout the Basin and Range region in the United States. Rift-zone activity is responsible for generating some unique volcanism, such as the Ol Doinyo Lengai in Tanzania. This volcano erupts lava consisting largely of **carbonatite**, a relatively cold, liquid carbonate mineral.

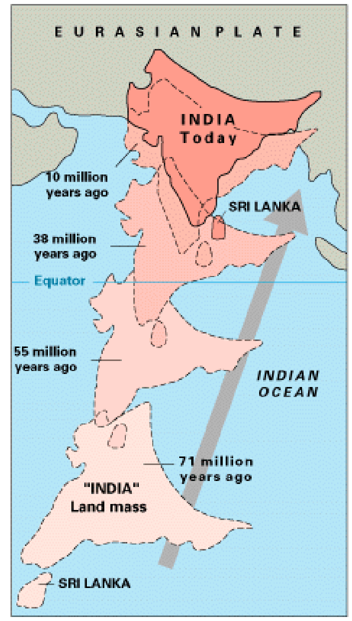

Figure 2.43: India colliding into Eurasia to create the modern day Himalayas. Figure description available at the end of the chapter.

2.4.2. Mid-Ocean Ridges

Figure 2.44: Progression from rift to mid-ocean ridge. Figure description available at the end of the chapter.

As rifting and volcanic activity progress, the continental lithosphere becomes more mafic (see Chapter 4) and thinner, with the eventual result transforming the plate under the rifting area into oceanic lithosphere. This is the process that gives birth to a new ocean, much like the narrow Red Sea emerging with the movement of Arabia away from Africa. As the oceanic lithosphere continues to diverge, a mid-ocean ridge is formed.

Mid-ocean ridges, also known as spreading centers, have several distinctive features. They are the only places on Earth that create new oceanic lithosphere. **Decompression melting** in the rift zone changes asthenosphere material into new lithosphere, which oozes up through cracks in oceanic plate. The amount of new lithosphere being created at mid-ocean ridges is highly significant. These undersea rift volcanoes produce more lava than all other types of volcanism combined. Despite this, most mid-oceanic ridge volcanism remains unmapped because the volcanoes are located deep on the ocean floor.

In rare cases, such as a few locations in Iceland, rift zones display the type of volcanism, spreading, and ridge formation found on the ocean floor.

The ridge feature is created by the accumulation of hot lithosphere material, which is lighter than the dense underlying asthenosphere. This chunk of isostatically buoyant lithosphere sits partially submerged and partially exposed on the asthenosphere, like an ice cube floating in a glass of water.

As the ridge continues to spread, the lithosphere material is pulled away from the area of volcanism and becomes colder and denser. As it continues to spread and cool, the lithosphere settles into wide swaths of relatively featureless topography called abyssal plains with lower topography.

This model of ridge formation suggests the sections of lithosphere furthest away from the mid-ocean ridges will be the oldest. Scientists have tested this idea by comparing the ages of rocks located in various locations on the ocean floor. Rocks found near ridges are younger than those found far away from any ridges. Sediment-accumulation patterns also confirm the idea of seafloor spreading. Sediment layers tend to be thinner near mid-ocean ridges, indicating it has had less time to build up.

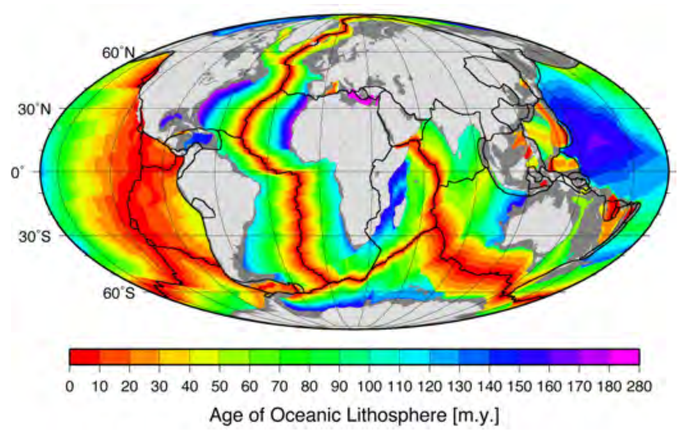

Figure 2.45: Age of oceanic lithosphere, in millions of years. Notice the differences in the Atlantic Ocean along the coasts of the continents. Figure description available at the end of the chapter.

As mentioned in the section on paleomagnetism and the development of plate tectonic theory, scientists noticed that mid-ocean ridges contained unique magnetic anomalies that show up as symmetrical striping on both sides of the ridge. The Vine-Matthews-Morley hypothesis proposes these alternating reversals are created by the Earth's magnetic field being imprinted into magma after it emerges from the ridge. Very hot magma has no magnetic field. As the oceanic plates get pulled apart, the magma cools below the Curie point—the temperature below which a magnetic field gets locked into magnetic minerals. The alternating magnetic reversals in the rocks reflects the periodic swapping of Earth's magnetic north and south poles. This paleomagnetic pattern provides a great historical record of ocean-floor movement and is used to reconstruct past tectonic activity and determine rates of ridge spreading.

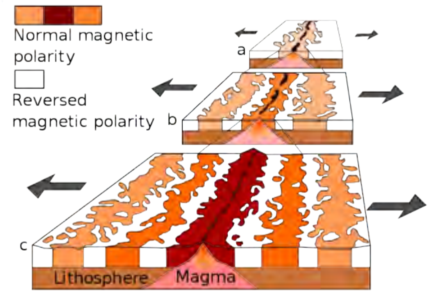

Figure 2.46: A time progression (with "a" being youngest and "c" being oldest) showing a spreading center getting wider while recording changes in the magnetic field of the Earth. Figure description available at the end of the chapter.

Video 2.2: Pangea breakup and formation of the northern Atlantic Ocean

Access this YouTube video by scanning the QR code. ["PANGEA Breakup" by ProfessorManganelli | https://www.youtube.com/watch?v=6o1HawAOTEI]

Thanks to their distinctive geology, mid-ocean ridges are home to some of the most unique ecosystems ever discovered. The ridges are often studded with **hydrothermal** vents, which are deep fissures that allow seawater to circulate through the upper portions of the oceanic plate and interact with hot rock. The super-heated seawater rises back up to the surface of the plate, carrying dissolved gases and minerals as well as small particulates. The hydrothermal water emitted as a result looks like black underwater smoke.

Scientists had known about these geothermal areas on the ocean floor for some time. However, it was not until 1977 that scientists piloting a deep submergence vehicle, the Alvin, discovered a thriving community of organisms clustered around these hydrothermal vents. These unique organisms, which include ten-foot-long tube worms taller than people, live in the complete darkness of the ocean floor, deprived of oxygen and sunlight. They use geothermal energy provided by the vents and a process called bacterial **chemosynthesis** to feed on sulfur compounds. Before this discovery, scientists believed life on Earth could not exist without photosynthesis, a process that requires sunlight. Some scientists suggest this type of environment could have been the origin of life on Earth and perhaps even **extraterrestrial** life elsewhere in the galaxy, such as on Jupiter's moon Europa.

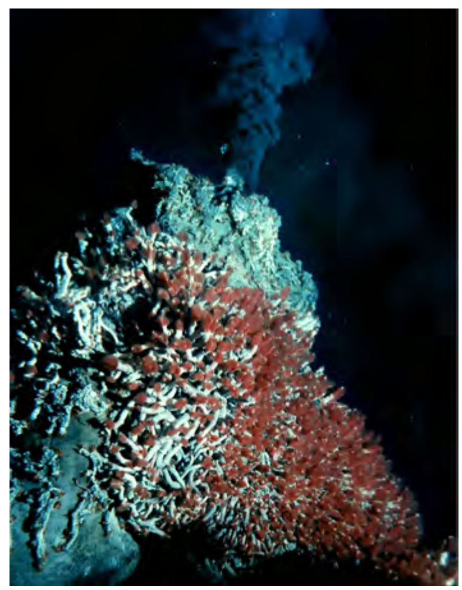

Figure 2.47: Black smoker hydrothermal vent with a colony of giant (6'+) tube worms. Figure description available at the end of the chapter.

Take this quiz to check your comprehension of this section.

Access the quiz for Section 2.4 by scanning the QR code.

2.5 Transform Boundaries

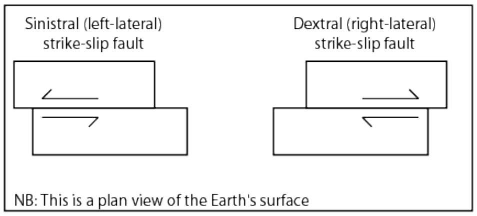

Figure 2.48: The two types of transform/strike-slip faults. Figure description available at the end of the chapter.

A transform boundary, sometimes called a **strike-slip** or conservative boundary, is where the lithospheric plates slide past each other in the horizontal plane. This movement is described based on the perspective of an observer standing on one of the plates, looking across the boundary at the opposing plate. **Dextral**, also known as right-lateral, movement describes the opposing plate moving to the right. **Sinistral**, also known as left-lateral, movement describes the opposing plate moving to the left.

Most transform boundaries are found on the ocean floor around mid-ocean ridges. These boundaries form **aseismic fracture zones** filled with earthquake-free transform faults to accommodate different rates of spreading occurring at the ridge.

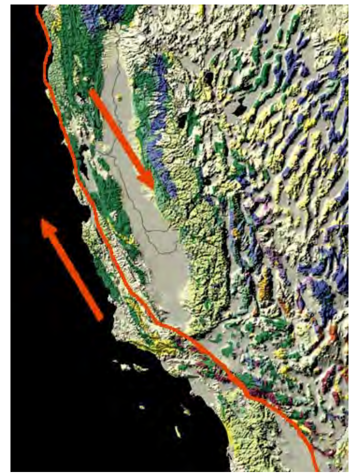

Figure 2.49: Map of the San Andreas fault showing relative motion. Figure description available at the end of the chapter.

Some transform boundaries produce significant seismic activity, primarily as earthquakes, with very little mountain-building or volcanism. This type of transform boundary may contain a single fault or series of faults, which develop in places where plate tectonic stresses are transferred to the surface. As with other types of active boundaries, if the plates are unable to **shear** past each other, the tectonic forces will continue to build up. If the built-up energy between the plates is suddenly released, the result is an earthquake.

In the eyes of humanity, the most significant transform faults occur within continental plates and have a shearing motion that frequently produces moderate-to-large magnitude earthquakes. Notable examples include the San Andreas fault in California, Northern and Eastern Anatolian faults in Turkey, Altyn Tagh fault in Central Asia, and Alpine fault in New Zealand.

2.5.1 Transpression and Transtension

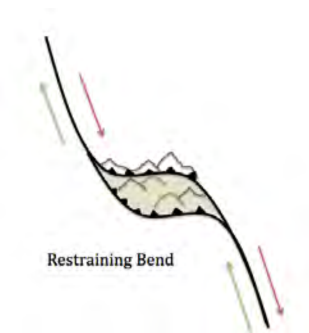

Figure 2.50: A transpressional strike-slip fault, causing uplift called a restraining bend. Figure description available at the end of the chapter.

Bends along transform faults may create compressional or extensional forces that cause secondary faulting zones. **Transpression** occurs where there is a component of **compression** in addition to the **shearing** motion. These forces build up around the area of the bend, where the opposing plates are restricted from sliding past each other. As the forces continue to build up, they create mountains in the restraining bend around the fault. The Big Bend area, located in the southern part of the San Andreas fault, includes a large area of transpression where many mountains have been built, moved, and even rotated.

Transtension zones require a fault that includes a releasing bend, where the plates are pulled apart by extensional forces. Depressions and sometimes volcanism develop in the releasing bend along the fault. The Dead Sea between Israel and Jordan and the Salton Sea of California are examples of basins formed by transtensional forces.

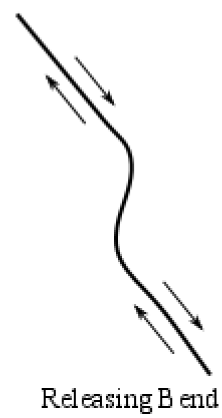

Figure 2.51: A transtensional strike-slip fault, causing a restraining bend. In the center of the fault, a depression with extension would be found. Figure description available at the end of the chapter.

2.5.2 Piercing Points

When a geological feature is cut by a fault, it is called a **piercing point**. Piercing points are very useful for recreating past fault movement, especially along transform boundaries. Transform faults are unique because their horizontal motion keeps a geological feature relatively intact, preserving the record of what happened. Other types of faults—normal and reverse—tend to be more destructive, obscuring or destroying these features. The best type of piercing point includes unique patterns, which are used to match the parts of a geological feature separated by fault movement. Detailed studies of piercing points show the San Andreas fault has experienced over 225 km of movement in the last 20 million years, and this movement occurred at three different fault traces.

Figure 2.52: Wallace Creek (dry) on the Cariso Plain, California. Note that, as the creek flows from the northern mountainous part of the image, it takes a sharp right (as viewed from the flow of water), then a sharp left. This is caused by the San Andreas Fault cutting roughly perpendicular to the creek and shifting the location of the creek over time. The fault can be seen about halfway down, trending left to right, as a change in the topography. Figure description available at the end of the chapter.

Video 2.3: Video of the origin of the San Andreas fault. As the mid-ocean ridge subducts, the relative motion between the remaining plates become transform, forming the fault system. Note that, because the motion of the plates is not exactly parallel to the fault, it causes divergent motion in the interior of North America.

Access this YouTube video by scanning the QR code. ["Plate Tectonics in a Nutshell (Tanya Atwater)" by VIP Voice | https://www.youtube.com/watch?v=IDTBY5WDELg]

Take this quiz to check your comprehension of this section.

Access the quiz for Section 2.5 by scanning the QR code.

2.6 The Wilson Cycle

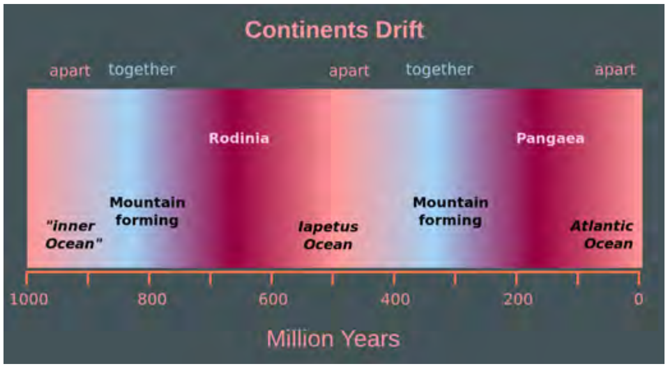

Figure 2.53: Diagram of the Wilson cycle, showing rifting and collision phases. Figure description available at the end of the chapter.

The **Wilson cycle** is named for J. Tuzo Wilson, who first described it in 1966, and it outlines the ongoing origin and breakup of supercontinents, such as Pangea and Rodinia. Scientists have determined this cycle has been operating for at least three billion years and possibly longer.

There are a number of hypotheses about how the Wilson cycle works. One mechanism proposes that rifting happens because continental plates reflect the heat much better than oceanic plates. When continents congregate together, they reflect more of the Earth's heat back into the mantle, generating more vigorous convection currents that then start the continental rifting process. Some geologists believe mantle plumes are remnants of these periods of increased mantle temperature and convection upwelling, studying them for clues about the origin of continental rifting.

The mechanism behind how supercontinents are created is still largely a mystery. There are three schools of thought about what continues to drive the continents further apart and eventually bring them together. The ridge-push hypothesis suggests after the initial rifting event, plates continue to be pushed apart by mid-ocean spreading centers and their underlying convection currents. The slab-pull hypothesis proposes the plates are pulled apart by descending slabs in the subduction zones of the oceanic-continental margins. A third idea, gravitational sliding, attributes the movement to gravitational forces pulling the lithospheric plates down from the elevated mid-ocean ridges and across the underlying asthenosphere. Current evidence seems to support slab pull more than ridge push or gravitational sliding.

2.7 Hotspots

The Wilson cycle provides a broad overview of tectonic plate movement. To analyze plate movement more precisely, scientists study hotspots. First postulated by J. Tuzo Wilson in 1963, a **hotspot** is an area in the lithospheric plate where molten magma breaks through and creates a volcanic center—islands in the ocean and mountains on land. As the plate moves across the hotspot, the volcano center becomes extinct because it is no longer over an active magma source. Instead, the magma emerges through another area in the plate to create a new active volcano. Over time, the combination of moving plate and stationary hotspot creates a chain of islands or mountains. Conventionally, hotspots were thought not to move, although recent evidence suggests that there may be exceptions.

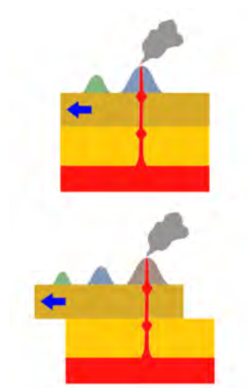

Figure 2.54: Diagram showing a nonmoving source of magma (mantle plume) and a moving overriding plate. Figure description available at the end of the chapter.

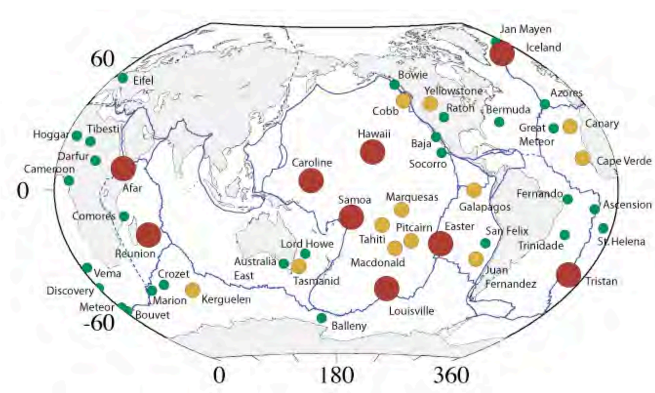

Figure 2.55: Map of world hotspots. Larger circles indicate more active hotspots. Figure description available at the end of the chapter.

Hotspots are the only types of volcanism not associated with subduction or rifting zones at plate boundaries; they seem totally disconnected from any plate tectonics processes, such as earthquakes. However, there are relationships between hotspots and plate tectonics. There are several hotspots, current and former, that are believed to have begun at the time of rifting. In addition, scientists use the age of volcanic eruptions and shape of the chain to quantify the rate and direction of plate movement relative to the hotspot.

Scientists are divided over how magma is generated in hotspots. Some suggest that hotspots originate from super-heated material that originates from as deep as the core and that reaches the Earth's crust as a **mantle plume**. Others argue the molten material that feeds hotspots is sourced from the mantle. Of course, it is difficult to collect data from these deep-Earth features due to the extremely high pressure and temperature.

The initiation of hotspots is another highly debated subject. The prevailing mechanism considers hotspots as starting in divergent boundaries during supercontinent rifting. Scientists have identified a number of current and past hotspots believed to have begun this way. Subducting slabs have also been named as causing mantle plumes and hotspot volcanism. Some geologists have suggested another geological process not involving plate tectonics may be involved, such as large space objects crashing into Earth. Regardless of how they are formed, there are dozens on the Earth. Some well-known examples include the Tahiti Islands, Afar Triangle, Easter Island, Iceland, Galapagos Islands, and Samoan Islands. The United States is home to two of the largest and best-studied hotspots: Hawai'i and Yellowstone.

2.7.1 Hawaiian Hotspot

The active volcanoes in Hawai'i represent one of the most active hotspot sites on Earth. Scientific evidence indicates the Hawaiian hotspot is at least 80 million years old. Geologists believe it is actually much older; however any rocks capable of proving this have been subducted under the ocean floor. The big island of Hawai'i sits atop a large mantle plume that marks the active hotspot. The Kilauea volcano is the main **vent** for this hotspot and has been actively erupting since 1983.

This enormous volcanic island chain, much of which is underwater, stretches across the Pacific for almost 6,000 km. The seamount chain's most striking feature is a sharp 60-degree bend located at the midpoint, which marks a significant change in plate movement direction that occurred 50 million years ago. The change in direction has commonly been linked to a plate reconfiguration but also to other things like plume migration.

In an attempt to map the Hawaiian mantle plume as far down as the lower mantle, scientists have used **tomography**, a type of three-dimensional seismic imaging. This information—along with other evidence gathered from rock ages, vegetation types, and island size—indicate the oldest islands in the chain are located the furthest away from the active hotspot.

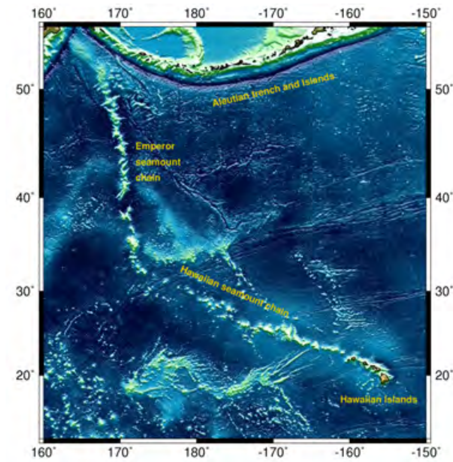

Figure 2.56: The Hawaiian–Emperor seamount and island chain. Figure description available at the end of the chapter.

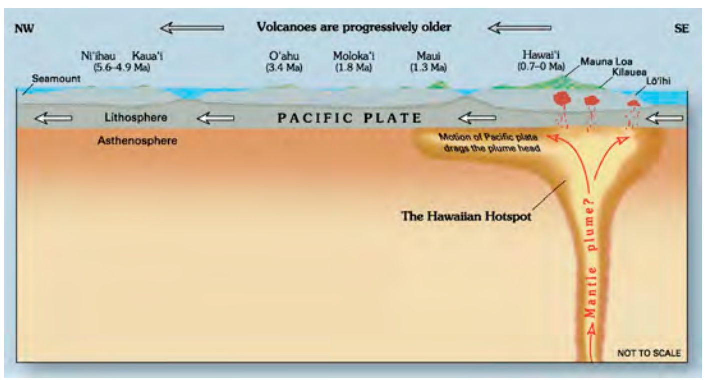

Figure 2.57: Diagram of the Hawaiian hotspot and islands that it formed. Figure description available at the end of the chapter.

2.7.2 Yellowstone Hotspot

Like the Hawaiian version, the Yellowstone hotspot is formed by magma rising through the lithosphere. What makes this hotspot different, however, is its location under a thick continental plate. Hawai'i sits on a thin oceanic plate, which is easily breached by magma coming to the surface. At Yellowstone, the thick continental plate presents a much more difficult barrier for magma to penetrate. When it does emerge, the eruptions are generally much more violent. Thankfully, they are also less frequent.

More than 15 million years of eruptions by this hotspot have carved a curved path across the Western United States. It has been suggested the Yellowstone hotspot is connected to the much older Columbia River flood basalts and even to 70-million-year-old volcanism found in the Yukon region of Canada.

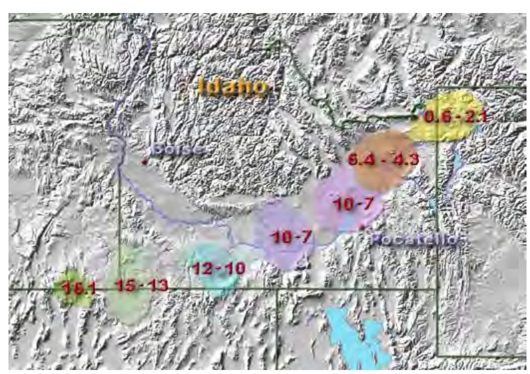

Figure 2.58: The track of the Yellowstone hotspot, which shows the age of different eruptions in millions of years ago. Figure description available at the end of the chapter.

The most recent major eruption of this hotspot created the Yellowstone Caldera and Lava Creek tuff formation approximately 631,000 years ago. The eruption threw 1,000 cubic kilometers of **ash** and magma into the atmosphere, some of which was found as far away as Mississippi. Should the hotspot erupt again, scientists predict it will be another massive event. This would be a calamity, reaching far beyond the Western United States. These supervolcanic eruptions fill the Earth's atmosphere with so much gas and ash that they block sunlight from reaching the Earth. Not only would this drastically alter climates and environments around the globe, it could affect worldwide food production.

Figure 2.59: Several prominent ash beds found in North America, including three Yellowstone eruptions shaded pink (Mesa Falls, Huckleberry Ridge, and Lava Creek), the Bisho Tuff ash bed (brown dashed line), and the modern May 18th, 1980, ash fall (yellow). Figure description available at the end of the chapter.

Take this quiz to check your comprehension of this section.

Access the quiz for Sections 2.6 and 2.7 by scanning the QR code.

Summary

Video 2.4: Plate tectonics

Access this YouTube video by scanning the QR code. ["Plate Tectonics Basics 1" by UTD IGLAB | https://www.youtube.com/watch?v=6wJBOk9xjto]

Plate tectonics is a unifying theory; it explains nearly all of the major geologic processes on Earth. Since its early inception in the 1950s and 1960s, geologists have been guided by this revolutionary perception of the world. The theory of plate tectonics states that the surface layer of the Earth is broken into a network of solid, relatively brittle plates. Underneath the plates is a much hotter and more ductile layer that contains zones of convective upwelling generated by the interior heat of Earth. These convection currents move the surface plates around—bringing them together, pulling them apart, and shearing them side-by-side. Earthquakes and volcanoes form at the boundaries where the]plates interact, with the exception of volcanic hotspots, which are not caused by plate movement.

Take this quiz to check your comprehension of this chapter.

Access the quiz for Chapter 2 by scanning the QR code.

Chapters URLs

- Audio pronunciation of Mohorovičić: https:/ /www.merriam-webster.com/dictionary/Mohorovicic%20discontinuity
- Animation 1: Basin and Range Structures. How do they form? [Video: 0:52] https://www.youtube.com/watch?v=TvvWqAdNV84
- Animation 2: Basin & Range: Extension, Erosion, Sedimentation. [Video: 0:31] https://www.youtube.com/watch?v=7DxcAMmNeZk

Text References

1. Aitta, A. (2006). Iron melting curve with a tricritical point. *J. Stat. Mech., 2006*(12), P12015.
2. Alfè, D., Gillan, M.J., and Price, G.D. (2002). Composition and temperature of the Earth's core constrained by combining ab initio calculations and seismic data. *Earth Planet. Sci. Lett., 195*(1), 91–98.
3. Atwater, T. (1970). Implications of plate tectonics for the Cenozoic tectonic evolution of Western North America. *Geol. Soc. Am. Bull., 81*(12), 3513–3536. doi: 10.1130/0016-7606(1970)81[3513:IOPTFT]2.0.CO;2.
4. Bacon, F., and Montagu, B. (1848), *The works of Francis Bacon, Lord Chancellor of England: With a life of the author:* Parry & McMillan.
5. Benioff, H. (1949). Seismic evidence for the fault origin of oceanic deeps. *Geological Society of America Bulletin, 60*(12), 1837–1856., doi: 10.1130/0016-7606(1949)60[1837:SEFTFO]2.0.CO;2.
6. Birch, F. (1952). Elasticity and constitution of the Earth's interior. *J. Geophys. Res., 57*(2), 227–286. doi: 10.1029/ JZ057i002p00227.
7. Birch, F. (1964). Density and composition of mantle and core. *J. Geophys. Res., 69*(20), 4377–4388.
8. Bott, M.H.P. (1993). Modelling the plate-driving mechanism. *Journal of the Geological Society, 150*(5), 941–951. doi: 10.1144/ gsjgs.150.5.0941.
9. Coats, R.R. (1962). Magma type and crustal structure in the Aleutian Arc, in The crust of the Pacific Basin. *American Geophysical Union*, 92–109. doi: 10.1029/GM006p0092.
10. Conrad, C.P., and Lithgow-Bertelloni, C. (2002). How mantle slabs drive plate tectonics. *Science, 298*(5591), 207–209. doi: 10.1126/science.1074161.
11. Corliss, J.B., Dymond, J.G., Gordon, L.I., Edmond, J.M., von Heezen, R.P., Ballard, R.D., Green, K., Williams, D.L., Bain-bridge, A., Crane, K., and van Andel, T.H. (1979). Submarine thermal springs on the Galapagos Rift. *Science, 203,* 107321083.
12. Davis, E.E., and Lister, C.R.B. (1974). Fundamentals of ridge crest topography. *Earth Planet. Sci. Lett., 21*(4), 405–413.
13. Dawson, J.B., Pinkerton, H., Norton, G.E., and Pyle, D.M. (1990). Physicochemical properties of alkali carbonatite lavas: Data from the 1988 eruption of Oldoinyo Lengai, Tanzania. *Geology, 18*(3), 260–263.
14. Drake, E.T. (1976). Alfred Wegener's reconstruction of Pangea. *Geology, 4*(1), 41–44. doi: 10.1130/ 0091-7613(1976)4<41:AWROP>2.0.CO;2
15. Engdahl, E.R., Flynn, E.A., and Masse, R.P. (1974). Differential PkiKP travel times and the radius of the core. *Geophysical J Royal Astro Soc, 40*, 457–463.
16. Ewing, M., Ewing, J.I., and Talwani, M. (1964). Sediment distribution in the oceans: The Mid-Atlantic Ridge. *Geol. Soc. Am. Bull., 75*(1), 17–36. doi: 10.1130/0016-7606(1964)75[17:SDITOT]2.0.CO;2.
17. Ewing, M., Houtz, R., and Ewing, J. (1969). South Pacific sediment distribution. *J. Geophys. Res., 74*(10), 2477–2493. doi: 10.1029/ JB074i010p02477.
18. Fernandez, L.M., and Careaga, J. (1968). The thickness of the crust in Central United States and La Paz, Bolivia, from the spectrum of longitudinal seismic waves. *Bull. Seismol. Soc. Am., 58*(2), 711–741.
19. Fluegel, von H.W. (1980). Wegener-Ampferer-Schwinner. Ein Beitrag zur Geschichte der Geologie in Österreich. *Mitt. Oesterr. Geol. Ges., 73*, 237–254.
20. Forsyth, D.W. (1975). The early structural evolution and anisotropy of the oceanic upper mantle. *Geophys. J. Int., 43*(1), 103–162. doi: 10.1111/j.1365-246X.1975.tb00630.x.
21. Frankel, H. (1982). The development, reception, and acceptance of the Vine-Matthews-Morley hypothesis. *Hist. Stud. Phys. Biol. Sci., 13*(1), 1–39.
22. Fukao, Y., and Obayashi, M. (2013). Subducted slabs stagnant above, penetrating through, and trapped below the 660 km discontinuity. *J. Geophys. Res. [Solid Earth], 118*(11), 2013JB010466.
23. Hagstrum, J.T. (2005). Antipodal hotspots and bipolar catastrophes: Were oceanic large-body impacts the cause? *Earth Planet. Sci. Lett., 236*(1–2), 13–27.
24. Hanks, T.C., and Anderson, D.L. (1969). The early thermal history of the earth. *Phys. Earth Planet. Inter., 2*(1), 19–29.
25. Heezen, B.C., and Tharp, M. (1965). Tectonic fabric of the Atlantic and Indian Oceans and continental drift. *Philosophical Transactions of the Royal Society of London A: Mathematical, Physical and Engineering Sciences, 258*(1088), 90–106. doi: 10.1098/rsta.1965.0024.
26. Heller, P.L., Bowdler, S.S., Chambers, H.P., Coogan, J.C., Hagen, E.S., Shuster, M.W., Winslow, N.S., and Lawton, T.F. (1986). Time of initial thrusting in the Sevier orogenic belt, Idaho-Wyoming and Utah. *Geology, 14*(5), 388–391.
27. Herak, D., and Herak, M. (2007). Andrija Mohorovičić (1857-1936)—On the occasion of the 150th anniversary of his birth. *Seismol. Res. Lett., 78*(6), 671–674.
28. Hess, H.H. (1962). History of ocean basins. *Petrologic Studies, 4*, 599–620.

29. Hutson, P., Middleton, J., and Miller, D. (2003). Collision Zones. Online, http://www.geosci.usyd.edu.au/users/prey/ ACSGT/EReports/eR.2003/GroupD/Report1/web%20pages/contents.html, accessed June 2017.
30. Isacks, B., Oliver, J., and Sykes, L.R. (1968). Seismology and the new global tectonics. *J. Geophys. Res., 73*(18), 5855–5899.
31. Ito, E., and Takahashi, E. (1989). Postspinel transformations in the system Mg2SiO4-Fe2SiO4 and some geophysical implications. *J. Geophys. Res. [Solid Earth], 94*(B8), 10637–10646.
32. Jacoby, W.R. (1981). Modern concepts of Earth dynamics anticipated by Alfred Wegener in 1912. *Geology, 9*(1), 25–27. doi: 10.1130/ 0091-7613(1981)92.0.CO;2">10.1130/ 0091-7613(1981)9<25:MCOEDA>2.0.CO;2.
33. Jakosky, B.M., Grebowsky, J.M., Luhmann, J.G., Connerney, J., Eparvier, F., Ergun, R., Halekas, J., Larson, D., Mahaffy, P., McFadden, J., Mitchell, D.F., Schneider, N., Zurek, R., Bougher, S., et al. (2015). MAVEN observations of the response of Mars to an interplanetary coronal mass ejection. *Science, 350*(6261), aad0210.
34. James, D.E., Fouch, M.J., Carlson, R.W., and Roth, J.B. (2011). Slab fragmentation, edge flow and the origin of the Yellowstone hotspot track. *Earth Planet. Sci. Lett., 311*(1–2), 124–135.
35. Ji, Y., and Nataf, H.-C. (1998). Detection of mantle plumes in the lower mantle by diffraction tomography. *Earth Planet. Sci. Lett., 159*(3–4), 99–115.
36. Johnston, S.T., Jane Wynne, P., Francis, D., Hart, C.J.R., Enkin, R.J., and Engebretson, D.C. (1996). Yellowstone in Yukon: The Late Cretaceous Carmacks Group. *Geology, 24*(11), 997–1000.
37. Kearey, P., Klepeis, K.A., and Vine, F.J. (2009). *Global tectonics:* Wiley Blackwell.
38. Le Pichon, X. (1968). Sea-floor spreading and continental drift. *J. Geophys. Res., 73*(12), 3661–3697.
39. Lehmann, I. (1936). P'. *Bur. Centr. Seism. Internat. A*(14), 87–115.
40. Mantovani, R. (1889). Les fractures de l'écorce terrestre et la théorie de Laplace. *Bull. Soc. Sc. et Arts Réunion*, 41–53.
41. Mason, R.G. (1958). A magnetic survey off the west coast of the United States between latitudes 32-degrees-N and 36-degrees-N longitudes 121-degrees-W and 128-degrees-W. *Geophysical Journal of the Royal Astronomical Society, 1*(4), 320.
42. Mason, R.G., and Raff, A.D. (1961). Magnetic survey off the West Coast of North America, 32° N. latitude to 42° N. latitude. *Geological Society of America Bulletin, 72*(8), 1259–1265. doi: 10.1130/ 0016-7606(1961)72[1259:MSOTWC]2.0.CO;2.
43. McCollom, T.M. (1999). Methanogenesis as a potential source of chemical energy for primary biomass production by autotrophic organisms in hydrothermal systems on Europa. *J. Geophys. Res., 104*(E12), 30729–30742., doi: 10.1029/1999JE001126.
44. McKenzie, D.P., and Parker, R.L. (1967), The North Pacific: An example of tectonics on a sphere. *Nature, 216,* 1276–1280. doi: 10.1038/ 2161276a0.
45. Miller, A.R., Densmore, C.D., Degens, E.T., Hathaway, J.C., Manheim, F.T., McFarlin, P.F., Pocklington, R., and Jokela, A. (1966). Hot brines and recent iron deposits in deeps of the Red Sea. *Geochimica et Cosmochimica Acta, 30*(3), 341–359. doi: 10.1016/ 0016-7037(66)90007-X.
46. Morgan, W.J. (1968). Rises, trenches, great faults, and crustal blocks. *J. Geophys. Res., 73*(6), 1959–1982. doi: 10.1029/JB073i006p01959.
47. Mueller, S., and Phillips, R.J. (1991). On the initiation of subduction. *J. Geophys. Res. [Solid Earth], 96*(B1), 651–665.
48. Oldham, R.D. (1906). The constitution of the interior of the Earth, as revealed by earthquakes. *Q. J. Geol. Soc. London, 62*(1–4), 456–475.
49. Pasyanos, M.E. (2010). Lithospheric thickness modeled from long-period surface wave dispersion. *Tectonophysics, 481* (1–4), 38–50.
50. Powell, R.E., and Weldon, R.J. (1992) Evolution of the San Andreas fault. *Annu. Rev. Earth Planet. Sci., 20,* 431.
51. Raff, A.D., and Mason, R.G. (1961). Magnetic survey off the West Coast of North America, 40 N. latitude to 52 N. latitude. *Geological Society of America Bulletin, 72*(8), 1267–1270. doi: 10.1130/ 0016-7606(1961)72[1267:MSOTWC]2.0.CO;2.
52. Runcorn, S.K. (1965). Palaeomagnetic comparisons between Europe and North America. *Philosophical Transactions of the Royal Society of London A: Mathematical, Physical and Engineering Sciences, 258*(1088), 1–11.
53. Saito, T., Ewing, M., and Burckle, L.H. (1966). Tertiary sediment from the Mid-Atlantic ridge. *Science, 151*(3714), 1075–1079. doi: 10.1126/ science.151.3714.1075.
54. Satake, K., and Atwater, B.F. (2007). Long-term perspectives on giant earthquakes and tsunamis at subduction zones. *Annu. Rev. Earth Planet. Sci., 35*, 349–374.
55. Scheidegger, A.E. (1953). Examination of the physics of theories of orogenesis. *Geol. Soc. Am. Bull., 64*(2), 127–150. doi: 10.1130/ 0016-7606(1953)64[127:EOTPOT]2.0.CO;2.
56. Simpson, G.G. (1943). Mammals and the nature of continents. *Am. J. Sci., 241*(1), 1–31.
57. Starr, A.M. (2015). *Ambient resonance of rock arches:* University of Utah.
58. Stern, R.J. (1998). A subduction primer for instructors of introductory geology courses and authors of introductory-geology textbooks. *J. Geosci. Educ., 46,* 221.
59. Stern, R.J. (2004) Subduction initiation: spontaneous and induced. *Earth Planet. Sci. Lett., 226*(3–4), 275–292.
60. Stich, D., Mancilla, F. de L., Pondrelli, S., and Morales, J. (2007). Source analysis of the February 12th, 2007, Mw 6.0 Horseshoe earthquake: Implications for the 1755 Lisbon earthquake. *Geophys. Res. Lett., 34*(12), L12308.
61. Tatsumi, Y. (2005). The subduction factory: How it operates in the evolving Earth. *GSA Today, 15*(7), 4.
62. Todo, Y., Kitazato, H., Hashimoto, J., and Gooday, A.J. (2005). Simple foraminifera flourish at the ocean's deepest point. *Science, 307*(5710), 689. doi: 10.1126/science.1105407.
63. Tolstoy, I., and Ewing, M. (1949). North Atlantic hydrography and the Mid-Atlantic ridge. *Geol. Soc. Am. Bull., 60*(10), 1527–1540. doi: 10.1130/0016-7606(1949)60[1527:NAHATM]2.0.CO;2.
64. Vine, F.J., and Matthews, D.H. (1963). Magnetic anomalies over oceanic ridges. *Nature, 199*(4897), 947–949.
65. Wächtershäuser, G. (1990). Evolution of the first metabolic cycles. *Proc. Natl. Acad. Sci. U. S. A., 87*(1), 200–204.

66. Wadati, K. (1935). On the activity of deep-focus earthquakes in the Japan Islands and neighbourhoods. *Geophys. Mag., 8*(3–4), 305–325.
67. Waszek, L., Irving, J., and Deuss, A. (2011). Reconciling the hemispherical structure of Earth's inner core with its superrotation. *Nat. Geosci., 4*(4), 264–267. doi: 10.1038/ngeo1083.
68. Wegener, A. (1912). Die Entstehung der Kontinente. *Geol. Rundsch., 3*(4), 276–292. doi: 10.1007/BF02202896.
69. Wegener, A. (1920). Die entstehung der kontinente und ozeane. *Рипол Классик.*
70. Wells, H.G., Huxley, J., and Wells, G.P. (1931). The science of life. *Philosophy, 6*(24), 506–507.
71. White, I.C., and Moreira, C. (1908). *Commissão de estudos das minas de Carvão de Pedra do Brazil.*
72. de Wijs, G.A., Kresse, G., Vočadlo, L., Dobson, D., Alfè, D., Gillan, M.J., and Price, G.D. (1998). The viscosity of liquid iron at the physical conditions of the Earth's core. *Nature, 392*(6678), 805–807. doi: 10.1038/33905.
73. Wilson, J.T. (1966). Did the Atlantic close and then re-open? *Nature, 211,* 676–681.
74. Wilson, M. (1993). Plate-moving mechanisms: constraints and controversies. *Journal of the Geological Society, 150*(5), 923–926. doi: 10.1144/gsjgs.150.5.0923.
75. Wyllie, P.J. (1970) Ultramafic rocks and the upper mantle, in Morgan, B.A. (ed.) *Fiftieth anniversary symposia: Mineralogy and petrology of the Upper Mantle; Sulfides; Mineralogy and geochemistry of non-marine evaporites:* Mineralogical Society of America, 3–32.
76. Zhou, Z. (2004). The origin and early evolution of birds: Discoveries, disputes, and perspectives from fossil evidence. *Naturwissenschaften, 91*(10), 455–471.

Figure References

Figure 2.1: Detailed map of all known plates, their boundaries, and movements. Eric Gaba. 2006-10, updated 2015-09. CC BY-SA 2.5. https://commons.wikimedia.org/wiki/File:Tectonic_plates_boundaries_detailed-en.svg

Figure 2.2: Wegener later in his life, ca. 1924–1930. Author unknown. ca. 1924 and 1930. Public domain. https://commons.wikimedia.org/wiki/File:Alfred_Wegener_ca.1924-30.jpg

Figure 2.3: Snider-Pellegrini's map showing the continental fit and separation, 1858. Antonio Snider-Pellegrini. 1858. Public domain. https://commons.wikimedia.org/wiki/File:Antonio_Snider-Pellegrini_Opening_of_the_Atlantic.jpg

Figure 2.4: Map of world elevations. Tahaisik. 2013. CC BY-SA 3.0. https://commons.wikimedia.org/wiki/File:Tahacik.jpg

Figure 2.5: Image showing fossils that connect the continents of Gondwana (the southern continents of Pangea). Osvaldocangaspadilla. 2010. Public domain. https://commons.wikimedia.org/wiki/File:Snider-Pellegrini_Wegener_fossil_map.svg

Figure 2.6: Animation of the basic idea of convection: an uneven heat source in a fluid causes rising material next to the heat and sinking material far from the heat. Oni Lukos. 2006. CC BY-SA 3.0. https://commons.wikimedia.org/wiki/File:Convection.gif

Figure 2.7: GPS measurements of plate motions. NASA. Public domain. https://cddis.nasa.gov/docs/2009/HTS_0910.pdf

Figure 2.8: The complex chemistry around mid-ocean ridges. National Oceanic and Atmospheric Administration (NOAA). https://oceanexplorer.noaa.gov/explorations/04fire/background/chemistry/media/chemistry_600.html

Figure 2.9: The magnetic field of Earth, simplified as a bar magnet. Zureks. 2012. Public domain. https://commons.wikimedia.org/wiki/File:Earth%27s_magnetic_field,_schematic.png

Figure 2.10: This animation shows how the magnetic poles have moved over 400 years. United States Geological Survey (USGS). 2010. Public domain. https://commons.wikimedia.org/wiki/File:Earth_Magnetic_Field_Declination_from_1590_to_1990.gif

Figure 2.11: The iron in the solidifying rock preserves the current magnetic polarity as new oceanic plates form at mid-ocean ridges. USGS. 2011. Public domain. https://commons.wikimedia.org/wiki/File:Mid-ocean_ridge_topography.gif

Figure 2.12: The Wadati-Benioff zone, showing earthquakes following the subducting slab down. USGS. 2013. Public domain. https://commons.wikimedia.org/wiki/File:Benioff_zone_earthquake_focus.jpg

Figure 2.13: J. Tuzo Wilson. Stephen Morris. 1992. CC BY-SA 3.0. https://commons.wikimedia.org/wiki/File:John_Tuzo_Wilson_in_1992.jpg

Figure 2.14: The layers of the Earth. Drlauraguertin. 2015. CC BY-SA 3.0. https://wiki.seg.org/wiki/File:Earthlayers.png#file

Figure 2.15: The global map of the depth of the Moho. AllenMcC. 2013. CC BY-SA 3.0. https://commons.wikimedia.org/wiki/File:Mohomap.png

Figure 2.16: This mantle xenolith containing olivine (green) is chemically weathering by hydrolysis and oxidation into the pseudomineral iddingsite, which is a complex of water, clay, and iron oxides. Matt Affolter. 2010. CC BY-SA 3.0. https://commons.wikimedia.org/wiki/File:Iddingsite.JPG

Figure 2.17: A polished fragment of iron-rich Toluca meteorite with octahedral Widmanstätten pattern. H. Raab. 2005. CC BY-SA 3.0. https://commons.wikimedia.org/wiki/File:TolucaMeteorite.jpg

Figure 2.18: Map of the major plates and their motions along boundaries. Scott Nash via USGS. 1996. Public domain. https://commons.wikimedia.org/wiki/File:Plates_tect2_en.svg

Figure 2.19: The lithosphere–asthenosphere boundary changes with certain tectonic situations. Nealey Sims. 2015. CC BY-SA 3.0. https://commons.wikimedia.org/wiki/File:Earth%27s_Inner_Layers_denoting_the_LAB.png

Figure 2.20: General perovskite structure. Perovskite silicates (i.e., bridgmenite, (Mg,Fe)SiO3) are thought to be the main component of the lower mantle, making it the most common mineral in or on Earth. Cadmium. 2006. Public domain. https://en.wikipedia.org/wiki/File:Perovskite.jpg

Figure 2.21: Lehmann in 1932. Even Neuhaus. 1932. Public domain. https://commons.wikimedia.org/wiki/File:Inge_Lehman.jpg

Figure 2.22: The outer core's spin causes our protective magnetic field. NASA. 2017. Public domain. https://www.nasa.gov/mission_pages/sunearth/news/gallery/earths-dynamiccore.html

Figure 2.23: Passive margin. Joshua Doubek. 2013. CC BY-SA 3.0. https://commons.wikimedia.org/wiki/File:Passive_Contiental_Margin.jpg

Figure 2.24: Schematic of plate boundary types. NOAA via USGS. Public domain. https://oceanexplorer.noaa.gov/facts/plate-boundaries.html

Figure 2.25: Geologic provinces, with the shield (orange) and platform (pink) comprising the craton, the stable interior of continents. USGS. 2005. Public domain. https://commons.wikimedia.org/wiki/File:World_geologic_provinces.jpg

Figure 2.26: Diagram of ocean-continent subduction. K. D. Schroeder. 2016. CC-BY-SA 4.0. https://commons.wikimedia.org/wiki/File:Subduction-en.svg

Figure 2.27: Microcontinents can become part of the accretionary prism of a subduction zone. MagentaGreen. 2014. CC BY-SA 3.0. https://commons.wikimedia.org/wiki/File:Volcanic_Arc_System_SVG_en.svg

Figure 2.28: Accreted terranes of Western North America. Modified from illustration provided by *Oceanus Magazine*; original figure by Jack Cook, Woods Hole Oceanographic Institution; adapted by USGS. Used under fair use.

Figure 2.29: Location of the large (Mw 8.5-9.0) 1755 Lisbon earthquake. USGS. 2014. Public domain. https://commons.wikimedia.org/wiki/File:1755_Lisbon_Earthquake_Location.png

Figure 2.30: Earthquakes along the Sunda megathrust subduction zone along the island of Sumatra, showing the 2006 Mw 9.1-9.3 Indian Ocean earthquake as a star. USGS. 2007. Public domain. https://commons.wikimedia.org/wiki/File:SundaMegathrustSeismicity.PNG

Figure 2.31: Various parts of a subduction zone. USGS. 2006. Public domain. https://commons.wikimedia.org/wiki/File:Volcanic_Arc_System.png

Figure 2.32: Shallow subduction during the Laramide orogeny. Melanie Moreno. 2006. Public domain. https://commons.wikimedia.org/wiki/File:Shallow_subduction_Laramide_orogeny.png

Figure 2.33: Subduction of an oceanic plate beneath a continental plate, forming a trench and volcanic arc. USGS. 1999. Public domain. https://commons.wikimedia.org/wiki/File:Oceanic-continental_convergence_Fig21oceancont.gif

Figure 2.34: Subduction of an oceanic plate beneath another oceanic plate, forming a trench and an island arc. USGS. 2005. Public domain. https://commons.wikimedia.org/wiki/File:Oceanic-oceanic_convergence_Fig21oceanocean.gif

Figure 2.35: Two continental plates colliding. USGS. 2005. Public domain. https://commons.wikimedia.org/wiki/File:Continental-continental_convergence_Fig21contcont.gif

Figure 2.36: A reconstruction of Pangea, showing approximate positions of modern continents. Kieff. 2009. CC BY-SA 3.0. https://commons.wikimedia.org/wiki/File:Pangaea_continents.svg

Figure 2.37: The tectonics of the Zagros Mountains. Mikenorton. 2010. CC BY-SA 3.0. https://commons.wikimedia.org/wiki/File:Zagros-FTB.png

Figure 2.38: Pillow lavas, which only form under water, from an ophiolite in the Apennine Mountains of Central Italy. Matt Affolter (Qfl247). 2010. CC BY-SA 3.0. https://commons.wikimedia.org/wiki/File:ItalyPillowBasalt.jpg

Figure 2.39: Animation of India crashing into Asia. Raynaldi rji. 2015. CC BY-SA 4.0. https://en.wikipedia.org/wiki/File:India-Eurasia_collision.gif

Figure 2.40: Faulting that occurs in divergent boundaries. USGS; adapted by Gregors. 2011. Public domain. https://commons.wikimedia.org/wiki/File:Fault-Horst-Graben.svg

Figure 2.41: The Afar Triangle (center) has the Red Sea ridge (center to upper left), Gulf of Aden ridge (center to right), and East African Rift (center to lower left) form a triple junction that are about 120° apart. Koba-chan. 2005. CC BY-SA 3.0. https://commons.wikimedia.org/wiki/File:Topographic30deg_N0E30.png

Figure 2.42: NASA image of the Basin and Range horsts and grabens across central Nevada. NASA. 2005. Public domain. https://commons.wikimedia.org/wiki/File:Basin_range_province.jpg

Figure 2.43: India colliding into Eurasia to create the modern day Himalayas. USGS. 2007. Public domain. https://commons.wikimedia.org/wiki/File:Himalaya-formation.gif

Figure 2.44: Progression from rift to mid-ocean ridge. Hannes Grobe, Alfred Wegener Institute for Polar and Marine Research; adapted by Lichtspiel. 2011. CC BY-SA 2.5. https://commons.wikimedia.org/wiki/File:Ocean-birth.svg

Figure 2.45: Age of oceanic lithosphere, in millions of years. Muller, R.D., Sdrolias, M., Gaina, C., and Roest W.R. (2008). Age, spreading rates and spreading symmetry of the world's ocean crust. Geochem. Geophys. Geosyst, 9(Q04006). doi:10.1029/2007GC001743. CC BY-SA 3.0. https://commons.wikimedia.org/wiki/File:Age_of_oceanic_lithosphere.jpg

Figure 2.46: A time progression (with "a" being youngest and "c" being oldest) showing a spreading center getting wider while recording changes in the magnetic field of the Earth. Chmee2. 2012. Public domain. https://commons.wikimedia.org/wiki/File:Oceanic.Stripe.Magnetic.Anomalies.Scheme.svg

Figure 2.47: Black smoker hydrothermal vent with a colony of giant (6'+) tube worms. NOAA. 2006. Public domain. https://commons.wikimedia.org/wiki/File:Main_Endeavour_black_smoker.jpg

Figure 2.48: The two types of transform/strike-slip faults. Cferrero. 2003. CC BY-SA 3.0. https://commons.wikimedia.org/wiki/File:Strike_slip_fault.png

Figure 2.49: Map of the San Andreas fault showing relative motion. Kate Barton, David Howell, and Joe Vigil via USGS. 2006. Public domain. https://commons.wikimedia.org/wiki/File:Sanandreas.jpg

Figure 2.50: A transpressional strike-slip fault, causing uplift called a restraining bend. GeoAsh. 2015. CC BY-SA 4.0. https://commons.wikimedia.org/wiki/File:Restraining_Bend.png

Figure 2.51: A transtensional strike-slip fault, causing a restraining bend. In the center of the fault, a depression with extension would be found. K. Martin. 2013. CC BY-SA 3.0. https://commons.wikimedia.org/wiki/File:Releasing_bend.png

Figure 2.52: Wallace Creek (dry) on the Cariso Plain, California. Robert E. Wallace via USGS. 2014. Public domain. https://commons.wikimedia.org/wiki/File:Wallace_Creek_offset_across_the_San_Andreas_Fault.png

Figure 2.53: Diagram of the Wilson cycle, showing rifting and collision phases. Hannes Grobe. 2007. CC BY-SA 2.5. https://commons.wikimedia.org/wiki/File:Wilson-cycle_hg.png

Figure 2.54: Diagram showing a nonmoving source of magma (mantle plume) and a moving overriding plate. Los688. 2008. Public domain. https://commons.wikimedia.org/wiki/File:Hotspot(geology)-1.svg

Figure 2.55: Map of world hotspots. Foulger. 2011. Public domain. https://commons.wikimedia.org/wiki/File:CourtHotspots.png

Figure 2.56: The Hawaii–Emperor seamount and island chain. Ingo Wölbern. 2008. Public domain. https://commons.wikimedia.org/wiki/File:Hawaii-Emperor_engl.png

Figure 2.57: Diagram of the Hawaiian hotspot and islands that it formed. Joel E. Robinson via USGS. 2006. Public domain. https://commons.wikimedia.org/wiki/File:Hawaii_hotspot_cross-sectional_diagram.jpg

Figure 2.58: The track of the Yellowstone hotspot, which shows the age of different eruptions in millions of years ago. Kelvin Case. 2013. CC BY 3.0. https://commons.wikimedia.org/wiki/File:HotspotsSRP_update2013.JPG

Figure 2.59: Several prominent ash beds found in North America, including three Yellowstone eruptions shaded pink (Mesa Falls, Huckleberry Ridge, and Lava Creek), the Bisho Tuff ash bed (brown dashed line), and the modern May 18th, 1980, ash fall (yellow). USGS. 2005. Public domain. https://commons.wikimedia.org/wiki/File:Yellowstone_volcano_-_ash_beds.svg

Figure Descriptions

Figure 2.1: World map with Pacific Ocean centered in the middle. Numerous tectonic plates are color-coded by outline: lavender outlines convergent boundaries, red outlines divergent boundaries, green outlines transform boundaries, and blue with triangles outlines subduction zones. The cardinal direction of plate movements are shown by small black arrows that are labeled with a number in millimeters per year.

Figure 2.2: Black and white headshot of a man in a suit and tie.

Figure 2.3: Two black and white illustrations side-by-side: the left illustration shows the world globe with eastern South America and western Africa connected, labeled as "Avant la separation." The right illustration shows the world globe with South America and Africa separated by an ocean, labeled as "Apres la separation."

Figure 2.4: World map color-coded by elevation. The ocean basins are dark blue except for the mid-ocean ridges and ocean margins which are light blue. The continents are green at low elevations and red to brown at higher elevations.

Figure 2.5: Illustration showing five continents connected. From the left to right, there are South America, Africa, India above Antarctica, and Australia. Overlain on the continents are color-coded tracks of various fossil evidence: a tan band across South America and Africa shows the extent of fossil evidence for Cynognathus, a Triassic therapsid approximately 3 meters long. A gray band across southern Africa, India, and Antarctica shows the extent of fossil evidence for the Triassic therapsid Lystrosaurus. A green band across southern South America, southern Africa, India, Antarctica, and Australia (all of the southern continents) shows the extent of fossil evidence for the fern Glossopteris. A blue band across southern South America and southern Africa shows the extent of fossil evidence for the freshwater reptile Mesosaurus.

Figure 2.6: An animation showing two circles rotating next to each other. The left circle is rotating counterclockwise while the right circle is rotating clockwise. At the bottom center of the animation is an animated flame that represents a heat source from below.

Figure 2.7: World map that has many red dots in various places around the world. Each dot is connected to a black arrow of variable length that represents the plate motion measured at the dot in centimeters per year.

Figure 2.8: Diagram showing a cross section of a mid-ocean ridge underwater. Volcanic heat is coming out of the mid-ocean ridge which is drawn like a cloud. Inside the cloud are many different chemicals. There are also arrows going from the water into the ridge, labeled "seawater" where it enters the ground and labeled "evolved seawater" as it reaches the mid- ocean ridge axis. The arrows are also labeled with many different chemicals. Deeper below the ridge is a red oval shape labeled "Magma 1200 degrees C."

Figure 2.9: World globe with a dipole bar magnet superimposed on it, aligned roughly with Earth's axis of rotation. The north end of the magnet points toward the South Pole while the south end of the magnet points toward the North Pole. There are also black curved lines coming out of the Earth's axis, forming magnetic loops.

Figure 2.10: Animation of magnetic field lines superimposed on a world map. The lines move on the map as the animation goes from the year 1590 to 1990.

Figure 2.11: Animated gif depicting a mid-ocean ridge with two oceanic plates moving away from the center of the ridge. As the movement progresses, symmetrical magnetic stripes appear on each side of the ridge.

Figure 2.12: Cross section of an oceanic tectonic plate colliding with a continental tectonic plate. There's a diagonal zone of red X's that descend from the trench at the surface, labeled "Benioff Zone." Each X represents an earthquake focus.

Figure 2.13: Headshot of an older man wearing a suit and tie.

Figure 2.14: From core to surface: Inner core (solid), outer core (liquid), mantle (including asthenosphere), crust (including lithosphere)

Figure 2.15: World map with the Moho depth color coded on the map: red is the deepest while blue is the shallowest. The Moho is deepest under central Asia and western South America, and the Moho is shallowest under the world ocean basins.

Figure 2.16: Photograph of a piece of basalt with a xenolith on top, sitting on a black and white scale with inches on the left and centimeters on the right. The xenolith consists of olive-green crystals and the basalt is gray-black. The entire sample is approximately 1.5 inches long.

Figure 2.17: Photograph of a cut and polished face of a silvery gray meteorite. There is a distinct pattern of criss-crossing lines on the polished surface.

Figure 2.18: World map with the largest tectonic plates outlined and filled in with a different color for each plate: the Eurasian Plate is colored green, the North American Plate is gray, the Australian Plate is orange, the Filipino Plate is red, the Pacific Plate is yellow, the Juan de Fuca and Cocos Plates are blueish purple, the Nazca Plate is light blue, the Antarctic Plate is dark blue, the Scotia Plate is medium blue, the Caribbean plate is pinkish orange, the South American Plate is purple, the African Plate is dark orange, the Arabian Plate is yellow, and the Indian Plate is dark red.

Figure 2.19: From core to surface: Inner core, outer core, asthenosphere (part of ductile mantle), LAB, upper solid mantle, lithosphere, oceanic crust, continental crust. Mid ocean ridges form from the asthenosphere.

Figure 2.20: Array of atoms in a cubic three-dimensional framework of an imaginary perovskite. The red atoms are oxygen anions which are connected to the blue central atoms, which designate smaller cations. There are also green atoms organized in rows in the blank space which represent the larger cations.

Figure 2.21: Antique photo of young woman wearing a sweater.

Figure 2.22: Diagram of Earth as a globe with a pie-shaped piece cut out of the crust to act as a window to view the interior. The mantle is inside of the crust, the liquid outer core is inside of the mantle, and the solid inner core is inside the innermost part of the globe. The diagram also shows the solid inner core rotating in a counterclockwise direction as viewed from the North Pole. There are black lines extending from the inner core toward the North Pole and they are fanned out, each showing the yearly locations of the magnetic North Pole from 1990 to 1996.

Figure 2.23: Cross section of a passive margin under water. Continental crust is in pink on the left-hand side with a line labeled "Paleozoic DFW" pointing to the continental crust. Connected to the right of the continental crust is transitional crust in orange, and connected to that is oceanic crust in brown. A yellow wedge of passive margin sediments lays on top of the crust and a double-sided arrow is above the passive margin sediments that's labeled "Hinge Zone." An arrow points to the passive margin sediments that says "Thickest section of sediments are deposited adjacent to the continents, above the transitional crust, in the region that becomes the hinge zone. Can be up to 20 km thick."

Figure 2.24: 3D diagram showing a cross section into Earth's crust. On the left-hand side is a convergent plate boundary, with a plate of oceanic crust colliding into another plate of oceanic crust. The oceanic crust on the right-hand side subducts toward the left and a line of volcanoes forms on the overriding oceanic plate as a volcanic island arc. To the right of that, there is a shield volcano on the lithosphere beneath the ocean with a hot spot feeding the volcano from below. To the right of the shield volcano, there is a divergent plate boundary where two oceanic plates move away from each other. There is a transform plate boundary labeled to the left of the divergent boundary. To the right of the divergent boundary, oceanic crust moves toward the right, colliding with continental crust. The oceanic crust subducts beneath the continental crust, forming a chain of continental volcanoes on top of the continental crust. To the farthest right of the diagram, there is a continental rift zone where the continental crust is splitting apart.

Figure 2.25: World map with geologic provinces color-coded: Shield are colored orange and are seen on northern North America, eastern South America, northwestern Europe, northern and southern Asia, northwestern Australia, and sub-Saharan and southern Africa. Platform are colored pink and are seen near the same locations as shield with the exception of large platforms covering most of northern Asia and Europe. Orogen are colored cyan and are seen along western North America, western South America, the northwestern edge of Africa, southern Europe, southeastern Australia, and southern, central, and northeastern Asia. Basin are colored blue and are seen as thin strips in central-west North America, central-west South America, southern and northeastern Asia, and small spots in central and northwestern Africa. Large igneous province is colored purple and are seen as small blobs in western North America, eastern South America, Iceland, eastern Africa, central India, and northern Asia. Extended Crust are colored yellow and are seen on the margins of all of the continents.

Figure 2.26: 3D diagram showing oceanic crust moving toward the right where it collides with continental crust and subducts down beneath it. Above the contact between the two plates, there is an ocean trench and accretionary prism to the right of the trench. There is a volcanic arc on top of the continental plate, above where the oceanic crust has subducted beneath it. Rising diapirs are labeled below the volcanic arc. The Moho discontinuity is marked by a green line at the base of the crust in both tectonic plates, above the solid uppermost mantle.

Figure 2.27: Cross section schematic showing oceanic crust subducting beneath another tectonic plate. Above the contact between the two plates, there is an ocean trench and accretionary prism. There is a volcanic front on top of the overriding plate which makes up a microcontinent, above where the oceanic crust has subducted beneath it. Ascending diapirs are labeled below the volcanic front. There are ocean basins on either side of the microcontinent.

Figure 2.28: Color-coded tectonic map of western North America and the eastern Pacific Ocean, showing accreted terranes and plate tectonic motion. The color coding is as follows: continental interior of North America is tan, attached fragments of land are green, ancient ocean floor that accreted is blue, submarine deposits that accreted are yellow, and island arcs that accreted are pink.

Figure 2.29: Map of the western coast of Portugal, Spain, and Morocco, showing an east-west trending fault that goes through the Strait of Gibraltar. A red star labels the location of the epicenter of the 1755 earthquake, located just south of the fault line in the North Atlantic Ocean.

Figure 2.30: Color-coded tectonic map centered on the island of Sumatra with numerous dots showing the locations of earthquakes along a northwest- southeast-trending subduction zone. The color coding is as follows: shallow earthquakes are orange and yellow dots, and deep earthquakes are blue, purple, and red dots. Generally, shallow earthquakes are toward the southwest while deep earthquakes are toward the northeast. An orange star marks the location of the 2006 Indian Ocean earthquake.

Figure 2.31: Cross sectional diagram showing a mid-ocean ridge on the left-hand side. On the right-hand side is oceanic floor moving toward the left which subducts when it collides with the other oceanic crustal plate. Above the subduction zone in the center of the diagram, a volcanic front forms, which are volcanic islands on oceanic crust. At the top of the diagram are the following labels from left to right: ocean basin, backarc, volcanic front, forearc, ocean basin.

Figure 2.32: Block diagram showing oceanic crust moving toward the right where it collides with continental crust and subducts down beneath it. Because the angle of subduction is shallow, the ocean crust travels inland before creating a volcanic arc on top of the continental plate, above where the oceanic crust has subducted beneath it–these are the Rocky Mountains.

Figure 2.33: Block diagram showing oceanic crust moving toward the right where it collides with continental crust and subducts down beneath it. Above the contact between the two plates, there is an ocean trench. There is a volcanic arc on top of the continental plate, above where the oceanic crust has subducted beneath it.

Figure 2.34: Block diagram showing an oceanic plate moving toward the right where it collides with another oceanic plate and subducts down beneath it. Above the contact between the two plates, there is an ocean trench. There is a volcanic island arc on top of the overriding oceanic plate, above where the oceanic crust has subducted beneath it.

Figure 2.35: Block diagram showing a continental plate moving toward the right where it collides with another continental plate and collides with it. Above the contact between the two plates, there is a mountain range with a high plateau. There is no subduction or volcanism occurring.

Figure 2.36: Map of crescent-shaped Pangaea with all of the modern continents placed together: Eurasia is located at the top of the map, followed by North America to the lower left of Eurasia, South America below North America, Africa to the right of South America, India to the right of Africa, Antarctica below India and Africa, and Australia to the lower right of Antarctica and India.

Figure 2.37: Annotated satellite image of the Arabian Plate next to the Eurasian Plate with the Persian Gulf Basin and Mesopotamian Basin between the two plates. Tectonic faults run northwest-to-southeast on the image and are labeled and colored as follows: the Main Zagros Reverse Fault in yellow on the Eurasian Plate, the Main Recent Fault in orange on the Eurasian plate, and the High Zagros Fault in lavender on the Eurasian Plate.

Figure 2.38: An outcrop of medium-gray rocks that have bulbous texture which are old cooled pillow lavas.

Figure 2.39: Animation of India crashing into Asia. The animation begins at 60 million years ago, progressing every 5 million years until present day. Throughout the animation, the Indian plate travels toward the rest of the Asian plate until it begins colliding around 45 million years ago. After colliding, a collision zone between the Indian Plate and Asia Plate grows a mountain range which is the present-day Himalayas.

Figure 2.40: Block diagram showing flat-lying layers being pulled apart, forming normal faults throughout the diagram that allow some blocks to drop down called grabens between high blocks called horsts.

Figure 2.41: Topographic map showing the Afar Triangle, a low area bordering on the Red Sea. It is part of the Great Rift Valley in East Africa. The area overlaps the borders of Eritrea, Djibouti and the entire Afar region of Ethiopia. The connecting three arms form a triple junction. The northernmost branching arm extends north through the Red Sea and into the Dead Sea, while the eastern arm extends through the Gulf of Aden and connects to the Mid-Indian Ocean ridge further to the east. Both of these rifting arms are below sea level and are similar to a mid-ocean ridge. The third rifting arm runs south through the countries of Kenya, Uganda, the Democratic Republic of Congo, Rwanda, Burundi, Tanzania, Zambia, Malawi and Mozambique.

Figure 2.42: Satellite photo of a tan landscape that has long ridges and valleys.

Figure 2.43: Drawing of a map showing the northward path that the India land mass and Sri Lanka took from 71 million years ago to today. The path shows the India land mass moving closer and closer to the Eurasian plate until it collides. Sri Lanka is located just south of the India land mass and also travels in the same path, but has not collided with the Eurasian plate.

Figure 2.44: Three cross sectional diagrams showing the progression from a rift valley to a mid-ocean ridge. In the first diagram, the cross section shows a rift that's splitting apart a land mass with the analogy of the present-day African rift valley. In the second diagram, the cross section shows a new ocean basin after the rift has spread enough that sea water fills it in, with the analogy of the present-day Red Sea. In the third and final diagram, the cross section shows a mature ocean basin after the rift has spread so far that the spreading center has now become a mid-ocean ridge, with the analogy of the present-day Atlantic Ocean.

Figure 2.45: Color-coded world map that shows the various ages of oceanic lithosphere. Continents are in gray. The color-coding and locations are as follows: the youngest oceanic lithosphere is 0 million years old and runs along the centers of the ocean basins where there are mid-ocean ridges, colored in red. Oceanic lithosphere ages get older away from the mid- ocean ridges, and the oldest oceanic lithosphere is 280 million years old near continental margins, colored purple.

Figure 2.46: A series of 3 block diagrams showing a time progression of a spreading center getting wider and wider while the magnetic field of the Earth flips back and forth, being recorded in the currently-forming igneous rocks at the mid-ocean ridge.

Figure 2.47: A black smoker hydrothermal vent at the bottom of the sea floor. There is a plume of black smoke coming from a cone-shaped extrusion of rock and a colony of tube worms are attached to the cone-shaped rock.

Figure 2.48: Sinistral (left-lateral) strike-slip fault: top block moves left and overhangs bottom block that is moving right. Dextraal (right-lateral) strike-slip fault: top block moves right and overhangs bottom block that is moving left.

Figure 2.49: Map of western North America annotated with the location of the main San Andreas fault which runs from northwest of the Canadian coast, through western California, and southeast through Mexico. There are arrows on either side of the fault line showing relative movement: on the east side of the fault, movement is toward the lower right and on the west side of the fault, movement is toward the upper left.

Figure 2.50: Line drawing of an overhead view of a transpressional strike-slip fault. The fault has a bend in it, causing separation of the line with an uplift inside. The left-hand side of the drawing shows the plate moving to the upper left while the right-hand side of the drawing shows the plate moving to the lower right.

Figure 2.51: Line drawing of an overhead view of a transtensional strike-slip fault. The fault has a bend in it. The left-hand side of the drawing shows the plate moving to the upper left while the right-hand side of the drawing shows the plate moving to the lower right.

Figure 2.52: Aerial photo of a landscape in California. A dry creek flows from the northern mountainous part of the image, then takes a sharp right as viewed from the flow of water, then a sharp left, caused by the San Andreas Fault cutting roughly perpendicular to the creek. The fault can be seen about halfway down, trending left to right, as a change in the topography.

Figure 2.53: Rectangular diagram with a scale bar along the bottom labeled "million years." On the left end of the scale is the number 1,000 and on the right end is the number 0 (present day). Starting at the left-hand side, the following labels are on the diagram: "inner ocean" around 950 million years, "mountain forming" around 800 million years, "Rodinia" around 660 million years, "Iapetus Ocean" around 500 million years, "Mountain forming" around 300 million years, "Pangaea" around 180 million years, and "Atlantic Ocean" around 50 million years.

Figure 2.54: Two cross sectional diagrams: the top diagram shows horizontal layers with a magma plume rising vertically through them and a volcano on top of the layers. The second diagram shows horizontal layers with the top layer moving toward the left; a magma plume rises vertically through them and a chain of volcanoes is formed on the top layer which is moving toward the left as the magma plume creates volcanoes on top.

Figure 2.55: World map showing locations of hot spots with various sizes according to how active they are. The largest circles are located in the following places on the map: there are five large circles in the Pacific Ocean including Hawaii, there are two large circles in the Atlantic Ocean including Iceland, and there are two large circles in/near the Indian Ocean including the Afar Triangle. Smaller dots are scattered throughout the world ocean basins with some on continental interiors such as Yellowstone.

Figure 2.56: Map of the Hawaii-Emperor seamount chain and seafloor topography. The Aleutian trench and islands run approximately east-to-west along the top of the map, the Emperor seamount chain runs approximately north-to- south near the left-hand side of the map, and the Hawaiian seamount chain runs approximately west-northwest-to-east-southeast near the bottom of the map.

Figure 2.57: Cross sectional diagram showing the Pacific plate moving toward the left of the diagram with the labels "NW" at the far left and "SE" at the far right. At the right-hand side of the diagram, a vertical mantle plume rises up from deep down, through the asthenosphere, and spreads laterally outward when it reaches the base of the lithosphere. Smaller vertical magma intrusions rise through the lithosphere, creating three volcanoes labeled Mauna Loa, Kilauea, and Lo'ihi. Arrows on the lithosphere point toward the left, indicating the direction that the Pacific Plate is traveling over the mantle plume. Along the top of the diagram is the label "Volcanoes are progressively older" with arrows to the left. There is a chain of volcanic islands on top of the Pacific Plate: from left to right or oldest to youngest, they are Ni'hau and Kaua'i which are labeled 5.6-4.9 Ma, O'ahu labeled 3.4 Ma, Moloka'i labeled 1.8 Ma, Maui labeled 1.3 Ma, and Hawai'i labeled 0.7-0 Ma.

Figure 2.58: Shaded relief map centered on Idaho, with small portions of the surrounding states shown too. The track of a hot spot is annotated on the map and color-coded at each past location. The hotspot started near the Idaho-Oregon-Nevada border with the label 16.1 which indicates it was there 16.1 million years ago, then moved relatively east-northeastward toward its present location near the Wyoming-Idaho-Montana border which is labeled 0.6-2.1 which indicates it has been there 2.1 to 0.6 million years ago. Note that the North American plate was moving over the hot spot, not that the hot spot was moving under North America.

Figure 2.59: Map of the United States with state borders outlined. Prominent ash beds are outlined and color-coded, including three Yellowstone eruptions shaded pink. One of the pink outlines is labeled Mesa Falls ash bed and encircles most of the states of Wyoming, Colorado, Kansas, and Nebraska, and partially encircles the states Montana, South Dakota, Oklahoma, and Texas. Another pink outline is labeled Huckleberry Ridge ash bed and encircles the a large western portion of the United States. The third pink outline is labeled Lava Creek ash bed and encircles most of the western half of the United States. There is also a brown dashed outline labeled "Bishop ash bed"

which encircles the entire southwest portion of the United States. There is a yellow elongated outline labeled "Mount St. Helens ash 1980" which covers a east-west-trending portion of southern Washington state.

3. MINERALS

Learning Objectives

By the end of this chapter, students should be able to:

- Define mineral.
- Describe the basic structure of the atom.
- Derive basic atomic information from the periodic table of elements.
- Describe chemical bonding related to minerals.
- Describe the main ways minerals form.
- Describe the silicon-oxygen tetrahedron and how it forms common silicate minerals.
- List common nonsilicate minerals in oxide, sulfide, sulfate, and carbonate groups.
- Identify minerals using physical properties and identification tables.

The term "minerals" as used in nutrition labels and pharmaceutical products is not the same as a mineral in a geological sense. In geology, the classic definition of a **mineral** is: 1) naturally occurring, 2) inorganic, 3) solid at room temperature, 4) regular crystal structure, and 5) defined chemical composition. A naturally occurring substance that resembles a mineral but lacks a crystalline structure does not meet all the criteria to be classified as a mineral and is therefore referred to as a **mineraloid**. Common examples include coal, pearl, opal, and obsidian.

A rock is a substance that contains one or more minerals or mineraloids. As is discussed in later chapters, there are three types of rocks composed of minerals: igneous (rocks crystallizing from molten material), sedimentary (rocks composed of products of **mechanical weathering**, such as sand or gravel, and **chemical weathering**, i.e., precipitates from solution), and metamorphic (rocks produced by alteration of other rocks by heat and pressure).

3.1 Chemistry of Minerals

Rocks are composed of minerals that have a specific chemical composition. To understand mineral chemistry, it is essential to examine the fundamental unit of all matter, the atom.

3.1.1 The Atom

Video 3.1: Atomic orbitals

Access this YouTube video by scanning the QR code. ["Atomic orbitals – Periodic table" by Nicolae Sfetcu | https://www.youtube.com/watch?v=RF-1_JaND68]

Matter is made of atoms. Atoms consist of subatomic particles—protons, neutrons, and electrons. A simple model of the atom has a central nucleus composed of **protons**, which have positive charges, and **neutrons**, which have no charge. A cloud of negatively charged **electrons** surrounds the nucleus, with the number of electrons equaling the number of protons, thus balancing the positive charge of the protons for a neutral atom. Protons and neutrons each have a mass number of 1. The mass of an electron is less than 1/1000 that of a proton or neutron, meaning most of the atom's mass is in the nucleus.

3.1.2 Periodic Table of the Elements

Matter is composed of **elements**, which are atoms that have a specific number of protons in the nucleus. This number of protons is called the atomic number for the element. For example, an oxygen atom has eight protons, and an iron atom has 26 protons. An element cannot be broken down chemically into a simpler form and retains unique chemical and physical properties. Each element behaves in a unique manner in nature. This uniqueness led scientists to develop a periodic table of the elements, a tabular arrangement of all known elements listed in order of their atomic numbers.

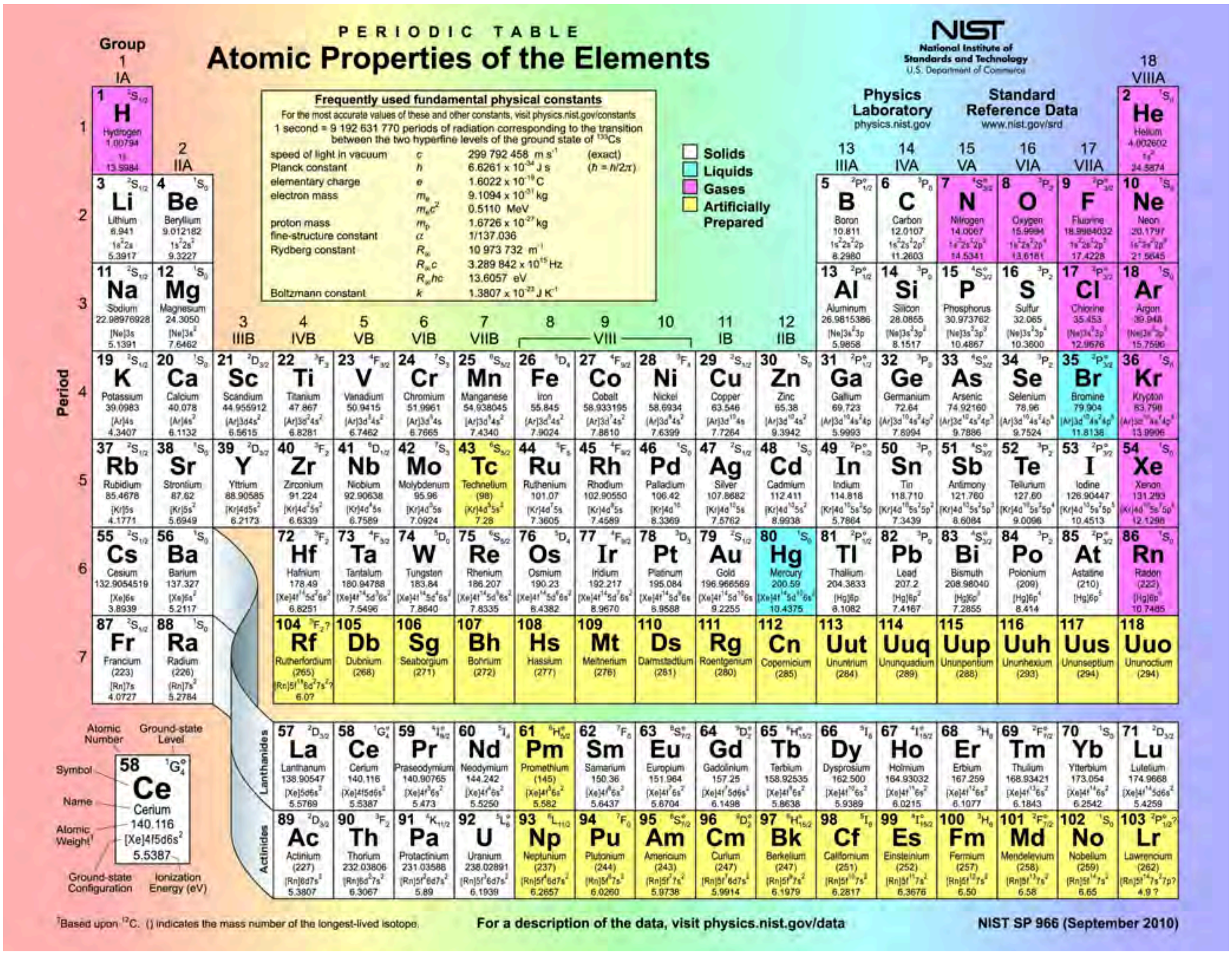

Figure 3.1: The periodic table of the elements. Figure description available at the end of the chapter.

The first arrangement of elements into a periodic table was done by Dmitri Mendeleev in 1869 using the elements known at the time. In the periodic table, each element has a chemical symbol, name, atomic number, and atomic mass. The chemical symbol is an abbreviation for the element, often derived from a Latin or Greek name for the substance. The atomic number is the number of protons in the nucleus. The atomic mass is the number of protons and neutrons in the nucleus, each with a mass number of 1. Since the mass of electrons is so much less than the protons and neutrons, the atomic mass is effectively the number of protons plus neutrons.

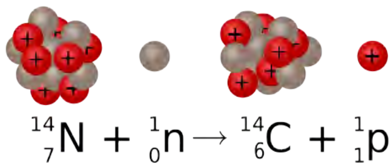

Figure 3.2: Formation of carbon-14 from nitrogen-14. Figure description available at the end of the chapter.

The atomic mass of natural elements represents an average mass of the atoms comprising that substance in nature and is usually not a whole number as seen on the periodic table; this means that, in nature, the element's atoms have different amounts of neutrons. The differing number of neutrons affects the mass of an element in nature, and the atomic mass number represents this average. This gives rise to the concept of isotope. **Isotopes** are forms of an element with the same number of protons but different numbers of neutrons. There are usually several isotopes for a particular element. For example, 98.9% of carbon atoms have six protons and six neutrons. This isotope of carbon is called carbon-12 (^{12}C). A few carbon atoms, carbon-13 (^{13}C), have six protons and seven neutrons. A trace amount of carbon atoms, carbon-14 (^{14}C), has six protons and eight neutrons.

Among the 118 known elements, the heaviest are fleeting human creations known only in high energy particle accelerators, and they decay rapidly. The heaviest naturally occurring element is uranium, atomic number 92. The eight most abundant elements in Earth's continental crust are shown in Table 1. These elements are found in the most common rock-forming minerals.

Element	Symbol	Abundance %
Oxygen	O	47%
Silicon	Si	28%
Aluminum	Al	8%
Iron	Fe	5%
Calcium	Ca	4%
Sodium	Na	3%
Potassium	K	3%
Magnesium	Mg	2%

Table 3.1: Eight most abundant elements in the Earths continental crust by weight. All other elements are less than 1. (Source USGS)

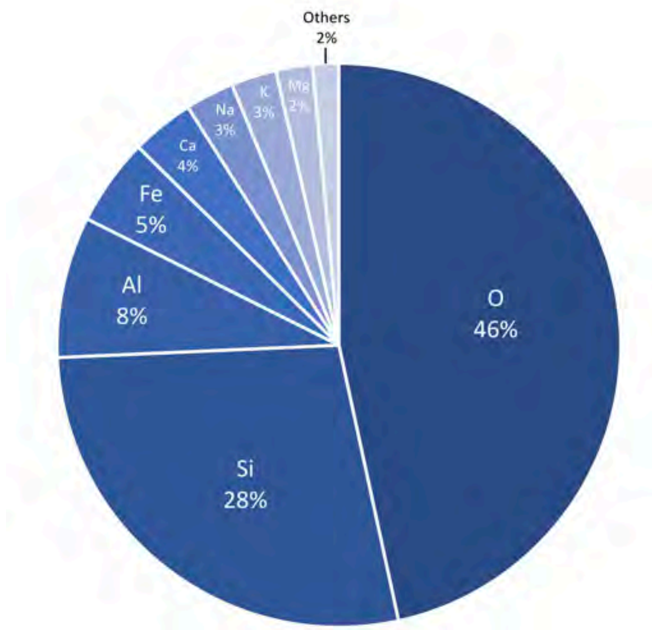

Figure 3.3: Element abundance pie chart for Earth's crust. Figure description available at the end of the chapter.

3.1.3 Chemical Bonding

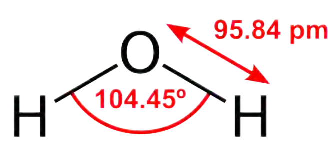

Figure 3.4: A model of a water molecule, showing the bonds between the hydrogen and oxygen. Figure description available at the end of the chapter.

Most substances on Earth are compounds containing multiple elements. Chemical bonding describes how these atoms attach with each other to form compounds, such as sodium and chlorine combining to form NaCl, common table salt. Compounds that are held together by chemical **bonds** are called molecules. Water is a compound of hydrogen and oxygen in which two hydrogen atoms are covalently bonded with one oxygen, making the water molecule. The oxygen we breathe is formed when one oxygen atom covalently bonds with another oxygen atom to make the molecule O_2. The subscript 2 in the chemical formula indicates the molecule contains two atoms of oxygen.

Most minerals are also compounds of more than one element. The common mineral **calcite** has the chemical formula $CaCO_3$, indicating the molecule consists of one calcium, one carbon, and three oxygen atoms. In calcite, one carbon and three oxygen atoms are held together by covalent bonds to form a molecular ion, called carbonate, which has a negative charge. Calcium as an ion has a positive charge of plus two. The two oppositely charged ions attract each other and combine to form the mineral calcite, $CaCO_3$. The name of the chemical compound is calcium carbonate, where calcium is Ca and carbonate refers to the molecular ion CO_3^{-2}.

The mineral **olivine** has the chemical formula $(Mg,Fe)_2SiO_4$, in which one silicon and four oxygen atoms are bonded with two atoms of either magnesium or iron. The comma between iron (Fe) and magnesium (Mg) indicates the two elements can occupy the same location in the crystal structure and substitute for one another.

Valence and Charge

The electrons around the atom's nucleus are located in shells representing different energy levels. The outermost shell is called the valence shell. Electrons in the valence shell are involved in chemical bonding. In 1913, Niels Bohr proposed a simple model of the atom that states atoms are more stable when their outermost shell is full. Atoms of most elements thus tend to gain or lose electrons so that the outermost shell is full. In Bohr's model, the innermost shell can have a maximum of two electrons and the second and third shells can have a maximum of eight electrons. When the innermost shell is the valence shell, as in the case of hydrogen and helium, it obeys the octet rule when it is full with two electrons. For elements in higher rows, the **octet rule** of eight electrons in the valence shell applies.

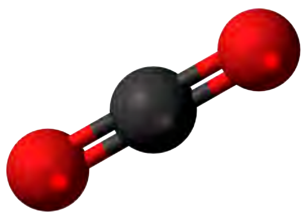

Figure 3.5: The carbon dioxide molecule. Since oxygen is -2 and carbon is +4, the two oxygens bond to the carbon to form a neutral molecule. Figure description available at the end of the chapter.

The rows in the periodic table present the elements in order of atomic number, and the columns organize elements with similar characteristics, such as the same number of electrons in their valence shells. Columns are often labeled from left to right with Roman numerals I to VIII and Arabic numerals 1 through 18. The elements in Columns I and II have one and two electrons in their respective valence shells, and the elements in Columns VI and VII have six and seven electrons in their respective valence shells.

In Row 3 and Column I, sodium (Na) has 11 protons in the nucleus and 11 electrons in three shells—two electrons in the inner shell, eight electrons in the second shell, and one electron in the valence shell. To maintain a full outer shell of eight electrons per the octet rule, sodium readily gives up that one electron so there are ten total electrons. With 11 positively charged protons in the nucleus and ten negatively charged electrons in two shells, sodium is an ion with an overall net charge of +1 when forming chemical bonds.

All elements in Column I have a single electron in their valence shell and a valence of one. These other Column I elements also readily give up this single valence electron and thus become ions with a +1 charge. Elements in Column II readily give up two electrons and end up as ions with a charge of +2. Note that elements in Columns I and II, which readily give up their valence electrons, often form bonds with elements in Columns VI and VII, which readily take up these electrons. Elements in Columns III through XV are usually involved in covalent bonding. Column XVIII (18)—the last column—contains the noble gases. These elements are chemically inert because the valence shell is already full with eight electrons, so they do not gain or lose electrons. An example is the noble gas helium, which has two valence electrons in the first shell. Its valence shell is therefore full. All elements in Column VIII possess full valence shells and do not form bonds with other elements.

As seen above, an atom with a net positive or negative charge as a result of gaining or losing electrons is called an **ion**. In general, the elements on the left side of the table lose electrons and become positive ions, which are called cations because they are attracted to the cathode in an electrical device. The elements on the right side tend to gain electrons. These are called **anions** because they are attracted to the anode in an electrical device. The elements in the center of the periodic table, Columns III through XV, do not consistently follow the octet rule. These are called transition elements. A common example is iron, which has a +2 or +3 charge depending on the oxidation state of the element. Oxidized Fe^{+3} carries a +3 charge and reduced Fe^{+2} is +2. These two different oxidation states of iron often impart dramatic colors to rocks containing their minerals—the oxidized form producing red colors and the reduced form producing green.

Ionic Bonding

Ionic bonds, also called electron-transfer bonds, are formed by the electrostatic attraction between atoms that have opposite charges. Atoms of two opposite charges attract each other electrostatically and form an ionic bond in which the positive ion transfers its electron (or electrons) to the negative ion. Through this transfer, both atoms thus achieve a full valence shell. For example, one atom of sodium (Na^{+1}) and one atom of chlorine (Cl^{-1}) form an ionic bond to make the compound sodium chloride (NaCl). This is also known as the mineral **halite**, or common table salt. Another example is calcium (Ca^{+2}) and chlorine (Cl^{-1}) combining to make the compound calcium chloride ($CaCl_2$). The subscript 2 indicates two atoms of chlorine are ionically bonded to one atom of calcium.

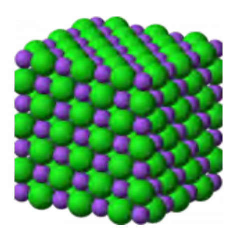

Figure 3.6: Cubic arrangement of sodium (purple) and chlorine (green) in halite. Figure description available at the end of the chapter.

Covalent Bonding

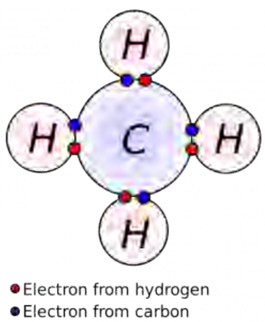

Figure 3.7: Methane molecule. Figure description available at the end of the chapter.

Ionic bonds are usually formed between a metal and a nonmetal. Another type, called a covalent or electron-sharing bond, commonly occurs between nonmetals. Covalent bonds share electrons between ions to complete their valence shells. For example, oxygen (atomic number 8) has eight electrons—two in the inner shell and six in the valence shell. Gases like oxygen often form diatomic molecules by sharing valence electrons. In the case of oxygen, two atoms attach to each other and share two electrons to fill their valence shells, becoming the common oxygen molecule we breathe (O_2). Methane (CH_4) is another covalently bonded gas. The carbon atom needs four electrons and each hydrogen needs one. Each hydrogen shares its electron with the carbon to form a molecule, as shown in the figure.

Take this quiz to check your comprehension of this section.

Access the quiz for Section 3.1 by scanning the QR code.

3.2 Formation of Minerals

Minerals form when atoms bond together in a crystalline arrangement. Three main ways this occurs in nature are: (1) precipitation directly from an aqueous (water) solution with a temperature change, (2) crystallization from a magma with a temperature change, and (3) biological precipitation by the action of organisms.

3.2.1 Precipitation from Aqueous Solution

Figure 3.8: Calcium carbonate deposits from hard water. Figure description available at the end of the chapter.

Solutions consist of ions or molecules, known as solutes, dissolved in a medium or solvent. In nature, this solvent is usually water. Many minerals can be dissolved in water, such as halite or table salt, in which the Na^{+1} and Cl^{-1} ions separate and disperse into the solution.

Precipitation is the reverse process, in which ions in solution come together to form solid minerals. Precipitation is dependent on the concentration of ions in solution and other factors such as temperature and pressure. The point at which a solvent cannot hold any more solute is called **saturation**. Precipitation can occur when the temperature of the solution falls, when the solute evaporates, or when chemical conditions change in a solution. An example of precipitation occurs in our homes when water evaporates and leaves behind a rind of minerals on faucets, shower heads, and drinking glasses.

In nature, changes in environmental conditions may cause the minerals dissolved in water to form bonds and grow into crystals or to cement grains of sediment together. In Utah, deposits of tufa formed from mineral-rich springs that emerged into Lake Bonneville in the last ice age. Now exposed in dry valleys, this porous tufa was a natural insulation used by pioneers to build their homes with a natural protection against summer heat and winter cold. The travertine **terraces** at Mammoth Hot Springs in Yellowstone Park are another example formed by calcite precipitation at the edges of the shallow **spring**-fed ponds.

Another example of precipitation occurs in the Great Salt Lake, Utah, where the concentration of sodium chloride and other salts is nearly eight times greater than in the world's oceans. **Streams** carry salt ions into the lake from the surrounding mountains. With no other outlet, the water in the lake evaporates and the concentration of salt increases until saturation is reached and the minerals precipitate out as sediments. Similar salt deposits include halite and other precipitates, occurring in other lakes like Mono Lake in California and the Dead Sea.

Figure 3.9: The salt flats of Badwater Basin in Death Valley National Park. Figure description available at the end of the chapter.

3.2.2 Crystallization From Magma

Heat is energy that causes atoms in substances to vibrate. Temperature is a measure of the intensity of the vibration. If the vibrations are violent enough, chemical bonds are broken and the crystals melt, releasing the ions into the melt. Magma is molten rock with freely moving ions. When magma is emplaced at depth or extruded onto the surface (then called lava), it starts to cool and mineral crystals can form.

Figure 3.10: Lava—magma at the Earth's surface. Figure description available at the end of the chapter.

3.2.3 Precipitation by Organisms

Figure 3.11: Ammonite shell made of calcium carbonate embedded in sedimentary rock. Figure description available at the end of the chapter.

Many organisms build bones, shells, and body coverings by extracting ions from water and precipitating minerals biologically. The most common mineral precipitated by organisms is calcite, or calcium carbonate ($CaCO_3$). Calcite is often precipitated by organisms as a polymorph called aragonite. **Polymorphs** are crystals with the same chemical formula but different crystal structures. Marine invertebrates such as corals and clams precipitate aragonite or calcite for their shells and structures. Upon death, their hard parts accumulate on the ocean floor as sediments and may eventually become the sedimentary rock **limestone**. Though limestone can form inorganically, the vast majority is formed by this biological process. Another example is marine organisms called radiolaria, which are zooplankton that precipitate silica for their microscopic external shells. When the organisms die, the shells accumulate on the ocean floor and can form the sedimentary rock **chert**. An example of biologic precipitation from the vertebrate world is bone, which is composed mostly of a type of apatite, a mineral in the phosphate group. The apatite found in bones contains calcium and water in its structure and is called hydroxycarbonate apatite, $Ca_5(PO_4)_3(OH)$. As mentioned above, such substances are not technically minerals until the organism dies and these hard parts become fossils.

Take this quiz to check your comprehension of this section.

Access the quiz for Section 3.2 by scanning the QR code.

3.3 Silicate Minerals

Minerals are categorized based on their composition and structure. Silicate minerals are built around a molecular ion called the silicon-oxygen tetrahedron. A tetrahedron has a pyramid-like shape with four sides and four corners. **Silicate** minerals form the largest group of minerals on Earth, comprising the vast majority of the Earth's mantle and crust. Of the nearly four thousand known minerals on Earth, most are rare. There are only a few that make up most of the rocks likely to be encountered by surface dwelling creatures like us. These are generally called the rock-forming minerals.

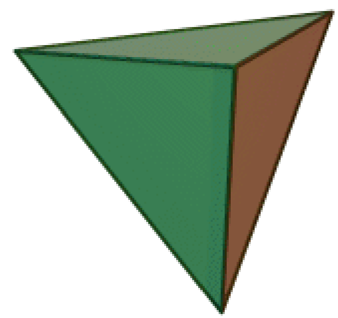

Figure 3.12: Rotating animation of a tetrahedra. Figure description available at the end of the chapter.

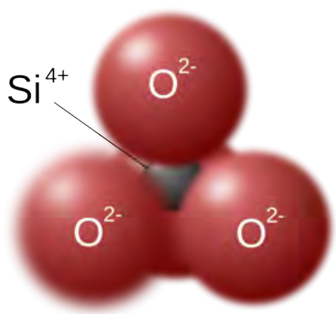

Figure 3.13: Silicate tetrahedron. Figure description available at the end of the chapter.

The **silicon-oxygen tetrahedron** (SiO_4) consists of a single silicon atom at the center and four oxygen atoms located at the four corners of the tetrahedron. Each oxygen ion has a -2 charge, and the silicon ion has a +4 charge. The silicon ion shares one of its four valence electrons with each of the four oxygen ions in a covalent bond to create a symmetrical, four-sided geometric pyramid figure. Only half of the oxygen's valence electrons are shared, giving the silicon-oxygen tetrahedron an ionic charge of -4. This silicon-oxygen tetrahedron forms bonds with many other combinations of ions to form the large group of silicate minerals.

The silicon ion is much smaller than the oxygen ions (see the figures) and fits into a small space in the center of the four large oxygen ions, visible if the top ball is removed (as shown in Figure 3.13). Because only one of the valence electrons of the corner oxygens is shared, the silicon-oxygen tetrahedron has chemically active corners available to form bonds with other silica tetrahedra or other positively charged ions such as Al^{+3}, $Fe^{+2,+3}$, Mg^{+2}, K^{+1}, Na^{+1}, and Ca^{+2}. Depending on many factors, such as the original magma chemistry, silica-oxygen tetrahedra can combine with other tetrahedra in several different configurations. For example, tetrahedra can be isolated, attached in chains, sheets, or three-dimensional structures. These combinations and others create the chemical structure in which positively charged ions can be inserted for unique chemical compositions, forming silicate mineral groups.

3.3.1 The Dark Ferromagnesian Silicates

Olivine Family

Olivine is the primary mineral component in mantle rock such as peridotite and basalt. It is characteristically green when not weathered. The chemical formula is $(Fe,Mg)_2SiO_4$. As previously described, the comma between iron (Fe) and magnesium (Mg) indicates these two elements occur in a solid solution. Unlike a liquid solution, a **solid solution** occurs when two or more elements have similar properties and can freely substitute for each other in the same location in the crystal structure.

Figure 3.14: Olivine crystals in basalt. Figure description available at the end of the chapter.

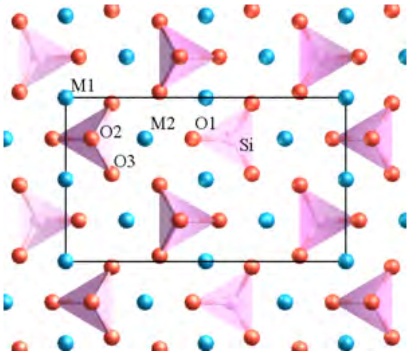

Figure 3.15: Tetrahedral structure of olivine. Figure description available at the end of the chapter.

Olivine is referred to as a mineral family because iron and magnesium have the ability to substitute for each other. Iron and magnesium in the olivine family indicates a solid solution forming a compositional series within the mineral group, which can form crystals of all iron as one endmember, all mixtures of iron and magnesium in between, and all magnesium as the other endmember. Different mineral names are applied to compositions between these end members. In the olivine series of minerals, the iron and magnesium ions in the solid solution are about the same size and charge, so either atom can fit into the same location in the growing crystals. Within the cooling magma, the mineral crystals continue to grow until they solidify into igneous rock. The relative amounts of iron and magnesium in the parent magma determine which minerals in the series form. Other rarer elements with properties similar to iron or magnesium, like manganese (Mn), can substitute into the olivine crystalline structure in small amounts. Such ionic substitutions in mineral crystals give rise to the great variety of minerals and are often responsible for differences in color and other properties within a group or family of minerals. Olivine has a pure iron endmember (called fayalite) and a pure magnesium endmember (called forsterite). Chemically, olivine is mostly silica, iron, and magnesium and therefore is grouped among the dark-colored ferromagnesian (iron = *ferro-*, magnesium = *magnesian*) or mafic minerals, a contraction of their chemical symbols Ma and Fe. Ferromagnesian silicates tend to be more dense than nonferromagnesian silicates. This difference in density ends up being important in controlling the behavior of the igneous rocks that are built from these minerals; whether a tectonic plate subducts or not is largely governed by the density of its rocks, which are in turn controlled by the density of the minerals that comprise them.

The crystal structure of olivine is built from independent silica tetrahedra. Minerals with independent tetrahedral structures are called neosilicates (or orthosilicates). In addition to olivine, other common neosilicate minerals include garnet, topaz, kyanite, and zircon.

Two other similar arrangements of tetrahedra are close in structure to the neosilicates and grade toward the next group of minerals, the pyroxenes. In a variation on independent tetrahedra called sorosilicates, there are minerals that share one oxygen between two tetrahedra, such as the pistachio-green epidote, a gemstone. Another variation are the cyclosilicates, which as the name suggests, consist of tetrahedral rings and include gemstones such as beryl, emerald, aquamarine, and tourmaline.

Pyroxene Family

Pyroxene is another family of dark ferromagnesian minerals, typically black or dark green in color. Members of the pyroxene family have a complex chemical composition that includes iron, magnesium, aluminum, and other elements bonded to polymerized silica tetrahedra. Polymers are chains, sheets, or three-dimensional structures and are formed by multiple tetrahedra covalently bonded via their corner oxygen atoms. Pyroxenes are commonly found in mafic igneous rocks such as peridotite, basalt, and **gabbro**, as well as metamorphic rocks like **eclogite** and blue schist.

Figure 3.16: Crystals of diopside, a member of the pyroxene family. Figure description available at the end of the chapter.

Pyroxenes are built from long, single chains of polymerized silica tetrahedra in which tetrahedra share two corner oxygens. The silica chains are bonded together into crystal structures by metal cations. A common member of the pyroxene family is augite, itself containing several solid solution series with a complex chemical formula—$(Ca,Na)(Mg,Fe,Al,Ti)(Si,Al)_2O_6$—that gives rise to a number of individual mineral names.

This single-chain crystalline structure bonds with many elements that can also freely substitute for each other. The generalized chemical composition for pyroxene is $XZ(Al,Si)_2O_6$. X represents the ions Na, Ca, Mg, or Fe, and Z represents Mg, Fe, or Al. These ions have similar ionic sizes, which allows many possible substitutions among them. Although the cations may freely substitute for each other in the crystal, they carry different ionic charges that must be balanced out in the final crystalline structure. For example, Na has a charge of +1, but Ca has charge of +2. If a Na^+ ion substitutes for a Ca^{+2} ion, it creates an unequal charge that must be balanced by other ionic substitutions elsewhere in the crystal. Note that ionic size is more important than ionic charge for substitutions to occur in solid solution series in crystals.

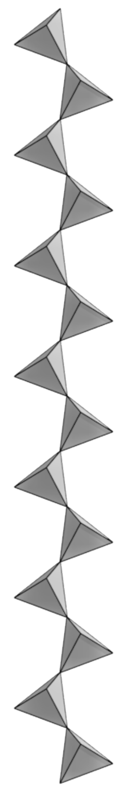

Figure 3.17: Single-chain tetrahedral structure in pyroxene. Figure description available at the end of the chapter.

Amphibole Family

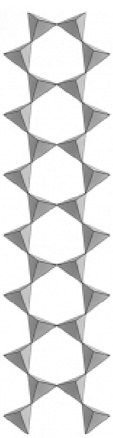

Figure 3.20: Double-chain structure. Figure description available at the end of the chapter.

Figure 3.18: Elongated crystals of hornblende in orthoclase. Figure description available at the end of the chapter.

Amphibole minerals are built from polymerized double silica chains, and they are also referred to as inosilicates. Imagine two pyroxene chains that connect together by sharing a third oxygen on each tetrahedra. Amphiboles are usually found in igneous and metamorphic rocks and typically have a long-bladed **crystal habit**. The most common amphibole, hornblende, is usually black; however, it can come in a variety of colors depending on its chemical composition. The metamorphic rock amphibolite is primarily composed of amphibole minerals.

Figure 3.19: Hornblende crystals. Figure description available at the end of the chapter.

Amphiboles are composed of iron, magnesium, aluminum, and other cations bonded with silica tetrahedra. These dark ferromagnesian minerals are commonly found in gabbro, baslt, diorite, and often form the black specks in granite. Their chemical formula is very complex and generally written as $(RSi_4O_{11})_2$, where R represents many different cations. For example, it can also be written more exactly as $AX_2Z_5((Si,Al,Ti)_8O_{22})(OH,F,Cl,O)_2$. In this formula, A may be Ca, Na, K, Pb, or nothing; X equals Li, Na, Mg, Fe, Mn, or Ca; and Z is Li, Na, Mg, Fe, Mn, Zn, Co, Ni, Al, Cr, Mn, V, Ti, or Zr. The substitutions create a wide variety of colors such as green, black, colorless, white, yellow, blue, or brown. Amphibole crystals can also include hydroxide ions (OH^-), which occur from an interaction between the growing minerals and water dissolved in magma.

3.3.2 Sheet Silicates

Figure 3.21: Sheet crystals of biotite mica. Figure description available at the end of the chapter.

Sheet silicates are built from tetrahedra that share all three of their bottom corner oxygens thus forming sheets of tetrahedra with their top corners available for bonding with other atoms. Micas and clays are common types of sheet silicates, also known as phyllosilicates. **Mica** minerals are usually found in igneous and metamorphic rocks, while clay minerals are more often found in sedimentary rocks. Two frequently found micas are dark-colored biotite, frequently found in granite, and light-colored muscovite, found in the metamorphic rock called **schist**.

Figure 3.22: Crystal of muscovite mica. Figure description available at the end of the chapter.

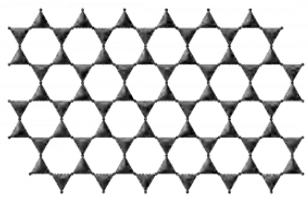

Figure 3.23: Sheet structure of mica. Figure description available at the end of the chapter.

Chemically, sheet silicates usually contain silicon and oxygen in a 2:5 ratio (Si_4O_{10}). Micas contain mostly silica, aluminum, and potassium. Biotite mica has more iron and magnesium and is considered a ferromagnesian silicate mineral. Muscovite micas belong to the **felsic** silicate minerals. Felsic is a contraction of **feldspar**, the dominant mineral in felsic rocks.

The illustration of the crystalline structure of mica shows the corner O atoms bonded with K, Al, Mg, Fe, and Si atoms, forming polymerized sheets of linked tetrahedra, with an octahedral layer of Fe, Mg, or Al between them. The yellow potassium ions form Van der Waals bonds (attraction and repulsion between atoms, molecules, and surfaces) and hold the sheets together. Van der Waals bonds differ from covalent and ionic bonds; they exist between the sandwiches, holding them together as a stack of sandwiches. The Van der Waals bonds are weak compared to the bonds within the sheets, allowing the sandwiches to be separated along the potassium layers. This gives mica its characteristic property of easily cleaving into sheets.

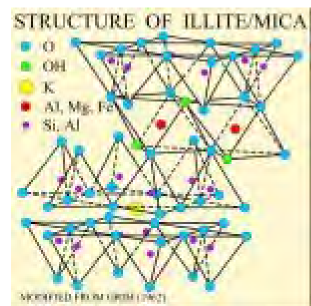

Figure 3.24: Crystal structure of a mica. Figure description available at the end of the chapter.

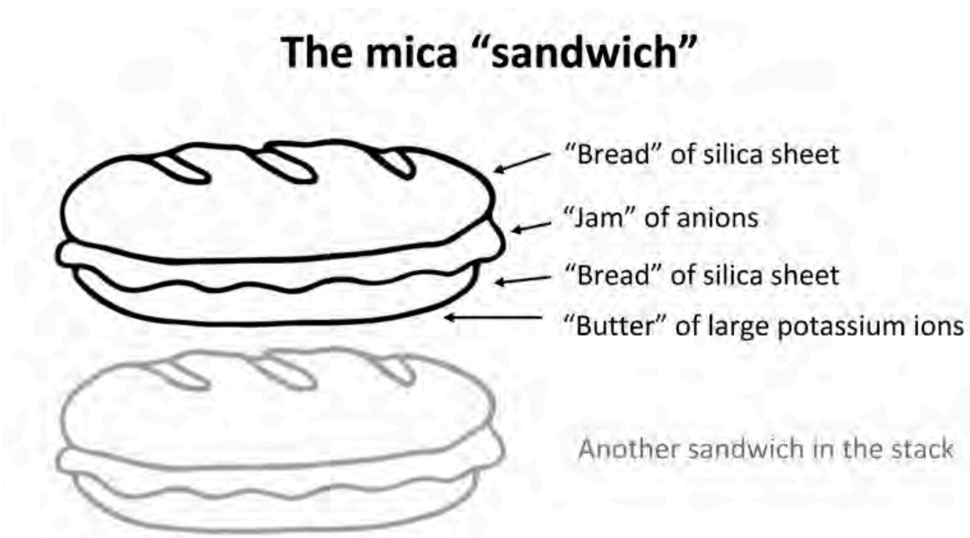

Figure 3.25: Mica "silica sandwich" structure. In this analogy, you may start with one "sandwich," where the top bun is a silica sheet, a "jam" of anions is the sandwich filling, and the bottom bun is another silica sheet. If you were to then place this sandwich on top of an existing sandwich, you could use butter to hold the two sandwiches together. This butter would be the large potassium ions forming Van der Waals bonds that hold the two sandwiches' bottom and top buns (silica sheets) together. Figure description available at the end of the chapter.

Clays minerals occur in sediments formed by the weathering of rocks and are another family of silicate minerals with a tetrahedral sheet structure. Clay minerals form a complex family and are an important component of many sedimentary rocks. Other sheet silicates include serpentine and chlorite, which are found in metamorphic rocks.

Clay minerals are composed of hydrous aluminum silicates. One type of clay, kaolinite, has a structure like an open-faced sandwich, with the bread being a single layer of silicon-oxygen tetrahedra and a layer of aluminum as the spread in an octahedral configuration with the sheets' top oxygens.

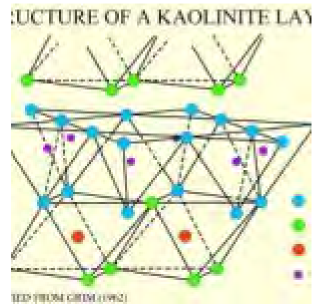

Figure 3.26: Structure of kaolinite. Figure description available at the end of the chapter.

3.3.3 Framework Silicates

Figure 3.27: Freely growing quartz crystals showing crystal faces. Figure description available at the end of the chapter.

Quartz and **feldspar** are the two most abundant minerals in the continental crust. In fact, feldspar itself is the single most abundant mineral in the Earth's crust. There are two types of feldspar—one containing potassium and abundant in felsic rocks of the continental crust, and the other with sodium and calcium abundant in the mafic rocks of oceanic crust. Together with quartz, these minerals are classified as framework silicates. They are built with a three-dimensional framework of silica tetrahedra in which all four corner oxygens are shared with adjacent tetrahedra. Within these frameworks in feldspar are holes and spaces into which other ions like aluminum, potassium, sodium, and calcium can fit, giving rise to a variety of mineral compositions and mineral names.

Feldspars are usually found in igneous rocks, such as granite, rhyolite, and basalt, as well as metamorphic rocks and detrital sedimentary rocks. **Detrital** sedimentary rocks are composed of mechanically weathered rock particles, like sand and gravel. Quartz is especially abundant in detrital sedimentary rocks because it is very resistant to disintegration by weathering. While quartz is the most abundant mineral on the Earth's surface due to its durability, feldspar minerals are the most abundant minerals in the Earth's crust, comprising roughly 50% of the total minerals that make up the crust.

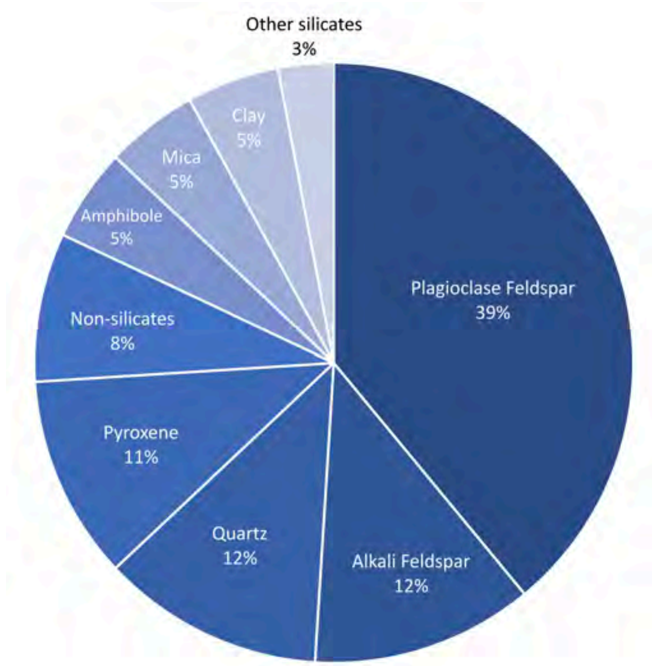

Figure 3.28: Mineral abundance pie chart in Earth's crust. Figure description available at the end of the chapter.

Figure 3.29: Pink orthoclase crystals. Figure description available at the end of the chapter.

Quartz is composed of pure silica, SiO_2, with the tetrahedra arranged in a three-dimensional framework. Impurities consisting of atoms within this framework give rise to many varieties of quartz, among which are gemstones like amethyst, rose quartz, and citrine. Feldspars are mostly silica with aluminum, potassium, sodium, and calcium. Orthoclase feldspar ($KAlSi_3O_8$), also called potassium feldspar or K-spar, is made of silica, aluminum, and potassium. Quartz and orthoclase feldspar are felsic minerals. **Felsic** is the compositional term applied to continental igneous minerals and rocks that contain an abundance of silica. Another feldspar is plagioclase, with the formula $(Ca,Na)AlSi_3O_8$). The solid solution (Ca,Na) indicates a series of minerals, with one end of the series with calcium ($CaAl_2Si_2O_8$), called anorthite, and the other end with sodium $NaAlSi_3O_8$, called albite. Note how the mineral accommodates the substitution of Ca^{++} and Na^{+}. Minerals in this solid solution series have different mineral names.

Aluminum, which has a similar ionic size to silicon, can substitute for silicon inside the tetrahedra. Because potassium ions are so much larger than sodium and calcium ions, which are very similar in size, the inability of the crystal lattice to accommodate both potassium and sodium/calcium gives rise to the two families of feldspar, orthoclase and plagioclase, respectively. Framework silicates are called tectosilicates and include the alkali metal-rich feldspathoids and zeolites.

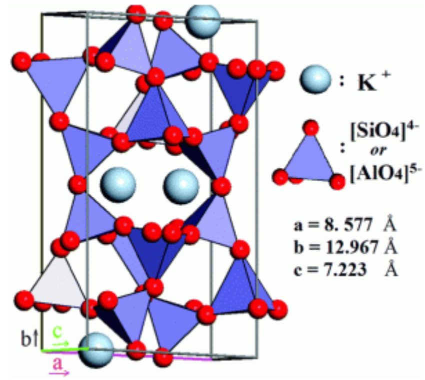

Figure 3.30: Crystal structure of feldspar. Figure description available at the end of the chapter.

Take this quiz to check your comprehension of this section.

Access the quiz for Section 3.3 by scanning the QR code.

3.4 Nonsilicate Minerals

The crystal structure of nonsilicate minerals (see table) does not contain silica-oxygen tetrahedra. Many nonsilicate minerals are economically important and provide **metallic** resources such as copper, lead, and iron. They also include valuable nonmetallic products such as salt, construction materials, and fertilizer.

Figure 3.31: Hanksite, $Na_{22}K(SO_4)_9(CO_3)_2Cl$, one of the few minerals that is considered a carbonate and a sulfate. Figure description available at the end of the chapter.

Mineral group	Examples	Formula	Uses
Native elements	Gold, silver, copper	Au, Ag, Cu	Jewelry, coins, industry
Carbonates	Calcite, dolomite	$CaCO_3$, $CaMg(CO_3)_2$	Lime, Portland cement
Oxides	Hematite, magnetite, bauxite	Fe_2O_3, Fe_3O_4, a mixture of aluminum oxides	Ores of iron & aluminum, pigments
Halides	Halite, sylvite	NaCl, KCl	Table salt, fertilizer
Sulfides	Galena, chalcopyrite, cinnabar	PbS, $CuFeS_2$, HgS	Ores of lead, copper, mercury
Sulphates	Gypsum, epsom salts	$CaSo_4 \cdot 2H_2O$, $MgSO_4 \cdot 7H_2O$	Sheetrock, therapeutic soak
Phosphates	Apatite	$Ca_5(PO_4)_3$(F,Cl,OH)	Fertilizer, teeth, bones

Table 3.2: Common nonsilicate mineral groups.

3.4.1 Carbonates

Figure 3.32: Calcite crystal in shape of rhomb. Note the double-refracted word "Calcite" in the center of the figure due to birefringence. Figure description available at the end of the chapter.

Calcite ($CaCO_3$) and dolomite ($CaMg(CO_3)_2$) are the two most frequently occurring carbonate minerals and usually occur in sedimentary rocks, such as limestone and dolostone rocks, respectively. Some carbonate rocks, such as calcite and dolomite, are formed via evaporation and precipitation. However, most carbonate-rich rocks, such as limestone, are created by the lithification of fossilized marine organisms. These organisms, ranging from microscopic to larger, more visible organisms, have shells or exoskeletons consisting of calcium carbonate ($CaCO_3$). When these organisms die, their remains accumulate on the floor of the water body in which they live, and the soft body parts decompose and dissolve away. The calcium carbonate hard parts become included in the sediments, eventually becoming the sedimentary rock called limestone. While limestone may contain large, easy-to-see fossils, most limestones contain the remains of microscopic creatures and originate from biological processes.

Figure 3.33: Limestone with small fossils. Figure description available at the end of the chapter.

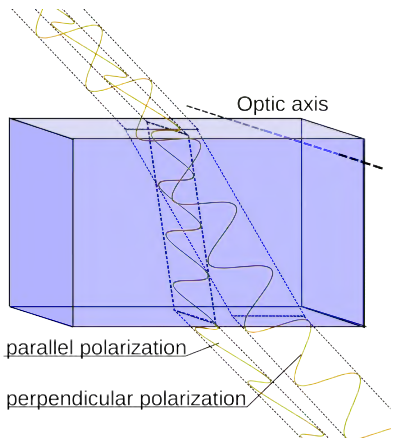

Figure 3.34: Bifringence in calcite crystals. Figure description available at the end of the chapter.

Calcite crystals show an interesting property called birefringence, meaning they polarize light into two wave components vibrating at right angles to each other. As the two light waves pass through the crystal, they travel at different velocities and are separated by refraction into two different travel paths. In other words, the crystal produces a double image of objects viewed through it. Because they polarize light, calcite crystals are used in special petrographic microscopes for studying minerals and rocks.

Many nonsilicate minerals are referred to as salts. The term salts here refers to compounds made by replacing the hydrogen in natural acids. The most abundant natural acid is **carbonic acid** that forms by the solution of carbon dioxide in water. Carbonate minerals are salts built around the carbonate ion (CO_3^{-2}) where calcium and/or magnesium replace the hydrogen in carbonic acid (H_2CO_3). Calcite and a closely related polymorph aragonite are secreted by organisms to form shells and physical structures like corals. Many such creatures draw both calcium and carbonate from dissolved bicarbonate ions (HCO_3^-) in ocean water. As seen in the mineral identification section below, calcite is easily dissolved in acid and thus effervesces in dilute hydrochloric acid (HCl). Small dropper bottles of dilute hydrochloric acid are often carried by geologists in the field are are also commonly used in mineral identification labs.

Other salts include halite (NaCl), in which sodium replaces the hydrogen in hydrochloric acid, and gypsum ($Ca[SO_4] \cdot 2H_2O$), in which calcium replaces the hydrogen in sulfuric acid. Note that some water molecules are also included in the gypsum crystal. Salts are often formed by evaporation and are called **evaporite** minerals.

The figure shows the crystal structure of calcite ($CaCO_3$). Like silicon, carbon has four valence electrons. The carbonate unit consists of carbon atoms (tiny white dots) covalently bonded to three oxygen atoms (red), with one oxygen sharing two valence electrons with the carbon and the other two sharing one valence electron each with the carbon, thus creating triangular units with a charge of -2. The negatively charged carbonate unit forms an ionic bond with the Ca ion (blue), which has a charge of +2.

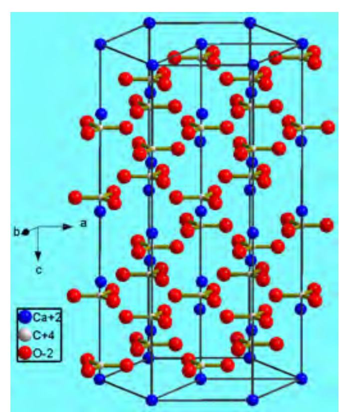

Figure 3.35: Crystal structure of calcite. Figure description available at the end of the chapter.

3.4.2 Oxides, Halides, and Sulfides

Figure 3.36: Limonite, a hydrated oxide of iron. Figure description available at the end of the chapter.

After carbonates, the next most common nonsilicate minerals are the oxides, halides, and sulfides.

Oxides consist of metal ions covalently bonded with oxygen. The most familiar oxide is rust, which is a combination of iron oxides (Fe_2O_3) and hydrated oxides. Hydrated oxides form when iron is exposed to oxygen and water. Iron oxides are important for producing metallic iron. When iron oxide or ore is smelted, it produces carbon dioxide (CO_2) and metallic iron.

When the color red appears in rocks, it is usually due to the presence of iron oxides. For example, the red sandstone cliffs in Zion National Park and throughout Southern Utah consist of white or colorless grains of quartz coated with iron oxide, which serve as cementing agents that hold the grains together.

Other iron oxides include limonite, magnetite, and hematite. Hematite occurs in many different crystal forms. The **massive** form shows no external structure. Botryoidal hematite shows large concentric blobs. Specular hematite looks like a mass of shiny metallic crystals. Oolitic hematite looks like a mass of dull-red fish eggs. These different forms of hematite are polymorphs and all have the same formula, Fe_2O_3.

Figure 3.37: Oolitic hematite. Figure description available at the end of the chapter.

Other common oxide minerals include:

- ice (H_2O), an oxide of hydrogen
- **bauxite** ($Al_2H_2O_4$), an ore for producing metallic aluminum, made up of hydrated oxides of aluminum
- corundum (Al_2O_3), which includes ruby and sapphire gemstones

Figure 3.38: Halite crystal showing cubic habit. Figure description available at the end of the chapter.

The **halides** consist of halogens in Column VII, usually fluorine or chlorine, ionically bonded with sodium or other cations. These include halite, or sodium chloride (NaCl); sylvite, or potassium chloride (KCl); and fluorite, or calcium fluoride (CaF_2).

Halide minerals usually form from the evaporation of seawater or other isolated bodies of water. A well-known example of halide mineral deposits created by evaporation is the Bonneville Salt Flats, located west of the Great Salt Lake in Utah.

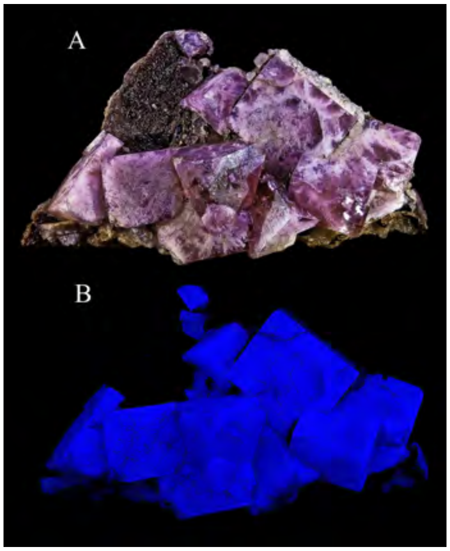

Figure 3.39: (A) Fluorite. (B) Fluorescence of fluorite under UV light. Figure description available at the end of the chapter.

Figure 3.40: Cubic crystals of pyrite. Figure description available at the end of the chapter.

Figure 3.41: Pyrite does not always form large, perfect cubes; rather, it can have an array of different crystal habits, including cubic, dodecahedral, octahedral, and massive. Figure description available at the end of the chapter.

Many important metal ores are **sulfides**, in which metals are bonded to sulfur. Significant examples include galena (lead sulfide), sphalerite (zinc sulfide), pyrite (iron sulfide, sometimes called "fool's gold"), and chalcopyrite (iron-copper sulfide). Sulfides are well known for being important ore minerals. For example, galena is the main source of lead, sphalerite is the main source of zinc, and chalcopyrite is the main copper ore mineral mined in porphyry deposits, like the Bingham mine (see Chapter 16). The largest sources of nickel, antimony, molybdenum, arsenic, and mercury are also sulfides.

3.4.3 Sulfates

Figure 3.42: Gypsum crystal. Figure description available at the end of the chapter.

Sulfate minerals contain a metal ion, such as calcium, bonded to a sulfate ion. The sulfate ion is a combination of sulfur and oxygen (SO_4^{2-}). The sulfate mineral **gypsum** ($CaSO_4 \cdot 2H_2O$) is used in construction materials such as plaster and drywall. Gypsum is often formed from evaporating water and usually contains water molecules in its crystalline structure. The $2H_2O$ in the formula indicates the water molecules are whole H_2O. This is different from minerals like amphibole, which contain a hydroxide ion (OH^-) that is derived from water but is missing a hydrogen ion (H^+). The calcium sulfate without water is a different mineral than gypsum called anhydrite ($CaSO_4$).

3.4.4 Phosphates

Phosphate minerals have a tetrahedral phosphate unit (PO_4^{-3}) combined with various anions and cations. In some cases, arsenic or vanadium can substitute for phosphorus. Phosphates are an important ingredient of fertilizers as well as detergents, paint, and other products. The best known phosphate mineral is apatite, $Ca_5(PO_4)_3(F,Cl,OH)$, variations of which are found in teeth and bones. The gemstone turquoise [$CuAl_6(PO_4)_4(OH)_8 \cdot 4H2O$] is a copper-rich phosphate mineral that, like gypsum, contains water molecules.

Figure 3.43: Apatite crystal. Figure description available at the end of the chapter.

3.4.5 Native Element Minerals

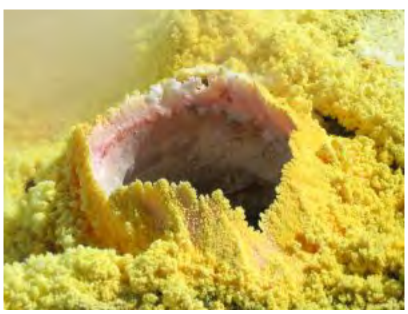

Figure 3.44: Native sulfur deposited around a volcanic fumarole. Figure description available at the end of the chapter.

Native element minerals, usually metals, occur in nature in a pure or nearly pure state. Gold is an example of a native element mineral; it is not very reactive and rarely bonds with other elements, so it is usually found in an isolated or pure state. The nonmetallic and poorly reactive mineral carbon is often found as a native element, such as graphite and diamonds. Mildly reactive metals like silver, copper, platinum, mercury, and sulfur sometimes occur as native element minerals. Reactive metals such as iron, lead, and aluminum almost always bond to other elements and are rarely found in a native state.

Figure 3.45: Native copper. Figure description available at the end of the chapter.

Take this quiz to check your comprehension of this section.

Access the quiz for Section 3.4 by scanning the QR code.

3.5 Identifying Minerals

Geologists identify minerals by their physical properties. In the field, where geologists may have limited access to advanced technology and powerful machines, they can still identify minerals by testing several physical properties: luster and color, streak, hardness, crystal habit, cleavage and fracture, and some special properties. Only a few common minerals make up the majority of Earth's rocks and are usually seen as small grains in rocks. Of the several properties used for identifying minerals, it is good to consider which will be most useful for identifying them in small grains surrounded by other minerals.

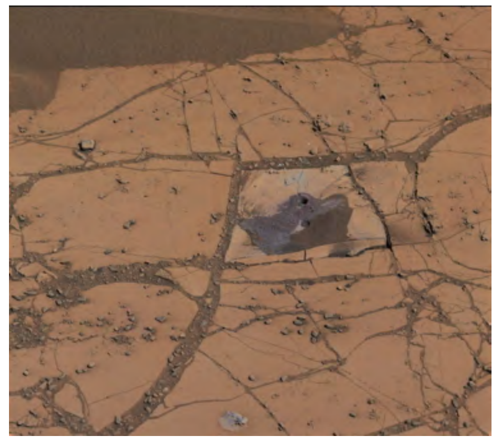

Figure 3.46: The rover Curiosity drilled a hole in this rock from Mars and confirmed the mineral hematite, as mapped from satellites. Figure description available at the end of the chapter.

3.5.1 Luster and Color

Figure 3.47: 15 mm metallic hexagonal molybdenite crystal from Quebec. Figure description available at the end of the chapter.

The first thing to notice about a mineral is its surface appearance, specifically luster and color. **Luster** describes how the mineral looks. Metallic luster looks like a shiny metal such as chrome, steel, silver, or gold. Submetallic luster has a duller appearance, as seen in pewter.

Nonmetallic luster doesn't look like a metal and may be described as vitreous (glassy), earthy, silky, pearly, and other surface qualities. Nonmetallic minerals may be shiny, although their vitreous shine is different from metallic luster. See the table for descriptions and examples of nonmetallic luster.

Figure 3.48: Submetallic luster shown on an antique pewter plate. Figure description available at the end of the chapter.

Luster	Description	Image	Image description
Vitreous/ glassy	Surface is shiny like glass.		Quartz crystals showing vitreous luster
Earthy/dull	Dull, like dried mud or clay		Kaolin specimen showing dull or earthy luster
Silky	Soft shine, like silk fabric	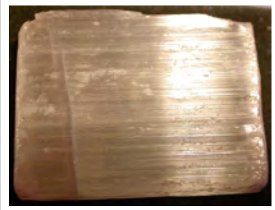	Gypsum specimen showing silky luster
Pearly	Like the inside of a clam shell or mother-of-pearl		Mica specimen showing pearly luster
Submetallic	Has the appearance of dull metal, like pewter. These minerals would usually still be considered metallic. Submetallic appearance can occur in metallic minerals because of weathering.		Sphalerite specimen showing submetallic luster

Table 3.3: Nonmetallic luster descriptions and examples.

Surface color may be helpful in identifying minerals, although it can be quite variable within the same mineral family. Mineral colors are affected by the main elements as well as by impurities in the crystals. These impurities may be rare elements—like manganese, titanium, chromium, or lithium—and even other molecules that are not normally part of the mineral formula. For example, the incorporation of water molecules gives quartz, which is normally clear, a milky color.

Some minerals predominantly show a single color. Malachite and azurite are green and blue, respectively, because of their copper content. Other minerals have a predictable range of colors due to elemental substitutions, usually via a solid solution. Feldspars, the most abundant minerals in the Earth's crust, are complex, have solid solution series, and present several colors, including pink, white, green, gray and others. Other minerals also come in several colors, influenced by trace amounts of several elements. The same element may show up as different colors in different minerals. With notable exceptions, color is usually not a definitive property of minerals. For identifying many minerals, a more reliable indicator is streak, which is the color of the powdered mineral.

Figure 3.49: Azurite is ALWAYS a dark blue color and has been used for centuries for blue pigment. Figure description available at the end of the chapter.

3.5.2 Streak

Figure 3.50: Different minerals may have different streaks. Figure description available at the end of the chapter.

Streak is related to the color of a powdered mineral and can be seen when a mineral sample is scratched or scraped on an unglazed porcelain streak plate. A paper page in a field notebook may also be used for the streak of some minerals. Minerals that are harder than the streak plate will not show streak but will scratch the porcelain. In such a case, a streak test can be obtained by powdering the mineral with a hammer and smearing the powder across a streak plate or notebook paper.

While mineral surface colors and appearances may vary, their streak colors can be diagnostically useful. An example of this property is seen in the iron-oxide mineral hematite. Hematite occurs in a variety of forms, colors, and lusters, from shiny metallic silver to earthy red-brown, as well as other differences in physical appearance. A hematite streak is consistently reddish brown, no matter what the original specimen looks like. Iron sulfide, or pyrite, is a brassy metallic yellow. Commonly called fool's gold, pyrite has a characteristic black to greenish-black streak.

3.5.3 Hardness

Hardness measures the ability of a mineral to scratch other substances. The Mohs hardness scale gives a number showing the relative scratch-resistance of minerals when compared to a standardized set of minerals of increasing hardness. The Mohs scale was developed by German geologist Fredrick Mohs in the early twentieth century, although the idea of identifying minerals by hardness goes back thousands of years. Mohs hardness values are determined by the strength of a mineral's atomic bonds.

Figure 3.51 shows the minerals associated with specific hardness values, together with some common items readily available for use in field testing and mineral identification. The hardness values run from 1 to 10, with 10 being the hardest; however, the scale is not linear. Diamond demonstrates a hardness of 10 and is actually about four times harder than corundum, which is 9. A steel pocketknife blade, which has a hardness value of 5.5, distinguishes between hard and soft minerals on many mineral identification keys.

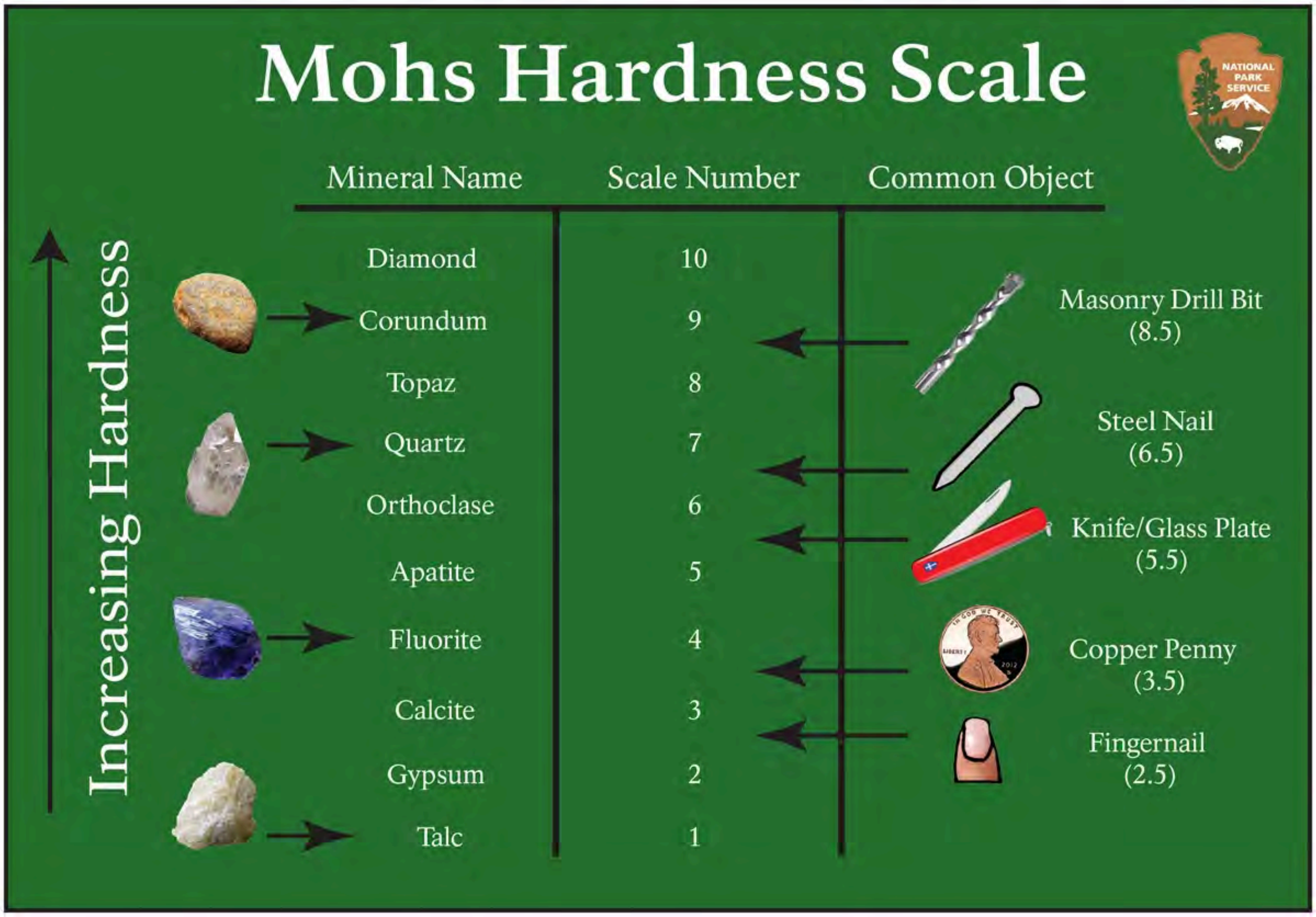

Figure 3.51: Mohs hardness scale. Figure description available at the end of the chapter.

3.5.4 Crystal Habit

Minerals can be identified by **crystal habit**—how their crystals grow and appear in rocks. Crystal shapes are determined by the arrangement of the atoms within the crystal structure. For example, a cubic arrangement of atoms gives rise to a cubic-shaped mineral crystal. Crystal habit refers to typically observed shapes and characteristics; however, it can be affected by other minerals crystallizing in the same rock. When minerals are constrained so they do not develop their typical crystal habit, they are called **anhedral**. **Subhedral** crystals are partially formed shapes. For some minerals, characteristic crystal habit is to grow crystal faces even when surrounded by other crystals in rock. An example is garnet. Minerals grown freely, where the crystals are unconstrained and can take characteristic shapes, often form crystal faces. A **euhedral** crystal has a perfectly formed, unconstrained shape. Some minerals crystallize in such tiny crystals that they do not show a specific crystal habit to the naked eye. Other minerals, like pyrite, can have an array of different crystal habits, including cubic, dodecahedral, octahedral, and massive. Table 3.4 lists typical crystal habits of various minerals.

Habit	Image	Examples
Bladed Long and flat crystals	 Kyanite	Kyanite, amphibole, gypsum
Botryoidal/mammillary Blobby, circular crystals	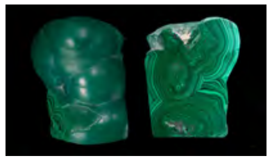 Malachite	Hematite, malachite, smithsonite
Coating/laminae/druse Crystals that are small and coat surfaces	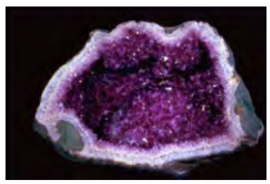 Quartz (var. amethyst) geode	Quartz, calcite, malachite, azurite
Cubic Cube-shaped crystals	 Calcite, galena	Pyrite, galena, halite
Dodecahedral Twelve-sided polygon shapes	 Pyrite	Garnet, pyrite
Dendritic Branching crystals	 Manganese dendrites, scale in mm	Mn-oxides, copper, gold

Habit	Image	Examples
Equant Crystals that do not have a long direction	 Olivine	Olivine, garnet, pyroxene
Fibrous Thin, very long crystals	 Tremolite, a type of amphibole	Serpentine, amphibole, zeolite
Layered, sheets Stacked, very thin, flat crystals	 Muscovite	Mica (biotite, muscovite, etc.)
Lenticular/platy Crystals that are platelike	 Orange wulfenite on calcite	Selenite roses, wulfenite, calcite
Hexagonal Crystals with six sides	 Hanksite	Quartz, hanksite, corundum
Massive/granular Crystals with no obvious shape, microscopic crystals	 Limonite, a hydrated oxide of iron	Limonite, pyrite, azurite, bornite

Habit	Image	Examples
Octahedral Four-sided double-pyramid crystals	 Fluorite	Diamond, fluorite, magnetite, pyrite
Prismatic/columnar Very long, cylindrical crystals	 Tourmaline var. elbaite with quartz & lepidolite on cleavelandite	Tourmaline, beryl, barite
Radiating Crystals that grow from a point and fan out	 Pyrophyllite	Pyrite "suns", pyrophyllite
Rhombohedral Crystals shaped like slanted cubes	 Calcite	Calcite, dolomite
Tabular/blocky/stubby Sharp-sided crystals with no long direction	 Diopside, a member of the pyroxene family	Feldspar, pyroxene, calcite
Tetrahedral Three-sided, pyramid-shaped crystals	 Tetrahedrite	Magnetite, spinel, tetrahedrite

Table 3.4: Typical crystal habits of various minerals.

Figure 3.52: Gypsum with striations. Figure description available at the end of the chapter.

Another crystal habit that may be used to identify minerals is striations, which are dark and light parallel lines on a crystal face. Twinning is another, which occurs when the crystal structure replicates in mirror images along certain directions in the crystal.

Figure 3.53: Twinned staurolite found at Fairy Stone State Park, located in Patrick County, Virginia. Figure description available at the end of the chapter.

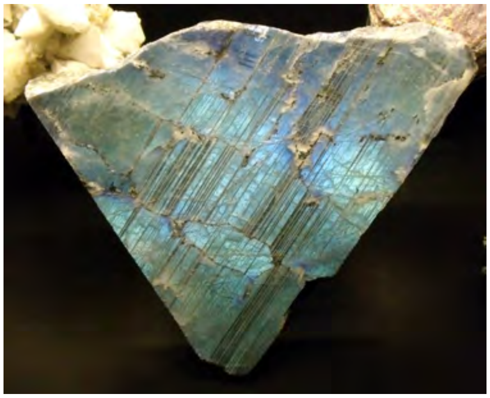

Figure 3.54: Striations on plagioclase. Figure description available at the end of the chapter.

Striations and twinning are related properties in some minerals that include plagioclase feldspar. Striations are optical lines on a cleavage surface. Because of twinning in the crystal, striations show up on one of the two cleavage faces of the plagioclase crystal.

3.5.5 Cleavage and Fracture

Minerals often show characteristic fracture patterns—patterns of breaking along specific cleavage planes. Cleavage planes are smooth, flat, parallel planes within the crystal. The cleavage planes may show as reflective surfaces on the crystal, as parallel cracks that penetrate into the crystal, or on the edge or side of the crystal as a series of steps similar to rice terraces. **Cleavage** arises in crystals where the atomic bonds between atomic layers are weaker along some directions than others, meaning they will break preferentially along these planes. Because they develop on atomic surfaces in the crystal, cleavage planes are optically smooth and reflect light, although the actual break on the crystal may appear jagged or uneven. In such cleavages, the cleavage surface may resemble mountainside rice terraces that all reflect sunlight from a particular sun angle. Some minerals have a strong cleavage, while some only have weak cleavage or do not typically demonstrate cleavage.

Figure 3.55: Citrine, a variety of quartz showing conchoidal fracture. Figure description available at the end of the chapter.

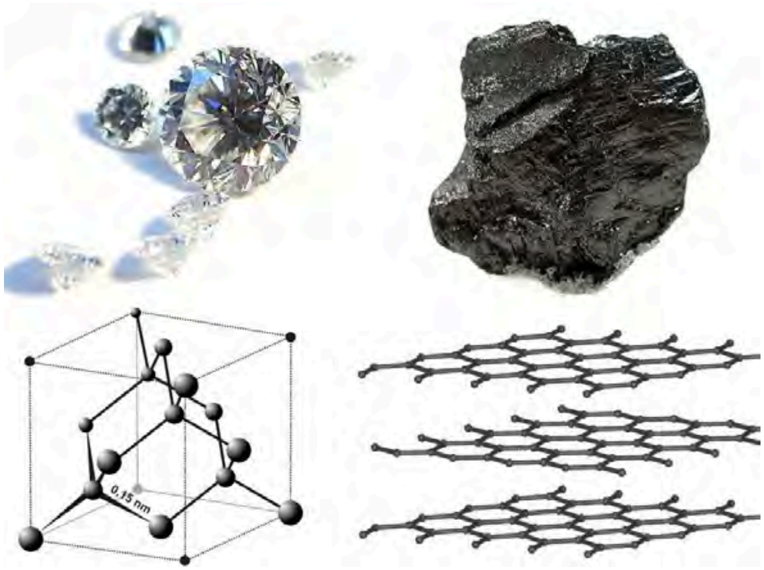

Figure 3.56: Photos and crystal structures of diamond and graphite. Both are composed entirely of carbon but have different physical properties due to their distinct crystal structures. Figure description available at the end of the chapter.

For example, quartz and olivine rarely show cleavage and typically break into conchoidal fracture patterns.

Graphite has its carbon atoms arranged into layers with relatively strong bonds within the layer and very weak bonds between the layers. Thus, graphite cleaves readily between the layers and the layers slide easily over one another, giving graphite its lubricating quality.

Mineral **fracture** surfaces may be rough and uneven, or they may show conchoidal fracture. Uneven fracture patterns are described as irregular, splintery, and fibrous. A **conchoidal** fracture has a smooth, curved surface like a shallow bowl or conch shell, often with curved ridges. Natural volcanic glass, called **obsidian**, breaks with this characteristic conchoidal pattern.

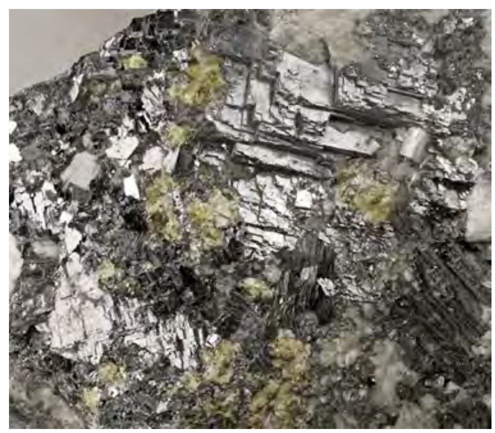

Figure 3.57: Cubic cleavage of galena; note how the cleavage surfaces show up as different but parallel layers in the crystal. Figure description available at the end of the chapter.

To work with cleavage, it is important to remember that cleavage is a result of bonds separating along planes of atoms in the crystal structure. On some minerals, cleavage planes may be confused with crystal faces. This will usually not be an issue for crystals of minerals that grew together within rocks. The act of breaking the rock to expose a fresh face will most likely break the crystals along cleavage planes. Some cleavage planes are parallel with crystal faces but many are not.

Figure 3.58: Freely growing quartz crystals showing crystal faces. Figure description available at the end of the chapter.

In some minerals, distinguishing cleavage planes from crystal faces may be challenging for the student. Understanding the nature of cleavage and referring to the number of cleavage planes and cleavage angles on identification keys should provide the student with enough information to distinguish cleavages from crystal faces. Cleavage planes may show as multiple parallel cracks or flat surfaces on the crystal. Cleavage planes may be expressed as a series of steps like terraced rice paddies. Cleavage planes arise from the tendency of mineral crystals to break along specific planes of weakness within the crystal favored by atomic arrangements. The number of cleavage planes, the quality of the cleavage surfaces, and the angles between them are diagnostic for many minerals, making cleavage one of the most useful properties for identifying minerals. Learning to recognize cleavage is an especially important and useful skill in studying minerals.

As an identification property of minerals, cleavage is usually given in terms of the quality of the cleavage (categorized as *perfect*, *imperfect*, or *none*), the number of cleavage surfaces, and the angles between the surfaces. The most common number of cleavage plane directions in the common rock-forming minerals are: one perfect cleavage (as in mica), two cleavage planes (as in feldspar, pyroxene, and amphibole), and three cleavage planes (as in halite, calcite, and galena). One perfect cleavage (as in mica) develops on the top and bottom of the mineral specimen, with many parallel cracks showing on the sides but no angle of intersection. Two cleavage planes intersect at an angle. Common cleavage angles are 60˚, 75˚, 90˚, and 120˚. Amphibole has two cleavage planes at 60˚ and 120˚. Galena and halite have three cleavage planes at 90˚ (known as cubic cleavage). Calcite cleaves readily in three directions, producing a cleavage figure called a rhomb that looks like a cube squashed toward one corner, giving rise to the approximately 75˚ cleavage angles. Pyroxene has an imperfect cleavage with two planes at 90˚.

Figure 3.59: Steps of cleavage along the same cleavage direction. Figure description available at the end of the chapter.

Cleavages on common rock-forming minerals:

- Quartz: none (conchoidal fracture)
- Olivine: none (conchoidal fracture)
- Mica: 1 perfect
- Feldspar: 2 perfect at 90˚
- Pyroxene: 2 imperfect at 90˚
- Amphibole: 2 perfect at 60˚/120˚
- Calcite: 3 perfect at approximately 75˚
- Halite, galena, pyrite: 3 perfect at 90˚

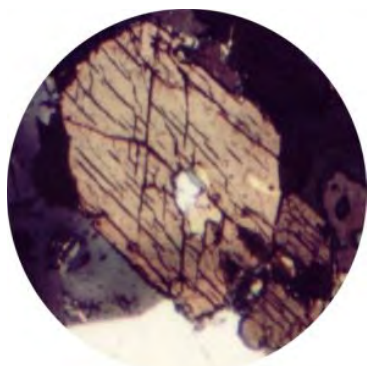

Figure 3.60: Photomicrograph showing 120/60° cleavage within a grain of amphibole. Figure description available at the end of the chapter.

3.5.6 Special Properties

Special properties are unique and identifiable characteristics that are used to identify minerals or that allow some minerals to be used for special purposes. Ulexite has a fiber-optic property that can project images through the crystal like a high-definition television screen (see Figure 3.61). A simple identifying special property is taste, such as the salty flavor of halite or common table salt (NaCl). Sylvite is potassium chloride (KCl) and has a more bitter taste.

Figure 3.61: A demonstration of ulexite's image projection. Figure description available at the end of the chapter.

Another property geologists may use to identify minerals is a property related to **density** called specific gravity. **Specific gravity** measures the weight of a mineral specimen relative to the weight of an equal volume of water. The value is expressed as a ratio between the mineral and water weights. To measure specific gravity, a mineral specimen is first weighed in grams then submerged in a graduated cylinder filled with pure water at room temperature. The rise in water level is noted using the cylinder's graduated scale. Since the weight of water at room temperature is one gram per cubic centimeter, the ratio of the two weights gives the specific gravity. Specific gravity is easy to measure in the laboratory but is less useful for mineral identification in the field than other more easily observed properties, except in a few rare cases such as the very dense galena or native gold. The high density of these minerals gives rise to a qualitative property called heft. Experienced geologists can roughly assess specific gravity by heft, a subjective quality of how heavy the specimen feels in one's hand relative to its size.

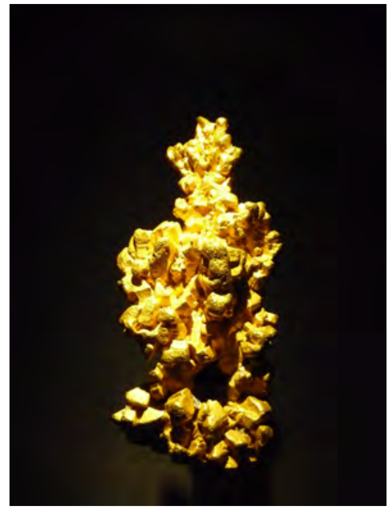

Figure 3.62: Native gold has one of the highest specific gravities. Figure description available at the end of the chapter.

A simple test for identifying calcite and dolomite is to drop a bit of dilute hydrochloric acid (10–15% HCl) on the specimen. If the acid drop effervesces or fizzes on the surface of the rock, the specimen is calcite. If it does not, the specimen is scratched to produce a small amount of powder and tested with acid again. If the acid drop fizzes slowly on the powdered mineral, the specimen is dolomite. The difference between these two minerals can be seen in the video. Geologists who work with carbonate rocks carry a small dropper bottle of dilute HCl in their field kit. Vinegar, which contains acetic acid, can be used for this test and is used to distinguish non-calcite fossils from limestone. While acidic, vinegar produces less of a fizzing reaction because acetic acid is a weaker acid.

Video 3.2: Calcite and dolomite reacting with hydrochloric acid

Access this YouTube video via the QR code. ["Calcite and Dolomite Reacting with Hydrochloric Acid
" by AZ Geology | https://www.youtube.com/watch?v=DX6ZMPbA09U]

Figure 3.63: Paperclips attach to lodestone (magnetite). Figure description available at the end of the chapter.

Some iron-oxide minerals are magnetic and are attracted to magnets. A common name for a naturally magnetic iron oxide is lodestone. Others include magnetite (Fe_3O_4) and ilmenite ($FeTiO_3$). Magnetite is strongly attracted to magnets and can be magnetized. Ilmenite and some types of hematite are weakly magnetic.

Some minerals and mineraloids scatter light via a phenomenon called iridescence. This property occurs in labradorite (a variety of plagioclase) and opal. It is also seen in biologically created substances like pearls and seashells. Cut diamonds show iridescence, and the jeweler's diamond cut is designed to maximize this property.

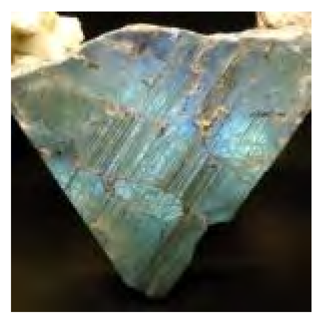

Figure 3.64: Plagioclase showing iridescence as well as striations on the cleavage surface. Figure description available at the end of the chapter.

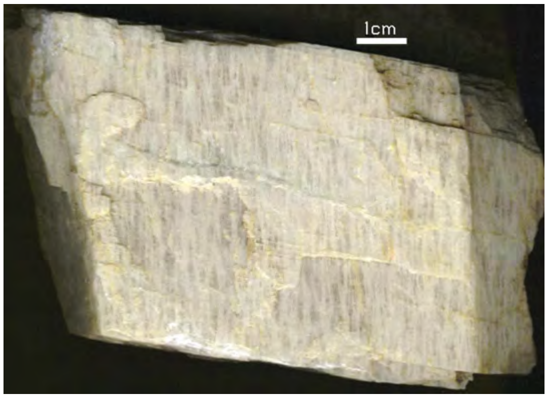

Figure 3.65: Exsolution lamellae within potassium feldspar. Figure description available at the end of the chapter.

Striations on mineral cleavage faces are an optical property that can be used to separate plagioclase feldspar from potassium feldspar (K-spar). A process called twinning creates parallel zones in the crystal that are repeating mirror images. The actual cleavage angle in plagioclase is slightly different than 90˚, and the alternating mirror images in these twinned zones produce a series of parallel lines on one of plagioclase's two cleavage faces. Light reflects off these twinned lines at slightly different angles, which then appear as light and dark lines called striations on the cleavage surface. Potassium feldspar does not exhibit twinning or striations but may show linear features called exsolution lamellae, also known as perthitic **lineation** or simply perthite. Because sodium and potassium do not fit into the same feldspar crystal structure, the lines are created by small amounts of sodium feldspar (albite) separating from the dominant potassium feldspar (K-spar) within the crystal structure. The two different feldspars crystallize out into roughly parallel zones within the crystal, which are seen as these linear markings.

One of the most interesting special mineral properties is fluorescence. Certain minerals, or trace elements within them, give off visible light when exposed to ultraviolet radiation or black light. Many mineral exhibits have a fluorescence room equipped with black lights so this property can be observed. An even rarer optical property is phosphorescence. Phosphorescent minerals absorb light and then slowly release it, much like a glow-in-the-dark sticker.

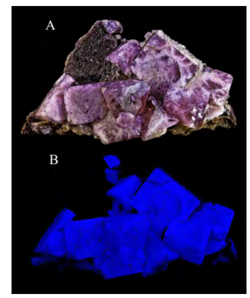

Figure 3.66: (A) Fluorite. (B) Fluorescence of fluorite under UV light. Figure description available at the end of the chapter.

Take this quiz to check your comprehension of this section.

Access the quiz for Section 3.5 by scanning the QR code.

Summary

Minerals are the building blocks of rocks and are essential to understanding geology. Mineral properties are determined by their atomic bonds. Most minerals begin in a fluid and either crystallize out of cooling magma or precipitate as ions and molecules out of a saturated solution. The silicates are largest group of minerals on Earth by number of varieties and relative quantity, making up a large portion of the crust and mantle. Based on the silicon-oxygen tetrahedra, the crystal structure of silicates reflects the fact that silicon and oxygen are Earth's top two most abundant elements. Nonsilicate minerals are also economically important, providing many types of construction and manufacturing materials. Minerals are identified by their unique physical properties, including luster, color, streak, hardness, crystal habit, fracture, cleavage, and special properties.

Take this quiz to check your comprehension of this chapter.

Access the quiz for Chapter 3 by scanning the QR code.

Text References

1. Clarke, F.W, and Washington, H.S. (1927). The composition of the Earth's crust. Professional Paper, United States Geological Survey.
2. Gordon, L.M., and Joester, D. (2011). Nanoscale chemical tomography of buried organic-inorganic interfaces in the chiton tooth. *Nature, 469*(7329), 194–197.
3. Lambeck, K. (1986). Planetary evolution: Banded iron formations. *320*(6063), 574–574.
4. Scerri, E.R. (2007). *The periodic table: Its story and its signiácance:* Oxford University Press, USA.
5. Thomson, J.J. (1897) XL. cathode rays. *Philosophical Magazine Series 5, 44*(269), 293–316.
6. Trenn, T.J., Geiger, H., Marsden, E., and Rutherford, E. (1974). The Geiger-Marsden scattering results and Rutherford's atom, July 1912 to July 1913: The shifting significance of scientific evidence. *Isis, 65*(1), 74–82.
7. Wedepohl, K.H. (1995). The composition of the continental crust. *Geochim. Cosmochim. Acta, 59*(7), 1217–1232.

Figure References

Figure 3.1: The periodic table of the elements. R.A. Dragoset, A. Musgrove, C.W. Clark, and W.C. Martin — NIST, Physical Measurement Laboratory. 2010. Public domain. https://commons.wikimedia.org/wiki/File:Periodic_Table_-_Atomic_Properties_of_the_Elements.png

Figure 3.2: Formation of carbon-14 from nitrogen-14. Sgbeer; adapted by NikNaks. 2011. CC BY-SA 3.0. https://commons.wikimedia.org/wiki/File:Carbon_14_formation_and_decay.svg

Figure 3.3: Element abundance pie chart for Earth's crust. Kindred Grey. 2022. CC BY 4.0.

Figure 3.4: A model of a water molecule, showing the bonds between the hydrogen and oxygen. Dan Craggs. 2009. Public domain. https://commons.wikimedia.org/wiki/File:H2O_2D_labelled.svg

Figure 3.5: The carbon dioxide molecule. Jynto. 2011. Public domain. https://commons.wikimedia.org/wiki/File:Carbon_dioxide_3D_ball.png

Figure 3.6: Cubic arrangement of sodium and chlorine in halite. Benjah-bmm27. 2006. Public domain. https://commons.wikimedia.org/wiki/File:Sodium-chloride-3D-ionic.png

Figure 3.7: Methane molecule. DynaBlast. 2006. CC BY-SA 2.5. https://commons.wikimedia.org/wiki/File:Covalent.svg

Figure 3.8: Calcium carbonate deposits from hard water. Bbypnda. 2014. CC BY-SA 3.0. https://commons.wikimedia.org/wiki/File:Hard_Water_Calcification.jpg

Figure 3.9: The salt flats of Badwater Basin in Death Valley National Park. Laura Neser. March 2022. CC BY-NC.

Figure 3.10: Lava—magma at the Earth's surface. Hawaii Volcano Observatory (DAS). 2003. Public domain. https://commons.wikimedia.org/wiki/File:Pahoehoe_toe.jpg

Figure 3.11: Ammonite shell made of calcium carbonate embedded in sedimentary rock. Laura Neser. March 2016. CC BY-NC.

Figure 3.12: Rotating animation of a tetrahedra. Kjell André. 2005. CC BY-SA 3.0. https://commons.wikimedia.org/wiki/File:Tetrahedron.gif

Figure 3.13: Silicate tetrahedron. Helgi. 2013. CC BY-SA 3.0. https://commons.wikimedia.org/wiki/File:Silicate_tetrahedron_%2B.svg

Figure 3.14: Olivine crystals in basalt. Vsmith. 2005. CC BY-SA 3.0. https://commons.wikimedia.org/wiki/File:Peridot_in_basalt.jpg

Figure 3.15: Tetrahedral structure of olivine. Matanya (usurped). 2005. Public domain. https://commons.wikimedia.org/wiki/File:Atomic_structure_of_olivine_1.png

Figure 3.16: Crystals of diopside, a member of the pyroxene family. Robert M. Lavinsky. 2010. CC BY-SA 3.0. https://commons.wikimedia.org/wiki/File:Diopside-172005.jpg

Figure 3.17: Single-chain tetrahedral structure in pyroxene. Bubenik. 2012. CC BY-SA 3.0. https://en.wikipedia.org/wiki/File:Pyroxferroite-chain.png

Figure 3.18: Elongated crystals of hornblende in orthoclase. Dave Dyet. 2007. Public domain. https://commons.wikimedia.org/wiki/File:Orthoclase_Hornblende.jpg

Figure 3.19: Hornblende crystals. Saperaud~commonswiki. 2005. Public domain. https://commons.wikimedia.org/wiki/File:Amphibole.jpg

Figure 3.20: Double-chain structure. Bubenik. 2012. CC BY-SA 3.0. https://commons.wikimedia.org/wiki/File:Jimthompsonite-chain.png

Figure 3.21: Sheet crystals of biotite mica. Fred Kruijen. 2005. CC BY-SA 3.0 NL. https://commons.wikimedia.org/wiki/File:Biotite_aggregate_-_Ochtendung,_Eifel,_Germany.jpg

Figure 3.22: Crystal of muscovite mica. Saperaud~commonswiki. 2005. Public domain. https://commons.wikimedia.org/wiki/File:MicaSheetUSGOV.jpg

Figure 3.23: Sheet structure of mica. Benjah-bmm27. 2007. Public domain. https://en.wikipedia.org/wiki/File:Silicate-sheet-3D-polyhedra.png

Figure 3.24: Crystal structure of a mica. Rosarinagazo. 2006. Public domain. https://commons.wikimedia.org/wiki/File:Illstruc.jpg

Figure 3.25: Mica "silica sandwich" structure. Kindred Grey. 2022. CC BY 4.0. Includes Sandwich by Alex Muravev from Noun Project (Noun Project license).

Figure 3.26: Structure of kaolinite. United States Geological Survey (USGS). Public domain. https://pubs.usgs.gov/of/2001/of01-041/htmldocs/clays/kaogr.htm

Figure 3.27: Freely growing quartz crystals showing crystal faces. JJ Harrison. 2009. CC BY-SA 2.5. https://en.wikipedia.org/wiki/File:Quartz,_Tibet.jpg

Figure 3.28: Mineral abundance pie chart in Earth's crust. Kindred Grey. 2022. CC BY 4.0.

Figure 3.29: Pink orthoclase crystals. Didier Descouens. 2009. CC BY-SA 4.0. https://commons.wikimedia.org/wiki/File:OrthoclaseBresil.jpg

Figure 3.30: Crystal structure of feldspar. Taisiya Skorina and Antoine Allanore (DOI:10.1039/C4GC02084G). 2015. CC BY 3.0. https://www.researchgate.net/figure/fig1_273641498

Figure 3.31: Hanksite, $Na_{22}K(SO_4)_9(CO_3)_2Cl$, one of the few minerals that is considered a carbonate and a sulfate. Matt Affolter(QFL247). 2009. CC BY-SA 3.0. https://commons.wikimedia.org/wiki/File:Hanksite.JPG

Figure 3.32: Calcite crystal in shape of rhomb. Note the double-refracted word "Calcite" in the center of the figure due to birefringence. Alkivar. 2005. Public domain. https://commons.wikimedia.org/wiki/File:Calcite-HUGE.jpg

Figure 3.33: Limestone with small fossils. Laura Neser. September 2024. CC BY-NC.

Figure 3.34: Bifringence in calcite crystals. Mikael Häggström. 2010. Public domain. https://commons.wikimedia.org/wiki/File:Positively_birefringent_material.svg

Figure 3.35: Crystal structure of calcite. Materialscientist. 2009. CC BY-SA 3.0. https://commons.wikimedia.org/wiki/File:Calcite.png

Figure 3.36: Limonite, a hydrated oxide of iron. USGS. 2005. Public domain. https://commons.wikimedia.org/wiki/File:LimoniteUSGOV.jpg

Figure 3.37: Oolitic hematite. Dave Dyet. 2007. Public domain. https://en.wikipedia.org/wiki/File:Hematite_-_oolitic_with_shale_Iron_Oxide_Clinton,_Oneida_County,_New_York.jpg

Figure 3.38: Halite crystal showing cubic habit. Saperaud~commonswiki. 2005. Public domain. https://en.wikipedia.org/wiki/File:ImgSalt.jpg

Figure 3.39: (A) Fluorite. (B) Fluorescence of fluorite under UV light. Didier Descouens. 2009. CC BY-SA 4.0. https://commons.wikimedia.org/wiki/File:FluoriteUV.jpg

Figure 3.40: Cubic crystals of pyrite. CarlesMillan. 2009. CC BY-SA 3.0. https://commons.wikimedia.org/wiki/File:2780M-pyrite1.jpg

Figure 3.41: Pyrite does not always form large, perfect cubes; rather, it can have an array of different crystal habits, including cubic, dodecahedral, octahedral, and massive. Laura Neser. September 2024. CC BY-NC.

Figure 3.42: Gypsum crystal. USGS. 2004. Public domain. https://commons.wikimedia.org/wiki/File:SeleniteGypsumUSGOV.jpg

Figure 3.43: Apatite crystal. Didier Descouens. 2010. CC BY-SA 4.0. https://commons.wikimedia.org/wiki/File:Apatite_Canada.jpg

Figure 3.44: Native sulfur deposited around a volcanic fumarole. Brisk g. 2006. Public domain. https://commons.wikimedia.org/wiki/File:Fumarola_Vulcano.jpg

Figure 3.45: Native copper. Jonathan Zander (Digon3); adapted by Materialscientist. 2009. CC BY-SA 2.5. https://commons.wikimedia.org/wiki/File:NatCopper.jpg

Figure 3.46: The rover Curiosity drilled a hole in this rock from Mars and confirmed the mineral hematite, as mapped from satellites. NASA/JPL-Caltech/MSSS. Public domain. https://www.nasa.gov/jpl/msl/pia19036/

Figure 3.47: 15 mm metallic hexagonal molybdenite crystal from Quebec. John Chapman. 2008. CC BY-SA 4.0. https://commons.wikimedia.org/wiki/File:Molly_Hill_molybdenite.JPG

Figure 3.48: Submetallic luster shown on an antique pewter plate. Unknown author. ca. 1770 and 1810. Public domain. https://commons.wikimedia.org/wiki/File:Pewter_Plate.jpg

Table 3.3: Nonmetallic luster descriptions and examples. Quartz Brésil by Didier Descouens, 2010 (CC BY-SA 4.0, https://commons.wikimedia.org/wiki/File:Quartz_Br%C3%A9sil.jpg). KaolinUSGOV by Saperaud~commonswiki, 2005 (Public domain, https://commons.wikimedia.org/wiki/File:KaolinUSGOV.jpg). Selenite Gips Marienglas by Ra'ike, 2006 (CC BY-SA 3.0, https://commons.wikimedia.org/wiki/File:Selenite_Gips_Marienglas.jpg). Mineral Mica GDFL006 by Luis Miguel Bugallo Sánchez, 2005 (CC BY-SA 3.0, https://commons.wikimedia.org/wiki/File:Mineral_Mica_GDFL006.JPG). Sphalerite4 by Andreas Früh, 2005 (CC BY-SA 3.0, https://commons.wikimedia.org/wiki/File:Sphalerite4.jpg).

Figure 3.49: Azurite is ALWAYS a dark blue color and has been used for centuries for blue pigment. Graeme Churchard. 2013. CC BY 2.0. https://en.wikipedia.org/wiki/File:Azurite_in_siltstone,_Malbunka_mine_NT.jpg

Figure 3.50: Different minerals may have different streaks. Ra'ike. 2010. CC BY-SA 3.0. https://commons.wikimedia.org/wiki/File:Streak_plate_with_Pyrite_and_Rhodochrosite.jpg

Figure 3.51: Mohs hardness scale. NPS. Public domain (full license here). https://www.nps.gov/articles/mohs-hardness-scale.htm

Table 3.4: Typical crystal habits of various minerals. Elbaite-Lepidolite-Quartz-gem7-x1a by Robert M. Lavinsky, 2010 (CC BY-SA 3.0, https://commons.wikimedia.org/wiki/File:Elbaite-Lepidolite-Quartz-gem7-x1a.jpg). Pyrophyllite-290575 by Robert M. Lavinsky, 2010 (CC BY-SA 3.0, https://commons.wikimedia.org/wiki/File:Pyrophyllite-290575.jpg). Kyanite crystals by Aelwyn, 2006 (CC BY-SA 3.0, https://commons.wikimedia.org/wiki/File:Kyanite_crystals.jpg). Malachite Kolwezi Katanga Congo by Didier Descouens, 2012 (CC BY-SA 3.0, https://commons.wikimedia.org/wiki/File:Malachite_Kolwezi_Katanga_Congo.jpg). Ametyst-geode by Juppi66, 2009 (Public domain, https://commons.wikimedia.org/wiki/File:Ametyst-geode.jpg). Calcite-Galena-elm56c by Robert M. Lavinsky, before March 2010 (CC BY-SA 3.0, https://commons.wikimedia.org/wiki/File:Calcite-Galena-elm56c.jpg). Pyrite elbe by Didier Descouens, 2011 (CC BY-SA 4.0, https://commons.wikimedia.org/wiki/File:Pyrite_elbe.jpg). Dendrites01 by Wilson44691, 2008 (Public domain, https://commons.wikimedia.org/wiki/File:Dendrites01.jpg). Peridot2 by S kitahashi, 2006 (CC BY-SA 3.0, https://commons.wikimedia.org/wiki/File:Peridot2.jpg). Tremolite Campolungo by Didier Descouens, 2009 (CC BY-SA 4.0, https://en.wikipedia.org/wiki/File:Tremolite_Campolungo.jpg). Muscovite-Albite-122887 by Robert M. Lavinsky, 2010 (CC BY-SA 3.0, https://en.wikipedia.org/wiki/File:Muscovite-Albite-122887.jpg). Calcite-Wulfenite-tcw15a by Robert M. Lavinsky, 2010 (CC BY-SA 3.0, https://commons.wikimedia.org/wiki/File:Calcite-Wulfenite-tcw15a.jpg). Hanksite by Matt Affolter(QFL247), 2009 (CC BY-SA 3.0, https://commons.wikimedia.org/wiki/File:Hanksite.JPG). LimoniteUSGOV by USGS, unknown date (Public domain, https://en.wikipedia.org/wiki/File:LimoniteUSGOV.jpg). Fluorite crystals 270×444 by Ryan Salsbury, 2004 (CC BY-SA 3.0, https://commons.wikimedia.org/wiki/File:Fluorite_crystals_270x444.jpg). Calcite-HUGE by Alkivar, 2005 (Public domain, https://commons.wikimedia.org/wiki/File:Calcite-HUGE.jpg). Diopside-172005 by Robert M. Lavinsky, before March 2010 (CC BY-SA 3.0, https://commons.wikimedia.org/wiki/File:Diopside-172005.jpg). Tetrahedrite-Chalcopyrite-Sphalerite-251531 by Robert M. Lavinsky, before March 2010 (CC BY-SA 3.0, https://commons.wikimedia.org/wiki/File:Tetrahedrite-Chalcopyrite-Sphalerite-251531.jpg).

Figure 3.52: Gypsum with striations. Didier Descouens. 2009. CC BY-SA 4.0. https://commons.wikimedia.org/wiki/File:Gypse_Caresse.jpg

Figure 3.53: Twinned staurolite. Virginia State Parks. 2013. CC BY 2.0. https://flic.kr/p/WxNWqi

Figure 3.54: Striations on plagioclase. Mike Beauregard. 2011. CC BY 2.0. https://flic.kr/p/9xh4MS

Figure 3.55: Citrine, a variety of quartz showing conchoidal fracture. James St. John. 2021. CC BY 2.0. https://flic.kr/p/2ky61rb

Figure 3.56: Photos and crystal structures of diamond as compared to graphite. Itub; adapted by Materialscientist. 2009. CC BY-SA 3.0. https://commons.wikimedia.org/wiki/File:Diamond_and_graphite2.jpg

Figure 3.57: Cubic cleavage of galena; note how the cleavage surfaces show up as different but parallel layers in the crystal. Modris Baum. 2012. Public domain. https://commons.wikimedia.org/wiki/File:Argentiferous_Galena-458851.jpg

Figure 3.58: Freely growing quartz crystals showing crystal faces. JJ Harrison. 2009. CC BY-SA 2.5. https://en.wikipedia.org/wiki/File:Quartz,_Tibet.jpg

Figure 3.59: Steps of cleavage along the same cleavage direction. USGS; adapted by David Remahl. 2004. Public domain. https://commons.wikimedia.org/wiki/File:WollastoniteUSGOV.jpg

Figure 3.60: Photomicrograph showing 120/60° cleavage within a grain of amphibole. Eurico Zimbres. 1990. CC BY-SA 2.5. https://en.wikipedia.org/wiki/File:Amphibol.jpg

Figure 3.61: A demonstration of ulexite's image projection. Dave Merrill. 2005. CC BY-SA 2.0. https://commons.wikimedia.org/wiki/File:Ulexite_on_flickr_%2821734610%29.jpg

Figure 3.62: Native gold has one of the highest specific gravities. Gump Stump. 2008. CC BY-SA 3.0. https://commons.wikimedia.org/wiki/File:Latrobe_gold_nugget_Natural_History_Museum.jpg

Figure 3.63: Paperclips attach to lodestone (magnetite). Ryan Somma. 1980. CC BY-SA 2.0. https://commons.wikimedia.org/wiki/File:Magnetite_Lodestone.jpg

Figure 3.64: Plagioclase showing iridescence as well as striations on the cleavage surface. Mike Beauregard. 2011. CC BY 2.0. https://flic.kr/p/9xh4MS

Figure 3.65: Exsolution lamellae within potassium feldspar. Jstuby. 2009. Public domain. https://commons.wikimedia.org/wiki/File:Perthitic_feldspar_Dan_Patch_SD.jpg

Figure 3.66: (A) Fluorite. (B) Fluorescence of fluorite under UV light. Didier Descouens. 2009. CC BY-SA 4.0. https://commons.wikimedia.org/wiki/File:FluoriteUV.jpg

Figure Descriptions

Figure 3.1: An organized grid-like structure known as the periodic table of elements. It consists of rows and columns that contain symbols and numbers representing different chemical elements. The elements are arranged in increasing order based on their atomic number, from left to right and top to bottom. Each element is depicted by its symbol, such as H for hydrogen, followed by its atomic number and atomic weight. The table is color-coded to group elements with similar properties.

Figure 3.2: 3D diagram showing the formation of carbon-14 from nitrogen-14 from left to right. On the left side of the diagram is a drawing of a nitrogen-14 atom with 7 spherical neutrons and 7 spherical protons stuck together. Next to that diagram is a single sphere that represents a single neutron being added to the nitrogen-14 atom. To the right of that is the resulting carbon- 14 atom represented as 6 spherical protons and 8 spherical neutrons stuck together, next to a single sphere that represents a single proton that's leftover from the reaction.

Figure 3.3: Oxygen: 46%, Silicon: 28%, Aluminum: 8%, Iron: 5%, Calcium: 4%, Sodium: 3%, Potassium: 3%, Magnesium: 2%, Others: 2%.

Figure 3.4: Simple diagram of a water molecule with the letter O at the center and an individual letter H branching out on either side of the O. One letter H is to to the lower left of the letter O with a line connecting them and the other letter H is to the lower right of the letter O with a line connecting them. The angle between the two connecting lines is 104.45 degrees. Along one of the connecting lines is the label "95.84 pm."

Figure 3.5: Carbon dioxide molecule with a carbon ion in the center and two oxygen ions on either side, each sharing two electrons with the carbon.

Figure 3.6: 3-D diagram of a crystal model of halite with spherical ions of sodium and chlorine arranged in a cubic structure. Chlorine atoms are colored green and sodium atoms are smaller than the chlorine atoms, colored purple.

Figure 3.7: 2-D diagram showing a methane molecule with carbon labeled as the letter "C" at the center in a circle and four circular hydrogen atoms labeled as the letter "H" surrounding the carbon atom. Each hydrogen atom is sharing an electron at its contact with carbon and the carbon atom is sharing four electrons, one at each hydrogen atom connection.

Figure 3.8: Encrusted whitish calcium carbonate (lime) deposits on a faucet head.

Figure 3.9: Three people standing on a flat white expanse with a steep hill rising to the right side of the photo.

Figure 3.10: Glowing orange-to-yellow molten lava flowing next to black solid volcanic rock.

Figure 3.11: A spiral-shaped outline of an ammonite shell embedded in a tan rock.

Figure 3.12: Animation of a rotating pyramid shape with a triangular base. The sides of the shape are green and brown.

Figure 3.13: 3-D diagram of four red balls labelled O-2-negative stacked in a pyramid shape with one small gray ball labeled Si-4-positive in the center.

Figure 3.14: A rock sample that shows many small granular crystals of the green mineral olivine in a gray basalt.

Figure 3.15: Grayscale diagram of the atomic scale structure of olivine looking along the a axis (Pbnm setting) with the long b axis across the page and the short c axis up the page. Oxygen is shown in red, silicon in pink, and magnesium/iron in blue; the three inequivalent oxygen and two inequivalent metal sites are marked O and M respectively. A projection of the unit cell is shown by a black rectangle.

Figure 3.16: A sample of elongated dark green crystals clustered together in the same sample.

Figure 3.17: Grayscale diagram of a single vertical chain of tetrahedra in pyroxene, alternating with adjacent corner oxygens bonded. The outer corners are active to bond with other anions.

Figure 3.18: A crystal of tan-to-pink orthoclase (potassium feldspar) with elongated dark brown crystals of hornblende embedded in the sample.

Figure 3.19: Two shiny black crystals of hornblende

Figure 3.20: Diagram of a vertical double chain structure of amphibole; two single chains laying next to each other with the inner corners of each tetrahedron bonded and the outer corners active to bond with anions.

Figure 3.21: Glassy, dark brown crystals of biotite mica showing sheet-like habit.

Figure 3.22: Sample of tan-to-brown muscovite mica showing sheet structure of the mineral. It appears as thin sheets stacked on top of each other which are part of a single sample.

Figure 3.23: Diagram of continuous sheets of tetrahedra with all three base corners bonded to each other; the top corner active to bond with anions. Each corner of the tetrahedra is labeled with a red dot.

Figure 3.24: Diagram of mica crystal structure with the sheets of tetrahedra inverted onto each other into sandwiches with the active corners bonded with anions. The sandwiches are connected together with large potassium ions that form weak bonds which are easily separated so the crystal comes apart into sheets.

Figure 3.25: The mica sandwich. Bread of silica sheet, jam of anions, bread of silica sheet, butter of large potassium ions.

Figure 3.26: Crystal structure of a kaolinite layer with one octahedral sheet condensed with one tetrahedral sheet beneath it.

Figure 3.27: Glassy, transparent prismatic crystals growing together.

Figure 3.28: Plagioclase feldspar: 39%, alkali feldspar: 12%, quartz: 12%, pyroxene: 11%, non-silicates: 8%, amphibole: 5%, mica: 5%, clay: 5%, other silicates: 3%.

Figure 3.29: A group of crystals of pink potassium feldspar growing together.

Figure 3.30: Framework structure of feldspar with all corners of tetrahedra shared with adjacent tetrahedra; there are holes in the structure in which large anions like potassium and sodium/calcium fit.

Figure 3.31: The mineral is hexagonal and clear.

Figure 3.32: A clear, glassy calcite crystal in a rhombohedral shape. Text that says "calcite" is visible through the crystal which has been double-refracted.

Figure 3.33: Piece of limestone full of small fossils.

Figure 3.34: Block diagram of a calcite crystal polarizing light into two waves that vibrate at right angles to each other and pass through the crystal in different paths. One path is labeled "parallel polarization" and the other path is labeled "perpendicular polarization."

Figure 3.35: Crystal structure of calcite showing the carbonate units of carbon surrounded by three oxygen ions and bonded to calcium ions.

Figure 3.36: Sample of limonite which has a dull, yellow color.

Figure 3.37: Piece of brick red hematite that has tiny white spheres embedded within the sample.

Figure 3.38: Whitish glassy sample of halite with cubic crystals visible.

Figure 3.39: Purplish crystals of fluorite. The second image shows the deep blue fluorescence of fluorite under ultraviolet light.

Figure 3.40: Metallic gold-colored cubic crystals of pyrite.

Figure 3.41: Massive-looking chunk of metallic gold-colored mineral.

Figure 3.42: Whitish glassy sample of gypsum that is transparent.

Figure 3.43: An elongated prismatic crystal of dark green apatite.

Figure 3.44: Yellow native sulfur deposited around the vent of a volcanic fumarole.

Figure 3.45: Metallic native copper.

Figure 3.46: Reddish-brown rock that has a small hole drilled through it.

Figure 3.47: A gray metallic crystal.

Figure 3.48: Antique gold-colored pewter plate showing a more dull submetallic luster.

Figure 3.49: There are two dark blue disks on white siltstone.

Figure 3.50: Gold-colored metallic piece of pyrite with a black streak on a white streak plate and pinkish red-colored piece of rhodochrosite with a white streak on a black streak plate.

Figure 3.51: Higher numbers indicate increasing hardness. 10: diamond (mineral). 9: corundum (mineral). 8.5: masonry drill bit. 8: topaz (mineral). 7: quartz (mineral). 6.5: steel nail. 6: orthoclase (mineral). 5.5: knife/glass plate. 5: apatite (mineral). 4: fluorite (mineral). 3.5: copper penny. 3: calcite (mineral). 2.5: fingernail. 2: gypsum (mineral). 1: talc (mineral).

Figure 3.52: Glassy, clear mineral that has many horizontal lines on it.

Figure 3.53: The brown minerals are replicated in different directions and connected in the middle

Figure 3.54: Striations or parallel dark lines on one cleavage surface on plagioclase feldspar that has an iridescent blue-green sheen.

Figure 3.55: Clear, glassy sample that has a fracture with smooth, curved surfaces, slightly concave, with concentric undulations resembling the lines of a seashell.

Figure 3.56: Samples and crystal structure diagrams of diamond and graphite next to each other. On the left is a photo of shiny diamond gemstones, below which is the crystal structure of diamond: it has isometric structure, which means the carbon atoms are all bonded in the same way in all direction. On the right is a photo of submetallic graphite, below which is the crystal structure of graphite: it consists of layers of carbon atoms separated by a gap with weak bonds holding the layers together.

Figure 3.57: Dark gray metallic sample of galena; cubic cleavage is visible in various layers of the sample.

Figure 3.58: Glassy, transparent prismatic crystals growing together.

Figure 3.59: White, vitreous, opaque sample of wollastonite which has visible step-like cleavage all along the same cleavage direction. A penny sits on top of the sample for scale.

Figure 3.60: Photomicrograph showing 120/60 degree cleavage as seen by thin black criss-crossing black lines in tan amphibole grain.

Figure 3.61: The word on the page can be seen through the mineral, and is slightly magnified.

Figure 3.62: Bright gold nugget.

Figure 3.63: Series of three paper clips together that stick into the air from one end touching the tan sample of lodestone.

Figure 3.64: Striations or parallel dark lines on one cleavage surface on plagioclase feldspar that has an iridescent blue-green sheen.

Figure 3.65: Whitish sample with vertical gray linear features throughout. The sample has a pearly luster.

Figure 3.66: Purplish crystals of fluorite. The second image shows the deep blue fluorescence of fluorite under ultraviolet light.

4. IGNEOUS PROCESSES AND VOLCANOES

Learning Objectives

By the end of this chapter, students should be able to:

- Explain the origin of magma as it relates to plate tectonics.
- Describe how the Bowen's reaction series relates mineral crystallization and melting temperatures.
- Explain how cooling of magma leads to rock compositions and textures and how these are used to classify igneous rocks.
- Analyze the features of common igneous landforms and how they relate to their origin.
- Describe how silica content affects magma viscosity and eruptive style of volcanoes.
- Describe volcano types, eruptive styles, composition, and their plate tectonic settings.
- Describe volcanic hazards.

Igneous rock is formed when liquid rock freezes into a solid rock. This molten material is called magma when it is in the ground and lava when it is on the surface. Only the Earth's outer core is liquid; the Earth's mantle and crust are naturally solid. However, there are a few minor pockets of magma that form near the surface where geologic processes cause melting. It is this magma that becomes the source for volcanoes and igneous rocks. This chapter will describe the classification of igneous rocks, the unique processes that form magmas, types of volcanoes and volcanic processes, volcanic hazards, and igneous landforms.

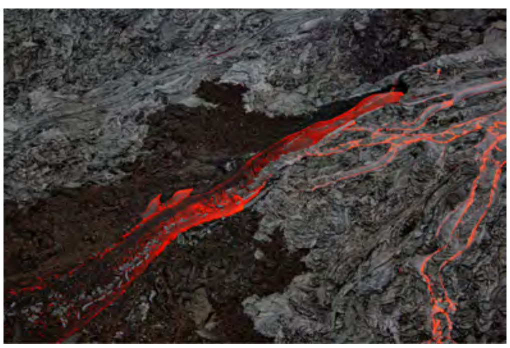

Figure 4.1: Lava flow in Hawai'i. Figure description available at the end of the chapter.

Lava cools quickly on the surface of the Earth and forms tiny microscopic crystals. These are known as fine-grained extrusive, or volcanic, **igneous** rocks. Extrusive rocks are often **vesicular**, filled with holes from escaping gas bubbles. Volcanism is the process in which lava erupts. Depending on the properties of the lava that erupts, the volcanism can be drastically different, from smooth and gentle to dangerous and explosive. This leads to different types of volcanoes and different volcanic hazards.

In contrast, magma that cools slowly below the Earth's surface forms larger crystals which can be seen with the naked eye. These are known as coarse-grained intrusive, or plutonic, igneous rocks. This relationship between cooling rates and grain sizes of the solidified minerals in igneous rocks is important for interpreting the rock's geologic history.

Figure 4.2: Half Dome in Yosemite National Park, California, is a part of the Sierra Nevada batholith, which is mostly made of granite. Figure description available at the end of the chapter.

4.1 Classification of Igneous Rocks

Igneous rocks are classified based on texture and composition. **Texture** describes the physical characteristics of the minerals, such as grain size. This relates to the cooling history of the molten magma from which it came. Composition refers to the rock's specific mineralogy and chemical composition. Cooling history is also related to changes that can occur to the composition of igneous rocks.

4.1.1 Texture

If magma cools slowly, deep within the crust, the resulting rock is called **intrusive**, or plutonic. The slow cooling process allows crystals to grow large, giving intrusive igneous rock a coarse-grained **phaneritic** texture. The individual crystals in phaneritic texture are readily visible to the unaided eye.

Figure 4.3: Granite is a classic coarse-grained (phaneritic) intrusive igneous rock. The different colors are unique minerals, with the black likely composed of two or three different minerals. Figure description available at the end of the chapter.

Figure 4.4: Basalt is a classic fine-grained extrusive igneous rock. Figure description available at the end of the chapter.

When lava is extruded onto the surface or intruded into shallow fissures near the surface and cools, the resulting igneous rock is called **extrusive**, or volcanic. Extrusive igneous rocks have a fine-grained **aphanitic** texture, in which the grains are too small to see with the unaided eye. The fine-grained texture indicates the quickly cooling lava did not have time to grow large crystals. These tiny crystals can be viewed under a petrographic microscope. In some cases, extrusive lava cools so rapidly it does not develop crystals at all. This noncrystalline material is not classified as minerals but as volcanic glass. This is a common component of volcanic ash and rocks like obsidian.

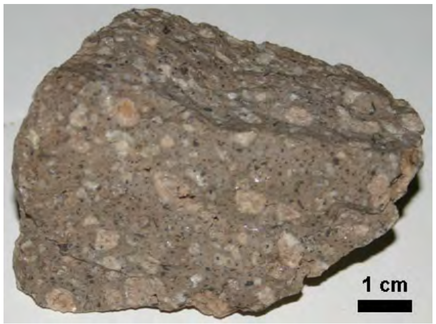

Figure 4.5: Porphyritic texture. Figure description available at the end of the chapter.

Some igneous rocks have a mix of coarse-grained minerals surrounded by a matrix of fine-grained material in a texture called **porphyritic**. The large crystals are called **phenocrysts**, and the fine-grained matrix is called the **groundmass** (often referred to as simply the "matrix"). Porphyritic texture indicates the magma body underwent a multi-stage cooling history, cooling slowly while deep under the surface and later rising to a shallower depth or to the surface, where it cooled more quickly.

Figure 4.6: Pegmatitic texture. Figure description available at the end of the chapter.

Residual molten material expelled from igneous intrusions may form veins or masses containing very large crystals of minerals like feldspar, quartz, beryl, tourmaline, and mica. This texture, which indicates a very slow crystallization, is called pegmatitic. A rock that chiefly consists of pegmatitic texture is known as a **pegmatite**. To give an example of how large these crystals can get, transparent cleavage sheets of pegmatitic muscovite mica were used as windows during the Middle Ages.

All magmas contain gases dissolved in solution called **volatiles**. As the magma rises to the surface, the drop in pressure causes the dissolved volatiles to come bubbling out of solution, like the fizz in an opened bottle of soda. The gas bubbles become trapped in the solidifying lava to create a vesicular texture, with the holes specifically called vesicles. The type of volcanic rock with common vesicles is called scoria.

Figure 4.7: Scoria. Figure description available at the end of the chapter.

Figure 4.8: Pumice. Figure description available at the end of the chapter.

An extreme version of scoria occurs when volatile-rich lava is very quickly quenched and becomes a meringue-like froth of glass called **pumice**. Some pumice is so full of vesicles that the density of the rock drops low enough that it will float.

Lava that cools extremely quickly may not form crystals at all, even microscopic ones. The resulting rock is called volcanic glass. Obsidian is a rock consisting of volcanic glass. Obsidian as a glassy rock shows an excellent example of conchoidal fracture similar to the mineral quartz (see Chapter 3).

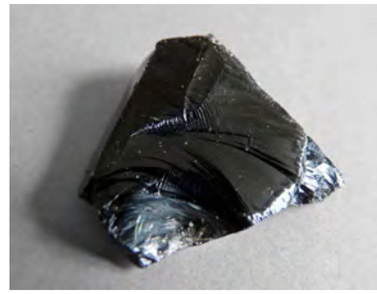

Figure 4.9: Obsidian (volcanic glass). Note conchoidal fracture. Figure description available at the end of the chapter.

Figure 4.10: Welded tuff. Figure description available at the end of the chapter.

When volcanoes erupt explosively, vast amounts of lava, rock, ash, and gases are thrown into the atmosphere. The solid parts, called **tephra**, settle back to Earth and cool into rocks with **pyroclastic** textures. *Pyro-*, meaning fire, refers to the igneous source of the tephra, and *–clastic* refers to the rock fragments. Tephra fragments are named based on size—**ash** (<2 mm), **lapilli** (2–64 mm), and **bombs** or blocks (>64 mm). Pyroclastic texture is usually recognized by the chaotic mix of crystals, angular glass shards, and rock fragments. Rock formed from large deposits of tephra fragments is called **tuff**. If the fragments accumulate while still hot, the heat may deform the crystals and weld the mass together, forming a welded tuff.

4.1.2 Composition

Composition refers to a rock's chemical and mineral makeup. For igneous rock, composition is divided into four groups: felsic, intermediate, mafic, and ultramafic. These groups refer to differing amounts of silica, iron, and magnesium found in the minerals that make up the rocks. It is important to realize these groups do not have sharp boundaries in nature but rather lie on a continuous spectrum with many transitional compositions and names that refer to specific quantities of minerals. As an example, **granite** is a commonly used term but has a very specific definition that involves exact quantities of minerals like feldspar and quartz. Rocks labeled as "granite" in laymen applications can be several other rocks, including syenite, tonalite, and monzonite. To avoid these complications, Figure 4.11 presents a simplified version of igneous rock nomenclature focusing on the four main groups, which is adequate for an introductory student.

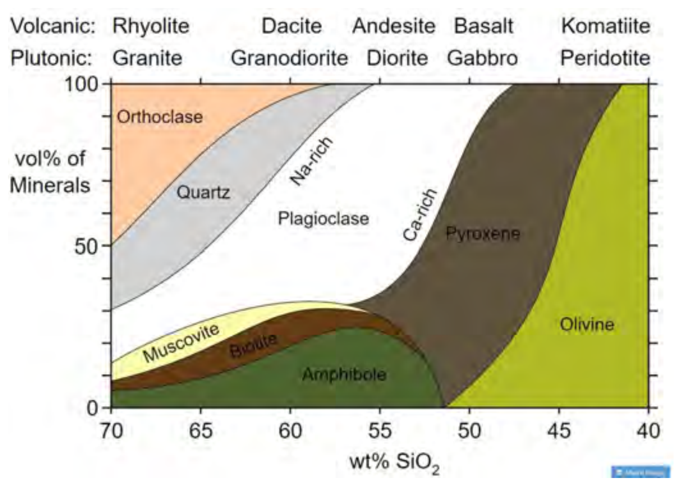

Figure 4.11: Mineral composition of common igneous rocks. Percentage of minerals is shown on the vertical axis. Percentage of silica is shown on the horizontal axis. Rock names at the top include a continuous spectrum of compositions, grading from one into another. Figure description available at the end of the chapter.

Felsic refers to a predominance of the light-colored (felsic) minerals **fel**dspar and **si**lica in the form of quartz. These light-colored minerals have more silica as a proportion of their overall chemical formulas. Minor amounts of dark-colored (mafic) minerals like amphibole and biotite mica may be present as well. Felsic igneous rocks are rich in silica (in the 65–75% range, meaning the rock would be 65–75% weight percent SiO_2) and poor in iron and magnesium.

Intermediate is a composition between felsic and mafic. It usually contains roughly equal amounts of light and dark minerals, including light grains of plagioclase feldspar and dark minerals like amphibole. It is intermediate in silica in the 55–60% range.

Mafic refers to an abundance of ferromagnesian minerals (with magnesium and iron, chemical symbols **M**g and **F**e) plus plagioclase feldspar. It is mostly made of dark minerals like pyroxene and olivine, which are rich in iron and magnesium and relatively poor in silica. Mafic rocks are low in silica, in the 45–50% range.

Ultramafic refers to the extremely mafic rocks composed of mostly olivine and some pyroxene, which have even more magnesium and iron and even less silica. These rocks are rare on the surface but make up peridotite, the rock of the upper mantle. It is poor in silica, in the 40% or less range.

The top of Figure 4.11 has both plutonic and volcanic igneous rocks arranged in a continuous spectrum from felsic on the left to intermediate, mafic, and ultramafic toward the right. **Rhyolite** thus refers to the volcanic and felsic igneous rocks, and **granite** thus refers to intrusive and felsic igneous rocks. **Andesite** and **diorite** likewise refer to extrusive and intrusive intermediate rocks (with dacite and granodiorite applying to those rocks with compositions between felsic and intermediate). **Basalt** and **gabbro** are the extrusive and intrusive names for mafic igneous rocks, and **peridotite** is ultramafic, with komatiite as the fine-grained extrusive equivalent. Komatiite is a rare rock because volcanic material that comes directly from the mantle is not common, although some examples can be found in ancient Archean rocks. Nature rarely has sharp boundaries and the classification and naming of rocks often imposes what appear to be sharp boundary names onto a continuous spectrum.

To identify a rock, match the texture (below) with the composition (right)	Composition			
Texture	**Felsic** • >10% quartz • >50% feldspar • <15% mafic minerals	**Intermediate** • >10% quartz • >50% plagioclase • >10% orthoclase • <50% mafic minerals	**Mafic** • 20–85% plagioclase • 15–50% pyroxene • >35% olivine	**Ultramafic** Olivine & pyroxene
Phaneritic Coarse grained	**Granite**	**Diorite**	**Gabbro**	**Peridotite**
Aphanitic Fine grained	**Rhyolite**	**Andesite**	**Basalt**	X
Porphyritic Large crystals in a fine matrix	**Porphyritic rhyolite**	**Porphyritic andesite**	**Porphyritic basalt**	X
Vesicular Bubbly or frothy	**Pumice**	X	**Scoria**	X
Glassy	**Obsidian**	X	X	X
Pyroclastic Fragmental	**Rhyolitic tuff or volcanic breccia**	**Andesitic tuff or volcanic breccia**	**Basaltic tuff or volcanic breccia**	X

Figure 4.12: Igneous rock classification table with composition as vertical columns and texture as horizontal rows. Figure description available at the end of the chapter.

Aphanitic/phaneritic rock types	
Felsic composition	
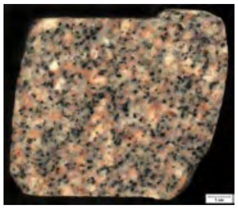 Granite	 Rhyolite
Granite is a course crystalline felsic intrusive rock. The presence of quartz is a good indicator of granite. Granite commonly has large amounts of salmon pink potassium feldspar and white plagioclase crystals that have visible cleavage planes. Granite is a good approximation for the continental crust, both in density and composition.	Rhyolite is a fine-grained crystalline felsic extrusive rock. Rhyolite is commonly pink and will often have glassy quartz phenocrysts. Because felsic lava is less mobile, it is less common than granite. Examples of rhyolite include several lava flows in Yellowstone National Park and the altered rhyolite that makes up the Grand Canyon of the Yellowstone.
Intermediate composition	
 Diorite	 Andesite
Diorite is a coarse crystalline intermediate intrusive igneous rock. Diorite is identifiable by its Dalmatian-like appearance of black hornblende and biotite and white plagioclase feldspar. It is found in the Andes Mountains as well as the Henry and Abajo Mountains of Utah.	Andesite is a fine-grained crystalline intermediate extrusive rock. It is commonly grey and porphyritic. It can be found in the Andes Mountains and in some island arcs (see Chapter 2). It is the fine-grained compositional equivalent of diorite.
Mafic composition	
 Gabbro	 Vesicular basalt
Gabbro is a coarse-grained mafic igneous rock, made with mainly mafic minerals like pyroxene and only minor plagioclase. Because mafic lava is more mobile, it is less common than basalt. Gabbro is a major component of the lower oceanic crust.	Basalt is a fine-grained mafic igneous rock. It is commonly vesicular and aphanitic. When porphyritic, it often has either olivine or plagioclase phenocrysts. Basalt is the main rock formed at mid-ocean ridges and is therefore the most common rock on the Earth's surface, making up the entirety of the ocean floor (except where covered by sediment).

Table 4.1: Aphanitic and phaneritic rock types with images.

4.1.3 Igneous Rock Bodies

Igneous rocks are common in the geologic record, but surprisingly, it is intrusive rocks that are more common. Extrusive rocks, because of their small crystals and glass, are less durable. Plus, they are, by definition, exposed to the elements of erosion immediately. Intrusive rocks, forming underground with larger, stronger crystals, are more likely to last. Therefore, most landforms and rock groups that owe their origin to igneous rocks are intrusive bodies. A significant exception to this is active volcanoes, which are discussed in a later section on volcanism. This section will focus on the common igneous bodies found in many places within the **bedrock** of Earth.

When magma intrudes into a weakness like a crack or fissure and solidifies, the resulting cross-cutting feature is called a **dike** (sometimes spelled dyke). Because of this, dikes are often vertical or at an angle relative to the preexisting rock layers that they intersect. Dikes are therefore discordant intrusions, not following any layering that was present. Dikes are important to geologists, not only for the study of igneous rocks themselves but also for dating rock sequences and interpreting the geologic history of an area. The dike is younger than the rocks it cuts across and, as discussed in the chapter on geologic time (Chapter 7), may be used to assign actual numeric ages to sedimentary sequences, which are notoriously difficult to age date.

Figure 4.13: Dike of olivine gabbro cutting across Baffin Island in the Canadian Arctic. Figure description available at the end of the chapter.

Figure 4.14: Igneous sill intruding between Paleozoic strata in Nova Scotia. Figure description available at the end of the chapter.

Sills are another type of intrusive structure. A sill is a concordant intrusion that runs parallel to the sedimentary layers in the country rock. They are formed when magma exploits a weakness between these layers, shouldering them apart and squeezing between them. As with dikes, sills are younger than the surrounding layers and may be radioactively dated to study the age of sedimentary strata.

A **magma chamber** is a large underground reservoir of molten rock. The path of rising magma is called a **diapir**. The processes by which a diapir intrudes into the surrounding native or country rock are not well understood and are the subject of ongoing geological inquiry. For example, it is not known what happens to the preexisting country rock as the diapir intrudes. One theory is the overriding rock gets shouldered aside, displaced by the increased volume of magma. Another proposes that the native rock is melted and consumed into the rising magma or broken into pieces that settle into the magma, a process known as **stoping**. It has also been proposed that diapirs are not a real phenomenon but just a series of dikes that blend into each other. The dikes may intrude over millions of years, but since they may be made of similar material, they would appear to have formed at the same time. Regardless, when a diapir cools, it forms an mass of intrusive rock called a **pluton**. Plutons can have irregular shapes but can often be somewhat round.

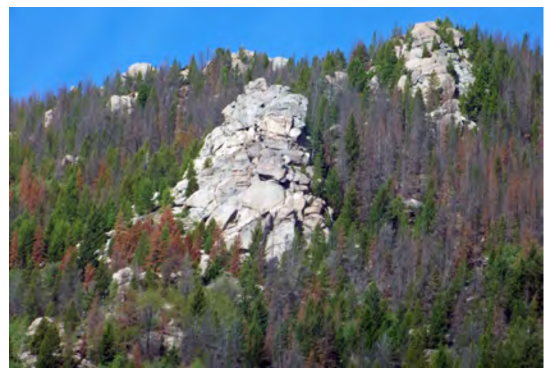

Figure 4.15: Quartz monzonite from the Cretaceous in Montana, USA. Figure description available at the end of the chapter.

Figure 4.16: Half Dome in Yosemite National Park, California, is a part of the Sierra Nevada batholith, which is mostly made of granite. Figure description available at the end of the chapter.

When many plutons merge together in an extensive single feature, it is called a **batholith**. Batholiths are found in the cores of many mountain ranges, including the granite formations of Yosemite National Park in the Sierra Nevada of California. They are typically more than 100 km^2 in area, associated with subduction zones, and mostly felsic in composition. A stock is a type of pluton with less surface exposure than a batholith and may represent a narrower neck of material emerging from the top of a batholith. Batholiths and stocks are discordant intrusions that cut across and through surrounding country rock.

Figure 4.17: The Henry Mountains in Utah are interpreted to be a laccolith, exposed by erosion of the overlying layers. Figure description available at the end of the chapter.

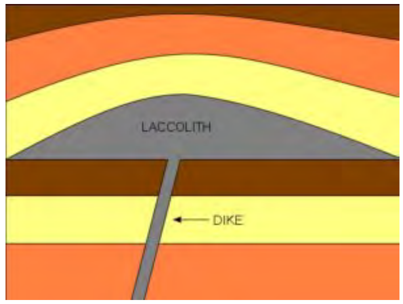

Figure 4.18: Laccolith forms as a blister between sedimentary strata. Figure description available at the end of the chapter.

Laccoliths are blister-like, concordant intrusions of magma that form between sedimentary layers. The Henry Mountains of Utah are a famous topographic landform formed by this process. Laccoliths bulge upwards; a similar downward-bulging intrusion is called a **lopolith**.

Complete this interactive activity to check your understanding. Click on the plus signs on the illustration for descriptions of several igneous features.

Access this interactive activity by scanning the QR code.

Take this quiz to check your comprehension of this section.

Access the quiz for Section 4.1 by scanning the QR code.

4.2 Bowen's Reaction Series

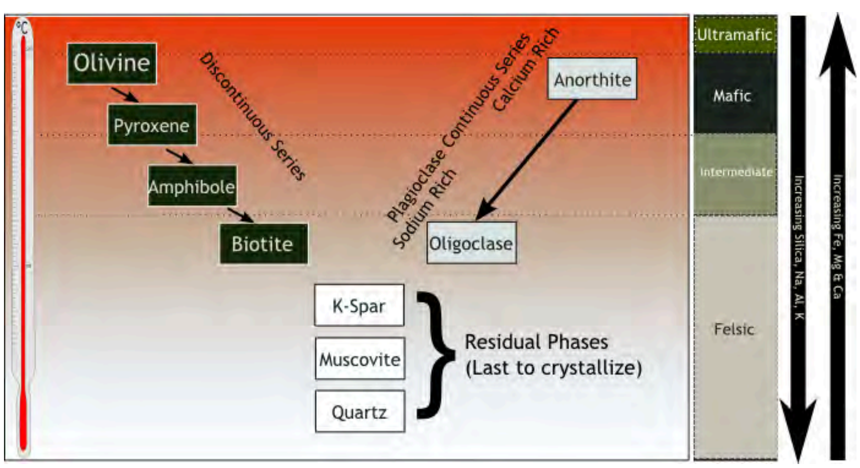

Figure 4.19: Bowen's reaction series. Higher-temperature minerals shown at top (olivine) and lower-temperature minerals shown at bottom (quartz). Figure description available at the end of the chapter.

Figure 4.20: Olivine, the first mineral to crystallize in a melt. Figure description available at the end of the chapter.

Bowen's reaction series describes the temperature at which minerals crystallize when cooled or melt when heated. The low end of the temperature scale, where all minerals crystallize into solid rock, is approximately 700˚C (1292˚F). The upper end of the range, where all minerals exist in a molten state, is approximately 1250˚C (2282˚F). These numbers reference minerals that crystallize at standard sea level pressure, 1 bar. The values will be different for minerals located deep below the Earth's surface due to the increased pressure, which affects crystallization and melting temperatures. However, the order and relationships are maintained.

In Figure 4.19, the righthand column lists the four groups of igneous rock from top to bottom: ultramafic, mafic, intermediate, and felsic. The down-pointing arrow on the far right shows increasing amounts of silica, sodium, aluminum, and potassium as the mineral composition goes from ultramafic to felsic. The up-pointing arrow shows increasing ferromagnesian components, specifically iron, magnesium, and calcium. To the far left of the diagram is a temperature scale. Minerals near the top of diagram, such as olivine and anorthite (a type of plagioclase), crystallize at higher temperatures. Minerals near the bottom, such as quartz and muscovite, crystallize at lower temperatures.

Figure 4.21: Norman L. Bowen. Figure description available at the end of the chapter.

The most important aspect of Bowen's reaction series is to notice the relationships between minerals and temperature. Norman L. Bowen (1887–1956) was an early twentieth century geologist who studied igneous rocks. He noticed that, in igneous rocks, certain minerals always occur together and that these mineral assemblages exclude other minerals. Curious as to why, and in consideration of the hypothesis that it had to do with the temperature at which the rocks cooled, he set about conducting experiments on igneous rocks in the early 1900s, grinding combinations of rocks into powder, sealing the powders into metal capsules, heating them to various temperatures, and then cooling them.

Figure 4.22: Norman L. Bowen and his colleague working at the Carnegie Institution of Washington Geophysical Laboratory. Figure description available at the end of the chapter.

When he opened the quenched capsules, he found a glass surrounding mineral crystals that he could identify under his petrographic microscope. The results of many of these experiments, conducted at different temperatures over a period of several years, showed that the common igneous minerals crystallize from magma at different temperatures. He also saw that minerals occur together in rocks with others that crystallize within similar temperature ranges and never crystallize with other minerals. This relationship can explain the main difference between mafic and felsic igneous rocks. Mafic igneous rocks contain more mafic minerals and therefore crystallize at higher temperatures than felsic igneous rocks. This is even seen in lava flows, with felsic lavas erupting hundreds of degrees cooler than their mafic counterparts. Bowen's work laid the foundation for understanding igneous **petrology** (the study of rocks) and resulted in his book *The Evolution of the Igneous Rocks* in 1928.

Take this quiz to check your comprehension of this section.

Access the quiz for Section 4.2 by scanning the QR code.

4.3 Magma Generation

Magma and lava contain three components: melt, solids, and volatiles. The melt is made of ions from minerals that have liquefied. The solids are made of crystallized minerals floating in the liquid melt, which may be minerals that have already cooled. Volatiles are gaseous components—such as water vapor, carbon dioxide, sulfur, and chlorine—dissolved in the magma. The presence and amount of these three components affect the physical behavior of the magma and will be discussed more below.

4.3.1 Geothermal Gradient

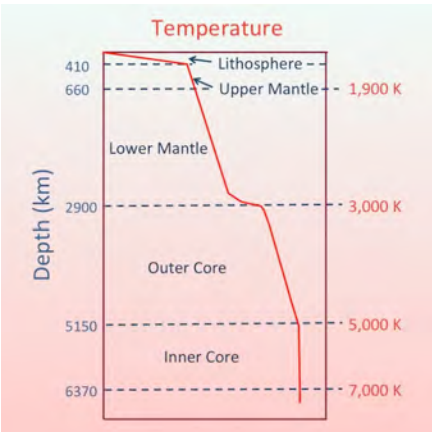

Figure 4.23: Geothermal gradient. Figure description available at the end of the chapter.

Below the surface, the temperature of the Earth rises. This heat is caused by residual heat left from the formation of Earth and ongoing radioactive decay. The rate at which temperature increases with depth is called the **geothermal gradient**. The average geothermal gradient in the upper 100 km (62 mi) of the crust is about 25˚C per kilometer of depth. So for every kilometer of depth, the temperature increases by about 25˚C.

The depth-temperature graph (see Figure 4.23) illustrates the relationship between the geothermal gradient (geotherm, red line) and the start of rock melting (solidus, green line). The geothermal gradient changes with depth (which has a direct relationship to pressure) through the crust into the upper mantle. The area to the left of the green line includes solid components; to the right is where liquid components start to form. The temperature will increase with depth, and, at about 125 kilometers (78 miles), the natural geothermal gradient is closest to the solidus.

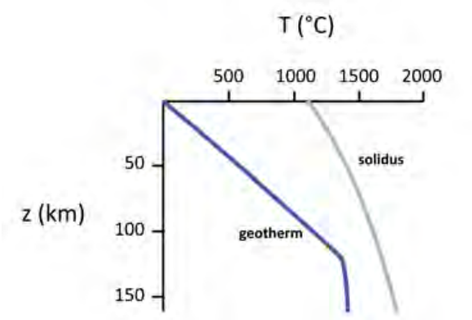

Figure 4.24: Pressure-temperature diagram showing temperature in degrees Celsius on the x-axis and depth below the surface in kilometers (km) on the y-axis. The dark blue line is the geothermal gradient, and the light blue solidus line represents the temperature and pressure regime at which melting begins. Rocks at pressures and temperatures left of the light blue line are solid. If pressure/temperature conditions change so that rocks pass to the right of the light blue line, then they will start to melt. Figure description available at the end of the chapter.

The temperature at 100 km (62 mi) deep is about 1,200˚C (2,192˚F). At bottom of the crust, 35 km (22 mi) deep, the pressure is about 10,000 bars. A bar is a measure of pressure, with 1 bar being normal atmospheric pressure at sea level. At these pressures and temperatures, the crust and mantle are solid. To a depth of 150 km (93 mi), the geothermal gradient line stays to the left of the solidus line. This relationship continues through the mantle to the core-mantle boundary, at 2,880 km (1,790 mi).

The solidus line slopes to the right because the melting temperature of any substance depends on pressure. The higher pressure created at greater depth increases the temperature needed to melt rock. In another example, water boils at 100˚C at sea level with an atmospheric pressure close to 1 bar; but if the pressure is lowered, as shown on the video below, water boils at a much lower temperature.

Video 4.1: Boiling water at room temperature

Access this YouTube video by scanning the QR code. ["Boiling water at room temperature – science experiment" by Coolphysicsvideos Physics | https://www.youtube.com/watch?v=Ks4VuXTTKmo]

There are three principal ways rock behavior crosses to the right of the green solidus line to create molten magma: (1) decompression melting caused by lowering the pressure, (2) flux melting caused by adding volatiles (see more below), and (3) heat-induced melting caused by increasing the temperature. The Bowen's reaction series shows that minerals melt at different temperatures. Since magma is a mixture of different minerals, the solidus boundary is more of a fuzzy zone rather than a well-defined line; some minerals are melted and some remain solid. This type of rock behavior is called **partial melting** and represents real-world magmas, which typically contain solid, liquid, and volatile components.

4.4 Volcanism

When magma emerges onto the Earth's surface, the molten rock is called lava. A volcano is a type of land **formation** created when lava solidifies into rock. Volcanoes have been an important part of human society for centuries, though our understanding of them was limited until plate tectonics made them less mysterious. This section describes volcano location, type, hazards, and monitoring.

4.4.1. Distribution and Tectonics

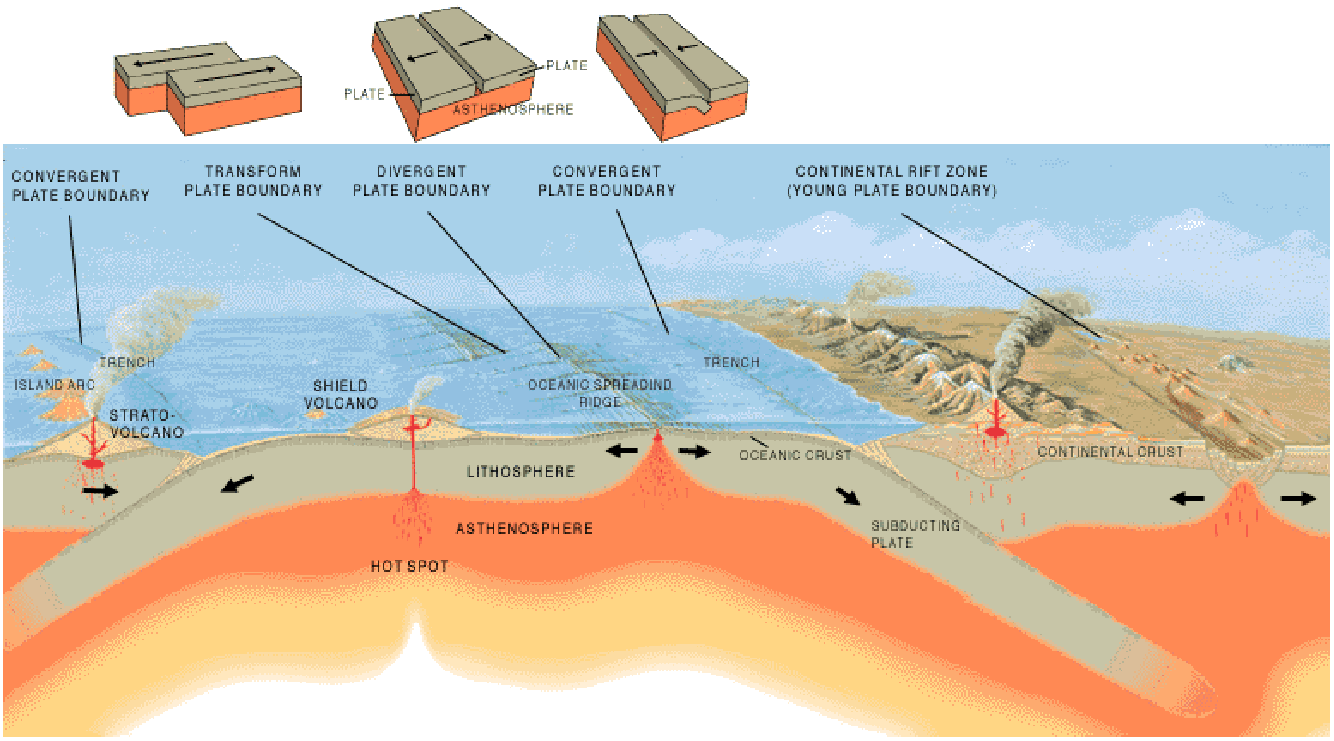

Figure 4.25: Association of volcanoes with plate boundaries. Figure description available at the end of the chapter.

Most volcanoes are interplate volcanoes. **Interplate** volcanoes are located at active plate boundaries created by volcanism at mid-ocean ridges, subduction zones, and continental rifts. The prefix *inter-* means between. Some volcanoes are **intraplate** volcanoes. The prefix *intra-* means within, and intraplate volcanoes are located within tectonic plates, far removed from plate boundaries. Many intraplate volcanoes are formed by hotspots.

Volcanoes at Mid-Ocean Ridges

Most volcanism on Earth occurs on the ocean floor along mid-ocean ridges, a type of divergent plate boundary (see Chapter 2). These interplate volcanoes are also the least observed and famous, since most of them are located under 3,000–4,500 m (10,000–15,000 ft) of ocean, and the eruptions are slow, gentle, and oozing. One exception is the interplate volcanoes of Iceland. The diverging and thinning oceanic plates allow hot mantle rock to rise, releasing pressure and causing decompression melting. Ultramafic mantle rock, consisting largely of peridotite, partially melts and generates magma that is basaltic. Because of this, almost all volcanoes on the ocean floor are basaltic. In fact, most oceanic lithosphere is basaltic near the surface, with phaneritic gabbro and ultramafic peridotite underneath.

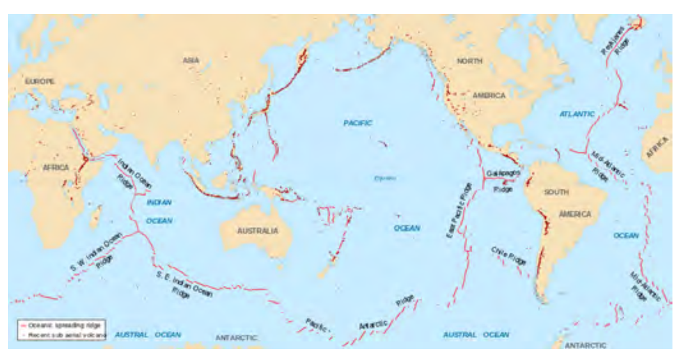

Figure 4.26: Map of spreading ridges throughout the world. Figure description available at the end of the chapter.

When basaltic lava erupts underwater, it emerges in small explosions and/or forms pillow-shaped structures called pillow basalts. These seafloor eruptions enable entire underwater ecosystems to thrive in the deep ocean around mid-ocean ridges. These ecosystems exist around deep-sea hydrothermal vents—also known as **black smokers**—which emit hot, black, mineral-rich water.

Figure 4.27: Pillow basalt on seafloor near Hawai'i. Figure description available at the end of the chapter.

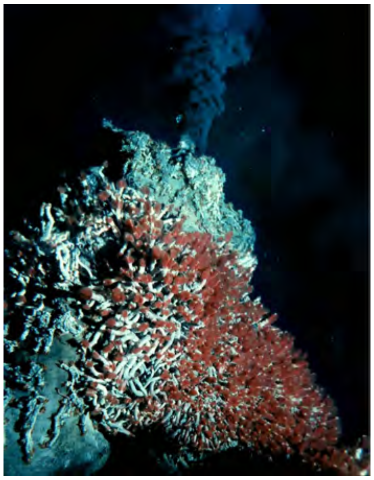

Figure 4.28: Black smoker hydrothermal vent with a colony of giant (6'+) tube worms. Figure description available at the end of the chapter.

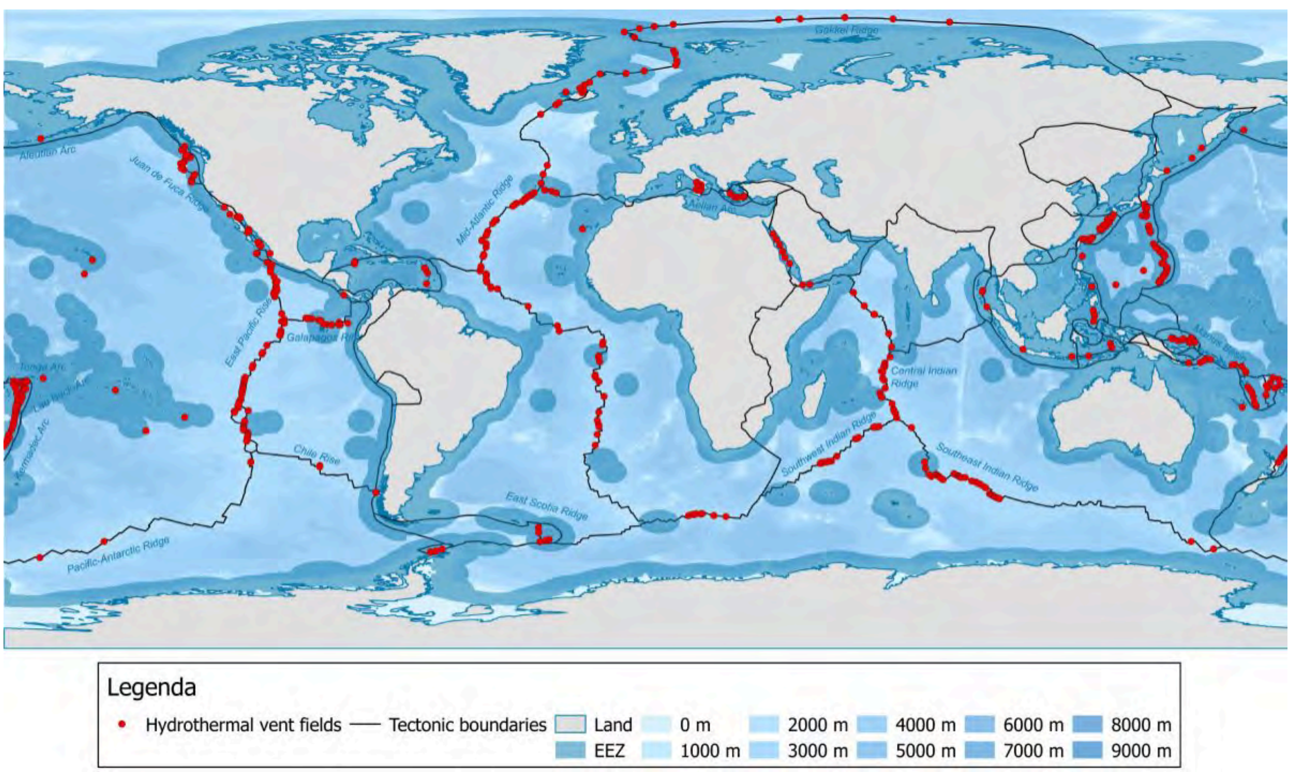

Figure 4.29: Distribution of hydrothermal vent fields. Figure description available at the end of the chapter.

Without sunlight to support photosynthesis, these organisms instead utilize a process called **chemosynthesis**. Certain bacteria are able to turn hydrogen sulfide (H_2S), a gas that smells like rotten eggs, into life-supporting nutrients and water. Larger organisms may eat these bacteria or absorb nutrients and water produced by bacteria living symbiotically inside their bodies. The videos show some of the ecosystems found around deep-sea hydrothermal vents.

Video 4.2: Updating the deep-diving submarine at 50-years-old

Access this YouTube video by scanning the QR code. ["The Alvin Submarine Part 1: Updating the Deep-Diving Submarine at 50 Years Old – WIRED" by WIRED | https://www.youtube.com/watch?v=a5aQ4W9GbpU]

Video 4.3: Incredible views on board the deep-sea vessel

Access this YouTube video by scanning the QR code. ["The Alvin Submarine Part 2: Incredible Views On-Board the Deep-Sea Vessel" by WIRED | https://www.youtube.com/watch?v=dXOQFnU-49k]

Volcanoes at Subduction Zones

The second most common location for volcanism is adjacent to subduction zones, a type of convergent plate boundary (see Chapter 2). The process of subduction expels water from hydrated minerals in the descending slab, which causes flux melting in the overlying mantle rock. Because subduction volcanism occurs in a volcanic arc, the thickened crust promotes partial melting and magma differentiation. These evolve the mafic magma from the mantle into more silica-rich magma. The Ring of Fire surrounding the Pacific Ocean, for example, is dominated by subduction-generated eruptions of mostly silica-rich lava; the volcanoes and plutons consist largely of intermediate-to-felsic rock such as andesite, rhyolite, pumice, and tuff.

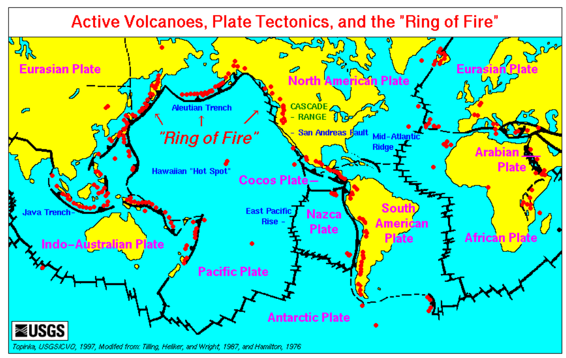

Figure 4.30: Distribution of volcanoes on the planet. An interactive map of volcano distributions can be found here: https://www.ncei.noaa.gov/maps/hazards. Figure description available at the end of the chapter.

Volcanoes at Continental Rifts

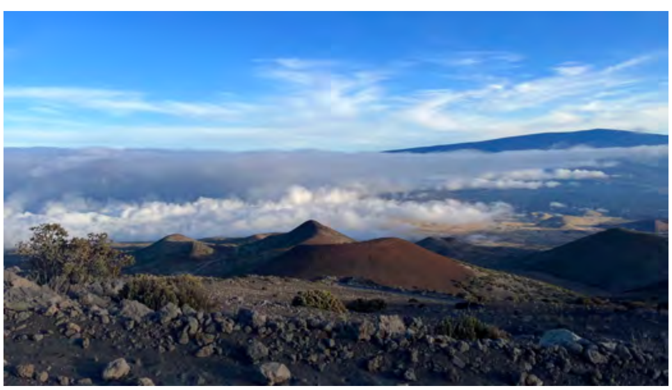

Figure 4.31: Basaltic cinder cones on the flank of Mauna Kea. Mauna Kea is a shield volcano on the north end of Hawai'i Island. Figure description available at the end of the chapter.

Some volcanoes are created at continental rifts, where crustal thinning is caused by diverging lithospheric plates, such as the East African rift basin in Africa. Volcanism caused by crustal thinning without continental rifting is found in the Basin and Range Province in North America. In this location, volcanic activity is produced by rising magma that stretches the overlying crust. Lower crust or upper mantle material rises through the thinned crust, releases pressure, and undergoes decompression-induced partial melting. This magma is less dense than the surrounding rock and continues to rise through the crust to the surface, erupting as basaltic lava. These eruptions usually result in flood basalts, cinder cones, and basaltic lava flows (see Video 4.4). Relatively young cinder cones of basaltic lava can be found in south-central Utah's Black Rock Desert volcanic field, which is part of the zone of Basin and Range crustal extension. These Utah cinder cones and lava flows started erupting around six million years ago, with the last eruption occurring 720 years ago.

Video 4.4: Basin and range volcanic processes

Access this YouTube video by scanning the QR code. ["Basin & Range Volcanic Processes (Educational)
" by IRIS Earthquake Science | https://www.youtube.com/watch?v=4VgMe-JXOAM]

Hotspots

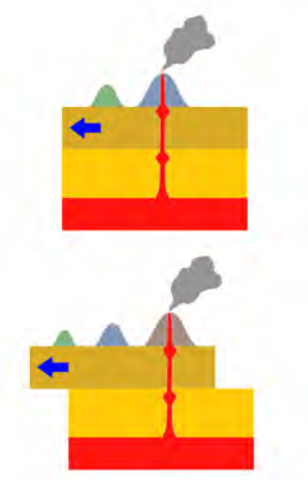

Figure 4.32: Diagram showing a nonmoving source of magma (mantle plume) and a moving overriding plate. Figure description available at the end of the chapter.

Hotspots are the main source of intraplate volcanism. Hotspots occur when lithospheric plates glide over a hot mantle plume, an ascending column of solid heated rock originating from deep within the mantle. The mantle plume generates melts as material rises, with the magma rising even more. When the ascending magma reaches the lithospheric crust, it spreads out into a mushroom-shaped head that is tens to hundreds of kilometers across.

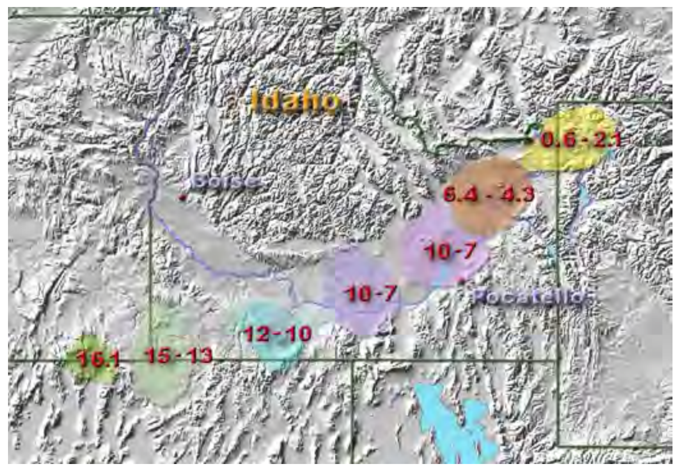

Figure 4.33: The track of the Yellowstone hotspot, which shows the age of different eruptions in millions of years ago. Figure description available at the end of the chapter.

Since most mantle plumes are located beneath the oceanic lithosphere, the early stages of intraplate volcanism typically take place underwater. Over time, basaltic volcanoes may build up from the seafloor into islands, such as the Hawaiian Islands. In the location where a hotspot is found under a continental plate, contact with the hot mafic magma may cause the overlying felsic rock to melt and mix with the mafic material below, forming intermediate magma. Or the felsic magma may continue to rise and cool into a granitic batholith or erupt as a felsic volcano. The Yellowstone Caldera is an example of hotspot volcanism that resulted in an explosive eruption.

A zone of actively erupting volcanism connected to a chain of extinct volcanoes indicates intraplate volcanism located over a hotspot. These volcanic chains are created by the overriding oceanic plate slowly moving over a hotspot mantle plume. These chains are seen on the seafloor and continents and include volcanoes that have been inactive for millions of years. The Hawaiian Islands on the Pacific Oceanic plate are the active end of a long volcanic chain that extends from the northwest Pacific Ocean to the Emperor Seamounts, all the way to the subduction zone beneath the Kamchatka Peninsula. The overriding North American continental plate moved across a mantle plume hotspot for several million years, creating a chain of volcanic calderas that extends from Southwestern Idaho to the presently active Yellowstone Caldera in Wyoming.

Video 4.5 illustrates hotspot volcanoes.

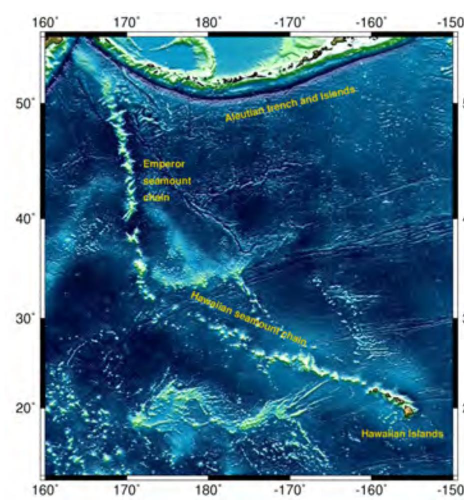

Figure 4.34: The Hawaiian–Emperor seamount and island chain. Figure description available at the end of the chapter.

Video 4.5: What is a volcanic hotspot?

Access this YouTube video by scanning the QR code. [“What is a Volcanic Hotspot? (Educational)” by IRIS Earthquake Science | https://www.youtube.com/watch?v=AhSaE0omw9o]

4.4.2 Volcano Features and Types

Volcanoes are categorized based on their shape, eruption style, magmatic composition, and other aspects.

Complete this interactive activity to check your understanding.

Access this interactive activity by scanning the QR code.

Figure 4.35 shows the main features of a typical stratovolcano: (1) magma chamber, (2) upper layers of lithosphere, (3) the **conduit** or narrow pipe through which the lava erupts, (4) the base or edge of the volcano, (5) a sill of magma between layers of the volcano, (6) a diapir or feeder tube to the sill, (7) layers of tephra (ash) from previous eruptions, (8) & (9) layers of lava erupting from the vent and flowing down the sides of the volcano, (10) the **crater** at the top of the volcano, (11) layers of lava and tephra on (12), a **parasitic cone** (a small volcano located on the flank of a larger volcano, such as Shastina on Mount Shasta. Kilauea, sitting on the flank of Mauna Loa, is not considered a parasitic cone because it has its own separate magma chamber), (13) the vents of the parasite and the main volcano, (14) the rim of the crater, (15) clouds of ash blown into the sky by the eruption that settle back onto the volcano and surrounding land.

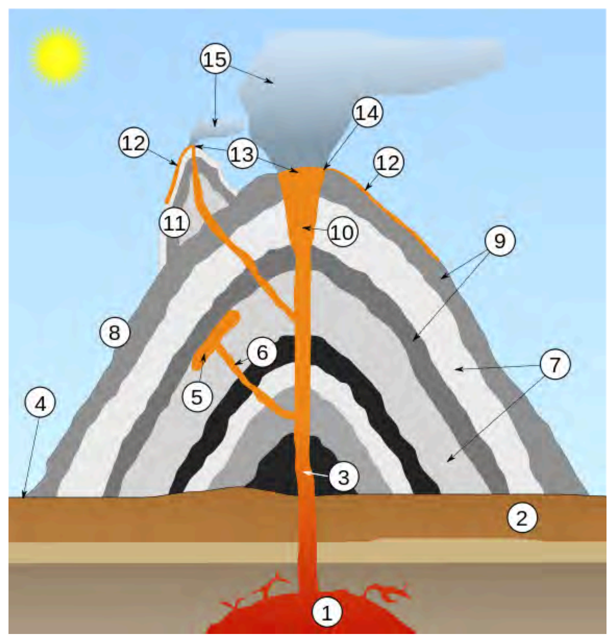

Figure 4.35: Stratovolcano. Figure description available at the end of the chapter.

Figure 4.36: Oregon’s Crater Lake was formed about 7,700 years ago after the eruption of Mount Mazama. Figure description available at the end of the chapter.

The largest craters are called calderas, such as the Crater Lake Caldera in Oregon. Many volcanic features are produced by viscosity, a basic property of a lava. **Viscosity** is the resistance to flowing by a fluid. Low-viscosity magma flows easily, more like syrup, as seen in the basaltic volcanism that occurs in Hawai’i on shield volcanoes. High viscosity means a thick and sticky magma, typically felsic or intermediate, that flows slowly, similar to toothpaste.

Shield Volcano

Figure 4.37: Kilauea Summit in Hawai'i. Figure description available at the end of the chapter.

The largest volcanoes are **shield volcanoes**. They are characterized by broad, low-angle flanks, small vents at the top, and mafic magma chambers. The name comes from the side view, which resembles a medieval warrior's shield. They are typically associated with hotspots, mid-ocean ridges, or continental rifts with rising upper-mantle material. The low-angle flanks are built up slowly from numerous low-viscosity basaltic lava flows that spread out over long distances. The basaltic lava erupts effusively, meaning the eruptions are small, localized, and predictable.

Typically, shield volcano eruptions are not much of a hazard to human life—although nonexplosive eruptions of Kilauea (Hawai'i) in 2018 produced uncharacteristically large lavas that damaged roads and structures. Mauna Loa and Kilauea in Hawai'i are examples of shield volcanoes. Shield volcanoes are also found in Iceland, the Galapagos Islands, Northern California, Oregon, and the East African Rift.

Figure 4.38: Eruption of Kilauea in 2018 produced high-viscosity lava, shown here crossing a road. This eruption caused much property damage. Figure description available at the end of the chapter.

Figure 4.39: Olympus Mons, an enormous shield volcano on Mars, the largest volcano in the solar system, standing about two-and-a-half times higher than Everest is above sea level. Figure description available at the end of the chapter.

The largest volcanic edifice in the Solar System is Olympus Mons on Mars. This (possibly extinct) shield volcano covers an area the size of the state of Arizona. This may indicate the volcano erupted over a hotspot for millions of years, which means Mars had little, if any, plate tectonic activity.

Basaltic lava forms special landforms based on magma temperature, composition, and content of dissolved gases and water vapor. The two main types of basaltic volcanic rock have Hawaiian names—*pahoehoe* and *aa*. **Pahoehoe** might come from low-viscosity lava that flows easily into ropey strands.

Figure 4.40: Ropey pahoehoe lava cooled into basalt. Figure description available at the end of the chapter.

Figure 4.41: Blocky aa lava. Figure description available at the end of the chapter.

Aa (sometimes spelled a'a or ʻaʻā and pronounced "ah-ah") is more viscous and has a crumbly, blocky appearance. The exact details of what forms the two types of flows are still up for debate. Felsic lavas have lower temperatures and more silica; as a result, they have higher viscosity. These also form aa-style flows.

Low-viscosity, fast-flowing basaltic lava tends to harden on the outside, forming a tube while continuing to flow internally. Once lava flow subsides, the empty outer shell may be left as a lava tube. Lava tubes, with or without collapsed roofs, form famous caves in Hawai'i, Northern California, the Columbia River basalt plateau of Washington and Oregon, El Malpais National Monument in New Mexico, and Craters of the Moon National Monument in Idaho.

Fissures are cracks that commonly originate from shield-style eruptions. Lava emerging from fissures is typically mafic and very fluid. The 2018 Kiluaea eruption included fissures associated with the lava flows. Some fissures are caused by volcanic seismic activity rather than lava flows. Some fissures are influenced by plate tectonics, such as the common fissures located parallel to the divergent boundary in Iceland.

Figure 4.42: Devils Tower in Wyoming has columnar jointing. Figure description available at the end of the chapter.

Figure 4.43: Columnar jointing on Giant's Causeway in Ireland. Figure description available at the end of the chapter.

Cooling lava can contract into columns with semi-hexagonal cross sections called columnar jointing. This feature forms the famous Devils Tower in Wyoming, possibly an ancient volcanic vent from which the surrounding layers of lava and ash have been removed by erosion. Another well-known exposed example of columnar jointing is the Giant's Causeway in Ireland.

Congealed magma, along with fragmental volcanic and wallrock materials, can be preserved in the feeding conduits of a volcano upon cessation of activity. These preserved rocks form crudely cylindrical masses, from which dikes radiate outward; they may be visualized as the "fossil" remains of the innards of a volcano (the so-called "volcanic plumbing system") and are referred to as **volcanic necks** or plugs.

Figure 4.44: Shiprock, located in New Mexico, is the erosional remnant of the throat of a volcano, referred to as a volcanic neck. Figure description available at the end of the chapter.

Stratovolcano

Figure 4.45: Mount Rainier towers over Tacoma, Washington. Figure description available at the end of the chapter.

A **stratovolcano**, also called a composite cone volcano, has steep flanks, a symmetrical cone shape, and a distinct crater, rising prominently above the surrounding landscape. The term composite refers to the alternating layers of pyroclastic fragments, like ash and bombs, and solidified lava flows of varying composition. Examples include Mount Rainier in Washington State and Mount Fuji in Japan.

Figure 4.46: Mount Fuji in Japan is a typical stratovolcano: symmetrical, increasing slope, visible crater at the top. Figure description available at the end of the chapter.

Stratovolcanoes usually have felsic-to-intermediate magma chambers but can even produce mafic lavas. Stratovolcanoes have viscous lava flows and domes, punctuated by explosive eruptions. This produces volcanoes with steep flanks.

Lava Domes

Figure 4.47: Lava domes have started the rebuilding process at Mount St. Helens, Washington. Figure description available at the end of the chapter.

Lava domes are accumulations of silica-rich volcanic rock, such as rhyolite and obsidian. Too viscous to flow easily, the felsic lava tends to pile up near the vent in blocky masses. Lava domes often form in a vent within the collapsed crater of a stratovolcano and grow by internal expansion. As the dome expands, the outer surface cools, hardens, and shatters, spilling loose fragments down the sides. Mount St. Helens has a good example of a lava dome inside of a collapsed stratovolcano crater. Examples of standalone lava domes are Chaiten in Chile and Mammoth Mountain in California.

Caldera

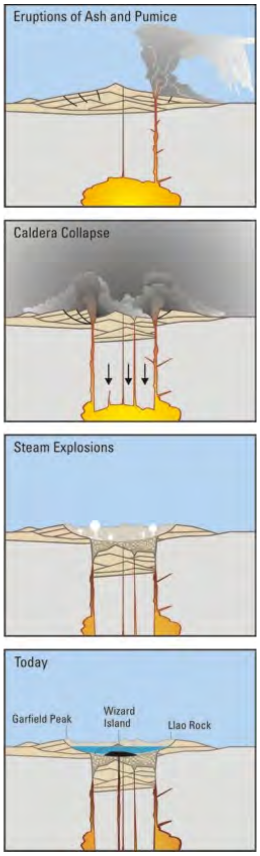

Figure 4.48: Timeline of events at Mount Mazama. Figure description available at the end of the chapter.

Calderas are steep-walled, basin-shaped depressions formed by the collapse of a volcanic edifice into an empty magma chamber. Calderas are generally very large, with **diameters** of up to 25 km (15.5 mi). The term caldera specifically refers to a volcanic vent; however, it is frequently used to describe a volcano type. Caldera volcanoes are typically formed by eruptions of high-viscosity felsic lava with high volatiles content.

Figure 4.49: Wizard Island sits in the caldera at Crater Lake. Figure description available at the end of the chapter.

Crater Lake, Yellowstone, and the Long Valley Caldera are good examples of this type of volcanism. The caldera at Crater Lake National Park in Oregon was created about 6,800 years ago when Mount Mazama, a composite volcano, erupted in a huge explosive blast. The volcano ejected large amounts of volcanic ash and rapidly drained the magma chamber, causing the top to collapse into a large depression that later filled with water. Wizard Island in the middle of the lake is a later resurgent lava dome that formed within the caldera basin.

The Yellowstone volcanic system erupted three times in the recent geologic past—2.1, 1.3, and 0.64 million years ago—leaving behind three caldera basins. Each eruption created large rhyolite lava flows as well as pyroclastic flows that solidified into tuff formations. Each extra-large eruption rapidly emptied its magma chamber, causing the roof to collapse and form a caldera. The youngest of the three calderas contains most of Yellowstone National Park, as well as two resurgent lava domes. The calderas are difficult to see today due to the amount of time since their eruptions and subsequent erosion and glaciation.

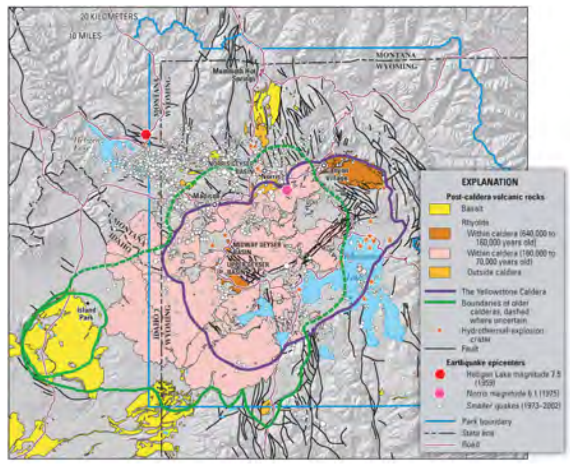

Figure 4.50: Map of calderas and related rocks around Yellowstone. Figure description available at the end of the chapter.

Yellowstone volcanism started about 17 million years ago as a hotspot under the North American lithospheric plate near the Oregon/Nevada border. As the plate moved to the southwest over the stationary hotspot, it left behind a track of past volcanic activities. Idaho's Snake River Plain was created from volcanism that produced a series of calderas and lava flows. The plate eventually arrived at its current location in northwestern Wyoming, where hotspot volcanism formed the Yellowstone calderas.

The Long Valley Caldera near Mammoth, California, is the result of a large volcanic eruption that occurred 760,000 years ago. The explosive eruption dumped enormous amounts of ash across the United States in a manner similar to the Yellowstone eruptions. The Bishop Tuff deposit near Bishop, California, is made of ash from this eruption. The current caldera basin is 17 km by 32 km (10 mi by 20 mi), large enough to contain the town of Mammoth Lakes, a major ski resort, airport, major highway, resurgent dome, and several hot springs.

Figure 4.51: Several prominent ash beds found in North America, including three Yellowstone eruptions shaded pink (Mesa Falls, Huckleberry Ridge, and Lava Creek), the Bisho Tuff ash bed (brown dashed line), and the modern May 18th, 1980, ash fall (yellow). Figure description available at the end of the chapter.

Cinder Cone

Figure 4.52: Sunset Crater in Arizona is a cinder cone. Figure description available at the end of the chapter.

Cinder cones are small volcanoes with steep sides and are made of pyroclastic fragments that have been ejected from a pronounced central vent. The small fragments are called cinders, and the largest are volcanic **bombs**. The eruptions are usually short-lived events, typically consisting of mafic lavas with a high content of volatiles. Hot lava is ejected into the air, cooling and solidifying into fragments that accumulate on the flank of the volcano. Cinder cones are found throughout western North America.

Figure 4.54: Lava from Parícutin covered the local church and destroyed the town of San Juan, Mexico. Figure description available at the end of the chapter.

Figure 4.53: Soon after the birth of Parícutin in 1943. Figure description available at the end of the chapter.

A recent and striking example of a cinder cone is the eruption near the village of Paricutin, Mexico, that started in 1943. The cinder cone started explosively shooting cinders out of the vent in the middle of a farmer's field. The volcanism quickly built up the cone to a height of over 90 m (300 ft) within a week and reached 365 m (1,200 ft) within the first eight months. After the initial explosive eruption of gases and cinders, basaltic lava poured out from the base of the cone. This is a common order of events for cinder cones: violent eruption, cone and crater formation, low-viscosity lava flow from the base. The cinder cone is not strong enough to support a column of lava rising to the top of the crater, so the lava breaks through and emerges near the bottom of the volcano. During nine years of eruption activity, the ashfall covered about 260 km^2 (100 mi^2) and destroyed the nearby town of San Juan.

Flood Basalts

A rare volcanic eruption type, unobserved in modern times, is the flood basalt. **Flood basalts** are some of the largest and lowest viscosity eruptions known. Since no such eruption has occurred in human history, their exact mechanisms of eruption are still mysterious. Some famous examples include the Columbia River flood basalts in Washington, Oregon, and Idaho, the **Deccan Traps**, which cover about a third of the country of India, and the Siberian Traps, which may have been involved in the Earth's largest mass extinction (see Chapter 8).

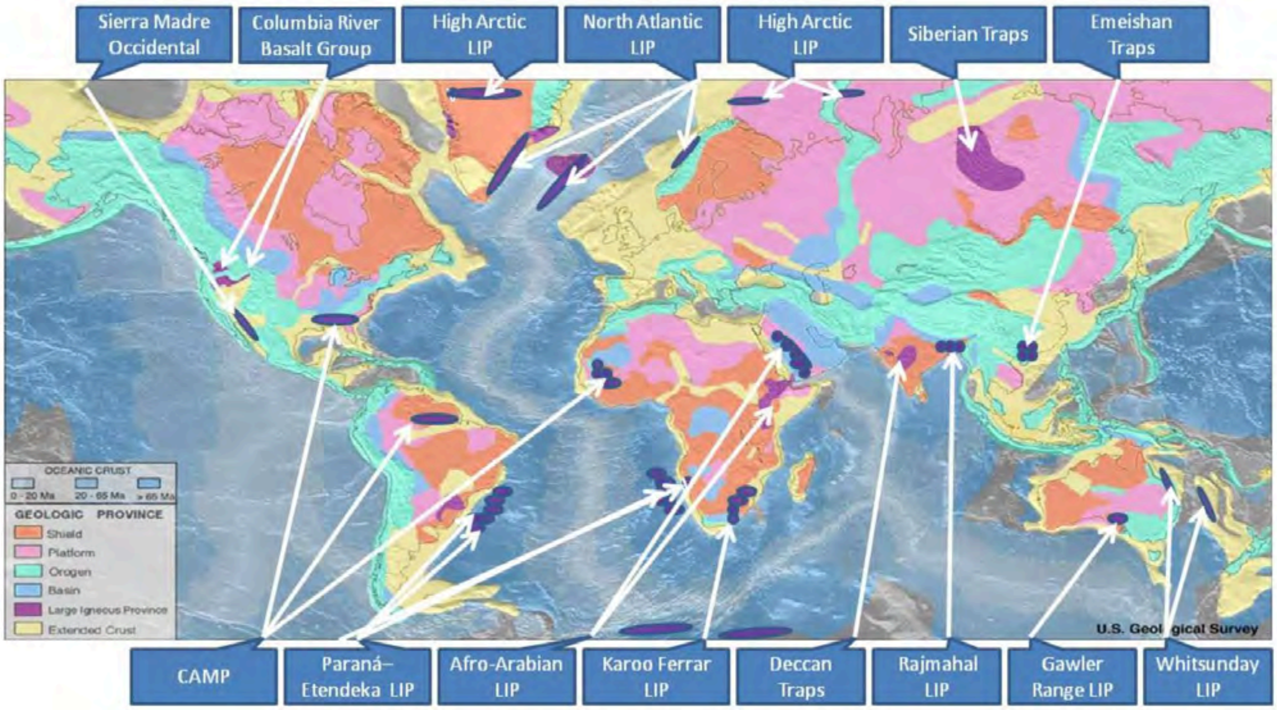

Figure 4.55: World map of flood basalts. Note the largest is the Siberian Traps. Figure description available at the end of the chapter.

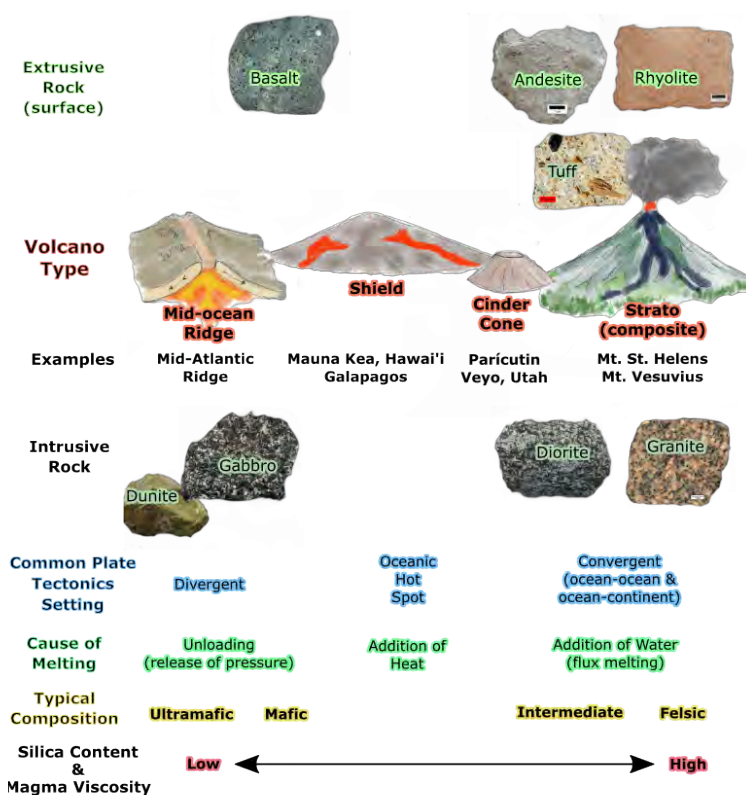

Figure 4.56: Igneous rock types and related volcano types. Mid-ocean ridges and shield volcanoes represent more mafic compositions, and strato (composite) volcanoes generally represent a more intermediate or felsic composition and a convergent plate tectonic boundary. Note that there are exceptions to this generalized layout of volcano types and igneous rock composition. Figure description available at the end of the chapter.

4.4.3 Volcanic Hazards and Monitoring

While the most obvious volcanic hazard is lava, the dangers posed by volcanoes go far beyond lava flows. For example, on May 18, 1980, Mount St. Helens (Washington, United States) erupted with an explosion and landslide that removed the upper 400 m (1,300 ft) of the mountain. The initial explosion was immediately followed by a lateral blast, which produced a pyroclastic flow that covered nearly 600 km^2 (230 mi^2) of forest with hot ash and debris. The pyroclastic flow moved at speeds of 80–130 kph (50–80 mph), flattening trees and ejecting clouds of ash into the air. The USGS video provides an account of this explosive eruption that killed 57 people.

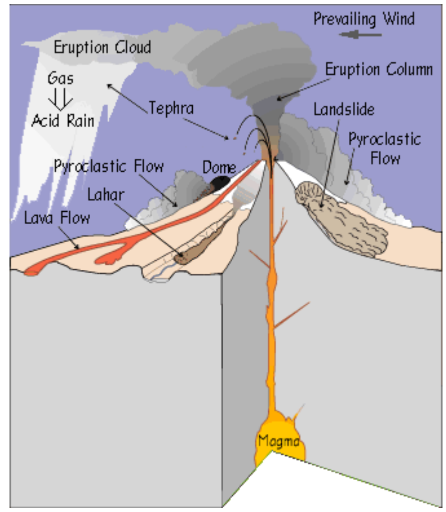

Figure 4.57: General diagram of volcanic hazards. Figure description available at the end of the chapter.

Video 4.6: Mount St. Helens

Access this YouTube video by scanning the QR code. ["Mount St. Helens: May 18, 1980" by USGS | https://www.youtube.com/watch?v=Ec30uU0G56U]

Figure 4.58: Human remains from the 79 CE eruption of Vesuvius. Figure description available at the end of the chapter.

In 79 CE, Mount Vesuvius, located near Naples, Italy, violently erupted, sending a pyroclastic flow over the Roman countryside, including the cities of Herculaneum and Pompeii. The buried towns were discovered in an archeological expedition in the eighteenth century. Pompeii famously contains the remains of people (in the form of **casts**) suffocated by ash and covered by 3 m (10 ft) of ash, pumice lapilli, and collapsed roofs.

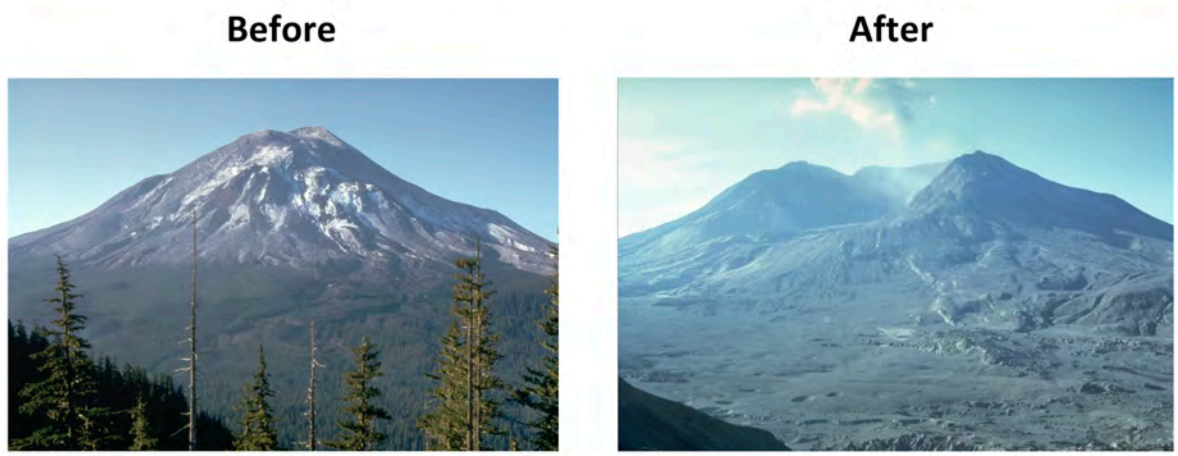

Figure 4.59: Mount St. Helens, the day before the May 18th, 1980, eruption (left) and four months after the major eruption (right). Figure description available at the end of the chapter.

Figure 4.60: Image from the May 18, 1980, eruption of Mount St. Helens, Washington. Figure description available at the end of the chapter.

Pyroclastic Flows

Figure 4.61: The material coming down from the eruption column is a pyroclastic flow. Figure description available at the end of the chapter.

The most dangerous volcanic hazard are **pyroclastic flows**. These flows are a mix of lava blocks, pumice, ash, and hot gases between 200˚C–700˚C (400˚F–1300˚F). The turbulent cloud of ash and gas races down the steep flanks at high speeds up to 193 kph (120 mph) into the valleys around composite volcanoes. Most explosive, silica-rich, high-viscosity magma volcanoes such as composite cones usually have pyroclastic flows. The rocks tuff and welded tuff are often formed from these pyroclastic flows.

There are numerous examples of deadly pyroclastic flows. In 2014, the Mount Ontake pyroclastic flow in Japan killed 47 people. The flow was caused by magma heating groundwater into steam, which then rapidly ejected with ash and volcanic bombs. Some people were killed by inhalation of toxic gases and hot ash, while others were struck by volcanic bombs. Another example is the Caribbean Island of Martinique, where, in 1902, Mount Pelee erupted with a violent pyroclastic flow that destroyed the entire town of St. Pierre and killed 28,000 people in moments. Video 4.7 documents an eye witness account in the early 1900s, when Mount Unzen erupted several times with pyroclastic flows. The pyroclastic flow shown in this famous short video killed 41 people.

Figure 4.62: The remains of St. Pierre. Figure description available at the end of the chapter.

Video 4.7: Dome collapse and pyroclastic flow at Unzen Volcano

Access this YouTube video by scanning the QR code. ["Dome collapse and pyroclastic flow at Unzen Volcano" by DrChristopher-Gomez | https://www.youtube.com/watch?v=Cvjwt9nnwXY]

Landslides and Landslide-Generated Tsunamis

The steep and unstable flanks of a volcano can lead to slope failure and dangerous landslides. These landslides can be **triggered** by magma movement, explosive eruptions, large earthquakes, and/or heavy rainfall. During the 1980 Mount St. Helens eruption, the entire north flank of the volcano collapsed and released a huge landslide that moved at speeds of 160–290 kph (100–180 mph).

If enough landslide material reaches the ocean, it may cause a tsunami. In 1792, a landslide caused by an Mount Unzen eruption reached the Ariaka Sea, generating a tsunami that killed 15,000 people. When Mount Krakatau in Indonesia erupted in 1883, it generated ocean waves that towered 40 m (131 ft) above sea level. The tsunami killed 36,000 people and destroyed 165 villages.

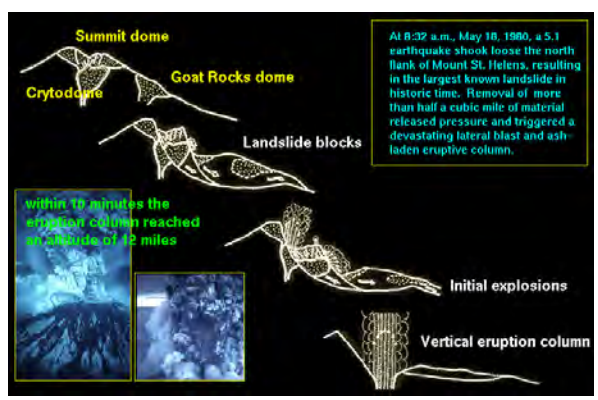

Figure 4.63: Sequence of events for Mount St. Helens, May 18th, 1980. Note that an earthquake caused a landslide, which caused the "uncorking" of the mountain and started the eruption. Figure description available at the end of the chapter.

Tephra

Figure 4.64: A man sweeps ash from an eruption of Kelud, Indonesia. Figure description available at the end of the chapter.

Volcanoes, especially composite volcanoes, eject large amounts of tephra (ejected rock materials), most notably ash (tephra fragments less than 2 mm [0.08 in]). Larger tephra is heavier and falls closer to the vent. Larger blocks and bombs pose hazards to those close to the eruption, as was the case with the 2014 Mount Ontake disaster in Japan discussed earlier.

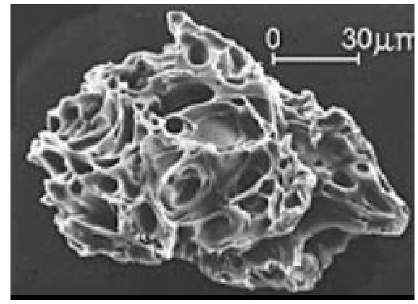

Figure 4.65: Micrograph of silica particle in volcanic ash. A cloud of these is capable of destroying an aircraft or automobile engine. Figure description available at the end of the chapter.

Hot ash poses an immediate danger to people, animals, plants, machines, roads, and buildings located close to the eruption. Ash is fine grained (< 2mm) and can travel airborne long distances away from the eruption site. Heavy accumulations of ash can cause buildings to collapse. In people, it may cause respiratory issues like silicosis. Ash is destructive to aircraft and automobile engines, capable of disrupting transportation and shipping services. In 2010, the Eyjafjallajökull volcano in Iceland emitted a large ash cloud into the upper atmosphere, causing the largest air-travel disruption in Northern Europe since World War II. No one was injured, but the service disruption was estimated to have cost the world economy billions of dollars.

Volcanic Gases

As magma rises to the surface, the confining pressure decreases and allows dissolved gases to escape into the atmosphere. Even volcanoes that are not actively erupting may emit hazardous gases, such as carbon dioxide (CO_2), sulfur dioxide (SO_2), hydrogen sulfide (H_2S), and hydrogen halides (HF, HCl, or HBr).

Carbon dioxide tends to sink and accumulate in depressions and basins. In volcanic areas known to emit carbon dioxide, low-lying areas may trap hazardous concentrations of this colorless and odorless gas. The Mammoth Mountain Ski Resort in California is located within the Long Valley Caldera, which is one such area of carbon dioxide-producing volcanism. In 2006, three ski patrol members died of suffocation caused by carbon dioxide after falling into a snow depression near a fumarole (info).

In rare cases, volcanism may create a sudden emission of gases without warning. Limnic eruptions (*limne* is Greek for lake) occur in crater lakes associated with active volcanism. The water in these lakes is supercharged with high concentrations of dissolved gases. If the water is physically jolted by a landslide or earthquake, it may trigger an immediate and massive release of gases out of solution. An analogous example would be what happens to a vigorously shaken bottle of carbonated soda when the cap is opened. An infamous limnic eruption occurred in 1986 at Lake Nyos, Cameroon. Almost 2,000 people were killed by a massive release of carbon dioxide.

Lahars

Lahar is an Indonesian word used to describe a volcanic mudflow that forms from rapidly melting snow or glaciers. Lahars are slurries resembling wet concrete and consisting of water, ash, rock fragments, and other debris. These mudflows flow down the flanks of volcanoes or mountains covered with freshly erupted ash and on steep slopes can reach speeds of up to 80 kph (50 mph).

Figure 4.66: Mud line shows the extent of lahars around Mount St. Helens. Figure description available at the end of the chapter.

Several major cities, including Tacoma, are located on prehistoric lahar flows that extend for many kilometers across the flood plains surrounding Mount Rainier in Washington (see Figure 4.67). A map of Mount Baker in Oregon shows a similar potential hazard for lahar flows. A tragic scenario played out recently, in 1985, when a lahar from the Nevado del Ruiz volcano in Colombia buried the town of Armero and killed an estimated 23,000 people.

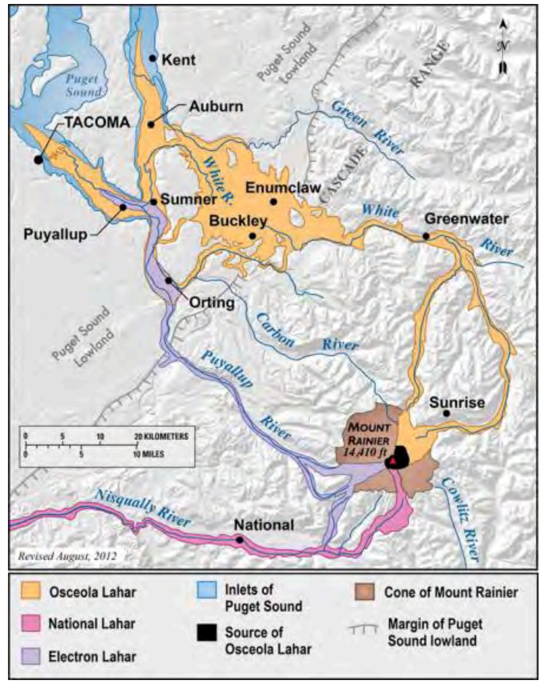

Figure 4.67: Old lahars around Tacoma, Washington. Figure description available at the end of the chapter.

Monitoring

Geologists use various instruments to detect changes or indications that an eruption is imminent. Videos 4.8 through 4.10 show different types of volcanic monitoring used to predict eruptions: (1) earthquake activity, (2) increases in gas emission, and (3) changes in land surface orientation and elevation.

One video shows how monitoring earthquake frequency, especially special vibrational earthquakes called harmonic tremors, can detect magma movement and possible eruption. Another video shows how gas monitoring may be used to predict an eruption. A rapid increase of gas emission may indicate magma that is actively rising to surface and releasing dissolved gases out of solution and that an eruption is imminent. The last video shows how a GPS unit and tiltmeter can detect land surface changes, indicating that magma is moving underneath it.

Video 4.8: Earthquake signals

Access this YouTube video by scanning the QR code. ["Volcano Monitoring—Earthquake signals (educational)" by IRIS Earthquake Science | https://www.youtube.com/watch?v=nlo-2JoNHrw]

Video 4.9: Measuring gas emissions

Access this YouTube video by scanning the QR code. ["Volcano Monitoring—Measuring Gas emmisions
" by IRIS Earthquake Science | https://www.youtube.com/watch?v=owk4fWbw4qM]

Video 4.10: Using tiltmeters and GPS to monitor a volcano

Access this YouTube video by scanning the QR code. ["Volcano Monitoring_Deformation measured with tilt meter and GPS" by IRIS Earthquake Science | https://www.youtube.com/watch?v=sNYQkxxd_0Q]

Take this quiz to check your comprehension of this section.

Access the quiz for Section 4.4 by scanning the QR code.

Summary

Igneous rock is divided into two major groups: intrusive rock that solidifies from underground magma and extrusive rock that forms from lava that erupts and cools on the surface. Magma is generated from mantle material in several plate tectonic situations by three types of melting: decompression melting, flux melting, or heat-induced melting. Magma composition is determined by differences in the melting temperatures of the mineral components (Bowen's reaction series). The processes affecting magma composition include partial melting, magmatic differentiation, assimilation, and collision. Volcanoes come in a wide variety of shapes and sizes and are classified by multiple factors, including magma composition and plate tectonic activity. Because volcanism presents serious hazards to human civilization, geologists carefully monitor volcanic activity to mitigate or avoid the dangers it presents.

Take this quiz to check your comprehension of this chapter.

Access the quiz for Chapter 4 by scanning the QR code.

Chapter URLs

- Ski patrol's fatal fall into a volcanic fumarole: https://pubmed.ncbi.nlm.nih.gov/19364170

Text References

1. Arndt, N.T. (1994). Chapter 1: Archean Komatiites, in K.C. Condie (ed.), *Developments in Precambrian Geology:* Elsevier, p. 11–44.
2. Bateman, P.C., and Chappell, B.W. (1979). Crystallization, fractionation, and solidification of the Tuolumne Intrusive Series, Yosemite National Park, California. *Geological Society of America Bulletin, 90*(5), 465–482. doi: 10.1130/0016-7606(1979)90<465:CFASOT>2.0.CO;2
3. Boehler, R. (1996). Melting temperatures of the Earth's mantle and core: Earth's thermal structure. *Annual Review of Earth and Planetary Sciences, 24*(1), 15–40., doi: 10.1146/annurev.earth.24.1.15.
4. Bowen, N.L. (1922). The reaction principle in petrogenesis. *J. Geol., 30*(3), 177–198.
5. Bowen, N.L. (1928). *The evolution of the igneous rocks:* Dover Publications.
6. Carr, M.H. (1975). Geologic map of the Tharsis Quadrangle of Mars. *IMAP.*
7. Earle, S. (2015). *Physical Geology OER textbook:* BC Campus OpenEd.
8. EarthScope (2014). Mount Ontake Volcanic Eruption. Online, http://www.earthscope.org/science/geo-events/mount-ontakevolcanic-eruption, accessed July 2016.
9. Frankel, C. (2005). *Worlds on fire: Volcanoes on the Earth, the Moon, Mars, Venus and Io:* Cambridge University Press.
10. Glazner, A.F., Bartley, J.M., Coleman, D.S., Gray, W., and Taylor, R.Z. (2004). Are plutons assembled over millions of years by amalgamation from small magma chambers? *GSA Today, 14*(4), 4. doi: 10.1130/1052-5173(2004)014<0004:APAOMO>2.0.CO;2.
11. Luongo, G., Perrotta, A., Scarpati, C., De Carolis, E., Patricelli, G., and Ciarallo, A. (2003). Impact of the AD 79 explosive eruption on Pompeii, II. Causes of death of the inhabitants inferred by stratigraphic analysis and areal distribution of the human casualties. *J. Volcanol. Geotherm. Res., 126*(3–4), 169–200.
12. Mueller, S., and Phillips, R.J. (1991). On the initiation of subduction. *J. Geophys. Res. [Solid Earth], 96*(B1), 651–665.
13. Peacock, M.A. (1931). Classification of igneous rock series. *The Journal of Geology, 39*(1), 54–67.
14. Perkins, S. (2011). 2010's volcano-induced air travel shutdown was justified. Online, http://www.sciencemag.org/ news/2011/04/

2010s-volcano-induced-air-travel-shutdown-was-justified, accessed July 2016.
15. Peterson, D.W., and Tilling, R.I. (1980). Transition of basaltic lava from pahoehoe to aa, Kilauea Volcano, Hawaii: Field observations and key factors – ScienceDirect. *J. Volcanol. Geotherm. Res., 7*(3–4), 271–293.
16. Petrini, K., and Podladchikov, Y. (2000). Lithospheric pressure–depth relationship in compressive regions of thickened crust. *Journal of Metamorphic Geology, 18*(1), 67–77. doi: 10.1046/j.1525-1314.2000.00240.x.
17. Reid, J.B., Evans, O.C., and Fates, D.G. (1983). Magma mixing in granitic rocks of the central Sierra Nevada, California. *Earth and Planetary Science Letters, 66*, 243–261. doi: 10.1016/0012-821X(83)90139-5.
18. Rhodes, J.M., and Lockwood, J.P. (1995). Mauna Loa revealed: Structure, composition, history, and hazards. *Washington DC American Geophysical Union Geophysical Monograph Series,* 92.
19. Scandone, R., Giacomelli, L., and Gasparini, P. (1993). Mount Vesuvius: 2000 years of volcanological observations. *Journal of Volcanology and Geothermal Research, 58*, 5–25.
20. Stovall, W.K., Wilkins, A.M., Mandeville, C.W., and Driedger, C.L. (2016). Fact Sheet. United States Geological Survey.
21. Thorarinsson, S. (1969). The Lakagigar eruption of 1783. *Bull. Volcanol., 33*(3), 910–929.
22. Tilling, R.I. (2008). The critical role of volcano monitoring in risk reduction. *Adv. Geosci., 14*, 3–11.
23. United States Geological Survey (1999). Exploring the deep ocean floor. Online, http://pubs.usgs.gov/gip/dynamic/exploring.html, accessed July 2016.
24. United States Geological Survey (2012) Black Rock Desert volcanic field. Online, http://volcanoes.usgs.gov/volcanoes/black_rock_desert/, accessed July 2016.
25. United States Geological Survey (1997). Other volcanic structures. Online, https://pubs.usgs.gov/gip/volc/structures.html, accessed September 2024.
26. United States Geological Survey (2001). Dual volcanic tragedies in the Caribbean led to founding of HVO. Online, http://hvo.wr.usgs.gov/volcanowatch/archive/2001/01_05_03.html, accessed July 2016.
27. United States Geological Survey (2011). Volcanoes: Principal types of volcanoes. Online, http://pubs.usgs.gov/gip/volc/types.html, accessed July 2016.
28. United States Geological Survey (2012a). USGS: Volcano hazards program. Online, https://volcanoes.usgs.gov/vhp/hazards.html, accessed July 2016.
29. United States Geological Survey (2012b). Yellowstone Volcano Observatory: Online, https://volcanoes.usgs.gov/volcanoes/yellowstone/yellowstone_geo_hist_52.html, accessed July 2016.
30. United States Geological Survey (2016). Volcanoes general – What are the different types of volcanoes? Online, https://www2.usgs.gov/faq/cat-egories/ 9819/2730, accessed March 2017.
31. USGS (2017). The volcanoes of Lewis and Clark – Mount St. Helens. Online, https://volcanoes.usgs.gov/observatories/ cvo/Historical/LewisClark/Info/summary_mount_st_helens.shtml, accessed March 2017.
32. Wallace, P.J. (2005). Volatiles in subduction zone magmas: Concentrations and fluxes based on melt inclusion and volcanic gas data. *Journal of Volcanology and Geothermal Research, 140*(1–3), 217–240. doi: 10.1016/j.jvolgeo-res.2004.07.023.
33. Williams, H. (1942). *The geology of Crater Lake National Park, Oregon: With a reconnaissance of the Cascade Range southward to Mount Shasta:* Carnegie institution.

Figure References

Figure 4.1: Lava flow in Hawai'i. Brocken Inaglory. 2007. CC BY-SA 3.0. https://commons.wikimedia.org/wiki/File:P%C4%81hoehoe_and_Aa_flows_at_Hawaii.jpg

Figure 4.2: Half Dome, an intrusive igneous batholith in Yosemite National Park. Jon Sullivan. 2004. Public domain. https://commons.wikimedia.org/wiki/File:Yosemite_20_bg_090404.jpg

Figure 4.3: Granite is a classic coarse-grained (phaneritic) intrusive igneous rock. Laura Neser. September 2024. CC BY-NC.

Figure 4.4: Basalt is a classic fine-grained extrusive igneous rock. James St. John. 2019. CC BY 2.0. https://commons.wikimedia.org/wiki/File:Basalt_3_(48674276863).jpg

Figure 4.5: Porphyritic texture. Jstuby. 2008. Public domain. https://commons.wikimedia.org/wiki/File:Olearyandesite.jpg

Figure 4.6: Pegmatitic texture. Jstuby. 2007. Public domain. https://commons.wikimedia.org/wiki/File:We-pegmatite.jpg

Figure 4.7: Scoria. Jonathan Zander (Digon3). 2008. CC BY-SA 3.0. https://commons.wikimedia.org/wiki/File:Scoria_Macro_Digon3.jpg

Figure 4.8: Pumice. deltalimatrieste. 2008. Public domain. https://commons.wikimedia.org/wiki/File:Pomice_di_veglia.jpg

Figure 4.9: Obsidian (volcanic glass). Note conchoidal fracture. Ji-Elle. 2011. CC BY-SA 3.0. https://commons.wikimedia.org/wiki/File:Lipari-Obsidienne_(5).jpg

Figure 4.10: Welded tuff. Wilson44691. 2010. Public domain. https://commons.wikimedia.org/wiki/File:HoleInTheWallTuff.jpg

Figure 4.11: Mineral composition of common igneous rocks. Woudloper. 2009. Public domain. https://commons.wikimedia.org/wiki/File:Mineralogy_igneous_rocks_EN.svg

Figure 4.12: Igneous rock classification table with composition as vertical columns and texture as horizontal rows. Kindred Grey. 2022. Adapted from Belinda Madsen, *An Introduction to Geology*. OpenStax. Salt Lake Community College. CC BY-NC-SA 4.0.

Table 4.1: Aphanitic and phaneritic rock types with images. Quartz monzonite 36mw1037 by B.W. Hallett, V. F. Paskevich, L.J. Poppe, S.G. Brand, and D.S. Blackwood via USGS (Public domain, https://commons.wikimedia.org/wiki/File:Quartz_monzonite_36mw1037.jpg). PinkRhyolite by Michael C. Rygel, 2014 (CC BY-SA 3.0, https://commons.wikimedia.org/wiki/File:PinkRhyolite.tif). Diorite MA by Amcyrus2012, 2015 (CC BY 4.0, https://commons.wikimedia.org/wiki/File:Diorite_MA.JPG). Andesite by James St. John, 2014 (CC BY 2.0, https://flic.kr/p/oBkKSy). GabbroRockCreek1 by Mark A. Wilson, 2008 (Public domain, https://commons.wikimedia.org/wiki/File:Gabbro-RockCreek1.jpg). VesicularBasalt1 by Jstuby, 2008 (Public domain, https://commons.wikimedia.org/wiki/File:VesicularBasalt1.jpg).

Figure 4.13: Dike of olivine gabbro cutting across Baffin Island in the Canadian Arctic. Mike Beauregard. 2012. CC BY 2.0. https://en.wikipedia.org/wiki/File:Franklin_dike_on_northwestern_Baffin_Island.jpg

Figure 4.14: Igneous sill intruding between Paleozoic strata in Nova Scotia. Mikenorton. 2010. CC BY-SA 3.0. https://commons.wikimedia.org/wiki/File:Horton_Bluff_mid-Carboniferous_sill.JPG

Figure 4.15: Quartz monzonite from the Cretaceous in Montana, USA. James St. John. 2010. CC BY 2.0. https://commons.wikimedia.org/wiki/File:Butte_Quartz_Monzonite_(Late_Cretaceous,_76_Ma;_Rampart_Mountain,_northeast_of_Butte,_Montana,_USA)_1.jpg

Figure 4.16: Half Dome in Yosemite National Park, California, is a part of the Sierra Nevada batholith, which is mostly made of granite. Jon Sullivan. 2004. Public domain. https://commons.wikimedia.org/wiki/File:Yosemite_20_bg_090404.jpg

Figure 4.17: The Henry Mountains in Utah are interpreted to be a laccolith, exposed by erosion of the overlying layers. Steven Mahoney. 2005. CC BY-SA 2.5. https://commons.wikimedia.org/wiki/File:Henry_Mountains,_Utah,_2005-06-01.jpg

Figure 4.18: Laccolith forms as a blister between sedimentary strata. Erimus and Stannered. 2007. Public domain. https://commons.wikimedia.org/wiki/File:Laccolith.svg

Figure 4.19: Bowen's reaction series. Colivine. 2011. Public domain. https://commons.wikimedia.org/wiki/File:Bowen%27s_Reaction_Series.png

Figure 4.20: Olivine, the first mineral to crystallize in a melt. S kitahashi. 2006. CC BY-SA 3.0. https://commons.wikimedia.org/wiki/File:Peridot2.jpg

Figure 4.21: Norman L. Bowen. Unknown author. 1909. Public domain. https://commons.wikimedia.org/wiki/File:NormanLBowen_1909.jpg

Figure 4.22: Norman L. Bowen and his colleague working at the Carnegie Institution of Washington Geophysical Laboratory. Smithsonian Institution. 2010. Public domain. https://commons.wikimedia.org/wiki/File:(left_to_right)-_Norman_Levi_Bowen_(1887-1956)_and_Orville_Frank_Tuttle_(1916-1983)_(4730112454)_(cropped).jpg

Figure 4.23: Geothermal gradient. Bkilli1. 2013. CC BY-SA 3.0. https://commons.wikimedia.org/wiki/File:Temperature_schematic_of_inner_Earth.jpg

Figure 4.24: Pressure-temperature diagram showing temperature in degrees Celsius on the x-axis and depth below the surface in kilometers (km) on the y-axis. Kindred Grey. 2022. CC BY-SA 3.0. Adapted from Partial melting asthenosphere EN by Woudloper, 2010 (CC BY-SA 3.0, https://commons.wikimedia.org/wiki/File%3APartial_melting_asthenosphere_EN.svg).

Figure 4.25: Association of volcanoes with plate boundaries. Jose F. Vigil via USGS. 1997. Public domain. https://commons.wikimedia.org/wiki/File:Tectonic_plate_boundaries.png

Figure 4.26: Map of spreading ridges throughout the world. Eric Gaba. 2006. CC BY-SA 2.5. https://commons.wikimedia.org/wiki/File:Spreading_ridges_volcanoes_map-fr.svg

Figure 4.27: Pillow basalt on seafloor near Hawai'i. National Oceanic and Atmospheric Administration (NOAA). 1988. Public domain. https://commons.wikimedia.org/wiki/File:Nur05018-Pillow_lavas_off_Hawaii.jpg

Figure 4.28: Black smoker hydrothermal vent with a colony of giant (6'+) tube worms. NOAA. 2006. Public domain. https://commons.wikimedia.org/wiki/File:Main_Endeavour_black_smoker.jpg

Figure 4.29: Distribution of hydrothermal vent fields. DeDuijn. 2016. CC BY-SA 4.0. https://commons.wikimedia.org/wiki/File:Distribution_of_hydrothermal_vent_fields.png

Figure 4.30: Distribution of volcanoes on the planet. USGS. 2007. Public domain. https://commons.wikimedia.org/wiki/File:Map_plate_tectonics_world.gif

Figure 4.31: Basaltic cinder cones on the flank of Mauna Kea. Laura Neser. June 2022. CC BY-NC.

Figure 4.32: Diagram showing a nonmoving source of magma (mantle plume) and a moving overriding plate. Los688. 2008. Public domain. https://en.wikipedia.org/wiki/File:Hotspot(geology)-1.svg

Figure 4.33: The track of the Yellowstone hotspot, which shows the age of different eruptions in millions of years ago. Kelvin Case. 2013. CC BY 3.0. https://commons.wikimedia.org/wiki/File:HotspotsSRP_update2013.JPG

Figure 4.34: The Hawaiian–Emperor seamount and island chain. Ingo Wölbern. 2008. Public domain. https://commons.wikimedia.org/wiki/File:Hawaii-Emperor_engl.png

Figure 4.35: Stratovolcano. MesserWoland. CC BY-SA.

Figure 4.36: Oregon's Crater Lake was formed about 7,700 years ago after the eruption of Mount Mazama. Zainubrazvi. 2006. CC BY-SA 3.0. https://en.wikipedia.org/wiki/File:Crater_lake_oregon.jpg

Figure 4.37: Kilauea Summit in Hawai'i. Laura Neser. June 2022. CC BY-NC.

Figure 4.38: Eruption of Kilauea in 2018 produced high-viscosity lava, shown here crossing a road. USGS. 2018. Public domain. https://commons.wikimedia.org/wiki/File:USGS_K%C4%ABlauea_multimediaFile-1955.jpg

Figure 4.39: Olympus Mons, an enormous shield volcano on Mars, the largest volcano in the solar system, standing about two-and-a-half times higher than Everest is above sea level. NASA. 1978. Public domain. https://en.wikipedia.org/wiki/File:Olympus_Mons_alt.jpg

Figure 4.40: Ropey pahoehoe lava cooled into basalt. Laura Neser. June 2022. CC BY-NC.

Figure 4.41: Blocky aa lava. Librex. 2009. CC BY 2.0. https://commons.wikimedia.org/wiki/File:Lava_del_Volcan_Pacaya_2009-11-28.jpg

Figure 4.42: Devils Tower in Wyoming has columnar jointing. Laura Neser. 2012. CC BY-NC.

Figure 4.43: Columnar jointing on Giant's Causeway in Ireland. Udri. 2014. CC BY-NC-SA 2.0. https://flic.kr/p/2j1mgwE

Figure 4.44: Shiprock, located in New Mexico, is the erosional remnant of the throat of a volcano, referred to as a volcanic neck. Mary Lou Mortimer. March 2022. CC BY 3.0.

Figure 4.45: Mount Rainier towers over Tacoma, Washington. Lyn Topinka via USGS. 1984. Public domain. https://commons.wikimedia.org/wiki/File:Mount_Rainier_over_Tacoma.jpg

Figure 4.46: Mount Fuji in Japan is a typical stratovolcano: symmetrical, increasing slope, visible crater at the top. Alpsdake. 2016. CC BY-SA 4.0. https://commons.wikimedia.org/wiki/File:Numazu_and_Mount_Fuji.jpg

Figure 4.47: Lava domes have started the rebuilding process at Mount St. Helens, Washington. Willie Scott via United States Geological Survey (USGS). 2006. Public domain. https://commons.wikimedia.org/wiki/File:MSH06_aerial_crater_from_north_high_angle_09-12-06.jpg

Figure 4.48: Timeline of events at Mount Mazama. USGS and NPS. 2006. Public domain. https://commons.wikimedia.org/wiki/File:Mount_Mazama_eruption_timeline.PNG

Figure 4.49: Wizard Island sits in the caldera at Crater Lake. Don Graham. 2006. CC BY-SA 2.0. https://commons.wikimedia.org/wiki/File:Crater_Lake_National_Park,_OR_2006_(6539577313).jpg

Figure 4.50: Map of calderas and related rocks around Yellowstone. USGS. 1905. Public domain. https://www.usgs.gov/media/images/simplified-map-yellowstone-caldera

Figure 4.51: Several prominent ash beds found in North America, including three Yellowstone eruptions shaded pink (Mesa Falls, Huckleberry Ridge, and Lava Creek), the Bisho Tuff ash bed (brown dashed line), and the modern May 18th, 1980, ash fall (yellow). USGS. 2005. Public domain. https://commons.wikimedia.org/wiki/File:Yellowstone_volcano_-_ash_beds.svg

Figure 4.52: Sunset Crater, Arizona is a cinder cone. NPS. Unknown date. Public domain. https://commons.wikimedia.org/wiki/File:Sunset_Crater10.jpg

Figure 4.53: Soon after the birth of Parícutin in 1943. K. Segerstrom via USGS. 1943. Public domain. https://commons.wikimedia.org/wiki/File:Paricutin_30_612.jpg

Figure 4.54: Lava from Parícutin covered the local church and destroyed the town of San Juan, Mexico. Sparksmex. 2007. Public domain. https://commons.wikimedia.org/wiki/File:Paricutin2.jpg

Figure 4.55: World map of flood basalts. Williamborg. 2011. CC BY-SA 3.0. https://commons.wikimedia.org/wiki/File:Flood_Basalt_Map.jpg

Figure 4.56: Igneous rock types and related volcano types. Unknown author. Unknown date. Personal use. https://www.seekpng.com/ipng/u2t4y3r5o0r5r5w7_table-of-igneous-rocks-and-related-volcano-types

Figure 4.57: General diagram of volcanic hazards. USGS. 2008. Public domain. https://pubs.usgs.gov/fs/fs002-97/old%20html%20files

Figure 4.58: Human remains from the 79 CE eruption of Vesuvius. Gary Todd. 2019. Public domain. https://commons.wikimedia.org/wiki/File:Pompeii_Ruins_Cast_of_Human_Victim_at_Villa_of_the_Mysteries_(48445486616).jpg

Figure 4.59: Mount St. Helens, the day before the May 18th, 1980, eruption (left) and four months after the major eruption (right). Mount St. Helens, one day before the devastating eruption by Harry Glicken, USGS/CVO, 1980 (Public domain, https://commons.wikimedia.org/wiki/File:Mount_St._Helens,_one_day_before_the_devastating_eruption.jpg). MSH80 st helens from johnston ridge 09-10-80 by Harry Glicken via USGS (Public domain, https://commons.wikimedia.org/wiki/File:MSH80_st_helens_from_johnston_ridge_09-10-80.jpg).

Figure 4.60: Image from the May 18, 1980, eruption of Mount St. Helens, Washington. Austin Post via USGS. 1980. Public domain. https://commons.wikimedia.org/wiki/File:MSH80_eruption_mount_st_helens_05-18-80-dramatic-edit.jpg

Figure 4.61: The material coming down from the eruption column is a pyroclastic flow. C.G. Newhall via USGS. 1984. Public domain. https://en.wikipedia.org/wiki/File:Pyroclastic_flows_at_Mayon_Volcano.jpg#:~:text=English%3A%20Pyroclastic%20flows%20at%20Mayon,50%20km%20toward%20the%20west.

Figure 4.62: The remains of St. Pierre. Angelo Heilprin. 1902. Public domain. https://commons.wikimedia.org/wiki/File:Pelee_1902_3.jpg

Figure 4.63: Sequence of events for Mount St. Helens, May 18th, 1980. Lyn Topinka via USGS. 1998. Public domain. https://commons.wikimedia.org/wiki/File:Msh_may18_sequence.gif

Figure 4.64: A man sweeps ash from an eruption of Kelud, Indonesia. Crisco 1492. 2014. CC BY-SA 3.0. https://commons.wikimedia.org/wiki/File:Ash_in_Yogyakarta_during_the_2014_eruption_of_Kelud_01.jpg

Figure 4.65: Micrograph of silica particle in volcanic ash. USGS. 1980. Public domain. https://volcanoes.usgs.gov/volcanic_ash/components_ash.html

Figure 4.66: Mud line shows the extent of lahars around Mount St. Helens. USGS. 1980. Public domain. https://www.usgs.gov/media/images/lahars-resulting-may-18-1980-eruption-mount-st-helens

Figure 4.67: Old lahars around Tacoma, Washington. USGS. 1905. Public domain. https://www.usgs.gov/media/images/lahar-pathways-events-heading-mount-rainier-map-showing-t

Figure Descriptions

Figure 4.1: Stream of orange molten lava traveling down gently sloping hill of cooled black and gray volcanic rock.

Figure 4.2: The granite formation rises against a backdrop of blue sky and gray mountains. Half Dome's distinct shape, with its sheer vertical face on one side and smooth, rounded surface on the other, is prominently displayed.

Figure 4.3: Hand holding a rectangular chunk of rock that contains large, easily visible mineral grains of various colors including pink, white, gray, and black.

Figure 4.4: Sample of basalt that is dull black without any clearly visible grains.

Figure 4.5: Dull grayish tan rock sample that contains large. easily visible tan mineral grains embedded within a finer-grained grayish tan groundmass.

Figure 4.6: Tan-to-black rock sample containing very large shiny crystals.

Figure 4.7: A round-shaped sample of dull black lava rock full of small air holes.

Figure 4.8: A round-shaped sample of dull white lava rock full of small air holes.

Figure 4.9: An angular chunk of shiny black volcanic glass that has a conchoidal fracture.

Figure 4.10: Dull tan rock made from volcanic ash that contains numerous various- sized angular fragments of other volcanic materials embedded, ranging from tan to black in color.

Figure 4.11: Rectangular diagram with the following axis labels: on the left-hand vertical axis is "vol % of minerals" which increases from 0 at the bottom to 100 at the top; on the bottom horizontal axis is "wt% SiO2" which increases from 40 at the right-hand side to 70 at the left-hand side; and on the top horizontal axis are the following rock names: rhyolite and granite on the left, then dacite and granodiorite to the right of those, then andesite and diorite to the right of those, then basalt and gabbro to the right of those, and finally komatiite and peridotite to the far right. Inside the rectangular diagram are color-coded mineral names: tan orthoclase fills the upper left of the rectangle, then gray quartz is parallel to the right of orthoclase, then white plagioclase to the right of quartz, dark gray pyroxene to the right of that, and olive-green olivine filling the far right- hand side of the rectangle. At the lower left of the rectangle are cream- colored muscovite, dark brown biotite, and dark green amphibole.

Figure 4.12: To identify a rock, match the texture (below) with the composition (right). Textures: phaneritic (coarse grained), aphanitic (fine grained), porphyritic (large crystals in a fine matrix), vesicular (bubbly or frothy), glassy, pyroclastic (fragmental). Compositions. Felsic (>10% quartz, >50% feldspar, <15% mafic materials). Intermediate (>10% quartz, >50% plagioclase, >10% orthoclase, <50% mafic minerals). Mafic (20-85% plagioclase, 15-50% pyroxene, >35% olivine). Ultramafic (olivine & pyroxene). Granite: phaneritic, felsic. Diorite: phaneritic, intermediate. Gabbro: phaneritic, mafic. Peridotite: phaneritic, ultramafic. Rhyolite: aphanitic, felsic. Andesite: aphanitic, intermediate. Basalt: aphanitic, mafic. Porphyritic rhyolite: porphyritic, felsic. Porphyritic andesite: porphyritic, intermediate. Porphyritic basalt: porphyritic, mafic. Pumice: vesicular, felsic. Scoria: vesicular, mafic. Obsidian: glassy, felsic. Rhyolitic tuff or volcanic breccia: pyroclastic, felsic. Andesitic tuff or volcanic breccia: pyroclastic, intermediate. Basaltic tuff or volcanic breccia: pyroclastic, mafic.

Figure 4.13: Hilly landscape with dark red and gray hills made of flat-lying sedimentary layers, with a black igneous dike cutting perpendicular to the hill ridge that goes straight through the sedimentary layers.

Figure 4.14: Cliff that shows slightly angled parallel tan, gray, and black sedimentary layers, with a tan, white, and black-colored igneous sill visible between and parallel to the sedimentary layers.

Figure 4.15: White and light gray rock formations that stick out vertically from the surrounding hillside which is covered in green and brown trees.

Figure 4.16: The granite formation rises against a backdrop of blue sky and gray mountains. Half Dome's distinct shape, with its sheer vertical face on one side and smooth, rounded surface on the other, is prominently displayed.

Figure 4.17: Cross sectional diagram showing three flat-lying sedimentary layers colored orange, yellow, and brown stacked at the bottom of the diagram and three upward-arched sedimentary layers colored orange, yellow, and brown at the top of the diagram. A gray intrusion labeled "laccolith" fills the space between the arched sedimentary layers and the flat sedimentary layers with a nearly vertical thin gray intrusion labeled "dike" feeding it from below.

Figure 4.18: High mountains covered in snow that have an overall broad, dome- shaped top. There are green trees and shrubs in the foreground.

Figure 4.19: A rectangular diagram with a vertical axis representing temperature increasing upward on the left. On the right-hand side of the diagram are two arrows: one points downward and is labeled "Increasing Silica, Na, Al, K" and the other points upward with the label "Increasing Fe, Mg & K." Inside the diagram are various mineral labels; starting from the bottom to top, they are Quartz, Muscovite, and K-Spar with a bracket labeling them "Residual Phases (Last to crystallize)" and above those are two branches: the discontinuous series branching toward the upper left and the continuous series branching toward the upper right. The discontinuous series contains Biotite, then Amphibole to the upper left of that, then Pyroxene to the upper left, and then Olivine to the upper left; the continuous series contains Oligoclase, then Anorthite to the upper left. On the right of the diagram are the labels Felsic, Intermediate, Mafic, and Ultramafic from bottom to top.

Figure 4.20: Light green, glassy crystal of olivine.

Figure 4.21: Black and white photograph of Norman Bowen, a white man, in a suit with a black jacket and white collared shirt and white tie.

Figure 4.22: Black and white photograph of Norman Bowen, a white man sitting in a chair, in a suit, holding and looking at an angular object, while a colleague, a white man seated behind him with glasses and a pipe and looking over his shoulder, also holds an angular object.

Figure 4.23: Diagram showing temperature in kelvins increasing vertically downward with depth in km in the Earth. A red curve is drawn from the upper left corner of the diagram that shallowly dips down to the right until it reaches 410 km depth; this is labeled lithosphere. Below that, the curve steepens and goes deeper down until it shallows again around 2900 km depth. The part of the line from 410 to 660 km is labeled upper mantle and the line from 660 to 2900 km is labeled lower mantle. Below 2900 km, the curve steepens again down to 5150 km, and becomes vertical below 5150 km. From 2900 to 5150 km, the line is labeled outer core, and from 5150 to 6370 km, the line is labeled inner core.

Figure 4.24: Diagram showing pressure increasing down on the vertical axis and temperature increasing to the right on the horizontal axis. There are two diagonal lines on the diagram: one is dark blue, labeled geotherm, that is a straight line from the upper left (0 on both axes) toward the lower right until it reaches about 125 km depth and 1250 degrees C temperature, where it then steepens to a nearly vertical

line downward. The other line is light blue and is a slightly curved, steep line that goes from about 1100 degrees C and 0 km depth down steeply and slightly toward the right, labeled solidus.

Figure 4.25: 3D diagram showing a cross section into Earth's crust. On the left-hand side is a convergent plate boundary, with a plate of oceanic crust colliding into another plate of oceanic crust. The oceanic crust on the right-hand side subducts toward the left and a line of volcanoes forms on the overriding oceanic plate as a volcanic island arc. To the right of that, there is a shield volcano on the lithosphere beneath the ocean with a hot spot feeding the volcano from below. To the right of the shield volcano, there is a divergent plate boundary where two oceanic plates move away from each other. There is a transform plate boundary labeled to the left of the divergent boundary. To the right of the divergent boundary, oceanic crust moves toward the right, colliding with continental crust. The oceanic crust subducts beneath the continental crust, forming a chain of continental volcanoes on top of the continental crust. To the farthest right of the diagram, there is a continental rift zone where the continental crust is splitting apart.

Figure 4.26: World map with continents and oceans labeled. Multiple series of spreading ridges are drawn and labeled as red line segments on the map: major ones are found in an upside-down Y shape in the Indian Ocean, bordering the Pacific Ocean basin, running through the approximate center of the North and South Atlantic Ocean basins, and in the eastern corner of Africa. Small red dots mark the spots of recent subaerial volcanoes; they are found along the spreading ridge locations along with at hot spots and sparsely scattered on the Asian continent.

Figure 4.27: Underwater photo with a dark bluish hue of lumpy, bulbous chunks of black basalt on sea floor.

Figure 4.28: A black smoker hydrothermal vent at the bottom of the sea floor. There is a plume of black smoke coming from a cone-shaped extrusion of rock and a colony of tube worms are attached to the cone-shaped rock.

Figure 4.29: World map showing worldwide distribution of hydrothermal vent fields as red dots on the map; tectonic boundaries are drawn as thin black lines on the map. The hydrothermal vent fields are found along all of the mid- ocean ridges in the ocean basins.

Figure 4.30: World map showing with major tectonic plates labeled; plate boundaries are marked as black lines and active volcanoes are marked as red dots. Active volcanoes are shown along various plate boundaries, especially around the edts of the Pacific Ocean basin where they are labeled "Ring of Fire."

Figure 4.31: Gently sloping landscape with smaller rocky hills covered in black, brown, and red chunks of volcanic rock. A broad summit can be seen in the distant background.

Figure 4.32: Two cross sectional diagrams: the top diagram shows horizontal layers with a magma plume rising vertically through them and a volcano on top of the layers. The second diagram shows horizontal layers with the top layer moving toward the left; a magma plume rises vertically through them and a chain of volcanoes is formed on the top layer which is moving toward the left as the magma plume creates volcanoes on top.

Figure 4.33: Shaded relief map centered on Idaho, with small portions of the surrounding states shown too. The track of a hot spot is annotated on the map and color-coded at each past location. The hotspot started near the Idaho-Oregon-Nevada border with the label 16.1 which indicates it was there 16.1 million years ago, then moved relatively east-northeastward toward its present location near the Wyoming-Idaho-Montana border which is labeled 0.6-2.1 which indicates it has been there 2.1 to 0.6 million years ago. Note that the North American plate was moving over the hot spot, not that the hot spot was moving under North America.

Figure 4.34: Map of the Hawaii-Emperor seamount chain and seafloor topography. The Aleutian trench and islands run approximately east-to-west along the top of the map, the Emperor seamount chain runs approximately north-to- south near the left-hand side of the map, and the Hawaiian seamount chain runs approximately west-northwest-to-east-southeast near the bottom of the map.

Figure 4.35: Volcano with labels 1-15.

Figure 4.36: Aerial view of the top of a large mountain that has a large hole at its top, filled with deep blue lake water. There is a small cone-shaped island in the lake visible in the lower right of the photo.

Figure 4.37: Brown-to black rubble-covered foreground with a broad mountaintop visible in the background.

Figure 4.38: Blocky lava flowing over a road in Hawaii. A tree is on fire on the left-hand side of the photo.

Figure 4.39: Satellite view of enormous tan-to-brown volcano. It has a large round shape and some small craters visible in its flank and caldera.

Figure 4.40: Outcrop of black volcanic rock with an arced, undulating, ropey appearance. A person's blue shoe is standing on the outcrop.

Figure 4.41: Jagged, sharp-looking black volcanic rock with red hot lava showing underneath parts of the black rocks. There are three mountain peaks in the background.

Figure 4.42: High tower of rock composed of vertical polygonal columns that are tan in color. There are green trees surrounding the base of the tower.

Figure 4.43: Landscape composed of interlocking hexagonal tan, red, and brown basalt columns that vary in height.

Figure 4.44: Tan, flat landscape that has a vertical tan-brown rocky outcrop rising high above the surrounding landscape.

Figure 4.45: View of city buildings with towering snow-capped mountain in the background.

Figure 4.46: Tall, nearly-symmetrical snow-capped mountain.

Figure 4.47: Aerial view of the top of a large barren mountain that has a large hole at its top. There is a small bulbous shape growing in the hole with steam coming out of it.

Figure 4.48: Four cross sectional diagrams. The first diagram shows a blob of magma at the bottom with two narrow vents rising vertically from the blob, one near the center of the diagram and the other to the right of that one; at the surface is a layered volcano with ash and pumice erupting where the side vent reaches the surface. The second diagram shows the layered volcano has collapsed at its center with arrows pointing downward to show the collapse. The third diagram shows small amounts of steam rising from the surface where the layered volcano has collapsed. The fourth diagram is labeled "Today" and shows the modern-day volcano with Garfield Peak on the left side of the caldera and Llao Rock on the right side of the caldera, with a lake and Wizard Island in the center of the caldera.

Figure 4.49: View through a clearing in green trees of a lake with a cone-shaped island in it.

Figure 4.50: Shaded relief map centered on Wyoming, with small portions of the surrounding states shown too. The caldera and related volcanic rocks, along with faults and earthquake epicenters, are annotated on the map and color-coded. The Yellowstone Caldera is outlined in purple, located in the west-central portion of Wyoming. Boundaries of older calderas are outlined in green with a dashed line where uncertain; there's an older caldera near the Idaho-Wyoming border, located in Idaho. There's an uncertain caldera from just west of the Wyoming border into Wyoming, covering the west-central portion of the state. There are numerous earthquake epicenters scattered throughout the Yellowstone caldera and also clustered just northwest of the caldera.

Figure 4.51: Map of the United States with state borders outlined. Prominent ash beds are outlined and color-coded, including three Yellowstone eruptions shaded pink. One of the pink outlines is labeled Mesa Falls ash bed and encircles most of the states of Wyoming, Colorado, Kansas, and Nebraska, and partially encircles the states Montana, South Dakota, Oklahoma, and Texas. Another pink outline is labeled Huckleberry Ridge ash bed and encircles the a large western portion of the United States. The third pink outline is labeled Lava Creek ash bed and encircles most of the western half of the United States. There is also a brown dashed outline labeled "Bishop ash bed" which encircles the entire southwest portion of the United States. There is a yellow elongated outline labeled "Mount St. Helens ash 1980" which covers a east-west-trending portion of southern Washington state.

Figure 4.52: Aerial view of brown cinder cone volcano with large opening at top; the surrounding landscape is low, shrubby green vegetation.

Figure 4.53: Slightly grainy color photograph of a cinder cone volcano erupting an ash plume with a person wearing a brown plaid sombrero and red handkerchief looking on.

Figure 4.54: Grayish tan stone church tower and building surrounded by black and brown blocky volcanic rocks.

Figure 4.55: World map of flood basalts. Includes Sierra Madre occidental, Columbia River basalt group (2), High Arctic LIP (3), North Atlantic LIP (3), Siberian Traps, Emeishan Traps, CAMP (3), Parana-Etendeka LIP (4), Afro- Arabian LIP (2), Karoo Ferrar LIP, Deccan traps, Rajmahal LIP, Gawler Range LIP, Whitsunday LIP (2). Note the largest is the Siberian Traps.

Figure 4.56: Table of igneous rocks and related volcano types. Horizontal axis is arranged from low to high silica content (i.e. from ultramafic to felsic). First row shows the extrusive (surface) igneous rocks basalt, andesite, and rhyolite. Second row shows volcano types: mid-ocean ridge, shield, cinder cone, and strato (composite). Third row shows examples of each volcano: mid-atlantic ridge, Mauna Kea (Hawaii), Paricutin, and Mt. St. Helens. Fourth row shows intrusive rocks from mafic to felsic: Dunite, gabbro, diorige, granite. Fifth row shows common plate-tectonic settings: divergent oceanic hot spot, and convergent boundaries. Sixth row is typical composition: ultramafic, mafic, intermediate, and felsic.

Figure 4.57: Block diagram of a volcano with various hazards labeled: along the flanks of the volcano are a lava flow, lahar, two pyroclastic flows, and a landslide; erupting from the volcano are an eruption column and tephra with an eruption cloud, gas, and acid rain coming from the eruption column. There is a vent of magma feeding the volcano from below and a small lava dome on part of the side of the volcano.

Figure 4.58: The body is laying down, encased in a cast formed from grayish white ash.

Figure 4.59: Two photographs of a large volcano. The left photo is labeled "Before," showing a large, conical volcano with snow on its flanks

and a forest at its base. The right photo is labeled "After," showing the peak of the mountain has collapsed into a caldera and the landscape is barren.

Figure 4.60: Black and white photo of a large volcano erupting with billowing smoke and dark flows down its flanks.

Figure 4.61: Erupting volcano with billowing smoke erupting from its peak, traveling upward as well as laterally down the right flank of the volcano.

Figure 4.62: Black and white photo of a man sitting on a ridge, overlooking a destroyed city.

Figure 4.63: Series of four schematic diagrams of Mt. St. Helens in a diagonal line from upper left to lower right. Starting at the upper left, the diagram shows a volcano with three domes labeled: Summit dome at the top, Cryptodome in the center base of the summit, and Goat Rocks dome along the right flank. The second diagram shows a landslide that collapsed the right flank of the volcano; the third diagram shows the initial explosions that resulted, erupting upward and toward the right, and the fourth diagram shows a vertical eruption column coming from the now-collapsed right flank of the volcano. On the lower left of the figure is two black and white photos of the eruption column. On the upper right of the figure is the following text: At 8: 32 a.m., May 18, 1980, a 5.1 earthquake shook loose the north flank of Mount St. Helens, resulting in the largest known landslide in historic time. Removal of more than half a cubic mile of material released pressure and triggered a devastating lateral blast and ash-laden eruptive column.

Figure 4.64: A man wearing a surgical mask sweeping white ash off the street. He is also wearing a conical hat, a red jacket, and brown pants. There is abundant white ash covering the street around and behind him.

Figure 4.65: Grayscale micrograph of volcanic ash particle with abundant pore space throughout the particle. A scale bar labeled 0 to 30 micrometers is in the upper right of the image.

Figure 4.66: Barren trees with a noticeable horizontal line throughout them at the same height, below which the trees are grayish tan from being covered in mud and above which the brown bark of the trees is visible.

Figure 4.67: Shaded relief map with Tacoma, Washington, at the upper left of the map and Mount Rainier at the lower right of the map. Three lahars are colored on the map: the Osceola Lahar in yellow that goes from Mount Rainier to Tacoma, generally following the path of the White River; the National Lahar in pink that goes from the south side of Mount Rainier toward the left, generally following the path of the Nisqually River; and the Electron Lahar in lilac that goes from Mount Rainier to Puyallup, generally following the Puyallup River.

5. WEATHERING, EROSION, AND SEDIMENTARY ROCKS

Learning Objectives

By the end of this chapter, students will be able to:

- Describe how water is an integral part of all sedimentary rock formation.
- Explain how chemical and mechanical weathering turn bedrock into sediment.
- Differentiate the two main categories of sedimentary rocks: clastic rock formed from pieces of weathered bedrock and chemical rock that precipitates out of solution by organic or inorganic means.
- Explain the importance of sedimentary structures and analysis of depositional environments and how they provide insight into the Earth's history.

Sedimentary rock and the processes that create it, which include weathering, erosion, and lithification, are integral parts of understanding Earth science. This is because the majority of the Earth's surface is made up of sedimentary rocks and their common predecessor, sediments. Even though sedimentary rocks can form in drastically different ways, the origin and creation of each has one thing in common: water.

5.1 The Unique Properties of Water

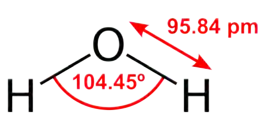

Figure 5.1: A model of a water molecule, showing the bonds between the hydrogen and oxygen. Figure description available at the end of the chapter.

Water plays a role in the formation of most sedimentary rock. It is one of the main agents involved in creating the minerals in chemical sedimentary rock. It also is a weathering and erosion agent, producing the grains that become detrital sedimentary rock. Several special properties make water an especially unique substance, that is integral to the production of sediments and sedimentary rock.

The water molecule consists of two hydrogen atoms covalently bonded to one oxygen atom, arranged in a specific and important geometry. The two hydrogen atoms are separated by an angle of about 105 degrees, and both are located on one side of the oxygen atom. This atomic arrangement, with the positively charged hydrogens on one side and negatively charged oxygen on the other side, gives the water molecule a property called **polarity**. Resembling a battery or a magnet, the molecule's positive-negative architecture leads to a whole suite of unique properties.

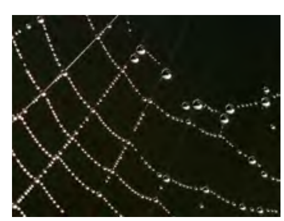

Figure 5.2: Dew on a spider's web. Figure description available at the end of the chapter.

Polarity allows water molecules to stick to other substances. This is called **adhesion**. Water is also attracted to itself, a property called **cohesion**, which results in water's most common form in the air, a droplet. Cohesion is responsible for creating surface tension, which various insects use to walk on water by distributing their weight across the surface.

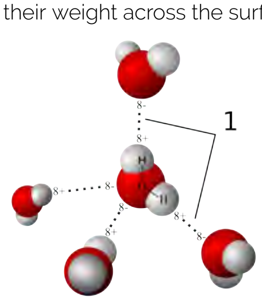

Figure 5.3: Hydrogen bonding between water molecules. Figure description available at the end of the chapter.

The fact that water is attracted to itself leads to another important property that is extremely rare in the natural world—its liquid form is denser than its solid form. The polarity of water creates a special type of weak bonding called **hydrogen bonds**. Hydrogen bonds allow the molecules in liquid water to sit close together. Water is densest at 4˚C and is less dense above or below that temperature. As water solidifies into ice, the molecules must move apart in order to fit into the crystal lattice, causing water to expand and become less dense as it freezes. Because of this, ice floats and water at 4˚C sinks, which keeps the oceans liquid and prevents them from freezing solid from the bottom up. This unique property of water keeps Earth, the water planet, habitable.

Even more critical for supporting life, water remains liquid over a very large range of temperatures, which is also a result of cohesion. Hydrogen bonding allows liquid water can absorb high amounts of energy before turning into vapor or gas. The wide range across which water remains a liquid, 0°C–100°C (32°F–212°F), is rarely exhibited in other substances. Without this high boiling point, liquid water as we know it would be constricted to narrow temperature zones on Earth; instead water is found from pole to pole. Further, water is the only substance that exists in all three phases—solid, liquid, and gas—in Earth's surface environments.

Water is a **universal solvent**, meaning it dissolves more substances than any other common, naturally occurring liquid. Water molecules use polarity and hydrogen bonds to pry ions away from the crystal lattice. Water is such a powerful solvent, it can dissolve even the strongest rocks and minerals given enough time.

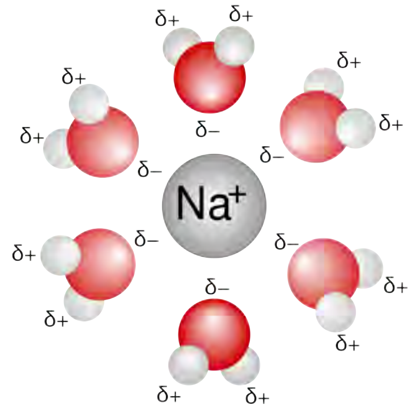

Figure 5.4: A sodium (Na) ion in solution. Figure description available at the end of the chapter.

Take this quiz to check your comprehension of this section.

Access the quiz for Section 5.1 by scanning the QR code.

5.2 Weathering and Erosion

Bedrock refers to the solid rock that makes up the Earth's outer crust. Weathering is a process that turns bedrock into smaller particles called **sediment**. Mechanical weathering includes pressure expansion, frost wedging, root wedging, and salt expansion. Chemical weathering includes carbonic acid and hydrolysis, dissolution, and oxidation.

Erosion is a mechanical process, usually driven by water, wind, gravity, or ice, that transports sediment (and soil) from the place of weathering. Liquid water is the main agent of erosion. Gravity and mass wasting processes (see Chapter 10) move rocks and sediment to new locations. Gravity and ice, in the form of glaciers (see Chapter 14), move large rock fragments as well as fine sediment.

Erosion resistance is important in the creation of distinctive geological features. This is well demonstrated in the cliffs of the Grand Canyon. The cliffs are made of rock left standing after less resistant materials have weathered and eroded away. Rocks with different levels of erosion resistance also create the unique-looking features called hoodoos in Bryce Canyon National Park and Goblin Valley State Park in Utah.

5.2.1 Mechanical Weathering

Mechanical weathering physically breaks bedrock into smaller pieces. The usual agents of mechanical weathering are pressure, temperature, the freezing/thawing cycle of water, plant or animal activity, and salt evaporation.

Pressure Expansion

Bedrock buried deep within the Earth is under high pressure and temperature. When uplift and erosion brings bedrock to the surface, its temperature drops slowly, while its pressure drops immediately. The sudden pressure drop causes the rock to rapidly expand and crack; this is called pressure expansion. Sheeting, or **exfoliation**, occurs when the rock surface spalls off in layers. **Spheroidal weathering** is a type of exfoliation that produces rounded features and is caused when chemical weathering moves along joints in the bedrock.

Figure 5.5: The outer layer of this granite is fractured and eroding away, known as exfoliation. Figure description available at the end of the chapter.

Frost Wedging

Frost wedging, also called ice wedging, uses the power of expanding ice to break apart rocks. Water works its way into various cracks, voids, and crevices. As the water freezes, it expands with great force, exploiting any weaknesses. When ice melts, the liquid water moves further into the widened spaces. Repeated cycles of freezing and melting eventually pry the rocks apart. The cycles can occur daily when temperatures fluctuate from freezing to melting between day and night.

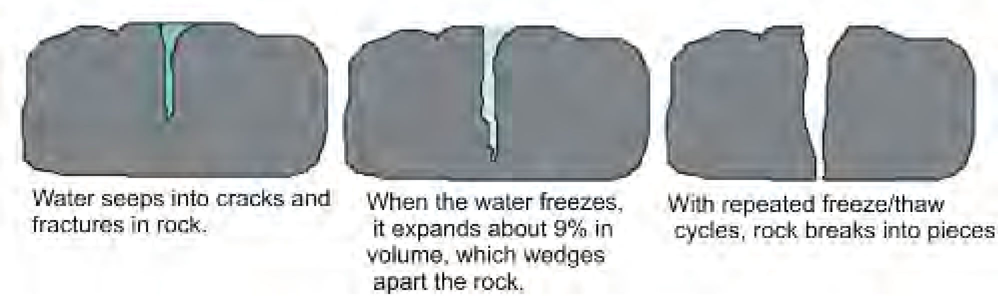

Figure 5.6: The process of frost wedging. Figure description available at the end of the chapter.

Root Wedging

Like frost wedging, **root wedging** happens when plant roots work themselves into cracks, prying the bedrock apart as they grow. Occasionally these roots may become fossilized. **Rhizolith** is the term for these roots when they are preserved in the rock record. Tunneling organisms such as earthworms, termites, and ants are biological agents that induce weathering similar to root wedging.

Figure 5.7: The roots of this tree are demonstrating the destructive power of root wedging. Though this picture features a man-made rock (asphalt), it works on typical rock as well. Figure description available at the end of the chapter.

Salt Expansion

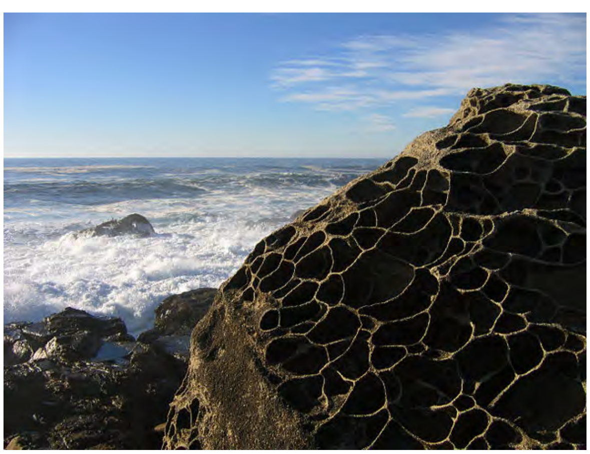

Figure 5.8: Tafoni from Salt Point, California. Figure description available at the end of the chapter.

Salt expansion, which works similarly to frost wedging, occurs in areas of high evaporation or near-marine environments. Evaporation causes salts to precipitate out of solution and then grow and expand into cracks in rock. Salt expansion is one of the causes of **tafoni**, a series of holes in rock. Tafonis, cracks, and holes are weak points that become susceptible to increased weathering. Another phenomena that occurs when salt water evaporates is that it can leave behind a square imprint preserved in a soft sediment, which is called a **hopper crystal**.

5.2.2 Chemical Weathering

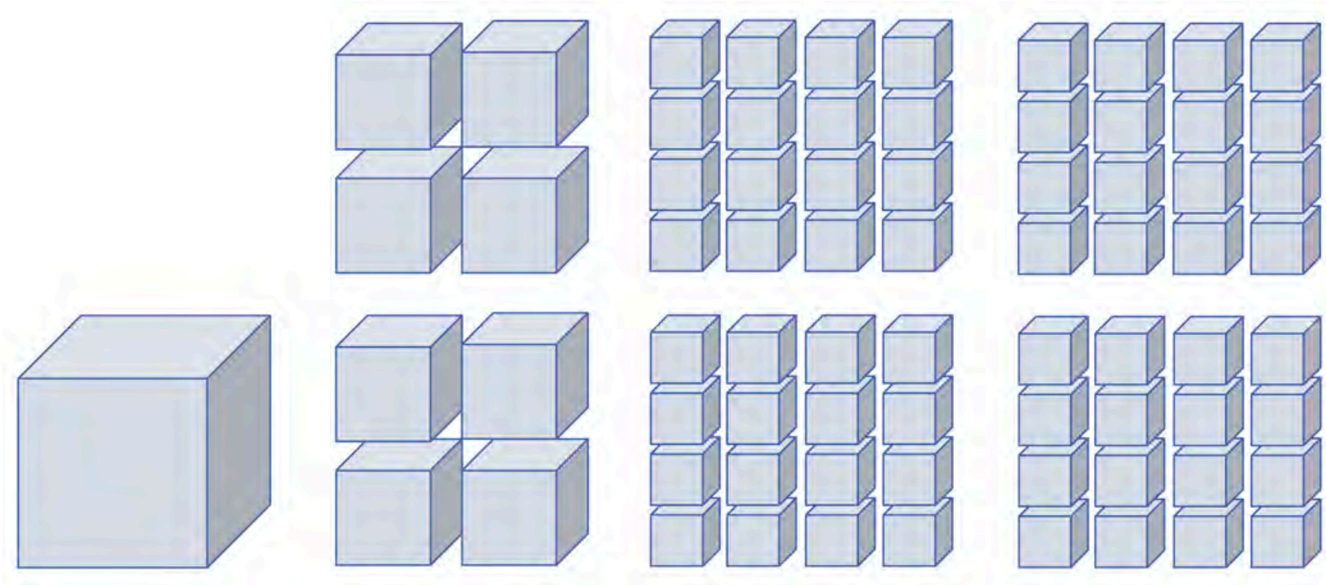

Figure 5.9: Each of these three groups of cubes has an equal volume. However, their surface areas are vastly different. On the left, the single cube has a length, width, and height of 4 units, giving it a surface area of $6(4 \times 4) = 96$ and a volume of $4^3 = 64$. The middle eight cubes have a length, width, and height of 2, meaning a surface area of $8(6(2 \times 2)) = 8 \times 24 = 192$. They also have a volume of $8(2^3) = 8 \times 8 = 64$. The 64 cubes on the right have a length, width, and height of 1, leading to a surface area of $64(6(1 \times 1)) = 64 \times 6 = 384$. The volume remains unchanged, because $64(1^3) = 64 \times 1 = 64$. The surface area to volume ratio (SA:V), which is related to the amount of material available for reactions, changes for each as well. On the left, it is 96/64 = 0.75 or 3:2. The center has a SA/V of 192/64 = 1.5, or 3:1. On the right, the SA:V is 384/64 = 6, or 6:1. Figure description available at the end of the chapter.

Chemical weathering is the dominant weathering process in warm, humid environments. It happens when water, oxygen, and other reactants chemically degrade the mineral components of bedrock and turn them into water-soluble ions, which can then be transported by water. Higher temperatures accelerate chemical weathering rates.

Chemical and mechanical weathering work hand in hand via a fundamental concept called surface-area-to-volume ratio. Chemical weathering only occurs on rock surfaces because water and reactants cannot penetrate solid rock. Mechanical weathering penetrates bedrock, breaking large rocks into smaller pieces and creating new rock surfaces. This exposes more surface area to chemical weathering, enhancing its effects. In other words, higher surface-area-to-volume ratios produce higher rates of overall weathering.

Carbonic Acid and Hydrolysis

Carbonic acid (H_2CO_3) forms when carbon dioxide, the fifth-most abundant gas in the atmosphere, dissolves in water. This happens naturally in clouds, which is why precipitation is normally slightly acidic. Carbonic acid is an important agent in two chemical weathering reactions, hydrolysis and dissolution.

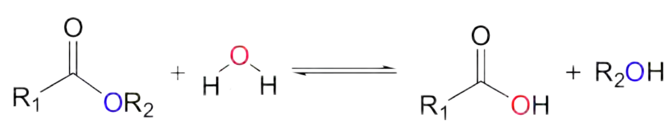

Figure 5.10: Generic hydrolysis diagram, where the mineral bonds in question would represent the left side of the diagram. Figure description available at the end of the chapter.

Hydrolysis occurs via two types of reactions. In one reaction, water molecules ionize into positively charged H^{+1} and OH^{-1} ions and replace mineral cations in the crystal lattice. In another type of hydrolysis, carbonic acid molecules react directly with minerals, especially those containing silicon and aluminum (i.e., feldspars), to form molecules of clay minerals.

Hydrolysis is the main process that breaks down silicate rock and creates clay minerals. The following is a hydrolysis reaction that occurs when silica-rich feldspar encounters carbonic acid, producing water-soluble clay and other ions:

feldspar + carbonic acid (in water) → clay + metal cations (Fe^{++}, Mg^{++}, Ca^{++}, Na^{+}, etc.) + bicarbonate anions (HCO_3^{-1}) + silica (SiO_2)

Clay minerals are platy silicates or phyllosilicates (see Chapter 3) similar to micas and are the main components of very fine-grained sediment. The dissolved substances may later precipitate into chemical sedimentary rocks like evaporite and limestone, as well as amorphous silica or chert nodules.

Dissolution

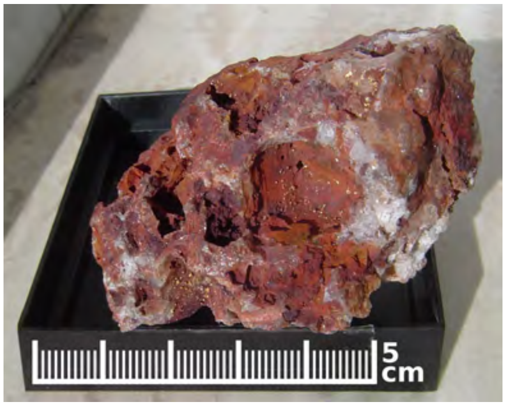

Figure 5.11: In this rock, a pyrite cube has dissolved (as shown by the negative "corner" impression in the rock), leaving behind small specks of gold. Figure description available at the end of the chapter.

Dissolution is a hydrolysis reaction that dissolves minerals in bedrock and leaves the ions in solution, usually in water. Some evaporites and carbonates, like salt and calcite, are more prone to this reaction; however, all minerals can be dissolved. Nonacidic water, with a neutral pH of 7, will dissolve any mineral, although it may happen very slowly. Water with higher levels of acid, naturally or manmade, dissolves rocks at a higher rate. Liquid water is normally slightly acidic due to the presence of carbonic acid and free H^+ ions. Natural rainwater can be highly acidic, with pH levels as low as 2. Dissolution can be enhanced by a biological agent, such as when organisms like lichen and bacteria release organic acids onto the rocks to which they are attached. Regions with high humidity (airborne moisture) and precipitation experience more dissolution due to rocks and water being in contact for longer.

The **Goldich dissolution series** shows chemical weathering rates are associated to crystallization rankings in the Bowen's reaction series (see Chapter 4). Minerals at the top of the Bowen series crystallize under high temperatures and pressures, as well as chemically weathering at a faster rate than minerals ranked at the bottom. Quartz, a felsic mineral that crystallizes at 700˚C, is very resistant to chemical weathering. High crystallization-point mafic minerals, such as olivine and pyroxene (1250˚C), weather relatively rapidly and more completely. Olivine and pyroxene are rarely found as end products of weathering because they tend to break down into elemental ions.

Figure 5.12: This mantle xenolith containing olivine (green) is chemically weathering by hydrolysis and oxidation into the pseudomineral iddingsite, which is a complex of water, clay, and iron oxides. The more altered side of the rock has been exposed to the environment longer. Figure description available at the end of the chapter.

Figure 5.13: Eroded karst topography in Minerve, France. Figure description available at the end of the chapter.

Dissolution is also noteworthy for the special geological features it creates. In places with abundant carbonate bedrock, dissolution weathering can produce a karst topography characterized by sinkholes or caves (see Chapter 10).

Timpanogos Cave National Monument in northern Utah is a well-known dissolution feature. The figure shows a cave formation created from dissolution followed by precipitation; that is, groundwater saturated with calcite seeped into the cavern, where evaporation caused the dissolved minerals to precipitate out.

Figure 5.14: A formation called the Great Heart of Timpanogos in Timpanogos Cave National Monument. Figure description available at the end of the chapter.

Oxidation

Oxidation, the chemical reaction that causes rust in metallic iron, occurs geologically when iron atoms in a mineral bond with oxygen. Any minerals containing iron can be oxidized. The resultant iron oxides may permeate a rock if it is rich in iron minerals. Oxides may also form a coating that covers rocks and grains of sediment or lines rock cavities and fractures. If the oxides are more susceptible to weathering than the original bedrock, they may create void spaces inside the rock mass or hollows on exposed surfaces.

Three commonly found minerals are produced by iron-oxidation reactions: red or grey hematite, brown goethite (pronounced "GUR-tite"), and yellow limonite. These iron oxides coat and bind mineral grains together into sedimentary rocks in a process called **cementation**, which often gives these rocks a dominant color. They color the rock layers of the Colorado Plateau, as well as Zion, Arches, and Grand Canyon National Parks. These oxides can permeate a rock that is rich in iron-bearing minerals or can be a coating that forms in cavities or fractures. When the minerals replacing existing minerals in bedrock are resistant to weathering, iron concretions may occur in the rock. When bedrock is replaced by weaker oxides, this process commonly results in void spaces and weakness throughout the rock mass and often leaves hollows on exposed rock surfaces.

Figure 5.15: Pyrite cubes are oxidized, becoming a new mineral, goethite. In this case, goethite is a pseudomorph after pyrite, meaning it has taken the form of another mineral. Figure description available at the end of the chapter.

5.2.3 Erosion

Figure 5.16: A hoodoo near Moab, Utah. Figure description available at the end of the chapter.

Erosion is a mechanical process, usually driven by water, gravity, (see Chapter 10), wind, or ice (see Chapter 14), that removes sediment from the place of weathering. Liquid water is the main agent of erosion.

Erosion resistance is important in the creation of distinctive geological features. This is well demonstrated in many areas of the American Southwest, such as the cliffs of the Grand Canyon and Zion National Park. The cliffs are made of rock left standing after less resistant materials have weathered and eroded away.

Figure 5.17: Court of the Patriarchs in Zion National Park, Utah. Figure description available at the end of the chapter.

5.2.4 Soil

Soil is a combination of air, water, minerals, and organic matter that forms at the transition between biosphere and geosphere. Soil is made when weathering breaks down bedrock and turns it into sediment. If erosion does not remove the sediment significantly, organisms can access the mineral content of the sediments. These organisms turn minerals, water, and atmospheric gases into organic substances that contribute to the soil.

Soil is an important reservoir for organic components necessary for plants, animals, and microorganisms to live. The organic component of soil, called **humus**, is a rich source of bioavailable nitrogen. Nitrogen is the most common element in the atmosphere, but it exists in a form most life forms are unable to use. Special bacteria found only in soil provide most nitrogen compounds that are usable—bioavailable—by life forms.

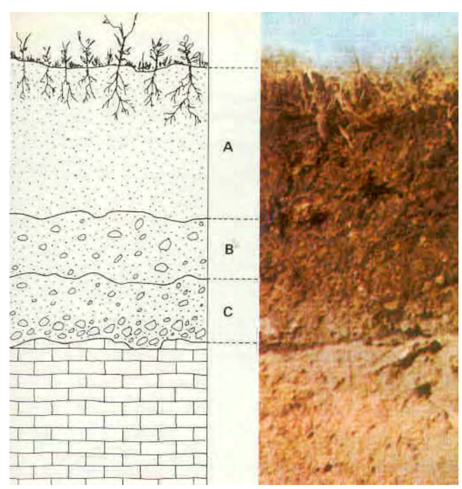

Figure 5.18: Sketch and picture of soil. Figure description available at the end of the chapter.

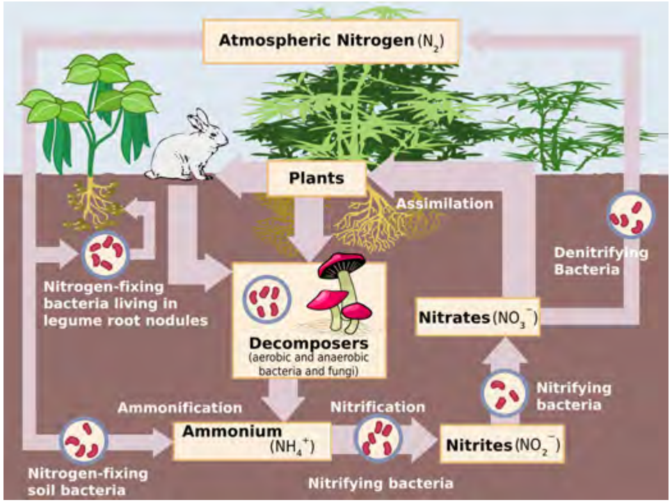

Figure 5.19: Schematic of the nitrogen cycle. Figure description available at the end of the chapter.

These nitrogen-fixing bacteria absorb nitrogen from the atmosphere and convert it into nitrogen compounds. These compounds are absorbed by plants and used to make DNA, amino acids, and enzymes. Animals obtain bioavailable nitrogen by eating plants, and this is the source of most of the nitrogen used by life. That nitrogen is an essential component of proteins and DNA. Soils range from poor to rich, depending on the amount of humus they contain. Soil productivity is determined by water and nutrient content. Freshly created volcanic soils, called andisols, and clay-rich soils that hold nutrients and water are examples of productive soils.

The nature of the soil, meaning its characteristics, is determined primarily by five components: (1) the mineralogy of the parent material, (2) topography, (3) weathering, (4) climate, and (5) the organisms that inhabit the soil. For example, soil tends to erode more rapidly on steep slopes, so soil layers in these areas may be thinner than in flood plains, where it tends to accumulate. The quantity and chemistry of organic matter of soil affects how much and what varieties of life it can sustain. Temperature and precipitation, two major weathering agents, are dependent on climate. Fungi and bacteria contribute organic matter and give soil the ability to sustain life, interacting with plant roots to exchange nitrogen and other nutrients.

In well-formed soils, there is a discernable arrangement of distinct layers called **soil horizons**. These soil horizons can be seen in road cuts that expose the layers at the edge of the cut. Soil horizons make up the **soil profile**. Each soil horizon reflects climate, topography, and other soil-development factors, as well as its organic material and mineral sediment composition. The horizons are assigned names and letters. Differences in naming schemes depend on the area, soil type, or research topic. Figure 5.21 shows a simplified soil profile that uses commonly designated names and letters.

Figure 5.20: Agricultural terracing, such as these created by the Inca culture from the Andes, helps reduce erosion and promote soil formation, leading to better farming practices. Figure description available at the end of the chapter.

O Horizon: The top horizon is a thin layer of predominantly organic material, such as leaves, twigs, and other plant parts that are actively decaying into humus.

A Horizon: The next layer, called **topsoil**, consists of humus mixed with mineral sediment. As precipitation soaks down through this layer, it leaches out soluble chemicals. In wet climates with heavy precipitation, this leaching produces a separate layer called Horizon E, the leaching or eluviation zone.

B Horizon: Also called **subsoil**, this layer consists of sediment mixed with humus removed from the upper layers. The subsoil is where mineral sediment is chemically weathered. The amount of organic material and degree of weathering decrease with depth. The upper subsoil zone, called **regolith**, is a porous mixture of humus and highly weathered sediment. In the lower zone, saprolite, scant organic material is mixed with largely unaltered parent rock.

C Horizon: Known as **substratum**, this is a zone of mechanical weathering. Here, bedrock fragments are physically broken but not chemically altered. This layer contains no organic material.

R Horizon: The final layer consists of unweathered parent bedrock and fragments.

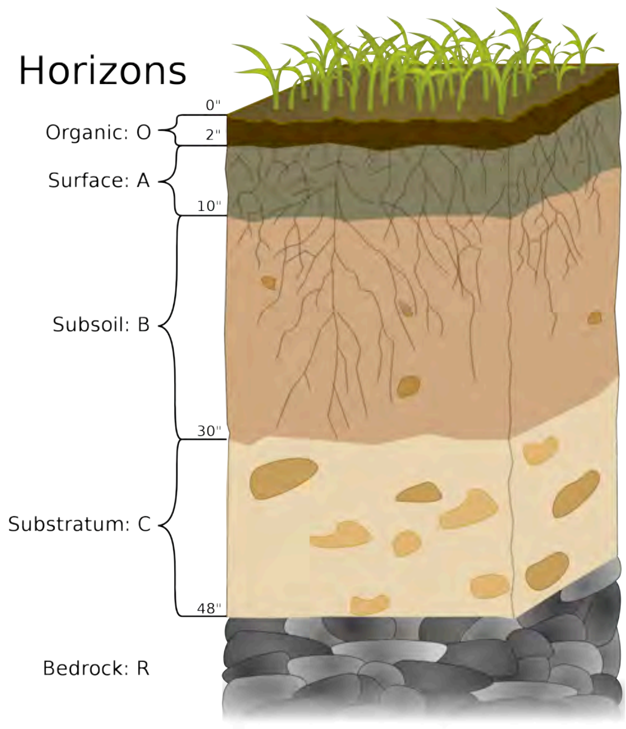

Figure 5.21: A simplified soil profile with labeled layers. Figure description available at the end of the chapter.

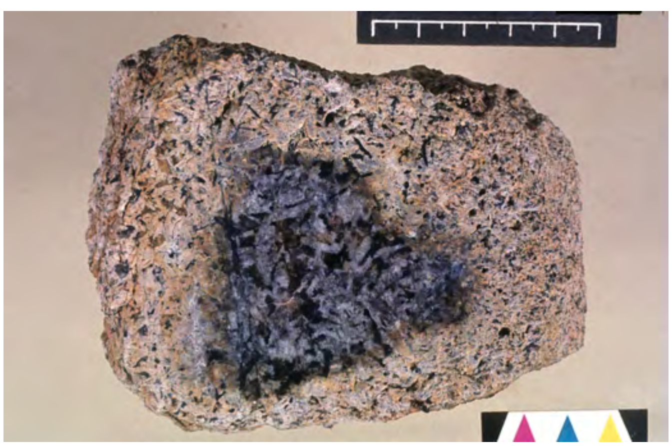

Figure 5.22: A sample of bauxite. Note the unweathered igneous rock in the center. Figure description available at the end of the chapter.

The United States governing body for agriculture, the USDA, identifies soil types through a taxonomic classification called soil orders. Oxisols, or laterite soils, are nutrient-poor soils found in tropical regions. While poorly suited for growing crops, oxisols are home to most of the world's mineable aluminum ore (bauxite). Ardisol forms in dry climates and can develop layers of hardened calcite called caliche. Andisols originate from volcanic ash deposits. Alfisols contain silicate clay minerals. These two soil orders are productive for farming due to their high content of mineral nutrients. In general, color can be an important factor in understanding soil conditions. Black soils tend to be anoxic, red oxygen-rich, and green oxygen-poor (i.e., reduced). This is true for many sedimentary rocks as well.

Figure 5.23: A dust storm approaches Stratford, Texas, in 1935. Figure description available at the end of the chapter.

Soil is not just essential to terrestrial life in nature but also to human civilization via agriculture. Careless or uninformed human activity can seriously damage soil's life-supporting properties. A prime example is the famous Dust Bowl disaster of the 1930s, which affected the Midwestern United States. The damage occurred because of large-scale attempts to develop prairieland in southern Kansas, Colorado, western Texas, and Oklahoma into farmland. Poor understanding of the region's geology, ecology, and climate led to farming practices that ruined the soil profile.

The prairie soils and native plants are well adapted to a relatively dry climate. With government encouragement, settlers moved in to homestead the region. They plowed vast areas of prairie into long, straight rows and planted grain. The plowing broke up the stable soil profile and destroyed the natural grasses and plants, which had long roots that anchored the soil layers. The grains they planted had shallower root systems and were plowed up every year, which made the soil prone to erosion. The plowed furrows were aligned in straight rows running downhill, which favored erosion and loss of topsoil.

The local climate does not produce sufficient precipitation to support non-native grain crops, so the farmers drilled wells and over-pumped water from the underground **aquifers**. The grain crops failed due to lack of water, leaving bare soil that was stripped from the ground by the prairie winds. Particles of midwestern prairie soil were deposited along the East Coast and as far away as Europe. Huge dust storms called black blizzards made life unbearable, and the once-hopeful homesteaders left in droves. Oklahoma during this time is the setting for John Steinbeck's famous novel and John Ford's film, *The Grapes of Wrath*. The lingering question is whether we have learned the lessons of the Dust Bowl to avoid creating it again.

Take this quiz to check your comprehension of this section.

Access the quiz for Section 5.2 by scanning the QR code.

5.3 Sedimentary Rocks

Sedimentary rock is classified into two main categories: clastic and chemical. **Clastic**, or **detrital**, sedimentary rocks are made from pieces of bedrock, sediment, derived primarily by mechanical weathering. Clastic rocks may also include chemically weathered sediment. Clastic rocks are classified by grain shape, grain size, and sorting. Chemical sedimentary rocks are precipitated from water saturated with dissolved minerals. Chemical rocks are classified mainly by composition of minerals in the rock.

5.3.1 Lithification and Diagenesis

Lithification turns loose sediment grains, created by weathering and transported by erosion, into clastic sedimentary rock via three interconnected steps. Deposition happens when friction and gravity overcome the forces driving sediment transport, allowing sediment to accumulate. **Compaction** occurs when material continues to accumulate on top of the sediment layer, squeezing the grains together and driving out water. The mechanical compaction is aided by weak attractive forces between the smaller grains of sediment. Groundwater typically carries cementing agents into the sediment. These minerals, such as calcite, amorphous silica, or oxides, may have a different composition than the sediment grains. **Cementation** is the process of gluing the minerals that coat sediments grains together into a fused rock.

Figure 5.24: Geologic unconformity seen at Siccar Point on the east coast of Scotland. Figure description available at the end of the chapter.

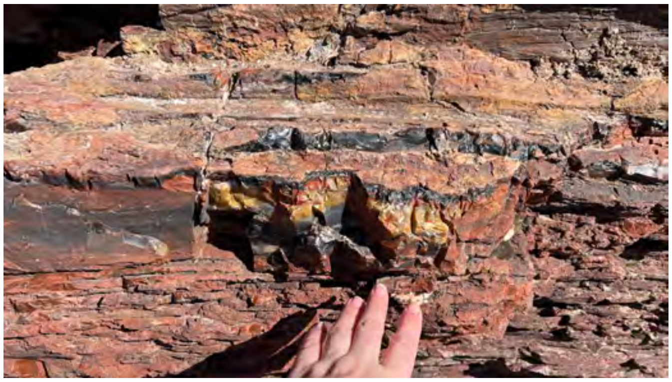

Figure 5.25: Permineralization in petrified wood. Figure description available at the end of the chapter.

Diagenesis is an accompanying process to lithification and is a low-temperature form of rock metamorphism (see Chapter 6). During diagenesis, sediments are chemically altered by heat and pressure. A classic example is aragonite ($CaCO_3$), a form of calcium carbonate that makes up most organic shells. When lithified aragonite undergoes diagenesis, the aragonite reverts to calcite ($CaCO_3$), which has the same chemical formula but a different crystalline structure. In sedimentary rock containing calcite and magnesium (Mg), diagenesis may transform the two minerals into dolomite ($CaMg(CO_3)_2$). Diagenesis may also reduce the **pore** space, or open volume, between sedimentary rock grains. The processes of cementation, compaction, and ultimately lithification occur within the realm of diagenesis, which includes the processes that turn organic material into fossils.

5.3.2 Detrital Sedimentary Rocks (Clastic)

Detrital, or **clastic**, sedimentary rocks consist of preexisting sediment pieces that comes from weathered bedrock. Most of this is mechanically weathered sediment, although some clasts may be pieces of chemical rocks. This creates some overlap between the two categories, since clastic sedimentary rocks may include chemical sediments. Detrital rocks are classified and named based on their grain size.

Grain Size

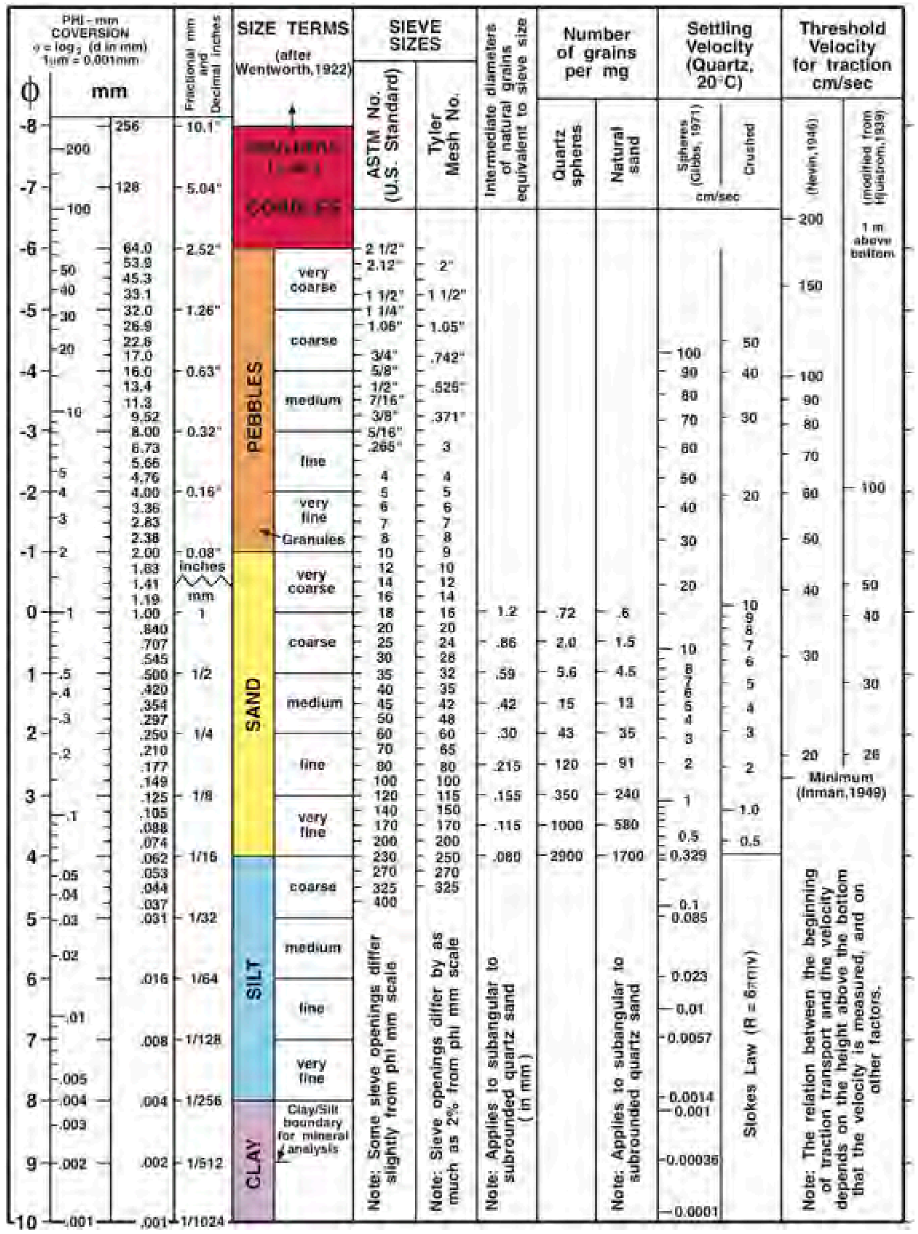

Figure 5.26: Size categories of sediments according to the Wentworth scale. Figure description available at the end of the chapter.

Detrital rock is classified according to sediment **grain size**, which is **graded** from large to small on the Wentworth scale (see Figure 5.26). Grain size is the average diameter of sediment fragments in sediment or rock. Grain sizes are delineated using a log base 2 scale. For example, the grain sizes in the pebble class are 2.52, 1.26, 0.63, 0.32, 0.16, and 0.08 inches, which correlate respectively to very coarse, coarse, medium, fine, and very fine granules. Large fragments, or clasts, include all grain sizes larger than 2 mm (5/64 in). These include boulders, cobbles, granules, and gravel. Sand has a grain size between 2 mm and 0.0625 mm, about the lower limit of the naked eye's resolution. Sediment grains smaller than sand are called silt. Silt is unique; the grains can be felt with a finger or as grit between your teeth but are too small to see with the naked eye.

Sorting and Rounding

Sorting describes the range of grain sizes within sediment or sedimentary rock. Geologists use the term "well sorted" to describe a narrow range of grain sizes, and "poorly sorted" for a wide range of grain sizes (see Figure 5.27). It is important to note that soil engineers use similar terms with opposite definitions; well-graded sediment consists of a variety of grain sizes, and poorly graded sediment has roughly the same grain sizes.

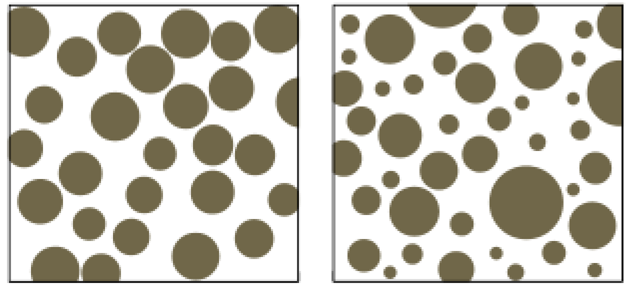

Figure 5.27: A well-sorted sediment (left) and a poorly sorted sediment (right). Figure description available at the end of the chapter.

When reading the story told by rocks, geologists use sorting to interpret erosion or transport processes, as well as deposition energy. For example, wind-blown sands are typically extremely well sorted, while glacial deposits are typically poorly sorted. These characteristics help identify the type of erosion process that occurred. Coarse-grained sediment and poorly sorted rocks are usually found nearer to the source of sediment, while fine sediments are carried farther away. In a rapidly flowing mountain stream, you would expect to see boulders and pebbles. In a lake fed by the stream, there should be sand and silt deposits. Finding large boulders in a lake may indicate the involvement of another sediment transport process, such as rockfall caused by ice or root wedging.

Rounding is created when angular corners of rock fragments are removed from a piece of sediment due to abrasion during transport. Well-rounded sediment grains are defined as being free of all sharp edges. Very angular sediment retains the sharp corners. Most clast fragments start with some sharp edges due to the bedrock's crystalline structure, and those points are worn down during transport. More-rounded grains imply a longer erosion time or transport distance or a more energetic erosional process. Mineral hardness is also a factor in rounding.

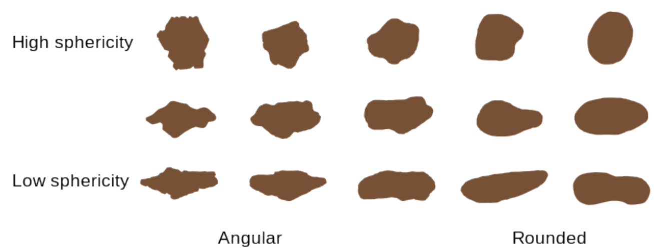

Figure 5.28: Degree of rounding in sediments. Sphericity refers to the spherical nature of an object, a completely different measurement unrelated to rounding. Figure description available at the end of the chapter.

Composition and Provenance

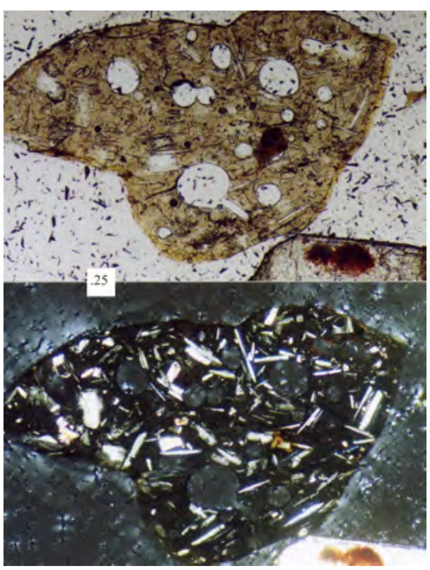

Figure 5.29: A sand grain made of basalt, known as a microlitic volcanic lithic fragment. Box is 0.25 mm. (Top) plane-polarized light. (Bottom) Cross-polarized light. Figure description available at the end of the chapter.

Composition describes the mineral components found in sediment or sedimentary rock and may be influenced by local geology, like **source rock** and hydrology. Other than clay, most sediment components are easily determined by visual inspection (see Chapter 3). The most commonly found sediment mineral is quartz because of its low chemical reactivity and high hardness, making it resistant to weathering, and its ubiquitous occurrence in continental bedrock. Other commonly found sediment grains include feldspar and lithic fragments. Lithic fragments are pieces of fine-grained bedrock and include mud chips, volcanic clasts, or pieces of slate.

Weathering of volcanic rock produces Hawai'i's famous black (basalt) and green (olivine) sand beaches, which are rare elsewhere on Earth. This is because the local rock is composed almost entirely of basalt and provides an abundant source of dark-colored clasts loaded with mafic minerals. According to the Goldich dissolution series, clasts high in mafic minerals are more easily destroyed compared to clasts composed of felsic minerals like quartz.

Geologists use **provenance** to discern the original source of sediment or sedimentary rock. Provenance is determined by analyzing mineral composition and types of fossils present, as well as textural features like sorting and rounding. Provenance is important for describing tectonic history, visualizing paleogeographic formations, unraveling an area's geologic history or reconstructing past supercontinents.

In quartz sandstone, sometimes called quartz arenite (SiO_2), provenance may be determined using a rare, durable clast mineral called **zircon** ($ZrSiO_4$). Zircon, or zirconium silicate, contains traces of uranium, which can be used for age-dating the source bedrock that contributed sediment to the lithified sandstone rock (see Chapter 7).

Figure 5.30: Hawaiian beach composed of black sand from weathering of nearby basaltic rock. Figure description available at the end of the chapter.

Classification of Clastic Rocks

Clastic rocks are classified according to the grain size of their sediment. Coarse-grained rocks contain clasts with a predominant grain size larger than sand. Typically, smaller sediment grains, collectively called groundmass or matrix, fill in much of the volume between the larger clasts, holding the clasts together. **Conglomerates** are rocks containing coarse rounded clasts, and breccias contain angular clasts (see Figure 5.31). Both conglomerates and breccias are usually poorly sorted.

Figure 5.31: Megabreccia in Titus Canyon, Death Valley National Park, California. Figure description available at the end of the chapter.

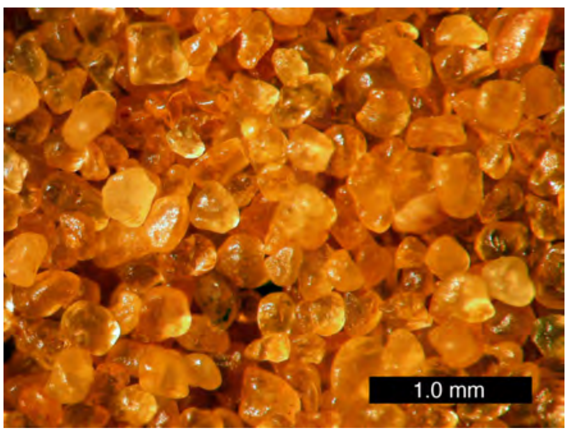

Figure 5.32: Enlarged image of frosted and rounded windblown sand grains. Figure description available at the end of the chapter.

Medium-grained rocks composed mainly of sand are called sandstone, or sometimes arenite if well sorted. Sediment grains in sandstone can have a wide variety of mineral compositions, roundness, and sorting. Some sandstone names indicate the rock's mineral composition. Quartz sandstone contains predominantly quartz sediment grains. **Arkose** is sandstone with significant amounts of feldspar, usually greater than 25%. Sandstone that contains feldspar, which weathers more quickly than quartz, is useful for analyzing the local geologic history. **Greywacke** is a term with conflicting definitions, referring to either sandstone with a muddy matrix or sandstone with many lithic fragments (small rock pieces).

Figure 5.33: The Rochester Shale, New York. Note the thin fissility in the layers. Figure description available at the end of the chapter.

Fine-grained rocks include mudstone, shale, siltstone, and claystone. **Mudstone** is a general term for rocks made of sediment grains smaller than sand (less than 2 mm). Rocks that are **fissile**—meaning they separate into thin sheets—are called shale. Rocks exclusively composed of silt or clay sediment are called **siltstone** or **claystone**, respectively. These last two rock types are rarer than mudstone or shale.

Figure 5.34: Claystone laminations from Glacial Lake Missoula. Figure description available at the end of the chapter.

Rock types found as a mixture between the main classifications may be named using the less-common component as a descriptor. For example, a rock containing some silt but mostly rounded sand and gravel is called a silty conglomerate. Sand-rich rock containing minor amounts of clay is called clayey sandstone.

5.3.3 Chemical, Biochemical, and Organic

Chemical sedimentary rocks are formed by processes that do not directly involve mechanical weathering and erosion. Chemical weathering may contribute the dissolved materials in water that ultimately form these rocks. Biochemical and organic sediments are clastic in the sense that they are made from pieces of organic material that is deposited, buried, and lithified; however, they are usually classified as being chemically produced.

Inorganic chemical sedimentary rocks are made of minerals precipitated from ions dissolved in solution and are created without the aid of living organisms. Inorganic chemical sedimentary rocks form in environments where ion concentration, dissolved gases, temperatures, or pressures are changing, which causes minerals to crystallize.

Biochemical sedimentary rocks are formed from shells and bodies of underwater organisms. The living organisms extract chemical components from the water and use them to build shells and other body parts. The components include silica and aragonite, a mineral similar to and commonly replaced by calcite.

Organic sedimentary rocks come from organic material that has been deposited and lithified, usually under water. The source materials are plant and animal remains that are transformed through burial and heat, ending up as **coal**, **oil**, and methane (**natural gas**).

Inorganic Chemical

Inorganic chemical sedimentary rocks are formed when minerals precipitate out of an aqueous solution, usually due to water evaporation. The precipitate minerals form various salts known as evaporites. For example, the Bonneville Salt Flats in Utah flood with winter rains and dry out every summer, leaving behind salts such as gypsum and halite. The deposition order of evaporite deposits is opposite to their solubility order—i.e., as water evaporates and increases the mineral concentration in solution, less-soluble minerals precipitate out sooner than the highly soluble minerals. The deposition order and saturation percentages are depicted in Table 5.1, bearing in mind the process in nature may vary from laboratory derived values.

Figure 5.35: Salt-covered plain known as the Bonneville Salt Flats, Utah. Figure description available at the end of the chapter.

Mineral sequence	Percent seawater remaining after evaporation
Calcite	50%
Gypsum/anhydrite	20%
Halite	10%
Various potassium and magnesium salts	5%

Table 5.1: Deposition order and saturation percentages.

Figure 5.36: Ooids from Joulter's Cay, The Bahamas. Figure description available at the end of the chapter.

Figure 5.37: Limestone tufa towers along the shores of Mono Lake, California. Figure description available at the end of the chapter.

Calcium carbonate-saturated water precipitates porous masses of calcite called **tufa**. Tufa can form near degassing water and in saline lakes. Waterfalls downstream of springs often precipitate tufa as the turbulent water enhances degassing of carbon dioxide, which makes calcite less soluble and causes it to precipitate. Saline lakes concentrate calcium carbonate through a combination of wave action causing degassing, springs in the lakebed, and evaporation. In salty Mono Lake in California, tufa towers were exposed after water was diverted and lowered the lake levels.

Figure 5.38: Travertine ground surface of Mammoth Hot Springs, Yellowstone National Park, USA. Figure description available at the end of the chapter.

Cave deposits like stalactites and stalagmites are another form of chemical precipitation of calcite, in a form called **travertine**. Calcite slowly precipitates from water to form the travertine, which often shows **banding**. This process is similar to the mineral growth on faucets in your home sink or shower that comes from hard (mineral-rich) water. Travertine also forms at hot springs such as Mammoth Hot Springs in Yellowstone National Park.

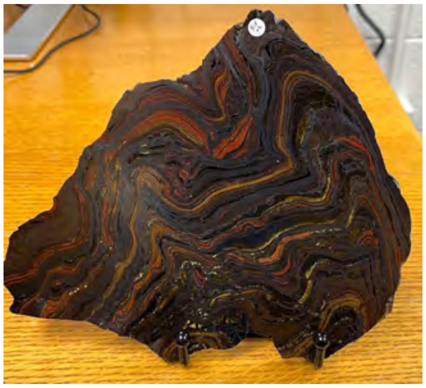

Figure 5.39: This sample of banded iron formation displays alternating bands of iron-rich and silica-rich mud, formed as oxygen combined with dissolved iron. Figure description available at the end of the chapter.

Banded iron formation deposits commonly formed early in Earth's history, but this type of chemical sedimentary rock is no longer being created. Oxygenation of the atmosphere and oceans caused free iron ions, which are water-soluble, to become oxidized and precipitate out of solution. The iron oxide was deposited, usually in bands alternating with layers of chert.

Figure 5.40: A type of chert, flint, shown with a lighter weathered crust. Figure description available at the end of the chapter.

Chert, another commonly found chemical sedimentary rock, is usually produced from silica (SiO_2) precipitated from groundwater. Silica is highly insoluble on the surface of Earth, which is why quartz is so resistant to chemical weathering. Water deep underground is subjected to higher pressures and temperatures, which helps dissolve silica into an aqueous solution. As the groundwater rises toward or emerges at the surface, the silica precipitates out, often as a cementing agent or into nodules. For example, the bases of the geysers in Yellowstone National Park are surrounded by silica deposits called geyserite, or sinter. The silica is dissolved in water that is thermally heated by a relatively deep magma source. Chert can also form biochemically and is discussed in the biochemical subsection. Chert has many synonyms, some of which may have gem value, such as jasper, flint, onyx, and agate, due to subtle differences in colors, striping, and other factors; however, chert is the more general term used by geologists for the entire group.

Figure 5.41: Ooids forming an oolite. Figure description available at the end of the chapter.

Oolites are among the few limestone forms created by an inorganic chemical process, similar to what happens in evaporite deposition. When water is oversaturated with calcite, the mineral precipitates out around a nucleus, a sand grain or shell fragment, and forms little spheres called **ooids** (see Figure 5.41). As evaporation continues, the ooids continue building concentric layers of calcite as they roll around in gentle currents.

Biochemical

Figure 5.42: Hokie Stone is a dolomite-limestone rock found near Blacksburg, Virginia, and is prominently displayed on the majority of buildings throughout the Blacksburg campus of Virginia Tech. (Top) Hokie Stone façade detail on Holden Hall. (Bottom) Polished sample of Hokie Stone next to rough cut sample. Figure description available at the end of the chapter.

Biochemical sedimentary rocks are not that different from chemical sedimentary rocks; they are also formed from ions dissolved in solution. However, biochemical sedimentary rocks rely on biological processes to extract the dissolved materials out of the water. Most macroscopic marine organisms use dissolved minerals, primarily aragonite (calcium carbonate), to build hard parts such as shells. When organisms die, the hard parts settle as sediment, which become buried, compacted, and cemented into rock.

This biochemical extraction and secretion is the main process for forming limestone, the most commonly occurring nonclastic sedimentary rock. Limestone is mostly made of calcite ($CaCO_3$) and sometimes includes dolomite ($CaMgCO_3$), a close relative. Solid calcite reacts with hydrochloric acid by effervescing or fizzing. Dolomite only reacts to hydrochloric acid when ground into a powder, which can be done by scratching the rock surface (see Chapter 3).

Limestone occurs in many forms, most of which originate from biological processes. Entire coral reefs and their ecosystems can be preserved in exquisite detail in limestone rock. **Fossiliferous** limestone contains many visible fossils. A type of limestone called **coquina** originates from beach sands made predominantly of shells that were lithified. Coquina is composed of loosely cemented shells and shell fragments. You can find beaches like this in modern tropical environments, such as the Bahamas. **Chalk** contains high concentrations of shells from a microorganism called a coccolithophore. **Micrite**, also known as microscopic calcite mud, is a very fine-grained limestone containing microfossils that can only be seen using a microscope.

Figure 5.43: Shell fragments make up the rock coquina. (Top) Hand sample. (Bottom) Close-up (different sample). Figure description available at the end of the chapter.

Biogenetic chert forms on the deep ocean floor, created from biochemical sediment made of microscopic organic shells. This sediment, called ooze, may be calcareous (calcium carbonate based) or siliceous (silica based) depending on the type of shells deposited. For example, the shells of radiolarians (zooplankton) and diatoms (phytoplankton) are made of silica, so they produce siliceous ooze.

Organic

Figure 5.44: Anthracite coal, the highest grade of coal. Figure description available at the end of the chapter.

Under the right conditions, intact pieces of organic material (or material derived from organic sources), is preserved in the geologic record. Although not derived from sediment, this lithified organic material is associated with sedimentary strata and created by similar processes—burial, compaction, and diagenesis. Deposits of these fuels develop in areas where organic material collects in large quantities. Lush swamplands can create conditions conducive to coal formation. Shallow-water, organic material-rich marine sediment can become highly productive petroleum and natural gas deposits. See Chapter 16 for a more in-depth look at these fossil-derived energy sources.

Classification of Chemical Sedimentary Rocks

In contrast to detrital sediment, the classification of chemical, biochemical, and organic sedimentary rocks is based on mineral composition. Most of these are monomineralic, composed of a single mineral, so the rock name is usually associated with the identifying mineral. Chemical sedimentary rocks consisting of halite are called rock salt. Rocks made of limestone (calcite) is an exception, having elaborate subclassifications and even two competing classification methods: Folk classification and Dunham classification. The Folk classification deals with rock grains and usually requires a specialized petrographic microscope. The Dunham classification is based on rock texture, which is visible to the naked eye or through the use of a hand lens and is easier for field applications. Most carbonate geologists use the Dunham system.

Figure 5.45: Gyprock, a rock made of the mineral gypsum. From the Castile Formation of New Mexico. Figure description available at the end of the chapter.

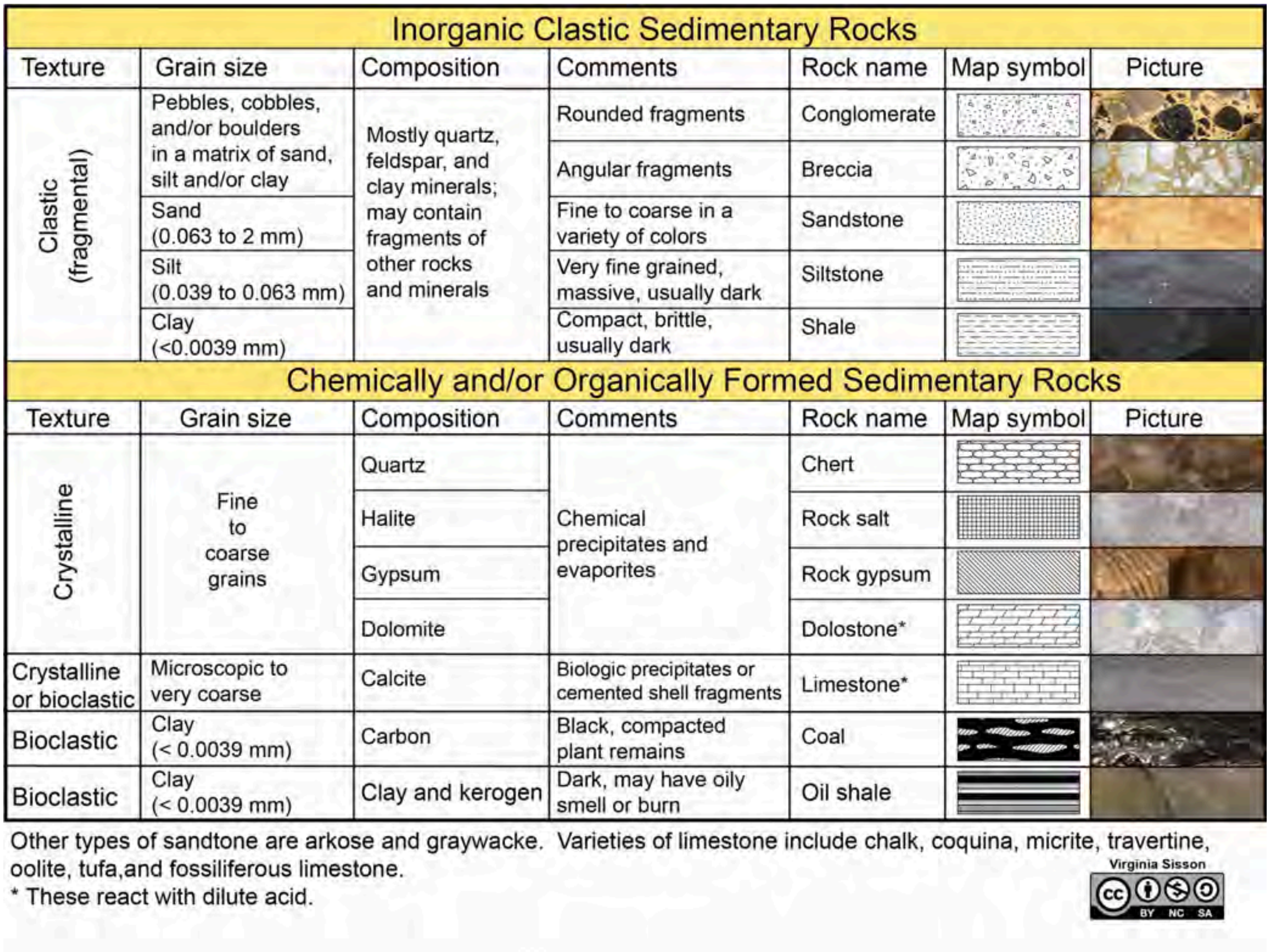

Inorganic Clastic Sedimentary Rocks						
Texture	Grain size	Composition	Comments	Rock name	Map symbol	Picture
Clastic (fragmental)	Pebbles, cobbles, and/or boulders in a matrix of sand, silt and/or clay	Mostly quartz, feldspar, and clay minerals; may contain fragments of other rocks and minerals	Rounded fragments	Conglomerate		
			Angular fragments	Breccia		
	Sand (0.063 to 2 mm)		Fine to coarse in a variety of colors	Sandstone		
	Silt (0.039 to 0.063 mm)		Very fine grained, massive, usually dark	Siltstone		
	Clay (<0.0039 mm)		Compact, brittle, usually dark	Shale		
Chemically and/or Organically Formed Sedimentary Rocks						
Texture	Grain size	Composition	Comments	Rock name	Map symbol	Picture
Crystalline	Fine to coarse grains	Quartz	Chemical precipitates and evaporites	Chert		
		Halite		Rock salt		
		Gypsum		Rock gypsum		
		Dolomite		Dolostone*		
Crystalline or bioclastic	Microscopic to very coarse	Calcite	Biologic precipitates or cemented shell fragments	Limestone*		
Bioclastic	Clay (< 0.0039 mm)	Carbon	Black, compacted plant remains	Coal		
Bioclastic	Clay (< 0.0039 mm)	Clay and kerogen	Dark, may have oily smell or burn	Oil shale		

Other types of sandtone are arkose and graywacke. Varieties of limestone include chalk, coquina, micrite, travertine, oolite, tufa,and fossiliferous limestone.
* These react with dilute acid.

Virginia Sisson

CC BY NC SA

Figure 5.46: Sedimentary rock identification chart. Figure description available at the end of the chapter.

Take this quiz to check your comprehension of this section.

Access the quiz for Section 5.3 by scanning the QR code.

5.4 Sedimentary Structures

Sedimentary structures are visible textures or arrangements of sediments within a rock. Geologists use these structures to interpret the processes that made the rock and the environment in which it formed. They use uniformitarianism to usually compare sedimentary structures formed in modern environments to lithified counterparts in ancient rocks. Below is a summary discussion of common sedimentary structures that are useful for interpretations in the rock record.

5.4.1 Bedding Planes

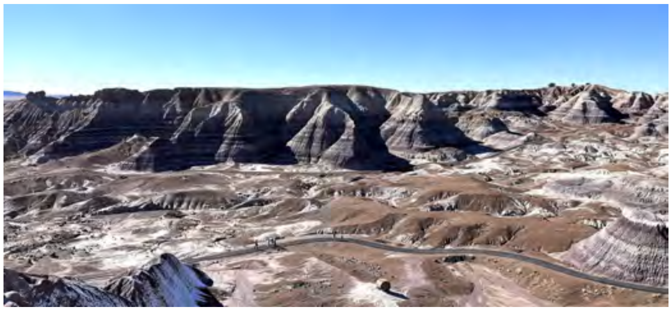

Figure 5.47: Sedimentary beds visible in Petrified Forest National Park. Figure description available at the end of the chapter.

The most basic sedimentary structure is **bedding** planes, the planes that separate the layers or strata in sedimentary and some volcanic rocks. Visible in exposed outcroppings, each bedding plane indicates a change in sediment deposition conditions. This change may be subtle; for example, if a section of underlying sediment firms up, this may be enough to create a layer that is dissimilar from the overlying sediment. Each layer is called a **bed**, or stratum, the most basic unit of **stratigraphy**, the study of sedimentary layering.

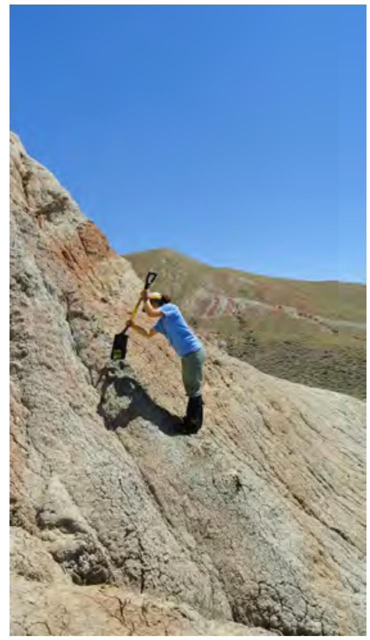

Figure 5.48: A student from the University of North Carolina digs into beds of Paleocene-Eocene sedimentary strata in northwestern Wyoming. Figure description available at the end of the chapter.

As would be expected, bed thickness can indicate sediment deposition quantity and timing. Technically, a bed is a bedding plane thicker than 1 cm (0.4 in) and the smallest mappable unit. A layer thinner than 1 cm (0.4 in) is called a lamina. **Varves** are bedding planes created when **laminae** and beds are deposited in repetitive cycles, typically occurring on a daily or seasonal basis. Varves are valuable geologic records of climatic histories, especially those found in lakes and glacial deposits.

5.4.2 Graded Bedding

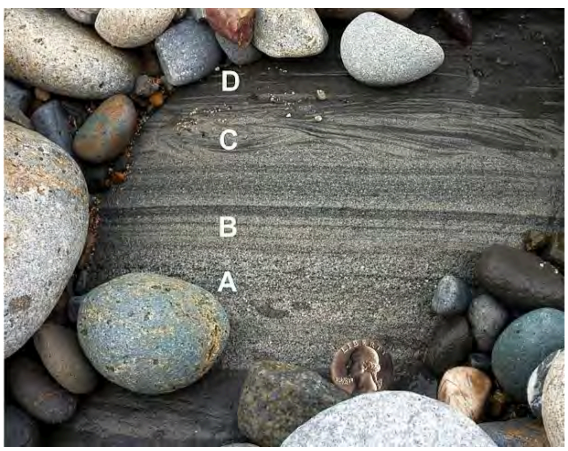

Figure 5.49: Image of the classic Bouma sequence. A = coarse- to fine-grained sandstone, possibly with an erosive base. B = laminated medium- to fine-grained sandstone. C = rippled fine-grained sandstone. D = laminated siltstone grading to mudstone. Figure description available at the end of the chapter.

Graded bedding refers to a sequence of increasingly coarse- or fine-grained sediment layers. Graded bedding often develops when sediment deposition occurs in an environment of decreasing energy. A **Bouma sequence** is graded bedding observed in clastic rock called **turbidite**. Bouma sequence beds are formed by offshore sediment gravity flows, which are underwater flows of sediment. These subsea density flows begin when sediment is stirred up by an energetic process and becomes a dense slurry of mixed grains. The sediment flow courses downward through submarine channels and **canyons** due to gravity acting on the density difference between the denser slurry and less dense surrounding seawater. As the flow reaches deeper ocean basins, it slows down, loses energy, and deposits sediment in a Bouma sequence of coarse grains first, followed by increasingly finer grains (see Figure 5.49).

5.4.3 Flow Regime and Bedforms

In fluid systems, such as moving water or wind, sand is the most easily transported and deposited sediment grain. Smaller particles like silt and clay are less movable by fluid systems because the tiny grains are chemically attracted to each other and stick to the underlying sediment. Under higher flow rates, the fine silt and clay sediment tends to stay in place, and the larger sand grains get picked up and moved.

Bedforms are sedimentary structures created by fluid systems working on sandy sediment. Grain size, flow velocity, and **flow regime** (or flow pattern) interact to produce bedforms that have unique, identifiable physical characteristics. Flow regimes are divided into upper and lower regimes, which are further divided into uppermost, upper, lower, and lowermost parts. The table below shows bedforms and their associated flow regimes. For example, the dunes bedform is created in the upper part of the lower flow regime.

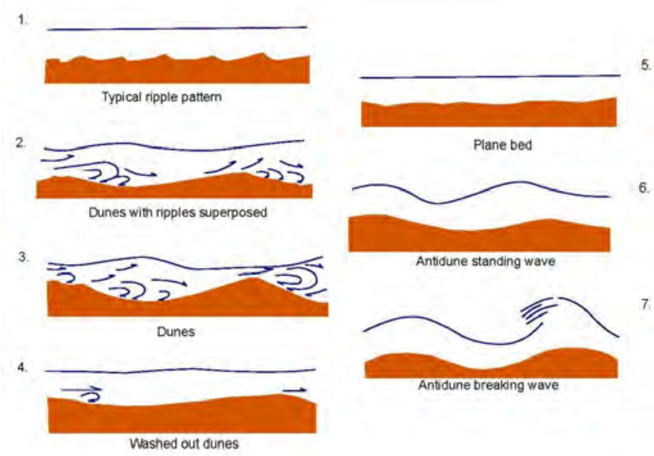

Figure 5.50: Bedforms under increasing flow velocities. Figure description available at the end of the chapter.

Flow regime (part)	Bedform	Description
Lower (lowest)	Plane bed	Lower plane bed, flat laminations
Lower (lower)	Ripples	Small (with respect to flow) inclined layers dipping downflow
Lower (upper)	Dunes	Larger inclined cross-beds, ±ripples, dipping downflow
Upper (lower)	Plane bed	Flat layers, can include lined-up grains (parting lineations)
Upper (upper)	Antidunes	Hard to preserve reverse dunes dipping shallowly upflow
Upper (uppermost)	Chutes/pools (rare)	Erosional, not really a bedform; rarely found preserved

Table 5.2: Bedforms and their associated flow regimes.

Plane Beds

Plane beds created in the lower flow regime are like bedding planes on a smaller scale. The flat, parallel layers form as sandy sediment piles and move on top of layers below. Even nonflowing fluid systems, such as lakes, can produce sediment plane beds. Plane beds in the upper flow regime are created by fast-flowing fluids. They may look identical to beds with lower flow regimes; however, they typically show **parting lineations**, slight alignments of grains in rows and swaths caused by high sediment transport rates that only occur in upper flow regimes.

Figure 5.51: Subtle lines across this sandstone (trending from the lower left to upper right) are parting lineations. Figure description available at the end of the chapter.

Figure 5.52: Modern current ripple in sand from the Netherlands. The flow creates a steep side down current. In this image, the flow is from right to left. Figure description available at the end of the chapter.

Ripples

Ripples are known by several names: ripple marks, ripple cross-beds, or ripple cross-laminates. The ridges or undulations in the bed are created as sediment grains pile on top of the plane bed. With the exception of dunes, the scale of these beds is typically measured in centimeters. Occasionally, large flows like glacial lake outbursts can produce ripples as tall as 20 m (66 ft).

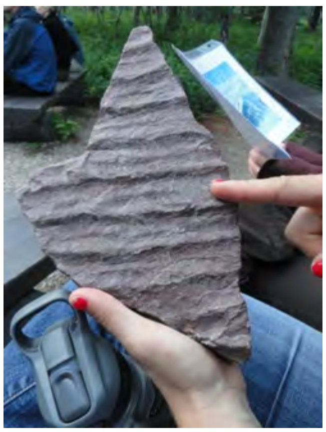

Figure 5.53: Ripple marks visible in 1.6-billion-year-old rock in Glacier National Park, Montana. Figure description available at the end of the chapter.

First scientifically described by Hertha Ayrton, ripple shapes are determined by flow type and can be straight-crested, sinuous, or complex. Asymmetrical ripples form in a unidirectional flow. Symmetrical ripples are the result of an oscillating back-and-forth flow typical of inter-tidal swash zones. Climbing ripples are created from high sedimentation rates and appear as overlapping layers of ripple shapes (see Figure 5.54).

Figure 5.54: Climbing ripple deposit from India. Figure description available at the end of the chapter.

Dunes

Dunes are very large and prominent versions of ripples, and they are typical examples of large cross-bedding. **Cross-bedding** happens when ripples or dunes pile atop one another, interrupting, and/or cutting into the underlying layers. Desert sand dunes are probably the first image conjured up by this category of bedform.

British geologist Ralph Agnold (1941) considered barchan and linear seif dunes as the only true dune forms. Other workers have recognized other types of dunes, including transverse and star dunes as well as **parabolic** and **linear** dunes anchored by plants, which are common in coastal areas.

Figure 5.55: Lithified cross-bedded dunes in Zion National Park, Utah. Figure description available at the end of the chapter.

Figure 5.56: Modern sand dune in Morocco. Figure description available at the end of the chapter.

Dunes are the most common sedimentary structure found within channelized flows of air or water. The biggest difference between river dunes and air-formed (desert) dunes is the depth of the fluid systems. Since the atmosphere's depth is immense when compared to a river channel, desert dunes are much taller than those found in rivers. Some famous air-formed dune landscapes include the Sahara Desert, Death Valley, and the Gobi Desert.

As airflow moves sediment along, the grains accumulate on the dune's windward (wind-facing) surface. The angle of the windward side is typically shallower than the leeward (downwind) side, down which the grains fall. This difference in slopes can be seen in a bed cross section and indicates the direction of the flow in the past. There are typically two styles of dune beds: the more common trough cross-beds with curved windward surfaces and rarer planar cross-beds with flat windward surfaces.

In tidal locations with strong in-and-out flows, dunes can develop in opposite directions. This produces a feature called herringbone cross-bedding.

Another dune formation variant occurs when very strong, hurricane-strength winds agitate parts of the usually undisturbed seafloor. These beds are called **hummocky cross-stratification** and have a 3-D architecture of hills and valleys, with inclined and declined layering that matches the dune shapes.

Figure 5.57: Herringbone cross-bedding from the Mazomanie Formation, from the Upper Cambrian in Minnesota. Figure description available at the end of the chapter.

Figure 5.58: Hummocky cross-stratification, seen as wavy lines throughout the middle of this rock face. Best example is just above the pencil in the center. Figure description available at the end of the chapter.

Antidunes

Antidunes are so named because they share similar characteristics with dunes but are formed by a different, opposing process. While dunes form in lower flow regimes, antidunes come from fast-flowing upper flow regimes. In certain conditions of high flow rates, sediment accumulates upstream of a subtle dip instead of traveling downstream (see Figure 5.59). Antidunes form in phase with the flow; in rivers, they are marked by rapids in the current. Antidunes are rarely preserved in the rock record because the high flow rates needed to produce the beds also accelerate erosion.

Figure 5.59: Antidunes forming in Urdaibai, Spain. [Figure description available at the end of the chapter](#).

5.4.4 Bioturbation

Figure 5.60: Bioturbated dolomitic siltstone from Kentucky. [Figure description available at the end of the chapter](#).

Bioturbation is the result of organisms burrowing through soft sediment, which disrupts the bedding layers. These tunnels are backfilled and eventually preserved when the sediment becomes rock. Bioturbation happens most commonly in shallow marine environments and can be used to indicate water depth.

5.4.5 Mudcracks

Mudcracks occur in clay-rich sediment that is submerged under water and later dries out. Water fills voids in the clay's crystalline structure, causing the sediment grains to swell. When this waterlogged sediment begins to dry out, the clay grains shrink. The sediment layer forms deep polygonal cracks with tapered openings toward the surface, which can be seen in profile. The cracks fill with new sediment and become visible veins running through the lithified rock. These dried-out clay beds are a major source of **mud chips**, small fragments of mud or shale that commonly become **inclusions** in sandstone and conglomerate. What makes this sedimentary structure so important to geologists is they only form in certain depositional environments, such as tidal flats that form underwater and are later exposed to air. Syneresis cracks are similar in appearance to mudcracks but much rarer; they are formed when subaqueous (underwater) clay sediment shrinks.

Figure 5.61: (Top) Modern mudcracks in Wyoming. (Bottom) Lithified mudcracks from Maryland. [Figure description available at the end of the chapter](#).

5.4.6 Sole Marks

Figure 5.62: This flute cast shows a flow direction toward the upper right of the image, as seen by the bulge extending down out of the layer above. The flute cast would have been scoured into a rock layer below that has been removed by erosion, leaving the sandy layer above to fill in the flute cast. [Figure description available at the end of the chapter](#).

Sole marks are small features typically found in river deposits. They form at the base of a bed (the sole), and on top of the underlying bed. They can indicate several things about the deposition conditions, such as flow direction or stratigraphic up-direction (see Geopetal Structures section). Flute casts or scour marks are grooves carved out by the forces of fluid flow and sediment loads. The upstream part of the flow creates steep grooves, while the downstream grooves are shallower. The grooves subsequently become filled by overlying sediment, creating a cast of the original hollow.

Formed similarly to flute casts but with a more regular and aligned shape, groove casts are produced by larger clasts or debris carried along in the water that scrape across the sediment layer. Tool marks come from objects like sticks carried in the fluid downstream or embossed into the sediment layer, leaving a depression that later fills with new sediment.

Figure 5.63: Groove casts at the base of a turbidite deposit in Italy. Figure description available at the end of the chapter.

Load casts, an example of **soft-sediment deformation**, are small indentations made by an overlying layer of coarse sediment grains or by clasts intruding into a softer, finer-grained sediment layer.

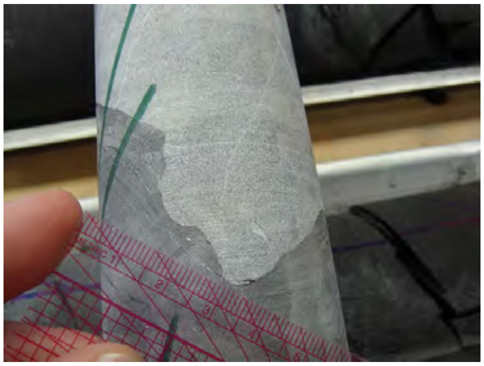

Figure 5.64: A drill core showing a load cast with light-colored sand extending down into dark mud. Figure description available at the end of the chapter.

5.4.7 Raindrop Impressions

Like their name implies, **raindrop impressions** are small pits or bumps found in soft sediment. While they are generally believed to be created by rainfall, they may be caused by other agents, such as escaping gas bubbles.

Figure 5.65: Mississippian raindrop impressions over wave ripples from Nova Scotia. Figure description available at the end of the chapter.

5.4.8 Imbrication

Figure 5.66: Cobbles in this conglomerate in Switzerland are positioned in a way that they are stacked on each other, which occurred as flow moved from left to right. Figure description available at the end of the chapter.

Imbrication is a stack of large and usually flat clasts—cobbles, gravels, mud chips, etc.—that are aligned in the direction of fluid flow. The clasts may be stacked in rows, with their edges dipping down and flat surfaces aligned to face the flow (see Figure 5.66), or their flat surfaces may be parallel to the layer and long axes aligned with flow. Imbrications are useful for analyzing **paleocurrents**, or currents found in the geologic past, especially in alluvial deposits.

5.4.9 Geopetal Structures

Geopetal structures, also called up-direction indicators, are used to identify which way was up when the sedimentary rock layers were originally formed. This is especially important in places where the rock layers have been deformed, tilted, or overturned. Well-preserved mudcracks, sole marks, and raindrop impressions can be used to determine up direction. Other useful geopetal structures include:

- Vugs—Small voids in the rock that usually become filled during diagenesis. If the void is partially filled or filled in stages, it serves as a permanent record of a level bubble, frozen in time.
- Cross-bedding—In places where ripples or dunes pile on top of one another, where one cross-bed interrupts and/or cuts below another, this shows a cross-cutting relationship that indicates up direction.
- Ripples, dunes—Sometimes the ripples are preserved well enough to differentiate between the crests (top) and troughs (bottom).
- Fossils—Body fossils in life position, meaning the body parts are not scattered or broken, and **trace fossils** like footprints (see Figure 5.68) can provide an up direction. Intact fossilized coral reefs are excellent up indicators because of their large sizes and easily distinguishable tops and bottoms. Index fossils, such as ammonites, can be used to age date strata and determine up direction based on relative rock ages.
- Vesicles—Lava flows eliminate gas upwards. An increase of vesicles toward the top of the flow indicates up.

Figure 5.67: This bivalve (clam) fossil was partially filled with tan sediment, partially empty. Later fluids filled in the fossil with white calcite minerals. The line between the sediment and the later calcite is paleo-horizontal. Figure description available at the end of the chapter.

Figure 5.68: Eubrontes trace fossil from Utah, showing that the geopetal direction is into the image. Figure description available at the end of the chapter.

Take this quiz to check your comprehension of this section.

Access the quiz for Section 5.4 by scanning the QR code.

5.5 Depositional Environments

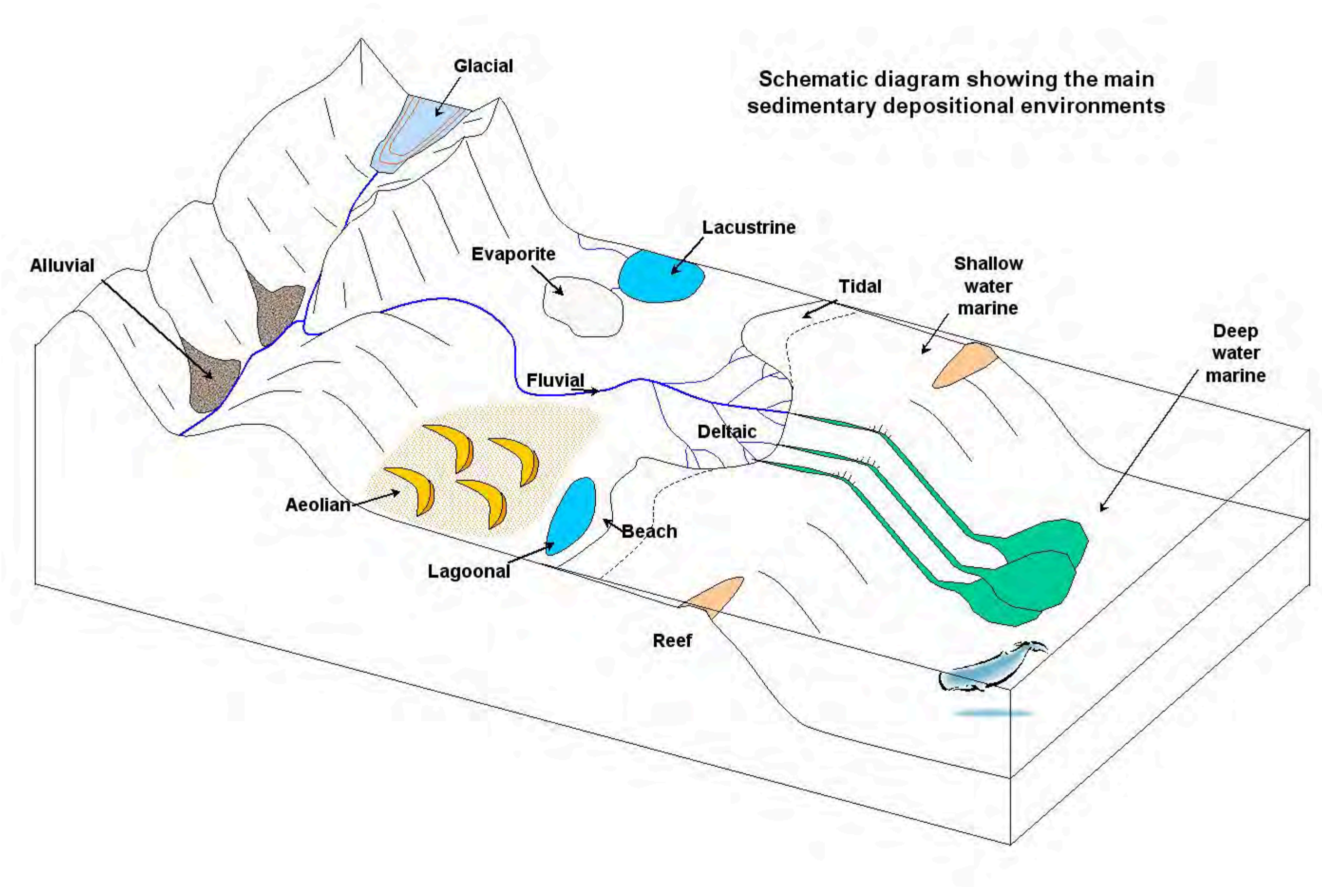

Figure 5.69: A representation of common depositional environments. Figure description available at the end of the chapter.

The ultimate goal of many stratigraphy studies is to understand the original **depositional environment**. Knowing where and how a particular sedimentary rock was formed can help geologists paint a picture of past environments—such as a mountain glacier, gentle floodplain, dry desert, or deep-sea ocean floor. The study of depositional environments is a complex endeavor; Table 5.3 shows a simplified version of what to look for in the rock record.

Location	Sediment	Common rock types	Typical fossils	Sedimentary structures
Abyssal	Very fine muds and oozes, diatomaceous earth	Chert	Diatoms	Few
Submarine fan	Graded Bouma sequences, alternating sand/mud	Clastic rocks	Rare	Channels, fan shape
Continental slope	Mud, possible sand, countourites	Shale, siltstone, limestone	Rare	Swaths
Lower shoreface	Laminated sand	Sandstone	Bioturbation	Hummocky cross-beds
Upper shoreface	Planar sand	Sandstone	Bioturbation	Plane beds, cross-beds
Littoral (beach)	Very well-sorted sand	Sandstone	Bioturbation	Few
Tidal flat	Mud and sand with channels	Shale, mudstone, siltstone	Bioturbation	Mudcracks, symmetric ripples
Reef	Lime mud with coral	Limestone	Many, commonly coral	Few
Lagoon	Laminated mud	Shale	Many, bioturbation	Laminations
Delta	Channelized sand with mud, ±swamp	Clastic rocks	Many to few	Cross-beds
Fluvial (river)	Sand and mud, can have larger sediments	Sandstone, conglomerate	Bone beds (rare)	Cross-beds, channels, asymmetric ripples
Alluvial	Mud to boulders, poorly sorted	Clastic rocks	Rare	Channels, mud cracks
Lacustrine (lake)	Fine-grained laminations	Shale	Invertebrates, rare (deep) bone beds	Laminations
Paludal (swamp)	Plant material	Coal	Plant debris	Rare
Aeolian (dunes)	Very well-sorted sand and silt	Sandstone	Rare	Cross-beds (large)
Glacial	Mud to boulders, poorly sorted	Conglomerate (tillite)		Striations, drop stones

Table 5.3: Rock record and depositional environments.

5.5.1 Marine

Marine depositional environments are completely and constantly submerged in seawater. Their depositional characteristics are largely dependent on the depth of water, with two notable exceptions: submarine fans and turbidites.

Abyssal

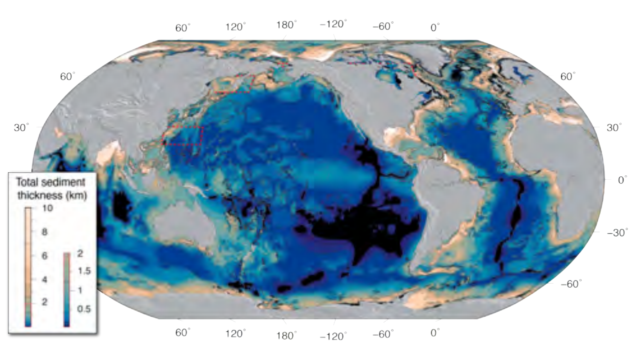

Figure 5.70: Marine sediment thickness. Note the lack of sediment away from the continents. Figure description available at the end of the chapter.

Abyssal sedimentary rocks form on the abyssal plain. The plain is made up of relatively flat ocean floor with some minor topographical features called abyssal hills. These small seafloor mounts range from 100 m to 20 km in diameter and are possibly created by extension. Most abyssal plains do not experience significant fluid movement, so sedimentary rock formed there are very fine grained.

There are three categories of abyssal sediment. Calcareous oozes consist of calcite-rich plankton shells that have fallen to the ocean floor. An example of this type of sediment is chalk. Siliceous oozes are also made of plankton debris, but these organisms build their shells using silica or hydrated silica. In some cases, such as with diatomaceous earth, sediment is deposited below the **calcite compensation depth**, a depth where calcite solubility increases. Any calcite-based shells are dissolved, leaving only silica-based shells. Chert is another common rock formed from these types of sediment. These two types of abyssal sediment are also classified as biochemical in origin (see Section 5.3.3).

The third sediment type is pelagic clay. Very fine-grained clay particles, typically brown or red, descend through the water column very slowly. Pelagic clay deposition occurs in areas of remote open ocean, where there is little plankton accumulation.

Figure 5.71: Diatomaceous earth. Figure description available at the end of the chapter.

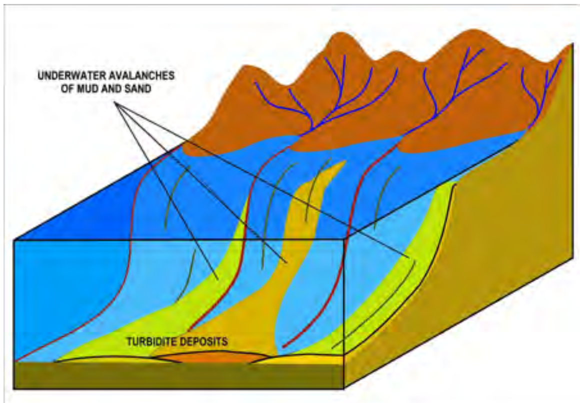

Figure 5.72: Turbidites interdeposited within submarine fans. Figure description available at the end of the chapter.

Two notable exceptions to the fine-grained nature of abyssal sediment are submarine fan and turbidite deposits. Submarine fans occur offshore at the base of large river systems. They are initiated during times of low sea level, when strong river currents carve **submarine canyons** into the **continental shelf**. When sea levels rise, sediment accumulates on the shelf, typically forming large, fan-shaped floodplains called **deltas**. Periodically, the sediment is disturbed, creating dense slurries that flush down the underwater canyons in large gravity-induced events called turbidites. The **submarine fan** is formed by a network of turbidites that deposit their sediment loads as the slope decreases, much like what happens above water at alluvial fans and deltas. This sudden flushing transports coarser sediment to the ocean floor where they are otherwise uncommon. Turbidites are also the typical origin of graded Bouma sequences (see Chapter 5).

Continental Slope

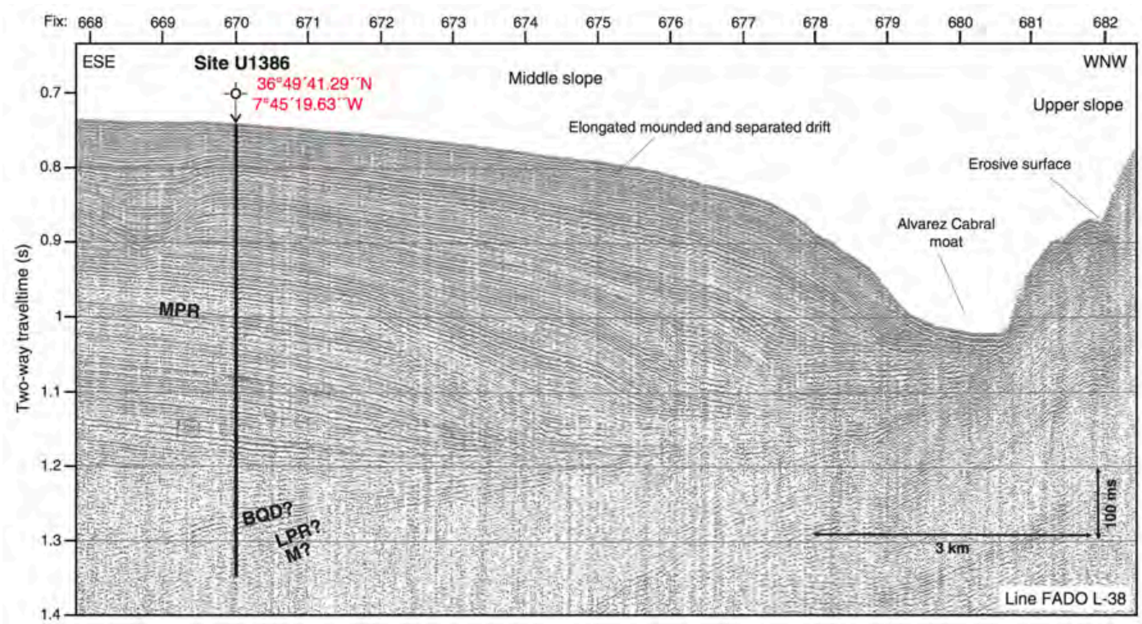

Figure 5.73: Contourite drift deposit imaged with seismic waves. Figure description available at the end of the chapter.

Continental slope deposits are not common in the rock record. The most notable type of continental slope deposits are contourites. Contourites form on the slope between the continental shelf and deep ocean floor. Deep-water ocean currents deposit sediment into smooth drifts of various architectures, sometimes interwoven with turbidites.

Lower Shoreface

The lower shoreface lies below the normal depth of wave agitation, so the sediment is not subject to daily winnowing and deposition. These sediment layers are typically finely laminated and may contain hummocky cross-stratification. Lower shoreface beds are affected by larger waves, such those as generated by hurricanes and other large storms.

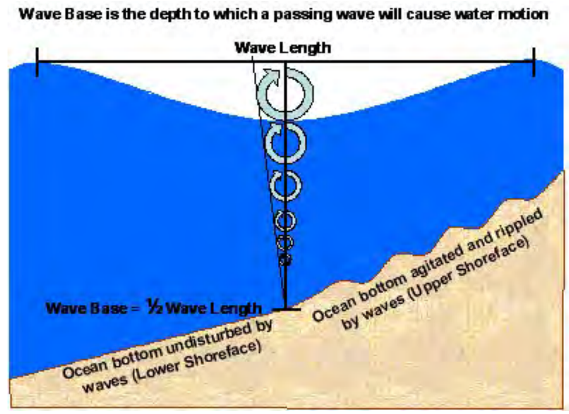

Figure 5.74: Diagram describing wavebase. Figure description available at the end of the chapter.

Upper Shoreface

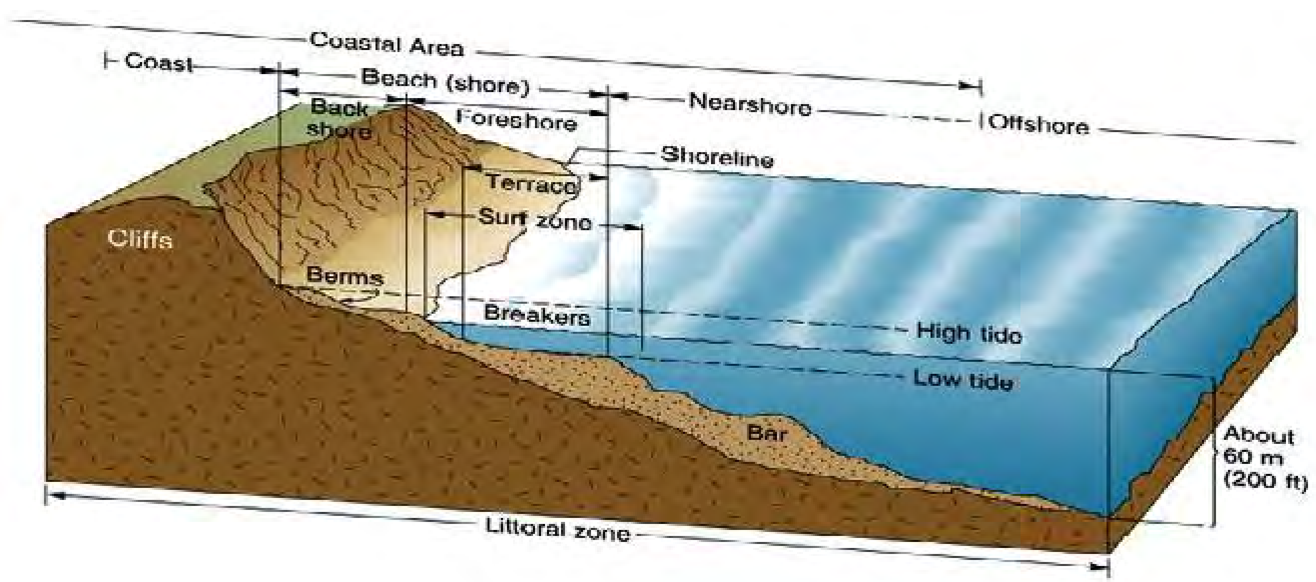

Figure 5.75: Diagram of zones of the shoreline. Figure description available at the end of the chapter.

The upper shoreface contains sediments within the zone of normal wave action, though still submerged below the beach environment. These sediments usually consist of very well-sorted, fine sand. The main sedimentary structure is planar bedding consistent with the lower part of the upper flow regime, but it can also contain cross-bedding created by longshore currents.

5.5.2 Transitional Coastline Environments

Transitional environments, more often called shoreline or **coastline** environments, are zones of complex interactions caused by ocean water hitting land. The sediment preservation potential is very high in these environments because deposition often occurs on the continental shelf and under water. Shoreline environments are an important source of hydrocarbon deposits (petroleum, natural gas).

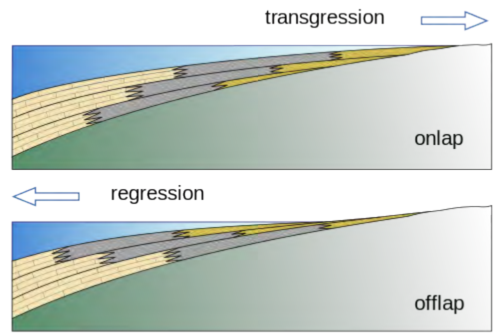

Figure 5.76: The rising sea levels of transgressions create onlapping sediments, while regressions create offlapping. Figure description available at the end of the chapter.

The study of shoreline depositional environments is called **sequence stratigraphy**. Sequence stratigraphy examines depositional changes and 3-D architectures associated with rising and falling sea levels, which is the main force at work in shoreline deposits. These sea-level fluctuations come from the daily **tides**, as well as climate changes and plate tectonics. A steady rise in sea level relative to the shoreline is called **transgression**. **Regression** is the opposite—a relative drop in sea level. Some common components of shoreline environments are littoral zones, tidal flats, reefs, lagoons, and deltas. For a more in-depth look at these environments, see Chapter 12.

Littorals

The **littoral** zone, better known as the beach, consists of highly weathered, homogeneous, well-sorted sand grains made mostly of quartz. There are beaches with black or other types of sand, but they tend to be unique exceptions rather than the rule. Because beach sands, past or present, are so highly evolved, the amount grain weathering can be discerned using the minerals zircon, tourmaline, and rutile, which is why the tool used to do so is called the ZTR index. The ZTR index is higher in more weathered beaches because these relatively rare and weather-resistant minerals become concentrated in older beaches. In some beaches, the ZTR index is so high the sand can be harvested as an economically viable source of these minerals. The beach environment has no sedimentary structures due to the constant bombardment of wave energy delivered by surf action. Beach sediment is moved around via multiple processes. Some beaches with high sediment supplies develop dunes nearby.

Figure 5.77: Heavy mineral layers (dark) in a quartz beach sand deposit in India. Figure description available at the end of the chapter.

Tidal Flats

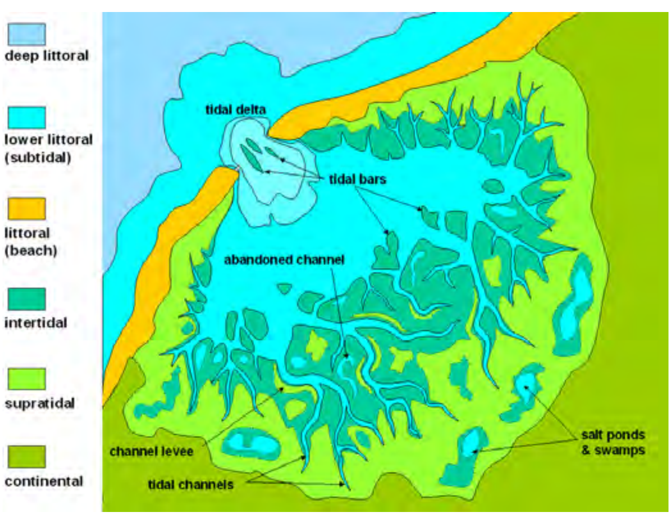

Figure 5.78: General diagram of a tidal flat and associated features. Figure description available at the end of the chapter.

Tidal flats, or mud flats, are sedimentary environments that are regularly flooded and drained by ocean tides. Tidal flats have large areas of fine-grained sediment but may also contain coarser sands. Tidal flat deposits typically contain gradational sediments and may include multi-directional ripple marks. Mudcracks are also commonly seen due to the sediment being regularly exposed to air during low tides; the combination of mudcracks and ripple marks is unique to tidal flats.

Tidal water carries in sediment, sometimes focusing the flow through a narrow opening called a tidal inlet. Tidal channels, creek channels influenced by tides, can also focus tidally induced flow. Areas of higher flow like inlets and tidal channels feature coarser grain sizes and larger ripples, which in some cases can develop into dunes.

Reefs

Figure 5.79: Waterpocket Fold, Capitol Reef National Park, Utah. Figure description available at the end of the chapter.

Reefs, which most people would immediately associate with tropical coral reefs found in the oceans, are not only made by living things. Natural buildups of sand or rock can also create reefs that are similar to barrier islands. Geologically speaking, a reef is any topographically elevated feature on the continental shelf located oceanward of and separate from the beach. The term reef can also be applied to **terrestrial** (atop the continental crust) features. Capitol Reef National Park in Utah contains a topographic barrier, a reef, called the Waterpocket Fold.

Most reefs, now and in the geologic past, originate from the biological processes of living organisms. The growth habits of coral reefs provide geologists important information about the past. The hard structures in coral reefs are built by soft-bodied marine organisms, which continually add new material and enlarge the reef over time. Under certain conditions, when the land beneath a reef is subsiding, the coral reef may grow around and through existing sediment, holding the sediment in place and thus preserving the record of the surrounding environmental and geological condition.

Figure 5.80: A modern coral reef. Figure description available at the end of the chapter.

Figure 5.81: The light-blue reef is fringing the island of Vanatinai. As the island erodes away, only the reef will remain, forming a reef-bound seamount. Figure description available at the end of the chapter.

Sediment found in coral reefs is typically fine-grained and mostly carbonate, and it tends to deposit between the intact coral skeletons. Water with high levels of silt or clay particles can inhibit reef growth because coral organisms require sunlight to thrive; they host symbiotic algae called zooxanthellae that provide the coral with nourishment via photosynthesis. Inorganic reef structures have much more variable compositions. Reefs have a big impact on sediment deposition in lagoon environments since they are natural storm breaks, buffering waves and storms, which allows fine grains to settle and accumulate.

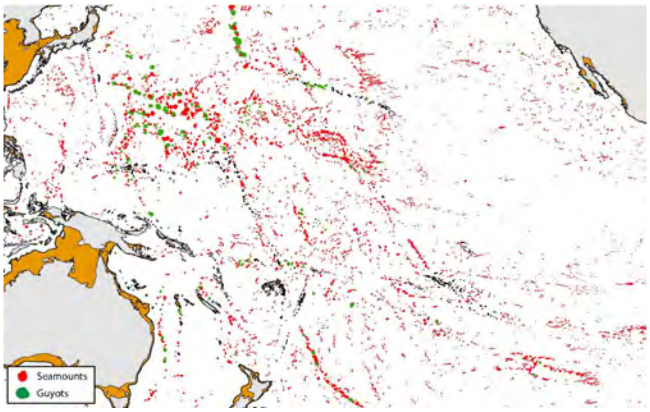

Figure 5.82: Seamounts and guyots in the North Pacific. Figure description available at the end of the chapter.

Reefs are found around shorelines and islands; coral reefs are particularly common in tropical locations. Reefs are also found around features known as **seamounts**, which are the bases of ocean islands left standing under water after the upper parts have been eroded away by waves. Examples include the Emperor seamounts, formed millions of years ago over the Hawaiian Hotspot. Reefs live and grow along the upper edge of these flat-topped seamounts. If the reef builds up above sea level and completely encircles the top of the seamount, it is called a coral-ringed atoll. If the reef is submerged, due to erosion, **subsidence**, or sea level rise, the seamount reef structure is called a guyot.

Lagoons

Lagoons are small bodies of seawater located inland from the shore or isolated by another geographic feature, such as a reef or **barrier island**. Because they are protected from the action of tides, currents, and waves, lagoon environments typically have very fine-grained sediments. Lagoons, as well as **estuaries**, are ecosystems with high biological productivity. Rocks from these environments often includes bioturbation marks or coal deposits. Around lagoons where evaporation exceeds water inflow, salt flats, also known as sabkhas, and sand dune fields may develop at or above the high tide line.

Figure 5.83: Kara-Bogaz Gol lagoon, Turkmenistan. Figure description available at the end of the chapter.

Deltas

Figure 5.84: The Nile Delta, in Egypt. Figure description available at the end of the chapter.

Deltas form where rivers enter lakes or oceans and are of three basic shapes: river-dominated deltas, wave-dominated deltas, and tide-dominated deltas. The name delta comes from the Greek letter Δ (delta, uppercase), which resembles the triangular shape of the Nile River Delta. The velocity of water flow is dependent on riverbed slope or **gradient**, which becomes shallower as the river descends from the mountains. At the point where a river enters an ocean or lake, its slope angle drops to zero degrees (0°). The flow velocity quickly drops as well, and sediment—from coarse clasts to fine sand and mud—is deposited to form the delta. As one part of the delta becomes overwhelmed by sediment, the slow-moving flow gets diverted back and forth, over and over, and forms a spread-out network of smaller distributary channels.

Figure 5.85: Birdfoot river-dominated delta of the Mississippi River. Figure description available at the end of the chapter.

Deltas are organized by the dominant process that controls their shape: tide-dominated, wave-dominated, or river-dominated. Wave-dominated deltas generally have smooth coastlines and beach ridges on the land that represent previous shorelines. The Nile River Delta is a wave-dominated type (see Figure 5.84).

The Mississippi River Delta is a river-dominated delta shaped by levees along the river and its distributaries that confine the flow, forming a shape called a birdfoot delta. Other times, the tides or the waves can be a bigger factor and can reshape the delta in various ways.

A tide-dominated delta is dominated by tidal currents. During flood stages when rivers have lots of water available, the delta develops distributaries that are separated by sand bars and sand ridges. The tidal delta of the Ganges River is the largest delta in the world.

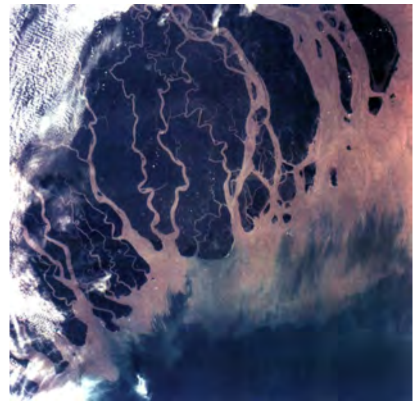

Figure 5.86: Tidal delta of the Ganges River. Figure description available at the end of the chapter.

5.5.3 Terrestrial

Terrestrial depositional environments are diverse. Water—either in a liquid or frozen state—is a major factor in these environments, even when there is a lack of water, creating arid conditions.

Fluvial

Fluvial (river) systems are formed by water flowing in channels over the land. They generally come in two main varieties: meandering or braided. In meandering streams, the flow carries sediment grains via a single channel that wanders back and forth across the floodplain. The floodplain sediment away from the channel is mostly fine-grained material that only gets deposited during floods.

Figure 5.87: The Cauto River in Cuba. Note the sinuosity in the river, which is meandering. Figure description available at the end of the chapter.

Braided fluvial systems generally contain coarser sediment grains and form a complicated series of intertwined channels that flow around gravel and sand bars (see Chapter 11).

Figure 5.88: The braided Waimakariri River in New Zealand. Figure description available at the end of the chapter.

Alluvial

A distinctive characteristic of **alluvial** systems is the intermittent flow of water. Alluvial deposits are common in arid places with little soil development. Lithified alluvial beds are the primary basin-filling rock found throughout the Basin and Range region of the Western United States. The most distinctive alluvial sedimentary deposit is the alluvial fan, a large cone of sediment formed by streams flowing out of dry mountain valleys into a wider and more open dry area. Alluvial sediments are typically poorly sorted and coarse grained and are often found near playa lakes or aeolian deposits (see Chapter 13).

Figure 5.89: An alluvial fan spreads out into a broad alluvial plain. From Red Rock Canyon State Park, California. Figure description available at the end of the chapter.

Lacustrine

Lake systems and deposits known as **lacustrine** deposits form via processes somewhat similar to marine deposits but on a much smaller scale. Lacustrine deposits are found in lakes in a wide variety of locations. Lake Baikal in southeast Siberia (Russia) is in a tectonic basin. Crater Lake (Oregon) sits in a volcanic caldera. The Great Lakes (northern United States) came from glacially carved and deposited sediment. Ancient Lake Bonneville (Utah) formed in a pluvial setting during a climate that was relatively wetter and cooler than that of modern Utah. **Oxbow** lakes, named for their curved shapes, originated in fluvial floodplains. Lacustrine sediment tends to be very fine grained and thinly laminated, with only minor contributions from wind-blown, current, and tidal deposits. When lakes dry out or evaporation outpaces precipitation, **playas** form. Playa deposits resemble those of normal lake deposits but contain more evaporite minerals. Certain tidal flats can have playa-type deposits as well.

Figure 5.90: Oregon's Crater Lake was formed about 7,700 years ago after the eruption of Mount Mazama. Figure description available at the end of the chapter.

Paludal

Paludal systems, which include bogs, marshes, swamps, or other wetlands, usually contain lots of organic matter. Paludal systems typically develop in coastal environments but are common in humid, low-lying, low-latitude, warm zones with large volumes of flowing water. A characteristic paludal deposit is a peat bog, a deposit rich in organic matter that can be converted into coal when lithified. Paludal environments may be associated with tidal, deltaic, lacustrine, and/or fluvial deposition.

Aeolian

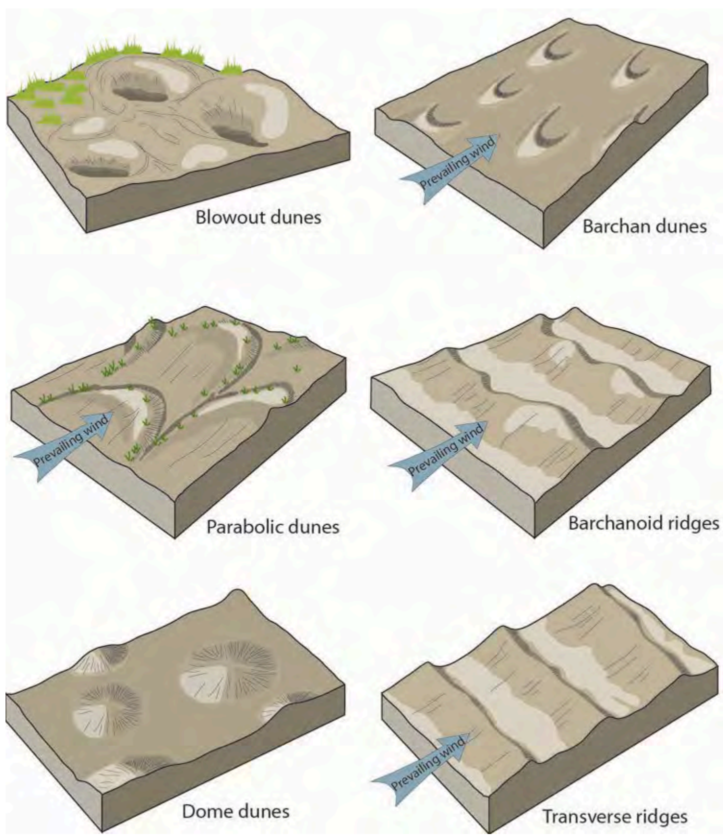

Figure 5.91: Formation and types of dunes. Figure description available at the end of the chapter.

Aeolian, sometimes spelled eolian or œolian, refers to deposits of windblown sediments. Since wind has a much lower carrying capacity than water, aeolian deposits typically consists of clast sizes from fine dust to sand. Fine silt and clay can cross very long distances, even entire oceans, suspended in air.

With sufficient sediment influx, aeolian systems can potentially form large dunes in dry or wet conditions. Figure 5.91 shows dune features and various types.

Layers of wind-blown sediment can become compacted into what is known as **loess**. Loess commonly starts as finely ground rock flour created by glaciers. Such deposits cover thousands of square miles in the Midwestern United States. Loess may also form in desert regions (see Chapter 13). Silt for the Loess Plateau in China came from the Gobi Desert in China and Mongolia.

Figure 5.92: Loess Plateau in China. The loess is so highly compacted that buildings and homes have been carved in it. Figure description available at the end of the chapter.

Glacial

Figure 5.93: Wide range of sediments near Athabaska Glacier, Jasper National Park, Alberta, Canada. Figure description available at the end of the chapter.

Glacial sedimentation is very diverse and generally consists of the most poorly sorted sediment deposits found in nature. The main clast type is called **diamictite**, which literally means "two sizes," referring to the unsorted mix of large and small rock fragments found in glacial deposits. Many glacial tills, glacially derived diamictites, include very finely pulverized rock flour along with giant erratic boulders. The surfaces of larger clasts typically have striations from the rubbing, scraping, and polishing of surfaces by abrasion during the movement of glacial ice. Glacial systems are so large and produce so much sediment that they frequently create multiple, individualized depositional environments, such as fluvial, deltaic, lacustrine, pluvial, alluvial, and/or aeolian (see Chapter 14).

5.5.4 Facies

In addition to mineral composition and lithification process, geologists also classify sedimentary rock by its depositional characteristics, collectively called **facies** or lithofacies. Sedimentary facies consist of physical, chemical, and/or biological properties, including relative changes in these properties in adjacent beds of the same layer or geological age. Geologists analyze sedimentary rock facies to interpret the original deposition environment, as well as disruptive geological events that may have occurred after the rock layers were established.

It boggles the imagination to think of all the sedimentary deposition environments working next to each other at the same time in any particular region on Earth. The resulting sediment beds develop characteristics reflecting contemporaneous conditions at the time of deposition, which later may become preserved into the rock record. For example, in the Grand Canyon, rock strata of the same geologic age include many different depositional environments: beach sand, tidal flat silt, offshore mud, and farther offshore limestone. In other words, each sedimentary or stratigraphic facies presents recognizable characteristics that reflect specific, and different, depositional environments that were present at the same time.

Facies may also reflect depositional changes in the same location over time. During periods of rising sea level, called marine transgression, the shoreline moves inland as seawater covers what was originally dry land and creates new offshore depositional environments. When these sediment beds turn into sedimentary rock, the vertical stratigraphy sequence reveals beach lithofacies buried by offshore lithofacies.

Biological facies are remnants (coal, diatomaceous earth) or evidence (fossils) of living organisms. **Index fossils** are fossilized life forms specific to a particular environment and/or geologic time period, serving as an example of biological facies. The horizontal assemblage and vertical distribution of fossils are particularly useful for studying species evolution because transgression, deposition, burial, and compaction processes happen over a considerable geologic time range.

Fossil assemblages that show evolutionary changes greatly enhance our interpretation of Earth's ancient history by illustrating the correlation between stratigraphic sequence and geologic timescale. During the middle Cambrian Period (see Chapter 7), regions around the Grand Canyon experienced marine transgression in a southeasterly direction (relative to current maps). This shift of the shoreline is reflected in the Tapeats Sandstone beach facies, Bright Angle Shale near-offshore mud facies, and Muav Limestone far-offshore facies. Marine organisms had plenty of time to evolve and adapt to their slowly changing environment; these changes are reflected in the biological facies, which show older life forms in the western regions of the canyon and younger life forms in the east.

Take this quiz to check your comprehension of this section.

Access the quiz for Section 5.5 by scanning the QR code.

Summary

Sedimentary rocks are grouped into two main categories: clastic (detrital) and chemical. Clastic (detrital) rocks are made of mineral clasts or sediment that lithifies into solid material. Sediment is produced by the mechanical or chemical weathering of bedrock and transported away from the source via erosion. Sediment that is deposited, buried, compacted, and sometimes cemented becomes clastic rock. Clastic rocks are classified by grain size; for example, sandstone is made of sand-sized particles. Chemical sedimentary rocks come from minerals precipitated out of an aqueous solution and is classified according to mineral composition. The chemical sedimentary rock limestone is made of calcium carbonate. Sedimentary structures have textures and shapes that give insight into depositional histories. Depositional environments depend mainly on fluid transport systems and encompass a wide variety of underwater and above ground conditions. Geologists analyze depositional conditions, sedimentary structures, and rock records to interpret the paleogeographic history of a region.

Take this quiz to check your comprehension of this chapter.

Access the quiz for Chapter 5 by scanning the QR code.

Text References

1. Affolter, M.D. (2004). *On the nature of volcanic lithic fragments:* Definition source and evolution.
2. Ashley, G.M. (1990). Classification of large-scale subaqueous bedforms: A new look at an old problem-SEPM bedforms and bedding structures. *J. Sediment. Res., 60*(1).
3. Ayrton, H. (1910). The origin and growth of ripple-mark. *Proceedings of the Royal Society of London. Series A, Containing Papers of a Mathematical and Physical Character, 84*(571), 285–310.
4. Bagnold, R.A. (1941). *The physics of blown sand and desert dunes:* Methum.
5. Blatt, H., Middleton, G.V., and Murray, R. (1980). *Origin of Sedimentary Rocks:* Prentice-Hall, Inc.
6. Bouma, A.H., Kuenen, P.H., and Shepard, F.P. (1962). *Sedimentology of some flysch deposits: A graphic approach to facies interpretation:* Elsevier Amsterdam.
7. Cant, D.J. (1982). *Fluvial facies models and their application.*
8. Dickinson, W.R., and Suczek, C.A. (1979). Plate tectonics and sandstone compositions. *AAPG Bull., 63*(12), 2164–2182.
9. Dunham, R.J. (1962). *Classification of carbonate rocks according to depositional textures.*
10. Eisma, D. (1998). *Intertidal deposits: River mouths, tidal flats, and coastal lagoons:* CRC Marine Science, Taylor & Francis.
11. Folk, R.L. (1974). *Petrography of sedimentary rocks:* Univ. Texas, Hemphill.
12. Goldich, S.S. (1938). A study in rock-weathering. *J. Geol., 46*(1), 17–58.
13. Hubert, J.F. (1962). A zircon-tourmaline-rutile maturity index and the interdependence of the composition of heavy mineral assemblages with the gross composition and texture of sandstones. *J. Sediment. Res., 32*(3).
14. Johnson, C.L., Franseen, E.K., and Goldstein, R.H. (2005). The effects of sea level and palaeotopography on lithofacies distribution and geometries in heterozoan carbonates, south-eastern Spain. *Sedimentology, 52*(3), 513–536. doi: 10.1111/j.1365-3091.2005.00708.x.
15. Karátson, D., Sztanó, O., and Telbisz, T. (2002). Preferred clast orientation in volcaniclastic mass-flow deposits: Application of a new photo-statistical method. *J. Sediment. Res., 72*(6), 823–835.
16. Klappa, C.F. (1980). Rhizoliths in terrestrial carbonates: Classification, recognition, genesis and significance. *Sedimentology, 27*(6), 613–629.
17. Longman, M.W. (1981). *A process approach to recognizing facies of reef complexes.*
18. Mckee, E.D., and Weir, G.W. (1953). Terminology for stratification and cross-stratification in sedimentary rocks. *Geol. Soc. Am. Bull., 64*(4), 381–390.
19. Metz, R. (1981). Why not raindrop impressions? *J. Sediment. Res., 51*(1).

20. Nichols, M.M., Biggs, R.B., and Davies, R.A. Jr. (1985). Estuaries, in *Coastal Sedimentary Environments: Springer-Verlag:* New York, p. 77–173.
21. Normark, W.R. (1978). Fan valleys, channels, and depositional lobes on modern submarine fans: Characters for recognition of sandy turbidite environments. *AAPG Bull., 62*(6), 912–931.
22. Pettijohn, F.J., and Potter, P.E. (2012). *Atlas and glossary of primary sedimentary structures.*
23. Plummer, P.S., and Gostin, V.A., 1981, Shrinkage cracks: desiccation or synaeresis? *J. Sediment. Res.,* v. 51, no. 4.
24. Reinson, G.E. (1984). Barrier-island and associated strand-plain systems, in Walker, R.G. (ed.). *Facies Models: Geoscience Canada Reprint Series 1,* p. 119–140.
25. Stanistreet, I.G., and McCarthy, T.S. (1993). The Okavango Fan and the classification of subaerial fan systems. *Sediment. Geol., 85*(1), p. 115–133.
26. Stow, D.A.V., Faugères, J.-C., Viana, A., and Gonthier, E. (1998). Fossil contourites: A critical review. *Sediment. Geol., 115*(1–4), 3–31.
27. Stow, D.A.V., and Piper, D.J.W. (1984). Deep-water fine-grained sediments: Facies models. *Geological Society, London, Special Publications, 15*(1), 611–646.
28. Udden, J.A. (1914). Mechanical composition of clastic sediments. *Geol. Soc. Am. Bull., 25*(1), 655–744.
29. Wentworth, C.K. (1922). A scale of grade and class terms for clastic sediments. *J. Geol., 30*(5), 377–392.
30. Yin, D., Peakall, J., Parsons, D., Chen, Z., Averill, H.M., Wignall, P., and Best, J. (2016). Bedform genesis in bedrock substrates: Insights into formative processes from a new experimental approach and the importance of suspension-dom-inated abrasion. *Geomorphology, 255,* 26–38.

Figure References

Figure 5.1: A model of a water molecule, showing the bonds between the hydrogen and oxygen. Dan Craggs. 2009. Public domain. https://commons.wikimedia.org/wiki/File:H2O_2D_labelled.svg

Figure 5.2: Dew on a spider's web. Luc Viatour. 2007. CC BY-SA 3.0. https://commons.wikimedia.org/wiki/File:Spider_web_Luc_Viatour.jpg

Figure 5.3: Hydrogen bonding between water molecules. Qwerter. 2011. Public domain. https://commons.wikimedia.org/wiki/File:3D_model_hydrogen_bonds_in_water.svg

Figure 5.4: A sodium (Na) ion in solution. Taxman. 2006. Public domain. https://commons.wikimedia.org/wiki/File:Na%2BH2O.svg

Figure 5.5: The outer layer of this granite is fractured and eroding away, known as exfoliation. Wing-Chi Poon. 2005. CC BY-SA 2.5. https://en.m.wikipedia.org/wiki/File:GeologicalExfoliationOfGraniteRock.jpg

Figure 5.6: The process of frost wedging. Julie Sandeen. 2010. CC BY-SA 3.0. https://commons.wikimedia.org/wiki/File:Mechanical_weathering.png

Figure 5.7: The roots of this tree are demonstrating the destructive power of root wedging. Arseny Khakhalin. 2006. CC BY 3.0. https://commons.wikimedia.org/wiki/File:Pine-tree_roots_digging_through_the_asphalt_-_panoramio.jpg

Figure 5.8: Tafoni from Salt Point, California. Dawn Endico. 2005. CC BY-SA 2.0. https://commons.wikimedia.org/wiki/File:Tafoni_03.jpg

Figure 5.9: Each of these three groups of cubes has an equal volume. Kindred Grey. 2022. CC BY 4.0.

Figure 5.10: Generic hydrolysis diagram, where the mineral bonds in question would represent the left side of the diagram. Unknown author. 2014. CC BY-SA 4.0. https://commons.wikimedia.org/wiki/File:Hydrolysis.png

Figure 5.11: In this rock, a pyrite cube has dissolved (as shown by the negative "corner" impression in the rock), leaving behind small specks of gold. Matt Affolter (QFL247). 2009. CC BY-SA 3.0. https://commons.wikimedia.org/wiki/File:GoldinPyriteDrainage_acide.JPG

Figure 5.12: This mantle xenolith containing olivine (green) is chemically weathering by hydrolysis and oxidation into the pseudomineral iddingsite, which is a complex of water, clay, and iron oxides. Matt Affolter. 2010. CC BY-SA 3.0. https://commons.wikimedia.org/wiki/File:Iddingsite.JPG

Figure 5.13: Eroded karst topography in Minerve, France. Hugo Soria. 2005. CC BY-SA 3.0. https://commons.wikimedia.org/wiki/File:Karst_minerve.jpg

Figure 5.14: A formation called the Great Heart of Timpanogos in Timpanogos Cave National Monument. Sleeping Bear Dunes National Lakeshore. 2012. CC BY 2.0. https://commons.wikimedia.org/wiki/File:Tica_(7563200350).jpg

Figure 5.15: Pyrite cubes are oxidized, becoming a new mineral, goethite. Matt Affolter (QFL247). 2010. CC BY-SA 3.0. https://commons.wikimedia.org/wiki/File:PyOx.JPG

Figure 5.16: A hoodoo near Moab, Utah. Qfl247. 2010. GNU Free Documentation License. https://en.wikipedia.org/wiki/File:Moab-Hoodoo.JPG

Figure 5.17: Court of the Patriarchs in Zion National Park, Utah. Laura Neser. March 2022. CC BY-NC.

Figure 5.18: Sketch and picture of soil. Carlosblh. 2006. CC BY-SA 3.0. https://commons.wikimedia.org/wiki/File:Estructura-suelo.jpg

Figure 5.19: Schematic of the nitrogen cycle. Johann Dréo. 2009. CC BY-SA 3.0. https://commons.wikimedia.org/wiki/File:Nitrogen_Cycle.svg

Figure 5.20: Agricultural terracing, such as these created by the Inca culture from the Andes, helps reduce erosion and promote soil formation, leading to better farming practices. Unknown author. 2007. Public domain. https://commons.wikimedia.org/wiki/File:Pisac006.jpg

Figure 5.21: A simplified soil profile with labeled layers. Wilsonbiggs. 2021. CC BY-SA 4.0. https://commons.wikimedia.org/wiki/File:Soil_Horizons.svg

Figure 5.22: A sample of bauxite. Werner Schellmann. 1965. CC BY-SA 2.5. https://commons.wikimedia.org/wiki/File:Bauxite_with_unweathered_rock_core._C_021.jpg

Figure 5.23: A dust storm approaches Stratford, Texas, in 1935. George E. Marsh Album via National Oceanic and Atmospheric Administration (NOAA). 1935. Public domain. https://commons.wikimedia.org/wiki/File:Dust_Storm_Texas_1935.jpg

Figure 5.24: Geologic unconformity seen at Siccar Point on the east coast of Scotland. dave souza. 2008. CC BY-SA 4.0. https://commons.wikimedia.org/wiki/File:Siccar_Point_red_capstone_closeup.jpg

Figure 5.25: Permineralization in petrified wood. Laura Neser. March 2022. CC BY-NC.

Figure 5.26: Size categories of sediments according to the Wentworth scale. Jeffress Williams, Matthew A. Arsenault, Brian J. Buczkowski, Jane A. Reid, James G. Flocks, Mark A. Kulp, Shea Penland, and Chris J. Jenkins via USGS. 2011. Public domain. https://commons.wikimedia.org/wiki/File:Wentworth_scale.png

Figure 5.27: A well-sorted sediment (left) and a poorly sorted sediment (right). Woudloper. 2009. CC BY-SA 3.0. https://commons.wikimedia.org/wiki/File:Sorting_in_sediment.svg

Figure 5.28: Degree of rounding in sediments. Woudloper. 2009. Public domain. https://commons.wikimedia.org/wiki/File:Rounding_%26_sphericity_EN.svg

Figure 5.29: A sand grain made of basalt, known as a microlitic volcanic lithic fragment. Matt Affolter (QFL247). 2009. CC BY-SA 3.0. https://commons.wikimedia.org/wiki/File:LvMS-Lvm.jpg

Figure 5.30: Hawaiian beach composed of black sand from weathering of nearby basaltic rock. Laura Neser. June 2022. CC BY-NC.

Figure 5.31: Megabreccia in Titus Canyon, Death Valley National Park, California. NPS. Unknown date. Public domain. https://commons.wikimedia.org/wiki/File:Titus_Canyon_Narrows.jpg

Figure 5.32: Enlarged image of frosted and rounded windblown sand grains. Wilson44691. 2008. Public domain. https://commons.wikimedia.org/wiki/File:CoralPinkSandDunesSand.jpg

Figure 5.33: The Rochester Shale, New York. Wilson44691. 2015. Public domain. https://en.m.wikipedia.org/wiki/File:Rochester_Shale_Niagara_Gorge.jpg

Figure 5.34: Claystone laminations from Glacial Lake Missoula. Matt Affolter. 2010. CC BY-SA 3.0. https://commons.wikimedia.org/wiki/File:GLMsed.jpg

Figure 5.35: Salt-covered plain known as the Bonneville Salt Flats, Utah. Michael Pätzold. 2008. CC BY-SA 4.0. https://commons.wikimedia.org/wiki/File:Bonneville_salt_flats_pilot_peak.jpg

Figure 5.36: Ooids from Joulter's Cay, The Bahamas. Wilson44691. 2010. Public domain. https://commons.wikimedia.org/wiki/File:Ooids,_Joulter_Cays,_Bahamas.jpg

Figure 5.37: Limestone tufa towers along the shores of Mono Lake, California. Yukinobu Zengame. 2005. CC BY 2.0. https://commons.wikimedia.org/wiki/File:Limestone_towers_at_Mono_Lake,_California.jpg

Figure 5.38: Travertine ground surface of Mammoth Hot Springs, Yellowstone National Park, USA. Laura Neser. 2012. CC BY-NC.

Figure 5.39: This sample of banded iron formation displays alternating bands of iron-rich and silica-rich mud, formed as oxygen combined with dissolved iron. Laura Neser. September 2024. CC BY-NC.

Figure 5.40: A type of chert, flint, shown with a lighter weathered crust. Ra'ike. 2014. CC BY-SA 3.0. https://commons.wikimedia.org/wiki/File:Flint_with_weathered_crust.JPG

Figure 5.41: Ooids forming an oolite. Unknown author. 2008. Public domain. https://commons.wikimedia.org/wiki/File:OoidSurface01.jpg

Figure 5.42: Hokie Stone is a dolomite-limestone rock found near Blacksburg, Virginia, and is prominently displayed on the majority of buildings throughout the Blacksburg campus of Virginia Tech. Both photos by Laura Neser. October 2024. CC BY-NC.

Figure 5.43: Shell fragments make up the rock coquina. (Top) Hand sample. (Bottom) Close-up (different sample). Top photo: Laura Neser. September 2024. CC BY-NC. Bottom photo: Wilson44691. 2008. Public domain. https://commons.wikimedia.org/wiki/File:Coquina-Close.jpg

Figure 5.44: Anthracite coal, the highest grade of coal. United States Geological Survey (USGS). 2007. Public domain. https://commons.wikimedia.org/wiki/File:Coal_anthracite.jpg

Figure 5.45: Gyprock, a rock made of the mineral gypsum. James St. John. 2016. CC BY 2.0. https://commons.wikimedia.org/wiki/File:Gyprock_(Castile_Formation,_Upper_Permian_Eddy_County,_New_Mexico.jpg

Figure 5.46: Sedimentary rock identification chart. Virginia Sisson. Unknown date. CC BY-NC-SA 4.0. Figure 2.13 from https://uhlibraries.pressbooks.pub/historicalgeologylab/chapter/chapter02-earthmaterials

Figure 5.47: Sedimentary beds visible in Petrified Forest National Park. Laura Neser. June 2022. CC BY-NC.

Figure 5.48: A student from the University of North Carolina digs into beds of Paleocene-Eocene sedimentary strata in northwestern Wyoming. Laura Neser. 2011. CC BY-NC.

Figure 5.49: Image of the classic Bouma sequence. Mikesclark. 2013. CC BY-SA 3.0. https://commons.wikimedia.org/wiki/File:Turbidite_from_Pigeon_Pt_Fm_at_Pescadero_Beach,_CA.jpg

Figure 5.50: Bedforms under increasing flow velocities. US Dept. of Transportation Federal Highway Administration. 2013. Public domain. https://commons.wikimedia.org/wiki/File:Bedforms_under_various_flow_regimes.pdf

Figure 5.51: Subtle lines across this sandstone (trending from the lower left to upper right) are parting lineations. Matt Affolter (a.k.a. QFL247). 2010. CC BY-SA 3.0. https://commons.wikimedia.org/wiki/File:PartingLineation.JPG

Figure 5.52: Modern current ripple in sand from the Netherlands. Heinz-Josef Lücking. 2007. CC BY-SA 3.0 DE. https://commons.wikimedia.org/wiki/File:Rippelbildungen_am_Strand_von_Spiekeroog.JPG

Figure 5.53: Ripple marks visible in 1.6-billion-year-old rock in Glacier National Park, Montana. Laura Neser. August 2014. CC BY-NC.

Figure 5.54: Climbing ripple deposit from India. DanHobley. 2011. CC BY-SA 3.0. https://commons.wikimedia.org/wiki/File:Climbing_ripples.JPG

Figure 5.55: Lithified cross-bedded dunes in Zion National Park, Utah. Laura Neser. June 2022. CC BY-NC.

Figure 5.56: Modern sand dune in Morocco. Rosino. 2005. CC BY-SA 2.0. https://en.wikipedia.org/wiki/File:Morocco_Africa_Flickr_Rosino_December_2005_84514010.jpg

Figure 5.57: Herringbone cross-bedding from the Mazomanie Formation, from the Upper Cambrian in Minnesota. James St. John. 2015. CC BY 2.0. https://commons.wikimedia.org/wiki/File:Herringbone_cross-stratified_quartzose_sandstones_with_trace_fossils_(Mazomanie_Formation,_Upper_Cambrian;_riverside_cliff,_western_side_of_the_St._Croix_River,_northeast_of_Lookout_Point,_Minnesota,_USA)_4_(18812079220).jpg

Figure 5.58: Hummocky cross-stratification, seen as wavy lines throughout the middle of this rock face. Matt Affolter (QFL247). 2010. CC BY-SA 3.0. https://commons.wikimedia.org/wiki/File:HumXSec.JPG

Figure 5.59: Antidunes forming in Urdaibai, Spain. Kol35. 2011. CC BY-SA 4.0. https://commons.wikimedia.org/wiki/File:Antidunes_(Urdaibai_estuary).JPG

Figure 5.60: Bioturbated dolomitic siltstone from Kentucky. Jstuby. 2010. Public domain. https://en.wikipedia.org/wiki/File:Saluda_bioturbation.jpg

Figure 5.61: (Top) Modern mudcracks in Wyoming. (Bottom) Lithified mudcracks from Maryland. Top: Laura Neser. 2009. CC BY-NC. Bottom: Jstuby. 2009. Public domain. https://en.wikipedia.org/w/index.php?title=File:Mudcracks_roundtop_hill_MD.jpg

Figure 5.62: This flute cast shows a flow direction toward the upper right of the image, as seen by the bulge extending down out of the layer above. Matt Affolter (QFL247). 2010. CC BY-SA 3.0. https://commons.wikimedia.org/wiki/File:FluteCast.jpg

Figure 5.63: Groove casts at the base of a turbidite deposit in Italy. Mikenorton. 2006. CC BY-SA 3.0. https://commons.wikimedia.org/wiki/File:Groove_casts.jpg

Figure 5.64: A drill core showing a load cast showing light-colored sand extending down into dark mud. Matt Affolter. 2010. CC BY-SA 3.0. https://commons.wikimedia.org/wiki/File:LoadCast.jpg

Figure 5.65: Mississippian raindrop impressions over wave ripples from Nova Scotia. Rygel, M.C. 2006. CC BY-SA 3.0. https://commons.wikimedia.org/wiki/File:Raindrop_impressions_mcr1.jpg

Figure 5.66: Cobbles in this conglomerate in Switzerland are positioned in a way that they are stacked on each other, which occurred as flow moved from left to right. Laura Neser. September 2023. CC BY-NC.

Figure 5.67: This bivalve (clam) fossil was partially filled with tan sediment, partially empty. Matt Affolter. 2009. CC BY-SA 3.0. https://commons.wikimedia.org/wiki/File:Geopetal.jpg

Figure 5.68: Eubrontes trace fossil from Utah, showing that the geopetal direction is into the image. Wilson44691. 2008. Public domain. https://commons.wikimedia.org/wiki/File:Eubrontes01.jpg

Figure 5.69: A representation of common depositional environments. Mikenorton. 2008. CC BY-SA 3.0. https://en.wikipedia.org/wiki/File:SedimentaryEnvironment.jpg

Figure 5.70: Marine sediment thickness. Note the lack of sediment away from the continents. NOAA. 2019. Public domain. https://ngdc.noaa.gov/mgg/sedthick

Figure 5.71: Diatomaceous earth. James St. John. 2013. CC BY 2.0. https://commons.wikimedia.org/wiki/File:Diatomite_(diatomaceous_earth)_Monterey_Formation_at_a_diatomite_quarry_just_south_of_Lompoc.jpg

Figure 5.72: Turbidites interdeposited within submarine fans. Oggmus. 2016. CC BY-SA 4.0. https://commons.wikimedia.org/wiki/File:Turbidite_formation.jpg

Figure 5.73: Contourite drift deposit imaged with seismic waves. Integrated Ocean Drilling Program. 2012. CC BY-SA 3.0. https://en.wikipedia.org/wiki/File:Contourite_sparker_seismic_elongate_drift.png

Figure 5.74: Diagram describing wavebase. GregBenson. 2004. CC BY-SA 3.0. https://en.wikipedia.org/wiki/File:Wavebase.jpg

Figure 5.75: Diagram of zones of the shoreline. US Government. 2012. Public domain. https://commons.wikimedia.org/wiki/File:Littoral_Zones.jpg

Figure 5.76: The rising sea levels of transgressions create onlapping sediments, and regressions create offlapping. Woudloper. 2009. CC BY-SA 1.0. https://commons.wikimedia.org/wiki/File:Offlap_%26_onlap_EN.svg

Figure 5.77: Heavy mineral layers (dark) in a quartz beach sand deposit in India. Mark A. Wilson. 2008. Public domain. https://commons.wikimedia.org/wiki/File:HeavyMineralsBeachSand.jpg

Figure 5.78: General diagram of a tidal flat and associated features. Foxbat deinos. 2009. Public domain. https://commons.wikimedia.org/wiki/File:Tidal_flat_general_sketch.png

Figure 5.79: Waterpocket Fold, Capitol Reef National Park, Utah. Bobak Ha'Eri. 2008. CC BY 3.0. https://commons.wikimedia.org/wiki/File:2008-0914-CapitolReef-WaterpocketFold1.jpg

Figure 5.80: A modern coral reef. Toby Hudson. 2010. CC BY-SA 3.0. https://commons.wikimedia.org/wiki/File:Coral_Outcrop_Flynn_Reef.jpg

Figure 5.81: The light-blue reef is fringing the island of Vanatinai. NASA image by Jesse Allen and Rob Simmon, using data provided by the United States Geological Survey. 2002. Public domain. https://en.m.wikipedia.org/wiki/File:Vanatinai,_Louisiade_Archipelago.jpg

Figure 5.82: Seamounts and guyots in the North Pacific. PeterTHarris. 2015. CC BY-SA 3.0. https://commons.wikimedia.org/wiki/File:Distribution_of_seamounts_and_guyots_in_the_North_Pacific.pdf

Figure 5.83: Kara-Bogaz Gol lagoon, Turkmenistan. NASA. 1995. Public domain. https://commons.wikimedia.org/wiki/File:Kara-Bogaz_Gol_from_space,_September_1995.jpg

Figure 5.84: The Nile Delta, in Egypt. Jacques Descloitres, MODIS Rapid Response Team, NASA/sh. 2003. Public domain. https://commons.wikimedia.org/wiki/File:Nile_River_and_delta_from_orbit.jpg

Figure 5.85: Birdfoot river-dominated delta of the Mississippi River. NASA. 2001. Public domain. https://commons.wikimedia.org/wiki/File:Mississippi_delta_from_space.jpg

Figure 5.86: Tidal delta of the Ganges River. NASA. 1994. Public domain. https://commons.wikimedia.org/wiki/File:Ganges_River_Delta,_Bangladesh,_India.jpg

Figure 5.87: The Cauto River in Cuba. Not home~commonswiki. 2007. Public domain. https://commons.wikimedia.org/wiki/File:Rio-cauto-cuba.jpg

Figure 5.88: The braided Waimakariri River in New Zealand. Greg O'Beirne. 2016. CC BY 2.5. https://commons.wikimedia.org/wiki/File:Waimakariri01_gobeirne.jpg

Figure 5.89: An alluvial fan spreads out into a broad alluvial plain. Matt Affolter. 2010. CC BY-SA 3.0. https://commons.wikimedia.org/wiki/File:AlluvialPlain.jpg

Figure 5.90: Oregon's Crater Lake was formed about 7,700 years ago after the eruption of Mount Mazama. Zainubrazvi. 2006. CC BY-SA 3.0. https://en.wikipedia.org/wiki/File:Crater_lake_oregon.jpg

Figure 5.91: Formation and types of dunes. NPS Natural Resources. 2016. Public domain. https://flic.kr/p/GAn1Pj

Figure 5.92: Loess Plateau in China. Till Niermann. 1987. CC BY-SA 3.0. https://en.wikipedia.org/wiki/File:Loess_landscape_china.jpg

Figure 5.93: Wide range of sediments near Athabaska Glacier, Jasper National Park, Alberta, Canada. Wing-Chi Poon. 2006. CC BY-SA 2.5. https://commons.wikimedia.org/wiki/File:Glacial_Transportation_and_Deposition.jpg

Figure Descriptions

Figure 5.1: Simple diagram of a water molecule with the letter O at the center and an individual letter H branching out on either side of the O. One letter H is to to the lower left of the letter O with a line connecting them and the other letter H is to the lower right of the letter O with a line connecting them. The angle between the two connecting lines is 104.45 degrees. Along one of the connecting lines is the label "95.84 pm."

Figure 5.2: Spider web with detailed square structure. Water droplets stick to the web.

Figure 5.3: 3D model of four water molecules attaching to a single water molecule in the center; in each water molecule, the single larger oxygen atom is colored red with two smaller gray hydrogen atoms attached; two water molecules attach to the center one from a positively charged hydrogen atom to a negatively charged oxygen atom and two water molecules attach to the center one from a negatively charged oxygen atom to a positively charged hydrogen atom.

Figure 5.4: Diagram with a sodium atom at the center and six water molecules surrounding the sodium atom. The center atom is gray, labeled "Na+". The surrounding molecules each have one red oxygen and two gray hydrogen atoms with the Greek symbol delta labeling each atom; the hydrogen atoms each have delta+ while the oxygen atoms which all face the center sodium atom each have delta-.

Figure 5.5: A layer of broken slabs of rock lying on top of a larger landscape of domed rock. The rocks are reddish-tan and gray.

Figure 5.6: Water seeps into cracks and fractures in rock. When the water freezes, it expands about 9% in volume, which wedges apart the rock. With repeated freeze/thaw cycles, rock breaks into pieces.

Figure 5.7: Roots of a tree are visible rising and breaking through asphalt.

Figure 5.8: Tan rock with many holes resembling honeycomb with crashing ocean waves in the background.

Figure 5.9: The left side has one large cube, the middle has 8 medium cubes, the right side has 64 small cubes. Each group has the same overall volume.

Figure 5.10: Diagram showing hydrolysis; on the left hand side are two molecules, one of which is water; on the right hand side are two new molecules, resulting after water has broken the first molecule's chemical bond.

Figure 5.11: Chunk of brick red rock with white crystals; tiny gold flecks can be seen in void spaces of the rock; approximately 5 centimeters in size.

Figure 5.12: Photograph of a piece of basalt with a xenolith on top, sitting on a black and white scale with inches on the left and centimeters on the right. The xenolith consists of olive-green crystals and the basalt is gray-black. The entire sample is approximately 1.5 inches long.

Figure 5.13: White-gray cliffside with numerous caves and holes throughout; the base and top of the cliffs are covered in green vegetation.

Figure 5.14: Cream-colored rock formation attached to a cave ceiling that resembles a human heart.

Figure 5.15: Chunk of dull tan rock with two dark brown glassy cubic crystals growing from it.

Figure 5.16: Tower of brick red rock with visible horizontal layers; the tower thins upward except for a larger, flat rock capping the top of the tower.

Figure 5.17: Three large vertical rock outcrops side by side consisting of brownish tan flat-lying layers. There is green vegetation in the foreground and at the base of the cliffs.

Figure 5.18: Black and white cross sectional sketch of soil profiles: the top layer has plants on top with shallow roots and is filled in with small dots, labeled A; the layer below has small dots and larger grains drawn, labeled B; the layer below has more larger grains clustered along the base of the layer and also small dots throughout labeled C, and the bottom layer has a brick pattern labeled C. On the right of the sketch is a color photograph of those soil profiles in real life, with brown to tan soil matching each layer of the sketch.

Figure 5.19: A schematic diagram representing the nitrogen cycle; it consists of interconnected arrows and labeled boxes, showcasing the various stages and transformations of nitrogen. The cycle begins with atmospheric nitrogen (N2), which is converted into ammonium (NH4+) through nitrogen fixation, represented by an arrow pointing through nitrogen-fixing soil bacteria in the subsurface. The ammonium then undergoes nitrification, shown by arrows leading through nitrifying bacteria in the ground to a box labeled Nitrites (NO2-) and an arrow from that box leading through more nitrifying bacteria leading to a box labeled Nitrates (NO3-). From there, the nitrates are taken up by plants, indicated by an arrow labeled Assimilation, pointing towards a labeled plants box. The nitrogen can then move through the food chain as organisms consume the plants, depicted by an arrow leading to a rabbit. Plants and animals that die are consumed by Decomposers, represented by arrows from the Plants box and rabbit drawing that leads into the ground to a box labeled Decomposers. Denitrification, represented by an arrow leading from Nitrates, through denitrifying bacteria, and pointing back to atmospheric nitrogen, completes the cycle.

Figure 5.20: A mountain slope has been made into artificial steps for farming, covered in low green vegetation.

Figure 5.21: Block diagram of soil horizons: the top layer goes from 0 inches at the surface down to 2 inches into the ground and has plants on top; the layer is dark brown in color, labeled Organic: O. The layer below goes from 2 to 10 inches depth and has abundant plant roots branching down through the layer; the layer is gray in color, labeled Surface: A. The layer below goes from 10 to 30 inches depth and has fewer, deeper roots branching through the layer and also contains sparse larger rock clasts; the layer is dark tan in color, labeled Subsoil: B. The layer below goes from 30 to 48 inches depth and does not contain any plant roots but does have more abundant rock clasts than the layer above; the layer is light tan in color, labeled Substratum: C. The bottom layer goes below 48 inches depth and only consists of rock clasts; the layer is dark gray to black in color, labeled Bedrock: R.

Figure 5.22: Chunk of heavily weathered tan and porous rock that has unweathered elongated gray and black crystals in the center.

Figure 5.23: Black and white photo of a few houses on flat land along with two people standing near a house; a giant wall of dust is seen approaching in the background of the photo.

Figure 5.24: On the right hand side is a series of dark brown rock layers that are vertical. As you look toward the left, the vertical layers are capped by gently-dipping reddish brown sedimentary layers. The ocean is seen in the background.

Figure 5.25: The rock has distinct colorful layers that are yellow, red, black, and tan, in the shape of a tree log. A person's hand is outstretched touching the rock.

Figure 5.26: Chart with the following columns from left to right: phi, mm, Fractional mm and Decimal Inches, Size Terms, Sieve Sizes, Intermediate diameters of natural grains equivalent to sieve size, Number of grains per mg, Settling Velocity (Quartz, 30 degrees C), and Threshold Velocity for traction cm/sed. Grain sizes are delineated using a log base 2 scale; the grain sizes in the boulder class are larger than 10.1 inches; the grain sizes in the cobble class are 2.52 to 10.1 inches; the grain sizes in the pebble class are 2.52 to 0.08 inches, which include the size terms very coarse, coarse, medium, fine, and very fine granules; the grain sizes in the sand class are 1 mm to 1/16 mm, which include the size terms very coarse, coarse, medium, fine, and very fine; the grain sizes in the silt class are 1/16 mm to 1/256 mm, which include the size terms coarse, medium, fine, and very fine; and the grain sizes in the clay class are 1/256 mm to 1/1024 mm, which do not have specific size terms.

Figure 5.27: The sediment on the left is all about the same size. The sediment on the right is many sizes.

Figure 5.28: Series of three rows that each contain five drawn grain shapes; the top row is labeled High sphericity and contains rounded to more square- shaped grains while the bottom row is labeled Low sphericity and contains elongated to oval-shaped grains; the columns toward the left are labeled Angular and have pointed, jagged edges along each grain edge, while the columns toward the right are labeled Rounded and have smoothed, rounded corners along each grain edge.

Figure 5.29: Two microscopic photos of the same sand grain made of basalt with a photo length of 0.25 mm. The top picture is plane-polarized light and shows a tan grain with numerous highlighted holes throughout it while the bottom is cross-polarized light and shows a black grain with numerous highlighted elongated grains throughout it.

Figure 5.30: Beach cove with green sand and numerous people; surrounding the cove are black layers of volcanic rock.

Figure 5.31: Cliff face alongside a curving gravel road; numerous large, angular dark gray boulder fragments are embedded throughout the white cliffside rock.

Figure 5.32: Close-up photo of unconsolidated amber-colored glassy grains with rounded edges; a scale bar at the lower right says 1.0 mm.

Figure 5.33: Outcrop of gray rocks with a slope of broken rocks leading up to a vertical cliff of very thinly layered rocks; a group of six people stand at the top of the slope inspecting the rocks at the base of the cliff.

Figure 5.34: Light tan to gray chalky-looking rock cliff face with extremely thin laminations visible; a rock hammer leans against the outcrop for scale.

Figure 5.35: A flat white expanse with a mountain range in the distant background.

Figure 5.36: Zoomed-in photo of a cluster of pearly white smooth, rounded grains; a scale bar at the lower right says 0.50 mm.

Figure 5.37: Whitish gray limestone towers stick vertically out of the ground, resembling thin spires with rough rounded sides.

Figure 5.38: White to tan chalky-looking ground surface with a dead tree in the center; there is some standing liquid around the dead tree and orangeish step-like deposits in the background.

Figure 5.39: A slice of rock, showing red and brown curvy layers with glittering dots throughout.

Figure 5.40: The flint is black, and the weathered crust around it is light tan. The overall shape is blobby, resembling the shape of a potato.

Figure 5.41: Zoomed-in photo of a cluster of dull tan smooth, rounded grains, with a slightly larger star-shaped grain laying in the cluster as well; a scale bar at the lower right says 1.50 mm.

Figure 5.42: The top photo is an exterior building wall covered in differently-sized bricks of gtrey and tan natural rock; there is a black sign with brassy lettering that says Holden Hall. The bottom photo shows two pieces of rock; the left piece is nearly square, approximately 2 centimeters and has a glossy tan surface, while the right piece is chunky, approximately 10 centimeters and has a rough reddish surface.

Figure 5.43: Top is a hand holding a rectangular block of light tan rock composed entirely of small broken shell pieces; bottom is a close-up of fragments of light tan broken shells with a scale bar at the lower left that says 1.0 cm.

Figure 5.44: Chunk of black, very shiny rock.

Figure 5.45: Cross sectional view of a rock with alternating thicker white and thinner brown layers.

Figure 5.46: Inorganic clastic sedimentary rocks include Conglomerate, Breccia, Sandstone, Siltstone, and shale. They all have classic (fragmental) texture and a composition of mostly quartz, feldspar, and clay minerals; may contain fragments of other rocks and minerals. Conglomerate: rounded fragments; grain size are pebbles, cobbles, and/or boulders in a matrix of sand, silt, and/or clay. Breccia: angular fragments; grain size are pebbles, cobbles, and/or boulders in a matrix of sand, silt, and/or clay. Sandstone: fine to coarse in a variety of colors; grain size is sand (0.063-2mm). Siltstone: very fine grained, massive, usually dark; grain size is silt (0.039- 0.063mm). Shale is compact, brittle, usually dark; grain size is clay (<0. 0039mm). Chemically and/or organically formed sedimentary rocks include chert, rock salt, rock gypsum, dolostone, limestone, coal, and oil shale. Chert: crystalline texture, fine to coarse grains, quartz composition, chemical precipitates and evaporites. Rock salt: crystalline texture, fine to coarse grains, halite composition, chemical precipitates and evaporites. Rock gypsum: crystalline texture, fine to coarse grains, gypsum composition, chemical precipitates and evaporites. Dolostone: crystalline texture, fine to coarse grains, dolomite composition, chemical precipitates and evaporites. Limestone: crystalline or bioclastic texture, microscopic to very coarse grain size, calcite composition, biologic precipitates or cemented shell fragments. Coal: bioclastic texture, clay grain size, carbon composition, black and compacted plant remains. Oil shale: bioclastic texture, clay grain size, clay and kerogen composition, dark and may have oily smell or burn.

Figure 5.47: Barren tan and white landscape in the foreground with a paved path running from left to right; in the background are slopes of black, white, and gray rock that are layered in a horizontal manner, leading up to a relatively flat top.

Figure 5.48: A woman is standing on a tan, gray, and red crumbly hillslope holding a shovel pointed downward.

Figure 5.49: Rock with the following layers labeled from bottom to top: layer labeled A is coarse-to fine-grained tan and gray sandstone; layer labeled B is finely laminated medium-to fine-grained gray and black sandstone; layer labeled C is black and gray rippled fine-grained

sandstone; and the layer labeled D is finely laminated black siltstone grading to mudstone. There are also rounded cobbles lying around the described rock.

Figure 5.50: Series of seven side-view diagrams; diagram 1 is labeled Typical ripple pattern and has a tan bed with six ridges along the top with a flat water line above the bed; diagram 2 is labeled Dunes with ripples superposed and has a tan bed with two elongated ridges along the top with a slightly curved water line above the bed and numerous curved arrows generally moving from left to right; diagram 3 is labeled Dunes and has a tan bed with two elongated, high ridges along the top with a more curved water line above the bed and numerous curved arrows generally moving from right to left with some swirls; diagram 4 is labeled Washed out dunes and has a tan bed with a gently sloping ridge along the top with a nearly flat water line above the bed and two arrows pointing from left to right; diagram 5 is labeled Plane bed and has a tan bed with three low, gently sloping ridges along the top with a flat water line above the bed; diagram 6 is labeled Antidune standing wave and has a tan bed with two elongated ridges along the top with a curved water line that matches the shape of the ridges above the bed; and diagram 7 is labeled Antidune breaking wave and has a tan bed with two domed ridges along the top with a curved water line that matches the shape of the ridges and also has a wave crashing on the right side.

Figure 5.51: There are slight grooves in a very grainy-looking whitish tan rock; a pocket knife rests on the rock for scale.

Figure 5.52: Close-up photo of ripples in sand; there's a visible steeper side on the left of each sand ripple, and a more gentle slope on the right side of each ripple.

Figure 5.53: Sample of reddish-brown rock that has visible parallel ridges and valleys on its surface; a person is holding the sample in one hand and pointing at a ripple with the other hand.

Figure 5.54: Cross sectional view of rock containing a series of elongated ridges and troughs that appear to be ascending or climbing toward the upper right; a rock hammer rests at the base of the outcrop for scale.

Figure 5.55: Tall cliff with tan to brown beds visible along the cliff face; on the face of the cliff the bedding planes are visible as nearly horizontal, with smaller parallel tan lines between each bedding plane angled down toward the left.

Figure 5.56: The tan sand dune is rippled on the left, steeper side and smooth on the right side.

Figure 5.57: A cross sectional view of thin cross beds that create a V-shape with the V opening toward the left of the photo.

Figure 5.58: Tan rock with visible bumpy and undulating lines in the rock; a pencil rests vertically against the rock face for scale.

Figure 5.59: A shallow stream of water flows over a sandy bank toward a larger pool; the water stream has small waves in it as it travels over depressions in the sand.

Figure 5.60: Slab of gray rock with lighter gray ovals and lines visible in darker gray matrix; a scale bar in the upper right says 1 cm.

Figure 5.61: Two photos; the top photo shows dried tan mud that has polygonal cracks running throughout it with a person standing on it toward the background. Bottom photo shows grayish brown solid rock that has filled-in cracks that go in several directions, forming polygonal shapes with a pair of hiking boots is seen on top of the rock.

Figure 5.62: A view of the bottom of a tan rock layer with a bulge sticking out of the base toward the observer; a pen is next to the rock for scale.

Figure 5.63: A view of the bottom of a tan and gray rock with visible narrow, parallel ridges that go across the base of the rock.

Figure 5.64: A cylindrical piece of gray rock; light-colored gray rock with sand-sized grains is sticking down into dark gray rock with mud-sized grains.

Figure 5.65: Gray rock with round circle impressions dotted along the surface; a scale bar at the upper right says 3 cm.

Figure 5.66: Tan, brown, and white conglomerate with rounded cobbles embedded parallel and stacked on each other in a slanted manner.

Figure 5.67: Gray rock that contains a cross sectional view of a clam fossil that is partially filled with tan sediment and partially filled with white calcite; the line between the sediment and calcite is roughly horizontal; a person's finger points to the fossil.

Figure 5.68: Tan rock with a cast of a dinosaur footprint that has three elongated toes; a scale bar at the upper right says 5.0 cm.

Figure 5.69: Block diagram of various depositional environments; there is a mountain range with two environments labeled Alluvial and Glacial; at the base of the mountains is flat land with four environments labeled Aeolian, Fluvial, Evaporite, and Lacustrine; the flat land ends at the shoreline which has four environments labeled Lagoonal, Beach, Deltaic, and Tidal; from the shoreline into the ocean there's a continental shelf, the top of which has two environments labeled Reef and Shallow water marine; and at the base of the continental shelf is a deep ocean basin with one environment labeled Deep water marine.

Figure 5.70: World map with ocean basins color-coded according to the sediment thickness on the ocean floor; the thickest sediment is tan in color with a darker gradient for thinner sediment, while the thinnest sediment id deep blue in color with a lighter gradient for thicker sediment. The sediment is thickest around the ocean margins near the continents while the sediment is thinnest away from the continents in the deepest ocean basins and trenches.

Figure 5.71: Chunk of white, fine-grained, powdery-looking rock.

Figure 5.72: Block diagram showing continental shelf sloping down toward deep ocean water with underwater avalanches of mud and sand labeled on the slope and lumps at the base labeled Turbidite Deposits.

Figure 5.73: 2D seismic diagram with two-way traveltime on the vertical axis increasing downward and distance on the horizontal axis increasing toward the right, from ESE on the left to WNW on the right. Thin layers are visible in the image, sloping shallowly toward the right; the ground surface above the layers also slopes down toward the right with a moat visible near the far right and then a steep upward slope past that.

Figure 5.74: Cross sectional diagram of sand sloping upward toward the right with shallowing ocean water above; there is a horizontal line between two successive ocean wave crests labeled Wave Length; at the top of the diagram it says "Wave base is the depth to which a passing wave will cause water motion." There are circular arrows stacked vertically at the wave trough with the largest circle at the top and smaller and smaller circles toward the bottom until there are no more circles; at the bottom of the circular arrows is the label "Wave Base = 1/2 Wave Length." Along the sloping sand are two labels: on the side dipping below the vertical stack of arrows, the sand is smooth and there is the label "Ocean bottom undisturbed by waves (Lower Shoreface);" on the side dipping upward above the vertical stack of arrows, the sand is rippled and there is the label "Ocean bottom agitated and rippled by waves (Upper Shoreface)."

Figure 5.75: Block diagram of shoreline zones: on land is the Coast; there is gently sloping sand coming from the bases of cliffs along the coast; this includes the labels Beach, Backshore, and Berms; in the shallowest part of the ocean water are the labels Foreshore, Terrace, Surf zone, and Breakers. A line labeled Shoreline points to the contact between the edge of the ocean water and the beach. In deeper water is the label Nearshore and then in the deepest water is the label Offshore. The high tide and low tide line are drawn on the diagram as well, and there is a deposit on the continental slope labeled Bar. Across the entire diagram is the label Littoral zone. The deepest part of the water is about 60 m.

Figure 5.76: Two cross sectional diagrams; the top diagram shows onlap with layers of sediments being deposited on top of each other, with each successive upper layer being deposited toward inland; there is an arrow pointing toward the right-hand side labeled transgression; the bottom diagram shows offlap with layers of sediments being deposited on top of each other, with each successive upper layer being deposited toward the ocean; there is an arrow pointing toward the left-hand side labeled regression.

Figure 5.77: Side view of a sand deposit that has layers of tan sand interbedded with layers of gray and black sand; a penny is stuck into the sand for scale.

Figure 5.78: Generalized map view of a tidal flat with labeled and color-coded features: deep littoral is colored blue and found to the upper left of the diagram; lower littoral (subtidal) is colored cyan and next to the deep littoral zone; littoral (beach) is colored marigold and is a strip alongside the lower littoral zone, however the beach has a gap in it; in the gap of the beach there are tidal bars colored turquoise to match the intertidal label; other turquoise intertidal zones are found inland from the beach; supratidal is colored lime green and surrounds the intertidal zones behind the beach; and continental is colored olive green and surrounds the supratidal zone as well as the areas behind the beach along the edges of the diagram.

Figure 5.79: Aerial view of a long, thin whitish ridge that runs through the surrounding tan to brown landscape.

Figure 5.80: Colorful coral reef underwater in light blue, shallow water.

Figure 5.81: Satellite image of an elongate dark green island that's surrounded by deep blue water. A reef can be seen as a lighter blue ring outside of the island.

Figure 5.82: The left side of the map shows part of Australia and Asia while the right side of the map shows the west-southwestern coast of North America. The Pacific Ocean is white, with numerous red dots, ranging from tiny to small, scattered throughout the ocean; guyots are shown as slightly larger green dots and are less abundant than seamounts.

Figure 5.83: Satellite image of a brown, barren landscape with a large blue rounded body of water on the land; to the left of that body of water is a deeper blue larger water body, the Caspian Sea.

Figure 5.84: Satellite view of a land-sea boundary with a green fan-shaped delta between the edge of tan land and deep blue ocean, widening toward the ocean.

Figure 5.85: Satellite view of light blue water with a green dendritic or birdfoot-shaped delta branching out into the water.

Figure 5.86: Satellite view of numerous roughly parallel tan-colored rivers leading to a larger body of tan water that becomes deep blue away from the mouths of the rivers.

Figure 5.87: Sinuous tan river running through roughly flat green terrain.

Figure 5.88: Many channels that braid back and forth among each other; between channels are tan sediment deposits.

Figure 5.89: Landscape with a broad, tan valley dotted with low scrubby vegetation; a river from distant ridges splits and runs in numerous branches down the broad valley.

Figure 5.90: A large hole in the top of a mountain that is filled with a lake. There is also an island in the lake.

Figure 5.91: Six block diagrams of various dune shapes: blowout dunes which are sandy depressions; parabolic dunes which are U-shaped with the wind blowing in the direction of the curve of the U; dome dunes which are dome-shaped rising from the land; barchan dunes which are a narrow U- shape with the wind blowing in the direction of the arms of the U; barchanoid ridges which are elongate wavy ridges with the wind blowing from the shallowly sloping side toward the steeper sloped side; and transverse ridges which are linear ridges with the wind blowing from the shallowly sloping side toward the steeper sloped side.

Figure 5.92: Tan landscape of plateaus and canyons with buildings carved into the stone.

Figure 5.93: Along the edge of glacial ice, numerous broken pieces of tan, gray, and black rocks lay along the edge, ranging in size from large boulders to tiny bits.

6. METAMORPHIC ROCKS

Contributing Author: Dr. Peter Davis, Pacific Lutheran University

Learning Objectives

By the end of this chapter, students will be able to:

- Describe the temperature and pressure conditions of the metamorphic environment.
- Identify and describe the three principal metamorphic agents.
- Describe what recrystallization is and how it affects mineral crystals.
- Explain what foliation is and how it results from directed pressure and recrystallization.
- Explain the relationships among slate, phyllite, schist, and gneiss in terms of metamorphic grade.
- Define index mineral.
- Explain how metamorphic facies relate to plate tectonic processes.
- Describe what a contact **aureole** is and how contact metamorphism affects surrounding rock.
- Describe the role of hydrothermal metamorphism in forming mineral deposits and ore bodies.

Metamorphic rock—*meta*- meaning change and –*morphos* meaning form—is one of the three rock categories in the rock cycle (see Chapter 1). Metamorphic rock material has been changed by temperature, pressure, and/or fluids. The rock cycle shows that both igneous and sedimentary rocks can become metamorphic rocks. Metamorphic rocks themselves can be re-metamorphosed. Because metamorphism is caused by plate tectonic motion, metamorphic rock provides geologists with a history book of how past tectonic processes shaped our planet.

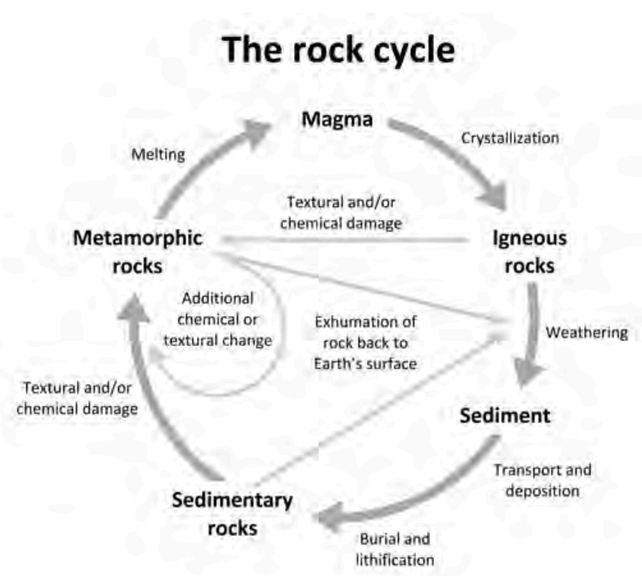

Figure 6.1: Rock cycle showing the five materials (such as igneous rocks and sediment) and the processes by which one changes into another (such as weathering). Figure description available at the end of the chapter.

6.1 Metamorphic Processes

Metamorphism occurs when solid rock changes in composition and/or texture without the mineral crystals melting, which is how igneous rock is generated. Metamorphic source rocks, the rocks that experience the metamorphism, are called the parent rock or **protolith**, from *proto*– meaning first and *lithos*- meaning rock. Most metamorphic processes take place deep underground, inside the Earth's crust. During metamorphism, protolith chemistry is mildly changed by increased temperature (heat), a type of pressure called confining pressure, and/or chemically reactive fluids. Rock texture is changed by heat, confining pressure, and a type of pressure called **directed stress**.

6.1.1 Temperature (Heat)

Temperature measures a substance's energy, with an increase in temperature representing an increase in energy. Temperature changes affect the chemical equilibrium in minerals. At high temperatures, atoms may vibrate so vigorously they jump from one position to another within the crystal lattice, which remains intact. In other words, this atom swapping can happen while the rock is still solid.

The temperatures of metamorphic rock are located between surficial processes (as in sedimentary rock) and magma in the rock cycle. Heat-driven metamorphism begins at temperatures as low as 200˚C and can continue to occur at temperatures as high as 700˚C–1100˚C. Higher temperatures would create magma, and thus, would no longer be a metamorphic process. Temperature increases with increasing depth in the Earth along a geothermal gradient (see Chapter 4), and metamorphic rock records these depth-related temperature changes.

6.1.2 Pressure

Pressure is the force exerted over a unit area on a material. Like heat, pressure can affect the chemical equilibrium of minerals in a rock. The pressure that affects metamorphic rocks can be grouped into confining pressure and directed stress. **Stress** is a scientific term indicating a force. **Strain** is the result of this stress, including metamorphic changes within minerals.

Confining Pressure

Pressure is exerted on rocks under the surface due to the simple fact that rocks lie on top of one another. When pressure is exerted from rocks above, it is balanced from below and from the sides in what is called confining, or lithostatic, pressure. Confining pressure has equal pressure on all sides (see Figure 6.2) and is responsible for causing chemical reactions to occur just like heat. These chemical reactions will cause new minerals to form.

Confining pressure is measured in bars and ranges from 1 bar at sea level to around 10,000 bars at the base of the crust. For metamorphic rocks, pressures range from a relatively low pressure of 3,000 bars to around 50,000 bars, which occurs around 15–35 kilometers below the surface.

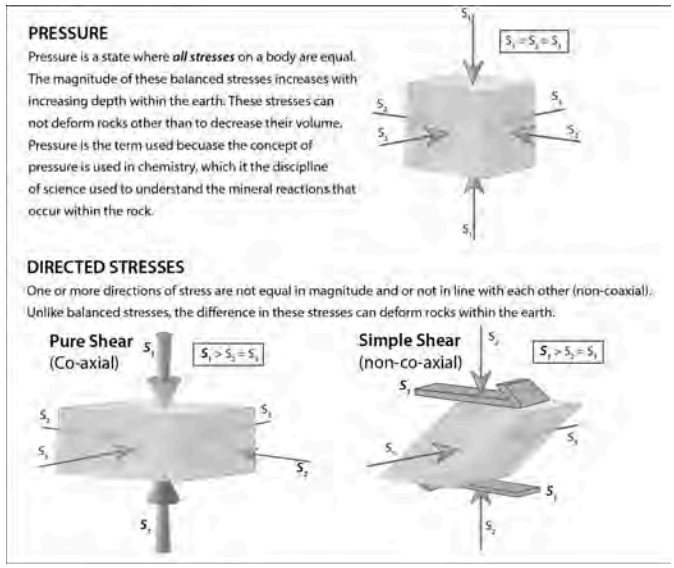

Figure 6.2: Difference between pressure and stress and how they deform rocks. Pressure (or confining pressure) has equal stress (forces) in all directions and increases with depth under the Earth's surface. Under directed stress, some stress directions (forces) are stronger than others, and this can deform rocks. Figure description available at the end of the chapter.

Directed Stress

Figure 6.3: Pebbles (that used to be spherical or close to spherical) in quartzite deformed by directed stress. Figure description available at the end of the chapter.

Directed stress, also called differential or tectonic stress, is an unequal balance of forces on a rock in one or more directions (see previous figure). Directed stresses are generated by the movement of lithospheric plates. In contrast to confining pressure, directed stress occurs at much lower pressures and does not generate chemical reactions that change mineral composition and atomic structure. Instead, directed stress modifies the parent rock at a mechanical level, changing the arrangement, size, and/or shape of the mineral crystals. These crystalline changes create identifying textures, which is shown in the figure below comparing the phaneritic texture of igneous granite with the foliated texture of metamorphic gneiss.

Directed stresses produce rock textures in many ways. Crystals can be **rotated**, changing their orientation in space. Crystals can get fractured, reducing their grain size. Conversely, they may grow larger as atoms migrate. Crystal shapes also become deformed. These mechanical changes occur via **recrystallization**, which is when minerals dissolve from an area of rock experiencing high stress and then precipitate or regrow in a location with lower stress. For example, recrystallization increases grain size much like adjacent soap bubbles coalesce to form larger ones. Recrystallization rearranges mineral crystals without fracturing the rock structure, deforming the rock like Silly Putty; these changes provide important clues to understanding the creation and movement of deep underground rock faults.

Figure 6.4: An igneous rock, granite (left), and foliated high-temperature and high-pressure metamorphic rock, gneiss (right), illustrating a metamorphic texture. Figure description available at the end of the chapter.

6.1.3 Fluids

A third metamorphic agent is chemically reactive fluids that are expelled by crystallizing magma and created by metamorphic reactions. These reactive fluids are made of mostly water (H_2O) and carbon dioxide (CO_2), as well as smaller amounts of potassium (K), sodium (Na), iron (Fe), magnesium (Mg), calcium (Ca), and aluminum (Al). These fluids react with minerals in the protolith, changing its chemical equilibrium and mineral composition in a process similar to the reactions driven by heat and pressure. In addition to using elements found in the protolith, the chemical reaction may incorporate substances contributed by the fluids to create new minerals. In general, this style of metamorphism, in which fluids play an important role, is called hydrothermal metamorphism or hydrothermal alteration. Water actively participates in chemical reactions and allows extra mobility of the components in hydrothermal alteration.

Fluid-activated metamorphism is frequently involved in creating economically important mineral deposits that are located next to igneous intrusions or magma bodies. For example, the mining districts in the Cottonwood Canyons and Mineral Basin of northern Utah produce valuable ores such as argentite (silver sulfide), galena (lead sulfide), and chalcopyrite (copper iron sulfide), as well as the native element gold. These mineral deposits were created from the interaction between a granitic intrusion called the Little Cottonwood Stock and country rock consisting of mostly limestone and dolostone. Hot, circulating fluids expelled by the crystallizing granite reacted with and dissolved the surrounding limestone and dolostone, precipitating new minerals created by the chemical reaction. Hydrothermal alternation of mafic mantle rock, such as olivine and basalt, creates the metamorphic rock **serpentinite**, a member of the serpentine subgroup of minerals. This metamorphic process happens at mid-ocean spreading centers, where newly formed oceanic crust interacts with seawater.

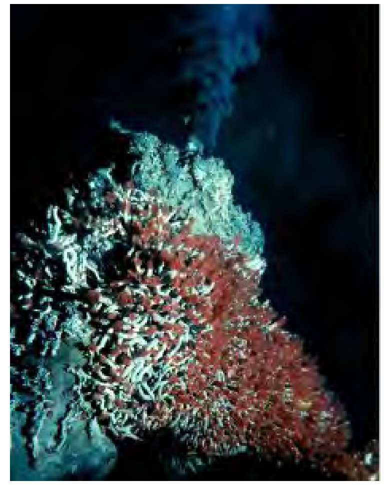

Figure 6.5: Black smoker hydrothermal vent with a colony of giant (6'+) tube worms. Figure description available at the end of the chapter.

Some hydrothermal alterations remove elements from the parent rock rather than deposit them. This happens when seawater circulates down through fractures in the fresh, still-hot basalt, reacting with and removing mineral ions from it. The dissolved minerals are usually ions that do not fit snugly in the silicate crystal structure, such as copper. The mineral-laden water emerges from the seafloor via hydrothermal vents called black smokers, named after the dark-colored precipitates produced when the hot vent water meets cold seawater (see Chapter 4). Ancient black smokers were an important source of copper ore for the inhabitants of Cyprus (Cypriots) as early as 4,000 BCE, and later for the Romans.

Take this quiz to check your comprehension of this section.

Access the quiz for Section 6.1 by scanning the QR code.

6.2 Metamorphic Textures

Metamorphic texture is the description of the shape and orientation of mineral grains in a metamorphic rock. Metamorphic rock textures are foliated, nonfoliated, or lineated, each of which is described below.

Identify rock's foliation		Textural features	Mineral composition	Rock name	Parent rock
Foliated (layered texture)	Fine-grained or no visible grains	Flat, slaty cleavage is well developed. Dense, microscopic grains may exhibit slight sheen (or dull luster). Clanky sound when struck. Breaks into hard, flat sheets.	Fine, microscopic clay or mica	Slate	Shale
		Finely crystalline; micas hardly discernible but impart a sheen or luster. Breaks along wavy surfaces.	Dark silicates and micas	Phyllite	Siltstone or shale
	Medium- to coarse-grained	Schistose texture. Foliation formed by alignment of visible crystals. Rock breaks along scaly foliation surfaces. Medium- to fine-grained. Sparkling appearance.	Common minerals include chlorite, biotite, muscovite, garnet, and hornblende. Recognizable minerals used as part of rock name. Porphyroblasts common.	Mica schist	Siltstone or shale
				Garnet schist	
		Gneissic banding. Coarse-grained. Foliation present as minerals arranged into alternating light and dark layers giving the rock a banded texture in side view. Crystalline texture. No cleavage.	Light-colored quartz and feldspar; dark ferromagnesian minerals	Gneiss	Shale or granitic rocks
Nonfoliated (no layered texture)	Fine-grained or no visible grains	Medium- to coarse-grained crystalline structure.	Crystals of amphibole (hornblende) in blade-like crystals	Amphibolite	Basalt, gabbro, or ultramafic igneous rocks
		Microcrystalline texture. Glassy black sheen. Conchoidal fracture. Low density.	Fine, tar-like, organic makeup	Anthracite coal	Coal
		Dense and dark-colored. Fine or microcrystalline texture. Very hard. Color can range from gray, gray-green to black.	Microscopic dark silicates	Hornfels	Many rock types
		Microcrystalline or no visible grains, with smooth, wavy surfaces. May be dull or glossy. Usually shades of green.	Serpentine. May have fibrous asbestos visible.	Serpentinite	Ultramafic igneous rocks or peridotite
	Fine- to coarse-grained	Microcrystalline or no visible grains. Can be scratched with a fingernail. Shades of green, gray, brown, or white. Soapy feel.	Talc	Soapstone or talc schist	Ultramafic igneous rocks
		Crystalline. Hard (scratches glass). Breaks across grains. Sandy or sugary texture. Color variable; can be white, pink, buff, brown, red, purple.	Quartz grains fused together. Grains will not rub off like sandstone.	Quartzite	Quartz sandstone
		Finely crystalline (resembling a sugar cube) to medium or coarse texture. Color variable; white, pink, gray, among others. Fossils in some varieties.	Calcite or dolomite crystals tightly fused together. Calcite effervesces with HCl; dolomite effervesces only when powdered.	Marble	Limestone or dolostone
		Texture of conglomerate but breaks across clasts as easily as around them. Pebbles may be stretched (lineated) or cut by rock cleavage.	Granules or pebbles are commonly granitic or jasper, chert, quartz, or quartzite.	Meta-conglomerate	Conglomerate

Table 6.1: Metamorphic rock identification table.

6.2.1 Foliation and Lineation

Foliation is a term that describes minerals lined up in planes. Certain minerals, most notably the mica group, are mostly thin and planar by default. Foliated rocks typically appear as if the minerals are stacked like pages of a book, thus the use of the term *folia*, like a leaf. Other minerals, with hornblende being a good example, are longer in one direction, linear like a pencil or a needle rather than a planar-shaped book. These linear objects can also be aligned within a rock. This is referred to as a **lineation**. Linear crystals, such as hornblende, tourmaline, or stretched quartz grains, can be arranged as part of a foliation, a lineation, or foliation/lineation together. If minerals lie on a plane with mica but with no common or preferred direction, this is foliation. If the minerals line up and point in a common direction but with no planar fabric, this is lineation. When minerals lie on a plane AND point in a common direction; this is both foliation and lineation.

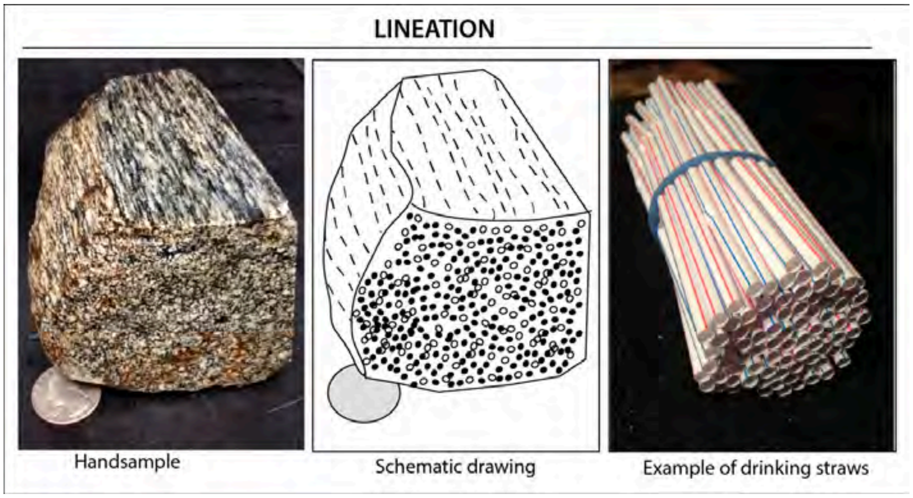

Figure 6.6: Example of lineation in which minerals are aligned like a stack of straws or pencils. Figure description available at the end of the chapter.

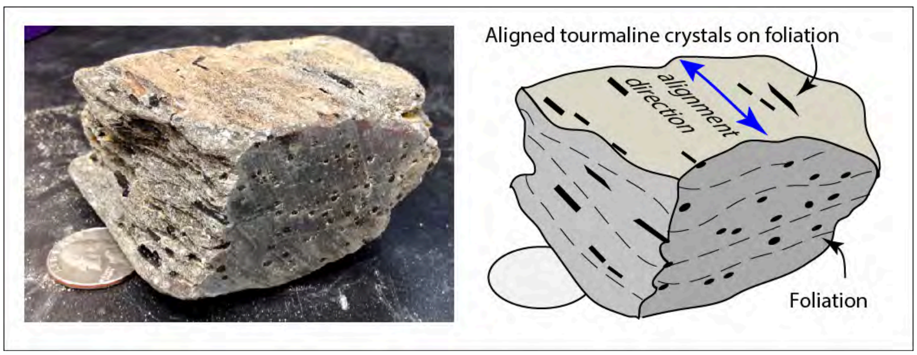

Figure 6.7: An example of foliation WITH lineation. Figure description available at the end of the chapter.

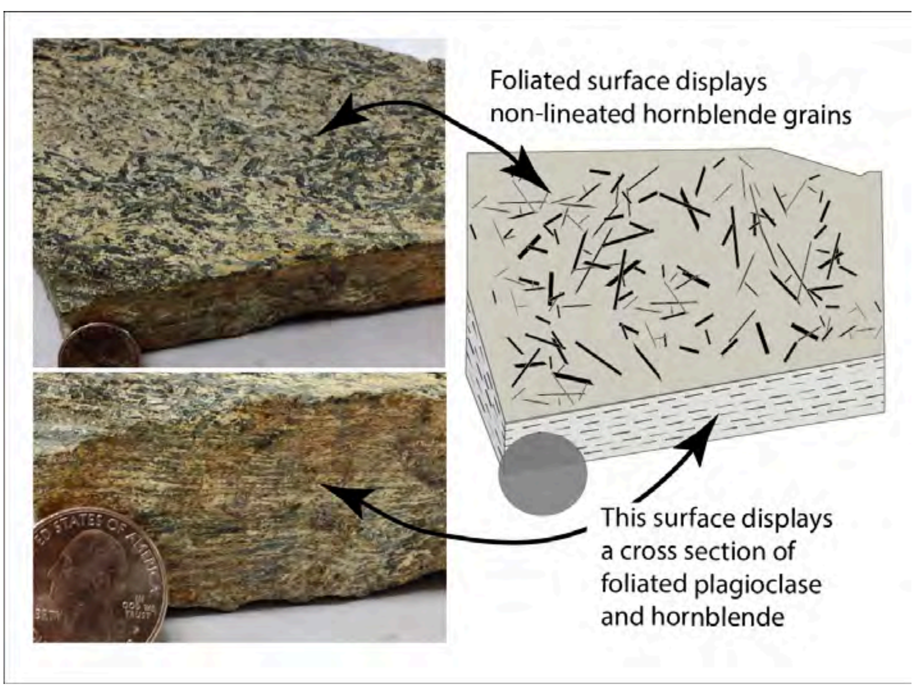

Figure 6.8: An example of foliation WITHOUT lineation. Figure description available at the end of the chapter.

Foliated metamorphic rocks are named based on the style of their foliations. Each type has a specific texture that defines and distinguishes it, with their descriptions listed below.

Slate is a fine-grained metamorphic rock that exhibits a foliation called **slaty cleavage**, which refers to the flat orientation of the small platy crystals of mica and chlorite forming perpendicular to the direction of stress. The minerals in slate are too small to see with the unaided eye. The thin layers in slate may resemble sedimentary bedding, but they are a result of directed stress and may lie at angles to the original strata. In fact, original sedimentary layering may be partially or completely obscured by the foliation. Thin slabs of slate are often used as a building material for roofs and tiles.

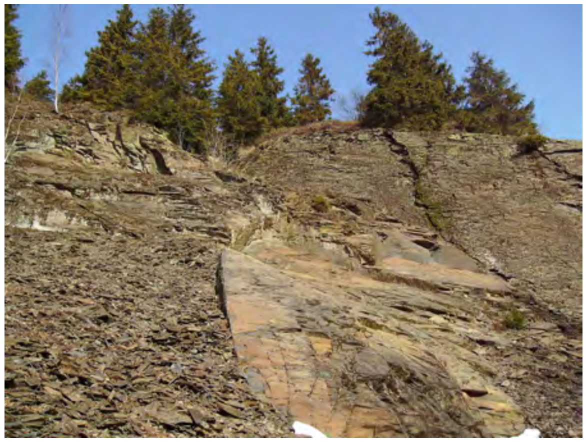

Figure 6.9: Rock breaking along flat, even planes. Figure description available at the end of the chapter.

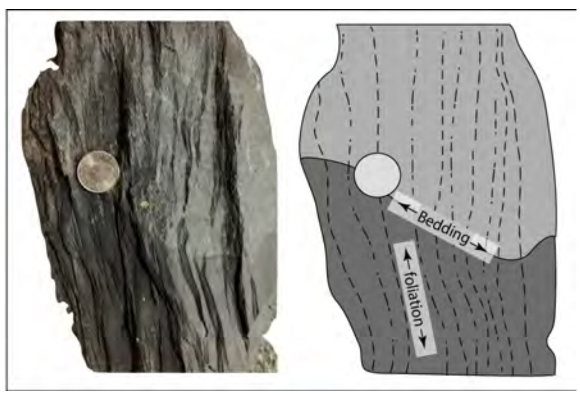

Figure 6.10: Foliation versus bedding. Foliation is caused by metamorphism. Bedding is a result of sedimentary processes. They do not have to align. Figure description available at the end of the chapter.

Phyllite is a foliated metamorphic rock in which platy minerals have grown larger and the surface of the foliation shows a sheen from light reflecting from the grains, perhaps even taking on a wavy appearance called crenulations. Similar to phyllite, but with even larger grains, is the foliated metamorphic rock schist, which has large platy grains visible as individual crystals. Common minerals are muscovite, biotite, and porphyroblasts of garnets (a porphyroblast is a large crystal of a particular mineral surrounded by small grains). **Schistosity** is a textural description of foliation created by the parallel alignment of platy visible grains. Some schists are named for their minerals, such as mica schist (mostly micas), garnet schist (mica schist with garnets), and staurolite schist (mica schists with staurolite).

Figure 6.11: Phyllite with a small fold. Figure description available at the end of the chapter.

Figure 6.12: Schist. Figure description available at the end of the chapter.

Figure 6.13: Garnet staurolite muscovite schist. Figure description available at the end of the chapter.

Figure 6.14: Gneiss. Figure description available at the end of the chapter.

Gneissic banding is a metamorphic foliation in which visible silicate minerals separate into dark and light bands, or lineations. These grains tend to be coarse and are often folded. A rock with this texture is called **gneiss**. Since gneisses form at the highest temperatures and pressures, some partial melting may occur. This partially melted rock is a transition between metamorphic and igneous rocks called a **migmatite**.

Migmatites appear as dark- and light-banded gneiss that may be swirled or twisted to some extent since some minerals started to melt. Thin accumulations of light-colored rock layers can occur in a darker rock that are parallel to each other and can even cut across the gneissic foliation. The lighter-colored layers are interpreted to be the result of the separation of a felsic igneous melt from the adjacent highly metamorphosed darker layers, or they can result from the injection of a felsic melt from some distance away.

Figure 6.15: Migmatite, a rock which was partially molten. Figure description available at the end of the chapter.

6.2.2 Nonfoliated

Figure 6.16: Marble. Figure description available at the end of the chapter.

Figure 6.17: Baraboo quartzite. Figure description available at the end of the chapter.

Nonfoliated textures do not have lineations, foliations, or other alignments of mineral grains. **Nonfoliated** metamorphic rocks are typically composed of just one mineral and therefore usually show the effects of metamorphism with recrystallization in which crystals grow together but with no preferred direction. The two most common examples of nonfoliated rocks are quartzite and marble. **Quartzite** is a metamorphic rock from the protolith sandstone. In quartzites, the quartz grains from the original sandstone are enlarged and interlocked by recrystallization. A defining characteristic for distinguishing quartzite from sandstone is that quartz crystals, when broken with a rock hammer, break across the grains. In a sandstone, only a thin mineral cement holds the grains together, meaning that a broken piece of sandstone will leave the grains intact. Because most sandstones are rich in quartz, a mechanically and chemically durable substance, quartzite is very hard and resistant to weathering.

Figure 6.18: Connemara marble, a variety of green marble from Connemara, Ireland. Figure description available at the end of the chapter.

Marble is metamorphosed limestone (or dolostone) composed of calcite (or dolomite). Recrystallization typically generates larger interlocking crystals of calcite or dolomite. Marble and quartzite often look similar, but these minerals are considerably softer than quartz. Another way to distinguish marble from quartzite is to apply a drop of dilute hydrochloric acid. Marble will effervesce (fizz) if it is made of calcite.

A third nonfoliated rock is **hornfels**, which is identified by its dense, fine-grained, hard, blocky or splintery texture composed of several silicate minerals. Crystals in hornfels grow smaller with metamorphism, becoming so small that specialized study is required to identify them. These commonly occur around intrusive igneous bodies. The protolith of hornfels can be even harder to distinguish, as it can be anything from mudstone to basalt.

Figure 6.19: Macro view of quartzite. Note the interconnectedness of the grains. Figure description available at the end of the chapter.

Take this quiz to check your comprehension of this section.

Access the quiz for Section 6.2 by scanning the QR code.

6.3 Metamorphic Grade

Metamorphic grade refers to the range of metamorphic change a rock undergoes, progressing from low grade (little metamorphic change) to high grade (significant metamorphic change). Low-grade metamorphism begins at temperatures and pressures just above sedimentary rock conditions. The sequence slate → phyllite → schist → gneiss illustrates an increasing metamorphic grade.

Geologists use **index minerals** that form at certain temperatures and pressures to identify metamorphic grade. These index minerals also provide important clues to a rock's sedimentary protolith and the metamorphic conditions that created it. Chlorite, muscovite, biotite, garnet, and staurolite are index minerals representing a respective sequence of low-to-high grade rock. The following interactive activity shows a **phase diagram** of three index minerals—sillimanite, kyanite, and andalusite—with the same chemical formula (Al_2SiO_5) but having different crystal structures (**polymorphism**) created by different pressure and temperature conditions.

Figure 6.20: Garnet schist. Figure description available at the end of the chapter.

Complete this interactive activity to check your understanding.

Access this interactive activity by scanning the QR code.

Some metamorphic rocks are named based on the highest grade of index mineral present. Chlorite schist includes the low-grade index mineral chlorite. Muscovite schist contains the slightly higher-grade muscovite, indicating a greater degree of metamorphism. Garnet schist includes the high-grade index mineral garnet, indicating it has experienced much higher pressures and temperatures than chlorite.

Take this quiz to check your comprehension of this section.

Access the quiz for Section 6.3 by scanning the QR code.

6.4 Metamorphic Environments

As with igneous processes, metamorphic rocks form at different zones of pressure (depth) and temperature, as shown on the pressure-temperature (P-T) diagram. The term facies is an objective description of a rock. In metamorphic rocks, facies are groups of minerals called mineral assemblages. The names of **metamorphic facies** on the pressure-temperature diagram reflect minerals and mineral assemblages that are stable at these pressures and temperatures, providing information about the metamorphic processes that have affected the rocks. This is useful when interpreting the history of a metamorphic rock.

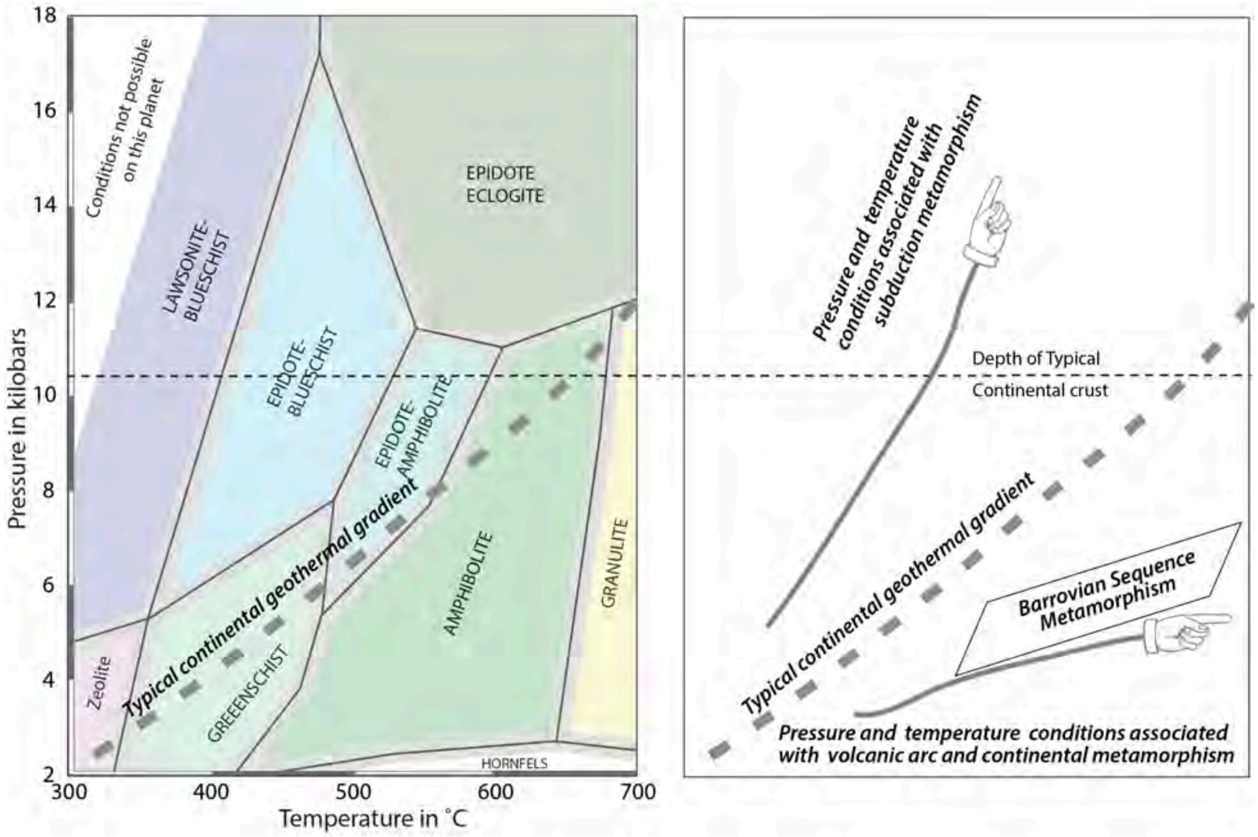

Figure 6.21: Pressure-temperature graphs of various metamorphic facies. Figure description available at the end of the chapter.

In the late 1800s, British geologist George Barrow mapped zones of index minerals in different metamorphic zones of an area that underwent regional metamorphism. Barrow outlined a progression of index minerals, named the Barrovian sequence, that represents increasing metamorphic grade: chlorite (slates and phyllites) → biotite (phyllites and schists) → garnet (schists) → staurolite (schists) → kyanite (schists) → sillimanite (schists and gneisses).

The first in the Barrovian sequence has a mineral group that is commonly found in the metamorphic greenschist facies. Greenschist rocks form under relatively low pressure and temperatures and represent the fringes of regional metamorphism. The "green" part of the name is derived from green minerals like chlorite, serpentine, and epidote, and the "schist" part is applied due to the presence of platy minerals such as muscovite.

Many different styles of metamorphic facies are recognized, and these are due to different geologic and tectonic processes. Recognizing these facies is the most direct way to interpret the metamorphic history of a rock. A simplified list of major metamorphic facies is given below.

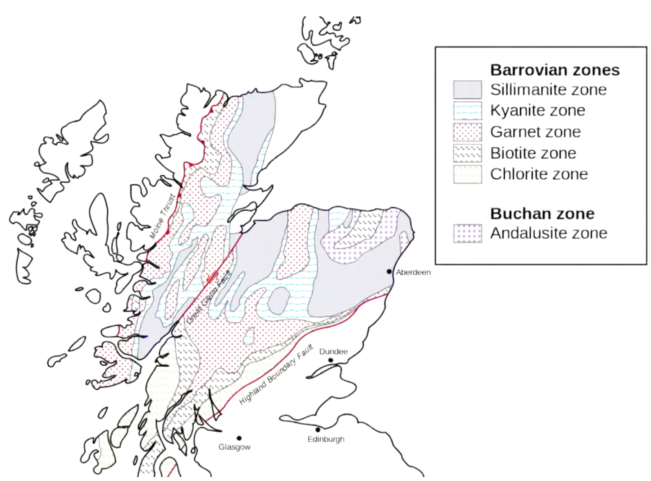

Figure 6.22: Barrovian sequence in Scotland. Figure description available at the end of the chapter.

6.4.1 Burial Metamorphism

Burial metamorphism occurs when rocks are deeply buried at depths of more than 2,000 meters (1.24 miles). Burial metamorphism commonly occurs in sedimentary basins, where rocks are buried deeply by overlying sediments. As an extension of diagenesis, a process that occurs during lithification (Chapter 5), burial metamorphism can cause clay minerals, such as smectite, in shales to change to another clay mineral, illite, or it can cause quartz sandstone to metamorphose into quartzite, such as in the Big Cottonwood Formation in the Wasatch range of Utah. This formation was deposited as ancient near-shore sands in the late Proterozoic (see Chapter 7), deeply buried and metamorphosed to quartzite, folded, and later exposed at the surface in the Wasatch range today. The increase of temperature with depth in combination with an increase of confining pressure produces low-grade metamorphic rocks with a mineral assemblages indicative of a zeolite facies.

6.4.2 Contact Metamorphism

Contact metamorphism occurs in rock exposed to high temperature and low pressure, as might happen when hot magma intrudes into or lava flows over preexisting protolith. This combination of high temperature and low pressure produces numerous metamorphic facies. The lowest pressure conditions produce hornfels facies, while higher pressure creates greenschist, amphibolite, or granulite facies.

As with all metamorphic rock, the parent rock texture and chemistry are major factors in determining the final outcome of the metamorphic process, including what index minerals are present. Fine-grained shale and basalt, which happen to be chemically similar, characteristically recrystallize to produce hornfels. Sandstone (silica) surrounding an igneous intrusion becomes quartzite via contact metamorphism, and limestone (carbonate) becomes marble.

When contact metamorphism occurs deeper in the Earth, metamorphism can be seen as rings of facies around the intrusion, resulting in aureoles. These differences in metamorphism appear as distinct bands surrounding the intrusion, as can be seen around the Alta stock in Little Cottonwood Canyon, Utah. The Alta stock is a granite intrusion surrounded first by rings of the index minerals amphibole (tremolite) and olivine (forsterite), with a ring of talc (dolostone) located further away.

Figure 6.23: Contact metamorphism in outcrop. Figure description available at the end of the chapter.

6.4.3 Regional Metamorphism

Regional metamorphism occurs when parent rock is subjected to increased temperature and pressure over a large area. This often occurs in mountain ranges created by converging continental crustal plates. This is the setting for the Barrovian sequence of rock facies, with the lowest grade of metamorphism occurring on the flanks of the mountains and the highest grade near the core of the mountain range, closest to the convergent boundary.

An example of an old regional metamorphic environment is visible in the northern Appalachian Mountains while driving east from New York State through Vermont and into New Hampshire. Along this route, the degree of metamorphism gradually increases from sedimentary parent rock to low-grade metamorphic rock, then higher-grade metamorphic rock, and eventually the igneous core. The rock sequence is sedimentary rock, slate, phyllite, schist, gneiss, migmatite, and granite. In fact, New Hampshire is nicknamed the Granite State. The reverse sequence can be seen heading east, from eastern New Hampshire to the coast.

6.4.4 Subduction Zone Metamorphism

Figure 6.24: Blueschist. Figure description available at the end of the chapter.

In **subduction zone metamorphism**, a type of regional metamorphism, oceanic crust is pushed downward into the mantle. Due to the oceanic crust's relatively cooler temperatures, especially along the upper surface (seafloor), it stays cooler than the surrounding mantle. This creates a metamorphic environment of high pressure and low temperature. Glaucophane, which has a distinctive blue color, is an index mineral found in blueschist facies (see metamorphic facies diagram, Figure 6.21). **Blueschist** typically forms in subduction zones then transforms into eclogite at even deeper depths (about 35 km) and sinks into the mantle, almost never resurfacing. However, in a few places in the world, subduction-zone metamorphic rocks have returned to the surface, such as in the California Coast Range near San Francisco. The range has blueschist-facies rocks created by subduction-zone metamorphism, which include rocks made of blueschist, eclogite, greenstone, and red chert. Greenstone, which is metamorphized basalt, gets its color from the index mineral chlorite.

Figure 6.25: Eclogite. Figure description available at the end of the chapter.

6.4.5 Fault Metamorphism

There are a range of metamorphic rocks made along faults. Near the surface, rocks are involved in repeated brittle faulting, which produces a material called rock flour, which is rock that has been ground up into the particle size of flour used for food. At lower depths, faulting create cataclastites, chaotically crushed mixes of rock material with little internal texture. At depths below **cataclasites**, where strain becomes ductile, mylonites are formed. **Mylonites** are metamorphic rocks created by dynamic recrystallization through directed shear forces, generally resulting in a reduction of grain size. When larger, stronger crystals (like feldspar, quartz, or garnet) embedded in a metamorphic matrix are sheared into an asymmetrical eye-shaped crystal, an **augen** is formed.

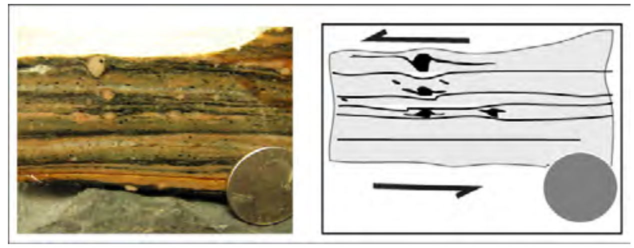

Figure 6.26: Mylonite. Figure description available at the end of the chapter.

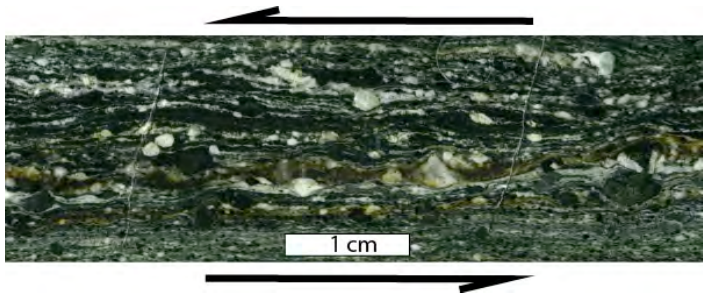

Figure 6.27: Examples of augens. Figure description available at the end of the chapter.

6.4.6 Shock Metamorphism

Shock metamorphism (also known as impact metamorphism) is metamorphism resulting from a high-pressure shock event, such as a **meteor** or other **bolide** impact. Shock metamorphism is the result of very high pressures (and higher but less extreme temperatures) delivered relatively rapidly. Shock metamorphism produces planar deformation features, tektites, shatter cones, and quartz polymorphs. Shock metamorphism produces planar deformation features (shock laminae), which are narrow planes of glassy material with distinct orientations found in silicate mineral grains. Shocked quartz has planar deformation features.

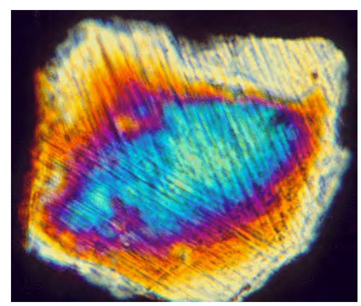

Figure 6.28: Shock lamellae in a quartz grain. Figure description available at the end of the chapter.

Figure 6.29: Meteor Crater is an impact crater that is 1.2 km across and about 180 m deep in the desert of Northern Arizona. Figure description available at the end of the chapter.

Figure 6.30: Shatter cone. Figure description available at the end of the chapter.

Shatter cones are cone-shaped pieces of rock created by dynamic branching fractures caused by impacts. While not strictly a metamorphic structure, they are common around shock metamorphism. Their diameter can range from microscopic to several meters. Fine-grained rocks with shatter cones show a distinctive horsetail pattern.

Shock metamorphism can also produce index minerals, though they are typically only found via microscopic analysis. The quartz polymorphs coesite and stishovite are indicative of impact metamorphism. As discussed in Chapter 3, polymorphs are minerals with the same composition but different crystal structures. Intense pressure (> 10 GPa) and moderate-to-high temperatures (700–1200°C) are required to form these minerals.

Shock metamorphism can also produce glass. Tektites are gravel-size glass grains ejected during an impact event. They resemble volcanic glass but, unlike volcanic glass, tektites contain no water or phenocrysts and have a different bulk and isotopic chemistry. Tektites contain partially melted inclusions of shocked mineral grains. Although all are melt glasses, tektites are also chemically distinct from trinitite (produced from thermonuclear detonations) and fulgurites (produced by lightning strikes). All geologic glasses not derived from volcanoes can be called with the general term pseudotachylytes, a name which can also be applied to glasses created by faulting. The term *pseudo-* in this context means “false” or “in the appearance of” a volcanic rock called tachylite because the material observed looks like a volcanic rock but is produced by significant shear heating.

Figure 6.31: Tektites. Figure description available at the end of the chapter.

Take this quiz to check your comprehension of this section.

Access the quiz for Section 6.4 by scanning the QR code.

Video 6.1: Identifying metamorphic rocks

Access this YouTube video by scanning the QR code. [“Metamorphic Rocks (& toast)” by GeoScience Videos | https://www.youtube.com/watch?v=Ncr-46YX-N0]

Video 6.2: Identifying metamorphic rocks

Access this YouTube video by scanning the QR code. [“Identifying Metamorphic Rocks — Earth Rocks!” by Earth Rocks! | https://www.youtube.com/watch?v=HUydPhIaQQU]

Summary

Metamorphism is the process that changes existing rocks (called protoliths) into new rocks with new minerals and new textures. Increases in temperature and pressure are the main causes of metamorphism, with fluids adding important mobilization of materials. The primary way metamorphic rocks are identified is by texture. Foliated textures come from platy minerals forming planes in a rock, while nonfoliated metamorphic rocks have no internal fabric. Grade describes the amount of metamorphism in a rock, and facies are a set of minerals that can help guide an observer to an interpretation of the metamorphic history of a rock. Different tectonic or geologic environments cause metamorphism, including collisions, subduction, faulting, and even impacts from space.

Take this quiz to check your comprehension of this chapter.

Access the quiz for Chapter 6 by scanning the QR code.

Text References

1. Bucher, K., and Grapes, R. (2011). *Petrogenesis of metamorphic rocks:* Springer.
2. Jeong, I.-K., Heffner, R.H., Graf, M.J., and Billinge, S.J.L. (2003). Lattice dynamics and correlated atomic motion from the atomic pair distribution function. *Phys. Rev. B Condens. Matter, 67*(10), 104301.
3. Marshak, S. (2009). *Essentials of Geology, 3rd or 4th Edition.*
4. Proctor, B.P., McAleer, R., Kunk, M.J., and Wintsch, R.P. (2013). Post-Taconic tilting and Acadian structural overprint of the classic Barrovian metamorphic gradient in Dutchess County, New York. *Am. J. Sci., 313*(7), 649–682.
5. Timeline of Art History (2007). *Reference Reviews, v. 21*(8), 45–45.

Figure References

Figure 6.1: Rock cycle showing the five materials (such as igneous rocks and sediment) and the processes by which one changes into another (such as weathering). Kindred Grey. 2022. CC BY 4.0.

Figure 6.2: Difference between pressure and stress and how they deform rocks. Peter Davis. 2017. CC BY-NC-SA 4.0. https://slcc.pressbooks.pub/introgeology/chapter/6-metamorphic-rocks

Figure 6.3: Pebbles (that used to be spherical or close to spherical) in quartzite deformed by directed stress. Peter Davis. 2017. CC BY-NC-SA 4.0. https://slcc.pressbooks.pub/introgeology/chapter/6-metamorphic-rocks

Figure 6.4: An igneous rock, granite (left), and foliated high-temperature and high-pressure metamorphic rock, gneiss (right), illustrating a metamorphic texture. Peter Davis. 2017. CC BY-NC-SA 4.0. https://slcc.pressbooks.pub/introgeology/chapter/6-metamorphic-rocks

Figure 6.5: Black smoker hydrothermal vent with a colony of giant (6'+) tube worms. National Oceanic and Atmospheric Administration (NOAA). 2006. Public domain. https://commons.wikimedia.org/wiki/File:Main_Endeavour_black_smoker.jpg

Table 6.1: Metamorphic rock identification table. Kindred Grey. 2022. Table data from Belinda Madsen's graphic in CH 6 of An Introduction to Geology. OpenStax. Salt Lake Community College. CC BY-NC-SA 4.0.

Figure 6.6: Example of lineation in which minerals are aligned like a stack of straws or pencils. Peter Davis. 2017. CC BY-NC-SA 4.0. https://slcc.pressbooks.pub/introgeology/chapter/6-metamorphic-rocks

Figure 6.7: An example of foliation WITH lineation. Peter Davis. 2017. CC BY-NC-SA 4.0. https://slcc.pressbooks.pub/introgeology/chapter/6-metamorphic-rocks

Figure 6.8: An example of foliation WITHOUT lineation. Peter Davis. 2017. CC BY-NC-SA 4.0. https://slcc.pressbooks.pub/introgeology/chapter/6-metamorphic-rocks

Figure 6.9: Rock breaking along flat even planes. Uta Baumfelder. 2010. Public domain. https://commons.wikimedia.org/wiki/File:Ehemaliger_Schiefertagebau_am_Brand.jpg

Figure 6.10: Foliation versus bedding. Peter Davis. 2017. CC BY-NC-SA 4.0. https://slcc.pressbooks.pub/introgeology/chapter/6-metamorphic-rocks

Figure 6.11: Phyllite with a small fold. Peter Davis. 2017. CC BY-NC-SA 4.0. https://slcc.pressbooks.pub/introgeology/chapter/6-metamorphic-rocks

Figure 6.12: Schist. Michael C. Rygel. 2012. CC BY-SA 3.0. https://commons.wikimedia.org/wiki/File:Schist_detail.jpg

Figure 6.13: Garnet staurolite muscovite schist. Peter Davis. 2017. CC BY-NC-SA 4.0. https://slcc.pressbooks.pub/introgeology/chapter/6-metamorphic-rocks

Figure 6.14: Gneiss. Laura Neser. September 2024. CC BY-NC.

Figure 6.15: Migmatite, a rock which was partially molten. Peter Davis. 2017. CC BY-NC-SA 4.0. https://slcc.pressbooks.pub/introgeology/chapter/6-metamorphic-rocks

Figure 6.16: Marble. Peter Davis. 2017. CC BY-NC-SA 4.0. https://slcc.pressbooks.pub/introgeology/chapter/6-metamorphic-rocks

Figure 6.17: Baraboo quartzite. Peter Davis. 2017. CC BY-NC-SA 4.0. https://slcc.pressbooks.pub/introgeology/chapter/6-metamorphic-rocks

Figure 6.18: Connemara marble, a variety of green marble from Connemara, Ireland. Laura Neser. September 2024. CC BY-NC.

Figure 6.19: Macro view of quartzite. Manishwiki15. 2012. CC BY-SA 3.0. https://commons.wikimedia.org/wiki/File:Sample_of_Quartzite.jpg

Figure 6.20: Garnet schist. Graeme Churchard (GOC53). 2005. CC BY 2.0. https://commons.wikimedia.org/wiki/File:Garnet_Mica_Schist_Syros_Greece.jpg

Figure 6.21: Pressure–temperature graphs of various metamorphic facies. Peter Davis. 2017. CC BY-NC-SA 4.0. https://slcc.pressbooks.pub/introgeology/chapter/6-metamorphic-rocks

Figure 6.22: Barrovian sequence in Scotland. Woudloper. 2009. CC BY-SA 3.0. https://commons.wikimedia.org/wiki/File:Scotland_metamorphic_zones_EN.svg

Figure 6.23: Contact metamorphism in outcrop. Random Tree. 2012. Public domain. https://commons.wikimedia.org/wiki/File:Metamorphic_Aureole_in_the_Henry_Mountains.jpg

Figure 6.24: Blueschist. Peter Davis. 2017. CC BY-NC-SA 4.0. https://slcc.pressbooks.pub/introgeology/chapter/6-metamorphic-rocks

Figure 6.25: Eclogite. Laura Neser. September 2024. CC BY-NC.

Figure 6.26: Mylonite. Peter Davis. 2017. CC BY-NC-SA 4.0. https://slcc.pressbooks.pub/introgeology/chapter/6-metamorphic-rocks

Figure 6.27: Examples of augens. Peter Davis. 2017. CC BY-NC-SA 4.0. https://slcc.pressbooks.pub/introgeology/chapter/6-metamorphic-rocks

Figure 6.28: Shock lamellae in a quartz grain. Glen A. Izett. 2000. Public domain. https://commons.wikimedia.org/wiki/File:820qtz.jpg

Figure 6.29: Meteor Crater is an impact crater that is 1.2 km across and about 180 m deep in the desert of Northern Arizona. Laura Neser. March 2022. CC BY-NC.

Figure 6.30: Shatter cone. JMGastonguay. 2014. CC BY-SA 4.0. https://commons.wikimedia.org/wiki/File:ShatterConeCharlevoix1.jpg

Figure 6.31: Tektites. Brocken Inaglory. 2007. CC BY-SA 3.0. https://en.wikipedia.org/wiki/File:Two_tektites.jpg

Figure Descriptions

Figure 6.1: The rock cycle (clockwise). Magma turns to Igneous rock through crystallization. Igneous rocks turn to sediment through weathering. Sediment turns to sedimentary rocks through transport and deposition and burial and lithification. Sedimentary rocks turn to metamorphic rocks through textural and or chemical damage. Metamorphic rocks turn to magma through melting. Igneous rocks turn to metamorphic rocks through textural and/or chemical damage. metamorphic and sedimentary rocks endure weathering by exhumation of rock back to Earth's surface.

Figure 6.2: Three 3-D diagrams: the top diagram is labeled Pressure and shows a cube with a single arrow pointing inward on each face, labeled S1, S2, and S3 which correlate with the Z-axis, Y-axis, and X-axis, respectively. The text next to this diagram says "Pressure is a state where all stresses on a body are equal. The magnitude of these balanced stresses increases with increasing depth within the earth. These stresses can not deform rocks other than to decrease their volume. Pressure is the term used because the concept of pressure is used in chemistry, which it the discipline of science used to understand the mineral reactions that occur within the rock." The lower two diagrams are labeled Directed Stresses with the accompanying text "One or more directions of stress are not equal in magnitude and or not in line with each other (non-coaxial). Unlike balanced stresses, the difference in these stresses can deform rocks within the earth." One

of these diagrams is labeled Pure Shear (co-axial) and shows a stretched cuboid with S1 arrows pointing downward toward the top face and upward toward the bottom face; the other diagram is labeled Simple Shear (non-co-axial) and shows a sheared cube with S1 shear force arrows parallel to the top and bottom faces pointed in opposite directions; for both of these diagrams, S1 is greater than S2 and S3, with S2 equaling S3.

Figure 6.3: Thinly layered rock with flattened parallel pebbles embedded throughout.

Figure 6.4: Two coarse-grained rock samples that both contain pink, white, and black minerals; one rock sample has random alignment of minerals while the other sample has dark minerals forming thin, black parallel lines with pink and white minerals elongated in the same direction.

Figure 6.5: A black smoker hydrothermal vent at the bottom of the sea floor. There is a plume of black smoke coming from a cone-shaped extrusion of rock and a colony of tube worms are attached to the cone-shaped rock.

Figure 6.6: Three images: on the left is a photo of a rock sample with elongated tan and black linear minerals visible along on the sides which are seen as dots where they terminate at the rock face perpendicular to the lines; in the middle is a schematic black and white drawing of the rock sample; and on the right is a photo of a bundle of plastic drinking straws that are held together with a rubber band wrapped around them.

Figure 6.7: Two images: on the left is a photo of a grayish tan rock sample with visible layering and elongated linear mineral alignment along the sides; on the face perpendicular to the lineations, layering is still visible but the lineations appear as dots; the right image shows a grayscale schematic drawing of the rock with arrows that label foliation, aligned tourmaline crystals on foliation, and alignment direction.

Figure 6.8: Three images: on the left are two photos of a rock sample, one viewed from the top and one viewed from the side; along the top, elongate black crystals have random orientation embedded within tan matrix but on the side, the black crystals have visible layering with the tan matrix; on the right is a schematic grayscale drawing of the rock sample with two arrows: one pointing to the top labeled "Foliated surface displays non-lineated hornblende grains" and another pointing to the side labeled "This surface displays a cross section of foliated plagioclase and hornblende."

Figure 6.9: Outcrop of tan to brown thinly layered rock.

Figure 6.10: Two images: on the left is a photo of a gray rock sample with visible thin layering that runs vertically through the sample and also a bedding plane that runs roughly left to right; the right image shows a grayscale schematic drawing of the rock with arrows that label the foliation direction and bedding direction.

Figure 6.11: Sample of tan rock with a slight sheen that has a small fold and thin layering; a US quarter rests on top of it for scale.

Figure 6.12: Sample of grayish-tan rock with a silky sheen that has thin layering; a scale bar rests on the sample that says 3 cm.

Figure 6.13: Two photos of similar rocks that have visible foliation: the rocks have a silvery sheen and sparse small glassy brown crystals throughout. Arrows labeled "Garnet staurolite muscovite schist" point to the small brown crystals.

Figure 6.14: Hand holding blocky chunk of rock that has distinct black and white parallel bands throughout.

Figure 6.15: Rock that has distinct black and white swirling bands; a person's finger points to the rock for scale.

Figure 6.16: Two chunks of rock, one pink in color and the other white in color; both have interlocking crystals; a US quarter rests on the pink sample for scale.

Figure 6.17: Chunk of pinkish tan rock with interlocking crystals; a US quarter rests on the sample for scale.

Figure 6.18: Six pieces of rock on a wooden shelf; all pieces contain shades of green with some being interfingered with white and black.

Figure 6.19: Zoomed-in view of a chunk of pinkish tan rock with interlocking glassy crystals.

Figure 6.20: Rock with a silvery sheen and large polygonal brown crystals scattered throughout; a Euro coin rests on the outcrop for scale.

Figure 6.21: Pressure increases upward on the vertical axis and temperature increases toward the right on the horizontal axis. High pressure with high temperature is associated with subduction metamorphism while low pressure and high temperature is associated with volcanic arc and continental metamorphism.

Figure 6.22: Map of Scotland with metamorphic zones highlighted; metamorphic grade increases toward the northwest, away from the Highland Boundary Fault in the southeast.

Figure 6.23: Outcrop of thick beds of flat-lying dull tan rock on top of pink rock with a chalky appearance.

Figure 6.24: Sample of dark blue rock with dark green bands throughout; silvery mica grains can also be seen sparsely throughout the sample; a US quarter rests on the sample for scale.

Figure 6.25: Chunk of rock consisting of a dark olive green matrix and brownish red garnet crystals embedded throughout.

Figure 6.26: Two images: on the left is a side view of a rock sample with thin parallel layers and rounded grains embedded in some places, around which the layers are slightly offset; a US quarter rests against the sample for scale; on the right is a grayscale drawing of the sample with arrows pointing in the direction of stress: the arrow above the sample points toward the left and the arrow below the sample points toward the right.

Figure 6.27: Cross sectional view of a rock sample that shows distinct thin layering of dark gray, brown, and black minerals; rounded white crystals that do not deform as easily form lens-shapes among the layers; an arrow above the sample points toward the left and an arrow below the sample points toward the right; a scale bar near the bottom of the sample says 1 cm.

Figure 6.28: A microscopic view of a grain that has visible thin lines forming a V-shape through the grain; it has a prismatic inside with a blue center, purple ring around the center, and yellow outer ring; outside of the ring the mineral is white.

Figure 6.29: A huge bowl-shaped crater ringed with brownish tan rocks, lightly dusted in snow. Three people can be seen standing on an overlook on the left side of the photo with their arms in the air.

Figure 6.30: Person holding a cone-shaped rock with lines running along the exterior that converge toward the point of the cone.

Figure 6.31: Two elongated dark brownish black shiny rocks, one resembling the shape of a dumbbell and the other resembling the shape of a teardrop.

7. GEOLOGIC TIME

Learning Objectives

By the end of this chapter, students should be able to:

- Explain the difference between relative time and numeric time.
- Describe the five principles of stratigraphy.
- Apply relative dating principles to a block diagram, and interpret the sequence of geologic events.
- Define an isotope, and explain alpha decay, beta decay, and electron capture as mechanisms of radioactive decay.
- Describe how radioisotopic dating is accomplished, and list the four key isotopes used.
- Explain how carbon-14 forms in the atmosphere and how it is used in dating recent events.
- Explain how scientists know the numeric age of the Earth and other events in Earth history.
- Explain how sedimentary sequences can be dated using radioisotopes and other techniques.
- Define a fossil, and describe types of fossils preservation.
- Outline how natural selection takes place as a mechanism of evolution.
- Describe stratigraphic correlation.
- List the eons, eras, and periods of the geologic timescale, and explain the purpose behind the divisions.
- Explain the relationship between time units and corresponding rock units—chronostratigraphy versus lithostratigraphy.

The geologic timescale and basic outline of Earth's history were worked out long before we had any scientific means of assigning numerical age units, like years, to events in that history. Working out Earth's history depended on realizing some key principles of relative time. Nicolas Steno (1638–1686) introduced basic principles of stratigraphy, the study of layered rocks, in 1669. William Smith (1769–1839), working with the strata of English coal mines, noticed that strata and their sequences were consistent throughout the region. Eventually he produced the first national geologic map of Britain, becoming known as "the Father of English Geology." Nineteenth-century scientists developed a relative timescale using Steno's principles, with names derived from the characteristics of the rocks in those areas. The figure of this geologic timescale shows the names of the units and subunits. Using this scale, geologists can place all events of Earth history in order without ever knowing their numerical ages. The specific events within Earth history are discussed in Chapter 8.

Figure 7.1: Nicolas Steno, ca. 1670. Figure description available at the end of the chapter.

7.1 Relative Dating

Relative dating is the process of determining if one rock or geologic event is older or younger than another without knowing their specific ages—i.e., how many years ago the object was formed. The principles of relative time are simple, even obvious now, but were not generally accepted by scholars until the Scientific Revolution of the seventeenth and eighteenth centuries. James Hutton (see Chapter 1) realized geologic processes are slow, and his ideas on uniformitarianism (i.e., "the present is the key to the past") provided a basis for interpreting rocks of the Earth using scientific principles.

EON	ERA	PERIOD	MILLIONS OF YEARS AGO
Phanerozoic	Cenozoic	Quaternary	1.6
		Tertiary	66
	Mesozoic	Cretaceous	138
		Jurassic	205
		Triassic	240
	Paleozoic	Permian	290
		Pennsylvanian	330
		Mississippian	360
		Devonian	410
		Silurian	435
		Ordovician	500
		Cambrian	570
Proterozoic	Late Proterozoic Middle Proterozoic Early Proterozoic		2500
Archean	Late Archean Middle Archean Early Archean		3800?
Pre-Archean			

Figure 7.2: Geologic timescale. Figure description available at the end of the chapter.

7.1.1 Relative Dating Principles

Stratigraphy is the study of layered sedimentary rocks. This section discusses principles of relative time used in all of geology, though they are especially useful in stratigraphy.

Principle of superposition: In an otherwise undisturbed sequence of sedimentary strata, or rock layers, the layers on the bottom are the oldest and layers above them are younger.

Principle of original horizontality: Layers of rocks deposited from above, such as sediments and lava flows, are originally laid down horizontally. The exception to this principle is seen at the margins of basins, where the strata can slope slightly downward into the basin.

Figure 7.3: Lower strata are older than those on top of them. Figure description available at the end of the chapter.

Figure 7.4: Lateral continuity. Figure description available at the end of the chapter.

Principle of lateral continuity: Within the depositional basin, strata are continuous in all directions until they thin out at the edge of that basin. Of course, all strata eventually end, either by hitting a geographic barrier, such as a ridge, or when the depositional process extends too far from its source, either a sediment source or a volcano. Strata that are cut by a canyon remain continuous on either side of the canyon.

Figure 7.5: Dark dike cutting across older rocks, the lighter of which is younger than the grey rock. Figure description available at the end of the chapter.

Principle of cross-cutting relationships: Deformation events like folds, faults, and igneous intrusions that cut across rocks are younger than the rocks they cut across.

Principle of inclusions: When one rock formation contains pieces or **inclusions** of another rock, the included rock is older than the host rock.

Principle of fossil succession: Evolution has produced a succession of unique fossils that correlate to the units of the geologic timescale. Assemblages of fossils contained in strata are unique to the time they lived, and they can be used to correlate rocks of the same age across a wide geographic distribution. Assemblages of fossils are groups of several unique fossils occurring together.

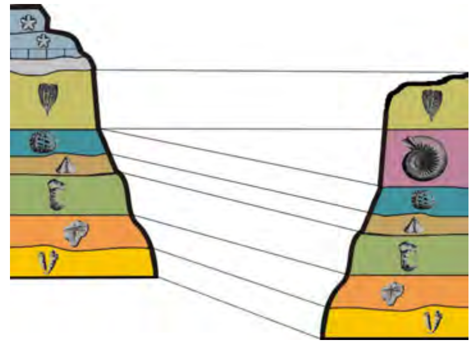

Figure 7.6: Fossil succession showing correlation among strata. Figure description available at the end of the chapter.

7.1.2 Grand Canyon Example

Figure 7.7: The Grand Canyon of Arizona. Figure description available at the end of the chapter.

The Grand Canyon of Arizona illustrates the stratigraphic principles. Figure 7.7 shows layers of rock on top of one another in order from the oldest at the bottom to the youngest at the top, based on the principle of superposition. The predominant white layer just below the canyon rim is the Coconino Sandstone. This layer is laterally continuous, even though the intervening canyon separates its outcrops. The rock layers exhibit the principle of lateral continuity, as they are found on both sides of the Grand Canyon carved by the Colorado River.

Figure 7.8 shows a cross section of the rocks exposed on the walls of the Grand Canyon, illustrating the principle of cross-cutting relationships, superposition, and original horizontality. In the lowest parts of the Grand Canyon are the oldest sedimentary formations, with igneous and metamorphic rocks at the bottom. The principle of cross-cutting relationships shows the sequence of these events. The metamorphic schist (#16) is the oldest rock formation, and the cross-cutting granite intrusion (#17) is younger. As seen in the figure, the other layers on the walls of the Grand Canyon are numbered in reverse order, with #15 being the oldest and #1 the youngest. This illustrates the principle of superposition. The Grand Canyon region lies in the Colorado Plateau, which is characterized by horizontal or nearly horizontal strata that follow the principle of original horizontality. These rock strata have been barely disturbed from their original deposition, except by a broad regional uplift.

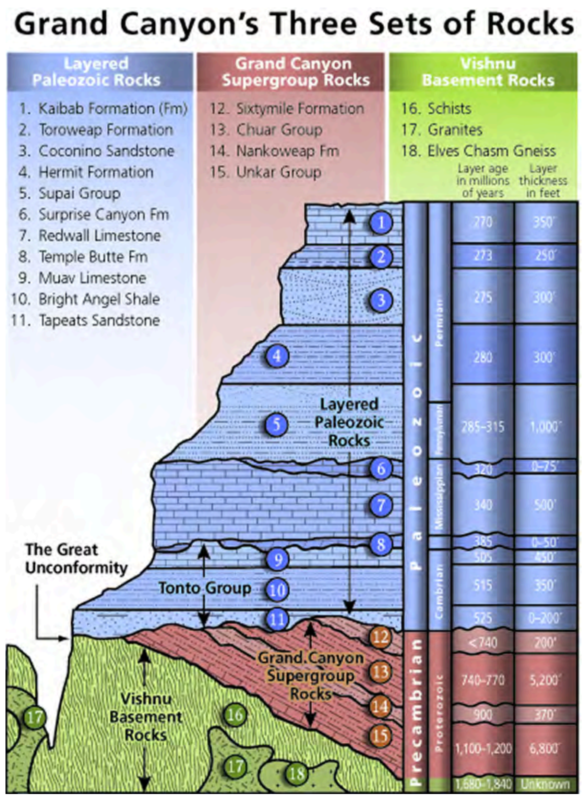

Figure 7.8: The rocks of the Grand Canyon. Figure description available at the end of the chapter.

The photo of the Grand Canyon here shows strata that were originally deposited in a flat layer on top of older igneous and metamorphic "basement" rocks, per the original horizontality principle. Because the formation of the basement rocks and the deposition of the overlying strata is not continuous—instead broken by events of metamorphism, intrusion, and erosion—the contact between the strata and the older basement is termed an unconformity. An **unconformity** represents a period during which deposition did not occur or erosion removed rock that had been deposited, resulting in the absence of rocks that represent events of Earth history during that span of time at that place. Unconformities appear in cross sections and stratigraphic columns as wavy lines between formations.

Figure 7.9: The red, layered rocks of the Grand Canyon Supergroup overlying the dark-colored rocks of the Vishnu schist represents a type of unconformity called a nonconformity. Figure description available at the end of the chapter.

7.1.3 Unconformities

Figure 7.10: All three of these formations have a disconformity at the two contacts between them. The pinching Temple Butte is the easiest to see the erosion, but even between the Muav and Redwall, there is an unconfomity. Figure description available at the end of the chapter.

There are three types of unconformities: nonconformity, disconformity, and angular unconformity. A **nonconformity** occurs when sedimentary rock is deposited on top of igneous and metamorphic rocks, as is the case with the contact between the strata and basement rocks at the bottom of the Grand Canyon.

The strata in the Grand Canyon represent alternating marine transgressions and regressions during which sea level rose and fell over millions of years. When the sea level was high, marine strata formed. When sea level fell, the land was exposed to erosion, creating an unconformity. In the Grand Canyon cross section, this erosion is shown as heavy wavy lines between the various numbered strata. This is a type of unconformity called a **disconformity**, where either nondeposition or erosion took place. In other words, layers of rock that could have been present are absent. The time that could have been represented by such layers is instead represented by the disconformity.

The Phanerozoic strata in most of the Grand Canyon are horizontal. However, near the bottom, horizontal strata overlie tilted strata. This is known as the Great Unconformity and is an example of an angular unconformity. The lower strata were tilted by tectonic processes that disturbed their original horizontality and caused the strata to be eroded. Later, horizontal strata were deposited on top of the tilted strata, creating the angular unconformity.

Figure 7.11: In the lower part of the picture is an angular unconformity in the Grand Canyon known as the Great Unconformity. Note flat-lying strata over dipping strata. Figure description available at the end of the chapter.

Here are graphical illustrations of the three types of unconformity.

Disconformity involves a break or stratigraphic absence between strata in an otherwise parallel sequence of strata.

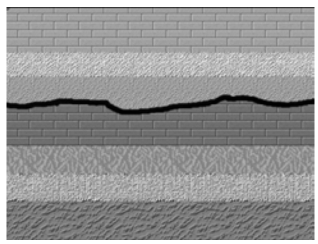

Figure 7.12: Disconformity. Figure description available at the end of the chapter.

Nonconformity involves sedimentary strata deposited on crystalline (igneous or metamorphic) rocks.

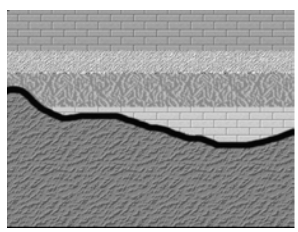

Figure 7.13: Nonconformity (the lower rocks are igneous or metamorphic). Figure description available at the end of the chapter.

Angular unconformity involves sedimentary strata deposited on a terrain developed on sedimentary strata that have been deformed by tilting, folding, and/or faulting that makes them no longer horizontal.

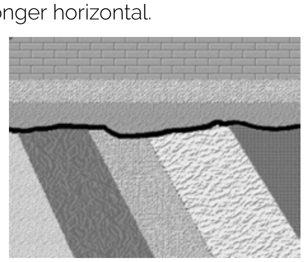

Figure 7.14: Angular unconformity. Figure description available at the end of the chapter.

7.1.3 Applying Relative Dating Principles

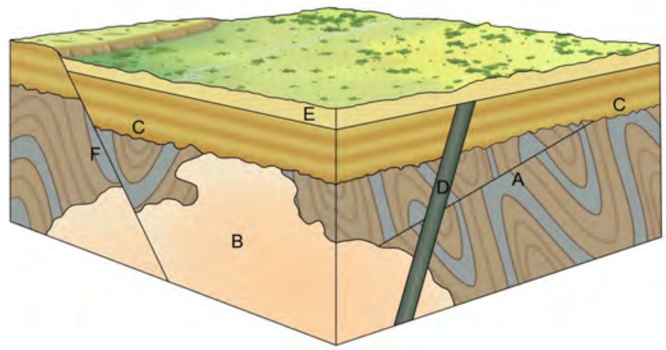

Figure 7.15: Block diagram to apply relative dating principles. The wavy rock is an old metamorphic gneiss, A and F are faults, B is an igneous granite, D is a basaltic dike, and C and E are sedimentary strata. Figure description available at the end of the chapter.

In the block diagram, the sequence of geological events can be determined by using the relative-dating principles and known properties of igneous, sedimentary, and metamorphic rock (see Chapter 4, Chapter 5, and Chapter 6). The sequence begins with the folded metamorphic gneiss on the bottom. Next, the gneiss is cut and displaced by the fault labeled A. Both the gneiss and fault A are cut by the igneous granitic intrusion called batholith B; its irregular outline suggests it is an igneous granitic intrusion emplaced as magma into the gneiss. Since batholith B cuts both the gneiss and fault A, batholith B is younger than the other two rock formations. Next, the gneiss, fault A, and batholith B were eroded, forming a nonconformity shown with the wavy line. This unconformity was actually an ancient landscape surface on which sedimentary rock C was subsequently deposited, perhaps by a marine transgression. Next, igneous basaltic dike D cuts through all rocks except sedimentary rock E. This shows that there is a disconformity between sedimentary rocks C and E. The top of dike D is level with the top of layer C, which establishes that erosion flattened the landscape prior to the deposition of layer E, creating a disconformity between rocks D and E. Fault F cuts across all of the older rocks B, C and E, producing a **fault scarp**, which is the low ridge on the upper-left side of the diagram. The final events affecting this area are current erosion processes working on the land surface, rounding off the edge of the fault scarp and producing the modern landscape at the top of the diagram.

Take this quiz to check your comprehension of this section.

Access the quiz for Section 7.1 by scanning the QR code.

7.2 Absolute Dating

Figure 7.16: Canada's Nuvvuagittuq Greenstone Belt may have the oldest rocks and oldest evidence of life on Earth, according to recent studies. Figure description available at the end of the chapter.

Relative time allows scientists to tell the story of Earth events but does not provide specific numeric ages and thus does not show the rate at which geologic processes operate. Based on Hutton's principle of uniformitarianism (see Chapter 1), early geologists surmised geological processes work slowly and the Earth is very old. Scientists interpreted Earth history through relative dating principles until the end of the nineteenth century. Because science advances as technology advances, the discovery of radioactivity in the late 1800s provided scientists with a new scientific tool called radioisotopic dating. Using this new technology, they could assign specific time units, in this case years, to mineral grains within a rock. These numerical values are not dependent on comparisons with other rocks, such as with relative dating, so this dating method is called **absolute dating**. There are several types of absolute dating discussed in this section, but radioisotopic dating is the most common and therefore is the focus on this section.

7.2.1 Radioactive Decay

All elements on the periodic table of elements (see Chapter 3) contain isotopes. An isotope is an atom of an element with a different number of neutrons. For example, hydrogen (H) always has one proton in its nucleus (the atomic number), but the number of neutrons can vary among the isotopes (0, 1, 2). Recall that the number of neutrons added to the atomic number gives the atomic mass. When hydrogen has one proton and zero neutrons, it is sometimes called protium (^{1}H), when hydrogen has one proton and one neutron, it is called deuterium (^{2}H), and when hydrogen has one proton and two neutrons, it is called tritium (^{3}H).

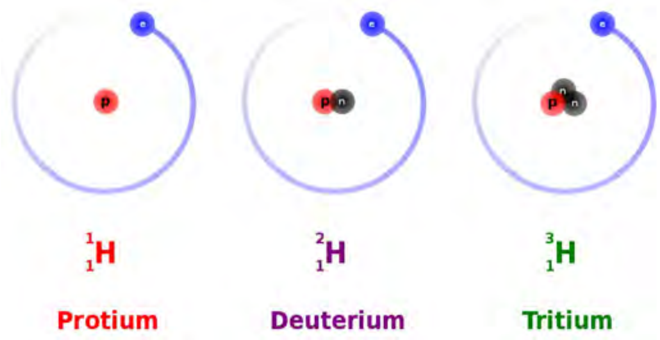

Figure 7.17: Three isotopes of hydrogen. Figure description available at the end of the chapter.

Many elements have both stable and unstable isotopes. For the hydrogen example, ^{1}H and ^{2}H are stable, but ^{3}H is unstable. Unstable isotopes, called **radioactive** isotopes, spontaneously decay over time, releasing subatomic particles or energy in a process called radioactive decay. When this occurs, an unstable isotope becomes a more stable isotope of another element. For example, carbon-14 (^{14}C) decays to nitrogen-14 (^{14}N).

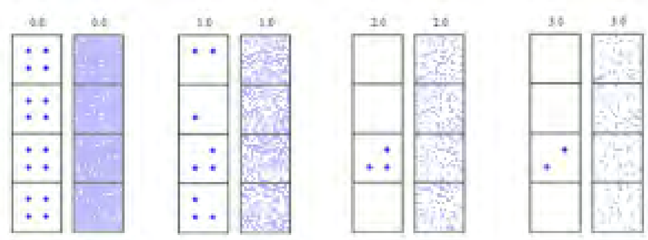

Figure 7.18: Simulation of half-life. On the left, four simulations with only a few atoms. On the right, four simulations with many atoms. Figure description available at the end of the chapter.

The radioactive decay of any individual atom is a completely unpredictable and random event. However, some rock specimens have enormous numbers of radioactive isotopes, perhaps trillions of atoms, and this large group of radioactive isotopes does have a predictable pattern of radioactive decay. The radioactive decay of *half* of the radioactive isotopes in this group takes a specific amount of time. The time it takes for half of the atoms in a substance to decay is called the **half-life**. In other words, the half-life of an isotope is the amount of time it takes for half of a group of unstable isotopes to decay to a stable isotope. The half-life is constant and measurable for a given radioactive isotope, so it can be used to calculate the age of a rock. For example, the half-life uranium-238 (^{238}U) is 4.5 billion years, and the half-life of ^{14}C is 5,730 years.

The principles behind this dating method require two key assumptions. First, the mineral grains containing the isotope formed at the same time as the rock, such as minerals in an igneous rock that crystallized from magma. Second, the mineral crystals remain a closed system, meaning they are not subsequently altered by elements moving in or out of them.

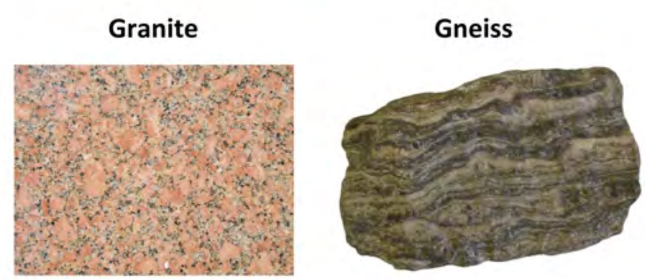

Figure 7.19: Granite (left) and gneiss (right). Dating a mineral within the granite would give the crystallization age of the rock, while dating the gneiss might reflect the timing of metamorphism. Figure description available at the end of the chapter.

These requirements place some constraints on the kinds of rock suitable for dating, with igneous rock being the best. Metamorphic rocks are crystalline, but the processes of metamorphism may reset the clock, and derived ages may represent a smear of different metamorphic events rather than the age of original crystallization. Detrital sedimentary rocks contain clasts from separate parent rocks from unknown locations and derived ages are thus meaningless. However, sedimentary rocks with precipitated minerals, such as evaporites, may contain elements suitable for radioisotopic dating. Igneous pyroclastic layers and lava flows within a sedimentary sequence can be used to date the sequence. Cross-cutting igneous rocks and sills can be used to bracket the ages of affected older sedimentary rocks. The resistant mineral zircon, found as clasts in many ancient sedimentary rocks, has been successfully used for establishing very old dates, including the age of Earth's oldest known rocks. Knowing that zircon minerals in metamorphosed sediments came from older rocks that are no longer available for study, scientists can date zircon to establish the age of the pre-metamorphic source rocks.

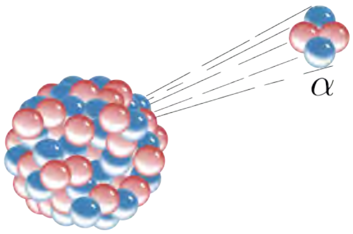

Figure 7.20: Alpha decay in which two protons and two neutrons leave the nucleus. Figure description available at the end of the chapter.

There are several ways radioactive atoms decay. We will consider three of them here—alpha decay, beta decay, and electron capture. **Alpha decay** is when an alpha particle, which consists of two protons and two neutrons, is emitted from the nucleus of an atom. This also happens to be the nucleus of a helium atom; helium gas may get trapped in the crystal lattice of a mineral in which alpha decay has taken place. When an atom loses two protons from its nucleus, lowering its atomic number, it is transformed into an element that is two atomic numbers lower on the periodic table of the elements.

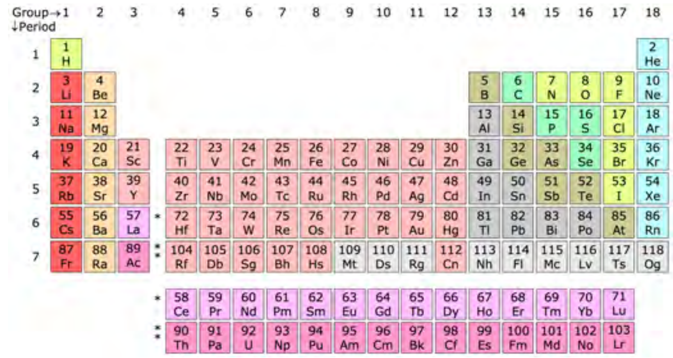

Figure 7.21: Periodic table of the elements. Figure description available at the end of the chapter.

The loss of four particles, in this case two neutrons and two protons, also lowers the mass of the atom by four. For example alpha decay takes place in the unstable isotope ^{238}U, which has an atomic number of 92 (92 protons) and mass number of 238 (total of all protons and neutrons). When ^{238}U spontaneously emits an alpha particle, it becomes thorium-234 (^{234}Th). The radioactive decay product of an element is called its **daughter isotope**, and the original element is called the **parent isotope**. In this case, ^{238}U is the parent isotope and ^{234}Th is the daughter isotope. The half-life of ^{238}U is 4.5 billion years, i.e., the time it takes for half of the parent isotope atoms to decay into the daughter isotope. This isotope of uranium, ^{238}U, can be used for absolute dating the oldest materials found on Earth and even meteorites and materials from the earliest events in our Solar System.

Beta Decay

Beta decay is when a neutron in its nucleus splits into an electron and a proton. The electron is emitted from the nucleus as a beta ray. The new proton increases the element's atomic number by one, forming a new element with the same atomic mass as the parent isotope. For example, ^{234}Th is unstable and undergoes beta decay to form protactinium-234 (^{234}Pa), which also undergoes beta decay to form uranium-234 (^{234}U). Notice these are all isotopes of different elements, but they have the same atomic mass of 234. The decay process of radioactive elements like uranium keeps producing radioactive parents and daughters until a stable, or nonradioactive, daughter is formed. Such a series is called a **decay chain**. The decay chain of the radioactive parent isotope ^{238}U progresses through a series of alpha (red arrows on the adjacent figure) and beta decays (blue arrows), until it forms the stable daughter isotope, lead-206 (^{206}Pb).

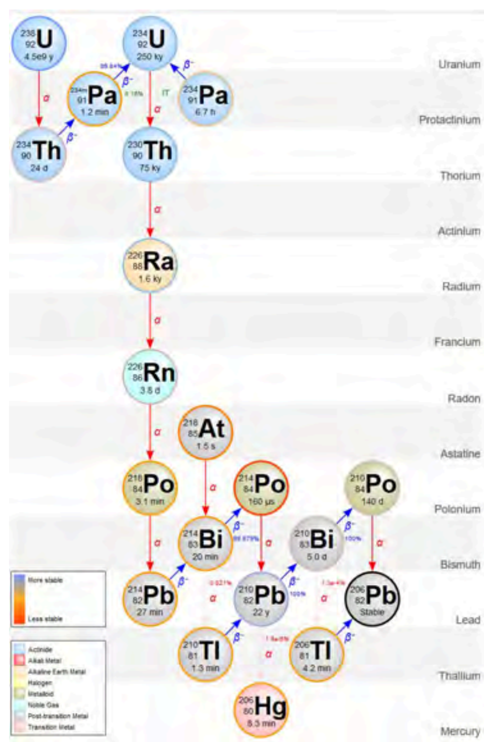

Figure 7.22: Decay chain of U-238 to stable Pb-206 through a series of alpha and beta decays. Figure description available at the end of the chapter.

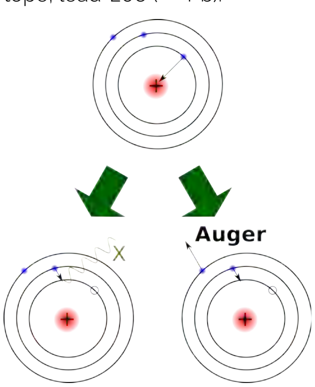

Figure 7.23: The two paths of electron capture. Figure description available at the end of the chapter.

Electron capture is when a proton in the nucleus captures an electron from one of the electron shells and becomes a neutron. This produces one of two different effects: an electron jumps in to fill the missing spot of the departed electron and emits an X-ray, or in what is called the Auger process, another electron is released and changes the atom into an ion. The atomic number is reduced by one, and mass number remains the same. An example of an element that decays by electron capture is potassium-40 (^{40}K). Radioactive ^{40}K makes up a tiny percentage (0.012%) of naturally occurring potassium, most of which is not radioactive. ^{40}K decays to argon-40 (^{40}Ar) with a half-life of 1.25 billion years, so it is very useful for dating geological events. Below is a table of some of the more commonly used radioactive dating isotopes and their half-lives.

Elements	Parent symbol	Daughter symbol	Half-life
Uranium-238/Lead-206	^{238}U	^{206}Pb	4.5 billion years
Uranium-235/Lead-207	^{235}U	^{207}Pb	704 million years
Potassium-40/Argon-40	^{40}K	^{40}Ar	1.25 billion years
Rubidium-87/Strontium-87	^{87}Rb	^{87}Sr	48.8 billion years
Carbon-14/Nitrogen-14	^{14}C	^{14}N	5,730 years

Table 7.1: Some common isotopes used for radioisotopic dating.

7.2.2 Radioisotopic Dating

For a given a sample of rock, how is the dating procedure carried out? The parent and daughter isotopes are separated out of the mineral using chemical extraction. In the case of uranium, ^{238}U and ^{235}U isotopes are separated out together, as are the ^{206}Pb and ^{207}Pb with an instrument called a **mass spectrometer**.

Figure 7.24: Mass spectrometer instrument. Figure description available at the end of the chapter.

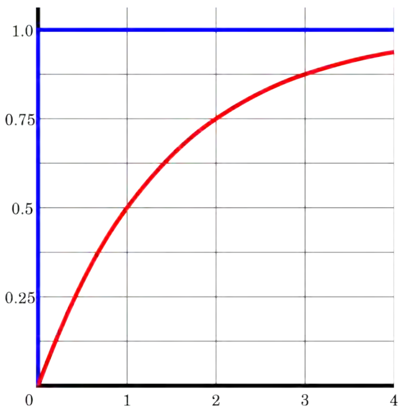

Figure 7.25: Graph of the amount of half-life versus the amount of daughter isotope. Figure description available at the end of the chapter.

Here is a simple example of age calculation using the daughter-to-parent ratio of isotopes. When the mineral initially forms, it consists of 0% daughter and 100% parent isotope, so the daughter-to-parent ratio (D/P) is 0. After one half-life, half the parent has decayed, so there is 50% daughter and 50% parent, a 50/50 ratio, with D/P = 1. After two half-lives, there is 75% daughter and 25% parent, a 75/25 ratio, with D/P = 3. This can be further calculated for a series of half-lives as shown in the table. The table does not show more than ten half-lives because after about ten half-lives, the amount of remaining parent is so small it becomes too difficult to accurately measure via chemical analysis. Modern applications of this method have achieved remarkable accuracies of plus or minus two million years in 2.5 billion years (that's ±0.055%). Applying the uranium/lead technique in any given sample analysis provides two separate clocks running at the same time, ^{238}U and ^{235}U. The existence of these two clocks in the same sample creates a cross-check between the two. Many geological samples contain multiple parent/daughter pairs, so cross-checking the clocks confirms that radioisotopic dating is highly reliable.

Half lives (#)	Parent present (%)	Daughter present (%)	Daughter/parent ratio	Parent/daughter ratio
Start the clock	100	0	0	Infinite
1	50	50	1	1
2	25	75	3	0.33
3	12.5	87.5	7	0.143
4	6.25	93.75	15	0.0667
5	3.125	96.875	31	0.0325
10	0.098	99.9	1023	0.00098

Table 7.2: Ratio of parent to daughter in terms of half-life.

Another radioisotopic dating method involves carbon and is useful for dating archaeologically important samples containing organic substances like wood or bone. Radiocarbon dating, also called carbon dating, uses the unstable isotope carbon-14 (^{14}C) and the stable isotope carbon-12 (^{12}C). Carbon-14 is constantly being created in the atmosphere through the interaction of cosmic particles with atmospheric nitrogen-14 (^{14}N). Cosmic particles such as neutrons strike the nitrogen nucleus, kicking out a proton but leaving the neutron in the nucleus. The collision reduces the atomic number by one, changing it from seven to six, changing the nitrogen into carbon with the same mass number of 14. The ^{14}C quickly bonds with oxygen (O) in the atmosphere to form carbon dioxide ($^{14}CO_2$) that mixes with other atmospheric carbon dioxide ($^{12}CO_2$); this mix of gases is incorporated into living matter. While an organism is alive, the ratio of $^{14}C/^{12}C$ in its body doesn't really change since CO_2 is constantly exchanged with the atmosphere. However, when it dies, the radiocarbon clock starts ticking as the ^{14}C decays back to ^{14}N by beta decay, which has a half-life of 5,730 years. The radiocarbon dating technique is thus useful for 57,300 years or so, about ten half-lives back.

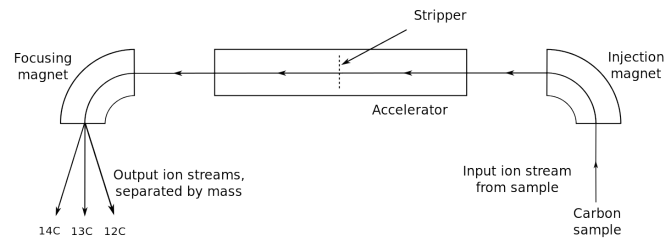

Figure 7.26: Schematic of carbon going through a mass spectrometer. Figure description available at the end of the chapter.

Radiocarbon dating relies on daughter-to-parent ratios derived from a known quantity of parent ^{14}C. Early applications of carbon dating assumed the production and concentration of ^{14}C in the atmosphere remained fairly constant for the last 50,000 years. However, it is now known that the amount of parent ^{14}C levels in the atmosphere has varied. Comparisons of carbon ages with tree-ring data and other data for known events have allowed reliable calibration of the radiocarbon dating method. Considering that carbon-14's baseline levels can be calibrated against other reliable dating methods, carbon dating has been shown to be a reliable method for dating archaeological specimens and very recent geologic events.

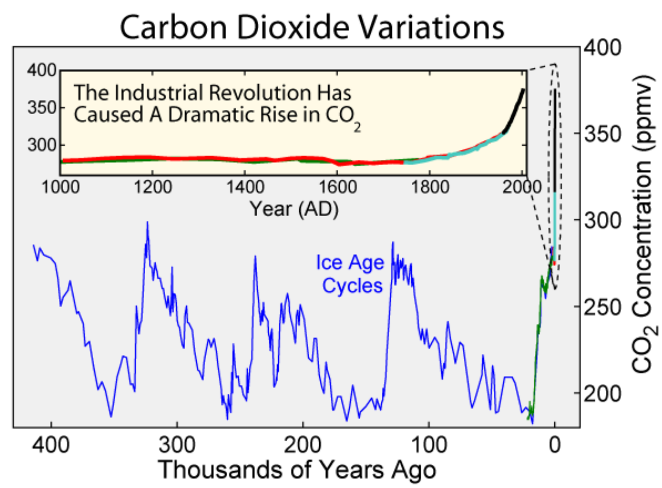

Figure 7.27: Carbon dioxide concentrations over the last 400,000 years. Figure description available at the end of the chapter.

7.2.3 Age of the Earth

Figure 7.28: Artist's impression of the Earth in the Hadean. Figure description available at the end of the chapter.

The work of Hutton and other scientists gained attention after the Renaissance (see Chapter 1), spurring exploration into the idea of an ancient Earth. In the late nineteenth century, William Thompson, a.k.a. Lord Kelvin, applied his knowledge of physics to develop the assumption that the Earth started as a hot molten sphere. He estimated the Earth is 98 million years old, but because of uncertainties in his calculations, stated the age as a range of between 20 and 400 million years. This animation illustrates how Kelvin calculated this range and why his numbers were so far off, which has to do with unequal heat transfer within the Earth. It has also been pointed out that Kelvin failed to consider pliability and convection in the Earth's mantle as a heat-transfer mechanism. Kelvin's estimate for Earth's age was considered plausible but not without challenge, and the discovery of radioactivity provided a more accurate method for determining ancient ages.

In the 1950s, Clair Patterson (1922–1995) thought he could determine the age of the Earth using radioactive isotopes frommeteorites, which he considered to be early Solar System remnants that were present at the time Earth was forming. Patterson analyzed meteorite samples for uranium and lead using a mass spectrometer. He used the uranium/lead dating technique in determining the age of the Earth to be 4.55 billion years, give or take about 70 million (± 1.5%). The current estimate for the age of the Earth is 4.54 billion years, give or take 50 million (± 1.1%). It is remarkable that Patterson, who was still a graduate student at the University of Chicago, came up with a result that has barely changed in over 60 years, even as technology has improved dating methods.

7.2.4 Dating Geological Events

Radioactive isotopes of elements that are common in mineral crystals are useful for radioisotopic dating. The uranium/lead method, with its two cross-checking clocks, is most often used with crystals of the mineral zircon ($ZrSiO_4$) where uranium can substitute for zirconium in the crystal lattice. Zircon is resistant to weathering, which makes it useful for dating geological events in ancient rocks. During metamorphic events, zircon crystals may form multiple crystal layers, with each layer recording the isotopic age of an event, thus tracing the progress of the several metamorphic events.

Figure 7.29: Photomicrograph of zircon crystal. Figure description available at the end of the chapter.

Geologists have used zircon grains in some amazing studies that illustrate how scientific conclusions can change with technological advancements. Zircon crystals from Western Australia that formed when the crust first differentiated from the mantle 4.4 billion years ago have been determined to be the oldest known rocks. The zircon grains were incorporated into metasedimentary host rocks, which are sedimentary rocks showing signs of having undergone partial metamorphism. The host rocks were not very old, but the embedded zircon grains were created 4.4 billion years ago and survived the subsequent processes of weathering, erosion, deposition, and metamorphism. From other properties of the zircon crystals, researchers concluded not only that continental rocks were exposed above sea level but also that conditions on the early Earth were cool enough for liquid water to exist on the surface. The presence of liquid water allowed the processes of weathering and erosion to take place. Researchers at UCLA studied 4.1-billion-year-old zircon crystals and found carbon in the zircon crystals that may be biogenic in origin, meaning that life may have existed on Earth much earlier than previously thought.

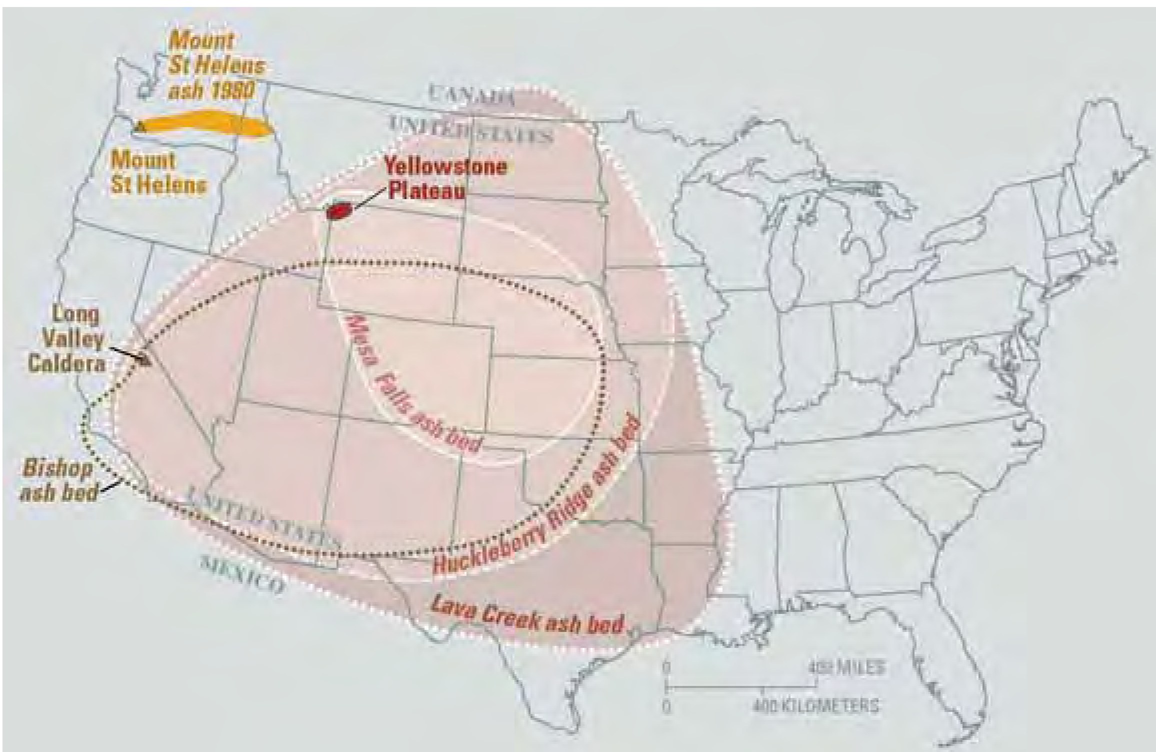

Figure 7.30: Several prominent ash beds found in North America, including three Yellowstone eruptions shaded pink (Mesa Falls, Huckleberry Ridge, and Lava Creek), the Bisho Tuff ash bed (brown dashed line), and the modern May 18th, 1980, ash fall (yellow). Figure description available at the end of the chapter.

Igneous rocks are best suited for radioisotopic dating because their primary minerals provide dates of crystallization from magma. Metamorphic processes tend to reset the clocks and smear the igneous rock's original date. Detrital sedimentary rocks are less useful because they are made of minerals derived from multiple parent sources with many potential dates. However, scientists can use igneous events to date sedimentary sequences. For example, if sedimentary strata are between a lava flow and volcanic ash bed with radioisotopic dates of 54 million years and 50 million years, then geologists know the sedimentary strata and the fossils formed between 54 and 50 million years ago. Another example would be a 65-million-year-old volcanic dike that cut across sedimentary strata. This provides an upper-limit age on the sedimentary strata, so this strata would be older than 65 million years. Potassium is common in evaporite sediments and has been used for potassium/argon dating. Primary sedimentary minerals containing radioactive isotopes like ^{40}K have provided dates for important geologic events.

7.2.5 Other Absolute Dating Techniques

Luminescence (a.k.a. thermoluminescence): Radioisotopic dating is not the only way scientists determine numeric ages. Luminescence dating measures the time elapsed since some silicate minerals, such as coarse sediments of silicate minerals, were last exposed to light or heat at the surface of Earth. All buried sediments are exposed to radiation from normal background radiation from the decay process described above. Some of these electrons get trapped in the crystal lattice of silicate minerals like quartz. When exposed at the surface, ultraviolet radiation and heat from the Sun releases these electrons, but when the minerals are buried just a few inches below the surface, the electrons get trapped again. Samples of coarse sediments collected just a few feet below the surface are analyzed by stimulating them with light in a lab. This stimulation releases the trapped electrons as a photon of light in a process called luminescence. The amount luminescence released indicates how long the sediment has been buried. Luminescence dating is only useful for dating young sediments that are less than one million years old. In Utah, luminescence dating is used to determine when coarse-grained sediment layers were buried near a fault. This is one technique used to determine the recurrence interval of large earthquakes on faults like the Wasatch fault that primarily cut coarse-grained material and lack buried organic soils for radiocarbon dating.

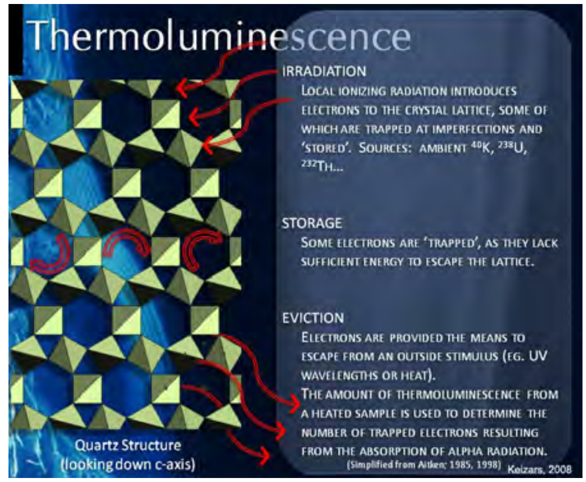

Figure 7.31: Thermoluminescence, a type of luminescence dating. Figure description available at the end of the chapter.

Fission Track: Fission track dating relies on damage to the crystal lattice produced when unstable ^{238}U decays to the daughter product ^{234}Th and releases an alpha particle. These two decay products move in opposite directions from each other through the crystal lattice, leaving a visible track of damage. This is common in uranium-bearing mineral grains such as apatite. The tracks are large and can be visually counted under an optical microscope. The number of tracks correspond to the age of the grains. Fission track dating works from about 100,000 to two billion (1×10^5 to 2×10^9) years ago. Fission track dating has also been used as a second clock to confirm dates obtained by other methods.

Figure 7.32: Apatite from Mexico. Figure description available at the end of the chapter.

Take this quiz to check your comprehension of this section.

Access the quiz for Section 7.2 by scanning the QR code.

7.3 Fossils and Evolution

Fossils are any evidence of past life preserved in rocks. They may be actual remains of body parts (rare), impressions of soft body parts, **casts** and **molds** of body parts (more common), body parts replaced by mineral (common), or evidence of animal behavior such as footprints and burrows. The body parts of living organisms range from the hard bones and shells of animals, soft cellulose of plants, soft bodies of jellyfish, down to single cells of bacteria and algae. Which body parts can be preserved? The vast majority of life today consists soft-bodied and/or single-celled organisms, and these are not likely be preserved in the geologic record except under unusual conditions. The best environment for preservation is the ocean, yet marine processes can dissolve hard parts and scavenging can reduce or eliminate remains. Thus, even under ideal conditions in the ocean, the likelihood of preservation is quite limited. For terrestrial life, the possibility of remains being buried and preserved is even more limited. In other words, the fossil record is incomplete and records only a small percentage of life that existed. Although incomplete, fossil records are used for stratigraphic correlation using the **principle of faunal succession** and provide a method used for establishing the age of a formation on the geologic timescale.

Figure 7.33: Archaeopteryx lithographica specimen displayed at the Museum für Naturkunde in Berlin. Figure description available at the end of the chapter.

7.3.1 Types of Preservation

Figure 7.34: The trilobite had a hard exoskeleton and is an early arthropod, the same group that includes modern insects, crustaceans, and arachnids. Figure description available at the end of the chapter.

Remnants or impressions of hard parts, such as a marine clam shell or dinosaur bone, are the most common types of fossils. The original material has almost always been replaced with new minerals that preserve much of the shape of the original shell, bone, or cell. The common types of fossil preservation are actual preservation, permineralization, molds and casts, carbonization, and trace fossils.

Actual preservation is a rare form of fossilization where the original materials or hard parts of the organism are preserved. Preservation of soft-tissue is very rare since these organic materials easily disappear through bacterial decay. Examples of actual preservation are unaltered biological materials like insects in amber or original minerals like mother-of-pearl on the interior of a shell. Another example is mammoth skin and hair preserved in post-glacial deposits in the Arctic regions. Rare mummification has left fragments of soft tissue, skin, and sometimes even blood vessels of dinosaurs, from which proteins have been isolated and evidence for DNA fragments have been discovered.

Figure 7.35: Mosquito preserved in amber. Figure description available at the end of the chapter.

Permineralization occurs when an organism is buried and then elements in groundwater completely impregnate all spaces within the body, even its cells. Soft body structures can be preserved in great detail, but stronger materials like bone and teeth are the most likely to be preserved. Petrified wood is an example of detailed cellulose structures in the wood being preserved. The University of California Berkeley website has more information on permineralization.

Figure 7.36: Permineralization in petrified wood at Petrified Forest National Park. Figure description available at the end of the chapter.

Molds and casts form when the original material of the organism dissolves and leaves a cavity in the surrounding rock. The shape of this cavity is an external mold. If the mold is subsequently filled with sediments or a mineral precipitate, the organism's external shape is preserved as a **cast**. Sometimes internal cavities of organisms, such internal casts of clams, snails, and even skulls, are preserved as internal casts that show details of soft structures. If the chemistry is right and burial is rapid, mineral nodules form around soft structures, preserving the three-dimensional detail. This is called **authigenic mineralization**.

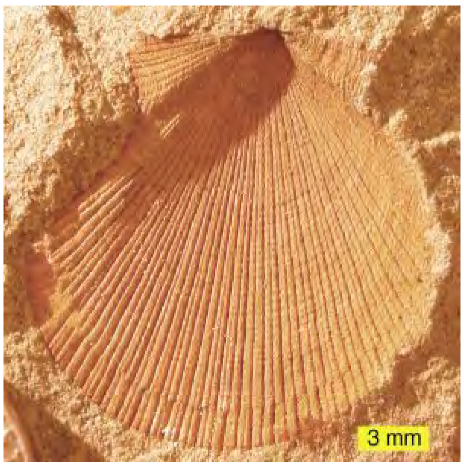

Figure 7.37: External mold of a clam. Figure description available at the end of the chapter.

Carbonization occurs when the organic tissues of an organism are compressed, the volatiles are driven out, and everything but the carbon disappears, leaving a carbon silhouette of the original organism. Leaf and fern fossils are examples of carbonization.

Figure 7.38: Carbonized leaf. Figure description available at the end of the chapter.

Figure 7.39: Dinosaur tracks as a record of its passing. Figure description available at the end of the chapter.

Trace fossils are indirect evidence left behind by an organism living its life, often in the form of burrows and footprints. Ichnology is specifically the study of prehistoric animal tracks. Dinosaur tracks testify to their presence and movement over an area and even provide information about their size, gait, speed, and behavior. Burrows dug by tunneling organisms tell of their presence and mode of life. Other trace fossils include fossilized feces called coprolites and stomach stones called gastroliths that provide information about diet and habitat.

Figure 7.40: Fossil animal droppings (coprolite). Figure description available at the end of the chapter.

7.3.2 Evolution

Evolution has created a variety of ancient fossils that are important to stratigraphic correlation (see Chapter 7 and Chapter 5) This section is a brief discussion of the process of evolution. The British naturalist Charles Darwin (1809–1882) recognized that life forms evolve into progeny life forms. He proposed natural selection—which operated on organisms living under environmental conditions that posed challenges to survival—was the mechanism driving the process of evolution forward.

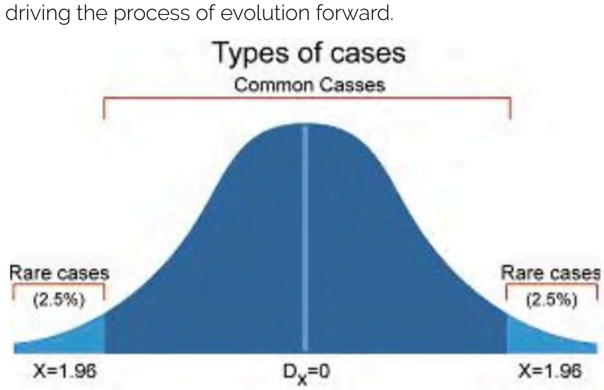

Figure 7.41: Variation within a population. Figure description available at the end of the chapter.

The basic classification unit of life is the species: a population of organisms that exhibit shared characteristics and are capable of reproducing fertile offspring. For a species to survive, each individual within a particular population is faced with challenges posed by the environment and must survive them long enough to reproduce. Within the natural variations present in the population, there may be individuals possessing characteristics that give them some advantage in facing the environmental challenges. These individuals are more likely to reproduce and pass these favored characteristics on to successive generations. If sufficient individuals in a population fail to surmount the challenges of the environment and the population cannot produce enough viable offspring, the species becomes extinct. The average lifespan of a species in the fossil record is around a million years. The fact that life still exists on Earth shows the role and importance of evolution as a natural process in meeting the continual challenges posed by our dynamic Earth. If the inheritance of certain distinctive characteristics is sufficiently favored over time, populations may become genetically isolated from one another, eventually resulting in the evolution of separate species. This genetic isolation may also be caused by a geographic barrier, such as an island surrounded by ocean. This theory of evolution by natural selection was elaborated by Darwin in his book *On the Origin of Species* (see Chapter 1). Since the time of Darwin's original ideas, technology has provided many tools and mechanisms to study how evolution and speciation take place, and this arsenal of tools is growing. Evolution is well beyond the hypothesis stage and is a well-established theory of modern science.

Variation within populations occurs through the natural mixing of genes through sexual reproduction or from naturally occurring mutations. Some of this genetic variation can introduce advantageous characteristics that increase the individual's chances of survival. While some species in the fossil record show little morphological change over time, others show gradual or punctuated changes, within which intermediate forms can be seen.

Take this quiz to check your comprehension of this section.

Access the quiz for Section 7.3 by scanning the QR code.

7.4 Correlation

Correlation is the process of establishing which sedimentary strata are of the same age but geographically separate. Correlation can be determined by using magnetic polarity reversals (Chapter 2), rock types, unique rock sequences, or index fossils. There are four main types of correlation: stratigraphic, lithostratigraphic, chronostratigraphic, and biostratigraphic.

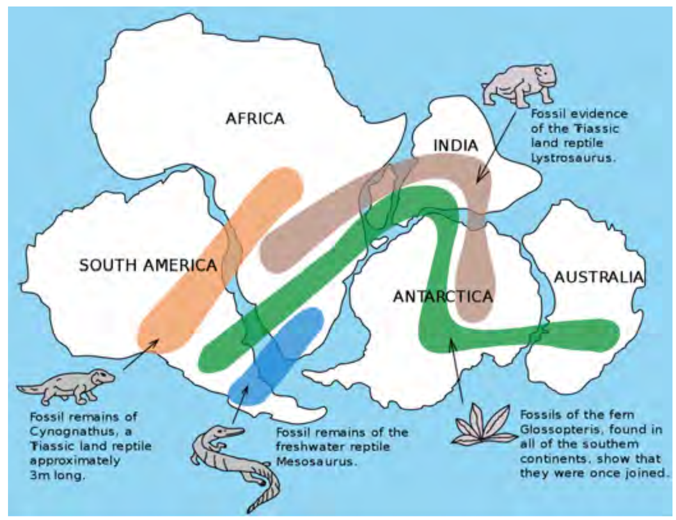

Figure 7.42: Image showing fossils that connect the continents of Gondwana (the southern continents of Pangea). Figure description available at the end of the chapter.

7.4.1 Stratigraphic Correlation

Stratigraphic correlation is the process of establishing which sedimentary strata are the same age between distant geographical areas by means of their stratigraphic relationship. Geologists construct geologic histories of areas by mapping and making stratigraphic columns—detailed descriptions of the strata from bottom to top. An example of stratigraphic relationships and correlation between Canyonlands National Park and Zion National Park in Utah. At Canyonlands, the Navajo Sandstone overlies the Kayenta Formation, which overlies the cliff-forming Wingate Formation. In Zion, the Navajo Sandstone overlies the Kayenta Formation which overlies the cliff-forming Moenave Formation. Based on the stratigraphic relationship, the Wingate and Moenave Formations correlate. These two formations have unique names because their compositions and outcrop patterns are slightly different. Other strata in the Colorado Plateau and their sequences can be recognized and correlated over thousands of square miles.

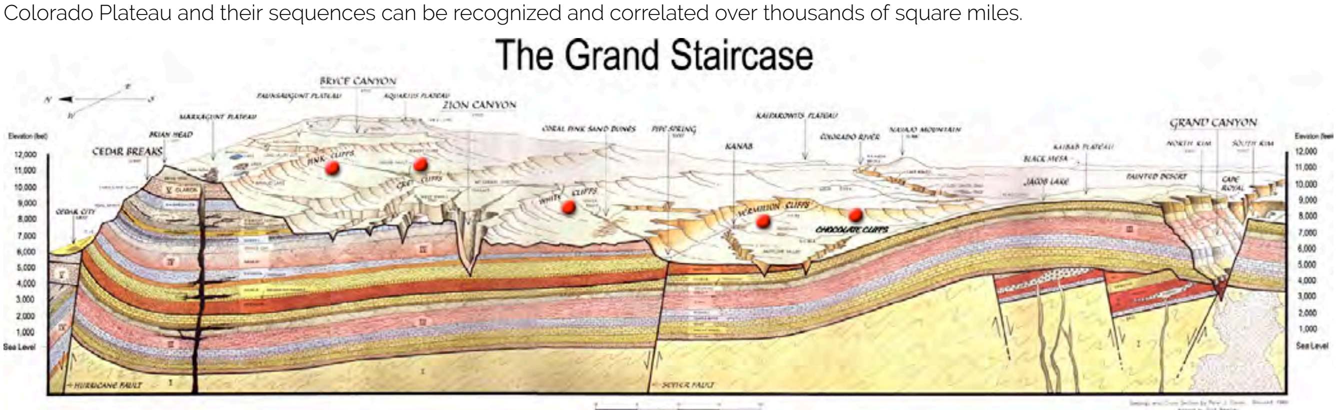

Figure 7.43: Correlation of strata along the Grand Staircase from the Grand Canyon to Zion Canyon, Bryce Canyon, and Cedar Breaks. Figure description available at the end of the chapter.

7.4.2 Lithostratigraphic Correlation

Figure 7.44: View of Navajo Sandstone in Zion National Park. Figure description available at the end of the chapter.

Lithostratigraphic correlation establishes a similar age of strata based on the lithology—the composition and physical properties of that strata. *Lithos* is Greek for stone, and *-logy* comes from the Greek word for doctrine or science. Lithostratigraphic correlation can be used to correlate whole formations over long distances or can be used to correlate smaller strata within formations to trace their extent and regional depositional environments.

Figure 7.45: Stevens Arch in the Navajo Sandstone at Coyote Gulch some 125 miles away from Zion National Park. Figure description available at the end of the chapter.

For example, the Navajo Sandstone, which makes up the prominent walls of Zion National Park, is the same Navajo Sandstone in Canyonlands because the lithology of the two are identical, even though they are hundreds of miles apart. Extensions of the same Navajo Sandstone formation are found miles away in other parts of southern Utah, including Capitol Reef and Arches National Parks. Further, this same formation is called the Aztec Sandstone in Nevada and Nugget Sandstone near Salt Lake City because they are lithologically distinct enough to warrant new names.

7.4.3 Chronostratigraphic Correlation

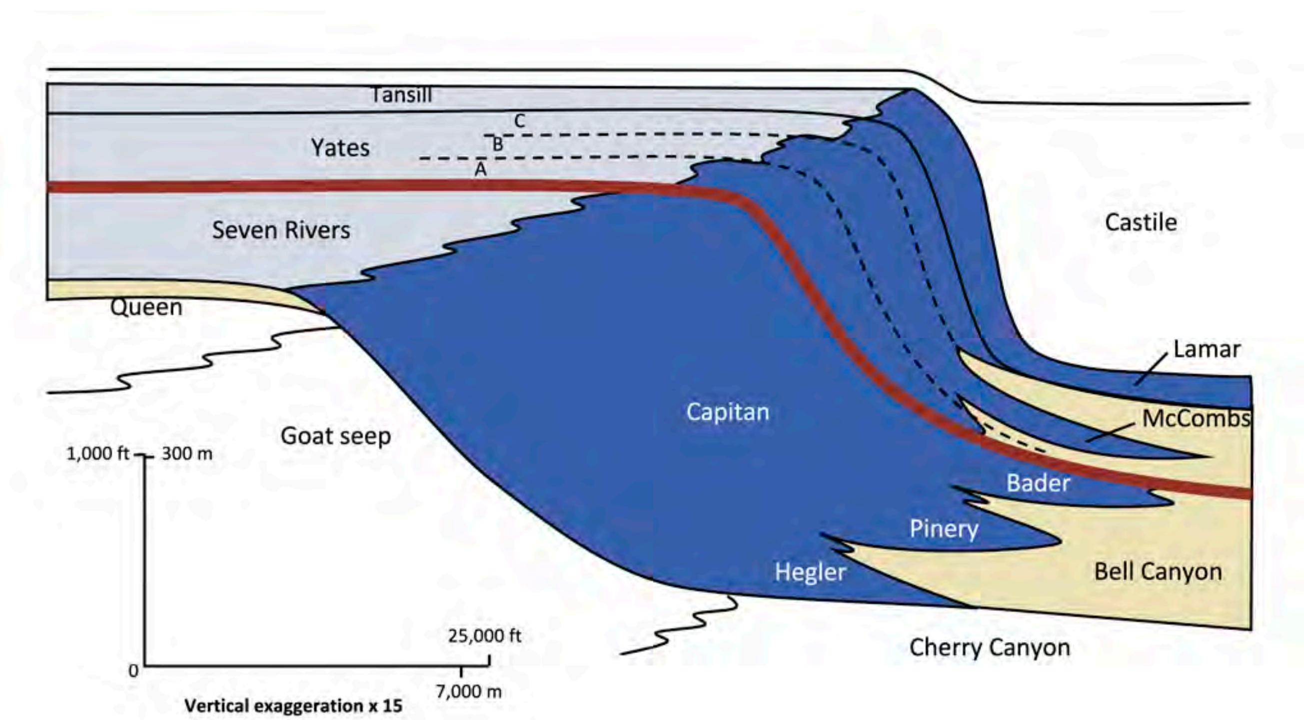

Figure 7.46: Cross section of the Permian El Capitan Reef at Guadalupe National Monument, Texas. The red line shows a chronostratigraphic time line that represents a snapshot in time in which the shallow marine lagoon/back reef area (light blue), main Capitan reef (dark blue), and deep marine silstones (yellow) were all being deposited at the same time. Figure description available at the end of the chapter.

Chronostratigraphic correlation matches rocks of the same age, even though they are made of different lithologies. Different lithologies of sedimentary rocks can form at the same time at different geographic locations because depositional environments vary geographically. For example, at any one time in a marine setting, there could be this sequence of depositional environments from beach to deep marine: beach, near shore area, shallow marine lagoon, reef, slope, and deep marine. Each depositional environment will have a unique sedimentary rock formation. On the figure of the Permian Capitan Reef at Guadalupe National Monument in West Texas, the red line shows a chronostratigraphic time line that represents a snapshot in time. The shallow-water marine lagoon/back reef area is light blue, the main Capitan reef is dark blue, and deep-water marine siltstone is yellow. All three of these unique lithologies were forming at the same time in the Permian along this red timeline.

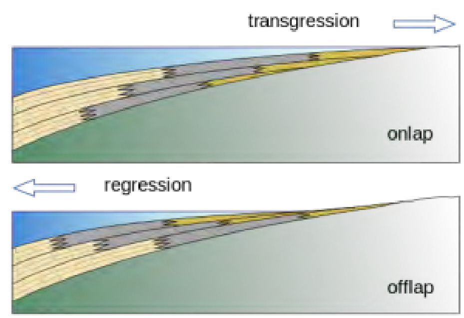

Figure 7.47: The rising sea levels of transgressions create onlapping sediments, while regressions create offlapping. Ocean water is shown in blue, so the time line is on the surface below the water. At the same time, sandstone (buff color), limestone (gray), and shale (mustard color) are all forming at different depths of water. Figure description available at the end of the chapter.

7.4.4 Biostratigraphic Correlation

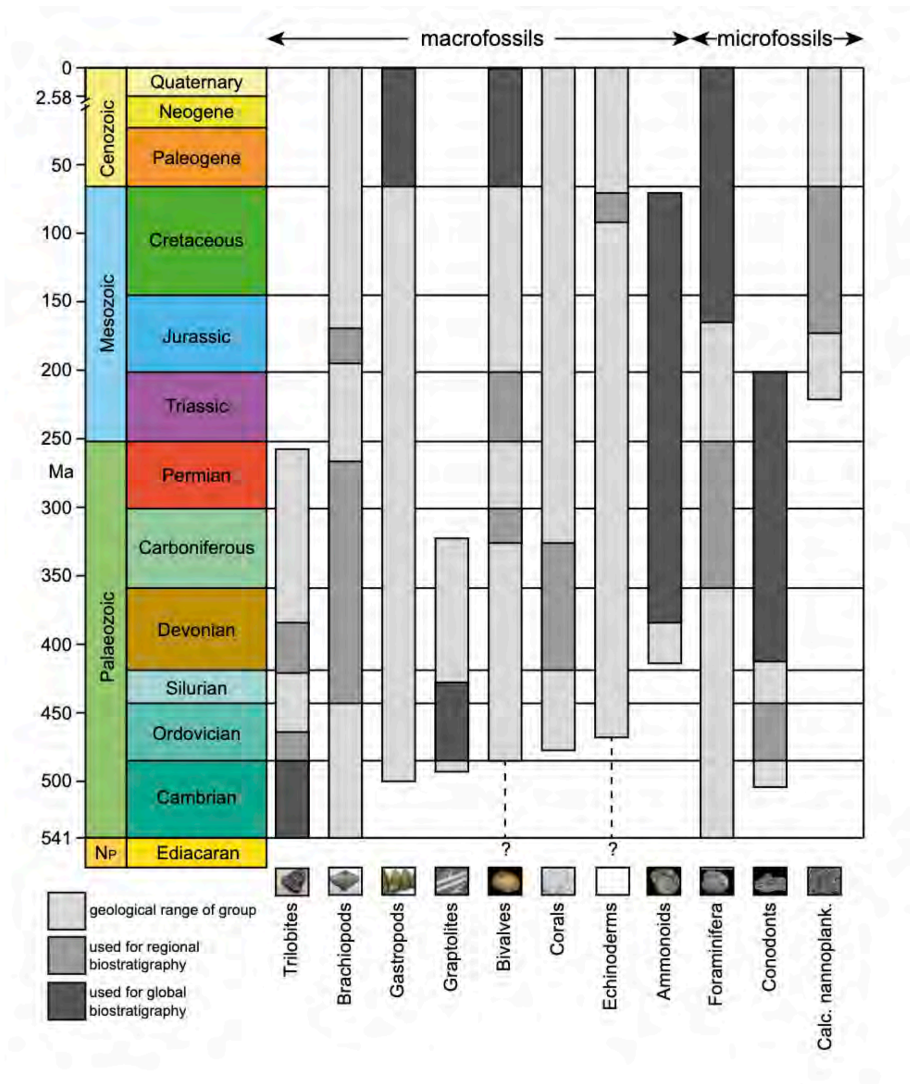

Figure 7.48: Index fossils used for biostratigraphic correlation. Figure description available at the end of the chapter.

Biostratigraphic correlation uses index fossils to determine strata ages. Index fossils represent assemblages or groups of organisms that were uniquely present during specific intervals of geologic time. Fossils allow geologists to assign a formation to an absolute date range, such as the **Jurassic** Period (199 to 145 million years ago) rather than a relative timescale. In fact, most of the geologic time ranges are mapped to fossil assemblages. The most useful index fossils come from life forms that were geographically widespread and had a species lifespan that was limited to a narrow time interval. In other words, index fossils can be found in many places around the world but only during a narrow time frame. Some of the best fossils for biostratigraphic correlation are microfossils, most of which came from single-celled organisms.

As with microscopic organisms today, they were widely distributed across many environments throughout the world. Some of these microscopic organisms had hard parts, such as exoskeletons or outer shells, making them better candidates for preservation.

Foraminifera, single-celled organisms with calcareous shells, are an example of an especially useful index fossil for the Cretaceous Period and Cenozoic Era.

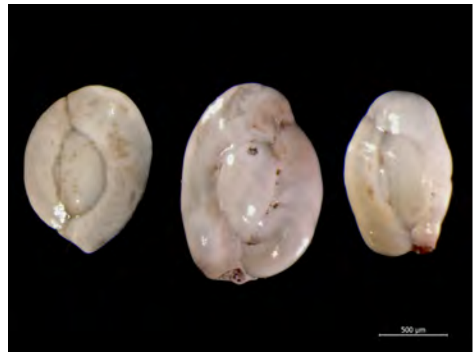

Figure 7.49: Foraminifera, microscopic creatures with hard shells. Figure description available at the end of the chapter.

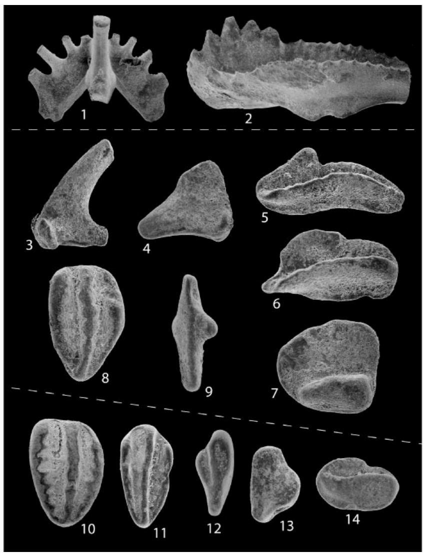

Figure 7.50: Conodonts. Figure description available at the end of the chapter.

Conodonts are another example of microfossils useful for biostratigraphic correlation of the **Cambrian** through **Triassic** Periods. Conodonts are toothlike phosphatic structures of an eel-like multicelled organism that had no other preservable hard parts. The conodont-bearing creatures lived in shallow marine environments all over the world. Upon death, the phosphatic hard parts were scattered into the rest of the marine sediments. These distinctive toothlike structures are easily collected and separated from limestone in the laboratory.

Because the conodont creatures were so widely abundant, rapidly evolving, and readily preserved in sediments, their fossils are especially useful for correlating strata, even though knowledge of the actual animal possessing them is sparse. Scientists in the 1960s carried out a fundamental biostratigraphic correlation that tied Triassic conodont zonation into ammonoids, which are extinct ancient cousins of the pearly nautilus. Up to that point, ammonoids were the only standard for Triassic correlation, so cross-referencing micro and macro index fossils enhanced the reliability of biostratigraphic correlation for either type. That conodont study went on to establish the use of conodonts to internationally correlate Triassic strata located in Europe, Western North America, and the Arctic islands of Canada.

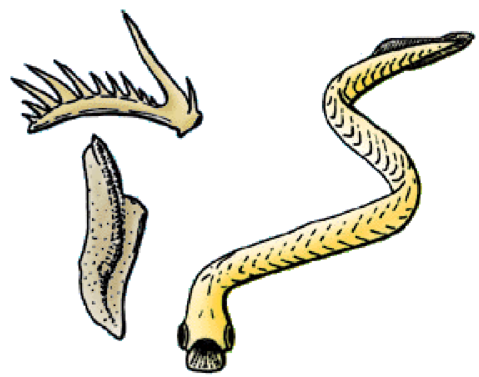

Figure 7.51: Artist reconstruction of the conodont animal. Figure description available at the end of the chapter.

7.4.5 Geologic Timescale

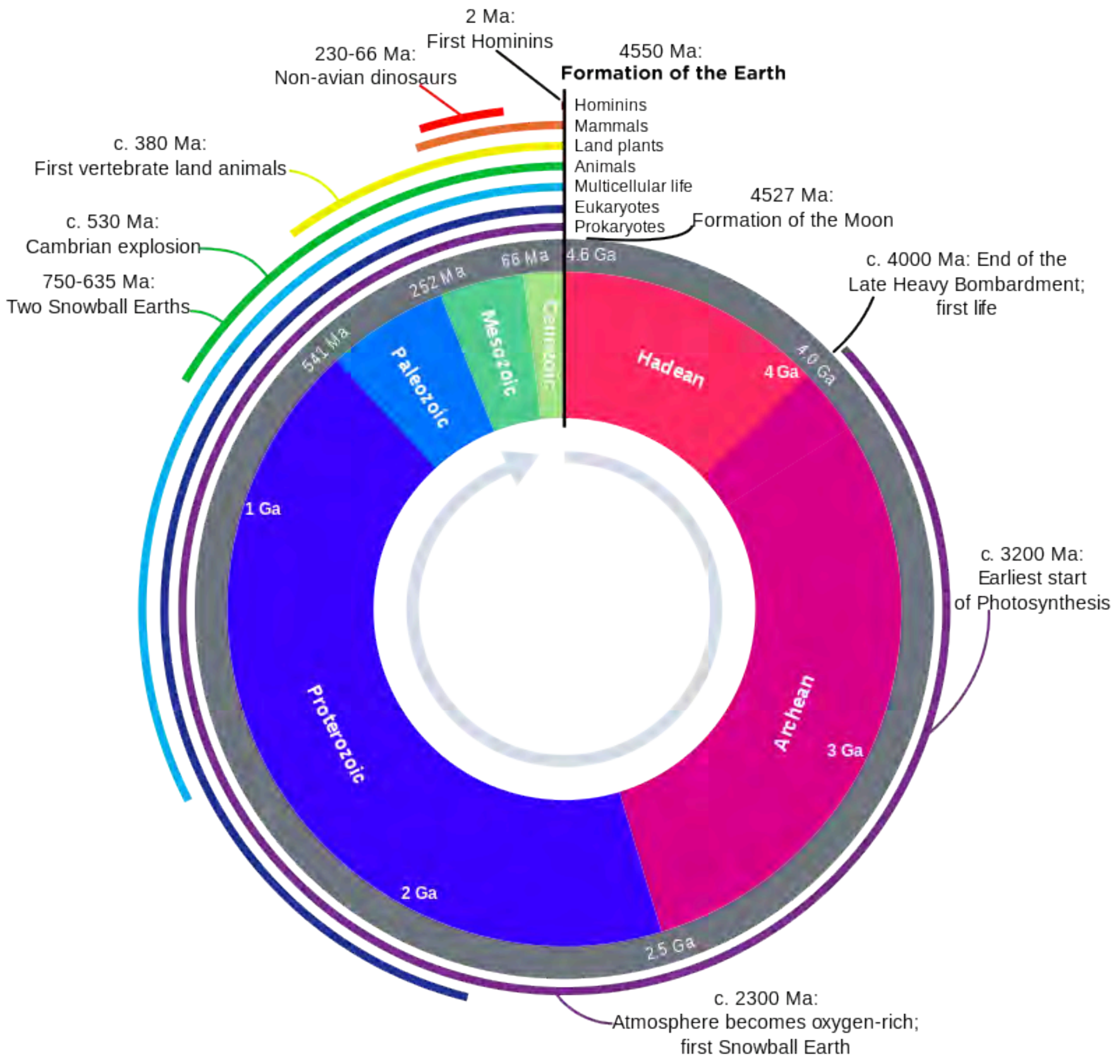

Figure 7.52: Geologic time on Earth, represented circularly, showing the individual time divisions and important events. Ga = billion years ago, Ma = million years ago. Figure description available at the end of the chapter.

Geologic time has been subdivided into a series of divisions by geologists. **Eon** is the largest division of time, followed by **era**, **period**, **epoch**, and age. The partitions of the geologic timescale are the same everywhere on Earth; however, rocks may or may not be present at a given location depending on the geologic activity during a particular period of time. Thus, we have the concept of time vs. rock, in which time is an unbroken continuum but rocks may be missing and/or unavailable for study. The figure of the geologic timescale represents time flowing continuously from the beginning of the Earth, with the time units presented in an unbroken sequence. But that does not mean there are rocks available for study from all of these time units.

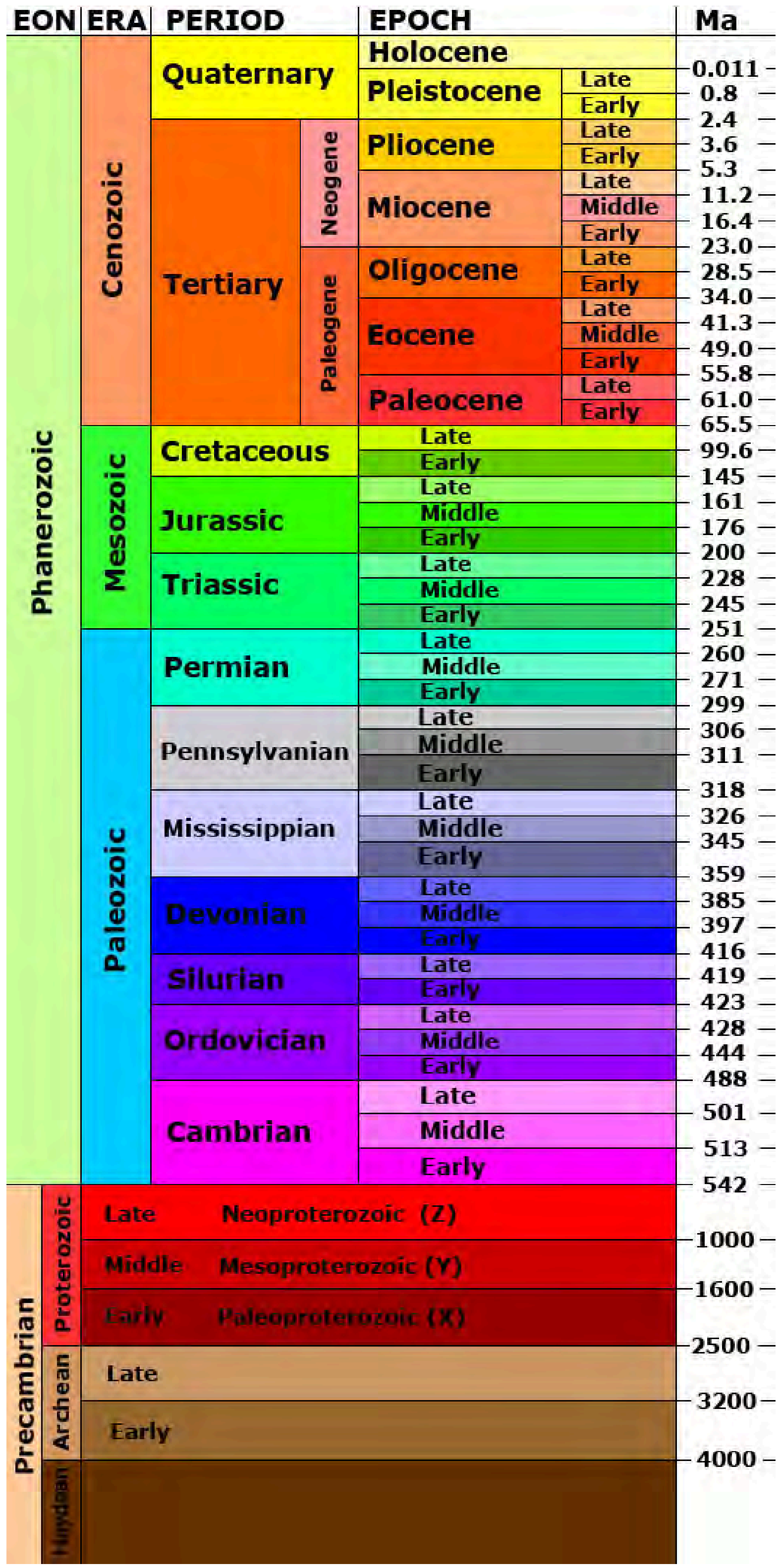

Figure 7.53: Geologic timescale with ages shown. Figure description available at the end of the chapter.

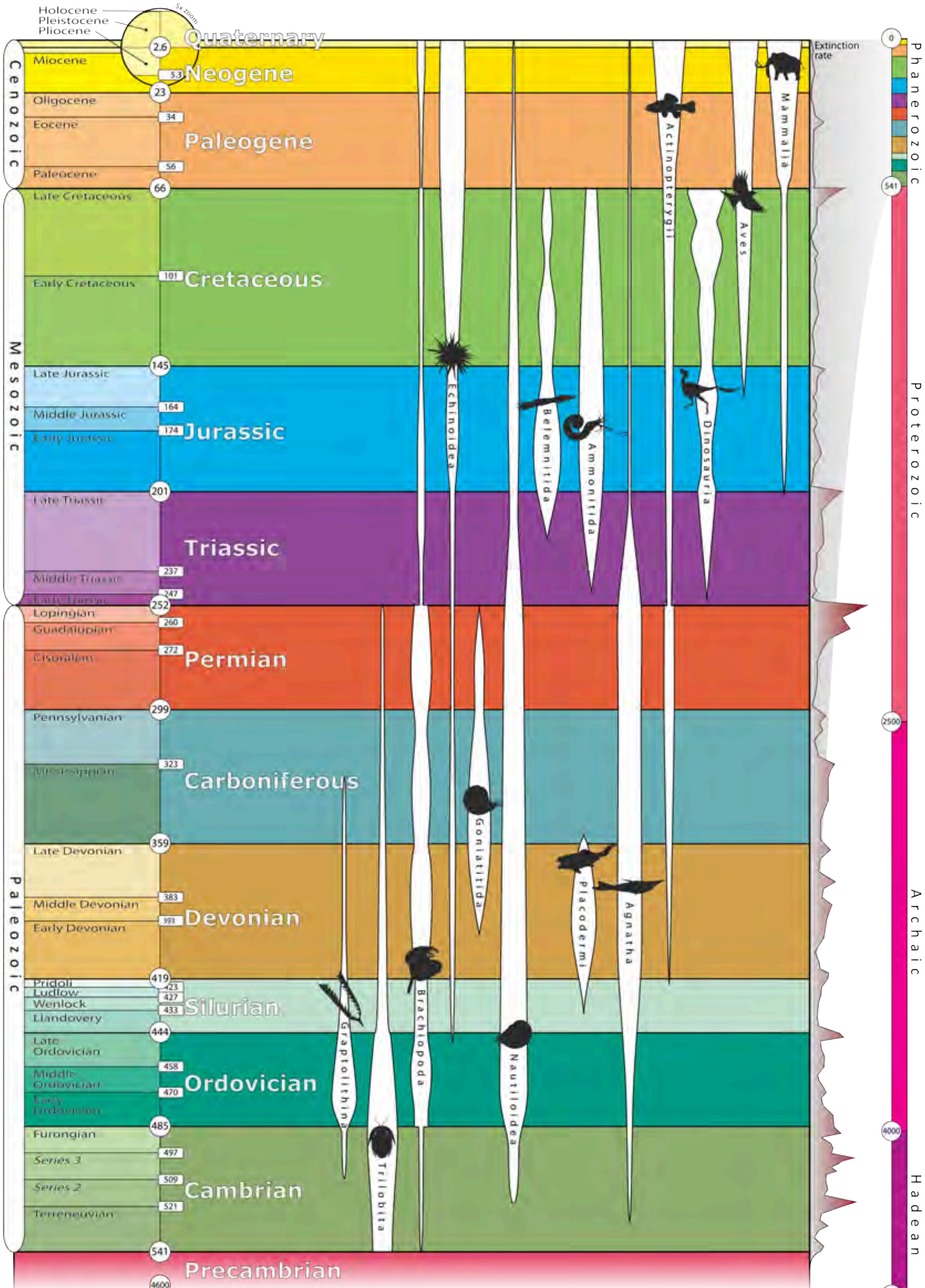

Figure 7.54: Names from the geologic timescale applied to taxonomical diversity of some major animal taxa. Figure description available at the end of the chapter.

The geologic timescale was developed during the nineteenth century using the principles of stratigraphy. The relative order of the time units was determined before geologist had the tools to assign numerical ages to periods and events. Biostratigraphic correlation uses fossils to assign era and period names to sedimentary rocks on a worldwide scale. With the expansion of science and technology, some geologists think the influence of humanity on natural processes has become so great they are suggesting a new geologic time period known as the **Anthropocene**.

Take this quiz to check your comprehension of this section.

Access the quiz for Section 7.4 by scanning the QR code.

Summary

Events in Earth history can be placed in sequence using the five principles of relative dating. The geologic timescale was completely worked out in the nineteenth century using these principles without knowing any actual numeric ages for the events. The discovery of radioactivity in the late 1800s enabled **absolute dating**, the assignment of numerical ages to events in the Earth's history, using the decay of unstable radioactive isotopes. Accurately interpreting radioisotopic dating data depends on the type of rock tested and accurate assumptions about isotope baseline values. With a combination of relative and absolute dating, the history of geological events, age of Earth, and a geologic timescale have been determined with considerable accuracy. Stratigraphic correlation is an additional tool used for understanding how depositional environments change geographically. Geologic time is vast, providing plenty of time for the evolution of various life forms, and some of these have become preserved as fossils that can be used for biostratigraphic correlation. The geologic timescale is continuous, although the rock record may be broken because rocks representing certain time periods may be missing.

Take this quiz to check your comprehension of this chapter.

Access the quiz for Chapter 7 by scanning the QR code.

Chapter URLs

- Animation 1: Why Is It Hot Underground? [Video: 1:49] https://www.youtube.com/watch?v=mOSpRzW2i_4
- The University of California Berkeley website: https://ucmp.berkeley.edu/paleo/fossils/permin.html

Text References

1. Allison, P.A., and Briggs, D.E.G. (1993). Exceptional fossil record: Distribution of soft-tissue preservation through the Phanerozoic. *Geology, 21*(6), 527–530.
2. Bell, E.A., Boehnke, P., Harrison, T.M., and Mao, W.L. (2015). Potentially biogenic carbon preserved in a 4.1 billion-year-old zircon. *Proc. Natl. Acad. Sci. U.S.A., 112*(47), 14518–14521.
3. Brent Dalrymple, G. (1994). *The age of the earth:* Stanford University Press.
4. Burleigh, R. (1981). W. F. Libby and the development of radiocarbon dating. *Antiquity, 55*(214), 96–98.
5. Christopher B. DuRoss, Stephen F. Personius, Anthony J. Crone, Susan S. Olig, and William R. Lund (2011). Integration of paleoseismic data from multiple sites to develop an objective earthquake chronology: Application to the Weber segment of the Wasatch fault zone, Utah. *Bulletin of the Seismological Society of America, v. 101*(6), 2765–2781. doi: 0.1785/0120110102.
6. Dass, C. (2007) Basics of mass spectrometry, in *Fundamentals of Contemporary Mass Spectrometry:* John Wiley & Sons, Inc., 1–14.
7. Elston, D.P., Billingsley, G.H., and Young, R.A. (1989). Geology of Grand Canyon, northern Arizona (with Colorado River guides): Lees Ferry to Pierce Ferry, Arizona. *Amer Geophysical Union.*
8. Erickson, J., Coates, D.R., and Erickson, H.P. (2014). An introduction to fossils and minerals: Seeking clues to the Earth's past. Facts on File science library, Facts on File, Incorporated.
9. Geyh, M.A., and Schleicher, H. (1990). *Absolute age determination: Physical and chemical dating methods and their application:* Springer-Verlag, New York.
10. Ireland, T. (1999). New tools for isotopic analysis. *Science, 286*(5448), 2289–2290.

11. Jackson, P.W., and G.S. of London. (2007). Four centuries of geological travel: The search for knowledge on foot, bicycle, sledge and camel. *Geological Society special publication, Geological Society.*
12. Jaffey, A.H., Flynn, K.F., Glendenin, L.E., Bentley, W.C., et al. (1971). Precision measurement of half-lives and specific activities of U 235 and U 238. *Phys. Rev. C Nucl. Phys.*
13. Léost, I., Féraud, G., Blanc-Valleron, M.M., and Rouchy, J.M. (2001). First absolute dating of Miocene Langbeinite evaporites by 40Ar/39Ar laser step-heating: [K2Mg2 (SO4) 3] Stebnyk Mine (Carpathian Foredeep Basin). *Geophys. Res. Lett., 28*(23), 4347–4350.
14. Mosher, L.C. (1968). Triassic conodonts from western North America and Europe and their correlation. *J. Paleontol., 42*(4), 895–946.
15. Oberthu ¨ r, T., Davis, D.W., Blenkinsop, T.G., and Höhndorf, A. (2002). Precise U–Pb mineral ages, Rb–Sr and Sm–Nd systematics for the Great Dyke, Zimbabwe—Constraints on late Archean events in the Zimbabwe craton and Limpopo belt. *Precambrian Res., 113*(3–4), 293–305.
16. Patterson, C. (1956). Age of meteorites and the earth. *Geochim. Cosmochim. Acta, 10*(4), 230–237.
17. Schweitzer, M.H., Wittmeyer, J.L., Horner, J.R., and Toporski, J.K. (2005). Soft-tissue vessels and cellular preservation in Tyrannosaurus rex. *Science, 307*(5717), 1952–1955.
18. Valley, J.W., Peck, W.H., King, E.M., and Wilde, S.A. (2002). A cool early Earth. *Geology, v. 30*(4), 351–354.
19. Whewell, W. (1837). *History of the inductive sciences: From the earliest to the present times:* J.W. Parker.
20. Wilde, S.A., Valley, J.W., Peck, W.H., and Graham, C.M. (2001). Evidence from detrital zircons for the existence of continental crust and oceans on the Earth 4.4 Gyr ago: *Nature, 409*(6817), 175–178.
21. Winchester, S. (2009). *The map that changed the world: William Smith and the birth of modern geology:* Harper-Collins.

Figure References

Figure 7.1: Nicolas Steno, ca. 1670. Justus Sustermans. ca. 1666–1677; uploaded in 2012. Public domain. https://commons.wikimedia.org/wiki/File:Portrait_of_Nicolas_Stenonus.jpg

Figure 7.2: Geologic timescale. United States Geological Survey (USGS). 1997. Public domain. https://pubs.usgs.gov/gip/fossils/numeric.html

Figure 7.3: Lower strata are older than those on top of them. Wilson44691. 2009. Public domain. https://commons.wikimedia.org/wiki/File:IsfjordenSuperposition.jpg

Figure 7.4: Lateral continuity. Roger Bolsius. 2013. CC BY-SA 3.0. https://en.wikipedia.org/wiki/File:Grand_Canyon_Panorama_2013.jpg

Figure 7.5: Dark dike cutting across older rocks, the lighter of which is younger than the grey rock. Thomas Eliasson of Geological Survey of Sweden. 2008. CC BY 2.0. https://commons.wikimedia.org/wiki/File:Multiple_Igneous_Intrusion_Phases_Kosterhavet_Sweden.jpg

Figure 7.6: Fossil succession showing correlation among strata. 2010 דקי. CC BY-SA 3.0. https://commons.wikimedia.org/wiki/File:Faunal_sucession.jpg

Figure 7.7: The Grand Canyon of Arizona. Jean-Christophe BENOIST. 2012. CC BY 3.0. https://commons.wikimedia.org/wiki/File:Grand_Canyon_-_Hopi_Point.jpg

Figure 7.8: The rocks of the Grand Canyon. NPS. 2018. Public domain. https://www.nps.gov/articles/age-of-rocks-in-grand-canyon.htm

Figure 7.9: The red, layered rocks of the Grand Canyon Supergroup overlying the dark-colored rocks of the Vishnu schist represents a type of unconformity called a nonconformity. Simeon87. 2012. CC BY-SA 3.0. https://commons.wikimedia.org/wiki/File:Grand_Canyon_with_Snow_4.jpg

Figure 7.10: All three of these formations have a disconformity at the two contacts between them. NPS. 2009. Public domain. https://commons.wikimedia.org/wiki/File:Redwall,_Temple_Butte_and_Muav_formations_in_Grand_Canyon.jpg

Figure 7.11: In the lower part of the picture is an angular unconformity in the Grand Canyon known as the Great Unconformity. Doug Dolde. 2008. Public domain. https://commons.wikimedia.org/wiki/File:View_from_Lipan_Point.jpg

Figure 7.12: Disconformity. 2008 .דקי. CC BY-SA 3.0. https://commons.wikimedia.org/wiki/File:Disconformity.jpg

Figure 7.13: Nonconformity (the lower rocks are igneous or metamorphic). 2008 .דקי. CC BY-SA 3.0. https://commons.wikimedia.org/wiki/File:Nonconformity.jpg

Figure 7.14: Angular unconformity. 2008 .דקי. CC BY-SA 3.0. https://commons.wikimedia.org/wiki/File:Angular_unconformity.jpg

Figure 7.15: Block diagram to apply relative dating principles. Woudloper. 2009. CC BY-SA 1.0. https://commons.wikimedia.org/wiki/File:Cross-cutting_relations.svg

Figure 7.16: Canada's Nuvvuagittuq Greenstone Belt may have the oldest rocks and oldest evidence of life on Earth, according to recent studies. NASA. 2008. Public domain. https://commons.wikimedia.org/wiki/File:Nuvvuagittuq_belt_rocks.jpg

Figure 7.17: Three isotopes of hydrogen. Dirk Hünniger. 2016. CC BY-SA 3.0. https://commons.wikimedia.org/wiki/File:Hydrogen_Deuterium_Tritium_Nuclei_Schmatic-en.svg

Figure 7.18: Simulation of half-life. Sbyrnes321. 2010. Public domain. https://commons.wikimedia.org/wiki/File:Halflife-sim.gif

Figure 7.19: Granite (left) and gneiss (right). Fjæregranitt3 by Friman, 2007 (CC BY-SA 3.0, https://commons.wikimedia.org/wiki/File:Fj%C3%A6regranitt3.jpg). Gneiss by Siim Sepp, 2005 (CC BY-SA 3.0, https://commons.wikimedia.org/wiki/File:Gneiss.jpg).

Figure 7.20: Alpha decay in which two protons and two neutrons leave the nucleus. Inductiveload. 2007. Public domain. https://commons.wikimedia.org/wiki/File:Alpha_Decay.svg

Figure 7.21: Periodic table of the elements. Sandbh. 2017. CC BY-SA 4.0. https://en.wikipedia.org/wiki/File:Periodic_Table_Chart_with_less_active_and_active_nonmetals.png

Figure 7.22: Decay chain of U-238 to stable Pb-206 through a series of alpha and beta decays. ThaLibster. 2017. CC BY-SA 4.0. https://en.wikipedia.org/wiki/File:Decay_Chain_of_Uranium-238.svg

Figure 7.23: The two paths of electron capture. Pamputt. 2015. CC BY-SA 4.0. https://en.wikipedia.org/wiki/File:Atomic_rearrangement_following_an_electron_capture.svg

Figure 7.24: Mass spectrometer instrument. Archives CAMECA. 2006. CC BY-SA 3.0. https://commons.wikimedia.org/wiki/File:IMS3F_pbmf.jpg

Figure 7.25: Graph of the amount of half-life versus the amount of daughter isotope. Krishnavedala. 2015. Public domain. https://en.wikipedia.org/wiki/File:Half_times.svg

Figure 7.26: Schematic of carbon going through a mass spectrometer. Mike Christie. 2013. CC BY-SA 3.0. https://commons.wikimedia.org/wiki/File:Accelerator_mass_spectrometer_schematic_for_radiocarbon.svg

Figure 7.27: Carbon dioxide concentrations over the last 400,000 years. Robert A. Rohde. 2011. CC BY-SA 3.0. https://commons.wikimedia.org/wiki/File:Carbon_Dioxide_400kyr.svg

Figure 7.28: Artist's impression of the Earth in the Hadean. Tim Bertelink. 2016. CC BY-SA 4.0. https://commons.wikimedia.org/wiki/File:Hadean.png

Figure 7.29: Photomicrograph of zircon crystal. Denniss. 2006. CC BY-SA 3.0. https://commons.wikimedia.org/wiki/File:Zircon_microscope.jpg

Figure 7.30: Several prominent ash beds found in North America, including three Yellowstone eruptions shaded pink (Mesa Falls, Huckleberry Ridge, and Lava Creek), the Bisho Tuff ash bed (brown dashed line), and the modern May 18th, 1980, ash fall (yellow). USGS. 2005. Public domain. https://commons.wikimedia.org/wiki/File:Yellowstone_volcano_-_ash_beds.svg

Figure 7.31: Thermoluminescence, a type of luminescence dating. Zkeizars. 2008. CC BY-SA 4.0. https://commons.wikimedia.org/wiki/File:Keizars_TLexplained2.jpg

Figure 7.32: Apatite from Mexico. Robert M. Lavinsky. Before March 2010. CC BY-SA 3.0. https://commons.wikimedia.org/wiki/File:Apatite-(CaF)-280343.jpg

Figure 7.33: Archaeopteryx lithographica specimen displayed at the Museum für Naturkunde in Berlin. H. Raab. 2009. CC BY-SA 3.0. https://commons.wikimedia.org/wiki/File:Archaeopteryx_lithographica_(Berlin_specimen).jpg

Figure 7.34: The trilobite had a hard exoskeleton and is an early arthropod, the same group that includes modern insects, crustaceans, and arachnids. Wilson44691. 2010. Public domain. https://commons.wikimedia.org/wiki/File:ElrathiakingiUtahWheelerCambrian.jpg

Figure 7.35: Mosquito preserved in amber. Didier Desouens. 2010. CC BY-SA 4.0. https://commons.wikimedia.org/wiki/File:Ambre_Dominique_Moustique.jpg

Figure 7.36: Permineralization in petrified wood at Petrified Forest National Park. Laura Neser. March 2022. CC BY-NC.

Figure 7.37: External mold of a clam. Wilson44691. 2007. Public domain. https://commons.wikimedia.org/wiki/File:Aviculopecten_subcardiformis01.jpg

Figure 7.38: Carbonized leaf. Wilson44691. 2008. Public domain. https://commons.wikimedia.org/wiki/File:ViburnumFossil.jpg

Figure 7.39: Dinosaur tracks as a record of its passing. Ballista. 2006. CC BY-SA 3.0. https://commons.wikimedia.org/wiki/File:Cheirotherium_prints_possibly_Ticinosuchus.jpg

Figure 7.40: Fossil animal droppings (coprolite). USGS. 2008. Public domain. https://commons.wikimedia.org/wiki/File:Coprolite.jpg

Figure 7.41: Variation within a population. Inglesenargentina. 2006. Public domain. https://en.wikipedia.org/wiki/File:Bell-shaped-curve.jpg

Figure 7.42: Image showing fossils that connect the continents of Gondwana (the southern continents of Pangea). Osvaldocangaspadilla. 2010. Public domain. https://commons.wikimedia.org/wiki/File:Snider-Pellegrini_Wegener_fossil_map.svg

Figure 7.43: Correlation of strata along the Grand Staircase from the Grand Canyon to Zion Canyon, Bryce Canyon, and Cedar Breaks. NPS. 2005. Public domain. https://commons.wikimedia.org/wiki/File:Grand_Staircase-big.jpg

Figure 7.44: View of Navajo Sandstone in Zion National Park. Laura Neser. March 2022. CC BY-NC.

Figure 7.45: Stevens Arch in the Navajo Sandstone at Coyote Gulch some 125 miles away from Zion National Park. G. Thomas. 2007. Public domain. https://en.wikipedia.org/wiki/File:StevensArchUT.jpg

Figure 7.46: Cross section of the Permian El Capitan Reef at Guadalupe National Monument, Texas. Kindred Grey. 2022. Adapted under fair use from Garber, R.A., Grover, G.A., & Harris, P.M. (1989). Geology of the Capitan Shelf Margin – Subsurface Data from the Northern Delaware Basin (DOI:10.2110/cor.89.13.0003).

Figure 7.47: The rising sea levels of transgressions create onlapping sediments, while regressions create offlapping. Woudloper. 2009. CC BY-SA 1.0. https://commons.wikimedia.org/wiki/File:Offlap_%26_onlap_EN.svg

Figure 7.48: Index fossils used for biostratigraphic correlation. David Bond. 2016. CC BY-SA 4.0. https://commons.wikimedia.org/wiki/File:Biostratigraphic_index_fossils_01.svg

Figure 7.49: Foraminifera, microscopic creatures with hard shells. Hans Hillewaert. 2011. CC BY-SA 4.0. https://en.wikipedia.org/wiki/File:Quinqueloculina_seminula.jpg

Figure 7.50: Conodonts. USGS. 2007. Public domain. https://commons.wikimedia.org/wiki/File:Conodonts.jpg

Figure 7.51: Artist reconstruction of the conodont animal. Philippe Janvier. 1997. CC BY 3.0. https://commons.wikimedia.org/wiki/File:Euconodonta.gif

Figure 7.52: Geologic time on Earth, represented circularly, showing the individual time divisions and important events. Woudloper; adapted by Hardwigg. 2010. Public domain. https://commons.wikimedia.org/wiki/File:Geologic_Clock_with_events_and_periods.svg

Figure 7.53: Geologic timescale with ages shown. USGS. 2009. Public domain. https://commons.wikimedia.org/wiki/File:Geologic_time_scale.jpg

Figure 7.54: Names from the geologic timescale applied to taxonomical diversity of some major animal taxa. Frederik Lerouge. 2015. CC BY-SA 4.0. https://commons.wikimedia.org/wiki/File:Geologic_Time_Scale.png

Figure Descriptions

Figure 7.1: Portrait painting of a young man in 1600s.

Figure 7.2: Quaternary period – 1.6 million years ago. tertiary period – 66 million years ago. these make up the cenozoic era. cretaceous period – 138 million years ago. jurassic period – 205 million years ago. triassic period – 240 million years ago. these make up the mesozoic era. permian period – 290 million years ago. pennsylvanian period – 330 million years ago. mississippian period – 360 million years ago. devonian period – 410 million years ago. silurian period – 435 million years ago. ordovician period – 500 million years ago. cambrian – 570 million years ago. these make up the paleozoic era. The cenozoic, mesozoic, and paleozoic eras make up the phanerozoic eon. The proterozoic eon includes late, middle, and early proterozoic eras – 2500 million years ago. The archean eon includes late, middle, and early archean eras – 3800? years ago.

Figure 7.3: Sloping cliffside with flat-lying layers of tan and brown sedimentary rocks.

Figure 7.4: Wide-angle view overlooking the Grand Canyon, in which you can see continuous flat-lying layers of white, tan, and gray sedimentary rock along the canyon walls.

Figure 7.5: Rock outcrop with a nearly vertical white-tan igneous rock cutting through a larger, gray domed rock; there's a second thin black vertical igneous intrusion cutting through both the white intrusion and gray domed rock.

Figure 7.6: Two cross sectional diagrams with the one on the left slightly higher than the one on the right; on each diagram there are seven flat-lying layers containing different fossils in each layer; six of the fossil layers match across both diagrams and there are lines correlating the strata that contain equivalent fossils.

Figure 7.7: Wide-angle view overlooking the Grand Canyon, in which you can see continuous flat-lying layers of tan, brown, and gray sedimentary rock along the canyon walls.

Figure 7.8: Rocks that make up the Grand Canyon. From top to bottom (newest to oldest rocks) in three layers. Top layer: layered paleozoic rocks including Kaibab formation (Fm), Toroweap formation, Coconino sandstone, Hermit formation, Supai group, Surprise canyon Fm, Redwall limestone, Temple butte Fm, Muav limestone, Bright angel shale, Tapeats sandstone. Middle layer: Grand canyon supergroup rocks including Sixtymile formation, Chuar group, Nankoweap Fm, Unkar group. Bottom layer: Vishnu basement rocks including schists, granites, elves chasm gneiss.

Figure 7.9: View of canyon walls of the Grand Canyon in which you can see flat-lying layers of reddish sedimentary rock overlying dark brownish rocks that don't have any layering.

Figure 7.10: Cliffside outcrop with reddish tan thick flat-lying layers at the top labeled "Redwall Limestone;" below the left part of the Redwall Limestone is a wedge-shaped brick red layer labeled "Temple Butte Formation;" below the right part of the Redwall Limestone and below the Temple Butte Formation are tannish brown flat-lying layers labeled "Muav Limestone."

Figure 7.11: View of canyon walls of the Grand Canyon in which you can see reddish and gray flat-lying sedimentary rock layers overlying shallowly dipping tan and gray sedimentary rock layers.

Figure 7.12: Grayscale cross sectional view of seven flat-lying sedimentary layers; between two of the layers in the middle is a thick, curved line representing a gap in time.

Figure 7.13: Grayscale cross sectional view of four flat-lying sedimentary layers sitting on top of crystalline rocks; along the contact of the sedimentary layers and crystalline rock is a thick, curved line representing a gap in time.

Figure 7.14: Grayscale cross sectional view of three flat-lying sedimentary layers sitting on top of a series of five steeply dipping sedimentary layers; along the bottom contact of the lowest flat-lying sedimentary layer, above the angled layers, is a thick, curved line representing a gap in time.

Figure 7.15: 3D block diagram, the top of which is the ground surface. There are flat-lying sedimentary layers near the surface which are cut by a steeply dipping igneous intrusion and a steeply dipping fault; below the sedimentary layers are crystalline metamorphic rocks which have a large bulbous igneous intrusion that has risen through them; a shallowly dipping fault cuts through the metamorphic rocks but not through any other rocks. A detailed explanation is provided in section 7.1.3 of the textbook.

Figure 7.16: An outcrop of gray and tan rocks on a shoreline.

Figure 7.17: Three atomic diagrams of different isotopes of hydrogen: on the left is protium with one proton and no neutrons in the nucleus; in the middle is deuterium with one proton and one neutron in the nucleus; on the right is tritium with one proton and two neutrons in the nucleus; all three diagrams have one electron orbiting each nucleus.

Figure 7.18: Two animated diagrams, each consisting of a column of four cubes stacked on each other; on the left diagram, there are four blue dots inside each of the cubes at the time of zero; as the time goes from zero to four, the dots disappear randomly until 50% are left at one half-life, 25% are left at two half-lives, 12.5% are left at three half-lives, and 6.25% are left at four half-lives. The right diagram has the same progression but with many more smaller blue dots filling each square at the beginning, decreasing by the same percentages at each half-life.

Figure 7.19: Two rock samples: the rock on the left has large pink grains and smaller black, gray, and white grains interlocked without any visible pattern; the rock on the right has banded layering of dark minerals and light minerals.

Figure 7.20: 3D diagram showing a cluster of two protons and two neutrons leaving a larger cluster of many more protons and neutrons; the cluster leaving is labeled with the Greek lowercase letter alpha.

Figure 7.21: An organized grid-like structure known as the periodic table of elements. It consists of rows and columns that contain symbols and numbers representing different chemical elements. The elements are arranged in increasing order based on their atomic number, from left to right and top to bottom. Each element is depicted by its symbol, such as H for hydrogen, followed by its atomic number and atomic weight. The table is color-coded to group elements with similar properties.

Figure 7.22: Decay chain of U-238 to stable Pb-206 which includes the following steps: U-238 emits an alpha particle to become Th-234, which then emits another alpha particle to become Pa-230. Pa-230 undergoes alpha decay to become U-226, followed by alpha decay to Ra-222. Ra-222 emits an alpha particle to become Rn-218, which further emits an alpha particle to become Po-214. Po-214 undergoes alpha decay to become Pb-210, which then undergoes beta decay to become Bi-210. Bi-210 emits a beta particle to become Po-210, which finally undergoes alpha decay to reach the stable state of Pb-206.

Figure 7.23: Three drawings of an atom arranged in a triangle shape with the bottom two diagrams coming from the top diagram: the top diagram shows an atom with a proton in the nucleus capturing an electron from the innermost of three electron shells circling the nucleus.

The bottom left diagram shows an electron jumping inward to fill the missing spot of the departed electron and also emitting an X-ray outward; the bottom right diagram shows the outermost electron being released outward while the middle electron jumps inward to fill the missing spot of the departed electron.

Figure 7.24: Photo of scientific instrument.

Figure 7.25: Graph shows exponential growth from 0 to 4.

Figure 7.26: Schematic diagram: on the far right a carbon sample enters a curved shape labeled injection magnet with it path labeled input ion stream from sample; arrows show the path of the carbon atom exiting the injection magnet toward the left, entering a rectangle labeled accelerator which has a dotted line cutting across it labeled Stripper; the arrows then show the atom exiting the accelerator and entering another curved shape labeled focusing magnet, after which it exits as three separate arrows labeled output ion streams, separated by mass. The left of the three arrows is labeled 14C, the center arrow is labeled 13C, and the right arrow is labeled 12C.

Figure 7.27: Graph titled Carbon Dioxide Variations; the horizontal axis is labeled Thousands of Years Ago and goes from 0 on the right-hand side to over 400 on the left-hand side; the vertical axis is labeled CO_2 concentration (ppmv) and goes from 0 on the bottom to 400 on the top; a jagged blue line shows repeating cycles of around 300 ppmv CO_2 to near 0 ppmv CO_2 until there is the highest peak occurring toward present-day which goes over 350 ppmv CO_2. An inset graph has a horizontal axis labeled Year (AD) which goes from 1000 on the left to over 2000 on the right and it shows exponential growth in CO_2 concentrations after around the year 1750 AD.

Figure 7.28: Digital rendering of a landscape view of Earth's surface covered in black volcanic rock with numerous lava flows and volcanoes erupting; the Sun is very large on the horizon, there is lightning striking the surface, and meteors are streaking through the sky.

Figure 7.29: Microscopic view of a single elongate prismatic crystal that is amber to clear in color with a glassy luster.

Figure 7.30: Map of the United States with state borders outlined. Prominent ash beds are outlined and color-coded, including three Yellowstone eruptions shaded pink. One of the pink outlines is labeled Mesa Falls ash bed and encircles most of the states of Wyoming, Colorado, Kansas, and Nebraska, and partially encircles the states Montana, South Dakota, Oklahoma, and Texas. Another pink outline is labeled Huckleberry Ridge ash bed and encircles the a large western portion of the United States. The third pink outline is labeled Lava Creek ash bed and encircles most of the western half of the United States. There is also a brown dashed outline labeled "Bishop ash bed" which encircles the entire southwest portion of the United States. There is a yellow elongated outline labeled "Mount St. Helens ash 1980" which covers a east-west-trending portion of southern Washington state.

Figure 7.31: Diagram of atomic structure of quartz looking down c-axis; three curvy red arrows enter the lattice from the upper right, labeled irradiation; three circular red arrows are drawn within three of the empty spaces in the crystal lattice near the center of the diagram labeled storage; three curvy red arrows leave the lattice out of the lower right, labeled eviction.

Figure 7.32: An elongated prismatic crystal of light green apatite with a glassy luster.

Figure 7.33: Archaeopteryx fossil embedded within flat face of tan sedimentary rock; the fossil shows features of reptiles, such as sharp teeth, fingers with claws, and a long bony tail, as well as features of birds, such as small, broad wings and the impression of feathers.

Figure 7.34: Top view of a black fossilized trilobite that has an overall oval shape with a segmented body covered in a pattern of fine ridges; a scale bar labeled 0.5 cm is in the lower right of the photo.

Figure 7.35: Mosquito encased in crystallized amber.

Figure 7.36: The rock is in the shape of a large circular tree trunk with red, yellow, and white minerals running throughout the rock showing the impression of ancient tree rings.

Figure 7.37: Impression of a clam shell preserved in tan sandstone.

Figure 7.38: Brown carbon-rich film of a flat leaf embedded in tan sedimentary rock; holes from insect damage and veins in the leaf are visible; a scale bar labeled 10 mm is in the lower left of the photo.

Figure 7.39: Impression of a series of three tracks of a four-toed dinosaur embedded in brown sedimentary rock.

Figure 7.40: Tan-brown elongated lumpy rock with a 15 cm scale bar sitting in front of it.

Figure 7.41: Bell-shaped curve showing how variation within a population is distributed with respect to characteristics. Most members group in the center with rarer members on the tails.

Figure 7.42: Illustration showing five continents connected. From the left to right, there are South America, Africa, India above Antarctica, and Australia. Overlain on the continents are color-coded tracks of various fossil evidence: a tan band across South America and Africa shows the extent of fossil evidence for Cynognathus, a Triassic therapsid approximately 3 meters long. A gray band across southern Africa, India, and Antarctica shows the extent of fossil evidence for the Triassic therapsid Lystrosaurus. A green band across southern South Amer-

ica, southern Africa, India, Antarctica, and Australia (all of the southern continents) shows the extent of fossil evidence for the fern Glossopteris. A blue band across southern South America and southern Africa shows the extent of fossil evidence for the freshwater reptile Mesosaurus.

Figure 7.43: Cross-section showing the same sedimentary strata from the Grand Canyon to Zion Canyon, Bryce Canyon, and Cedar Breaks.

Figure 7.44: Steep canyon with cliffs of horizontal tan and brown rock layers that match up on either side of the canyon.

Figure 7.45: Landscape view of thin layers of tan and brown sedimentary rocks with a thick layer of tan to brown rock on top, featuring a large hole in the rock that forms an arch.

Figure 7.46: Cross-section showing horizontal strata on the left which then steeply slopes toward the right and becomes flat again; three different rock strata with unique lithology are being deposited at the same time in nearby geographic areas, noted by a thick red line that goes through the layers.

Figure 7.47: Two cross sectional diagrams; the top diagram shows onlap with layers of sediments being deposited on top of each other, with each successive upper layer being deposited toward inland; there is an arrow pointing toward the right-hand side labeled transgression; the bottom diagram shows offlap with layers of sediments being deposited on top of each other, with each successive upper layer being deposited toward the ocean; there is an arrow pointing toward the left-hand side labeled regression.

Figure 7.48: Diagram of part of the geologic time scale, from the Ediacaran through the Quaternary, with a vertical age axis from over 541 to 0 million years; to the right are various index fossils with bars that extend partially or fully through the time scale.

Figure 7.49: Microscopic view of three shiny white oval-shaped shells; a scale bar labeled 500 micrometers is at the lower right.

Figure 7.50: Black and white photos of fourteen teeth-like conodont fossils; the fossils are separated into three groups, each with slightly different morphology.

Figure 7.51: Artist's rendering of what a conodont might have looked like, an eel-like creature with large eyes and an apparatus of conodonts as mouthparts.

Figure 7.52: From oldest to newest time divisions: Hadean, archean, proterozoic, paleozoic, mesozoic, cenozoic. 4550 Ma: formation of the earth. 4527 Ma: formation of the moon.4000 Ma: end of the late heavy bombardment; first life. 3200 Ma: earliest start of photosynthesis. 2300 Ma: atmosphere becomes oxygen-rich; first snowball earth. 750-635 Ma: two snowball earths. 530 Ma: cambrian explosion. 380 Ma: first vertebrate land animals. 230-66 Ma: Non-avian dinosaurs. 2 Ma: first hominins.

Figure 7.53: Precambrian eon is made up of haydean, archean, and proterozoic eons. Phanerozoic eon is made up of paleozoic (permian, pennsylvanian, mississippian, devonian, silurian, ordovician, cambrian periods), mesozoic (cretaceous, jurassic, triassic periods), and cenozoic eras (quaternary and tertiary periods).

Figure 7.54: Diagram of the geologic time scale, from the Periods Precambrian through the Quaternary, with a vertical age axis from 4600 to 0 million years; to the right are various index fossils with bars that extend partially or fully through the time scale.

8. EARTH HISTORY

Learning Objectives

By the end of this chapter, students should be able to:

- Describe the turbulent beginning of Earth during the Hadean and Archean Eons.
- Identify the transition to modern atmosphere, plate tectonics, and evolution that occurred in the Proterozoic Eon.
- Describe the Paleozoic evolution and extinction of invertebrates with hard parts, fish, amphibians, reptiles, tetrapods, and land plants, in addition to the tectonics and sedimentation associated with the supercontinent Pangea.
- Describe the Mesozoic evolution and extinction of birds, dinosaurs, and mammals, in addition to the tectonics and sedimentation associated with the breakup of Pangea.
- Describe the Cenozoic evolution of mammals and birds, the paleoclimate, and the tectonics that shaped the modern world.

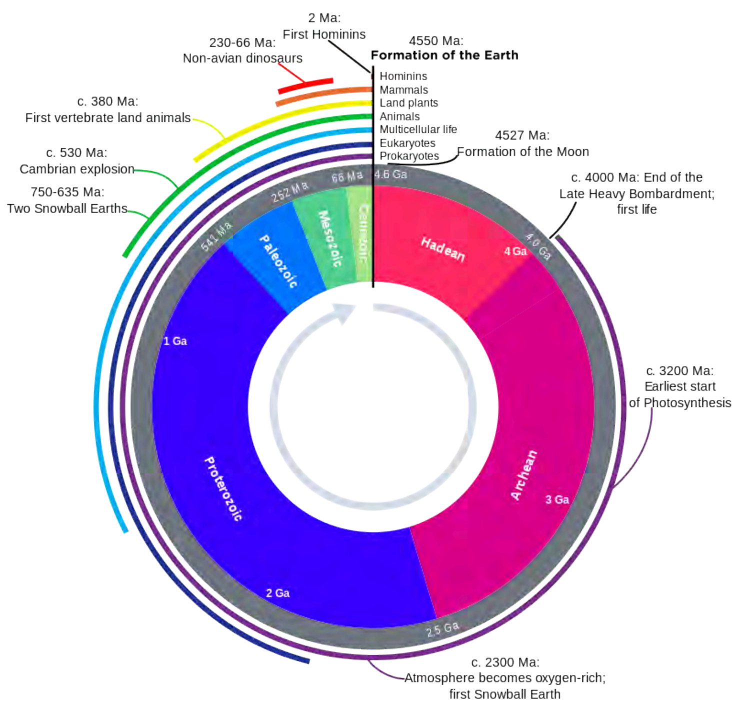

Figure 8.1: Geologic time on Earth, represented circularly, showing the individual time divisions and important events. Ga = billion years ago, Ma = million years ago. [Figure description available at the end of the chapter](#).

Entire courses and careers have been based on the wide-ranging topics covering Earth's history. Throughout the long history of Earth, change has been the norm. Looking back in time, an untrained eye would see many unfamiliar life forms and terrains. The main topics studied in Earth history are paleogeography, paleontology, paleoecology, and paleoclimatology—respectively, past landscapes, past organisms, past ecosystems, and past environments. This chapter will cover briefly the origin of the universe and the 4.6-billion-year history of Earth. This Earth history will focus on the major physical and biological events in each eon and era.

8.1 Hadean Eon

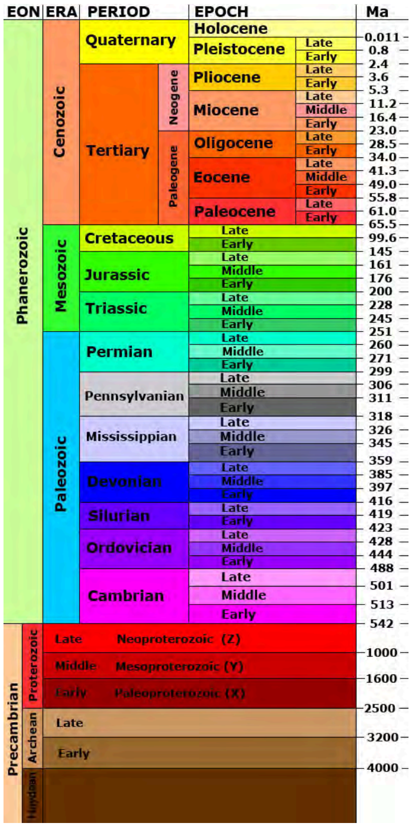

Figure 8.2: Geological timescale with ages shown. Figure description available at the end of the chapter.

Geoscientists use the geological timescale to assign relative age names to events and rocks, separating major events in Earth's history based on significant changes recorded in rocks and fossils. This section summarizes the most notable events of each major time interval. For a breakdown on how these time intervals are chosen and organized, see Chapter 7.

The **Hadean Eon**, named after the Greek god and ruler of the underworld Hades, is the oldest eon and dates from 4.5–4.0 billion years ago.

Figure 8.3: Artist's impression of the Earth in the Hadean. Figure description available at the end of the chapter.

This time represents Earth's earliest history, during which the planet was characterized by a partially molten surface, volcanism, and **asteroid** impacts. In addition to these impacts, several other mechanisms made the newly forming Earth incredibly hot, including gravitational compression and radioactive decay. Most of this initial heat still exists inside the Earth. The Hadean was originally defined as the birth of the planet occurring 4.0 billion years ago and preceding the existence of many rocks and life forms. However, geologists have dated minerals at 4.4 billion years, with evidence that liquid water was present. There is possibly even evidence of life existing over 4.0 billion years ago. However, the most reliable record for early life, the microfossil record, starts at 3.5 billion years ago.

8.1.1 Origin of Earth's Crust

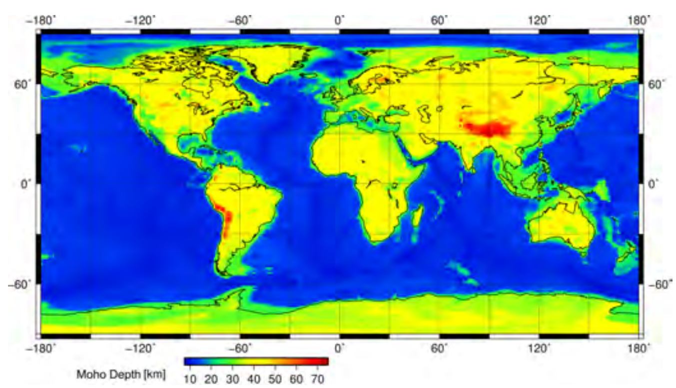

Figure 8.4: The global map of the depth of the Moho. Figure description available at the end of the chapter.

As Earth cooled from its molten state, minerals started to crystallize and settle, resulting in a separation of minerals based on density and the creation of the crust, mantle, and core. The earliest Earth was chiefly molten material and would have been rounded by gravitational forces, causing it to resemble a ball of lava floating in space. As the outer part of the Earth slowly cooled, the high melting-point minerals (see Bowen's reaction series in Chapter 4) formed solid slabs of early crust. These slabs were probably unstable and easily reabsorbed into the liquid magma until the Earth cooled enough to allow numerous larger fragments to form a thin, primitive crust. Scientists generally assume this crust was oceanic and mafic in composition and that it was littered with impacts, much like the Moon's current crust. There is still some debate over when plate tectonics started, which would have led to the formation of continental and felsic crust. Regardless of this, as Earth cooled and solidified, less-dense felsic minerals floated to the surface of the Earth to form the crust, while the denser mafic and ultramafic materials sank to form the mantle and the highest-density iron and nickel sank into the core. This differentiated the Earth from a homogeneous planet, making it heterogeneous, with layers of felsic crust, mafic crust, ultramafic mantle, and iron and nickel core.

8.1.2 Origin of the Moon

Figure 8.5: Far side of the Moon. Figure description available at the end of the chapter.

Several unique features of Earth's Moon have prompted scientists to develop the current hypothesis about its formation. The Earth and Moon are tidally locked, meaning that, as the Moon orbits, one side always faces the Earth and the opposite side is not visible to us. Most importantly, the chemical compositions of the Earth and Moon show nearly identical isotope ratios and volatile content. Apollo missions returned from the Moon with rocks that allowed scientists to conduct very precise comparisons between Moon and Earth rocks. Other bodies in the Solar System and meteorites do not share the same degree of similarity and show much higher variability. If the Moon and Earth formed together, this would explain why they are so chemically similar.

Figure 8.6: Artist's concept of the giant impact from a Mars-sized object that could have formed the moon. Figure description available at the end of the chapter.

Many ideas have been proposed for the origin of the Moon. The Moon could have been captured from another part of the Solar System and formed in place together with the Earth, or the Moon could have been ripped out of the early Earth. No proposed explanations have been able to account for all the evidence. The currently prevailing hypothesis is the **giant impact hypothesis**, which proposes a body about half of Earth's size must have shared at least parts of Earth's orbit and collided with it, resulting in a violent mixing and scattering of material from both objects. Both bodies would be composed of a combination of materials, with more of the lower-density splatter coalescing into the Moon. This may explain why the Earth has a higher density and thicker core than the Moon.

Video 8.1: Evolution of the Moon

Access this YouTube video by scanning the QR code. ["NASA | Evolution of the Moon" by NASA Goddard | https://www.youtube.com/watch?v=UIKmSQqp8wY]

8.1.3 Origin of Earth's Water

Explanations for the origin of Earth's water include volcanic outgassing, comets, and meteorites. The volcanic outgassing hypothesis states that Earth's water originated from inside the planet and emerged via tectonic processes as vapor associated with volcanic eruptions. Since all volcanic eruptions contain some water vapor, at times more than 1% of the volume, these alone could have created Earth's surface water. Another likely source of water was space. Comets are a mixture of dust and ice, with some or most of that ice being frozen water. Seemingly dry meteors can contain small but measurable amounts of water, usually trapped in their mineral structures. During heavy bombardment periods later in Earth's history, its cooled surface was pummeled by comets and meteorites, which could be why so much water exists above ground. There isn't a definitive answer for what process resulted in ocean water. Earth's water isotopically matches water found in meteorites much better than water from comets. However, it is hard to know if Earth processes could have changed the water's isotopic signature over the last four-plus billion years. It is possible that all three sources contributed to the origin of Earth's water.

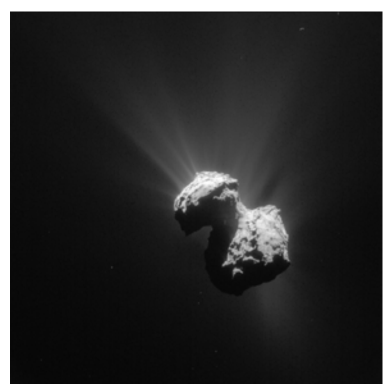

Figure 8.7: Water vapor leaves comet 67P/Churyumov–Gerasimenko. Figure description available at the end of the chapter.

Take this quiz to check your comprehension of this section.

Access the quiz for Section 8.1 by scanning the QR code.

8.2 Archean Eon

The **Archean Eon**, which lasted from 4.0–2.5 billion years ago, is named after the Greek word for beginning. This eon represents the beginning of the rock record. Although there is current evidence that rocks and minerals existed during the Hadean Eon, the Archean has a much more robust rock and fossil record.

Figure 8.8: Artist's impression of the Archean. Figure description available at the end of the chapter.

8.2.1 Late Heavy Bombardment

Figure 8.9: 2015 image from NASA's New Horizons probe of Pluto. The lack of impacts found on the Tombaugh Regio (the heart-shaped plain, lower right) has been inferred to be younger than the Late Heavy Bombardment and the surrounding surface due to its lack of impacts. Figure description available at the end of the chapter.

Objects were chaotically flying around at the start of the Solar System, building the **planets** and **moons**. There is evidence that after the planets formed about 4.1–3.8 billion years ago, a second large spike of asteroids and comets impacted the Earth and Moon in an event called the **Late Heavy Bombardment**. Meteorites and comets in stable or semi-stable orbits became unstable and started impacting objects throughout the Solar System; as this is when the Moon received most of its craters, this event is also known as the lunar cataclysm. During the Late Heavy Bombardment, the Earth, Moon, and all planets in the Solar System were pummeled by material from the Asteroid Belt and Kuiper Belt. Evidence of this bombardment was found within samples collected from the Moon.

It is universally accepted that the Solar System experienced extensive asteroid and comet bombardment at its start; however, some other process must have caused the second increase in impacts hundreds of millions of years later. A leading theory blames gravitational resonance between Jupiter and Saturn for disturbing orbits within the Asteroid and Kuiper Belts, a notion based on a similar process observed in the Eta Corvi star system.

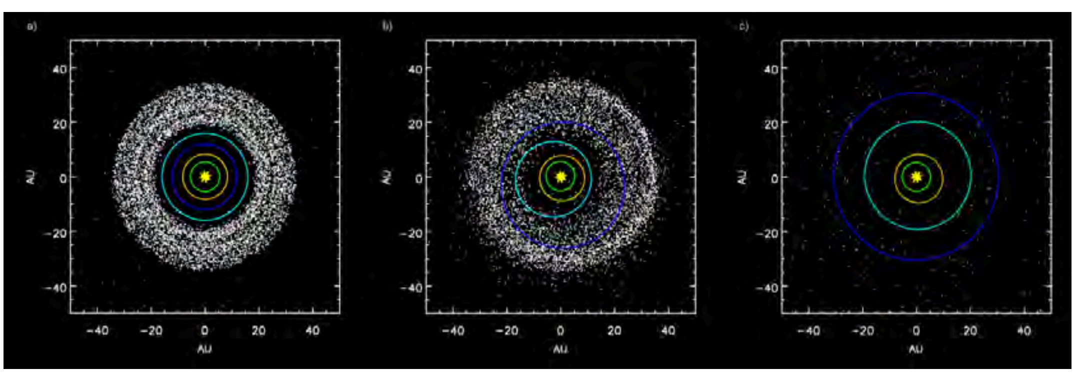

Figure 8.10: Simulation of before, during, and after the Late Heavy Bombardment. Figure description available at the end of the chapter.

8.2.2 Origin of the Continents

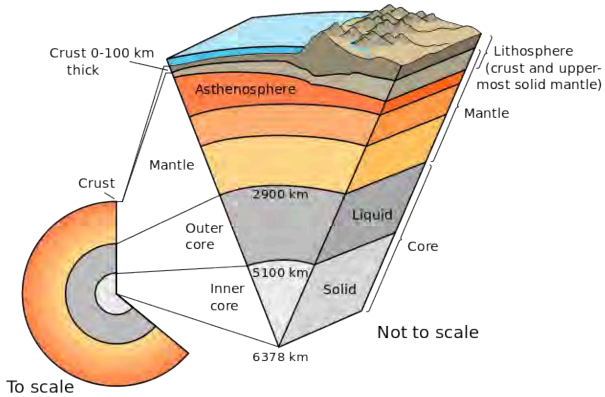

Figure 8.11: The layers of the Earth. Physical layers include lithosphere and asthenosphere; chemical layers are crust, mantle, and core. Figure description available at the end of the chapter.

Continents are a crucial part of plate tectonics working as they do currently. However, the easiest way to create continental material is via **assimilation** and differentiation of existing continents (see Chapter 4). This chicken-and-egg quandary over how continents were made in the first place is not easily answered because of the great age of continental material and how much evidence has been lost during tectonics and erosion. While the timing and specific processes are still debated, volcanic action must have brought the first continental material to the Earth's surface during the Hadean, 4.4 billion years ago. This model does not solve the problem of continent formation, since **magmatic differentiation** seems to need thicker crust. Nevertheless, the continents formed by some incremental process during the early history of Earth. The leading idea is that density differences allowed lighter felsic materials to float upward and heavier ultramafic materials and metallic iron to sink. These density differences led to the layering of the Earth, adding the layers that are now detected by seismic studies. Early protocontinents accumulated felsic materials as developing plate-tectonic processes brought lighter material from the mantle to the surface.

The first solid evidence of modern plate tectonics is found at the end of the Archean, indicating that at least some continental lithosphere must have been in place. This evidence does not necessarily mark the starting point of plate tectonics; remnants of earlier tectonic activity could have been erased by the rock cycle.

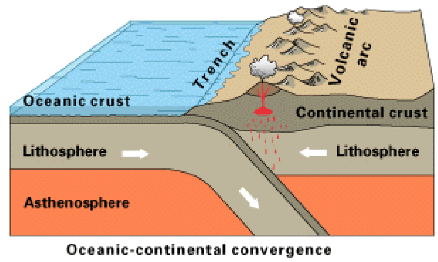

Figure 8.12: Subduction of an oceanic plate beneath another oceanic plate, forming a trench and an island arc. Several island arcs might combine and eventually evolve into a continent. Figure description available at the end of the chapter.

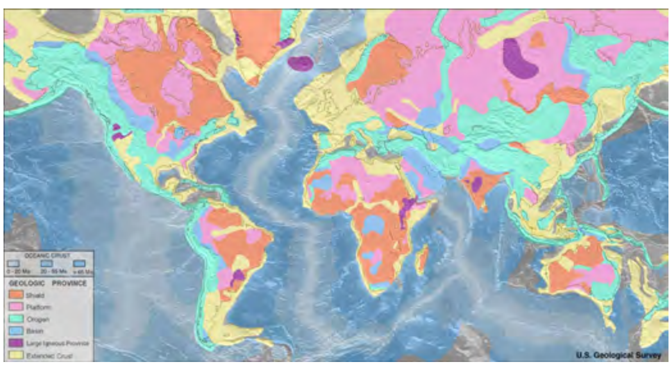

Figure 8.13: Geologic provinces, with the shield (orange) and platform (pink) comprising the craton, the stable interior of continents. Figure description available at the end of the chapter.

The stable interiors of the current continents are called cratons and were mostly formed in the Archean Eon. A craton has two main parts: the **shield**, which is crystalline basement rock near the surface, and the **platform** made of sedimentary rocks covering the shield. Most cratons have remained relatively unchanged, with most tectonic activity having occurred around cratons instead of within them. Whether they were created by plate tectonics or another process, Archean continents gave rise to the Proterozoic continents that now dominate our planet.

The general guidelines as to what constitutes a continent and differentiates oceanic from continental crust are under some debate. At passive margins, continental crust grades into oceanic crust at passive margins, making a distinction difficult. Even island-arc and hotspot material can seem more closely related to continental crust than oceanic. Continents usually have a craton in the middle with felsic igneous rocks. There is evidence that submerged masses like Zealandia, which includes present-day New Zealand, would be considered a continent. Continental crust that does not contain a craton is called a continental fragment, such as the island of Madagascar off the east coast of Africa.

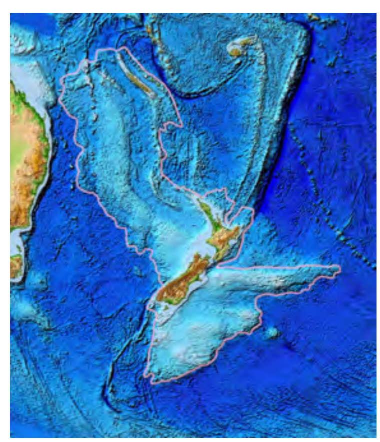

Figure 8.14: The continent of Zealandia. Figure description available at the end of the chapter.

8.2.3 First Life on Earth

Figure 8.15: Fossils of microbial mats from Sweden. Figure description available at the end of the chapter.

Life most likely started during the late Hadean or early Archean Eons. The earliest evidence of life are chemical signatures, microscopic filaments, and **microbial** mats. Carbon found in 4.1-billion-year-old zircon grains have a chemical signature suggesting an organic origin. Other evidence of early life are 3.8–4.3 billion-year-old microscopic filaments from a hydrothermal vent deposit in Quebec, Canada. While the evidence of chemical and microscopic filaments is not as robust as fossils, there is significant fossil evidence for life at 3.5 billion years ago. These first well-preserved fossils are photosynthetic microbial mats called **stromatolites**, found in Australia.

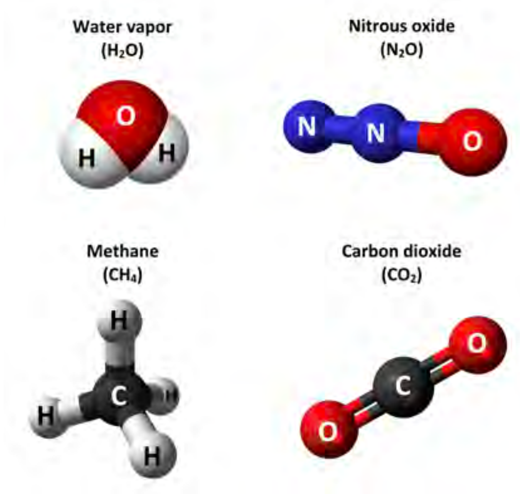

Figure 8.16: Greenhouse gases were more common in Earth's early atmosphere. Figure description available at the end of the chapter.

Although the origin of life on Earth is unknown, hypotheses include a chemical origin in the early atmosphere and ocean, deep-sea hydrothermal vents, and delivery to Earth by comets or other objects. One hypothesis is that life arose from the chemical environment of the Earth's early atmosphere and oceans, which was very different than today. The oxygen-free atmosphere produced a reducing environment with abundant methane, carbon dioxide, sulfur, and nitrogen compounds. This is what the atmosphere is like on other bodies in the Solar System. In the famous Miller-Urey experiment, researchers simulated early Earth's atmosphere and lightning within a sealed vessel. After igniting sparks within the vessel, they discovered the formation of amino acids, the fundamental building blocks of proteins. In 1977, when scientists discovered an isolated ecosystem around hydrothermal vents on a deep-sea mid-ocean ridge (see Chapter 4), it opened the door for another explanation of the origin of life. The hydrothermal vents have a unique ecosystem of life forms that use chemosynthesis as the foundation of the food chain instead of photosynthesis. The ecosystem derives its energy from hot chemical-rich waters pouring out of underground towers. This suggests that life could have started on the deep ocean floor and derived energy from the heat of the Earth's interior via chemosynthesis. Scientists have since expanded the search for life to more unconventional places, like Jupiter's icy moon Europa.

Video 8.2: Animation of the original Miller-Urey 1959 experiment that simulated the early atmosphere and created amino acids from simple elements and compounds

Access this YouTube video by scanning the QR code. ["Miller-Urey experiment" by Forsyth Tech CTLE | https://www.youtube.com/watch?v=qyt6IlcOJLo]

Another possibility is that life or its building blocks came to Earth from space, carried aboard comets or other objects. Amino acids, for example, have been found within comets and meteorites. This intriguing possibility also implies a high likelihood of life existing elsewhere in the cosmos.

Take this quiz to check your comprehension of this section.

Access the quiz for Section 8.2 by scanning the QR code.

8.3 Proterozoic Eon

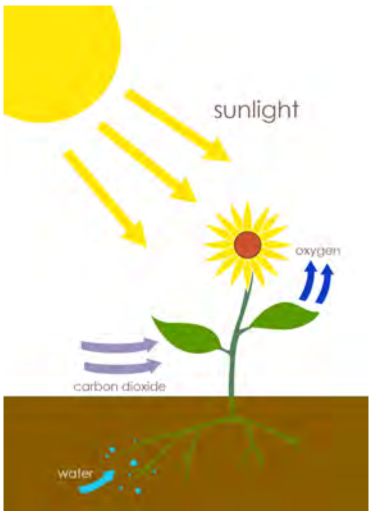

Figure 8.17: Diagram showing the main products and reactants in photosynthesis. The one product that is not shown is sugar, which is the chemical energy that goes into constructing the plant, and the energy that is stored in the plant, which is used later by the plant or by animals that consume the plant. Figure description available at the end of the chapter.

The **Proterozoic ("earlier life") Eon** comes after the Archean Eon and lasted from 2.5 billion years ago to 541 million years ago. During this time, most of the central parts of the continents had formed and plate tectonic processes had started. Photosynthesis by **microbial** organisms, such as single-celled cyanobacteria, had been slowly adding oxygen to the oceans. As cyanobacteria evolved into multicellular organisms, they completely transformed the oceans and later the atmosphere by adding massive amounts of free oxygen gas (O_2) and initiated what is called the **Great Oxygenation Event** (GOE). This drastic environmental change decimated the anaerobic bacteria, which could not survive in the presence of free oxygen. On the other hand, aerobic organisms could thrive in ways they could not earlier.

An oxygenated world also changed the chemistry of the planet in significant ways. For example, iron remained in solution in the nonoxygenated environment of the earlier Archean Eon. In chemistry, this is known as a reducing environment. Once the environment was oxygenated, iron combined with free oxygen to form solid precipitates of iron oxide, such as the minerals hematite or magnetite. These precipitates accumulated into large mineral deposits with red chert known as banded-iron formations, which are dated at about two billion years.

Figure 8.18: This sample of banded iron formation displays alternating bands of iron-rich and silica-rich mud, formed as oxygen combined with dissolved iron. Figure description available at the end of the chapter.

The formation of iron oxide minerals and red chert (see Figure 8.18) in the oceans lasted a long time and prevented oxygen levels from increasing significantly since precipitation took the oxygen out of the water and deposited it into the rock strata. As oxygen continued to be produced and mineral precipitation leveled off, dissolved oxygen gas eventually saturated the oceans and started bubbling out into the atmosphere. Oxygenation of the atmosphere is the single biggest event that distinguishes the Archean and Proterozoic environments. In addition to changing mineral and ocean chemistry, the GOE is also identified as triggering Earth's first glaciation event around 2.1 billion years ago, the Huron glaciation. Free oxygen reacted with methane in the atmosphere to produce carbon dioxide. Carbon dioxide and methane are called greenhouse gases because they trap heat within the Earth's atmosphere, like the insulated glass of a greenhouse. Methane is a more effective insulator than carbon dioxide, so as the proportion of carbon dioxide in the atmosphere increased, the greenhouse effect decreased and the planet cooled.

8.3.1 Rodinia

By the Proterozoic Eon, lithospheric plates had formed and were moving according to plate tectonic forces that were similar to current times. As the moving plates collided, the ocean basins closed to form a supercontinent called **Rodinia**. The supercontinent formed about one billion years ago and broke up about 750 to 600 million years ago, at the end of the Proterozoic. One of the resulting fragments was a continental mass called **Laurentia** that would later become North America. Geologists have reconstructed Rodinia by matching and aligning ancient mountain chains, assembling the pieces like a jigsaw puzzle and using paleomagnetics to orient to magnetic north.

The disagreements over these complex reconstructions is exemplified by geologists proposing at least six different models for the breakup of Rodinia to create Australia, Antarctica, parts of China, the Tarim craton north of the Himalayas, Siberia, or the Kalahari craton of Eastern Africa. This breakup created lots of shallow-water, biologically favorable environments that fostered the evolutionary breakthroughs marking the start of the next eon, the Phanerozoic.

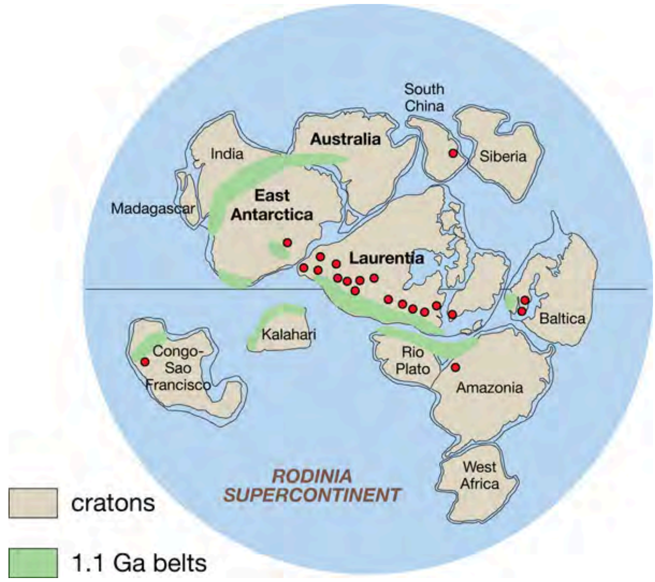

Figure 8.19: One possible reconstruction of Rodinia 1.1 billion years ago. [Figure description available at the end of the chapter].

8.3.2 Life Evolves

Figure 8.20: Modern cyanobacteria (as stromatolites) in Shark Bay, Australia. [Figure description available at the end of the chapter].

Life in the Archean and before is poorly documented in the fossil record. Based on chemical evidence and evolutionary theory, scientists propose this life would have been single-celled photosynthetic organisms, such as the cyanobacteria that created stromatolites. Cyanobacteria produced free oxygen in the atmosphere through photosynthesis. Cyanobacteria, archaea, and bacteria are **prokaryotes**—primitive organisms made of single cells that lack cell nuclei and other organelles.

A large evolutionary step occurred during the Proterozoic Eon with the appearance of **eukaryotes** around 2.1 to 1.6 billion years ago. Eukaryotic cells are more complex, having nuclei and organelles. The nuclear DNA is capable of more complex replication and regulation than that of prokaryotic cells. The organelles include mitochondria for producing energy and chloroplasts for photosynthesis. The eukaryote branch in the tree of life gave rise to fungi, plants, and animals.

Figure 8.21: Fossil stromatolites in Saratoga Springs, New York. [Figure description available at the end of the chapter].

Another important event in Earth's biological history occurred about 1.2 billion years ago when eukaryotes began sexual reproduction. Sharing genetic material from two reproducing individuals, male and female, greatly increased genetic variability in their offspring. This genetic mixing accelerated evolutionary change, contributing to more complexity among individual organisms and within ecosystems (see Chapter 7).

Proterozoic land surfaces were barren of plants and animals, and geologic processes actively shaped the environment differently because land surfaces were not protected by leafy and woody vegetation. For example, rain and rivers would have caused erosion at much higher rates on land surfaces devoid of plants. This resulted in thick accumulations of pure quartz sandstone from the Proterozoic Eon, such as the extensive quartzite formations in the core of the Uinta Mountains in Utah.

Fauna during the Ediacaran Period, 635.5 to 541 million years ago, are known as the **Ediacaran fauna** and offer a first glimpse at the diversity of ecosystems that evolved near the end of the Proterozoic. These soft-bodied organisms were among the first multicellular life forms and were probably wormlike or similar to jellyfish. Ediacaran fauna did not have hard parts like shells and were not well preserved in the rock records. However, studies suggest they were widespread in the Earth's oceans. Scientists still debate how many species were evolutionary dead-ends that became extinct and how many were ancestors of modern groupings. The transition of soft-bodied Ediacaran life forms to life forms with hard body parts occurred at the end of the Proterozoic and beginning of the Phanerozoic Eons. This evolutionary explosion of biological diversity made a dramatic difference in scientists' ability to understand the history of life on Earth.

Figure 8.22: Dickinsonia, a typical Ediacaran fossil. Figure description available at the end of the chapter.

Take this quiz to check your comprehension of this section.

Access the quiz for Section 8.3 by scanning the QR code.

8.4 Phanerozoic Eon: Paleozoic Era

Figure 8.23: The trilobite had a hard exoskeleton and is an early arthropod, the same group that includes modern insects, crustaceans, and arachnids. Figure description available at the end of the chapter.

The **Phanerozoic Eon** is the most recent, spanning 541 million years ago to today. Its name means "visible life" because the Phanerozoic rock record is marked by an abundance of fossils. Phanerozoic organisms had hard body parts like claws, scales, shells, and bones that were more easily preserved as fossils. Rocks from the older Precambrian time are less commonly found and rarely include fossils because those organisms had soft body parts. Phanerozoic rocks are younger, more common, and contain the majority of extant fossils. The study of rocks from this eon yields much greater detail. The Phanerozoic is subdivided into three eras; from oldest to youngest, they are **Paleozoic** ("ancient life"), **Mesozoic** ("middle life"), and **Cenozoic** ("recent life"), and the remaining three sections in this chapter cover three important eras.

Life in the early Paleozoic Era was dominated by marine organisms, but by the middle of the era, plants and animals evolved to live and reproduce on land. Fish evolved jaws, and fins evolved into jointed limbs. The development of lungs allowed animals to emerge from the sea and become the first air-breathing tetrapods (four-legged animals), such as amphibians. From amphibians evolved reptiles with the amniotic egg. From reptiles evolved an early ancestor to birds and mammals, and their scales became feathers and fur. Near the end of the Paleozoic Era, the **Carboniferous** Period had some of the most extensive forests in Earth's history. Their fossilized remains became the **coal** that powered the Industrial Revolution.

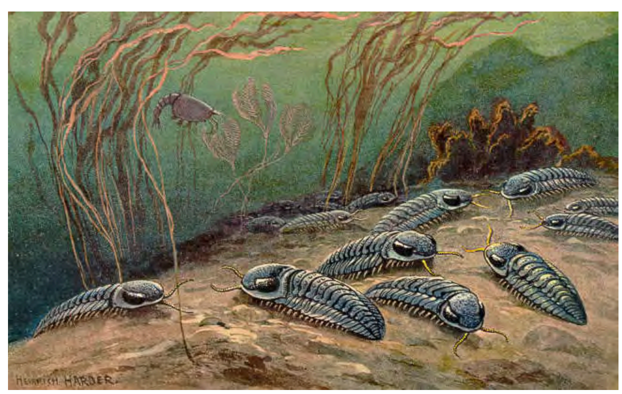

Figure 8.24: Trilobites, by Heinrich Harder, 1916. Figure description available at the end of the chapter.

8.4.1 Paleozoic Tectonics and Paleogeography

Figure 8.25: Laurentia, which makes up the North American craton. [Figure description available at the end of the chapter](#).

During the Paleozoic Era, sea levels rose and fell four times. With each sea level rise, the majority of North America was covered by a shallow tropical ocean. Evidence of these submersions is found in the abundant marine sedimentary rocks such as limestone with fossils corals and ooids. Extensive sea level falls are documented by widespread unconformities. Today, the midcontinent has extensive marine sedimentary rocks from the Paleozoic and western North America has thick layers of marine limestone on block-faulted mountain ranges such as Mount Timpanogos near Provo, Utah.

Figure 8.26: A reconstruction of Pangea, showing approximate positions of modern continents. [Figure description available at the end of the chapter](#).

The assembly of the supercontinent Pangea, sometimes spelled Pangaea, was completed by the late Paleozoic Era. The name Pangea was originally coined by Alfred Wegener and means "all land." Pangea describes when all of the major continents were grouped together as one by a series of tectonic events including subduction island-arc accretion, continental collisions, and ocean-basin closures. In North America, these tectonic events occurred on the east coast and are known as the Taconic, Acadian, Caledonian, and Alleghanian orogenies. The Appalachian Mountains are the erosional remnants of these mountain-building events in North America. Surrounding Pangea was a global ocean basin known as the Panthalassa. Continued plate movement extended the ocean into Pangea, forming a large bay called the Tethys Sea that eventually divided the land mass into two smaller supercontinents, Laurasia and Gondwana. Laurasia consisted of Laurentia and Eurasia, and Gondwana consisted of the remaining continents of South America, Africa, India, Australia, and Antarctica.

Video 8.3: Animation of plate movement the last 3.3 billion years. Pangea occurs at the 4:40 mark.

Access this [YouTube video](#) by scanning the QR code. ["Continental Drift" by Algol | https://www.youtube.com/watch?v=ovT90wYrVk4]

While the east coast of North America was tectonically active during the Paleozoic Era, the west coast remained mostly inactive as a passive margin during the early Paleozoic. The western edge of the North American continent was near the present-day Nevada-Utah border and was an expansive, shallow continental shelf near the paleoequator. However, by the Devonian Period, the Antler orogeny started on the west coast and lasted until the Pennsylvanian Period. The Antler orogeny was a volcanic island arc that was accreted onto western North America, with the subduction direction away from North America. This created a mountain range on the west coast of North America called the Antler highlands and was the first part of building the land in the west that would eventually make most of the California, Oregon, and Washington states. By the late Paleozoic, the Sonoma orogeny began on the west coast and was another collision of an island arc. The Sonoma orogeny marks the change in subduction direction to be toward North America with a volcanic arc along the entire west coast of North America by the late Paleozoic to early Mesozoic Eras.

By the end of the Paleozoic Era, the east coast of North America had a very high mountain range due to continental collision and the creation of Pangea. The west coast of North America had smaller and isolated volcanic highlands associated with island arc accretion. During the Mesozoic Era, the size of the mountains on either side of North America would flip, with the west coast being a more tectonically active plate boundary and the east coast changing into a passive margin after the breakup of Pangea.

8.4.2 Paleozoic Evolution

The beginning of the Paleozoic Era is marked by the first appearance of hard body parts like shells, spikes, teeth, and scales; it is also marked by the appearance in the rock record of most animal phyla known today. That is, most basic animal body plans appeared in the rock record during the **Cambrian** Period. This sudden appearance of biological diversity is called the **Cambrian explosion**. Scientists debate whether this sudden appearance is more from a rapid evolutionary diversification as a result of a warmer climate following the late Proterozoic glacial environments, from the better preservation and fossilization of hard parts, or due to artifacts of a more complete and recent rock record. For example, fauna may have been diverse during the Ediacaran Period, setting the stage for the Cambrian explosion, but they lacked hard body parts and would have left few fossils behind. Regardless, the Cambrian Period 541–485 million years ago marked the appearance of most animal phyla.

Figure 8.27: Anomalocaris reconstruction by the MUSE science museum in Italy. Figure description available at the end of the chapter.

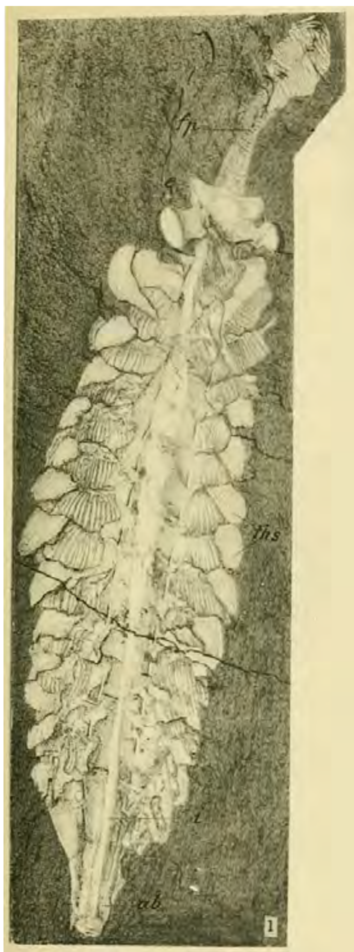

Figure 8.28: Original plate from Walcott's 1912 description of Opabinia, with labels: *fp* = frontal appendage, *e* = eye, *ths* = thoracic somites, *i* = intestine, *ab* = abdominal segment. Figure description available at the end of the chapter.

One of the best fossil sites for the Cambrian explosion was discovered in 1909 by Charles Walcott (1850–1927) in the Burgess Shale in Western Canada. The Burgess Shale is a **Lagerstätte**, a site of exceptional fossil preservation that includes impressions of soft body parts. This discovery allowed scientists to study Cambrian animals in immense detail because soft body parts are not normally preserved and fossilized. Other Lagerstätte sites of similar age in China and Utah have allowed scientist to form a detailed picture of Cambrian biodiversity. The biggest mystery surrounds animals that do not fit existing lineages and are unique to that time. This includes many famous fossilized creatures: the first compound-eyed trilobites; *Wiwaxia*, a creature covered in spiny plates; *Hallucigenia*, a walking worm with spikes; *Opabinia*, a five-eyed arthropod with a grappling claw; and *Anomalocaris*, the alpha predator of its time, complete with grasping appendages and circular mouth with sharp plates. Most notably appearing during the Cambrian is an important ancestor to humans. A segmented worm called *Pikaia* is thought to be the earliest ancestor of the **Chordata** phylum that includes vertebrates, animals with backbones.

Figure 8.29: A modern coral reef. Figure description available at the end of the chapter.

By the end of the Cambrian, mollusks, brachiopods, nautiloids, gastropods, graptolites, echinoderms, and trilobites covered the seafloor. Although most animal phyla appeared by the Cambrian, the biodiversity at the family, genus, and species levels was low until the **Ordovician** Period. During the Great Ordovician Biodiversification Event, vertebrates and invertebrates (animals without backbone) became more diverse and complex at the family, genus, and species levels. The cause of the rapid speciation event is still debated, but some likely causes are a combination of warm temperatures, expansive continental shelves near the equator, and more volcanism along the mid-ocean ridges. Some have shown evidence that an asteroid breakup event and consequent heavy meteorite impacts correlate with this diversification event. The additional volcanism added nutrients to ocean water, helping support a robust ecosystem. Many life forms and ecosystems that would be recognizable in current times appeared at this time. Mollusks, corals, and arthropods in particular multiplied to dominate the oceans.

Figure 8.30: Guadalupe National Park is made of a giant fossil reef. Figure description available at the end of the chapter.

One important evolutionary advancement during the Ordovician Period was reef-building organisms, mostly colonial coral. Corals took advantage of the ocean chemistry, using calcite to build large structures that resembled modern reefs like the Great Barrier Reef off the coast of Australia. These reefs housed thriving ecosystems of organisms that swam around, hid in, and crawled over them. Reefs are important to paleontologists because of their preservation potential, massive size, and in-place ecosystems. Few other fossils offer more diversity and complexity than reef assemblages.

According to evidence from glacial deposits, a small ice age caused sea levels to drop and led to a major mass extinction by the end of the Ordovician. This is the earliest of five mass extinction events documented in the fossil record. During this mass extinction, an unusually large number of species abruptly disappear in the fossil record (see video below).

Video 8.4: Three-minute video describing mass extinctions and how they are defined

Access this YouTube video by scanning the QR code. ["How Many Mass Extinctions Have There Been?" by MinuteEarth | https://www.youtube.com/watch?v=aO9mOAKXvJs]

Life bounced back during the **Silurian** Period. The period's major evolutionary event was the development of jaws from the forward pair of gill arches in bony fishes and sharks. Hinged jaws allowed fish to exploit new food sources and ecological niches. This period also included the introduction of armored fishes, known as the placoderms. In addition to fish and jaws, Silurian rocks provide the first evidence of terrestrial, or land-dwelling, plants and animals. The first vascular plant, *Cooksonia,* had woody tissues, pores for gas exchange, and veins for water and food transport. Insects, spiders, scorpions, and crustaceans began to inhabit moist, freshwater terrestrial environments.

Figure 8.31: The placoderm Bothriolepis panderi from the Devonian in Russia. Figure description available at the end of the chapter.

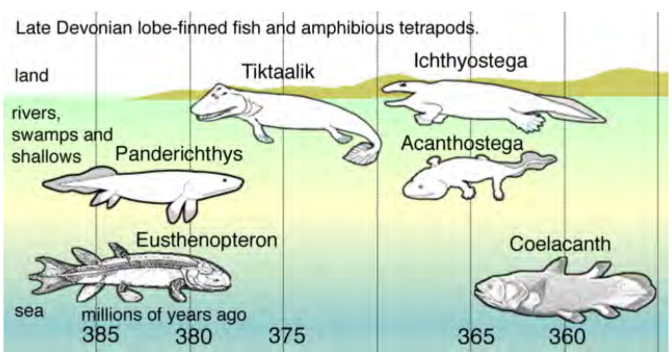

Figure 8.32: Several different types of fish and amphibians that led to walking on land. Figure description available at the end of the chapter.

The **Devonian** Period is called the Age of Fishes due to the rise in plated, jawed, and lobe-finned fishes. The lobe-finned fishes, which were related to the modern lungfish and coelacanth, are important for their eventual evolution into tetrapods—four-limbed vertebrate animals that can walk on land. The first lobe-finned land-walking fish, named *Tiktaalik*, appeared about 385 million years ago and serves as a transition fossil between fish and early tetrapods. Though *Tiktaalik* was clearly a fish, it had some tetrapod structures as well. Several fossils from the Devonian are more tetrapodlike than fishlike, but these weren't fully terrestrial. The first fully terrestrial tetrapod arrived in the Mississippian (early Carboniferous) Period. By the Mississippian Period, tetrapods had evolved into two main groups, amphibians and amniotes, from a common tetrapod ancestor. The amphibians were able to breathe air and live on land but still needed water to nurture their soft eggs. The first reptile (an amniote) could live and reproduce entirely on land with hard-shelled eggs that wouldn't dry out.

Land plants had also evolved into the first trees and forests. Toward the end of the Devonian, another mass extinction event occurred. This extinction, while severe, is the least temporally defined, with wide variations in the timings of the event or events. Reef-building organisms were the hardest hit, leading to dramatic changes in marine ecosystems.

The next time period is called the **Carboniferous** (North American geologists have subdivided this into the Mississippian and Pennsylvanian Periods). This period saw the highest levels of oxygen ever known, with forests (e.g., ferns, club mosses) and swamps dominating the landscape. This helped cause the largest arthropods ever, like the millipede *Arthropleura*, at 2.5 meters (6.4 feet) long! It also saw the rise of a new group of animals, the reptiles. The evolutionary advantage that reptiles have over amphibians is the amniote egg (egg with a protective shell), which allows them to rely on nonaquatic environments for reproduction. This widened the terrestrial reach of reptiles compared to amphibians. This period's booming life, especially plant life, created cooling temperatures as carbon dioxide was removed from the atmosphere. By the middle Carboniferous, these cooler temperatures led to an ice age (called the Karoo glaciation) and less-productive forests. The reptiles fared much better than the amphibians, leading to their diversification. This glacial event lasted into the early Permian.

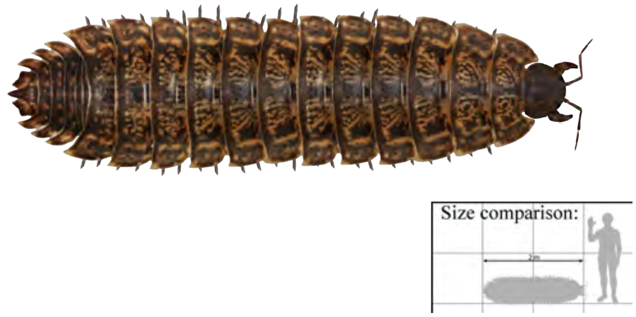

Figure 8.33: A reconstruction of the giant arthropod (insects and their relatives) Arthropleura. Figure description available at the end of the chapter.

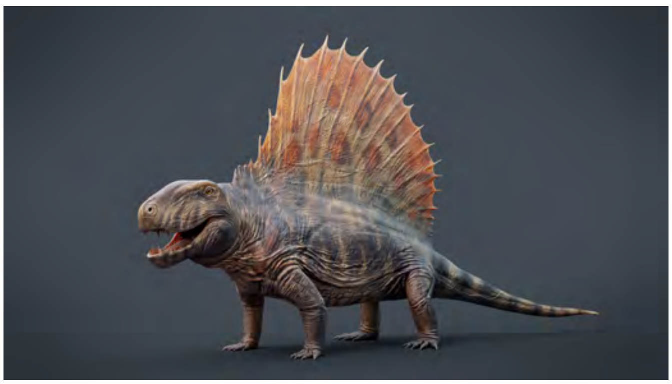

Figure 8.34: Reconstruction of Dimetrodon. Figure description available at the end of the chapter.

By the **Permian**, the now-assembled Pangea supercontinent led to a dryer climate and even more diversification and domination by the reptiles. The groups that developed in this warm climate eventually radiated into dinosaurs. Another group, known as the synapsids, eventually evolved into mammals. Synapsids, including the famous sail-backed *Dimetrodon,* are commonly confused with dinosaurs. Pelycosaurs (of the Pennsylvanian to early Permian, like *Dimetrodon)* are the first group of synapsids that exhibit the beginnings of mammalian characteristics, such as well-differentiated dentition: incisors, highly developed canines in lower and upper jaws, and cheek teeth, premolars, and molars. Starting in the late Permian, a second group of synapsids, called the therapsids (or mammal-like reptiles) evolve and become the ancestors to mammals.

Permian Mass Extinction

The end of the Paleozoic Era is marked by the largest mass extinction in Earth history. The Paleozoic Era had two smaller mass extinctions, but these were not as large as the **Permian Mass Extinction**, also known as the Permian-Triassic Extinction Event. It is estimated that up to 96% of marine species and 70% of land-dwelling (terrestrial) vertebrates went extinct. Many famous organisms, like sea scorpions and trilobites were never seen again in the fossil record. What caused such a widespread extinction event? The exact cause is still debated, though the leading idea relates to extensive volcanism associated with the **Siberian Traps**, which are one of the largest deposits of flood basalts known on Earth, dating to the time of the extinction event. The eruption size is estimated at over three million cubic kilometers—approximately four million times larger than the famous 1980 Mount St. Helens eruption in Washington. The unusually large volcanic eruption would have contributed a large amount of toxic gases, aerosols, and greenhouse gases into the atmosphere. Further, some evidence suggests that the volcanism burned vast coal deposits, releasing methane (a greenhouse gas) into the atmosphere. As discussed in Chapter 15, greenhouse gases cause the climate to warm. This extensive addition of greenhouse gases from the Siberian Traps may have caused a runaway greenhouse effect that rapidly changed the climate, acidified the oceans, disrupted food chains, disrupted carbon cycling, and caused the largest mass extinction.

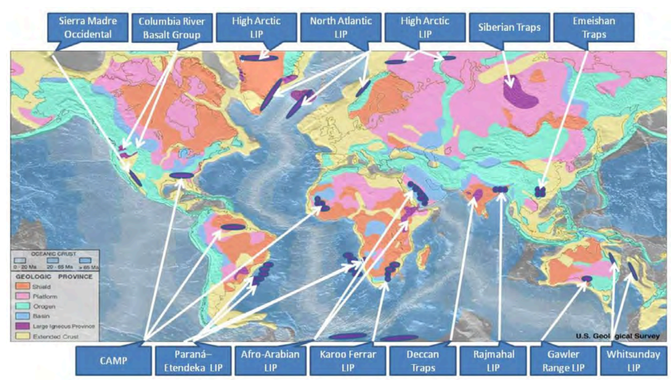

Figure 8.35: World map of flood basalts. Note the largest is the Siberian Traps. Figure description available at the end of the chapter.

Take this quiz to check your comprehension of this section.

Access the quiz for Section 8.4 by scanning the QR code.

8.5 Phanerozoic Eon: Mesozoic Era

Following the Permian Mass Extinction, the **Mesozoic** ("middle life") was from 252 million years ago to 66 million years ago. As Pangea started to break apart, mammals, birds, and flowering plants developed. The Mesozoic is probably best known as the Age of Reptiles, most notably, the dinosaurs.

Figure 8.36: Perhaps the greatest fossil ever found, a velociraptor attacked a protoceratops, and both were fossilized mid-sequence. Figure description available at the end of the chapter.

8.5.1 Mesozoic Tectonics and Paleogeography

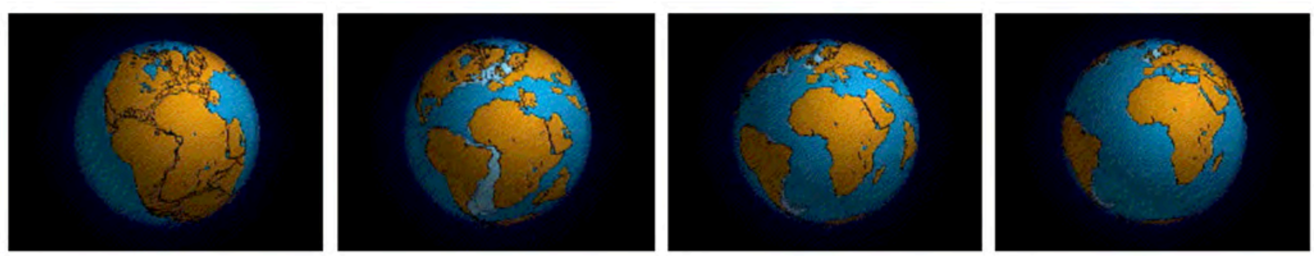

Figure 8.37: Animation showing Pangea breaking up. Figure description available at the end of the chapter.

Pangea started breaking up (in a region that would become eastern Canada and United States) around 210 million years ago in the Late Triassic. Clear evidence for this includes the age of the sediments in the Newark Supergroup rift basins and the Palisades sill of the eastern part of North America and the age of the Atlantic ocean floor. Due to seafloor spreading, the oldest rocks on the Atlantic's floor are along the coast of northern Africa and the east coast of North America, while the youngest are along the mid-ocean ridge.

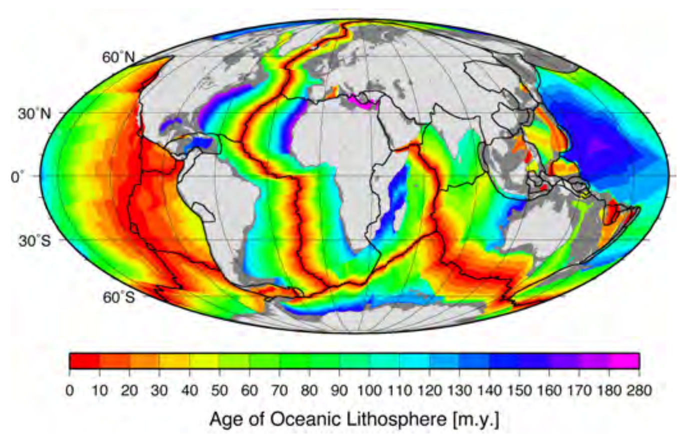

Figure 8.38: Age of oceanic lithosphere, in millions of years. Note the differences in the Atlantic Ocean along the coasts of the continents. Figure description available at the end of the chapter.

This age pattern shows how the Atlantic Ocean opened as the young Mid-Atlantic Ridge began to create the seafloor. This means the Atlantic Ocean started opening and was first formed here. The southern Atlantic opened next, with South America separating from Central and Southern Africa. Finally, after the Mesozoic ended, Greenland and Scandinavia parted ways in the northern-most Atlantic. The breaking points of each rifted plate margin eventually turned into the passive plate boundaries of the east coast of the Americas today.

Video 8.5: Video of Pangea breaking apart and plates moving to their present locations

Access this YouTube video by scanning the QR code. ["PANGEA Breakup" by ProfessorManganelli | https://www.youtube.com/watch?v=6o1HawAOTEI]

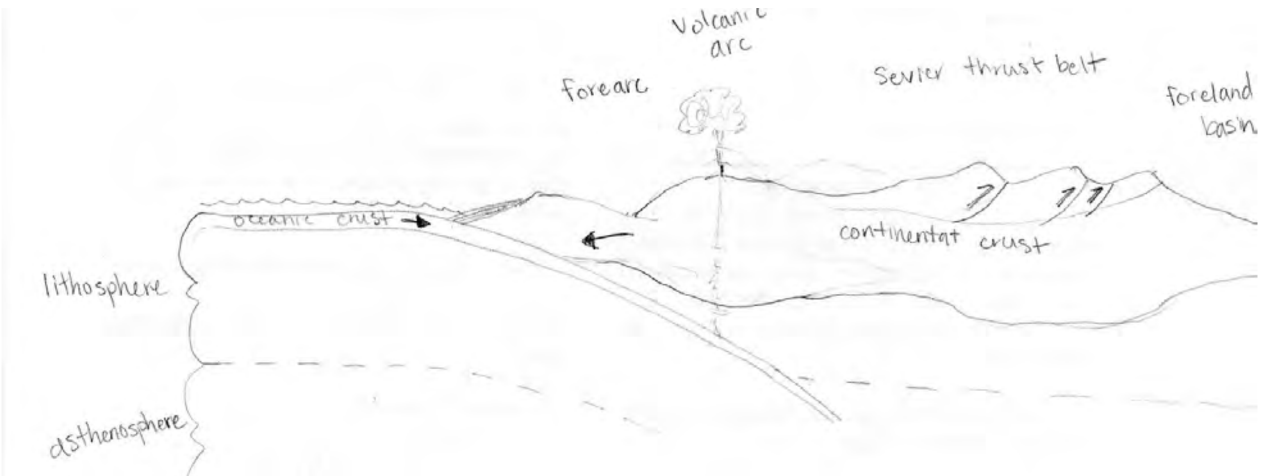

Figure 8.39: Sketch of the major features of the Sevier orogeny. Figure description available at the end of the chapter.

In western North America, an active plate margin had started with subduction, controlling most of the tectonics of that region in the Mesozoic. Another possible island-arc collision created the Sonoman orogeny in Nevada during the latest Paleozoic to the Triassic. In the Jurassic, another island-arc collision caused the Nevadan orogeny, a large Andean-style volcanic arc and thrust belt. The Sevier orogeny followed in the Cretaceous, which was mainly a volcanic arc to the west and a thin-skinned fold and thrust belt to the east, meaning stacks of shallow faults and folds built up the topography. Many of the structures in the Rocky Mountains today date from this orogeny.

Tectonics had an influence in one more important geographic feature in North America: the Cretaceous Western Interior Foreland Basin, which flooded during high sea levels, forming the **Cretaceous Interior Seaway**. Subduction from the west was the Farallon plate, an oceanic plate connected to the Pacific plate (seen today in remnants such as the Juan de Fuca plate, off the coast of the Pacific Northwest). Subduction was shallow at this time because a very young, hot, and less dense portion of the Farallon plate was subducted. This shallow subduction caused a downwarping in the central part of North America. Additional contributors to the high sea levels include shallow subduction and increasing rates of seafloor spreading and subduction, high temperatures, and melted ice. These factors allowed a shallow epicontinental seaway that extended from the Gulf of Mexico to the Arctic Ocean, dividing North America into two separate land masses, Laramidia to the west and Appalachia to the east, for 25 million years. Many of the coal deposits in Utah and Wyoming formed from swamps along the shores of this seaway. By the end of the Cretaceous, cooling temperatures caused the seaway to regress.

Figure 8.40: The Cretaceous Interior Seaway in the mid-Cretaceous. Figure description available at the end of the chapter.

8.5.2 Mesozoic Evolution

Figure 8.41: A Mesozoic scene from the Late Jurassic. Figure description available at the end of the chapter.

The Mesozoic Era was dominated by reptiles—more specifically, the dinosaurs. The Triassic saw devastated ecosystems that took over 30 million years to fully re-emerge after the Permian Mass Extinction. The first appearance of many modern groups of animals that would later flourish occurred at this time. This includes frogs (amphibians), turtles (reptiles), marine ichthyosaurs and plesiosaurs (marine reptiles), mammals, and the archosaurs. The archosaurs ("ruling reptiles") include ancestral groups that went extinct at the end of the Triassic, as well as the flying pterosaurs, crocodilians, and the dinosaurs. Archosaurs, like the placental mammals after them, occupied all major environments: terrestrial (dinosaurs), airborne (pterosaurs), aquatic (crocodilians) and even fully marine habitats (marine crocodiles). The pterosaurs, the first vertebrate group to take flight, started small in the Triassic, like the dinosaurs and mammals.

At the end of the Triassic, another mass extinction event occurred, the fourth major mass extinction in the geologic record. This was perhaps caused by the Central Atlantic Magmatic Province flood basalt. The end-Triassic extinction made certain lineages go extinct and helped spur the evolution of survivors like mammals, pterosaurs (flying reptiles), ichthyosaurs/plesiosaurs/mosasaurs (marine reptiles), and dinosaurs.

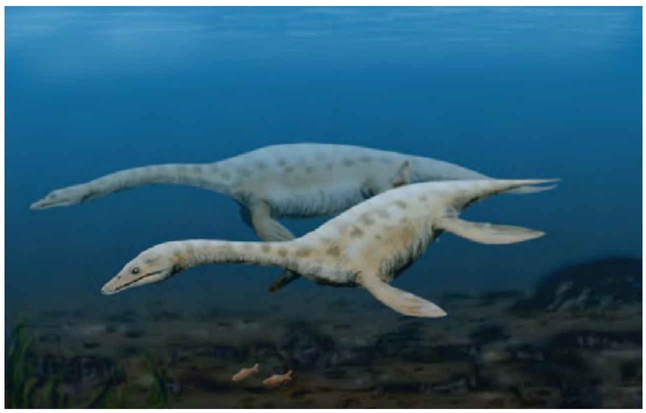

Figure 8.42: A drawing of the early plesiosaur Augustasaurus from the Triassic of Nevada. Figure description available at the end of the chapter.

Mammals, as previously mentioned, got their start from a reptilian synapsid ancestor that possible lived in the late Paleozoic. Mammals stayed small, in mainly nocturnal niches, with insects being their largest prey. The development of warm-blooded circulation and fur may have been a response to this lifestyle.

In the Jurassic, species that were previously common flourished due to a warmer and more tropical climate. The dinosaurs were relatively small animals in the Triassic Period of the Mesozoic but became truly massive in the Jurassic. Dinosaurs are split into two groups based on their hip structure, i.e., orientation of the pubis and ischium bones in relationship to each other. This is referred to as the "reptile-hipped" saurischians and the "bird-hipped" ornithischians. This has recently been brought into question by a new idea for dinosaur lineage.

Figure 8.43: Reconstruction of the small (<5") Megazostrodon, one of the first animals considered to be a true mammal. Figure description available at the end of the chapter.

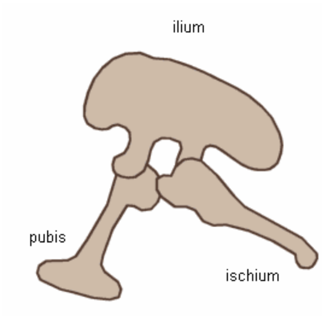

Figure 8.45: Open structure of a saurischian hip, which is similar to a lizard's. Figure description available at the end of the chapter.

Most of the dinosaurs of the Triassic were saurischians, but all of them were bipedal. The major adaptive advantage of dinosaurs was changes in the hip and ankle bones, enabling the tucking of the legs under the body for improved locomotion as opposed to the semi-erect gait of crocodiles or the sprawling posture of reptiles. In the Jurassic, limbs (or a lack thereof) were also important to another group of reptiles, leading to the evolution of *Eophis*, the oldest snake.

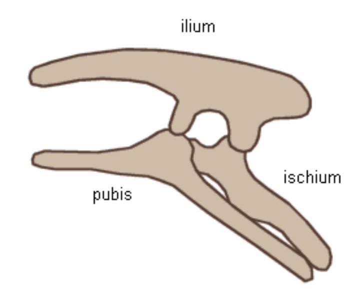

Figure 8.44: Closed structure of a ornithischian hip, which is similar to a bird's. Figure description available at the end of the chapter.

There is a paucity of dinosaur fossils from the Early and Middle Jurassic, but by the Late Jurassic, they were dominating the planet. The saurischians diversified into giant herbivorous (plant-eating) long-necked sauropods weighing up to 100 tons and into theropods that were bipedal and carnivorous, with the possible exception of the genus *Therizinosaurus*. All of the ornithischians (e.g., *Stegosaurus, Iguanodon, Triceratops, Ankylosaurus, Pachycephhlosaurus*) were herbivorous, with a strong tendency to have a "turtle-like" beak at the tips of their mouths.

Figure 8.46: Therizinosaurs, like Beipiaosaurus (shown in this restoration), are known for their enormous hand claws. Figure description available at the end of the chapter.

Figure 8.47: Archaeopteryx lithographica specimen displayed at the Museum für Naturkunde in Berlin. Figure description available at the end of the chapter.

The pterosaurs grew and diversified in the Jurassic, and another notable arial organism developed and thrived in the Jurassic: birds. When the seeming dinosaur-bird hybrid *Archeopteryx* was found in the Solnhofen Lagerstätte of Germany, it started the conversation on the origin of birds. The idea that birds evolved from dinosaurs occurred very early in the history of research into evolution, only a few years after Darwin's *On the Origin of Species*. This study used a remarkable fossil of *Archeopteryx* from a transitional animal between dinosaurs and birds. Small meat-eating theropod dinosaurs were likely the branch that became birds due to their similar features. A significant debate still exists over how and when powered flight evolved. Some have stated a running-start model, while others have favored a tree-leaping gliding model or even a semi-combination: flapping to aid in climbing.

The **Cretaceous** saw a further diversification, specialization, and domination of the dinosaurs and other fauna. One of the biggest changes on land was the transition to angiosperm-dominated flora. Angiosperms, which are plants with flowers and seeds, had originated in the Cretaceous, switching many plains to grasslands by the end of the Mesozoic. By the end of the period, they had replaced gymnosperms (evergreen trees) and ferns as the dominant plant in the world's forests. Haplodiploid eusocial insects (bees and ants) are descendants of wasplike ancestors from the Jurassic that co-evolved with the flowering plants during this time period. The breakup of Pangea not only shaped our modern world's geography but biodiversity at the time as well. Throughout the Mesozoic, animals on the isolated, now-separated island continents (formerly parts of Pangea) took strange evolutionary turns. This includes giant titanosaurian sauropods (*Argentinosaurus*) and theropods (*Giganotosaurus*) from South America.

Figure 8.48: Reconstructed skeleton of Argentinosaurus, from Naturmuseum Senckenberg in Germany. Figure description available at the end of the chapter.

K-T Extinction

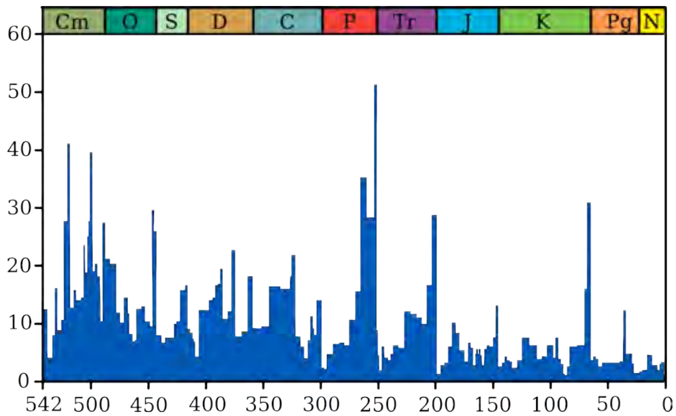

Figure 8.49: Graph of the rate of extinctions. Note the large spike at the end of the Cretaceous (labeled as K). Figure description available at the end of the chapter.

Similar to the end of the Paleozoic Era, the Mesozoic Era ended with the K-Pg Mass Extinction (previously known as the **K-T extinction**) 66 million years ago. This extinction event was likely caused by a large **bolide** (an extraterrestrial impactor such as an **asteroid**, **meteoroid**, or **comet**) that collided with Earth. Ninety percent of plankton species, 75% of plant species, and all the dinosaurs went extinct at this time.

Figure 8.50: Artist's depiction of an impact event. Figure description available at the end of the chapter.

One of the strongest pieces of evidence comes from the element iridium. Quite rare on Earth and more common in meteorites, it has been found all over the world in higher concentrations at a particular layer of rock that formed at the time of the K-T boundary. Soon other scientists started to find evidence to back up the claim. Melted rock spheres—a special type of "shocked" quartz called stishovite, found only at impact sites—were found in many places around the world. The huge impact created a strong thermal pulse that could be responsible for global forest fires, strong acid rains, a corresponding abundance of ferns, the first colonizing plants after forest fires, enough debris thrown into the air to significantly cool temperatures afterward, and a two-kilometer-high tsunami inferred from deposits found from Texas to Alabama.

Figure 8.51: The land expression of the Chicxulub crater. The other side of the crater is within the Gulf of Mexico. Figure description available at the end of the chapter.

Still, with all this evidence, one large piece remained missing: the crater where the bolide impacted. It was not until 1991 that the crater was confirmed using petroleum company geophysical data. Even though it is the third-largest confirmed crater on Earth at roughly 180 km wide, the **Chicxulub crater** was hard to find due to being partially underwater and partially obscured by the dense forest canopy of the Yucatan Peninsula. Coring of the center of the impact, called the peak ring, contained granite, indicating the impact was so powerful that it lifted basement sediment from the crust several miles toward the surface. In 2010, an international team of scientists reviewed 20 years of research and blamed the impact for the extinction.

With all of this information, it seems like the case would be closed. However, there are other events at this time which could have partially aided the demise of so many organisms. For example, sea levels are known to have been slowly decreasing at the time of the K-T event, which is tied to marine extinctions, though any study on gradual vs. sudden changes in the fossil record is flawed due to the incomplete nature of the fossil record. Another big event at this time was the **Deccan Traps** flood basalt volcanism in India. At over 1.3 million cubic kilometers of material, it was certainly a large source of material hazardous to ecosystems at the time, and it has been suggested to be at least partially responsible for the extinction. Some have found the impact and eruptions too much of a coincidence and have even linked the two together.

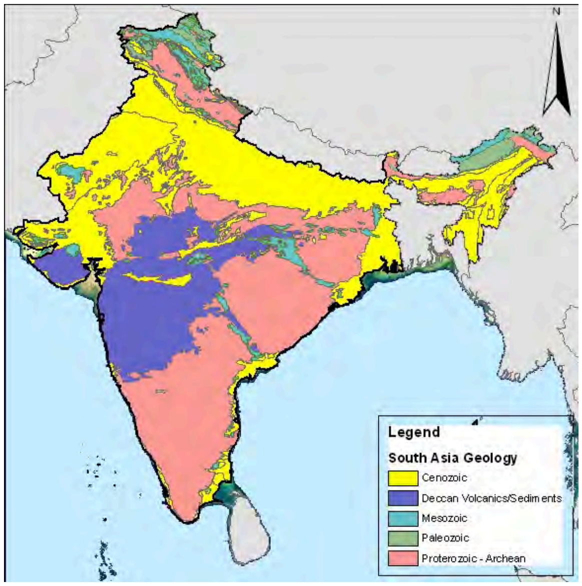

Figure 8.52: Geology of India, with purple representing Deccan Traps-related rocks. Figure description available at the end of the chapter.

Take this quiz to check your comprehension of this section.

Access the quiz for Section 8.5 by scanning the QR code.

8.6 Phanerozoic Eon: Cenozoic Era

The **Cenozoic**, meaning "new life," is known as the Age of Mammals because it is in this era that mammals came to be a dominant and large life form, including human ancestors. Birds also flourished in the open niches left by the dinosaur's demise. Most of the Cenozoic has been relatively warm, with the main exception being the ice age that started about 2.558 million years ago and (despite recent warming) continues today. Tectonic shifts in the west caused volcanism but eventually changed the long-standing subduction zone into a transform boundary.

Figure 8.53: Paraceratherium, seen in this reconstruction, was a massive (15–20 ton, 15-foot-tall) ancestor of rhinos. Figure description available at the end of the chapter.

8.6.1 Cenozoic Tectonics and Paleogeography

Video 8.6: Animation of the last 38 million years of movement in western North America. Note that after the ridge is subducted, convergent turns to transform (with divergent inland).

Access this YouTube video by scanning the QR code. ["Plate Tectonics in a Nutshell (Tanya Atwater)" by VIP Voice | https://www.youtube.com/watch?v=IDTBY5WDELg]

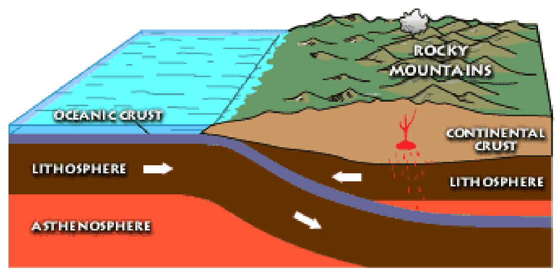

Figure 8.54: Shallow subduction during the Laramide orogeny. Figure description available at the end of the chapter.

In the Cenozoic, the plates of the Earth moved into more familiar places, with the biggest change being the closing of the Tethys Sea with collisions such as the Alps, Zagros, and Himalayas, a collision that started about 57 million years ago and continues today. Maybe the most significant tectonic feature that occurred in the Cenozoic of North America was the conversion of the west coast of California from a convergent boundary subduction zone to a transform boundary. Subduction off the coast of the western United States, which had occurred throughout the Mesozoic, had continued in the Cenozoic. After the Sevier orogeny in the late Mesozoic, a subsequent orogeny called the Laramide orogeny, occurred in the early Cenozoic. The Laramide was thick-skinned, different than the Sevier orogeny. It involved deeper crustal rocks and produced bulges that would become mountain ranges like the Rockies, Black Hills, Wind River Range, Uinta Mountains, and the San Rafael Swell. Instead of descending directly into the mantle, the subducting plate shallowed out and moved eastward beneath the continental plate, affecting the overlying continent hundreds of miles east of the continental margin and building high mountains. This occurred because the subducting plate was so young and near the spreading center, meaning the density of the plate was low and subduction was hindered.

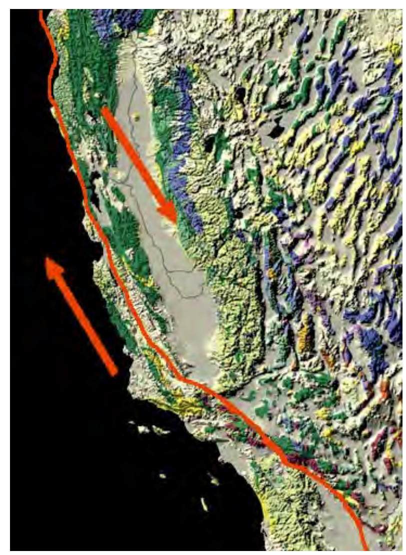

Figure 8.55: Map of the San Andreas fault, showing relative motion. Figure description available at the end of the chapter.

As the mid-ocean ridge itself started to subduct, the relative motion had changed. Subduction caused a relative convergence between the subducting Farallon plate and the North American plate. On the other side of the mid-ocean ridge from the Farallon plate was the Pacific plate, which was moving away from the North American plate. Thus, as the subduction zone consumed the mid-ocean ridge, the relative movement became transform instead of convergent, which went on to become the San Andreas fault system. As the San Andreas grew, it caused east-west directed extensional forces to spread over the Western United States, creating the Basin and Range Province. The transform fault switched position over the last 18 million years, twisting the mountains around Los Angeles, and new faults in the southeastern California deserts may become a future San Andreas-style fault. During this switch from subduction to transform, the nearly horizontal Farallon slab began to sink into the mantle. This caused magmatism as the subducting slab sank, allowing asthenosphere material to rise around it. This event is called the Oligocene ignimbrite flare-up, which was one of the most significant periods of volcanism ever, including the largest single confirmed eruption, the 5,000 cubic kilometer Fish Canyon Tuff.

8.6.2 Cenozoic Evolution

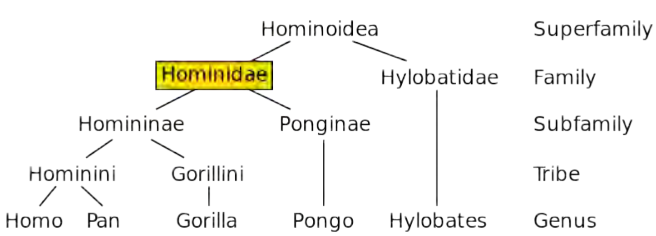

Figure 8.56: Family tree of hominids (Hominidae). Figure description available at the end of the chapter.

There are five groups of early mammals in the fossil record, based primarily on fossil teeth, the hardest bone in vertebrate skeletons. For the purpose of this text, the most important group are the Eupantotheres, which diverged into the two main groups of mammals, the marsupials (like *Sinodelphys*) and placentals or eutherians (like *Eomaia*) in the Cretaceous and then diversified in the Cenozoic. The marsupials dominated on the isolated island continents of South America and Australia, and many went extinct in South America with the introduction of placental mammals. Some well-known mammal groups have been highly studied with interesting evolutionary stories in the

Cenozoic. For example, horses started small, with four toes, and ended up larger, with just one toe. Cetaceans (marine mammals like whales and dolphins) started on land from small bearlike (mesonychids) creatures in the early Cenozoic and gradually took to water. However, no form of evolution has been more studied than human evolution. Hominids, the name for humanlike primates, started in Eastern Africa several million years ago.

The first critical event in this story is an environmental change from jungle to more of a savanna, probably caused by changes in Indian Ocean circulation. While bipedalism is known to have evolved before this shift, it is generally believed that our bipedal ancestors (like *Australopithecus*) had an advantage by covering ground more easily in a more open environment compared to their non-bipedal evolutionary cousins. There is also a growing body of evidence, including the famous Australopithecine fossil "Lucy," that our early ancestors lived in trees. Arboreal animals usually demand a high intelligence to navigate through a three-dimensional world. It is from this lineage that humans evolved, using the capability of endurance running as a means to acquire more resources and possibly even hunt. This can explain many uniquely human features, from our long legs, strong achilles, lack of lower gut protection, and our wide range of running efficiencies.

Figure 8.57: Lucy skeleton, showing real fossil (brown) and reconstructed skeleton (white). Figure description available at the end of the chapter.

Figure 8.58: The hypothesized movement of the Homo genus. Years are marked as to the best guess of the timing of movement. Figure description available at the end of the chapter.

Once the hands were freed up, the next big step was a large brain. There have been arguments that a switch to eating more meat, cooking with fire, tool use, and even the construct of society itself can explain this increase in brain size. Regardless of how, it was this increased cognitive power that allowed humans to reign as their ancestors moved out of Africa and explored the world, ultimately entering the Americas through land bridges like the Bering land bridge. The details of this worldwide migration and the different branches of the hominid evolutionary tree are very complex and best reserved for their own course.

Anthropocene and Extinction

Humans have had an influence on the Earth, its ecosystems, and climate. Yet human activity cannot explain all of the changes that have occurred in the recent past. The start of the Quaternary Period, the last and current period of the Cenozoic, is marked by the start of our current ice age 2.58 million years ago. During this time period, ice sheets advanced and retreated, most likely due to Milankovitch cycles (see Chapter 15). Also at this time, various cold-adapted megafauna emerged (like giant sloths, saber-tooth cats, and woolly mammoths), and most of them went extinct as the Earth warmed from the most recent glacial maximum. A long-standing debate concerns the cause of these and other extinctions. Is climate warming to blame, or were they caused by humans? Certainly, we know of recent human extinctions of animals like the dodo or passenger pigeon. Can we connect modern extinctions to extinctions in the recent past? If so, there are several ideas as to how this happened. Possibly the most widely accepted and oldest is the hunting/overkill hypothesis. The idea behind this hypothesis is that humans hunted large herbivores for food, then as a result, carnivores could not find food; human arrival times in locations have been shown to be tied to increased extinction rates in many cases.

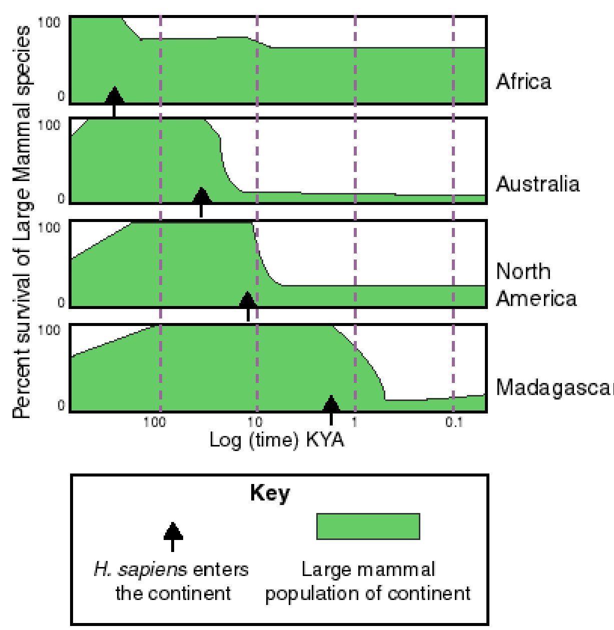

Figure 8.59: Graph showing abundance of large mammals and the introduction of humans. Figure description available at the end of the chapter.

Modern human impact on the environment and the Earth as a whole is unquestioned. In fact, many scientists are starting to suggest that the rise of human civilization ended and/or replaced the **Holocene** Epoch and defines a new geologic time interval: the **Anthropocene**. Evidence for this change includes extinctions, increased tritium (hydrogen with two neutrons) due to nuclear testing, rising pollutants like carbon dioxide, the emergence of more than 200 never-before seen mineral species that have occurred only in this epoch, materials such as plastic and metals which will be long-lasting "fossils" in the geologic record, and large amounts of earthen material moved. The biggest scientific debate with this topic is the starting point. Some say that humans' invention of agriculture would be recognized in geologic strata and that should be the starting point, around 12,000 years ago. Others link the start of the Industrial Revolution and the subsequent addition of vast amounts of carbon dioxide in the atmosphere. Either way, the idea is that alien geologists visiting Earth in the distant future would easily recognize the impact of humans on the Earth as the beginning of a new geologic period.

Figure 8.60: Bingham Canyon Mine, Utah. This open pit mine is the largest man-made removal of rock in the world. Figure description available at the end of the chapter.

Take this quiz to check your comprehension of this section.

Access the quiz for Section 8.6 by scanning the QR code.

Summary

The changes that have occurred since the inception of Earth are vast and significant. From the oxygenation of the atmosphere, the progression of life forms, and the assembly and deconstruction of several supercontinents, to the extinction of more life forms than exist today, having a general understanding of these changes can put present change into a more rounded perspective.

Take this quiz to check your comprehension of this chapter.

Access the quiz for Chapter 8 by scanning the QR code.

Text References

1. Alvarez, L.W., Alvarez, W., Asaro, F., and Michel, H.V. (1980). Extraterrestrial cause for the Cretaceous-tertiary extinction. *Science, 208*(4448), 1095–1108.
2. Beerling, D. (2008). *The emerald planet: How plants changed Earth's history:* OUP Oxford.
3. Boyce, J.W., Liu, Y., Rossman, G.R., Guan, Y., Eiler, J.M., Stolper, E.M., and Taylor, L.A. (2010). Lunar apatite with terrestrial volatile abundances. *Nature, 466*(7305), 466–469.
4. Brueckner, H.K., and Snyder, W.S. (1985). Structure of the Havallah sequence, Golconda allochthon, Nevada: Evidence for prolonged evolution in an accretionary prism. *Geol. Soc. Am. Bull., 96*(9), 1113–1130.
5. Brusatte, S.L., Benton, M.J., Ruta, M., and Lloyd, G.T. (2008). The first 50 Myr of dinosaur evolution: Macroevolutionary pattern and morphological disparity. *Biol. Lett., 4*(6), 733–736.
6. Canup, R.M., and Asphaug, E. (2001). Origin of the Moon in a giant impact near the end of the Earth's formation. *Nature, 412*(6848), 708–712.
7. Clack, J.A. (2009). The fish-tetrapod transition: New fossils and interpretations. *Evolution: Education and Outreach, 2*(2), 213–223. doi:

10/cz257q.
8. Cohen, K.M., Finney, S.C., Gibbard, P.L., and Fan, J.-X. (2013). The ICS international chronostratigraphic chart. *Episodes, 36*(3), 199–204.
9. Colbert, E.H., and Morales, M.A. (1991). *History of the backboned animals through time:* Wiley.
10. De Laubenfels, M.W. (1956). Dinosaur extinction: One more hypothesis. *J. Paleontol.*
11. Gomes, R., Levison, H.F., Tsiganis, K., and Morbidelli, A. (2005). Origin of the cataclysmic late heavy bombardment period of the terrestrial planets. *Nature, 435*(7041), 466–469.
12. Hatcher, R.D., Jr, Thomas, W.A., and Viele, G.W. (1989). *The Appalachian-Ouachita orogen in the United States:* Geological Society of America.
13. Hosono, N., Karato, S., Makino, J., and Saitoh, T.R. (2019). Terrestrial magme ocean origin of the Moon. *Nature Geoscience,* p. 1. doi: 10.1038/s41561-019-0354-2.
14. Hsiao, E. (2004). Possibility of life on Europa.
15. Hubble, E. (1929). A relation between distance and radial velocity among extragalactic nebulae. *Proc. Natl. Acad. Sci. U.S.A., 15*(3), 168–173.
16. Ingersoll, R.V. (1982). Triple-junction instability as cause for late Cenozoic extension and fragmentation of the western United States. *Geology, 10*(12), 621–624.
17. Johnson, C.M. (1991). Large-scale crust formation and lithosphere modification beneath Middle to Late Cenozoic calderas and volcanic fields, western North America. *J. Geophys. Res. [Solid Earth], 96*(B8), 13485–13507.
18. Kass, M.S. (1999). Prognathodon stadtmani: (Mosasauridae) a new species from the Mancos shale (lower Campanian) of western Colorado. *Vertebrate Paleontology in Utah, Utah Geological.*
19. Livaccari, R.F. (1991). Role of crustal thickening and extensional collapse in the tectonic evolution of the Sevier-Laramide orogeny, western United States. *Geology, 19*(11). 1104–1107.
20. McMenamin, M.A., and Schulte McMenamin, D.L. (1990). *The emergence of animals: The Cambrian breakthrough:* Columbia University Press.
21. Mitrovica, J.X., Beaumont, C., and Jarvis, G.T. (1989). Tilting of continental interiors by the dynamical effects of subduction. *Tectonics.*
22. Ru ̈ cklin, M., Donoghue, P.C.J., Johanson, Z., Trinajstic, K., Marone, F., and Stampanoni, M. (2012). Development of teeth and jaws in the earliest jawed vertebrates. *Nature, 491*(7426), 748–751.
23. Sahney, S., and Benton, M.J. (2008). Recovery from the most profound mass extinction of all time. *Proc. Biol. Sci., 275*(1636), 759–765.
24. Salaris, M., and Cassisi, S. (2005). *Evolution of stars and stellar populations:* John Wiley & Sons.
25. Schoch, R.R. (2012). *Amphibian evolution: The life of early land vertebrates:* Wiley-Blackwell.
26. Sharp, B.J. (1958). Mineralization in the intrusive rocks in Little Cottonwood Canyon, Utah. *GSA Bulletin, 69*(11), 1415–1430. doi: 10.1130/0016-7606(1958)69[1415:MITIRI]2.0.CO;2.
27. Wiechert, U., Halliday, A.N., Lee, D.C., Snyder, G.A., Taylor, L.A., and Rumble, D. (2001). Oxygen isotopes and the moon-forming giant impact. *Science, 294*(5541), 345–348.
28. Wilde, S.A., Valley, J.W., Peck, W.H., and Graham, C.M. (2001). Evidence from detrital zircons for the existence of continental crust and oceans on the Earth 4.4 Gyr ago. *Nature, 409*(6817), 175–178.
29. Wood, R.A. (2019). The rise of Animals. *Scientific American, 320*(6), 24–31.

Figure References

Figure 8.1: Geologic time on Earth, represented circularly, showing the individual time divisions and important events. Woudloper; adapted by Hardwigg. 2010. Public domain. https://commons.wikimedia.org/wiki/File:Geologic_Clock_with_events_and_periods.svg

Figure 8.2: Geological timescale with ages shown. United States Geological Survey (USGS). 2009. Public domain. https://commons.wikimedia.org/wiki/File:Geologic_time_scale.jpg

Figure 8.3: Artist's impression of the Earth in the Hadean. Tim Bertelink. 2016. CC BY-SA 4.0. https://commons.wikimedia.org/wiki/File:Hadean.png

Figure 8.4: The global map of the depth of the Moho. AllenMcC. 2013. CC BY-SA 3.0. https://commons.wikimedia.org/wiki/File:Mohomap.png

Figure 8.5: Far side of the Moon. Apollo 16 astronauts via NASA. 1972. Public domain. https://en.wikipedia.org/wiki/File:Back_side_of_the_Moon_AS16-3021.jpg

Figure 8.6: Artist's concept of the giant impact from a Mars-sized object that could have formed the moon. NASA/JPL-Caltech. 2017. Public domain. https://www.nasa.gov/multimedia/imagegallery/image_feature_1454.html

Figure 8.7: Water vapor leaves comet 67P/Churyumov–Gerasimenko. ESA/Rosetta/NAVCAM. 2015. CC BY-SA 3.0 IGO. https://commons.wikimedia.org/wiki/File:Comet_on_7_July_2015_NavCam.jpg

Figure 8.8: Artist's impression of the Archean. Tim Bertelink. 2017. CC BY-SA 4.0. https://commons.wikimedia.org/wiki/File:Archean.png

Figure 8.9: 2015 image from NASA's New Horizons probe of Pluto. NASA/Johns Hopkins University Applied Physics Laboratory/Southwest Research Institute. 2015. Public domain. https://commons.wikimedia.org/wiki/File:Nh-pluto-in-true-color_2x_JPEG-edit-frame.jpg

Figure 8.10: Simulation of before, during, and after the Late Heavy Bombardment. Kesäperuna. 2019. CC BY-SA 3.0. https://commons.wikimedia.org/wiki/File:Lhborbits.png

Figure 8.11: The layers of the Earth. Drlauraguertin. 2015. CC BY-SA 3.0. https://wiki.seg.org/wiki/File:Earthlayers.png

Figure 8.12: Subduction of an oceanic plate beneath another oceanic plate, forming a trench and an island arc. USGS. 1999. Public domain. https://commons.wikimedia.org/wiki/File:Oceanic-continental_convergence_Fig21oceancont.gif

Figure 8.13: Geologic provinces, with the shield (orange) and platform (pink) comprising the craton, the stable interior of continents. USGS. 2005. Public domain. https://commons.wikimedia.org/wiki/File:World_geologic_provinces.jpg

Figure 8.14: The continent of Zealandia. National Oceanic and Atmospheric Administration (NOAA). 2006. Public domain. https://commons.wikimedia.org/wiki/File:Zealandia_topography.jpg

Figure 8.15: Fossils of microbial mats from Sweden. Smith609. 2008. CC BY-SA 3.0. https://commons.wikimedia.org/wiki/File:Runzelmarken.jpg

Figure 8.16: Greenhouse gases were more common in Earth's early atmosphere. Kindred Grey. 2022. CC BY 4.0. Water molecule 3D by Dbc334, 2006 (Public domain, https://commons.wikimedia.org/wiki/File:Water_molecule_3D.svg). Nitrous-oxide-dimensions-3D-balls by Ben Mills, 2007 (Public domain, https://commons.wikimedia.org/wiki/File:Nitrous-oxide-dimensions-3D-balls.png). Methane-CRC-MW-3D-balls by Ben Mills, 2009 (Public domain, https://en.m.wikipedia.org/wiki/File:Methane-CRC-MW-3D-balls.png). Carbon dioxide 3D ball by Jynto, 2011 (Public domain, https://commons.wikimedia.org/wiki/File:Carbon_dioxide_3D_ball.png).

Figure 8.17: Diagram showing the main products and reactants in photosynthesis. At09kg. 2011. CC BY-SA 3.0. https://commons.wikimedia.org/wiki/File:Photosynthesis.gif

Figure 8.18: This sample of banded iron formation displays alternating bands of iron-rich and silica-rich mud, formed as oxygen combined with dissolved iron. Laura Neser. September 2024. CC BY-NC.

Figure 8.19: One possible reconstruction of Rodinia 1.1 billion years ago. John Goodge. 2011. Public domain. https://commons.wikimedia.org/wiki/File:Rodinia_reconstruction.jpg

Figure 8.20: Modern cyanobacteria (as stromatolites) in Shark Bay, Australia. Paul Harrison. 2005. CC BY-SA 3.0. https://en.wikipedia.org/wiki/File:Stromatolites_in_Sharkbay.jpg

Figure 8.21: Fossil stromatolites in Saratoga Springs, New York. Rygel, M.C. 2005. CC BY-SA 3.0. https://commons.wikimedia.org/wiki/File:Stromatolites_hoyt_mcr1.jpg

Figure 8.22: Dickinsonia, a typical Ediacaran fossil. Verisimilus. 2007. CC BY-SA 3.0. https://commons.wikimedia.org/wiki/File:Dickinsonia-Costata.jpg

Figure 8.23: The trilobite had a hard exoskeleton and is an early arthropod, the same group that includes modern insects, crustaceans, and arachnids. Wilson44691. 2010. Public domain. https://commons.wikimedia.org/wiki/File:ElrathiakingiUtahWheelerCambrian.jpg

Figure 8.24: Trilobites, by Heinrich Harder, 1916. Heinrich Harder. 1916. Public domain. https://commons.wikimedia.org/wiki/File:Trilobite_Heinrich_Harder.jpg

Figure 8.25: Laurentia, which makes up the North American craton. USGS. 2005. Public domain. https://commons.wikimedia.org/wiki/File:North_america_craton_nps.gif

Figure 8.26: A reconstruction of Pangea, showing approximate positions of modern continents. Kieff. 2009. CC BY-SA 3.0. https://commons.wikimedia.org/wiki/File:Pangaea_continents.svg

Figure 8.27: Anomalocaris reconstruction by the MUSE science museum in Italy. Matteo De Stefano/MUSE. 2016. CC BY-SA 3.0. https://commons.wikimedia.org/wiki/File:Anomalocaris_canadensis_-_reconstruction_-_MUSE.jpg

Figure 8.28: Original plate from Walcott's 1912 description of Opabinia, with labels: *fp* = frontal appendage, *e* = eye, *ths* = thoracic somites, *i* = intestine, *ab* = abdominal segment. Charles Doolittle Walcott. 1912. Public domain. https://commons.wikimedia.org/wiki/File:Opabinia_regalis_-_Walcott_Cambrian_Geology_and_Paleontology_II_plate_28_.jpg

Figure 8.29: A modern coral reef. Toby Hudson. 2010. CC BY-SA 3.0. https://commons.wikimedia.org/wiki/File:Coral_Outcrop_Flynn_Reef.jpg

Figure 8.30: Guadalupe National Park is made of a giant fossil reef. Zereshk. 2007. CC BY-SA 3.0. https://commons.wikimedia.org/wiki/File:Guadalupe_Nima2.jpg

Figure 8.31: The placoderm Bothriolepis panderi from the Devonian in Russia. Haplochromis. 2007. CC BY-SA 3.0. https://commons.wikimedia.org/wiki/File:Bothriolepis_panderi.jpg

Figure 8.32: Several different types of fish and amphibians that led to walking on land. Dave Souza; adapted by Pixelsquid. 2020. CC BY-SA 3.0. https://commons.wikimedia.org/wiki/File:Fishapods.svg

Figure 8.33: A reconstruction of the giant arthropod (insects and their relatives) Arthropleura. Tim Bertelink. 2016. CC BY-SA 4.0. https://commons.wikimedia.org/wiki/File:Arthropleura.png

Figure 8.34: Reconstruction of Dimetrodon. Max Bellomio. 2019. CC BY-SA 4.0. https://commons.wikimedia.org/wiki/File:Dimetrodon_grandis_3D_Model_Reconstruction.png

Figure 8.35: World map of flood basalts. Williamborg. 2011. CC BY-SA 3.0. https://commons.wikimedia.org/wiki/File:Flood_Basalt_Map.jpg

Figure 8.36: Perhaps the greatest fossil ever found, a velociraptor attacked a protoceratops, and both were fossilized mid-sequence. Yuya Tamai. 2014. CC BY 2.0. https://commons.wikimedia.org/wiki/File:Fighting_dinosaurs_(1).jpg

Figure 8.37: Animation showing Pangea breaking up. USGS. 2005. Public domain. https://commons.wikimedia.org/wiki/File:Pangea_animation_03.gif

Figure 8.38: Age of oceanic lithosphere, in millions of years. Muller, R.D., Sdrolias, M., Gaina, C., and Roest W.R. (2008). Age, spreading rates and spreading symmetry of the world's ocean crust. Geochem. Geophys. Geosyst, 9(Q04006). doi:10.1029/2007GC001743. CC BY-SA 3.0. https://commons.wikimedia.org/wiki/File:Age_of_oceanic_lithosphere.jpg

Figure 8.39: Sketch of the major features of the Sevier orogeny. Pinkcorundum. 2011. Public domain. https://commons.wikimedia.org/wiki/File:Sevierorogeny.jpg

Figure 8.40: The Cretaceous Interior Seaway in the mid-Cretaceous. By William A. Cobban and Kevin C. McKinney, USGS. 2004. Public domain. https://commons.wikimedia.org/wiki/File:Cretaceous_seaway.png

Figure 8.41: A Mesozoic scene from the Late-Jurassic. Gerhard Boeggemann. 2006. CC BY-SA 2.5. https://commons.wikimedia.org/wiki/File:Europasaurus_holgeri_Scene_2.jpg

Figure 8.42: A drawing of the early plesiosaur Agustasaurus from the Triassic of Nevada. Nobu Tamura. 2008. CC BY 3.0. https://commons.wikimedia.org/wiki/File:Augustasaurus_BW.jpg

Figure 8.43: Reconstruction of the small (<5″) Megazostrodon, one of the first animals considered to be a true mammal. Theklan. 2017. CC BY-SA 4.0. https://commons.wikimedia.org/wiki/File:Megazostrodon_sp._Natural_History_Museum_-_London.jpg

Figure 8.44: Closed structure of a ornithischian hip, which is similar to a bird's. Fred the Oyster. 2014. CC BY-SA 4.0. https://commons.wikimedia.org/wiki/File:Ornithischia_pelvis_structure.svg

Figure 8.45: Open structure of a saurischian hip, which is similar to a lizard's. Fred the Oyster. 2014. CC BY-SA 4.0. https://commons.wikimedia.org/wiki/File:Saurischia_pelvis_structure.svg

Figure 8.46: Therizinosaurs, like Beipiaosaurus (shown in this restoration), are known for their enormous hand claws. Matt Martyniuk. 2009. CC BY-SA 3.0. https://commons.wikimedia.org/wiki/File:Beipiao1mmartyniuk.png

Figure 8.47: Archaeopteryx lithographica specimen displayed at the Museum für Naturkunde in Berlin. H. Raab. 2009. CC BY-SA 3.0. https://commons.wikimedia.org/wiki/File:Archaeopteryx_lithographica_(Berlin_specimen).jpg

Figure 8.48: Reconstructed skeleton of Argentinosaurus, from Naturmuseum Senckenberg in Germany. Eva K. 2010. CC BY-NC-ND 3.0. https://commons.wikimedia.org/wiki/File:Argentinosaurus_DSC_2943.jpg

Figure 8.49: Graph of the rate of extinctions. Smith609. 2008. CC BY-SA 3.0. https://commons.wikimedia.org/wiki/File:Extinction_intensity.svg

Figure 8.50: Artist's depiction of an impact event. Made by Fredrik. Cloud texture from public domain NASA image. 2004. Public domain. https://commons.wikimedia.org/wiki/File:Impact_event.jpg

Figure 8.51: The land expression of the Chicxulub crater. NASA/JPL-Caltech. 2000. Public domain. https://commons.wikimedia.org/wiki/File:Yucatan_chix_crater.jpg

Figure 8.52: Geology of India, with purple representing Deccan Traps-related rocks. CamArchGrad. 2007. Public domain. https://en.wikipedia.org/wiki/File:India_Geology_Zones.jpg

Figure 8.53: Paraceratherium, seen in this reconstruction, was a massive (15-20 ton, 15 foot tall) ancestor of rhinos. Tim Bertelink. 2016. CC BY-SA 4.0. https://commons.wikimedia.org/wiki/File:Indricotherium.png

Figure 8.54: Shallow subduction during the Laramide orogeny. Melanie Moreno, USGS. 2006. Public domain. https://commons.wikimedia.org/wiki/File:Shallow_subduction_Laramide_orogeny.png

Figure 8.55: Map of the San Andreas fault, showing relative motion. Kate Barton, David Howell, and Joe Vigil via USGS. 2006. Public domain. https://commons.wikimedia.org/wiki/File:Sanandreas.jpg

Figure 8.56: Family tree of hominids (Hominidae). Fred the Oyster. 2014. CC BY-SA 4.0. https://commons.wikimedia.org/wiki/File:Hominidae_chart.svg

Figure 8.57: Lucy skeleton, showing real fossil (brown) and reconstructed skeleton (white). Andrew. 2007. CC BY-SA 2.0. https://commons.wikimedia.org/wiki/File:Lucy_Skeleton.jpg

Figure 8.58: The hypothesized movement of the Homo genus. NordNordWest. 2014. Public domain. https://commons.wikimedia.org/wiki/File:Spreading_homo_sapiens_la.svg

Figure 8.59: Graph showing abundance of large mammals and the introduction of humans. ElinWhitneySmith. 2006. Public domain. https://commons.wikimedia.org/wiki/File:Extinctions_Africa_Austrailia_NAmerica_Madagascar.gif

Figure 8.60: Bingham Canyon Mine, Utah. Doc Searls. 2016. CC BY 2.0. https://commons.wikimedia.org/wiki/File:Bingham_Canyon_mine_2016.jpg

Figure Descriptions

Figure 8.1: From oldest to newest time divisions: Hadean, archean, proterozoic, paleozoic, mesozoic, cenozoic. 4550 Ma: formation of the earth. 4527 Ma: formation of the moon.4000 Ma: end of the late heavy bombardment; first life. 3200 Ma: earliest start of photosynthesis. 2300 Ma: atmosphere becomes oxygen-rich; first snowball earth. 750-635 Ma: two snowball earths. 530 Ma: cambrian explosion. 380 Ma: first vertebrate land animals. 230-66 Ma: Non-avian dinosaurs. 2 Ma: first hominins.

Figure 8.2: Precambrian eon is made up of haydean, archean, and proterozoic eons. Phanerozoic eon is made up of paleozoic (permian, pennsylvanian, mississippian, devonian, silurian, ordovician, cambrian periods), mesozoic (cretaceous, jurassic, triassic periods), and cenozoic eras (quaternary and tertiary periods).

Figure 8.3: Dark sky, fire and lighting everywhere. Volcanoes on the surface. Large sun in the background.

Figure 8.4: World map with the Moho depth color coded on the map: red is the deepest while blue is the shallowest. The Moho is deepest under central Asia and western South America, and the Moho is shallowest under the world ocean basins.

Figure 8.5: The far side of the Moon, gray in color and covered in numerous craters.

Figure 8.6: The Earth and a Mars-sized object are colliding in a giant explosion.

Figure 8.7: Gray dumbbell-shaped comet that has gaseous jets coming off of the comet's surface.

Figure 8.8: Landscape shows clear water with numerous algal mats; in the distance is a large erupting volcano, meteors streaking through the sky, and the moon very large at the horizon.

Figure 8.9: Planet covered in ice with numerous craters dotting the surface, with the exception of a smooth white plain covering a large portion of the lower right part of the planet.

Figure 8.10: Three diagrams showing a progressive simulation of the outer planets and the Kuiper Belt with a horizontal scale of negative 50 to positive 50 labeled AU and a vertical scale of negative 50 to positive 50 labeled AU; the first diagram shows closely clustered white dots surrounding the drawn circular orbits of the four outer planets; the second diagram shows that the white dots have scattered outward but are still clustered in a ring and the outer four planets have changed their orbits; the third diagram shows that the white dots are completely scattered and the four outer planets' orbits are drawn as they occur today.

Figure 8.11: From core to surface: Inner core (solid), outer core (liquid), mantle (including asthenosphere), crust (including lithosphere)

Figure 8.12: Block diagram showing an oceanic plate moving toward the right where it collides with another oceanic plate and subducts down beneath it. Above the contact between the two plates, there is an ocean trench. There is a volcanic island arc on top of the overriding oceanic plate, above where the oceanic crust has subducted beneath it.

Figure 8.13: World map with geologic provinces color-coded: Shield are colored orange and are seen on northern North America, eastern South America, northwestern Europe, northern and southern Asia, northwestern Australia, and sub-Saharan and southern Africa. Platform are colored pink and are seen near the same locations as shield with the exception of large platforms covering most of northern Asia and Europe. Orogen are colored cyan and are seen along western North America, western South America, the northwestern edge of Africa, southern Europe, southeastern Australia, and southern, central, and northeastern Asia. Basin are colored blue and are seen as thin strips in central-west North America, central-west South America, southern and northeastern Asia, and small spots in central and northwestern Africa. Large igneous province is colored purple and are seen as small blobs in western North America, eastern South America, Iceland, eastern Africa, central India, and northern Asia. Extended Crust are colored yellow and are seen on the margins of all of the continents.

Figure 8.14: Relief map centered on New Zealand with a pink outline extending north and southeast of New Zealand that represents the extent of the continent of New Zealandia.

Figure 8.15: Rocks with a wrinkled texture, formed by microbial mats; the rocks are both gray and green in color and a rock hammer rests on the outcrop for scale.

Figure 8.16: Four diagrams showing various greenhouse gas molecules: water vapor consists of a red oxygen atom with two white hydrogen atoms attached on the bottom left and bottom right; nitrous oxide consists of two blue nitrogen atoms and a red oxygen atom connected in a straight line; methane consists of a black carbon atom at the center with four white hydrogen atoms connected to the carbon atom in a pyramidal shape; and carbon dioxide consists of a red oxygen atom, a black carbon atom, and another red oxygen atom connected in a straight line.

Figure 8.17: Water enters through the plants roots. Carbon dioxide enters through the plants leaves. Sunlight enters through the plants leaves. Oxygen leaves the plants leaves.

Figure 8.18: A slice of rock, showing red and brown curvy layers with glittering dots throughout.

Figure 8.19: Circular world map showing multiple gray cratons arranged together in the following way: just above the equator on the left is Madagascar, India, and East Antarctica; Laurentia spans across the equator with Australia, South China, and Siberia above it; Baltica is to the right of Laurentia, also across the equator; below Laurentia and Baltica are Rio Plato, Amazonia, and West Africa. There are two island cratons below the equator and toward the left: Congo-Sao Francisco and Kalahari. There are green strips across East Antarctica, Laurentia, and Congo-Sao Francisco that represent 1.1 Ga belts.

Figure 8.20: Brown, blobby stromatolites are slightly sticking out of the shallow water of the ocean.

Figure 8.21: Concentric round structures in gray limestone.

Figure 8.22: Oval fossil that resembles a leaf imprinted in tan sandstone.

Figure 8.23: Top view of a black fossilized trilobite that has an overall oval shape with a segmented body covered in a pattern of fine ridges; a scale bar labeled 0.5 cm is in the lower right of the photo.

Figure 8.24: Illustration of trilobites crawling on the seafloor.

Figure 8.25: Color-coded map of North America; covering the majority of the United States and Canada it is brown with the label North American Craton-continental crust that has remained relatively stable for the past 600 million years; there is a purple wedge in the American southwest that extends as a thin strip along the margins of the North American Craton labeled Deformed Craton; along the western edge of North America it is green with the label Accretionary Belt-welded to the North American continental margin within the last 600 million years; along the east coast and extending into the oceans it is blue with the label Coastal Plain.

Figure 8.26: One supercontinent in the shape of a crescent. From top to bottom: Eurasia, North america, Africa, South america, India, Antarctica, Australia.

Figure 8.27: Elongate reddish brown animal with swimming flaps running along its body, large compound eyes, and a single pair of segmented frontal appendages.

Figure 8.28: Elongate white fossil animal with a segmented trunk that has flaps along the sides and a fan-shaped tail.

Figure 8.29: Colorful coral reef underwater in light blue, shallow water.

Figure 8.30: A mountain with steep cliffs rising from vegetation-covered slopes; the mountain has a blunt, nearly flat top.

Figure 8.31: Tan fish fossil that is covered with natural plate-like armor.

Figure 8.32: Late Devonian lobe-finned fish and amphibious tetrapods. Land: Tiktaalik (375 million years ago), Ichthyostega (365 million years ago). Rivers, swamps, and shallows: Panderichthys (380 million years ago), acanthostega (365 million years ago). Sea: Eusthenopteron (385 million years ago), coelacanth (360 million years ago)

Figure 8.33: Top view of a 2-meter long brown millipede with segmented body; an inset diagram shows the millipede size compared with a human.

Figure 8.34: Four-legged brownish-black animal with a distinct tan sail-like structure on its back; it has a reptile-like body, covered in scaly skin, and its head features a long snout with sharp teeth. The sail on its back is composed of bony projections connected by a thin membrane.

Figure 8.35: World map with geologic provinces color-coded: Shield are colored orange and are seen on northern North America, eastern South America, northwestern Europe, northern and southern Asia, northwestern Australia, and sub-Saharan and southern Africa. Platform are colored pink and are seen near the same locations as shield with the exception of large platforms covering most of northern Asia and Europe. Orogen are colored cyan and are seen along western North America, western South America, the northwestern edge of Africa, southern Europe, southeastern Australia, and southern, central, and northeastern Asia. Basin are colored blue and are seen as thin strips in central-west North America, central-west South America, southern and northeastern Asia, and small spots in central and northwestern Africa. Large igneous province is colored purple and are seen as small blobs in western North America, eastern South America, Iceland, eastern Africa, central India, and northern Asia. Extended Crust are colored yellow and are seen on the margins of all of the continents.

Figure 8.36: Two well-preserved dinosaur fossils interlocked in a battle pose: one dinosaur is a Velociraptor, a smaller predator with sharp claws and teeth, while the other is a Protoceratops, an herbivorous dinosaur with a beak-like snout and a frilled neck.

Figure 8.37: GIF showing the progression of Pangea separating to become the continents in their current configuration.

Figure 8.38: Color-coded world map that shows the various ages of oceanic lithosphere. Continents are in gray. The color-coding and locations are as follows: the youngest oceanic lithosphere is 0 million years old and runs along the centers of the ocean basins where there are mid-ocean ridges, colored in red. Oceanic lithosphere ages get older away from the mid-ocean ridges, and the oldest oceanic lithosphere is 280 million years old near continental margins, colored purple.

Figure 8.39: Cross sectional sketch of an oceanic plate moving toward the right, subducting beneath continental crust; a volcanic arc forms on the continental crust above the subducting oceanic crust with a forearc in front of the volcanic arc; to the right of the volcanic arc is a series of mountain ridges thrusting upward labeled Sevier thrust belt; behind that is the foreland basin.

Figure 8.40: Map of North America showing multiple seaways: the Western Interior Seaway spans north to south across the western part of Canada, the United States, and eastern Mexico where it connects to the Gulf of Mexico; the Hudson Seaway spans central Canada and connects to the Western Interior Seaway when it reaches the United States; and the Labrador Seaway spans east to west across the northernmost part of Canada; both the Western Interior Seaway and the Hudson Seaway connect to the Labrador Seaway at the northern ends.

Figure 8.41: Illustration of several dinosaurs walking on sandy beach with lush green forest in the foreground and background.

Figure 8.42: Illustration of two animals swimming underwater with long and streamlined bodies; their four limbs resemble paddle-like structures; their heads are elongated, featuring a pointed snout and sharp teeth; their bodies are covered in a smooth gray and tan skin texture.

Figure 8.43: A small shrew-like animal covered in white fur.

Figure 8.44: Drawing of the ilium bone; the pubis bone and ischium bone are each connected to the ilium bone; the bones of the pubis and ischium are close to each other.

Figure 8.45: Drawing of the ilium bone; the pubis bone and ischium bone are each connected to the ilium bone; the bones of the pubis and ischium are pointed away from each other.

Figure 8.46: A four-legged animal in a bipedal stance with a long tail and slender body; its head is characterized by a long snout and sharp teeth; its body is covered in white feathers and it has long claws at the end of each leg.

Figure 8.47: Archaeopteryx fossil embedded within flat face of tan sedimentary rock; the fossil shows features of reptiles, such as sharp teeth, fingers with claws, and a long bony tail, as well as features of birds, such as small, broad wings and the impression of feathers.

Figure 8.48: A massive four-legged dinosaur skeleton, with a long neck extending upwards and a massive body supported by sturdy legs; the head is small in proportion to its body.

Figure 8.49: Bar graph with a horizontal axis going from the Cambrian to present toward the right and vertical axis going from 0 to 60 upward. There are multiple spikes with one spike at the end of the Cretaceous.

Figure 8.50: Massive rock on fire slamming into the earth.

Figure 8.51: Two satellite images of the Yucatan Peninsula; the second image has a dashed semicircle overlain on a faint semi-circular land

imprint at the northern part of the peninsula labeled Trough, along with three black arrows pointing to small dot-shaped features labeled Cenotes (sinkholes).

Figure 8.52: Map of south Asia with the geology of India color-coded: yellow Cenozoic rocks are found in northern India and in small slivers along the eastern coast; purple Deccan Volcanic rocks are found in west-central India; teal Mesozoic rocks are found in small slivers in northern India and central India; green Paleozoic rocks are found in small slivers in northern India; and pink Proterozoic-Archean rocks cover southern and eastern India with a large chunk in northern India as well.

Figure 8.53: A four-legged animal that resembles a rhinoceros with a long neck and a robust body supported by sturdy legs; the head is large and elongated, featuring a hornless snout; the skin texture is gray, thick, and wrinkled.

Figure 8.54: Block diagram showing oceanic crust moving toward the right where it collides with continental crust and subducts down beneath it. Because the angle of subduction is shallow, the ocean crust travels inland before creating a volcanic arc on top of the continental plate, above where the oceanic crust has subducted beneath it–these are the Rocky Mountains.

Figure 8.55: Map of western North America annotated with the location of the main San Andreas fault which runs from northwest of the Canadian coast, through western California, and southeast through Mexico. There are arrows on either side of the fault line showing relative movement: on the east side of the fault, movement is toward the lower right and on the west side of the fault, movement is toward the upper left.

Figure 8.56: Superfamily: hominoidea. Family: Hominidae and hylobatidae. Hominidae has 2 subfamilies: homininae and ponginae. Ponginae has genus pongo. homininae has 2 tribes: hominini (genuses homo and pan) and gorillini (genus gorilla)

Figure 8.57: Human-like skeleton in glass case. Skeleton is 1/2 fossil and 1/2 reconstructed skeleton.

Figure 8.58: Homo genus originated in southern africa and moved north through europe and asia, south through australia, and through greenland/alaska to north america and south america.

Figure 8.59: Four graphs stacked on top of each other labeled Africa, Australia, North America, and Madagascar; each graph shows the large mammal population of the continent with an arrow to label when H. sapiens enters the continent; the horizontal axis is labeled Log (time) KYA and goes from over 100 on the left to below 0.1 on the right; the vertical axis is labeled Percent survival of Large Mammal species and goes from 0 on the bottom to 100 on the top. In each of the graphs, the large mammal population decreases after H. sapiens enters the continent.

Figure 8.60: Immense terraced dirt-lined open pit with snow-covered mountains visible around the back of the mine.

9. CRUSTAL DEFORMATION AND EARTHQUAKES

Learning Objectives

By the end of this chapter, students should be able to:

- Differentiate between stress and strain.
- Identify the three major types of stress.
- Differentiate between brittle, ductile, and elastic deformation.
- Describe the geological map symbol used for strike and dip of strata.
- Name and describe different fold types.
- Differentiate the three major fault types, and describe their associated movements.
- Explain how elastic rebound relates to earthquakes.
- Describe different seismic wave types and how they are measured.
- Explain how humans can induce seismicity.
- Describe how seismographs work to record earthquake waves.
- Locate the epicenter of an earthquake from seismograph records.
- Explain the difference between earthquake magnitude and intensity.
- List earthquake factors that determine ground shaking and destruction.
- Identify secondary earthquake hazards.
- Describe notable historical earthquakes.

Crustal deformation occurs when applied forces exceed the internal strength of rocks, physically changing their shapes. These forces are called stress, and the physical changes they create are called strain. Forces involved in tectonic processes, as well as gravity and igneous pluton emplacement, produce strains in rocks that include folds, fractures, and faults. When rock experiences large amounts of shear stress and breaks with rapid, brittle deformation, energy is released in the form of **seismic waves**, commonly known as an earthquake.

9.1 Stress and Strain

Stress is the force exerted per unit area, and **strain** is the physical change that results in response to that force. When applied stress is greater than the internal strength of rock, strain results in the form of deformation of the rock. Strain in rocks can be represented as a change in rock volume and/or rock shape, as well as fracturing of the rock. There are three types of stress: tensional, compressional, and shear. Tensional stress involves forces pulling in opposite directions, which results in strain that stretches and thins rock. Compressional stress involves forces pushing together, and compressional strain shows up as rock folding and thickening. Shear stress involves transverse forces; the strain shows up as opposing blocks or regions of material moving past each other.

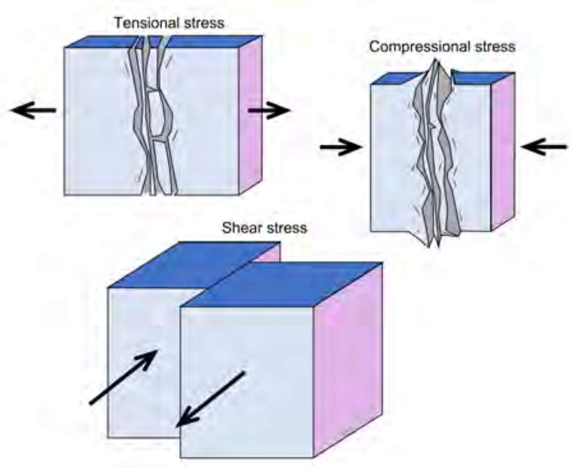

Figure 9.1: Types of stress. (Clockwise from top left): tensional stress, compressional stress, and shear stress. Figure description available at the end of the chapter.

Type of stress	Associated plate boundary type (see Chapter 2)	Resulting strain	Associated fault and offset types
Tensional	Divergent	Stretching and thinning	Normal
Compressional	Convergent	Shortening and thickening	Reverse
Shear	Transform	Tearing	Strike-slip

Table 9.1: Types of stress and resulting strain.

Take this quiz to check your comprehension of this section.

Access the quiz for Section 9.1 by scanning the QR code.

9.2 Deformation

When rocks are stressed, the resulting strain can be elastic, ductile, or brittle. This change is generally called deformation. **Elastic deformation** is strain that is reversible after a stress is released. For example, when you stretch a rubber band, it elastically returns to its original shape after you release it. **Ductile deformation** occurs when enough stress is applied to a material that the changes in its shape are permanent, and the material is no longer able to revert to its original shape. For example, if you bend a metal bar too far, it can be permanently bent out of shape. The point at which elastic deformation is surpassed and strain becomes permanent is called the **yield point**. In Figure 9.2, the yield point is where the line transitions from elastic deformation to ductile deformation (the end of the dashed line). **Brittle deformation** is another critical point of no return, when rock integrity fails and the rock fractures under increasing stress.

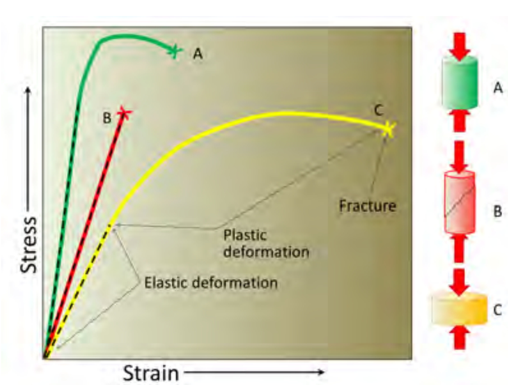

Figure 9.2: Different materials deform differently when stress is applied. Material "A" has relatively little deformation when undergoing large amounts of stress, before undergoing plastic deformation and finally brittlely failing. Material "B" only elastically deforms before brittlely failing. Material "C" undergoes significant plastic deformation before finally failing brittlely. Figure description available at the end of the chapter.

The type of deformation a rock undergoes depends on pore pressure, strain rate, rock strength, temperature, stress intensity, time, and confining pressure. Pore pressure is exerted on the rock by fluids in the open spaces or pores embedded within rock or sediment. Strain rate measures how quickly a material is deformed. For example, applying stress slowly makes it is easier to bend a piece of wood without breaking it. Rock strength measures how easily a rock deforms under stress. Shale has low strength, and granite has high strength. Removing heat or decreasing temperature makes materials more rigid and susceptible to brittle deformation. On the other hand, heating materials make them more ductile and less brittle. Heated glass can be bent and stretched.

Factor	Strain response
Increase temperature	More ductile
Increase strain rate	More brittle
Increase rock strength	More brittle

Table 9.2: Relationship between factors operating on rock and the resulting strains.

Take this quiz to check your comprehension of this section.

Access the quiz for Section 9.2 by scanning the QR code.

9.3 Geological Maps

Geologic maps are two-dimensional (2-D) representations of geologic formations and structures at the Earth's surface, including **formations**, faults, folds, inclined strata, and rock types. Formations are recognizable rock units. Geologists use geologic maps to represent where geologic formations, faults, folds, and inclined rock units are. Each formation on the map is indicated by a color and a label. For examples of geologic maps, see the Utah Geological Survey (UGS) geologic map viewer.

Formation labels include symbols that follow a specific protocol. The first one or more letters are uppercase and represent the geologic time period of the formation. More than one uppercase letter indicates the formation is associated with multiple time periods. The following lowercase letters represent the formation name, abbreviated rock description, or both.

9.3.1 Cross Sections

Cross sections are subsurface interpretations made from surface and subsurface measurements. Maps display geology in the horizontal plane, while cross sections show subsurface geology in the vertical plane. For more information on cross sections, check out the AAPG wiki.

9.3.2 Strike and Dip

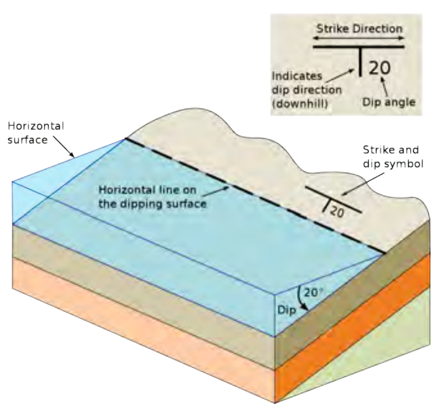

Figure 9.3: "Strike" and "dip" are words used to describe the orientation of rock layers with respect to north/south and horizontal. Figure description available at the end of the chapter.

Geologists use a special symbol called strike and dip to represent inclined beds. Strike and dip map symbols look like the capital letter *T*, with a short trunk and extra-wide top line. The short trunk represents the dip, and the top line represents the strike. **Dip** is the angle that a bed plunges into the Earth from the horizontal. A number next to the symbol represents dip angle. One way to visualize the **strike** is to think about a line made by standing water on the inclined layer. That line is horizontal and lies on a compass direction that has some angle with respect to true north or south (see Figure 9.3). The strike angle is measured by a special compass—e.g., N 30° E (read north 30 degrees east) means the horizontal line points northeast at an angle of 30° from true north. The strike and dip symbol is drawn on the map at the strike angle with respect to true north on the map. The dip of the inclined layer represents the angle down to the layer from horizontal; in the figure, this is 45° SE (read dipping 45 degrees to the southeast). The direction of dip would be the direction a ball would roll if set on the layer and released. A horizontal rock bed has a dip of 0°, and a vertical bed has a dip of 90°. Strike and dip considered together are called rock attitude.

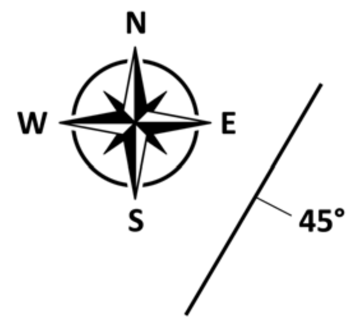

Figure 9.4: Attitude symbol on geologic map (with compass directions for reference) showing strike of N30°E and dip of 45° to the SE. Figure description available at the end of the chapter.

This video illustrates geologic structures and associated map symbols.

Video 9.1: Folds, dip, and strike

Access this YouTube video by scanning the QR code. ["Folds, Dip and Strike" by wvannorden | https://www.youtube.com/watch?v=UzZFMWH-lSQ]

Take this quiz to check your comprehension of this section.

Access the quiz for Section 9.3 by scanning the QR code.

9.4 Folds

Geologic **folds** are layers of rock that are curved or bent by ductile deformation. Folds are most commonly formed by compressional forces at depth, where hotter temperatures and higher confining pressures allow ductile deformation to occur.

Folds are described by the orientation of their axes, axial planes, and limbs. The plane that splits the fold into two halves is known as the **axial plane**. The fold axis is the line along which the bending occurs and is where the axial plane intersects the folded strata. The hinge line follows the line of greatest bend in a fold. The two sides of the fold are the fold limbs.

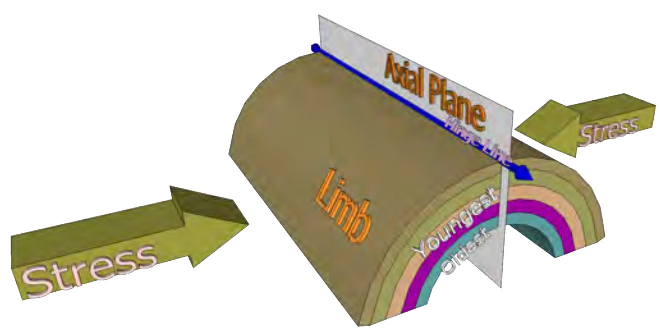

Figure 9.5: Model of anticline. Oldest beds are in the center, and the youngest are on the outside. The axial plane intersects the center angle of bend. The hinge line follows the line of greatest bend, where the axial plane intersects the outside of the fold. Figure description available at the end of the chapter.

Symmetrical folds have a vertical axial plane, and limbs have equal but opposite dips. Asymmetrical folds have dipping, nonvertical axial planes where the limbs dip at different angles. Overturned folds have steeply dipping axial planes, and the limbs dip in the same direction but usually at different dip angles. Recumbent folds have horizontal or nearly horizontal axial planes. When the axis of the fold plunges into the ground, the fold is called a plunging fold. Folds are classified into five categories: anticline, syncline, monocline, dome, and basin.

9.4.1 Anticline

Anticlines are archlike, or A-shaped, folds that are convex-upward in shape. They have downward curving limbs and beds that dip down and away from the central fold axis. In anticlines, the oldest rock strata are in the center of the fold, along the axis, and the younger beds are on the outside. Since geologic maps show the intersection of surface topography with underlying geologic structures, an anticline on a geologic map can be identified by both the attitude of the strata forming the fold and the older age of the rocks inside the fold. An antiform has the same shape as an anticline, but the relative ages of the beds in the fold cannot be determined. Oil geologists are interested in anticlines because they can form oil **traps**, where oil migrates up along the limbs of the fold and accumulates in the high point along the fold axis.

Figure 9.6: An anticline near Bcharre, Lebanon. Figure description available at the end of the chapter.

9.4.2 Syncline

3D Model 9.1: Synclinal fold

Access this interactive 3D model by scanning the QR code.

Synclines are troughlike, or U-shaped, folds that are concave-upward in shape. They have beds that dip down and in toward the central fold axis. In synclines, older rock is on the outside of the fold and the youngest rock is inside of the fold axis. A synform has the shape of a syncline but, like an antiform, does not have distinguishable age zones.

9.4.3 Monocline

Monoclines are steplike folds in which flat rocks are upwarped or downwarped then continue flat. Monoclines are relatively common on the Colorado Plateau, where they form "reefs," which are ridges that act as topographic barriers and should not be confused with ocean reefs (see Chapter 5). Capitol Reef is an example of a monocline in Utah. Monoclines can be caused by bending of shallower sedimentary strata as faults grow below them. These faults are commonly called "blind faults" because they end before reaching the surface and can be either normal or reverse faults.

Figure 9.7: Monocline at Colorado National Monument. Figure description available at the end of the chapter.

9.4.4 Dome

A dome is a symmetrical to semisymmetrical upwarping of rock beds. Domes have a shape like an inverted bowl, similar to an architectural dome on a building. Examples of domes in Utah include the San Rafael Swell, Harrisburg Junction Dome, and Henry Mountains. Domes are formed from compressional forces, underlying igneous intrusions (see Chapter 4), salt diapirs, or even impacts, like upheaval dome in Canyonlands National Park.

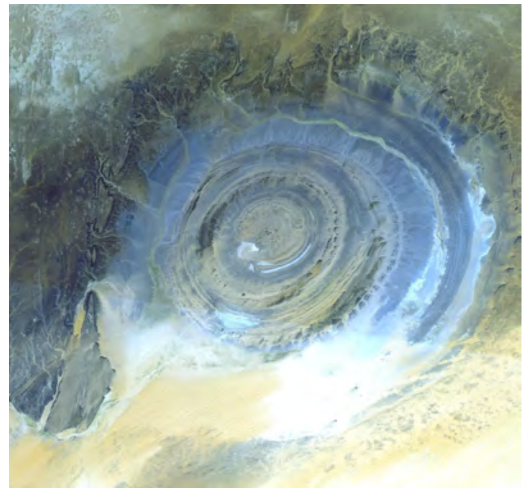

Figure 9.8: This prominent circular feature in the Sahara Desert of Mauritania has attracted attention since the earliest space missions because it forms a conspicuous bull's-eye in the otherwise rather-featureless expanse of the desert. Initially interpreted as a meteorite impact structure because of its high degree of circularity, it is now thought to be merely a symmetrical uplift (circular anticline) that has been laid bare by erosion. Figure description available at the end of the chapter.

9.4.5 Basin

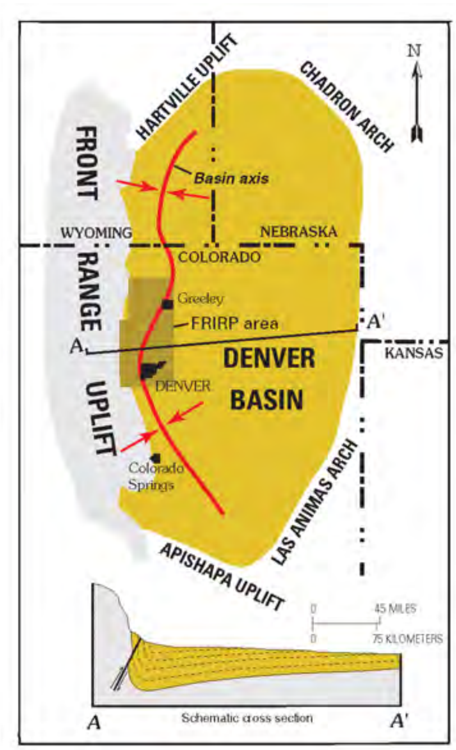

Figure 9.9: The Denver Basin is an active sedimentary basin at the eastern extent of the Rocky Mountains. As sediment accumulates, the basin subsides, creating a basin-shape of beds that all dip toward the center of the basin. Figure description available at the end of the chapter.

A basin is the inverse of a dome, a bowl-shaped depression in a rock bed. The Uinta Basin in Utah is an example of a basin. Some **structural basins** are also sedimentary basins that collect large quantities of sediment over time. Sedimentary basins can form as a result of folding but are much more commonly produced in mountain building, forming between mountain blocks or via faulting. Regardless of the cause, as the basin sinks or subsides, it can accumulate more sediment because the weight of the sediment causes more subsidence in a positive-feedback loop. There are active **sedimentary basins** all over the world. An example of a rapidly subsiding basin in Utah is the Oquirrh Basin, dated to the Pennsylvanian-Permian age, which has accumulated over 9,144 m (30,000 ft) of fossiliferous sandstones, shales, and limestones. These strata can be seen in the Wasatch Mountains along the east side of Utah Valley, especially on Mount Timpanogos and in Provo Canyon.

Take this quiz to check your comprehension of this section.

Access the quiz for Section 9.4 by scanning the QR code.

9.5 Faults

Faults are the places in the crust where brittle deformation occurs as two blocks of rocks move relative to one another. Normal and reverse faults display vertical, also known as **dip-slip**, motion. Dip-slip motion consists of relative up-and-down movement along a dipping fault between two blocks, the hanging wall and footwall. In a dip-slip system, the **footwall** is below the fault plane and the **hanging wall** is above the fault plane. A good way to remember this is to imagine a mine tunnel running along a fault; the hanging wall would be where a miner would hang a lantern, and the footwall would be at the miner's feet.

Faulting as a term refers to the rupture of rocks. Such ruptures occur at plate boundaries but can also occur in plate interiors. Faults slip along the fault plane. The fault scarp is the **offset** of the surface produced by the fault breaking through the surface. **Slickensides** are polished, often grooved surfaces along the fault plane created by friction during the movement.

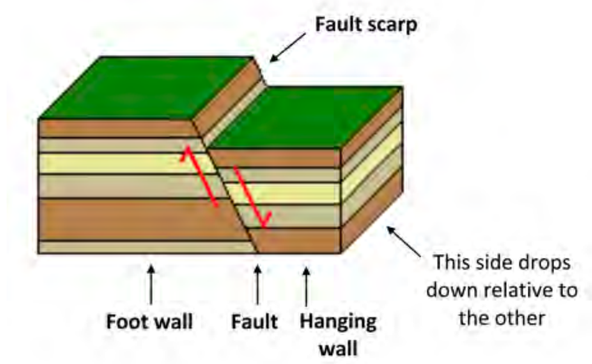

Figure 9.10: Common terms used for normal faults. Normal faults form when the hanging wall moves down relative to the footwall. Figure description available at the end of the chapter.

A joint or fracture is a plane of brittle deformation in rock created by movement that is not offset or sheared. Joints can result from many processes, such as cooling, depressurizing, or folding. Joint systems may be regional, affecting many square miles.

9.5.1 Normal Faults

Normal faults move by a vertical motion in which the hanging wall moves downward relative to the footwall along the dip of the fault. Normal faults are created by tensional forces in the crust. Normal faults and tensional forces commonly occur at divergent plate boundaries, where the crust is being stretched by tensional stresses (see Chapter 2). Examples of normal faults in Utah are the Wasatch fault, the Hurricane fault, and other faults bounding the valleys in the Basin and Range Province.

Figure 9.11: Example of a normal fault in an outcrop of the Pennsylvanian Honaker Trail Formation near Moab, Utah. Figure description available at the end of the chapter.

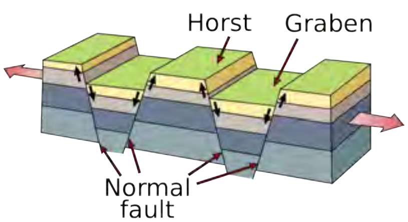

Figure 9.12: Faulting that occurs in the crust under tensional stress. Figure description available at the end of the chapter.

Grabens, horsts, and half-grabens are blocks of crust or rock bounded by normal faults (see Chapter 2). Grabens drop down relative to adjacent blocks and create valleys. Horsts rise up relative to adjacent down-dropped blocks and become areas of higher topography. In places where they occur together, horsts and grabens create a symmetrical pattern of valleys surrounded mountains and normal faults on both sides. **Half-grabens** are a one-sided version of a horst and graben, where blocks are tilted by a normal fault on one side, creating an asymmetrical valley-mountain arrangement. The mountain-valleys of the Basin and Range Province of Western Utah and Nevada consist of a series of full and half-grabens from the Salt Lake Valley to the Sierra Nevada Mountains.

Normal faults do not continue clear into the mantle. In the Basin and Range Province, the dip of a normal fault tends to decrease with depth, i.e., the fault angle becomes shallower and more horizontal as it goes deeper. Such decreasing dips happen when large amounts of extension occur along very low-angle normal faults, known as **detachment faults**. The normal faults of the Basin and Range, produced by tension in the crust, appear to become detachment faults at greater depths.

9.5.2 Reverse Faults

In **reverse faults**, compressional forces cause the hanging wall to move up relative to the footwall. A thrust fault is a reverse fault where the fault plane has a low dip angle of less than 45°. Thrust faults carry older rocks on top of younger rocks and can even cause repetition of rock units in the stratigraphic record.

Convergent plate boundaries with subduction zones create a special type of "reverse" fault called a **megathrust fault**, where denser oceanic crust drives down beneath less-dense overlying crust. Megathrust faults cause the largest magnitude earthquakes ever measured and commonly cause massive destruction and tsunamis.

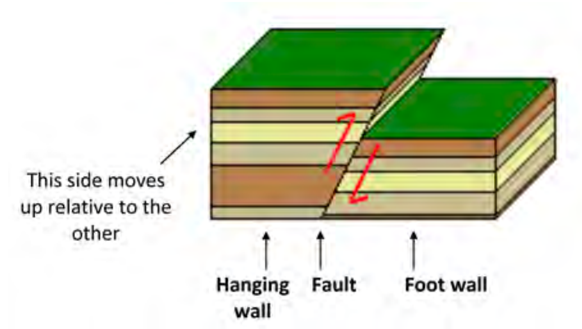

Figure 9.13: Simplified block diagram of a reverse fault. Figure description available at the end of the chapter.

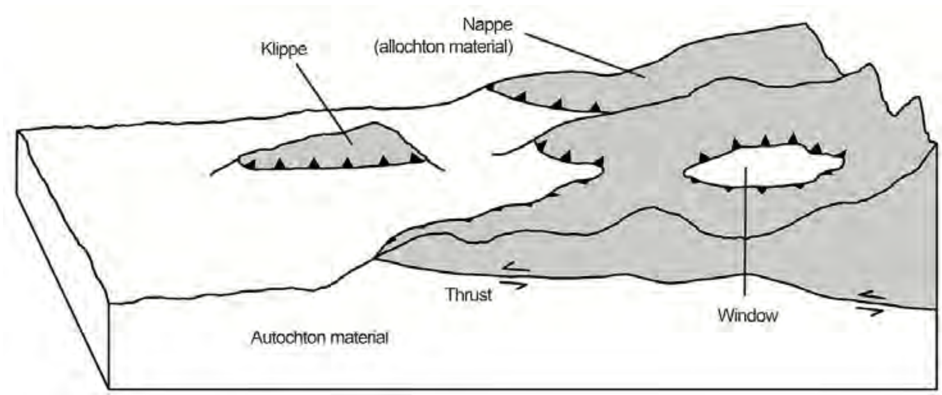

Figure 9.14: Terminology of thrust faults (low-angle reverse faults). A klippe is the remnant of the hanging wall (a.k.a. nappe) where the surrounding material has eroded away. A window is where part of the hanging wall has eroded away to expose the footwall (autochton). Note the symbol showing flags on the overlying thrust plate. Figure description available at the end of the chapter.

Figure 9.15: Thrust fault in the northern Qilian Mountains (Qilian Shan). The blueish rock is a thick fault gouge of basement, and the reddish material is above the fault plane, all of which has been thrust above the brown quaternary conglomerates (right). The fault plane dips 65° to the south. Figure description available at the end of the chapter.

9.5.3 Strike–Slip Faults

Strike-slip faults have side-to-side motion. Strike-slip faults are most commonly associated with transform plate boundaries and are prevalent in transform fracture zones along mid-ocean ridges. In pure strike-slip motion, fault blocks on either side of the fault do not move up or down relative to each other; rather, they move laterally, side to side. The direction of strike-slip movement is determined by an observer standing on a block on one side of the fault. If the block on the opposing side of the fault moves left relative to the observer's block, this is called **sinistral** motion. If the opposing block moves right, it is **dextral** motion.

Video 9.2: Video showing motion in a strike-slip fault

Access this YouTube video by scanning the QR code. ["Strike-Slip Fault" by USGS | https://www.youtube.com/watch?v=NqzKvzkZrWQ]

Bends along strike-slip faults create areas of **compression** or **tension** between the sliding blocks (see Chapter 2). Tensional stresses create transtensional features with normal faults and basins, such as the Salton Sea in California. Compressional stresses create transpressional features with reverse faults and cause small-scale mountain building, such as the San Gabriel Mountains in California. The faults that splay off transpression or transtension features are known as **flower structures**.

An example of a dextral, right-lateral strike-slip fault is the San Andreas fault, which denotes a transform boundary between the North American and Pacific plates. An example of a sinistral, left-lateral strike-slip fault is the Dead Sea fault in Jordan and Israel.

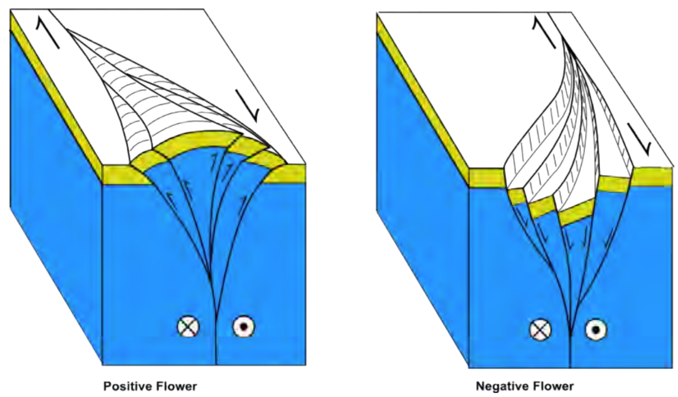

Figure 9.16: Flower structures created by strike-slip faults. Depending on the relative movement in relation to the bend in the fault, flower structures can create basins or mountains. Figure description available at the end of the chapter.

Video 9.3: Video showing how faults are classified

Access this YouTube video by scanning the QR code. ["Classification of Faults" by GeoScience Videos | https://www.youtube.com/watch?v=qlk7IfYMufs]

Take this quiz to check your comprehension of this section.

Access the quiz for Section 9.5 by scanning the QR code.

9.6 Earthquake Essentials

Earthquakes are felt at the surface of the Earth when energy is released by blocks of rock sliding past each other, evidence that faulting has occurred. Seismic energy thus released travels through the Earth in the form of seismic waves. Most earthquakes occur along active plate boundaries, but intraplate earthquakes (not along plate boundaries) occur and are still poorly understood. The USGS Earthquakes Hazards Program has a real-time map showing the most recent earthquakes.

9.6.1 How Earthquakes Happen

The release of seismic energy is explained by the **elastic rebound** theory. When rock is strained to the point that it undergoes brittle deformation, the place where the initial offsetting rupture takes place between the fault blocks is called the **focus**. This offset propagates along the fault, which is known as the fault plane.

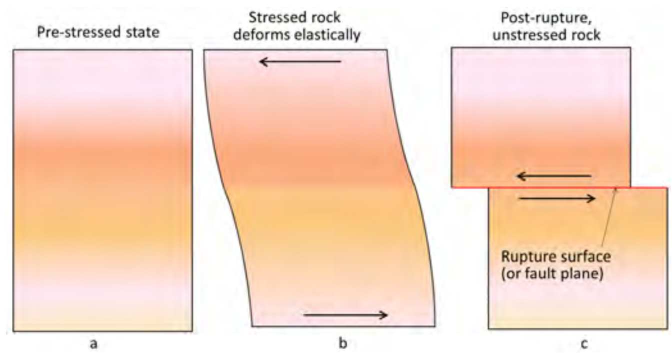

Figure 9.17: Process of elastic rebound: (a) Undeformed state, (b) accumulation of elastic strain, and (c) brittle failure and release of elastic strain. Figure description available at the end of the chapter.

The fault blocks of persistent faults like the Wasatch fault (Utah), showing recurring movements, are locked together by friction. Over hundreds to thousands of years, stress builds up along the fault until it overcomes frictional resistance, rupturing the rock and initiating fault movement. The deformed unbroken rocks snap back toward their original shape in a process called elastic rebound**.** Think of bending a stick until it breaks; stored energy is released, and the broken pieces return to near their original orientation.

Bending, the ductile deformation of the rocks near a fault, reflects a buildup of stress. In earthquake-prone areas like California, strain gauges are used to measure this bending and help seismologists, scientists who study earthquakes, understand more about predicting them. In locations where the fault is not locked, seismic stress causes continuous, gradual displacement between the fault blocks, which is called fault **creep**. Fault creep occurs along some parts of the San Andreas fault (California).

After an initial earthquake, continuous application of stress in the crust causes elastic energy to begin to build again during a period of inactivity along the fault. The accumulating elastic strain may be periodically released to produce small earthquakes called foreshocks on or near the main fault. Foreshocks can occur hours or days before a large earthquake or may not occur at all. The main release of energy during the major earthquake is known as the **mainshock**. **Aftershocks** may follow the mainshock to adjust new strain produced during the fault movement and generally decrease over time.

9.6.2 Focus and Epicenter

The earthquake focus, also called hypocenter, is the initial point of rupture, and displacement of the rock moves from the hypocenter along the fault surface. The earthquake focus is the point along the fault plane from which initial seismic waves spread outward and is always located at some depth below the ground surface. From the focus, rock displacement propagates up, down, and laterally along the fault plane. This displacement produces shock waves called seismic waves. The larger the displacement between the opposing fault blocks and the further the displacement propagates along the fault surface, the more seismic energy is released and the greater the amount and duration of shaking. The **epicenter** is the location on the Earth's surface vertically above the focus. This is the location that most news reports give because it is the center of the area where people are affected.

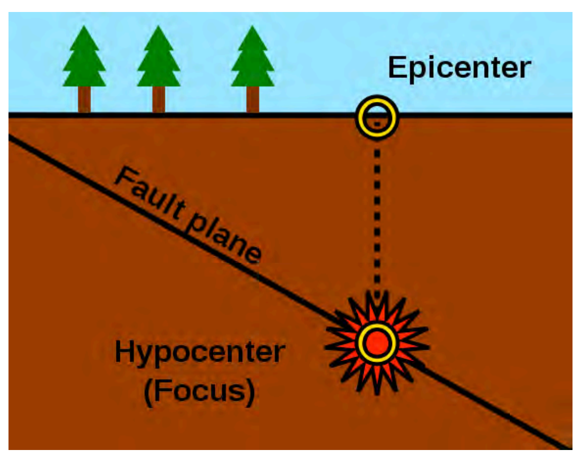

Figure 9.18: The hypocenter is the point along the fault plane in the subsurface from which seismic energy emanates. The epicenter is the point on land surface vertically above the hypocenter. Figure description available at the end of the chapter.

9.6.3 Seismic Waves

To understand earthquakes and how earthquake energy moves through the Earth, consider the basic properties of waves. Waves describe how energy moves through a medium, such as rock or unconsolidated sediments in the case of earthquakes. Wave **amplitude** indicates the magnitude or height of earthquake motion. **Wavelength** is the distance between two successive peaks of a wave. Wave frequency is the number of repetitions of the motion over a period of time in the form of cycles per time unit. Period, which is the amount of time a wave takes to travel one wavelength, is the inverse of frequency. When multiple waves combine, they can interfere with each other (see Figure 9.19). When waves combine in sync, they produce constructive interference, where the influence of one wave adds to and magnifies the other. If waves are out of sync, they produce destructive interference, which diminishes the amplitudes of both waves. If two combined waves have the same amplitude and frequency but are one half-wavelength out of sync, the resulting destructive interference can eliminate each wave. These processes of wave amplitude, frequency, period, and constructive and destructive interference determine the magnitude and intensity of earthquakes.

Seismic waves are the physical expression of energy released by the elastic rebound of rock within displaced fault blocks and are felt as an earthquake. Seismic waves occur as body waves and surface waves. **Body waves** pass underground through the Earth's interior body and are the first seismic waves to propagate out from the focus. Body waves include primary (P) waves and secondary (S) waves. **P waves** are the fastest body waves and move through rock via compression, very much like sound waves move through air. Rock particles move forward and back during passage of the P waves, enabling them to travel through solids, liquids, plasma, and gases. **S waves** travel more slowly, following P waves, and propagate as shear waves that move rock particles from side to side. Because they are restricted to lateral movement, S waves can only travel through solids but not liquids, plasma, or gases.

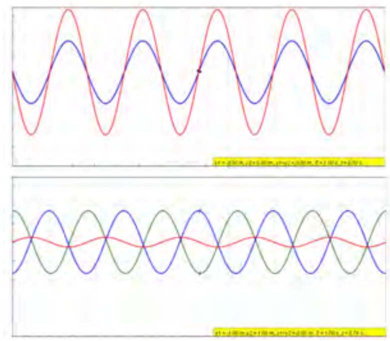

Figure 9.19: Example of constructive and destructive interference. Note the red line representing the results of interference. Figure description available at the end of the chapter.

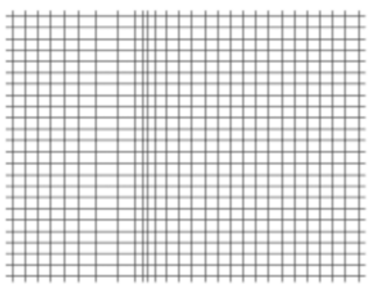

Figure 9.20: P waves are compressional. Figure description available at the end of the chapter.

During an earthquake, body waves pass through the Earth and into the mantle as a subspherical wave front. Considering a point on a wave front, the path followed by a specific point on the spreading wave front is called a seismic ray, and a seismic ray reaches a specific seismograph located at one of thousands of seismic monitoring stations scattered over the Earth. Density increases with depth in the Earth, and since seismic velocity increases with density, a process called **refraction** causes earthquake rays to curve away from the vertical and bend back toward the surface, passing through different bodies of rock along the way.

Surface waves are produced when body waves from the focus strike the Earth's surface. Surface waves travel along the Earth's surface, radiating outward from the epicenter. Surface waves take the form of rolling waves called **Rayleigh waves** [watch wave propagation animation video] and side-to-side waves called **Love waves** [watch wave propagation animation video]. Surface waves are produced primarily as the more energetic S waves strike the surface from below, with some surface wave energy contributed by P waves. Surface waves travel more slowly than body waves, and because of their complex horizontal and vertical movement, surface waves are responsible for most of the damage caused by an earthquake. Love waves produce predominantly horizontal ground shaking and, ironically for their name, are the most destructive. Rayleigh waves produce an elliptical motion with longitudinal dilation and compression, like ocean waves. However, Rayleigh waves cause rock particles to move in a direction opposite to that of water particles in ocean waves.

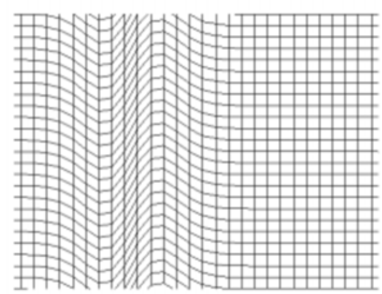

Figure 9.21: S waves are shear. Figure description available at the end of the chapter.

The Earth has been described as ringing like a bell after an earthquake, with earthquake energy reverberating inside it. Like other waves, seismic waves refract (bend) and bounce (reflect) when passing through rocks of differing densities. S waves, which cannot move through liquid, are blocked by the Earth's liquid outer core, creating an S wave shadow zone on the side of the planet opposite to the earthquake focus. P waves, on the other hand, pass through the core but are refracted into the core by the difference of density at the core-mantle boundary. This has the effect of creating a cone-shaped P wave shadow zone on parts of the other side of the Earth from the focus.

Video 9.4: Body and surface waves of 2011 Tohoku earthquake

Access this video by scanning the QR code. ["2011 Tohoku Earthquake, Mag. 9.0. Body and Surface Waves" by seismicsoundlab | https://vimeo.com/153300296]

9.6.4 Induced Seismicity

Earthquakes known as **induced seismicity** occur near natural gas extraction sites because of human activity. Injection of waste fluids in the ground, commonly a byproduct of an extraction process for **natural gas** known as **fracking**, can increase the outward pressure that liquid in the pores of a rock exerts, known as pore pressure. The increase in pore pressure decreases the frictional forces that keep rocks from sliding past each other, essentially lubricating fault planes. This effect is causing earthquakes to occur near injection sites in a human-induced activity known as induced seismicity. The significant increase in drilling activity in the Central United States has spurred the requirement for the disposal of significant amounts of waste drilling fluid, resulting in a measurable change in the cumulative number of earthquakes experienced in the region.

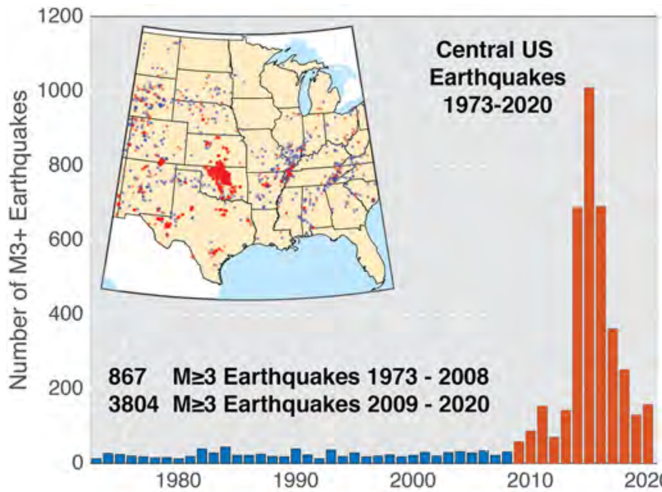

Figure 9.22: Frequency of earthquakes in the Central United States. Note the sharp increase in the number of earthquakes from 2010 to 2020. Figure description available at the end of the chapter.

Take this quiz to check your comprehension of this section.

Access the quiz for Section 9.6 by scanning the QR code.

9.7 Measuring Earthquakes

9.7.1 Seismographs

Video 9.5: Animation of a horizontal seismograph

Access this YouTube video by scanning the QR code. ["Horizontal Seismograph Slowed" by IRIS Earthquake Science | https://www.youtube.com/watch?v=83GOKn7kWXM]

People feel approximately one million earthquakes a year, usually when they are close to the source and the earthquake registers a moment magnitude of at least 2.5. Major earthquakes of moment magnitude 7.0 and higher are extremely rare. The US Geological Survey (USGS) Earthquakes Hazards Program real-time map shows the location and magnitude of recent earthquakes around the world.

To accurately study seismic waves, geologists use **seismographs** that can measure even the slightest ground vibrations. Early twentieth-century seismograms use a weighted pen (pendulum) suspended by a long spring above a recording device fixed solidly to the ground. The recording device is a rotating drum mounted with a continuous strip of paper. During an earthquake, the suspended pen stays motionless and records ground movement on the paper strip. The resulting graph is known as a seismogram. Digital versions use magnets, wire coils, electrical sensors, and digital signals instead of mechanical pens, springs, drums, and paper. A seismograph array is multiple seismographs configured to measure vibrations in three directions: north-south (x-axis), east-west (y-axis), and up-down (z-axis).

Video 9.6: Animation of a vertical seismograph

Access this YouTube video by scanning the QR code. [“Vertical Seismograph” by IRIS Earthquake Science | https://www.youtube.com/watch?v=DX5VXGmdnAg]

To pinpoint the location of an earthquake epicenter, seismologists use the differences in arrival times of the P, S, and surface waves. After an earthquake, P waves will appear first on a seismogram, followed by S waves, and finally surface waves, which have the largest amplitude. It is important to note that surface waves lose energy quickly, so they are not measurable at great distances from the epicenter. These time differences determine the distance but not the direction of the epicenter. By using wave arrival times recorded on seismographs at multiple stations, seismologists can apply triangulation to pinpoint the location of the epicenter of an earthquake. At least three seismograph stations are needed for triangulation. The distance from each station to the epicenter is plotted as the radius of a circle. The epicenter is demarked where the circles intersect. This method also works in 3-D, using multi-axis seismographs and sphere radii to calculate the underground depth of the focus.

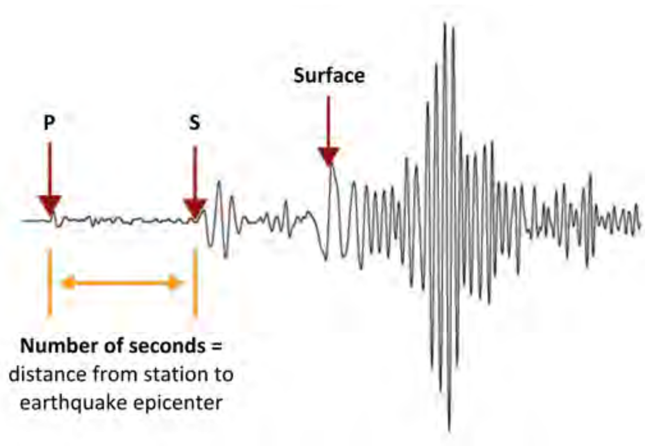

Figure 9.23: A seismogram showing the arrivals of the P, S, and surface waves. Figure description available at the end of the chapter.

Video 9.7: Method of triangulation used to locate the epicenter of an earthquake

Access this YouTube video by scanning the QR code. [“Earthquake Epicenter Location” by Mike Sammartano | https://www.youtube.com/watch?v=oBS7BKqHRhs]

9.7.2 Seismograph Network

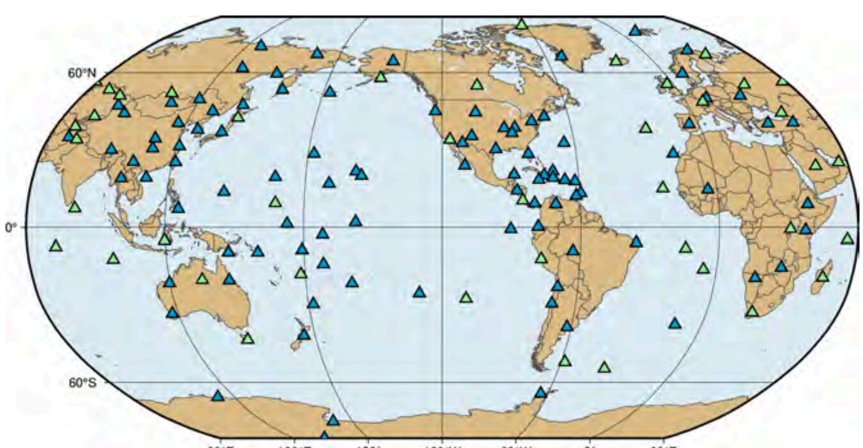

Figure 9.24: Global network of seismic stations. Note that this map does not show all of the world’s seismic stations, just one of the networks of stations scientists use to measure seismic activity. Figure description available at the end of the chapter.

The International Registry of Seismograph Stations lists more than 20,000 seismographs on the planet. By comparing data from multiple seismographs, scientists can map the properties of the inside of the Earth, detect detonations of large explosive devices, and predict tsunamis. The Global Seismic Network, a worldwide set of linked seismographs that electronically distribute real-time data, includes more than 150 stations that meet specific design and precision standards. The USArray is a network of hundreds of permanent and transportable seismographs in the United States that are used to map the subsurface activity of earthquakes (see Video 9.8).

Along with monitoring for earthquakes and related hazards, the Global Seismograph Network helps detect nuclear weapons testing, which is monitored by the Comprehensive Nuclear Test Ban Treaty Organization. Most recently, seismographs have been used to determine nuclear weapons testing by North Korea.

Video 9.8: Nepal earthquake (M7.9) ground motion visualization

Access this YouTube video by scanning the QR code. [“Nepal Earthquake M7.9 Ground Motion Visualization” by EarthScope | https://www.youtube.com/watch?v=5xc-rNOISQE]

9.7.3 Seismic Tomography

Very much like a CT (computed tomography) scan uses X-rays at different angles to image the inside of a body, seismic tomography uses seismic rays from thousands of earthquakes that occur each year, passing at all angles through masses of rock, to generate images of internal Earth structures.

Using the assumption that the Earth consists of homogenous layers, geologists developed a model of expected properties of Earth materials at every depth called the PREM (preliminary reference earth model). These properties include seismic wave transmission velocity, which is dependent on rock density and elasticity. In the mantle, temperature differences affect rock density. Cooler rocks have a higher density and therefore transmit seismic waves more quickly. Warmer rocks have a lower density and transmit earthquake waves more slowly. When the arrival times of seismic rays at individual seismic stations are compared to arrival times predicted by PREM, differences are called **seismic anomalies** and can be measured for bodies of rock within the Earth from seismic rays passing through them at seismic network stations. Because seismic rays travel at all angles from many earthquakes and arrive at many stations, variations in the properties of the rock bodies allow 3-D images to be constructed of the rock bodies through which the rays passed. Seismologists are thus able to construct 3-D images of the interior of the Earth.

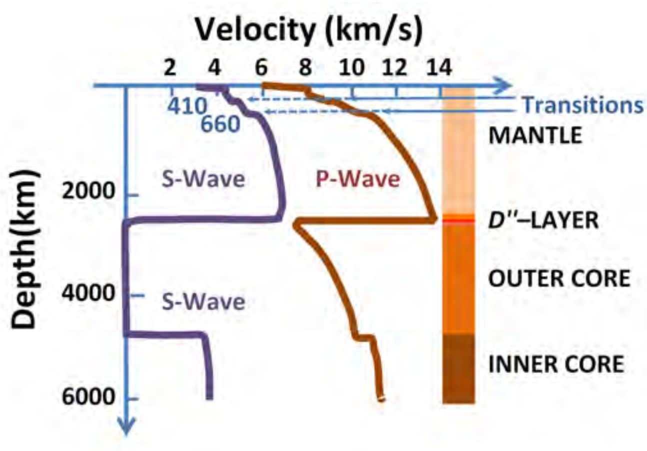

Figure 9.25: Speed of seismic waves with depth in the Earth. Two thousand kilometers is 1,240 miles. Figure description available at the end of the chapter.

For example, seismologists have mapped the Farallon plate, a tectonic plate that subducted beneath North America during the last several million years, and the Yellowstone magma chamber, which is a product of the Yellowstone hotspot under the North American continent. Peculiarities of the Farallon plate subduction are thought to be responsible for many features of western North America, including the Rocky Mountains (see Chapter 8).

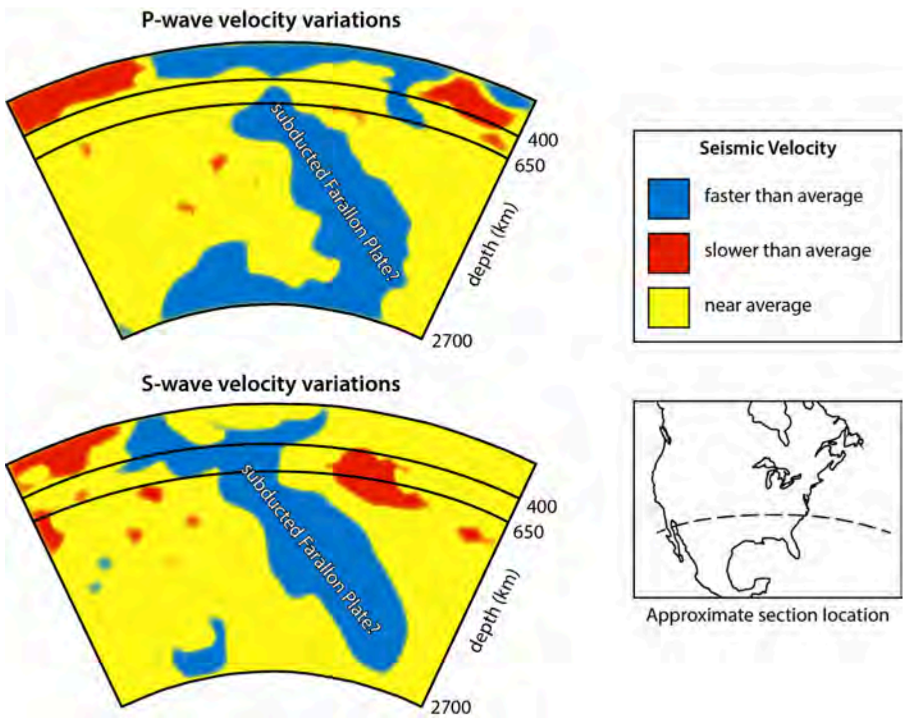

Figure 9.26: Simplified and interpreted P- and S-wave velocity variations in the mantle across southern North America, showing the subducted Farallon plate. Figure description available at the end of the chapter.

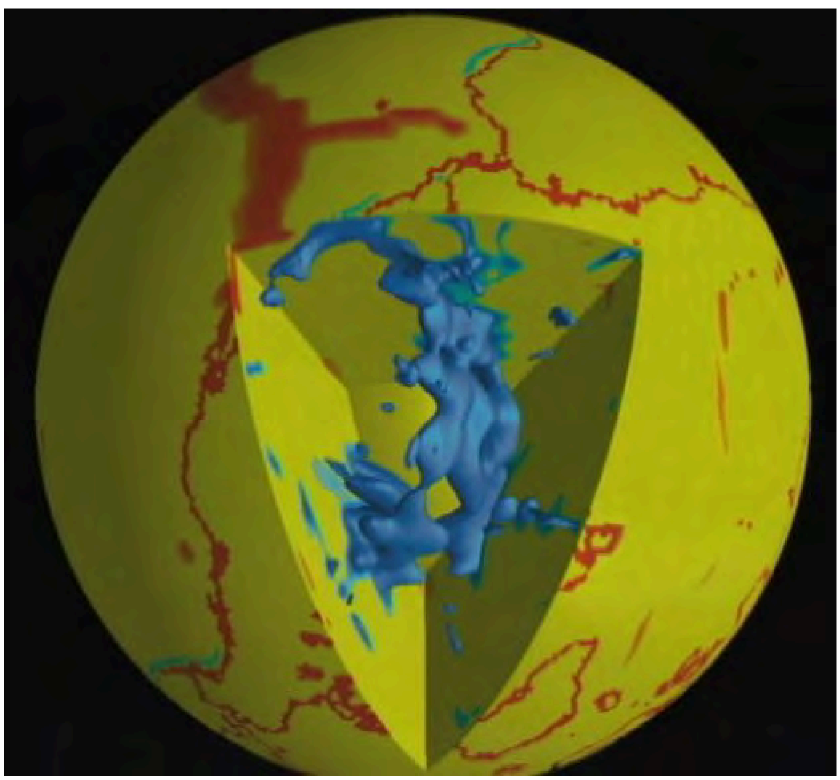

Figure 9.27: Tomographic image of the Farallon plate in the mantle below North America. Figure description available at the end of the chapter.

9.7.4 Earthquake Magnitude and Intensity

Richter Scale

Magnitude is the measure of the energy released by an earthquake. The **Richter scale**, the first and most well-known magnitude scale, was developed by Charles F. Richter (1900–1985) at the California Institute of Technology. This was the magnitude scale used historically by early seismologists. Richter magnitude (M_L) is determined from the maximum amplitude of the pen tracing on the seismogram recording. Adjustments for epicenter distance from the seismograph are made using the arrival-time differences of S and P waves.

The Richter scale is logarithmic, based on powers of 10. This means an increase of one Richter unit represents a tenfold increase in seismic-wave amplitude; in other words, a magnitude 6 earthquake shakes the ground ten times more than a magnitude 5. However, the *actual energy released* for each magnitude unit is 32 times greater, which means a magnitude 6 earthquake releases 32 times more energy than a magnitude 5.

The Richter scale was developed for earthquakes in Southern California, using local seismographs. It has limited applications for larger distances and very large earthquakes. Therefore, most agencies no longer use the Richter scale. **Moment magnitude** (M_W), which is measured using seismic arrays and generates values comparable to the Richter scale, is more accurate for measuring earthquakes across the Earth, including large earthquakes, although they require more time to calculate. News media often report Richter magnitudes right after an earthquake occurs, even though scientific calculations now use moment magnitudes.

Moment Magnitude Scale

The moment magnitude scale depicts the absolute size of earthquakes, comparing information from multiple locations and using a measurement of actual energy released calculated from the cross-sectional area of rupture, amount of slippage, and the rigidity of the rocks. Because each earthquake occurs in a unique geologic setting and the rupture area is often hard to measure, estimates of moment magnitude can take days or even months to calculate.

Like the Richter scale, the moment magnitude scale is logarithmic. Magnitude values of the two scales are approximately equal, except for very large earthquakes. Both scales are used for reporting earthquake magnitude. The Richter scale provides a quick magnitude estimate immediately following the quake. Moment magnitude calculations take much longer but are more accurate and thus, more useful for scientific analysis.

Video 9.9: Moment magnitude explained

Access this YouTube video by scanning the QR code. ["Moment Magnitude Explained—What Happened to the Richter Scale?" by IRIS Earthquake Science | https://www.youtube.com/watch?v=HL3KGK5eqaw]

Modified Mercalli Intensity Scale

The **modified Mercalli intensity (MMI) scale** is a qualitative rating of ground-shaking intensity based on observable structural damage and people's perceptions. This scale uses a *I* (Roman numeral one) rating for the lowest intensity and *X* (ten) for the highest (see Table 9.3) and can vary depending on epicenter location and population density, such as urban versus rural settings. Historically, scientists used the MMI scale to categorize earthquakes before they developed quantitative measurements of magnitude. Intensity maps show locations of the most severe damage based on residential questionnaires, local news articles, and onsite assessment reports.

Intensity	Shaking	Description/damage
I	Not felt	Not felt except by a very few under especially favorable conditions.
II	Weak	Felt only by a few persons at rest, especially on upper floors of buildings.
III	Weak	Felt quite noticeably by persons indoors, especially on upper floors of buildings. Many people do not recognize it as an earthquake. Standing motor cars may rock slightly. Vibrations similar to the passing of a truck. Duration estimated.
IV	Light	Felt indoors by many, outdoors by few during the day. At night, some awakened. Dishes, windows, doors disturbed; walls make cracking sound. Sensation like heavy truck striking building. Standing motor cars rocked noticeably.
V	Moderate	Felt by nearly everyone; many awakened. Some dishes, windows broken. Unstable objects overturned. Pendulum clocks may stop.
VI	Strong	Felt by all, many frightened. Some heavy furniture moved; a few instances of fallen plaster. Damage slight.
VII	Very strong	Damage negligible in buildings of good design and construction; slight to moderate in well-built ordinary structures; considerable damage in poorly built or badly designed structures; some chimneys broken.
VIII	Severe	Damage slight in specially designed structures; considerable damage in ordinary substantial buildings with partial collapse. Damage great in poorly built structures. Fall of chimneys, factory stacks, columns, monuments, walls. Heavy furniture overturned.
IX	Violent	Damage considerable in specially designed structures; well-designed frame structures thrown out of plumb. Damage great in substantial buildings, with partial collapse. Buildings shifted off foundations.
X	Extreme	Some well-built wooden structures destroyed; most masonry and frame structures destroyed with foundations. Rails bent.

Table 9.3: Abridged Mercalli scale. (Source: USGS General Interest Publication. 1989, 288-913.)

Shake Maps

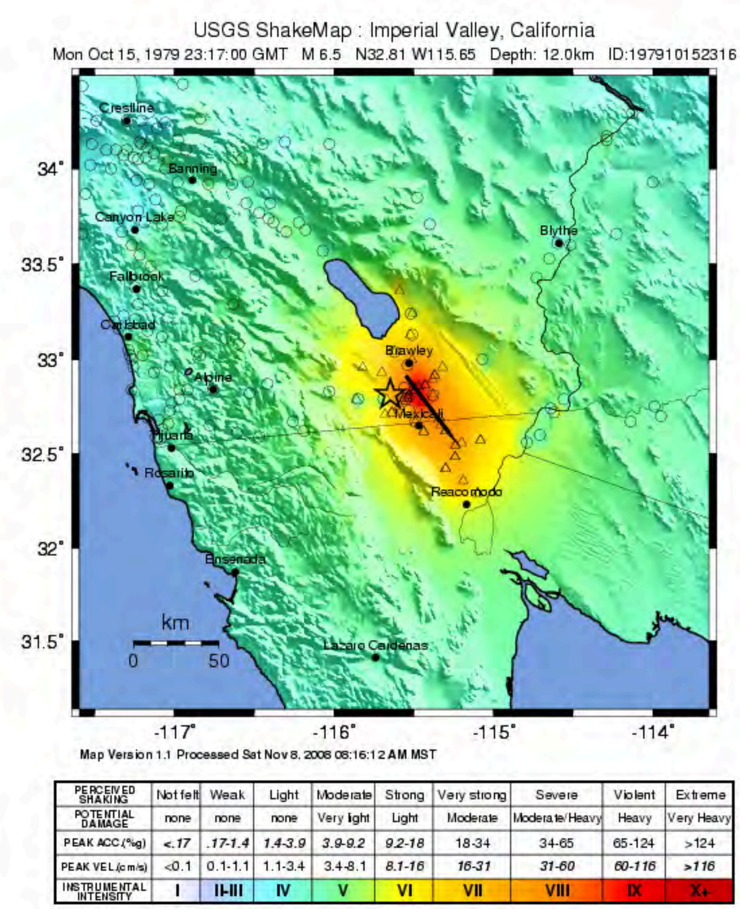

Figure 9.28: Example of a shake map. Figure description available at the end of the chapter.

Shake maps, written ShakeMaps by the USGS, use high-quality, computer-interpolated data from seismograph networks to show areas of intense shaking. Shake maps are useful in the crucial minutes after an earthquake, as they show emergency personnel where the greatest damage likely occurred and help them locate possibly damaged gas lines and other utility facilities.

Take this quiz to check your comprehension of this section.

Access the quiz for Section 9.7 by scanning the QR code.

9.8 Earthquake Risk

9.8.1 Factors That Determine Shaking

Earthquake magnitude is an absolute value that measures pure energy release. However, intensity (i.e., how much the ground shakes) is determined by several factors.

Earthquake magnitude: In general, the larger the magnitude, the stronger the shaking and the longer the shaking will last.

This table is taken from the USGS and shows scales of magnitude and Mercalli intensity, as well as descriptions of shaking and resulting damage.

Magnitude	Modified Mercalli intensity	Shaking/damage description
1.0-3.0	I	Only felt by a very few.
3.0-3.9	II-III	Noticeable indoors, especially on upper floors.
4.0-4.9	IV-V	Most to all feel it. Dishes, doors, cars shake and possibly break.
5.0-5.9	VI-VII	Everyone feels it. Some items knocked over or broken. Building damage possible.
6.0-6.9	VII-IX	Frightening amounts of shaking. Significant damage especially with poorly constructed buildings.
≥ 7.0	≥ VIII	Significant destruction of buildings. Potential for objects to be thrown in air from shaking.

Table 9.4: Mercalli intensity as it relates to magnitude.

Location and direction: Shaking is more severe closer to the epicenter. The severity of shaking is influenced by the location of the observer relative to epicenter, direction of rupture propagation, and path of greatest rupture.

Local geologic conditions: Seismic waves are affected by the nature of the ground materials through which they pass. Different materials respond differently to an earthquake. Think of shaking a block of Jell-O versus a meatloaf—one will jiggle much more when hit by waves of the same amplitude. The ground's response to shaking depends on the degree of substrate consolidation. Solid sedimentary, igneous, or metamorphic bedrock shakes less than unconsolidated sediments.

Video 9.10: How different substrates behave in response to different seismic waves and their potential for destruction

Access this YouTube video by scanning the QR code. ["Amplification and Liquefaction Animation (Educational)" by IRIS Earthquake Science | https://www.youtube.com/watch?v=536xSZ_XkSs]

Seismic waves move fastest through consolidated bedrock, slower through unconsolidated sediments, and slowest through unconsolidated sediments with a high water content. Seismic energy is transmitted by wave velocity and amplitude. When seismic waves slow down, energy is transferred to the amplitude, increasing the motion of surface waves, which in turn amplifies ground shaking.

Focus depth: Deeper earthquakes cause less surface shaking because much of their energy, transmitted as body waves, is lost before reaching the surface. Recall that surface waves are generated by P and S waves impacting the Earth's surface.

9.8.2 Factors That Determine Destruction

Just as certain conditions will impact intensity of ground shaking, several factors affect how much destruction is caused.

Building materials: The flexibility of a building material determines its resistance to earthquake damage. Unreinforced masonry (URM) is the material most devastated by ground shaking. Wood framing fastened with nails bends and flexes during seismic wave passage and is more likely to survive intact. Steel also has the ability to deform elastically before brittle failure. The Fix the Bricks campaign in Salt Lake City, Utah, has good information on URMs and earthquake safety.

Figure 9.29: Example of devastation on unreinforced masonry by seismic motion. Figure description available at the end of the chapter.

Intensity and duration: Greater shaking and duration of shaking causes more destruction than lower and shorter shaking.

Resonance: Resonance occurs when seismic wave frequency matches a building's natural shaking frequency and increases the shaking. This happened in the 1985 Mexico City earthquake, where buildings of heights between six and 15 stories were especially vulnerable to earthquake damage. Skyscrapers designed with earthquake resilience have dampers and base isolation features to reduce resonance.

Resonance is influenced by the properties of the building materials. Changes in the structural integrity of a building can alter resonance. Conversely, changes in measured resonance can indicate a potentially altered structural integrity.

These two videos discuss why buildings fall during earthquakes and a modern procedure to reduce potential earthquake destruction for larger buildings.

Video 9.11: Why do buildings fall in earthquakes?

Access this YouTube video by scanning the QR code. ["Why do buildings fall in earthquakes? – Vicki V. May" by TED-Ed | https://www.youtube.com/watch?v=H4VQul_SmCg]

Video 9.12: Base isolators

Access this YouTube video by scanning the QR code. ["Utah State Capital Building – Base Isolators" by ReadySetPrepShow | https://www.youtube.com/watch?v=DP7fB1I7UwE]

9.8.3 Earthquake Recurrence

A long hiatus in activity along a fault segment with a history of recurring earthquakes is known as a **seismic gap**. The lack of activity may indicate the fault segment is locked, which may produce a buildup of strain and higher probability of an earthquake recurring. Geologists dig earthquake trenches across faults to estimate the frequency of past earthquake occurrences. Trenches are effective for faults with relatively long **recurrence** intervals of roughly 100s to 10,000s of years between significant earthquakes. Trenches are less useful in areas with more frequent earthquakes because they usually have more recorded data.

Figure 9.30: Fault trench near Teton Fault. Trenches allow geologists to see a cross section of a fault and to use dating techniques to determine how frequently earthquakes occur. Figure description available at the end of the chapter.

9.8.4 Earthquake Distribution

Like volcanoes, earthquakes tend to aggregate around active boundaries of tectonic plates. The exception is intraplate earthquakes, which are comparatively rare.

Below are five areas where different sizes of earthquakes occur.

Subduction zones: Subduction zones, found at convergent plate boundaries, are where megathrust earthquakes, the largest and deepest earthquakes, occur. Examples of subduction-zone earthquake areas include the Sumatran Islands, Aleutian Islands, west coast of South America, and Cascadia subduction zone off the coast of Washington and Oregon. See Chapter 2 for more information about subduction zones.

Collision zones: Collisions between converging continental plates create broad earthquake zones that may generate deep, large earthquakes from the remnants of past subduction events or other deep-crustal processes. The Himalayan Mountains (northern border of the Indian subcontinent) and Alps (southern Europe and Asia) are active regions of collision-zone earthquakes. See Chapter 2 for more information about collision zones.

Transform boundaries: Strike-slip faults created at transform boundaries produce moderate-to-large earthquakes that usually have a maximum moment magnitude of about 8. The San Andreas fault (California) is an example of a transform-boundary earthquake zone. Other examples of transform faults include Haiti's Enriquillo-Plantain Garden fault system, which caused the 2010 earthquake near Port-au-Prince (see below), and Septentrional fault, which destroyed Cap-Haïtien in 1842 and shook Cuba in 2020, as well as the Alpine fault (New Zealand) and Anatolian faults (Turkey). See Chapter 2 for more information about transform boundaries.

Divergent boundaries: Continental rifts and mid-ocean ridges found at divergent boundaries generally produce moderate earthquakes. Examples of active earthquake zones include the East African Rift System (southwestern Asia through eastern Africa), Iceland, and Basin and Range Province (Nevada, Utah, California, Arizona, and northwestern Mexico). See Chapter 2 for more information about divergent boundaries.

Intraplate earthquakes: Intraplate earthquakes are not found near tectonic plate boundaries but generally occur in areas of weakened crust or concentrated tectonic stress. The New Madrid seismic zone, which covers Missouri, Illinois, Tennessee, Arkansas, and Indiana, is thought to represent the failed Reelfoot rift. The failed rift zone weakened the crust, making it more responsive to tectonic plate movement and interaction. Geologists theorize the infrequently occurring earthquakes are produced by low strain rates

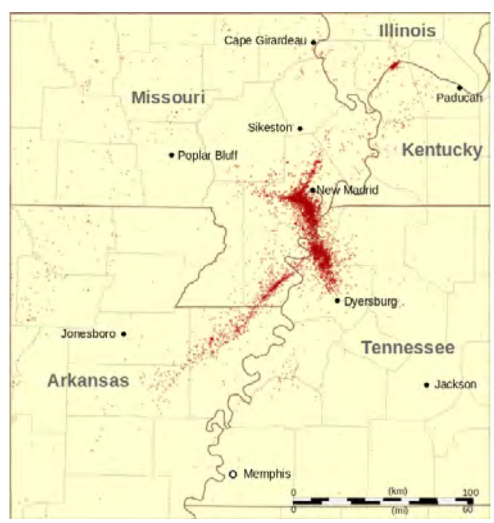

Figure 9.31: High density of earthquakes in the New Madrid seismic zone. Figure description available at the end of the chapter.

9.8.5 Secondary Hazards Caused by Earthquakes

Most earthquake damage is caused by ground shaking and fault block displacement. In addition, there are secondary hazards that endanger structures and people, in some cases after the shaking stops.

Buildings toppled from liquefaction during a 7.5 magnitude earthquake in Japan.

Liquefaction: Liquefaction occurs when water-saturated, unconsolidated sediments, usually silt or sand, become fluidlike from shaking. The shaking breaks the cohesion between grains of sediment, creating a slurry of particles suspended in water. Buildings settle or tilt in the liquified sediment, which looks very much like quicksand from the movies. Liquefaction also creates sand volcanoes, cone-shaped features created when liquefied sand is squirted through an overlying and usually finer-grained layer.

Figure 9.32: Buildings toppled from liquefaction during a 7.5 magnitude earthquake in Japan. Figure description available at the end of the chapter.

Video 9.13: How liquefaction takes place

Access this YouTube video by scanning the QR code. ["Liquefaction Demonstrated" by Illinois State Geological Survey | https://www.youtube.com/watch?v=b_aIm5oi5eA]

This video shows liquefaction occurring during the 2011 earthquake in Japan.

Video 9.14: Liquefaction during the 2011 earthquake in Japan

Access this YouTube video by scanning the QR code. ["Great Eastern Japan Earthquake – Liquefaction in Makuhari" by Brent Kooi | https://www.youtube.com/watch?v=rn3oAvmZY8k]

Tsunamis: Among the most devastating natural disasters are **tsunamis**, earthquake-induced ocean waves. When the seafloor is offset by fault movement or an underwater landslide, the ground displacement lifts a volume of ocean water and generates the tsunami wave. Ocean wave behavior, which includes tsunamis, is covered in Chapter 12. Tsunami waves are fast-moving with low amplitude in deep ocean water, but their amplitude grows significantly in the shallower waters approaching shore. When a tsunami is about to strike land, the drawback of the trough preceding the wave crest causes the water to recede dramatically from shore. Tragically, curious people wander out and follow the disappearing water, only to be overcome by an oncoming wall of water that can be upwards of a 30 m (100 ft) high. Early warning systems help mitigate the loss of life caused by tsunamis.

Figure 9.33: As the ocean depth becomes shallower, the wave slows down and piles up on top of itself, making large, high-amplitude waves. Figure description available at the end of the chapter.

Landslides: Shaking can trigger landslides (see Chapter 10). In 1992, a moment magnitude 5.9 earthquake in St. George, Utah, caused a landslide that destroyed several structures in the Balanced Rock Hills subdivision in Springville, Utah.

Seiches: Seiches are waves generated in lakes by earthquakes. The shaking may cause water to slosh back and forth, or sometimes change the lake depth. Seiches in Hebgen Lake during a 1959 earthquake caused major destruction to nearby structures and roads.

This video shows a seich generated in a swimming pool by an earthquake in Nepal in 2015.

Figure 9.34: Schoolhouse in Thistle, Utah, destroyed by a landslide. Figure description available at the end of the chapter.

Video 9.15: A seich generated in a swimming pool by an earthquake in Nepal in 2015

Access this YouTube video by scanning the QR code. ["Nepal Earthquake Today Live Video – Swimming Pool CCTV Footage" by Movie Talkies | https://www.youtube.com/watch?v=muLgPPu6c_I]

Land elevation changes: Elastic rebound and displacement along the fault plane can cause significant land elevation changes, such as subsidence or upheaval. The 1964 Alaska earthquake produced significant land elevation changes, with the differences in height between the hanging wall and footwall ranging from one to several meters (3–30 ft). The Wasatch Mountains in Utah represent an accumulation of fault scarps created a few meters at a time, over a few million years.

Take this quiz to check your comprehension of this section.

Access the quiz for Section 9.8 by scanning the QR code.

9.9 Case Studies

Video 9.16 explains the seismic activity and hazards of the Intermountain seismic belt and the Wasatch fault, a large intraplate area of seismic activity.

Video 9.16: Activities of the Intermountain seismic belt and the Wasatch fault.

Access this YouTube video by scanning the QR code. ["Wasatch Fault Fly By Video (high quality)" by Utah Geological Survey | https://www.youtube.com/watch?v=DByPiCkznE0]

9.9.1 North American Earthquakes

Basin and Range earthquakes: Earthquakes in the Basin and Range Province, from the Wasatch fault (Utah) to the Sierra Nevada (California), occur primarily in normal faults created by tensional forces. The Wasatch fault, which defines the eastern extent of the Basin and Range Province, has been studied as an earthquake hazard for more than 100 years.

New Madrid earthquakes (1811–1812): Historical accounts of earthquakes in the New Madrid seismic zone date as far back as 1699, and earthquakes continue to be reported in modern times. A sequence of large (M_W >7) occurred from December 1811 to February 1812 in the New Madrid area of Missouri. The earthquakes damaged houses in St. Louis, affected the stream course of the Mississippi River, and leveled the town of New Madrid. These earthquakes were the result of intraplate seismic activity.

Charleston (1886): The 1886 earthquake in Charleston, South Carolina, was a moment magnitude 7.0, with a Mercalli intensity of X. It caused significant ground motion and killed at least 60 people. This intraplate earthquake was likely associated with ancient faults created during the breakup of Pangea. The earthquake caused significant liquefaction. Scientists estimate the recurrence of destructive earthquakes in this area with an interval of approximately 1,500 to 1,800 years.

Great San Francisco earthquake and eire (1906): On April 18, 1906, a large earthquake with an estimated moment magnitude of 7.8 and MMI of X occurred along the San Andreas fault near San Francisco, California. There were multiple aftershocks followed by devastating fires, resulting in about 80% of the city being destroyed. Geologists G.K. Gilbert and Richard L. Humphrey, working independently, arrived the day following the earthquake and took measurements and photographs**.**

Figure 9.35: Remains of San Francisco after the 1906 earthquake and fire. Figure description available at the end of the chapter.

Alaska (1964): The 1964 Alaska earthquake, moment magnitude 9.2, was one of the most powerful earthquakes ever recorded. The earthquake originated in a megathrust fault along the Aleutian subduction zone. The earthquake caused large areas of land subsidence and uplift, as well as significant mass wasting.

The following video from the USGS describes the 1964 Alaska earthquake.

Video 9.17: The 1964 Alaska earthquake

Access this YouTube video by scanning the QR code. ["1964 Quake: The Great Alaska Earthquake" by USGS | https://www.youtube.com/watch?v=lE2j10xyOgI]

Loma Prieta (1989): The Loma Prieta, California, earthquake was created by movement along the San Andreas fault. The moment magnitude 6.9 earthquake was followed by a magnitude 5.2 aftershock. It caused 63 deaths, buckled portions of the several freeways, and collapsed part of the San Francisco-Oakland Bay Bridge.

This video shows how shaking propagated across the Bay Area during the 1989 Loma Prieta earthquake.

Video 9.18: How shaking propagated across the Bay Area during the 1989 Loma Prieta earthquake

Access this YouTube video by scanning the QR code. ["1989 Loma Prieta Earthquake – Shaking Intesity Animation" by LiveScience | https://www.youtube.com/watch?v=VuQSs7QHL28]

This video shows destruction caused by the 1989 Loma Prieta earthquake.

Video 9.19: Destruction caused by the 1989 Loma Prieta earthquake

Access this YouTube video by scanning the QR code. ["Loma Prieta Earthquake, CA, 1989, Part 1" by Lin Kerns | https://www.youtube.com/watch?v=L6jYgqLyIPw]

9.9.2 Global Earthquakes

Many of history's largest earthquakes occurred in megathrust zones, such as the Cascadia subduction zone (Washington and Oregon coasts) and Mount Rainier (Washington).

Shaanxi, China (1556): On January 23, 1556, an earthquake of an approximate moment magnitude 8 hit Central China, killing approximately 830,000 people in what is considered the most deadly earthquake in history. The high death toll was attributed to the collapse of cave dwellings (*yaodong*) built in loess deposits, which are large banks of windblown, compacted sediment (see Chapter 5). Earthquakes in this are region believed to have a recurrence interval of 1,000 years.

Lisbon, Portugal (1755): On November 1, 1755, an earthquake with an estimated moment magnitude range of 8–9 struck Lisbon, Portugal, killing between 10,000 to 17,400 people. The earthquake was followed by a tsunami, which brought the total death toll to between 30,000–70,000 people.

Valdivia, Chile (1960): The May 22, 1960, earthquake was the most powerful earthquake ever measured, with a moment magnitude 9.4–9.6 and lasting an estimated ten minutes. It triggered tsunamis that destroyed houses across the Pacific Ocean in Japan and Hawai'i and caused vents to erupt on the Puyehue-Cordón Caulle (Chile).

Below is a video describing the tsunami produced by the 1960 Chile earthquake.

Video 9.20: Tsunami produced by the 1960 Chile earthquake

Access this YouTube video by scanning the QR code. ["Tsunami Animation: Valdivia, Chile, 1960 (rotating globe)" by PacificTWC | https://www.youtube.com/watch?v=RHYbprZAIWo]

Tangshan, China (1976): Just before 4 a.m. (Beijing time) on July 28, 1976, a moment magnitude 7.8 earthquake struck Tangshan (Hebei Province), China, and killed more than 240,000 people. The high death toll is attributed to people still being asleep or at home and most buildings being made of unreinforced masonry.

Sumatra, Indonesia (2004): On December 26, 2004, slippage of the Sunda megathrust fault generated a moment magnitude 9.0–9.3 earthquake off the coast of Sumatra, Indonesia. This megathrust fault is created by the Australia plate subducting below the Sunda plate in the Indian Ocean. The resultant tsunamis created massive waves as tall as 24 m (79 ft) when they reached the shore and killed more than an estimated 200,000 people along the Indian Ocean coastline.

Haiti (2010): The moment magnitude 7 earthquake that occurred on January 12, 2010, was followed by many aftershocks of magnitude 4.5 or higher. More than 200,000 people are estimated to have died as result of the earthquake. The widespread infrastructure damage and crowded conditions contributed to a cholera outbreak, which is estimated to have caused thousands more deaths.

Tōhoku, Japan (2011): Because most Japanese buildings are designed to tolerate earthquakes, the moment magnitude 9.0 earthquake on March 11, 2011, was not as destructive as the tsunami it created. The tsunami caused more than 15,000 deaths and tens of billions of dollars in damage, including the destructive meltdown of the Fukushima nuclear power plant.

Take this quiz to check your comprehension of this section.

Access the quiz for Section 9.9 by scanning the QR code.

Summary

Geologic stress, applied force, comes in three types: tension, shear, and compression. Strain is produced by stress and results in three types of deformation: elastic, ductile, and brittle. Geological maps are two-dimensional representations of surface formations, which are the surface expression of three-dimensional geologic structures in the subsurface. The map symbol called strike and dip, or rock attitude, indicates the orientation of rock strata with reference to north-south and horizontal. Folded rock layers are categorized by the orientation of their limbs—fold axes and axial planes. Faults result when stress forces exceed rock integrity and friction, leading to brittle deformation and breakage. The three major fault types are described by the movement of their fault blocks: normal, strike-slip, and reverse.

Earthquakes, or seismic activity, are caused by sudden brittle deformation accompanied by elastic rebound. The release of energy from an earthquake focus is generated as seismic waves. P and S waves travel through the Earth's interior. When they strike the outer crust, they create surface waves. Human activities, such as mining and nuclear detonations, can also cause seismic activity. Seismographs measure the energy released by an earthquake using a logarithmic scale of magnitude units; the moment magnitude scale has replaced the original Richter scale. Earthquake intensity is the perceived effects of ground shaking and physical damage. The location of earthquake foci is determined from triangulation readings from multiple seismographs.

Earthquake rays passing through rocks of the Earth's interior and measured at the seismographs of the worldwide Seismic Network allow 3-D imaging of buried rock masses as seismic tomographs.

Earthquakes are associated with plate tectonics. They usually occur around the active plate boundaries, including zones of subduction, collision, and transform and divergent boundaries. Areas of intraplate earthquakes also occur. The damage caused by earthquakes depends on a number of factors, including magnitude, location and direction, local conditions, building materials, intensity and duration, and resonance. In addition to damage directly caused by ground shaking, secondary earthquake hazards include liquefaction, tsunamis, landslides, seiches, and elevation changes.

Take this quiz to check your comprehension of this chapter.

Access the quiz for Chapter 9 by scanning the QR code.

Chapter URLs

- UGS geologic map viewer: https://geomap.geology.utah.gov
- AAPG wiki: https://wiki.aapg.org/Cross_section
- USGS Earthquakes Hazards Program: https://earthquake.usgs.gov/earthquakes/map
- Rayleigh waves: Propagation of Seismic Waves: Rayleigh waves. [Video: 0:15] https://www.youtube.com/watch?v=6yXgfYHAS7c
- Love waves: Propagation of Seismic Waves: Love waves. [Video: 0:15] https://www.youtube.com/watch?v=t7wJu0Kts7w
- International Registry of Seismograph Stations: https://www.isc.ac.uk/registries
- Global Seismic Network: https://www.usgs.gov/programs/earthquake-hazards/gsn-global-seismographic-network
- USArray: http://www.usarray.org
- Comprehensive Nuclear Test Ban Treaty Organization: https://www.ctbto.org

Text References

1. Christenson, G.E. (1995). The September 2, 1992, ML 5.8 St. George earthquake, Washington County, Utah. *Utah Geological Survey Circular 88.*
2. Coleman, J.L., and Cahan, S.M. (2012). Preliminary catalog of the sedimentary basins of the United States. *United States Geological Survey Open-File Report 1111.*
3. Earle, S. (2015). *Physical geology OER textbook:* BC Campus OpenEd.
4. Feldman, J. (2012). *When the Mississippi ran backwards: Empire, intrigue, murder, and the New Madrid earthquakes of 1811 and 1812:* Free Press.
5. Fuller, M.L. (1912). The New Madrid earthquake. *Central United States Earthquake Consortium Bulletin 494*, 129.
6. Gilbert, G.K., and Dutton, C.E. (1877). Report on the geology of the Henry Mountains: U.S. Government Printing Office, 160.
7. Hildenbrand, T.G., and Hendricks, J.D. (1995). Geophysical setting of the Reelfoot rift and relations between rift structures and the New Madrid seismic zone. *United States Geological Survey Professional Paper 1538*-E, 36.
8. Means, W.D. (1976). *Stress and strain – Basic concepts of continuum mechanics:* Springe.
9. Ressetar, R. (ed.). (2013). The San Rafael Swell and Henry Mountains Basin: Geologic centerpiece of Utah. Utah Geological Association, 250.
10. Satake, K., and Atwater, B.F. (2007). Long-term perspectives on giant earthquakes and tsunamis at subduction zones. *Annual Review of Earth and Planetary Sciences, 35*(1), 349–374. doi: 10.1146/annurev.earth.35.031306.140302.
11. Talwani, P., and Cox, J. (1985). Paleoseismic evidence for recurrence of Earthquakes near Charleston, South Carolina. *Science, 229*(4711), 379–381.

Figure References

Figure 9.1: Types of stress. Michael Kimberly, North Carolina State University via United States Geological Survey (USGS). 2021. Adapted by Laura Neser. Public domain. https://www.usgs.gov/media/images/stresstypesgif

Figure 9.2: Different materials deform differently when stress is applied. Steven Earle. 2019. CC BY. Figure 12.1.1 from https://opentextbc.ca/physicalgeology2ed/chapter/12-1-stress-and-strain

Figure 9.3: "Strike" and "dip" are words used to describe the orientation of rock layers with respect to north/south and horizontal. CrunchyRocks. 2018. CC BY 4.0. https://commons.wikimedia.org/wiki/File:Strike_and_dip_on_bedding.svg

Figure 9.4: Attitude symbol on geologic map (with compass directions for reference) showing strike of N30°E and dip of 45° to the SE. Kindred Grey. 2022. CC BY 4.0. Includes Compass Rose by NAPISAH from Noun Project (Noun Project license).

Figure 9.5: Model of anticline. Speleotherm. 2016. CC BY-SA 4.0. https://commons.wikimedia.org/wiki/File:Anticline.png

Figure 9.6: An anticline near Bcharre, Lebanon. Not home. 2005. Public domain. https://commons.wikimedia.org/wiki/File:Anticline-lebanon.jpg

Figure 9.7: Monocline at Colorado National Monument. Anky-man. 2007. CC BY-SA 3.0. https://commons.wikimedia.org/wiki/File:Monocline.jpg

Figure 9.8: This prominent circular feature in the Sahara Desert of Mauritania has attracted attention since the earliest space missions because it forms a conspicuous bull's-eye in the otherwise rather-featureless expanse of the desert. NASA/GSFC/MITI/ERSDAC/JAROS, and US/Japan ASTER Science Team. 2000. Public domain. https://commons.wikimedia.org/wiki/File:ASTER_Richat.jpg

Figure 9.9: The Denver Basin is an active sedimentary basin at the eastern extent of the Rocky Mountains. Daniel H. Knepper, Jr. (ed.), USGS. 2002. Public domain. https://commons.wikimedia.org/wiki/File:Denver_Basin_Location_Map.png

Figure 9.10: Common terms used for normal faults. Kindred Grey. 2022. CC BY-SA 3.0. Includes Faults6 by Actualist, 2013 (CC BY-SA 3.0, https://commons.wikimedia.org/wiki/File:Faults6.png).

Figure 9.11: Example of a normal fault in an outcrop of the Pennsylvanian Honaker Trail Formation near Moab, Utah. James St. John. 2007. CC BY 2.0. https://commons.wikimedia.org/wiki/File:Faults_in_Moenkopi_Formation_Moab_Canyon_Utah_USA_01.jpg

Figure 9.12: Faulting that occurs in the crust under tensional stress. USGS; adapted by Gregors. 2011. Public domain. https://commons.wikimedia.org/wiki/File:Fault-Horst-Graben.svg

Figure 9.13: Simplified block diagram of a reverse fault. Kindred Grey. 2022. CC BY-SA 3.0. Includes Faults6 by Actualist, 2013 (CC BY-SA 3.0, https://commons.wikimedia.org/wiki/File:Faults6.png).

Figure 9.14: Terminology of thrust faults (low-angle reverse faults). Woudloper. 2006. Public domain. https://commons.wikimedia.org/wiki/File:Thrust_system_en.jpg

Figure 9.15: Thrust fault in the northern Qilian Mountains (Qilian Shan). Jide. 2006. CC BY-SA 3.0. https://commons.wikimedia.org/wiki/File:Thrust_fault_Qilian_Shan.jpg

Figure 9.16: Flower structures created by strike-slip faults. Mikenorton. 2009. CC BY-SA 3.0. https://commons.wikimedia.org/wiki/File:Flowerstructure1.png

Figure 9.17: Process of elastic rebound: (a) Undeformed state, (b) accumulation of elastic strain, and (c) brittle failure and release of elastic strain. Steven Earle. Unknown date. CC BY 4.0. Figure 11.2 from https://open.maricopa.edu/physicalgeology/chapter/11-1-what-is-an-earthquake

Figure 9.18: The hypocenter is the point along the fault plane in the subsurface from which seismic energy emanates. Derived from original work by Sam Hocevar. 2014. CC BY-SA 1.0. https://commons.wikimedia.org/wiki/File:Epicenter_Diagram.svg

Figure 9.19: Example of constructive and destructive interference. Note the red line representing the results of interference. Lookangmany, thanks to author of original simulation, Wolfgang Christian, and to Francisco Esquembre, author of Easy Java Simulation. 2015. CC BY-SA 4.0. https://commons.wikimedia.org/wiki/File:Waventerference.gif

Figure 9.20: P waves are compressional. Christophe Dang Ngoc Chan. 2006. CC BY-SA 3.0. https://commons.wikimedia.org/wiki/File:Onde_compression_impulsion_1d_30_petit.gif

Figure 9.21: S waves are shear. Christophe Dang Ngoc Chan. 2006. CC BY-SA 3.0. https://commons.wikimedia.org/wiki/File:Onde_cisaillement_impulsion_1d_30_petit.gif

Figure 9.22: Frequency of earthquakes in the Central United States. USGS. 2019. Public domain. https://commons.wikimedia.org/wiki/File:Cumulative_induced_seismicity.png

Figure 9.23: A seismogram showing the arrivals of the P, S, and surface waves. Kindred Grey. 2022. CC BY 4.0. Adapted from USGS (Public domain, https://www.usgs.gov/media/images/seismic-wave-showing-p-wave-and-s-wave-initiation).

Figure 9.24: Global network of seismic stations. USGS. 2022. Public domain. https://www.usgs.gov/media/images/global-seismographic-network-gsn-stations

Figure 9.25: Speed of seismic waves with depth in the Earth. Brews ohare. 2010. CC BY-SA 3.0. https://commons.wikimedia.org/wiki/File:Speeds_of_seismic_waves.png

Figure 9.26: Simplified and interpreted P- and S-wave velocity variations in the mantle across southern North America, showing the subducted Farallon plate. Oilfieldvegetarian. 2016. CC BY-SA 4.0. https://commons.wikimedia.org/wiki/File:FarallonTomoSlice.png

Figure 9.27: Tomographic image of the Farallon plate in the mantle below North America. Stuart A. Snodgrass and Hans-Peter Bunge via NASA. 2002. Public domain. https://commons.wikimedia.org/wiki/File:Farallon_Plate.jpg

Figure 9.28: Example of a shake map. USGS. 2012. Public domain. https://en.wikipedia.org/wiki/File:USGS_Shakemap_-_1979_Imperial_Valley_earthquake.jpg

Figure 9.29: Example of devastation on unreinforced masonry by seismic motion. M. Mehrain, Dames, and Moore via NOAA/NGDC. 2012. Public domain. https://commons.wikimedia.org/wiki/File:Collapse_of_Unreinforced_Masonry_Buildings,_Iran_(Persia)_-_1990_Manjil_Roudbar_Earthquake.jpg

Figure 9.30: Fault trench near Teton Fault. Jaime Delano via USGS. 2017. Public domain. https://www.usgs.gov/media/images/teton-fault-4

Figure 9.31: High density of earthquakes in the New Madrid seismic zone. Kbh3rd. 2011. CC BY-SA 3.0. https://commons.wikimedia.org/wiki/File:New_Madrid_Seismic_Zone_activity_1974-2011.svg

Figure 9.32: Buildings toppled from liquefaction during a 7.5 magnitude earthquake in Japan. Ungtss. 1964. Public domain. https://commons.wikimedia.org/wiki/File:Liquefaction_at_Niigata.jpg

Figure 9.33: As the ocean depth becomes shallower, the wave slows down and piles up on top of itself, making large, high-amplitude waves. Régis Lachaume. 2005. CC BY-SA 3.0. https://commons.wikimedia.org/wiki/File:Propagation_du_tsunami_en_profondeur_variable.gif

Figure 9.34: Schoolhouse in Thistle, Utah, destroyed by a landslide. Jenny Bauman. 2006. CC BY-SA 2.0. https://commons.wikimedia.org/wiki/File:Thistle-School_house.jpg

Figure 9.35: Remains of San Francisco after the 1906 earthquake and fire. Lester C. Guernsey. 1906. Public domain. https://commons.wikimedia.org/wiki/File:San_Francisco_1906_earthquake_Panoramic_View.jpg

Figure Descriptions

Figure 9.1: Tensional stress where dominant stresses are pulling away from the object, compressional stress where dominant stress is pushing in towards the object, and shear, where part of the object is pushed and part of the object is pulled (stresses in opposite directions)

Figure 9.2: Chart with Stress increasing upward and Strain increasing toward the right; three color-coded curves are on the graph: curve A is green and increases upward with little movement toward the right until it ends near the top; curve B is red and increases upward before abruptly ending; and curve C is yellow and has a broad arc up and to the right before ending toward the far right of the chart.

Figure 9.3: Block diagram showing three stacked sedimentary layers gently dipping with a transparent horizontal surface overlain on top of the layers; there is a dashed line where the horizontal layer intersects the dipping layers with the label Horizontal line on the dipping surface; the angle between the horizontal layer and the dipping layers is 20 degrees and labeled Dip; on the top of the dipping layers is a T-shaped symbol labeled Strike and dip symbol, with the number 20 in the lower right. In the upper right of the figure is a T-shaped symbol with an arrow along the longest part labeled Strike Direction; at the lower right of the T is the number 20, labeled Dip angle; and the smaller part of the symbol is labeled Indicates dip direction (downhill).

Figure 9.4: A compass rose showing N, E, S, and W; a T-shaped strike and dip symbol is next to it with the longest part oriented roughly northeast-southwest. The shortest part of the strike and dip symbol points toward the southeast and is labeled 45 degrees.

Figure 9.5: Model of anticline. Oldest beds are in the center and youngest on the outside. The axial plane intersects the center angle of bend. The hinge line follows the line of greatest bend, where the axial plane intersects the outside of the fold; two arrows point inward toward the axial plane labeled Stress.

Figure 9.6: View of a hillside with exposed sedimentary layers that form an arch shape.

Figure 9.7: View of a cliffside with a series of tan to red sedimentary layers visible; they are horizontal on the left-hand side and angle downward toward the right.

Figure 9.8: View of a dome from space. The upwarped beds of rock form concentric circles, where the center of the dome has been eroded away.

Figure 9.9: Schematic map of the Denver Basin, a sedimentary basin under under northeastern Colorado, southeastern Wyoming, and southwestern Nebraska; the Front Range Uplift runs approximately north to south along the left side of the basin. The map includes a cross section of the area, showing yellow sedimentary beds folding downward into a syncline.

Figure 9.10: Block diagram of a normal fault. The footwall is the block on the left which has moved upward and the hanging wall is the block on the right which has moved downward; a fault runs from upper left to lower right between the blocks; the exposed side of the foot wall along the surface is labeled Fault scarp.

Figure 9.11: Roadcut cliffside outcrop of multicolor sedimentary beds offset by a normal fault; on either side of the fault, the rocks on the right-side hanging wall have moved downward relative to the rocks on the left-side foot wall.

Figure 9.12: Block diagram showing a series of three uplifted horsts with a downthrown graben between each horst; the entire area extends with arrows pointing outward; there are normal faults at each of the contacts between horsts and grabens.

Figure 9.13: Block diagram of a reverse fault. The hanging wall is the block on the left which has moved upward and the footwall is the block on the right which has moved downward; a fault runs from upper right to lower left between the blocks.

Figure 9.14: Block diagram of a landscape with numerous thrust fault features: the base of the landscape is the footwall, labeled Autochton material and colored white; on the left-hand side of the diagram, a gray oval-shaped piece of land is on top of the landscape with a thrust fault at its base, labeled klippe; gray hills sit on top of the white landscape on the right-hand side of the diagram with a thrust fault at its base, labeled Nappe; there is a white oval-shaped exposure in the gray hills labeled Window.

Figure 9.15: View of a cliffside with gray rocks on the left-hand side; red rocks are to the right of the gray rock with a fault plane visible below the red rocks, angled from the lower left to upper right; below and on the right side of the fault are brown sedimentary rocks.

Figure 9.16: Two block diagrams: the left diagram shows mountains that have formed on the surface as a result of a strike-slip fault causing wedges of rock to move upward, labeled Positive Flower; the right diagram shows basins that have formed on the surface as a result of a strike-slip fault causing wedges of rock to move downward, labeled Negative Flower.

Figure 9.17: A (prestressed state): rectangle with no movement. B (stressed rock deforms elastically): rectangle has curvy movement in the middle from top being pulled left and bottom being pulled right. C (post-rupture, unstressed rock): rectangle split in the middle on the rupture surface or fault plane. top moves left, bottom moves right.

Figure 9.18: The hypocenter is the point from which seismic energy emanates. The epicenter is the point on land surface vertically above the hypocenter.

Figure 9.19: Animated GIF showing green waves moving toward the right and blue waves of equal amplitude and wavelength moving toward the left; a red wave shows the resulting wave amplitude as the waves interact: when their wave crests match up, the total wave amplitude increases; when one wave crest matches with the other wave trough, the wave amplitude goes to zero.

Figure 9.20: Animated GIF showing a an approximately 30 by 30 grid with a compressional wave traveling through the grid, pushing the vertical lines closer together as it travels.

Figure 9.21: Animated GIF showing a an approximately 30 by 30 grid with a shear wave traveling through the grid, creating s-shaped curves as it travels.

Figure 9.22: A bar graph: the y-axis is "Number of M3+ Earthquakes" with a scale of 0 to 1200, and the x-axis is the year in question with a scale of 1970 to 2020. The bars spike sharply up after the year 2009, with the highest bar peak in 2015. There is also an inset map of the central United States that has dots of locations of earthquakes during this period, color-coded by magnitude. The densest cluster is in Oklahoma.

Figure 9.23: Squiggly lines along a horizontal axis. When the P-wave arrives, a small amplitude squiggle shows up. Then the S-wave arrives, and another small-amplitude squiggle shows. Finally, the surface-waves arrive, and large-amplitude waves show up, two to three times the amplitude of the body waves. Then the wave taper off and the line becomes essentially horizontal again.Number of seconds between the P and S waves is the distance from station to earthquake epicenter.

Figure 9.24: World map showing the distribution of Global Seismographic Network (GSN) stations. USGS GSN site locations are shown as blue triangles and IRIS/IDA station locations are shown as green triangles; the stations are spread across the entire globe.

Figure 9.25: Graph showing velocity of seismic waves in km/s increasing toward the right from 0 to 14 and depth in km increasing downward from 0 to 6000. S-wave is plotted in purple and increases velocity downward from approximately 3 km/s at 0 km depth to 6.5 km/s at 2900 km depth; at 2900 km the S-wave curve goes down to 0 km/s until it reaches 4600 km depth, where it increases to 4 km/s downward from there. P-wave is plotted in brown and increases velocity downward from approximately 6 km/s at 0 km depth to 14 km/s at 2900 km depth; at 2900 km the S-wave curve goes down to 7 km/s and begins increasing downward to 11 km/s at 6000 km depth. On the right-hand side of the diagram is a vertical bar with Mantle labeled at 0 to 2900 km depth, D"-layer labeled at 2900 to 3000 km depth, Outer Core labeled at 3000 to 5100 km, and Inner Core labeled at 5100 km to the bottom of the graph.

Figure 9.26: Two cross sections across the United States with the following color-coded seismic velocities: blue represents faster than average, red represents slower than average, and yellow represents near average. The top cross section is labeled P-wave velocity variations and there is a visible angled slab colored in blue that goes from about 420 km depth down toward the bottom of the diagram at 2700 km depth, labeled subducted Farallon Plate?; there is also blue along the top of the diagram near the center, with red blobs on the left and right near the surface; the rest is colored yellow. The bottom cross section is labeled S-wave velocity variations and there is a visible angled slab colored in blue that goes from the surface down toward the bottom of the diagram and ends at 2600 km depth, labeled subducted Farallon Plate?; there are small red blobs on the left near the surface as well as toward the right at depths of 400 to 700 km; the rest is colored yellow.

Figure 9.27: 3D yellow sphere centered on North America with red plate tectonic boundaries drawn on the surface; there is a wedge-shaped slice cut out which reveals a blue blobby slab visible at depth, representing the Farallon plate in the mantle.

Figure 9.28: Square shaded relief map centered over the Imperial Valley of southern California with latitude and longitude labeled around the edges of the map. Near the center of the map is star that marks an earthquake epicenter on the edge of a small red area shaded on the map; radiating outward from the red area are lighter red to orange to yellow areas, representing less and less shaking felt away from the epicenter of the earthquake. At the bottom of the figure is a chart showing the Mercalli Scale (described in the text).

Figure 9.29: Color photograph of rubble from the remains of a collapsed building; in the background are vegetation-covered mountains.

Figure 9.30: 5 people in bright vests stand at the bottom of a trench.

Figure 9.31: Map centered on southeastern Missouri, western Kentucky, northwestern Tennessee, southern Illinois, and northeastern Arkansas; earthquake epicenters are marked as red dots with a visible concentration near the border of southeastern Missouri, northwestern Tennessee, and northeastern Arkansas.

Figure 9.32: Three rows of rectangular-shaped buildings with the second and third rows of buildings having fallen over.

Figure 9.33: Animated gif showing large wavelength, low-amplitude waves in the deep ocean and high-amplitude, low-wavelength waves in the shallow ocean. Frequency decreases with depth.

Figure 9.34: Extremely damaged brick structure with only an archway remaining.

Figure 9.35: Panoramic black-and-white photo of rubble and the remains of buildings, some still smoking.

10. MASS WASTING

Learning Objectives

By the end of this chapter, students should be able to:

- Explain what mass wasting is and why it occurs on a slope.
- Explain the basic triggers of mass-wasting events and how they occur.
- Identify types of mass wasting.
- Identify risk factors for mass-wasting events.
- Evaluate landslides and their contributing factors.

This chapter discusses the fundamental processes driving mass wasting, types of mass wasting, examples and lessons learned from famous mass-wasting events, how mass wasting can be predicted, and how people can be protected from this potential hazard. **Mass wasting** is the downhill movement of rock and soil material due to gravity. The term landslide is often used as a synonym for mass wasting, but mass wasting is a much broader term referring to all movement downslope. Geologically, landslide is a general term for mass wasting that involves fast-moving geologic material; such an event typically involves the movement of loose material and overlying soils. Moving blocks of bedrock are called rock topples, rock slides, or rock falls, depending on the dominant motion of the blocks. Movements of dominantly liquid material are called flows. Movement by mass wasting can be slow or rapid. Rapid movement can be dangerous, as is often the case during **debris flows**. Areas with steep topography and rapid rainfall, such as the California coast, Rocky Mountain Region, and Pacific Northwest, are particularly susceptible to hazardous mass-wasting events.

10.1 Slope Strength

Mass wasting occurs when a slope fails. A slope fails when it is too steep and unstable for existing materials and conditions. Slope stability is ultimately determined by two principal factors: the slope angle and the strength of the underlying material. Force of gravity, which plays a part in mass wasting, is constant on the Earth's surface for the most part, although small variations exist depending on the elevation and density of the underlying rock. In Figure 10.1, a block of rock situated on a slope is pulled down toward the Earth's center by the force of gravity (*fg*). The gravitational force acting on a slope can be divided into two components: the shear or driving force (*fs*) pushing the block down the slope, and the normal or resisting force (*fn*) pushing into the slope, which produces friction. The relationship between **shear force** and **normal force** is called **shear strength**. When the normal force (i.e., friction) is greater than the shear force, then the block does *not* move downslope. However, if the slope angle becomes steeper or if the earth material is weakened, shear force exceeds normal force, compromising shear strength, and downslope movement occurs.

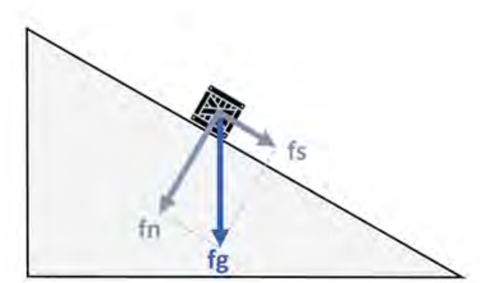

Figure 10.1: Forces on a block on an inclined plane (*fg* = force of gravity; *fn* = normal force; *fs* = shear force). Figure description available at the end of the chapter.

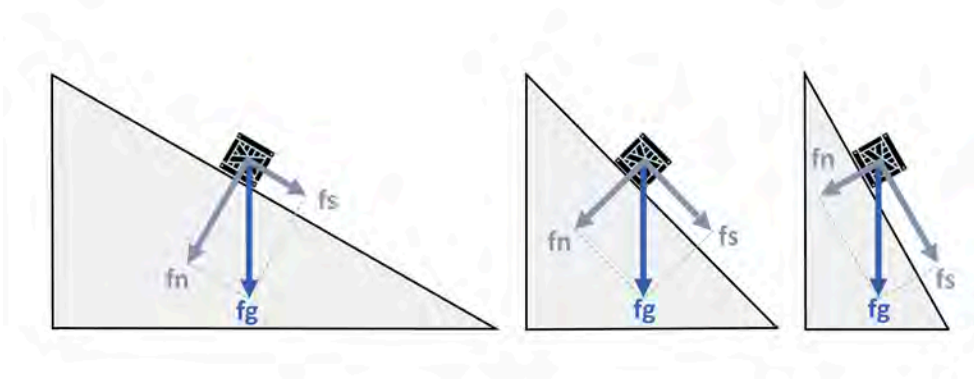

Figure 10.2: As slope increases, the force of gravity (*fg*) stays the same and the normal force decreases while the shear force proportionately increases. Figure description available at the end of the chapter.

In the figure, the force vectors change as the slope angle increases. The gravitational force doesn't change, but the shear force increases while the normal force decreases. The steepest angle at which rock and soil material is stable and will *not* move downslope is called the angle of repose. The angle of repose is measured relative from the horizontal. When a slope is at the angle of repose, the shear force is in equilibrium with the normal force. If the slope becomes just slightly steeper, the shear force exceeds the normal force, and the material starts to move downhill. The angle of repose varies for all material and slopes depending on many factors, such as grain size, grain composition, and water content. The figure shows the angle of repose for sand that is poured into a pile on a flat surface. The sand grains cascade down the sides of the pile until they come to a rest at the angle of repose. At that angle, the base and height of the pile continue to increase, but the angle of the sides remains the same.

Figure 10.3: Angle of repose in a pile of sand. Figure description available at the end of the chapter.

Water is a common factor that can significantly change the shear strength of a particular slope. Water is located in pore spaces, which are empty air spaces between the grains in sediments or rocks. For example, assume a dry sand pile has an angle of repose of 30 degrees. If water is added to the sand, the angle of repose will increase, possibly to 60 degrees or even 90 degrees, such as a sandcastle being built at a beach. But if too much water is added to the pore spaces of the sandcastle, the water decreases the shear strength and lowers the angle of repose, and the sandcastle collapses.

Another factor influencing shear strength are planes of weakness in sedimentary rocks. Bedding planes (see Chapter 5) can act as significant planes of weakness when they are parallel to the slope but less so if they are perpendicular to the slope. At locations A and B in Figure 10.4, the bedding is nearly perpendicular to the slope and relatively stable. At location D, the bedding is nearly parallel to the slope and quite unstable. At location C, the bedding is nearly horizontal, and the stability is intermediate between the other two extremes. Additionally, if clay minerals form along bedding planes, they can absorb water and become slick. When a bedding plane of shale (clay and silt) becomes saturated, it can lower the shear strength of the rock mass and cause a landslide, such as at the 1925 Gros Ventre, Wyoming, rock slide. See the case studies section for details on this and other landslides.

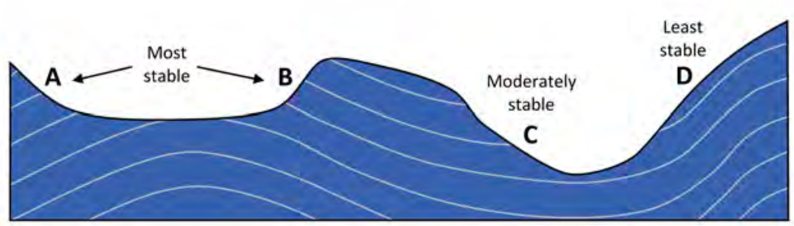

Figure 10.4: Locations A and B have bedding nearly perpendicular to the slope, making for a relatively stable slope. Location D has bedding nearly parallel to the slope, increasing the risk of slope failure. Location C has bedding nearly horizontal, and the stability is relatively intermediate. Figure description available at the end of the chapter.

Take this quiz to check your comprehension of this section.

Access the quiz for Section 10.1 by scanning the QR code.

10.2 Mass-Wasting Triggers & Mitigation

Mass-wasting events often have a **trigger**; something changes that causes a landslide to occur at a specific time. It could be rapid snowmelt, intense rainfall, earthquake shaking, volcanic eruption, storm waves, rapid-stream erosion, or human activities, such as grading a new road. Increased water content within the slope is the most common mass-wasting trigger. Water content can increase due to rapidly melting snow or ice or an intense rain event. Intense rain events can occur more often during El Niño years, when the west coast of North America receives more precipitation than normal and landslides become more common. Additional water can be added to a slope through changes in surface-water conditions resulting from earthquakes, previous slope failures that dam up streams, or human structures that interfere with runoff, such as buildings, roads, or parking lots. In the case of the 1959 Hebgen Lake rockslide in Madison Canyon, Montana, the shear strength of the slope may have been weakened by earthquake shaking. Most landslide **mitigation** diverts and drains water away from slide areas. Tarps and plastic sheeting are often used to drain water off of slide bodies and prevent **infiltration** into the slide. Drains are used to dewater landslides and shallow wells are used to monitor the water content of some active landslides.

An **oversteepened** slope may also trigger landslides. Slopes can be made excessively steep by natural processes of erosion or when humans modify the landscape for building construction. An example of how a slope may be oversteepened during development occurs where the bottom of the slope is cut into, perhaps to build a road or level a building lot, and the top of the slope is modified by depositing excavated material from below. If done carefully, this practice can be very useful in land development, but in some cases, this can result in devastating consequences. For example, this might have been a contributing factor in the 2014 North Salt Lake City, Utah, landslide. A former gravel pit was regraded to provide a road and several building lots. These activities may have oversteepened the slope, which resulted in a slow-moving landslide that destroyed one home at the bottom of the slope. Natural processes such as excessive stream erosion from a flood or coastal erosion during a storm can also oversteepen slopes. For example, natural undercutting of the riverbank was proposed as part of the trigger for the famous 1925 Gros Ventre, Wyoming, rock slide.

Slope reinforcement can help prevent and mitigate landslides. For rockfall-prone areas, sometimes it is economical to use long steel bolts. Bolts, drilled a few meters into a rock face, can secure loose pieces of material that could pose a hazard. Shockcrete, a reinforced spray-on form of concrete, can strengthen a slope face when applied properly. Buttressing a slide (adding weight at the toe of the slide and removing weight from the head) can stabilize a landslide. Terracing, which creates a stairstep topography, can be applied to help with slope stabilization, but it must be applied at the proper scale to be effective.

A different approach in reducing landslide hazard is to shield, catch, and divert the runout material. Sometimes the most economical way to deal with a landslide hazard is to divert and slow the falling material. Special stretchable fencing can be applied in areas where rockfall is common to protect pedestrians and vehicles. Runout channels, diversion structures, and check **dams** can be used to slow debris flows and divert them around structures. Some highways have special tunnels that divert landslides over the highway. In all of these cases, the shielding has to be engineered to a scale that is greater than the slide, or catastrophic loss in property and life could result.

Take this quiz to check your comprehension of this section.

Access the quiz for Section 10.2 by scanning the QR code.

10.3 Landslide Classification & Identification

Mass-wasting events are classified by type of movement and type of material, and there are several ways to classify these events. Figure 10.5 and Table 10.1 show terms used. In addition, mass-wasting types often share common morphological features observed on the surface, such as the head scarp (commonly seen as crescent shapes on a cliff face), hummocky or uneven surfaces; accumulations of **talus** (loose rocky material falling from above), and toe of slope, which covers existing surface material.

10.3.1 Types of Mass Wasting

The most common mass-wasting types are falls, rotational and translational slides, flows, and creep. Falls are abrupt rock movements that detach from steep slopes or cliffs. Rocks separate along existing natural breaks such as fractures or bedding planes. Movement occurs as free-falling, bouncing, and rolling. Falls are strongly influenced by gravity, mechanical weathering, and water. **Rotational slides** commonly show slow movement along a curved rupture surface. **Translational slides** are often rapid movements along a plane of distinct weakness between the overlying slide material and more-stable underlying material. Slides can be further subdivided into rock slides, debris slides, or earth slides depending on the type of the material involved (see table).

Type of movement	Primary material type and common name of slide		
	Bedrock	*Soil: mostly coarse-grained*	*Soil: mostly fine-grained*
Falls	Rockfall		
Rock avalanche	Rock avalanche		
Rotational slide (slump)		Rotational debris slide (slump)	Rotational Earth slide (slump)
Transitional slide	Transitional rock slide	Transitional debris slide	Transitional Earth slide
Flows		Debris flow	Earth flow
Soil creep		Creep	Creep

Table 10.1: Mass wasting types.

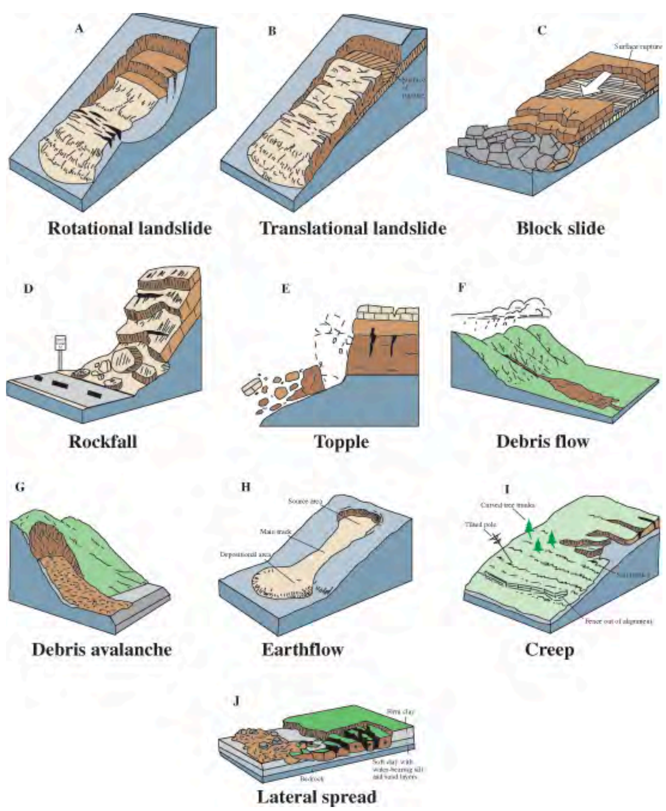

Figure 10.5: Examples of some of the types of landslides. Figure description available at the end of the chapter.

Flows are rapidly moving mass-wasting events in which the loose material is typically mixed with abundant water, creating long runouts at the slope base. Flows are commonly separated into debris flow (coarse material) and earthflow (fine material) depending on the type of material involved and the amount of water. Some of the largest and fastest flows on land are called **sturzstroms**, or long-runout landslides. They are still poorly understood but are known to travel for long distances, even in places without significant atmospheres, like the Moon.

Creep is the imperceptibly slow downward movement of material caused by a regular cycle of nighttime freezing followed by daytime thawing in unconsolidated material such as soil. During the freeze, expansion of ice pushes soil particles out away from the slope, while the day following the thaw, gravity pulls them directly downward. The net effect is a gradual movement of surface soil particles downhill. Creep is indicated by curved tree trunks, bent fences or retaining walls, tilted poles or fences, and small soil ripples or ridges. A special type of **soil creep** is solifluction, which is the slow movement of soil lobes on low-angle slopes due to soil seasonally freezing and thawing in high-latitude, typically sub-Arctic, Arctic, and Antarctic locations.

Video 10.1: Landslide hazards

Access this YouTube video by scanning the QR code. ["Landslide Hazards" by USGS | https://www.youtube.com/watch?v=MVwSpGVfWVo]

10.3.2 Parts of a Landslide

Landslides have several identifying features that can be common across the different types of mass wasting. Note that there are many exceptions, and a landslide does not have to have these features. Displacement of material by landslides causes the absence of material uphill and the deposition of new material downhill, and careful observation can identify the evidence of that displacement. Other signs of landslides include tilted or offset structures or natural features that would normally be vertical or in place.

Many landslides have escarpments or scarps. Landslide scarps, like fault scarps, are steep terrain created when movement of the adjacent land exposes a part of the subsurface. The most prominent scarp is the main scarp, which marks the uphill extent of the landslide. As the disturbed material moves out of place, a step slope forms and develops a new hillside escarpment for the undisturbed material. Main scarps are formed by movement of the displaced material away from the undisturbed ground and are the visible part of the slide rupture surface.

Complete this interactive activity to check your understanding.

Access this interactive activity by scanning the QR code.

The slide rupture surface is the boundary of the landslide's body of movement. The geologic material below the slide surface does not move and is marked on the sides by the flanks of the landslide and at the end by the toe of the landslide.

The toe of the landslide marks the end of the moving material. The toe marks the runout, or maximum distance traveled, of the landslide. In rotational landslides, the toe is often a large, disturbed mound of geologic material that forms as the landslide moves past its original rupture surface.

Rotational and **translational landslides** often have extensional cracks, sag ponds, hummocky terrain, and pressure ridges. Extensional cracks form when a landslide's toe moves forward faster than the rest of landslide, resulting in tensional forces. Sag ponds are small bodies of water filling depressions formed where landslide movement has impounded drainage. Hummocky terrain is undulating and uneven topography that results from the ground being disturbed. Pressure ridges develop on the margins of the landslide, where material is forced upward into a ridge structure.

Take this quiz to check your comprehension of this section.

Access the quiz for Section 10.3 by scanning the QR code.

10.4 Examples of Landslides

10.4.1 Landslides in United States

Gros Ventre, Wyoming (1925): On June 23, 1925, a 38 million cubic meter (50 million cu yd) translational rockslide occurred next to the Gros Ventre River (pronounced "grow vont") near Jackson Hole, Wyoming. Large boulders dammed the Gros Ventre River and ran up the opposite side of the valley several hundred vertical feet. The dammed river created Slide Lake, and two years later in 1927, lake levels rose high enough to destabilize the dam. The dam failed and caused a catastrophic flood that killed six people in the small downstream community of Kelly, Wyoming.

Figure 10.6: Scar of the Gros Ventre landslide in background with landslide deposits in the foreground. Figure description available at the end of the chapter.

Figure 10.7: Lower Slide Lake was created on June 23, 1925, when the Gros Ventre landslide dammed the Gros Ventre River. It is located in Bridger-Teton National Forest, in the US state of Wyoming. Figure description available at the end of the chapter.

A combination of three factors caused the rock slide: (1) heavy rains and rapidly melting snow saturated the Tensleep sandstone, causing the underlying shale of the Amsden Formation to lose its shear strength; (2) the Gros Ventre River cut through the sandstone, creating an oversteepened slope; and (3) soil on top of the mountain became saturated with water due to poor drainage. The cross-section diagram shows how the parallel bedding planes between the Tensleep sandstone and Amsden Formation offered little friction against the slope surface as the river undercut the sandstone. Lastly, the rockslide may have been triggered by an earthquake.

Madison Canyon, Montana (1959): In 1959, the largest earthquake in Rocky Mountain recorded history, magnitude 7.5, struck the Hebgen Lake area of Montana, causing a destructive seiche on the lake (see Chapter 9). The earthquake caused a rock avalanche that dammed the Madison River, creating Quake Lake, and ran up the other side of the valley hundreds of vertical feet. Today, there are still house-sized boulders visible on the slope opposite their starting point. The slide moved at a velocity of up to 160.9 kph (100 mph), creating an incredible air blast that swept through the Rock Creek Campground. The slide killed 28 people, most of whom were in the campground and remain buried there. In a manner like the Gros Ventre slide, foliation planes of weakness in metamorphic rock outcrops were parallel with the surface, compromising shear strength.

Figure 10.8: Road damage from the August 1959 Hebgen Lake (Montana-Yellowstone) earthquake. Figure description available at the end of the chapter.

Mount Saint Helens, Washington (1980): On May 18, 1980, a 5.1 magnitude earthquake triggered the largest landslide observed in the historical record. This landslide was followed by the lateral eruption of Mount St. Helens volcano, and the eruption was followed by volcanic debris flows known as lahars. The volume of material moved by the landslide was 2.8 cubic kilometers (0.67 mi^3).

La Conchita, California (1995 and 2005): On March 4, 1995, a fast-moving earthflow damaged nine houses in the Southern California coastal community of La Conchita. A week later, a debris flow in the same location damaged five more houses. Surface-tension cracks at the top of the slide gave early warning signs in the summer of 1994. During the rainy winter season of 1994/1995, the cracks grew larger. The likely trigger of the 1995 event was unusually heavy rainfall during the winter of 1994/1995 and rising groundwater levels. Ten years later, in 2005, a rapid-debris flow occurred at the end of a 15-day period of near-record rainfall in Southern California. Vegetation remained relatively intact, as it was rafted on the surface of the rapid flow, indicating that much of the landslide mass simply was being carried on a presumably much more saturated and fluidized layer beneath. The 2005 slide damaged 36 houses and killed ten people.

Figure 10.9: Oblique lidar image of La Conchita after the 2005 landslide, with the 1995 landslide outlined in blue and the 2005 landslide in yellow; arrows show examples of other landslides in the area; red line outlines main scarp of an ancient landslide for the entire bluff. Figure description available at the end of the chapter.

Figure 10.10: 1995 La Conchita slide. Figure description available at the end of the chapter.

Figure 10.11: 2014 Oso slide in Washington killed 43 people and buried many homes. [Figure description available at the end of the chapter](#).

Oso, Washington (2014): On March 22, 2014, a landslide of approximately 18 million tons (10 million yd^3) traveled at 64 kph (40 mph), extended for nearly 1.6 km (1 m), and dammed the North Fork of the Stillaguamish River. The landslide covered 40 homes and killed 43 people in the Steelhead Haven community near Oso, Washington. It produced a volume of material equivalent to 600 football fields covered in material 3 m (10 ft) deep. The winter of 2013–2014 was unusually wet, with almost double the average amount of precipitation. The landslide occurred in an area of the Stillaguamish River Valley historically active with many landslides, but previous events had been small.

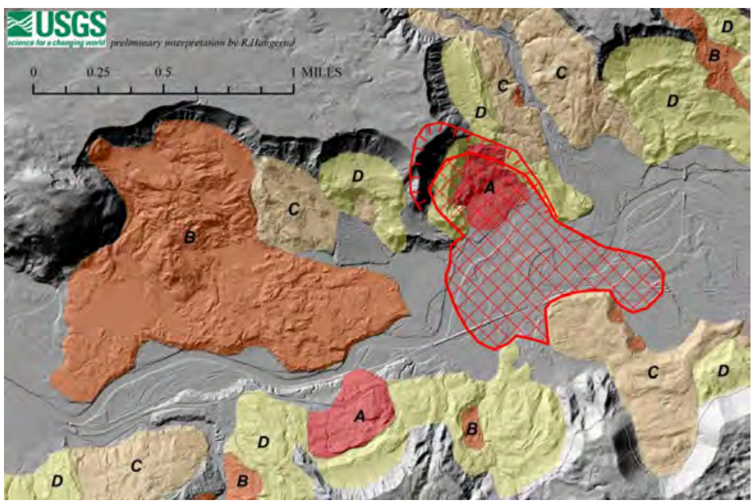

Figure 10.12: Annotated lidar map of 2014 Oso slide in Washington. [Figure description available at the end of the chapter](#).

Yosemite National Park rock falls: The steep cliffs of Yosemite National Park cause frequent **rockfalls**. Fractures created to tectonic stresses and exfoliation and expanded by frost wedging can cause house-sized blocks of granite to detach from the cliff-faces of Yosemite National Park. The park models potential runout—the distance landslide material travels—to better assess the risk posed to the millions of park visitors.

Video 10.2: Rock fall in Yosemite

Access this [YouTube video](https://www.youtube.com/watch?v=H0YhlqP1BgE) by scanning the QR code. ["Yosemite Nature Notes – 10 – Rock Fall" by yosemitenationalpark | https://www.youtube.com/watch?v=H0YhlqP1BgE]

10.4.2 Landslides in Utah

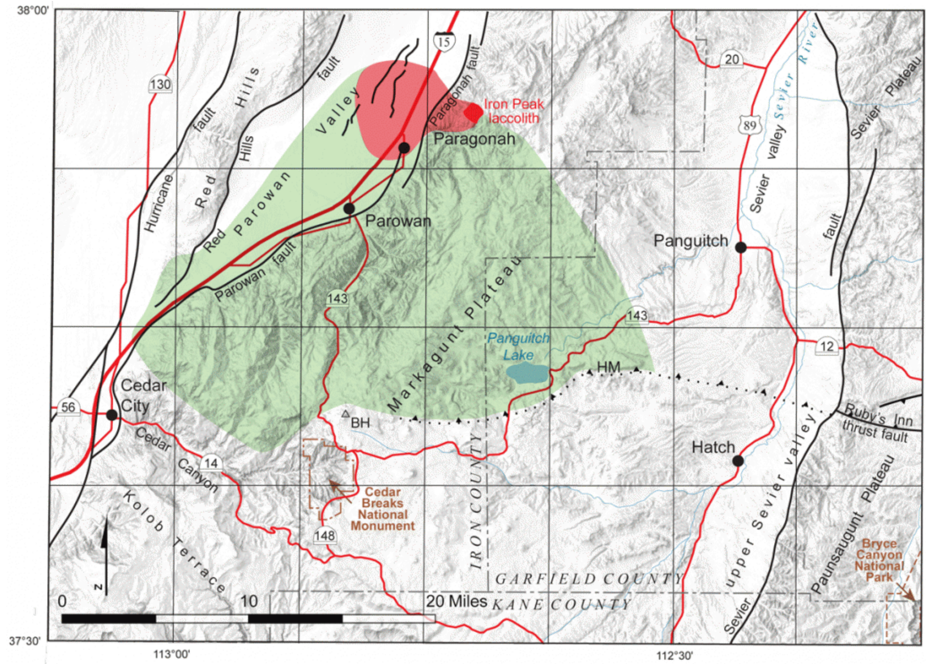

Figure 10.13: Approximate extent of Markagunt gravity slide. Figure description available at the end of the chapter.

Markagunt gravity slide: About 21–22 million years ago, one of the biggest land-based landslides yet discovered in the geologic record displaced more than 1,700 cu km (408 cu mi) of material in one relatively fast event. Evidence for this slide includes breccia conglomerates (see Chapter 5), glassy pseudotachylytes, (see Chapter 6), slip surfaces, similar to faults (see Chapter 9), and dikes (see Chapter 7). The landslide is estimated to encompass an area the size of Rhode Island and to extend from near Cedar City, Utah, to Panguitch, Utah. This landslide was likely the result of material released from the side of a growing laccolith (a type of igneous intrusion; see Chapter 4), after being triggered by an eruption-related earthquake.

Figure 10.14: The 1983 Thistle landslide (foreground) dammed the Spanish Fork river, creating a lake. Figure description available at the end of the chapter.

Thistle slide (1983): Starting in April of 1983 and continuing into May of that year, a slow-moving landslide traveled 305 m (1,000 ft) downhill and blocked Spanish Fork Canyon with an earthflow dam 61 m (200 ft) high. This caused disastrous flooding upstream in the Soldier Creek and Thistle Creek valleys, submerging the town of Thistle. As part of the emergency response, a spillway was constructed to prevent the newly formed lake from breaching the dam. Later, a tunnel was constructed to drain the lake, and currently the river continues to flow through this tunnel. The rail line and US6 highway had to be relocated at a cost of more than $200 million.

Figure 10.15: House before and after destruction from 2013 Rockville rockfall. Figure description available at the end of the chapter.

Rockville rockfall (2013): Rockville, Utah, is a small community near the entrance to Zion National Park. In December of 2013, a 2,700 ton (1,400 yd^3) block of Shinarump Conglomerate fell from the Rockville Bench cliff, landed on the steep 35-degree slope below, and shattered into several large pieces that continued downslope at a high speed. These boulders completely destroyed a house located 375 feet below the cliff (see Figure 10.15) and killed two people inside the home. The topographic map shows other rockfalls in the area prior to this catastrophic event.

North Salt Lake slide (2014): In August 2014, after a particularly wet period, a slow-moving rotational landslide destroyed one home and damaged nearby tennis courts. Reports from residents suggested that ground cracks had been seen near the top of the slope at least a year prior to the catastrophic movement. The presence of easily drained sands and gravels overlying more **impermeable** clays weathered from volcanic ash, along with recent regrading of the slope, may have been contributing causes of this slide. Local heavy rains seem to have provided the trigger. In the two years after the landslide, the slope has been partially regraded to increase its stability. Unfortunately, as of January 2017, parts of the slope had shown reactivation movement. Similarly, in 1996 residents in a nearby subdivision started reporting distress to their homes. This distress continued until 2012, when 18 homes became uninhabitable due to extensive damage and were removed. A geologic park was constructed in the now-vacant area.

Figure 10.16: Scarp and displaced material from the North Salt Lake (Parkview) slide of 2014. Figure description available at the end of the chapter.

Video 10.3: North Salt Lake landslide

Access this YouTube video by scanning the QR code. ["EXCLUSIVE: Time lapse video of landslide in North Salt Lake neighborhood" by KUTV 2 News Salt Lake City | https://www.youtube.com/watch?v=NQs_OWgNshg]

Bingham Canyon Copper Mine landslide, Utah (2013): At 9:30 p.m. on April 10, 2013, more than 65 million cubic meters of steep terraced mine wall slid down into the engineered pit of Bingham Canyon mine, making it one of the largest historic landslides not associated with volcanoes. Radar systems maintained by the mine operator warned of the wall's movement, preventing the loss of life and limiting the loss of property.

Complete this interactive activity to check your understanding.

Access this interactive activity by scanning the QR code.

Take this quiz to check your comprehension of this section.

Access the quiz for Section 10.4 by scanning the QR code.

Summary

Mass wasting is a geologic term describing all downhill rock and soil movement due to gravity. Mass wasting occurs when a slope is too steep to remain stable with existing material and conditions. Loose rock and soil, in a combination called regolith, are what typically move during a mass-wasting event. Slope stability is determined by two factors: the angle of the slope and the shear strength of the accumulated materials. Mass-wasting events are triggered by changes that oversteepen slope angles and weaken slope stability, such as rapid snow melt, intense rainfall, earthquake shaking, volcanic eruption, storm waves, stream erosion, and human activities. Excessive precipitation is the most common trigger. Mass-wasting events are classified by their type of movement and material, and they share common morphological surface features. The most common types of mass-wasting events are rockfalls, slides, flows, and creep.

Mass-wasting movement ranges from slow to dangerously rapid. Areas with steep topography and rapid rainfall, such as the California coast, Rocky Mountain Region, and Pacific Northwest, are particularly susceptible to hazardous mass-wasting events. By examining examples and lessons learned from famous mass-wasting events, scientists have a better understanding of how mass wasting occurs. This knowledge has brought them closer to predicting where and how these potentially hazardous events may occur and how people can be protected.

Take this quiz to check your comprehension of this chapter.

Access the quiz for Chapter 10 by scanning the QR code.

Text References

1. Haugerud, R.A. (2014). Preliminary interpretation of pre-2014 landslide deposits in the vicinity of Oso, Washington. *United States Geological Survey.*
2. Highland, L. (2004). Landslide types and processes. Online, http://pubs.er.usgs.gov.
3. Highland, L.M., and Bobrowsky, P. (2008). The landslide handbook – A guide to understanding landslide. *United States Geological Survey USGS Numbered Series 1325*, 147.
4. Highland, L.M., and Schuster, R.L. (2000). Significant landslide events in the United States. *United States Geological Survey.*
5. Hildenbrand, T.G., and Hendricks, J.D. (1995). Geophysical setting of the Reelfoot rift and relations between rift structures and the New Madrid seismic zone. *United States Geological Survey Professional Paper 1538*-E, 36.
6. Hungr, O., Leroueil, S., and Picarelli, L. (2013). The Varnes classification of landslide types, an update. *Landslides, 11*(2), 167–194.
7. Jibson, R.W. (2005). Landslide hazards at La Conchita, California. *United States Geological Survey Open-File Report 2005-1067.*
8. Lipman, P.W., and Mullineaux, D.R. (1981). The 1980 eruptions of Mount St. Helens, Washington. *United States Geological Survey Numbered Series 1250*, doi: 10.3133/pp1250.

9. Lund, W.R., Knudsen, T.R., and Bowman, S.D. (2014). Investigation of the December 12, 2013, Fatal Rock Fall at 368 West Main Street, Rockville, Utah. *Utah Geological Survey 273*, 24.
10. United States Forest Service (2016). A brief history of the Gros Ventre Slide geological site.

Figure References

Figure 10.1: Forces on a block on an inclined plane (*fg* = force of gravity; *fn* = normal force; *fs* = shear force). Kindred Grey. 2022. CC BY 4.0. Includes crate by Andrew Doane from Noun Project (Noun Project license).

Figure 10.2: As slope increases, the force of gravity (*fg*) stays the same and the normal force decreases while the shear force proportionately increases. Kindred Grey. 2022. CC BY 4.0. Includes crate by Andrew Doane from Noun Project (Noun Project license).

Figure 10.3: Angle of repose in a pile of sand. Captain Sprite. 2007. CC BY-SA 2.5. https://en.wikipedia.org/wiki/File:Angleofrepose.png

Figure 10.4: Locations A and B have bedding nearly perpendicular to the slope, making for a relatively stable slope. Location D has bedding nearly parallel to the slope, increasing the risk of slope failure. Location C has bedding nearly horizontal, and the stability is relatively intermediate. Kindred Grey. 2022. CC BY 4.0.

Figure 10.5: Examples of some of the types of landslides. R.L. Schuster, United States Geological Survey (USGS). 2004. Public domain. https://pubs.usgs.gov/fs/2004/3072/fs-2004-3072.html

Figure 10.6: Scar of the Gros Ventre landslide in background with landslide deposits in the foreground. Daniel Mayer. 2006. CC BY-SA 3.0. https://commons.wikimedia.org/wiki/File:Gros_Venture_Slide.jpg

Figure 10.7: Lower Slide Lake was created on June 23, 1925, when the Gros Ventre landslide dammed the Gros Ventre River. Daniel Mayer. 2006. CC BY-SA 3.0. https://commons.wikimedia.org/wiki/File:Lower_Slide_Lake.jpg

Figure 10.8: Road damage from the August 1959 Hebgen Lake (Montana-Yellowstone) earthquake. R.B. Colton via USGS. 1959. Public domain. https://commons.wikimedia.org/wiki/File:Roaddamage59quake.jpg

Figure 10.9: Oblique lidar image of La Conchita after the 2005 landslide. Todd Stennett via USGS. 2016. Public domain. https://www.usgs.gov/media/images/la-conchita

Figure 10.10: 1995 La Conchita slide. USGS. 2005. Public domain. https://commons.wikimedia.org/wiki/File:Laconchita1995landslide.jpg

Figure 10.11: 2014 Oso slide in Washington killed 43 people and buried many homes. Mark Reid, USGS. 2014. Public domain. https://commons.wikimedia.org/wiki/File:Oso_Landslide_aerial.jpg

Figure 10.12: Annotated lidar map of 2014 Oso slide in Washington. USGS. 2014. Public domain. https://commons.wikimedia.org/wiki/File:Oso_landslide_geomorphology_map.png

Figure 10.13: Approximate extent of Markagunt gravity slide. Used under fair use from *The Early Miocene Markagunt Megabreccia: Utah's Largest Catastrophic Landslide* by Robert F. Biek. https://geology.utah.gov/map-pub/survey-notes/the-early-miocene-markagunt-megabreccia

Figure 10.14: The 1983 Thistle landslide (foreground) dammed the Spanish Fork river creating a lake. R.L. Schuster, USGS. 1983. Public domain. https://en.wikipedia.org/wiki/File:Thistlelandslideusgs.jpg

Figure 10.15: House before and after destruction from 2013 Rockville rockfall. Used under fair use from *Investigation of the December 12, 2013, Fatal Rock Fall at 368 West Main Street, Rockville, Utah* by William R. Lund, Tyler R. Knudsen, and Steve D. Bowman. https://ugspub.nr.utah.gov/publications/reports_of_investigations/ri-273.pdf

Figure 10.16: Scarp and displaced material from the North Salt Lake (Parkview) slide of 2014. Used under fair use from Parkway Drive Landslide, North Salt Lake. https://geology.utah.gov/hazards/landslides/parkway_drive_landslide

Figure Descriptions

Figure 10.1: 2D diagram of a sloped plane with a crate sitting on top of the plane; a light blue arrow points downward from the side of crate parallel to the incline labeled fs, another light blue arrow points perpendicular to the inclined plane from the bottom of the crate labeled fn, and a dark blue arrow points vertically straight down from the bottom corner of the crate labeled fg.

Figure 10.2: As slope increases, the force of gravity (fg) stays the same and the normal force decreases while the shear force proportionately increases.

Figure 10.3: A pile of sand with two arrows: one arrow points upward along the slope of the pile and a second arrow points parallel to horizontal, with the angle between the two arrows labeled angle of repose.

Figure 10.4: At locations A and B, the bedding is nearly perpendicular to the slope and the bedding is relatively stable. At location D, the bedding is nearly parallel to the slope and the bedding is quite unstable. At location C the bedding is nearly horizontal and the stability is intermediate between the other two extremes.

Figure 10.5: Ten block diagrams showing the various types of landslides as described in the text. See surrounding text for more details.

Figure 10.6: Mountain in the background with a visible scar of missing vegetation on the slope with rubbly rock deposits in the foreground.

Figure 10.7: Sloping hillsides covered in vegetation with a lake in the foreground.

Figure 10.8: Road that is cracked and fully split apart.

Figure 10.9: Black and white LIDAR image of a hillside with landslides outlined: a blue oval outlines a vertical landslide scarp; it overlaps a yellow elongate outline of another vertical landslide; a red arc near the top of the slope with black arrows pointing downward denotes another landslide; neighborhood buildings are visible at the base of the slope.

Figure 10.10: Vegetated hillside with a large section that has slumped down onto several houses in a neighborhood at the base of the hillside.

Figure 10.11: Aerial photo of large slide scarp with debris at the bottom of the hillside covering an entire river and damming it.

Figure 10.12: Shaded relief map centered on the North Fork of the Stillaguamish River and State Highway 530 just east of Oso, Washington, with colored areas showing numerous recent landslides; the Oso landslide of 2014 is labeled A with red cross-hatching over the approximate area of runout, covering the river as well as the highway.

Figure 10.13: Index map centered on the Markagunt Plateau, showing extent of Markagunt Megabreccia in green which covers most of the plateau; the Iron Peak laccolith is a small red circular feature at the north end of the Markagunt Megabreccia.

Figure 10.14: Aerial photo of vegetated mountains with a river running through them; a large tan landslide can be seen covering the river and damming it, creating a lake.

Figure 10.15: Side-by-side images taken from the same place. Left: House in tact with a mountain in the background. Right: house destroyed by boulders and smaller rocks.

Figure 10.16: Vegetated hillside with a large slump of grass-lined material at the base of the hillside just above a row of houses; a tan sliver-shaped scarp can be seen in the hillside.

11. WATER

Learning Objectives

By the end of this chapter, students should be able to:

- Describe the processes of the water cycle.
- Describe drainage basins, watershed protection, and water budget.
- Describe reasons for water laws, who controls them, and how water is shared in the Western US.
- Describe zone of transport, zone of sediment production, zone of deposition, and equilibrium.
- Describe stream landforms: channel types, alluvial fans, floodplains, natural levees, deltas, entrenched meanders, and terraces.
- Describe the properties required for a good aquifer, and define confining layer water table.
- Describe three major groups of water contamination and three types of remediation.
- Describe karst topography, how it is created, and the landforms that characterize it.

All life on Earth requires water. The hydrosphere (Earth's water) is an important agent of geologic change. Water shapes our planet by depositing minerals, aiding lithification, and altering rocks after they are lithified. Water carried by subducted oceanic plates causes flux melting of upper mantle material. Water is among the volatiles in magma and emerges at the surface as steam in volcanoes.

Figure 11.1: Example of a Roman aqueduct in Segovia, Spain. Figure description available at the end of the chapter.

Figure 11.2: Chac mask in Mexico. Figure description available at the end of the chapter.

Humans rely on suitable water sources for consumption, agriculture, power generation, and many other purposes. In pre-industrial civilizations, those in power controlled water resources. As shown in the figures, two-thousand-year-old Roman aqueducts still grace European, Middle Eastern, and North African skylines. Ancient Mayan architecture depicts water imagery such as frogs, water lilies, and water fowl, illustrating the importance of water in their societies. In the drier lowlands of the Yucatan Peninsula, mask facades of the hooked-nosed rain god, Chac (or *Chaac)* are prominent on Mayan buildings such as the Kodz Poop (Temple of the Masks, sometimes spelled Coodz Poop) at the ceremonial site of Kabah. To this day, government controlled water continues to be an integral part of most modern societies.

11.1 Water Cycle

The water cycle is the continuous circulation of water in the Earth's atmosphere. During circulation, water changes between solid, liquid, and gas (water vapor) and changes location. The processes involved in the water cycle are evaporation, transpiration, condensation, precipitation, and runoff.

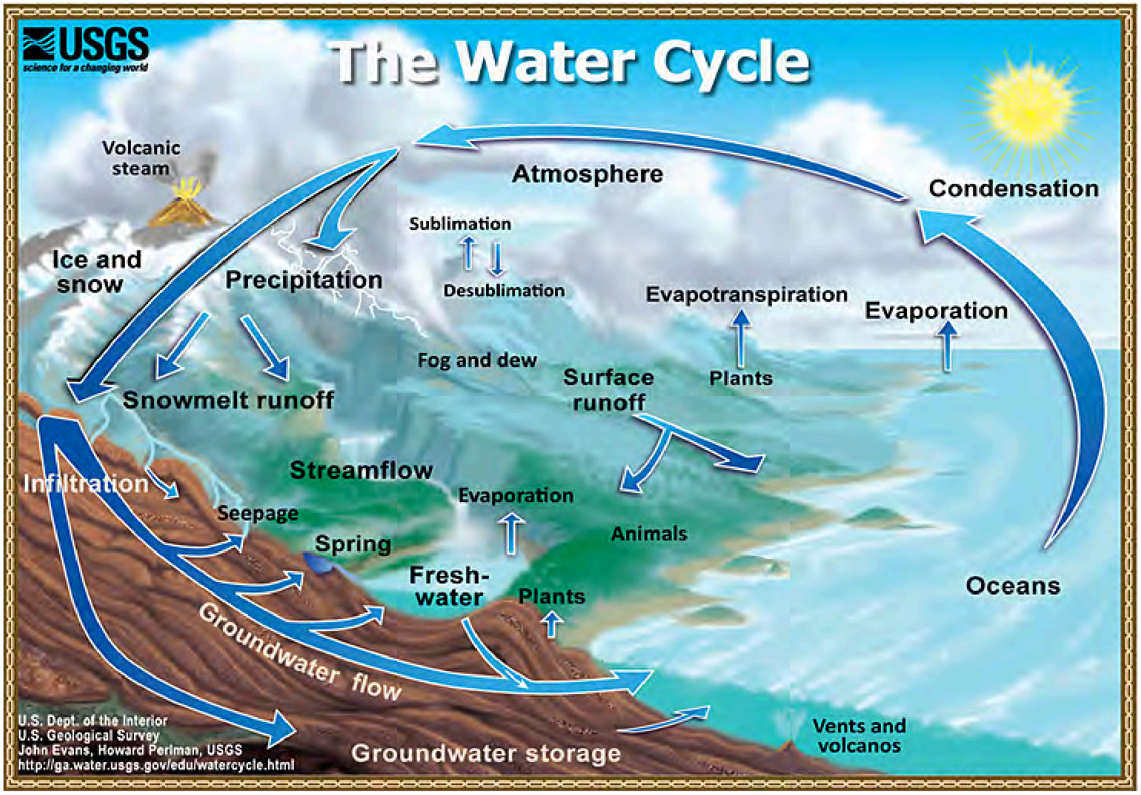

Figure 11.3: The water cycle. Figure description available at the end of the chapter.

Evaporation is the process by which a liquid is converted to a gas. Water evaporates when **solar energy** warms the water sufficiently to excite the water molecules to the point of vaporization. Evaporation occurs from oceans, lakes, streams, and the land surface. Plants contribute significant amounts of water vapor through transpiration, a byproduct of photosynthesis that occurs through the minute pores of plant leaves. The term **evapotranspiration** refers to these two sources of water entering the atmosphere and is commonly used by geologists.

Water vapor is invisible. Condensation is the process of water vapor transitioning to a liquid. Winds carry water vapor in the atmosphere long distances. When water vapor cools or when air masses of different temperatures mix, water vapor may condense back into droplets of liquid water. These water droplets usually form around a microscopic piece of dust or salt called condensation nuclei. These small droplets of liquid water suspended in the atmosphere become visible as in a cloud. Water droplets inside clouds collide and stick together, growing into larger droplets. Once the water droplets become big enough, they fall to Earth as rain, snow, hail, or sleet.

Once precipitation has reached the Earth's surface, it can evaporate or flow as **runoff** into streams, lakes, and eventually back to the oceans. Water in streams and lakes is called surface water. Water can also infiltrate into the soil and fill the pore spaces in the rock or sediment underground to become groundwater. Groundwater slowly moves through rock and unconsolidated materials. Some groundwater may reach the surface again, where it discharges as springs, streams, lakes, and the ocean. Since surface water in streams and lakes can infiltrate again to recharge groundwater, the surface water and groundwater systems are connected.

Video 11.1: Water cycle

Access this YouTube video by scanning the QR code. ["Water Cycle | How the Hydrologic Cycle Works" by National Science Foundation News | https://www.youtube.com/watch?v=al-do-HGuIk]

Take this quiz to check your comprehension of this section.

Access the quiz for Section 11.1 by scanning the QR code.

11.2 Water Basins and Budgets

The basic unit of division of the landscape is the **drainage basin**, also known as a catchment or watershed. It is the area of land that captures precipitation and contributes runoff to a stream or stream segment. **Drainage divides** are local topographic high points that separate one drainage basin from another. Water that falls on one side of the divide goes to one stream, and water that falls on the other side of the divide goes to a different stream. Each stream, **tributary**, and streamlet has its own drainage basin. In areas with flatter topography, drainage divides are not as easily identified, but they still exist.

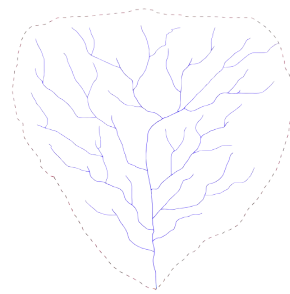

Figure 11.4: Map view of a drainage basin with main trunk streams and many tributaries with drainage divide in dashed red line. Figure description available at the end of the chapter.

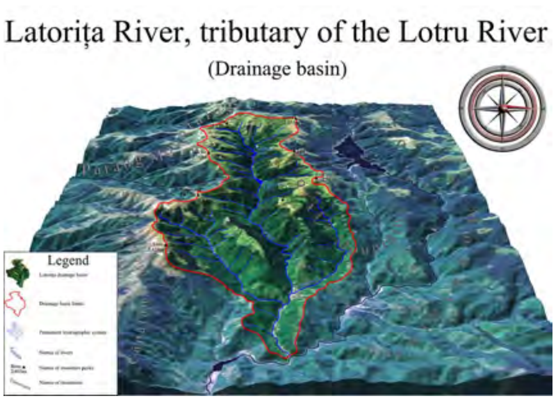

Figure 11.5: Oblique view of the drainage basin and divide of the Latorita River, Romania. Figure description available at the end of the chapter.

The headwater is where the stream begins. Smaller tributary streams combine downhill to make the larger trunk of the stream. The **mouth** is where the stream finally reaches its end. The mouth of most streams is at the ocean. However, a rare number of streams do not flow to the ocean but rather end in a **closed basin** (or endorheic basin), where the only outlet is evaporation. Most streams in the Great Basin of western North America end in endorheic basins. For example, in Salt Lake County, Utah, Little Cottonwood Creek and the Jordan River flow into the endorheic Great Salt Lake, where the water evaporates.

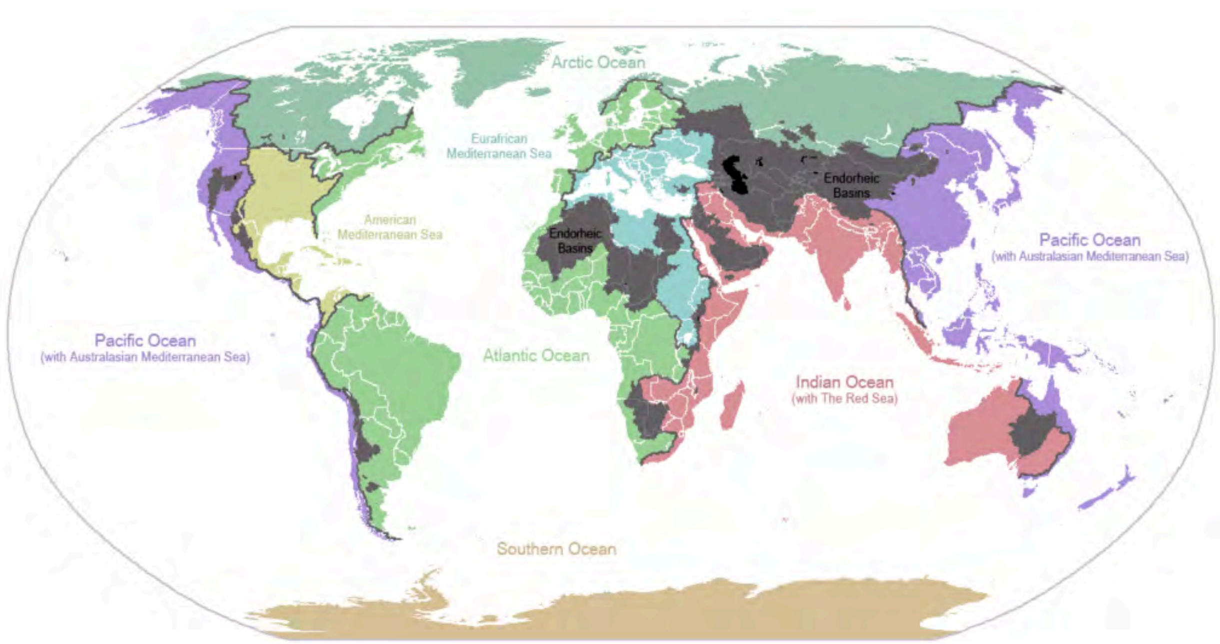

Figure 11.6: Major drainage basins color-coded to match the related ocean. Closed basins (or endorheic basins) are shown in gray. Figure description available at the end of the chapter.

Perennial streams flow all year round. Perennial streams occur in humid or temperate climates where there is sufficient rainfall and low evaporation rates. Water levels rise and fall with the seasons, depending on the discharge. **Ephemeral streams** flow only during rain events or the wet season. In arid climates, like Utah, many streams are ephemeral. These streams occur in dry climates with low amounts of rainfall and high evaporation rates. Their channels are often dry washes or arroyos for much of the year, and their sudden flow causes **flash floods**.

Along Utah's Wasatch Front, the urban area extending north to south from Brigham City to Provo, there are several watersheds that are designated as "watershed protection areas," which limits the type of use allowed in those drainages in order to protect culinary water. Dogs and swimming are limited in those watersheds because of the possibility of contamination by harmful bacteria and substances to the drinking supply of Salt Lake City and surrounding municipalities.

Water in the water cycle is very much like money in a personal budget. Income includes precipitation and inflow from streams and groundwater. Expenses include groundwater withdrawal, evaporation, and outflow from streams and groundwater. If the expenses outweigh the income, the water budget is not balanced. In this case, water is removed from savings, i.e., water storage, if available. Reservoirs, snow, ice, soil moisture, and aquifers all serve as storage in a water budget. In dry regions, the water is critical for sustaining human activities. Understanding and managing the water budget is an ongoing political and social challenge.

Hydrologists create groundwater budgets within any designated area, but they are generally made for watershed (basin) boundaries because groundwater and surface water are easier to account for within these boundaries. Water budgets can be created for state, county, or aquifer extent boundaries as well. The groundwater budget is an essential component of the hydrologic model; hydrologists use measured data with a conceptual workflow of the model to better understand the water system.

Take this quiz to check your comprehension of this section.

Access the quiz for Section 11.2 by scanning the QR code.

11.3 Water Use and Distribution

In the United States, 1,344 billion liters (355 billion gallons) of ground and surface water are used each day, of which 288 billion liters (76 billion gallons) are fresh groundwater. The state of California uses 16% of the national groundwater.

Utah is the second driest state in the United States. Nevada, with a mean statewide precipitation of 31 cm (12.2 inches) per year, is the driest. Utah also has the second highest per capita rate of total domestic water use of 632.16 liters (167 gallons) per person per day. With the combination of relatively high demand and limited quantity, Utah is at risk for water budget deficits.

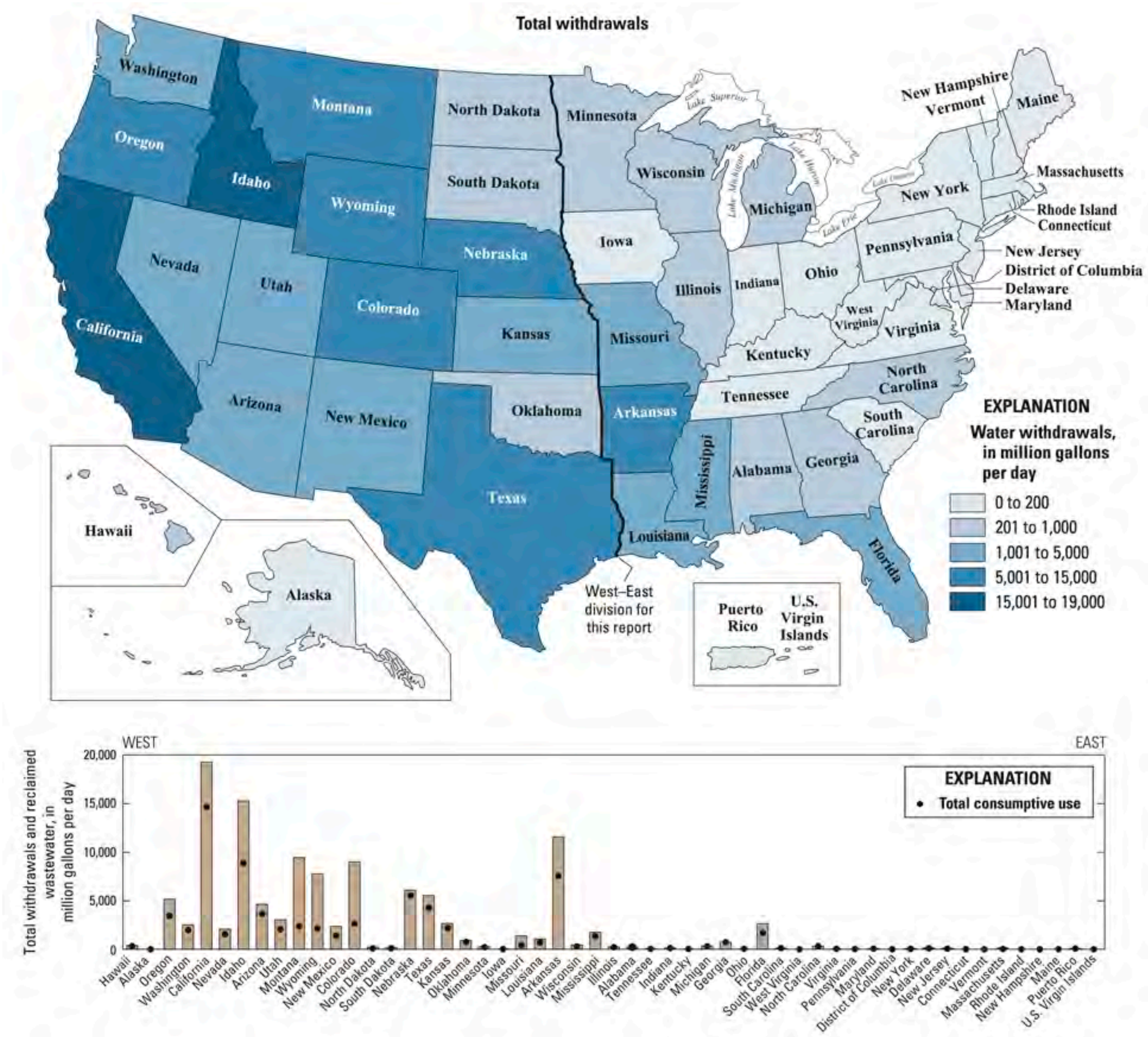

Figure 11.7: Agricultural water use in the United States by state. Figure description available at the end of the chapter.

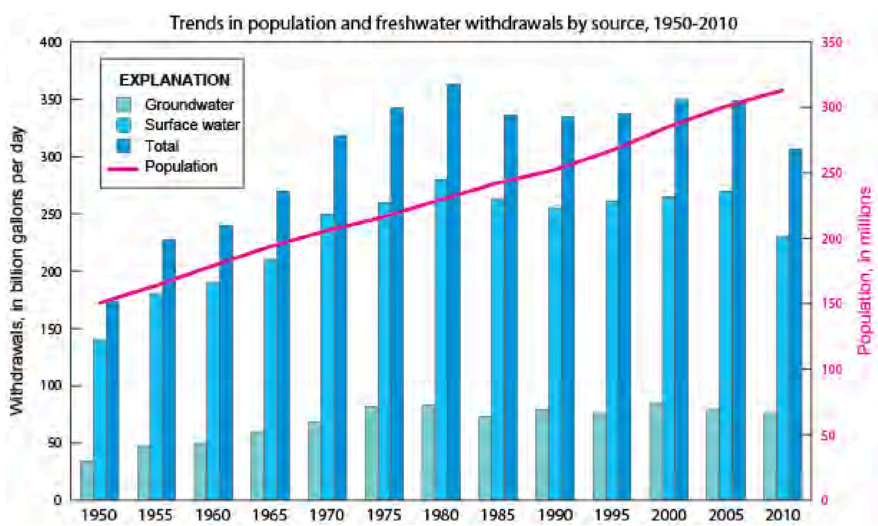

Figure 11.8: Trends in water use by source. Figure description available at the end of the chapter.

11.3.1 Surface Water Distribution

Fresh water is a precious resource and should not be taken for granted, especially in dry climates. Surface water makes up only 1.2% of the fresh water available on the planet, and 69% of that surface water is trapped in ground ice and permafrost. Stream water accounts for only 0.006% of all freshwater, and lakes contain only 0.26% of the world's fresh water.

Global circulation patterns are the most important factor in distributing surface water through precipitation. Due to the Coriolis effect and the uneven heating of the Earth, air rises near the equator and near latitudes 60° north and south. Air sinks at the poles and latitudes 30° north and south (see Chapter 13). Land masses near rising air are more prone to have humid and wet climates. Land masses near sinking air, which inhibits precipitation, are prone to dry conditions. Other factors that affect local climate patterns include prevailing winds, ocean circulation patterns (such as the Gulf Stream's effects on eastern North America), rain shadows (the dry leeward sides of mountains), and even the proximity of bodies of water. When this moist air collides with the nearby mountains, it rises and cools, and the moisture may fall out as snow or rain on nearby areas in a phenomenon known as "lake-effect precipitation."

Figure 11.9: Distribution of precipitation in the United States. The 100th meridian is approximately where the average precipitation transitions from relatively wet to dry. [Figure description available at the end of the chapter](#).

In the United States, the 100th meridian roughly marks the boundary between the humid and arid parts of the country. Growing crops west of the 100th meridian requires irrigation. In the west, surface water is stored in reservoirs and mountain snowpacks, then strategically released through a system of canals during times of high water use.

Some of the driest parts of the Western United States are in the Basin and Range Province. The Basin and Range has multiple mountain ranges that are oriented north to south. Most of the basin valleys in the Basin and Range are dry, receiving less than 30 cm (12 in) of precipitation per year. However, some of the mountain ranges can receive more than 1.52 m (60 in) of water as snow or snow-water equivalent. The snow-water equivalent is the amount of water that would result if the snow were melted, as the snowpack is generally much thicker than the equivalent amount of water that it would produce.

11.3.2 Groundwater Distribution

Water source	Water volume (cubic miles)	Fresh water (%)	Total water (%)
Oceans, seas, and bays	321,000,000	—	96.5%
Ica caps, glaciers, and permanent snow	5,773,000	68.7%	1.74%
Groundwater (total)	5,614,000	—	1.69%
Groundwater (fresh)	2,526,000	30.1%	0.76%
Groundwater (saline)	3,088,000	—	0.93%
Soil moisture	3,959	0.05%	0.001%
Ground ice and permafrost	71,970	0.86%	0.022%
Lakes (total)	42,320	—	0.013%
Lakes (fresh)	21,830	0.26%	0.007%
Lakes (saline)	20,490	—	0.006%
Atmosphere	3,095	0.04%	0.001%
Swamp water	2,752	0.03%	0.0008%
Rivers	509	0.006%	0.0002%
Biological water	269	0.003%	0.0001%

Table 11.1: Groundwater distribution.

Groundwater makes up 30.1% of the fresh water on the planet, making it the most abundant reservoir of fresh water accessible to most humans. The majority of fresh water, 68.7%, is stored in glaciers and ice caps as ice. As the glaciers and ice caps melt due to global warming, this fresh water is lost as it flows into the oceans.

Take this quiz to check your comprehension of this section.

Access the quiz for Section 11.3 by scanning the QR code.

11.4 Water Law

Federal and state governments have put laws in place to ensure the fair and equitable use of water. In the United States, the states are tasked with creating a fair and legal system for sharing water.

11.4.1 Water Rights

Because of the limited supply of water, especially in the Western United States, states disperse a system of legal **water rights** defined as a claim to a portion or all of a water source, such as a spring, stream, well, or lake. Federal law mandates that states control water rights, with the special exception of federally reserved water rights (such as those associated with national parks and Native American tribes) and navigation servitude that maintains navigable water bodies. Each state in the United States has a different way to disperse and manage water rights.

A person, entity, company, or organization must have a water right to legally extract or use surface or groundwater in their state. Water rights in some western states are dictated by the concept of prior appropriation, or "first in time, first in right," where the person with the oldest water right gets priority water use during times when there is not enough water to fulfill every water right.

The Colorado River and its tributaries pass through a desert region, including seven states (Wyoming, Colorado, Utah, New Mexico, Arizona, Nevada, California), Native American reservations, and Mexico. As the Western United States became more populated and while California was becoming a key agricultural producer, the states along the Colorado River realized that the river was important to sustaining life in the West.

To guarantee certain *perceived* water rights, these western states recognized that a water budget was necessary for the Colorado River Basin. Thus the Colorado River Compact was enacted in 1922 to ensure that each state got a fair share of the river water. The compact granted each state a specific volume of water based on the total measured flow at the time. However, in 1922, the flow of the river was higher than its long-term average flow; consequently, more water was allocated to each state than is typically available in the river.

Over the next several decades, lawmakers have made many other agreements and modifications regarding the Colorado River Compact, including the agreements that brought about the Hoover Dam (formerly Boulder Dam), the Glen Canyon Dam, and a treaty between the American and Mexican governments. Collectively, the agreements are referred to as "The Law of the River" by the United States Bureau of Reclamation. Despite adjustments to the Colorado River Compact, many believe that the Colorado River is still over-allocated, as the Colorado River's flow no longer reaches the Pacific Ocean, its original terminus (**base level**). Dams along the Colorado River have caused water to divert and evaporate, creating serious water budget concerns in the Colorado River Basin. Predicted drought associated with global warming is causing additional concerns about over-allocating the Colorado River flow in the future.

The Law of the River highlights the complex and prolonged nature of interstate water rights agreements, as well as the importance of water.

Video 11.2: The Colorado River Compact of 1922

Access this YouTube video by scanning the QR code. ["The Colorado River Compact of 1922" by Megan Damele | https://www.youtube.com/watch?v=MZrKW-Q9X8E]

The Snake Valley straddles the border of Utah and Nevada, with more of the irrigable land area lying on the Utah side of the border. In 1989, the Southern Nevada Water Authority (SNWA) submitted applications for water rights to pipe up to 191,189,707 cu m (155,000 ac-ft) of water per year (an acre-foot of water is one acre covered with water one foot deep) from Spring, Snake, Delamar, Dry Lake, and Cave valleys to Southern Nevada, mostly for Las Vegas. Nevada and Utah have attempted a comprehensive agreement, but negotiations have not yet been settled.

Listen to the NPR story on Snake Valley.

Read about the SNWA History.

Complete this interactive activity to check your understanding.

Access this interactive activity by scanning the QR code.

Video 11.3: Transporting Snake Valley water to satisfy a thirsty Las Vegas

Access this YouTube video by scanning the QR code. ["The Consequences: Transporting Snake Valley water to satisfy a thirsty Las Vegas" by Great Basin Water Network | https://www.youtube.com/watch?v=eCZ8KLrmUXo]

11.4.2 Water Quality and Protection

Two major federal laws that protect water quality in the United States are the Clean Water Act and the Safe Drinking Water Act. The Clean Water Act, an amendment of the Federal Water Pollution Control Act, protects navigable waters from dumping and point-source pollution. The Safe Drinking Water Act ensures that water provided by public water suppliers, like cities and towns, is safe to drink.

The US Environmental Protection Agency Superfund program ensures the cleanup of hazardous contamination and can be applied to situations of surface water and groundwater contamination. It is part of the Comprehensive Environmental Response, Compensation, and Liability Act of 1980. Under this act, state governments and the US Environmental Protection Agency can use the superfund to pay for remediation of a contaminated site and then file a lawsuit against the polluter to recoup the costs. Or to avoid being sued, the polluter that caused the contamination may take direct action or provide funds to remediate the contamination.

Take this quiz to check your comprehension of this section.

Access the quiz for Section 11.4 by scanning the QR code.

11.5 Surface Water

Geologically, a stream is a body of flowing surface water confined to a channel. Terms such as river, creek, and brook are social terms not used in geology. Streams erode and transport sediments, making them the most important agents of the Earth's surface, along with wave action (see Chapter 12), in eroding and transporting sediments. They create much of the surface topography and are an important water resource.

Several factors cause streams to erode and transport sediment, but the two main factors are stream-channel gradient and velocity. Stream-channel gradient is the slope of the stream, usually expressed in meters per kilometer or feet per mile. A steeper channel gradient promotes erosion. When tectonic forces elevate a mountain, the stream gradient increases, causing the mountain stream to erode downward and deepen its channel, eventually forming a valley. Stream-channel velocity is the speed at which channel water flows. Factors affecting channel velocity include channel gradient which decreases downstream, discharge and channel size which increase as tributaries coalesce, and channel roughness which decreases as sediment lining the channel walls decreases in size, reducing friction. The combined effect of these factors is that channel velocity actually increases from mountain brooks to the mouth of the stream.

11.5.1 Discharge

Stream size is measured in terms of **discharge**, the volume of water flowing past a point in the stream over a defined time interval. Volume is commonly measured in cubic units (length x width x depth), shown as cubic feet (ft^3) or cubic meters (m^3). Therefore, the units of discharge are cubic feet per second (ft^3/sec or cfs). Therefore, the units of discharge are cubic meters per second (m^3/s or cms), or cubic feet per second (ft^3/sec or cfs). **Stream discharge** increases downstream. Smaller streams have less discharge than larger streams. For example, the Mississippi River is the largest river in North America, with an average flow of about 16,990.11 cms (600,000 cfs). For comparison, the average discharge of the Jordan River at Utah Lake is about 16.25 cms (574 cfs), and for the annual discharge of the Amazon River (the world's largest river), annual discharge is about 175,565 cms (6,200,000 cfs).

Discharge can be expressed by the following equation:

Q = V A

- Q = discharge cms (or ft^3/sec)
- A = cross-sectional area of the stream channel [width times average depth] as m^2 (or in^2 or ft^2)
- V = average channel velocity m/s (or ft/sec)

At a given location along the stream, velocity varies with stream width, shape, and depth within the stream channel as well. When the stream channel narrows but discharge remains constant, the same volume of water must flow through a narrower space, causing the velocity to increase, similar to putting a thumb over the end of a backyard water hose. In addition, during rain storms or heavy snow melt, runoff increases, which increases stream discharge and velocity.

When the stream channel curves, the highest velocity will be on the outside of the bend. When the stream channel is straight and uniformly deep, the highest velocity is in the channel center at the top of the water, where it is the farthest from frictional contact with the stream's channel bottom and sides. In hydrology, the **thalweg** of a river is the line drawn that shows its natural progression and deepest channel, as is shown in the diagram.

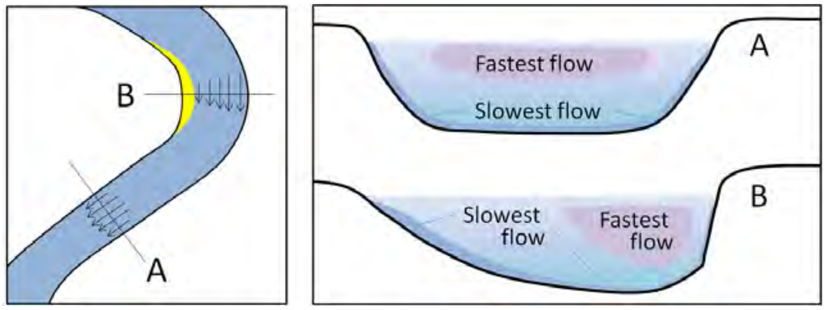

Figure 11.10: Thalweg of a river. In a river bend, the fastest moving water is on the outside of the bend, near the cut bank. Stream velocity is higher on the outside bend and on the water surface farthest from the friction of the stream bed. Longer arrows indicate faster velocity. Figure description available at the end of the chapter.

11.5.2 Runoff versus Infiltration

Factors that dictate whether water will **infiltrate** into the ground or run off over the land include the amount, type, and intensity of precipitation; the type and amount of vegetation cover; the slope of the land; the temperature and aspect of the land; preexisting conditions; and the type of soil in the infiltrated area. High-intensity rain will cause more runoff than the same amount of rain spread out over a longer duration. If the rain falls faster than the soil's properties allow it to infiltrate, then the water that cannot infiltrate becomes runoff. Dense vegetation can increase infiltration, as the vegetative cover slows the water particles' overland flow, giving them more time to infiltrate. If a parcel of land has more direct solar radiation or higher seasonal temperatures, there will be less infiltration and runoff, as evapotranspiration rates will be higher. As the land's slope increases, so does runoff because the water is more inclined to move downslope than infiltrate into the ground. Extreme examples are a basin and a cliff, where water infiltrates much more quickly into a basin than a cliff that has the same soil properties. Because saturated soil does not have the capacity to take more water, runoff is generally greater over saturated soil. Clay-rich soil cannot accept infiltration as quickly as gravel-rich soil.

11.5.3 Drainage Pattern

The pattern of tributaries within a region is called **drainage pattern**. They depend largely on the type of rock beneath and on structures within that rock (such as folds and faults). The main types of drainage patterns are dendritic, trellis, rectangular, radial, and deranged. Dendritic patterns are the most common and develop in areas where the underlying rock or sediments are uniform in character, mostly flat lying, and can be eroded equally easily in all directions. Examples are alluvial sediments or flat-lying sedimentary rocks. Trellis patterns typically develop where sedimentary rocks have been folded or tilted and then eroded to varying degrees depending on their strength. The Appalachian Mountains in the Eastern United States have many good examples of **trellis drainage**. **Rectangular** patterns develop in areas that have very little topography and a system of bedding planes, joints, or faults that form a rectangular network. A **radial** pattern forms when streams flow away from a central high point such as a mountain top or volcano, with the individual streams typically having **dendritic** drainage patterns. In places with extensive limestone deposits, streams can disappear into the groundwater via caves and subterranean drainage, and this creates a **deranged** pattern.

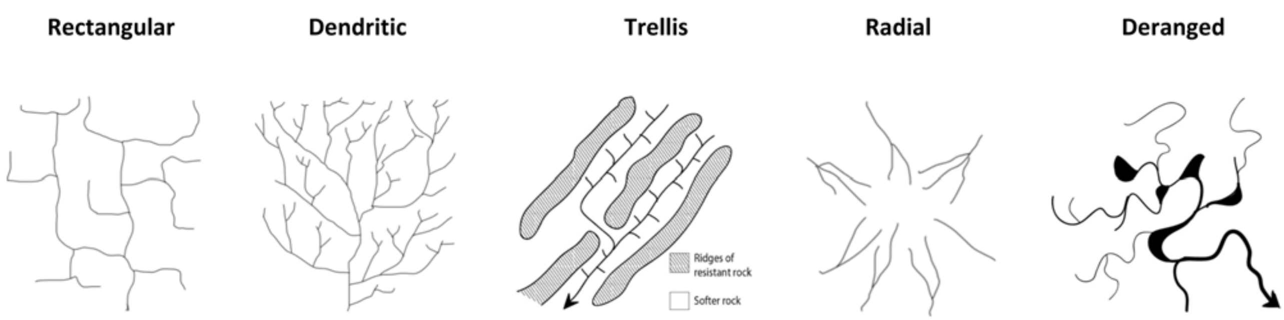

Figure 11.11: Various stream drainage patterns. Figure description available at the end of the chapter.

11.5.4 Fluvial Processes

Fluvial processes dictate how a stream behaves and include factors controlling fluvial sediment production, transport, and deposition. Fluvial processes include velocity, slope and gradient, erosion, transportation, deposition, stream equilibrium, and base level.

Streams can be divided into three main zones: the many smaller tributaries in the source area, the main trunk stream in the floodplain, and the distributaries at the mouth of the stream. Major stream systems like the Mississippi are composed of many source areas, many tributaries, and trunk streams, all coalescing into the one main stream that drains the region. The zones of a stream are defined as (1) the zone of sediment production (erosion), (2) the zone of transport, and (3) the zone of deposition. The zone of sediment production is located in the **headwaters** of the stream. In the zone of sediment transport, there is a general balance between erosion of the finer sediment in its channel and transport of sediment across the floodplain. Streams eventually flow into the ocean or end in quiet water with a delta, which is a zone of sediment deposition located at the mouth of a stream. The **longitudinal profile** of a stream is a plot of the elevation of the stream channel at all points along its course and illustrates the location of the three zones.

Zone of Sediment Production

The zone of sediment production is located in the headwaters of a stream, where rills and gullies erode sediment and contribute to larger tributary streams. These tributaries carry sediment and water further downstream to the main trunk of the stream. Tributaries at the headwaters have the steepest gradient; erosion there produces considerable sediment carried by the stream. Headwater streams tend to be narrow and straight, with small or nonexistent floodplains adjacent to the channel. Since the zone of sediment production is generally the steepest part of the stream, headwaters are generally located in relatively high elevations. The Rocky Mountains of Wyoming and Colorado west of the Continental Divide contain much of the headwaters for the Colorado River, which then flows from Colorado through Utah and Arizona to Mexico. Headwaters of the Mississippi River system lie east of the Continental Divide in the Rocky Mountains and west of the Appalachian Divide.

Zone of Sediment Transport

Streams transport sediment great distances from the headwaters to the ocean, the ultimate depositional basin. Sediment transportation is directly related to stream gradient and velocity. Faster and steeper streams can transport larger sediment grains. When velocity slows down, larger sediments settle to the channel bottom. When the velocity increases, those larger sediments are entrained and move again.

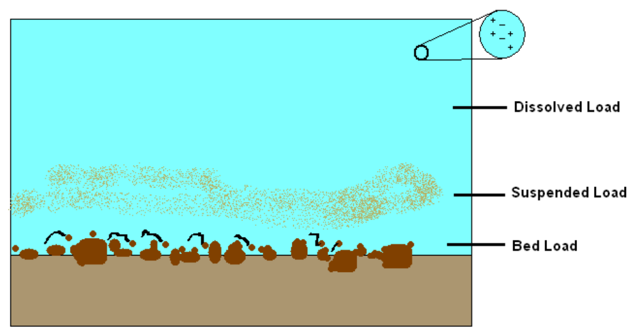

Figure 11.12: A stream carries dissolved load, suspended load, and bedload. Figure description available at the end of the chapter.

Transported sediments are grouped into bedload, suspended load, and dissolved load, as illustrated in the above image. Sediments that are moved along the channel bottom are the **bedload**, which typically consists of the largest and densest particles. Bedload is moved by saltation (bouncing) and traction (being pushed or rolled along by the force of the flow). Smaller particles are picked up by flowing water and carried in suspension as **suspended load**. The particle size that is carried in suspended and bedload depends on the flow velocity of the stream. **Dissolved load** in a stream is the total of the ions in solution from chemical weathering, including common ions such as bicarbonate (HCO_3^-), calcium (Ca^{+2}), chloride (Cl^{-1}), potassium (K^{+1}), and sodium (Na^{+1}). The amounts of these ions are not affected by flow velocity.

Video 11.4: Bedload sediment transport

Access this YouTube video by scanning the QR code. ["Bed load sediment transport" by CSDMS | https://www.youtube.com/watch?v=is-qcxrKKBI]

A **floodplain** is the flat area of land adjacent to a stream channel inundated with flood water on a regular basis. Stream flooding is a natural process that adds sediment to floodplains. A stream typically reaches its greatest velocity when it is close to flooding, known as the **bankfull stage**. As soon as the flooding stream overtops its banks and flows onto its floodplain, the velocity decreases. Sediment that was being carried by the swiftly moving water is deposited at the edge of the channel, forming a low ridge or **natural levee**. In addition, sediments are added to the floodplain during this flooding process, contributing to fertile soils.

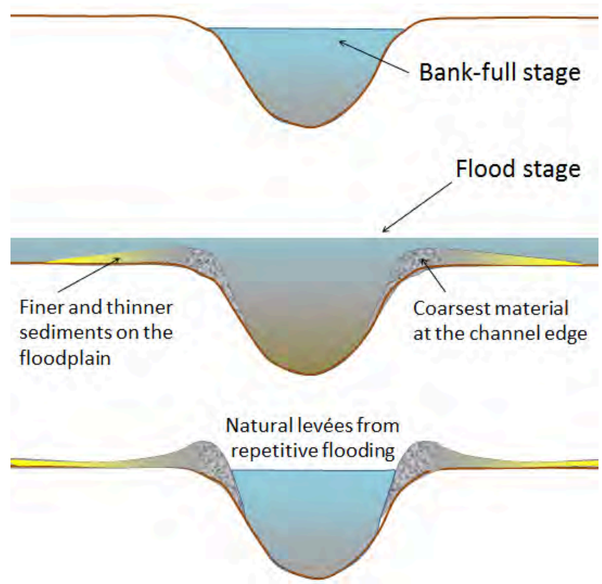

Figure 11.13: Profile of stream channel at bankfull stage, flood stage, and during deposition of natural levee. Figure description available at the end of the chapter.

Zone of Sediment Deposition

Deposition occurs when bedload and suspended load come to rest on the bottom of the stream channel, lake, or ocean due to decrease in stream gradient and reduction in velocity. While both deposition and erosion occur in the zone of transport, such as on point bars and cut banks, ultimate deposition occurs where the stream reaches a lake or ocean. Landforms called deltas form where the stream enters quiet water and are composed of the finest sediment such as fine sand, silt, and clay.

Equilibrium and Base Level

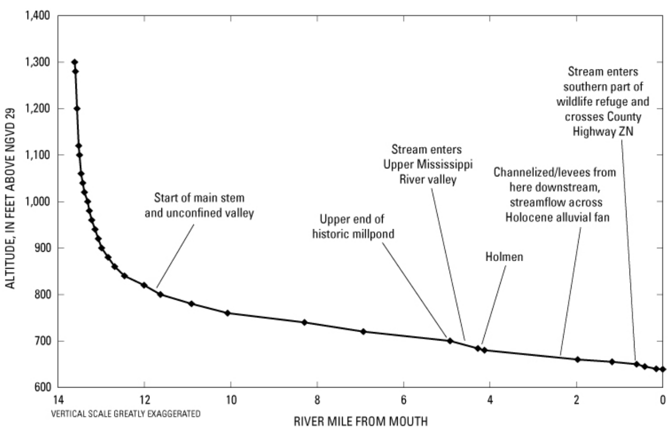

Figure 11.14: Example of a longitudinal profile of a stream; Halfway Creek, Indiana. Figure description available at the end of the chapter.

All three stream zones are present in the typical longitudinal profile of a stream, which plots the elevation of the channel at all points along its course (see Figure 11.14). All streams have a long profile. The long profile shows the stream gradient from headwater to mouth. All streams attempt to achieve an energetic balance among erosion, transport, gradient, velocity, discharge, and channel characteristics along the stream's profile. This balance is called equilibrium.

Another factor influencing equilibrium is base level, the elevation of the stream's mouth at the lowest level to which a stream can erode. The ultimate base level is, of course, sea level. A lake or reservoir may also represent base level for a stream entering it. The Great Basin of western Utah, Nevada, and parts of some surrounding states contains no outlets to the sea and provides internal base levels for streams within it. Base level for a stream entering the ocean changes if sea level rises or falls. Base level also changes if a natural or human-made dam is added along a stream's profile. When base level is lowered, a stream will cut down and deepen its channel. When base level rises, deposition increases as the stream adjusts in an attempt to establish a new state of equilibrium. A stream that has approximately achieved equilibrium is called a graded stream.

11.5.5 Fluvial Landforms

Stream landforms are the land features formed on the surface by either erosion or deposition. The stream-related landforms described here are primarily related to channel types.

Channel Types

Figure 11.15: The braided Waimakariri River in New Zealand. Figure description available at the end of the chapter.

Stream channels can be straight, braided, meandering, or entrenched. The gradient, sediment load, discharge, and location of base level all influence channel type. **Straight channels** are relatively straight, located near the headwaters, and have steep gradients, low discharge, and narrow V-shaped valleys. Examples of these are located in mountainous areas.

Braided streams have multiple channels splitting and recombining around numerous mid-channel bars. These are found in floodplains with low gradients in areas with nearby sources of coarse sediment such as trunk streams draining mountains or in front of glaciers.

Figure 11.16: Air photo of the meandering river Río Cauto, Cuba. Figure description available at the end of the chapter.

Meandering streams have a single channel that curves back and forth like a snake within its floodplain, emerging from its headwaters into the zone of transport. Meandering streams are dynamic, creating a wide floodplain by eroding and extending meander loops side to side. The highest velocity water is located on the outside of a meander bend. Erosion of the outside of the curve creates a feature called a **cut bank**, and the meander extends its loop wider by this erosion.

Figure 11.17: Point bar and cut bank on the Cirque de la Madeleine in France. Figure description available at the end of the chapter.

The thalweg of the stream is the deepest part of the stream channel. In the straight parts of the channel, the thalweg and highest velocity are in the center of the channel. But at the bend of a meandering stream, the thalweg shifts toward the cut bank. Opposite the cut bank on the inside bend of the channel is the lowest stream velocity, found in an area of deposition called a **point bar**.

In areas of tectonic uplift such as on the Colorado Plateau, meandering streams that once flowed on the plateau surface have become **entrenched** or incised as uplift occurred and the stream cut its meandering channel down into bedrock. Over the past several million years, the Colorado River and its tributaries have incised into the flat-lying rocks of the plateau by hundreds, even thousands of feet, creating deep canyons including the Grand Canyon in Arizona.

Figure 11.18: Horseshoe Bend is an entrenched meander of the Colorado River in Glen Canyon National Recreation Area near Page, Arizona. Figure description available at the end of the chapter.

Figure 11.19: Panoramic view of incised meanders of the San Juan River at Gooseneck State Park, Utah. Figure description available at the end of the chapter.

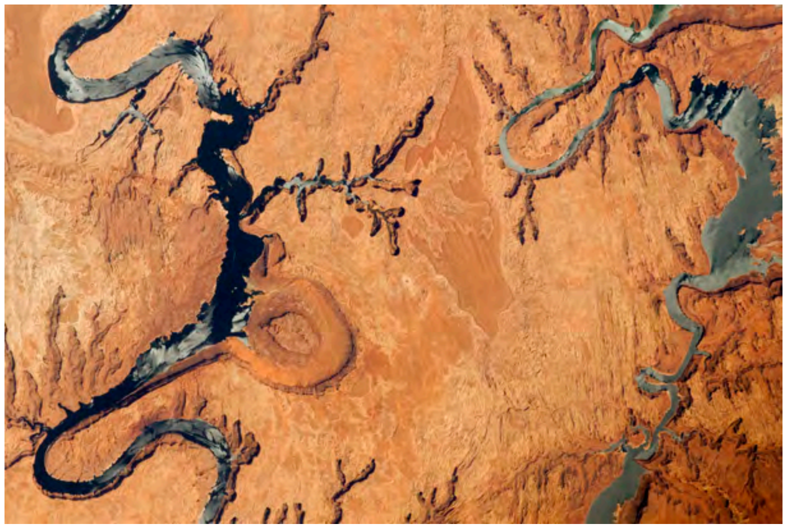

Figure 11.20: The Rincon is an abandoned meander loop on the entrenched Colorado River in Lake Powell. Figure description available at the end of the chapter.

Figure 11.21: Landsat image of Zambezi Flood Plain, Namibia. Figure description available at the end of the chapter.

Many fluvial landforms occur on a floodplain associated with a meandering stream. Meander activity and regular flooding contribute to widening the floodplain by eroding adjacent uplands. The stream channels are confined by natural levees that have been built up over many years of regular flooding. Natural levees can isolate and direct flow from tributary channels on the floodplain from immediately reaching the main channel. These isolated streams are called **yazoo streams** and flow parallel to the main trunk stream until there is an opening in the levee to allow for a belated confluence.

Video 11.5: How is a levee formed?

Access this YouTube video by scanning the QR code. ["How is a levee formed?" by Quentin Lister | https://www.youtube.com/watch?v=persGpc6-Dw]

To limit flooding, humans build artificial levees on flood plains. Sediment that breaches the levees during a flood stage is called **crevasse splays** and delivers silt and clay onto the floodplain. These deposits are rich in nutrients and often make good farmland. When floodwaters crest over human-made levees, the levees quickly erode, with potentially catastrophic impacts. Because of the good soils, farmers regularly return after floods and rebuild year after year.

Through erosion on the outsides of the meanders and deposition on the insides, the channels of meandering streams move back and forth across their floodplain over time. On very broad floodplains with very low gradients, the meander bends can become so extreme that they cut across themselves at a narrow neck called a cutoff (see Figure 11.22). The former channel becomes isolated and forms an oxbow lake, as seen on the right of the figure. Eventually the oxbow lake fills in with sediment and becomes a wetland and eventually a **meander scar**. Stream meanders can migrate and form oxbow lakes in a relatively short amount of time. **Scroll bars** are series of ridges that result from the continuous lateral migration of a meander, more common in mature rivers. The presence of scroll bars suggests that the water flow in the channel may have been sustained for a relatively long time before migrating. Where stream channels form geographic and political boundaries, this shifting of channels can cause conflicts.

Figure 11.22: Meander nearing cutoff on the Nowitna River in Alaska. You can see multiple series of scroll bars inside each meander, showing the former locations of the channel. Figure description available at the end of the chapter.

Video 11.6: Why do rivers curve?

Access this YouTube video by scanning the QR code. ["Why Do Rivers Curve?" by MinuteEarth | https://www.youtube.com/watch?v=8a3r-cG8Wic]

Alluvial fans are a depositional landform created where streams emerge from mountain canyons into a valley. The channel that had been confined by the canyon walls is no longer confined, and it slows down and spreads out, dropping its bedload of all sizes, forming a delta in the air of the valley. As distributary channels fill with sediment, the stream is diverted laterally, and the alluvial fan develops into a cone-shaped landform with distributaries radiating from the canyon mouth. Alluvial fans are common in the dry climates of the West, where ephemeral streams emerge from canyons in the ranges of the Basin and Range.

Figure 11.23: Alluvial fan in Iraq seen by NASA satellite. A stream emerges from the canyon and creates this cone-shaped deposit. Figure description available at the end of the chapter.

Complete this interactive activity to check your understanding.

Access this interactive activity by scanning the QR code.

A delta is formed when a stream reaches a quieter body of water, such as a lake or the ocean, and the bedload and suspended load is deposited. If wave erosion from the water body is greater than deposition from the river, a delta will not form. The largest and most famous delta in the United States is the Mississippi River Delta, formed where the Mississippi River flows into the Gulf of Mexico. The Mississippi River drainage basin is the largest in North America, draining 41% of the contiguous United States. Because of the large drainage area, the river carries a large amount of sediment. The Mississippi River is a major shipping route, and human engineering has ensured that the channel has been artificially straightened and remains fixed within the floodplain. The river is now 229 km shorter than it was before humans began engineering it. Because of these restraints, the delta is now focused on one trunk channel and has created a "bird's foot" pattern. The two NASA images of the delta below show how the shoreline has retreated and land was inundated with water while deposition of sediment was focused at end of the distributaries. These images have changed over a 25-year period from 1976 to 2001. These are stark changes illustrating sea-level rise and land subsidence from the compaction of peat due to the lack of sediment resupply.

Figure 11.24: Location of the Mississippi River drainage basin and Mississippi River Delta. Figure description available at the end of the chapter.

Complete this interactive activity to check your understanding.

Access this interactive activity by scanning the QR code.

The formation of the Mississippi River Delta started about 7,500 years ago, when postglacial sea level stopped rising. In the past 7,000 years, prior to **anthropogenic** modifications, the Mississippi River Delta formed several sequential lobes. The river abandoned each lobe for a more preferred route to the Gulf of Mexico. These delta lobes were reworked by the ocean waves of the Gulf of Mexico. After each lobe was abandoned by the river, isostatic depression and compaction of the sediments caused basin subsidence and made the land sink.

Figure 11.25: Delta in Quake Lake Montana. Deposition of this delta began in 1959, when the Madison River was dammed by the landslide caused by the 7.5 magnitude earthquake. Figure description available at the end of the chapter.

A clear example of how deltas form came from an earthquake. During the 1959 Madison Canyon 7.5 magnitude earthquake in Montana, a large landslide dammed the Madison River, forming Quake Lake, which is still there today. A small tributary stream that once flowed into the Madison River now flows into Quake Lake, forming a delta composed of coarse sediment actively eroded from the mountainous upthrown block to the north.

Deltas can be further categorized as wave-dominated or tide-dominated. Wave-dominated deltas occur where the tides are small and wave energy dominates. An example is the Nile River Delta in the Mediterranean Sea, which has the classic shape of the Greek character (Δ), from which the landform is named. A tide-dominated delta forms when ocean tides are powerful and influence the shape of the delta. For example, Ganges-Brahmaputra Delta in the Bay of Bengal (near India and Bangladesh) is the world's largest delta.

At the Sundarban Delta in Bangladesh, tidal forces create linear intrusions of seawater into the delta. This delta is also home to the world's largest mangrove swamp.

Figure 11.26: Sundarban Delta in Bangladesh, a tide-dominated delta of the Ganges River. Figure description available at the end of the chapter.

Figure 11.27: Nile Delta showing its classic "delta" shape. Figure description available at the end of the chapter.

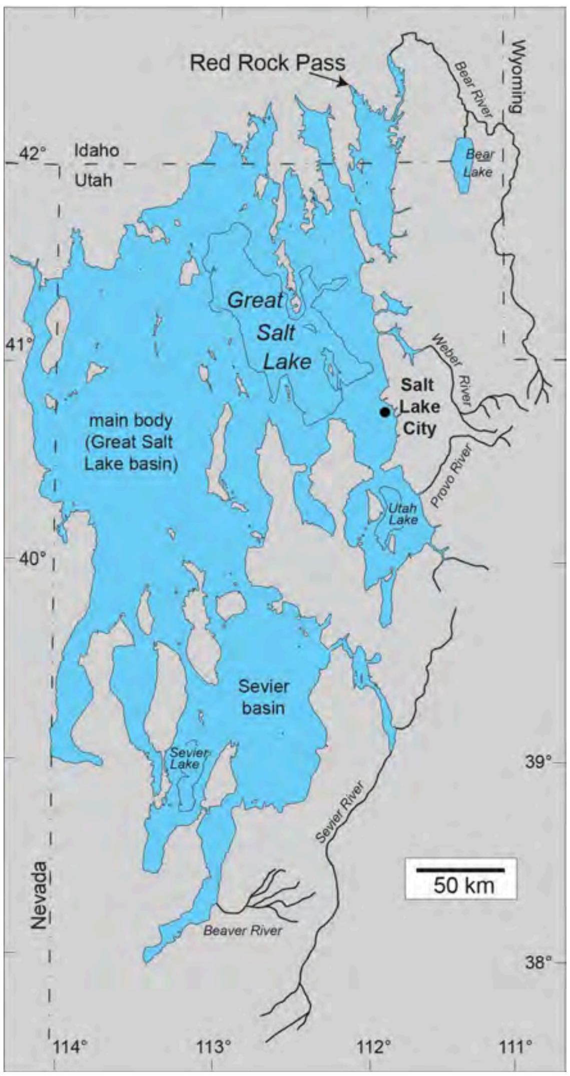

Figure 11.28: Map of Lake Bonneville, showing the outline of the Bonneville shoreline, the highest level of the lake. Figure description available at the end of the chapter.

Lake Bonneville was a large pluvial lake that occupied the western half of Utah and parts of eastern Nevada from about 30,000 to 12,000 years ago. The lake filled to a maximum elevation as great as approximately 5,100 feet above mean sea level, filling the basins and leaving the mountains exposed, many as islands. The presence of the lake allowed for deposition of both fine-grained lake mud and silt as well as coarse gravels from the mountains. Variations in lake level were controlled by regional climate and a catastrophic failure of Lake Bonneville's main outlet, Red Rock Pass. During extended periods of time in which the lake level remained stable, wave-cut terraces were produced that can be seen today on the flanks of many mountains in the region. Significant deltas formed at the mouths of major canyons in Salt Lake, Cache, and other Utah valleys. The Great Salt Lake is the remnant of Lake Bonneville and cities have built up on these delta deposits.

Figure 11.29: Deltaic deposits of Lake Bonneville near Logan, Utah; wave-cut terraces can be seen on the mountain slope. Figure description available at the end of the chapter.

Stream terraces are remnants of older floodplains located above the existing floodplain and river. Like entrenched meanders, stream terraces form when uplift occurs or base level drops and streams erode downward, their meanders widening a new floodplain. Stream terraces can also form from extreme flood events associated with retreating glaciers. Classic examples of multiple stream terraces can be found along the Snake River in Grand Teton National Park in Wyoming.

Figure 11.30: Terraces along the Snake River, Wyoming. Figure description available at the end of the chapter.

Take this quiz to check your comprehension of this section.

Access the quiz for Section 11.5 by scanning the QR code.

11.6 Groundwater

Groundwater is an important source of fresh water. It can be found at varying depths in all places under the ground but is limited by extractable quantity and quality.

Video 11.7: What is an aquifer?

Access this YouTube video by scanning the QR code. ["What is an Aquifer?" by GeoScience Videos | https://www.youtube.com/watch?v=g7R0yLX0V9E]

11.6.1 Porosity and Permeability

An **aquifer** is a rock unit that contains extractable ground water. A good aquifer must be both porous and permeable. **Porosity** is the space between grains that can hold water, expressed as the percentage of open space in the total volume of the rock. **Permeability** comes from connectivity of the spaces that allows water to move in the aquifer. Porosity can occur as primary porosity, as space between sand grains or vesicles in volcanic rocks, or as secondary porosity in the form of fractures or dissolved spaces in rock. Compaction and cementation during lithification of sediments reduces porosity (see Section 5.3).

A combination of a place to contain water (porosity) and the ability to move water (permeability) makes a good aquifer—a rock unit or sediment that allows extraction of groundwater. Well-sorted sediments have higher porosity because there are not smaller sediment particles filling in the spaces between the larger particles. Shales made of clays generally have high porosity, but the pores are poorly connected, thereby causing low permeability.

Video 11.8: Porosity and permeability

Access this YouTube video by scanning the QR code. ["Porosity and Permeability" by GeoScience Videos | https://www.youtube.com/watch?v=8mfBomrw0rs]

While permeability is an important measure of a porous material's ability to transmit water, hydraulic conductivity is more commonly used by geologists to measure how easily a fluid is transmitted. **Hydraulic conductivity** measures both the permeability of the porous material and the properties of the water (or whatever fluid is being transmitted, like oil or gas). Because hydraulic conductivity also measures the properties of the fluid, such as viscosity, it is used by both petroleum geologists and hydrogeologists to describe the production capability of oil reservoirs and of aquifers. High hydraulic conductivity indicates that fluid transmits rapidly through an aquifer.

11.6.2 Aquifers

Aquifers are rock layers with sufficient porosity and permeability to allow water to be both contained and move within them. For rock or sediment to be considered an aquifer, its pores must be at least partially filled with water and it must be permeable enough to transmit water. Drinking water aquifers must also contain potable water. Aquifers can vary dramatically in scale, spanning several formations that cover large regions to being a local formation in a limited area. Aquifers that are adequate for water supply are permeable, porous, and potable.

11.6.3 Groundwater Flow

When surface water infiltrates, or seeps, into the ground, it usually enters the unsaturated zone, also called the vadose zone or zone of aeration. The **vadose zone** is the volume of geologic material between the land surface and the zone of saturation, where the pore spaces are not completely filled with water. Plant roots inhabit the upper vadose zone, and fluid pressure in the pores is less than atmospheric pressure. Below the vadose zone is the capillary fringe. Capillary fringe is the usually thin zone below the vadose zone, where the pores are completely filled with water (saturation), but the fluid pressure is less than atmospheric pressure. The pores in the capillary fringe are filled because of capillary action, which occurs because of a combination of adhesion and cohesion. Below the capillary fringe is the saturated zone, or phreatic zone, where the pores are completely saturated and the fluid in the pores is at or above atmospheric pressure. The interface between the capillary fringe and the saturated zone marks the location of the **water table**.

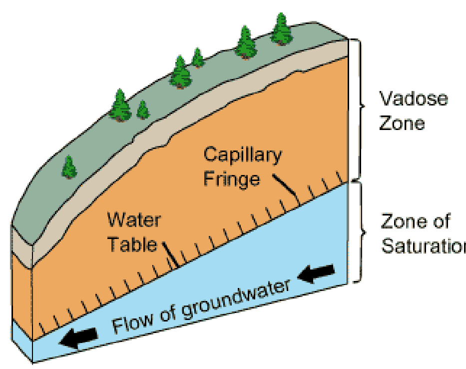

Figure 11.31: Zone of saturation. Figure description available at the end of the chapter.

Wells are conduits that extend into the ground, with openings to the aquifers that extract from, measure, and sometimes add water to the aquifer. Wells are generally the way that geologists and hydrologists measure the depth to groundwater from the land surface and withdraw water from aquifers.

Water is found throughout the pore spaces in sediments and bedrock. The water table is the area below which the pores are fully saturated with water. The simplest case of a water table is when the aquifer is unconfined, meaning it does not have a confining layer above it. Confining layers can pressurize aquifers by trapping water that is recharged at a higher elevation underneath the confining layer, allowing for a potentiometric surface higher than the top of the aquifer and sometimes higher than the land surface.

A **confining layer** is a low-permeability layer above and/or below an aquifer that restricts the water from moving in and out of the aquifer. Confining layers include **aquicludes**, which are so impermeable that no water travels through them, and **aquitards**, which significantly decrease the speed at which water travels through them. The **potentiometric surface** represents the height that water would rise in a well that is penetrating the pressurized aquifer system. Breaches in the pressurized aquifer system, like faults or wells, can cause springs or flowing wells, also known as artesian wells.

The water table will generally mirror surface topography, though more subdued, because hydrostatic pressure is equal to atmospheric pressure along the surface of the water table. If the water table intersects the ground surface, the result will be water at the surface in the form of a gaining stream, spring, lake, or wetland. The water table intersects the channel for gaining streams, which then gains water from the water table. The channels for losing streams lie below the water table, thus losing streams lose water to the water table. Losing streams may be seasonal during a dry season or ephemeral in dry climates, where they may normally be dry and carry water only after rainstorms. Ephemeral streams pose a serious danger of flash flooding in dry climates.

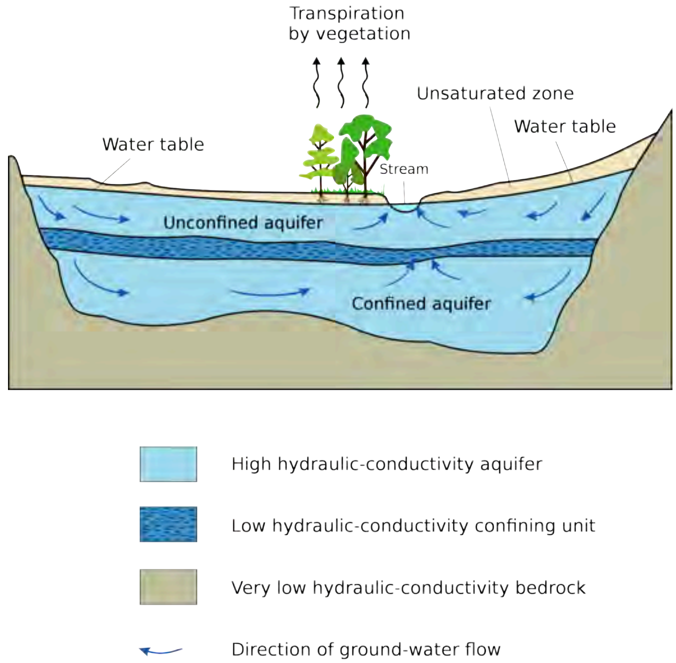

Figure 11.32: An aquifer cross section. This diagram shows two aquifers with one aquitard (a confining or impermeable layer) between them, surrounded by the bedrock aquiclude, which is in contact with a gaining stream (typical in humid regions). Figure description available at the end of the chapter.

Video 11.9: Where is the water table?

Access this YouTube video by scanning the QR code. ["Where is the Water Table?" by GeoScience Videos | https://www.youtube.com/watch?v=UfgyJkmZgK8]

Using wells, geologists measure the water table's height and the potentiometric surface. Graphs of the depth to groundwater over time are known as hydrographs and show changes in the water table over time. Well-water level is controlled by many factors and can change very frequently, even every minute, seasonally, and over longer periods of time.

In 1856, French engineer Henry Darcy developed a hypothesis to show how discharge through a porous medium is controlled by permeability, pressure, and cross-sectional area. To prove this relationship, Darcy experimented with tubes of packed sediment with water running through them. The results of his experiments empirically established a quantitative measure of hydraulic conductivity and discharge that is known as Darcy's law. The relationships described by Darcy's law have close similarities to Fourier's law in the field of heat conduction, Ohm's law in the field of electrical networks, or Fick's law in diffusion theory.

Q = KA(Δh/L)

- Q = flow (volume/time)
- K = hydraulic conductivity (length/time)
- A = cross-sectional area of flow (area)
- Δh = change in pressure head (pressure difference)
- L = distance between pressure (h) measurements (length)
- **Δh/**L is commonly referred to as the hydraulic gradient

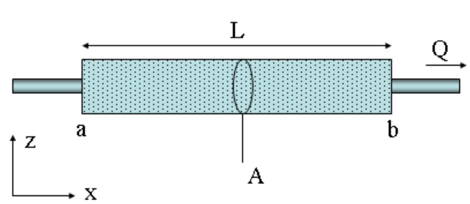

Figure 11.33: Pipe showing apparatus that would demonstrate Darcy's law. Δh would be measured across L from a to b. Figure description available at the end of the chapter.

Pumping water from an unconfined aquifer lowers the water table. Pumping water from a confined aquifer lowers the pressure and/or potentiometric surface around the well. In an unconfined aquifer, the water table is lowered as water is removed from the aquifer near the well, producing drawdown and a **cone of depression** (see Figure 11.34). In a confined aquifer, pumping on an **artesian well** reduces the pressure or potentiometric surface around the well.

When one cone of depression intersects another cone of depression or a barrier feature like an impermeable mountain block, drawdown is intensified. When a cone of depression intersects a recharge zone, the cone of depression is lessened.

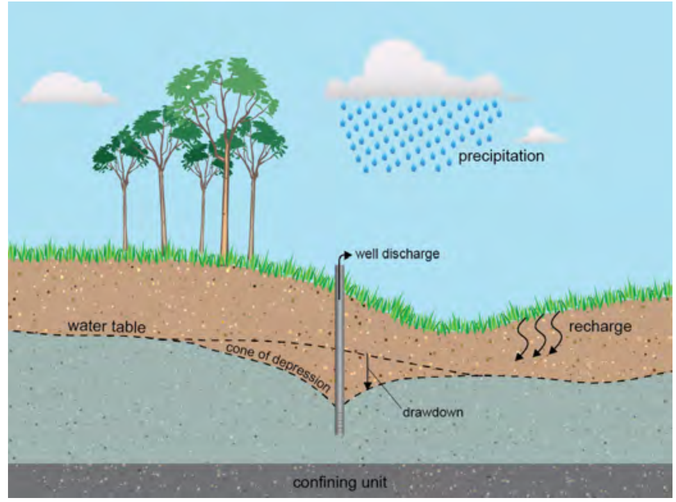

Figure 11.34: Cones of depression. Figure description available at the end of the chapter.

11.6.4 Recharge

The **recharge** area is where surface water enters an aquifer through the process of infiltration. Recharge areas are generally topographically high locations of an aquifer. They are characterized by losing streams and permeable rock that allows infiltration into the aquifer. Recharge areas mark the beginning of groundwater flow paths.

In the Basin and Range Province, recharge areas for the unconsolidated aquifers of the valleys are located along mountain foothills. In the foothills of Salt Lake Valley, losing streams contribute water to the gravel-rich deltaic deposits of ancient Lake Bonneville, in some cases feeding artesian wells in the Salt Lake Valley.

An aquifer management practice is to induce recharge through storage and recovery. Geologists and hydrologists can increase the recharge rate into an aquifer system using injection wells and infiltration galleries or basins. Injection wells pump water into an aquifer where it can be stored. Injection wells are regulated by state and federal governments to ensure that the injected water does not negatively impact the quality or supply of the existing groundwater in the aquifer. Some aquifers can store significant quantities of water, allowing water managers to use the aquifer system like a surface reservoir. Water is stored in the aquifer during periods of low water demand and high water supply and later extracted during times of high water demand and low water supply.

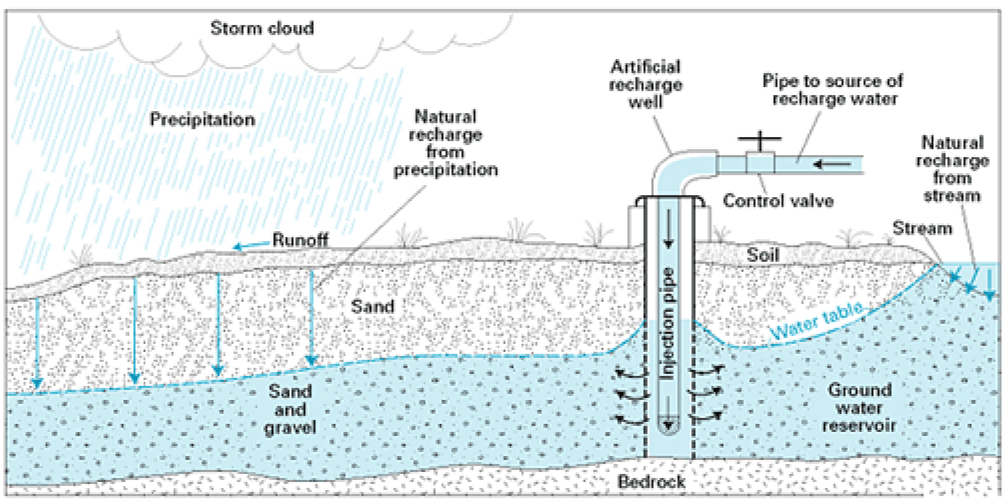

Figure 11.35: Different ways an aquifer can be recharged. Figure description available at the end of the chapter.

11.6.5 Discharge

Discharge areas are where the water table or potentiometric surface intersects the land surface. Discharge areas mark the end of groundwater flow paths. These areas are characterized by springs, flowing (artesian) wells, gaining streams, and playas in the dry valley basins of the Basin and Range Province of the Western United States.

11.6.6 Groundwater Mining and Subsidence

Like other natural resources on our planet, the quantity of fresh and potable water is finite. The only natural source of water on land is from the sky in the form of precipitation. In many places, groundwater is being extracted faster than it is being replenished. When groundwater is extracted faster than it is recharged, groundwater levels and potentiometric surfaces decline, and discharge areas diminish or dry up completely. Regional pumping-induced groundwater decline is known as **groundwater mining** or groundwater overdraft. Groundwater mining is a serious situation and can lead to dry wells, reduced spring and stream flow, and subsidence. Groundwater mining is happening in places where more water is extracted by pumping than is being replenished by precipitation and where the water table is continually lowered. In these situations, groundwater must be viewed as an ore body and, in its depletion, has the possibility of producing ghost towns.

Video 11.10: Groundwater

Access this YouTube video by scanning the QR code. ["Science Today: Groundwater | California Academy of Sciences" by California Academy of Sciences | https://www.youtube.com/watch?v=_DuwZjb3_DA]

In many places, water actually helps hold up an aquifer's skeleton by the water pressure exerted on the grains in an aquifer. This pressure is called pore pressure and comes from the weight of overlying water. If pore pressure decreases because of groundwater mining, the aquifer can compact, causing the surface of the ground to sink. Areas that are especially susceptible to this effect are aquifers made of unconsolidated sediments. Unconsolidated sediments with multiple layers of clay and other fine-grained material are at higher risk because, when water is drained, clay compacts considerably.

Subsidence from groundwater mining has been documented in southwestern Utah, notably Cedar Valley in Iron County. Groundwater levels have declined more than 100 feet in certain parts of Cedar Valley, causing earth fissures and measurable amounts of land subsidence.

This photo shows documentation of subsidence from pumping of groundwater for irrigation in the Central Valley in California. The pole shows subsidence from groundwater pumping over a period of time.

Figure 11.36: Evidence of land subsidence from pumping of groundwater shown by dates on a pole. Figure description available at the end of the chapter.

Take this quiz to check your comprehension of this section.

Access the quiz for Section 11.6 by scanning the QR code.

11.7 Water Contamination and Remediation

Water can be contaminated by natural features like mineral-rich geologic formations and by human activities such as agriculture, industrial operations, landfills, animal operations, and sewage treatment processes, among many other things. As water runs over the land or infiltrates into the ground, it dissolves material left behind by these potential contaminant sources. There are three major groups of contamination: organic chemicals, inorganic chemicals, and biological agents. Small sediments that cloud water, causing turbidity, is also an issue with some wells, but it is not considered contamination. The risks and type of **remediation** for a contaminant depends on the type of chemicals present.

Contamination occurs as point-source and nonpoint-source pollution. **Point source** pollution can be attributed to a single, definable source, while **nonpoint source** pollution is from multiple dispersed sources. Point sources include waste disposal sites, storage tanks, sewage treatment plants, and chemical spills. Nonpoint sources are dispersed and indiscreet, where the whole of the contribution of pollutants is harmful even if the individual components do not have harmful concentrations of pollutants. A good example of nonpoint pollution occurs in residential areas, where lawn fertilizer on one person's yard may not contribute much pollution to the system, but the combined effect of many residents using fertilizer can lead to significant nonpoint pollution. Other nonpoint sources include nutrients (nitrate and phosphate), herbicides, pesticides contributed by farming, nitrate contributed by animal operations, and nitrate contributed by septic systems.

Organic chemicals are common pollutants. They consist of strands and rings of carbon atoms, usually connected by covalent bonds. Other types of atoms, like chlorine, and molecules, like hydroxide (OH_{-}), are attached to the strands and rings. The number and arrangement of atoms will decide how the chemical behaves in the environment, its danger to humans or ecosystems, and where the chemical ends up in the environment. The different arrangements of carbon allow for tens of thousands of organic chemicals, many of which have never been studied for negative effects on human health or the environment. Common organic pollutants are herbicides and pesticides, pharmaceuticals, fuel, and industrial solvents and cleansers.

Organic chemicals include surfactants such as cleaning agents and synthetic hormones associated with pharmaceuticals, which can act as endocrine disruptors. Endocrine disruptors mimic hormones and can cause long-term effects in developing sexual reproduction systems in developing animals. Only very small quantities of endocrine disruptors are needed to cause significant changes in animal populations.

An example of organic chemical contamination is the Love Canal, Niagara Falls, New York. From 1942 to 1952, the Hooker Chemical Company disposed of over 21,337 metric tons (21,000 tons) of chemical waste, including chlorinated hydrocarbons, into a canal and covered it with a thin layer of clay. Chlorinated hydrocarbons are a large group of organic chemicals that have chlorine functional groups, most of which are toxic and carcinogenic to humans. The company sold the land to the New York School Board, who developed it into a neighborhood. After residents began to suffer from serious health ailments and pools of oily fluid started rising into residents' basements, the neighborhood had to be evacuated. This site became a US Environmental Protection Agency **Superfund site**, a site with federal funding and oversight to ensure its cleanup.

Inorganic chemicals are another set of chemical pollutants. They can contain carbon atoms but not in long strands or links. Inorganic contaminants include chloride, arsenic, and nitrate (NO_3). Nutrients can be from geologic material, like phosphorous-rich rock, but are most often sourced from fertilizer and animal and human waste. Untreated sewage and agricultural runoff contain concentrates of nitrogen and phosphorus, which are essential for the growth of microorganisms. Nutrients like nitrate and phosphate in surface water can promote growth of microbes, like blue-green algae (cyanobacteria), which in turn use oxygen and create toxins (microcystins and anatoxins) in lakes. This process is known as eutrophication.

Metals are common inorganic contaminants. Lead, mercury, and arsenic are some of the more problematic inorganic groundwater contaminants. Bangladesh has a well-documented case of arsenic contamination from natural geologic material dissolving into the groundwater. Acid-mine drainage can also cause significant inorganic contamination (see Chapter 16).

Salt, typically sodium chloride, is a common inorganic contaminant. It can be introduced into groundwater from natural sources, such as evaporite deposits like the Arapien Shale of Utah, or from anthropogenic sources like the salts applied to roads in the winter to keep ice from forming. Salt contamination can also occur near ocean coasts from salt water intruding into the cones of depression around fresh groundwater pumping, inducing the encroachment of saltwater into the freshwater body.

Figure 11.37: Acid mine drainage continues today from a coal mine that was shut down in 1935 near Blacksburg, Virginia, along the Coal Mining Heritage Loop Trail. The water's orange color is due to the high amounts of iron and sulfur. Figure description available at the end of the chapter.

Biological agents are another common groundwater contaminant and include harmful bacteria and viruses. A common bacteria contaminant is *Escherichia coli* (*E. coli*). Generally, harmful bacteria are not present in groundwater unless the groundwater source is closely connected with a contaminated surface source, such as a septic system. **Karst**—a landform created from dissolved limestone—is especially susceptible to this form of contamination because water moves relatively quickly through the conduits of dissolved limestone. Bacteria can also be used for remediation.

View [USGS tables on contaminants found in groundwater](#).

Remediation is the act of cleaning contamination. Hydrologists use three types of remediation: biological, chemical, and physical. Biological remediation uses specific strains of bacteria to break down a contaminant into safer chemicals. This type of remediation is usually used on organic chemicals but also works on reducing or oxidizing inorganic chemicals like nitrate. Phytoremediation is a type of bioremediation that uses plants to absorb the chemicals over time.

Chemical remediation uses chemicals to remove the contaminant or make it less harmful. One example is to use a reactive barrier, a permeable wall in the ground or at a discharge point that chemically reacts with contaminants in the water. Reactive barriers made of limestone can increase the pH of acid mine drainage, making the water less acidic and more basic, which removes dissolved contaminants by precipitation into solid form.

Physical remediation consists of removing the contaminated water and either treating it with filtration, called pump-and-treat, or disposing of it. All of these options are technically complex, expensive, and difficult, with physical remediation typically being the most costly.

Take this quiz to check your comprehension of this section.

Access the quiz for Section 11.7 by scanning the QR code.

11.8 Karst

Figure 11.38: Steep karst towers in China left as remnants from limestone dissolving away by acidic rain and groundwater. Figure description available at the end of the chapter.

Karst refers to landscapes and hydrologic features created by the dissolving of limestone. Karst can be found anywhere there is limestone and other soluble subterranean substances like salt deposits. Dissolving of limestone creates features like sinkholes, caverns, disappearing streams, and towers.

Figure 11.39: Sinkholes of the McCauley Sink in Northern Arizona, produced by collapse of Kaibab Limestone into caverns caused by the solution of underlying salt deposits. Figure description available at the end of the chapter.

The dissolution of underlying salt deposits has caused sinkholes to form in the Kaibab Limestone on the Colorado Plateau in Arizona.

Figure 11.40: This sinkhole caused by the collapse of surface into a underground cavern appeared in the front yard of this home in Florida. Figure description available at the end of the chapter.

Collapse of the surface into an underground cavern caused this sinkhole in the front yard of a home in Florida.

CO_2 in the atmosphere dissolves readily in the water droplets that form clouds, from which precipitation comes in the form of rain and snow. This precipitation is slightly acidic with carbonic acid. Karst forms when carbonic acid dissolves (calcium carbonate) in limestone.

$$\mathbf{H_2O + CO_2 = H_2CO_3}$$

water + carbon dioxide gas = carbonic acid in water

$$\mathbf{CaCO_3 + H_2CO_3 = Ca^{2+} + 2HCO_3^{\ -1}}$$

solid calcite + carbonic acid in water dissolved = calcium ion + dissolved bicarbonate ion

After the slightly acidic water dissolves the calcite, changes in temperature or gas content in the water can cause the water to redeposit the calcite as tufa (travertine) in a different place, often by a spring or in a cave. Speleothems are secondary deposits, typically made of travertine, deposited in a cave. Travertine speleothems form by water dripping through cracks and dissolved openings in caves and evaporating, leaving behind the travertine deposits. Speleothems commonly occur in the form of stalactites, which extend from the ceiling, and stalagmites, which rise up from the floor.

Figure 11.41: Mammoth Hot Springs, Yellowstone National Park. Figure description available at the end of the chapter.

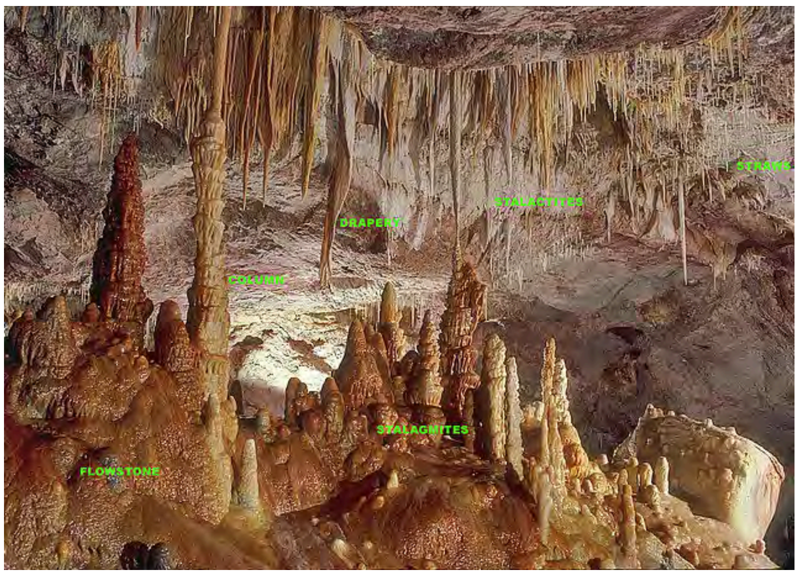

Figure 11.42: Varieties of speleothems. Figure description available at the end of the chapter.

Surface water enters the karst system through sinkholes, losing streams, and disappearing streams. Changes in base level can cause rivers running over limestone to dissolve the limestone and sink into the ground. As the water continues to dissolve its way through the limestone, it can leave behind intricate networks of caves and narrow passages. Often, dissolution will follow and expand fractures in the limestone. Water exits the karst system as springs and rises. In mountainous terrane, dissolution can extend all the way through the vertical profile of the mountain, with caverns dropping thousands of feet.

Figure 11.43: This stream disappears into a subterranean cavern system to re-emerge a few hundred yards downstream. Figure description available at the end of the chapter.

Take this quiz to check your comprehension of this section.

Access the quiz for Section 11.8 by scanning the QR code.

Summary

Water is essential for all living things. It continuously cycles through the atmosphere, over land, and through the ground. In much of the United States and other countries, water is managed through a system of regional laws and regulations and distributed on paper in a system collectively known as "water rights." Surface water follows a watershed, which is separated from other areas by its divides (highest ridges). Groundwater exists in the pores within rocks and sediment. It moves predominantly due to pressure and gravitational gradients through the rock. Human and natural causes can make water unsuitable for consumption. There are different ways to deal with this contamination. A karst occurs when limestone is dissolved by water, forming caves and sinkholes.

Take this quiz to check your comprehension of this chapter.

Access the quiz for Chapter 11 by scanning the QR code.

Chapter URLs

- NPR story on Snake Valley: https://www.npr.org/2007/06/12/10953190/las-vegas-water-battle-crops-vs-craps
- SNWA History: https://www.snwa.com/about/mission/index.html
- NASA images: https://earthobservatory.nasa.gov/images/8103/mississippi-river-delta
- USGS tables on contaminants found in groundwater: https://www.usgs.gov/special-topics/water-science-school/science/contamination-groundwater

Text References

1. Brush, L.M., Jr. (1961). Drainage basins, channels, and flow characteristics of selected streams in central Pennsylvania. Online, http://pubs.er.usgs.gov.
2. Charlton, R. (2007). *Fundamentals of fluvial geomorphology:* Taylor & Francis.
3. Cirrus Ecological Solutions (2009). Jordan River TMDL. Utah State Division of Water Quality.
4. Earle, S. (2015). *Physical geology OER textbook:* BC Campus OpenEd.
5. EPA (2009). Water on Tap—What You Need to Know: U.S. Environmental Protection Agency.
6. Fagan, B. (2012). *Elixir: A history of water and humankind:* Bloomsbury Press.
7. Fairbridge, R.W. (1968). Yazoo rivers or streams, in *Geomorphology: Springer Berlin Heidelberg Encyclopedia of Earth Science,* 1238–1239.
8. Freeze, A.R., and Cherry, J.A. (1979). *Groundwater:* Prentice Hall.
9. Galloway, D., Jones, D.R., and Ingebritsen, S.E. (1999). Land subsidence in the United States. *United States Geological Survey Circular 1182.*
10. Galloway, W.E., Whiteaker, T.L., and Ganey-Curry, P. (2011). History of Cenozoic North American drainage basin evolution, sediment yield, and accumulation in the Gulf of Mexico basin. *Geosphere, 7*(4), 938–973.
11. Gilbert, G.K. (1890). Lake Bonneville. *United States Geological Survey.*
12. Gleick, P.H. (1993). *Water in crisis: A guide to the world's fresh water resources:* Oxford University Press.
13. Hadley, G. (1735). Concerning the cause of the general trade-winds. *Philosophical Transactions, 39*(436–444), 58–62.

14. Halvorson, S.F., and James Steenburgh, W. (1999). *Climatology of lake-effect snowstorms of the Great Salt Lake:* University of Utah.
15. Heath, R.C. (1983). Basic ground-water hydrology: *United States Geological Survey Water-Supply Paper 2220.*
16. Hobbs, W.H., and Fisk, H.N. (1947). Geological investigation of the alluvial valley of the lower Mississippi River. *JSTOR.*
17. Knudsen, T., Inkenbrandt, P., Lund, W., Lowe, M., and Bowman, S. (2014). Investigation of land subsidence and earth fissures in Cedar Valley, Iron County, Utah. *Utah Geological Survey Special Study 150.*
18. Lorenz, E.N. (1955). Available potential energy and the maintenance of the general circulation. *Tell'Us, 7*(2), 157–167.
19. Marston, R.A., Mills, J.D., Wrazien, D.R., Bassett, B., and Splinter, D.K. (2005). Effects of Jackson lake dam on the Snake River and its floodplain, Grand Teton National Park, Wyoming, USA. *Geomorphology, 71*(1–2), 79–98.
20. Maupin, M.A., Kenny, J.F., Hutson, S.S., Lovelace, J.K., Barber, N.L., and Linsey, K.S. (2014). Estimated use of water in the United States in 2010. *United States Geological Survey.*
21. Myers, W.B., and Hamilton, W. (1964). The Hebgen Lake, Montana, earthquake of August 17, 1959. *U.S. Geol. Surv. Prof. Pap., 435*, 51.
22. Oviatt, C.G. (2015). Chronology of Lake Bonneville, 30,000 to 10,000 yr B.P. *Quat. Sci. Rev., 110*, 166–171.
23. Powell, J.W. (1879). *Report on the lands of the arid region of the United States with a more detailed account of the land of Utah with maps:* Monograph.
24. Reed, J.C., Love, D., and Pierce, K. (2003). Creation of the Teton landscape: A geologic chronicle of Jackson Hole and the Teton range. Online, http://pubs.er.usgs.gov.
25. Reese, R.S. (2014). Review of aquifer storage and recovery in the Floridan aquifer system of Southern Florida. *United States Geological Survey.*
26. Schele, L., Miller, M.E., Kerr, J., Coe, M.D., and Sano, E.J. (1992). *The blood of kings: Dynasty and ritual in Maya art:* George Braziller Inc.
27. Seaber, P.R., Kapinos, F.P., and Knapp, G.L. (1987). Hydrologic unit maps. *United States Geological Survey.*
28. Solomon, S. (2011). *Water: The epic struggle for wealth, power, and civilization:* Harper Perennial.
29. Törnqvist, T.E., Wallace, D.J., Storms, J.E.A., Wallinga, J., Van Dam, R.L., Blaauw, M., Derksen, M.S., Klerks, C.J.W., Meijneken, C., and Snijders, E.M.A. (2008). Mississippi Delta subsidence primarily caused by compaction of Holocene strata. *Nat. Geosci., 1*(3), 173–176.
30. Turner, R.E., and Rabalais, N.N. (1991). Changes in Mississippi River water quality this century. *Bioscience, 41*(3), 140–147.
31. United States Geological Survey (1967). The Amazon: Measuring a mighty river. *United States Geological Survey O-245-247.*
32. United States Environmental Protection Agency (2014). Cyanobacteria/Cyanotoxins.
33. United States Geological Survey (2012). Snowmelt – The Water Cycle, from USGS Water-Science School.
34. Utah/Nevada Draft Snake Valley Agreement (2013).

Figure References

Figure 11.1: Example of a Roman aqueduct in Segovia, Spain. Bernard Gagnon. 2009. CC BY-SA 3.0. https://en.wikipedia.org/wiki/File:Aqueduct_of_Segovia_08.jpg

Figure 11.2: Chac mask in Mexico. Bernard DUPONT. 1995. CC BY-SA 2.0. https://commons.wikimedia.org/wiki/File:Chac_Mask_(21784027699).jpg

Figure 11.3: The water cycle. John Evans and Howard Periman, United States Geological Survey (USGS). 2013. Public domain. https://commons.wikimedia.org/wiki/File:Watercyclesummary.jpg

Figure 11.4: Map view of a drainage basin with main trunk streams and many tributaries with drainage divide in dashed red line. Zimbres. 2005. CC BY-SA 2.5. https://commons.wikimedia.org/wiki/File:Hydrographic_basin.svg

Figure 11.5: Oblique view of the drainage basin and divide of the Latorita River, Romania. Asybaris01. 2011. Public domain. https://commons.wikimedia.org/wiki/File:EN_Bazinul_hidrografic_al_Raului_Latorita,_Romania.jpg

Figure 11.6: Major drainage basins color-coded to match the related ocean. Citynoise. 2007. Public domain. https://commons.wikimedia.org/wiki/File:Ocean_drainage.png

Figure 11.7: Agricultural water use in the United States by state. USGS. 2018. Public domain. https://www.usgs.gov/media/images/map-us-state-showing-total-water-withdrawals-2015

Figure 11.8: Trends in water use by source. USGS. 2018. Public domain. https://www.usgs.gov/media/images/trends-population-and-freshwater-withdrawals-source-1950-2015-0

Figure 11.9: Distribution of precipitation in the United States. United States Department of the Interior. 2006. Public domain. https://commons.wikimedia.org/wiki/File:Average_precipitation_in_the_lower_48_states_of_the_USA.png

Figure 11.10: Thalweg of a river. In a river bend, the fastest moving water is on the outside of the bend, near the cut bank. Steven Earle. 2021. CC BY. Figure 8.1.1 from https://openeducationalberta.ca/practicalgeology/chapter/8-1-stream-erosion-and-deposition/#fig8.1.1

Figure 11.11: Various stream drainage patterns. Kindred Grey. 2022. CC BY-SA 3.0. Includes Rectangular by Zimbres, 2006 (CC BY-SA 2.5, https://commons.wikimedia.org/wiki/File:Rectangular.png). Dendritic by Zimbres, 2006 (CC BY-SA 2.5, https://en.wikipedia.org/wiki/

File:Dendritic.png). Trellis drainage pattern by Tshf aee, 2007 (CC BY-SA 3.0, https://en.wikipedia.org/wiki/File:Trellis_drainage_pattern.jpg). Radial by Zimbres, 2006 (CC BY-SA 2.5, https://commons.wikimedia.org/wiki/File:Radial.png). Irregular drainage pattern by Tshf aee, 2007 (CC BY-SA 3.0, https://en.wikipedia.org/wiki/File:Irregular_drainage_pattern.jpg).

Figure 11.12: A stream carries dissolved load, suspended load, and bedload. PSUEnviroDan. 2008. Public domain. https://en.wikipedia.org/wiki/File:Stream_Load.gif

Figure 11.13: Profile of stream channel at bankfull stage, flood stage, and during deposition of natural levee. Steven Earle. 2021. CC BY. Figure 8.1.4 from https://openeducationalberta.ca/practicalgeology/chapter/8-1-stream-erosion-and-deposition/#retfig8.1.3

Figure 11.14: Example of a longitudinal profile of a stream; Halfway Creek, Indiana. USGS. 2008. Public domain. https://commons.wikimedia.org/wiki/File:HalfwayCreek_fig02.jpg

Figure 11.15: The braided Waimakariri River in New Zealand. Greg O'Beirne. 2007. CC BY 2.5. https://commons.wikimedia.org/wiki/File:Waimakariri01_gobeirne.jpg

Figure 11.16: Air photo of the meandering river, Rio Cauto, Cuba. Not home~commonswiki. 2007. Public domain. https://commons.wikimedia.org/wiki/File:Rio-cauto-cuba.jpg

Figure 11.17: Point bar and cut bank on the Cirque de la Madeleine in France. Jean-Christophe BENOIST. 2007. CC BY 2.5. https://commons.wikimedia.org/wiki/File:CirqueMadeleine.jpg

Figure 11.18: Horseshoe Bend is an entrenched meander of the Colorado River in Glen Canyon National Recreation Area near Page, Arizona. Laura Neser. March 2022. CC BY-NC.

Figure 11.19: Panoramic view of incised meanders of the San Juan River at Gooseneck State Park, Utah. Michael Rissi. 2006. CC BY-SA 3.0. https://commons.wikimedia.org/wiki/File:GooseNeckStateParkPanorama.jpg

Figure 11.20: The Rincon is an abandoned meander loop on the entrenched Colorado River in Lake Powell. NASA's Earth Observatory. 2012. CC BY 2.0. https://commons.wikimedia.org/wiki/File:Lake_Powell_and_The_Rincon,_Utah_-_NASA_Earth_Observatory.jpg

Figure 11.21: Landsat image of Zambezi Flood Plain, Namibia. Jesse Allen and Robert Simmon via NASA. 2010. Public domain. https://commons.wikimedia.org/wiki/File:Zambezi_Flood_Plain,_Namibia_(EO-1).jpg

Figure 11.22: Meander nearing cutoff on the Nowitna River in Alaska. Oliver Kurmis. 2002. CC BY-SA 2.0 DE. https://commons.wikimedia.org/wiki/File:Nowitna_river.jpg

Figure 11.23: Alluvial fan in Iraq seen by NASA satellite. NASA. 2004. Public domain. https://commons.wikimedia.org/wiki/File:Alluvial_fan_in_Iran.jpg

Figure 11.24: Location of the Mississippi River drainage basin and Mississippi River Delta. Shannon1. 2016. CC BY-SA 4.0. https://commons.wikimedia.org/wiki/File:Mississippiriver-new-01.png

Figure 11.25: Delta in Quake Lake Montana. Staplegunther. 2007. CC BY-SA 3.0. https://commons.wikimedia.org/wiki/File:Quakelakemontana.jpg

Figure 11.26: Sundarban Delta in Bangladesh, a tide-dominated delta of the Ganges River. NordNordWest. 2015. CC BY-SA 3.0 DE. https://commons.wikimedia.org/wiki/File:Bangladesh_adm_location_map.svg

Figure 11.27: Nile Delta showing its classic "delta" shape. NASA. 2018. Public domain. https://www.earthdata.nasa.gov/worldview/worldview-image-archive/the-nile-delta-from-space

Figure 11.28: Map of Lake Bonneville, showing the outline of the Bonneville shoreline, the highest level of the lake. Staplini. 2019. CC BY-SA 4.0. https://commons.wikimedia.org/wiki/File:Map_of_Lake_Bonneville.jpg

Figure 11.29: Deltaic deposits of Lake Bonneville near Logan, Utah; wave-cut terraces can be seen on the mountain slope. Staplini. 2019. CC BY-SA 4.0. https://commons.wikimedia.org/wiki/File:Image_of_Lake_Bonneville_shorelines.png

Figure 11.30: Terraces along the Snake River, Wyoming. Fredlyfish4. 2008. CC BY-SA 3.0. https://commons.wikimedia.org/wiki/File:Snake_River_Overlook.jpg

Figure 11.31: Zone of saturation. USGS. 2011. Public domain. https://commons.wikimedia.org/wiki/File:Vadose_zone.gif

Figure 11.32: An aquifer cross section. Hans Hillewaert. 2007. CC BY-SA 3.0. https://commons.wikimedia.org/wiki/File:Aquifer_en.svg

Figure 11.33: Pipe showing apparatus that would demonstrate Darcy's law. Vectorised by Sushant savla from the work by Peter Kapitola. 2018. CC BY-SA 2.5. https://en.m.wikipedia.org/wiki/File:Darcy%27s_Law.svg

Figure 11.34: Cones of depression. USGS. 2018. Public domain. https://www.usgs.gov/media/images/cone-depression-pumping-a-well-can-cause-water-level-lowering

Figure 11.35: Different ways an aquifer can be recharged. USGS. Unknown date. Public domain. https://www.usgs.gov/media/images/groundwater-can-be-recharged-naturally-and-artificially

Figure 11.36: Evidence of land subsidence from pumping of groundwater shown by dates on a pole. Dr. Joseph F. Poland via USGS. 1977. Public domain. https://www.usgs.gov/media/images/location-maximum-land-subsidence-us-levels-1925-and-1977

Figure 11.37: Acid mine drainage continues today from a coal mine that was shut down in 1935 near Blacksburg, Virginia, along the Coal Mining Heritage Loop Trail. Laura Neser. September 2021. CC BY-NC.

Figure 11.38: Steep karst towers in China left as remnants of limestone dissolving away by acidic rain and groundwater. chensiyuan. 2011. CC BY-SA 4.0. https://commons.wikimedia.org/wiki/File:1_li_jiang_guilin_yangshuo_2011.jpg

Figure 11.39: Sinkholes of the McCauley Sink in Northern Arizona, produced by collapse of Kaibab Limestone into caverns caused by the solution of underlying salt deposits. Google Earth. Image retrieved 2022 by Kindred Grey. Public domain.

Figure 11.40: This sinkhole caused by the collapse of surface into a underground cavern appeared in the front yard of this home in Florida. Ann Tihansky via USGS. 2010. Public domain. https://www.usgs.gov/media/images/sinkholes-west-central-florida-freeze-event-2010-2

Figure 11.41: Mammoth hot springs, Yellowstone National Park. Brocken Inaglory. 2008. CC BY-SA 3.0. https://en.wikipedia.org/wiki/File:Dead_trees_at_Mammoth_Hot_Springs.jpg

Figure 11.42: Varieties of speleothems. Dave Bunnell/Under Earth Images. 2006. CC BY-SA 2.5. https://commons.wikimedia.org/wiki/File:Labeled_speleothems.jpg

Figure 11.43: This stream disappears into a subterranean cavern system to re-emerge a few hundred yards downstream. Martyn Gorman. 2007. CC BY-SA 2.0. https://www.geograph.org.uk/photo/471804

Figure Descriptions

Figure 11.1: Stone wall made up of two levels of thin arches

Figure 11.2: Mayan stone figure with a long elephant-like nose representing a water deity.

Figure 11.3: A diagram depicting the continuous movement and transformation of water on Earth. The diagram shows a circular process with labeled arrows and key components: starting with the evaporation process, an arrow indicates water vapor rising from bodies of water into the atmosphere; condensation is represented by arrows showing the transformation of water vapor into clouds; precipitation is denoted with arrows indicating the falling of rain or snow from clouds back to the Earth's surface; surface runoff and infiltration are demonstrated by arrows showing water flowing over the land or seeping into the ground; arrows depicting the processes of plant uptake and transpiration are shown where water is absorbed by plants and released into the atmosphere through their leaves.

Figure 11.4: Schematic map view of a drainage basin: the main trunk stream has many branching tributaries and the drainage divide encircles all of the streams as a dashed red line.

Figure 11.5: Oblique relief map of the Latorita River, a tributary of the Lotru River; North is toward the right of the map. The Latorita drainage basin is colored green and outlined in red; it encircles the main river as well as the tributary streams and surrounding land leading to the river.

Figure 11.6: World map with major drainage basins color-coded according to which ocean they lead to; the drainage basins leading to the Pacific Ocean are colored purple and cover western North America, a sliver along western South America, eastern and southeastern Asia, and northeastern and eastern Australia; the drainage basins leading to the Atlantic Ocean are colored green and cover eastern North America, central and eastern South America, western Europe, and western Africa; the drainage basins leading to the American Mediterranean Sea are colored olive green and cover central and southern North America and a tiny northern part of South America; the drainage basins leading to the Arctic Ocean are colored teal and cover northern North America, northern Europe, and northern Asia; the drainage basins leading to the Indian Ocean are colored pink and cover eastern Africa, southern Asia, and central and western Australia; the drainage basins leading to the Eurafrican Mediterranean Sea are colored blue and cover southern Europe and northern and central Africa; the drainage basins leading to the Southern Ocean are colored tan and covers all of Antarctica; and endorheic basins are colored gray and they are located in western and southern North America, southern South America, northern and central Africa, southern Africa, southern Asia, and central Australia.

Figure 11.7: Map of the United States with water withdrawals per state in different shades of blue; low water withdrawals are lighter shades of blue while higher water withdrawals are darker shades of blue; California and Idaho have the highest water withdrawals; Oregon, Montana, Colorado, Nebraska, Texas, and Arkansas also have high water withdrawals; Washington, Wyoming, Nevada, Utah, Arizona, New Mexico, Kansas, Missouri, Mississippi, and Florida have lower withdrawals, and the rest of the 50 states have the lowest water withdrawals.

Figure 11.8: Bar graph titled Trends in population and freshwater withdrawals by source, 1950-2010: the horizontal axis has years in 5-year intervals on the from 1950 to 2010; there are two vertical axes: the left vertical axis is labeled Withdrawals, in billion gallons per day and increases from 0 to 400, and the right vertical axis is labeled Population, in millions and increases from 0 to 350. Population increases over time while total water use increases at the beginning, peaks at 1980, and stays relatively steady until a decrease in 2010.

Figure 11.9: Map of the United States showing distribution of precipitation in the United States. The western half of the United States is much drier than the eastern half of the United States with the exception of the Pacific northwest which has abundant precipitation.

Figure 11.10: tream velocity is higher on the outside bend and the surface which is farthest from the friction of the stream bed. The inside of the bend is a shorter distance than the outside. Longer arrows indicate faster velocity.
In a river bend, the fastest moving particles are on the outside of the bend, near the cut bank.

Figure 11.11: Five schematic diagrams of stream drainage patterns: rectangular drainage shows streams curving at nearly right angles; dendritic drainage shows streams resembling tree branches; trellis drainage shows parallel ridge lines with streams between ridge lines; radial drainage shows streams radiating outward from a central high point; and deranged drainage shows curvy, erratic streams that appear and disappear.

Figure 11.12: 2D diagram with a brown stream bed at the bottom and a light blue stream above it; particles that move along the stream bed are labeled Bed load, particles that are carried in the stream without touching the stream bed are labeled Suspended load, and there is a label Dissolved load to show material dissolved in the water.

Figure 11.13: Profile of a stream channel at three stages: the Bank-full stage shows the water filling the channel without overflowing, the Flood stage shows the river overfilling the channel and spreading outward with sediments deposited on the top of the river banks, and deposition of natural levee shows the river within the channel due to natural levels forming that raised the stream banks higher.

Figure 11.14: Longitudinal profile of a creek in Indiana with altitude along the y-axis and river miles from mouth on the x-axis: it shows steep gradient in its headwaters the farthest away from its mouth and shallower gradients toward its mouth.

Figure 11.15: Many channels that braid back and forth among each other; between channels are tan sediment deposits.

Figure 11.16: Sinuous tan river running through roughly flat green terrain.

Figure 11.17: U-shaped river bend in France with sandy deposition at the inside of the bend labeled Point Bar and erosion on the outside of the bend labeled Cut Bank; there is lush green vegetation around the river and cliffs in the background.

Figure 11.18: Steep canyon with a river in a U-shape at the base; a man in a blue jacket is standing on top of the cliff outlook.

Figure 11.19: Panoramic view of an S-shaped meandering river that flows at the base of tall canyons.

Figure 11.20: Astronaut-taken photograph of two long branches of Lake Powell, which extends across southeastern Utah and northeastern Arizona. The serpentine surface of the reservoir is highlighted by gray regions of sunglint and follows the incised course of the canyon, surrounded by a tan landscape. The two branches of the lake are connected by a bend to the southwest which is cut off at the bottom of the photo.

Figure 11.21: Satellite image of a large flood plain; the main river branches into two on the right-hand side of the photo, then spreads out toward the left into numerous smaller meandering streams; fertile green land covers the wide area of branching streams.

Figure 11.22: River with extreme S-shaped curves surrounded by flat green landscape; two curves of the river nearly touch each other.

Figure 11.23: Satellite image of an alluvial fan in a tan desert landscape; a stream emerges from a canyon and creates a fan-shaped deposit that has rectangular green patches scattered at the edges of the deposit.

Figure 11.24: Map of central North America showing the main branch of the Mississippi River and the many tributaries that contribute to the river.

Figure 11.25: A lake surrounded by forest-covered mountain slopes.

Figure 11.26: Map of the Ganges River leading into a delta; there are also many smaller parallel streams also leading into the delta.

Figure 11.27: Satellite view of a land-sea boundary with a green fan-shaped delta between the edge of tan land and deep blue ocean, widening toward the ocean.

Figure 11.28: Map of Lake Bonneville in northwestern Utah; the modern Great Salt Lake is outlined in the northern part of Lake Bonneville and is much smaller than Lake Bonneville.

Figure 11.29: Satellite view of tan desert landscape with slopes on the left leading down to a flat white playa labeled Pilot Valley Playa on the right; the slopes are labeled Pilot Range; near the bottom of the image at the base of the slopes is the label Bonneville shoreline; near the top of the image at the base of the slopes are the labels offshore sediments of Lake Bonneville and Provo shoreline; leading from the base of the slopes to the playa is the label multiple unnamed shorelines on alluvial fans on the eastern piedmont of the Pilot Range with another label Stansbury shoreline.

Figure 11.30: Landscape with a winding river in the foreground and steep rocky mountains in the background. Three different levels of flat surfaces are visible in the foreground.

Figure 11.31: Cross sectional diagram that shows the subsurface below a vegetated ground surface that slopes downward toward the left; the upper part of the ground is labeled Vadose Zone and the part below that zone is labeled Zone of Saturation. The boundary between the zones is labeled Water Table and there is a small zone just above the Water Table labeled Capillary Fringe. The flow of groundwater is toward the left.

Figure 11.32: Cross section of aquifers: there are two aquifers with one aquitard between them, surrounded by the bedrock aquiclude. The lower aquifer is labeled Confined aquifer and the upper aquifer is labeled Unconfined aquifer; the boundary at the top of the Unconfined aquifer is labeled Water table and the ground above is labeled Unsaturated zone. The direction of groundwater flow is shown with arrows which flow toward the surface where a stream channel is located; trees at the surface are labeled Transpiration by vegetation.

Figure 11.33: Schematic diagram of a horizontal pipe: the pipe is a porous medium and the length of the pipe is labeled L. A cross sectional slice of the pipe is labeled A. The left end of the pipe is labeled a and the right end of the pipe is labeled b; a smaller pipe enters and exits the main pipe with an arrow pointing toward the right labeled Q.

Figure 11.34: Cross sectional diagram that shows the subsurface around where a water well is located. The shape of the water table around the well is cone- shaped, where groundwater level has the greatest drawdown near the well.

Figure 11.35: Cross sectional diagram that shows the the different ways an aquifer can be recharged: on the left side of the diagram there is a storm cloud releasing precipitation onto the ground surface with some water becoming runoff and some infiltrating and recharging the aquifer; near the center of the diagram there is an artificial recharge well that injects water directly into the aquifer; on the right side of the diagram there is a stream at the surface that naturally recharges the aquifer.

Figure 11.36: Man standing next to pole with signs showing approximate altitude of land surface in 1925 (highest sign on pole), 1955 (middle sign on pole), and 1977 (at ground level).

Figure 11.37: Orange-colored small stream flowing from left to right, emerging from a hole in a squared grey rock on the left; with small sticks and vegetation throughout the area.

Figure 11.38: River flowing across landscape of flat land with steep rock towers rising from the land.

Figure 11.39: Light tan landscape with numerous bowl-shaped sinkholes.

Figure 11.40: Dirt-lined sinkhole in front of a gray house; the sinkhole is cordoned off with caution tape.

Figure 11.41: White and brown natural steps with steam rising near the back; the brown steps have a coating of liquid and organic material while the white steps are dry and chalky in appearance. There are a few dead tree trunks in the springs.

Figure 11.42: Numerous cave formations hanging from the top and protruding from the base of a cave. Smooth, bulbous formations protruding from the base are labeled Flowstone and spires that rise from the base are labeled Stalagmites. Spires that hang from the ceiling are labeled Stalactites, small tubes hanging are labeled Straws, and ribbon-like formations hanging from the ceiling are labeled Drapery. One formation stretches from the ceiling of the cave to the base of the cave, labeled Column.

Figure 11.43: A stream disappears into gravel at the foreground of the photo.

12. EARTH'S COASTLINES AND OCEANS

Learning Objectives

By the end of this chapter, students should be able to:

- Describe how waves occur, move, and carry energy.
- Describe shoreline features and zones.
- Describe wave refraction and its contribution to longshore currents and longshore drift.
- Distinguish between submergent and emergent coasts, and describe coastal features associated with each.
- Describe the pattern of the main ocean currents, and explain the different factors involved in surface currents and deep ocean currents.
- Explain how ocean tides occur, and distinguish among diurnal, semidiurnal, and mixed tide patterns.
- Summarize ocean water properties and the reasons they may vary.
- Summarize the major ocean floor properties along with the methods scientists use to observe them.

Our planet is dominated by oceans, earning it the nickname "the blue planet." Approximately 71% of Earth's surface is covered in oceans, including marginal seas. The remaining 29% is all the land we know: continents and islands. **Oceanography** is an interdisciplinary study of all aspects of the world ocean. Oceanographers generally recognize five major ocean basins: the Pacific, Atlantic, Indian, Arctic, and Southern Ocean. Coastlines are the interfaces between land and ocean and, as such, are the longest visible boundaries on Earth. To understand the processes that occur at these boundaries, it is important to first understand wave energy.

12.1 Waves and Wave Processes

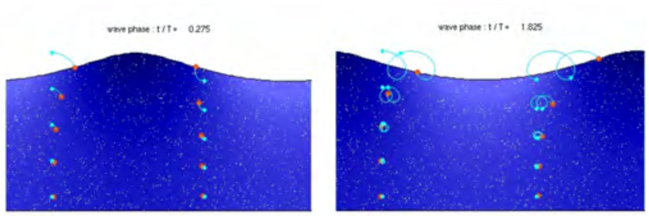

Figure 12.1: Particle motion within a wind-blown wave. Figure description available at the end of the chapter.

Wind blowing over the surface of water transfers energy to the water through friction. The energy transferred from wind to water causes waves to form. Waves move as individual oscillating particles of water. As the wave crest passes, the water is moving forward. As the **wave trough** passes, the water is moving backward. To see wave movement in action, watch a cork or any floating object as a wave passes.

There are several important terms to understand about the operation of waves. The **wave crest** is the highest point of the wave. The trough is the lowest point of the wave. **Wave height** is the vertical distance from the trough to the crest and is determined by wave energy. Wave amplitude is half the wave height, or the distance from either the crest or trough to the still water line. Wavelength is the horizontal distance between consecutive wave crests. **Wave velocity** is the speed at which a wave crest moves forward and is related to the wave's energy. **Wave period** is the time interval it takes for adjacent wave crests to pass a given point.

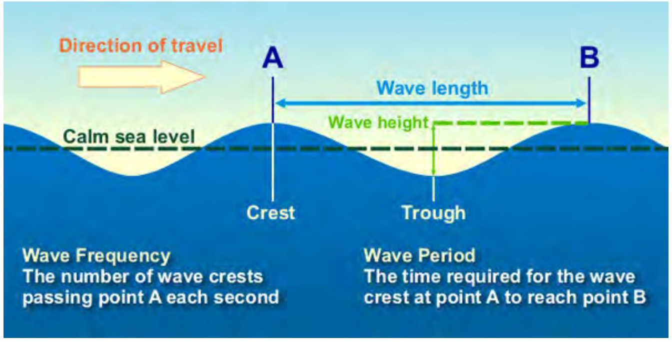

Figure 12.2: Aspects of water waves, labeled. Figure description available at the end of the chapter.

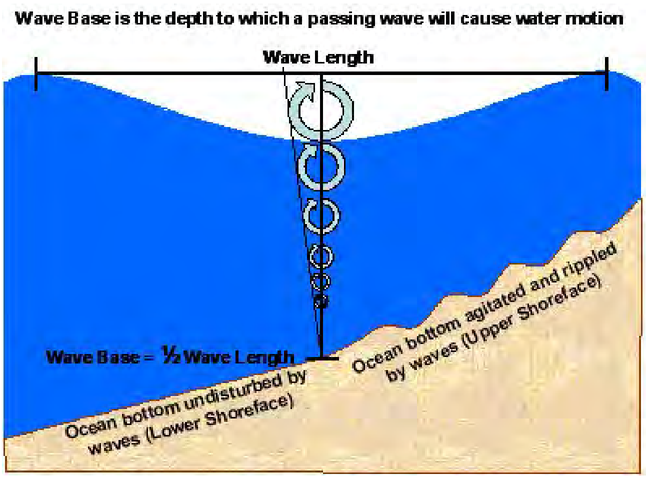

Figure 12.3: Diagram describing wavebase. Figure description available at the end of the chapter.

The circular motion of water particles diminishes with depth and is negligible at about one half-wavelength, an important dimension to remember in connection with waves. Wave base is the vertical depth at which water ceases to be disturbed by waves. In water shallower than the wave base, waves will disturb the bottom and ripple shore sand. Wave base is measured at a depth of about one half-wavelength, where the water particles' circular motion diminishes to zero. If waves approaching a beach have crests with intervals of about 6 m (~20 ft), this wave motion disturbs water to about 3 m (~10 ft) deep. This motion is known as **fair-weather wave base**. In strong storms such as hurricanes, both wavelength and wave base increase dramatically to a depth known as the **storm wave base**, which is approximately 91 m (~300 ft).

Waves are generated by wind blowing across the ocean surface. The amount of energy imparted to the water depends on wind velocity and the distance across which the wind is blowing. This distance is called **fetch**. Waves striking a shore are typically generated by storms hundreds of miles from the coast and have been traveling across the ocean for days.

Winds blowing in a relatively constant direction generate waves moving in that direction. Such a group of approximately parallel waves traveling together is called a **wave train**. A wave train coming from one fetch can produce various wavelengths. Longer wavelengths travel at a faster velocity than shorter wavelengths, so they arrive first at a distant shore. Thus, there is a wavelength-sorting process that takes place during the wave train's travel. This sorting process is called wave dispersion.

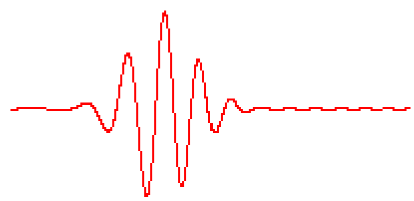

Figure 12.4: Wave train moving with dispersion. Figure description available at the end of the chapter.

A rogue wave is an unusual and rarer type of wave that is large, unexpected, and dangerous. Rogue, freak, or killer waves have been part of marine folklore for centuries but have only been accepted as real by scientists over the past few decades.

Figure 12.5: A rogue wave estimated at 18.3 meters (60 feet) in the Gulf Stream off of Charleston, South Carolina. At the time, surface winds were light at 15 knots. The wave was moving away from the ship after crashing into it moments before this photo was captured. Figure description available at the end of the chapter.

Known as extreme storm waves by scientists, **rogues** are waves that are more than twice the size of surrounding waves, are very unpredictable, and often come unexpectedly from directions other than prevailing wind and waves. Most reports of extreme storm waves say they look like "walls of water." They are often steep-sided, with unusually deep troughs. Since these waves are uncommon, measurement and analysis of this phenomenon is extremely rare. Exactly how and when rogue waves form is still under investigation, but there are several known causes, including constructive interference and focusing of wave energy.

Extreme waves often form because swells travel across the ocean at different speeds and directions. As these swells pass through one another, their crests, troughs, and lengths sometimes coincide and reinforce each other. This process can form unusually large, towering waves that quickly disappear, a type of constructive interference. If the swells are travelling in the same direction, these mountainous waves may last for several minutes before subsiding.

When waves formed by a storm develop in a water current against the normal wave direction, an interaction can take place that results in a shortening of the wave frequency, focusing the wave energy. This can cause the waves to dynamically join together, forming very big rogue waves. The currents where these are sometimes seen are the Gulf Stream and the Agulhas current. Extreme waves developed in this fashion tend to be longer lived.

12.1.1 Behavior of Waves Approaching Shore

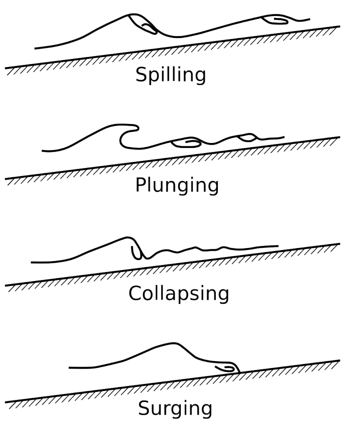

Figure 12.6: Types of breakers. Figure description available at the end of the chapter.

On the open sea, waves generally appear choppy because wave trains from many directions interact with each other, a process called wave interference. Constructive interference occurs where crests align with other crests. The aligned wave height is the sum of the individual wave heights, a process referred to as wave amplification. Constructive interference also produces hollows where troughs align with other troughs. Destructive interference occurs where crests align with troughs and cancel each other out. As waves approach shore and begin to make frictional contact with the seafloor at a depth of about one half-wavelength or less, they begin to slow down. However, the energy carried by the wave remains the same, so the waves build up higher. Remember that water moves in a circular motion as a wave passes, and each circle is fed from the trough in front of the advancing wave. As the wave encounters shallower water at the shore, there is eventually insufficient water in the trough in front of the wave to supply a complete circle, so the crest pours over, creating a breaker.

Figure 12.7: All waves, including tsunamis, slow down as they reach shallow water. This causes the wave to increase in height. Figure description available at the end of the chapter.

A special type of wave is called a tsunami, sometimes incorrectly called a tidal wave. Tsunamis are generated by energetic events affecting the seafloor, such as earthquakes, submarine landslides, and volcanic eruptions (see Chapters 4 and 9). During earthquakes, for example, tsunamis can be produced when the moving crustal rocks below the sea abruptly elevate a portion of the seafloor. Water is suddenly lifted, creating a bulge at the surface and a wave train spreads out in all directions, traveling at tremendous speeds—over 322 kph (200 mph)—and carrying enormous energy. Tsunamis may pass unnoticed in the open ocean because they move so fast, the wavelength is very long, and the wave height is very low. But, as the wave train approaches shore and each wave begins to interact with the shallow seafloor, friction increases and the wave slows down. Still carrying its enormous energy, wave height builds up, and the wave strikes the shore as a wall of water that can be over 30 m (~100 ft) high. The massive wave, called a tsunami runup, may sweep inland well beyond the beach, destroying structures far inland. Tsunamis can deliver a catastrophic blow to people at the beach. As the trough water in front of the tsunami wave is drawn back, the seafloor is exposed. Curious and unsuspecting people on the beach may run out to see exposed offshore sea life only to be overwhelmed when the breaking crest hits.

Take this quiz to check your comprehension of this section.

Access the quiz for Section 12.1 by scanning the QR code.

12.2 Shoreline Features

Coastlines are dynamic, high energy, and geologically complicated places where many different erosional and depositional features exist (see Chapter 5). They include all parts of the land-sea boundary directly affected by the sea, including land far above high tide and seafloor well below normal wave base. But the shoreline itself is the direct interface between water and land that shifts with the tides. This shifting interface at the shoreline is called the littoral zone. The combination of waves, currents, climate, coastal morphology, and gravity, acts on this land-sea boundary to create shoreline features.

12.2.1 Shoreline Zones

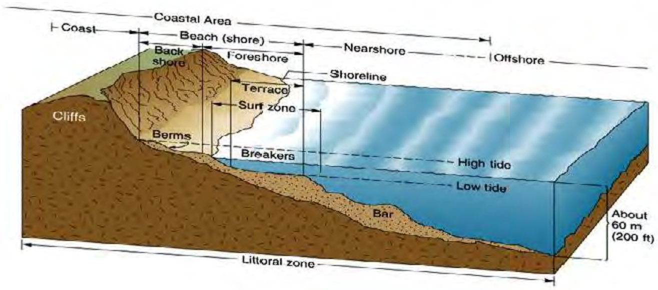

Figure 12.8: Diagram of zones of the shoreline. Figure description available at the end of the chapter.

Shorelines are divided into five primary zones—offshore, nearshore, surf, foreshore, and backshore. The **offshore** zone is below water, but it is still geologically active due to flows of **turbidity currents** that cascade over the continental slope and accumulate in the continental rise. The **nearshore** zone is the area of the shore affected by the waves where water depth is one half-wavelength or less. The width of this zone depends on the maximum wavelength of the approaching wave train and the slope of the seafloor. The nearshore zone includes the **shoreface**, which is where sand is disturbed and deposited. The shoreface is divided into upper and lower shoreface. Upper shoreface is affected by everyday wave action and consists of finely laminated and cross-bedded sand. The lower shoreface is the only area moved by storm waves and consists of hummocky cross-stratified sand. The **surf zone** is where the waves break.

The **foreshore** zone overlaps the surf zone and is periodically wet and dry due to waves and tides. The foreshore zone is where planer-laminated, well-sorted sand accumulates. The **beach face** is the part of the foreshore zone where the breaking waves swash up and the backwash flows back down. Low ridges above the beach face in the foreshore zone are called **berms**. During the summer in North America, the part of the beach where people spread their towels and umbrellas is the **summer berm**. Wave energy is typically lower in the summer, which allows sand to pile onto the beach. Behind the summer berm is a low ridge of sand called the **winter berm**. In winter, higher storm energy moves the summer berm sand off the beach and piles it in the nearshore zone. The next year, that sand is replaced on the beach and moved back onto the summer berm. The **backshore** zone is the area always above sea level in normal conditions. In the backshore zone, onshore winds may blow sand behind the beach and the berms, creating dunes.

12.2.2 Refraction, Longshore Currents, and Longshore Drift

As waves enter shallower water less than one half-wavelength depth, they slow down. Waves usually approach the shoreline at an angle, with the end of the waves nearest the beach slowing down first. This causes the wave crests to bend in a process called wave refraction. From the beach face, it looks like waves are approaching the beach straight on, parallel to the beach. However, as refracted waves actually approach the shoreline at a slight angle, they create a slight difference between the swash as it moves up the beach face at a slight angle and the backwash as it flows straight back down under gravity. This slight angle between swash and backwash along the beach causes beach sand to move down the beach in a sawtooth fashion referred to as beach drift. Parallel to the beach is an ocean current called the **longshore current**. Waves stir up sand in the surf zone and move it along the shore. **Longshore drift** along both the west and east coasts of North America moves sand north to south on average.

Longshore currents can carry longshore drift down a coast until it reaches a bay or inlet where it will deposit sand in the quieter water (see Chapter 11). Here, a **spit** can form. As the spit grows, it may extend across the mouth of the bay, forming a barrier called a **baymouth bar**. Where bays and inlets serve as boat anchorage, spits and baymouth bars are a severe inconvenience. Often, inconvenienced communities create methods to keep their bays and harbors open.

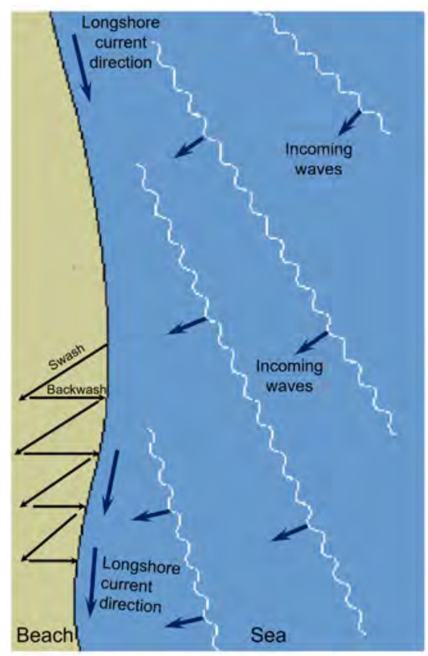

Figure 12.9: Longshore drift. Figure description available at the end of the chapter.

One way to keep a harbor open is to build a **jetty**, a long concrete or stone barrier constructed to deflect the sand away from a harbor mouth or other ocean waterway. If the jetty does not deflect the sand far enough out, sand may continue to flow along the shore, forming a spit around the end of the jetty. A more expensive but effective method to keep a bay mouth open is to dredge the sand from the growing spit, put it on barges, and deliver it back to the drift downstream of the harbor mouth. An even more expensive but more effective option is to install large pumps and pipes to draw in the sand upstream of the harbor, pump it through pipes, and discharge it back into the drift downstream of the harbor mouth. Because natural processes work continuously, human efforts to mitigate inconvenient spits and baymouth bars require ongoing modifications. For example, the community of Santa Barbara, California, tried several methods to keep their harbor open before settling on pumps and piping.

Figure 12.10: Jetties near Carlsbad, California. Note that the left jetty is loaded with sand, while the right jetty is lacking sand. This is due to the longshore drift going left to right. Figure description available at the end of the chapter.

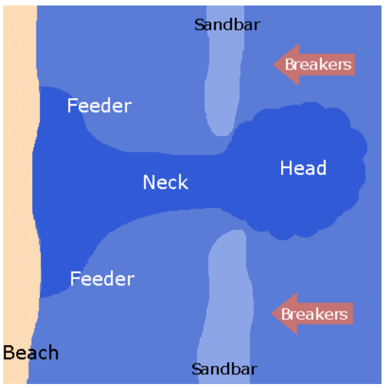

Figure 12.11: Animation of rip currents. Figure description available at the end of the chapter.

Rip currents are another coastal phenomenon related to longshore currents. Rip currents occur in the nearshore seafloor when wave trains come *straight* onto the shoreline. In areas where wave trains push water directly toward the beach face or where the shape of the nearshore seafloor refracts waves toward a specific point on the beach, the water piles up on the shore. But this water must find an outlet back to the sea. The outlet is relatively narrow, and rip currents carry the water directly away from the beach. Swimmers caught in rip currents are carried out to sea. Swimming back to shore directly against the strong current is fruitless. A solution for good swimmers is to ride out the current to where it dissipates, swim around it, and return to the beach. Another solution for average swimmers is to swim parallel to the beach until out of the current, then to return to the beach. Where rip currents are known to exist, warning signs are often posted. The best solution is to understand the nature of rip currents, have a plan before entering the water, or watch the signs and avoid them all together.

Figure 12.12: Rip currents sign at Canaveral National Seashore, Florida. Figure description available at the end of the chapter.

Like rip currents, undertow is a current that moves away from the shore. However, unlike rip currents, undertow occurs underneath the approaching waves and is strongest in the surf zone, where waves are high and water is shallow. Undertow is another return flow for water transported onshore by waves.

12.2.3 Emergent and Submergent Coasts

Figure 12.13: Island Arch, a sea arch in Victoria, Australia. Figure description available at the end of the chapter.

Emergent coasts occur where sea levels fall relative to land level. **Submergent coasts** occur where sea levels rise relative to land level. Tectonic shifts and sea-level changes cause the long-term rise and fall of sea level relative to land. Some features associated with emergent coasts include high cliffs, headlands, exposed bedrock, steep slopes, rocky shores, arches, stacks, tombolos, wave-cut platforms, and wave notches.

In emergent coasts, wave energy, wind, and gravity erode the coastline. The erosional features are elevated relative to the wave zone. Sea cliffs are persistent features formed by waves cutting away at their base and higher rocks calving off by mass wasting. Refracted waves that attack bedrock at the base of headlands may erode or carve out a sea arch, which can extend below sea level in a sea cave. When a sea arch collapses, it leaves one or more rock columns called stacks.

Figure 12.15: Wave notches carved by Lake Bonneville, Antelope Island, Utah. Figure description available at the end of the chapter.

Figure 12.14: This tombolo known as Angel Road connects the stack of Shodo Island, Japan. Figure description available at the end of the chapter.

A **stack** or nearshore island creates a quiet water zone behind it. Sand moving in the longshore drift accumulates in this quiet zone, forming a **tombolo**: a sand strip that connects the island or stack to the shoreline. Where sand supply is low, wave energy may erode a **wave-cut platform** across the surf zone, exposed as bare rock with tidal pools at low tide. This benchlike terrace extends to the cliff's base. When wave energy cuts into the base of a sea cliff, it creates a **wave notch**.

Submergent coasts occur where sea levels rise relative to land. This may be due to tectonic subsidence—when the Earth's crust sinks—or when sea levels rise due to glacier melt. Features associated with submergent coasts include flooded river mouths, fjords, barrier islands, lagoons, estuaries, bays, tidal flats, and tidal currents. In submergent coastlines, river mouths are flooded by the rising water, as is the case with the Chesapeake Bay. **Fjords** are glacial valleys flooded by post-ice age sea-level rise (see Chapter 14). Barrier islands are elongated bodies of sand that formed from old beach sands that used to parallel the shoreline. Often, lagoons lie behind barrier islands. Barrier island formation is controversial; some scientists believe that they formed when ice sheets melted after the last ice age, raising sea levels. Another hypothesis is that barrier islands formed from spits and bars accumulating far offshore.

Figure 12.16: Landsat image of Chesapeake Bay, Eastern United States. Note the barrier islands parallel to the coastline. Figure description available at the end of the chapter.

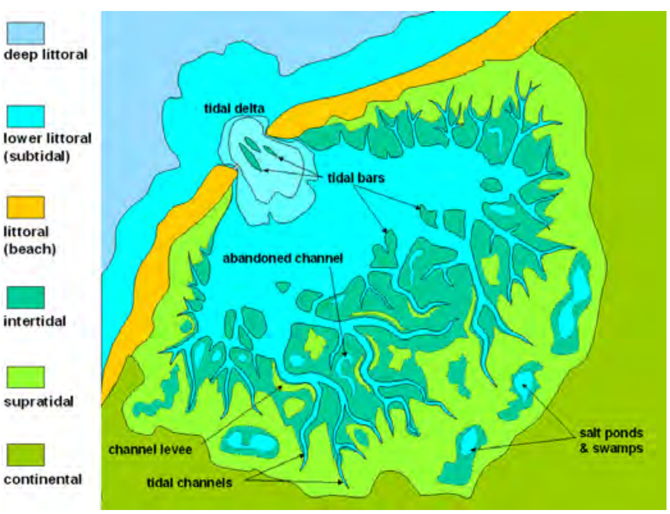

Figure 12.17: General diagram of a tidal flat and associated features. Figure description available at the end of the chapter.

Tidal flats, or mudflats, form where tides alternately flood and expose low areas along the coast. Tidal currents create combinations of symmetrical and asymmetrical ripple marks on mudflats, and drying mud creates mud cracks. In the central Wasatch Mountains of Utah, ancient tidal flat deposits are exposed in the Precambrian strata of the Big Cottonwood Formation. These ancient deposits provide an example of applying Hutton's principle of uniformitarianism (see Chapter 1). Sedimentary structures common on modern tidal flats indicate that these ancient deposits were formed in a similar environment; there were shorelines, tides, and shoreline processes acting at that time, yet the ancient age indicates that there were no land plants to hold products of mechanical weathering in place (see Chapter 5), so erosion rates would have been different.

Geologically, tidal flats are broken into three different sections: barren zones, marshes, and salt pans. These zones may be present or absent in each individual tidal flat. Barren zones are areas with strong flowing water and coarser sediment, with ripple marks and cross-bedding common. Marshes are vegetated with sand and mud. Salt pans or flats, less often submerged than the other zones, are the finest-grained parts of tidal flats, with silty sediment and mud cracks (see Chapter 5).

Lagoons are locations where spits, barrier islands, or other features partially cut off a body of water from the ocean. Estuaries are a vegetated type of lagoon where fresh water flows into the area, making the water **brackish**—a salinity between salt and fresh water. However, terms like lagoon, **estuary**, and even bay are often loosely used in place of one another. Lagoons and estuaries are certainly transitional between land and water environments where littoral (shallow shorelines), lacustrine (lakes or lagoons), and fluvial rivers or currents can overlap. For more information on lagoons and estuaries, see Chapter 5.

Figure 12.18: Kara-Bogaz Gol lagoon, Turkmenistan. Figure description available at the end of the chapter.

12.2.4 Human Impact on Coastal Beaches

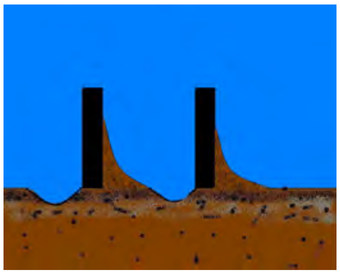

Figure 12.19: Bird's-eye view of groins gathering sediment from longshore drift (current flowing from right to left). Figure description available at the end of the chapter.

Humans impact coastal beaches when they build homes, condominiums, hotels, businesses, and harbors—and then again when they try to manage the natural processes of erosion. Waves, currents, longshore drift, and dams at river mouths deplete sand from expensive beachfront property and expose once calm harbors to high-wave energy. To protect their investment, keep sand on their beach, and maintain calm harbors, cities and landowners find ways to mitigate the damage by building jetties, groins, dams, and breakwaters.

Jetties are large manmade piles of boulders or concrete barriers built at river mouths and harbors. A jetty is designed to divert the current or tide, to keep a channel to the ocean open, and to protect a harbor or beach from wave action. Groins are similar but smaller than jetties. **Groins** are fences of wire, wood, or concrete built across the beach perpendicular to the shoreline and downstream of a property. Unlike jetties, groins are used to preserve sand on a beach rather than to divert it. Sand erodes on the downstream side of the groin and collects against the upstream side. Every groin on one property thus creates a need for another one on the property downstream. A series of groins along a beach develops a scalloped appearance along the shoreline.

Figure 12.20: Groin system on a coast in Virginia. Figure description available at the end of the chapter.

Inland streams and rivers flow to the ocean, carrying sand to the longshore current, which distributes it to beaches. When dams are built, they trap sand and keep sediment from reaching beaches. To replenish beaches, sand may be hauled in from other areas by trucks or barges and then dumped on the depleted beach. Unfortunately, this can disrupt the ecosystem that exists along the shoreline by exposing native creatures to foreign ecosystems and microorganisms and by introducing foreign objects to humans. For example, visitors to one replenished East Coast beach found munitions and metal shards in the sand, which had been dredged from abandoned military test ranges.

Figure 12.21: A tombolo formed behind the breakwater at Venice, CA. Figure description available at the end of the chapter.

An approach to protect harbors and moorings from high-energy wave action is to build a **breakwater**—an offshore structure against which the waves break, leaving calmer waters behind it. Unfortunately, breakwaters keep waves from reaching the beach and stop sand moving with longshore drift. When longshore drift is interrupted, sand is deposited in quieter water, and the shoreline builds out, forming a tombolo behind the breakwater. The tombolo eventually fills in the area behind the breakwater with sand. When the city of Venice, California, built a breakwater to create a quiet water harbor, longshore drift created a tombolo behind the breakwater, as seen in the image. The tombolo now acts as a large groin in the beach drift.

12.2.5 Submarine Canyons

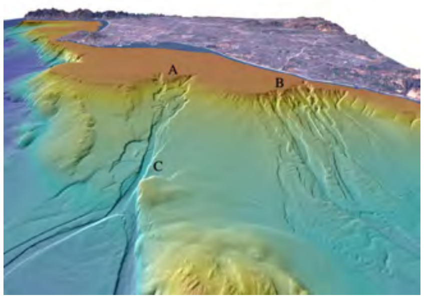

Figure 12.22: Submarine canyons off of Los Angeles. A = San Gabriel Canyon, B = Newport Canyon. At Point C, the canyon is 815 m wide and 25 m deep. Figure description available at the end of the chapter.

Submarine canyons are narrow, deep underwater canyons located on continental shelves. Submarine canyons typically form at the mouths of large landward river systems. They form when rivers cut down into the continental shelf during periods of low sea level and when material continually slumps or flows down from the mouth of a river or a delta. Underwater currents rich in sediment and more dense than seawater can flow down the canyons, even eroding and deepening them, then drain onto the ocean floor. Underwater landslides, called turbidity flows, occur when steep delta faces and underwater sediment flows are released down the continental slope. Turbidity flows in submarine canyons can continue to erode the canyon, and eventually, fan-shaped deposits develop at the mouth of the canyon on the continental rise. See Chapter 5 for more information on turbidity flows.

Take this quiz to check your comprehension of this section.

Access the quiz for Section 12.2 by scanning the QR code.

12.3 Currents and Tides

Ocean water moves as waves, currents, and tides. Ocean currents are driven by persistent global winds blowing over the water's surface and by water density. Ocean currents are part of Earth's heat engine, in which solar energy is absorbed by ocean water and distributed by ocean currents. Water has another unique property, high specific heat, that relates to ocean currents. Specific heat is the amount of heat necessary to raise a unit volume of a substance one degree. For water, it takes one calorie per cubic centimeter to raise its temperature one degree Celsius. This means the oceans, covering 71% of the Earth's surface, soak up solar heat with little temperature change and distribute that heat around the Earth by ocean currents.

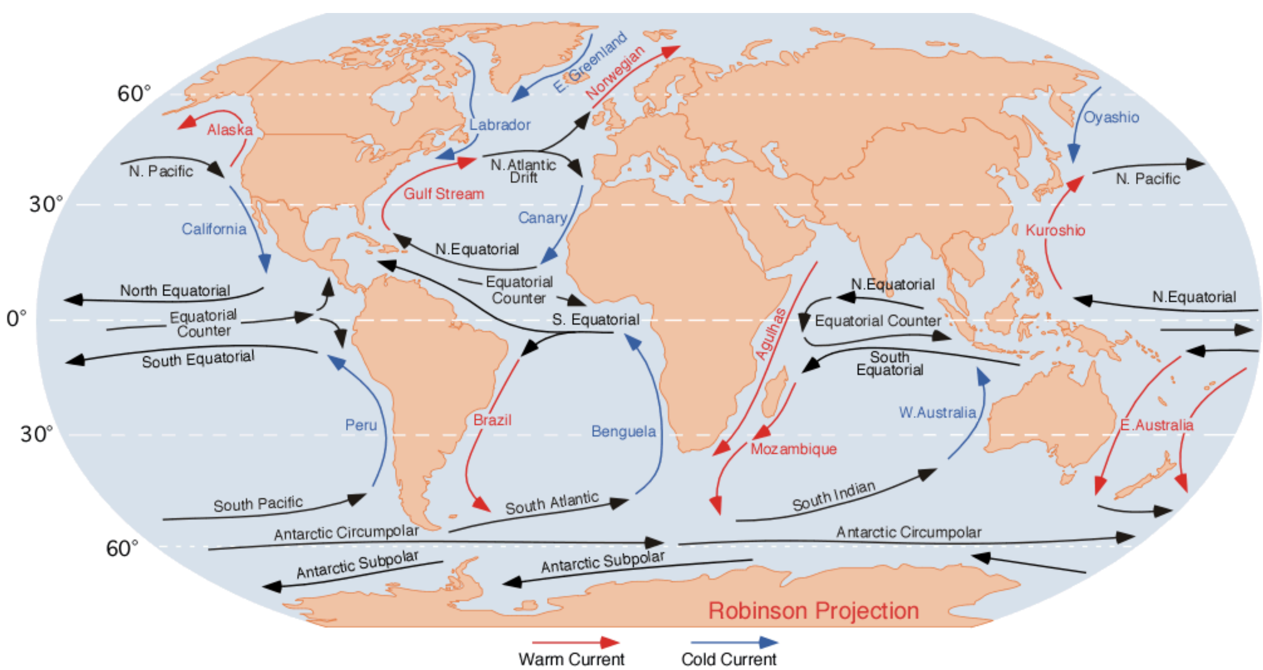

Figure 12.23: World ocean currents. Figure description available at the end of the chapter.

12.3.1 Surface Currents

The Earth's rotation and the Coriolis effect exert significant influence on ocean currents (see Chapter 13). In the figure, the black arrows show global surface currents. Notice the large circular currents in the Northern and Southern Hemispheres in the Atlantic, Pacific, and Indian Oceans. These currents are called **gyres** and are driven by atmospheric circulation—air movement. Gyres rotate clockwise in the Northern Hemisphere and counterclockwise in the Southern Hemisphere because of the Coriolis effect. Western boundary currents flow from the equator toward the poles, carrying warm water. They are key contributors to local climate. Western boundary currents are narrow and move poleward along the east coasts of adjacent continents. The Gulf Stream and the Kuroshio Currents in the Northern Hemisphere and the Brazil, Mozambique, and Australian Currents in the Southern Hemisphere are western boundary currents. Currents returning cold water toward the equator are broad and diffuse along the western coasts of adjacent land masses. These warm western boundary and cold eastern boundary currents affect climate of nearby lands, making them warmer or colder than other areas at equivalent latitudes. For example, the warm Gulf Stream makes Northern Europe much milder than similar latitudes in northeastern Canada and Greenland. Another example is the cool Humboldt Current, also called the Peru Current, flowing north along the west coast of South America. Cold currents limit evaporation in the ocean, which is one reason the Atacama Desert in Chile is cool and arid.

12.3.2 Deep Currents

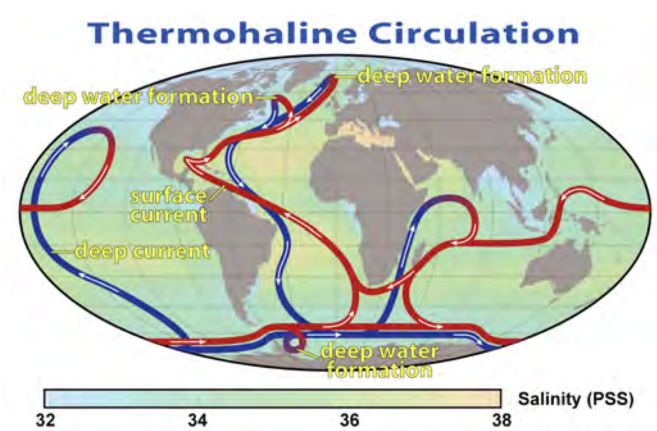

Figure 12.24: Global thermohaline circulation (PSS = practical salinity units). Figure description available at the end of the chapter.

Whether an ocean current moves horizontally or vertically depends on its density. The density of seawater is determined by temperature and salinity.

Evaporation and freshwater influx from rivers affect salinity and, therefore, the density of seawater. As the western boundary currents cool at high latitudes, salinity increases due to evaporation and ice formation (recall that ice floats; water is densest just above its freezing point). So the cold, denser water sinks to become the ocean's deep waters. Deep-water movement is called **thermohaline circulation** (*thermo-* referring to temperature and *-haline* referring to salinity). This circulation connects the world's deep ocean waters. Movement of the Gulf Stream illustrates the beginning of thermohaline circulation. Heat in the warm poleward-moving Gulf Stream promotes evaporation, which takes heat from the water, and as heat thus dissipates, the water cools. The resulting water is much colder, saltier, and denser. As the denser water reaches the North Atlantic and Greenland, it begins to sink and becomes a deep-water current. As shown in the illustration above, this worldwide connection between shallow and deep-ocean circulation overturns and mixes the entire world ocean, bringing nutrients to marine life with what is sometimes referred to as the global conveyor belt.

12.3.3 Tides

Tides are the rising and lowering of sea level during the day and are caused by the gravitational effects of the Sun and Moon on the oceans. The Earth rotates daily within the Moon and Sun's gravity fields. Although the Sun is much larger and its gravitational pull is more powerful, the Moon is closer to Earth; hence, the Moon's gravitational influence on tides is dominant. The magnitude of the tide at a given location and the difference between high and low tide—the tidal range—depends primarily on the configuration of the Moon and Sun with respect to the Earth orbit and rotation.

Spring tide occurs when the Sun, Moon, and Earth line up with each other at the full or new Moon; this is when the tidal range is at a maximum. **Neap tide** occurs approximately two weeks later, when the Moon and Sun are at right angles with the Earth, and the tidal range is at this point.

The Earth rotates within a tidal envelope, so tides rise and ebb daily. Tides are measured at coastal locations. These measurements and the tidal predictions based on them are published on the NOAA website. Tides rising and falling create tidal patterns at any given shore location. The three types of tidal patterns are diurnal, semidiurnal, and mixed**.**

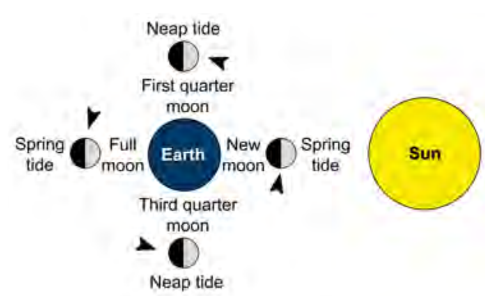

Figure 12.25: Diagram showing tides in relation to the Sun and Moon. Figure description available at the end of the chapter.

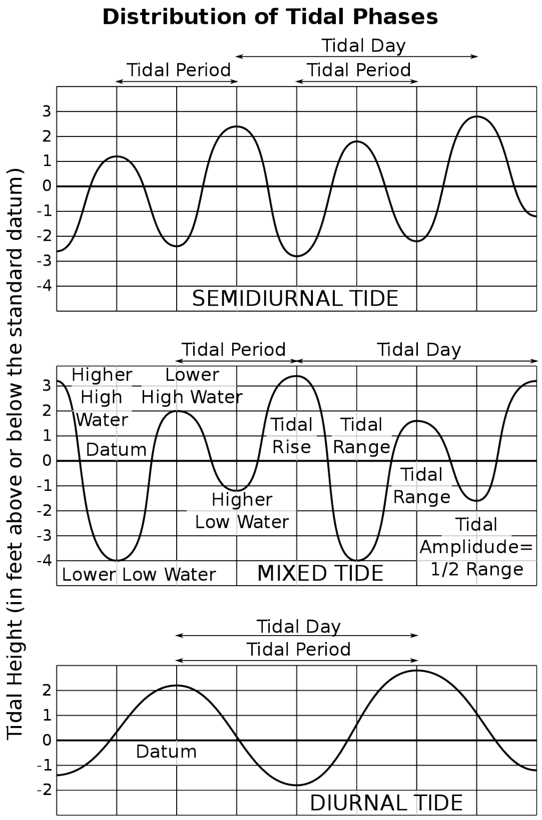

Figure 12.26: Different tide types. Figure description available at the end of the chapter.

Diurnal tides go through one complete cycle each tidal day. A **tidal day** is the amount of time it takes for the Moon to align with a point on the Earth as the Earth rotates, which is slightly longer than 24 hours. **Semidiurnal tides** go through two complete cycles in each tidal day—occurring approximately every 12 hours and 50 minutes, with the tidal range typically varying in each cycle. **Mixed tides** are a combination of diurnal and semidiurnal patterns and show two tidal cycles per tidal day, but the relative amplitudes of each cycle and their highs and lows vary during the tidal month. For example, there is a high-high tide and a high-low tide. The next day, there is a low-high tide and a low-low tide.

It is complicated to forecast the tidal pattern and the times tidal phases arrive at a given shore location and can be done for only a few days at a time.

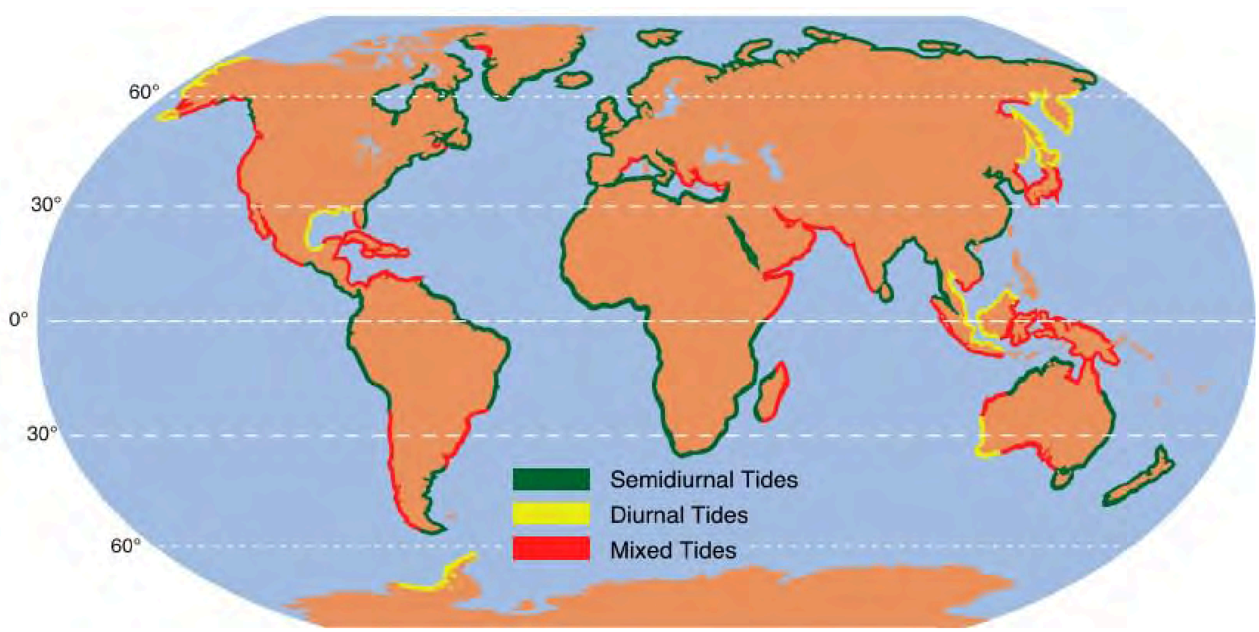

Figure 12.27: Global tide types. Figure description available at the end of the chapter.

Tidal phases are determined by **bathymetry**—the depth of ocean basins and the continental obstacles that are in the way of the tidal envelope within which the Earth rotates. Local tidal experts make 48-hour tidal forecasts using tidal charts based on daily observations, as can be seen in the chart of different tide types. A typical tidal range is approximately 1 m (3 ft). Extreme tidal ranges occur where the tidal wave enters a narrow restrictive zone that funnels the tidal energy. An example is the English Channel between Great Britain and the European continent where the tidal range is 7 to 9.75 m (23 to 32 ft). The Earth's highest tidal ranges occur at the Bay of Fundy, the funnel-like bay between Nova Scotia and New Brunswick, Canada, where the average range is nearly 12 m (40 ft) and the extreme range is around 18 m (60 ft). At extreme tidal range locations, a person who ventures out onto the seafloor exposed during ebb tide may not be able to outrun the advancing water during flood tide. NOAA has additional information on tides.

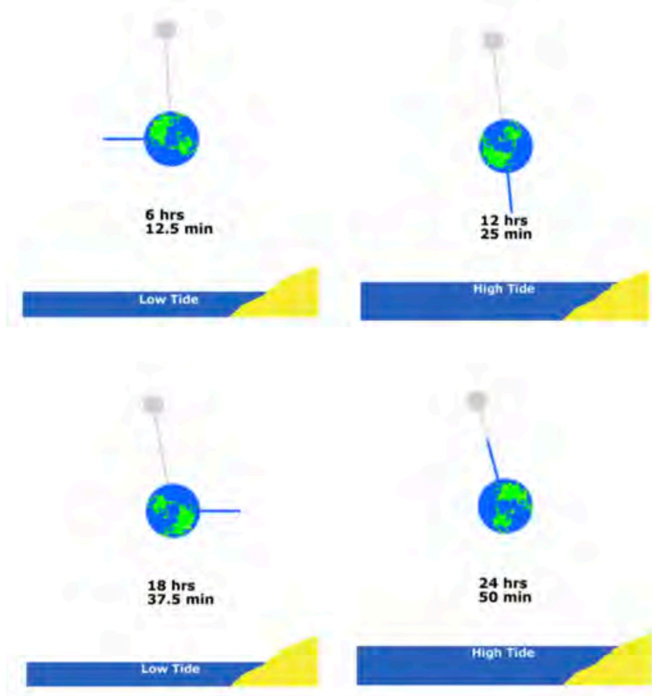

Figure 12.28: A tidal day lasts slightly longer than 24 hours. Figure description available at the end of the chapter.

Tidal forces push seawater into two tidal bulges on opposite sides of the Earth. These tidal bulges lag behind as Earth rotates, which causes friction between Earth's crust (the ocean floor) and the ocean itself, and that friction acts to slow down Earth's rotation. This process, known as **tidal braking**, occurs because the gravitational pull between the Earth and Moon creates resistance, gradually reducing Earth's rotational speed. This friction is slowing the Earth's rotation down by some 1.7 milliseconds every century, and in geologic time, this adds up; in fact, it's estimated that Earth began with a day lasting only four modern hours. Another consequence of this is that the Moon's distance from Earth is gradually increasing. As it moves farther away, it will orbit less quickly (just as planets farther from the Sun move more slowly in their orbits). Both the day and the month on Earth will continue to get longer, although bear in mind that the effects are very gradual. This has been confirmed by mirrors placed on the Moon by Apollo 11 astronauts, which show that the Moon is moving away by 3.8 centimeters per year. Ultimately, billions of years in the future, the day and the month will be the same length (about 47 of our present days).

Take this quiz to check your comprehension of this section.

Access the quiz for Section 12.3 by scanning the QR code.

12.4 Ocean Water Properties

Ocean water has several unique properties: it freezes at a slightly lower temperature than fresh water, has a slightly higher density than fresh water, conducts electricity significantly better than fresh water, and is mildly basic on the **pH scale**. Ocean water is also, of course, salty. By weight, it consists of about 3.5% dissolved mineral substances that are collectively termed salts. Salinity is the total amount of solid material dissolved in water. Temperature and density are basic ocean water properties that influence such things as deep-ocean circulation and the distribution and types of life forms.

12.4.1 Ocean Water Salinity

Oceanographers typically use parts per thousand (‰) to express salinity because dissolved substances in ocean water are present in such minute quantities. This means that for every 1,000 grams of seawater, on average, 35 grams are made up of dissolved salts. Consequently, the average salinity of seawater is 35‰. Most salt in seawater is sodium chloride (NaCl).

The salts in the ocean are delivered from two main sources. The first is chemical weathering of rocks on the continents, carried to the oceans via streams. A second major source of dissolved elements found in ocean water is from Earth's interior through volcanic eruptions in a process called outgassing. Despite rivers and volcanoes constantly adding new material to ocean water, the ocean's composition remains relatively stable. This stability is achieved because salt from seawater is continually deposited as sediment on the ocean floor, creating a balanced input and output system in the oceans.

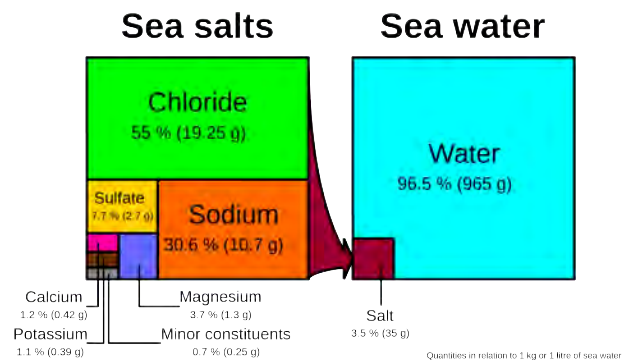

Figure 12.29: Proportions of water and dissolved components in a typical sample of seawater. Most of the salt in seawater is sodium chloride. Figure description available at the end of the chapter.

Various surface processes alter the salinity of ocean water regionally. Processes that add large amounts of fresh water to seawater, thereby decreasing salinity, include precipitation, runoff from land, icebergs melting, and sea-ice melting. Processes that remove large amounts of fresh water from seawater, increasing salinity, include evaporation and the formation of sea ice.

Latitude and seasons both affect seawater salinity as well. Salinity levels in the open ocean are higher at subtropical latitudes because these areas experience high evaporation rates. In contrast, regions with significant precipitation experience lower salinity levels due to the dilution of ocean waters. This occurs near the equator and in the midlatitudes between 35 and 60 degrees latitude. Seasonally, seawater freezes in the winter at the poles, and when it freezes, the ice itself is practically fresh water. That's because only the water molecules freeze out, leaving the salt behind and increasing the salinity of the remaining liquid seawater. During the summer, sea ice melts, thereby decreasing salinity.

12.4.2 Ocean Water Density

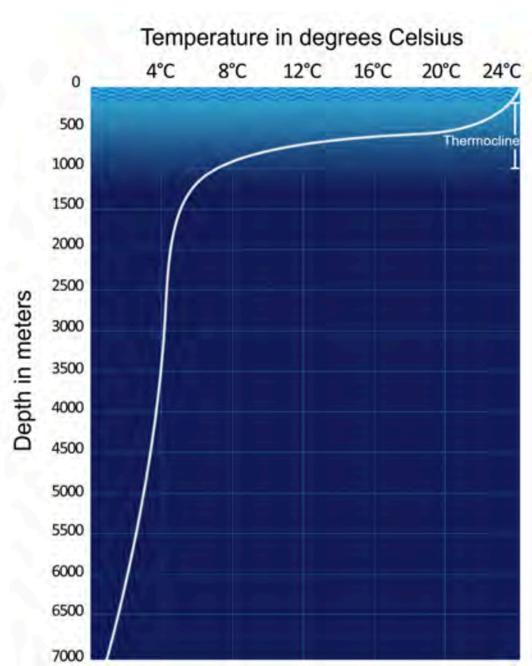

Figure 12.30: Variations in ocean-water temperature with depth for low-latitude regions. Figure description available at the end of the chapter.

Density is an important property of ocean water because it determines the water's vertical position in the ocean. Ocean water density is influenced by two main factors: salinity and temperature. An increase in salinity adds dissolved substances and results in an increase in seawater density. An increase in temperature, on the other hand, causes water to expand and results in a decrease in seawater density. Therefore, temperature and density have an inverse relationship: one variable decreases as the result of the other variable's increase. A sampling of the open ocean from the surface to the seafloor shows that both temperature and density change with depth and that the changes are not the same everywhere.

In regions closer to the equator, surface ocean water tends to have warmer temperatures, with temperature rapidly declining as depth increases due to limited penetration of sunlight into the ocean. The transition layer where temperature changes swiftly with depth is termed the **thermocline**. Conversely, in higher latitudes, where surface temperatures remain consistently cold, the thermocline is nonexistent.

The density of ocean water is also influenced by latitude. In equatorial regions, surface ocean water exhibits lower density due to higher surface temperatures. Similar to temperature trends, density increases with depth. The **pycnocline** is the layer of ocean water between approximately 300 meters and 1,000 meters, characterized by a rapid change in density with depth. The presence of a pycnocline serves as a barrier to the mixing of low-density water above and high-density water below. Conversely, in polar regions, where temperature gradients are less pronounced, there is no rapid density change with depth, resulting in the absence of a pycnocline.

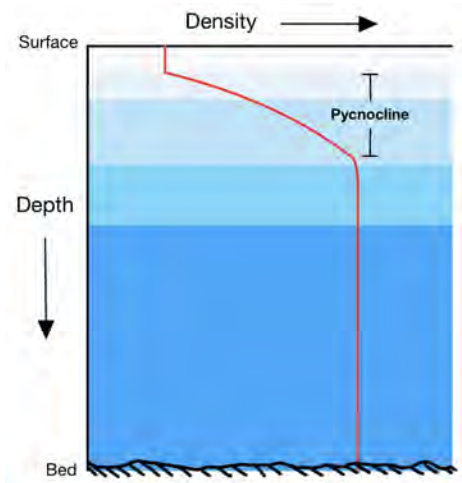

Figure 12.31: Variations in ocean-water density with depth for low-latitude regions. Figure description available at the end of the chapter.

12.4.3 Ocean Layering

Similar to Earth's interior, the ocean exhibits vertical zonation based on water density. Lower-density water occupies the surface layers, transitioning to denser water with increasing depth, with the densest seawater at the greatest depths. In the open ocean, a three-tiered structure can be recognized: a shallow surface mixed zone, transition zone, and deep zone.

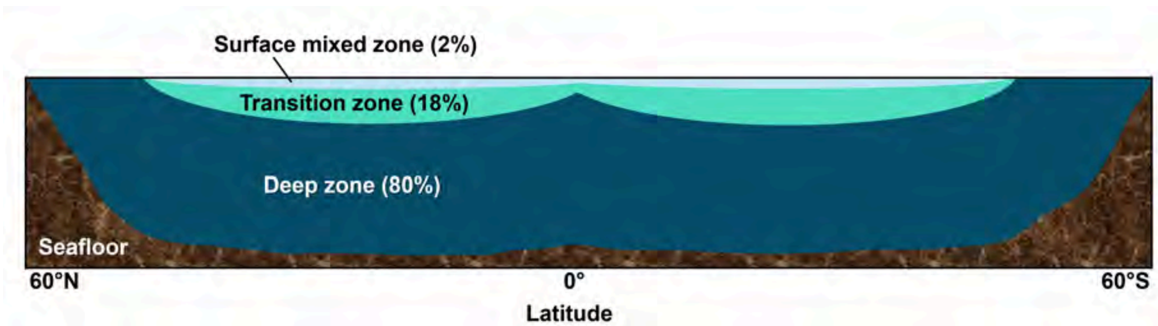

Figure 12.32: The ocean's layers. Figure description available at the end of the chapter.

Solar radiation serves as the primary source of heat for the ocean surface. Wind-driven waves, along with turbulence generated by currents and tides, facilitate the mixing of this surface layer, distributing heat through the shallow surface mixed zone. This zone comprises only about 2% of the total ocean volume, having slightly variable thickness and temperature depending on latitude and season. Below the shallow mixed zone, a sharp temperature decline marks the transition zone. This zone bridges the gap between the warm surface waters and the cold deep zone below. It includes a thermocline (and pycnocline) and accounts for roughly 18% of ocean water. Beyond the transition zone lies the vast deep zone, where sunlight doesn't reach and temperatures are just above freezing. This zone comprises about 80% of ocean water, maintaining consistently high density.

This three-layered structure is not universally applicable. At higher latitudes, the absence of a distinct thermocline and pycnocline negates the rapid changes in temperature and density with depth.

Take this quiz to check your comprehension of this section.

Access the quiz for Section 12.4 by scanning the QR code.

12.5 The Ocean Floor

There is a great variety of features at the bottom of our world ocean, including extensive chains of volcanoes, deep trenches, wide plains, and **oceanic plateaus**. Our understanding of the complex characteristics of the ocean floor remained largely unknown until the **HMS Challenger** expedition, a scientific voyage that made many foundational oceanographic discoveries which spanned from December 1872 to May 1876. The Challenger expedition marked the first attempt at a comprehensive scientific study of the global ocean; since then, advancements in oceanographic science have unveiled the vast ocean floors in much greater detail.

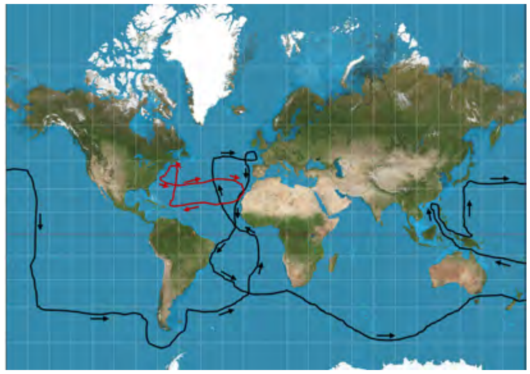

Figure 12.33: Approximate routes of the Challenger expedition of 1872–1876. Figure description available at the end of the chapter.

12.5.1 Mapping the Ocean Floor

Bathymetry refers to the measurement of ocean depths and the charting of the ocean floor's topography. The fundamental methodology for seafloor mapping leverages **sonar** (sound navigation and ranging), a technique that utilizes sound waves to navigate, communicate, or detect objects.

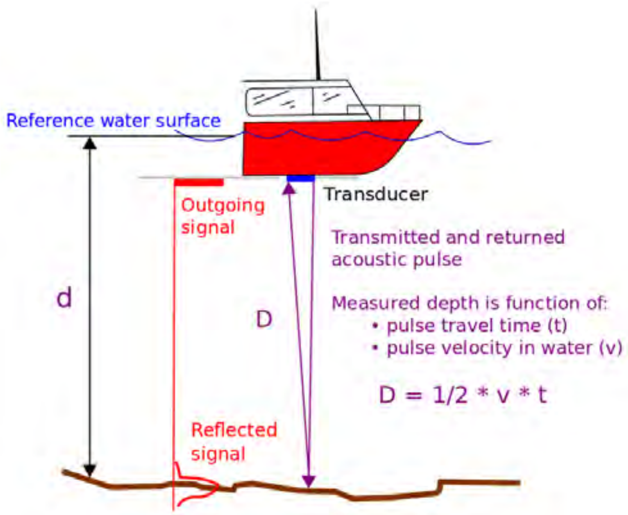

Figure 12.34: Diagram showing the basic principle of single-beam echo sounding. Figure description available at the end of the chapter.

In the early twentieth century, **echo sounders** were the first devices that used sound for water depth measurement. These devices functioned by transmitting an acoustic pulse, often called a "ping," into the water column. Upon encountering an object, such as a large marine animal or the seabed itself, the acoustic energy would reflect, generating an echo. A receiver at the surface would capture this reflected echo from the bottom, and a high-precision clock would measure the round-trip travel time down to fractions of a second. With this information, the depth to the ocean floor could be calculated. Continuous monitoring and subsequent depth determinations from these echoes were then plotted, creating a bathymetric profile of the seafloor. By combining numerous profiles from adjacent survey tracks, a comprehensive seafloor chart was produced.

Breakthroughs in technology have led to more detailed ocean floor maps. One such breakthrough involves measuring the shape of the ocean surface from space.

After accounting for waves, tides, currents, and atmospheric effects, it was found that the ocean surface is not perfectly "flat." Large seafloor features create stronger-than-average gravitational pulls, resulting in elevated areas on the ocean surface, while canyons and trenches cause slight depressions. Satellites equipped with radar **altimeters** can measure these subtle variations by transmitting and receiving **microwave** pulses that reflect off the ocean surface, detecting differences as small as a few centimeters. When combined with traditional sonar measurements, this data helps produce detailed maps of the ocean floor.

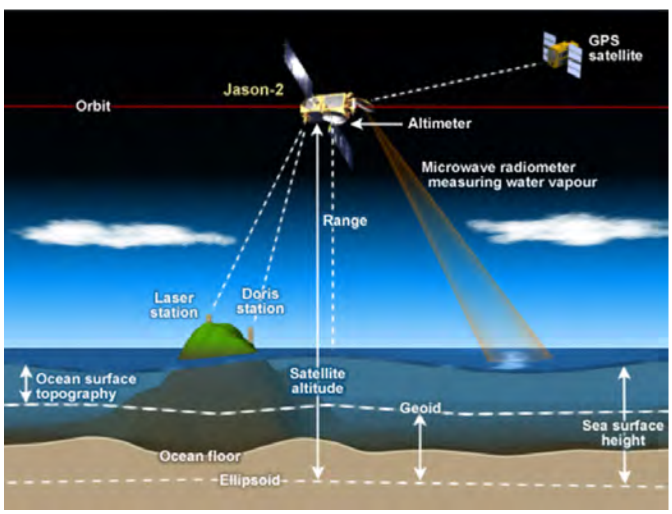

Figure 12.35: How satellite radar altimetry works. Figure description available at the end of the chapter.

12.5.2 Ocean Floor Provinces

Oceanographers studying the topography of the ocean floor have outlined three major areas, or provinces: continental margins, deep ocean basins, and mid-ocean ridges.

The edges of continents, where land transitions to the deep ocean, are called **continental margins**. These margins mark the spot where continental crust thins out and gives way to oceanic crust. There are two main types: passive and active margins.

Passive margins are geologically inactive, located far from plate boundaries. Consequently, these margins are not linked to strong earthquakes or volcanic activity. They form when continental blocks slowly rift apart by ongoing seafloor spreading. Passive margins are typically wide and collect massive amounts of sediment over time. They're made up of several key features: the continental shelf, the continental slope, and the continental rise. Most of the Atlantic Ocean and a significant part of the Indian Ocean are lined by passive margins.

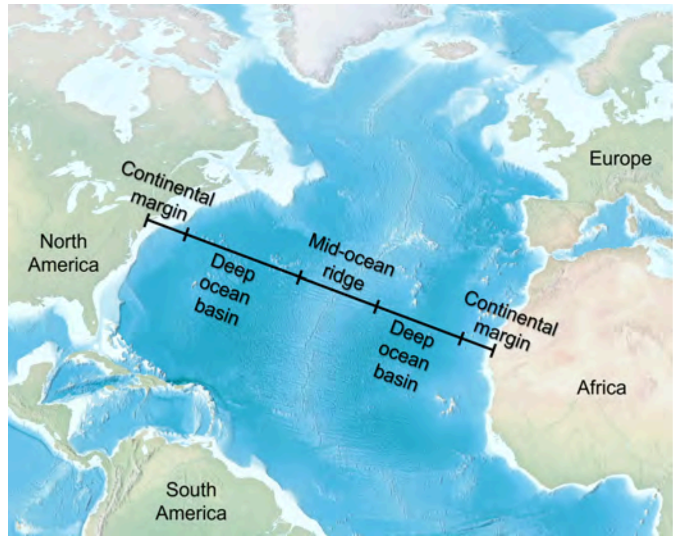

Figure 12.36: Major topographic provinces of the North Atlantic Ocean. Figure description available at the end of the chapter.

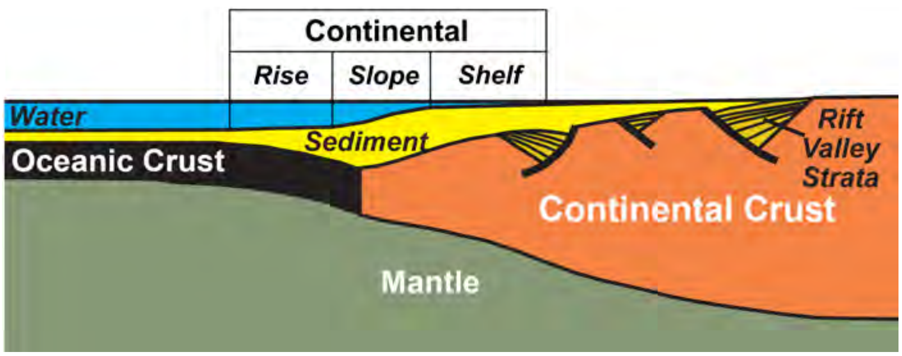

Figure 12.37: A passive continental margin. Figure description available at the end of the chapter.

Unlike the Atlantic and Indian Oceans, the majority of the Pacific Ocean is fringed by **active continental margins**, characterized by subduction zones where the denser oceanic plate is subducted under the less dense continental plate, creating a deep oceanic trench. Oceanic trenches surround most of the Pacific Rim.

Between the continental margin and the mid-ocean ridge lies the deep ocean basin. This region includes deep ocean trenches, abyssal plains, seamounts, and oceanic plateaus.

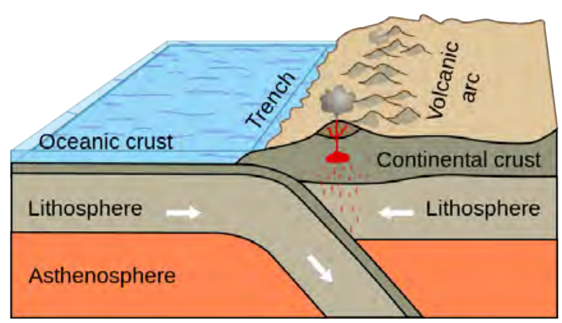

Figure 12.38: An active continental margin. Figure description available at the end of the chapter.

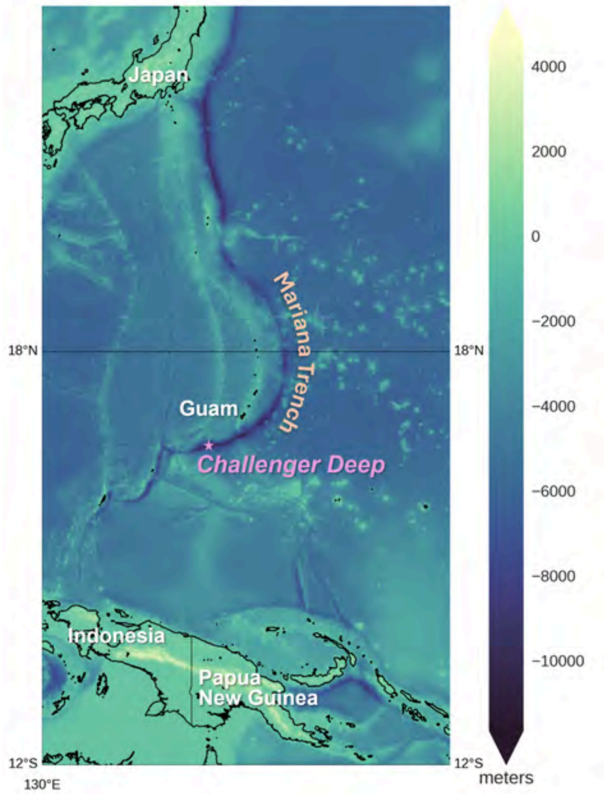

Figure 12.39: Bathymetry map of the Mariana Trench region. The Challenger Deep is the deepest known point of the ocean floor on Earth, with a depth of 10,920 ± 10 meters. Figure description available at the end of the chapter.

Most deep ocean trenches are extremely deep linear depressions on the ocean floor located in the Pacific Ocean, where some exceed 33,000 feet in depth.

Abyssal plains are incredibly flat regions present in all oceans. Due to its lack of oceanic trenches, the Atlantic Ocean has the most extensive abyssal plains which act as sediment traps, allowing more material to settle than in other major ocean basins. Submarine landforms known as seamounts rise from the ocean floor without reaching the surface, typically formed from extinct volcanoes that rise abruptly in a conical shape. While seamounts are found in all oceans, they are most common in the Pacific. An oceanic plateau is a massive, relatively flat feature that rises above the surrounding seafloor and has one or more steep sides, formed by extensive outpourings of basaltic lavas.

The mid-ocean ridge is a massive underwater mountain range that snakes its way through all the world's oceans. Formed along seafloor spreading centers where tectonic plates pull apart, it's Earth's longest interconnected mountain system at over 43,000 miles in length. It's a zone with frequent earthquakes, high heat flow from the Earth's interior, and volcanic mountains erupting on the newly formed oceanic crust.

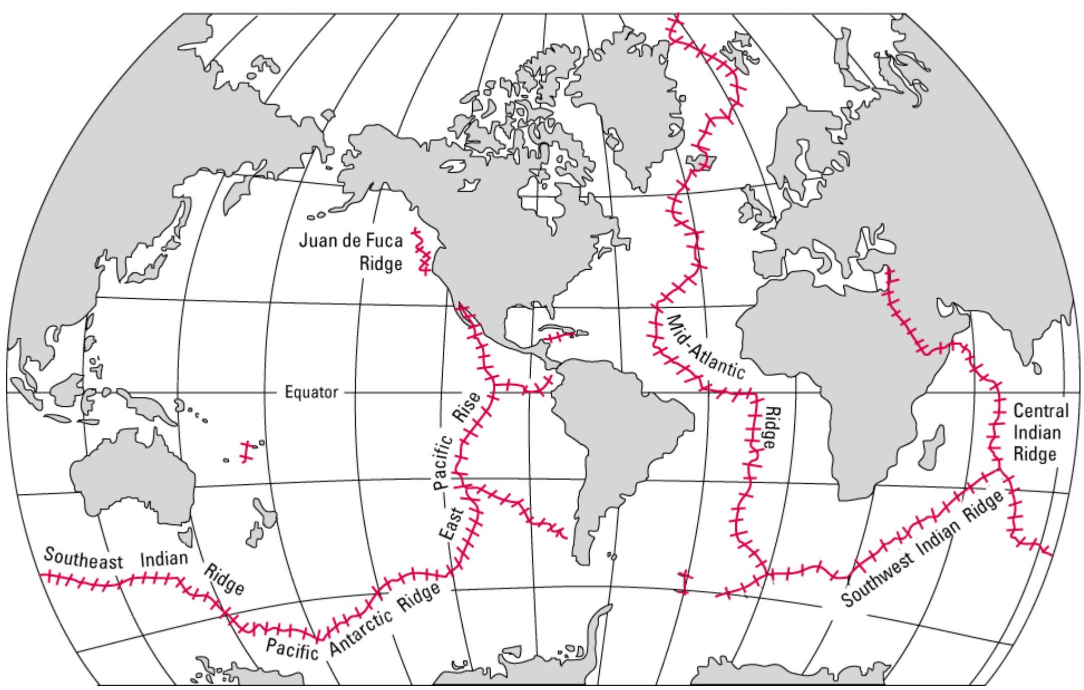

Figure 12.40: World distribution of mid-ocean ridges. Figure description available at the end of the chapter.

Take this quiz to check your comprehension of this section.

Access the quiz for Section 12.5 by scanning the QR code.

Summary

Shoreline processes are complex but are important for understanding coastal processes. Waves, currents, and tides are the main agents that shape shorelines. Most coastal landforms can be attributed to moving sand via longshore drift and to long-term rising or falling sea levels.

The shoreline is the interface between water and land and is divided into five zones. Processes at the shoreline are called littoral processes. Waves approach the beach at an angle, which cause the waves to bend toward the beach. This bending action is called wave refraction and is responsible for creating the longshore current and longshore drift—the process that moves sand along the coasts. When the longshore current deposits sand along the coast into quieter waters, the sand can accumulate, creating a spit or barrier called a baymouth bar, which often blocks bays and harbors. Inconvenienced humans create methods to keep their harbors open and preserve sand on their beaches by creating jetties and groins, which negatively affect natural beach processes.

Emergent coasts are created by sea levels falling, while submergent coasts are caused by sea levels rising. Oceans absorb solar energy, which is distributed by currents throughout the world. Circular surface currents, called gyres, rotate clockwise in the Northern Hemisphere and counterclockwise in the Southern Hemisphere. Thermohaline deep circulation connects the world's deep ocean waters; when shallow poleward moving warm water evaporates, the colder, saltier, and denser water sinks and becomes deep-water currents. The connection between shallow and deep-ocean circulation is called the global conveyor belt.

Tides are the rising and lowering of sea level during the day and are caused by the gravitational effects of the Sun and Moon on the oceans. There are three types of tidal patterns: diurnal, semidiurnal, and mixed. Typical tidal ranges are approximately 1 m (3 ft). Extreme tidal ranges are around 18 m (60 ft).

By weight, ocean water consists of about 3.5% dissolved mineral substances that are collectively termed salts. Salinity is the total amount of solid material dissolved in water. Temperature and density are basic ocean water properties that influence such things as deep-ocean circulation and the distribution and types of life forms. Surface processes, latitude, and seasons alter the salinity of ocean water regionally. Ocean water density is influenced by two main factors: salinity and temperature. The ocean exhibits a three-tiered vertical zonation based on water density: a shallow surface mixed zone, transition zone, and deep zone.

There is a great variety of features at the bottom of our world ocean, including extensive chains of volcanoes, deep trenches, wide plains, and oceanic plateaus. The fundamental methodology for seafloor mapping leverages sonar, a technique that utilizes sound waves to navigate, communicate, or detect objects. Oceanographers studying the topography of the ocean floor have outlined three major provinces: continental margins, deep ocean basins, and mid-ocean ridges.

Take this quiz to check your comprehension of this chapter.

Access the quiz for Chapter 12 by scanning the QR code.

Chapter URLs

- Tide measurements and predictions: https://tidesandcurrents.noaa.gov/tide_predictions.html
- National Oceanic and Atmospheric Administration (NOAA): https://tidesandcurrents.noaa.gov

Text References

1. Colling, A. (2001). *Ocean circulation* (eds. Open University Course Team): Butterworth-Heinemann.
2. Davis, R.A., Jr., and Fitzgerald, D.M. (2009). *Beaches and coasts:* John Wiley & Sons.
3. Davis, R.A. (1997). *The evolving coast:* Scientific American Library New York.
4. Greene, Paul, Follett, G., and Henker, C. (2009). Munitions and dredging experience on the United States coast. *Marine Technology Society Journal, 43*(4), 127–31.
5. Jackson, N.L., Harley, M.D., Armaroli, C., and Nordstrom, K.F. (2015). Beach morphologies induced by breakwaters with different orientations. *Geomorphology, 239*(June), 48–57.
6. Littoral Bypassing and Beach Restoration in the Vicinity of Port Hueneme, California. (n.d.). In *Coastal Engineering* (1966).
7. Munk, W.H. (1950). On the wind-driven ocean circulation. *Journal of Meteorology, 7*(2), 80–93.
8. Normark, W.R., and Carlson, P.R. (2003). Giant submarine canyons: Is size any clue to their importance in the rock record? *Geological Society of America Special Papers 370*(January), 175–90.
9. Reineck, H-E, and Singh, I.B. (2012). *Depositional sedimentary environments: With reference to terrigenous clastics:* Springer Science & Business Media.
10. Rich, J.L. (1951). Three critical environments of deposition, and criteria for recognition of rocks deposited in each of them. *Geological Society of America Bulletin, 62*(1), 1–20.
11. Runyan, K., and Griggs, G. (2005). Implications of harbor dredging for the Santa Barbara littoral cell. In *California and the World Ocean '02*, 121–35: American Society of Civil Engineers.
12. Schwiderski, E.W. (1980). On charting global ocean tides. *Reviews of Geophysics, 18*(1), 243–68.
13. Stewart, R.H. (2008). Introduction to Physical Oceanography. Texas A & M University Texas.
14. Stommel, H., and Arons, A.B. (2017). On the abyssal circulation of the world ocean: I. Stationary Planetary Flow Patterns on a Sphere. ScienceDirect. http://www.sciencedirect.com/science/article/pii/0146631359900656.
15. NOAA. Why is the ocean salty, but rivers flowing into it are not? National Ocean Service website, updated on 01/18/24. https://oceanservice.noaa.gov/facts/riversnotsalty.html.
16. Earle, S. (2019). *Physical geology – 2nd edition:* BCcampus. Retrieved from https://opentextbc.ca/physicalgeology2ed

Figure References

Figure 12.1: Particle motion within a wind-blown wave. Kraaiennest. 2008. CC BY-SA 4.0. https://commons.wikimedia.org/wiki/File:Deep_water_wave.gif

Figure 12.2: Aspects of water waves, labeled. National Oceanic and Atmospheric Administration (NOAA). Unknown date. Public domain. https://oceanservice.noaa.gov/education/tutorial_currents/media/supp_cur03a.html

Figure 12.3: Diagram describing wavebase. GregBenson. 2004. CC BY-SA 3.0. https://en.wikipedia.org/wiki/File:Wavebase.jpg

Figure 12.4: Wave train moving with dispersion. Fffred~commonswiki. 2006. Public domain. https://commons.wikimedia.org/wiki/File:Wave_packet_(dispersion).gif

Figure 12.5: A rogue wave estimated at 18.3 meters (60 feet) in the Gulf Stream off of Charleston, South Carolina. NOAA. 2024. Public domain. https://oceanservice.noaa.gov/facts/roguewaves.html

Figure 12.6: Types of breakers. Kraaiennest. 2015. CC BY-SA 3.0. https://commons.wikimedia.org/wiki/File:Breaking_wave_types.svg

Figure 12.7: All waves, including tsunamis, slow down as they reach shallow water. Régis Lachaume. 2005. CC BY-SA 3.0. https://commons.wikimedia.org/wiki/File:Propagation_du_tsunami_en_profondeur_variable.gif

Figure 12.8: Diagram of zones of the shoreline. US Navy. 2006. Public domain. https://commons.wikimedia.org/wiki/File:Littoral_Zones.jpg

Figure 12.9: Longshore drift. United States Geological Survey (USGS). 2006. Adapted by Laura Neser. Public domain. https://commons.wikimedia.org/wiki/File:Longshore_i18n.png

Figure 12.10: Jetties near Carlsbad, California. USGS. 2005. Public domain. https://commons.wikimedia.org/wiki/File:Jetty_break2_new(USGS).jpg

Figure 12.11: Animation of rip currents. NOAA. 2008. Public domain. https://www.nws.noaa.gov/mdl/rip_current

Figure 12.12: Rip currents sign at Canaveral National Seashore, Florida. Laura Neser. 2018. CC BY-NC.

Figure 12.13: Island Arch, a sea arch in Victoria, Australia. Diliff. 2008. CC BY-SA 3.0. https://commons.wikimedia.org/wiki/File:Island_Archway,_Great_Ocean_Rd,_Victoria,_Australia_-_Nov_08.jpg

Figure 12.14: This tombolo known as Angel Road connects the stack of Shodo Island, Japan. 663highland. 2012. CC BY-SA 3.0. https://commons.wikimedia.org/wiki/File:Angel_Road_Shodo_Island_Japan01s3.jpg

Figure 12.15: Wave notches carved by Lake Bonneville, Antelope Island, Utah. Wilson44691. 2008. Public domain. https://commons.wikimedia.org/wiki/File:WaveCutPlatformsAntelopeIslandUT.jpg

Figure 12.16: Landsat image of Chesapeake Bay, Eastern United States. USGS, NASA. 2009. Public domain. https://www.usgs.gov/media/images/chesapeake-bay-landsat

Figure 12.17: General diagram of a tidal flat and associated features. Foxbat deinos. 2009. Public domain. https://en.m.wikipedia.org/wiki/File:Tidal_flat_general_sketch.png

Figure 12.18: Kara-Bogaz Gol lagoon, Turkmenistan. NASA. 1995. Public domain. https://commons.wikimedia.org/wiki/File:Kara-Bogaz_Gol_from_space,_September_1995.jpg

Figure 12.19: Bird's-eye view of groins gathering sediment from longshore drift (current is flowing from right to left). Archer0630. 2013. CC BY-SA 3.0. https://commons.wikimedia.org/wiki/File:Groin_effect-3.jpg

Figure 12.20: Groin system on a coast in Virginia. Internet Archive Book Images. 1958. Public domain. https://commons.wikimedia.org/wiki/File%3AThe_Annual_bulletin_of_the_Beach_Erosion_Board_(1958)_(18396945096).jpg

Figure 12.21: A tombolo formed behind the breakwater at Venice, CA. Internet Archive Book Images. 1948. Public domain. https://flic.kr/p/wRSfxb

Figure 12.22: Submarine canyons off of Los Angeles. A = San Gabriel Canyon, B = Newport Canyon. At Point C, the canyon is 815 m wide and 25 m deep. USGS. 2012. Public domain. https://commons.wikimedia.org/wiki/File:Canyons_off_LA.jpg

Figure 12.23: World ocean currents. Dr. Michael Pidwirny. 2007. Public domain. https://commons.wikimedia.org/wiki/File:Corrientes-oceanicas.png

Figure 12.24: Global thermohaline circulation. NASA. 2008. Public domain. https://commons.wikimedia.org/wiki/File:Thermohaline_Circulation_2.png

Figure 12.25: Diagram showing tides in relation to the Sun and Moon. Snubcube. 2013. Public domain. Adapted by Laura Neser. https://commons.wikimedia.org/wiki/File:Tide_type.svg

Figure 12.26: Different tide types. Snubcube. 2013. Public domain. https://commons.wikimedia.org/wiki/File:Tide_type.svg

Figure 12.27: Global tide types. KVDP. 2009. Public domain. https://commons.wikimedia.org/wiki/File:Diurnal_tide_types_map.jpg

Figure 12.28: A tidal day lasts slightly longer than 24 hours. NOAA. Unknown date. Public domain. https://oceanservice.noaa.gov/education/tutorial_tides/tides05_lunarday.html

Figure 12.29: Proportions of water and dissolved components in a typical sample of seawater. Tcncv. 2008. Public domain. https://en.wikipedia.org/wiki/Seawater#/media/File:Sea_salt-e-dp_hg.svg

Figure 12.30: Variations in ocean-water temperature with depth for low-latitude regions. Praveenron. 2014. Adapted by Laura Neser. Public domain. https://commons.wikimedia.org/wiki/File:THERMOCLINE.png

Figure 12.31: Variations in ocean-water density with depth for low-latitude regions. Ebmwtreng. 2023. Public domain. https://commons.wikimedia.org/wiki/File:Pycnocline_illustrative_drawing_03_13_22.jpg

Figure 12.32: The ocean's layers. Laura Neser. Public domain.

Figure 12.33: Approximate routes of the the Challenger expedition of 1872–1876. rehemat24. Adapted by Laura Neser. Accessed June 7, 2024. CC BY. https://diatoms.myspecies.info/file-colorboxed/86

Figure 12.34: Diagram showing the basic principle of single-beam echo sounding. Brandon T. Fields (cdated) via the US Army Corps of Engineers. 2012. Public domain. https://commons.wikimedia.org/wiki/File:Principle_of_SBES.svg

Figure 12.35: How satellite radar altimetry works. NOAA/STAR. Accessed June 7, 2024. Public domain. https://www.star.nesdis.noaa.gov/socd/lsa/AltBathy

Figure 12.36: Major topographic provinces of the North Atlantic Ocean. Tom Patterson. 2020. Adapted by Laura Neser. 2024. Public domain. https://commons.wikimedia.org/wiki/File:North_Atlantic_seafloor.jpg

Figure 12.37: A passive continental margin. NPGallery. 2019. Adapted by Laura Neser. 2024. Public domain. https://npgallery.nps.gov/AssetDetail/8869db4c-3c8b-403f-ae44-128352ca73c6

Figure 12.38: An active continental margin. Booyabazooka. 1999. Public domain. https://commons.wikimedia.org/wiki/File:Active_Margin.svg.

Figure 12.39: Bathymetry map of the Mariana Trench region. Astrobob. 2017. Adapted by Laura Neser. 2024. CC BY-SA. https://commons.wikimedia.org/wiki/File:Mariana_trench.png

Figure 12.40: World distribution of mid-ocean ridges. J M Watson, USGS. 1999. Public domain. https://pubs.usgs.gov/gip/dynamic/baseball.html

Figure Descriptions

Figure 12.1: The red circles are the present positions of massless particles, moving with the flow velocity. The light-blue line gives the path of these particles, and the light-blue circles the particle position after each wave period. The white dots are fluid particles, also followed in time. In the case shown here, the mean Eulerian horizontal velocity below the wave trough is zero. Observe that the wave period, experienced by a fluid particle near the free surface, is different from the wave period at a fixed horizontal position (as indicated by the light-blue circles). This is due to the Doppler shift.

Figure 12.2: Diagram of water waves: the peak of the wave is labeled Crest, the lowest part is labeled Trough, and the Wave height is the distance between the crest and trough. The distance between two successive crests is labeled Wavelength; a horizontal dashed line halfway between the crest and trough is labeled Calm sea level.

Figure 12.3: Cross sectional diagram of sand sloping upward toward the right with shallowing ocean water above; there is a horizontal line between two successive ocean wave crests labeled Wave Length; at the top of the diagram it says "Wave base is the depth to which a passing wave will cause water motion." There are circular arrows stacked vertically at the wave trough with the largest circle at the top and smaller and smaller circles toward the bottom until there are no more circles; at the bottom of the circular arrows is the label "Wave Base = 1/2 Wave Length." Along the sloping sand are two labels: on the side dipping below the vertical stack of arrows, the sand is smooth and there is the label "Ocean bottom undisturbed by waves (Lower Shoreface);" on the side dipping upward above the vertical stack of arrows, the sand is rippled and there is the label "Ocean bottom agitated and rippled by waves (Upper Shoreface)."

Figure 12.4: Simple animation of a series of waves moving as a group from left to right.

Figure 12.5: Forward view on top of a ship that's in dark blue water and there is a high steep wave in front of the ship.

Figure 12.6: Four diagrams of breakers. The top diagram is labeled Spilling and shows waves breaking long and slow, losing its energy as it spills from the crest down the front of the wave. The second diagram is labeled Plunging and shows waves becoming steeper than a spilling breaker and the crest falling as a well-defined curl. The third diagram is labeled Collapsing and shows waves becoming steeper and then the crest collapsing. The fourth diagram is labeled Surging and shows a long wave period, low amplitude wave that doesn't spill or curl, but instead builds up and then slides rapidly up the beach.

Figure 12.7: Animated gif showing large wavelength, low-amplitude waves in the deep ocean and high-amplitude, low-wavelength waves in the shallow ocean. Frequency decreases with depth.

Figure 12.8: Block diagram of shoreline zones: on land is the Coast; there is gently sloping sand coming from the bases of cliffs along the coast; this includes the labels Beach, Backshore, and Berms; in the shallowest part of the ocean water are the labels Foreshore, Terrace, Surf zone, and Breakers. A line labeled Shoreline points to the contact between the edge of the ocean water and the beach. In deeper water is the label Nearshore and then in the deepest water is the label Offshore. The high tide and low tide line are drawn on the diagram as well, and there is a deposit on the continental slope labeled Bar. Across the entire diagram is the label Littoral zone. The deepest part of the water is about 60 m.

Figure 12.9: Schematic diagram of waves approaching a beach with arrows showing the direction of flow: on the beach, arrows show flow downcurrent onto the sand labeled swash and then straight back out to sea labeled backwash. In the water, arrows show incoming waves approaching the beach at an angle toward the left and downward; the water flows parallel to the beach front down the diagram labeled longshore current.

Figure 12.10: Two parallel jetties extending into the ocean; on the left side of the left jetty is a buildup of sand while the other sides of the jetties do not have the same buildup.

Figure 12.11: Animation of a rip current: as ocean water approaches shore, a narrow current of water, the rip current, rushes outwards between two sandbars into deeper water. The thin part of the rip current is labeled neck and it expands into a plume in deeper water, labeled Head.

Figure 12.12: Photograph of a white rectangular metal sign that says Rip Currents: Break the Grip of the Rip! Below the text is a cartoon drawing of an overhead view of the ocean as seen from the shore with black arrows converging and creating a thin current moving out from the shore to deeper water, with a swimmer at the end of the current. There are green arrows labeled Escape that point parallel to the shoreline in both directions away from the rip current. Near the bottom of the sign is the text: If caught in a rip current: don't fight the current; swim out of the current, then to shore; if you can't escape, float or tread water; and if you need help, call or wave for assistance. The very bottom of the sign states: Safety: know how to swim; never swim alone; and if in doubt, don't go out.

Figure 12.13: The arch is a rock formation in a cove of water with a hole in the middle which allows water to pass through; the surrounding landscape is composed of vertical tan cliffs.

Figure 12.14: People walking along an elongate sand deposit that extends from the mainland out to a large vegetation-covered rock in the ocean.

Figure 12.15: Panoramic view of erosional notches in a brown hillside with a white playa and part of a lake in the foreground.

Figure 12.16: Landsat image of the east coast of the United States, centered on the Chesapeake Bay; there are numerous branching rivers leading to the bay and thing, elongate barrier islands located just off the eastern coast.

Figure 12.17: Generalized map view of a tidal flat with labeled and color-coded features: deep littoral is colored blue and found to the upper left of the diagram; lower littoral (subtidal) is colored cyan and next to the deep littoral zone; littoral (beach) is colored marigold and is a strip alongside the lower littoral zone, however the beach has a gap in it; in the gap of the beach there are tidal bars colored turquoise to match the intertidal label; other turquoise intertidal zones are found inland from the beach; supratidal is colored lime green and surrounds the intertidal zones behind the beach; and continental is colored olive green and surrounds the supratidal zone as well as the areas behind the beach along the edges of the diagram.

Figure 12.18: Satellite image of a brown, barren landscape with a large blue rounded body of water on the land; to the left of that body of water is a deeper blue larger water body, the Caspian Sea.

Figure 12.19: Schematic top-down view of two parallel groins extending perpendicular outward from the shoreline. Sand is built up on beach on the right side of each groin and sand is eroded away from the beach on the left side of each groin.

Figure 12.20: Black and white aerial photo of a series of parallel groins extending perpendicular outward from the shoreline with buildings visible on the mainland; sand is built up on beach on the left side of each groin and sand is eroded away from the beach on the right side of each groin.

Figure 12.21: Black and white aerial photo of a breakwater that was built in shallow ocean water parallel to the shoreline but currently has sand built up from the beach all the way to the structure. Buildings are visible on the mainland.

Figure 12.22: Perspective view looking north over two submarine canyons. The distance across the bottom of the image is about 17 km with a vertical exaggeration of 6x. Newport Canyon is labeled B and is composed of individual channels that braid down the slope over a width of about 9 km. The San Gabriel Canyon is labeled A and begins as a series of channels that join together midway down the slope and then split into two channels at the base of the slope. The width of San Gabriel Canyon about halfway down the slope, labeled C, is 815 m and incises about 25 m into the slope.

Figure 12.23: World map of ocean currents; in the northern hemisphere, large-scale gyres flow in a clockwise pattern in each ocean basin; in the southern hemisphere, large-scale gyres flow in a counterclockwise pattern in each ocean basin. Cool currents are generally found along the west coasts of continents and are blue in color; warm currents are generally found along the east coasts of continents and are red in color; the rest of the currents are black.

Figure 12.24: World map of thermohaline circulation currents in the oceans; deep water formation occurs near the poles and surface currents occur near the equators. In the Atlantic Ocean, a blue deep water current forms in the Arctic and travels south along the west margin of the ocean until it reaches Antarctica and flows toward the east; from Antarctica, a red surface current flows from northward off the west coast of Africa, crossing westward toward the northeast coast of South America, and flows northward along the west margin of the ocean until it reaches the Arctic. In the Pacific Ocean, a blue deep water current forms near Antarctica and travels northwestward through the center of the Pacific Ocean until it becomes a red surface current, loops around in a clockwise direction in the northern Pacific Ocean, and travels westward toward southeast Asia; the red surface current continues westward through southeast Asia until it reaches Madagascar,

flows westward around the southern tip of Africa, and joins the red surface current that flows northward along the west margin of the Atlantic Ocean. A blue deep water current flows eastward along the margin of Antarctica.

Figure 12.25: Schematic diagram of the types of tides that occur on Earth as the Moon travels around the Earth; the Sun is to the right-hand side of the diagram. The New Moon occurs when the Moon is located between the Earth and Sun, during which there is a Spring tide; the First Quarter Moon occurs when the Moon travels a quarter of the way counterclockwise around Earth, making a right angle between the Moon, Earth, and Sun, during which there is a Neap tide; the Full Moon occurs when the Moon travels another quarter of the way counterclockwise around Earth, causing the Earth, Moon, and Sun to be in a straight line, during which there is a Spring tide; the Third Quarter Moon travels another quarter of the way counterclockwise around Earth, making a right angle between the Moon, Earth, and Sun, during which there is a Neap tide.

Figure 12.26: Three graphs with tidal height along the vertical axis and time along the horizontal axis. The first graph shows semidiurnal tide, during which tides go through two complete cycles in each tidal day, with the tidal range varying slightly in each cycle. The second graph shows mixed tide, during which tides go through a combination of diurnal and semidiurnal patterns and show two tidal cycles per tidal day, but the relative amplitudes of each cycle and their highs and lows vary during the tidal month. The third graph shows diurnal tide, during which tides go through one complete cycle each tidal day with similar tidal ranges.

Figure 12.27: World map showing the three tidal types along the coasts: Semidiurnal tides are colored green, Diurnal tides are yellow, and Mixed tides are red. Semidiurnal tides are found along the east coast of the United States and Canada, the west coast of central America, the northwest coast of South America, the east and southeast coasts of South America, most of the European coasts with the exception of the northern Mediterranean coast, most of the African coasts with the exception of the horn of Africa, northern and southeastern Asia, northwestern and southeastern Australia, and New Zealand. Diurnal tides are found along the west coast of Alaska, the Gulf of Mexico, northeast Asia, southeast Asia, southwest Australia, and northwest Antarctica. Mixed tides are found along the west coast of North America, the Caribbean, northern South America, southwestern and southeastern South America, the northern Mediterranean, eastern Madagascar, the horn of Africa and northeast Africa, south-central Asia, southeast and east Asia, and northwestern, northeastern, and southern Australia.

Figure 12.28: GIF animation showing Earth rotating on a 24-hour cycle, the Moon revolving around Earth at a much slower rate, and tides at a shoreline fluctuating as a result. High tides and low tides each occur twice during one revolution of the Moon: low tides occur when the Earth, Moon, and Sun make a right angle with each other while high tides occur when the Earth, Moon, and Sun are in alignment. Because the Moon is revolving around Earth, a tidal day lasts slightly longer than 24 hours.

Figure 12.29: Diagram showing concentration of salt within seawater; it's 96.5% water and 3.5% salt. There is a pop-out diagram showing the concentrations of various salt ions within the seawater; the composition of the total salt component is: 55% chloride, 30.6% sodium, 7.7% sulfate, 3.7% magnesium , 1.2% calcium, 1.1% potassium, and 0.7% minor constituents.

Figure 12.30: A graph with temperatures in Celsius increasing toward the right along the x-axis, from 0 to 24 degrees. Depth in meters increases downward along the y-axis, from 0 to 7,000. A curve on the graph goes from 0 meters depth and 24 degrees Celsius downward and abruptly moves toward the left at approximately 100 meters depth until it reaches 6 degrees Celsius and 1000 meters depth; from there it changes to nearly vertical downward.

Figure 12.31: A unitless graph with density increasing toward the right along the x-axis and depth increasing downward along the y-axis. A curve on the graph goes from 0 depth and low density straight down until it abruptly moves toward the right at still shallow depth; after it reaches a deeper depth, it changes to nearly vertical downward.

Figure 12.32: Cross section of the ocean from 60 degrees North latitude on the left, 0 degrees latitude in the middle, and 60 degrees South latitude on the right. There are three colored areas within the ocean: a dark teal zone labeled the deep zone that takes up 80% of the filled-in area. This zone makes up the entire bottom of the ocean until the transition zone above, which is colored medium teal and takes up 18% of the area in the figure. Above the transition zone is a small light blue lens labeled surface mixed zone which takes up 2% of the area.

Figure 12.33: World map with a black loop running across the Pacific Ocean from west to east, traveling south of the tip of South America, then north through the Atlantic Ocean. When the line reaches the mid-North Atlantic, it curves back down off the west coast of Europe and then Africa, traveling southwest to the eastern coast of South America and then traveling toward the east where it passes south of Africa then south of Australia. It then turns back westward and travels among southeast Asian islands before continuing east across the Pacific where the loop is completed. A separate smaller red loop is shown circling around the north Atlantic Ocean.

Figure 12.34: Simple diagram showing a red and white boat on the surface of the ocean with a blue bar labeled transducer at the bottom of the boat. Two purple arrows go between the boat and ocean floor, labeled transmitted and returned acoustic pulse. The first arrow travels vertically down to the ocean floor from the boat and the second arrow points up from the ocean floor to the boat, labeled capital D. The diagram states Measured depth is function of: pulse travel time (t) and pulse velocity in water (v). Beneath the text is the following equation: D = 1/2*v*t

Figure 12.35: Diagram showing a GPS satellite receiving a signal from an altimeter device in low orbit above the ocean. There are three white dashed lines that travel from the altimeter to the surface: one travels vertically down to the ocean surface and the other two travel down to the surface of an island, labeled Laser station and Doris station.

Figure 12.36: Map of the North Atlantic Ocean with a black line drawn from northeast North America to West Africa. Along the line are five labels: at the edge of North America is the continental margin, toward the deeper ocean is the deep ocean basin, and in the middle of the ocean is the mid-ocean ridge. Continuing along the line there is another deep ocean basin east of the mid-ocean ridge and then another continental margin off the west coast of Africa.

Figure 12.37: Cross sectional diagram of black oceanic crust on the left transitioning to orange continental crust on the right, with olive green mantle beneath both. Above both the oceanic and continental crust is a yellow layer labeled sediment, and there is blue ocean water above that. Deep ocean is on the left, and it gets shallower toward the right as the sediment slopes upward. The continental rise is labeled where deep ocean water begins to get shallower, the continental slope is labeled where there's a steeper slope to the right of the rise, and the continental shelf is labeled where the slope of sediment flattens out again beneath shallow ocean water.

Figure 12.38: Block diagram showing tan oceanic lithosphere beneath the ocean on the left traveling toward the right and then sloping downward into the orange asthenosphere when it reaches continental crust on the right. Above the sloping lithosphere are red dashes moving vertically upward toward a volcano on the overriding continental crust, where there is a volcanic arc. Just off the coast of the continental crust is a deep groove at the bottom of the ocean labeled trench.

Figure 12.39: Depth map of Mariana Trench. Japan is labeled near the top of the map, colored light green to indicate above sea level; Indonesia and Papua New Guinea are labeled near the bottom of the map, all colored light green to indicate elevation above sea level reaching nearly 4,000 meters. Nearly vertical with a slight arch is the Mariana Trench at the center of the map. colored dark blue to indicate depth below sea level reaching over 10,000 meters deep. The Challenger Deep location is marked with a pink star near the southern part of the Mariana Trench.

Figure 12.40: Gray and white world map with interconnected red hatched lines marking the location of mid-ocean ridges. The lines are connected as follows: one line travels north to south through the Atlantic Ocean, connecting to a northeast-trending line south of Africa, connecting to a north to south line east of Africa and south of Asia, then traveling toward the east, south of Australia. The line continues east until it curves toward the north when it reaches west of South America. The north-trending line continues until it reaches the west coast of North America.

13. DESERTS AND GLACIERS

Learning Objectives

By the end of this chapter, students should be able to:

- Explain the defining characteristics of a desert, and distinguish among the broad categories of deserts.
- Explain how geographic features, latitude, atmospheric circulation, and Coriolis effect influence where deserts are located.
- List the primary desert weathering and erosion processes and resulting landforms.
- Identify desert landforms, and explain how they are formed by erosion and deposition.
- Describe the main types of sand dunes and the conditions that form them.
- Differentiate the different types of glaciers, and contrast them with sea icebergs.
- Describe how glaciers form, move, and create landforms.
- Describe glacial budget; describe the zones of accumulation, equilibrium, and melting.
- Describe the history and causes of past glaciations and their relationship to climate, sea-level changes, and isostatic rebound.

At first glance, deserts and glaciers may seem like opposites—one conjures images of endless heat and aridity, while the other evokes thoughts of frozen, icy expanses. However, both deserts and glaciers are part of a larger conversation about extreme environments shaped by similar geological forces. These landscapes are defined by scarcity, either of water or warmth, and both are profoundly influenced by processes of erosion, deposition, and weathering.

Deserts, which cover about one-third of the Earth's land surface, are characterized by their dry conditions, where evaporation exceeds precipitation. Although glaciers are composed of frozen water, they can be considered "frozen deserts" because they too exist in regions where precipitation is low, albeit in solid form. In both environments, the absence or freezing of water leads to unique landforms and geologic features. Understanding these landscapes not only enriches our appreciation of the diversity of Earth's environments but also highlights their vulnerability to climate change.

This chapter is divided into two parts; the first half explores the characteristics, formation, and geological processes of deserts, while the second half delves into the features and dynamics of glaciers.

13.1 The Origin of Deserts

Approximately 30% of the Earth's terrestrial surface consists of deserts, which are defined as locations of low precipitation. While temperature extremes are often associated with deserts, they do not define them. Deserts exhibit extreme temperatures because of the lack of moisture in the atmosphere, including low humidity and scarce cloud cover. Without cloud cover, the Earth's surface absorbs more of the Sun's energy during the day and emits more heat at night.

Figure 13.1: World hot deserts (BWh indicated in red). Figure description available at the end of the chapter.

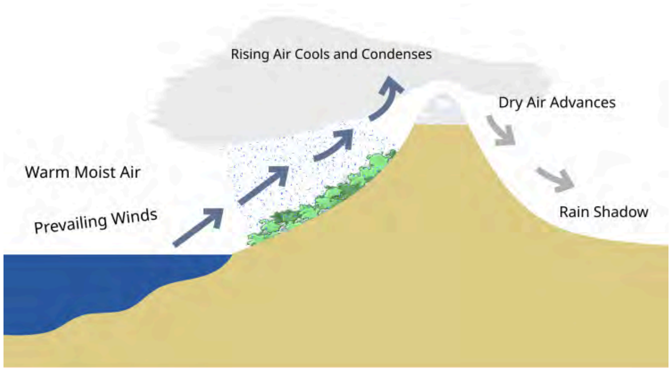

Figure 13.2: Mountainous areas in front of the prevailing winds create a rain shadow. Figure description available at the end of the chapter.

Deserts are not randomly located on the Earth's surface. Many deserts are located at latitudes between 15° and 30° in both hemispheres and at both the North and South Poles, created by prevailing wind circulation in the atmosphere. Sinking, dry air currents occurring at 30° north and south of the equator produce **trade wind deserts** like the African Sahara and Australian Outback.

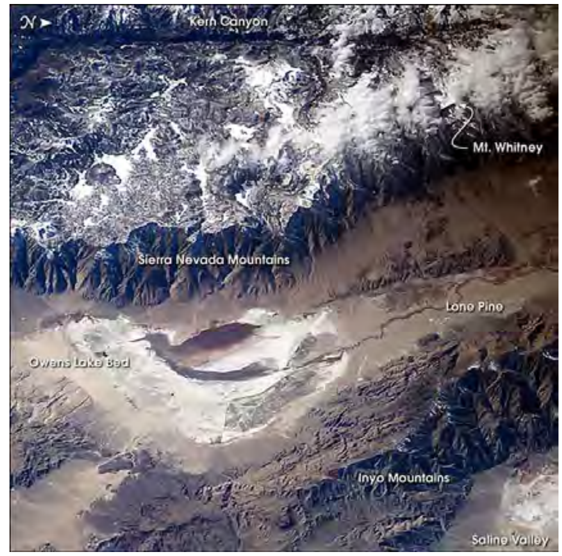

Figure 13.3: In this image from the ISS, the Sierra Nevada Mountains are perpendicular to prevailing westerly winds, creating a rain shadow to the east (bottom of the image). Note the dramatic decrease in snow on the Inyo Mountains. Figure description available at the end of the chapter.

Another type of desert is found in the rain shadow created from prevailing winds blowing over mountain ranges. As the wind drives air up and over mountains, atmospheric moisture is released as snow or rain. Atmospheric pressure is lower at higher elevations, causing the moisture-laden air to cool. Cool air holds less moisture than hot air, and precipitation occurs as the wind rises up the mountain. After releasing its moisture on the windward side of the mountains, the dry air descends on the leeward, or downwind, side of the mountains to create an arid region with little precipitation called a **rain shadow**. Examples of rain-shadow deserts include the Western Interior Desert of North America and Atacama Desert of Chile, which is the Earth's driest warm desert.

Finally, **polar deserts**, such as vast areas of the Antarctic and Arctic, are created from sinking cold air that is too cold to hold much moisture. Although they are covered with ice and snow, these deserts have very low average annual precipitation. As a result, Antarctica is Earth's driest continent.

Video 13.1: Rain shadow

Access this YouTube video by scanning the QR code. ["Rain Shadow" by University of Illinois Extension | https://www.youtube.com/watch?v=iMu4dShS74w]

13.1.1 Atmospheric Circulation

Geographic location, atmospheric circulation, and the Earth's rotation are the primary causal factors of deserts. Solar energy converted to heat is the engine that drives the circulation of air in the atmosphere and water in the oceans. The strength of the circulation is determined by how much energy is absorbed by the Earth's surface, which in turn is dependent on the average position of the Sun relative to the Earth. In other words, the Earth is heated unevenly depending on latitude and angle of incidence. Latitude is a line circling the Earth parallel to the equator and is measured in degrees. The equator is 0°, and the North and South Poles are 90° N and 90° S, respectively (see Figure 13.4 for a diagram of generalized atmospheric circulation on Earth). **Angle of incidence** is the angle made by a ray of sunlight shining on the Earth's surface. Tropical zones are located near the equator, where the latitude and angle of incidence are close to 0°, and receive high amounts of solar energy. The poles, which have latitudes and angles of incidence approaching 90°, receive little or almost no energy.

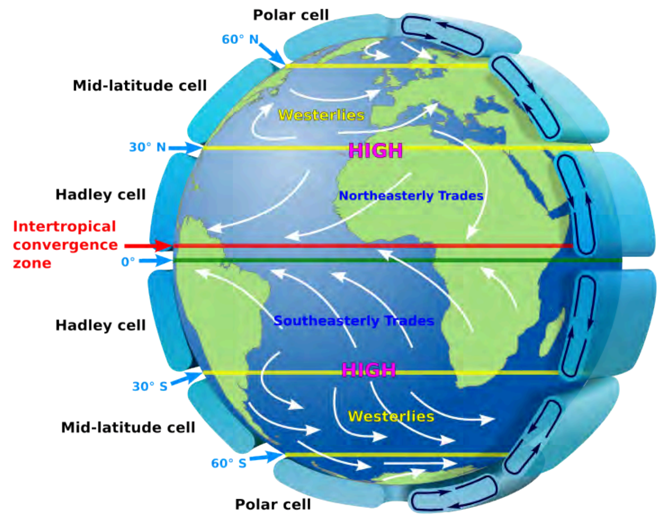

Figure 13.4: Generalized atmospheric circulation. Figure description available at the end of the chapter.

The figure shows the generalized air circulation within the atmosphere. Three cells of circulating air span the space between the equator and poles in both hemispheres, the Hadley cell, the Ferrel or midlatitude cell, and the polar cell. In the **Hadley cell**, located over the tropics and closest to the equatorial belt, the Sun heats the air and causes it to rise. The rising air cools and releases its contained moisture as tropical rain. The rising dried air spreads away from the equator and toward the North and South Poles, where it collides with dry air in the Ferrel cell. The combined dry air sinks back to the Earth at 30° latitude. This sinking drier air creates belts of predominantly high pressure at approximately 30° north and south of the equator, called the horse latitudes. Arid zones between 15° and 30° north and south of the equator thus exist, within which desert conditions predominate. The descending air flowing north and south in the Hadley and Ferrel cells also creates prevailing winds called **trade winds** near the equator and **westerlies** in the temperate zone. Note the arrows indicating general directions of winds in these zones.

Other deserts, like the Great Basin Desert that covers parts of Utah and Nevada, owe at least part of their origin to other atmospheric phenomena. The **Great Basin Desert**, while somewhat affected by sinking air effects from global circulation, is a rain-shadow desert. As westerly moist air from the Pacific rises over the Sierra Nevadas and other mountains, it cools and loses moisture as condensation and precipitation on the upwind, rainy side of the mountains.

Figure 13.5: USGS map of the Great Basin Desert. Figure description available at the end of the chapter.

Figure 13.6: Map of the Atacama Desert (yellow) and surrounding related climate areas (orange). Figure description available at the end of the chapter.

One of the driest places on Earth is the **Atacama Desert** of northern Chile. The Atacama Desert occupies a strip of land along Chile's coast just north of latitude 30°S, at the southern edge of the trade-wind belt. The desert lies west of the Andes Mountains, in the rain shadow created by prevailing trade winds blowing west. As this warm moist air crossing the Amazon basin meets the eastern edge of the mountains, it rises, cools, and precipitates much of its water out as rain. Once over the mountains, the cool, dry air descends onto the Atacama Desert. Onshore winds from the Pacific are cooled by the Peru (Humboldt) ocean current. This super-cooled air holds almost no moisture and, with these three factors, some locations in the Atacama Desert have received no measured precipitation for several years. This desert is the driest nonpolar location on Earth.

Notice in Figure 13.7 that the polar regions are also areas of predominantly high pressure created by descending cold dry air, the **polar cells**. As with the other cells, cold air, which holds much less moisture than warm air, descends to create polar deserts. This is why historically, land near the North and South Poles has always been so dry.

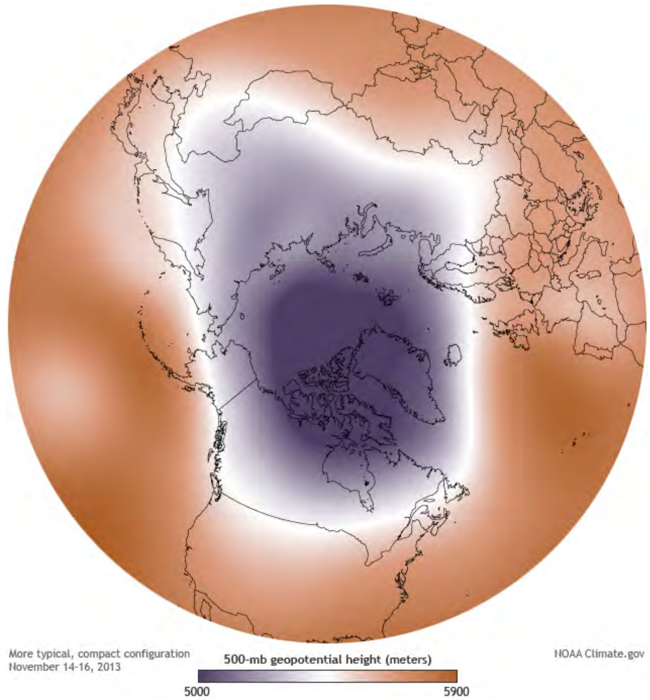

Figure 13.7: The polar vortex of mid-November, 2013. This cold, descending air (shown in purple) is characteristic of polar circulation. Figure description available at the end of the chapter.

13.1.2 Coriolis Effect

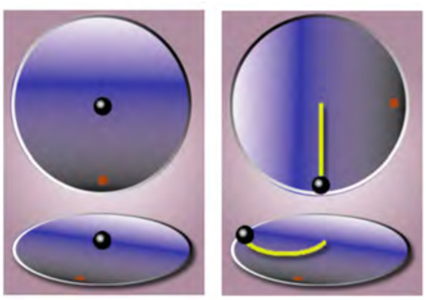

Figure 13.8: In the inertial frame of reference of the top picture, the ball moves in a straight line. The observer, represented as a red dot, standing in the rotating frame of reference sees the ball following a curved path. This perceived curvature is due to the Coriolis effect and centrifugal forces. Figure description available at the end of the chapter.

The Earth rotates toward the east, where the sun rises. Think of spinning a weight on a string around your head. The speed of the weight depends on the length of the string. The speed of an object on the rotating Earth depends on its horizontal distance from the Earth's axis of rotation. Higher latitudes are a smaller distance from the Earth's rotational axis and therefore do not travel as fast eastward as lower latitudes that are closer to the equator. When a fluid like air or water moves from a lower latitude to a higher latitude, the fluid maintains its momentum from moving at a higher speed, so it will travel relatively faster eastward than the Earth beneath at the higher latitudes. This factor causes deflection of movements that occur in north-south directions.

Another factor in the Coriolis effect also causes deflection of east-west movement due to the angle between the centripetal effect of Earth's spin and gravity pulling toward the Earth's center (see Figure 13.9). This produces a net deflection toward the equator. The total Coriolis deflection on a mass moving in any direction on the rotating Earth results from a combination of these two factors.

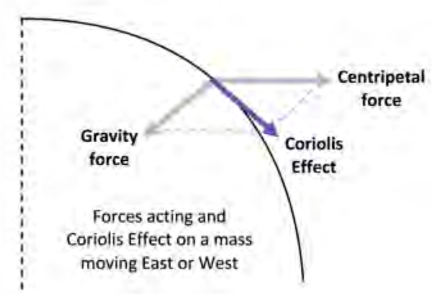

Figure 13.9: Forces acting on a mass moving east–west on the rotating Earth that produce the Coriolis effect. Figure description available at the end of the chapter.

Since each hemisphere has three atmospheric cells moving respectively north and south relative to the Earth beneath them, the Coriolis effect deflects these moving air masses to the right in the Northern Hemisphere and to the left in the Southern Hemisphere. The Coriolis effect also deflects moving masses of water in the ocean currents.

For example, in the Northern Hemisphere Hadley cell, the lower altitude air currents are flowing south toward the equator. These are deflected to the right (or west) by the Coriolis effect. This deflected air generates the prevailing trade winds that European sailors used to cross the Atlantic Ocean and reach South America and the Caribbean Islands in their tall ships. This air movement is mirrored in the Hadley cell in the Southern Hemisphere; the lower-altitude air current flowing toward the equator is deflected to the left, creating trade winds that blow to the northwest.

In the northern Ferrel, or midlatitude, cell, surface air currents flow from the horse latitudes (latitude 30˚) toward the North Pole, and the Coriolis effect deflects them toward the east or to the right, producing the zone of westerly winds. In the Southern Hemisphere Ferrel cell, the poleward flowing surface air is deflected to the left and flows southeast, creating the Southern Hemisphere westerlies.

Another Coriolis-generated deflection produces the polar cells. At 60˚ north and south latitude, relatively warmer rising air flows poleward, cooling and converging at the poles where it sinks in the polar high. This sinking dry air creates the polar deserts, the driest deserts on Earth. The persistence of ice and snow is a result of cold temperatures at these dry locations.

Figure 13.10: Inertia of air masses caused by the Coriolis effect in the absence of other forces. Figure description available at the end of the chapter.

The Coriolis effect operates on all motions on the Earth. Artillerymen must take the Coriolis effect into account on ballistic trajectories when making long-distance targeting calculations. Geologists note how its effect on air and oceanic currents creates deserts in designated zones around the Earth as well as creating the surface currents in the ocean. The Coriolis effect causes the ocean gyres to turn clockwise in the Northern Hemisphere and counterclockwise in the Southern. It also affects weather by creating high-altitude, polar jet streams that sometimes push lobes of cold arctic air into the temperate zone, down to as far as latitude 30˚ from the usual 60˚. It also causes low-pressure systems and intense tropical storms to rotate counterclockwise in the Northern Hemisphere and clockwise in the Southern Hemisphere.

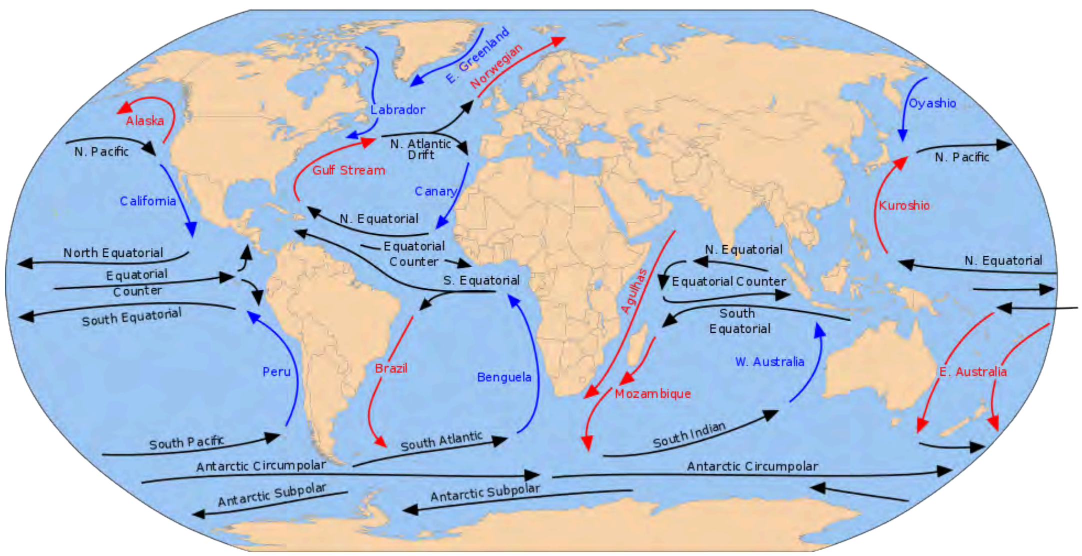

Figure 13.11: Gyres of the Earth's oceans. Figure description available at the end of the chapter.

Video 13.2: The Coriolis effect

Access this YouTube video by scanning the QR code. ["The Coriolis Effect Explained" by Atlas Pro | https://www.youtube.com/watch?v=HIyBpi7B-dE]

Take this quiz to check your comprehension of this section.

Access the quiz for Section 13.1 by scanning the QR code.

13.2 Desert Processes

13.2.1 Desert Weathering and Erosion

Figure 13.12: Weathering and erosion of Canyonlands National Park has created a unique landscape that includes arches, cliffs, and spires. Figure description available at the end of the chapter.

Weathering takes place in desert climates by the same means as other climates, only at a slower rate. While higher temperatures typically spur faster chemical weathering, water is the main agent of weathering, and lack of water slows both mechanical and chemical weathering. Low precipitation levels also mean less runoff as well as ice wedging. When precipitation does occur in the desert, it is often heavy and may result in flash floods in which a lot of material may be dislodged and moved quickly.

Figure 13.13: Newspaper Rock, located in Petrified Forest National Park, is a site with many petroglyphs carved into desert varnish. Figure description available at the end of the chapter.

One unique weathering product in deserts is **desert varnish**. Also known as desert patina or rock rust, this is thin dark-brown layers of clay minerals and iron and manganese oxides that form on very stable surfaces within arid environments. The exact way this material forms is still unknown, though cosmogenic and biologic mechanisms have been proposed.

Figure 13.14: A dust storm (haboob) hits Texas in 2019. Figure description available at the end of the chapter.

While water is still the dominant agent of erosion in most desert environments, wind is a notable agent of weathering and erosion in many deserts. This includes suspended sediment traveling in **haboobs**, or large dust storms, that frequent deserts. Deposits of windblown dust are called loesses. Loess deposits cover wide areas of the Midwestern United States, much of it from rock flour that melted out of the ice sheets during the last ice age. Loess was also blown from desert regions in the West. Possessing lower energy than water, wind transport nevertheless moves sand, silt, and dust. As noted in Chapter 11, the load carried by a fluid (air is a fluidlike water) is distributed among bedload and suspended load. As with water, in wind these components depend on wind velocity.

Sand-sized material moves by a process called **saltation** in which sand grains are lifted into the moving air and carried a short distance, where they drop and splash into the surface, dislodging other sand grains that are then carried a short distance and splash, dislodging still others.

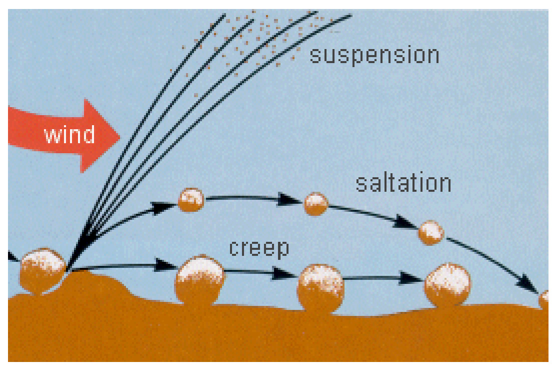

Figure 13.15: Diagram showing the mechanics of saltation. Figure description available at the end of the chapter.

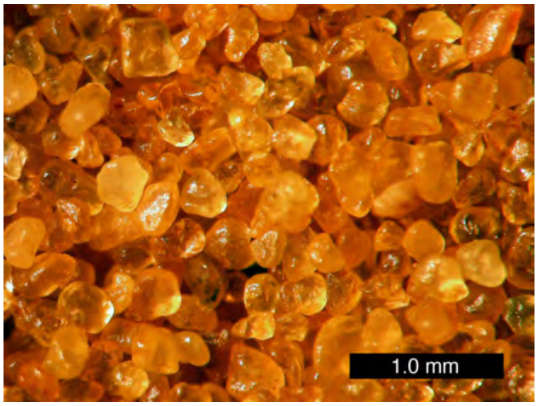

Figure 13.16: Enlarged image of frosted and rounded windblown sand grains. Figure description available at the end of the chapter.

Since saltating sand grains are constantly impacting other sand grains, wind-blown sand grains are commonly quite well rounded, with frosted surfaces. Saltation is a cascading effect of sand movement, creating a zone of windblown sand up to a meter or so above the ground. This zone of saltating sand is a powerful erosive agent in which bedrock features are effectively sandblasted. The fine-grained suspended load is effectively sorted from the sand near the surface, carrying the silt and dust into haboobs. Wind is thus an effective sorting agent separating sand and dust-sized (≤70 μm) particles (see Chapter 5). When wind velocity is high enough to slide or roll materials along the surface, the process is called creep.

Figure 13.17: A sailing stone at Racetrack Playa in Death Valley National Park, California. Figure description available at the end of the chapter.

One extreme version of sediment movement was shrouded in mystery for years: sliding stones. Also called **sailing stones** and sliding rocks, these are large boulders that move along flat surfaces in deserts, leaving trails. This includes the famous example of the Racetrack Playa in Death Valley National Park, California. For years, scientists and enthusiasts attempted to explain their movement, with few definitive results. In recent years, several experimental and observational studies have confirmed that the stones, embedded in thin layers of ice, are propelled by friction from high winds. These studies include measurements of actual movement, as well as recreations of the conditions, with resulting movement in the lab.

Figure 13.18: (Top) A yardang near Meadow, Texas. (Bottom) Blowout near Earth, Texas. Figure description available at the end of the chapter.

The zone of saltating sand is an effective agent of erosion through sand abrasion. A bedrock outcrop which has such a sandblasted shape is called a **yardang**. Rocks and boulders lying on the surface may be blasted and polished by saltating sand. When predominant wind directions shift, multiple sandblasted and polished faces may appear. Such wind-abraded desert rocks are called **ventifacts**.

In places with sand and silt accumulations, clumps of vegetation often anchor sediment on the desert surface. Yet, winds may be sufficient to remove materials not anchored by vegetation. The bowl-shaped depression remaining on the surface is called a **blowout**.

Figure 13.19: Wind-carved ventifact in White Desert National Park, Egypt. Figure description available at the end of the chapter.

13.2.2 Desert Landforms

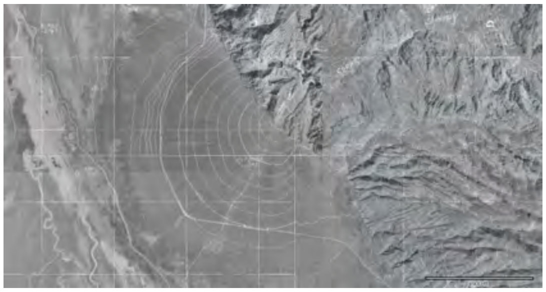

Figure 13.20: Aerial image of alluvial fan in Death Valley. Figure description available at the end of the chapter.

In the American Southwest, as streams emerge into the valleys from the adjacent mountains, they create desert landforms called alluvial fans. When a stream emerges from the narrow canyon, the flow is no longer constrained by the canyon walls and spreads out. At the lower slope angle, the water slows down and drops its coarser load. As the channel fills with this conglomeratic material, the stream is deflected around it. This deposited material deflects the stream into a system of radial distributary channels in a process similar to a delta's formation by a river entering a body of water. This process develops a system of radial distributaries and constructs a fan-shaped alluvial fan.

Figure 13.21: Bajada along Frisco Peak in Utah. Figure description available at the end of the chapter.

Alluvial fans continue to grow and may eventually coalesce with neighboring fans to form an apron of **alluvium** along the mountain front called a **bajada**.

Figure 13.22: Inselbergs in the Western Sahara. Figure description available at the end of the chapter.

As the mountains erode away and their sediment accumulates first in alluvial fans, then bajadas, the mountains eventually are buried in their own erosional debris. Such buried mountain remnants are called **inselbergs**, "island mountains," as first described by the German geologist Wilhelm Bornhardt (1864–1946).

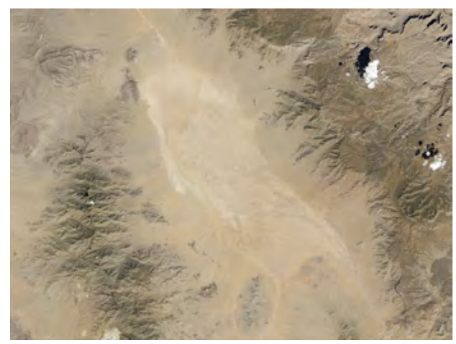

Figure 13.23: Satellite image of desert playa surrounded by mountains. Figure description available at the end of the chapter.

Where the desert valley is an enclosed basin—i.e., streams entering it do not drain out—the water is removed by evaporation and a dry lake bed called a playa is formed.

Figure 13.24: (Top) Dry wash (or ephemeral stream). (Bottom) Flash flood in a (different) dry wash. Figure description available at the end of the chapter.

Playas are among the flattest of all landforms. Such a dry lake bed may cover a large area and be filled after a heavy thunderstorm to only a few inches deep. Playa lakes and desert streams that contain water only after rainstorms are called intermittent or ephemeral. Because of intense thunderstorms, the volume of water transported by ephemeral drainage in arid environments can be substantial during a short period of time. Desert soil structures lack organic matter that promotes infiltration by absorbing water. Instead of percolating into the soil, the runoff compacts the ground surface, making the soil hydrophobic (i.e., water-repellant). Because of this hardpan surface, ephemeral streams may gather water across large areas, suddenly filling with water from storms many miles away.

High-volume ephemeral flows, called flash floods, may move as sheet flows or **sheetwash**; they can also be channeled through normally dry arroyos or canyons. Flash floods are a major factor in desert deposition. Dry channels can fill quickly with ephemeral drainage, creating a mass of water and debris that charges down the **arroyo**, even overflowing the banks. Flash floods pose a serious hazard for desert travelers because the storm activity feeding the runoff may be miles away. People hiking or camping in arroyos that have been bone dry for months or years have been swept away by sudden flash floods.

Figure 13.25: Antelope Canyon is a slot canyon in Arizona formed by the erosion of Navajo Sandstone. It is susceptible to flash flooding, even from rain falling miles away. Figure description available at the end of the chapter.

13.2.3 Sand

Figure 13.26: A sand sea or erg in the Sahara Desert. Figure description available at the end of the chapter.

The popular concept of a typical desert is a broad expanse of sand. Geologically, deserts that are defined by a lack of water and arid regions resembling seas of sand belong to the category of desert called an **erg**. An erg consists of fine-grained, loose sand grains, often blown by wind, or aeolian forces, into dunes. Probably the best known erg is the Rub' al Khali, which means empty quarter, of the Arabian Peninsula. Ergs are also found in the Great Sand Dunes National Park (Colorado), Little Sahara Recreation Area (Utah), White Sands National Monument (New Mexico), and parts of Death Valley National Park (California). Ergs are not restricted to deserts but may form anywhere there is a substantial supply of sand, including as far north as 60° N in Saskatchewan, Canada, in the Athabasca Sand Dunes Provincial Park. Coastal ergs exist along lakes and oceans as well, and examples are found in Oregon, Michigan, and Indiana.

An internal cross section of a sand dune shows a feature called cross-bedding. As wind blows up the windward side of the dune, it carries sand to the dune crest, depositing layers of sand parallel to the windward (or "stoss") side. The sand builds up the crest of the dune and pours over the top until the leeward (downwind or slip) face of the dune reaches the **angle of repose**, the maximum angle which will support the slip face. Dunes are unstable features and move as the sand erodes from the stoss side and continues to drop down the leeward side, covering previous stoss and slip-face layers and creating the cross-beds. Mostly, these are reworked over and over again, but occasionally, the features are preserved in a depression, then lithified. Shifting wind directions and abundant sand sources create chaotic patterns of cross-beds like those seen in Zion National Park of Utah.

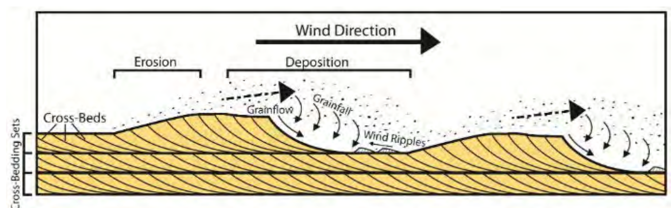

Figure 13.27: Formation of cross-bedding in sand dunes. Figure description available at the end of the chapter.

In the Mesozoic Era, Utah was covered by a series of ergs, with the thickest being in southern Utah, which lithified into sandstone (see Chapter 5). Perhaps the best known of these sandstone formations is the Navajo Sandstone of Jurassic age. This sandstone formation consists of dramatic cliffs and spires in Zion National Park and covers a large part of the Colorado Plateau. In Arches National Park, a later series of sand dunes covered the Navajo Sandstone and lithified to become the Entrada Formation also during the Jurassic. Erosion of overlying layers exposed fins of the underlying Entrada Sandstone and carved out weaker parts of the fins forming the arches.

Figure 13.28: Cross-beds in the Navajo Sandstone at Zion National Park. Figure description available at the end of the chapter.

As the cements that hold the grains together in these modern sand cliffs disintegrate and the freed grains gather at the base of the cliffs and move down the washes, sand grains may be recycled and redeposited. These Mesozoic sand ergs may represent ancient quartz sands recycled many times from igneous origins in the early Precambrian, just passing now through another cycle of erosion and deposition. An example of this is Coral Pink Sand Dunes State Park in southwestern Utah, which contains sand that is being eroded from the Navajo Sandstone to form new dunes.

13.2.4 Dune Types

Figure 13.29: NASA image of barchan dune field in coastal Brazil. Figure description available at the end of the chapter.

Dunes are complex features formed by a combination of wind direction and sand supply, in some cases interacting with vegetation. There are several types of dunes representing variables of wind direction, sand supply, and vegetative anchoring. Crescent-shaped **barchan dunes** form where sand supply is limited and there is a fairly constant wind direction. Barchans move downwind and develop a crescent shape with wings on either side of a dune crest. Barchans are known to actually move over homes, even towns.

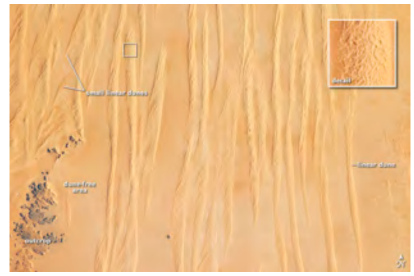

Figure 13.30: Satellite image of longitudinal dunes in Egypt. Figure description available at the end of the chapter.

Longitudinal dunes, or **linear dunes**, form where sand supply is greater and the wind blows a dominant direction in a back-and-forth manner. They may form ridges tens of meters high lined up with the predominant wind directions.

Parabolic dunes form where vegetation anchors parts of the sand and unanchored parts blow out. Parabolic dune shape may be similar to barchan dunes but usually reversed, and it is determined more by the anchoring vegetation than a strict parabolic form.

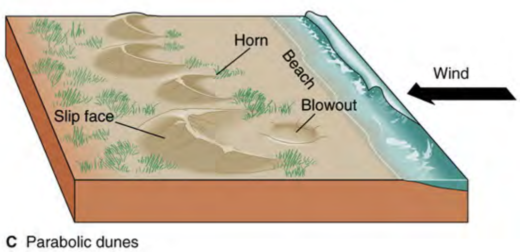

Figure 13.31: Parabolic dunes. Figure description available at the end of the chapter.

Star dunes form where the wind direction is variable in all directions. Sand supply can range from limited to quite abundant. It is the variation in wind direction that forms the star.

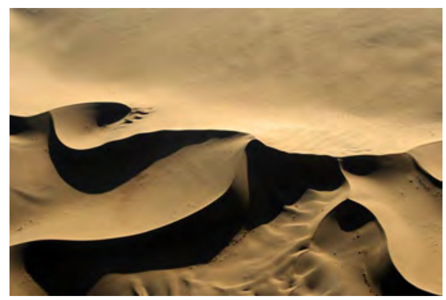

Figure 13.32: Star dune in Namib Desert. Figure description available at the end of the chapter.

Take this quiz to check your comprehension of this section.

Access the quiz for Section 13.2 by scanning the QR code.

13.3 The Great Basin and the Basin and Range

The Great Basin is the largest area of interior drainage in North America, meaning there is no outlet to the ocean and all precipitation remains in the basin or is evaporated. It covers western Utah, most of Nevada, and extends into southeastern California, southern Oregon, and southern Idaho. Because there is no outlet to the ocean, streams in the Great Basin deliver runoff to lakes and playas within the basin. A subregion within the Great Basin is the Basin and Range, which extends from the Wasatch Front in Utah west across Nevada to the Sierra Nevada Mountains of California. The basins and ranges referred to in the name are horsts and grabens, formed by normal fault blocks from crustal extension, as discussed in Chapters 2 and 9. The lithosphere of the entire area has stretched by a factor of about 2, meaning from end to end, the distance has doubled over the past 30 million years or so. Valleys without outlets form individual basins, each of which is filled with alluvial sediments leading into playa depositional environments. During the recent ice age, the climate was more humid, and while glaciers were forming in some of the mountains, pluvial lakes formed over large areas. During the ice age, valleys in much of western Utah and eastern Nevada were covered by Lake Bonneville. As the climate became arid after the ice age, Lake Bonneville dried, leaving as a remnant the Great Salt Lake in Utah.

Figure 13.33: The Great Basin. [Figure description available at the end of the chapter](#).


Figure 13.34: Typical Basin and Range scene. Ridgecrest, CA, sits just east of the southern Sierra Nevada Mountains. [Figure description available at the end of the chapter](#).

The desert of the Basin and Range extends from about 35˚ to near 40˚ and results from a rain shadow effect created by westerly winds from the Pacific rising and cooling over the Sierras, becoming depleted of moisture by precipitation on the western side. The result is relatively dry air descending across Nevada and western Utah.

A journey from the Wasatch Front southwest to the Pacific Ocean will show stages of desert landscape evolution from the fault block mountains of Utah with sharp peaks and alluvial fans at the mouths of canyons, through landscapes in Southern Nevada with bajadas along the mountain fronts, to the landscapes in the Mojave Desert of California with subdued inselbergs sticking up through a sea of coalesced bajadas. These landscapes illustrate the evolutionary stages of desert landscape development.

13.3.1 Desertification

When previously arable land suitable for agriculture transforms into desert, this process is called **desertification**. Plants and humus-rich soil (see Chapter 5) promote groundwater infiltration and water retention. When an area becomes more arid due to changing environmental conditions, the plants and soil become less effective in retaining water, creating a positive feedback loop of desertification. This self-reinforcing loop spirals into increasingly arid conditions and further enlarges the desert regions.

Desertification may be caused by human activities, such as unsustainable crop-cultivation practices, overgrazing by livestock, overuse of groundwater, and global climate change. Human-caused desertification is a serious worldwide problem. The world map figure above shows what areas are most vulnerable to desertification. Note the red and orange areas in the Western and Midwestern regions of the United States, which also cover large areas of arable land used for raising food crops and animals. The creation of the Dust Bowl in the 1930s (see Chapter 5) is a classic example of a high-vulnerability region impacted by human-caused desertification. As demonstrated in the Dust Bowl, conflicts may arise between agricultural practices and conservation measures. Mitigating desertification while allowing farmers to make a survivable living requires public and individual education to create community support and understanding of sustainable agriculture alternatives.

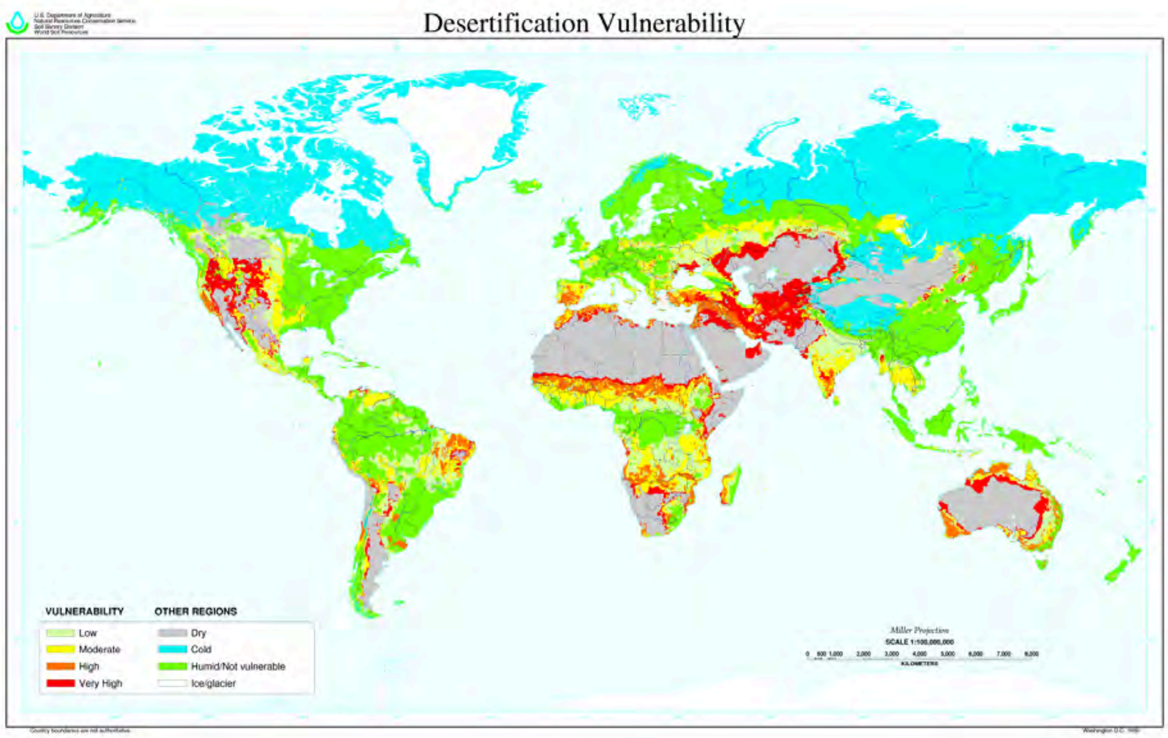

Figure 13.35: World map showing desertification vulnerability. Figure description available at the end of the chapter.

Take this quiz to check your comprehension of this section.

Access the quiz for Section 13.3 by scanning the QR code.

13.4 Glaciers

The Earth's cryosphere, or ice, has a unique set of erosional and depositional features compared to its hydrosphere, or liquid water. This ice exists primarily in two forms, glaciers and icebergs. **Glaciers** are large accumulations of ice that exist year-round on the land surface. In contrast, masses of ice floating on the ocean are icebergs, although they may have had their origin in glaciers.

Figure 13.36: Glacier in the Bernese Alps. Figure description available at the end of the chapter.

Glaciers cover about 10% of the Earth's surface and are powerful erosional agents that sculpt the planet's surface. These enormous masses of ice usually form in mountainous areas that experience cold temperatures and high precipitation. Glaciers also occur in low-lying areas such as Greenland and Antarctica that remain extremely cold year-round.

13.4.1 Glacier Formation

Figure 13.37: Alpine glaciers of the Alps visible from an airplane en route from Milan, Italy, to Munich, Germany. Figure description available at the end of the chapter.

Glaciers form when repeated annual snowfall accumulates as deep layers of snow that are not completely melted in the summer. Thus there is an accumulation of snow that builds up into deep layers. Perennial snow is a snow accumulation that lasts all year. A thin accumulation of perennial snow is a snow field. Over repeated seasons of perennial snow, the snow settles, compacts, and bonds with underlying layers. The amount of void space between the snow grains diminishes. As the old snow gets buried by more new snow, the older snow layers compact into **firn**, or névé, a granular mass of ice crystals. As the firn continues to be buried, compressed, and recrystallizes, the void spaces become smaller and the ice becomes less porous, eventually turning into glacier ice. Solid glacial ice still retains a fair amount of void space that traps air. These small air pockets provide records of the past atmosphere composition.

There are three general types of glaciers: alpine or **valley glaciers**, ice sheets, and ice caps. Most **alpine glaciers** are located in the world's major mountain ranges such as the Andes, Rockies, Alps, and Himalayas, usually occupying long, narrow valleys. Alpine glaciers may also form at lower elevations in areas that receive high annual precipitation such as the Olympic Peninsula in Washington State.

Ice sheets, also called **continental glaciers**, form across millions of square kilometers of land and are thousands of meters thick. Earth's largest ice sheets are located on Greenland and Antarctica. The Greenland ice sheet is the largest ice mass in the Northern Hemisphere, with an extensive surface area of over 2 million sq km (1,242,700 sq mi) and an average thickness of up to 1,500 meters (5,000 ft, almost a mile).

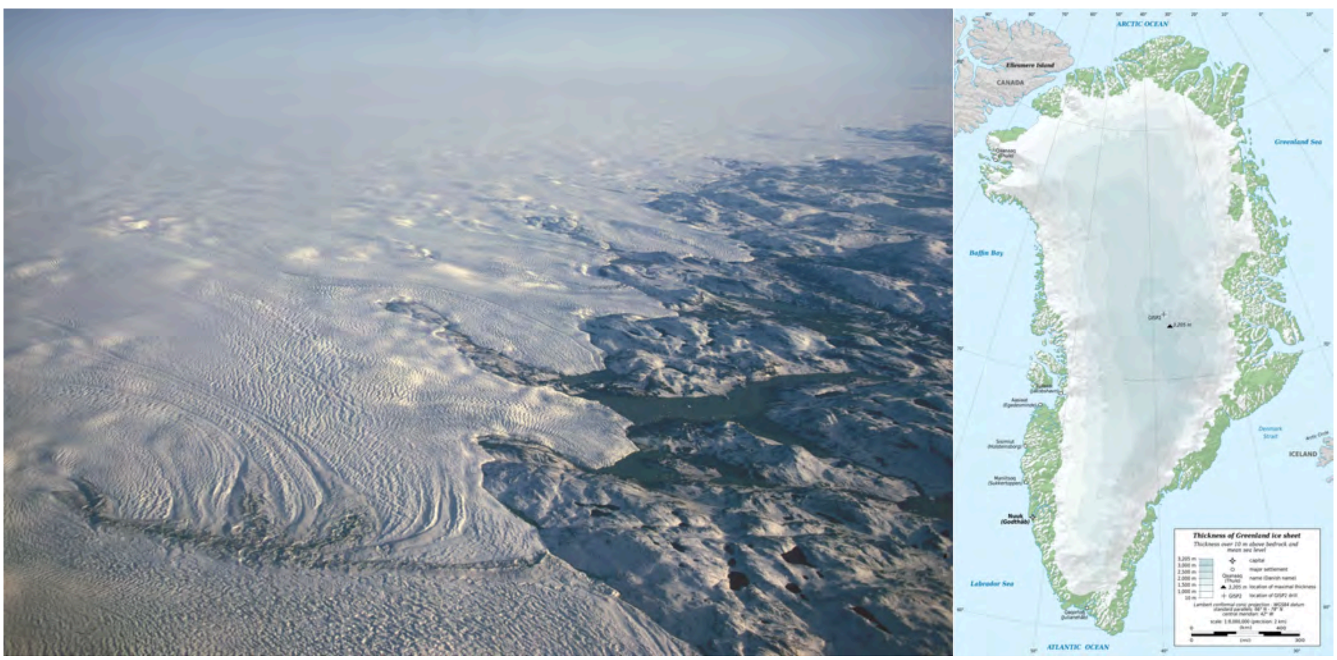

Figure 13.38: (Left) Greenland ice sheet. (Right) Map showing the thickness of the Greenland ice sheet in meters. Figure description available at the end of the chapter.

The Antarctic ice sheet is even larger and covers almost the entire continent. The thickest parts of the Antarctic ice sheet are over 4,000 meters thick (>13,000 ft or 2.5 mi). Its weight depresses the Antarctic bedrock to below sea level in many places. The cross-sectional diagram comparing the Greenland and Antarctica ice sheets illustrates the size difference between the two.

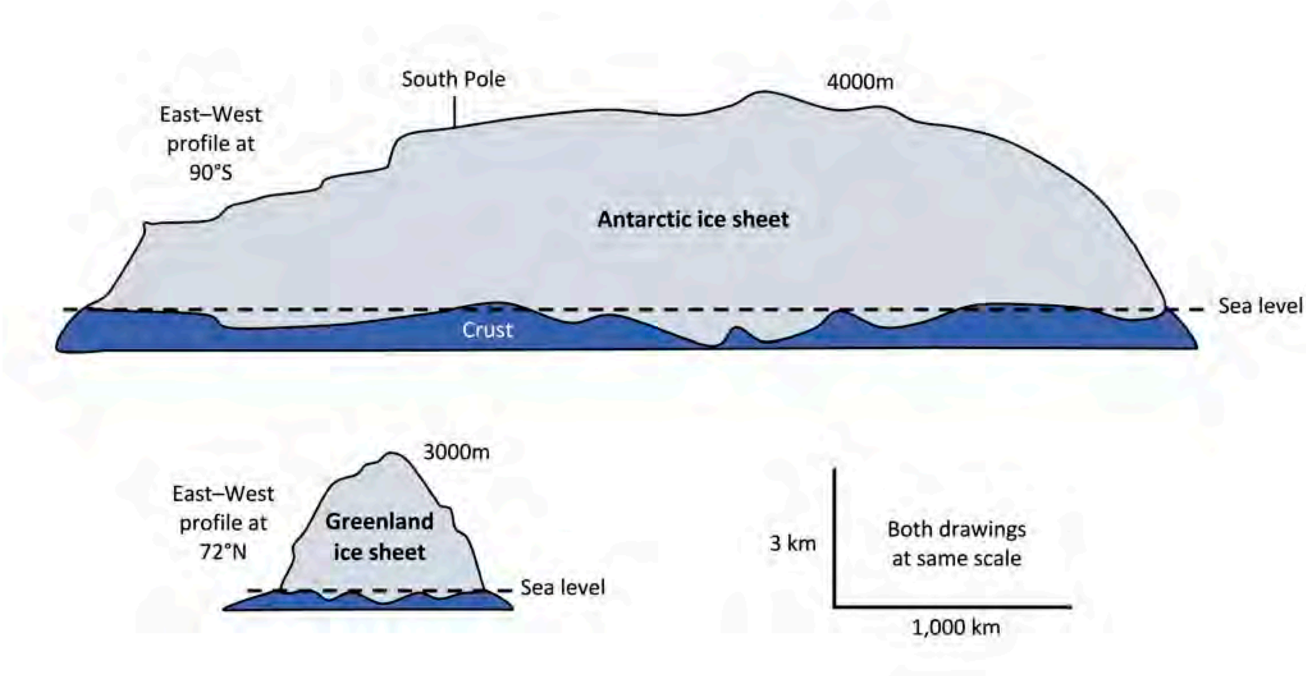

Figure 13.39: Cross-sectional view of both Greenland and Antarctic ice sheets drawn to scale for size comparison. Figure description available at the end of the chapter.

Ice cap glaciers are smaller versions of ice sheets that cover less than 50,000 km^2, usually occupy higher elevations, and may cover tops of mountains. There are several ice caps on Iceland. A small ice cap called Snow Dome is near Mount Olympus on the Olympic Peninsula in the state of Washington.

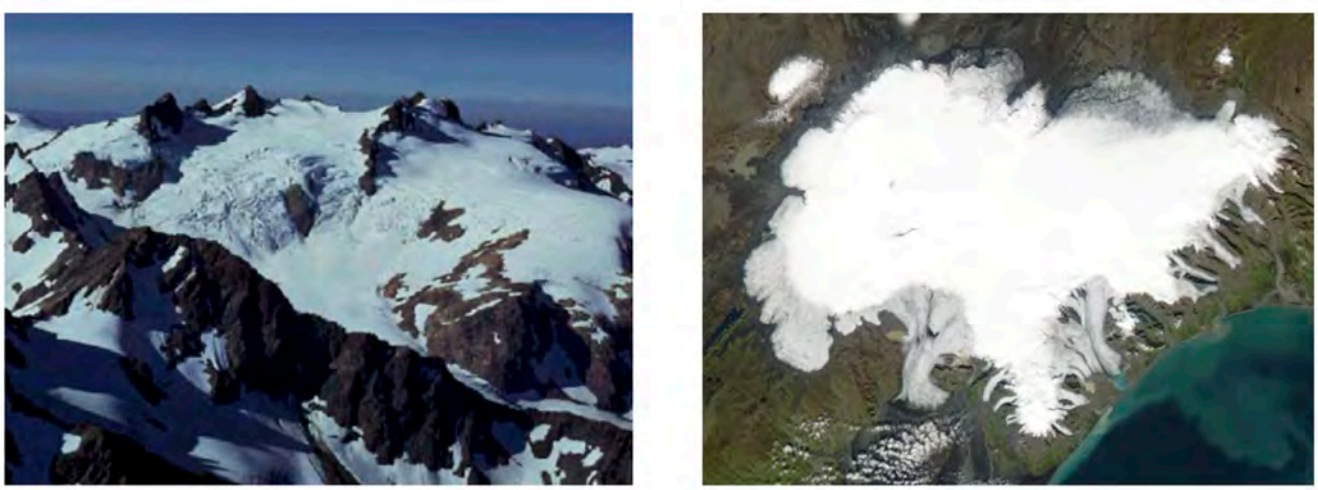

Figure 13.40: Snow Dome ice cap near Mount Olympus, Washington (left), and Vatnajökull ice cap in Iceland (right). Figure description available at the end of the chapter.

Figure 13.41: Maximum extent of Laurentide ice sheet. Figure description available at the end of the chapter.

The figure shows the size of the ancient Laurentide ice sheet in the Northern Hemisphere. This ice sheet was present during the last glacial maximum event, also known as the last ice age.

Take this quiz to check your comprehension of this section.

Access the quiz for Section 13.4 by scanning the QR code.

13.5 Glacier Dynamics

13.5.1 Glacier Movement

Figure 13.42: Glacial crevasses (left) and crevasse on the Easton Glacier in the North Cascades (right). Figure description available at the end of the chapter.

As the ice accumulates, it begins to flow downward under its own weight. In 1948, glaciologists installed hollow vertical rods in the Jungfraufirn Glacier in the Swiss Alps to measure changes in its movement over two years. This study showed that the ice at the surface was fairly rigid and ice within the glacier was actually flowing downhill. The cross-sectional diagram of an alpine (valley) glacier shows that the rate of ice movement is slow near the bottom and fastest in the middle, with the top ice being carried along on the ice below.

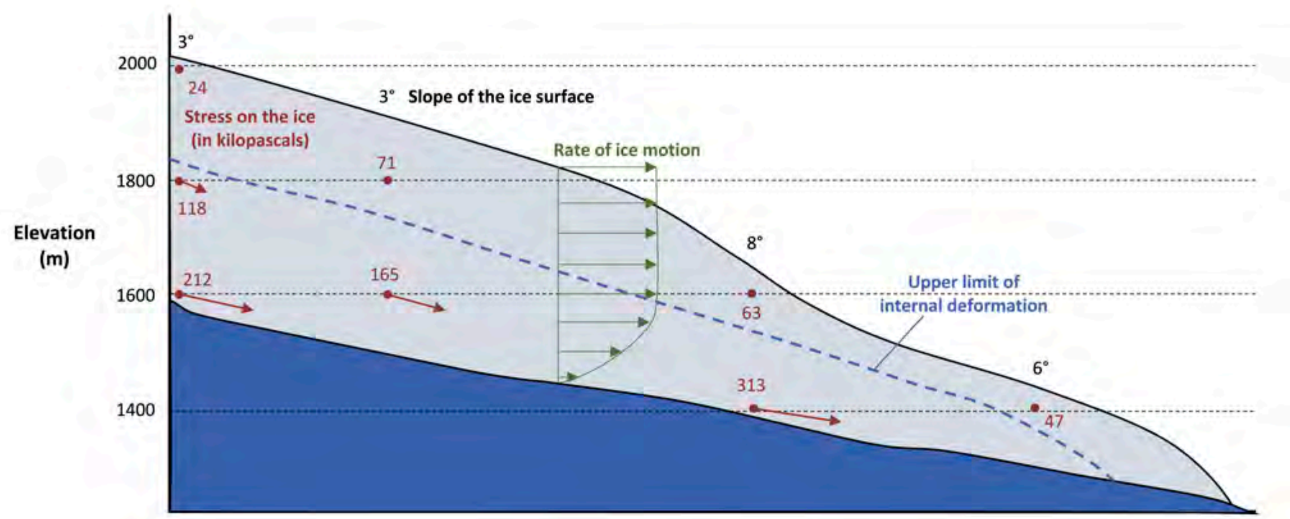

Figure 13.43: Cross section of a valley glacier showing stress (red numbers) increase with depth under the ice. The ice will deform and flow where the stress is greater than 100 kilopascals, and the relative extent of that deformation is depicted by the red arrows. Downslope movement is shown with blue arrows. The upper ice above the red dashed line does not flow but is pushed along en masse. Figure description available at the end of the chapter.

One of the unique properties of ice is that it melts under pressure. About half of the overall glacial movement was from sliding on a film of meltwater along the bedrock surface, with the other half from internal flow. Ice near the surface of the glacier is rigid and brittle to a depth of about 50 m (165 ft). In this brittle zone, large ice cracks called **crevasses** form on the glacier's moving surface. These crevasses can be covered and hidden by a snow bridge and are a hazard for glacier travelers.

Below the brittle zone, the pressure typically exceeds 100 kilopascals (kPa), which is approximately 100,000 times atmospheric pressure. Under this applied force, the ice no longer breaks, but rather it bends or flows in a zone called the plastic zone. This plastic zone represents the great majority of glacier ice. The plastic zone contains a fair amount of sediment of various grades from boulders to silt and clay. As the bottom of the glacier slides and grinds across the bedrock surface, these sediments act as grinding agents and create a zone of significant erosion.

13.5.2 Glacial Budget

A **glacial budget** is like a bank account, with the ice being the existing balance. If there is more income (snow accumulating in winter) than expense (snow and ice melting in summer), then the glacial budget shows growth. A positive or negative balance of ice in the overall glacial budget determines whether a glacier advances or retreats, respectively. The area in which the ice balance grows is called the **zone of accumulation**. The area where ice balance is shrinking is called the zone of ablation.

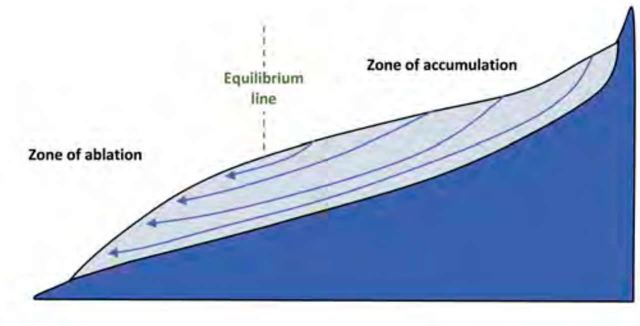

Figure 13.44: Cross-sectional view of an alpine glacier showing internal flow lines, zone of accumulation, snow line, and zone of ablation. Figure description available at the end of the chapter.

The diagram shows these two zones and the equilibrium line. In the zone of accumulation, the snow-accumulation rate exceeds the snow-melting rate and the ice surface is always covered with snow. The equilibrium line, also called the **snowline** or firnline, marks the boundary between the zones of accumulation and ablation. Below the equilibrium line in the zone of ablation, the melting rate exceeds snow accumulation, leaving the bare ice surface exposed. The position of the firnline changes during the season and from year to year as a reflection of a positive or negative ice balance in the glacial budget. Of the two variables affecting a glacier's budget, winter accumulation and summer melt, summer melt matters most to a glacier's budget. Cool summers promote glacial advance, and warm summers promote glacial retreat.

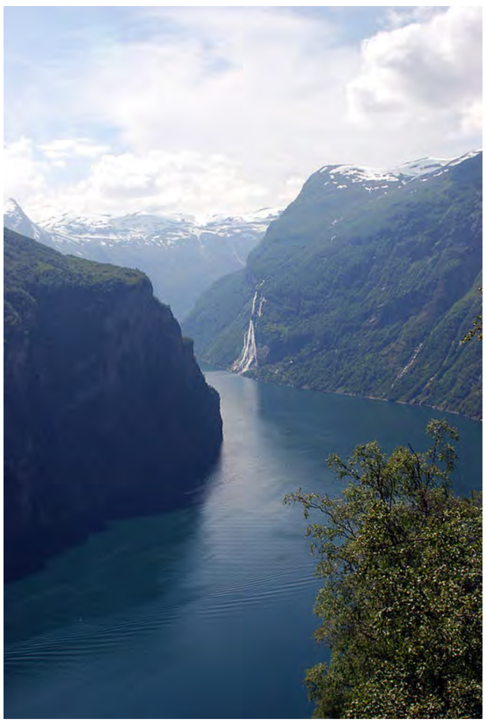

Figure 13.45: Fjord. Figure description available at the end of the chapter.

If a handful of warmer summers promote glacial retreat, then global climate warming over decades and centuries will accelerate glacial melting and retreat even faster. Global warming due to human burning of fossil fuels is causing the ice sheets to lose, in years, an amount of mass that would normally take centuries. Current glacial melting is contributing to sea levels rising more quickly than expected based on previous history.

As the Antarctica and Greenland ice sheets melt during global warming, they become thinner or deflate. The edges of the ice sheets break off and fall into the ocean in a process called **calving**, becoming floating icebergs. A fjord is a steep-walled valley flooded with seawater. The narrow shape of a fjord has been carved out by a glacier during a cooler climate period. During a warming trend, glacial meltwater may raise the sea level in fjords and flood formerly dry valleys. Glacial retreat and deflation are well illustrated in the 2009 TED Talk "Time-lapse proof of extreme ice loss" by James Balog.

Video 13.3: Time-lapse proof of extreme ice loss, by James Balog

Access this YouTube video by scanning the QR code. ["Time-lapse proof of extreme ice loss – James Balog" by TED-Ed | https://www.youtube.com/watch?v=yTDdY1UG7ug]

Take this quiz to check your comprehension of this section.

Access the quiz for Section 13.5 by scanning the QR code.

13.6 Glacial Landforms

Both alpine and continental glaciers create two categories of landforms: erosional and depositional. Erosional landforms are formed by the removal of material. Depositional landforms are formed by the addition of material. Because glaciers were first studied by eighteenth- and nineteenth-century geologists in Europe, the terminology applied to glaciers and glacial features contains many terms derived from European languages.

13.6.1 Erosional Glacial Landforms

Erosional landforms are created when moving masses of glacial ice slide and grind over bedrock. Glacial ice contains large amounts of poorly sorted sand, gravel, and boulders that have been plucked and pried from the bedrock. As the glaciers slide across the bedrock, they grind the sediments into a fine powder called rock flour. Rock flour acts as fine grit that polishes the surface of the bedrock to a smooth finish called **glacial polish**. Larger rock fragments scrape over the surface, creating elongated grooves called **glacial striations**.

Figure 13.46: Glacial striations on granite in Whistler, Canada (left), and glacial striations in Mount Rainier National Park (right). Figure description available at the end of the chapter.

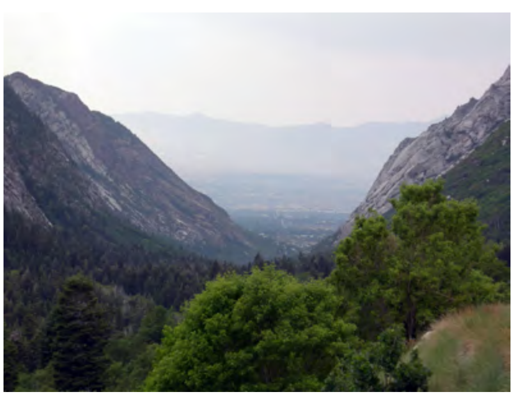

Figure 13.47: The U-shape of the Little Cottonwood Canyon, Utah, as it enters the Salt Lake Valley. Figure description available at the end of the chapter.

Alpine glaciers produce a variety of unique erosional landforms, such as U-shaped valleys, arêtes, cirques, tarns, horns, cols, hanging valleys, and truncated spurs. In contrast, stream-carved canyons have a V-shaped profile when viewed in cross section. Glacial erosion transforms a former V-shaped stream valley into a U-shaped one. Glaciers are typically wider than streams of similar length, and since glaciers tend to erode both at their bases and their sides, they erode V-shaped valleys into relatively flat-bottomed broad valleys with steep sides and a distinctive U shape. As seen in the images, Little Cottonwood Canyon near Salt Lake City, Utah, was occupied by an ice age glacier that extended down to the mouth of the canyon and into Lake Bonneville. Today, that U-shaped valley hosts many erosional landforms, including polished and striated rock surfaces. In contrast, Big Cottonwood Canyon to the north of Little Cottonwood Canyon has retained the V-shape in its lower portion, indicating that its glacier did not extend clear to its mouth but was confined to its upper portion.

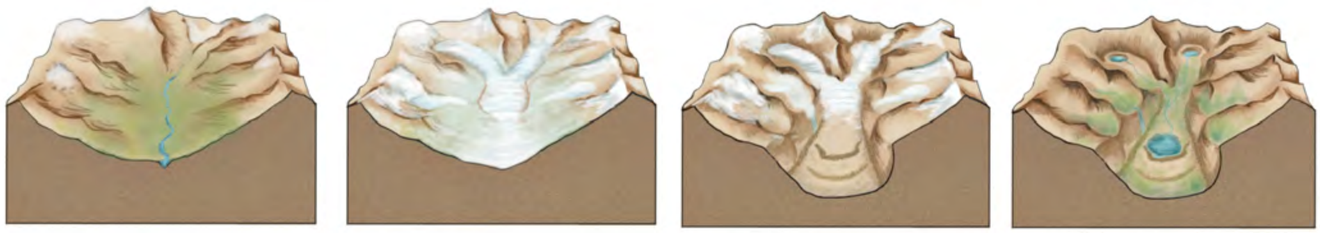

Figure 13.48: Formation of a glacial valley. Glaciers change the shape of the valley from a "V" shape to a "U." Figure description available at the end of the chapter.

When glaciers carve two U-shaped valleys adjacent to each other, the ridge between them tends to be sharpened into a sawtooth feature called an **arête**. At the head of a glacially carved valley is a bowl-shaped feature called a **cirque**. The cirque represents where the head of the glacier eroded the mountain by plucking rock away from it and the weight of the thick ice eroded out a bowl. After the glacier is gone, the bowl at the bottom of the cirque often fills with precipitation and is occupied by a lake called a tarn. When three or more mountain glaciers erode headward at their cirques, they produce **horns**—steep-sided, spire-shaped mountains. Low points along arêtes or between horns are mountain passes termed cols. Where a smaller tributary glacier flows into a larger trunk glacier, the smaller glacier cuts down less. Once the ice has gone, the tributary valley is left as a hanging valley, sometimes with a waterfall plunging into the main valley. As the trunk glacier straightens and widens a V-shaped valley and as it erodes the ends of side ridges, a steep triangle-shaped cliff is formed called a **truncated spur**.

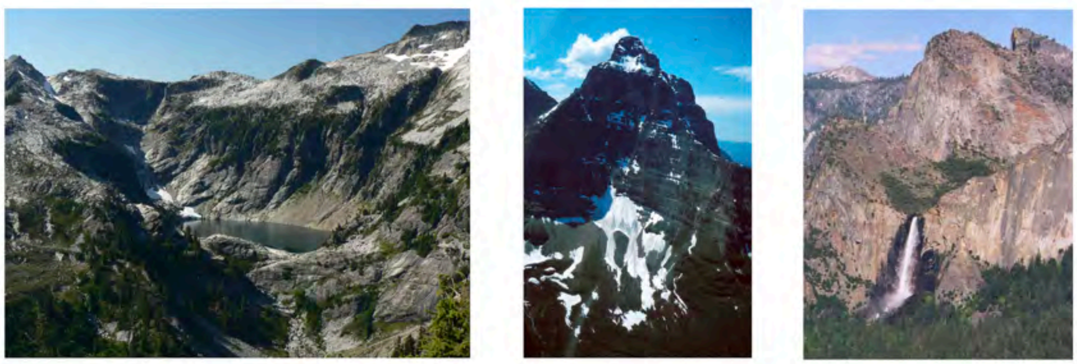

Figure 13.49: Cirque with Upper Thornton Lake in the North Cascades National Park, Washington (left). An example of a horn, Kinnerly Peak, Glacier National Park, Montana (center). Bridalveil Falls in Yosemite National Park, California (right) is a good example of a hanging valley. Figure description available at the end of the chapter.

13.6.2 Depositional Glacial Landforms

Depositional landforms and materials are produced from deposits left behind by a retreating glacier. All glacial deposits are called drift. These include till, tillites, diamictites, terminal moraines, recessional moraines, lateral moraines, medial moraines, ground moraines, silt, outwash plains, glacial erratics, kettles, kettle lakes, crevasses, eskers, kames, and drumlins.

Glacial ice carries a lot of sediment, which is called **till** when deposited by a melting glacier. Till is poorly sorted, with grain sizes ranging from clay and silt to pebbles and boulders. These clasts may be striated. Many depositional landforms are composed of till. The term **tillite** refers to lithified rock having glacial origins. Diamictite refers to a lithified rock that contains a wide range of clast sizes; this includes glacial till but is a more objective and descriptive term for any rock with a wide range of clast sizes.

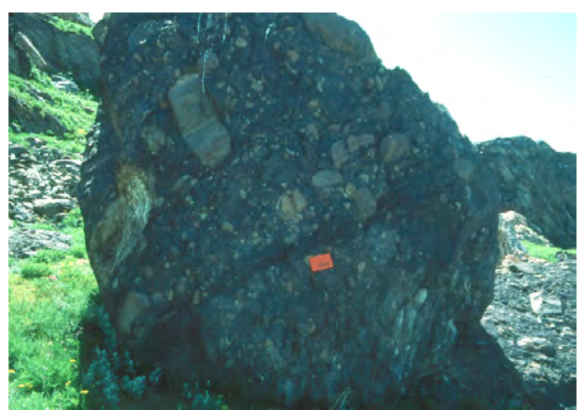

Figure 13.50: Boulder of diamictite of the Mineral Fork Formation, Antelope Island, Utah, United States. Figure description available at the end of the chapter.

Moraines are mounded deposits consisting of glacial till carried in the glacial ice and rock fragments dislodged by mass wasting from the U-shaped valley walls. The glacier acts like a conveyor belt, carrying and depositing sediment at the end of and along the sides of theice flow. Because the ice in the glacier always flows downslope, every glacier has **moraines** built up at its terminus, even if it is not advancing.

Moraines are classified by their location with respect to the glacier. A **terminal moraine** is a ridge of till located at the end or terminus of the glacier. **Recessional moraines** are left by retreating glaciers pausing in their retreats. **Lateral moraines** accumulate along the sides of the glacier from material mass wasted from the valley walls. When two tributary glaciers merge, the two lateral moraines combine to form a **medial moraine** running down the center of the combined glacier. **Ground moraine** is a veneer of till left on the land as the glacier melts.

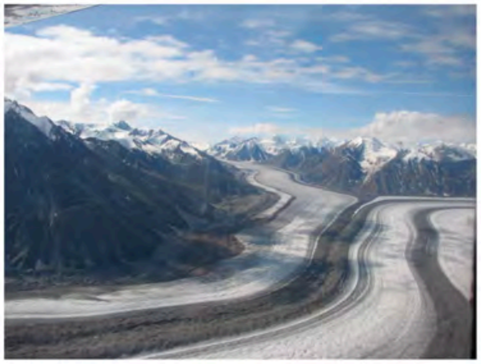

Figure 13.51: (Left) Lateral moraines of Kaskawulsh Glacier within Kluane National Park in the Canadian territory of Yukon. (Right) Medial moraines in northwestern Greenland where tributary glaciers meet. At least seven tributary glaciers from upstream have joined to form the trunk glacier flowing out of the upper left of the picture. Figure description available at the end of the chapter.

In addition to moraines, glaciers leave behind other depositional landforms. Silt, sand, and gravel produced by the intense grinding process are carried by streams of water and deposited in front of the glacier in an area called the **outwash plain**. Retreating glaciers may leave behind large boulders that don't match the local bedrock. These are called **glacial erratics**. When continental glaciers retreat, they can leave behind large blocks of ice within the till. These ice blocks melt and create a depression in the till called a **kettle**. If the depression later fills with water, it is called a kettle lake.

If meltwater flowing over the ice surface descends into crevasses in the ice, it may find a channel and continue to flow in sinuous channels within or at the base of the glacier. Within or under continental glaciers, these streams carry sediments. When the ice recedes, the accumulated sediment is deposited as a long sinuous ridge known as an **esker**. Meltwater descending down through the ice or over the margins of the ice may deposit mounds of till in hills called kames.

Drumlins are common in continental glacial areas of Germany, New York, and Wisconsin, where they are typically found in fields with great numbers. A drumlin is an elongated, asymmetrical teardrop-shaped hill reflecting ice movement with its steepest side pointing upstream to the flow of ice and its streamlined, low-angled side pointing downstream in the direction of ice movement.

Glacial scientists debate the origins of drumlins. A leading idea is that drumlins are created from accumulated till being compressed and sculpted under a glacier that retreated then advanced again over its own ground moraine. Another idea is that meltwater catastrophically flooded under the glacier and carved the till into these streamlined mounds. Still another proposes that the weight of the overlying ice statically deformed the underlying till.

Figure 13.52: A small group of Ice Age drumlins in Germany. Figure description available at the end of the chapter.

Complete this interactive activity to check your understanding.

Access this interactive activity by scanning the QR code.

13.6.3 Glacial Lakes

Glacial lakes are commonly found in alpine environments. A lake confined within a glacial cirque is called a tarn. A tarn forms when the depression in the cirque fills with precipitation after the ice is gone. Examples of tarns include Silver Lake near Brighton ski resort in Big Cottonwood Canyon, Utah, and Avalanche Lake in Glacier National Park, Montana.

Figure 13.53: Cracker Lake in Glacier National Park, Montana, is an example of a tarn. Figure description available at the end of the chapter.

Figure 13.54: Paternoster lakes. Figure description available at the end of the chapter.

When recessional moraines create a series of isolated basins in a glaciated valley, the resulting chain of lakes is called **paternoster lakes**. Lakes filled by glacial meltwater often look milky due to finely ground material called rock flour suspended in the water.

Figure 13.55: Satellite view of Finger Lakes region of New York. Figure description available at the end of the chapter.

Long, glacially carved depressions filled with water are known as **finger lakes**. **Proglacial lakes** form along the edges of all the largest continental ice sheets, such as Antarctica and Greenland. The crust is depressed isostatically by the overlying ice sheet, and these basins fill with glacial meltwater. Many such lakes, some of them huge, existed at various times along the southern edge of the Laurentide ice sheet. Lake Agassiz, Manitoba, Canada, is a classic example of a proglacial lake. Lake Winnipeg serves as the remnant of a much larger proglacial lake.

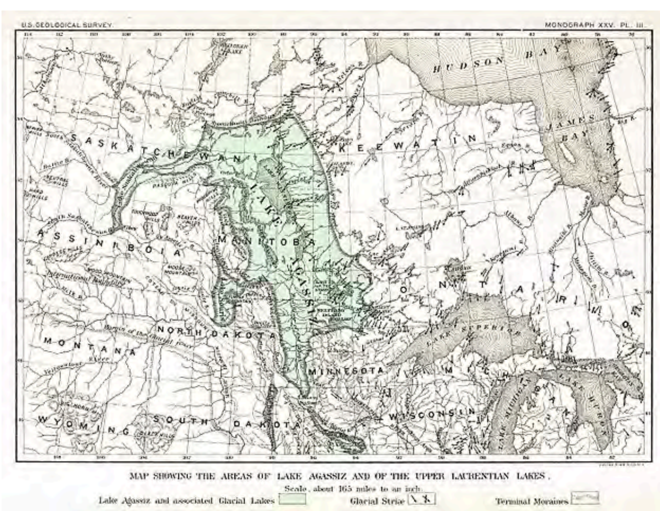

Figure 13.56: Extent of Lake Agassiz. Figure description available at the end of the chapter.

Other proglacial lakes were formed when glaciers dammed rivers and flooded the river valley. A classic example is Lake Missoula, which formed when a lobe of the Laurentide ice sheet blocked the Clark Fork River about 18,000 years ago. Over about 2,000 years, the ice dam holding back Lake Missoula failed several times. During each breach, the lake emptied across parts of eastern Washington, Oregon, and Idaho into the Columbia River Valley and eventually the Pacific Ocean. After each breach, the dam reformed and the lake refilled. Each breach produced a catastrophic flood over a few days. Scientists estimate that this cycle of ice dam, proglacial lake, and torrential massive flooding happened at least 25 times over a span of 20 centuries. The rate of each outflow is believed to have equaled the combined discharge of all of Earth's current rivers combined.

The landscape produced by these massive floods is preserved in the Channeled Scablands of Idaho, Washington, and Oregon.

Figure 13.57: View of Channeled Scablands in central Washington showing huge potholes and massive erosion. Figure description available at the end of the chapter.

Pluvial lakes form in humid environments that experience low temperatures and high precipitation. During the last glaciation, the climate of most of the Western United States was cooler and more humid than today. Under these low-evaporation conditions, many large lakes, called pluvial lakes, formed in the basins of the Basin and Range Province. Two of the largest were Lake Bonneville and Lake Lahontan. Lake Lahontan was in northwestern Nevada, while Bonneville occupied much of western Utah and eastern Nevada. Figure 13.58 illustrates the tremendous size of Lake Bonneville. The lake level fluctuated greatly over the centuries, leaving several pronounced old shorelines marked by wave-cut terraces. These old shorelines can be seen on mountain slopes throughout the western portion of Utah, including the Salt Lake Valley, indicating that the now heavily urbanized valley was once filled with hundreds of feet of water. Lake Bonneville's level peaked around 18,000 years ago when a breach occurred at Red Rock Pass in Idaho and water spilled into the Snake River. The flooding rapidly lowered the lake level and scoured the Idaho landscape across the Pocatello Valley, the Snake River Plain, and Twin Falls. The floodwaters ultimately flowed into the Columbia River across part of the scablands area at an incredible discharge rate of about 4,750 cu km/sec (1,140 cumi/sec).

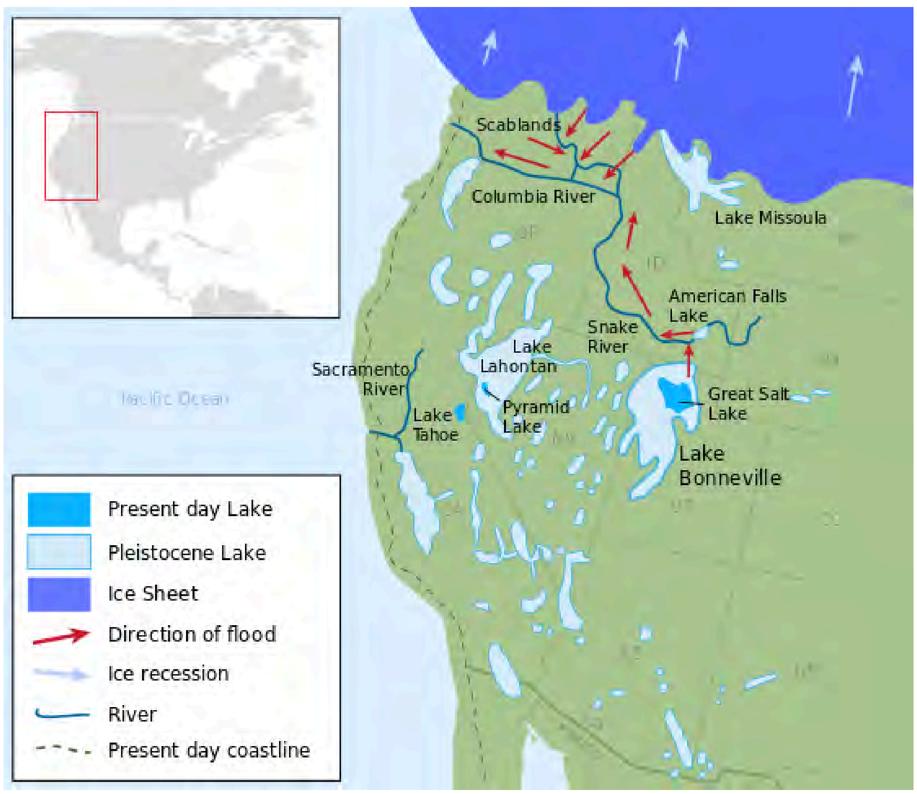

Figure 13.58: Pluvial lakes in the Western United States. Figure description available at the end of the chapter.

For comparison, this discharge rate would drain the volume of Lake Michigan completely dry within a few days.

The five Great Lakes in North America's Upper Midwest are proglacial lakes that originated during the last ice age. The lake basins were originally carved by the encroaching continental ice sheet. The basins were later exposed as the ice retreated about 14,000 years ago and were then filled by precipitation.

Figure 13.59: The Great Lakes. Figure description available at the end of the chapter.

Take this quiz to check your comprehension of this section.

Access the quiz for Section 13.6 by scanning the QR code.

13.7 Ice Age Glaciations

A **glaciation** (or ice age) occurs when the Earth's climate becomes cold enough that continental ice sheets expand, covering large areas of land. Four major, well-documented]glaciations have occurred in Earth's history: one during the Archean-early Proterozoic Eon, ~2.5 billion years ago; another in late Proterozoic Eon, ~700 million years ago; another in the Pennsylvanian, 323 to 300 million years ago; and most recently during the Pliocene-Pleistocene epochs, starting 2.5 million years ago (Chapter 8). Some scientists also recognize a minor glaciation around 440 million years ago in Africa.

The best-studied glaciation is, of course, the most recent. This infographic illustrates the glacial and climate changes over the last 20,000 years, ending with those caused by human actions since the Industrial Revolution. The Pliocene-Pleistocene glaciation was a series of several glacial cycles, possibly 18 in total. Antarctic ice-core records exhibit especially strong evidence for eight glacial advances occurring within the last 420,000 years. The last of these is known in popular media as "The Ice Age," but geologists refer to it as the Last Glacial Maximum. The glacial advance reached its maximum between 26,500 and 19,000 years ago.

13.7.1 Causes of Glaciations

Glaciations occur due to both long-term and short-term factors. In the geologic sense, long-term means a scale of tens to hundreds of millions of years and short-term means a scale of hundreds to thousands of years.

Long-term causes include plate tectonics breaking up the supercontinents (see Wilson cycle, Chapter 2), moving land masses to high latitudes near the North or South Poles and changing ocean circulation. For example, the closing of the Panama Strait and isolation of the Pacific and Atlantic Oceans may have triggered a change in precipitation cycles, which combined with a cooling climate to help expand the ice sheets.

Short-term causes of glacial fluctuations are attributed to the cycles in the Earth's rotational axis and to variations in the Earth's orbit around the Sun that affect the distance between Earth and the Sun. Called **Milankovitch cycles**, these cycles affect the amount of incoming solar radiation, causing short-term cycles of warming and cooling.

During the Cenozoic Era, carbon dioxide levels steadily decreased from a maximum in the Paleocene, causing the climate to gradually cool. By the Pliocene, ice sheets began to form. The effects of the Milankovitch cycles created short-term cycles of warming and cooling within the larger glaciation event.

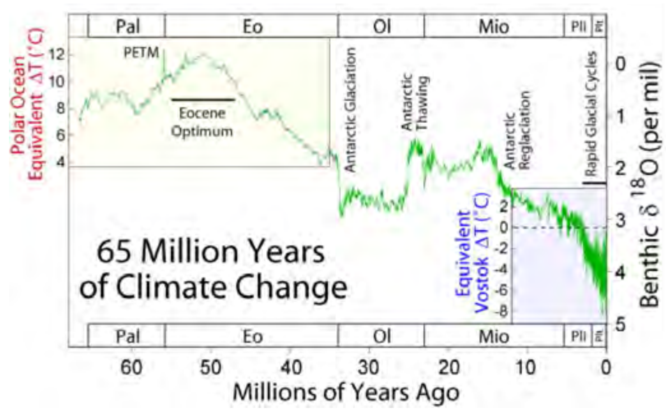

Figure 13.60: Atmospheric CO_2 has declined during the Cenozoic from a maximum in the Paleocene–Eocene that lasted up to the Industrial Revolution. Figure description available at the end of the chapter.

Milankovitch cycles are three orbital changes named after the Serbian astronomer Milutan Milankovitch. The three orbital changes are called precession, obliquity, and eccentricity. **Precession** is the wobbling of Earth's axis with a period of about 21,000 years; **obliquity** is changes in the angle of Earth's axis with a period of about 41,000 years; and **eccentricity** is variations in the Earth's orbit around the Sun leading to changes in distance from the Sun with a period of 93,000 years. These orbital changes created a 41,000-year-long glacial-interglacial Milankovitch cycle from 2.5 to 1 million years ago, followed by another longer cycle of about 100,000 years from 1 million years ago to today (see the Wikipedia page on Milankovitch cycles).

Complete this interactive activity to check your understanding.

Access this interactive activity by scanning the QR code.

Watch the video to see summaries of the ice ages, including their characteristics and causes.

Video 13.4: Ice ages and climate cycles

Access this YouTube video by scanning the QR code. ["Ice Ages & Climate Cycles" by GeoScience Videos | https://www.youtube.com/watch?v=yNiMhjPHPu0]

13.7.2 Sea-Level Change and Isostatic Rebound

When glaciers melt and retreat, two things happen: water runs off into the ocean, causing sea levels to rise worldwide, and the land, released from its heavy covering of ice, rises due to isostatic rebound. Since the Last Glacial Maximum about 19,000 years ago, sea level has risen about 125 m (400 ft). A global change in sea level is called **eustatic** sea-level change. During a warming trend, sea level rises due to more water being added to the ocean and also because of thermal expansion of seawater. About half of the Earth's eustatic sea level rise during the last century has been the result of glaciers melting and about half due to thermal expansion. Thermal expansion describes how a solid, liquid, or gas expands in volume with an increase in temperature. This 30-second video demonstrates thermal expansion with the classic brass ball and ring experiment.

Video 13.5: Thermal expansion

Access this YouTube video by scanning the QR code. ["Ball and Ring: Rate of Expansion and Contraction" by North Carolina School of Science and Mathematics | https://www.youtube.com/watch?v=QNoE5IoRheQ]

Relative sea-level change includes vertical movement of both eustatic sea level and continents on tectonic plates. In other words, sea-level change is measured relative to land elevation. For example, if the land rises a lot and sea level rises only a little, then the relative sea level would appear to drop.

Continents sitting on the lithosphere can move vertically upward as a result of two main processes, tectonic uplift and isostatic rebound. Tectonic uplift occurs when tectonic plates collide (see Chapter 2). **Isostatic rebound** describes the upward movement of lithospheric crust sitting on top of the asthenospheric layer below it. Continental crust bearing the weight of continental ice sinks into the asthenosphere, displacing it. After the ice sheet melts away, the asthenosphere flows back in and continental crust floats back upward. Erosion can also create isostatic rebound by removing large masses like mountains and transporting the sediment away (think of the Mesozoic removal of the Alleghanian Mountains and the uplift of the Appalachian Plateau; Chapter 8), albeit this process occurs more slowly than relatively rapid glacier melting.

The isostatic-rebound map in Figure 13.61 shows rates of vertical crustal movement worldwide. The highest rebound rate is indicated by the blue-to-purple zones (top end of the scale). The orange-to-red zones (bottom end of the scale) surrounding the high-rebound zones indicate isostatic lowering as adjustments in displaced subcrustal material have taken place.

Most glacial isostatic rebound occurs where continental ice sheets rapidly melted about 19,000 years ago, such as in Canada and Scandinavia. Its effects can be seen wherever ice age ice or water bodies are or were present on continental surfaces and in terraces on river floodplains that cross these areas. Isostatic rebound occurred in Utah when the water from Lake Bonneville drained away. North America's Great Lakes also exhibit **emergent coastline** features caused by isostatic rebound since the continental ice sheet retreated.

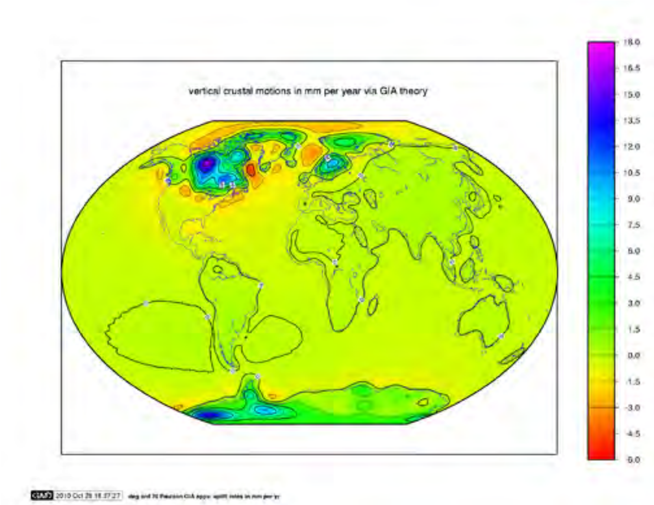

Figure 13.61: Rate of isostatic rebound. Figure description available at the end of the chapter.

Take this quiz to check your comprehension of this section.

Access the quiz for Section 13.7 by scanning the QR code.

Summary

Approximately 30% of Earth's surface is arid lands shaped by factors such as latitude, atmospheric circulation, and terrain. Deserts between 15° and 30° latitude are formed by descending air masses in the atmosphere's major cells, including the Sahara and deserts of the Middle East. Other deserts, like those in western North America and the Atacama in South America, form in rain shadows behind mountain ranges. Dry, descending air also creates polar deserts at the poles.

Atmospheric circulation, involving the Hadley, Ferrel, and polar cells, drives desert formation. Warm air rises in the tropics, dries out, and descends in the arid zones of both hemispheres. The Earth's rotation deflects air masses, producing prevailing winds like the trade winds and westerlies. Complex interactions of latitude, rain shadows, and ocean currents make the Atacama Desert the driest place on Earth.

In deserts, weathering occurs slowly due to low moisture, with unique features like desert varnish and wind-driven erosion. Wind transports sand, shaping landforms like dunes and eroded bedrock features. Poor land management can accelerate desertification, a global problem that degrades once-productive land into desert.

Glaciers form when snowfall exceeds melting, compressing snow into ice. They can be classified into alpine glaciers in valleys, ice sheets covering continents, and ice caps over smaller areas at high elevations. As glaciers grow, they flow under their own weight, with the upper brittle ice cracking into crevasses, while the lower plastic zone bends and flows. Rock debris, known as moraine, gets carried along, grinding against bedrock and causing significant erosion.

Glaciers have a budget that balances accumulation and ablation. If more ice accumulates than melts, the glacier advances; if melting exceeds accumulation, the glacier recedes, a trend seen globally due to warming. Glaciers shape landscapes by carving U-shaped valleys and depositing features like moraines, drumlins, and kettle lakes. Their meltwater forms outwash plains and can create massive floods, as seen with ice age lakes like Lake Missoula, which caused widespread erosion in areas like the Channeled Scablands.

Take this quiz to check your comprehension of this chapter.

Access the quiz for Chapter 13 by scanning the QR code.

Chapter URLs

- Infographic: Infographic. "A Timeline of Earth's Average Temperature since the Last Ice Age Glaciation" https://xkcd.com/1732
- Milankovitch cycles: https://en.wikipedia.org/wiki/Milankovitch_cycles

Text References

1. Allen, P.A., and Etienne, J.L. (2008). Sedimentary challenge to snowball Earth. *Nat. Geosci., 1*(12), 817–825.
2. Bagnold, R. A. (1941). *The physics of blown sand and desert dunes:* Methum, 265.
3. Berner, R.A. (1998). The carbon cycle and carbon dioxide over Phanerozoic time: The role of land plants. *Philos. Trans. R. Soc. Lond. B Biol. Sci., 353*(1365), 75–82.
4. Boggs, S. (2006). *Principles of sedimentology and stratigraphy:* Pearson Prentice Hall. http://agris.fao.org/agrissearch/search.do?recordID=US201300110702.
5. Clements, T. (1952). Wind-blown rocks and trails on Little Bonnie Claire Playa, Nye County, Nevada. *Journal of Sedimentary Research, 22*(3). Society for Sedimentary Geology. http://archives.datapages.com/data/sepm/journals/v01-32/data/022/022003/0182.htm.
6. Collado, G.A., Valladares, M.A., and Méndez, M.A. (2013). Hidden diversity in spring snails from the Andean Altiplano, the second highest plateau on Earth, and the Atacama Desert, the driest place in the world. *Zoological Studies, 52*(1), 50.
7. Cunningham, W.L., Leventer, A., Andrews, J.T., Jennings, A.E., and Licht, K.J. (1999). Late Pleistocene–Holocene marine conditions in the Ross Sea, Antarctica: Evidence from the diatom record. *The Holocene, 9*(2), 129–139.
8. Deynoux, M., Miller, J.M.G., and Domack, E.W. (2004). *Earth's glacial record: World and regional geology:* Cambridge University Press, World and Regional Geology.
9. Earle, S. (2015). *Physical geology OER textbook:* BC Campus OpenEd.
10. Easterbrook, D.J. (1999). *Surface processes and landforms:* Pearson College Division.
11. Eyles, N., and Januszczak, N. (2004). "Zipper-rift": A tectonic model for Neoproterozoic glaciations during the breakup of Rodinia after 750 Ma. *Earth-Sci. Rev. 65*(1–2), 1–73.
12. Francey, R.J., Allison, C.E., Etheridge, D.M., Trudinger, C.M., et al. (1999). A 1000-year high precision record of $\delta 13C$ in atmospheric $CO2$. *Tellus B Chem. Phys. Meteorol.*
13. Geist, H. (2005). *The causes and progression of desertification:* Ashgate Aldershot.
14. Grayson, D.K. (1993). *The desert's past: A natural prehistory of the Great Basin:* Smithsonian Institute Press.
15. Gutro, R. (2005). NASA – What's the difference between weather and climate? Online, http://www.nasa.gov/mission_pages/noaa-n/

climate/climate_weather.html, accessed September 2016.
16. Hadley, G. (1735). Concerning the cause of the general trade-winds: *Philosophical Transactions, 39*(436-444). The Royal Society, 58–62.
17. Hartley, A.J., and Chong, G. (2002). Late Pliocene age for the Atacama Desert: Implications for the Desertification of Western South America. *Geology, 30*(1), 43–46. http://geology.gsapubs.org.
18. Hedin, S.A. (1903). *Central Asia and Tibet. Vol. 1:* Hurst and Blackett, limited.
19. Hoffman, P.F., Kaufman, A.J., Halverson, G.P., and Schrag, D.P. (1998). A neoproterozoic snowball Earth. *Science, 281*(5381), 1342–1346.
20. Hooke, R.L. (1967). Processes on arid-region alluvial fans. *The Journal of Geology, 75*(4), 438–60.
21. King, L.C. (1953). Canons of landscape evolution. *Geological Society of America Bulletin 64*(7), 721–52.
22. Kletetschka, G., Hooke, R.L., Ryan, A., Fercana, G., McKinney, E. and Schwebler, K.P. (2013). Sliding stones of Racetrack Playa, Death Valley, USA: The roles of rock thermal conductivity and fluctuating water levels. *Geomorphology, 195*(August), 110–17.
23. Kopp, R.E., Kirschvink, J.L., Hilburn, I.A., and Nash, C.Z. (2005). The Paleoproterozoic snowball Earth: A climate disaster triggered by the evolution of oxygenic photosynthesis. *Proc. Natl. Acad. Sci. U.S.A., 102*(32), 11131–11136.
24. Laity, J.E. (2009). Landforms, landscapes, and processes of aeolian erosion, in *Geomorphology of desert environments,* (Parsons, A.J., and Abrahams, A.D., eds.): Springer Netherlands, 597–627.
25. Lean, J., Beer, J., and Bradley, R. (1995). Reconstruction of solar irradiance since 1610: Implications for climate change. *Geophys. Res. Lett., 22*(23), 3195–3198.
26. Levitus, S., Antonov, J.I., Wang, J., Delworth, T.L., Dixon, K.W., and Broccoli, A.J. (2001). Anthropogenic warming of Earth's climate system. *Science, 292*(5515), 267–270.
27. Lindsey, R. (2009). Climate and Earth's energy budget: Feature articles. NASA. Online, http://earthobservatory.nasa.gov, accessed September 2016.
28. Littell, E., and Littell, R.S. (1846). *Littell's living age:* T.H. Carter & Company.
29. Livingstone, I., and Warren, A. (1996). *Aeolian geomorphology: An introduction:* Longman.
30. Muhs, D.R., and Bettis, E.A. (2003). Quaternary Loess-Paleosol Sequences as Examples of Climate-Driven Sedimentary Extremes." Special Papers-Geological Society of America. Boulder, Colo.; Geological Society of America; 1999, 53–74.
31. Norris, R.D., Norris, J.M., Lorenz, R.D., Ray, J., and Jackson, B. (2014). Sliding rocks on Racetrack Playa, Death Valley National Park: First observation of rocks in motion. *PloS One, 9*(8), e105948. http://journals.plos.org.
32. North Carolina State University (2013a). Composition of the atmosphere.
33. North Carolina State University (2013b). Composition of the atmosphere. Online, http://climate.ncsu.edu/edu/k12/.AtmComposition, accessed September 2016.
34. Oreskes, N. (2004). The scientific consensus on climate change. *Science, 306*(5702), 1686–1686.
35. Pachauri, R.K., Allen, M.R., Barros, V.R., Broome, J., Cramer, W., Christ, R., Church, J.A., Clarke, L., Dahe, Q., Dasgupta, P., Dubash, N.K., Edenhofer, O., Elgizouli, I., Field, C.B., et al. (2014). Climate change 2014: Synthesis report. Contribution of Working Groups I, II and III to the Fifth Assessment Report of the Intergovernmental Panel on Climate Change (R. K. Pachauri & L. Meyer, eds.): Geneva, Switzerland, IPCC.
36. Santer, B.D., Mears, C., Wentz, F.J., Taylor, K.E., Gleckler, P.J., Wigley, T.M.L., Barnett, T.P., Boyle, J.S., Bru ̈ ggemann, W., Gillett, N.P., Klein, S.A., Meehl, G.A., Nozawa, T., Pierce, D.W., et al. (2007). Identification of human-induced changes in atmospheric moisture content. *Proc. Natl. Acad. Sci. U.S.A., 104*(39), 15248–15253.
37. Schopf, J.W., and Klein, C. (1992). Late-Proterozoic low-latitude global glaciation: The snowball Earth, in Schopf, J.W., and Klein, C. (eds.). *The Proterozoic biosphere: A multidisciplinary study:* Cambridge University Press, p. 51–52.
38. Shao, Y. (2008). *Physics and modelling of wind erosion:* Springer Science & Business Media.
39. Stanley, G.M. (1955). Origin of playa stone tracks, racetrack playa, Inyo County, California. *Geological Society of America Bulletin, 66*(11), 1329–50. http://gsabulletin.gsapubs.org.
40. Walker, A.S. (1996). *Deserts: Geology and resources:* U.S. Government Printing Office. https://pubs.er.usgs.gov/publication/7000004.
41. Webb, T., and Thompson, W. (1986). Is vegetation in equilibrium with climate? How to interpret late-Quaternary pollen data. *Vegetatio, 67*(2), 75–91.
42. Weissert, H. (2000). Deciphering methane's fingerprint. *Nature, 406*(6794), 356–357.
43. Whitlock, C., and Bartlein, P.J. (1997). Vegetation and climate change in northwest America during the past 125 kyr. *Nature, 388*(6637), 57–61.
44. Wilson, I.G. (1971). Desert sandflow basins and a model for the development of ergs. *The Geographical Journal, 137*(2), 180–99.
45. Wolpert, S. (2009). New NASA temperature maps provide a 'whole new way of seeing the moon'. Online, http://newsroom. ucla.edu/releases/new-nasa-temperature-maps-provide-102070, accessed February 2017.
46. Zachos, J., Pagani, M., Sloan, L., Thomas, E., and Billups, K. (2001). Trends, rhythms, and aberrations in global climate. 65 Ma to present. *Science, 292*(5517), 686–693.

Figure References

Figure 13.1: World hot deserts (Koppen BWh). M.C. Peel, B.L. Finlayson, and T.A. McMahon; adapted by Me ne frego. 2011. CC BY-SA 3.0. https://en.wikipedia.org/wiki/File:Koppen_World_Map_BWh.png

Figure 13.2: Mountainous areas in front of the prevailing winds create a rain shadow. domdomegg. 2015. CC BY 4.0. https://commons.wikimedia.org/wiki/File:Rainshadow_copy.svg

Figure 13.3: In this image from the ISS, the Sierra Nevada Mountains are perpendicular to prevailing westerly winds, creating a rain shadow to the east (bottom of the image). NASA. 2003. Public domain. https://earthobservatory.nasa.gov/images/3273/southern-sierra-nevada-and-owens-lake

Figure 13.4: Generalized atmospheric circulation. NASA. 2009. Public domain. https://commons.wikimedia.org/wiki/File:Earth_Global_Circulation.jpg

Figure 13.5: USGS map of the Great Basin Desert. United States Geological Survey (USGS). 2012. Public domain. https://commons.wikimedia.org/wiki/File:Central_Basin_and_Range_ecoregion.gif

Figure 13.6: Map of the Atacama Desert (yellow) and surrounding related climate areas (orange). cobaltcigs. 2010. CC BY-SA 3.0. https://en.wikipedia.org/wiki/File:Atacama_map.svg

Figure 13.7: The polar vortex of mid-November, 2013. National Oceanic and Atmospheric Administration (NOAA). 2014. Public domain. https://commons.wikimedia.org/wiki/File:November2013_polar_vortex_geopotentialheight_mean_Large.jpg

Figure 13.8: In the inertial frame of reference of the top picture, the ball moves in a straight line. Hubi. 2003. CC BY-SA 3.0. https://commons.wikimedia.org/wiki/File:Corioliskraftanimation.gif

Figure 13.9: Forces acting on a mass moving east–west on the rotating Earth that produce the Coriolis effect. Kindred Grey. 2022. CC BY 4.0.

Figure 13.10: Inertia of air masses caused by the Coriolis effect in the absence of other forces. Kes47. 2015. CC BY-SA 3.0. https://commons.wikimedia.org/wiki/File:Coriolis_effect.svg

Figure 13.11: Gyres of the Earth's oceans. Canuckguy; adapted by Shadowxfox and Popadius. 2012. Public domain. https://commons.wikimedia.org/wiki/File:Corrientes-oceanicas-en.svg

Figure 13.12: Weathering and erosion of Canyonlands National Park has created a unique landscape that includes arches, cliffs, and spires. Rick. 2005. CC BY 2.0. https://commons.wikimedia.org/wiki/File:Mesa_Arch_Canyonlands_National_Park.jpg

Figure 13.13: Newspaper Rock, located in Petrified Forest National Park, is a site with many petroglyphs carved into desert varnish. Laura Neser. March 2022. CC BY-NC.

Figure 13.14: A dust storm (haboob) hits Texas in 2019. Jakeorin. 2019. CC BY-SA 4.0. https://commons.wikimedia.org/wiki/File:Haboob_in_Big_Spring,_TX.jpg

Figure 13.15: Diagram showing the mechanics of saltation. NASA. 2002. Public domain. https://commons.wikimedia.org/wiki/File:Saltation-mechanics.gif

Figure 13.16: Enlarged image of frosted and rounded windblown sand grains. Wilson44691. 2008. Public domain. https://commons.wikimedia.org/wiki/File:CoralPinkSandDunesSand.jpg

Figure 13.17: A sailing stone at Racetrack Playa in Death Valley National Park, California. Lgcharlot. 2006. CC BY-SA 4.0. https://commons.wikimedia.org/wiki/File:Racetrack_Playa_in_Death_Valley_National_Park.jpg

Figure 13.18: (Top) A yardang near Meadow, Texas. (Bottom) Blowout near Earth, Texas. Yardang: United States Department of Agriculture. 2000. Public domain. https://commons.wikimedia.org/wiki/File:Yardang_Lea-Yoakum_Dunes.jpg, Blowout: Leaflet. 1996. CC BY-SA 3.0. https://commons.wikimedia.org/wiki/File:Blowout_Earth_TX.jpg

Figure 13.19: Wind-carved ventifact in White Desert National Park, Egypt. Christine Schultz. 2003. Public domain. https://commons.wikimedia.org/wiki/File:Weisse_W%C3%BCste.jpg

Figure 13.20: Aerial image of alluvial fan in Death Valley. USGS. 2005. Public domain. https://commons.wikimedia.org/wiki/File:Alluvial_Fan.jpg

Figure 13.21: Bajada along Frisco Peak in Utah. GerthMichael. 2010. CC BY-SA 3.0. https://commons.wikimedia.org/wiki/File:FriscoMountainUT.jpg

Figure 13.22: Inselbergs in the Western Sahara. Nick Brooks. 2007. CC BY 2.0. https://commons.wikimedia.org/wiki/File:Breast-Shaped_Hill.jpg

Figure 13.23: Satellite image of desert playa surrounded by mountains. Robert Simmon, using Landsat data from the USGS and NASA. 2013. Public domain. https://earthobservatory.nasa.gov/images/80913/eye-exam-for-a-satellite

Figure 13.24: (Top) Dry wash (or ephemeral stream). (Bottom) Flash flood in a (different) dry wash. Top: Finetooth. 2010. CC BY-SA 3.0.

https://commons.wikimedia.org/wiki/File:Dry_Wash_in_PEFO_NP.jpg Bottom: USGS. 2016. Public domain. https://www.usgs.gov/media/images/a-flooded-river-australia

Figure 13.25: Antelope Canyon is a slot canyon in Arizona formed by the erosion of Navajo Sandstone. It is susceptible to flash flooding, even from rain falling miles away. Laura Neser. March 2022. CC BY-NC.

Figure 13.26: A sand sea or erg in the Sahara Desert. Wsx. 2004. CC BY-SA 3.0. https://commons.wikimedia.org/wiki/File:Sahara_Desert_in_Jalu,_Libya.jpeg

Figure 13.27: Formation of cross-bedding in sand dunes. David Tarailo, GSA, GeoCorps Program. 2015. Public domain. https://commons.wikimedia.org/wiki/File:Formation_of_cross-bedding.jpg

Figure 13.28: Cross-beds in the Navajo Sandstone at Zion National Park. Laura Neser. March 2022. CC BY-NC.

Figure 13.29: NASA image of barchan dune field in coastal Brazil. NASA. 2003. Public domain. https://earthobservatory.nasa.gov/images/3889/coastal-dunes-brazil

Figure 13.30: Satellite image of longitudinal dunes in Egypt. NASA. 2012. Public domain. https://earthobservatory.nasa.gov/images/78151/linear-dunes-great-sand-sea-egypt

Figure 13.31: Parabolic dunes. Po ke jung. 2011. CC BY 3.0. https://commons.wikimedia.org/wiki/File:Parabolic_dune.jpg

Figure 13.32: Star dune in Namib Desert. Dave Curtis. 2005. CC BY-NC-ND 2.0. https://flic.kr/p/4N5Fa

Figure 13.33: The Great Basin. Kmusser; adapted by Hike395. 2022. CC BY-SA 3.0. https://commons.wikimedia.org/wiki/File:Great_Basin_map.gif

Figure 13.34: Typical Basin and Range scene. Matt Affolter (QFL247). 2010. CC BY-SA 3.0. https://commons.wikimedia.org/wiki/File:RidgecrestCA.jpg

Figure 13.35: World map showing desertification vulnerability. USDA. 1998. Public domain. https://commons.wikimedia.org/wiki/File:Desertification_map.png

Figure 13.36: Glacier in the Bernese Alps. Dirk Beyer. 2005. CC BY-SA 3.0. https://commons.wikimedia.org/wiki/File:Grosser_Aletschgletscher_3178.jpg

Figure 13.37: Alpine glaciers of the Alps visible from an airplane en route from Milan, Italy, to Munich, Germany. Laura Neser. September 2023. CC BY-NC.

Figure 13.38: (Left) Greenland ice sheet. (Right) Map showing the thickness of the Greenland ice sheet in meters. Left: Greenland ice sheet. Hannes Grobe. 1995. CC BY-SA 2.5. https://commons.wikimedia.org/wiki/File:Greenland-ice_sheet_hg.jpg. Right: Eric Gaba. 2011. CC BY-SA 3.0. https://commons.wikimedia.org/wiki/File:Greenland_ice_sheet_AMSL_thickness_map-en.svg

Figure 13.39: Cross-sectional view of both Greenland and Antarctic ice sheets drawn to scale for size comparison. Kindred Grey. 2022. CC BY 4.0. Adapted from Steve Earle (CC BY 4.0). https://opengeology.org/textbook/14-glaciers/14-2_steve-earle_antarctic-greenland-2-300×128

Figure 13.40: Snow Dome ice cap near Mount Olympus, Washington (left), and Vatnajökull ice cap in Iceland (right). Left: Mount Olympus Washington by United States National Park Service. 2004. Public domain. https://commons.wikimedia.org/wiki/File:Mount_Olympus_Washington.jpg. Right: Vatnajökull by NASA. 2004. Public domain. https://commons.wikimedia.org/wiki/File:Vatnaj%C3%B6kull.jpeg

Figure 13.41: Maximum extent of Laurentide ice sheet. USGS. 2005. Public domain. https://commons.wikimedia.org/wiki/File:Pleistocene_north_ice_map.jpg

Figure 13.42: Glacial crevasses (left) and cravasse on the Easton Glacier in the North Cascades (right). chevron crevasse by Bethan Davies, 2015 (CC BY-NC-SA 3.0, https://www.antarcticglaciers.org/glacier-processes/structural-glaciology/chevron-crevasse). Glaciereaston by Mauri S. Pelto, 2005 (Public domain, https://en.wikipedia.org/wiki/File:Glaciereaston.jpg).

Figure 13.43: Cross section of a valley glacier showing stress (red numbers) increase with depth under the ice. Kindred Grey. 2022. CC BY 4.0. Adapted from Steve Earle (CC BY 4.0). https://opengeology.org/textbook/14-glaciers/14-2_steve-earle_ice-flow-and-stress

Figure 13.44: Cross-sectional view of an alpine glacier showing internal flow lines, zone of accumulation, snow line, and zone of melting. Kindred Grey. 2022. CC BY 4.0. Adapted from Steven Earle (CC BY 4.0). https://opentextbc.ca/geology/chapter/16-2-how-glaciers-work

Figure 13.45: Fjord. Frédéric de Goldschmidt. 2007. CC BY-SA 3.0. https://sco.wikipedia.org/wiki/File:Geirangerfjord_(6-2007).jpg

Figure 13.46: Glacial striations on granite in Whistler, Canada (left), and glacial striations in Mount Rainier National Park (right). Glacial striations by Amezcackle, 2003 (Public domain, https://en.m.wikipedia.org/wiki/File:Glacial_striations.jpg). Glacial striation 21149 by Walter Siegmund, 2007 (CC BY-SA 3.0, https://commons.wikimedia.org/wiki/File:Glacial_striation_21149.jpg).

Figure 13.47: The U-shape of the Little Cottonwood Canyon, Utah, as it enters into the Salt Lake Valley. Wilson44691. 2008. Public domain. https://commons.wikimedia.org/wiki/File:UshapedValleyUT.jpg

Figure 13.48: Formation of a glacial valley. Cecilia Bernal. 2015. CC BY-SA 4.0. https://commons.wikimedia.org/wiki/File:Glacier_Valley_formation-_Formaci%C3%B3n_Valle_glaciar.gif

Figure 13.49: Cirque with Upper Thornton Lake in the North Cascades National Park, Washington (left). Thornton Lakes 25929 by Walter Siegmund, 2007 (CC BY-SA 3.0, https://commons.wikimedia.org/wiki/File:Thornton_Lakes_25929.jpg). Kinnerly Peak by USGS, 1982 (Public domain, https://uk.wikipedia.org/wiki/%D0%A4%D0%B0%D0%B9%D0%BB:Kinnerly_Peak.jpg). Closeup of Bridalveil Fall seen from Tunnel View in Yosemite NP by Daniel Mayer, 2003 (CC BY-SA 1.0, https://commons.wikimedia.org/wiki/File:Closeup_of_Bridalveil_Fall_seen_from_Tunnel_View_in_Yosemite_NP.jpg).

Figure 13.50: Boulder of diamictite of the Mineral Fork Formation, Antelope Island, Utah, United States. Jstuby. 2002. Public domain. https://commons.wikimedia.org/wiki/File:Diamictite_Mineral_Fork.jpg

Figure 13.51: (Left) Lateral moraines of Kaskawulsh Glacier within Kluane National Park in the Canadian territory of Yukon. Kluane Icefield 1 by Steffen Schreyer, 2005 (CC BY-SA 2.0 DE, https://commons.wikimedia.org/wiki/File:Kluane_Icefield_1.jpg). Nuussuaq-peninsula-moraines by Algkalv, 2010 (CC BY-SA 3.0, https://commons.wikimedia.org/wiki/File:Nuussuaq-peninsula-moraines.jpg).

Figure 13.52: A small group of Ice Age drumlins in Germany. Martin Groll. 2009. CC BY 3.0 DE. https://commons.wikimedia.org/wiki/File:Drumlin_1789.jpg

Figure 13.53: Cracker Lake in Glacier National Park, Montana, is an example of a tarn. Laura Neser. 2014. CC BY-NC.

Figure 13.54: Paternoster lakes. wetwebwork. 2007. CC BY-SA 2.0. https://en.wikipedia.org/wiki/File:View_from_Forester_Pass.jpg

Figure 13.55: Satellite view of Finger Lakes region of New York. NASA. 2004. Public domain. https://commons.wikimedia.org/wiki/File:New_York%27s_Finger_Lakes.jpg

Figure 13.56: Extent of Lake Agassiz. USGS. 1895. Public domain. https://commons.wikimedia.org/wiki/File:Agassiz.jpg

Figure 13.57: Pluvial lakes in central Washington showing huge potholes and massive erosion. DKRKaynor. 2019. CC BY-SA 4.0. https://commons.wikimedia.org/wiki/File:Channeled_Scablands.jpg

Figure 13.58: Pluvial lakes in the Western United States. Fallschirmjäger. 2013. CC BY-SA 3.0. https://en.wikipedia.org/wiki/File:Lake_bonneville_map.svg

Figure 13.59: The Great Lakes. SeaWiFS Project, NASA/Goddard Space Flight Center, and ORBIMAGE. 2000. Public domain. https://commons.wikimedia.org/wiki/File:Great_Lakes_from_space.jpg

Figure 13.60: Atmospheric CO_2 has declined during the Cenozoic from a maximum in the Paleocene–Eocene that lasted up to the Industrial Revolution. Robert A. Rohde. 2005. CC BY-SA 3.0. https://commons.wikimedia.org/wiki/File:65_Myr_Climate_Change.png

Figure 13.61: Rate of isostatic rebound. NASA. 2010. Public domain. https://commons.wikimedia.org/wiki/File:PGR_Paulson2007_Rate_of_Lithospheric_Uplift_due_to_post-glacial_rebound.png

Figure Descriptions

Figure 13.1: World map showing the location of hot deserts in red: the hot deserts are located near 30 north or south latitude; hot deserts are seen in southwest North America, western South America, Saharan Africa and southern Africa, the Middle East and southern Asia, and central-western Australia.

Figure 13.2: Mountain with water body on the left. From left to right: Prevailing winds carry warm moist air up the mountain. At top: rising air cools and condenses. On the way down the mountain: dry air advances and casts a rain shadow.

Figure 13.3: Photo taken from the ISS showing the Sierra Nevada Mountains running from left to right; the mountain range on the upward side of the image are snow capped while the mountain slopes and basin at the base of the range on the downward side of the image are tan and lack vegetation, indicating a rain shadow. The Inyo Mountains are near the bottom of the photo which lack snow due to the rain shadow.

Figure 13.4: An illustration of the Earth with three generalized circulation cells shown for each hemisphere; the Polar cell is located above 50 degrees north and south latitude, the Mid-latitude cell is located between 30 and 50 degrees north and south latitude, and the Hadley

cell is located between 0 and 30 degrees north and south latitude. On the globe, arrows show the general wind directions in each cell: polar winds flow outward from each pole in the Polar cells, westerlies flow from west to east, toward the poles in the Mid-latitude cells, northeasterly trades flow from the northeast to southwest in the northern Hemisphere Hadley cell, and southeasterly trades flow from the southeast to northwest in the southern Hemisphere Hadley cell.

Figure 13.5: Map of the Great Basin Desert, located across most of Nevada, Western Utah, southeastern Idaho, and eastern California. The Humboldt River runs approximately east to west in the northern part of the desert and the Great Salt Lake is located near the eastern edge of the desert.

Figure 13.6: Map of South America with the Atacama Desert colored yellow and orange: the desert is located along the coast of west-central South America.

Figure 13.7: Circular map of the northern hemisphere centered on the North Pole. The map is color coded according to geopotential height, with cold, descending air in purple over the Arctic.

Figure 13.8: Animation illustrating a ball thrown on a rotating disc viewed from two perspectives: from the inertial frame of reference and from a stationary viewer on the disc. Viewed from the inertial frame of reference, the ball moves in a straight line from the center of the disc to the bottom of the image as the disc rotates counterclockwise. Viewed from the perspective of a stationary viewer on the disc, the ball appears to follow a curved path from the center outward toward the left of the viewer.

Figure 13.9: Schematic diagram showing forces acting on a mass moving East or West on the rotating Earth. As the Earth rotates, centripetal force pushes the mass outward while gravity force pulls the mass toward the center of Earth; combined, the Coriolis effect is between these two forces.

Figure 13.10: Illustration of the Earth with circular arrows pointing clockwise in the Northern Hemisphere and counterclockwise in the Southern Hemisphere, which equates to Coriolis deflection to the right in the Northern Hemisphere and to the left in the Southern Hemisphere.

Figure 13.11: World map of ocean currents; in the northern hemisphere, large-scale gyres flow in a clockwise pattern in each ocean basin; in the southern hemisphere, large-scale gyres flow in a counterclockwise pattern in each ocean basin. Cool currents are generally found along the west coasts of continents and are blue in color; warm currents are generally found along the east coasts of continents and are red in color; the rest of the currents are black.

Figure 13.12: Photo through a sandstone arch of a desert landscape with steep sandstone cliffs, distant spires, and a flat basin.

Figure 13.13: The rock is dark brown with tan petroglyphs carved into it.

Figure 13.14: A few trucks on dry, flat land. From ground to sky is a dark brown dust cloud that you cannot see through.

Figure 13.15: 2D diagram showing how sand grains can travel by wind blowing on a sandy ground surface: the largest grains move along the ground surface and are labeled creep, slightly smaller particles bounce along the surface and are labeled saltation, and tiny particles that move through the air are labeled suspension.

Figure 13.16: Close-up photo of unconsolidated amber-colored glassy grains with rounded edges; a scale bar at the lower right says 1.0 mm.

Figure 13.17: A large gray rock has slid over the light tan playa surface leaving a track in the playa.

Figure 13.18: Top photo shows sand-covered ground that has a sandstone rock resting on top of a base that has been worn away by sandblasting. Bottom photo shows man standing in bowl-shaped sandy depression.

Figure 13.19: Column of sand with larger sand boulder capping the column; the boulder has multiple flattened and faceted surfaces.

Figure 13.20: Black and white aerial image with white elevation contour lines overlain on the image. The contour lines show a semi-circular fan-shaped deposit where a stream emerges from a canyon in Death Valley.

Figure 13.21: Photo of mountains where alluvial fans have coalesced into a single apron of sediment along the mountain front.

Figure 13.22: Single dome-shaped mountain rising from a flat desert landscape.

Figure 13.23: Satellite image of a flat tan desert playa surrounded by mountains on either side.

Figure 13.24: Top photo shows a dry sandy stream bed surrounded by a desert landscape with scrubby vegetation, while the bottom photo shows a tan muddy water flooding in the desert.

Figure 13.25: Left photo shows a tan sandy desert landscape with a yellow sign that states warning flash flood area. Right photo shows a person standing in a very narrow tan sandy canyon.

Figure 13.26: Vast tan, sandy desert landscape. A single person and a white vehicle can be seen in the distance.

Figure 13.27: Cross sectional diagram showing wind blowing toward the right and sand moving as a result. There are three flat-lying sedimentary beds with smaller cross beds angled from upper left to lower right across the beds. Erosion happens on the gently-sloping left-hand side of the bed surface while deposition happens on the steeper right-hand side of the bed surface.

Figure 13.28: Tan sandstone with many thinly-bedded layers at various angles visible along the cliff face.

Figure 13.29: Satellite image of a field of barchan dunes, each showing characteristic crescent shapes with the wings pointing in the direction of prevailing winds.

Figure 13.30: Satellite image of long, linear parallel dune ridges in a tan sandy landscape.

Figure 13.31: Block diagram of a beach with wind blowing toward the left. Parabolic dunes form in the sand that have a crescent shape, with the horns anchored in vegetation and pointing toward the right. A bowl-shaped blowout forms in the sand where there is no vegetation.

Figure 13.32: Tan sand dune with a central peak and multiple ridges branching outward in various directions.

Figure 13.33: Map of the Great Basin Desert, located across most of Nevada, Western Utah, southeastern Idaho, eastern California, and south-central Oregon. Multiple streams begin and end within the basin.

Figure 13.34: Desert landscape covered in low scrubby vegetation. A town can be seen in the distance.

Figure 13.35: World map color coded according to desert vulnerability: low vulnerability is light green, moderate is yellow, high is orange, and very high is red. Regions with high and moderate vulnerability include western and southwestern U.S., eastern and south-central South America, sub- Saharan Africa and southern Africa, the Middle East, and the coastal regions of Australia. Other regions either have low to moderate vulnerability or are classified as other regions: dry, cold, humid/not vulnerable, or ice/glacier.

Figure 13.36: A long sheet of ice filling an alpine valley with parallel lines of sediment running lengthwise along the ice. In the background is a thick deposit of ice higher up in a mountain cirque.

Figure 13.37: Aerial photo of a mountainous terrain; the mountain slopes are dark brown, capped with a large expanse of white snow and ice; a deep blue lake can be seen in a valley on the right side of the photo.

Figure 13.38: Left image is an aerial photo of a broad expanse of white snow and ice. There are numerous waterways off the right side of the ice sheet. Right image is a map of Greenland showing the thickness of the ice sheet that covers nearly the entire country. The ice is thickest near the center of Greenland with a maximum thickness of 3,205 meters and gets thinner outward toward the coasts.

Figure 13.39: Antarctic ice sheet is very wide (roughly 6,000km). Greenland ice sheet is narrower (roughly 1,000 km). Both ice sheets have roughly the same height. Crust of each ice sheet remains at or below sea level.

Figure 13.40: Two photos: the left photo shows the side profile of a rocky mountain that is covered with an ice cap. The right photo is an aerial view of a white ice cap covering a large area of land.

Figure 13.41: Map centered over the North Pole, showing the maximum extent of the Laurentide ice sheet. The ice sheet covers Greenland, Canada, the northern United States, northern Europe, and northern Asia.

Figure 13.42: Two photos: the left photo shows deep cracks in a sheet of glacial ice and the right photo shows a person stepping over a deep crack in a sheet of glacial ice.

Figure 13.43: Cross sectional diagram of a glacier on a slope with elevation on the vertical axis. The glacier flows downhill at different rates with red numbers showing the stress on the ice in kilopascals and arrows showing the relative extent of deformation. In general, the stress increases deeper below the glacier surface and deforms most along the base of the glacier.

Figure 13.44: A cross sectional diagram of an alpine glacier on a slope with internal flow lines shown as blue arrows that point downhill parallel to the slope. The zone of accumulation and zone of melting are separated by a vertical equilibrium line, with the zone of accumulation being upslope and the zone of ablation downslope.

Figure 13.45: Water-filled valley with steep side walls.

Figure 13.46: Two photos: the left photo shows a big, smooth rock with parallel linear grooves and the right photo shows smoothed, polished rock with parallel linear grooves abraded.

Figure 13.47: A U-shaped valley with steep ridges on the sides and a wide curved valley at the base.

Figure 13.48: Animated GIF of the formation of a glacial valley: the valley begins as a V- shaped valley with a river running through it. As ice forms on the mountains and fills the valley, the glacier then carves away at the base of the valley, changing it into a U-shaped valley. At the end of the animation, the ice melts away and leaves behind a U-shaped glacial valley with a few rivers and a lake at the base.

Figure 13.49: Three photos: the left photo shows a steep rocky mountain that has an amphitheatre-like valley carved out of the top of the mountain, with a lake at the base. The middle photo shows a steep and pointy rocky mountain top. The right photo shows a steep rocky mountain with a U-shaped valley halfway up the slope; a large waterfall flows out of the mid-height valley onto the valley below.

Figure 13.50: A large boulder, dark in color, with smaller lighter colored clasts of a range of sizes inside of it.

Figure 13.51: Two photos: the left photo shows a long sheet of ice at the base of mountains with parallel lines of sediment running lengthwise along the ice, resembling an ice road. The right photo shows two long sheets of ice at the base of mountains that meet in a Y-shape; both sheets have parallel lines of sediment running lengthwise along the ice, resembling an ice road.

Figure 13.52: Aerial photograph of a small town surrounded by green landscape; numerous elongated asymmetrical teardrop-shaped hills are seen surrounding the town, which is also located on a small ridge.

Figure 13.53: An elongated green valley with a light milky blue lake at the valley base. There are steep brown mountain cliffs in the background that have white snow covering part of them.

Figure 13.54: Series of elongate lakes between moraines within an alpine glacial valley.

Figure 13.55: Satellite view of a series of long, finger-shaped lakes next to each other over a large area.

Figure 13.56: Map showing a large lake covering southeastern Manitoba, northwestern Ontario, northern Minnesota, eastern North Dakota, and Saskatchewan.

Figure 13.57: Aerial photo of a barren and pockmarked terrain.

Figure 13.58: Map of the western United States showing present day lakes, Pleistocene lakes, and the Pleistocene ice sheet; Lake Bonneville is a Pleistocene lake in northwestern Utah and arrows show that it floods toward the northwest, along the Snake River, until it reaches the Scablands of eastern Washington; the modern Great Salt Lake is in the northern part of Lake Bonneville and is much smaller than Lake Bonneville. The ice sheet is located in Canada and the northern United States; it also floods toward the Scablands. Other smaller Pleistocene lakes are scattered across the western U.S.

Figure 13.59: Aerial view of the five great lakes (Superior, Huron, Michigan, Erie, Ontario) that occupy basins left by the ice sheet in the Ice Age.

Figure 13.60: A graph of atmospheric CO_2 levels over time. The vertical axis shows Benthic O-18 in per mil, decreasing upward; the horizontal axis shows the time from 65 to 0 million years ago. During the Cenozoic Era, carbon dioxide levels steadily decreased from a maximum in the Paleocene, causing the climate to gradually cool. By the Pliocene, ice sheets began to form. There are short-term cycles of warming and cooling within the larger glaciation event.

Figure 13.61: World map, color coded by vertical crustal motions in mm per year. The highest rebound rate is 18.0 mm per year and high motions are indicated the blue-to-purple zones (top end of the scale). The lowest rebound rate is negative 6.0 mm per year, indicating isostatic lowering; these are orange- to-red zones (bottom end of the scale). Most glacial isostatic rebound is occurring where continental ice sheets rapidly melted about 19,000 years ago, such as in Canada, Scandinavia, and western Antarctica, and most isostatic lowering is occurring in the northern Atlantic Ocean and Arctic Ocean, with small spots of lowering off the coast of western Antarctica.

14. METEOROLOGY

Learning Objectives

By the end of this chapter, students should be able to:

- Understand the structure and composition of the atmosphere.
- Explain how energy travels through Earth's atmosphere.
- Describe the various aspects and elements of weather, including atmospheric water, air masses, and weather fronts.
- List the various physical controls on weather.
- Understand the causes and effects of severe weather events including thunderstorms, tornadoes, hurricanes, blizzards, and heat waves.

If someone across the country asks you what the weather is like today, you need to consider several factors. Air temperature, humidity, wind speed, the amount and types of clouds, and precipitation are all part of a thorough weather report. It's also important to consider the difference between weather and climate.

Weather is what is going on in the atmosphere at a particular place at a particular time. Weather is the change we experience from day to day. Weather can change rapidly. A location's weather depends on air temperature, air pressure, fog, humidity, cloud cover, precipitation, and wind speed and direction. All of these are directly related to the amount of energy that is in the system and where that energy is. The ultimate source of this energy is the Sun. As defined by the National Oceanic and Atmospheric Administration (NOAA), **meteorology** is the science concerned with the Earth's atmosphere and its physical processes. A meteorologist is a physical scientist who observes, studies, or forecasts the weather.

Climate is the average of a region's weather over time. The climate for a particular place is steady and changes only very slowly. Climate is determined by many factors, including the angle of the Sun, the likelihood of cloud cover, topography, and air pressure. These factors are related to the amount of solar energy and precipitation that a region experiences over time. Climate is the long-term average of weather in a particular spot. Although the weather for a particular winter day in Tucson, Arizona, may include snow, the climate of Tucson is generally warm and dry. The next chapter, Global Climate Change, describes the Earth systems involved in climate change, the geologic evidence of past climate changes, and the human role in today's climate change.

14.1 The Atmosphere

Earth's atmosphere is a thin blanket of gases and tiny particles—together called air. We are most aware of air when it moves and creates wind. All living things need some of the gases in air for life support. Without an atmosphere, Earth would likely be just another lifeless rock. Earth's atmosphere, along with the abundant liquid water at Earth's surface, are the keys to our planet's unique place in the Solar System. Much of what makes Earth exceptional depends on the atmosphere. Let's consider some of the reasons we are lucky to have an atmosphere.

Without the atmosphere, Earth would look a lot more like the Moon. Atmospheric gases, especially carbon dioxide (CO_2) and oxygen (O_2), are extremely important for living organisms. In photosynthesis, plants use CO_2 and create O_2. Photosynthesis is responsible for nearly all of the oxygen currently found in the atmosphere. By creating oxygen and food, plants have made an environment that is favorable for animals. In respiration, animals use oxygen to convert sugar into food energy they can use. Plants also go through respiration and consume some of the sugars they produce.

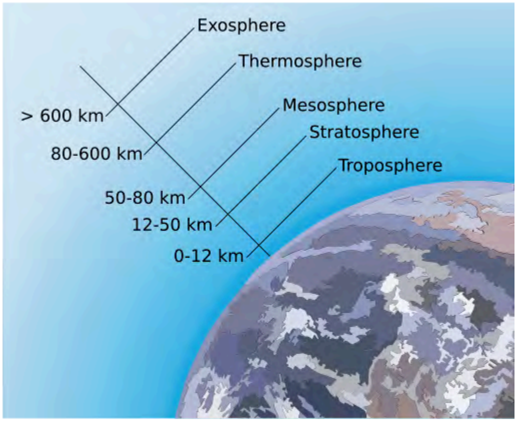

Figure 14.1: Layers of Earth's atmosphere. Figure description available at the end of the chapter.

The relationship between the atmosphere and water vapor is a crucial part of the hydrologic cycle. Water spends a lot of time in the atmosphere, mostly as water vapor. All weather takes place in the atmosphere, and virtually all of it happens in the lower atmosphere. The amount of water vapor present in different areas of the planet has a dynamic effect on the weather that occurs in different areas. Areas that are prone to regularly occurring water-rich storms have quite different ecosystems than drier areas that receive less moisture. Species are adapted to the conditions in which they live. Drier areas may have species of plants and animals that have strategies that allow them to thrive, whereas more temperate areas with more moisture have species that would not fare as well in drier climates. Thus, life depends on the climate and weather that occur in the zones in which life occurs.

Ozone is a molecule composed of three oxygen atoms (O_3). Ozone in the upper atmosphere absorbs high-energy ultraviolet (UV) radiation coming from the Sun. This protects living things on Earth's surface from the Sun's most harmful rays. Without ozone for protection, only the simplest life forms would be able to live on Earth. Along with the oceans, the atmosphere keeps Earth's temperatures within an acceptable range. Greenhouse gases trap heat in the atmosphere, so they help to moderate global temperatures. Without an atmosphere with greenhouse gases, Earth's temperatures would be frigid at night and scorching during the day. Important greenhouse gases include carbon dioxide, methane, water vapor, and ozone.

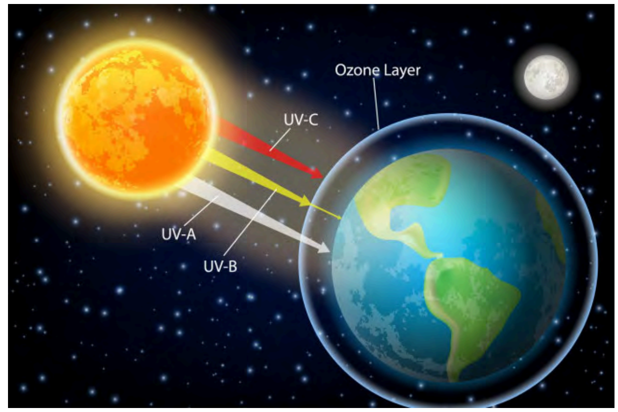

Figure 14.2: The ozone layer absorbs a portion of the radiation from the Sun, preventing it from reaching the planet's surface. Most importantly, it absorbs the portion of UV light called UVB, which has been linked to many harmful effects, including skin cancers, cataracts, and harm to some crops and marine life. Figure description available at the end of the chapter.

14.1.1 Atmospheric Gases

Nitrogen and oxygen together make up 99 percent of the planet's atmosphere. The rest of the gases are minor components but sometimes are very important. Humidity is the amount of water vapor in the air. Humidity varies from place to place and season to season. This fact is obvious if you compare a summer day in Atlanta, Georgia, where humidity is high, with a winter day in Phoenix, Arizona, where humidity is low. When the air is very humid, it feels heavy or sticky. Dry air usually feels more comfortable. Higher humidity is found around the equatorial regions because air temperatures are higher and warm air can hold more moisture than cooler air. Of course, humidity is lower near the polar regions because air temperature is lower.

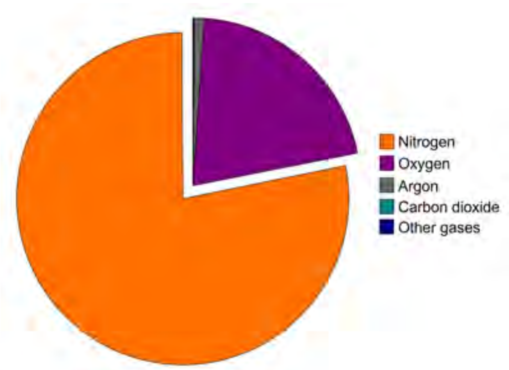

Figure 14.3: Pie chart of Earth's atmospheric composition. Figure description available at the end of the chapter.

Some of what is in the atmosphere is not gas. Particles of dust, soil, fecal matter, metals, salt, smoke, ash, and other solids make up a small percentage of the atmosphere. Particles provide starting points (or nuclei) for water vapor to condense on and form raindrops, and some particles are pollutants.

The atmosphere has different properties at different elevations above sea level, or altitudes. The air density (the number of molecules in a given volume) decreases with increasing altitude. This is why people who climb tall mountains, such as Mount Everest, have to set up camp at different elevations to let their bodies get used to the decreased air density.

Why does air density decrease with altitude? Gravity pulls the gas molecules toward Earth's center. The pull of gravity is stronger at sea level due to being closer to the center of the Earth than at higher altitudes. Air is denser at sea level where the gravitational pull is greater. Gases at sea level are also compressed by the weight of the atmosphere above them. The force of the air weighing down over a unit of area is known as its atmospheric pressure. The reason why we are not crushed by this weight is because the molecules inside our bodies are pushing outward to compensate. Atmospheric pressure is felt from all directions, not just from above.

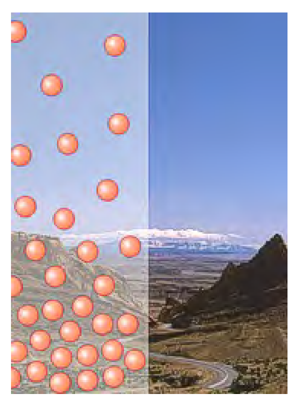

Figure 14.4: Atmospheric pressure decreases as altitude increases. Figure description available at the end of the chapter.

At higher altitudes, the atmospheric pressure is lower and the air is less dense than at higher altitudes. If your ears have ever "popped," you have experienced a change in air pressure. Gas molecules are found inside and outside your ears. When you change altitude quickly, like when an airplane is descending, your inner ear keeps the density of molecules at the original altitude. Eventually the air molecules inside your ear suddenly move through a small tube in your ear to equalize the pressure. This sudden rush of air is felt as a popping sensation.

Although the density of the atmosphere changes with altitude, the composition stays the same with altitude, with one exception. In the ozone layer, at about 20 km to 40 km above the surface, there is a greater concentration of ozone molecules than in other portions of the atmosphere.

14.1.2 Layers of the Atmosphere

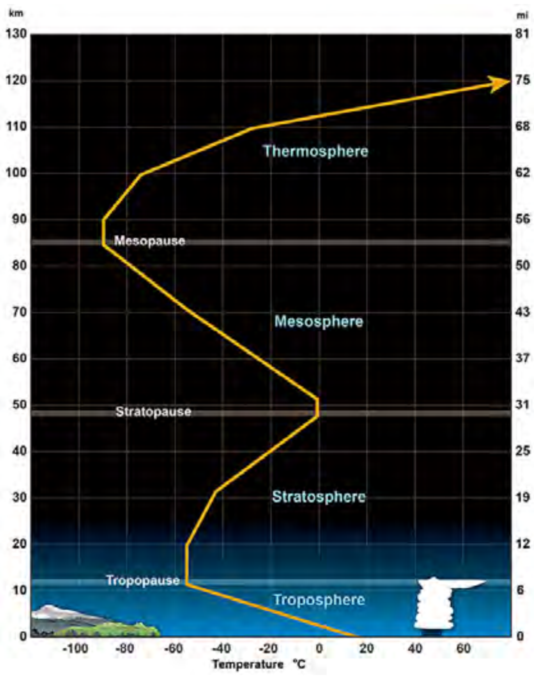

Figure 14.5: Layers of Earth's atmosphere with associated temperature changes. Figure description available at the end of the chapter.

The atmosphere's layers correspond with how the atmosphere's temperature changes with altitude. By understanding the way temperature changes with altitude, we can learn a lot about how the atmosphere works. While weather takes place in the lower atmosphere, interesting things, such as the aurora, happen higher in the atmosphere.

Warm air rises because gas molecules are able to move freely in the atmosphere. When gas molecules are warm, they move vigorously and take up more space. When gas molecules are cool, they are sluggish and do not take up as much space. With the same number of molecules in less space, both air density and air pressure are higher. Warmer, lighter air is more buoyant than the cooler air above it, so it rises. The cooler air then sinks down because it is denser than the air beneath it. This is the process of convection.

The property that changes most strikingly with altitude is air temperature. Unlike the change in pressure and density, which decrease with altitude, changes in air temperature are not regular. A change in temperature with distance is called a temperature gradient. The atmosphere is divided into layers based on how the temperature in that layer changes with altitude, which is known as the layer's temperature gradient. In some layers, temperature increases with altitude, and in others it decreases. The temperature gradient in each layer is determined by the heat source of the layer. Most of the important processes of the atmosphere take place in the lowest two layers: the troposphere and the stratosphere.

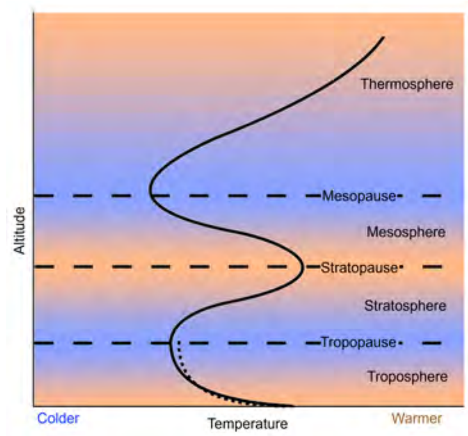

Figure 14.6: Thermal profile of Earth's atmosphere, showing the major divisions based on temperature. Figure description available at the end of the chapter.

The temperature of the troposphere is highest near the surface of the Earth and decreases with altitude. On average, the temperature gradient of the troposphere is 6.5°C per 1,000 m (3.6°F per 1,000 ft) of altitude. Earth's surface is a major source of heat for the troposphere, although nearly all of that heat comes from the Sun. Rock, soil, and water on Earth absorb the Sun's light and radiate it back into the atmosphere as heat. The temperature is also higher near the surface because of the greater density of gases. In the troposphere, warmer air is beneath cooler air, a condition that is unstable. The warm air near the surface rises while cool air higher in the troposphere sinks, resulting in mixing. This mixing causes the temperature gradient to vary with time and place. The rising and sinking of air in the troposphere also means that nearly all of the planet's weather takes place in the troposphere.

14.1.3 Atmospheric Energy, Temperature, and Heat

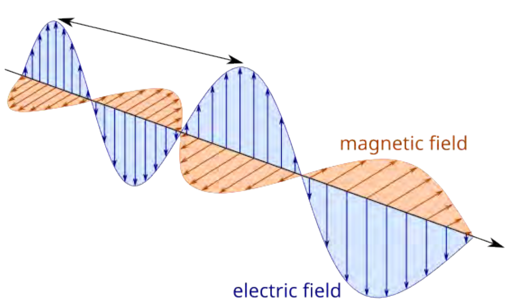

Figure 14.7: Oscillations of electric and magnetic fields of an electromagnetic wave. Figure description available at the end of the chapter.

Energy travels through space or material. This is obvious when you stand near a fire and feel its warmth or when you feel heat in the handle of a metal pot even though the handle is not sitting directly on the hot stove. Invisible energy waves can travel through air, glass, and even the vacuum of outer space. These waves have electrical and magnetic properties, so they are called electromagnetic waves. The transfer of energy from one object to another through electromagnetic waves is known as radiation. Different wavelengths of energy create different types of electromagnetic waves.

The wavelengths humans can see are known as visible light. These wavelengths appear to us as the colors of the rainbow. The longest wavelengths of visible light appear red. Infrared wavelengths are longer than visible red. We feel infrared energy as heat. Wavelengths that are shorter than violet are called ultraviolet.

Reflection is when light (or another wave) bounces back from a surface. **Albedo** is a measure of how well a surface reflects light. A surface with high albedo, for example a snow field, reflects a large percentage of light. One important fact to remember is that energy cannot be created or destroyed; it can only be changed from one form to another. This is such a fundamental fact of nature that it is a law: the law of conservation of energy. In photosynthesis, for example, plants convert solar energy into **chemical energy** that they can use. They do not create new energy. When energy is transformed, some nearly always becomes heat. Heat transfers from warmer objects to cooler ones easily. If no more heat is added, eventually all of a material will reach the same temperature.

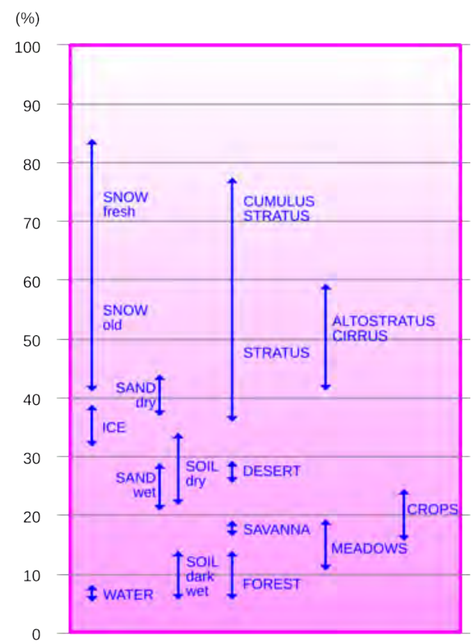

Figure 14.8: The percentage of diffusely reflected sunlight relative to various surface conditions. Figure description available at the end of the chapter.

Temperature is a measure of how fast the atoms in a material are vibrating. High temperature particles vibrate faster than low temperature particles. Rapidly vibrating atoms smash together, which generates heat. As a material cools down, the atoms vibrate more slowly and collide less frequently. As a result, they emit less heat. Temperature measures how fast a material's atoms are vibrating, while heat measures the material's total energy.

Heat is taken in or released when an object changes state, changing from a gas to a liquid or a liquid to a solid. This heat is called latent heat. When a substance changes state, latent heat is released or absorbed. A substance changing its state of matter does not change temperature. All of the energy that is released or absorbed goes toward changing the material's state. Substances also differ in their specific heat, which is the amount of energy needed to raise the temperature of one gram of the material by 1°C (1.8°F). Water has a very high specific heat, which means it takes a lot of energy to change the temperature of water.

14.1.4 Energy from the Sun

The Earth constantly tries to maintain an energy balance with the atmosphere. Most of the energy that reaches the Earth's surface comes from the Sun. About 44% of solar radiation is in the visible light wavelengths, but the Sun also emits infrared, ultraviolet, and other wavelengths. When viewed together, all of the wavelengths of visible light appear white. Of the solar energy that reaches the outer atmosphere, UV wavelengths have the greatest energy. Only about 7% of solar radiation is in the UV wavelengths. The remaining solar radiation is the longest wavelength, infrared. Most objects radiate infrared energy, which we feel as heat.

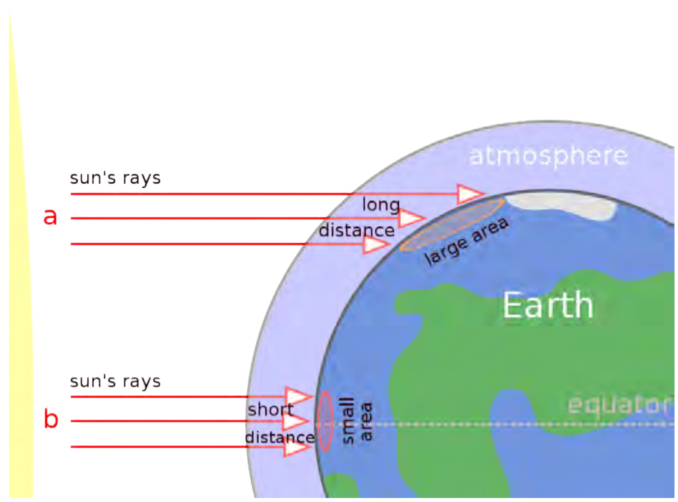

Figure 14.9: Solar radiation is strongest near the equator and weaker at the poles. Figure description available at the end of the chapter.

Heat moves in the atmosphere the same way it moves through the solid Earth or another medium. Radiation is the transfer of energy between two objects by electromagnetic waves. Heat radiates from the ground into the lower atmosphere. In conduction, heat moves from areas of more heat to areas of less heat by direct contact. Warmer molecules vibrate rapidly and collide with other nearby molecules, transferring their energy. In the atmosphere, conduction is more effective at lower altitudes, where air density is higher; this transfers heat upward to where the molecules are spread farther apart or transfers heat laterally from warmer to cooler spots, where the molecules move less vigorously. Heat transfer by movement of heated materials is called convection. Heat that radiates from the ground initiates convection cells in the atmosphere.

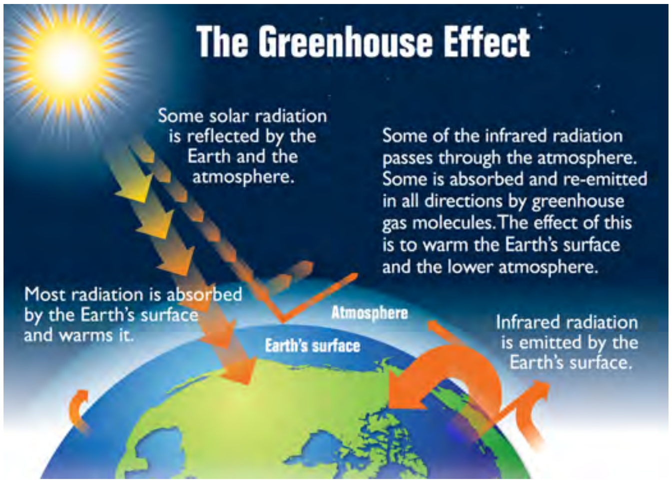

Figure 14.10: Earth's greenhouse effect. Figure description available at the end of the chapter.

Earth is not getting warmer or cooler due to incoming solar radiation, which means that the planet's heat budget is in balance, although the amount of incoming solar energy is different at different latitudes. The difference in solar energy received at different latitudes drives atmospheric circulation. The exception to Earth's temperature being in balance is caused by greenhouse gases. Greenhouse gases warm the atmosphere by trapping heat. Some of the heat radiation from the ground is trapped by greenhouse gases in the troposphere. Like a blanket on a sleeping person, greenhouse gases act as insulation for the planet. The warming of the atmosphere because of insulation by greenhouse gases is called the **greenhouse effect**. Greenhouse gases are the component of the atmosphere that moderate Earth's temperatures. Greenhouse gases include carbon dioxide (CO_2), water vapor (H_2O), methane (CH_4), ozone (O_3), nitrous oxides (N_2O), and chlorofluorocarbons (CFCs). All of these gases are a normal part of the atmosphere except manmade CFCs.

Different greenhouse gases have different abilities to trap heat. For example, one methane molecule traps 30 times as much heat as one carbon dioxide molecule. One CFC-12 molecule (a type of CFC) traps 10,600 times as much heat as one CO_2 molecule. Still, CO_2 is a very important greenhouse gas because it is much more abundant in the atmosphere. Human activity has significantly raised the levels of many of greenhouse gases in the atmosphere. Methane levels are about 2.5 times higher as a result of human activity. Carbon dioxide has increased more than 35%. CFCs have only recently existed. This is a concern because, as atmospheric greenhouse gas levels increase, more greenhouse gases trap more heat and warm the atmosphere. The increase or decrease of greenhouse gases in the atmosphere affect climate and weather over the entire Earth.

Take this quiz to check your comprehension of this section.

Access the quiz for Section 14.1 by scanning the QR code.

14.2 Weather Processes

The energy in our atmosphere creates temperature differences, and these temperature differences cause air rising, sinking, and moving across Earth's surface. This movement causes wind, storms, rain, and drought. In the following sections, we will explore the processes that control our weather.

14.2.1 Water in the Atmosphere

Humidity is the amount of water vapor in the air in a particular spot. We usually use the term to mean relative humidity, the percentage of water vapor a certain volume of air is holding relative to the maximum amount it can contain. If the humidity today is 80%, it means that the air contains 80% of the total amount of water it can hold at that temperature. If the humidity increases to more than 100%, the excess water condenses and forms precipitation. Since warm air can hold more water vapor than cool air, raising or lowering the temperature can change air's relative humidity. The temperature at which air becomes saturated with water is called the air's dew point. This term makes sense, because water condenses from the air as dew if the air cools down overnight and reaches 100% humidity.

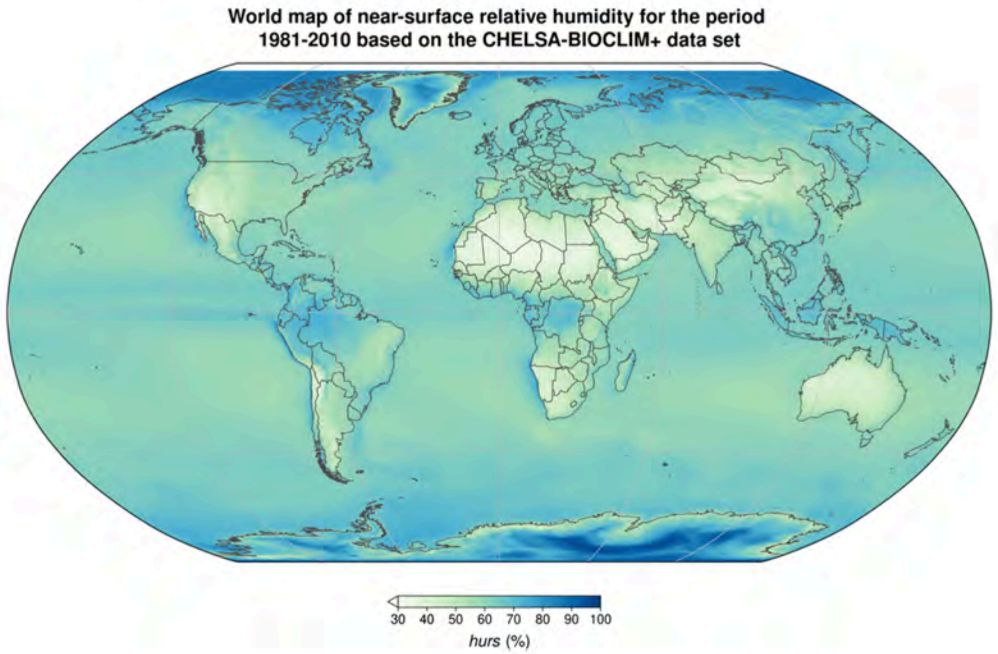

Figure 14.11: Global distribution of relative humidity at the surface, averaged over the years 1981–2010. Figure description available at the end of the chapter.

Clouds influence weather in a few ways: by preventing solar radiation from reaching the ground, by absorbing warmth that is re-emitted from the ground, and as a source of precipitation. When there are no clouds, there is less insulation. As a result, cloudless days can be extremely hot, and cloudless nights can be very cold. For this reason, cloudy days tend to have a lower range of temperatures than clear days. There are a variety of conditions needed for clouds to form; for instance, clouds form when air reaches its dew point. This can happen in two ways: (1) air temperature stays the same but humidity increases, common in locations that are warm and humid; (2) humidity can remain the same, but temperature decreases. When the air cools enough to reach 100% humidity, water droplets form. Air cools when it comes into contact with a cold surface or when it rises.

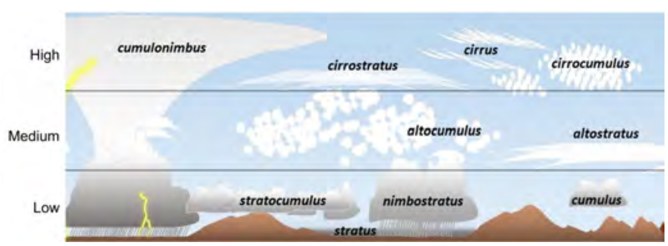

Figure 14.12: Tropospheric clouds. Figure description available at the end of the chapter.

Water vapor is not visible unless it condenses to become a cloud. Water vapor condenses around a nucleus, such as dust, smoke, or a salt crystal. This forms a tiny liquid droplet. Billions of these water droplets together make a cloud. Clouds are classified in several ways. While clouds appear in infinite shapes and sizes, they fall into some basic forms. From his *Essay of the Modifications of Clouds* (1803), Luke Howard divided clouds into three categories: cirrus, cumulus, and stratus, plus a fourth special type, nimbus. The most common classification used today divides clouds into these four separate cloud groups, which are determined by their altitude and whether precipitation is occurring or not.

High-level clouds, such as cirrus, cirrostratus, and cirrocumulus, form from ice crystals where the air is extremely cold and can hold little water vapor. Middle-level clouds, including altocumulus and altostratus clouds, may be made of water droplets, ice crystals, or both, depending on the air temperatures. Low-level clouds are nearly all water droplets. Stratus, and stratocumulus clouds are common low clouds. A special rain cloud category combines the three forms—cumulo, cirro, and stratus—referred to as a nimbo-form cloud (from *nimbus*, the Latin word for rain). The vast majority of precipitation occurs from nimbo-form clouds, and therefore these clouds are generally the thickest.

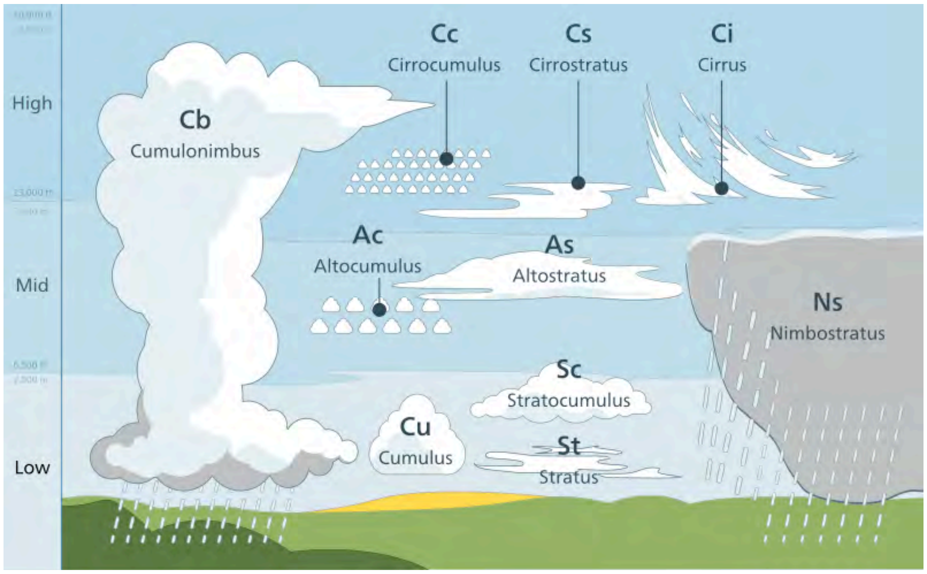

Figure 14.13: Cloud types. Figure description available at the end of the chapter.

Fog is a cloud located at or near the ground. When humid air near the ground cools below its dew point, fog is formed. The several types of fog each form in a different way. Radiation fog forms at night when skies are clear and the relative humidity is high. As the ground cools, the bottom layer of air cools below its dew point. Tule fog is an extreme form of radiation fog found in some regions. San Francisco, California, is famous for its summertime advection fog. Warm, moist Pacific Ocean air blows over the cold California Current and cools below its dew point. Sea breezes bring the fog onshore. Steam fog appears in autumn when cool air moves over a warm lake. Water evaporates from the lake surface and condenses as it cools, appearing like steam. Warm, humid air travels up a hillside and cools below its dew point to create upslope fog.

Figure 14.14: Advection fog layer in San Francisco with the Golden Gate Bridge and skyline in the background. Figure description available at the end of the chapter.

Precipitation is an extremely important part of weather. Some precipitation forms in place. The most common precipitation comes from clouds. Rain or snow droplets grow as they ride air currents in a cloud and collect other droplets. They fall when they become heavy enough to escape from the rising air currents that hold them up in the cloud. One million cloud droplets will combine to make only one rain drop. If temperatures are cold, the droplet will hit the ground as a snowflake.

14.2.2 Air Masses

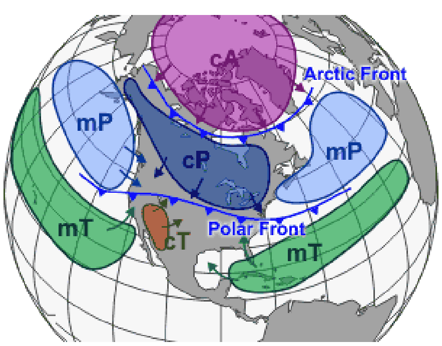

Figure 14.15: North American air masses. Figure description available at the end of the chapter.

An air mass is a large body of air that covers a relatively wide area and exhibits horizontally uniform properties of moisture and temperature. The location where an air mass receives its characteristics of temperature and humidity is called the source region. Air masses are slowly pushed along by high-level winds, and when an air mass moves over a new region, it shares its temperature and humidity with that region, which means that the temperature and humidity of a particular location depends partly on the characteristics of the air mass above it. Storms arise if the air mass and the region it moves over have different characteristics. For example, when a colder air mass moves over warmer ground, the bottom layer of air is heated. That air rises, forming clouds, rain, and sometimes thunderstorms.

In general, cold air masses tend to flow toward the equator and warm air masses tend to flow toward the poles. This brings heat to cold areas and cools down areas that are warm. It is one of the many processes that act toward balancing out the planet's temperatures. An air mass is classified by its temperature and moisture and is identified by using a letter code system. The first letter is always lowercase and determines the moisture content within the air mass: m (maritime) is moist and c (continental) is dry. The second letter is always capital and determines latitude: E (equatorial) is hot, T (tropical) is warm, P (polar) is cold, and A (arctic) is very cold.

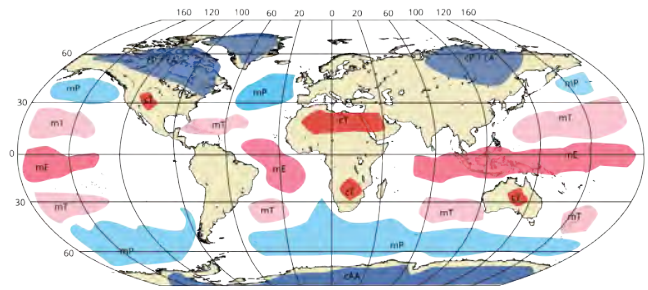

Figure 14.16: Source regions of global air masses. [Figure description available at the end of the chapter.]

14.2.3 Weather Fronts

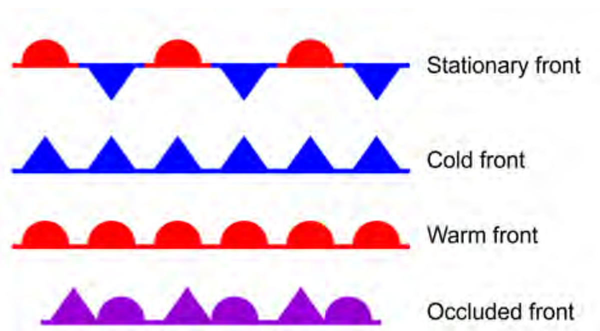

Figure 14.17: Guide to weather map symbols for weather fronts. [Figure description available at the end of the chapter].

A weather front is a transition zone between two air masses of relatively different densities, temperatures, and moisture. When two air masses come into contact with each other, they do not like to mix well because of their different densities (much like water and oil). Along a weather front, the warmer, less dense air rises over the colder, denser air to form clouds. There are several types of weather fronts: stationary fronts, cold fronts, warm fronts, and occluded fronts.

A stationary front occurs when two contrasting air masses of moisture and temperature connect, but neither of them will ground the other. In many ways, the two air masses are at a stalemate until one of them begins to give ground to the other. Typically, but not always, stationary fronts produce mild but prolonged precipitation.

Cold fronts are zones separating two distinct air masses, of which the colder, denser mass is advancing and replacing the warmer. The colder, denser air pushes under the warm air, forcing the warm, lighter air upward. If the warm air rising is unstable enough, massive thunderstorms are likely to occur. Cumulous and cumulonimbus clouds are common.

Warm fronts mark the boundary between a warm air mass that is replacing a colder air mass. When a warm air mass advances over a cold air mass, the warm air rises over but at a gentler rate than a cold front. Since the warm air does not rise as fast as a cold front, more stratus clouds form and precipitation is not as heavy.

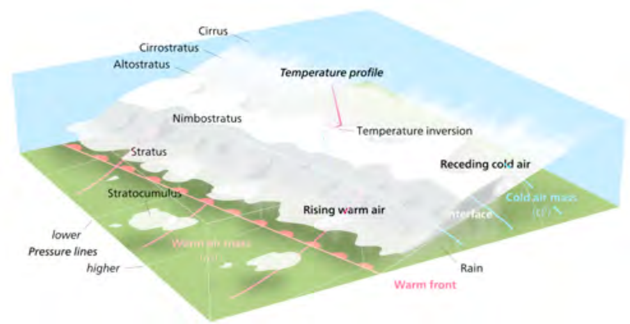

Figure 14.18: Illustration of a warm front. [Figure description available at the end of the chapter].

Finally, occluded fronts occur when a cold front overtakes a warm front, causing the warmer air to rise above and meet up with another cold air mass. The air masses, in order from front to back, are cold, warm, and then cold again. The Coriolis effect curves the boundary where the two fronts meet toward the pole. If the air mass that arrives third is colder than either of the first two air masses, that air mass slip beneath them both. This is called a cold occlusion. If the air mass that arrives third is warm, that air mass rides over the other air mass, called a warm occlusion. The weather at an occluded front is especially fierce right at the occlusion. Precipitation and shifting winds are typical.

14.2.4 Physical Controls on Weather and Climate

Several controlling factors determine global temperatures. The first and most significant factor controlling Earth's weather patterns is latitude. Because of the Earth's shape and the angle at which the Sun hits the planet, temperatures are highest near the equator and decrease toward the poles. In fact, at the equator, more energy is absorbed from the Sun than is radiated back into space. At the poles, more energy is radiated back into space than is absorbed by the Sun. The purpose of weather and ocean currents is to balance out these two extremes.

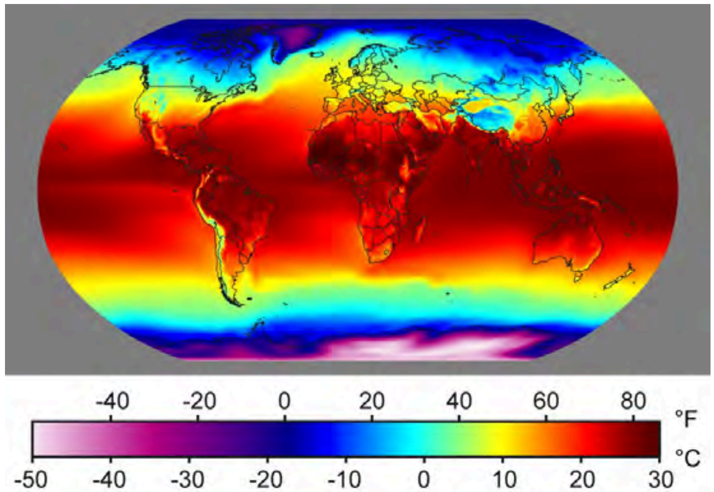

Figure 14.19: Global map of the annually averaged near-surface air temperature from 1961 to 1990. Figure description available at the end of the chapter.

The next impact on temperature is the land-water distribution on the planet. Places near the ocean tend to have milder climates year-round versus regions surrounded by land. This is because land can heat up and cool down faster and with more significant fluctuation than the ocean. The reason is that sunlight must heat a larger volume of area in the ocean since light can pass through water. Water requires five times more energy to rise in heat by one degree Celsius than for landmasses (water has a high specific heat). Thus, the temperatures of regions near large bodies of water change more slowly compared to land.

Ocean currents are also vital controls in transferring heat around the planet. In the Northern Hemisphere, ocean currents rotate clockwise, bringing cold water from the North Pole toward the equator and warm water from the equator toward the North Pole. The opposite occurs in the Southern Hemisphere, where ocean currents rotate counterclockwise. This results in overall cooler temperatures along the west coasts of continents and warmer temperatures along the east coasts.

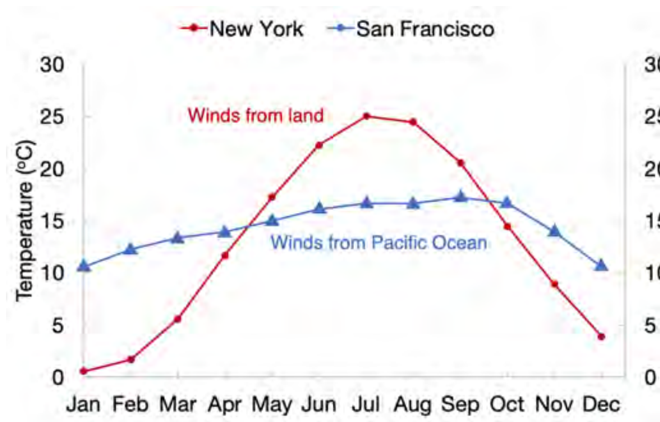

Figure 14.20: Average air temperatures in New York City and San Francisco. Winds from the west influence the climates of San Francisco and New York, but San Francisco has gentle seasons thanks to the cooling influence from the Pacific Ocean. Figure description available at the end of the chapter.

The last control of temperature is elevation. On average, atmospheric temperature decreases 3.5°F per 1,000 feet rise in elevation (6.4°C/km). This is called the normal lapse rate (a.k.a. temperature lapse rate).

Take this quiz to check your comprehension of this section.

Access the quiz for Section 14.2 by scanning the QR code.

14.3 Severe Weather

Severe weather is classified as "a series of events that can cause destructive or deadly effects on the ground" (NOAA). Severe weather can occur under a variety of situations, but three characteristics are generally needed: a temperature or moisture boundary, moisture, and (in the event of severe, precipitation-based events) instability in the atmosphere.

14.3.1 Thunderstorms

Weather happens every day, but only some days have storms. Storms vary immensely depending on whether they're warm or cold, coming off the ocean or off a continent, occurring in summer or winter, and many other factors. The effects of storms also vary depending on whether they strike a populated area or a natural landscape. Hurricane Katrina is a good example, since the flooding after the storm severely damaged New Orleans, while a similar storm in an unpopulated area would have done little damage. Thunderstorms are extremely common, with 14 million happening around the world every year; that's 40,000 per day! Most drop a lot of rain on a small area quickly, but some are severe and highly damaging. They form when ground temperatures are high, ordinarily in the late afternoon or early evening in spring and summer.

Figure 14.21: A thunderstorm with a classic anvil at the top. Figure description available at the end of the chapter.

All thunderstorms go through a three-stage life cycle. The first stage is called the cumulus stage, where an air parcel is forced to rise, cool, and condense—occurring at the lower condensation level—to develop into a cumulus cloud. The process of water vapor condensing into liquid water releases large quantities of latent heat, which makes the air within the cloud warmer and unstable, causing the cloud to continue to grow upward like a hot air balloon. These rising air parcels, called updrafts, prevent precipitation from falling from the cloud. But once the precipitation becomes too heavy for the updrafts to hold up, the moisture begins to fall, creating downdrafts within the cloud. The downdrafts also begin to pull cold, dry air from outside the cloud toward the ground in a process called entrainment.

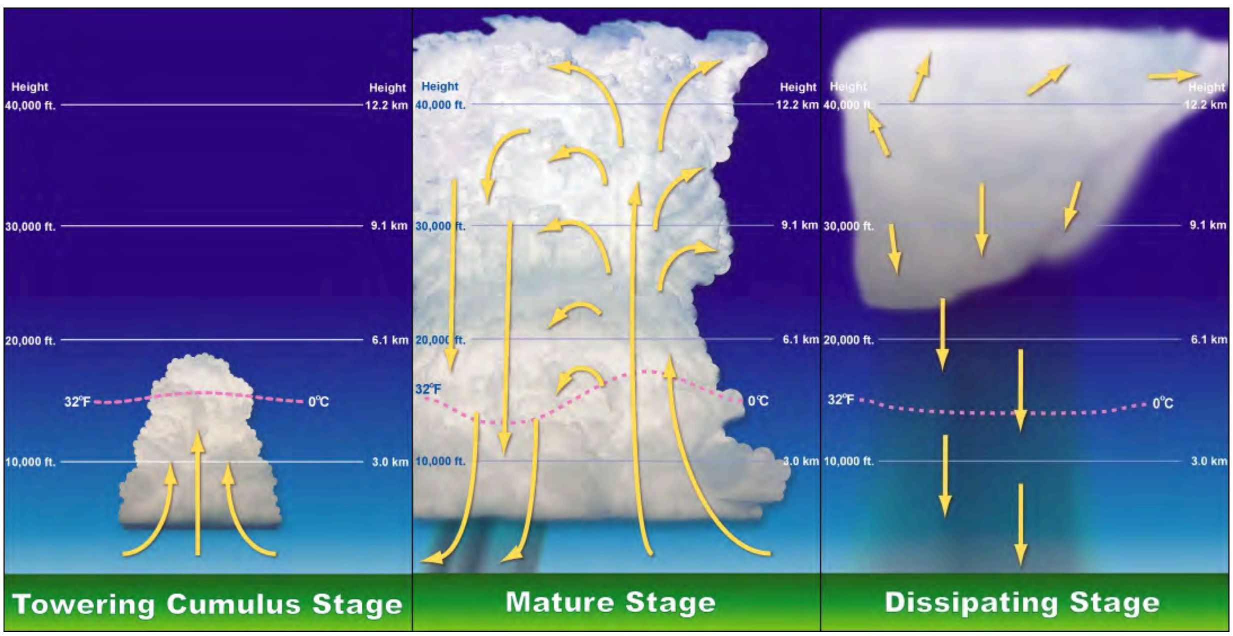

Figure 14.22: A diagram of thunderstorm formation. Figure description available at the end of the chapter.

Once the precipitation begins to fall from the cloud, the storm has reached the mature stage. During this stage, updrafts and downdrafts exist side-by-side and the cumulonimbus is called a cell. If the updrafts reach the top of the troposphere, the cumulus cloud will begin to spread outward, creating a defined anvil. At the same time, the downdrafts spread within the cloud and at first widen the cloud but eventually overtake the updrafts. Cool downdrafts form when precipitation and the cool air from entrainment are dragged down to the lower regions of a thunderstorm. It is also during the mature stage that the storm is most intense, producing strong, gusting winds, heavy precipitation, lightning, and possibly small hail.

Once the downdrafts overtake the updrafts, which also prevents the release of latent heat energy, the thunderstorm will begin to weaken into the third and final stage, called the dissipating stage. During this stage, light precipitation and downdrafts become the dominant feature within the cloud as it weakens. In all, only 20% of the moisture within the cloud fell as precipitation, whereas the other 80% evaporates back into the atmosphere.

The downdrafts of severe thunderstorms are so intense that, when they hit the ground, it sends warm air from the ground upward into the storm. The warm air gives the convection cells more energy. Rain and hail grow huge before gravity pulls them to Earth. Severe thunderstorms can last for hours and can cause a lot of damage because of high winds, flooding, intense hail, and tornadoes. Thunderstorms can form individually or in squall lines along a cold front. In the United States, squall lines form in spring and early summer in the Midwest, where the maritime tropical (mT) air mass from the Gulf of Mexico meets the continental polar (cP) air mass from Canada. So much energy collects in cumulonimbus clouds that a huge release of electricity, called lightning, may result. The electrical discharge may be between one part of the cloud and another, two clouds, or a cloud and the ground.

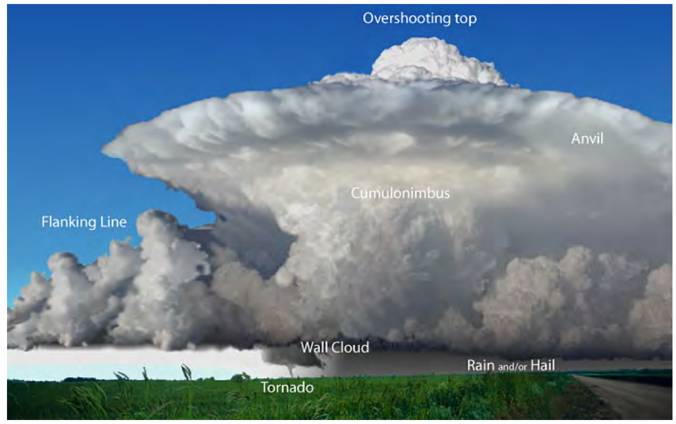

Figure 14.23: Some of the features found in a supercell storm. Every storm is different. Not all storms will display all of the features of a classic supercell. Figure description available at the end of the chapter.

14.3.2 Tornadoes

Figure 14.24: F5 tornado (upgraded from initial estimate of F4) viewed from the southeast as it approached Elie, Manitoba, on June 22nd, 2007. Figure description available at the end of the chapter.

Tornadoes, also called twisters, are fierce products of severe thunderstorms. As air in a thunderstorm rises, the surrounding air races in to fill the gap, forming a funnel. A tornado lasts from a few seconds to several hours. The average wind speed is about 177 kph (110 mph), but some winds are much faster. A tornado travels over the ground at about 45 kph (28 mph) and goes about 25 km (16 m) before losing energy and disappearing. An individual tornado may strike a small area, but it can destroy everything in its path. Most injuries and deaths from tornadoes are caused by flying debris. In the United States, an average of 90 people are killed by tornadoes each year. The most violent two percent of tornadoes account for 70% of the deaths by tornadoes.

The anatomy and development of tornadoes are not fully understood, but they form from cold fronts, severe thunderstorms, squall lines, supercells, and hurricanes. Geography also plays a crucial role in determining where tornadoes can and cannot form. The majority of thunderstorms in the United States form in the Midwest, which includes an area known as Tornado Alley. This region is where continental polar (cP) air masses from Canada collide with maritime tropical (mT) air from the Gulf of Mexico. This wind shear creates unstable atmospheric conditions and a rotating corkscrew column of air.

Figure 14.25: A diagram of the location of Tornado Alley and the related weather systems. Figure description available at the end of the chapter.

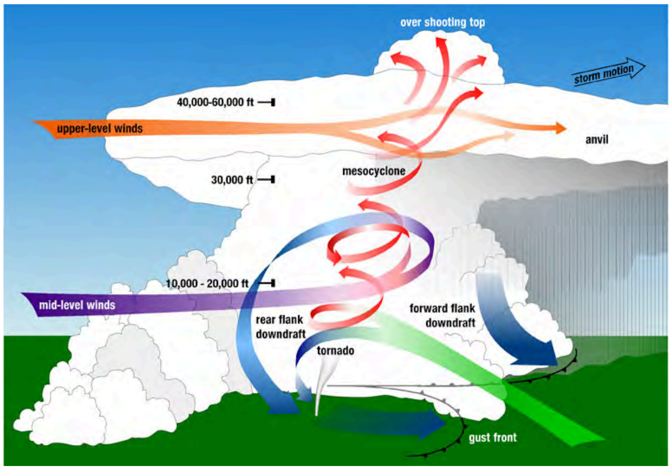

Figure 14.26: Tornadic supercell. Figure description available at the end of the chapter.

As the ground heats up through the day, updrafts pick up the rotating air into a portion of the thunderstorm to develop what is called a rotating mesocyclone. The updrafts stretch and tighten the now vertical column of air, causing it to rotate faster, much like an ice skater tightens to spin faster. As the rotating updrafts rise, a rotating wall cloud begins to form from the base of a mesocyclone. Sometimes a funnel cloud may begin to descend from the mesocyclone; it may even become a tornado if it reaches the ground.

Although there is an average of 770 tornadoes annually, the number of tornadoes each year varies greatly. In late April 2011, the situation was ripe for the deadliest set of tornadoes in 25 years. In addition to the meeting of cP and mT mentioned above, the jet stream was blowing strongly in from the west. The result was more than 40 tornadoes confirmed each day of the outbreak, with a one-day record of 223 on April 27. The entire region was alerted to the possibility of tornadoes in those late April days. But meteorologists can only predict tornado danger over a very wide region. No one can tell exactly where and when a tornado will touch down. Once a tornado is sighted on radar, its path is predicted and a warning is issued to people in that area. The exact path is unknown because tornado movement is not very predictable.

The intensity of tornadoes is measured on the enhanced Fujita scale, which assigns a value based on wind speed and damage. The enhanced Fujita scale, or EF scale, which became operational on February 1, 2007, is used to assign a tornado a rating based on estimated wind speeds and related damage. When tornado-related damage is surveyed, it is compared to a list of damage indicators (DIs) and degrees of damage (DoD), which help estimate better the range of wind speeds the tornado likely produced. From that, a rating (from EF0 to EF5) is assigned. The EF scale was revised from the original Fujita scale to reflect better examinations of tornado damage surveys so as to align wind speeds more closely with associated storm damage. The new scale has to do with how most structures are designed.

EF SCALE	
EF Rating	3 Second Gust (mph)
0	65-85
1	86-110
2	111-135
3	136-165
4	166-200
5	Over 200

Figure 14.27: The enhanced Fujita scale (EF scale). Figure description available at the end of the chapter.

14.3.3 Hurricanes

Tropical cyclones are considered some of the most powerful weather systems on the planet because of their size, strength, and potential loss to life and property. Tropical cyclones go by different names depending on geographic location. In North and Central America, they are called hurricanes. In the northwestern portion of the Pacific Ocean near China and Japan, they are called typhoons. Furthermore, in the Indian Ocean and Australia, they are called cyclones.

By any name, they are the most damaging storms on Earth. Hurricanes arise in the tropical latitudes (between 10° and 25° N) in summer and autumn when sea surface temperatures are 28°C (82°F) or higher. The warm seas create a large humid air mass. The warm air rises and forms a low-pressure cell, known as a tropical depression. Thunderstorms materialize around the tropical depression. If the temperature reaches or exceeds 28°C (82°F), the air begins to rotate around the low pressure (counterclockwise in the Northern Hemisphere and clockwise in the Southern Hemisphere). As the air rises, water vapor condenses, releasing energy from latent heat. If wind shear is low, the storm builds into a hurricane within two to three days.

Figure 14.28: Tropical cyclone Hurricane Florence in 2018 as viewed from International Space Station. The eye, eyewall, and surrounding rainbands are characteristics of tropical cyclones. Figure description available at the end of the chapter.

Hurricanes are huge systems with high winds. The exception is the relatively calm eye of the storm, where air rises upward. Rainfall can be as high as 2.5 cm (1 in) per hour, resulting in about 20 billion metric tons of water released daily in a hurricane. The release of latent heat generates enormous amounts of energy, nearly the total annual electrical power consumption of the United States from one storm. Hurricanes can also generate tornadoes.

The structure of a hurricane is fairly simple, though the processes involved are quite complex. As a low-pressure disturbance forms, the warm, moist air rushes toward the low pressure in order to rise upward to form towering thunderstorms. Around the low-pressure disturbance is a wall of clouds called an eye wall. Within the eye wall, the wind speeds are greatest, the clouds are the tallest, atmospheric pressure is at its lowest, and precipitation is most intense.

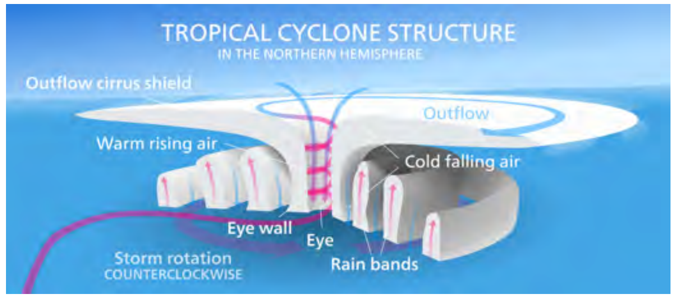

Figure 14.29: Diagram of a tropical cyclone (hurricane) in the Northern Hemisphere. Figure description available at the end of the chapter.

At the center, or heart, of the hurricane is the eye. Within the eye of a hurricane, winds are light, precipitation is minimal, and occasionally the skies above are clear. It is the calm region of the tropical storm, but that is what makes it so dangerous. Many people tend to go outside as the eye moves overhead because they believe the storm is over. But what some don't realize is that "round two" is coming from behind. Moving away from the eye wall are organized, intense thunderstorms called spiral rain bands, which rotate around and toward the storm's eye wall.

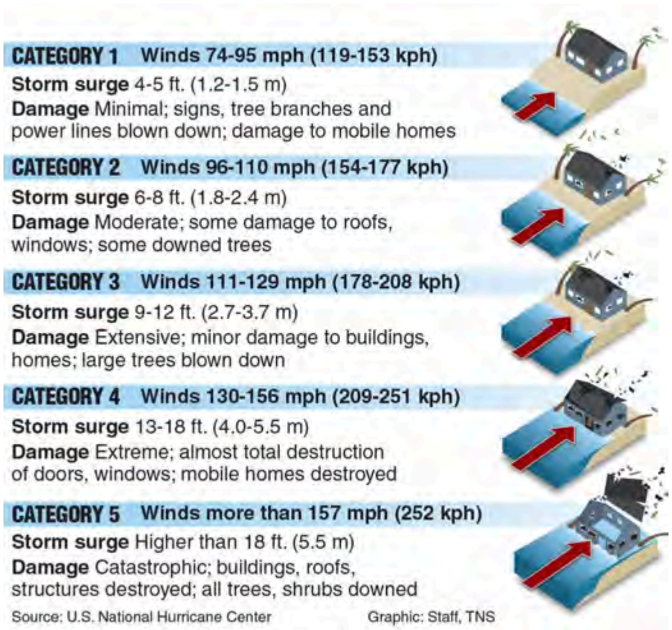

Figure 14.30: The Saffir-Simpson hurricane wind scale is a 1 to 5 rating based on a hurricane's sustained wind speed. Figure description available at the end of the chapter.

Hurricanes are assigned to categories based on their wind speed and estimated damage. The Saffir-Simpson scale was created to determine the strength and intensity of hurricanes. Just like the Fujita scale, it ranges from 1 to 5, with Category 5 being the strongest. The intensity of a hurricane increases as the atmospheric pressure near the eye decreases and the pressure-gradient force becomes steeper (atmospheric pressure decreases rapidly toward the eye), causing the winds to intensify, resulting in the potential for more damage.

For many years, hurricanes were named based on where they struck land. For example, the Galveston hurricane hit Galveston, Texas, in 1900. In the early 1900s, scientists started naming hurricanes using female names—clearly a sexist action by mostly white, male scientists at the time. But by the 1950s, the National Hurricane Center started naming hurricanes alphabetically, starting with the letter A and using male and female names. If the first year started the letter A with a female name, the following year, the first name would be male. The names are also determined six years in advance so that politics do not get involved with the naming of these deadly storms.

Hurricanes move with the prevailing winds. In the Northern Hemisphere, they originate in the trade winds and move to the west. When they reach the latitude of the westerlies, they switch direction and travel toward the north or northeast. Hurricanes may cover 800 km (500 mi) in one day.

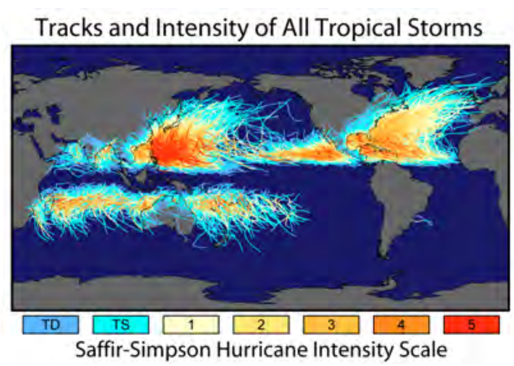

Figure 14.31: The common paths of all tropical storms, based on all storm tracks available from the National Hurricane Center and the Joint Typhoon Warning Center through September 2006. Figure description available at the end of the chapter.

Hurricanes typically last between five and ten days. Over cooler water or land, the hurricane's latent heat source shut downs and the storm weakens. When a hurricane disintegrates, it is replaced with intense rains and tornadoes. There are about 100 hurricanes around the world each year, plus many smaller tropical storms and tropical depressions. As people develop coastal regions, property damage from storms continues to rise. However, scientists are becoming better at predicting the paths of these storms and fatalities are decreasing.

The National Hurricane Center (NHC) is the division of the United States' National Oceanic and Atmospheric Administration (NOAA)/National Weather Service (NWS) responsible for tracking and predicting tropical weather systems between the prime meridian and the 140th meridian west poleward to the 30th parallel north in the northeast Pacific Ocean and the 31st parallel north in the northern Atlantic Ocean. Although the NHC is an agency of the United States, the World Meteorological Organization has designated it as the Regional Specialized Meteorological Center for the North Atlantic and eastern Pacific, making it the epicenter for tropical cyclone forecasts and observations occurring in these areas.

Damage from hurricanes comes from the high winds, rainfall, and storm surge. Storm surge occurs as the storm's low-pressure center comes onto land, causing the sea level to rise unusually high. A storm surge is often made worse by the hurricane's high winds blowing seawater across the ocean onto the shoreline. Flooding can be devastating, especially along low-lying coastlines such as the Atlantic and Gulf Coasts. Hurricane Camille in 1969 had a 7.3 m (24 ft) storm surge that traveled 200 km (125 mi) inland.

Figure 14.32: Hurricane Camille historical marker along US Route 29 and Virginia State Route 6 (Thomas Nelson Highway) near Woods Mill in Nelson County, Virginia. Figure description available at the end of the chapter.

14.3.4 Winter Storms and Blizzards

Blizzards are dangerous winter storms that are a combination of blowing snow and wind, resulting in very low visibilities. While heavy snowfalls and severe cold often accompany blizzards, they are not required. Sometimes strong winds pick up snow that has already fallen, creating a ground blizzard. Officially, the National Weather Service defines a blizzard as a storm which contains large amounts of snow *or* blowing snow, with winds in excess of 35 mph and visibilities of less than a quarter-mile for an extended period of time (at least three hours).

Figure 14.33: On March 29, 1881, snowdrifts in Minnesota were higher than locomotives. Figure description available at the end of the chapter.

Blizzards happen across the middle latitudes and toward the poles, usually as part of a mid-latitude cyclone. Blizzards are most common in winter, when the jet stream has traveled south and a cold, northern air mass comes into contact with a warmer, semitropical air mass. The very strong winds develop because of the pressure gradient between the low-pressure storm and the higher pressure west of the storm. Snow produced by the storm gets caught in the winds and blows nearly horizontally. Blizzards can also produce sleet or freezing rain.

Blizzards can create life-threatening conditions. Traveling by automobile can become difficult or even impossible due to "whiteout" conditions and drifting snow. Whiteout conditions occur most often with major storms that produce drier, more powdery snow. In this situation, it doesn't even need to be snowing to produce whiteout conditions, as the snow already on the ground is blown around, reducing the visibility to near zero at times.

The strong winds and cold temperatures accompanying blizzards can combine to create another danger. The wind chill factor is the amount of cooling one feels due to the combination of wind and temperature. During blizzards, with the combination of cold temperatures and strong winds, very low wind chill values can occur. It is not uncommon in the Midwest to have wind chills below -60°F during blizzard conditions. Blizzards also can cause a variety of other problems. Power outages can occur due to strong winds and heavy snow. Pipes can freeze and regular fuel sources may be cut off.

Figure 14.34: Heavy snow during the January 2016 United States blizzard. Figure description available at the end of the chapter.

14.3.5 Heat Waves

Another potentially deadly weather phenomena is a heat wave. A heat wave is different for different locations; it is a long period of hot weather, at least 86°F (30°C) for at least three days in cooler locations but much more in hotter locations. Heat waves can occur with or without high humidity. They have potential to cover a large area, exposing a high number of people to hazardous heat.

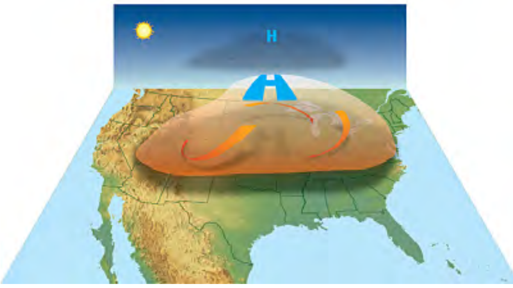

Figure 14.35: A high-pressure system in the upper atmosphere traps heat near the ground, forming a heat wave (for North America in this example). Figure description available at the end of the chapter.

Heat waves form when a high-pressure area in the upper atmosphere strengthens and remains over a region for several days and up to several weeks. This traps heat near the Earth's surface. It is usually possible to forecast heat waves, thus allowing authorities to issue a warning in advance. Heat waves have become more frequent and more intense over land, affecting almost every area on Earth since the 1950s.

Heat waves have an impact on the economy. They can reduce labor productivity, disrupt agricultural and industrial processes, and damage infrastructure. Severe heat waves have caused catastrophic crop failures and thousands of deaths from hyperthermia. They have increased the risk of wildfires in areas with drought. They can lead to widespread electricity outages because more air conditioning is used.

Category	Risk of Heat-Related Impacts
Green 0	Little to no risk from expected heat.
Yellow 1	Minor - This level of heat affects primarily those individuals extremely sensitive to heat, especially when outdoors without effective cooling and/or adequate hydration.
Orange 2	Moderate - This level of heat affects most individuals sensitive to heat, especially those without effective cooling and/or adequate hydration. Impacts possible in some health systems and in heat-sensitive industries.
Red 3	Major - This level of heat affects anyone without effective cooling and/or adequate hydration. Impacts likely in some health systems, heat-sensitive industries and infrastructure.
Magenta 4	Extreme - This level of rare and/or long-duration extreme heat with little to no overnight relief affects anyone without effective cooling and/or adequate hydration. Impacts likely in most health systems, heat-sensitive industries and infrastructure.

Figure 14.36: The National Weather Service risk categories for NWS HeatRisk. Figure description available at the end of the chapter.

Heat poses danger to human health and there are a variety of heat related illnesses that can occur. During extremely hot and humid weather, your body's ability to cool itself is challenged. When the body heats too rapidly to cool itself properly, or when too much fluid or salt is lost through dehydration or sweating, body temperature rises. You or someone you care about may experience a heat-related illness. It is important to know the symptoms of excessive heat exposure and the appropriate responses. The Centers for Disease Control and Prevention (CDC) provides a list of warning signs and symptoms of heat illness, and recommended first aid steps, which can be viewed here.

Take this quiz to check your comprehension of this section.

Access the quiz for Section 14.3 by scanning the QR code.

Summary

Weather is defined as the short-term atmospheric conditions at a specific time and place, influenced by variables like air temperature, pressure, and humidity. In contrast, climate refers to the long-term average weather patterns of a region, shaped by factors such as solar energy, geographic location, and altitude. Both weather and climate are directly affected by the Sun's energy and how it interacts with the atmosphere. The troposphere, where nearly all weather occurs, is influenced by processes like convection and the greenhouse effect, which help trap heat and maintain the planet's temperature balance. The atmosphere plays a vital in maintaining life on Earth by regulating temperature, supporting the water cycle, and protecting the planet from harmful solar radiation.

Key atmospheric processes such as the formation of clouds, precipitation, and the dynamics of air masses and weather fronts contribute to daily weather patterns and broader climate dynamics. The movement of air masses and the interactions at weather fronts play a critical role in shaping storms and other weather phenomena. Heat moves through various types of energy transfer including radiation, conduction, and convection.

Severe weather events like thunderstorms, tornadoes, hurricanes, and blizzards are driven by atmospheric instability, temperature differences, and moisture levels, with each event posing significant risks to both human life and property. It is important to understand these processes not only to predict weather more accurately but also to mitigate the effects of increasingly severe weather events exacerbated by climate change.

Take this quiz to check your comprehension of this chapter.

Access the quiz for Chapter 14 by scanning the QR code.

Chapter URLs

- List of warning signs and symptoms of heat illness, and recommended first aid steps from the Centers for Disease Control and Prevention (CDC): https://www.weather.gov/safety/heat-illness

Text References

1. Dastrup, R.A. (2020). *Physical geography and natural disasters OER textbook:* Salt Lake Community College. Creative Commons Attribution NonCommercial ShareAlike. Text adapted (remixed) by Laura Neser for clarification and formatting purposes only. https://slcc.pressbooks.pub/physicalgeography
2. Estrada, C., Michel, C.L., Wilson, M., Simpson, Je., Santoro, M., and Megivern, K.J. (2021). *Dynamic planet: Exploring geological disasters and environmental change OER textbook:* Maricopa CommunityColleges. Creative Commons Attribution-NonCommercial-ShareAlike 4.0 International License. Text adapted (remixed) by Laura Neser for clarification and formatting purposes only. https://open.maricopa.edu/hazards/frontmatter/introduction
3. National Oceanic & Atmospheric Administration, Severe weather. Public domain. https://www.nesdis.noaa.gov/our-environment/severe-weather
4. National Oceanic & Atmospheric Administration, Winter storms and blizzards. Public domain. https://www.weather.gov/fgz/WinterStorms
5. Solada, K., and Daniels, K.S. (2021). *Principles of Earth science OER textbook:* Open Oregon Educational Resources. Creative Commons Attribution-NonCommercial-ShareAlike 4.0 International License. Text adapted (remixed) by Laura Neser for clarification and formatting purposes only. https://openoregon.pressbooks.pub/earthscience
6. Wikipedia, Heat wave. CC-BY-SA. https://en.wikipedia.org/wiki/Heat_wave
7. Wikipedia, List of severe weather phenomena. CC-BY-SA. https://en.wikipedia.org/wiki/List_of_severe_weather_phenomena
8. Wikipedia, National Hurricane Center. CC-BY-SA. https://en.wikipedia.org/wiki/National_Hurricane_Center

Figure References

Figure 14.1: Layers of Earth's atmosphere. Medium69. 2014. CC BY-SA. https://commons.wikimedia.org/wiki/File:Atmosphere_structure-en.svg

Figure 14.2: The ozone layer absorbs a portion of the radiation from the Sun, preventing it from reaching the planet's surface. Felton Davis. 2020. CC BY. https://www.flickr.com/photos/felton-nyc/50768574522

Figure 14.3: Pie chart of Earth's atmospheric composition. Dbc334. 2015. Public domain. https://commons.wikimedia.org/wiki/File:Composizione_dell%27atmosfera_terrestre.svg

Figure 14.4: Atmospheric pressure decreases as altitude increases. National Oceanic and Atmospheric Administration (NOAA). Last updated 18 December 2023. Public domain. https://www.noaa.gov/jetstream/atmosphere/air-pressure

Figure 14.5: Layers of Earth's atmosphere with associated temperature changes. NOAA. Last updated Aug 20, 2024. Public domain. https://www.noaa.gov/jetstream/atmosphere/layers-of-atmosphere

Figure 14.6: Thermal profile of Earth's atmosphere, showing the major divisions based on temperature. Benjamin J. Burger. 3 June 2020. CC BY-SA. https://commons.wikimedia.org/wiki/File:Thermal-Profile-of-Earths-Atmosphere.gif

Figure 14.7: Oscillations of electric and magnetic fields of an electromagnetic wave. Piotr Fita. 30 Jan 2023. Public domain. https://commons.wikimedia.org/wiki/File:Electromagnetic_wave_EN.svg

Figure 14.8: The percentage of diffusely reflected sunlight relative to various surface conditions. Wereon. 16 August 2006. CC BY-SA. https://en.wikipedia.org/wiki/Albedo#/media/File:Albedo-e_hg.svg

Figure 14.9: Solar radiation is strongest near the equator and weaker at the poles. Peter Halasz. 26 June 2007. CC BY-SA. https://commons.wikimedia.org/wiki/File:Oblique_rays_02_Pengo.svg

Figure 14.10: Earth's greenhouse effect. EPA. 2012. Public domain. https://upload.wikimedia.org/wikipedia/commons/8/8e/Earth's_greenhouse_effect_(US_EPA,_2012).png

Figure 14.11: Global distribution of relative humidity at the surface, averaged over the years 1981–2010. Greenmind1980. 4 July 2022. CC BY-SA. https://en.wikipedia.org/wiki/Humidity#/media/File:RH_wiki.png

Figure 14.12: Tropospheric clouds. Petr Hykš. 12 December 2018. CC BY-NC 2.0. https://www.flickr.com/photos/violetplanet/46239433602

Figure 14.13: Cloud types. Valentin de Bruyn. 3 January 2012. CC BY-SA. https://commons.wikimedia.org/wiki/File:Cloud_types_en.svg

Figure 14.14: Advection fog layer in San Francisco with the Golden Gate Bridge and skyline in the background. Brocken Inaglory. 26 September 2009. CC BY-SA. https://en.wikipedia.org/wiki/Fog#/media/File:San_francisco_in_fog_with_rays.jpg

Figure 14.15: North American air masses. NOAA. Last updated 5 June 2023. Public domain. https://www.noaa.gov/jetstream/synoptic/air-masses

Figure 14.16: Source regions of global air masses (NASA). NASA. 15 November 2008. Public domain. https://commons.wikimedia.org/wiki/File:Air_masses.svg

Figure 14.17: Guide to weather map symbols for weather fronts. -xfi-. 14 August 2006. Adapted by Laura Neser. CC BY-SA. https://commons.wikimedia.org/wiki/File:Weather_fronts.svg

Figure 14.18: Illustration of a warm front. Kelvinsong. 31 December 2014. CC BY-SA. https://commons.wikimedia.org/wiki/User:IsadoraofIbiza#/media/File:Warm_front.svg

Figure 14.19: Global map of the annually averaged near-surface air temperature from 1961 to 1990. Robert A. Rohde. 15 February 2008. Adapted by Laura Neser. CC BY-SA. https://commons.wikimedia.org/wiki/File:Annual_Average_Temperature_Map.jpg

Figure 14.20: Average air temperatures in New York City and San Francisco. Jturner20. 9 November 2021. Adapted by Laura Neser. CC BY-SA. https://commons.wikimedia.org/wiki/File:Ocean_influence_on_climate_at_four_example_locations.png

Figure 14.21: A thunderstorm with a classic anvil at the top. Griffinstorm. 16 August 2014. CC BY-SA. https://en.wikipedia.org/wiki/Thunderstorm#/media/File:Single-cell_Thunderstorm_in_a_No-shear_Environment.jpg

Figure 14.22: A diagram of thunderstorm formation. NOAA. 7 June 2010. Public domain. https://en.wikipedia.org/wiki/Thunderstorm#/media/File:Thunderstorm_formation.jpg

Figure 14.23: Some of the features to be found in a supercell storm. NOAA. Accessed September 2024. Public domain. https://www.nssl.noaa.gov/education/svrwx101/thunderstorms/types

Figure 14.24: F5 tornado (upgraded from initial estimate of F4) viewed from the southeast as it approached Elie, Manitoba, on June 22nd, 2007. Justin1569. 22 June 2007. CC BY-SA. https://en.wikipedia.org/wiki/Tornado#/media/File:F5_tornado_Elie_Manitoba_2007.jpg

Figure 14.25: A diagram of the location of Tornado Alley and the related weather systems. Dan Craggs. 18 September 2009. CC BY-SA. https://commons.wikimedia.org/wiki/File:Tornado_Alley_Diagram.svg

Figure 14.26: Tornadic supercell. NOAA. 4 April 2007. Public domain. https://commons.wikimedia.org/wiki/File:Tornadic_supercell.jpg

Figure 14.27: The enhanced Fujita scale (EF scale). National Weather Service. Accessed September 2024. Public domain. https://www.weather.gov/oun/efscale

Figure 14.28: Tropical cyclone Hurricane Florence in 2018 as viewed from International Space Station. NASA Goddard Space Flight Center. 12 September 2018. CC BY. https://en.wikipedia.org/wiki/Tropical_cyclone#/media/File:Dramatic_Views_of_Hurricane_Florence_from_the_International_Space_Station_From_9_12_(42828603210).jpg

Figure 14.29: Diagram of a tropical cyclone (hurricane) in the Northern Hemisphere. Kelvinsong. 16 December 2012. CC BY. https://en.wikipedia.org/wiki/Tropical_cyclone#/media/File:Hurricane-en.svg

Figure 14.30: The Saffir-Simpson hurricane wind scale is a 1 to 5 rating based on a hurricane's sustained wind speed. Thomas Cizauskas. 8 September 2017. Public domain. https://www.flickr.com/photos/cizauskas/36294300853

Figure 14.31: The common paths of all tropical storms, based on all storm tracks available from the National Hurricane Center and the Joint Typhoon Warning Center through September 2006. NASA earth Observatory. Image of the Day for 2 November 2006. Public domain. https://earthobservatory.nasa.gov/images/7079/historic-tropical-cyclone-tracks

Figure 14.32: Hurricane Camille historical marker along US Route 29 and Virginia State Route 6 (Thomas Nelson Highway) near Woods Mill in Nelson County, Virginia. Famartin. 27 May 2016. CC BY-SA. https://commons.wikimedia.org/wiki/File:2016-05-27_09_07_16_Hurricane_Camille_historical_marker_along_U.S._Route_29_and_Virginia_State_Route_6_%28Thomas_Nelson_Highway%29_near_Woods_Mill_in_Nelson_County,_Virginia.jpg

Figure 14.33: On March 29, 1881, snowdrifts in Minnesota were higher than locomotives. Minnesota Historical Society. 29 March 1881. Public domain. https://en.wikipedia.org/wiki/Blizzard#/media/File:Train_stuck_in_snow.jpg

Figure 14.34: Heavy snow during the January 2016 United States blizzard. NOAA. 23 January 2016. CC BY. https://en.wikipedia.org/wiki/Blizzard#/media/File:Blizzard3_-_NOAA.jpg

Figure 14.35: A high-pressure system in the upper atmosphere traps heat near the ground, forming a heat wave (for North America in this example). US National Weather Service/National Ocean Service. 21 July 2011. Public domain. https://en.wikipedia.org/wiki/Heat_wave#/media/File:Heat_Wave.jpg

Figure 14.36: The National Weather Service risk categories for NWS HeatRisk. National Weather Service. Accessed September 2024. Public domain. https://www.wpc.ncep.noaa.gov/heatrisk

Figure Descriptions

Figure 14.1: Illustration of Earth as seen from space, with the layers of the atmosphere and their altitude ranges labeled along a straight line outward from Earth's surface. The troposphere is closest to Earth's surface, labeled 0-12 km; the stratosphere is above the troposphere, labeled 12-50 km; the mesosphere is above the stratosphere, labeled 50-80 km, the thermosphere is above the mesosphere, labeled 80-600 km, and the exosphere is the outermost layer, labeled greater than 600 km.

Figure 14.2: Illustration of the Sun on the left and Earth on the right with three colored arrows of different lengths pointing from the Sun to Earth. The lowermost arrow is white, labeled UV-A, and extends through Earth's atmosphere to Earth's surface; the middle arrow is yellow, labeled UV-B, and extends to a layer above Earth's surface labeled Ozone Layer with a smaller yellow arrow traveling through the Ozone layer to the surface of Earth; and the top arrow is red, labeled UV-C, and extends to the top of the Ozone Layer.

Figure 14.3: A color-coded pie chart showing the percentage of Earth's atmospheric gases. 78% of the pie chart is orange for nitrogen, 21% is purple for oxygen, 1% is gray for argon, less than 1% is teal for carbon dioxide, and less than 1% is navy blue for other gases.

Figure 14.4: Photograph of a desert area with an expanse of blue sky above the area; the image is split in half vertically and the left half has a partially transparent overlay of tan cartoon bubbles with a higher density of bubbles at the bottom, decreasing in density upwards.

Figure 14.5: Graph with temperature along the bottom horizontal axis labeled Temperature in degrees Celsius that goes from more than -100 on the left to over 60 on the right. The vertical axes represent altitude above Earth's surface with the left vertical axis labeled from 0 upward to 130 km above the surface and the right vertical axis labeled from 0 upward to 81 mi above the surface. The temperature is plotted as a yellow arrow that increases in altitude; at 0 km altitude, the arrow starts at about 18 degrees Celsius, decreasing in temperature upward until 12 km where it reaches about -58 degrees Celsius, and this section is labeled Troposphere with the Tropopause labeled at its top. The yellow arrow continues upward vertically until about 20 km altitude, then begins increasing in temperature until it reaches about 0 degrees Celsius at 50 km altitude and this section is labeled Stratosphere with the Stratopause labeled at its top. The yellow arrow continues upward vertically until about 52 km altitude, then begins decreasing in temperature until it reaches about -90 degrees Celsius at 80 km altitude and this section is labeled Mesosphere with the Mesopause labeled at its top. The yellow arrow continues upward vertically until about 90 km altitude, then begins rapidly increasing in temperature until it reaches over 70 degrees Celsius at 120 km altitude with the arrow pointing off the graph and this section is labeled Thermosphere.

Figure 14.6: Graph with temperature along the bottom horizontal axis that goes from colder on the left to warmer on the right. The vertical axis is labeled altitude. The temperature is plotted as a black curved line; at the bottom of the graph, the line starts just to the right of the center of the horizontal axis, decreasing in temperature with altitude in a section labeled Troposphere until the Tropopause labeled at its top. The black line then curves toward the right, increasing in temperature in a section labeled Stratosphere until the Stratopause labeled at its top. The black line then begins decreasing in temperature in a section labeled Mesosphere until it reaches the Mesopause labeled at its top. The black line then begins increasing in temperature in a section is labeled Thermosphere until it reaches the top of the graph.

Figure 14.7: Color-coded line graph with with two perpendicular waves that oscillate in unison: a red horizontal sine wave labeled magnetic field and a blue vertical sine wave labeled electric field. The line axis goes from left to right, indicating the waves' propogation direction to the right.

Figure 14.8: A pink chart that is labeled % along the left vertical side, going from 0 at the bottom to 100 at the top. Various surface conditions

are plotted with double-pointed vertical blue arrows as follows: on the far left is forms of water, with snow plotted from 40 to 85% and fresh snow labeled near the top and old snow labeled near the bottom; ice from 32-39%; and water from 6-9%. To the right of those arrows is dry sand from 38 to 44% and wet sand from 7 to 14. To the right of those arrows is dry soil from 22 to 34% and dark wet soil from 6 to 14%. To the right is an arrow from 36 to 78% with cumulus stratus labeled near the top and stratus labeled near the bottom; an arrow from 27-29% labeled desert; an arrow from 18-19% labeled savanna; and an arrow from 6 to 14% labeled forest. To the right of those arrows is altostratus cirrus from 41 to 59% and meadows from 11 to 19%.To the right of those arrows is crops from 15 to 25%.

Figure 14.9: Cartoon of the Earth in the lower right corner with a lavender shell around it labeled atmosphere and white outer space outside of that; the Sun is just barely showing to the left of the figure. There are three red horizontal arrows pointing from the Sun to the upper part of Earth labeled sun's rays, and the arrows span a circle on Earth's surface labeled large area. There are three other red horizontal arrows pointing from the Sun to the equatorial part of Earth labeled sun's rays, and the arrows span a smaller circle on Earth's surface labeled small area.

Figure 14.10: A cartoon of the Earth at the bottom of the figure and the Sun in the upper left. Two lines of blocky arrows point from the Sun to the Earth; one line consists of thicker blocky arrows reaching the Earth's surface, labeled Most radiation is absorbed by the Earth's surface and warms it. The set of lines to the right are thinner, labeled Some solar radiation is reflected by the Earth and the atmosphere; the line of arrows divides into two sets when they enter Earth's atmosphere with one set reflecting from the middle of the atmosphere and the other set reflecting from the Earth's surface. There is a very thick curved arrow that exits from Earth's surface, makes a U-turn in the atmosphere, and then points back to Earth's surface, labeled Infrared radiation is emitted by the Earth's surface.

Figure 14.11: World map color-coded according to relative humidity; the legend shows a color gradient with light bluish yellow representing approximately 30% humidity and navy blue representing 100% humidity. There are dark blue areas at the poles on the map and lighter areas everywhere else; notable regions with the lowest humidities include northern Africa, the Middle East, Australia, southwestern South America, and southwestern North America.

Figure 14.12: An illustrated chart of common cloud types depicted against a blue sky with brown land at the bottom, arranged in three categories based on their altitude. High clouds are the top row with cirrostratus depicted as thin, veil- like layers, cirrus depicted as thin, wispy streak, and cirrocumulus depicted as small, fluffy patches. Medium clouds are the middle row with altocumulus depicted as white slightly larger puffy clusters and altostratus depicted as a uniform, whitish sheet. Low clouds are the bottom row with stratocumulus depicted as low, lumpy layers, stratus depicted as flat, uniform gray layers near the surface, nimbostratus depicted as thick, dark rain clouds, and cumulus depicted as puffy, gray-white clouds with flat bases. One type of cloud spans low, medium, and high, labeled cumulonimbus, which has thick gray stormy clouds near the surface, thinning out to white clouds above, and spreading to a white anvil-shape with lightning at the top.

Figure 14.13: An illustrated chart of common cloud types depicted against a blue sky with green land at the bottom, arranged in three categories based on their altitude. High clouds are the top row at 23,000 to 40,000 feet altitude with cirrostratus (Cs) depicted as thin, veil-like layers, cirrus (Ci) depicted as thin, wispy streak, and cirrocumulus (Cc) depicted as small, fluffy patches. Mid clouds are the middle row at 6,500 to 23,000 feet altitude with altocumulus (Ac) depicted as white slightly larger puffy clusters and altostratus (As) depicted as a uniform, whitish sheet. Low clouds are the bottom row at 0 to 6,500 feet altitude with stratocumulus (Sc) depicted as lumpy layers, stratus (St) depicted as flat, low layers near the surface, cumulus (Cu) depicted as puffy, gray-white clouds with flat bases, and nimbostratus (Ns) spanning both Low and Mid levels depicted as thick, dark rain clouds. One type of cloud spans low, medium, and high, labeled cumulonimbus (Cb), which has thick gray stormy clouds near the surface, thinning out to white clouds above, and spreading to a white anvil-shape with lightning at the top.

Figure 14.14: Photograph of low-lying thick white cloud cover with the Golden Gate Bridge visible in the background rising out of the fog.

Figure 14.15: Grayscale illustration of the upper half of Earth with a grid overlain and colored partially transparent air masses labeled on top. The North pole is covered by a pink nearly circular air mass labeled Ca; there is a curved blue line with teeth pointing southward labeled Arctic Front around the southern border of the Ca air mass over northern North America. Just south of the curved blue line is a navy-blue air mass labeled cP that covers most of Canada with blue arrows pointing southward from the air mass. South of the cP air mass is another blue line with teeth pointing southward labeled Polar Front from the air mass; south of the blue line is a small orange air mass labeled cT in southwest North America. There are two light blue air masses labeled mP, one over the Pacific Ocean off the Pacific northwest coast of North America, and the other over the Atlantic Ocean off the northeast coast of North America. Lastly, there are two green air masses labeled mT, one over the Pacific Ocean off the Pacific southwest coast of North America, and the other over the Atlantic Ocean off the southeast coast of North America.

Figure 14.16: A world map with a grid overlain and color-coded air masses labeled on top. Navy-blue areas are labeled cA and/or cP, located over Antarctica, Greenland, northern North America, and north-central Asia. Light blue areas are labeled mP, located over the northern Atlantic Ocean, northern Pacific Ocean, southern Atlantic Ocean, and southern Pacific Ocean. Pink areas are labeled mT, located over the mid-northern Atlantic Ocean, mid- northern Pacific Ocean, mid-southern Atlantic Ocean, and mid-southern Pacific Ocean. Dark pink areas are labeled mE, located over the mid- Atlantic Ocean and mid-Pacific Ocean. Red areas are labeled cT, located over northern Africa and the Middle East, south-central Africa, central Australia, and west-central North America.

Figure 14.17: Four horizontal lines with triangles and/or semicircles along the length of each line according to the type of front. The top line has alternating red semicircles on top and blue triangles pointing downward, labeled stationary front. The second line has blue triangles on top pointing upward, labeled cold front. The third line has red semicircles on top, labeled warm front. The bottom line is purple and has alternating purple semicircles on top and purple triangles on top pointing upward, labeled occluded front.

Figure 14.18: Block diagram of thick white clouds hovering over green land with a blue sky in the background. There is a red line in front of the clouds with red semicircles along the line pointing toward the clouds labeled warm front. In front of that line are red arrows pointing in the direction of the clouds labeled Warm air mass (mT). The front portion of the clouds is labeled Rising warm air, and the clouds include the labels of specific cloud types within them including stratus and nimbostratus at the front, altostratus in the middle, and cirrostratus and cirrus at the back of the set of clouds; stratocumulus clouds are visible separately in front of the heavy cloud cover. The back side of the cloud cover is labeled Receding cold air, with a blue Cold air mass (cP) located there.

Figure 14.19: World map color-coded according to temperature; the legend shows a color gradient with light pink to white representing approximately -50 degrees Celsius, changing to deep blue around -25 degrees Celsius, light blue at 0 degree Celsius, yellow to orange from 10-15 degrees Celsius, and red up to 30 degrees Celsius. In terms of extremes, there is only one whitish-pink area over part of Antarctica, there are two dark blue areas at the poles on the map, and red areas cover the equator toward the midlatitudes.

Figure 14.20: Graph with temperature in degrees Celsius along the vertical axis from 0 at the bottom to 30 at the top. The months of the year are along the horizontal axis, starting with January at the left and December at the right. Two locations are plotted: New York is in red, starting at nearly 0 degrees in January, increasing smoothly to about 25 degrees in July, then decreasing to about 4 degrees in December; San Francisco is in blue, starting at 10 degrees in January, increasing slightly to about 17 degrees in September, then decreasing slightly to 10 degrees in December.

Figure 14.21: Photograph of a massive white cloud in the distance that includes smaller fluffy clouds at the base and a thick vertical column that rises upward, spreading into a wide flat top. There is a road and trees in the foreground.

Figure 14.22: A set of three diagrams showing the land surface at the bottom and altitude labeled upward to over 40,000 feet. The first diagram on the left is labeled towering cumulus stage and features a fluffy white cloud with a flat base at approximately 5,000 feet altitude and the top at approximately 19,000 feet altitude; there are three yellow arrows rising from the ground upward into the cloud and there is a nearly horizontal dashed line crossing near the top of the cloud labeled 0 degrees Celsius. The second diagram in the middle is labeled mature stage and features a towering high cloud with a flat base at approximately 5,000 feet altitude and the top at over 40,000 feet altitude; on the right half of the cloud there are many yellow arrows rising from the ground upward into the cloud and on the left half of the cloud there are yellow arrows pointing from the top of the cloud downward toward the ground where rain is occurring. There is a curvy dashed line crossing the cloud at approximately 15,000 feet altitude labeled 0 degrees Celsius. The third diagram on the right is labeled dissipating stage and features a high cloud with a curved base at approximately 22,000 feet altitude and a flat top at over 40,000 feet altitude; there are multiple yellow arrows pointing from the cloud downward toward the ground where rain is occurring and a few yellow arrows pointing up and to the right near the top of the cloud. There is a nearly horizontal dashed line below the cloud at approximately 15,000 feet altitude labeled 0 degrees Celsius.

Figure 14.23: Photograph of a massive set of clouds in the distance that includes smaller fluffy clouds at the base labeled flanking line, spreading into a single large wide cloud labeled cumulonimbus, with a smaller fluffy cloud on the top labeled overshooting top. The bottom of the set of clouds is labeled wall cloud and there is a tornado visible coming off the bottom; there is also rain and/or hail falling from the center base of the set of clouds. There is a road and a green field in the foreground.

Figure 14.24: Photograph of a whitish grey funnel cloud rising from the ground upward into the dark grey clouds above; there are visible bits of debris flying around the base of the tornado.

Figure 14.25: Map of the United States with color-coded weather systems overlain; there is a blue area labeled cold dry air over the northwest-central U.S. with an arrow pointing southeast toward the central U.S. An orange area labeled warm dry air is over the southwest U.S. with an arrow pointing east-northeast toward the central U.S. A light green area labeled warm moist air is over the southern U.S. with an arrow pointing northward toward the central U.S. A red area labeled tornado alley covers the central U.S. where the arrows converge.

Figure 14.26: A diagram of a towering cloud with mid-level winds entering from the left at an altitude of 10,000 to 20,000 feet and upper-level winds entering from the left at an altitude of 40,000 to 60,000 feet. There are spiraled arrows rising from the ground through the center of the cloud complex, exiting through the over shooting top. A tornado is drawn at the base of those arrows.

Figure 14.27: A two-column chart describing the Enhanced Fujita (EF) Scale with the left column titled EF Rating and the right column titled 3 Second Gust (mph). EF rating 0 corresponds with 65-85 mph 3 second gusts; EF rating 1 corresponds with 86-110 mph 3 second gusts; EF rating 2 corresponds with 111-135 mph 3 second gusts; EF rating 3 corresponds with 136-165 mph 3 second gusts; EF rating 4 corresponds with 166-200 mph 3 second gusts; and EF rating 5 corresponds with over 200 mph 3 second gusts.

Figure 14.28: Photograph of part of the Earth as seen from space with a massive, swirling cloud system with a well-defined, circular eye at its center, with parts of the International Space Station visible on the left-hand side of the photo.

Figure 14.29: Cartoon diagram of a hurricane cloud system in the northern hemisphere cut vertically in half to show the structure. There is a column of white cloud at the center labeled eye wall with blue arrows decreasing along the outer edge labeled cold falling air; a spiraling pink arrow points upward through the empty middle, labeled eye; the eye wall widens at its top to a flat- topped cloud labeled outflow cirrus shield. Surrounding the eye wall are three separate circular bands of clouds labeled rain bands, with pink arrows rising through each labeled warm rising air. The storm rotation is counterclockwise.

Figure 14.30: A chart describing the Saffir-Simpson Hurricane Wind Scale categories from 1 to 5 in text along with graphics showing the extent of damage. Category 1 is described as having wind speeds of 74-95 mph with a storm surge of 4-5 feet, causing minimal damage. Category 2 is described as having wind speeds of 96-110 mph with a storm surge of 6-8 feet, causing moderate damage. Category 3 is described as having wind speeds of 111-129 mph with a storm surge of 9-12 feet, causing extensive damage. Category 4 is described as having wind speeds of 130-156 mph with a storm surge of 13-18 feet, causing extreme damage. Lastly, Category 5 is described as having wind speeds of 157+ mph with a storm surge of higher than 18 feet, causing catastrophic damage.

Figure 14.31: A world map with grey continents and dark blue oceans, with the tracks of tropical storms overlain, color-coded by their intensity. Tropical depressions are blue, tropical storms are cyan, category 1 hurricanes are light yellow, category 2 are yellow, category 3 are marigold, category 4 are orange, and category 5 are red. The areas covered by these tracks include the following parts of the Pacific Ocean: a dense, large set of tracks off the eastern coast of Asia with all colors represented; off the eastern coast of Australia with all colors except red represented; and off the western and southwestern coast of North America with all colors represented. The northern half of the Atlantic Ocean is nearly completely covered by storm tracks with all colors represented. The Indian Ocean is covered in both its northern and southern ends by storm tracks. There is one minor storm track off the east coast of South America.

Figure 14.32: Photograph of a historic marker sign titled R 51 Hurricane Camille with the following text: on 20 Aug. 1969, torrential rains, following remnants of Hurricane Camille, devastated this area. A rainfall in excess of 25 inches, largely within a five-hour period, swept away or buried many miles of roads, more than 100 bridges, and more than 900 buildings. 125 people died in Nelson County. The damage totaled more than $100,000,000, and Virginia was declared a disaster area.

Figure 14.33: Old photograph of a black train with white snow drifts on either side rising above the top of the train; a man in black stands on one of the train cars.

Figure 14.34: Photograph of a snow-covered part of a city with cars parked along either side of the street, covered in snow, and bare trees lining either side of the snow-covered road. A few people are barely visible in the distance due to the snowy conditions.

Figure 14.35: A diagram drawn in the style of a shadow box with a map of the United States and part of Mexico and Canada laying on the bottom of the shadow box with blue sky and sunshine on the background of the shadow box. There is a large, orange-shaded bubble covering a large portion of the interior of the United States labeled H, with three curved orange arrows circulating in a clockwise manner within the bubble.

Figure 14.36: A two-column chart describing the risk categories for people experiencing heat with the left column titled Category and the right column titled Risk of Heat-Related Impacts; each row is color-coded. The top row is Green Category 0 with little to no risk from expected heat. The second row is Yellow Category 1 with minor risk; this level of heat affects primarily those individuals extremely sensitive to heat, especially when outdoors without effective cooling and/or adequate hydration. The third row is Orange Category 2 with moderate risk; this level of heat affects most individuals sensitive to heat, especially those without effective cooling and/or adequate hydration; impacts possible in some health systems and in heat- sensitive industries. The fourth row is Red Category 3 with major risk; this level of heat affects anyone without effective cooling and/or adequate hydration; impacts likely in some health systems, heat-sensitive industries and infrastructure. The fifth final row is magenta Category 5 with extreme risk; this level of rare and/or long-duration extreme heat with little to no overnight relief affects anyone without effective cooling and/or adequate hydration; impacts likely in most health systems, heat-sensitive industries and infrastructure.

15. GLOBAL CLIMATE CHANGE

Learning Objectives

By the end of this chapter, students should be able to:

- Describe the role of greenhouse gases in climate change.
- Describe the sources of greenhouse gases.
- Explain Earth's energy budget and global temperature changes.
- Explain how positive and negative feedback mechanisms can influence climate.
- Explain how we know about climates of the geologic past.
- Accurately describe which aspects of the environment are changing due to anthropogenic climate change.
- Describe the causes of recent climate change, particularly the role of humans in the overall climate balance.
- Describe projected climatic changes and the various options we have for decreasing greenhouse gas emissions.

This chapter describes the Earth systems involved in climate change, the geologic evidence of past climate changes, and the human role in today's climate change. In science, a system is a group of interacting objects and processes. Earth system science is the study of these systems: **geosphere** (rocks), **atmosphere** (gases), **hydrosphere** (water), **cryosphere** (ice), and **biosphere** (living things). Earth science studies these systems and how they interact and change in response to natural cycles and **anthropogenic** (human-driven) forces. Changes in one Earth system affect other systems.

It is critically important for us to be aware of the geologic context of climate change processes and how these Earth systems interact, first, for us to understand how and why human activities cause present-day climate change and, second, to distinguish between natural processes and human processes in the geologic past's climate record.

A significant part of this chapter introduces and discusses various processes from these Earth systems, how they influence each other, and how they impact global climate. For example, Earth's temperature and climate largely change based on atmospheric gas composition, ocean circulation, and the land-surface characteristics of rocks, glaciers, and plants.

As previously mentioned in the Meteorology chapter, understanding climate change requires the ability to distinguish between climate and weather. Weather is the short-term temperature and precipitation patterns that occur in days and weeks. Climate is the variable range of temperature and precipitation patterns averaged over the long-term for a particular region (see Section 13.1). Thus, a single cold winter does not mean that the entire globe is cooling; indeed, the United States' cold winters of 2013 and 2014 occurred while the rest of the Earth was experiencing record warm-winter temperatures. To avoid these generalizations, many scientists use a 30-year average as a good baseline. Therefore, climate change refers to slow temperature and precipitation changes and trends over the long term for a particular area or the Earth as a whole.

15.1 Earth's Temperature

Without an atmosphere, Earth would have huge temperature fluctuations between day and night, as the Moon does. Daytime temperatures would be hundreds of degrees Celsius above normal, and nighttime temperatures would be hundreds of degrees below normal. Because the Moon doesn't have much of an atmosphere, its daytime temperatures are around 106˚C (223˚F) and nighttime temperatures are around -183˚C (-298˚F). That is an astonishing 289˚C (521˚F) degree range between the Moon's light side and dark side. This section describes how Earth's atmosphere is involved in regulating the Earth's temperature.

15.1.1 Composition of Atmosphere

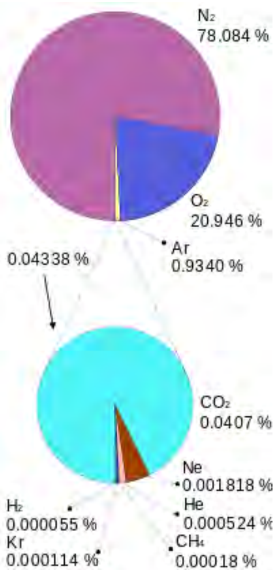

Figure 15.1: Composition of the atmosphere. Figure description available at the end of the chapter.

The atmosphere's composition is a key component in regulating the planet's temperature. The atmosphere is 78% nitrogen (N_2), 21% oxygen (O_2), 1% argon (Ar), and less than 1% trace components, which are all other gases. Trace components include carbon dioxide (CO_2), water vapor (H_2O), neon, helium, and methane. Water vapor is highly variable, mostly based on region, and composes about 1% of the atmosphere. Trace component gases include several important greenhouse gases, which are the gases responsible for warming and cooling the plant. On a geologic scale, volcanoes and the weathering process, which bury CO_2 in sediments, are the atmosphere's CO_2 sources. Biological processes both add and subtract CO_2 from the atmosphere.

Greenhouse gases trap heat in the atmosphere and warm the planet by absorbing some of the longer-wave outgoing infrared radiation that is emitted from Earth, thus keeping heat from being lost to space. More greenhouse gases in the atmosphere absorb more longwave heat and make the planet warmer. Greenhouse gases have little effect on shorter-wave incoming solar radiation.

The most common greenhouse gases are water vapor (H_2O), carbon dioxide (CO_2), methane (CH_4), and nitrous oxide (N_2O). Water vapor is the most abundant greenhouse gas, but its atmospheric abundance does not change much over time. Carbon dioxide is much less abundant than water vapor, but carbon dioxide is being added to the atmosphere by human activities such as burning fossil fuels, land-use changes, and deforestation. Further, natural processes such as volcanic eruptions add carbon dioxide, but this occurs at an insignificant rate compared to human-caused contributions.

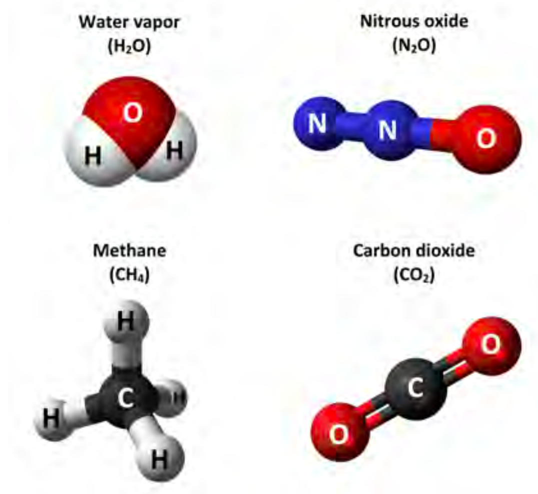

Figure 15.2: Common greenhouse gases. Figure description available at the end of the chapter.

There are two important reasons why carbon dioxide is the most important greenhouse gas. First, carbon dioxide stays in the atmosphere and does not go away for hundreds of years. Second, most of the additional carbon dioxide is "fossil" in origin, which means that it is released by burning fossil fuels. For example, coal and petroleum are fossil fuels. **Coal** and **oil** are made from long-dead plant material, which was originally created by photosynthesis millions of years ago and stored in the ground. Photosynthesis combines sunlight and carbon dioxide to create the substances of plants. This transformation occurs over millions of years as a slow process, accumulating fossil carbon in rocks and sediments. So, when we burn coal and oil, we instantaneously release the stored solar energy and fossil carbon dioxide that took millions of years to accumulate in the first place. The rate of release is critical to comprehend current climate change.

15.1.2 Carbon Cycle

Understanding global climate change requires an understanding of the carbon cycle and how Earth's own carbon-balancing system is being rapidly thrown off balance by human-driven activities. Earth has two important carbon cycles: the biological and the geological. In the biological cycle, living organisms—mostly plants—consume carbon dioxide from the atmosphere to make their tissues and substances through photosynthesis. Then, after the organisms die and then decay over years or decades, that carbon is released back into the atmosphere. The following is the general equation for photosynthesis.

$CO_2 + H_2O + sunlight \rightarrow sugars + O_2$

In the geological carbon cycle, a portion of the biological-cycle carbon becomes part of the geological carbon cycle: plant materials into coal and petroleum, tiny fragments and molecules into organic-rich shale, and the carbonate-bearing calcareous shells and other parts of marine organisms into limestone. Such materials become buried and become part of the slow geologic formation of coal and other sedimentary materials. This cycle actually involves most of Earth's carbon and operates very slowly.

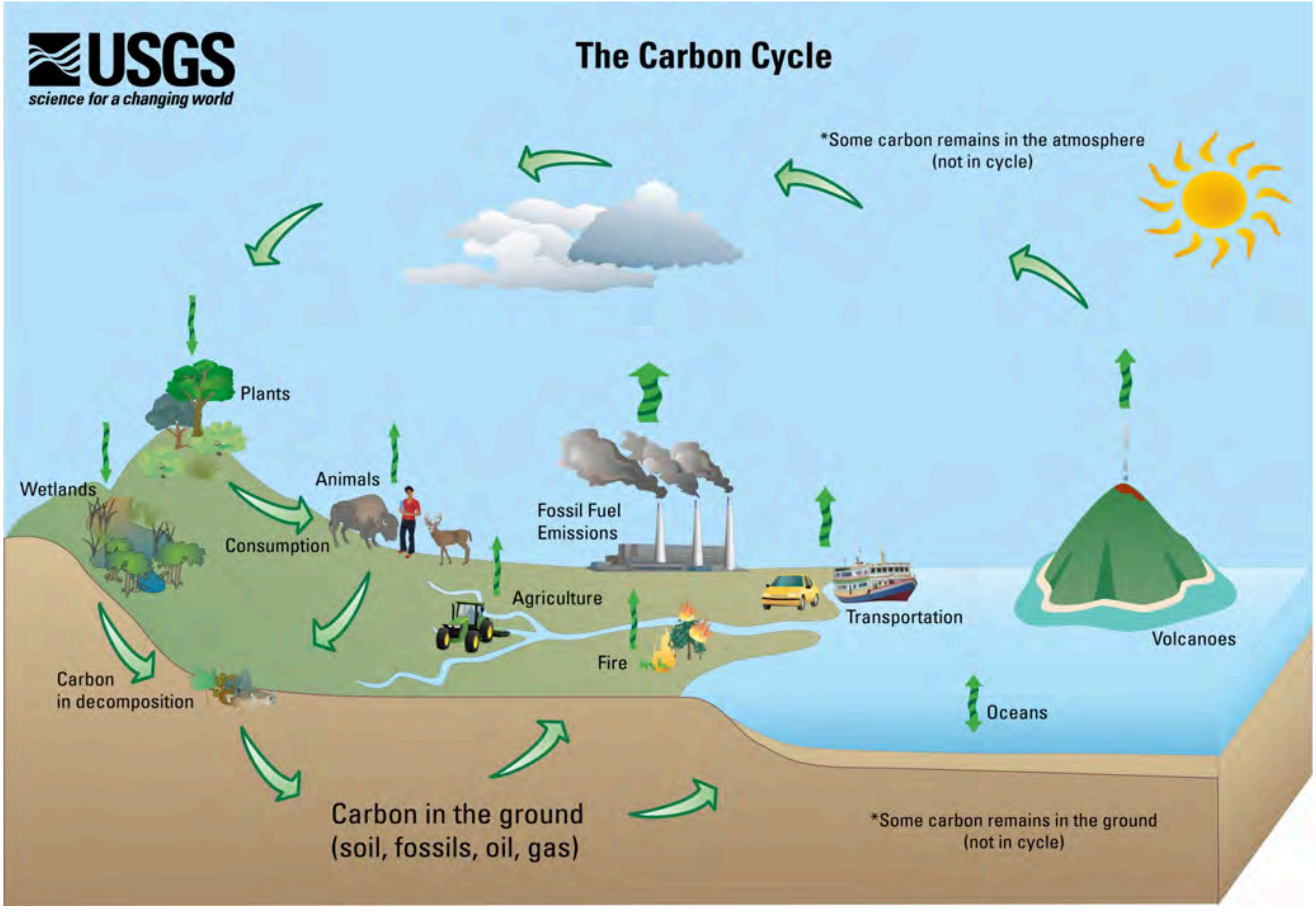

Figure 15.3: Carbon cycle. Figure description available at the end of the chapter.

The following are geological carbon-cycle storage reservoirs:

- Organic matter from plants is stored in peat, coal, and permafrost for thousands to millions of years.
- Silicate-mineral weathering converts atmospheric carbon dioxide to dissolved bicarbonate, which is stored in the oceans for thousands to tens of thousands of years.
- Marine organisms convert dissolved bicarbonate to forms of calcite, which is stored in carbonate rocks for tens to hundreds of millions of years.
- Carbon compounds are directly stored in sediments for tens to hundreds of millions of years; some end up in petroleum deposits.
- Carbon-bearing sediments are transferred by subduction to the mantle, where the carbon may be stored for tens of millions to billions of years.
- Carbon dioxide from within the Earth is released back to the atmosphere during volcanic eruptions, where it is stored for years to decades.

During much of Earth's history, the geological carbon cycle has been balanced by volcanoes releasing carbon at approximately the same rate that carbon is stored by the other processes. Under these conditions, Earth's climate has remained relatively stable. However, in Earth's history, there have been times when that balance has been upset. This can happen during prolonged stretches of above-average volcanic activity. One example is the Siberian Traps eruption around 250 million years ago, which contributed to strong climate warming over a few million years.

A carbon imbalance is also associated with significant mountain-building events. For example, the Himalayan Range has been forming for about 40 million years, and over that time—and still today—the rate of weathering on Earth has been enhanced because the huge mountains and extensive range present a greater surface area on which weathering takes place. The weathering of these rocks—most importantly the hydrolysis of feldspar—has resulted in consumption of atmospheric carbon dioxide and transfer of the carbon to the oceans and to ocean-floor carbonate-rich sediments. The steady drop in carbon dioxide levels over the past 40 million years, which contributed to the Pliocene-Pleistocene glaciations, is partly attributable to the formation of the Himalayan Range.

Another, nongeological form of carbon-cycle imbalance is happening today on a very rapid timescale. In just a few decades, humans have extracted volumes of fossil fuels, such as coal, oil, and gas stored in rocks over the past several hundred million years, and converted these fuels to energy and carbon dioxide. By doing so, we are changing the climate faster than has ever happened in the past. Remember, carbon dioxide stays in the atmosphere and does not go away for hundreds of years. The more greenhouse gases in the atmosphere, the more heat is trapped and the warmer the planet becomes.

15.1.3 Greenhouse Effect

The greenhouse effect is the reason our global temperature is rising, but it's important to understand what this effect is and how it occurs. The greenhouse effect occurs because greenhouse gases are present in the atmosphere. The greenhouse effect is named after a similar process that warms a greenhouse or a car on a hot summer day. Sunlight passes through the glass of the greenhouse or car, reaches the interior, and changes into heat. The heat radiates upward and gets trapped by the glass windows. The greenhouse effect for the Earth can be explained in three steps.

Step 1: Solar radiation from the Sun is composed of mostly ultraviolet (UV) light, visible light, and infrared (IR) radiation. Components of solar radiation include parts with a shorter wavelength than visible light, like ultraviolet light, and parts of the spectrum with longer wavelengths, like IR and others. Some of the radiation gets absorbed, scattered, or reflected by the atmospheric gases, but about half of the solar radiation eventually reaches the Earth's surface.

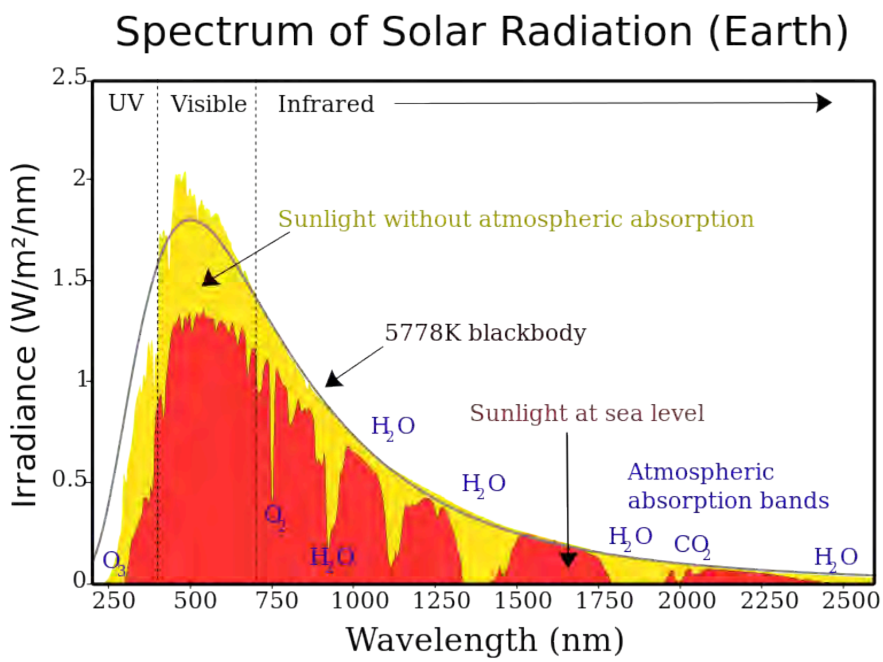

Figure 15.4: Incoming radiation absorbed, scattered, and reflected by atmospheric gases. Figure description available at the end of the chapter.

Step 2: The visible, UV, and IR radiation that reaches the surface converts to heat energy. Most students have experienced sunlight warming a surface such as pavement, a patio, or deck. When this occurs, the warmer surface then emits thermal radiation, which is a type of IR radiation. Then there is a conversion from visible, UV, and IR to just thermal IR. This thermal IR is what we experience as heat. If you have ever felt heat radiating from a fire or a hot stovetop, then you have experienced thermal IR.

Step 3: Thermal IR radiates from the Earth's surface back into the atmosphere. But since it is thermal IR instead of UV, visible, or regular IR, this thermal IR gets trapped by greenhouse gases. In other words, the Sun's energy leaves the Earth at a different wavelength than it enters, so the Sun's energy is not absorbed in the lower atmosphere when energy is coming in, rather occurring when the energy is going out. The gases that are mostly responsible for this energy blocking on Earth include carbon dioxide, water vapor, methane, and nitrous oxide. The presence of more greenhouse gases in the atmosphere results in more thermal IR being trapped. Explore this external link to an interactive animation on the greenhouse effect from the National Academy of Sciences.

15.1.4 Earth's Energy Budget

The solar radiation that reaches Earth is relatively uniform over time. Earth is warmed, and energy or heat radiates from the Earth's surface and lower atmosphere back to space. This flow of incoming and outgoing energy is Earth's energy budget. For Earth's temperature to be stable over long stretches of time, incoming energy and outgoing energy have to be equal on average so that the energy budget at the top of the atmosphere balances. About 29% of the incoming solar energy arriving at the top of the atmosphere is reflected back to space by clouds, atmospheric particles, or reflective ground surfaces like sea ice and snow. About 23% of incoming solar energy is absorbed in the atmosphere by water vapor, dust, and ozone. The remaining 48% passes through the atmosphere and is absorbed at the surface. Thus, about 71% of the total incoming solar energy is absorbed by the Earth system.

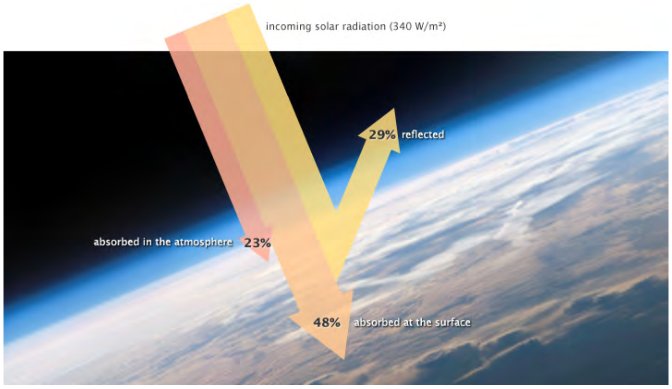

Figure 15.5: Incoming solar radiation filtered by the atmosphere. Figure description available at the end of the chapter.

When this energy reaches Earth, the atoms and molecules that make up the atmosphere and surface absorb the energy, and Earth's temperature increases. If this material *only* absorbed energy, then the temperature of the Earth would continue to increase and eventually overheat. For example, if you continuously run a faucet in a stopped-up sink, the water level rises and eventually overflows. However, temperature does not infinitely rise because the Earth is not just absorbing sunlight; it is also radiating thermal energy or heat back into the atmosphere. If thetemperature of the Earth rises, the planet emits an increasing amount of heat to space, and this is the primary mechanism that prevents Earth from continually heating.

Some of the thermal infrared heat radiating from the surface is absorbed and trapped by greenhouse gases in the atmosphere, which act like a giant canopy over Earth. The more greenhouse gases in the atmosphere, the more outgoing heat Earth retains and the less thermal infrared heat dissipates to space.

Factors beyond greenhouse gases can affect the Earth's energy budget. Increasing solar energy can increase the energy Earth receives. However, these increases are very small over time. In addition, land and water will absorb more sunlight when there is less ice and snow to reflect the sunlight back to the atmosphere. For example, the ice covering the Arctic Sea reflects sunlight back to the atmosphere; this reflected light is called **albedo**. Furthermore, aerosols (dust particles) produced from burning coal, diesel engines, and volcanic eruptions can reflect incoming solar radiation and actually cool the planet.

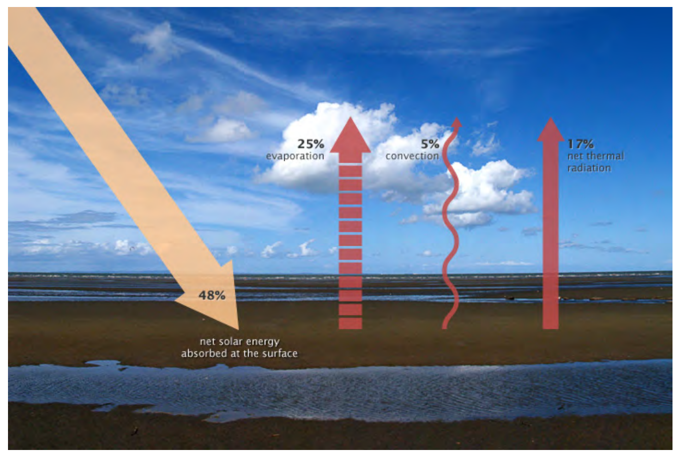

Figure 15.6: Some of the thermal infrared energy (heat) radiated from the surface into the atmosphere is trapped by gases in the atmosphere. Figure description available at the end of the chapter.

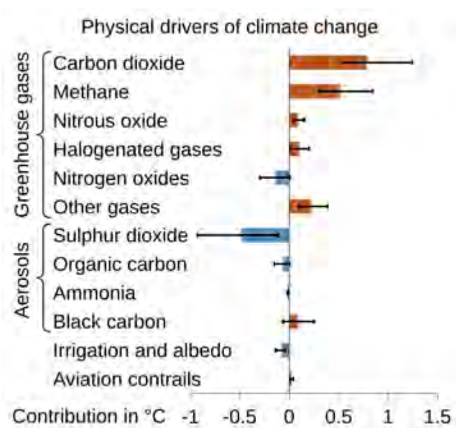

Figure 15.7: Contribution to observed climate change from 12 different drivers, as taken from the Summary for Policymakers of the Sixth IPCC Assessment Report. Future global warming potential for long-lived drivers like carbon dioxide emissions is not represented. Whiskers on each bar show the very likely range. Time period is 1850–1900 to 2010–2019. All contributions are from human activity, as natural variance and forcings have not contributed to warming in this time period. Figure description available at the end of the chapter.

While the effect of anthropogenic aerosols on the climate's system is weak, the effect of human-produced greenhouse gases is not weak. Thus, the net effect of human activity is warming due to more anthropogenic greenhouse gases associated with fossil fuel combustion.

An effect that changes the planet can trigger feedback mechanisms that amplify or suppress the original effect. A **positive feedback** mechanism occurs when the output or effect of a process enhances the original stimulus or cause. Thus, it increases the ongoing effect. For example, the loss of sea ice at the North Pole makes that area less reflective, reducing albedo. This allows the surface air and ocean to absorb more energy in an area that was once covered by sea ice. Another example is melting permafrost. **Permafrost** is permanently frozen soil located in the high latitudes, mostly in the Northern Hemisphere. As the climate warms, more permafrost thaws, and the thick deposits of organic matter are exposed to oxygen and begin to decay. This oxidation process releases carbon dioxide and methane, which in turn causes more warming, which melts more permafrost, and so on.

A **negative feedback** mechanism occurs when the output or effect reduces the original stimulus or cause. For example, in the short term, more carbon dioxide (CO_2) is expected to cause forest canopies to grow, which absorb more CO_2. Another example for the long term is that increased carbon dioxide in the atmosphere will cause more carbonic acid and chemical weathering, which results in the transportation of dissolved bicarbonate and other ions to the oceans, which are then stored in sediment.

Global warming is evidence that Earth's energy budget is not balanced. Positive feedback on Earth's temperature is now greater than negative feedback.

Take this quiz to check your comprehension of this section.

Access the quiz for Section 15.1 by scanning the QR code.

15.2 Evidence of Recent Climate Change

While climate has changed often in the past due to natural causes (see Section 14.5.1 and Section 15.3), the scientific consensus is that human activity is causing very rapid climate change. While this seems like a new idea, it was suggested more than 75 years ago. This section describes the evidence of what most scientists agree is anthropogenic or human-caused climate change. For more information, watch the video below on climate change by two professors at the North Carolina State University.

Video 15.1: Evidence for climate change

Access this YouTube video by scanning the QR code. ["Evidence for Climate Change" by GeoScience Videos | https://www.youtube.com/watch?v=dquECwUfIQg]

15.2.1 Global Temperature Rise

The land-ocean temperature index, 1880 to present, compared to a base reference time of 1951–1980, shows ocean temperatures steadily rising. The solid black line is the global annual mean, and the solid red line is the five-year Lowess smoothing. The blue uncertainty bars (95% confidence limit) account only for incomplete spatial sampling.

Since 1880, Earth's surface-temperature average has trended upward, with most of that warming occurring since 1970 (see this NASA animation). Surface temperatures include both land and ocean because water absorbs much additional trapped heat. Changes in land-surface or ocean-surface temperatures compared to a reference period from 1951 to 1980, where the long-term average remained relatively constant, are called temperature anomalies. A temperature anomaly thus represents the difference between the measured temperature and the average value during the reference period. Climate scientists calculate long-term average temperatures over thirty years or more, which identified the reference period from 1951 to 1980. Another common range is a century, for example, 1900–2000. Therefore, an anomaly of 1.25˚C (2.25˚F) for 2015 means that the average temperature for 2015 was 1.25˚C (2.25˚F) greater than the 1900–2000 average. In 1950, the temperature anomaly was -0.28˚C (-0.504˚F), so this is -0.28˚C (-0.504˚F) lower than the 1900–2000 average. These temperatures are annual average measured surface temperatures.

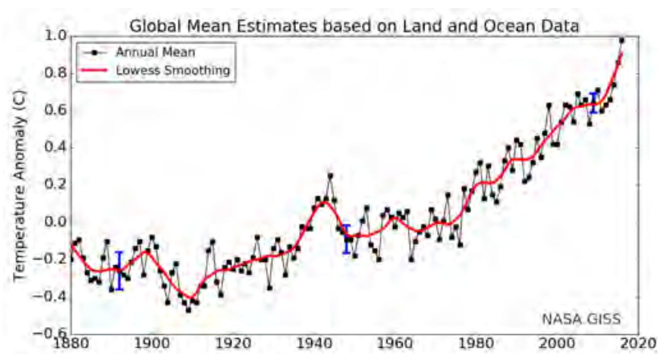

Figure 15.8: Land-ocean temperature index, 1880 to present, with a base time 1951–1980. The solid black line is the global annual mean, and the solid red line is the five-year Lowess smoothing. The blue uncertainty bars (95% confidence limit) account only for incomplete spatial sampling. The graph shows that Earth's temperature is rising. Figure description available at the end of the chapter.

This video of temperature anomalies shows worldwide temperature changes since 1880. The more blue, the cooler; the more yellow and red, the warmer.

Video 15.2: Earth's long-term warming trend can be seen in this visualization of NASA's global temperature record, which shows how the planet's temperatures are changing over time, compared to a baseline average from 1951 to 1980. The record is shown as a running five-year average.

Access this YouTube video by scanning the QR code. ["Global Warming from 1880 to 2021" by NASA Climate Change | https://www.youtube.com/watch?v=haBG2IlbwbA]

In addition to average land-surface temperatures rising, the ocean has absorbed much heat. Because oceans cover about 70 percent of the Earth's surface and have such a high specific heat value, they provide a large opportunity to absorb energy. The ocean has been absorbing about 80-to-90 percent of human activities' additional heat. As a result, the top 700 meters (2,300 feet) of the global ocean has warmed about 0.83˚C (1.5˚F) since 1901 (watch this three-minute video by NASA JPL on the ocean's heat capacity). The reason the ocean has warmed less than the atmosphere, while still taking on most of the heat, is due to water's very high specific heat, which means that water can absorb a lot of heat energy with a small temperature increase. In contrast, the lower specific heat of the atmosphere means it has a higher temperature increase, as it absorbs less heat energy.

Some scientists suggest that anthropogenic greenhouse gases do not cause global warming because between 1998 and 2013, Earth's surface temperatures did not increase much, despite greenhouse gas concentrations continuing to increase. However, since the oceans are absorbing most of the heat, decade-scale circulation changes in the ocean, similar to La Niña, push warmer water deeper under the surface. Once the ocean's absorption and circulation is accounted for and this heat is added back into surface temperatures, then temperature increases become apparent. Also, the ocean's heat storage is temporary, as reflected in the record-breaking warm years of 2014–2016. Indeed, with this temporary ocean-storage effect, 15 of the twenty-first century's first 16 years were the hottest in recorded history.

15.2.2 Carbon Dioxide

Anthropogenic greenhouse gases, mostly carbon dioxide (CO_2), have increased since the Industrial Revolution, when humans dramatically increased burning fossil fuels. These levels are unprecedented in the last 800,000-year Earth history as recorded in geologic sources such as ice cores. Carbon dioxide has increased by 40 percent since 1750, and the rate of increase has been the fastest during the last decade. For example, since 1750, $2,040^9$ tonnes (2,040 gigatons) of CO_2 have been added to the atmosphere; about 40 percent has remained in the atmosphere, while the remaining 60 percent has been absorbed into the land by plants and soil or into the oceans. Indeed, during the lifetime of most young adults, the total atmospheric CO_2 has increased by 50 ppm, or 15 percent.

Charles Keeling, an oceanographer with Scripps Institution of Oceanography in San Diego, California, was the first person to regularly measure atmospheric CO_2. Using his methods, scientists at the Mauna Loa Observatory, Hawai'i, have constantly measured atmospheric CO_2 since 1957. NASA regularly publishes these measurements at https://keelingcurve.ucsd.edu. Go there now to see the very latest measurement. Keeling's measured values have been posted in a curve of increasing values, called the Keeling curve. This curve varies up and down in a regular annual cycle, from summer when the plants in the Northern Hemisphere use CO_2 to winter when they are dormant. But the curve shows a steady CO_2 increase over the past several decades. This curve increases exponentially, not linearly, showing that the rate of CO_2 increase is itself increasing.

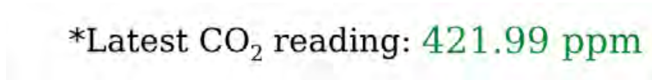

Figure 15.9: Latest CO_2 reading as of September 25, 2024. [Figure description available at the end of the chapter](#).

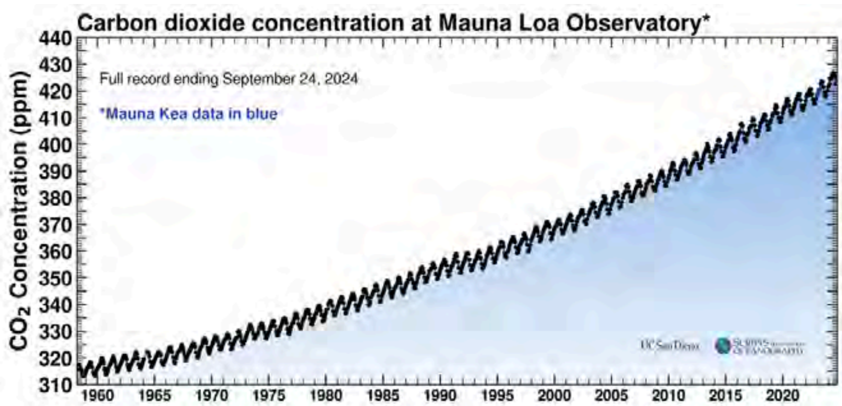

Figure 15.10: Keeling curve graph of the carbon dioxide concentration at Mauna Loa Observatory as of September 25, 2024. [Figure description available at the end of the chapter](#).

The following video shows how atmospheric CO_2 has varied recently and over the last 800,000 years, as determined by an increasing number of CO_2 monitoring stations (shown on the insert map). It is also instructive to watch the video's Keeling portion of how CO_2 varies by latitude. This shows that most human CO_2 sources are in the Northern Hemisphere, which is home to most of the land and most of the developed nations.

Video 15.3: History of atmospheric CO_2 from 800,000 years ago until January 2016

Access this [YouTube video](#) by scanning the QR code. Visit https://gml.noaa.gov/ccgg/trends for more information. ["Pumphandle 2016" by CarbonTracker | https://www.youtube.com/watch?v=gH6fQh9eAQE]

15.2.3 Melting Glaciers and Shrinking Sea Ice

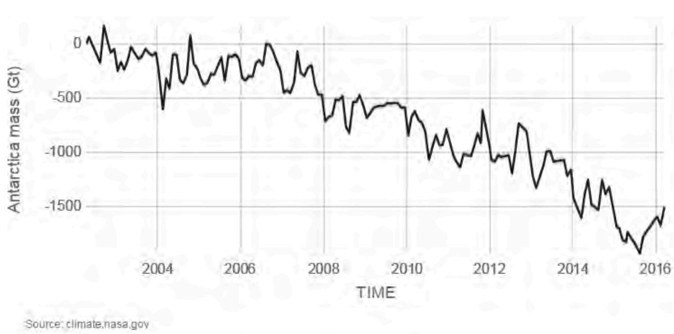

Figure 15.11: Decline of Antarctic ice mass from 2002 to 2016. [Figure description available at the end of the chapter](#).

Glaciers are large ice accumulations that exist year-round on the land's surface. In contrast, icebergs are masses of floating sea ice, although they may have had their origin in glaciers (see Glaciers chapter). Alpine glaciers, ice sheets, and sea ice are all melting. Explore melting glaciers at [NASA's interactive Global Ice Viewer](#). Satellites have recorded that Antarctica is melting at 1,189 tonnes (118 gigatons) per year, and Greenland is melting at 2,819 tonnes (281 gigatons) per year; 1 metric tonne is 1,000 kilograms (1 gigaton is over 2 trillion pounds). Almost all major alpine glaciers are shrinking, deflating, and retreating. The ice-mass loss rate is unprecedented—never observed before—since the 1940s, when quality records for glaciers began.

Before anthropogenic warming, glacial activity was variable with some retreating and some advancing. Now, spring snow cover is decreasing, and sea ice is shrinking. Most sea ice is at the North Pole, which is only occupied by the Arctic Ocean and sea ice. The NOAA animation shows how perennial sea ice has declined from 1987 to 2015. The oldest ice is white, and the youngest, seasonal ice is dark blue. The amount of old ice has declined from 20% in 1985 to 3% in 2015.

Video 15.4: This animation tracks the relative amount of ice of different ages from 1987 through early November 2015. The oldest ice is white; the youngest (seasonal) ice is dark blue. Key patterns are the export of ice from the Arctic through Fram Strait and the melting of old ice as it passes through the warm waters of the Beaufort Sea. Sea ice age is estimated by tracking of ice parcels using satellite imagery and drifting ocean buoys.

Access this YouTube video by scanning the QR code. ["Watch 25 Years of Arctic Sea Ice Disappear in 1 Minute" by climatecentral | https://www.youtube.com/watch?v=Fw7GfNR5PLA]

15.2.4 Rising Sea Level

Sea level is rising 3.4 millimeters (0.13 inches) per year and rose 0.19 meters (7.4 inches) from 1901 to 2010. This is largely thought to be from both glaciers melting and thermal expansion of seawater. Thermal expansion means that, as objects such as solids, liquids, and gases heat up, they expand in volume.

Below is a classic video demonstration (30 second) on thermal expansion with brass ball and ring (North Carolina School of Science and Mathematics).

Video 15.5: Thermal expansion

Access this YouTube video by scanning the QR code. ["Ball and Ring: Rate of Expansion and Contraction" by North Carolina School of Science and Mathematics | https://www.youtube.com/watch?v=QNoE5IoRheQ]

15.2.5 Ocean Acidification

Since 1750, about 40 percent of new anthropogenic carbon dioxide has remained in the atmosphere. The remaining 60 percent gets absorbed by the ocean and vegetation. The ocean has absorbed about 30 percent of that carbon dioxide. When carbon dioxide gets absorbed in the ocean, it creates carbonic acid. This makes the ocean more acidic, which then has an impact on marine organisms that secrete calcium carbonate shells. Recall that hydrochloric acid reacts by effervescing with limestone rock made of calcite, which is calcium carbonate. A more acidic ocean is associated with climate change and is linked to thinning the carbonate shells of some sea snails (pteropods) and small protozoan zooplanktons (foraminifera) and to ocean coral reefs' declining growth rates. Small animals like protozoan zooplankton are an important component at the base of the marine ecosystem. Combined with warmer temperature and lower oxygen levels, acidification is expected to have severe impacts on marine ecosystems and human-harvested fisheries, possibly affecting our ocean-derived food sources.

Video 15.6: Ocean acidification: The other carbon dioxide problem

Access this YouTube video by scanning the QR code. ["Ocean Acidification: The Other Carbon Dioxide Problem [1080p]" by djx-atlanta | https://www.youtube.com/watch?v=bvg0FajepzU]

15.2.6 Extreme Weather Events

Extreme weather events such as hurricanes, precipitation, and heat waves are increasing and becoming more intense. Since the 1980s, hurricanes, which are generated from warm ocean water, have increased in frequency, intensity, and duration and are likely connected to a warmer climate. Since 1910, average precipitation has increased by 10 percent in the contiguous United States, and much of this increase is associated with heavy precipitation events. However, the distribution is not even, and more precipitation is projected for the Northern United States, while less precipitation is projected for the already dry Southwest. Also, heat waves have increased, and rising temperatures are already affecting crop yields in northern latitudes. Increased heat allows for greater moisture capacity in the atmosphere, increasing the potential for more extreme events.

Take this quiz to check your comprehension of this section.

Access the quiz for Section 15.2 by scanning the QR code.

15.3 Prehistoric Climate Change

Over Earth's history, the climate has changed a lot. For example, during the Mesozoic Era, the Age of Dinosaurs, the climate was much warmer, and carbon dioxide was abundant in the atmosphere. However, throughout the Cenozoic Era, 65 million years ago to today, the climate has been gradually cooling. This section summarizes some of these major past climate changes.

Figure 15.12: Maximum extent of Laurentide ice sheet. Figure description available at the end of the chapter.

15.3.1 Past Glaciations

Through geologic history, climate has changed slowly over millions of years. Before the most recent Pliocene-**Quaternary** glaciation, there were other major glaciations. The oldest, known as the Huronian, occurred toward the end of the Archean Eon-early Proterozoic Eon, about 2.5 billion years ago. The Great Oxygenation Event (see Chapter 8) occurred during that time and is most commonly associated with causing that glaciation. The increased oxygen is thought to have reacted with the potent greenhouse gas methane, causing cooling.

The end of the Proterozoic Eon, about 700 million years ago, had other glaciations. These ancient Precambrian glaciations are included in the snowball Earth hypothesis. Widespread global rock sequences from these ancient times contain evidence that glaciers existed even in low latitudes. Two examples are limestone rock—usually formed in tropical marine environments—and glacial deposits—usually formed in cold climates—from this time that have been found together in many regions around the world. One example is in Utah. Evidence of continental glaciation is seen in interbedded limestone and glacial deposits (diamictites) on Antelope Island in the Great Salt Lake.

The controversial **snowball Earth hypothesis** suggests that a runaway albedo effect—where ice and snow reflect solar radiation and increasingly spread from polar regions toward the equator—caused land and ocean surfaces to completely freeze and biological activity to collapse. Since carbon dioxide could not enter the then-frozen ocean, the ice covering Earth could only melt when volcanoes emitted high enough carbon dioxide into the atmosphere to cause greenhouse heating. Some studies estimate that, because of the frozen ocean surface, carbon dioxide 350 times higher than today's concentration was required. Because biological activity did survive, the complete freezing and its extent in the snowball Earth hypothesis are controversial. A competing hypothesis is the slushball Earth hypothesis, in which some regions of the equatorial ocean remained open. Differing scientific conclusions about the stability of Earth's magnetic poles, impacts on ancient rock evidence from subsequent metamorphism, and alternate interpretations of existing evidence keep the idea of snowball Earth controversial.

Glaciations also occurred in the Paleozoic Era, notably the Andean-Saharan glaciation in the late Ordovician, about 440–460 million years ago, which coincided with a major extinction event, and the Karoo ice age during the Pennsylvanian Period, 323–300 million years ago. This glaciation was one of the evidences cited by Wegener for his continental drift hypothesis as his proposed Pangea drifted into south polar latitudes. The Karoo glaciation was associated with an increase of oxygen and a subsequent drop in carbon dioxide, most likely produced by the evolution and rise of land plants.

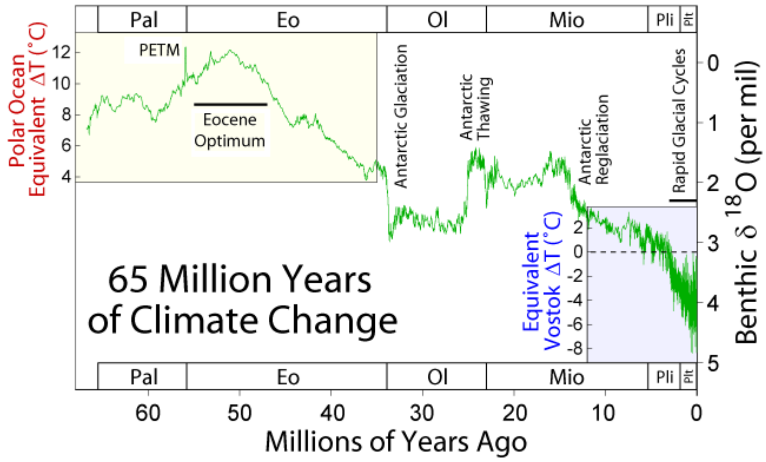

Figure 15.13: Global average surface temperature over the past 65 million years. Figure description available at the end of the chapter.

During the Cenozoic Era—the last 65 million years—climate started out warm and gradually cooled to its current state. This warm time is called the **Paleocene-Eocene thermal maximum**, and Antarctica and Greenland were ice-free during this time. Since the Eocene, tectonic events during the Cenozoic Era have caused the planet to persistently and significantly cool. For example, the Indian plate and Asian plate collided, creating the Himalaya Mountains, which increased the rate of weathering and erosion of silicate minerals, especially feldspar. Increased weathering consumes carbon dioxide from the atmosphere, which reduces the greenhouse effect, resulting in long-term cooling.

About 40 million years ago, the narrow gap between the South American plate and the Antarctica plate widened, which opened the Drake Passage. This opening allowed the water around Antarctica—the Antarctic Circumpolar Current—to flow unrestrictedly west to east, which effectively isolated the Southern Ocean from the warmer waters of the Pacific, Atlantic, and Indian Oceans. The region cooled significantly, and by 35 million years ago, during the Oligocene Epoch, glaciers had started to form on Antarctica.

Around 15 million years ago, subduction-related volcanoes between Central and South America created the Isthmus of Panama, which connected North and South America. This prevented water from flowing between the Pacific and Atlantic Oceans and reduced heat transfer from the tropics to the poles. This reduced heat transfer created a cooler Antarctica and larger Antarctic glaciers. As a result, the ice sheet expanded on land and water, increased Earth's reflectivity, and enhanced the albedo effect, which created a positive feedback loop: more reflective glacial ice, more cooling, more ice, more cooling, and so on.

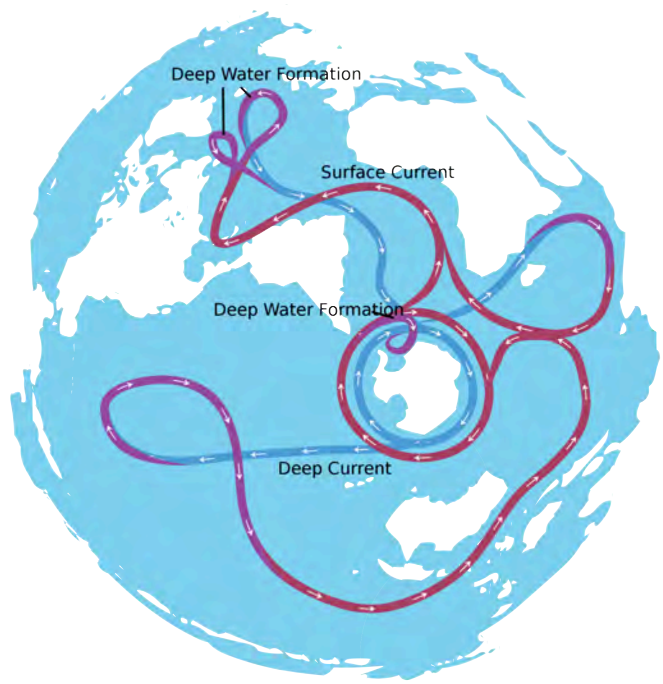

Figure 15.14: The Antarctic Circumpolar Current. Figure description available at the end of the chapter.

By five million years ago, during the Pliocene Epoch, ice sheets had started to grow in North America and Northern Europe. The most intense part of the current glaciation is the Pleistocene Epoch's last million years. The Pleistocene's temperature varies significantly through a range of almost 10°C (18°F) on timescales of 40,000 to 100,000 years, and ice sheets expand and contract correspondingly. These variations are attributed to subtle changes in Earth's orbital parameters, called Milankovitch cycles.

As described in the Glaciers chapter, Milankovitch cycles are three orbital changes named after the Serbian astronomer Milutan Milankovitch. The three orbital changes are called precession, obliquity, and eccentricity. Precession is the wobbling of Earth's axis with a period of about 21,000 years; obliquity is changes in the angle of Earth's axis with a period of about 41,000 years; and eccentricity is variations in the Earth's orbit around the Sun leading to changes in distance from the Sun with a period of 93,000 years. These orbital changes created a 41,000-year-long glacial-interglacial Milankovitch cycle from 2.5 to 1.0 million years ago, followed by another longer cycle of about 100,000 years from 1.0 million years ago to today (see Milankovitch cycles). Over the past million years, the glaciation cycles occurred approximately every 100,000 years, with many glacial advances occurring in the last two million years.

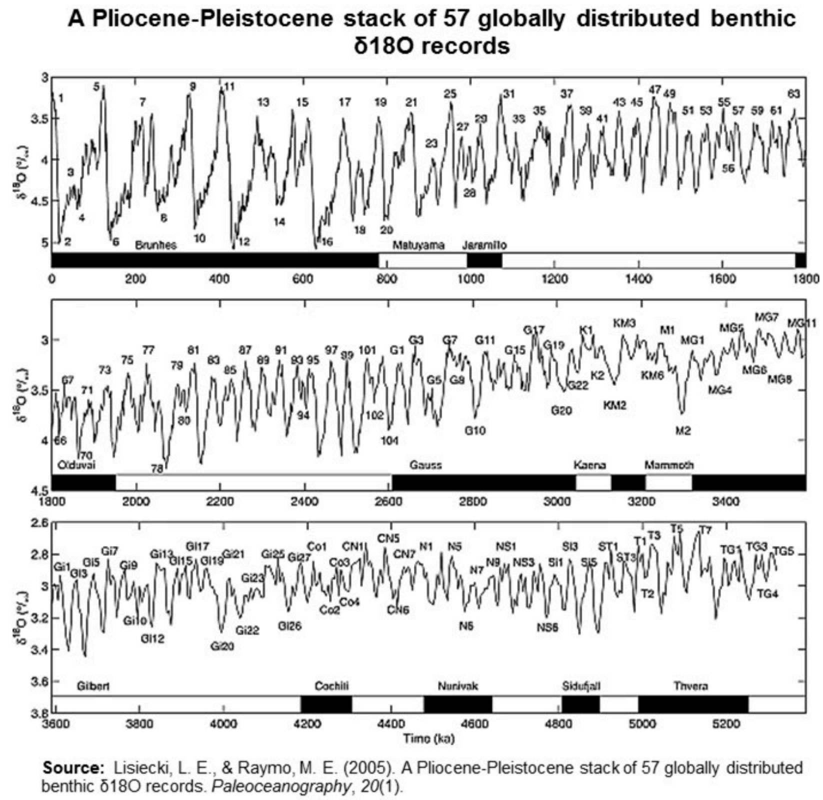

Figure 15.15: A Pliocene–Pleistocene stack of 57 globally distributed benthic δ18O records. Figure description available at the end of the chapter.

During an ice age, periods of warming climate are called **interglacials**; during interglacials, very brief periods of even warmer climate are called **interstadials**. These warming upticks are related to Earth's climate variations, like Milankovitch cycles, which are changes to the Earth's orbit that can fluctuate climate (see Glaciers chapter). In the last 500,000 years, there have been five or six interglacials, with the most recent belonging to our current time, the **Holocene** Epoch.

The two more recent climate swings, the Younger Dryas and the Holocene climatic optimum, demonstrate complex changes. These events are more recent yet have conflicting information. The Younger Dryas' cooling is widely recognized in the Northern Hemisphere, though the event's timing, about 12,000 years ago, does not appear to be equal everywhere. Also, it is difficult to find in the Southern Hemisphere. The Holocene climatic optimum is a warming around 6,000 years ago; it was not universally warmer, not as warm as current warming, and not warm at the same time everywhere.

15.3.2 Proxy Indicators of Past Climates

How do we know about past climates? Geologists use proxy indicators to understand past climate. A **proxy indicator** is a biological, chemical, or physical signature preserved in the rock, sediment, or ice record that acts like a fingerprint of something in the past. Thus, they are an *indirect* indicator of climate. An indirect indicator of ancient glaciations from the Proterozoic Eon and Paleozoic Era is the Mineral Fork Formation in Utah, which contains rock formations of glacial sediments such as diamictite (tillite); this dark rock has many fine-grained components plus some large out-sized clasts like a modern glacial till.

Deep-sea sediment is an indirect indicator of climate change during the Cenozoic Era. Researchers from the Ocean Drilling Program, an international research collaboration, collect deep-sea sediment cores that record continuous sediment accumulation. The sediment provides detailed chemical records of stable carbon and oxygen isotopes obtained from deep-sea benthic foraminifera shells that accumulated on the ocean floor over millions of years. The oxygen isotopes are a proxy indicator of deep-sea temperatures and continental ice volume.

Sediment Cores: Stable Oxygen Isotopes

Figure 15.16: Sediment core from the Greenland continental slope. Figure description available at the end of the chapter.

How do oxygen isotopes indicate past climate? The two main stable oxygen isotopes are ^{16}O and ^{18}O. They both occur in water (H_2O) and in the calcium carbonate ($CaCO_3$) shells of foraminifera, acting as both of those substances' oxygen component. The most abundant and lighter isotope is ^{16}O. Since it is lighter, it evaporates more readily from the ocean's surface as water vapor, which later turns to clouds and precipitation on the ocean and land. This evaporation is enhanced in warmer seawater and slightly increases the concentration of ^{18}O in the surface seawater from which the plankton derives the carbonate for its shells. Thus, the ratio of ^{16}O and ^{18}O in the fossilized shells in seafloor sediment is a proxy indicator of the temperature and evaporation of seawater.

Keep in mind, it is harder to evaporate the heavier water and easier to condense it. As evaporated water vapor drifts toward the poles and tiny droplets form clouds and precipitation, droplets of water with ^{18}O tend to form more readily than droplets of the lighter form and then precipitate out, leaving the drifting vapor depleted in ^{18}O. During geologic times when the climate is cooler, more of this lighter precipitation that falls on land is locked in the form of glacial ice. Consider that the giant ice sheets were more than a mile thick and covered a large part of North America during the last ice age only 14,000 years ago. During glaciation, the glaciers effectively lock away more ^{16}O, thus the ocean water and foraminifera shells become enriched in ^{18}O. Therefore, the ratio of ^{18}O to ^{16}O ($\delta^{18}O$) in calcium carbonate shells of foraminifera is a proxy indicator of past climate. The sediment cores from the Ocean Drilling Program record a continuous accumulation of these fossils in the sediment and provide a record of glacials, interglacials and interstadials.

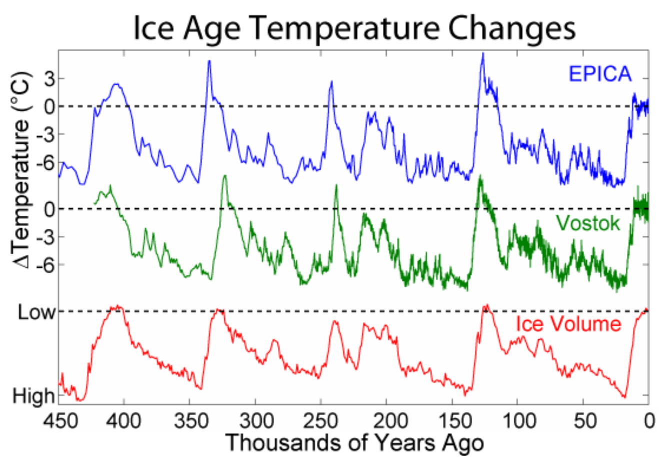

Figure 15.17: Antarctic temperature changes during the last few glaciations compared to global ice volume. The first two curves are based on the deuterium (heavy hydrogen) record from ice cores (EPICA Community Members, 2004; Petit et al., 1999). The bottom line is ice volume based on oxygen isotopes from a composite of deep-sea sediment cores (Lisiecki and Raymo, 2005). Figure description available at the end of the chapter.

Sediment Cores: Boron-Isotopes and Acidity

Ocean acidity is affected by carbonic acid and is a proxy for past atmospheric CO_2 concentrations. To estimate the ocean's pH (acidity) over the past 60 million years, researchers collected deep-sea sediment cores and examined the ancient planktonic foraminifera shells' boron-isotope ratios. Boron has two isotopes: ^{11}B and ^{10}B. In aqueous compounds of boron, the relative abundance of these two isotopes is sensitive to pH (acidity), hence CO_2 concentrations. In the early Cenozoic, around 60 million years ago, CO_2 concentrations were over 2,000 ppm and had higher pH, and they then started falling around 55 to 40 million years ago, with a noticeable drop in pH indicated by boron isotope ratios. The drop was possibly due to reduced CO_2 outgassing from ocean ridges, volcanoes and metamorphic belts, and due to increased carbon burial resulting from subduction and the Himalaya Mountains uplift. By the Miocene Epoch, about 24 million years ago, CO_2 levels were below 500 ppm, and by 800,000 years ago, CO_2 levels didn't exceed 300 ppm.

Carbon Dioxide Concentrations in Ice Cores

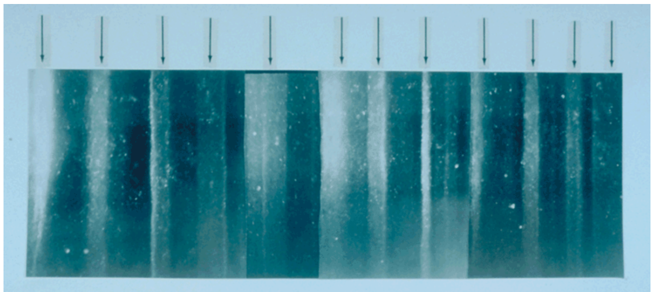

Figure 15.18: Nineteen-centimeter-long section of ice core showing 11 annual layers with summer layers (arrowed) sandwiched between darker winter layers. Figure description available at the end of the chapter.

For the recent Pleistocene Epoch's climate, researchers get a more detailed and direct chemical record of the last 800,000 years by extracting and analyzing ice cores from the Antarctic and Greenland ice sheets. Snow accumulates on these ice sheets and creates yearly layers. Oxygen isotopes are collected from these annual layers, and the ratio of ^{18}O to ^{16}O ($\delta^{18}O$) is used to determine temperature as discussed above. In addition, the ice contains small bubbles of atmospheric gas as the snow turns to ice. Analysis of these bubbles reveals the composition of the atmosphere at these previous times.

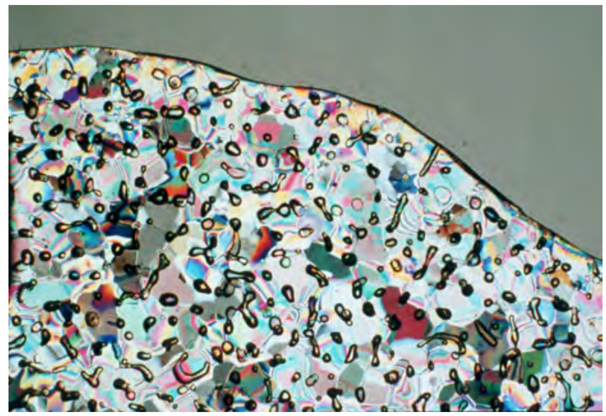

Figure 15.19: Antarctic ice showing hundreds of tiny trapped air bubbles from the atmosphere thousands of years ago. Figure description available at the end of the chapter.

Small pieces of this ice are crushed, and the ancient air is extracted into a mass spectrometer that can detect the ancient atmosphere's chemistry. Carbon dioxide levels are recreated from these measurements. Over the last 800,000 years, the maximum carbon dioxide concentration during warm times was about 300 parts per million (ppm), and the minimum was about 170 ppm during cold stretches. Currently, the Earth's atmospheric carbon dioxide content is over 410 ppm.

Oceanic Microfossils

Microfossils like foraminifera, diatoms, and radiolarians can be used as proxies to interpret past climate record. Different species of microfossils are found in the sediment core's different layers. Microfossil groups are called assemblages and their compositions differ depending on the climatic conditions when they lived. One assemblage consists of species that lived in cooler ocean water, such as in glacial times, while at a different level in the same sediment core, another assemblage consists of species that lived in warmer waters.

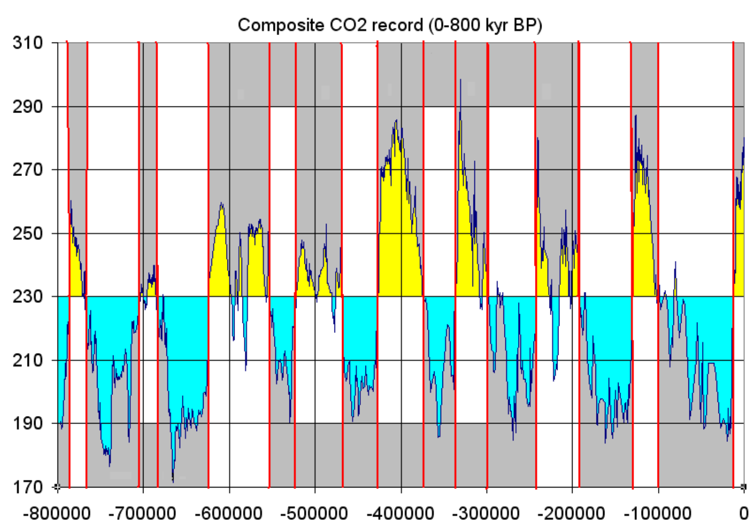

Figure 15.20: Composite carbon dioxide record from last 800,000 years based on ice core data from EPICA Dome C Ice Core. Figure description available at the end of the chapter.

Video 15.7: What sediment cores from the world's oceans reveal about climate patterns.

Access this YouTube video by scanning the QR code. ["Climatic Evidence From Sediments – Exploring the Science of Climate (3/5)" by OpenLearn from The Open University | https://www.youtube.com/watch?v=Yvu-g8BkkIg]

Tree Rings

Tree rings, which form every year as a tree grows, are another past climate indicator. Rings that are thicker indicate wetter years, and rings that are thinner and closer together indicate dryer years. Every year, a tree will grow one ring with a light section and a dark section. The rings vary in width. Since trees need much water to survive, narrower rings indicate colder and drier climates. Since some trees are several thousand years old, scientists can use their rings for regional paleoclimatic reconstructions—for example, to reconstruct past temperature, precipitation, vegetation, streamflow, sea-surface temperature, and other climate-dependent conditions. Paleoclimatic study means relating to a distinct past geologic climate. Dead trees, such as those found in Puebloan ruins, can be used to extend this proxy indicator by showing long-term droughts in the region, possibly explaining why villages were abandoned.

Figure 15.21: Tree rings form every year. Rings that are farther apart are from wetter years, and rings that are closer together are from dryer years. Figure description available at the end of the chapter.

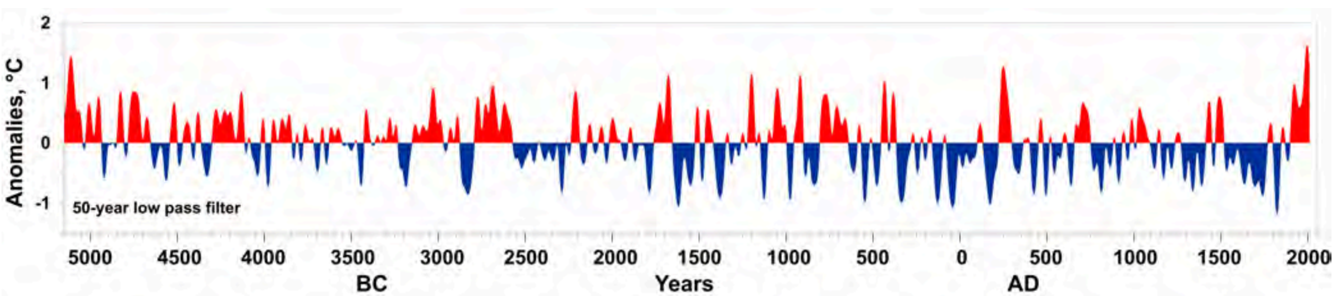

Figure 15.22: Summer temperature anomalies for the past 7,000 years. Figure description available at the end of the chapter.

Pollen

Pollen is also a proxy climate indicator. Flowering plants produce pollen grains. Pollen grains are distinctive when viewed under a microscope. Sometimes, pollen is preserved in lake sediments that accumulate in layers every year. Lake-sediment cores can reveal ancient pollen. Fossil-pollen assemblages are pollen groups from multiple species, such as spruce, pine, and oak. Through time, via the sediment cores and radiometric age-dating techniques, the pollen assemblages change, revealing the plants that lived in the area at the time. Thus, pollen assemblages are a past climate indicator, since different plants will prefer different climates. For example, in the Pacific Northwest, east of the Cascades in a region close to grassland and forest borders, scientists tracked pollen over the last 125,000 years, covering the last two glaciations. Pollen assemblages with more pine tree pollen are found during glaciations, and pollen assemblages with less pine tree pollen are found during interglacial times.

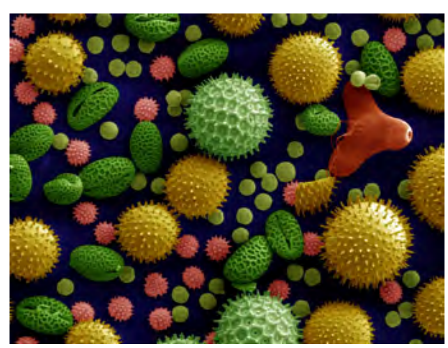

Figure 15.23: Scanning electron microscope image of modern pollen with false color added to distinguish plant species. Figure description available at the end of the chapter.

Other Proxy Indicators

Paleoclimatologists study many other phenomena to understand past climates, such as human historical accounts, human instrument records from the recent past, lake sediments, cave deposits, and corals.

Take this quiz to check your comprehension of this section.

Access the quiz for Section 15.3 by scanning the QR code.

15.4 Anthropogenic Causes of Climate Change

As shown in the previous section, prehistoric climate changes occur slowly over many millions of years. The climate changes observed today are rapid and largely human caused. Evidence shows that climate is changing, but what is causing that change? Since the late 1800s, scientists have suspected that human-produced (i.e., anthropogenic) changes in atmospheric greenhouse gases would likely cause climate change because changes in these gases have been the cause every time in the geologic past. By the middle 1900s, scientists began conducting systematic measurements, which confirmed that human-produced carbon dioxide was accumulating in the atmosphere and other Earth systems, such as forests and oceans. By the end of the 1900s and into the early 2000s, scientists solidified the theory of **anthropogenic climate change** when evidence from thousands of ground-based studies and continuous land and ocean satellite measurements mounted, revealing the expected temperature increase. The theory of anthropogenic climate change states that humans are causing most of the current climate changes by burning fossil fuels such as coal, oil, and natural gas. Theories evolve and transform as new data and new techniques become available, and they represent a particular field's state of thinking. This section summarizes the scientific consensus of anthropogenic climate change.

15.4.1 Scientific Consensus

The overwhelming majority of climate studies indicate that human activity is causing rapid changes to the climate, which will cause severe environmental damage. There is strong scientific consensus on the issue. Studies published in peer-reviewed scientific journals show that 97 percent of climate scientists agree that climate warming is caused from human activities. There is no alternative explanation for the observed link between human-produced greenhouse gas emissions and changing modern climate. Most leading scientific organizations endorse this position, including the US National Academy of Science, which was established in 1863 by an act of Congress under President Lincoln. Congress charged the National Academy of Science "with providing independent, objective advice to the nation on matters related to science and technology." Therefore, the National Academy of Science is the leading authority when it comes to policy advice related to scientific issues.

One way we know that the increased greenhouse gas emissions are from human activities is through isotopic fingerprints. For example, fossil fuels, representing plants that lived millions of years ago, have a stable carbon-13 to carbon-12 ($^{13}C/^{12}C$) ratio that is different from today's atmospheric stable-carbon ratio (radioactive ^{14}C is unstable). Isotopic carbon signatures have been used to identify anthropogenic carbon in the atmosphere since the 1980s. Isotopic records from the Antarctic ice sheet show stable isotopic signatures from ~1000 CE to ~1800 CE and a steady isotopic signature gradually changing since 1800, followed by a more rapid change after 1950 as burning of fossil fuels dilutes the CO_2 in the atmosphere. These changes show the atmosphere as having a carbon isotopic signature increasingly more similar to that of fossil fuels.

15.4.2 Anthropogenic Sources of Greenhouse Gases

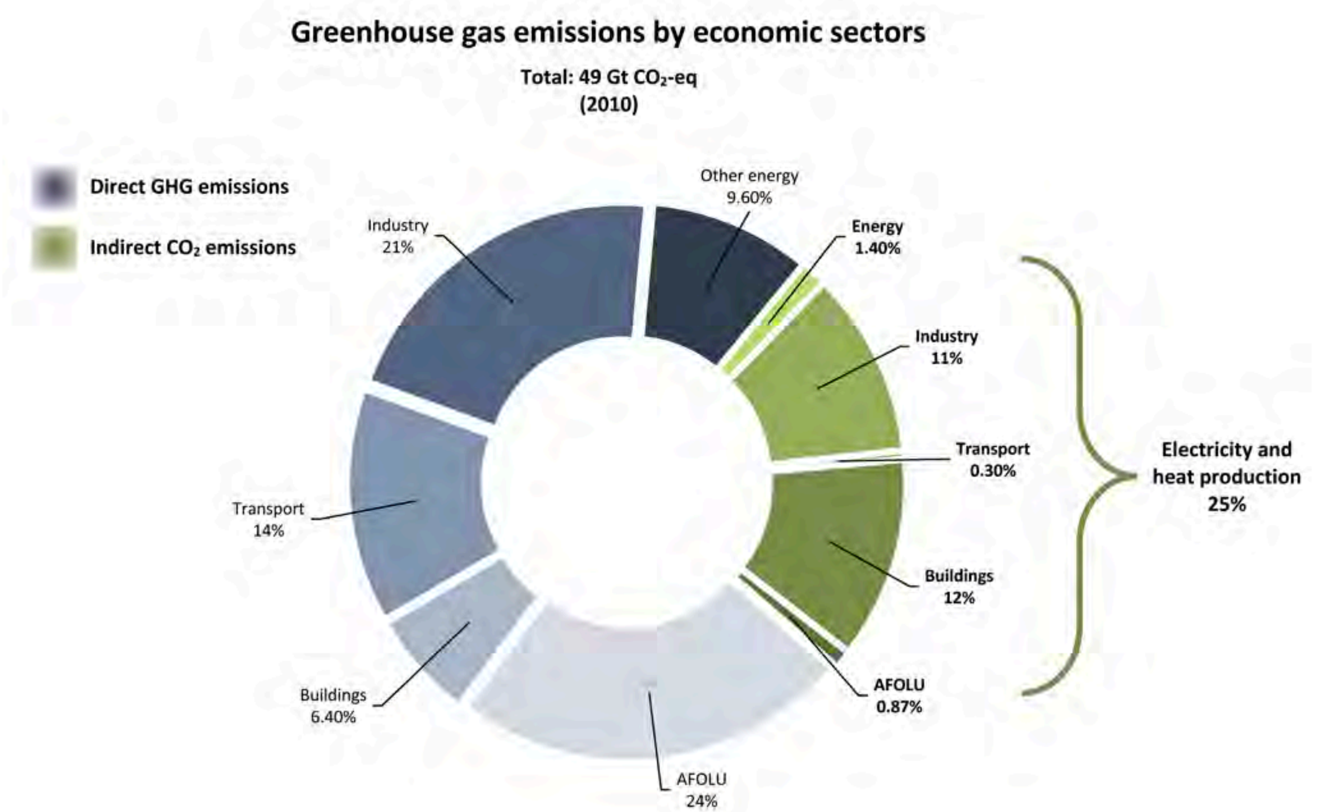

Figure 15.24: Total anthropogenic greenhouse gas emissions (gigatonne of CO_2-equivalent per year, $GtCO_2$-eq/yr) from economic sectors in 2010. The circle shows the shares of direct GHG emissions (in % of total anthropogenic GHG emissions) from five economic sectors in 2010. The pull-out shows how shares of indirect CO_2 emissions (in % of total anthropogenic GHG emissions) from electricity and heat production are attributed to sectors of final energy use. Figure description available at the end of the chapter.

Anthropogenic emissions of greenhouse gases have increased since pre-industrial times due to global economic growth and population growth. Atmospheric concentrations of the leading greenhouse gas, carbon dioxide, are at unprecedented levels that haven't been observed in at least the last 800,000 years. The pre-industrial level of carbon dioxide was at about 278 parts per million (ppm). In 2016, carbon dioxide was, for the first time, above 400 ppm for the entirety of the year. Measurements of atmospheric carbon at the Mauna Loa Carbon Dioxide Observatory show a continuous increase from 315 ppm since 1957 when the observatory was established to over 420 ppm in 2024. The daily reading today can be seen at Daily CO_2. Based on the ice core record over the past 800,000 years, carbon dioxide ranged from about 185 ppm during ice ages to 300 ppm during warm times. View the data-accurate NOAA animation below of carbon dioxide trends over the last 800,000 years.

What is the source of these anthropogenic greenhouse gas emissions? Fossil fuel combustion and industrial processes have contributed 78 percent of all emissions since 1970. The economic sectors responsible for most of this include electricity and heat production (25%); agriculture, forestry, and land use (24%); industry (21%); transportation, including automobiles (14%); other energy production (9.6%); and buildings (6.4%). More than half of greenhouse gas emissions have occurred in the last 40 years, and 40% of these emissions have stayed in the atmosphere. Unfortunately, despite scientific consensus, efforts to mitigate climate change require political action. Despite growing climate change concern, mitigation efforts, legislation, and international agreements have only reduced emissions in some places, while the less-developed world's continual economic growth has increased global greenhouse gas emissions. In fact, the years 2000 to 2010 saw the largest increases since 1970.

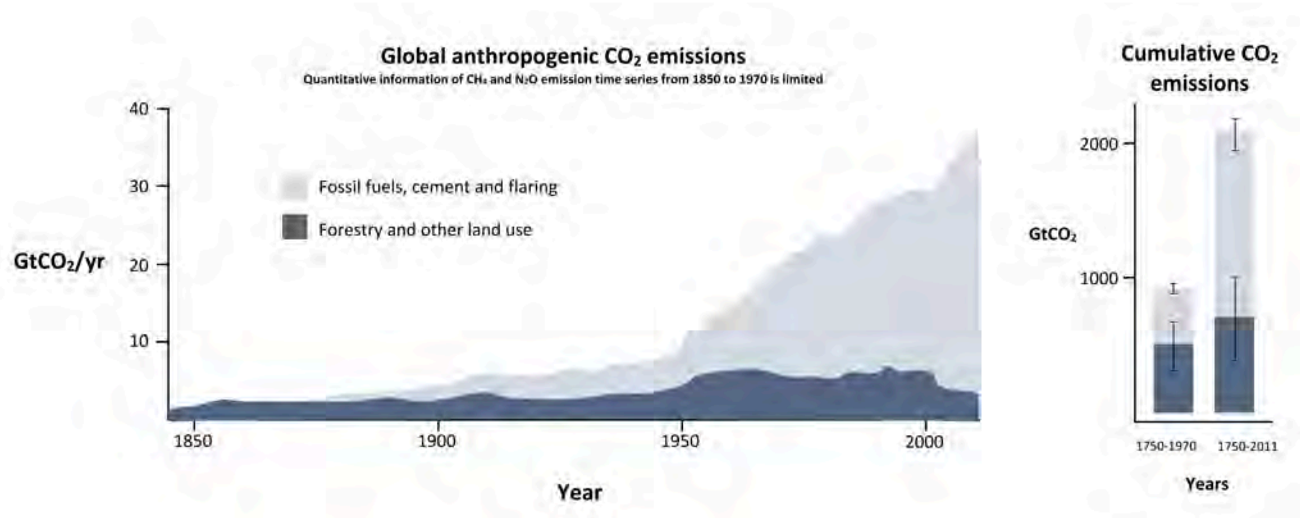

Figure 15.25: Annual global anthropogenic carbon dioxide (CO_2) emissions in gigatonne of CO_2-equivalent per year ($GtCO_2/yr$) from fossil fuel combustion, cement production and flaring, and forestry and other land use (FOLU), 1750–2011. Cumulative emissions and their uncertainties are shown as bars and whiskers. Figure description available at the end of the chapter.

15.4.3 Predicting Future Warming

Climate change can be a naturally occurring process and has created environments much warmer than today, such as the early Cretaceous Period. During this time, life thrived even in polar regions, such as the interior of Antarctica, which is uninhabitable today.

One misconception is that the threat of climate change has to do with the absolute warmth of the Earth. The concern for scientists has more to do with the rate of change of that temperature increase. Living organisms, including humans, can quickly adapt to substantial changes in climate if the changes take place slowly, over thousands of years. However, adapting to changes that are taking place on timescales of decades is far more challenging. The Earth is warming at such a rate that most species will struggle to adapt and evolve quickly enough to the coming warmer climates.

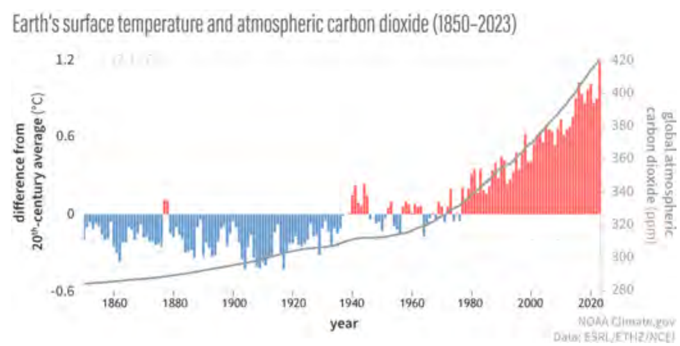

Figure 15.26: (Bar graph) Yearly temperature compared to the twentieth-century average from 1850–2023. Red bars mean warmer-than-average years; blue bars mean colder-than-average years. (Line graph) Atmospheric carbon dioxide amounts: 1850–1958 from IAC, 1959–2023 from NOAA Global Monitoring Lab. Figure description available at the end of the chapter.

Prediction is difficult, especially about the future. This is also true for projections of future climate change, as they rely on assumptions about future **radiative forcings** such as anthropogenic emissions of greenhouse gases and aerosols, which are unknown. For this reason, they are called projections and not predictions.

Climate scientists believe that the best projections consider results from state-of-the-science climate models because they are syntheses of theoretical and empirical knowledge. However, climate models are imperfect. Uncertainties in future projections will therefore arise from assumptions about both future greenhouse gas emissions and climate model errors.

The Intergovernmental Panel on Climate Change (IPCC) is a United Nations body that evaluates climate change science and publishes comprehensive Assessment Reports, Special Reports, and Methodology Reports. The latest Assessment Report, AR6, includes contributions from three Working Groups finalized between August 2021 and April 2022 and from a Synthesis Report completed in March 2023. These reports provide insights into climate change, its impacts, risks, and **mitigation** options. They can be freely accessed online.

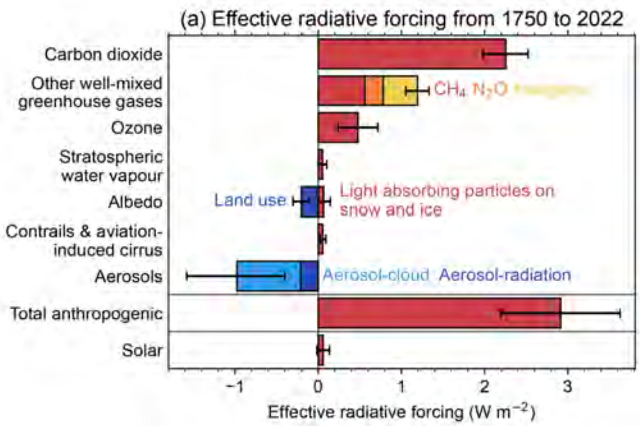

Figure 15.27: An assessment of effective radiative forcing in 2022 using a baseline year of 1750. Figure description available at the end of the chapter.

The most recent IPCC Assessment Report (AR6) uses future scenarios that specify anthropogenic radiative forcing and CO_2 concentrations. They are called Shared Socioeconomic Pathways (SSPs) and are followed by two numbers. The first indicates the socioeconomic narrative, and the second indicates the radiative forcing around the year 2100. For example, the scenario SSP5-8.5 uses the socioeconomic narrative 5 (Fossil Fueled Development) and reaches a radiative forcing of 8.5 W/m^2 in the year 2100, whereas scenario SSP1-1.9 uses the socioeconomic narrative 1 (Sustainability) and reaches a radiative forcing of 1.9 W/m^2 in the year 2100. The goal is to cover a range of possible futures. Note that the radiative forcing and CO_2 concentrations increase beyond the year 2100 for scenarios SSP3-7 and SSP5-8.5, whereas they stabilize for scenario SSP3-4.5 and decline for scenarios SSP1-1.9 and SSP1-2.6. Scenarios from the previous IPCC assessment report were called Representative Concentration Pathways (RCPs) and also used the radiative forcing in the year 2100 (e.g., RCP8.5 corresponds to SSP5-8.5).

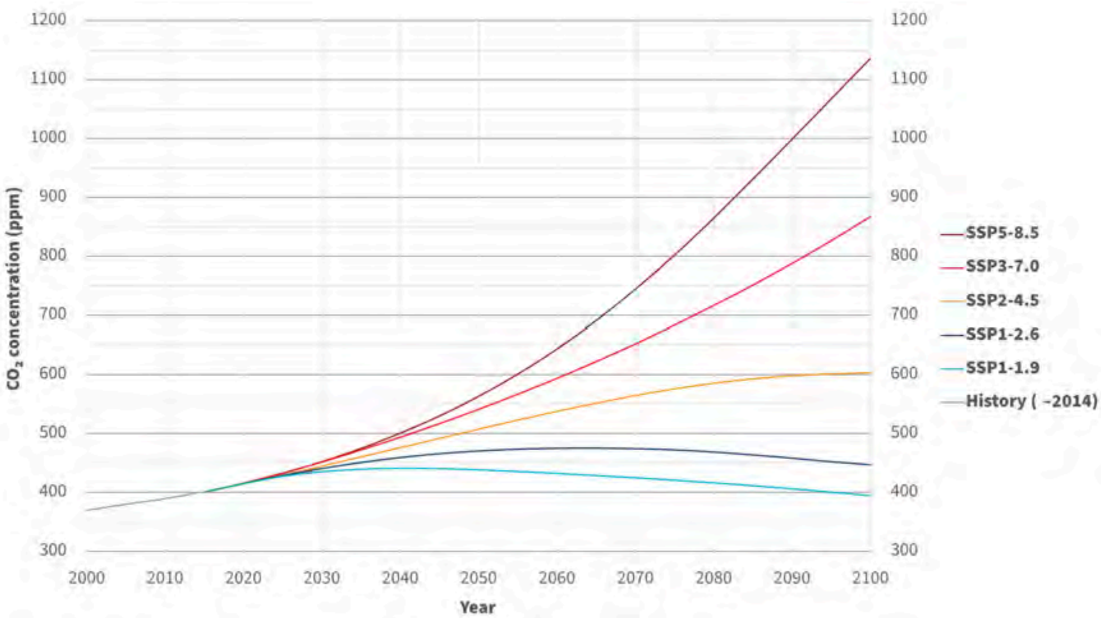

Figure 15.28: Atmospheric CO_2 concentrations by SSP across the twenty-first century (projected by MAGICC7, a simple/reduced complexity climate model). Figure description available at the end of the chapter.

CO_2 concentration pathways are used as input to comprehensive climate models, which project a range of global temperature responses. For scenarios SSP1-1.9 and SSP1-2.6, the models project further warming of less than 1°C above current levels by the year 2050 and subsequent stabilization or slow cooling. Scenarios SSP2-4.5 and SSP3-7 result in additional warming of about 2 to 3°C until 2100, whereas for the high-emission scenario SSP5-8.5 temperatures increase by 4°C by 2100. The latter is similar to the temperature difference between the Last Glacial Maximum and the pre-industrial. Note that the uncertainty is larger for higher-emission scenarios.

Carbon dioxide levels will continue to rise in the decades to come. However, the impacts will not be evenly distributed across the planet. Those impacts will depend on environmental and climate factors; other impacts will depend on whether the countries are developed or emerging. Climatologists and other scientists use sophisticated computer models to predict the causes, effects, and impacts of greenhouse gas increase on climate systems, both globally and for specific regions of the world.

It is essential to get a sound, data-driven understanding of climate change. Along with the IPCC, there are many organizations that study climate change, including the United Nations Environmental Programme (UNEP), World Health Organization, World Meteorological Organization (WMO), National Aeronautics and Space Administration (NASA), the National Oceanic and Atmospheric Administration (NOAA), and the US Environmental Protection Agency (EPA).

Take this quiz to check your comprehension of this section.

Access the quiz for Section 15.4 by scanning the QR code.

15.5 Solutions

Climate change is a difficult problem to solve because our modern society was built upon burning fossil fuels as an energy source. We still depend strongly on fossil fuel energy for everything from driving our cars and washing our laundry to charging our cell phones and heating our homes. In order to stabilize climate, however, we'll need to move to near-zero carbon emissions in the long run. Thus, the challenge is to decarbonize our economy. The longer we wait with this transformation, the larger the impacts of future climate change will be and the faster future emission reductions will need to be if the goal is to stay within a certain limit of global warming. And because it is a global problem, the whole world, or at least most of it, will need to cooperate to solve it. Moreover, because we're already committed to further climate change, we better prepare to adapt to it.

Historically, the increase in carbon emissions was caused by human population growth and an increase in the economy. The increased use of fossil fuel-based energy has lifted many people out of poverty and improved the lives of millions, although many people in the developing world remain in poverty today. **Energy intensity** of the **gross domestic product** (GDP) has been decreasing during the past 50 years, which has somewhat compensated for the increase in population and GDP per person, whereas carbon intensity has not changed as much as the other factors, according to the IPCC.

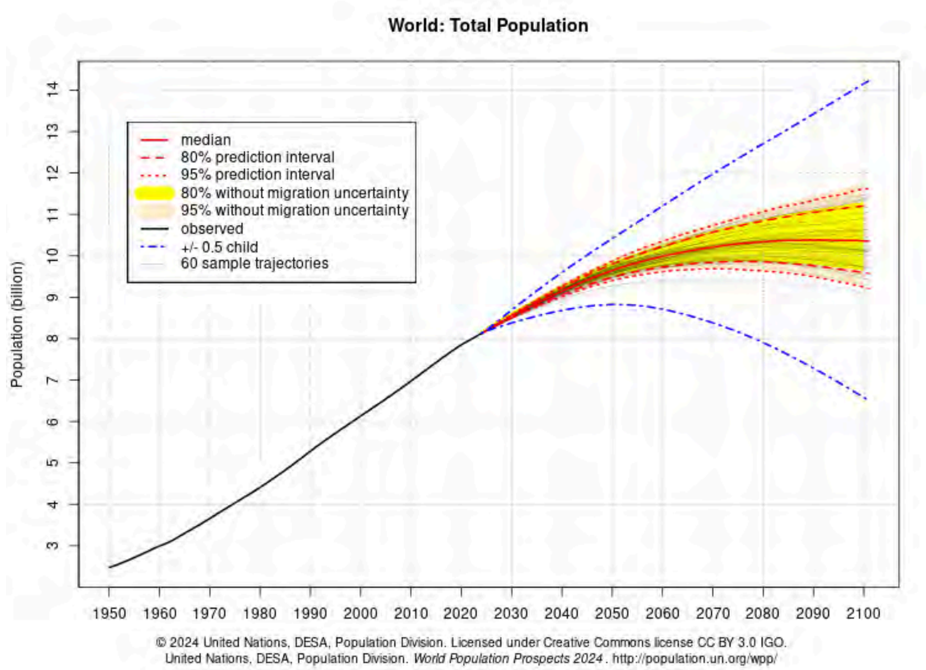

Figure 15.29: Estimates and probabilistic projections of the total population for the world. The population projections are based on the probabilistic projections of total fertility and life expectancy at birth. These probabilistic projections of total fertility and life expectancy at birth were carried out with a Bayesian hierarchical model. The figures display the probabilistic median, and the 80–95% prediction intervals of the probabilistic population projections, as well as the (deterministic) high and low variant (+/- 0.5 child). Figure description available at the end of the chapter.

Currently the world population is more than eight billion people, and it is expected to continue to increase, at least for the near future. This increase will continue to put more pressures on the Earth system; climate change is just one of them. Another example is the increased occupation of wild places by humans, which reduces habitats for many species of plants and animals or increasing demand for resources such as food and fresh water. Population growth could be efficiently reduced by educating and empowering women in the developing world and through poverty reduction. Reducing the GDP per person is probably not a good way to reduce emissions, because most people do not want to reduce their standard of living and energy consumption (although in many developed countries, a lot of waste could be cut without affecting the standard of living much). Since many people in the developing world hope to improve their standard of living, it will be desirable to further increase the average GDP per person in the future. But if carbon emissions could be reduced, for example, by shifting to non–fossil fuel energy sources that would reduce emissions without reducing GDP or energy consumption.

15.5.1 Technology

Current global energy production relies heavily on burning fossil fuels. The largest energy sources are oil, coal, and natural gas, all of which are fossil fuels, whereas all non–fossil fuel sources together account for only about 20% of the total. Most oil consumption powers internal combustion engines in cars and trucks, which have a very low efficiency. Only about 25% of all energy input into transportation is used to move vehicles, whereas most of the energy is wasted as heat. Coal is mainly used in power plants to generate electricity, which is also associated with a loss of a little over half. Note that this loss is less than the loss from internal combustion engines, which gives electric cars lower carbon footprints than internal combustion engine cars, even if the electricity is generated from coal. Most natural gas is used to generate electricity and to heat buildings. Hydropower and nuclear power are used exclusively to produce electricity, whereas **biomass** is used mostly for cooking and heating homes in the developing world. New renewables such as solar and wind supply only a small fraction of all energy.

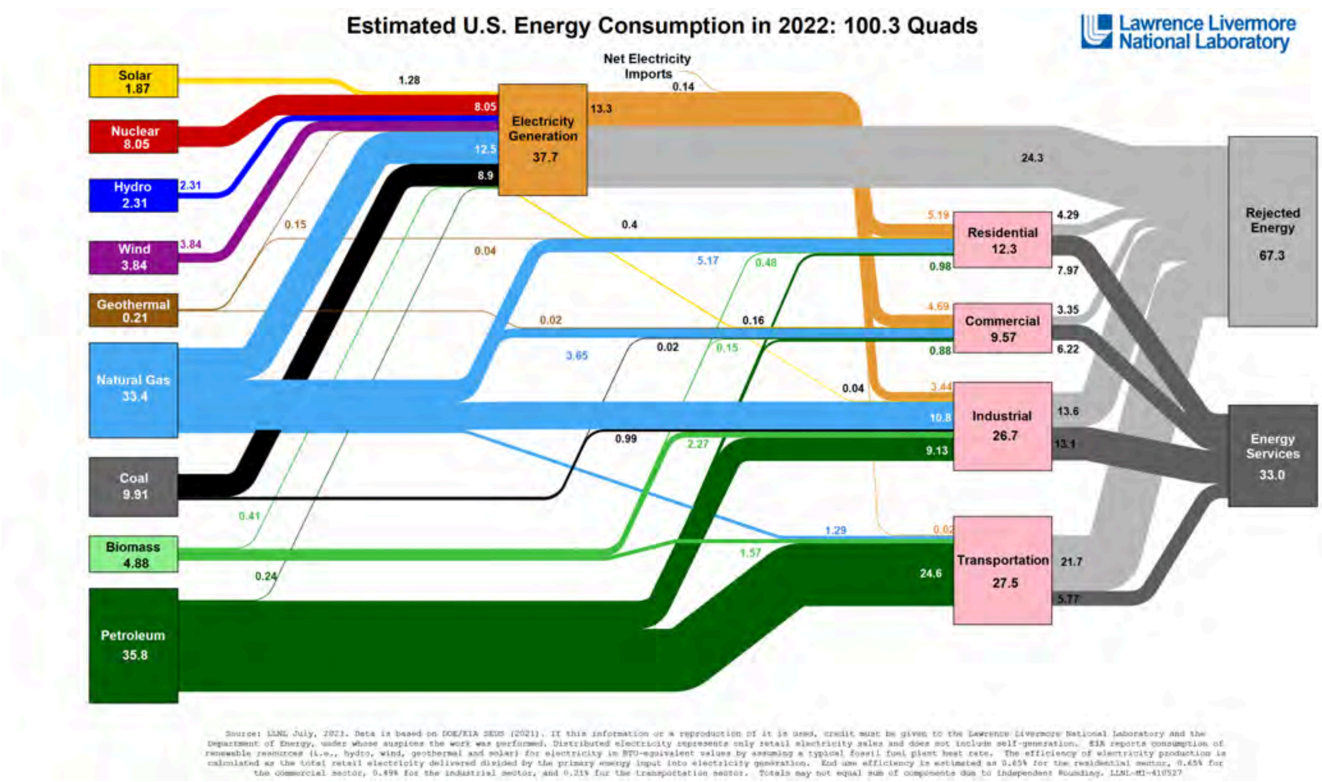

Figure 15.30: The 2022 energy flow chart released by Lawrence Livermore National Laboratory details the sources of energy production, how Americans are using energy, and how much waste exists. Figure description available at the end of the chapter.

However, in some countries, renewable energy sources have seen a rapid increase in recent years. Germany, for example, has increased renewables' contribution to total electricity production from 3% in 1990 to 45% in 2020, while its economy has been one of the strongest in Europe. Denmark plans to move to 100% renewable energy by 2050. In the United States, renewables currently account for 10% of total energy consumption and 15% of electricity production, and it is rapidly increasing. In 2016, for example, the US's solar power capacity doubled.

The advantage of renewables is an almost-unlimited potential supply with minimal carbon emissions (some emissions occur during the production and installation of solar panels and wind turbines); in addition, they are not associated with the dangers of nuclear power. Their disadvantage used to be their cost, particularly their high upfront investment cost. Once installed, however, solar panels and wind turbines operate with nearly no maintenance cost since solar energy and wind is free. During the past ten years, the cost for solar panels has decreased by 80%. Thus, if viewed over the lifetime of a system, renewables become competitive with fossil fuels. Other renewable energy sources are geothermal, tide and wave energy, and hydroelectric dams. An issue with renewables is their intermittent energy supply. Solar panels only work during the day, whereas wind turbines only work when the wind blows. However, a recent study showed that 80% of all electricity demand could easily be covered by wind and solar (Shaner et al., 2018).

Figure 15.31: Photograph of solar cell panels in the foreground, wind turbines in the middle ground, and electricity pylons in the background. Figure description available at the end of the chapter.

Figure 15.32: IAEA experts depart Unit 4 of TEPCO's Fukushima Daiichi Nuclear Power Station on April 17, 2013, as part of a mission to review Japan's plans to decommission the facility. Figure description available at the end of the chapter.

Nuclear plants also provide power that is fossil-free and does not cause carbon emissions (except during construction). For this reason, they are viewed by some as an important future energy source. However, nuclear power has disadvantages too. Not only are their plants expensive to build, they are also dangerous to operate and they produce radioactive waste for which currently no long-term repository exists. Catastrophic accidents—such as the nuclear meltdowns in 2011 at the Japanese Fukushima Daiichi plant and in 1986 at the Chernobyl reactor in what is now northern Ukraine—have shown the dangers associated with nuclear power production. Thus, nuclear power remains a controversial topic.

Currently, many companies are moving toward more electric cars or hybrid vehicles. Due to their much higher efficiencies (80–90%), their energy use is much smaller than for cars with internal combustion engines and their carbon footprint can be close to zero (considering there is some associated with vehicle production) if renewable energy sources are used for the electricity.

Figure 15.33: The BMW i3 is an electric car that was manufactured from 2013 to 2022. The i3 was BMW's first mass-produced zero emissions vehicle and was launched as part of BMW's electric vehicle BMW i subbrand. Figure description available at the end of the chapter.

Considering the large amounts of carbon emissions that currently come from the transportation sector and the large losses that occur there, shifting to an electric vehicle fleet could bring a tremendous reduction in future emissions. Even though electric cars are more expensive to purchase, their lifetime costs are lower than gasoline-powered cars. This is because the average cost for equivalent electricity is less than half the cost for a gallon of gas. Electric cars have other advantages too: no oil changes, no pollution, and more torque. Manufacturing electric cars, however, is not without environmental or human impacts, such as from the mining of raw materials used in the production of batteries.

Increasing energy efficiency is another cost-effective way to reduce carbon emissions. Residential and commercial buildings waste about half of their energy. Building insulation not only lowers its carbon emissions but also saves the owner money. Replacing old conventional electrical hot water heaters with inexpensive new heat pump water heaters also reduces electricity use, thereby saving money as well.

15.5.2 International Agreements

In 1992, the United Nations Framework Convention on Climate Change (UNFCCC) was adopted at the Rio Earth Summit. It was ratified by 197 countries (Parties to the Convention). Its Article 2 states:

> "The ultimate objective of this Convention and any related legal instruments that the Conference of the Parties may adopt is to achieve, in accordance with the relevant provisions of the Convention, stabilization of greenhouse gas concentrations in the atmosphere at a level that would prevent dangerous anthropogenic interference with the climate system. Such a level should be achieved within a time frame sufficient to allow ecosystems to adapt naturally to climate change, to ensure that food production is not threatened and to enable economic development to proceed in a sustainable manner."

The UNFCCC recognizes that the developed world is responsible for most historical carbon emissions and thus it should lead the way to reduce its emissions. The annual United Nations Climate Change Conferences, or COPs, are formal gatherings to assess and negotiate climate action, held under the UNFCCC. The **Kyoto Protocol**, an international agreement linked to the UNFCCC, commits its parties, which are developed countries, to binding carbon emission reduction targets. However, it was not successful in reducing global carbon emissions, presumably at least in part due to the United States never ratifying it, Canada exiting, and Russia not agreeing to emission reductions in its second phase (2013-2020). Under the administration of President George W. Bush, the US argued that it was not fair to reduce US emissions, while China was allowed to increase its emissions, even though per capita emissions in the US were much higher than those in China.

The **Paris Agreement** has the goal to limit global warming to well below 2°C, and it was ratified by 174 countries. It has made emission reductions essentially voluntary by soliciting pledges from each country and includes developing countries like China. However, resistance against any reduction in carbon emissions was evident when the US administration under President Trump withdrew from the agreement (although the next administration under President Biden re-entered the agreement).

Figure 15.34: Plenary session of the COP21 for the adoption of the Paris Accord, United Nations Climate Change Conference (Paris, Le Bourget). Figure description available at the end of the chapter.

15.5.3 Adaptation and Mitigation

While the situation surrounding global climate change is in serious need of our attention, it is important to realize that many scientists, leaders, and concerned citizens are making solutions to climate change part of their life's work. The two solutions to the problems caused by climate change are mitigation and adaptation, and we will likely need a combination of both in order to prosper in the future. We know that climate change is already occurring, as we can see and feel the effects of it. For this reason, it is essential to also adapt to our changing environment. This means that we must change our behaviors in response to the changing environment around us.

Figure 15.35: Lovett School, in north Atlanta, GA, has a rooftop garden with this mechanism for collecting water to use in irrigation. Figure description available at the end of the chapter.

Adaptation strategies will vary greatly by region, depending on the largest specific impacts in that area. For example, in the city of Delhi, India, a dramatic decrease in rainfall is projected over the next century. This city will likely need to implement policies and practices relating to conservation of water, for example, **rainwater harvesting**, water re-use, and increased irrigation efficiency. Rain-limited cities near oceans, such as Los Angeles, California, may choose to use **desalination** to provide drinking water to their citizens. Cities with low elevations near oceans may need to implement adaptation strategies for rising sea levels, from seawalls and levees to relocation of citizens. One adaptation strategy gaining use is the creation or conservation of wetlands, which provide natural protection against storm surges and flooding.

In general, a strategy to mitigate climate change is one that reduces the amount of greenhouse gases in the atmosphere or prevents additional emissions. Mitigation strategies attempt to "fix" the problems caused by climate change. Governmental regulations regarding fuel efficiency of vehicles is one example of an institutionalized mitigation strategy already in place in the United States and in many other countries around the world. Unlike some other countries, there are no carbon taxes or charges on burning fossil fuels in the United States. This is another governmental mitigation strategy that has been shown to be effective in many countries, including India, Japan, France, Costa Rica, Canada, and the United Kingdom.

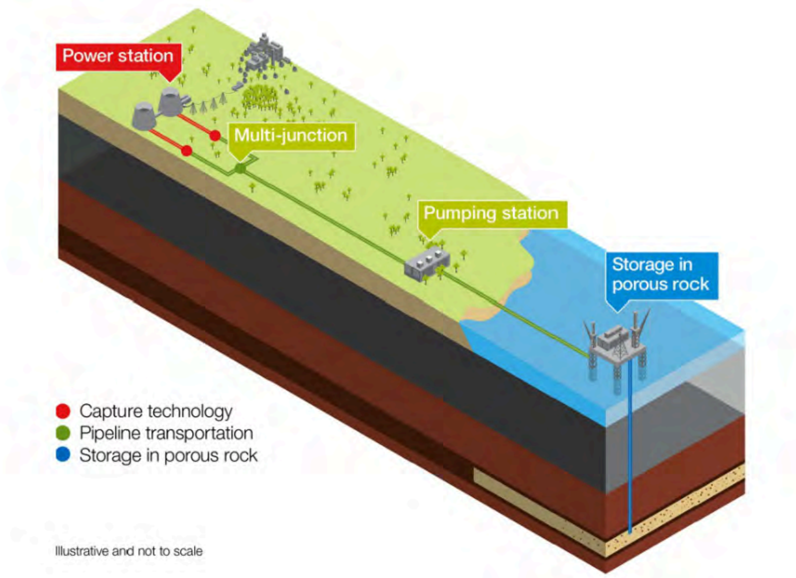

Figure 15.36: Graphic demonstrating the CCS process. Figure description available at the end of the chapter.

In addition to government measures and incentives, technology can also be harnessed to mitigate climate change. One strategy for this is the use of carbon capture and sequestration (CCS). Through CCS, 80–90% of the CO_2 that would have been emitted to the atmosphere from sources such as a coal-fired power plant is instead captured and then stored deep beneath the Earth's surface. The CO_2 is often injected and sequestered hundreds of miles underground into porous rock formations sealed below an impermeable layer, where it is stored permanently.

Scientists are also looking into the use of soils and vegetation for carbon storage potential. Proper management of soil and forest ecosystems has been shown to create additional carbon sinks for atmospheric carbon, reducing the overall atmospheric CO_2 burden. Increasing soil carbon further benefits communities by providing better-quality soil for agriculture and cultivation.

Technologies related to alternative energy sources mitigate climate change by providing people with energy not derived from the combustion of fossil fuels. Finally, energy conservation, choosing to walk or bike instead of driving, and disposing of waste properly are simple activities that, when done by large numbers of people, actively mitigate climate change by preventing carbon emissions.

Take this quiz to check your comprehension of this section.

Access the quiz for Section 15.5 by scanning the QR code.

Summary

Included in Earth Science is the study of the system of processes that affect surface environments and atmosphere of the Earth. Recent changes in atmospheric temperature and climate over intervals of decades have been observed. For Earth's climate to be stable, incoming radiation from the Sun and outgoing radiation from the Sun-warmed Earth must be in balance. Greenhouse gases in the atmosphere absorb the infrared thermal radiation from the Earth's surface, trapping that heat and warming the atmosphere in a process called the greenhouse effect. Thus, the energy budget is not now in balance and the Earth is warming. Human activity produces many greenhouse gases that have accelerated climate change. CO_2 from fossil fuel burning is one of the major such gases. While the atmosphere is mostly composed of nitrogen and oxygen, the greatest effect on global warming is had by trace components that include greenhouse gases (of which CO_2 and methane are the major examples).

A number of positive feedback mechanisms, processes whose results reinforce the original process, take place in the Earth system. An example of a PFM of great concern is permafrost melting, which causes decay of melting organic material, producing CO_2 and methane (both powerful greenhouse gases) that warm the atmosphere and promote more permafrost melting. Two carbon cycles affect Earth's atmospheric CO_2 composition, the biologic carbon cycle and the geologic carbon cycle. In the biologic cycle, organisms (mostly plants and also animals that eat them) remove CO_2 from the atmosphere for energy and to build their body tissues and return it to the atmosphere when they die and decay. The biologic cycle is a rapid cycle. In the geologic cycle, some organic matter is preserved in the form of petroleum and coal, while more is dissolved in seawater and captured in carbonate sediments, some of which is subducted into the mantle and returned by volcanic activity. The geologic carbon cycle is slow over geologic time.

Measurements of increasing atmospheric temperature have been made since the nineteenth century, but the upward temperature trend itself increased in the mid-twentieth century, showing the current trend is exponential. Because of the high specific heat of water, the oceans have absorbed most of the added heat. The temporary nature of this storage has been revealed by the record breaking warm years of the recent decade and the increase in intense storms and hurricanes. In 1957, the Mauna Loa CO_2 Observatory was established in Hawai'i, providing constant measurements of atmospheric CO_2 since 1958. The initial value was 315 ppm. The Keeling curve, named for the observatory founder, shows that value has steadily increased exponentially to over 420 ppm now. Compared to proxy data from atmospheric gases trapped in ice cores that show a maximum value for CO_2 of about 300 ppm over the last 800,000 years, the Keeling increase of over 100 ppm in 50 years is dramatic evidence of human-caused CO_2 increase and climate change. As Earth's temperature rises, glaciers and ice sheets are shrinking, resulting in sea level rise. Atmospheric CO_2 is also absorbed in seawater, producing increased concentrations of carbonic acid, which is raising the pH of the oceans, making it harder for marine life to extract carbonate for their skeletal materials.

Earth's climate has changed over geologic time with periods of major glaciations. There was a high temperature period in the Mesozoic shown by fossils in high latitudes and the Western Interior Seaway covering what is now the Midwest. However, climate has been cooling during the Cenozoic culminating in the most recent ice age. Since the ice age, several proxy indicators of ancient climate show that the rate and amount of current climate change is unique in geologic history and can only be attributed to human activity.

Addressing climate change is a challenging task, largely because our industrialized society has relied heavily on fossil fuels for energy and this dependency continues today. To stabilize the climate, we must aim for near-zero carbon emissions in the long term. Given the global nature of the problem, international cooperation is essential. Additionally, since some degree of climate change is inevitable, we must also prepare to adapt to its impacts.

Take this quiz to check your comprehension of this chapter.

Access the quiz for Chapter 15 by scanning the QR code.

Chapter URLs

- Interactive animation on the greenhouse effect: https://science.nasa.gov/resource/graphic-the-greenhouse-effect
- NASA animation: NASA Scientific Visualization Studio (2022), Global Temperature Anomalies from 1880 to 2021 https://svs.gsfc.nasa.gov/4964
- NASA video [3 min]: NASA JPL, Oceans of Climate Change https://science.nasa.gov/resource/video-oceans-of-climate-change
- Daily CO_2 Reading: https://www.co2.earth/daily-co2
- Milankovitch cycles: https://en.wikipedia.org/wiki/Milankovitch_cycles

Text References

1. Allen, P.A., and Etienne, J.L. (2008). Sedimentary challenge to snowball Earth. *Nat. Geosci., 1*(12), 817–825.
2. Berner, R.A. (1998). The carbon cycle and carbon dioxide over Phanerozoic time: The role of land plants. *Philos. Trans. R. Soc. Lond. B Biol. Sci., 353*(1365), 75–82.
3. Cunningham, W.L., Leventer, A., Andrews, J.T., Jennings, A.E., and Licht, K.J. (1999). Late Pleistocene–Holocene marine conditions in the Ross Sea, Antarctica: Evidence from the diatom record. *The Holocene, 9*(2), 129–139.
4. Dastrup, R.A. (2020). *Physical geography and natural disasters OER textbook:* Salt Lake Community College.
5. Deynoux, M., Miller, J.M.G., and Domack, E.W. (2004). *Earth's glacial record:* Cambridge University Press, World and Regional Geology.
6. Earle, S. (2015). *Physical geology OER textbook:* BCcampus OpenEd.
7. Eyles, N., and Januszczak, N. (2004). "Zipper-rift": A tectonic model for Neoproterozoic glaciations during the breakup of Rodinia after 750 Ma. *Earth-Sci. Rev., 65*(1–2), 1–73.

8. Francey, R.J., Allison, C.E., Etheridge, D.M., Trudinger, C.M., et al. (1999). A 1000-year high precision record of δ13C in atmospheric CO2. *Tellus B Chem. Phys. Meteorol.*
9. Gutro, R. (2005). NASA – What's the difference between weather and climate? Online, http://www.nasa.gov/mission_pages/noaa-n/climate/climate_weather.html, accessed September 2016.
10. Hoffman, P.F., Kaufman, A.J., Halverson, G.P., and Schrag, D.P. (1998). A neoproterozoic snowball Earth: *Science, 281*(5381), 1342–1346.
11. Kopp, R.E., Kirschvink, J.L., Hilburn, I.A., and Nash, C.Z. (2005). The Paleoproterozoic snowball Earth: A climate disaster triggered by the evolution of oxygenic photosynthesis. *Proc. Natl. Acad. Sci. U.S.A., 102*(32), 11131–11136.
12. Lean, J., Beer, J., and Bradley, R. (1995). Reconstruction of solar irradiance since 1610: Implications for climate change. *Geophys. Res. Lett., 22*(23), 3195–3198.
13. Levitus, S., Antonov, J.I., Wang, J., Delworth, T.L., Dixon, K.W., and Broccoli, A.J. (2001). Anthropogenic warming of Earth's climate system. *Science, 292*(5515), 267–270.
14. Lindsey, R. (2009). Climate and Earth's energy budget: Feature articles. NASA. Online, http://earthobservatory.nasa.gov, accessed September 2016.
15. North Carolina State University (2013a). Composition of the atmosphere.
16. North Carolina State University (2013b). Composition of the atmosphere: Online, http://climate.ncsu.edu/edu/k12/.AtmComposition, accessed September 2016.
17. Oreskes, N. (2004). The scientific consensus on climate change. *Science, 306*(5702), 1686–1686.
18. Pachauri, R.K., Allen, M.R., Barros, V.R., Broome, J., Cramer, W., Christ, R., Church, J.A., Clarke, L., Dahe, Q., Dasgupta, P.,Dubash, N.K., Edenhofer, O., Elgizouli, I., Field, C.B., et al. (2014). Climate change 2014: Synthesis report. Contribution of Working Groups I, II and III to the Fifth Assessment Report of the Intergovernmental Panel on Climate Change (Pachauri, R.K., and Meyer, L., eds.): IPCC.
19. Santer, B.D., Mears, C., Wentz, F.J., Taylor, K.E., Gleckler, P.J., Wigley, T.M.L., Barnett, T.P., Boyle, J.S., Bru ¨ ggemann, W., Gillett, N.P., Klein, S.A., Meehl, G.A., Nozawa, T., Pierce, D.W., et al. (2007). Identification of human-induced changes in atmospheric moisture content. *Proc. Natl. Acad. Sci. U.S.A., 104*(39), 15248–15253.
20. Schmittner, A. (2019). *Introduction to climate science OER textbook:* Oregon State University.
21. Schopf, J.W., and Klein, C. (1992). Late Proterozoic low-latitude global glaciation: The snowball Earth, in Schopf, J.W., and Klein, C. (eds.), *The Proterozoic biosphere: A multidisciplinary study:* Cambridge University Press, 51–52.
22. Webb, T., and Thompson, W. (1986). Is vegetation in equilibrium with climate? How to interpret late-Quaternary pollen data. *Vegetatio, 67*(2), 75–91.
23. Weissert, H. (2000). Deciphering methane's fingerprint. *Nature, 406*(6794), 356–357.
24. Whitlock, C., and Bartlein, P.J. (1997). Vegetation and climate change in northwest America during the past 125 kyr. *Nature, 388*(6637), 57–61.
25. Wolpert, S. (2009). New NASA temperature maps provide a 'whole new way of seeing the moon'. Online, http://newsroom.ucla.edu/releases/new-nasa-temperature-maps-provide-102070, accessed February 2017.
26. Zachos, J., Pagani, M., Sloan, L., Thomas, E., and Billups, K. (2001). Trends, rhythms, and aberrations in global climate 65 Ma to present. *Science, 292*(5517), 686–693.
27. Zehnder, C., Manoylov, K., Mutiti, S., Mutiti, C., VandeVoort, A., and Bennett, D. (2018). *Introduction to environmental science: 2nd edition OER textbook:* University System of Georgia.

Figure References

Figure 15.1: Composition of the atmosphere. NASA. 2019. Public domain. https://climate.nasa.gov/news/2915/the-atmosphere-getting-a-handle-on-carbon-dioxide/#:~:text=By%20volume%2C%20the%20dry%20air,methane%2C%20nitrous%20oxide%20and%20ozone.

Figure 15.2: Common greenhouse gases. Kindred Grey. 2022. CC BY 4.0. Water molecule 3D by Dbc334, 2006 (Public domain, https://commons.wikimedia.org/wiki/File:Water_molecule_3D.svg). Nitrous-oxide-dimensions-3D-balls by Ben Mills, 2007 (Public domain, https://commons.wikimedia.org/wiki/File:Nitrous-oxide-dimensions-3D-balls.png). Methane-CRC-MW-3D-balls by Ben Mills, 2009 (Public domain, https://en.m.wikipedia.org/wiki/File:Methane-CRC-MW-3D-balls.png). Carbon dioxide 3D ball by Jynto, 2011 (Public domain, https://commons.wikimedia.org/wiki/File:Carbon_dioxide_3D_ball.png).

Figure 15.3: Carbon cycle. United States Geological Survey (USGS). 2022. Public domain. https://www.usgs.gov/media/images/usgs-carbon-cycle

Figure 15.4: Incoming radiation absorbed, scattered, and reflected by atmospheric gases. Robert A. Rohde. 2013. CC BY-SA 3.0. https://commons.wikimedia.org/wiki/File:Solar_spectrum_en.svg

Figure 15.5: Incoming solar radiation filtered by the atmosphere. NASA illustration by Robert Simmon. Astronaut photograph ISS013-E-8948. 2009. Public domain. https://earthobservatory.nasa.gov/features/EnergyBalance/page4.php

Figure 15.6: Some of the thermal infrared energy (heat) radiated from the surface into the atmosphere is trapped by gases in the atmosphere. NASA illustration by Robert Simmon. Photograph by Cyron, 2006 (CC BY-NC 2.0). https://earthobservatory.nasa.gov/features/EnergyBalance/page5.php

Figure 15.7: Contribution to observed climate change from 12 different drivers, as taken from the Summary for Policymakers of the Sixth IPCC Assessment Report. Eric Fisk. 2021. CC BY-SA 4.0. https://en.wikipedia.org/wiki/Climate_change#/media/File:Physical_Drivers_of_climate_change.svg

Figure 15.8: Land-ocean temperature index, 1880 to present, with a base time 1951–1980. NASA. 2010. Public domain. https://commons.wikimedia.org/wiki/File:Global_Temperature_Trends.png

Figure 15.9: Latest CO_2 reading as of September 25, 2024. Scripps Institution of Oceanography at UC San Diego. 2024. Permissions statement. https://keelingcurve.ucsd.edu

Figure 15.10: Keeling curve graph of the carbon dioxide concentration at Mauna Loa Observatory as of September 25, 2024. Scripps Institution of Oceanography at UC San Diego. 2024. Permissions statement. https://keelingcurve.ucsd.edu

Figure 15.11: Decline of Antarctic ice mass from 2002 to 2016. NASA. 2017. Public domain. https://commons.wikimedia.org/wiki/File:ANTARCTICA_MASS_VARIATION_SINCE_2002.png

Figure 15.12: Maximum extent of Laurentide ice sheet. USGS. 2005. Public domain. https://commons.wikimedia.org/wiki/File:Pleistocene_north_ice_map.jpg

Figure 15.13: Global average surface temperature over the past 65 million years. Robert A. Rohde. 2005. CC BY-SA 3.0. https://commons.wikimedia.org/wiki/File:65_Myr_Climate_Change.png

Figure 15.14: The Antarctic Circumpolar Current. Avsa. 2009. CC BY-SA 3.0. https://commons.wikimedia.org/wiki/File:Conveyor_belt.svg

Figure 15.15: A Pliocene–Pleistocene stack of 57 globally distributed benthic **δ**18O records. Used under fair use from A Pliocene-Pleistocene stack of 57 globally distributed benthic **δ**18O records by Lorraine E. Lisiecki, Maureen E. Raymo (https://doi.org/10.1029/2004PA001071).

Figure 15.16: Sediment core from the Greenland continental slope. Hannes Grobe. 2008. CC BY 3.0. https://en.m.wikipedia.org/wiki/File:PS1920-1_0-750_sediment-core_hg.jpg

Figure 15.17: Antarctic temperature changes during the last few glaciations compared to global ice volume. This figure was produced by Robert A. Rohde from publicly available data and is incorporated into the Global Warming Art project. 2012. CC BY-SA 3.0. https://commons.wikimedia.org/wiki/File:Ice_Age_Temperature.png

Figure 15.18: 19-cm-long section of ice core showing 11 annual layers with summer layers (arrowed) sandwiched between darker winter layers. NOAA. 2005. Public domain. https://commons.wikimedia.org/wiki/File:GISP2_1855m_ice_core_layers.png?uselang=en-gb

Figure 15.19: Antarctic ice showing hundreds of tiny trapped air bubbles from the atmosphere thousands of years ago. Atmospheric Research, CSIRO. 2000. CC BY 3.0. https://commons.wikimedia.org/wiki/File:CSIRO_ScienceImage_518_Air_Bubbles_Trapped_in_Ice.jpg

Figure 15.20: Composite carbon dioxide record from last 800,000 years based on ice core data from EPICA Dome C Ice Core. Tomruen. 2011. CC BY-SA 3.0. https://commons.wikimedia.org/w/index.php?curid=16147504

Figure 15.21: Tree rings form every year. Arpingstone. 2005. Public domain. https://commons.wikimedia.org/wiki/File:Tree.ring.arp.jpg

Figure 15.22: Summer temperature anomalies for the past 7,000 years. R.M.Hantemirov. 2010. CC BY 3.0. https://commons.wikimedia.org/wiki/File:Yamal50.gif

Figure 15.23: Scanning electron microscope image of modern pollen with false color added to distinguish plant species. Dartmouth Electron Microscope Facility, Dartmouth College. 2011. Public domain. https://en.wikipedia.org/wiki/File:Misc_pollen_colorized.jpg

Figure 15.24: Total anthropogenic greenhouse gas emissions (gigatonne of CO_2-equivalent per year, $GtCO_2$-eq/yr) from economic sectors in 2010. Kindred Grey. 2022. CC BY 4.0. Data from IPCC, 2014: Climate Change 2014: Synthesis Report. Contribution of Working Groups I, II and III to the Fifth Assessment Report of the Intergovernmental Panel on Climate Change [Core Writing Team, R.K. Pachauri and L.A. Meyer (eds.)]. IPCC, Geneva, Switzerland, 151 pp. https://www.ipcc.ch/site/assets/uploads/2018/05/SYR_AR5_FINAL_full_wcover.pdf

Figure 15.25: Annual global anthropogenic carbon dioxide (CO_2) emissions in gigatonne of CO_2-equivalent per year ($GtCO_2$/yr) from fossil fuel combustion, cement production and flaring, and forestry and other land use (FOLU), 1750–2011. Kindred Grey. 2022. CC BY 4.0. Data from IPCC, 2014: Climate Change 2014: Synthesis Report. Contribution of Working Groups I, II, and III to the Fifth Assessment Report of the Intergovernmental Panel on Climate Change [Core Writing Team, R.K. Pachauri and L.A. Meyer (eds.)]. IPCC, Geneva, Switzerland, 151 pp. https://www.ipcc.ch/site/assets/uploads/2018/05/SYR_AR5_FINAL_full_wcover.pdf

Figure 15.26: Yearly temperature compared to the twentieth-century average from 1850–2023. Dr. Howard Diamond (NOAA ARL). 2024. Public domain. https://www.climate.gov/media/13840

Figure 15.27: An assessment of effective radiative forcing in 2022 using a baseline year of 1750. Piers M. Forster, Christopher J. Smith, Tristram Walsh, William F. Lamb, Robin Lamboll, Mathias Hauser, Aurélien Ribes, Debbie Rosen, Nathan Gillett, Matthew D. Palmer, Joeri Rogelj, Karina von Schuckmann, Sonia I. Seneviratne, Blair Trewin, Xuebin Zhang, Myles Allen, Robbie Andrew, Arlene Birt, Alex Borger, Tim Boyer, Jiddu A. Broersma, Lijing Cheng, Frank Dentener, Pierre Friedlingstein, José M. Gutiérrez, Johannes Gütschow, Bradley Hall, Masayoshi Ishii, Stuart Jenkins, Xin Lan, June-Yi Lee, Colin Morice, Christopher Kadow, John Kennedy, Rachel Killick, Jan C. Minx, Vaishali Naik, Glen P. Peters, Anna Pirani, Julia Pongratz, Carl-Friedrich Schleussner, Sophie Szopa, Peter Thorne, Robert Rohde, Maisa Rojas Corradi, Dominik Schumacher, Russell Vose, Kirsten Zickfeld, Valérie Masson-Delmotte, and Panmao Zhai. 8 June 2023. CC BY-SA 4.0. https://essd.copernicus.org/articles/15/2295/2023/essd-15-2295-2023.pdf

Figure 15.28: Atmospheric CO_2 concentrations by SSP across the twenty-first century (projected by MAGICC7, a simple/reduced complexity climate model). Sfdiversity. 9 February 2020. CC BY-SA 4.0. https://commons.wikimedia.org/wiki/File:Atmospheric_CO%E2%82%82_concentrations_by_SSP_across_the_21st_century.svg

Figure 15.29: Estimates and probabilistic projections of the total population for the world. 2024 United Nations, Department of Economic and Social Affairs (DESA), Population Division. United Nations, DESA, Population Division. World Population Prospects 2024. CC BY 3.0 IGO. http://population.un.org/wpp

Figure 15.30: The 2022 energy flow chart released by Lawrence Livermore National Laboratory. 2022. CC BY-NC-SA 4.0. https://flowcharts.llnl.gov

Figure 15.31: Photograph of solar cell panels in the foreground, wind turbines in the middle ground, and electricity pylons in the background. Kenueone. 2016. Public domain. https://commons.wikimedia.org/wiki/File:Renewable_Energy_on_the_Grid.jpg

Figure 15.32: IAEA experts depart Unit 4 of TEPCO's Fukushima Daiichi Nuclear Power Station on April 17, 2013, as part of a mission to review Japan's plans to decommission the facility. IAEA Imagebank. 2013. CC BY-SA 2.0. https://commons.wikimedia.org/wiki/File:IAEA_Experts_at_Fukushima_%2802813336%29.jpg

Figure 15.33: The BMW i3 is an electric car that was manufactured from 2013 to 2022. TTTNIS. 2014. Public domain. https://commons.wikimedia.org/wiki/File:BMW_i3_01.jpg

Figure 15.34: Plenary session of the COP21 for the adoption of the Paris Accord, United Nations Climate Change Conference (Paris, Le Bourget). UNclimatechange. 2015. CC BY 2.0. https://commons.wikimedia.org/wiki/File:They_did_it!_%2823692333176%29.jpg

Figure 15.35: Lovett School, in north Atlanta, GA, has a rooftop garden with this mechanism for collecting water to use in irrigation. Diane Cordell. 2011. CC BY-NC-ND 2.0. https://www.flickr.com/photos/dmcordell/6179788381

Figure 15.36: Graphic demonstrating the CCS process. Department of Energy and Climate Change. 2013. CC BY-ND 2.0. https://flic.kr/p/icqjsK

Figure Descriptions

Figure 15.1: This figure shows the proportion of atmospheric gases at 78% for nitrogen, 21% for oxygen, 1% for argon, and less than 1% for trace components.

Figure 15.2: Four diagrams showing various greenhouse gas molecules: water vapor consists of a red oxygen atom with two white hydrogen atoms attached on the bottom left and bottom right; nitrous oxide consists of two blue nitrogen atoms and a red oxygen atom connected in a straight line; methane consists of a black carbon atom at the center with four white hydrogen atoms connected to the carbon atom in a pyramidal shape; and carbon dioxide consists of a red oxygen atom, a black carbon atom, and another red oxygen atom connected in a straight line.

Figure 15.3: A diagram depicting the continuous movement and transformation of carbon on Earth. The diagram shows a circular process with labeled arrows and key components: starting with the emission of carbon into the atmosphere, arrows indicates carbon released from volcanoes, fossil fuel emissions from factories, agriculture, fire, transportation, oceans, and animals; arrows show carbon returning to Earth's surface through plants, oceans, and wetlands; an arrow shows consumption of carbon by animals; and arrows show carbon entering the ground in decomposition. There is an asterisked note in the sky that reads Some carbon remains in the atmosphere (not in cycle) and there is another asterisked note in the ground that says "Some carbon remains in the ground (not in cycle).

Figure 15.4: This graph shows the spectrum of solar radiation reaching Earth. The vertical axis show irradiance in Watts per square meter per nanometer increasing upward and the horizontal axis shows wavelength in nanometers increasing toward the right. A smooth and continuous curve shows the irradiance at each wavelength: the curve steeply rises starting at the bottom left of the graph at 0 nm wavelength in a section labeled UV, and the peak of the curve is around 500 nm wavelength and 1.75 irradiance in a section labeled Visible. Then the curve more gradually decreases toward the right in a section labeled Infrared, until it reaches near zero irradiance past 2600 nm wavelength.

Figure 15.5: This figure shows incoming solar radiation, 23% is absorbed in the atmosphere, 29% reflected, and 48% absorbed at the surface after passing through atmosphere.

Figure 15.6: Incoming solar radiation reaching the surface (48% net solar energy) and changing into longwave radiation (25% evaporation, 5% convection, 17% net thermal radiation) that radiates into the atmosphere.

Figure 15.7: Graph with contributions in degrees Celsius along the bottom horizontal axis and a vertical axis based at 0 degrees Celsius. Along the vertical axis are various drivers of climate change, each with a bar to show how much it cools or warms in degrees Celsius, with warming bars colored red and cooling bars colored blue. Starting from the bottom: aviation contrails has a red bar to less than 0.1 degrees and irrigation and albedo has a blue bar to nearly negative 0.1 degrees. The group above those is labeled aerosols which includes the following: black carbon has a red bar to nearly 0.1 degrees, ammonia has a blue bar to less than negative 0.1 degrees, organic carbon has a blue bar to nearly negative 0.1 degrees, sulphur dioxide has a blue bar to nearly negative 0.5 degrees. The group above aerosols is labeled greenhouse gases which includes the following: other gases has a red bar to 0.2 degrees, nitrogen oxides has a blue bar to negative 0.14 degrees, halogenated gases has a red bar to 0.1 degrees, nitrous oxide has a red bar to nearly 0.1 degrees, methane has a red bar to just over 0.5 degrees, and carbon dioxide has a red bar to nearly 0.8 degrees.

Figure 15.8: Graph of temperature anomaly on the vertical axis, from -0.6 to 1.0 degrees C, and time on the horizontal axis, from the year 1880 to 2016. The global annual mean land-ocean temperature is plotted on the graph as a solid black line and a solid red line is the five-year Lowess smoothing. The graph shows that the average mean temperature is rising over time, from -0.2 C temperature anomaly in 1880 to 0.98 C temperature anomaly in 2016 with minor fluctuations within the larger trend.

Figure 15.9: Latest CO_2 reading: 415.91 ppm.

Figure 15.10: Graph showing CO_2 concentration in ppm along the vertical axis, from 310 to 430, and year along the horizontal axis, from 1958 to 2022. The graph shows that the CO_2 concentration is rising over time, from 316 ppm in 1958 to 415.91 ppm in 2022 with minor seasonal fluctuations within each year in the larger trend.

Figure 15.11: Graph showing Antarctica ice mass in gigatons along the vertical axis, from negative 2000 to 0, and time along the horizontal axis, from the years 2002 to 2016. The graph shows that Antarctic ice mass has declined by 2000 gigatons from 2002 to 2016.

Figure 15.12: Map centered over the North Pole, showing the maximum extent of the Laurentide ice sheet. The ice sheet covers Greenland, Canada, the northern United States, northern Europe, and northern Asia.

Figure 15.13: A graph of atmospheric CO_2 levels over time. The vertical axis shows Benthic O-18 in per mil, decreasing upward; the horizontal axis shows the time from 65 to 0 million years ago. During the Cenozoic Era, carbon dioxide levels steadily decreased from a maximum in the Paleocene, causing the climate to gradually cool. By the Pliocene, ice sheets began to form. There are short-term cycles of warming and cooling within the larger glaciation event.

Figure 15.14: Map of bottom of earth showing Antarctic continent and an ocean current circulating clockwise around it.

Figure 15.15: Graph showing the oxygen isotope record for last 5 million years with regular minimum-maximum cycles. More pronounced glacial cycles are in the last 1 million years.

Figure 15.16: Image of 8 black, gray, brown, and tan sediment cores showing clear layering and vertical changes in color and composition.

Figure 15.17: This figure shows three graphs stacked vertically with the same horizontal axis: 450 thousand years ago on the left to present day on the right. The top two graphs are of Ice Age temperature anomalies over the last 450 thousand years to the present and the bottom graph shows changes in global ice volume over the last 450 thousand years to the present. Changes in global ice volume and changes in Antarctic temperature are highly correlated. Horizontal lines across each graph indicate modern temperature anomaly of 0 and ice volume of Low. The Antarctic temperature records indicate that the present interglacial is relatively cool compared to previous interglacials.

Figure 15.18: Photo of ice core with visible annual layers; 11 arrows point to lighter- colored summer layers sandwiched between darker winter layers.

Figure 15.19: A thin section of Antarctic ice showing hundreds of tiny trapped air bubbles. The ice is illuminated with polarized light, producing a colorful effect.

Figure 15.20: Graph of composite carbon dioxide record: the horizontal axis spans 800,000 years ago on the left to 0 years ago (present day) on the right and the vertical axis spans 170 at the bottom to 310 ppm at the top. CO_2 concentrations increase to around 290 ppm during warm periods and decrease to around 190 ppm during glacial periods with approximately 9 regular cycles throughout the graph.

Figure 15.21: Shows a tree cut in cross-section with tree rings. Each ring form in one year.

Figure 15.22: Graph of tree ring data: the horizontal axis is labeled Years and spans 5000 BC to 2000 AD; the vertical axis is labeled Anom-

alies, degrees C, and spans -1 degree Celsius to positive 2 degrees Celsius. Highs and lows fluctuate cyclically throughout time around the 0 degrees celsius line and the last few hundred years are slightly higher temperatures than earlier highs.

Figure 15.23: Scanning electron microscope image of pollen from a variety of common plants: sunflower are small spiky sphericals, colorized pink; morning glory are big sphericals with hexagonal cavities, colorized mint green; hollyhock are big spiky sphericals, colorized yellow; lily are bean shaped, colorized dark green; primrose are tripod shaped, colorized red; and castor bean are small smooth sphericals, colorized light green. The image is magnified some x500, so one bean shaped grain in the bottom left corner is about 50 μm long.

Figure 15.24: Pie chart shows greenhouse gas emissions by economic sectors. Total: 49 Gt CO_2-eq in 2010. 25% indirect CO_2 emissions: energy (1.4%), industry (11%), transport (0.3%), buildings (12%), AFOLU (0.87%). These make up electricity and heat production. 75% indirect CO_2 emissions: industry (21%), transport (14%), buildings (6.4%), AFOLU (24%).

Figure 15.25: Graph of global anthropogenic CO_2 emissions: the vertical axis is labeled $GtCO_2$ per year and spans 0 to 40; the horizontal axis is labeled Year and spans 1840 to 2011. The graph is color-coded according to fossil fuel emissions in light gray and forestry and other land use in dark gray. Carbon emissions from fossil fuel combustion increase notably around 1950 and continue to increase consistently until the graph ends in 2011, while forestry and other land use increase around 1950, remain relatively consistent until 2000, and then decrease. To the right of the main graph is a graphic labeled Cumulative CO_2 emissions, with two bar graphs labeled 1750-1970 and 1750-2011 and a shared horizontal axis labeled $GtCO_2$ that spans 0 to 2000. The bar graph for 1750-2011 reaches over 2000 $GtCO_2$ while the bar graph for 1750 to 1970 only reaches near 1000 $GtCO_2$. Like with the main graph, the emissions due to fossil fuels are much higher than the emissions due to forestry and other land use in the years 1750-2011.

Figure 15.26: Graph with the years 1850 to 2023 on the horizontal axis and two vertical axes. The left vertical axis is difference from twentieth century average in degrees Celsius, going from negative 0.6 to 1.2 upward, and the right vertical axis is global atmospheric carbon dioxide in parts per million, going from 280 to 410 upward. There is a horizontal line at 0 degrees Celsius to show the long-term average. A gray curve goes from the lower left to upper right, slowly traveling upward from the year 1850 to 1960 and then getting steeper upward from 1960 to 2023 in an exponential shape. There is a vertical bar for each year colored blue for cooler than average and red for warmer than average. From 1850 to 1939, nearly all of the bars are blue and below the average with the exception of years 1878 and 1879. From 1978 to 2023, all of the bars are red and above the average, increasing higher and higher in more recent years. The period between 1940 and 1977 has a mix of blue and red bars.

Figure 15.27: A bar chart showing effective radiative forcing in Watts per square meter on the horizontal axis from -1.6 on the left to 3.8 on the right. The nine plotted horizontal bars are color-coded so that red represents positive radiative forcing and blue represents negative radiative forcing. From bottom to top, the bars plotted are: Solar from 0 to 0.1 Watts per square meter, Total anthropogenic from 0 to 3 Watts per square meter, Aerosols from 0 to -1 Watts per square meter, Contrails & aviation-induced cirrus from 0 to 0.1 Watts per square meter, Albedo from -0.1 to 0.05 Watts per square meter, Stratospheric water vapor from 0 to 0.05 Watts per square meter, Ozone from 0 to 0.3 Watts per square meter, Other well-mixed greenhouse gases from 0 to 1.1 Watts per square meter, and Carbon dioxide from 0 to 2.2 Watts per square meter.

Figure 15.28: A graph showing CO_2 concentration in ppm on the vertical axis from 300 at the bottom to 1200 at the top and the Year on the horizontal axis from 2000 on the left to 2100 on the right. There are five colored lines on the graph showing various projection scenarios. In order from the flattest line that shows very little long-term change in CO_2 concentration to the year 2100 to the steepest line that shows the greatest long-term change in CO_2 concentration to the year 2100: blue represents SSP 1-1.9 and ends at just under 400 ppm in the year 2100, navy blue represents SSP 1-2.6 and ends at 450 ppm in the year 2100, yellow represents SSP 2-4.5 and ends at 600 ppm in the year 2100, red represents SSP 3-7.0 and ends at 870 ppm in the year 2100, and maroon represents SSP 5-8.5 and ends at 1140 ppm in the year 2100.

Figure 15.29: Graph with the years 1950 to 2100 along the horizontal axis and population in bilions from less than 3 to over 14 along the vertical axis. A black line goes from the bottom left under 3 billion people in the year 1950 toward the upper right and splits into multiple colored dashed curves at 8 billion people in the year 2024. There are two blue curved dashed lines that show the extreme projections, one continues the increase to over 14 billion people in the year 2100 and the other curves downward to less than 7 billion people in 2100. There are red dashed lines between the two blue dashed lines that show more moderate predictions, filled in with yellow.

Figure 15.30: A colorful flow chart that shows the various sources of energy production on the left, flowing in multiple pathways toward the right that split and recombine to end at two possible categories, rejected energy or energy services. The energy sources on the left are solar, nuclear, hydro, wind, geothermal, natural gas, coal, biomass, and petroleum, scaled in size according to how much energy they provide in the US. The two categories on the right are scaled in size with rejected energy being double the size of energy services.

Figure 15.31: Photograph of solar cell panels in the foreground, a much larger wind turbine in the middle ground, and electricity pylons in the more distant background.

Figure 15.32: Photograph of five people walking toward the camera, each dressed in white plastic-looking suits, wearing yellow hard hats, face masks, and black rubber boots. There is a partially destroyed white concrete and red brick building in the background.

Figure 15.33: Photo of a two-door car with a silver body and black hood.

Figure 15.34: Photo of five people dressed in business wear holding each others' hands in the air and smiling. Behind them is a sign that says "Nations Unies."

Figure 15.35: Photo of three blue-green buckets on vertical stilts of various heights with the tallest bucket directly below a roof drain. The buckets have spouts leading into the next smaller bucket and the smallest bucket spout leads into a cement irrigation structure.

Figure 15.36: Block diagram showing land leading to a body of water along the surface with multiple layers of earth below. Inland is a gray structure labeled power station that has two red lines that combine into a green dot labeled multi-junction. A single green line travels from the dot toward the shoreline and runs into a gray square labeled pumping station. The green line continues from the pumping station into the open body of water to a gray water platform titled storage in porous rock. A vertical blue line is drawn from the water platform down through three earth layers, ending a tan dotted layer representing porous rock.

16. ENERGY AND MINERAL RESOURCES

Learning Objectives

By the end of this chapter, students should be able to:

- Describe how a renewable resource is different from a nonrenewable resource.
- Compare the pros and cons of extracting and using fossil fuels and conventional and unconventional petroleum sources.
- Describe how metallic minerals are formed and extracted.
- Understand how society uses nonmetallic mineral resources.
- Compare the pros and cons of renewable energy sources, including solar, wind, hydroelectric, geothermal, and biomass.

Figure 16.1: A Mode 1 Oldowan tool used for chopping. Figure description available at the end of the chapter.

This text has previously discussed geology's pioneers such as scientists James Hutton and Charles Lyell, but the first real "geologists" were the hominids who picked up stones and began the Stone Age. Maybe stones were first used as curiosity pieces, maybe as weapons, but ultimately, they were used as tools. This was the Paleolithic Period, the beginning of geologic study, and it dates back 2.6 million years to East Africa.

In modern times, geologic knowledge is important for locating economically valuable materials for society's use. In fact, all things we use come from only three sources; they are farmed, hunted or fished, or mined. At the turn of the twentieth century, speculation was rampant that food supplies would not keep pace with world demand, suggesting the need to develop artificial fertilizers.

Fertilizer ingredients have multiple sources. Nitrogen is processed from the atmosphere using the Haber process for the manufacture of ammonia from atmospheric nitrogen and hydrogen; potassium comes from the hydrosphere, such as lakes or ocean evaporation; and phosphorus is mined from the lithosphere in minerals like apatite from phosphorite, which is found in Florida, North Carolina, Idaho, Utah, and around the world. Thus, without the mining and processing of natural materials, modern civilization would not exist. Indeed, geologists are essential in this process.

Figure 16.2: A container of phosphate from the Aurora mine in North Carolina. Figure description available at the end of the chapter.

Resources generally come in two major categories: renewable and nonrenewable. Renewable resources can be reused over and over, or their availability can be replicated over a short human life span; nonrenewable resources cannot.

16.1 Nonrenewable Resources

Nonrenewable resources cannot be replenished at a sustainable rate. They are finite within human time frames. Many nonrenewable resources come from planetary, tectonic, or long-term biologic processes and include materials such as gold, lead, copper, diamonds, marble, sand, natural gas, oil, and coal. Most nonrenewable resources include specific concentrated elements listed on the periodic table; some are compounds of those elements. For example, if society needs iron (Fe) sources, then an exploration geologist will search for iron-rich deposits that can be economically extracted. Nonrenewable resources may be abandoned when other materials become cheaper or serve a better purpose. For example, coal is abundantly available in England and other nations, but because oil and natural gas are available at a lower cost and lower environmental impact, coal use has decreased. Economic competition among nonrenewable resources is shifting use away from coal in many developed countries.

Figure 16.3: Natural octahedral shape of diamond. Figure description available at the end of the chapter.

16.1.1 Mining

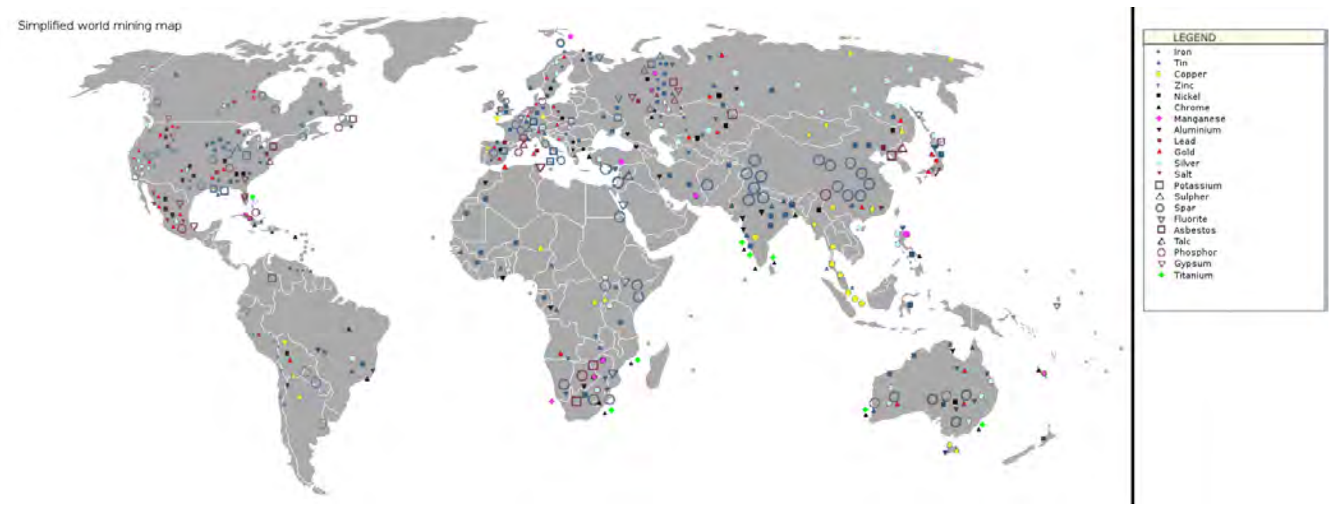

Figure 16.4: Map of world mining areas. Figure description available at the end of the chapter.

Mining is defined as extracting valuable materials from the Earth for society's use. Usually, these include solid materials such as gold, iron, coal, diamond, sand, and gravel, but materials can also include fluid resources such as oil and natural gas. Modern mining has a long relationship with modern society. The oldest **mine** dates back 40,000 years to the Lion Cavern in Swaziland, where there is evidence of concentrated digging into the Earth for hematite, an important iron ore used as red dye. Resources extracted by mining are generally considered to be nonrenewable.

16.1.2 Ore

Earth's materials include the periodic table elements. However, it is rare that these elements are concentrated to the point where it is profitable to extract and process the material into usable products. Any place where a valuable material is concentrated is a geologic and geochemical **anomaly**. A body of material from which one or more valuable substances can be mined at a profit is called an **ore** deposit. Typically, the term ore is used for only metal-bearing minerals, but it can be applied to valuable nonrenewable resource concentrations such as fossil fuels, building stones, and other nonmetal deposits, even groundwater. If a metal-bearing resource is not profitable to mine, it is referred to as a mineral deposit. The term natural resource is more common than the term ore for non-metal-bearing materials.

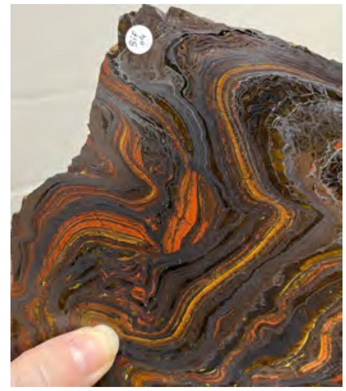

Figure 16.5: Banded-iron formations are an important ore of iron (Fe). Figure description available at the end of the chapter.

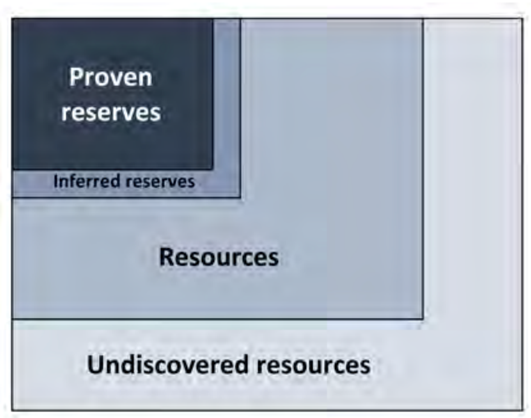

Figure 16.6: Diagram illustrating the relative abundance of proven reserves, inferred reserves, resources, and undiscovered resources. Figure description available at the end of the chapter.

It is implicit that the technology to mine is available, economic conditions are suitable, and political, social, and environmental considerations are satisfied in order to classify a natural resource deposit as ore. Depending on the substance, it can be concentrated in a narrow vein or distributed over a large area as a low-concentration ore. Some materials are mined directly from bodies of water (e.g., sylvite for potassium; water through desalination) and the atmosphere (e.g., nitrogen for fertilizers). These differences lead to various methods of mining and differences in terminology depending on the certainty. **Ore mineral resource** is used to describe an indication of ore that is potentially extractable, and the term **ore mineral reserve** is used for a well-defined (proven), profitable amount of extractable ore.

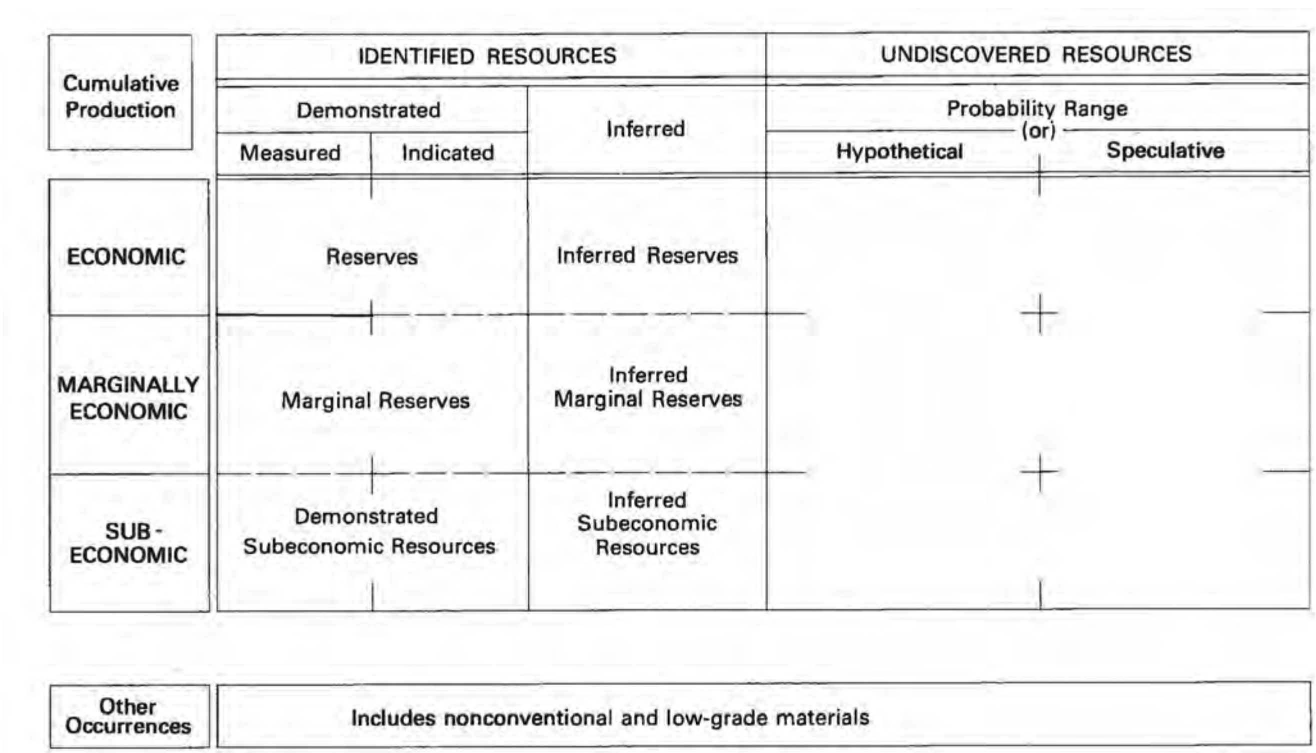

Figure 16.7: McKelvey diagram showing different definitions for different degrees of concentration and understanding of mineral deposits. Figure description available at the end of the chapter.

16.1.3 Mining Techniques

The mining style is determined by technology, social license, and economics. It is in the best interest of the company extracting the resources to do so in a cost-effective way. Fluid resources, such as oil and gas, are extracted by drilling wells and pumping. Over the years, drilling has evolved into a complex discipline in which directional drilling can produce multiple bifurcations and curves originating from a single drill collar at the surface. Using geophysical tools like seismic imaging, geologists can pinpoint resources and extract efficiently.

Solid resources are extracted by two principal methods of which there are many variants. **Surface mining** is used to remove material from the outermost part of the Earth. Underground mining accesses deep pockets of a resource through tunnels and shafts.

Open-pit mining is a type of surface mining that requires careful study of the ore body through surface mapping and drilling exploratory cores. The pit is progressively deepened through additional mining cuts to extract the ore. Typically, the pit's walls are as steep as can be safely managed. Once the pit is deepened, widening the top is very expensive. A steep wall is thus an engineering balance between efficient and profitable mining (from the company's point of view) and mass wasting (the angle of repose, from a safety point of view) so that there is less waste to remove. The waste is called nonvaluable rock or overburden, and moving it is costly. Occasionally, landslides do occur, such as the very large landslide in the Kennecott Bingham Canyon mine, Utah, in 2013. These events are costly and dangerous. The job of engineering geologists is to carefully monitor the mine; when company management heeds their warnings, there is ample time and action to avoid or prepare for any slide.

Figure 16.8: Bingham Canyon Mine, Utah. This open-pit mine is the largest manmade removal of rock in the world. Figure description available at the end of the chapter.

Figure 16.9: A surface coal mine in Wyoming. Figure description available at the end of the chapter.

Strip mining and **mountaintop mining** are surface mining techniques that are used to mine resources that cover large areas, especially layered resources such as coal. Strip mining uses large machines to remove layers of soil and rock, known as overburden, to expose the resource just below the surface. In mountaintop removal mining, an entire mountaintop is removed to access the ore below. After the mining is finished, the disturbed area can be re-covered with topsoil, and the area is replanted. However, the topography of the mountain is permanently altered. Surface mining can cause severe negative environmental impacts due to the large surface footprint that's disturbed. It has been known to destroy natural communities over large areas, trigger erosion, and pollute water, threatening the health and safety of nearby communities.

Figure 16.10: Underground mining of oil shale in Estonia. Figure description available at the end of the chapter.

Underground mining is a method often used to mine higher-grade, more localized, or very concentrated resources. In some examples, geologists mine some underground ore minerals by introducing chemical agents, which dissolve the target mineral. Then, they bring the solution to the surface, where precipitation extracts the material. But more often, a mining shaft tunnel or a large network of these shafts and tunnels is dug to access the material. The decision to mine underground or from Earth's surface is dictated by the ore deposit's concentration, depth, geometry, land-use policies, economics, surrounding rock strength, and physical access to the ore. For example, using surface mining techniques for deeper deposits might require removing too much material, the necessary method may be too dangerous or impractical, removing the entire overburden may be too expensive, or the mining footprint would be too large. These factors may prevent geologists from surface mining materials and cause a project to be mined underground. The mining method and its feasibility depends on the commodity's price and the cost of the technology needed to remove it and deliver it to market. Thus, mines and the towns that support them come and go as the commodity price varies. Conversely, technological advances and market demands may reopen mines and revive ghost towns.

There are also significant health effects and risks to miners. Traditional underground mining is risky to mine workers due to the risk of entrapment or death. Twenty-nine miners died on April 5, 2010, in an explosion at the Upper Big Branch coal mine in West Virginia, contributing to an uptick in mining-related deaths in the US between 2009 and 2010. In other countries with fewer safety regulations, accidents occur more frequently. In October 2022, for example, 41 were killed in a Turkish mine explosion. And in the same country just eight years prior, the Soma mine disaster took place on May 13, 2014, in which 301 people died. There is also risk of getting black lung disease (pneumoconiosis) in underground mining. This lung disease is caused by inhaling coal dust over a long time. It causes coughing and shortness of breath. If exposure is stopped, the outcome is good. However, the complicated form may cause shortness of breath that worsens.

16.1.4 Concentrating and Refining

Figure 16.11: A phosphate smelting operation in Alabama, 1942. Figure description available at the end of the chapter.

All ore minerals occur mixed with less desirable components called **gangue**. The process of physically separating gangue minerals from ore-bearing minerals is called concentrating. Separating a desired element from a host mineral by chemical means, including heating, is called **smelting**. Finally, taking a metal such as copper and removing other trace metals such as gold or silver is done through the refining process. Typically, **refining** is done one of three ways: (1) Materials can either be mechanically separated and processed based on the ore mineral's unique physical properties, such as recovering placer gold based on its high density; (2) Materials can be heated to chemically separate desired components, such as refining crude oil into gasoline; and (3) Materials can be smelted, in which controlled chemical reactions unbind metals from the minerals in which they are contained, such as when copper is taken out of chalcopyrite ($CuFeS_2$). Mining, concentrating, smelting, and refining processes require enormous energy. Continual advances in metallurgy and mining practice strive to develop more energy-efficient and environmentally benign processes and practices.

Take this quiz to check your comprehension of this section.

Access the quiz for Section 16.1 by scanning the QR code.

16.2 Fossil Fuels

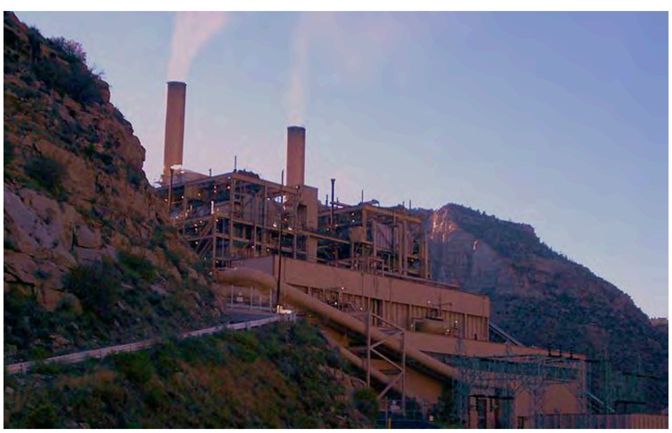

Figure 16.12: Coal power plant in Helper, Utah. Figure description available at the end of the chapter.

Fossil fuels are extractable sources of stored energy that were created by ancient ecosystems. The natural resources that typically fall under this category are coal, oil, and natural gas. These resources were originally formed via photosynthesis by living organisms such as plants, phytoplankton, algae, and cyanobacteria. This energy is actually fossil solar energy, since the Sun's ancient energy was converted by ancient organisms into tissues that preserved the **chemical energy** within the fossil fuel. Of course, as the energy is used, carbon enters the atmosphere as CO_2—just like photosynthetic respiration today—causing climate consequences (see Chapter 15). Today, humanity uses fossil fuels for most of the world's energy.

Converting solar energy by living organisms into hydrocarbon fossil fuels is a complex process. As organisms die, they decompose slowly, usually due to being buried rapidly, and the chemical energy stored within the organisms' tissues is buried within surrounding geologic materials. All fossil fuels contain carbon that was produced in an ancient environment. In environments rich with organic matter, such as swamps, coral reefs, and planktonic blooms, there is a higher potential for fossil fuels to accumulate. Indeed, there is some evidence that over geologic time, organic hydrocarbon fossil fuel material was highly produced globally. Lack of oxygen and moderate temperatures in the environment seem to help preserve these organic substances. The heat and pressure applied to organic material after it is buried contribute to transforming it into higher-quality materials, such as brown coal to anthracite and oil to gas. Heat and pressure can also cause mobile materials to migrate to conditions suitable for extraction.

Figure 16.13: Modern coral reefs and other highly productive shallow marine environments are thought to be the sources of most petroleum resources. Figure description available at the end of the chapter.

16.2.1 Oil and Gas

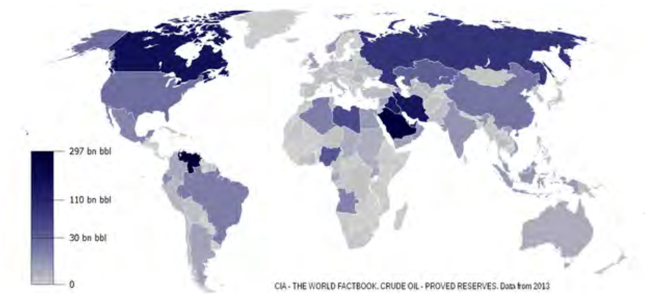

Figure 16.14: World oil reserves in 2013. Scale in billions of barrels. Figure description available at the end of the chapter.

Petroleum is principally derived from organic-rich shallow marine sedimentary deposits where the remains of microorganisms like plankton accumulated in fine-grained sediments. Petroleum's liquid component is called oil, and its gas component is called natural gas, which is mostly made up of methane (CH_4). As rocks such as shale, mudstone, or limestone lithify, the increasing pressure and temperature cause the oil and gas to be squeezed out and migrate from the source rock to a different rock unit higher in the rock column. Similar to the discussion of good aquifers in Chapter 11, if that rock is a sandstone, limestone, or other porous and permeable rock, and if it is involved in a suitable stratigraphic or structural trapping process, then that rock can act as an oil and gas reservoir.

A trap is a combination of a subsurface geologic structure, a porous and permeable rock, and an impervious layer that helps block oil and gas from moving further, which concentrates it for humans to extract later. A trap develops due to many different geologic situations. Examples include an anticline or domal structure, an impermeable salt dome, or a fault-bounded stratigraphic block, which is porous rock next to nonporous rock. The different traps have one thing in common: they pool fluid fossil fuels into a configuration in which extracting it is more likely to be profitable. The presence of oil or gas in strata outside of a trap renders it less viable to extract.

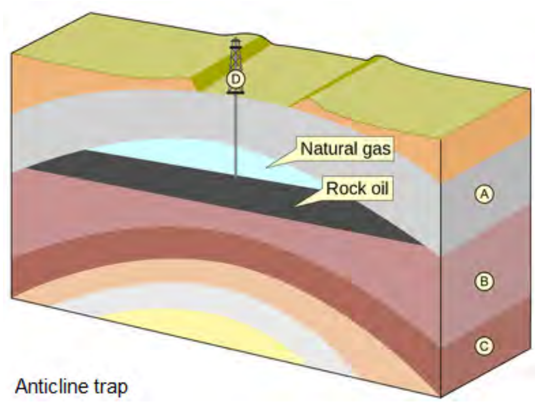

Figure 16.15: Examples of different forms of hydrocarbon traps in the core region of anticlines. Figure description available at the end of the chapter.

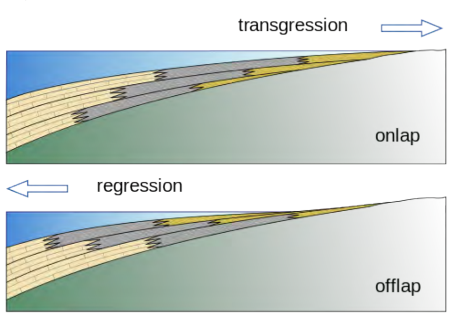

Figure 16.16: The rising sea levels of transgressions create onlapping sediments, and regressions create offlapping. Figure description available at the end of the chapter.

Sequence stratigraphy is a branch of geology that studies sedimentary facies both horizontally and vertically and is devoted to understanding how sea level changes create organic-rich shallow marine muds, carbonates, and sands in areas that are close to each other. For example, shoreline environments may have beaches, lagoons, reefs, nearshore and offshore deposits, all next to each other. Beach sand, lagoonal and nearshore muds, and coral reef layers accumulate into sediments that include sandstones—good reservoir rocks— next to mudstones and then limestones, both of which are potential source rocks. As sea level either rises or falls, the shoreline's location changes, and the sand, mud, and reef locations shift with it (see the figure). This places oil- and gas-producing rocks, such as mudstones and limestones, next to oil and gas reservoirs, such as sandstones and some limestones. Understanding how the lithology and the facies/stratigraphic relationships interplay is very important in finding new petroleum resources. Using sequence stratigraphy as a model allows geologists to predict favorable locations of the source rock and reservoir.

16.2.2 Tar Sands

Figure 16.17: Tar sandstone from the Miocene Monterey Formation of California. Figure description available at the end of the chapter.

Conventional oil and gas, which are pumped from a reservoir, are not the only way to obtain hydrocarbons. There are a few fuel sources known as unconventional petroleum sources. However, they are becoming more important as conventional sources become scarce. **Tar sands**, or oil sands, are sandstones that contain petroleum products that are highly viscous, like tar, and thus cannot be drilled and pumped out of the ground readily like conventional oil. This unconventional fossil fuel is bitumen, which can be pumped as a fluid only at very low recovery rates and only when heated or mixed with solvents. Therefore, using steam and solvent injections or directly mining tar sands to process later are ways to extract the tar from the sands. Alberta, Canada, is known to have the largest tar sand reserves in the world. As with ores, an energy resource becomes uneconomic if the total extraction and processing costs exceed the extracted material's sales revenue. Environmental costs may also contribute to a resource becoming uneconomic.

16.2.3 Oil Shale

Oil shale, or tight oil, is a fine-grained sedimentary rock that has significant petroleum or natural gas quantities locked tightly in the sediment. Shale has high porosity but very low permeability and is a common fossil fuel source rock. To extract the oil directly from the shale, the material has to be mined and heated, which, like with tar sands, is expensive and typically has a negative environmental impact.

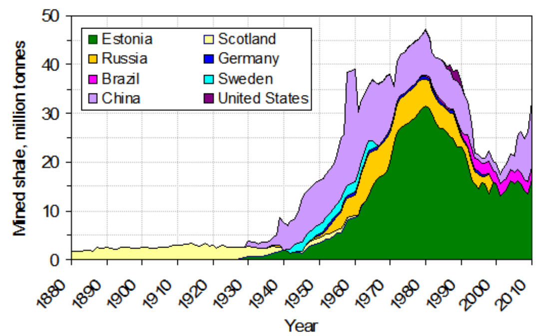

Figure 16.18: Global production of oil shale, 1880-2010. Figure description available at the end of the chapter.

16.2.4 Fracking

Another process used to extract the oil and gas from shale and other unconventional tight resources is called **hydraulic** fracturing, better known as fracking. In this method, high-pressure water, sand grains, and added chemicals are injected and pumped underground. The high pressure creates and holds open fractures in the rocks, which help release the hard-to-access mostly natural gas fluids. Fracking is more useful in tighter sediments, especially shale, which has a high porosity to store the hydrocarbons but low permeability to allow transmission of the hydrocarbons. Fracking has become controversial because its methods contaminate groundwater and induce seismic activity. This has created much controversy centered around public concerns, political concerns, and energy value.

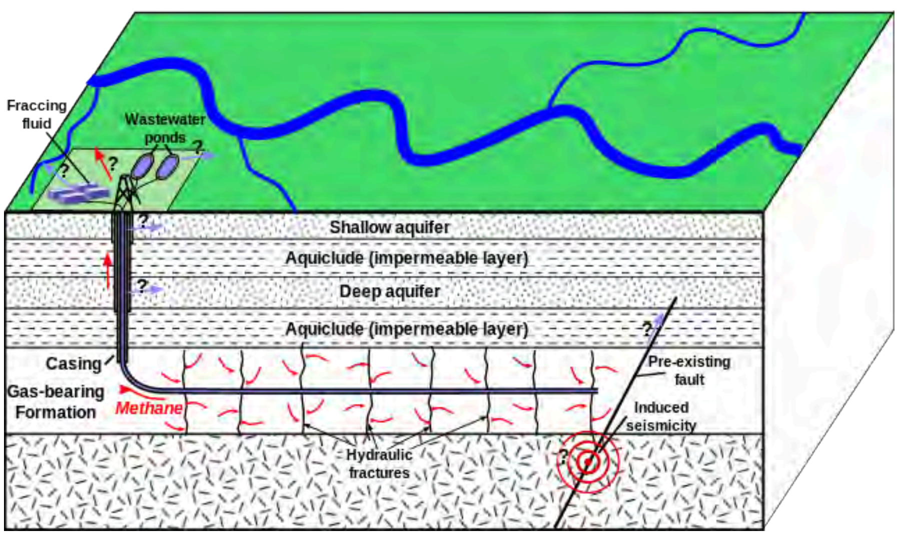

Figure 16.19: Schematic diagram of fracking. Figure description available at the end of the chapter.

16.2.5 Coal

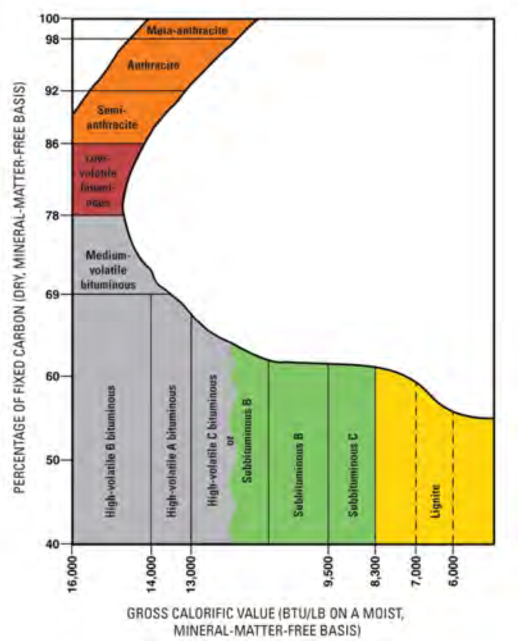

Figure 16.20: USGS diagram of different coal rankings. Figure description available at the end of the chapter.

Coal comes from fossilized swamps, though some older coal deposits that predate terrestrial plants are presumed to come from algal buildups. Coal is chiefly carbon, hydrogen, nitrogen, sulfur, and oxygen, with minor amounts of other elements. As plant material is incorporated into sediments, heat and pressure cause several changes that concentrate the fixed carbon, which is the coal's combustible portion. So, the more heat and pressure that coal undergoes, the greater its carbon concentration and fuel value and the more desirable its coal.

This is the general sequence of a swamp progressing through the various stages of coal formation and becoming more concentrated in carbon: Swamp → Peat → Lignite → Sub-bituminous → Bituminous → Anthracite → Graphite. As swamp materials collect on the swamp floor and are buried under accumulating materials, they first turn to peat.

Figure 16.21: Peat (also known as turf) consists of partially decayed organic matter. The Irish have long mined peat to be burned as fuel, though this practice is now discouraged for environmental reasons. Figure description available at the end of the chapter.

Peat itself is an economic fuel in some locations like the British Isles and Scandinavia. As lithification occurs, peat turns to lignite. With increasing heat and pressure, lignite turns to sub-bituminous coal, bituminous coal, and then, in a process like]metamorphism, anthracite. Anthracite is the highest metamorphic grade and most desirable coal since it provides the highest energy output. With even more heat and pressure driving out all the volatiles and leaving pure carbon, anthracite can become graphite.

Figure 16.22: Anthracite coal, the highest grade of coal. Figure description available at the end of the chapter.

Humans have used coal for at least 6,000 years, mainly as a fuel source. Coal resources in Wales are often cited as a primary reason for Britain's rise, and later, for the United States' rise during the Industrial Revolution. According to the US Energy Information Administration, US coal production has decreased due to competing energy sources' cheaper prices and due to society recognizing its negative environmental impacts, including increased very fine-grained particulate matter as an air pollutant, greenhouse gases, acid rain, and heavy metal pollution. Seen from this perspective, the coal industry as a source of fossil energy is unlikely to be revived.

As the world transitions away from fossil fuels like coal and as manufacturing seeks materials that are stronger, more flexible, and lighter than steel, including carbon fiber, for many applications, current research is exploring coal as a source of this carbon.

Take this quiz to check your comprehension of this section.

Access the quiz for Section 16.2 by scanning the QR code.

16.3 Mineral Resources

Mineral resources, while principally nonrenewable, are generally placed in two main categories: metallic, which contain metals, and nonmetallic, which contain other useful materials. Most mining has been traditionally focused on extracting metallic minerals. Human society has advanced significantly because we've developed the knowledge and technologies to yield metal from the Earth. This knowledge has allowed humans to build the machines, buildings, and monetary systems that dominate our world today. Locating and recovering these metals has been a key facet of geologic study since its inception. Every element across the periodic table has specific applications in human civilization. Metallic mineral mining is the source of many of these elements.

Figure 16.23: Gold-bearing quartz vein from California. Figure description available at the end of the chapter.

16.3.1 Types of Metallic Mineral Deposits

The various ways in which minerals and their associated elements concentrate to form ore deposits are too complex and numerous to fully review in this text. However, entire careers are built around them. In the following section, we describe some of the more common deposit types along with their associated elemental concentrations and world class occurrences.

Magmatic Processes

When a magmatic body crystallizes and differentiates (see Chapter 4), it can cause certain minerals and elements to concentrate. **Layered intrusions**, typically ultramafic to mafic, can host deposits that contain copper, nickel, platinum, palladium, rhodium, and chromium. The Stillwater Complex in Montana is an example of economic quantities of layered mafic intrusion. Associated deposit types can contain chromium or titanium-vanadium. The largest magmatic deposits in the world are the chromite deposits in the Bushveld Igneous Complex in South Africa. These rocks have an areal extent larger than the state of Utah. The chromite occurs in layers that resemble sedimentary layers, except these layers occur within a crystallizing magma chamber.

Figure 16.24: Layered intrusion of dark chromium-bearing minerals, Bushveld Complex, South Africa. Figure description available at the end of the chapter.

Figure 16.25: This pegmatite contains lithium-rich green elbaite (a tourmaline) and purple lepidolite (a mica). Figure description available at the end of the chapter.

Water and other volatiles that are not incorporated into mineral crystals when a magma crystallizes can become concentrated around the crystallizing magma's margins. Ions in these hot fluids are very mobile and can form exceptionally large crystals. Once crystallized, these large crystal masses are then called pegmatites. They form from magma fluids that are expelled from the solidifying magma when nearly the entire magma body has crystallized. In addition to minerals that are predominant in the main igneous mass, such as quartz, feldspar, and mica, pegmatite bodies may also have very large crystals of unusual minerals that contain rare elements like beryllium, lithium, tantalum, niobium, and tin, as well as native elements like gold. Such pegmatites are ores of these metals.

An unusual magmatic process is a **kimberlite** pipe, which is a volcanic conduit that transports ultramafic magma from within the mantle to the surface. Diamonds, which are formed at great temperatures and pressures of depth, are transported by kimberlite pipes to locations where they can be mined. The process that created these kimberlite ultramafic rocks is no longer common on Earth. Most known deposits are from the Archean Eon.

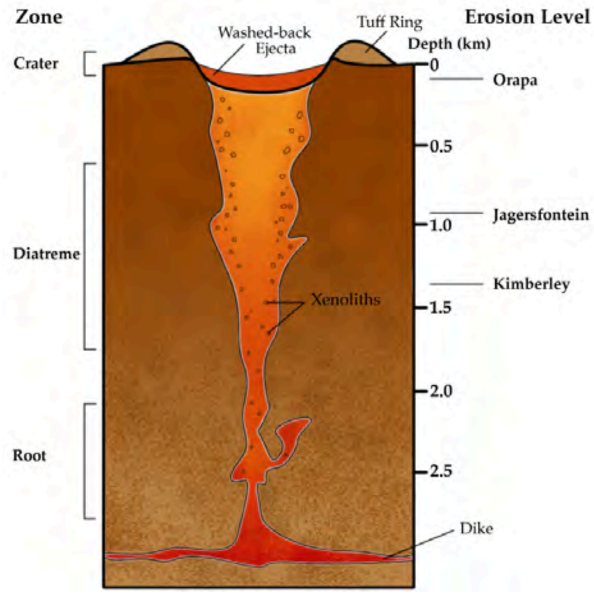

Figure 16.26: Schematic diagram of a kimberlite pipe. [Figure description available at the end of the chapter](#).

Hydrothermal Processes

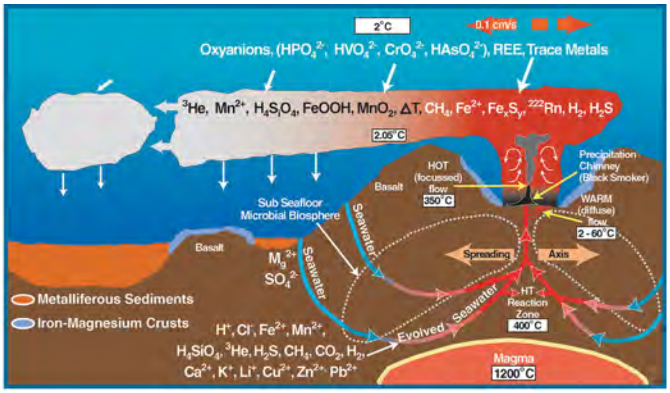

Figure 16.27: The complex chemistry around mid-ocean ridges. [Figure description available at the end of the chapter](#).

Fluids rising from crystallizing magmatic bodies or that are heated by the geothermal gradient cause many geochemical reactions that form various mineral deposits. The most active hydrothermal process today produces **volcanogenic massive sulfide** (VMS) deposits, which form from black smoker hydrothermal chimney activity near mid-ocean ridges all over the world. They commonly contain copper, zinc, lead, gold, and silver when found at the surface. Evidence from around 7000 BCE in a period known as the Chalcolithic shows copper was among the earliest metals smelted by humans as means of obtaining higher temperatures. The largest of these VMS deposits occur in Precambrian Period rocks. The Jerome deposit in central Arizona is a good example.

Another deposit type that draws on magma-heated water is a **porphyry** deposit. This is not to be confused with the porphyritic igneous texture, although the name is derived from the porphyritic texture that is nearly always present in the igneous rocks associated with a porphyry deposit. Several types of porphyry deposits exist, such as porphyry copper, porphyry molybdenum, and porphyry tin. These deposits contain low-grade disseminated ore minerals closely associated with intermediate and felsic intrusive rocks that are present over a very large area. Porphyry deposits are typically the largest mines on Earth. One of the largest, richest, and possibly best-studied mine in the world is Utah's Kennecott Bingham Canyon Mine. It's an open-pit mine, which, for over 100 years, has produced several elements, including copper, gold, molybdenum, and silver. Underground carbonate replacement deposits produce lead, zinc, gold, silver, and copper. In the mine's past, the open pit predominately produced copper and gold from chalcopyrite and bornite. Gold only occurs in minor quantities in the copper-bearing minerals, but because the Kennecott Bingham Canyon Mine produces on such a large scale, it is one of the largest gold mines in the US. In the future, this mine may produce more copper and molybdenum (molybdenite) from deeper underground mines.

Figure 16.28: The Morenci porphyry is oxidized toward its top (as seen in red rocks in the wall of the mine), creating supergene enrichment. [Figure description available at the end of the chapter](#).

Most porphyry copper deposits owe their high metal content and hence their economic value to weathering processes called **supergene enrichment**, which occurs when the deposit is uplifted, eroded, and exposed to oxidation. This process occurred millions of years after the initial igneous intrusion and hydrothermal expulsion ends. When the deposit's upper pyrite-rich portion is exposed to rain, the pyrite in the oxidizing zone creates an extremely acid condition that dissolves copper out of copper minerals, such as chalcopyrite, and converts the chalcopyrite to iron oxides, such as hematite or goethite. The copper minerals are carried downward in water until they arrive at the groundwater table and an environment where the primary copper minerals are converted into secondary higher-copper content minerals. Chalcopyrite (35% Cu) is converted to bornite (63% Cu) and ultimately chalcocite (80% Cu). Without this enriched zone, which is two-to-five times higher in copper content than the main deposit, most porphyry copper deposits would not be economic to mine.

If limestone or other calcareous sedimentary rocks are near the magmatic body, then another type of ore deposit called a **skarn** deposit forms. These metamorphic rocks form as magma-derived, highly saline metalliferous fluids react with carbonate rocks to create calcium-magnesium-silicate minerals like pyroxene, amphibole, and garnet, as well as high-grade iron, copper, zinc minerals, and gold. Intrusions that are genetically related to the intrusion that made the Kennecott Bingham Canyon deposit have also produced copper-gold skarns, which were mined by the early European settlers in Utah. When iron and/or sulfide deposits undergo metamorphism, the grain size commonly increases, which makes separating the gangue from the desired sulfide or oxide minerals much easier.

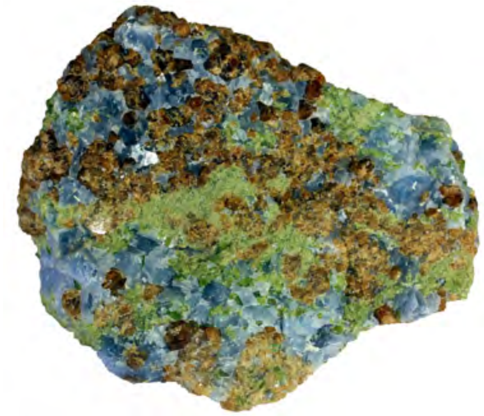

Figure 16.29: Garnet-augite skarn from Italy. Figure description available at the end of the chapter.

Figure 16.30: In this rock, a pyrite cube has dissolved (as shown by the negative "corner" impression in the rock), leaving behind small specks of gold. Figure description available at the end of the chapter.

Sediment-hosted disseminated gold deposits consist of low concentrations of microscopic gold as inclusions and disseminated atoms in pyrite crystals. These are formed via low-grade hydrothermal reactions, generally in the realm of diagenesis, that occur in certain rock types, namely muddy carbonates and limey mudstones. This hydrothermal alteration is generally far removed from a magma source but can be found in rocks situated with a high geothermal gradient. The Mercur deposit in Utah's Oquirrh Mountains was this type's earliest locally mined deposit. There, almost a million ounces of gold was recovered between 1890 and 1917. In the 1960s, a metallurgical process using cyanide was developed for these low-grade ore types. These deposits are also called Carlin-type deposits because the disseminated deposit near Carlin, Nevada, is where the new technology was first applied and where the first definitive scientific studies were conducted. Gold was introduced into these deposits by hydrothermal fluids that reacted with silty calcareous rocks, removing carbonate, creating additional permeability, and adding silica and gold-bearing pyrite in the pore space between grains. The Betze-Post mine and the Gold Quarry mine on the Carlin Trend are two of the largest disseminated gold deposits in Nevada. Similar deposits, but not as large, have been found in China, Iran, and Macedonia.

Nonmagmatic Geochemical Processes

Geochemical processes that occur at or near the surface without magma's aid also concentrate metals, but to a lesser degree than hydrothermal processes. One of the main reactions is **redox**, short for **reduction/oxidation** chemistry, which has to do with the amount of available oxygen in a system. Places with plentiful oxygen, as in the atmosphere today, are considered oxidizing environments, while oxygen-poor places are considered reducing environments. Uranium deposits are an example of where redox concentrated the metal. Uranium is soluble in oxidizing groundwater environments and precipitates as uraninite when encountering reducing conditions. Many of the deposits across the Colorado Plateau, such as in Moab, Utah, were formed by this method.

Figure 16.31: Underground uranium mine near Moab, Utah. Figure description available at the end of the chapter.

Redox reactions are also responsible for creating banded iron formations (BIFs), which are interbedded layers of iron oxide, composed of hematite and magnetite, chert, and shale beds. These deposits formed early in the Earth's history as the atmosphere was becoming oxygenated. Cycles of oxygenating iron-rich waters initiated precipitation of the iron beds. Because BIFs are generally Precambrian in age, happening at the event of atmospheric oxygenation, they are only found in some of the older exposed rocks in the United States, such as in Michigan's Upper Peninsula and northeast Minnesota.

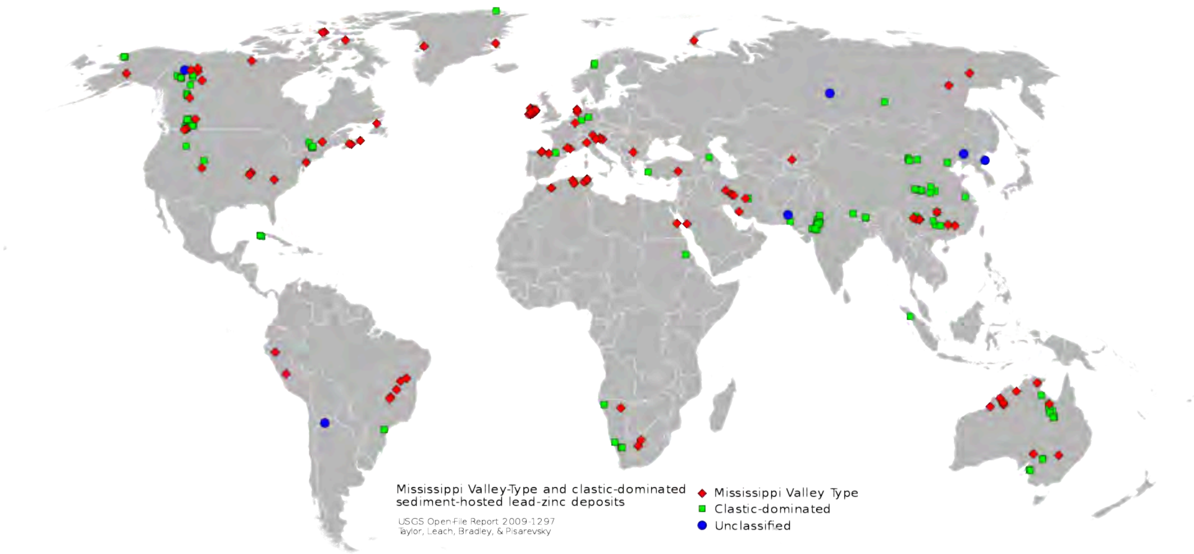

Figure 16.32: Map of Mississippi Valley-type ore deposits. Figure description available at the end of the chapter.

Deep, saline, **connate** fluids (trapped in pore spaces) within sedimentary basins may be highly metalliferous. When expelled outward and upward as basin sediments compacted, these fluids formed lead and zinc deposits in limestone by replacing or filling open spaces, such as caves and faults, and in sandstone by filling pore spaces. The most famous are called **Mississippi Valley-type** deposits. Also known as carbonate-hosted replacement deposits, they are large deposits of galena and sphalerite lead and zinc ores that form from hot fluids ranging from 100˚C to 200˚C (212˚F to 392˚F). Although they are named for occurring along the Mississippi River Valley in the US, they are found worldwide.

Sediment-hosted copper deposits occurring in sandstones, shales, and marls are enormous, and their contained resources are comparable to porphyry copper deposits. These deposits were most likely formed diagenetically by groundwater fluids in highly permeable rocks. Well-known examples are the Kupferschiefer in Europe, which has an areal coverage of >500,000 km^2, (310,685.596 mi^2) and the Zambian Copper Belt in Africa.

Soils and mineral deposits that are exposed at the surface experience deep and intense weathering, which can form surficial deposits. Bauxite, an aluminum ore, is preserved in karst topography and laterites, which are soils formed in wet tropical environments. Soils containing aluminum concentrate minerals, such as feldspar, and ferromagnesian minerals in igneous and metamorphic rocks undergo chemical weathering processes that concentrate the metals. Ultramafic rocks that undergo weathering form nickel-rich soils, and when the magnetite and hematite in banded iron formations undergo weathering, it forms goethite, a friable mineral that is easily mined for its iron content.

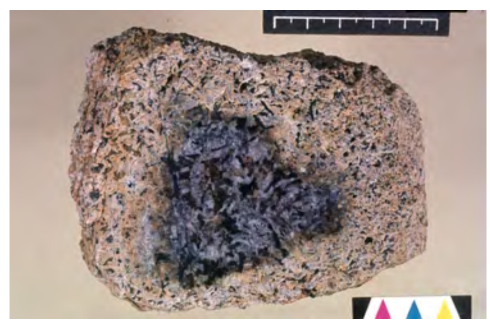

Figure 16.33: A sample of bauxite. Note the unweathered igneous rock in the center. Figure description available at the end of the chapter.

Surficial Physical Processes

Figure 16.34: Lithified heavy mineral sand (dark layers) from a beach deposit in India. Figure description available at the end of the chapter.

At the Earth's surface, mass wasting and moving water can cause hydraulic sorting, which forces high-density minerals to concentrate. When these minerals are concentrated in streams, rivers, and beaches, they are called **placer** deposits and occur in modern sands and ancient lithified rocks. Native gold, native platinum, zircon, ilmenite, rutile, magnetite, diamonds, and other gemstones can be found in placers. Humans have mimicked this natural process to recover gold manually by gold panning and by mechanized means such as dredging.

16.3.2 Environmental Impacts of Metallic Mineral Mining

Metallic mineral mining's primary impact comes from the mining itself, including disturbing the land surface, covering landscapes with tailings impoundments, and increasing mass wasting by accelerating erosion. In addition, many metal deposits contain pyrite, an uneconomic sulfide mineral that, when placed on waste dumps, generates **acid rock drainage** (ARD) during weathering, also commonly referred to as acid mine drainage. In oxygenated water, sulfides such as pyrite react and undergo complex reactions to release metal ions and hydrogen ions, which lowers pH to highly acidic levels. Mining and processing of mined materials typically increase the surface-area-to-volume ratio in the material, causing chemical reactions to occur even faster than would occur naturally. If not managed properly, these reactions lead to acidic streams and groundwater plumes that carry dissolved toxic metals. In mines where limestone is a waste rock or where carbonate minerals like calcite or dolomite are present, their acid-neutralizing potential helps reduce acid rock drainage. Although this is a natural process too, it is very important to isolate mine dumps and tailings from oxygenated water, to prevent the sulfides from dissolving and subsequently percolating the sulfate-rich water into waterways. Industry has taken great strides to prevent contamination in recent decades, but earlier mining projects are still causing problems with local ecosystems.

Figure 16.35: Acid mine drainage continues today from a coal mine that was shut down in 1935 near Blacksburg, Virginia, along the Coal Mining Heritage Loop Trail. The water's orange color is due to the high amounts of iron and sulfur. Figure description available at the end of the chapter.

16.3.3 Nonmetallic Mineral Deposits

While receiving much less attention, nonmetallic mineral resources, also known as industrial minerals, are just as vital to ancient and modern society as metallic minerals. The most basic is building stone. Limestone, travertine, granite, slate, and marble are common building stones and have been quarried for centuries. Even today, building stones are very popular for everything from slate roof tiles to granite countertops. In particular, pure limestone is ground up, processed, and reformed as plaster, cement, and concrete. Some nonmetallic mineral resources are not mineral specific; nearly any rock or mineral can be used. This is generally called aggregate, which is used in concrete, roads, and foundations. Gravel is one of the more common aggregates.

Figure 16.36: Carrara marble quarry in Italy, source to famous sculptures like Michelangelo's David. Figure description available at the end of the chapter.

Evaporites

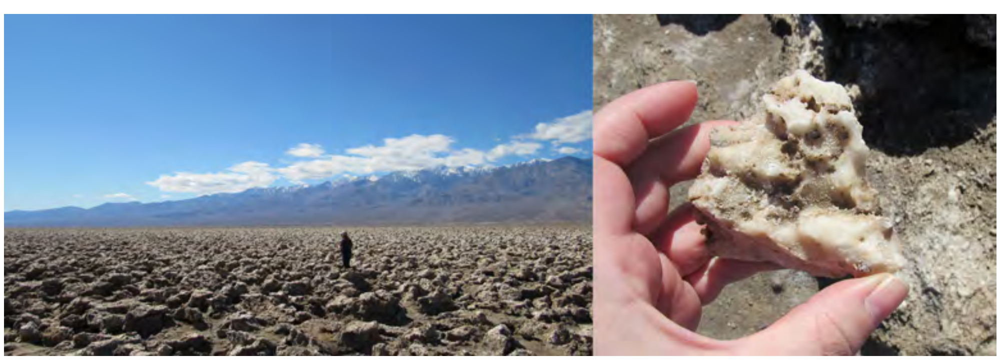

Figure 16.37: Crystallized salts compose the formations at Devils Golf Course in Death Valley National Park in the Western United States. Figure description available at the end of the chapter.

Evaporite deposits form in restricted basins where water evaporates faster than it recharges, such as the Death Valley saltpan in the Western United States or the Dead Sea, which borders Israel and Jordan. As the waters evaporate, soluble minerals are concentrated and become supersaturated, at which point they precipitate from the now highly saline waters. If these conditions persist for long stretches, thick rock salt, rock gypsum, and other mineral deposits accumulate (see Chapter 5).

Evaporite minerals, such as halite, are used in our food as common table salt. Salt was a vitally important food preservative and economic resource before refrigeration was developed. While still used in food, halite is now mainly mined as a chemical agent, water softener, or road de-icer. Gypsum is a common nonmetallic mineral used as a building material; it is the main component in dry wall. It is also used as a fertilizer. Other evaporites include sylvite (potassium chloride) and bischofite (magnesium chloride), both of which are used in agriculture, medicine, food processing, and other applications. Potash, a group of highly soluble potassium-bearing evaporite minerals, is used as a fertilizer. In hyper-arid locations, even more rare and complex evaporites like borax, trona, ulexite, and hanksite are mined. They can be found in places such as Searles Dry Lake and Death Valley, California, and in the Green River Formation's ancient evaporite deposits in Utah and Wyoming.

Figure 16.38: Hanksite, $Na_{22}K(SO_4)_9(CO_3)_2Cl$, one of the few minerals that is considered a carbonate and a sulfate. Figure description available at the end of the chapter.

Phosphorus

Phosphorus is an essential element that occurs in the mineral apatite, which is found in trace amounts in common igneous rocks. Phosphorite, or phosphate rock, is formed in sedimentary environments in the ocean, contains abundant apatite, and is mined to make fertilizer. Without phosphorus, life as we know it is not possible. Phosphorous is an important component of bone and DNA. Bone ash and guano are natural sources of phosphorus.

Figure 16.39: Apatite from Mexico. Figure description available at the end of the chapter.

Take this quiz to check your comprehension of this section.

Access the quiz for Section 16.3 by scanning the QR code.

16.4 Renewable Resources

Renewable resources are materials present in our environment that can be exploited and replenished. Some common renewable energy sources are linked with green energy sources because they are associated with relatively small or easily remediated environmental impact. For example, solar energy comes from **fusion** within the Sun, which radiates electromagnetic energy. This energy reaches the Earth constantly and consistently and should continue to do so for about five billion more years. **Wind energy**, also related to solar energy, is maybe the oldest renewable energy and is used to sail ships and power windmills. Both solar and wind-generated energy are variable on Earth's surface. These limitations are offset because we can use energy-storing devices, such as batteries or electricity exchanges between producing sites. The Earth's heat, known as geothermal energy, can be viable anywhere that geologists drill deeply enough. In practice, geothermal energy is more useful where heat flow is great, such as volcanic zones or regions with a thinner crust.

Hydroelectric dams provide energy by allowing water to fall through the dam under gravity, which activates turbines that produce the energy. Ocean tides are also a reliable energy source. All of these renewable resources provide energy that powers society. Other renewable resources are plant and animal matter, which are used for food, clothing, and other necessities but are being researched as possible energy sources.

Figure 16.40: Hoover Dam provides hydroelectric energy and stores water for Southern Nevada. Figure description available at the end of the chapter.

16.4.1 Solar Energy

Though only one billionth of the energy that leaves the Sun actually reaches the Earth's surface, this is more than enough to meet the world's energy requirements. In fact, almost all other sources of energy, renewable and nonrenewable, are actually stored forms of solar energy. **Solar energy** itself is a renewable energy source when energy from the Sun is converted to heat or electricity. The difficulties lie in harnessing the energy. Solar energy has been used for centuries to heat homes and water. Modern technology (e.g., photovoltaic cells) has provided a way to produce electricity from sunlight.

Figure 16.41: (Top) Aerial view of Apple Park, the corporate headquarters of Apple Inc., located in Cupertino, California, one of the biggest solar roofs in the world as of 2018. (Bottom) Closer image of solar panels made of photovoltaic cells on a flat roof. Figure description available at the end of the chapter.

There are two ways to harness solar energy. Passive systems are structures whose design, placement, or materials optimize the use of heat or light directly from the Sun. Active systems have devices to convert the Sun's energy into a more usable form, such as hot water or electricity.

In **passive solar systems**, strategic planning of building location, orientation, and materials provide great control over the inside temperature. Passive solar power manipulates the Sun's energy to provide heating or cooling without the use of special devices or modern technology. These heating and cooling strategies have been used historically, such as natural ventilation, solar heat gain, solar shading, and efficient insulation.

Active solar power systems harness the Sun's energy through the use of specialized devices that transform this energy into another form. Some of the more common examples of active solar devices include solar photovoltaic (PV) devices, solar thermal collectors, and solar thermal systems. The devices you are probably most used to seeing are solar **photovoltaic** devices, or solar cells, which change sunlight directly into electricity. Photovoltaics use semiconducting materials such as silicon to produce electricity from sunlight. When light hits the cells, the material produces free electrons that migrate across the cell, creating an electric current. Small PV cells can power calculators, watches, and other small electronic devices. Arrangements of many solar cells in PV panels and arrangements of multiple PV panels in PV arrays can produce electricity for an entire house or business. Some PV power plants have large arrays that cover many acres to produce electricity for thousands of homes. These are often termed "solar farms."

Though solar energy has great potential, there are also some downsides. Solar energy is not evenly distributed across the globe, making some locations better suited to solar energy investment than others. Even in locations with great solar potential, the solar energy can only be gathered while the Sun is shining. This means that little to no energy can be generated at night or on cloudy days. Since sunlight can't be stored and used on demand (like coal, oil, or even biomass), the challenge of intermittent power can be difficult to overcome. Still, many have found solar energy to be an excellent supplemental source of power, as demonstrated by the increasing popularity of installing solar panels on home, business, and municipal rooftops.

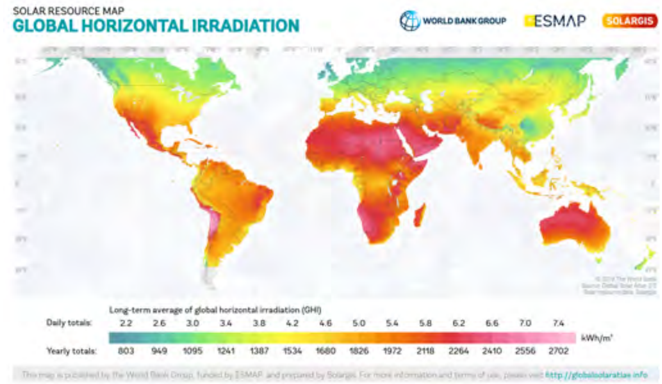

Figure 16.42: This solar resource map provides a summary of the estimated solar energy available for power generation and other energy applications. It represents the average daily/yearly totals of global horizontal irradiation (GHI), covering a period from 1994/1999/2007 (depending on the region) to 2018. Figure description available at the end of the chapter.

16.4.2 Wind Power

Wind power is a renewable energy source that uses the energy of moving air to generate electricity. Winds are caused by differences in atmospheric pressure across the globe. These pressure differentials themselves are largely caused by the temperature differences that result from uneven solar heating across the Earth. In this way, wind energy is an indirect form of solar energy. Similar to solar energy, some locations of the Earth's surface possess greater wind speeds and therefore a greater capacity for the harvesting of wind energy. Many locations with excellent wind power capacity are found on top of the ocean and are beginning to be utilized through the construction of offshore wind farms.

The most common way to collect and transform the wind's energy into a usable form is through wind **turbines**. These turbines use blades to collect the wind's **kinetic energy**. This technology has been in use for hundreds of years in the form of windmills. While traditional windmills used wind energy to pump water or grind grain, modern wind turbines convert this energy to electricity through the use of a generator. Wind flows over the blades of a turbine, creating lift (similar to the effect on airplane wings), which causes the blades to turn. The blades are connected to a drive shaft that turns an electric generator, which produces electricity.

Figure 16.43: (Left) A turbine and gear box are mounted in a casing called a nacelle, and rotor blades are attached to the turbine. The turbine localizes the energy of the turning rotor blades in a single rotating shaft that generates electricity. (Right) Wind turbine along the Allegheny Front in Grant County, West Virginia. Figure description available at the end of the chapter.

Wind turbines do not release emissions that pollute the air or water, and they do not require water for cooling. Since a wind turbine has a small physical footprint relative to the amount of electricity it produces, many wind farms are located on crop, pasture, forest land, or coastal areas. They contribute to economic sustainability by providing extra income to farmers and ranchers. Similar to PV solar systems, wind turbines are practical at the small scale and can be used in remote areas to generate electricity, even in the absence of electrical grid infrastructure. Similar to PV solar systems, it is impossible to store wind and use it on demand. Because of this, wind turbines may be intermittent in their production of power, only producing electricity when the wind is blowing.

Still, wind turbines do have a few environmental challenges. There are aesthetic concerns for some people who see them on the landscape ("Not In My Back Yard," or NIMBY, syndrome). A few wind turbines have caught on fire, and some have leaked lubricating fluids, though this is relatively rare. Wind turbines do produce noise pollution, which can impact both human and animal populations. Additionally, turbines have been found to cause bird and bat deaths, particularly if they are located along their migratory path. This is of particular concern if these are threatened or endangered species. There are ways to mitigate that impact, and they are currently being researched.

16.4.3 Hydroelectric Power

Hydroelectric power, also known as **hydropower**, is the second largest source of renewable energy used, next to biomass energy. Similar to wind power, hydropower has been used for hundreds of years as the kinetic energy from moving water was used to turn a mill and grind grain. For most types of hydropower, locations are limited to regions with rivers that are large enough and have a flow strong enough to support a hydropower station. At times when the river is low, there may not be sufficient flow to operate hydropower stations, causing this form of energy to be somewhat limited by both geographical and seasonal factors.

Figure 16.44: The Three Gorges Dam is the world's largest power station in terms of installed capacity (22,500 MW), located along the Yangtze River, Hubei Province, Central China. Figure description available at the end of the chapter.

The majority of hydropower in the world exists in the form of storage hydropower, in which dams are built across a river to block the flow of river water. The water stored behind the dam contains **potential energy**, and when released, the potential energy is converted to **kinetic energy** as the water rushes down. In addition to providing a source of hydroelectric power, the dam also creates a **reservoir**, or manmade lake, in the area upstream of the dam. Many of the largest power plants in the world are storage hydropower facilities, including the Three Gorges Dam in China, the world's largest power plant by installed capacity at 22,500 MW, and the Grand Coulee Dam in Washington, US, at over 6,800 MW.

Figure 16.45: Fish ladder at the Bonneville Dam along the Columbia River, Oregon. Figure description available at the end of the chapter.

Hydropower is a renewable source of energy since it does not directly produce emissions of air pollutants, it consumes no nonrenewable fuel sources, and the source of power is constantly regenerated. However, hydropower dams, reservoirs, and the operation of generators can have serious environmental impacts. For example, the migration of fish to their upstream spawning areas can be obstructed by dams. In areas where salmon must travel upstream to spawn, such as along the Columbia River in Washington and Oregon, the dams block their way. This problem can be partially alleviated by using "fish ladders" that help salmon get around the dams. Fish traveling downstream, however, can get killed or injured as water moves through turbines in the dam. Reservoirs and the operation of dams can also affect aquatic habitats due to changes in water temperatures, water depth, chemistry, flow characteristics, and sediment loads, all of which can lead to significant changes in the ecology and physical characteristics of the river both upstream and downstream. As reservoirs fill with water, it may cause natural areas, farms, cities, and archeological sites to be inundated and force populations to relocate.

16.4.4 Geothermal Energy

Geothermal energy uses heat from the Earth's internal geologic processes to produce electricity or provide heating. The subsurface temperature of the Earth provides an essentially endless energy resource. The energy harvested in a geothermal power plant is the same energy that forms geysers and hot springs. The heat from the Earth's core continuously flows outward. Sometimes the heat, as magma, reaches the surface as lava, but it usually remains below the Earth's crust, heating nearby rock and water, sometimes to levels as hot as 370°C. When water is heated by the Earth's heat, hot water or steam can be trapped in permeable and porous rocks under a layer of impermeable rock and a geothermal reservoir can form.

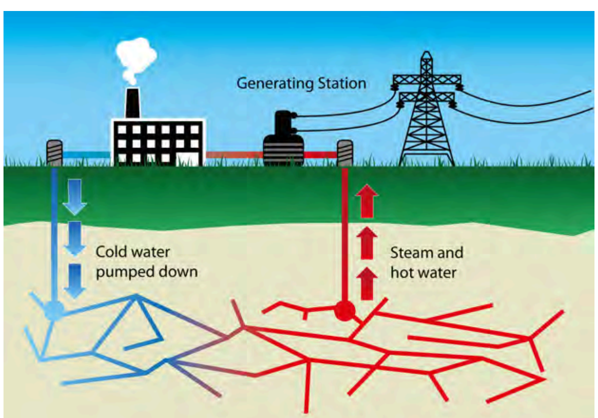

Figure 16.46: Geothermal energy production diagram. Figure description available at the end of the chapter.

A geothermal system requires heat, permeability, and water. To develop electricity from geothermal resources, wells are drilled in a location with high geothermal potential. This is typically a region containing naturally superheated groundwater. Groundwater percolates down through cracks in the subsurface rocks until it reaches rocks heated by underlying magma, and the heat converts the water to steam. Many areas with strong seismic activity, including earthquakes and volcanoes, also possess high geothermal potential. Examples include the country of Iceland and many regions of California and the North American Pacific Coast.

The environmental impact of geothermal energy depends on how it is being used. Direct use and heating applications have almost no negative impact on the environment. Geothermal power plants do not burn fuel to generate electricity, so their emission levels are very low. Some carbon dioxide and methane gas are emitted, but to a much smaller degree than the combustion of fossil fuels or biomass. Even though geothermal energy is renewable, not every plant built to capture this energy will be able to operate indefinitely because the energy relies on groundwater recharge. If the heated water is used faster than the recharge rate of]groundwater, the plant will eventually run out of water. Additionally, patterns of geothermal activity in the Earth's crust naturally shift over time, and an area that produces hot groundwater now may not always so do. The water of many hot springs is laced with salts and minerals that can corrode equipment, shorten the lifetime of plants, and increase maintenance costs.

16.4.5 Biomass Energy

Biomass energy, or bioenergy, is the energy stored in materials of biological origin such as plants and animals, and it is the oldest energy source used by humans. Until the Industrial Revolution prompted a shift to fossil fuels in the mid-eighteenth century, biomass energy was the world's dominant fuel source.

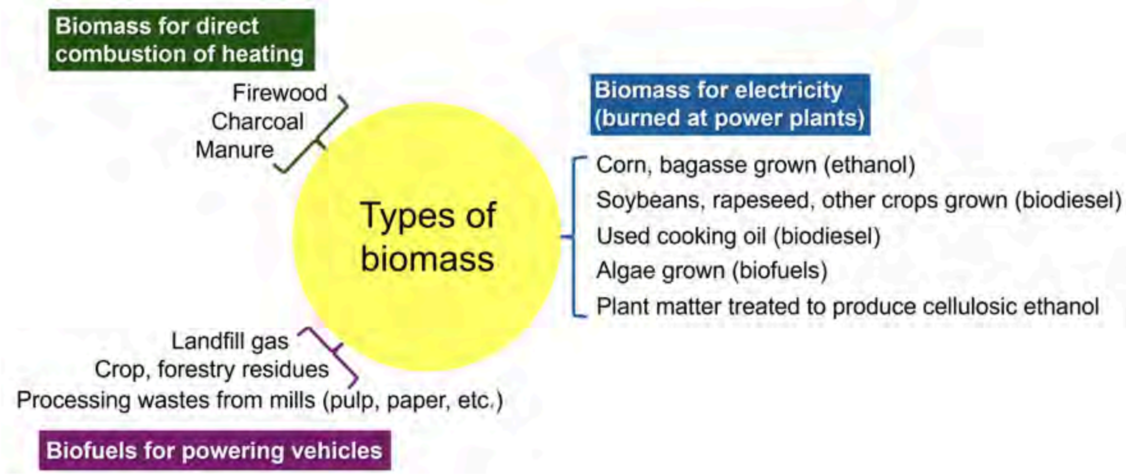

Figure 16.47: Sources and uses of bioenergy. Figure description available at the end of the chapter.

It includes direct combustion of solid biomass to provide energy for heating, cooking, and even generating electricity. Biomass can also be converted into liquid **biofuels** used to power vehicles, such as ethanol from corn, sugarcane residue, and soybeans (even used cooking oil can be repurposed as biodiesel). Biomass energy can also be harvested through gaseous biomass, sometimes called biogas, in the form of methane. Biomass is most frequently used as a fuel source in many less-industrialized nations, but with the decline of fossil fuel availability and the increase in fossil fuel prices, biomass is increasingly being used as a fuel source, even in more-industrialized nations.

A major challenge of biomass is determining if it is really a more sustainable option. The energy content of some biomass energy sources may not be as high as fossil fuels, so more must be burned to generate the same energy. It often takes energy to make energy, and biomass is one example where the processing required to make it may not be offset by the energy it produces. If conventional agriculture crops like corn or soybeans are used, they require major quantities of fossil fuel to manufacture fertilizer, run farm machines, and ship the fuel to markets, so these biofuels do not always offer significant net energy savings over gasoline and diesel fuel. Even if the environmental impact is net positive—for example, if renewable energy sources are used to make the biofuels—the economic and social effects of growing plants for fuels need to be considered. The land, fertilizers, water, and energy used to grow biofuel crops could be used to grow food crops instead. The competition between land for fuel and land for food can increase the price of food, which has a negative effect on society. It could also decrease the food supply and increase malnutrition and starvation globally.

Burning biomass directly (wood, manure, etc.) produces high-particulate material pollution, produces carbon dioxide, and deprives the soil of nutrients it normally would have received from the decomposition of the organic matter. In order to be used sustainably, one tree must be planted for every one cut down; however, trees that are cut for firewood are frequently not replanted. If too much biomass is taken, it can reduce forest and grassland contributions to ecosystem services. Each type of biomass energy source, therefore, must be evaluated for its full life-cycle impact in order to determine if it is really advancing sustainability and reducing environmental impacts.

Summary

Energy and mineral resources are vital to modern society, and it is the role of the geologist to locate these resources for human benefit. As environmental concerns have become more prominent, the value of the geologist has not decreased, as they are still vital in locating the deposits and identifying the least intrusive methods of extraction.

Energy resources are generally grouped as being renewable or nonrenewable. Geologists can aid in locating the best places to exploit renewable resources (e.g., locating a dam) but are commonly tasked with finding nonrenewable fossil fuels. Mineral resources are also grouped in two categories: metallic and nonmetallic. Minerals have a wide variety of processes that concentrate them to economic levels and are usually mined via surface or underground methods.

Take this quiz to check your comprehension of this chapter.

Access the quiz for Chapter 16 by scanning the QR code.

Text References

1. Ague, J.J., and Brimhall, G.H. (1989). Geochemical modeling of steady state fluid flow and chemical reaction during supergene enrichment of porphyry copper deposits. *Economic Geology and the Bulletin of the Society of Economic Geologists, 84*(3), 506–28. http://economicgeology.org.
2. Arndt, N.T. (1994). Chapter 1: Archean Komatiites, in Condie, K.C. (ed.), *Developments in Precambrian geology:* Elsevier, 11–74.
3. Bárdossy, György, and Aleva, G.J.J. (1990). *Lateritic Bauxites, Vol. 27:* Elsevier Science Ltd.
4. Barrie, C.T. (1999). Volcanic-associated massive sulfide deposits: Processes and examples in modern and ancient settings. *Reviews in Economic Geology, 8.* https://www.researchgate.net/pro.le/Michael_Per.t/publication/241276560_Geologic_petrologic_and_geochemical_relationships_between_magmatism_and_massive_sul.de_mineralization_along_the_eastern_Galapagos_Spreading_Center/links/02e7e51c8707bbfe9c000000.pdf.
5. Barrie, L. A., and Ho, R.M. (1984). The oxidation rate and residence time of sulphur dioxide in the Arctic atmosphere." *Atmospheric Environment, 18*(12), 2711–22.
6. Bauquis, P.-R. (1998). What future for extra heavy oil and bitumen: The Orinoco case, in paper presented by TOTAL at the World Energy Congress, 13:18.
7. Belloc, H. (1913). *The servile state:* T.N. Foulis.
8. Blander, M., Sinha, S., Pelton, A., and Eriksson, G. (2011). Calculations of the influence of additives on coal combustion deposits. Argonne National Laboratory, Lemont, Illinois, 315.
9. Boudreau, A.E. (2016). The Stillwater Complex, Montana–Overview and the significance of volatiles. *Mineralogical Magazine, 80*(4), 585–637.
10. Bromfield, C.S., Erickson, A.J., Haddadin, M.A., and Mehnert, H.H. (1977). Potassium-argon ages of intrusion, extrusion, and associated ore deposits, Park City Mining District, Utah. *Economic Geology and the Bulletin of the Society of Economic Geologists, 72*(5), 837–48.
11. Brown, V.J. (2007). Industry issues: Putting the heat on gas. *Environmental Health Perspectives, 115*(2), A76.
12. Cabri, L.J., Harris, D.C., and Weiser, T.W. (1996). Mineralogy and distribution of platinum-group mineral (PGM) placer deposits of the world. *Exploration and Mining Geology, 2*(5), 73–167.
13. Crutzen, P.J., and Lelieveld, J. (2001). Human impacts on atmospheric chemistry. *Annual Review of Earth and Planetary Sciences, 29*(1), 17–45.
14. Delaney, M.L. (1998). Phosphorus accumulation in marine sediments and the oceanic phosphorus cycle. *Global Biogeochemical Cycles, 12*(4), 563–72.
15. Demaison, G.J., and Moore, G.T. (1980). Anoxic environments and oil source bed genesis. *Organic Geochemistry, 2*(1), 9–31.
16. Dott, R.H., and Reynolds, M.J. (1969). *Sourcebook for petroleum geology:* American Association of Petroleum Geologists. http://archives.datapages.com/data/specpubs/methodo1/data/a072/a072/0001/0000/vi.htm.
17. Duffield, W.A. (2005). Volcanoes, Geothermal Energy, and the Environment, in *Volcanoes and the environment:* Cambridge University Press, 304.
18. Einaudi, M.T., and Burt, D.M. (1982). Introduction: Terminology, classification, and composition of skarn deposits. *Economic Geology and the Bulletin of the Society of Economic Geologists, 77*(4), 745–54.
19. Gandossi, L. (2013). An overview of hydraulic fracturing and other formation stimulation technologies for shale gas production." *Eur. Commission Jt. Res. Cent. Tech. Reports.* http://skalunudujos.lt/wp-content/uploads/an-overview-of-hydraulic-fracturing-and-other-stimulation-technologies.pdf.
20. Gordon, M., Jr., Tracey, J.I. Jr., and Ellis, M.W. (1958). *Geology of the Arkansas bauxite region.* http://pubs.er.usgs.gov. https://pubs.er.usgs.gov/publication/pp299.
21. Gordon, W.A. (1975). Distribution by latitude of Phanerozoic evaporite deposits. *The Journal of Geology, 83*(6), 671–84.
22. Haber, F. (2002). The synthesis of ammonia from its elements – Nobel lecture, June 2, 1920. *Resonance, 7*(9), 86–94.
23. Hawley, C.C. (2014). *A Kennecott story: Three mines, four men, and one hundred years, 1887-1997:* University of Utah Press.
24. Hirsch, R.L., Bezdek, R., and Wendling, R. (2006). Peaking of world oil production and its mitigation. *AIChE Journal. American Institute of Chemical Engineers, 52*(1), 2–8.
25. Hitzman, M., Kirkham, R., Broughton, D., Thorson, J., and Selley, D. (2005). The sediment-hosted stratiform copper ore system. *Economic Geology and the Bulletin of the Society of Economic Geologists.* http://eprints.utas.edu.au/705.
26. Hofstra, A.H., and Cline, J.S. (2000). Characteristics and models for Carlin-type gold deposits. *Reviews in Economic Geology, 13,* 163–220.

27. James, L.P. (1979). Geology, ore deposits, and history of the Big Cottonwood Mining District, Salt Lake County, Utah. *Utah Geological and Mineral Survey.* Utah Department of Natural Resources.
28. Kim, W-Y. (2013). Induced seismicity associated with fluid injection into a deep well in Youngstown, Ohio. *Journal of Geophysical Research, [Solid Earth], 118*(7), 3506–18.
29. Klein, C. (2005). Some Precambrian banded iron-formations (BIFs) from around the world: Their age, geologic setting, mineralogy, metamorphism, geochemistry, and origins. *The American Mineralogist, 90*(10), 1473–99.
30. Laylin, J.K. (1993). *Nobel Laureates in Chemistry, 1901-1992:* Chemical Heritage Foundation.
31. Leach, D. L., and Sangster, D.F. (1993). Mississippi Valley-type lead-zinc deposits. *Mineral Deposit Modeling: Geological.* https://www.researchgate.net/pro.le/Elisabeth_Rowan/publication/252527999_Genetic_link_between_Ouachita_foldbelt_tectonism_and_the_Mississippi_Valley-type_Leadzinc_deposits_of_the_Ozarks/links/00b7d53c97ac2d6fe7000000.pdf.
32. Lehmann, B. (2008). Uranium ore deposits. *Rev. Econ. Geol. AMS Online 2008,* 16–26.
33. London, D., and Kontak, D.J. (2012). Granitic pegmatites: Scientific wonders and economic bonanzas. *Elements, 8*(4), 257–61.
34. Mancuso, J.J., and Seavoy, R.E. (1981). Precambrian coal or anthraxolite: A source for graphite in high-grade schists and gneisses. *Economic Geology and the Bulletin of the Society of Economic Geologists, 76*(4), 951–54.
35. McKenzie, H., and Moore, B. (1970). Social origins of dictatorship and democracy. *JSTOR.* http://www.jstor.org/stable/27856441.
36. Needham, J., Wang, L., and Lu, G.D. (1963). *Science and Civilisation in China, Vol. 5:* Cambridge University Press.
37. Nuss, P., and Eckelman, M.J. (2014). Life cycle assessment of metals: A scientific synthesis. *PloS One, 9*(7), e101298.
38. Orton, E. (1889). *The Trenton limestone as a source of petroleum and inflammable gas in Ohio and Indiana:* U.S. Government Printing Office.
39. Palmer, M.A., Bernhardt, E.S., Schlesinger, W.H., Eshleman, K.N., Foufoula-Georgiou, E., Hendryx, M.S., Lemly, A.D., et al. (2010). Science and regulation. Mountaintop mining consequences. *Science, 327*(5962), 148–49.
40. Pratt, W.E. (1942). *Oil in the Earth:* University of Kansas Press.
41. Quéré, C. Le, Andres, R.J., Boden, T., Conway, T., Houghton, R.A., House, J.I., Marland, G., et al. (2013). The global carbon budget 1959–2011. *Earth System Science Data, 5*(1), 165–85.
42. Richards, J. P. (2003). Tectono-magmatic precursors for porphyry Cu-(Mo-Au) deposit formation. *Economic Geology and the Bulletin of the Society of Economic Geologists, 98*(8), 1515–33.
43. Rui-Zhong, H., Wen-Chao, S., Xian-Wu, B., Guang-Zhi, T., and Hofstra, A.H. (2002). Geology and geochemistry of Carlin-type gold deposits in China. *Mineralium Deposita, 37*(3-4), 378–92.
44. Schröder, K-P, and Smith, R.C. (2008). Distant future of the Sun and Earth revisited. *Monthly Notices of the Royal Astronomical Society, 386*(1), 155–63.
45. Semaw, S., Rogers, M.J., Quade, J., Renne, P.R., Butler, R.F., Dominguez-Rodrigo, M., Stout, D., Hart, W.S., Pickering, T., and Simpson, S.W. (2003). 2.6-million-year-old stone tools and associated bones from OGS-6 and OGS-7, Gona, Afar, Ethiopia." *Journal of Human Evolution, 45*(2), 169–77.
46. Tappan, H., and Loeblich, A.R. (1970). Geobiologic implications of fossil phytoplankton evolution and time-space distribution." *Geological Society of America Special Papers, 127*(January), 247–340.
47. Taylor, E.L., Taylor, T.N., and Krings, M. (2009). *Paleobotany: The biology and evolution of fossil plants:* Elsevier Science.
48. Tissot, B. (1979). Effects on prolific petroleum source rocks and major coal deposits caused by sea-level changes. *Nature, 277,* 463–65.
49. Vail, P.R., Mitchum, R.M., Jr, Thompson, S. III, Todd, R.G., Sangree, J.B., Widmier, J.M., Bubb, J.N., and Hatelid, W.G. (1977). Seismic stratigraphy and global sea level changes, in *Seismic stratigraphy-applications to hydrocarbon exploration* (Payton, C.E., ed.): American Association of Petroleum Geologists Memoir 26, 49–212.
50. Vogel, J.C. (1970). Groningen radiocarbon dates IX. *Radiocarbon, 12*(2), 444–71.
51. Willemse, J. (1969). The geology of the Bushveld igneous complex, the largest repository of magmatic ore deposits in the world." *Economic Geology Monograph 4,* 1–22.
52. Wrigley, E.A. (1990). *Continuity, chance and change: The character of the Industrial Revolution in England. Ellen McArthur lectures:* Cambridge University Press.
53. Youngquist, W. (1998). Shale oil–The elusive energy." Hubbert Center Newsletter 4.
54. Harris, E.P. (2023). *Introduction to environmental sciences and sustainability.* Creative Commons Attribution 4.0 International License. https://pressbooks.uwf.edu/envrioscience.
55. Zehnder, C. Manoylov, K., Mutiti, S., Mutiti, C., VandeVoort, A., and Bennett, D. (2018). *Introduction to environmental science: 2nd edition:* University System of Georgia. Creative Commons Attribution-NonCommercial-Share Alike 4.0 International License. https://alg.manifoldapp.org/projects/introduction-to-environmentalscience.
56. Environmental and Energy Study Institute (EESI). Accessed July 12, 2024. Solar Energy. Creative Commons Attribution License. https://www.eesi.org/topics/solar/description#:~:text=There%20are%20two%20ways%20to,as%20hot%20water%20or%20electricity.

Figure References

Figure 16.1: A Mode 1 Oldowan tool used for chopping. José-Manuel Benito Álvarez. 2007. Public domain. https://commons.wikimedia.org/wiki/File:Canto_tallado_2-Guelmim-Es_Semara.jpg

Figure 16.2: A container of phosphate from the Aurora mine in North Carolina. Melissa MB Wilkins. 2012. CC BY-NC 2.0. https://www.flickr.com/photos/melissambwilkins/8444130793

Figure 16.3: Natural octahedral shape of diamond. United States Geological Survey (USGS). 2003. Public domain. https://commons.wikimedia.org/wiki/File:Rough_diamond.jpg

Figure 16.4: Map of world mining areas. KVDP. 2009. Public domain. https://commons.wikimedia.org/wiki/File:Simplified_world_mining_map_1.png

Figure 16.5: Banded-iron formations are an important ore of iron (Fe). Laura Neser. September 2024. CC BY-NC.

Figure 16.6: Diagram illustrating the relative abundance of proven reserves, inferred reserves, resources, and undiscovered resources. Kindred Grey. 2022. CC BY 4.0.

Figure 16.7: McKelvey diagram showing different definitions for different degrees of concentration and understanding of mineral deposits. USGS. 1980. Public domain. https://commons.wikimedia.org/wiki/File:McKelveyDiagram.jpg

Figure 16.8: Bingham Canyon Mine, Utah. Doc Searls. 2016. CC BY 2.0. https://commons.wikimedia.org/wiki/File:Bingham_Canyon_mine_2016.jpg

Figure 16.9: A surface coal mine in Wyoming. Bureau of Land Management. Unknown date. Public domain. https://www.usgs.gov/news/science-snippet/earthword-thermal-maturity

Figure 16.10: Underground oil shale mining in Estonia. Kaupo Kikkas. 2011. CC BY-SA 4.0. https://commons.wikimedia.org/wiki/File:VKG_Ojamaa_kaevandus.jpg

Figure 16.11: A phosphate smelting operation in Alabama, 1942. Alfred T. Palmer. 1942. Public domain. https://commons.wikimedia.org/wiki/File:TVA_phosphate_smelting_furnace.jpg

Figure 16.12: Coal power plant in Helper, Utah. David Jolley. 2007. CC BY-SA 3.0. https://commons.wikimedia.org/wiki/File:Castle_Gate_Power_Plant,_Utah_2007.jpg

Figure 16.13: Modern coral reefs and other highly productive shallow marine environments are thought to be the sources of most petroleum resources. Toby Hudson. 2010. CC BY-SA 3.0. https://commons.wikimedia.org/wiki/File:Coral_Outcrop_Flynn_Reef.jpg

Figure 16.14: World oil reserves in 2013. GunnMap; generated with settings from Emilfaro and A5b. 2014. CC BY-SA 1.0. https://commons.wikimedia.org/wiki/File:Oil_Reserves.png

Figure 16.15: Examples of different forms of hydrocarbon traps in the core region of anticlines. MagentaGreen. 2014. CC BY-SA 4.0. https://commons.wikimedia.org/wiki/File:Anticlinal_Oil_trap.png

Figure 16.16: The rising sea levels of transgressions create onlapping sediments, and regressions create offlapping. Woudloper. 2009. CC BY-SA 1.0. https://commons.wikimedia.org/wiki/File:Offlap_%26_onlap_EN.svg

Figure 16.17: Tar sandstone from the Miocene Monterey Formation of California. James St. John. 2015. CC BY 2.0. https://flic.kr/p/rECMTD

Figure 16.18: Global production of oil shale, 1880–2010. USGS. 2011. Public domain. https://commons.wikimedia.org/wiki/File:Production_of_oil_shale.png

Figure 16.19: Schematic diagram of fracking. Mikenorton. 2012. CC BY-SA 3.0. https://en.wikipedia.org/wiki/File:HydroFrac.png

Figure 16.20: USGS diagram of different coal rankings. USGS. 2009. Public domain. https://commons.wikimedia.org/wiki/File:Coal_Rank_USGS.png

Figure 16.21: Peat (also known as turf) consists of partially decayed organic matter. David Stanley. 2019. CC BY 2.0. https://commons.m.wikimedia.org/wiki/File:Peat_(49302157252).jpg

Figure 16.22: Anthracite coal, the highest grade of coal. USGS. 2007. Public domain. https://commons.wikimedia.org/wiki/File:Coal_anthracite.jpg

Figure 16.23: Gold-bearing quartz vein from California. James St. John. 2014. CC BY 2.0. https://commons.wikimedia.org/wiki/File:Mother_Lode_Gold_OreHarvard_mine_quartz-gold_vein.jpg

Figure 16.24: Layered intrusion of dark chromium-bearing minerals, Bushveld Complex, South Africa. kevinzim/Kevin Walsh. 2006. CC BY 2.0. https://commons.wikimedia.org/wiki/File:Chromitite_Bushveld_South_Africa.jpg

Figure 16.25: This pegmatite contains lithium-rich green elbaite (a tourmaline) and purple lepidolite (a mica). Parent Géry. 2011. CC BY-SA 3.0. https://commons.wikimedia.org/wiki/File:Elba%C3%AFte_et_mica_(Br%C3%A9sil)_1.JPG

Figure 16.26: Schematic diagram of a kimberlite pipe. Asbestos. 2005. CC BY-SA 3.0. https://commons.wikimedia.org/wiki/File:VolcanicPipe.jpg

Figure 16.27: The complex chemistry around mid-ocean ridges. NOAA. 2011. Public domain. https://commons.wikimedia.org/wiki/File:Deep_Sea_Vent_Chemistry_Diagram.svg

Figure 16.28: The Morenci porphyry is oxidized toward its top (as seen in red rocks in the wall of the mine), creating supergene enrichment. Stephanie Salisbury. 2012. CC BY 2.0. https://commons.wikimedia.org/wiki/File:Morenci_Mine_2012.jpg

Figure 16.29: Garnet-augite skarn from Italy. Siim Sepp. 2012. CC BY-SA 3.0. https://commons.wikimedia.org/wiki/File:00031_6_cm_grossular_calcite_augite_skarn.jpg

Figure 16.30: In this rock, a pyrite cube has dissolved (as shown by the negative "corner" impression in the rock), leaving behind small specks of gold. Matt Affolter (QFL247). 2009. CC BY-SA 3.0. https://commons.wikimedia.org/wiki/File:GoldinPyriteDrainage_acide.JPG

Figure 16.31: Underground uranium mine near Moab, Utah. Matt Affolter. 2010. CC BY-SA 3.0. https://commons.wikimedia.org/wiki/File:UraniumMineUtah.JPG

Figure 16.32: Map of Mississippi Valley-type ore deposits. Kbh3rd. 2010. CC BY 3.0. https://commons.wikimedia.org/wiki/File:MV-Type_and_clastic_sediment-hosted_lead-zinc_deposits.svg

Figure 16.33: A sample of bauxite. Werner Schellmann. 1965. CC BY-SA 2.5. https://commons.wikimedia.org/wiki/File:Bauxite_with_unweathered_rock_core._C_021.jpg

Figure 16.34: Lithified heavy mineral sand (dark layers) from a beach deposit in India. Photograph taken by Mark A. Wilson (Department of Geology, The College of Wooster). 2008. Public domain. https://commons.wikimedia.org/wiki/File:HeavyMineralsBeachSand.jpg

Figure 16.35: Acid mine drainage continues today from a coal mine that was shut down in 1935 near Blacksburg, Virginia, along the Coal Mining Heritage Loop Trail. Laura Neser. September 2021. CC BY-NC.

Figure 16.36: Carrara marble quarry in Italy, source to famous sculptures like Michelangelo's David. Michele~commonswiki. 2006. CC BY-SA 3.0. https://commons.wikimedia.org/wiki/File:Carrara_Marble_quarry.jpg

Figure 16.37: Crystallized salts compose the formations at Devils Golf Course in Death Valley National Park in the Western United States. Laura Neser. March 2022. CC BY-NC.

Figure 16.38: Hanksite, $Na_{22}K(SO_4)_9(CO_3)_2Cl$, one of the few minerals that is considered a carbonate and a sulfate. Matt Affolter(QFL247). 2009. CC BY-SA 3.0.

Figure 16.39: Apatite from Mexico. Robert M. Lavinsky. Before March 2010. CC BY-SA 3.0. https://commons.wikimedia.org/wiki/File:Apatite-(CaF)-280343.jpg

Figure 16.40: Hoover Dam provides hydroelectric energy and stores water for Southern Nevada. Ubergirl. 2012. CC BY-SA 3.0. https://commons.wikimedia.org/wiki/File:Hoover_Dam,_Colorado_River.jpg

Figure 16.41: (Top) Aerial view of Apple Park, the corporate headquarters of Apple Inc., located in Cupertino, California, one of the biggest solar roofs in the world as of 2018. Daniel L. Lu. 2018. CC BY-SA. https://en.m.wikipedia.org/wiki/File:Aerial_view_of_Apple_Park_dllu.jpg. (Bottom) Closer image of solar panels made of photovoltaic cells on a flat roof. AleSpa. 2012. CC BY-SA.

Figure 16.42: This solar resource map provides a summary of the estimated solar energy available for power generation and other energy applications. Solargis. 2020. CC BY. https://commons.wikimedia.org/wiki/File:World_GHI_Solar-resource-map_GlobalSolarAtlas_World-Bank-Esmap-Solargis.png

Figure 16.43 (Left) Simplified diagram of a wind turbine. Tennessee Valley Authority. Unknown date. Public domain. https://commons.wikimedia.org/wiki/File:Wind_turbine_diagram.svg. (Right) Wind turbine along the Allegheny Front in Grant County, West Virginia. Famartin. 2016. CC BY. https://commons.wikimedia.org/wiki/File:2016-06-06_18_10_21_Wind_turbine_along_the_Allegheny_Front_near_Bismarck_in_Grant_County,_West_Virginia.jpg

Figure 16.44: The Three Gorges Dam. Sentinel Hub. 2019. CC BY. https://www.flickr.com/photos/sentinelhub/47007987002

Figure 16.45: Fish ladder at the Bonneville Dam along the Columbia River, Oregon. Don Graham. 2006. CC BY-SA. https://www.flickr.com/photos/23155134@N06/6506557507/in/photostream

Figure 16.46: Geothermal energy production diagram. Rxn111130. 2015. CC BY-SA. https://commons.wikimedia.org/wiki/File:Geothermal-energy.png

Figure 16.47: Sources and uses of bioenergy. Laura Neser, adapted from Shunkehe. 2024. CC BY-SA. https://commons.wikimedia.org/wiki/File:Biomass-types.webp

Figure Descriptions

Figure 16.1: A brown smooth rock that has chips flaked off of it on one side, sharpening it.

Figure 16.2: A clear rounded container full of dark gray pebbles and rocks.

Figure 16.3: Clear, glassy diamond with an octahedral shape embedded in a black chunk of rock.

Figure 16.4: A world map showing the locations of certain ores in the world. A specific focus has been put on metals and construction materials. The various resources are unevenly distributed across the globe.

Figure 16.5: A slice of rock, showing red, orange, yellow, and brown wavy layers with some layers being translucent. A thumb is seen at the lower left holding the sample.

Figure 16.6: Diagram shows the small box of "reserves" within a larger box of "resources". There is also an "inferred resources" box that is slightly larger than "proven reserves" box and an "undiscovered resources" box slightly larger than the resources box.

Figure 16.7: Graphical representation of mineral resource classification with respect to economics and geologic certainty. Three rows are labeled economic, marginally economic, and sub-economic. Two columns are labeled identified resources and undiscovered resources. The identified resources column is split into demonstrated and inferred columns, and the demonstrated column is further divided into measured and indicated columns. At the intersection of the demonstrated column and economic row, the box is labeled reserves; at the intersection of the demonstrated column and marginally economic row, the box is labeled marginal reserves; at the intersection of the demonstrated column and sub- economic row, the box is labeled demonstrated subeconomic resources. At the intersection of the inferred column and economic row, the box is labeled inferred reserves; at the intersection of the inferred column and marginally economic row, the box is labeled inferred marginal reserves; at the intersection of the inferred column and sub-economic row, the box is labeled inferred subeconomic resources. The boxes are blank under the column labeled undiscovered resources.

Figure 16.8: Immense terraced dirt-lined open pit with snow-covered mountains visible around the back of the mine.

Figure 16.9: A large yellow machine is removing black coal from a terraced slope.

Figure 16.10: A photo in an underground mine with horizontal layering visible in the mine walls; there is also a large yellow truck with a bucket attached to its front containing brown rocky material.

Figure 16.11: A man is operating a large machine that looks like a blast furnace.

Figure 16.12: A power plant with steam coming out, surrounded by rocky hills on either side.

Figure 16.13: Colorful coral reef underwater in light blue, shallow water.

Figure 16.14: World map showing oil reserves by nation in various shades of blue: darker blue nations richest in oil include Canada, Venezuela, and Saudi Arabia. Oil reserves vary geographically.

Figure 16.15: Block diagram showing upward-arching layers with petroleum pooling toward the top of the fold beneath the surface; natural gas forms above the petroleum; there is a well at the surface drilled down into the oil deposit.

Figure 16.16: Two cross sectional diagrams; the top diagram shows onlap with layers of sediments being deposited on top of each other, with each successive upper layer being deposited toward inland; there is an arrow pointing toward the right-hand side labeled transgression; the bottom diagram shows offlap with layers of sediments being deposited on top of each other, with each successive upper layer being deposited toward the ocean; there is an arrow pointing toward the left-hand side labeled regression.

Figure 16.17: Blocky chunk of sandstone that is black in color due to being filled with tar.

Figure 16.18: Graph of global production of oil shale: the horizontal axis is labeled Year and goes from 1880 to 2010; the vertical axis is labeled Mined shale, million tonnes and goes from 0 to 50. Eight countries' oil production is graphed and stacked to show world production: Estonia, Russia, Brazil, China, Scotland, Germany, Sweden, and United States. Total oil production remains low until around the year 1940, when it increases and peaks at 46 million tonnes around the year 1980; past 1980, the production decreases to 15 million tonnes around the year 2000. From 2000 to 2010, production increases again.

Figure 16.19: Block diagram showing fracking: a vertical well is drilled through numerous sedimentary layers until it reaches a layer labeled

Gas-bearing Formation. Then, the well turns horizontal where it extends throughout the gas-bearing formation. Fracking fluid is pumped from the surface into the well and cracks are formed along the horizontal portion of the well, labeled hydraulic fractures; methane flows from the cracks into the horizontal well segment and flows toward the surface. A preexisting fault is seen to the right of the end of the horizontal well, and an earthquake is shown labeled Induced seismicity.

Figure 16.20: Chart showing the coal rankings: the vertical axis is labeled percentage of fixed carbon and goes from 40 to 100; the horizontal axis is labeled gross calorific value (BTU/LB) and goes from 16,000 on the left to 5,000 on the right. Lignite is colored yellow and fills the chart from 40 to 60 percent carbon and 8,3000 to 5,000 calorific value; subbituminous is colored green and fills the chart from 40 to 60 percent carbon and around 12,000 to 8,3000 calorific value; high-volatile bituminous is colored lavender and fills the chart from 40 to 69 percent carbon and 16,000 to around 12,000 calorific value; medium-volatile bituminous is also colored lavender and fills the chart from 69 to 78 percent carbon and 16,000 to around 13,500 calorific value; low-volatile bituminous is colored red and fills the chart from 78 to 86 percent carbon and 16,000 to around 14,000 calorific value; semi-anthracite is colored orange and fills the chart from 86 to 92 percent carbon and 16,000 to around 13,500 calorific value; anthracite is also colored orange and fills the chart from 92 to 98 percent carbon and around 15,800 to around 12,500 calorific value; and meta-anthracite is also colored orange and fills the chart from 98 to 100 percent carbon and around 12,500 to around 12,000 calorific value.

Figure 16.21: A hand holding an elongated chunk of dull black peat, with a dirt-like texture and visible plant bits grown into it.

Figure 16.22: Chunk of black, very shiny rock.

Figure 16.23: Chunk of glassy white mineral with thin gold veins running through the sample.

Figure 16.24: Vertical outcrop of alternating tan and black horizontal layers.

Figure 16.25: Closeup view of rock with elongated glassy green crystals intergrown with light purple glassy grains.

Figure 16.26: Cross section of a kimberlite pipe: at depth of 0 (the surface) is a bowl- shaped crater filled with washed-back ejecta; surrounding the crater is a raised deposit labeled tuff ring. Deeper into the ground is a thin pipe of orange material that contains smaller grains labeled xenoliths; a bracket labels this section diatreme from 0.5 to 1.5 km depth. at the deepest part of the pipe, a horizontal intrusion of magma labeled dike feeds the vertical pipe; a bracket labels this section root from 2.0 to 2.6 km depth.

Figure 16.27: Cross section of a deep-sea vent; a bulbous pool of magma is beneath the vent, heating the crust and seawater entering through cracks on either side of the vent; the seawater entering from the sides becomes heated above the pool of magma and leaves the vent, releasing oxyanions, REE, and trace metals. There are complex chemical reactions occurring beneath and above the vent.

Figure 16.28: A large terraced open pit mine that contains both gray and red rocks; a haul truck is seen driving in the foreground.

Figure 16.29: A closeup photo of a chunk of rock made up of glassy amber-colored grains, olive green glassy grains, and a light blue glassy grains.

Figure 16.30: Chunk of brick red rock with flecks of gold left behind in a void. A 5 cm scale bar spans the width of the rock sample.

Figure 16.31: Dark mining shaft with rusted cart tracks leading into it. The shaft is carved into a cliffside composed of alternating red and whitish green sandstone and mudstone.

Figure 16.32: World map showing location of Mississippi Valley-Type and clastic- dominated sediment-hosted lead-zinc deposits. Mississippi Valley-Type locations are marked by red diamonds and are scattered across western Canada, the United States, eastern and western Greenland, western and eastern South America, Europe, southern and northeastern Africa, southern and eastern Asia, and Australia. Clastic-dominated deposits are marked by green squares and are located in western Canada, the United States, northern Greenland, the Caribbean, eastern South America, southwestern Africa, Europe, southern and eastern Asia, and Australia.

Figure 16.33: Chunk of heavily weathered tan and porous rock that has unweathered elongated gray and black crystals in the center.

Figure 16.34: Side view of a sand deposit that has layers of tan sand interbedded with layers of gray and black sand; a penny is stuck into the sand for scale.

Figure 16.35: Orange-colored small stream flowing from left to right, emerging from a hole in a squared grey rock on the left; with small sticks and vegetation throughout the area.

Figure 16.36: A quarry carved into a hillside with large blocks of gray and white marble removed.

Figure 16.37: Two photos; the left photo shows a flat expanse of jagged rocks with a person standing among them; there is a mountain range in the distant background. The right photo shows a hand holding a chunk of rough jagged whitish tan rock.

Figure 16.38: Cream-colored translucent crystal with 6 sides. A marker sits next to the sample for scale.

Figure 16.39: An elongated prismatic crystal of light green apatite with a glassy luster.

Figure 16.40: Aerial view of a large dam. The water level is much higher behind the dam than in front of it, and a road bridge runs across the canyon in front of the dam.

Figure 16.41: Two photos of photovoltaic cells on a roof. The top photo is an aerial photo of a circular series of photovoltaic cells with a large green area in the center of the circle and neighborhoods outside the circle. The bottom photo is a closer image of multiple photovoltaic cells which are dark blue rectangular panels with a checkered appearance.

Figure 16.42: World map with the average horizontal irradiation color coded on the map: red to pink areas experience the highest irradiation, up to 7.4 kilowatthours per square meter, while light to dark green areas experience the lowest irradiation, down to 2.2 kilowatthours per square meter. The areas experiencing the highest irradiation are southwest North America, western and easter South America, north-central Africa and southern Africa, the Arabian Peninsula, southwestern Asia, and a large portion of Australia. The areas experiencing the lowest irradation are located toward the poles.

Figure 16.43: Two images; the left is a simple diagram showing a side view of a wind turbine with the white rotor blades labeled and attached to a gray rectangle labeled nacelle that contains a green gear box and yellow cylindrical generator. The generator is attached to a red wire labeled power cables that runs down inside the white tower to the ground. The red wire ends at a tan box on the ground labeled transformer, which is connected by yellow wires to a series of three connected black power structures labeled switchyard. The right image is a photo of a white wind turbine with three blades rising from a green hillslope with low dark green vegetation covering its base.

Figure 16.44: A satellite image of a large river running from the top left toward the right of the image. A dam is visible as a tan line that runs across the river near the center of the image. On the left side of the dam is a large reservoir and on the right side of the dam is a thinner river. The river is surrounded by green landscape along with tan scarps, and there is a series of blue and tans buildings on the left of the dam alongside the river.

Figure 16.45: Photograph of a wide, very gently dipping waterway with visible small steps along its length. The waterway has metal fencing along its sides with a small group of people leaning along the fence looking at the waterway. There are a few trees on either side of the waterway and the rest of the ground around the waterway is paved.

Figure 16.46: Cross sectional diagram showing a black and white building that has a red line going into the building on the right and a blue line exiting the building on the left. The blue line goes down into the ground with arrows labeled cold water pumped down. The blue line branches into multiple segments and as those segments go toward the right, turn into red segments. A single red line goes up out of the ground with arrows labeled steam and hot water, where they enter a gray cylinder sitting on the surface. The gray cylinder is attached to a black cylinder labeled generating station which is connected to power lines above the surface.

Figure 16.47: A yellow circle at the center containing the text types of biomass. On the upper left of the circle is a green rectangle labeled Biomass for direct combustion of heating. Beneath that label are the terms firewood, charcoal, and manure, with a bracket connecting them pointing toward the yellow circle. On the right of the circle is a blue rectangle labeled Biomass for electricity (burned at power plants). Beneath that label are the terms corne, bagasse grown (ethanol), soybeans, rapeseed (biodiesel), used cooking oil (biodiesel), algae grown (biofuels), and plant matter treated to produce cellulosic ethanol, with a bracket connecting them pointing toward the yellow circle. On the lower left of the circle is a purple rectangle labeled Biofuels for powering vehicles. Above that label are the terms land fill gas, crop, forestry residues, and processing wastes from mills, with a bracket connecting them pointing toward the yellow circle.

17. ORIGIN OF THE UNIVERSE AND OUR SOLAR SYSTEM

Learning Objectives

By the end of this chapter, students should be able to:

- Explain the formation of the universe and how we observe it.
- Understand the origin of our Solar System.
- Describe how the objects in our Solar System are identified, explored, and characterized.
- Describe the types of bodies in our Solar System, their locations, and how they formed.
- Explain what influences the temperature of a planet's surface.
- Describe different methods for dating planets and the age of the Solar System.
- Discuss the assumption underlying the Copernican principle and outline its implications for modern-day astronomers.
- Identify where in the Solar System life is most likely sustainable and why.
- Understand the questions underlying the Fermi paradox.

The **universe** began 13.77 billion years ago when energy, matter, and space expanded from a single point. Evidence for the big bang is the cosmic "afterglow" from when the universe was still very dense, and red-shifted light from distant galaxies, which tell us the universe is still expanding.

The big bang produced hydrogen, helium, and lithium, but heavier elements come from nuclear **fusion** reactions in stars. Large stars make elements such as silicon, iron, and magnesium, which are important in forming terrestrial planets. Large stars explode as **supernovae** and scatter the elements into space.

Planetary systems begin with the collapse of a cloud of gas and dust. Material drawn to the center forms a star, and the remainder forms a disk around the star. Material within the disk clumps together to form planets. In our Solar System, rocky planets are closer to the Sun, and ice and gas giants are farther away. This is because temperatures near the Sun were too high for ice to form, but silicate minerals and metals could solidify.

Early Earth was heated by radioactive decay, collisions with bodies from space, and gravitational compression. Heating melted Earth, causing molten metal to sink to Earth's center and form a core, and causing silicate melt to float to the surface and form the mantle and crust. A collision with a planet the size of Mars knocked debris into orbit around Earth, and the debris coalesced into the Moon. Earth's atmosphere is the result of volcanic degassing, contributions by comets and meteorites, and photosynthesis.

The search for **exoplanets** has identified many Earth-sized rocky exoplanets, some of which are in the habitable zones of their stars. These are thought to be rocky worlds like Earth, but the compositions of these planets are not known for certain.

17.1 The Big Bang

According to the **big bang theory**, the universe blinked violently into existence 13.77 billion years ago. The big bang is often described as an explosion, but imagining it as an enormous fireball isn't accurate. The big bang involved a sudden expansion of matter, energy, and space from a single point. The kind of Hollywood explosion that might come to mind involves expansion of matter and energy within space, but during the big bang, space *itself* was created.

At the start of the big bang, the universe was too hot and dense to be anything but a sizzle of particles smaller than atoms, but as it expanded, it also cooled. Eventually some of the particles collided and stuck together. Those collisions produced the simplest elements, hydrogen and helium, which are also the most common elements in the universe, along with a small amount of lithium. Today, hydrogen is still the most abundant element in the universe with its simple structure of just one proton and one electron.

You may wonder how a universe can be created out of nothing or how we can know that the big bang happened at all. Creating a universe out of nothing is mostly beyond the scope of this chapter, but there is a way to think about it. The particles that make up the universe have opposites that cancel each other out, similar to the way that we can add the numbers 1 and −1 to get zero (also known as "nothing"). As far as the math goes, having zero is exactly the same as having a 1 and a −1. It is also exactly the same as having a 2 and a −2, a 3 and a −3, two −1s and a 2, and so on. In other words, *nothing* is really the potential for *something* if you divide it into its opposite parts. As for how we can know that the big bang happened at all, there are very good reasons to accept that it is indeed how our universe came to be.

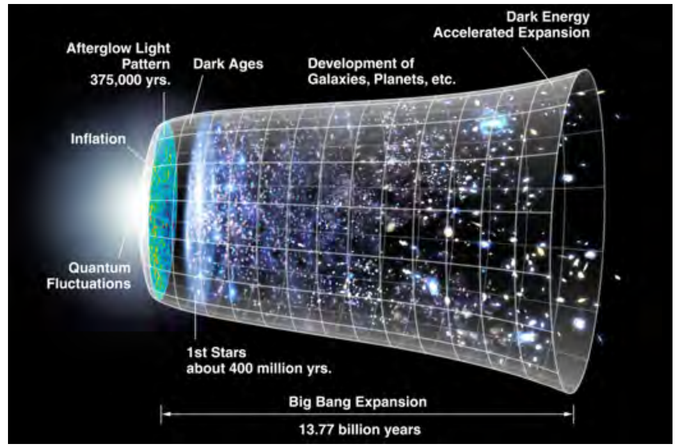

Figure 17.1: The big bang. The universe began 13.77 billion years ago with a sudden expansion of space, matter, and energy, and it continues to expand today. Figure description available at the end of the chapter.

17.1.1 Looking Back to the Early Stages of the Big Bang

The notion of seeing the past is often used metaphorically when we talk about ancient events, but in this case, it is meant literally. In our everyday experience, when we watch an event take place, we perceive that we are watching it as it unfolds in real time. In fact, this isn't true. To see the event, light from that event must travel to our eyes. Light travels very rapidly, but it does not travel instantly. If we were watching a digital clock one meter away from us change from 11:59 a.m. to 12:00 p.m., we would actually see it turn to 12:00 p.m. three billionths of a second after it happened. This isn't enough of a delay to cause us to be late for an appointment, but the universe is a very big place, and the "digital clock" in question is often much, much farther away. In fact, the universe is so big that it is convenient to describe distances in terms of **light years**, or the distance light travels in one year. What this means is that light from distant objects takes so long to get to us that we see those objects as they were at some considerable time in the past. For example, the star Proxima Centauri is 4.24 light years from the sun. If you viewed Proxima Centauri from Earth on January 1, 2015, you would actually see it as it appeared in early October 2010.

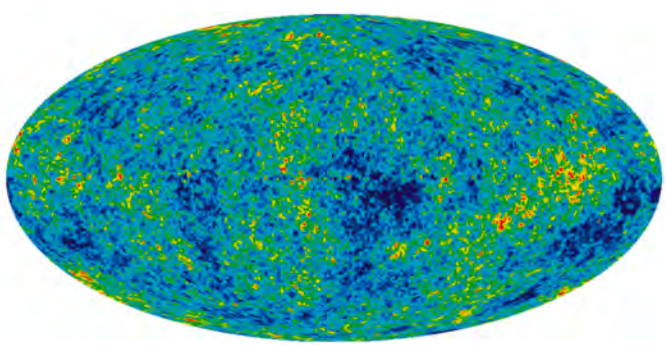

Figure 17.2: Cosmic microwave background (CMB) map of the sky, a baby picture of the universe. The CMB is light from 375,000 years after the big bang. The colors reveal variations in density. Red patches have the highest density, and blue patches have the lowest density. Regions of higher density eventually formed the stars, planets, and other objects seen in space today. Figure description available at the end of the chapter.

We now have tools that are powerful enough to look deep into space and see the arrival of light from early in the universe's history. Astronomers can detect light from approximately 375,000 years after the big bang is thought to have occurred. Physicists tell us that, if the big bang happened, then particles within the universe would still be very close together at this time. They would be so close that light wouldn't be able to travel far without bumping into another particle and getting scattered in another direction. The effect would fill the sky with glowing fog, the "afterglow" from the formation of the universe.

In fact, this is exactly what we see when we look at light from 375,000 years after the big bang. The fog is referred to as the **cosmic microwave background** (CMB), and it has been carefully mapped throughout the sky. The map displays the cosmic microwave background as temperature variations, but these variations translate to differences in the density of matter in the early universe. The red patches are the highest density regions, and the blue patches are the lowest density. Higher-density regions represent the eventual beginnings of stars and planets. The map has been likened to a baby picture of the universe.

17.1.2 The Big Bang is Still Happening, and We Can See the Universe Expanding

The expansion that started with the big bang never stopped. It continues today, and through observation, we can see large clusters of billions of stars (**galaxies**) moving away from us. Though the only exception is the Andromeda galaxy, with which we are on a collision course. The astronomer Edwin Hubble came to this conclusion when he observed that the light from other galaxies was redshifted. The **red shift** is a consequence of the **Doppler effect**. This refers to how we see waves when the object that is creating the waves is moving toward us or away from us.

Figure 17.3: Doppler effect. The ripples made in the direction the car is moving are closer together than the ripples behind the car. Figure description available at the end of the chapter.

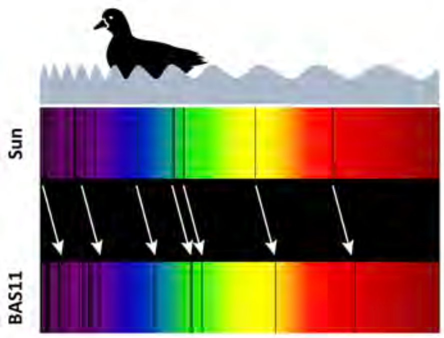

Figure 17.4: Red shift in light from the supercluster BAS11 compared to the sun's light. Black lines represent wavelengths absorbed by atoms (mostly H and He). For BAS11, the black lines are shifted toward the red end of the spectrum compared to the Sun. Figure description available at the end of the chapter.

Before we get to the Doppler effect as it pertains to the red shift, let's see how it works on something more tangible. The swimming duckling is generating waves as it moves through the water. It is generating waves that move forward as well as back, but notice that the ripples ahead of the duckling are closer to each other than the ripples behind the duckling. The distance from one ripple to the next is called the wavelength. The wavelength is shorter in the direction that the duckling is moving and longer as the duckling moves away.

As it pertains to air traveling in sound waves, the different wavelengths manifest as sounds with different pitches—the short wavelengths have a higher pitch, and the long wavelengths have a lower pitch. This is why the pitch of a car's engine changes as the car races past you.

Take this quiz to check your comprehension of this section.

Access the quiz for Section 17.1 by scanning the QR code.

17.2 Overview of Our Planetary System

The Solar System consists of the Sun and many smaller objects: the planets, their moons and rings, and such "debris" as asteroids, comets, and dust. Decades of observation and spacecraft exploration have revealed that most of these objects formed together with the Sun about 4.5 billion years ago. They represent clumps of material that condensed from an enormous cloud of gas and dust. The central part of this cloud became the Sun, and a small fraction of the material in the outer parts eventually formed the other objects.

During the past 50 years, we have learned more about the Solar System than anyone imagined before the Space Age. In addition to gathering information with powerful new telescopes, we have sent spacecraft directly to many members of the **planetary system**. Planetary astronomy is the only branch of our science in which we can, at least vicariously, travel to the objects we want to study. With evocative names such as Voyager, Pioneer, Curiosity, and Pathfinder, our robot explorers have flown past, orbited, or landed on every planet, returning images and data that have dazzled both astronomers and the public. In the process, we have also investigated two dwarf planets, hundreds of fascinating moons, four ring systems, a dozen asteroids, and several comets (smaller members of our Solar System that we will discuss later).

Our probes have penetrated the atmospheres of Jupiter and Saturn and landed on the surfaces of Venus, Mars, our Moon, Saturn's moon Titan, the asteroids Eros, Itokawa, Ryugu, and Bennu, and the comet Churyumov-Gerasimenko (usually referred to as 67P). Humans have set foot on the Moon and returned samples of its surface soil for laboratory analysis. We have flown a helicopter drone on Mars. We have even discovered other places in our Solar System that might be able to support some kind of life.

Section 17.2 is adapted from OpenStax's Astronomy 2e (2022). CC BY 4.0.
It can be accessed for free at https://openstax.org/books/astronomy-2e/pages/7-1-overview-of-our-planetary-system

17.2.1 An Inventory

The Sun, a star that is brighter than about 80% of the stars in the galaxy, is by far the most massive member of the Solar System. It is an enormous ball about 1.4 million kilometers in diameter, with surface layers of incandescent gas and an interior temperature of millions of degrees.

Object	Percentage of total mass of Solar System
Sun	99.8%
Jupiter	0.1%
Comets	0.0005–0.03% (estimate)
All other planets and dwarf planets	0.04%
Moons and rings	0.00005%
Asteroids	0.000002% (estimate)
Cosmic dust	0.0000001% (estimate)

Table 17.1: Mass of members of the Solar System. Note that the Sun is by far the most massive member of the Solar System.

Figure 17.5: Astronauts on the Moon. The lunar lander and surface rover from the Apollo 15 mission are seen in this view of the one place beyond Earth that has been explored directly by humans. Figure description available at the end of the chapter.

Most of the material of the planets in the Solar System is actually concentrated in the largest one, Jupiter, which is more massive than all the rest of the planets combined. Astronomers were able to determine the masses of the planets centuries ago using Kepler's laws of planetary motion and Newton's law of gravity to measure the planets' gravitational effects on one another or on moons that orbit them. Today, we make even more precise measurements of their masses by tracking their gravitational effects on the motion of spacecraft that pass near them.

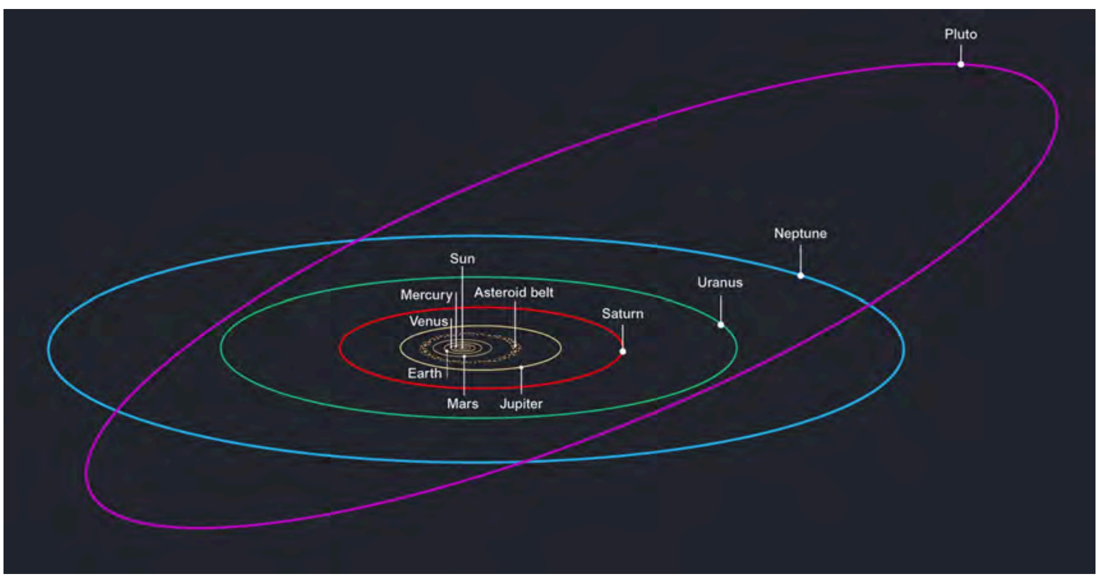

Figure 17.6: Orbits of the planets. All eight major planets orbit the Sun in roughly the same plane. Note that Pluto's orbit is not in the plane of the planets. Figure description available at the end of the chapter.

Beside Earth, five other planets were known to the ancients—Mercury, Venus, Mars, Jupiter, and Saturn—and two were discovered after the invention of the telescope: Uranus and Neptune. The eight planets all **revolve** in the same direction around the Sun. They orbit in approximately the same plane, like cars traveling on concentric tracks on a giant, flat racecourse. Each planet stays in its own "traffic lane," following a nearly circular orbit about the Sun and obeying the "traffic" laws discovered by Galileo, Kepler, and Newton. Besides these planets, we have also been discovering smaller worlds beyond Neptune that are called trans-Neptunian objects or TNOs. The first to be found, in 1930, was Pluto, but others have been discovered during the twenty-first century. One of them, Eris, is about the same size as Pluto and has at least one moon (Pluto has five known moons). The largest TNOs are also classed as dwarf planets, as is the largest asteroid, Ceres. To date, more than 2,600 of these TNOs have been discovered, and one, called Arrokoth, was explored by the New Horizons spacecraft.

Section 17.2 is adapted from OpenStax's Astronomy 2e (2022). CC BY 4.0.
It can be accessed for free at https://openstax.org/books/astronomy-2e/pages/7-1-overview-of-our-planetary-system

Each of the planets and **dwarf planets** also rotates (spins) about an axis running through it, and in most cases, the direction of rotation is the same as the direction of revolution about the Sun. The exceptions are Venus, which rotates backward (that is, in a retrograde direction), and Uranus and Pluto, which also have strange rotations, each spinning about an axis tipped nearly on its side. We do not yet know the spin orientations of the dwarf planets Eris, Haumea, and Makemake.

The rotation rates of the eight planets have been measured as follows. Mercury has a day that lasts 1,408 Earth hours, while Venus has the longest day of any planet at 5,832 Earth hours. Earth and Mars have similar day lengths, with Earth taking 24 hours to complete one rotation and Mars taking 25 hours. The gas giant rotate much faster than the terrestrial planets, with Jupiter having the shortest day at just 10 Earth hours for one rotation. Saturn is slightly slower, with a day length of 11 Earth hours. The two outermost planets, Uranus and Neptune, have day lengths of 17 Earth hours and 16 Earth hours, respectively.

The four planets closest to the Sun (Mercury through Mars) are called the inner, or terrestrial, planets. Often, the Moon is also discussed as a part of this group, bringing the total of terrestrial *objects* to five (we generally call Earth's satellite "the Moon," with a capital M, and the other satellites "moons," with lowercase m's). The terrestrial planets are relatively small worlds, composed primarily of rock and metal. All of them have solid surfaces that bear the records of their geological histories in the forms of craters, mountains, canyons, and volcanoes.

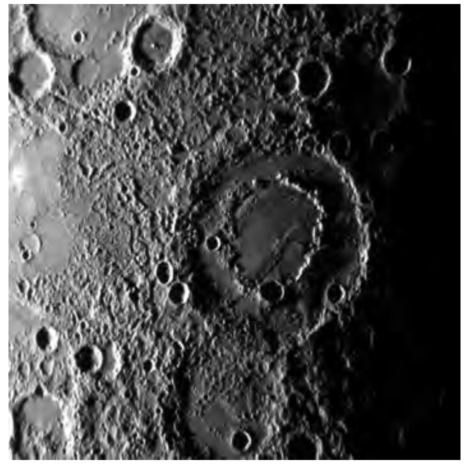

Figure 17.7: Surface of Mercury. The pockmarked face of the terrestrial world of Mercury is more typical of the inner planets than the watery surface of Earth. This image shows Caravaggio, a double-ring impact basin (approximately 160 kilometers in diameter), with another large impact crater on its south-southwestern side. Figure description available at the end of the chapter.

Figure 17.8: Mars Express orbiter view of Olympus Mons with its summit caldera, escarpment, and aureole. Figure description available at the end of the chapter.

Although the terrestrial planets share similar geological features, the size and abundance of these features vary on each planet. For instance, volcanic rock is present on all four inner planets, but Venus has the most volcanoes, with over 1,600 major ones and many smaller ones. In contrast, Mars has fewer than 20 named volcanoes, but it boasts the largest volcanoes in the Solar System, including Olympus Mons, the tallest of them all.

Mars is also home to the largest canyon in the Solar System, the Valles Marineris, which stretches over 3,000 km in length, spans up to 600 km in width, and reaches depths of up to 8 km. By comparison, the Earth's Grand Canyon in Arizona is 800 km long, 30 km across, and 1.8 km deep.

The next four planets (Jupiter through Neptune) are much larger and are composed primarily of lighter ices, liquids, and gases. We call these four the Jovian planets (after "Jove," another name for Jupiter in mythology) or giant planets—a name they richly deserve. About 1,300 Earths could fit inside Jupiter, for example. These planets do not have solid surfaces on which future explorers might land. They are more like vast, spherical oceans with much smaller, dense cores.

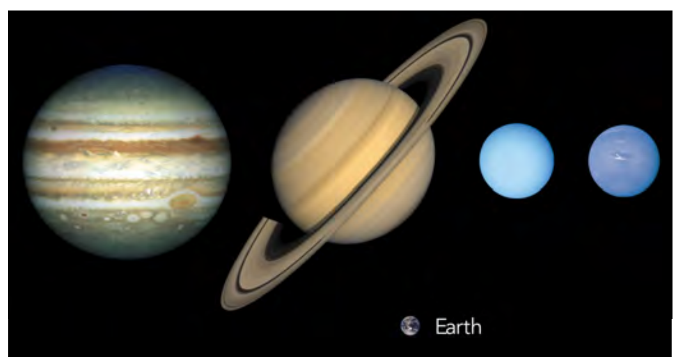

Figure 17.9: This montage shows the four giant planets: Jupiter, Saturn, Uranus, and Neptune. Below them, Earth is shown to scale in terms of size. Distance is not to scale. Figure description available at the end of the chapter.

Section 17.2 is adapted from OpenStax's Astronomy 2e (2022). CC BY 4.0.
It can be accessed for free at https://openstax.org/books/astronomy-2e/pages/7-1-overview-of-our-planetary-system

Name	Distance from Sun (AU)	Revolution period (y)	Diameter (km)	Mass (10^{23} kg)	Density (g/cm^3)
Mercury	0.39	0.24	4,878	3.3	5.4
Venus	0.72	0.62	12,120	48.7	5.2
Earth	1.00	1.00	12,756	59.8	5.5
Mars	1.52	1.88	6,787	6.4	3.9
Jupiter	5.20	11.86	142,984	18,991	1.3
Saturn	9.54	29.46	120,536	5,686	0.7
Uranus	19.18	84.07	51,118	866	1.3
Neptune	30.06	164.82	49,660	1,030	1.6

Table 17.2: The planets.

Near the outer edge of the system lies Pluto, which was the first of the distant icy worlds to be discovered beyond Neptune. Pluto was visited by a spacecraft, the NASA New Horizons mission, in 2015.

Figure 17.10: This intriguing image from the New Horizons spacecraft, taken when it flew by the dwarf planet Pluto in July 2015, shows some of its complex surface features. The rounded white area is called the Sputnik Plain, after humanity's first spacecraft. Figure description available at the end of the chapter.

The outermost part of the Solar System is known as the **Kuiper Belt**, which is a scattering of rocky and icy bodies. Beyond that is the **Oort cloud**, a zone filled with small and dispersed ice traces. These two locations are where most comets form and continue to orbit, and objects found here have relatively irregular orbits compared to the rest of the Solar System. Pluto, formerly the ninth planet, is located in this region of space. The XXVI General Assembly of the International Astronomical Union (IAU) stripped Pluto of planetary status in 2006 because scientists discovered an object more massive than Pluto, which they named Eris. The IAU decided against including Eris as a planet and therefore excluded Pluto as well.

The IAU narrowed the definition of a planet to three criteria: (1) it must orbit a star (in our cosmic neighborhood, the Sun), (2) it must be big enough to have enough gravity to force it into a spherical shape, and (3) it must be big enough that its gravity cleared away any other objects of a similar size near its orbit around the Sun. Pluto passed the first two parts of the definition but not the third. Pluto and Eris are currently classified as dwarf planets.

17.2.2 Smaller Members of the Solar System

Most of the planets are accompanied by one or more moons; only Mercury and Venus move through space alone. There are more than 210 known moons orbiting planets and dwarf planets, and undoubtedly many other small ones remain undiscovered. The largest of the moons are as big as small planets and just as interesting. In addition to our Moon, the Solar System also contains the four largest moons of Jupiter (called the Galilean moons, after their discoverer) and the largest moons of Saturn and Neptune (confusingly named Titan and Triton, respectively).

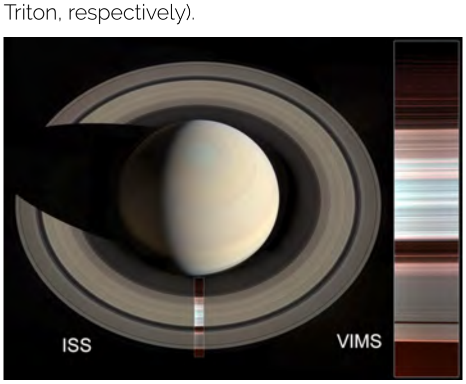

Figure 17.11: Saturn and its A, B, and C rings in visible and (inset) infrared light. In the false-color IR view, greater water ice content and larger grain size lead to blue-green color, while greater non-ice content and smaller grain size yield a reddish hue. Figure description available at the end of the chapter.

Each of the giant planets also has rings made up of countless small bodies ranging in size from mountains to mere grains of dust, all in orbit about the equator of the planet. The bright rings of Saturn are, by far, the easiest to see. They are among the most beautiful sights in the Solar System. However, all four ring systems are interesting to scientists because of their complicated forms, influenced by the pull of the moons that also orbit these giant planets.

The Solar System has many other less-conspicuous members. Another group is the asteroids, rocky bodies that orbit the Sun like miniature planets. Most asteroids are located in the Asteroid Belt, a region between the orbits of Mars and Jupiter (although some do cross the orbits of planets like Earth). A small percentage of asteroids are located outside the main Asteroid Belt. The Trojan asteroids travel along Jupiter's orbit in two loose groups that orbit the Sun, with one group always ahead of Jupiter and the other always behind. Most asteroids are remnants of the initial population of the Solar System that existed before the planets themselves formed. Some of the smallest moons of the planets, such as the moons of Mars, are very likely captured asteroids.

Section 17.2 is adapted from OpenStax's Astronomy 2e (2022). CC BY 4.0.
It can be accessed for free at https://openstax.org/books/astronomy-2e/pages/7-1-overview-of-our-planetary-system

Figure 17.12: Asteroid Eros. This small Earth-crossing asteroid image was taken by the NEAR-Shoemaker spacecraft from an altitude of about 100 kilometers. This view of the heavily cratered surface is about 10 kilometers wide. The spacecraft orbited Eros for a year before landing gently on its surface. Figure description available at the end of the chapter.

Another class of small bodies is composed mostly of ice made of frozen gases such as water, carbon dioxide, and carbon monoxide; these objects are called comets. Comets are also remnants from the formation of the Solar System, but they were formed and continue (with rare exceptions) to orbit the Sun in distant, cooler regions—stored in a sort of cosmic deep freeze. This is also the realm of the larger icy worlds called **dwarf planets**.

Finally, there are countless grains of broken rock, which we call cosmic dust, scattered throughout the Solar System. When these particles enter Earth's atmosphere (as millions do each day), they burn up, producing a brief flash of light in the night sky known as a meteor (meteors are often referred to as shooting stars). Occasionally, some larger chunk of rocky or metallic material survives its passage through the atmosphere and lands on Earth. Any piece that strikes the ground is known as a meteorite. You can see meteorites on display in many natural history museums and can sometimes even purchase pieces of them from gem and mineral dealers.

Figure 17.13: Comet Churyumov-Gerasimenko (67P). This approximately true-color image of the comet was taken by the Rosetta spacecraft on August 6, 2014, at a distance of 120 kilometers. There is surprisingly little color variation across the surface of the comet. Figure description available at the end of the chapter.

17.2.3 A Scale Model of the Solar System

Astronomy often deals with dimensions and distances that far exceed our ordinary experience. What does 1.4 billion kilometers—the distance from the Sun to Saturn—really mean to anyone? It can be helpful to visualize such large systems in terms of a scale model.

In our imaginations, let us build a scale model of the Solar System, adopting a scale factor of 1 billion (10^9)—that is, reducing the actual Solar System by dividing every dimension by a factor of 10^9. Earth, then, has a diameter of 1.3 centimeters, about the size of a grape. The Moon is a pea orbiting this at a distance of 40 centimeters, or a little more than a foot away. This Earth-Moon system fits into a standard backpack.

In this model, the Sun is nearly 1.5 meters in diameter, about the average height of an adult, and our Earth is at a distance of 150 meters—about one city block—from the Sun. Jupiter is five blocks away from the Sun, and its diameter is 15 centimeters, about the size of a very large grapefruit. Saturn is ten blocks from the Sun; Uranus, 20 blocks; and Neptune, 30 blocks. Pluto, with a distance that varies quite a bit during its 249-year orbit, is currently just beyond 30 blocks and getting farther with time. Most of the moons of the outer Solar System are the sizes of various kinds of seeds orbiting the grapefruit, oranges, and lemons that represent the outer planets.

In our scale model, a human is reduced to the dimensions of a single atom, and cars and spacecraft to the size of molecules. Sending the Voyager spacecraft to Neptune involves navigating a single molecule from the Earth-grape toward a lemon five kilometers away with an accuracy equivalent to the width of a thread in a spider's web.

If that model represents the Solar System, where would the nearest stars be? If we keep the same scale, the closest stars would be tens of thousands of kilometers away. If you built this scale model in the city where you live, you would have to place the representations of these stars on the other side of Earth or beyond.

By the way, model solar systems like the one we just presented have been built in cities throughout the world. In Sweden, for example, Stockholm's huge Globe Arena has become a model for the Sun, and Pluto is represented by a 12-centimeter sculpture in the small town of Delsbo, 300 kilometers away. Another model solar system is in Washington on the Mall between the White House and Congress (perhaps proving they are worlds apart?).

Section 17.2 is adapted from OpenStax's Astronomy 2e (2022). CC BY 4.0.
It can be accessed for free at https://openstax.org/books/astronomy-2e/pages/7-1-overview-of-our-planetary-system

Take this quiz to check your comprehension of this section.

Access the quiz for Section 17.2 by scanning the QR code.

17.3 Composition and Structure of Planets

The fact that there are two distinct kinds of planets—the rocky terrestrial planets and the gas-rich Jovian planets—leads us to believe that they formed under different conditions. Certainly their compositions are dominated by different elements. Let us look at each type in more detail.

17.3.1 The Terrestrial Planets

The terrestrial planets are quite different from the giants. In addition to being much smaller, they are composed primarily of rocks and metals. These, in turn, are made of elements that are less common in the universe as a whole. The most abundant rocks, called silicates, are made of silicon and oxygen, and the most common metal is iron. We can tell from their densities that Mercury has the greatest proportion of metals (which are denser) and the Moon has the lowest. Earth, Venus, and Mars all have roughly similar bulk compositions; about one-third of their mass consists of iron-nickel or iron-sulfur combinations, and two-thirds of the mass is from silicates. Because these planets are largely composed of oxygen compounds (such as the silicate minerals of their crusts), their chemistry is said to be oxidized.

When we look at the internal structure of each of the terrestrial planets, we find that the densest metals are in a central core, with the lighter silicates near the surface. If these planets were liquid, like the giant planets, we could understand this effect as the result the sinking of heavier elements due to the pull of gravity. This leads us to conclude that, although the terrestrial planets are solid today, they must have been hot enough to melt at one time.

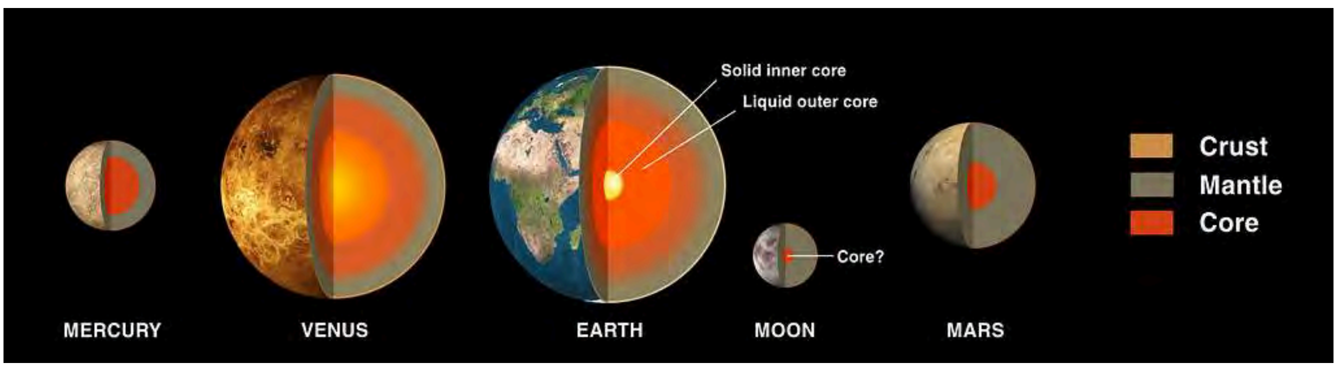

Figure 17.14: Generalized internal structure of terrestrial planets and our Moon. Figure description available at the end of the chapter.

Differentiation is the process by which gravity helps separate a planet's interior into layers of different compositions and densities. The heavier metals sink to form a core, while the lightest minerals float to the surface to form a crust. Later, when the planet cools, this layered structure is preserved. In order for a rocky planet to differentiate, it must be heated to the melting point of rocks, which is typically more than 1300 K.

17.3.2 The Giant Planets

The two largest planets, Jupiter and Saturn, have nearly the same chemical makeup as the Sun; they are composed primarily of the elements hydrogen and helium, with 75% of their mass being hydrogen and 25% helium. On Earth, both hydrogen and helium are gases, so Jupiter and Saturn are sometimes called gas planets. But this name is misleading. Jupiter and Saturn are so large that the gas is compressed in their interior until the hydrogen becomes a liquid. Because the bulk of both planets consists of compressed, liquefied hydrogen, we should really call them liquid planets.

Section 17.3 is adapted from OpenStax's Astronomy 2e (2022). CC BY 4.0.
It can be accessed for free at https://openstax.org/books/astronomy-2e/pages/7-2-composition-and-structure-of-planets

Under the force of gravity, the heavier elements sink toward the inner parts of a liquid or gaseous planet. Both Jupiter and Saturn, therefore, have cores composed of heavier rock, metal, and ice, but we cannot see these regions directly. We must infer the existence of the denser core inside these planets from studies of each planet's gravity. When we look down at each giant planet from above, all we see is a thick atmosphere with swirling clouds. The rapid rotations of Jupiter and Saturn create extreme weather patterns in their atmospheres. Jupiter's atmosphere, for example, features a counterclockwise rotating cyclonic storm in its southern hemisphere known as the **Great Red Spot**, which has been visible to humans for over 300 years.

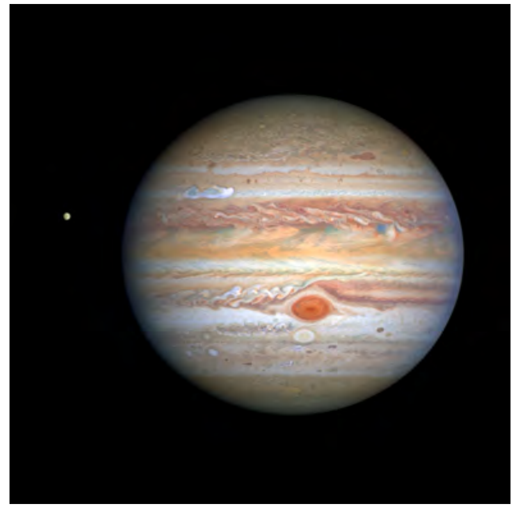

Figure 17.15: Jupiter with its moon Europa on the left. Earth's diameter is 11 times smaller than Jupiter, and four times larger than Europa. Figure description available at the end of the chapter.

Uranus and Neptune are much smaller than Jupiter and Saturn, but each also has a core of rock, metal, and ice. Uranus and Neptune were less efficient at attracting hydrogen and helium gas, so they have much smaller atmospheres in proportion to their cores.

Chemically, each giant planet is dominated by hydrogen and its many compounds. Nearly all the oxygen present is combined chemically with hydrogen to form water (H_2O). Chemists call such a hydrogen-dominated composition reduced. Throughout the outer Solar System, we find abundant water (mostly in the form of ice) and reducing chemistry.

17.3.3 Moons, Asteroids, and Comets

Chemically and structurally, Earth's Moon is like the terrestrial planets, but most moons are in the outer Solar System and have compositions similar to the cores of the giant planets around which they orbit. The four largest moons of Jupiter, known as the Galilean moons, are Ganymede, Callisto, Io, and Europa. They are named after the Italian astronomer Galileo Galilei, who first observed them through a telescope in 1610. The interiors of Ganymede, Io, and Europa have a layered structure. Io has a core, a mantle of partially molten rock, and a crust of solid rock coated with sulfur compounds. Both Europa and Ganymede have iron-rich cores, rocky mantles, and upper layers of water in both ice and liquid forms. Like Europa, Ganymede and Callisto have oceans, but these are deeper and less accessible than Europa's and their seafloors are covered with thick layers of ice.

Most of the asteroids and comets, as well as the smallest moons, were probably never heated to the melting point. However, some of the largest asteroids, such as Vesta, appear to be differentiated; others are fragments from differentiated bodies. Many of the smaller objects seem to be fragments or rubble piles that are the result of collisions. Because most asteroids and comets retain their original compositions, they represent relatively unmodified material dating back to the time of the formation of the Solar System. In a sense, they act as chemical fossils, helping us to learn about a long-ago time whose traces have been erased.

Figure 17.16: Jupiter's moon Ganymede. The brownish gray color of the surface indicates a dusty mixture of rocky material and ice. The bright spots are places where recent impacts have uncovered fresh ice from underneath. Figure description available at the end of the chapter.

17.3.4 Temperatures: Going to Extremes

Generally speaking, the farther a planet or moon is from the Sun, the cooler its surface. The planets are heated by the radiant energy of the Sun, which gets weaker with the square of the distance. You know how rapidly the heating effect of a fireplace or an outdoor radiant heater diminishes as you walk away from it; the same effect applies to the Sun. Mercury, the closest planet to the Sun, has a blistering surface temperature reaching 430°C on its sunlit side, whereas the surface temperature on Pluto is only about –220°C, colder than liquid air. Although it is the closest planet to the Sun, Mercury has no atmosphere to trap the heat, and thus the night side plunges to frigid lows of -180°C.

Mathematically, the temperatures decrease approximately in proportion to the square root of the distance from the Sun. Pluto is about 30 **astronomical units (AU)** at its closest to the Sun (or 100 times the distance of Mercury) and about 49 AU at its farthest from the Sun. Thus, Pluto's temperature is less than that of Mercury by the square root of 100, or a factor of 10: from 500 K to 50 K.

Section 17.3 is adapted from OpenStax's Astronomy 2e (2022). CC BY 4.0.
It can be accessed for free at https://openstax.org/books/astronomy-2e/pages/7-2-composition-and-structure-of-planets

In addition to its distance from the Sun, the surface temperature of a planet can be influenced strongly by its atmosphere. The extreme temperature swings between day and night on Mercury are caused by its lack of atmosphere. Venus's thick atmosphere of carbon dioxide acts as insulation, reducing the escape of heat built up at the surface, which results in an extreme greenhouse effect and temperatures greater than those on Mercury. Temperatures on Venus can reach 471˚C, making it the hottest planet in our Solar System.

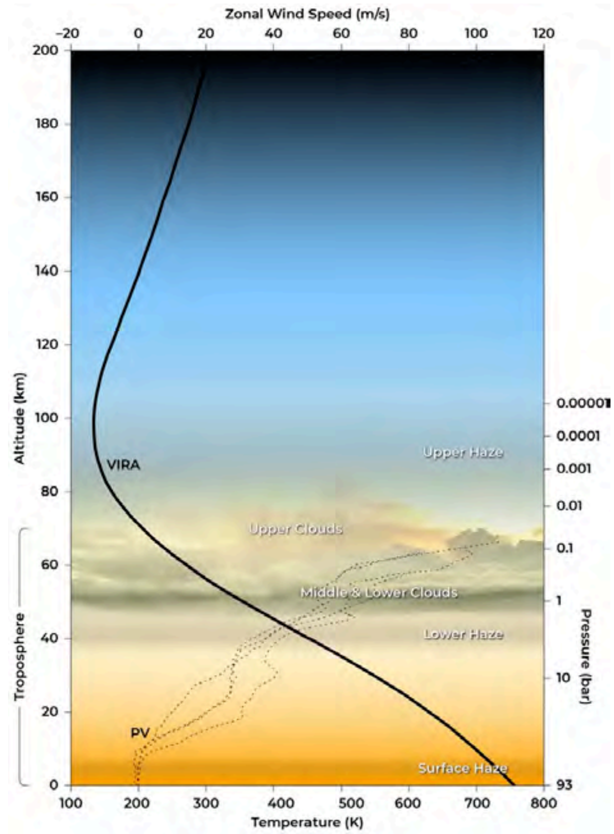

Figure 17.17: The present-day atmosphere of Venus. Black curves show an equatorial temperature profile from the Venus international reference atmosphere (solid) and zonal wind speeds from four Pioneer Venus entry probes (dashed). Figure description available at the end of the chapter.

Today, Earth is the only planet where surface temperatures generally lie between the freezing and boiling points of water. Without our atmospheric insulation (the greenhouse effect, which keeps the heat in), the oceans of Earth would be permanently frozen. As far as we know, Earth is the only planet to support life.

Conversely, if Mars once had a larger atmosphere in the past, it could have supported a more temperate climate than it has today. Today, Mars has a very thin atmosphere, 1% as dense as Earth's. Like Venus, it consists of mostly carbon dioxide along with small amounts of nitrogen, oxygen, and water vapor. However, due to the thin atmosphere, it cannot retain the heat trapped by atmospheric carbon dioxide. Consequently, Martian surface temperatures range from -153˚C to 20˚C.

17.3.5 Dating Planetary Surfaces

How do we know the age of the surfaces we see on planets and moons? If a world has a surface (as opposed to being mostly gas and liquid), astronomers have developed some techniques for estimating how long ago that surface solidified. Note that the age of these surfaces is not necessarily the age of the planet as a whole. On geologically active objects (including Earth), vast outpourings of molten rock or the erosive effects of water and ice, which we call planet weathering, have erased evidence of earlier epochs and present us with only a relatively young surface for investigation.

One way to estimate the age of a surface is by counting the number of impact craters. This technique works because the rate at which impacts have occurred in the Solar System has been roughly constant for several billion years. Thus, in the absence of forces to eliminate craters, the number of craters is simply proportional to the length of time the surface has been exposed. This technique has been applied successfully to many solid planets and moons.

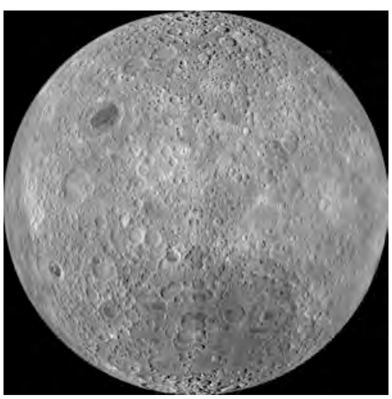
Figure 17.18: Our cratered Moon. This composite image of the Moon's surface was made from many smaller images taken between November 2009 and February 2011 by the Lunar Reconnaissance Orbiter (LRO) and shows craters of many different sizes. Figure description available at the end of the chapter.

Bear in mind that crater counts can tell us only the time since the surface experienced a major change that could modify or erase preexisting craters. Estimating ages from crater counts is a little like walking along a sidewalk in a snowstorm after the snow has been falling steadily for a day or more. You may notice that the snow is deep in front of one house, while next door the sidewalk may be almost clear. Do you conclude that less snow has fallen in front of Ms. Jones' house than Mr. Smith's? More likely, you conclude that Jones has recently swept the walk clean and Smith has not. Similarly, the numbers of craters indicate how long it has been since a planetary surface was last "swept clean" by ongoing lava flows or by molten materials ejected when a large impact happened nearby.

Still, astronomers can use the numbers of craters on different parts of the same world to provide important clues about how regions on that world evolved. On a given planet or moon, the more heavily cratered terrain will generally be older (that is, more time will have elapsed there since something swept the region clean).

Section 17.3.5 is adapted from OpenStax's Astronomy 2e (2022). CC BY 4.0.
It can be accessed for free at https://openstax.org/books/astronomy-2e/pages/7-3-dating-planetary-surfaces

17.3.6 Radioactive Rocks

Another way to trace the history of a solid world is to measure the age of individual rocks. After samples were brought back from the Moon by Apollo astronauts, the techniques that had been developed to date rocks on Earth were applied to rock samples from the Moon to establish a geological chronology for the Moon. Furthermore, a few samples of material from the Moon, Mars, and the large asteroid Vesta have fallen to Earth as meteorites and can be examined directly.

Scientists measure the age of rocks using the properties of natural radioactivity. Around the beginning of the twentieth century, physicists began to understand that some atomic nuclei are not stable but can split apart (decay) spontaneously into smaller nuclei. The process of radioactive decay involves the emission of particles such as electrons or of radiation in the form of **gamma rays**.

For any one radioactive nucleus, it is not possible to predict when the decay process will happen. Such decay is random in nature, like the throw of dice: as gamblers have found all too often, it is impossible to say when the dice will come up 7 or 11. But, for a very large number of dice tosses, we can calculate the odds that 7 or 11 will come up. Similarly, if we have a very large number of radioactive atoms of one type, there is a specific time period, called its half-life, during which the chances are fifty-fifty that decay will occur for any of the nuclei.

A particular nucleus may last a shorter or longer time than its half-life, but in a large sample, almost exactly half of the nuclei will have decayed after a time equal to one half-life. Half of the remaining nuclei will have decayed after two half-lives pass, leaving only one half of a half—or one quarter—of the original sample.

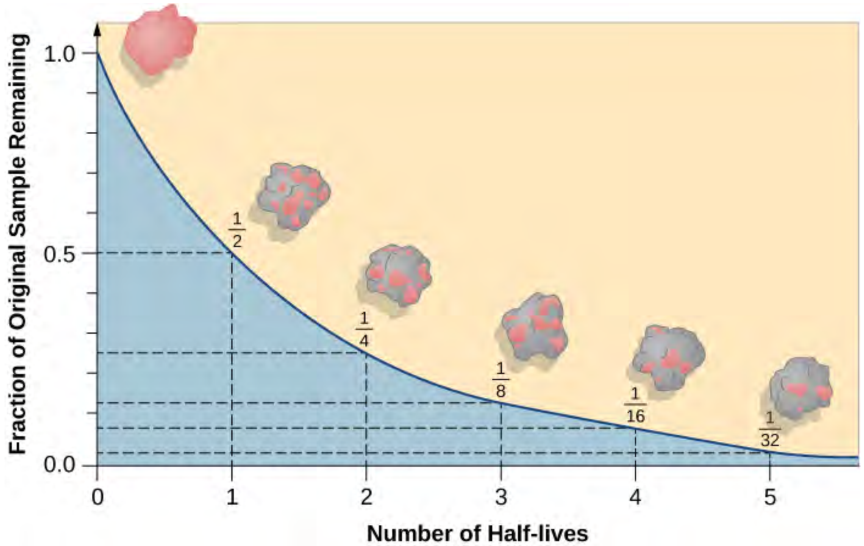

Figure 17.19: Radioactive decay. This graph shows (in pink) the amount of a radioactive sample that remains after several half-lives have passed. After one half-life, half the sample is left; after two half-lives, one half of the remainder (or one quarter) is left; and after three half-lives, one half of that (or one eighth) is left. Note that, in reality, the decay of radioactive elements in a rock sample would not cause any visible change in the appearance of the rock; the splashes of color are shown here for conceptual purposes only. Figure description available at the end of the chapter.

If you had one gram of pure radioactive nuclei with a half-life of 100 years, then after 100 years you would have 1/2 gram; after 200 years, 1/4 gram; after 300 years, only 1/8 gram; and so forth. However, the material does not disappear. Instead, the radioactive atoms are replaced with their decay products. Sometimes the radioactive atoms are called parents and the decay products are called daughter elements.

In this way, radioactive elements with half-lives we have determined can provide accurate nuclear clocks. By comparing how much of a radioactive parent element is left in a rock to how much of its daughter products have accumulated, we can learn how long the decay process has been going on and hence how long ago the rock formed. The following table summarizes the decay reactions used most often to date lunar and terrestrial rocks.

Section 17.3 is adapted from OpenStax's Astronomy 2e (2022). CC BY 4.0.
It can be accessed for free at https://openstax.org/books/astronomy-2e/pages/7-2-composition-and-structure-of-planets

Parent	Daughter	Half-life (billions of years)
Samarium-147	Neodymium-143	106
Rubidium-87	Strontium-87	48.8
Thorium-232	Lead-208	14
Uranium-238	Lead-206	4.47
Potassium-40	Argon-40	1.31

Table 17.3: Radioactive decay reaction used to date rocks. The number after each element is its atomic weight equal to the number of protons plus neutrons in its nucleus. This specifies the isotope of the element, as different isotopes of the same element differ in the number of neutrons.

When astronauts first flew to the Moon, one of their most important tasks was to bring back lunar rocks for radioactive age-dating. Until then, astronomers and geologists had no reliable way to measure the age of the lunar surface. Counting craters had let us calculate relative ages (for example, the heavily cratered lunar highlands were older than the dark lava plains), but scientists could not measure the actual age in years. Some thought that the ages were as young as those of Earth's surface, which has been resurfaced by many geological events. The Moon's surface being so young would imply active geology on our satellite. Only in 1969, when the first Apollo samples were dated, did we learn that the Moon is an ancient, geologically dead world. Using such dating techniques, we have been able to determine the ages of both Earth and the Moon; each was formed about 4.5 billion years ago (although, as we shall see, Earth probably formed earlier than the Moon). Similarly, radioactive dating of meteorites allowed scientists to determine that the Solar System itself is nearly 4.6 billion years old.

Figure 17.20: Sample from NASA's lunar surface collection at Johnson Space Center's vault in Houston, Texas. Figure description available at the end of the chapter.

We should also note that the decay of radioactive nuclei generally releases energy in the form of heat. Although the energy from a single nucleus is not very large (in human terms), the enormous numbers of radioactive nuclei in a planet or moon (especially early in its existence) can be a significant source of internal energy for that world. Geologists estimate that about half of Earth's current internal heat budget comes from the decay of radioactive isotopes in its interior.

Take this quiz to check your comprehension of this section.

Access the quiz for Section 17.3 by scanning the QR code.

17.4 Origin of the Solar System

Much of astronomy is motivated by a desire to understand the origin of things—to find at least partial answers to age-old questions of where the universe, the Sun, Earth, and we ourselves came from. Each planet and moon is a fascinating place that may stimulate our imagination as we try to picture what it would be like to visit. Taken together, the members of the Solar System preserve patterns that can tell us about the formation of the entire system. As we begin our exploration of the planets, we want to introduce our modern picture of how the Solar System formed.

The recent discovery of thousands of planets in orbit around other stars has shown astronomers that many exoplanetary systems can be quite different from our own Solar System. For example, it is common for these systems to include planets intermediate in size between our terrestrial and giant planets. These are often called superearths. Some exoplanet systems even have giant planets close to the star, reversing the order we see in our system.

Section 17.4 is adapted from OpenStax's Astronomy 2e (2022). CC BY 4.0.
It can be accessed for free at https://openstax.org/books/astronomy-2e/pages/7-4-origin-of-the-solar-system

17.4.1 Looking for Patterns

One way to approach our question of origin is to look for regularities among the planets. We found, for example, that all the planets lie in nearly the same plane and revolve in the same direction around the Sun. The Sun also spins in the same direction about its own axis. Astronomers interpret this pattern as evidence that the Sun and planets formed together from a spinning cloud of gas and dust that we call the **solar nebula**.

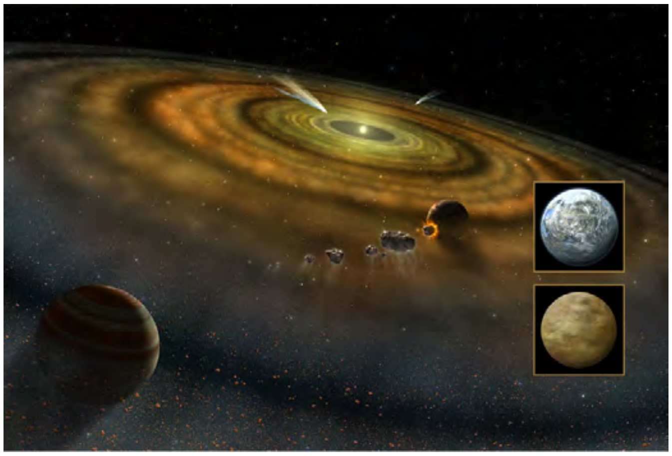

Figure 17.21: NASA artist's conception of various planet formation processes, including exocomets and other planetesimals, around Beta Pictoris, a very young type-AV star. Figure description available at the end of the chapter.

The composition of the planets gives another clue about origins. **Spectroscopic** analysis allows us to determine which elements are present in the Sun and the planets. The Sun has the same hydrogen-dominated composition as Jupiter and Saturn, and therefore it appears to have been formed from the same reservoir of material. In comparison, the terrestrial planets and our Moon are relatively deficient in the light gases and the various ices that form from the common elements oxygen, carbon, and nitrogen. Instead, on Earth and its neighbors, we see mostly the rarer heavy elements such as iron and silicon. This pattern suggests that the processes that led to planet formation in the inner Solar System must somehow have excluded much of the lighter materials that are common elsewhere. These lighter materials must have escaped, leaving a residue of heavy stuff.

The reason for this is not hard to guess, bearing in mind the heat of the Sun. The inner planets and most of the asteroids are made of rock and metal, which can survive heat, but they contain very little ice or gas, which evaporate when temperatures are high (to see what we mean, just compare how long a rock and an ice cube survive when they are placed in the sunlight). In the outer Solar System, where it has always been cooler, the planets and their moons are mostly composed of ice and gas, as are dwarf planets and comets.

17.4.2 The Evidence from Far Away

A second approach to understanding the origins of the Solar System is to look outward for evidence that other systems of planets are forming elsewhere. We cannot look back in time to the formation of our own system, but many stars in space are much younger than the Sun. In these systems, the processes of planet formation might still be accessible to direct observation. We observe that there are many other solar nebulas or circumstellar disks—flattened, spinning clouds of gas and dust surrounding young stars. These disks resemble our own Solar System's initial stages of formation billions of years ago.

Section 17.4 is adapted from OpenStax's Astronomy 2e (2022). CC BY 4.0.
It can be accessed for free at https://openstax.org/books/astronomy-2e/pages/7-4-origin-of-the-solar-system

17.4.3 Building Planets

Circumstellar disks are a common occurrence around very young stars, suggesting that disks and stars form together. Astronomers can use theoretical calculations to see how solid bodies might form from the gas and dust in these disks as they cool. These models show that material begins to coalesce first by forming smaller objects, precursors of planets, which we call **planetesimals**.

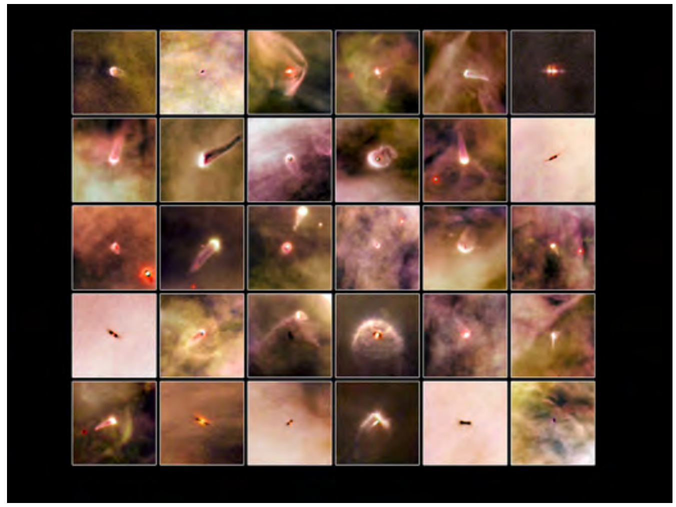

Figure 17.22: Atlas of planetary nurseries. These Hubble Space Telescope photos show sections of the Orion Nebula, a relatively close-by region where stars are currently forming. Each image shows an embedded circumstellar disk orbiting a very young star. Seen from different angles, some are energized to glow by the light of a nearby star, while others are dark and seen in silhouette against the bright glowing gas of the Orion Nebula. Each is a contemporary analog of our own solar nebula—a location where planets are probably being formed today. Credit: modification of work by NASA ESA/Hubble, L. Ricci (ESO). Figure description available at the end of the chapter.

Today's fast computers can simulate the way millions of planetesimals, probably no larger than 100 kilometers in diameter, might gather together under their mutual gravity to form the planets we see today. We are beginning to understand that this process was a violent one, with planetesimals crashing into each other and sometimes even disrupting the growing planets themselves. As a consequence of those violent impacts (and the heat from radioactive elements in them), all the planets were heated until they were liquid and gas and were therefore differentiated, which helps explain their present internal structures.

The process of impacts and collisions in the early Solar System was complex and, apparently, often random. The solar nebula model can explain many of the regularities we find in the Solar System, but the random collisions of massive collections of planetesimals could be the reason for some exceptions to the "rules" of solar system behavior. For example, why do the planets Uranus and Pluto spin on their sides? Why does Venus spin slowly and in the opposite direction from the other planets? Why does the composition of the Moon resemble Earth in many ways and yet exhibit substantial differences? The answers to such questions probably lie in enormous collisions that took place in the solar system long before life on Earth began.

Today, some 4.5 billion years after its origin, the Solar System is—thank goodness—a much less violent place. However, some planetesimals have continued to interact and collide, and their fragments move about the Solar System as roving "transients" that can make trouble for the established members of the Sun's family, such as our own Earth.

Take this quiz to check your comprehension of this section.

Access the quiz for Section 17.4 by scanning the QR code.

17.5 The Search for Life in the Universe

As we have learned more about the universe, we have naturally wondered whether there might be other forms of life out there. The ancient question "Are we alone in the universe?" connects us to generations of humans before us. While in the past, this question was in the realm of philosophy or science fiction, today we have the means to seek an answer through scientific inquiry. In this chapter, we will consider how life began on Earth, whether the same processes could have led to life on other worlds, and how we might seek evidence of life elsewhere. This is the science of **astrobiology**.

The search for life on other planets is not the same as the search for intelligent life, which (if it exists) is surely much rarer. Learning more about the origin, evolution, and properties of life on Earth aids us in searching for evidence of all kinds of life beyond that on our planet.

Astronomers and planetary scientists continue to search for life in the Solar System and the universe at large, with their searches falling into two categories. First is the direct exploration of planets within our own solar system, especially Mars and some of the icy moons of the outer Solar System. Second is the even more difficult task of searching for evidence of life—a **biomarker**—on planets circling other stars. As you will see, the approaches taken are very different, even though the goal of each is the same: to determine if life on Earth is unique in the universe.

Section 17.5 is adapted from OpenStax's Astronomy 2e (2022). CC BY 4.0.
It can be accessed for free at https://openstax.org/books/astronomy-2e/pages/30-thinking-ahead

17.5.1 The Cosmic Context for Life

As the universe aged following the big bang, processes within stars created the other elements, including those that make up Earth (such as iron, silicon, magnesium, and oxygen) and those required for life as we know it (such as carbon, oxygen, and nitrogen). These and other elements combined in space to produce a wide variety of compounds that form the basis of life on Earth.

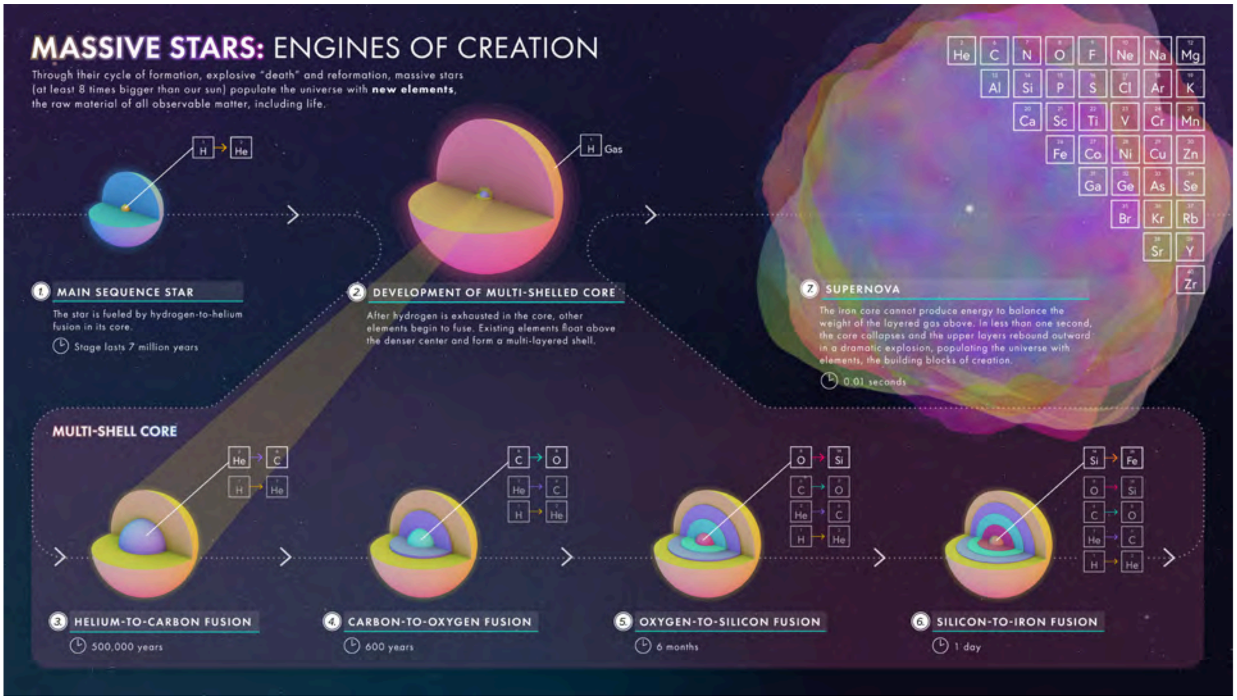

Figure 17.23: This illustration demonstrates how a massive star (at least eight times bigger than our sun) fuses heavier and heavier elements until exploding as a supernova and spreading those elements throughout space. Figure description available at the end of the chapter.

In particular, life on Earth is based on the presence of a key unit known as an **organic molecule**, a molecule that contains carbon. Especially important are the hydrocarbons, chemical compounds made up entirely of hydrogen and carbon, which serve as the basis for our biological chemistry, or **biochemistry**. While we do not understand the details of how life on Earth began, it is clear that, to make creatures like us possible, events like those described above must have occurred, resulting in what is called the chemical evolution of the universe.

The chemical variety and moderate conditions on Earth eventually led to the formation of molecules that could make copies of themselves (reproduce), which is essential for beginning life. Over the billions of years of Earth history, life evolved and became more complex. The course of evolution was punctuated by occasional planet-wide changes caused by collisions with some of the smaller bodies that did not make it into the Sun or one of its accompanying worlds. In fact, mammals may owe their domination of Earth's surface to just such a collision 65 million years ago, which led to the extinction of the dinosaurs (along with the majority of other living things). The details of such mass extinctions are currently the focus of a great deal of scientific interest.

Philosophers of science sometimes call the idea that there is nothing special about our place in the universe the **Copernican principle**. Following this principle, most scientists would be surprised if life were limited to our planet and had started nowhere else. There are billions of stars in our galaxy old enough for life to have developed on a planet around them, and there are billions of other galaxies as well. Astronomers and biologists have long conjectured that a series of events similar to those on the early Earth probably led to living organisms on many planets around other stars and possibly even on other bodies within our Solar System, such as Mars or the moon Europa.

The real scientific issue is whether organic biochemistry is likely or unlikely in the universe at large. Are we a fortunate and exceedingly rare outcome of chemical evolution, or is organic biochemistry a regular part of the chemical evolution of the cosmos? We do not yet know the answer to this question, but data, even an exceedingly small amount (like finding "unrelated to us" living systems on a world like Europa), will help us arrive at it.

17.5.2 Life on Mars

The possibility that Mars hosts (or has hosted) life has a rich history dating back to the "canals" that some people claimed to see on the Martian surface toward the end of the nineteenth century and the beginning of the twentieth. With the dawn of the Space Age came the possibility to address this question up close through a progression of missions to Mars that began with the first successful flyby of a robotic spacecraft in 1964 and have led to the deployment of capable rovers, like Curiosity and Perseverance, with instruments to look for organic chemistry.

The earliest missions to Mars provided some hints that liquid water—one of life's primary requirements—may once have flowed on the surface, and later missions have strengthened this conclusion.

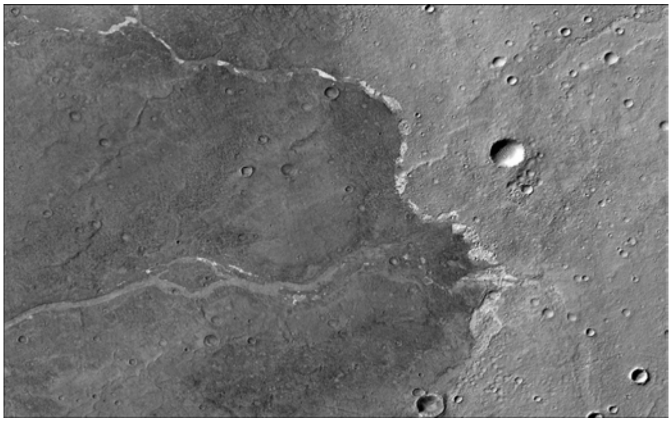

Figure 17.24: NASA's Mars Reconnaissance Orbiter used its Context Camera to capture this image of Bosporos Planum, a location on Mars. The white specks are salt deposits found within a dry channel. The largest impact crater in the scene is nearly one mile (1.5 kilometers) across. Figure description available at the end of the chapter.

The NASA Viking landers, whose purpose was to search directly for evidence of life on Mars, arrived on Mars in 1976. Viking's onboard instruments found no organic molecules (the stuff of which life is made), and no evidence of biological activity in the Martian soils it analyzed.

This result is not particularly surprising because, despite the evidence of flowing liquid water in the past, liquid water on the surface of Mars is generally not stable today. Over much of Mars, temperatures and pressures at the surface are so low that pure water would either freeze or boil away (under very low pressures, water will boil at a much lower temperature than usual). To make matters worse, unlike Earth, Mars has neither a magnetic field nor ozone layer to protect the surface from harmful solar ultraviolet radiation and energetic particles. However, Viking's analyses of the soil said nothing about whether life may have existed in Mars' distant past, when liquid water was more abundant. We do know that water in the form of ice exists in abundance on Mars, not so deep beneath its surface. Water vapor is also a constituent of the atmosphere of Mars.

Since the visit of Viking, our understanding of Mars has deepened spectacularly. Orbiting spacecraft have provided increasingly detailed images of the surface and detected the presence of minerals that could have formed only in the presence of liquid water. Multiple surface missions, including the Mars Exploration Rovers Spirit and Opportunity (2004), followed by the much larger Curiosity rover (2012) and Perseverance rover (2021), confirmed these remote-sensing data.

All of the rovers found abundant evidence for a past history of liquid water, revealed not only from the mineralogy of rocks they analyzed but also from the unique layering of rock formations. Curiosity has gone a step beyond evidence for water and confirmed the existence of habitable environments on ancient Mars. "Habitable" means not only that liquid water was present, but that life's requirements for energy and elemental raw materials could also have been met.

Figure 17.25: The hole that NASA's Curiosity Mars rover drilled into a mudstone. The diameter of the drill hole is about 0.6 inch (1.6 centimeters). The mudstone is interpreted to represent an ancient lake, and it preserves evidence of an environment that would have been suited to support microbes that get their energy by eating chemicals in rocks. Figure description available at the end of the chapter.

17.5.3 Life in the Outer Solar System

The massive gas and ice giant planets of the outer Solar System—Jupiter, Saturn, Uranus, and Neptune—are almost certainly not habitable for life as we know it, but some of their moons might be. Although these worlds in the outer Solar System contain abundant water, they receive so little warming sunlight in their distant orbits that it was long believed they would be "geologically dead" balls of hard, frozen ice and rock. However, missions to the outer Solar System have found something much more interesting.

Jupiter's moon Europa revealed itself to the Voyager and Galileo missions as an active world whose icy surface apparently conceals an ocean with a depth of tens to perhaps a hundred kilometers. As the moon orbits Jupiter, the planet's massive gravity creates tides on Europa—just as our own Moon's gravity creates our ocean tides—and the friction of all that pushing and pulling generates enough heat to keep the water in liquid form. Similar tides act upon other moons if they orbit close to the planet.

Europa has probably had an ocean for most or all of its history, but habitability requires more than just liquid water. Life also requires energy, and because sunlight does not penetrate below the kilometers-thick ice crust of Europa, this would have to be chemical energy.

Section 17.5 is adapted from OpenStax's Astronomy 2e (2022). CC BY 4.0.
It can be accessed for free at https://openstax.org/books/astronomy-2e/pages/30-thinking-ahead

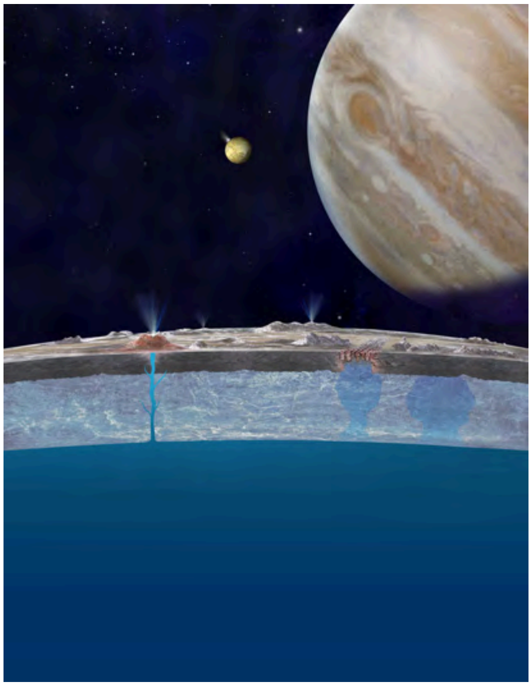

Figure 17.26: Based on new evidence from Jupiter's moon Europa, astronomers hypothesize that chloride salts bubble up from the icy moon's global liquid ocean and reach the frozen surface, where they are bombarded with sulfur from volcanoes on Jupiter's innermost large moon, Io. This illustration of Europa (foreground), Jupiter (right), and Io (middle) is an artist's concept. Figure description available at the end of the chapter.

One of Europa's key attributes from an astrobiology perspective is that its ocean is most likely in direct contact with an underlying rocky mantle, and the interaction of water and rocks—especially at high temperatures, as within Earth's hydrothermal vent systems—yields a reducing chemistry (where molecules tend to give up electrons readily) that is like half of a chemical battery. To complete the battery and provide energy that could be used by life requires the availability of an oxidizing chemistry (where molecules tend to accept electrons readily). On Earth, when chemically reducing vent fluids meet oxygen-containing seawater, the energy that becomes available often supports thriving communities of microorganisms and animals on the seafloor, far from the light of the Sun.

In 2005, the Cassini mission performed a close flyby of a small (500-kilometer diameter) moon of Saturn, Enceladus, and made a remarkable discovery. Plumes of gas and icy material were venting from the moon's south polar region at a collective rate of about 250 kilograms of material per second. Several observations, including the discovery of salts associated with the icy material, suggest that their source is a liquid water ocean beneath tens of kilometers of ice. Although it remains to be shown definitively whether the ocean is local or global, transient or long-lived, it does appear to be in contact with and have reacted to a rocky interior. As on Europa, this is probably a necessary—though not sufficient—condition for habitability. What makes Enceladus so enticing to planetary scientists, though, are those plumes of material that seem to come directly from its ocean: samples of the interior are there for the taking by any spacecraft sent flying through. For a future mission, such samples could yield evidence not only of whether Enceladus is habitable but, indeed, of whether it is home to life.

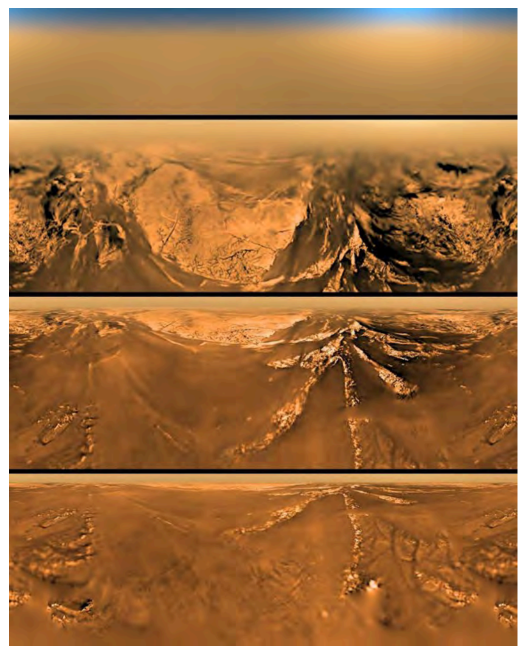

Figure 17.27: These images of Saturn's moon Titan were taken in 2005 by the Huygens probe at four different altitudes. The images are a flattened (Mercator) projection of the view from the descent imager/spectral radiometer on the probe as it landed on Titan's surface. Figure description available at the end of the chapter.

Saturn's big moon Titan is very different from both Enceladus and Europa. Although it may host a liquid water layer deep within its interior, it is the surface of Titan and its unusual chemistry that makes this moon such an interesting place.

Titan's thick atmosphere is composed mostly of nitrogen but also of about 5% methane. In the upper atmosphere, the Sun's ultraviolet light breaks apart and recombines these molecules into more complex organic compounds that are collectively known as **tholins**. The tholins shroud Titan in an orange haze, and imagery from Cassini and from the Huygens probe that descended to Titan's surface show that heavier particles appear to accumulate on the surface, even forming "dunes" that are cut and sculpted by flows of liquid hydrocarbons (such as liquid methane). Some scientists see this organic chemical factory as a natural laboratory that may yield some clues about the Solar System's early chemistry—perhaps even chemistry that could support the origin of life.

17.5.4 Habitable Planets Orbiting Other Stars

One of the most exciting developments in astronomy during the last two decades is the ability to detect **exoplanets**—planets orbiting other stars. Since the discovery of the first exoplanet in 1995, there have been thousands of confirmed detections and many more candidates that are not yet confirmed. These include several dozen possibly habitable exoplanets. Such numbers finally allow us to make some predictions about exoplanets and their life-hosting potential. The majority of stars with mass similar to the Sun appear to host at least one planet, with multi-planet systems like our own not unusual. How many of these planets might be habitable, and how could we search for life there?

In evaluating the prospect for life in distant planetary systems, astrobiologists have developed the idea of a **habitable zone**—a region around a star where suitable conditions might exist for life. This concept focuses on life's requirement for liquid water, and the habitable zone is generally thought of as the range of distances from the central star in which water could be present in liquid form at a planet's surface. In our own Solar System, for example, Venus has surface temperatures far above the boiling point of water and Mars has surface

Section 17.5 is adapted from OpenStax's Astronomy 2e (2022). CC BY 4.0.
It can be accessed for free at https://openstax.org/books/astronomy-2e/pages/30-thinking-ahead

temperatures that are almost always below the freezing point of water. Earth, which orbits between the two, has a surface temperature that is "just right" to keep much of our surface water in liquid form.

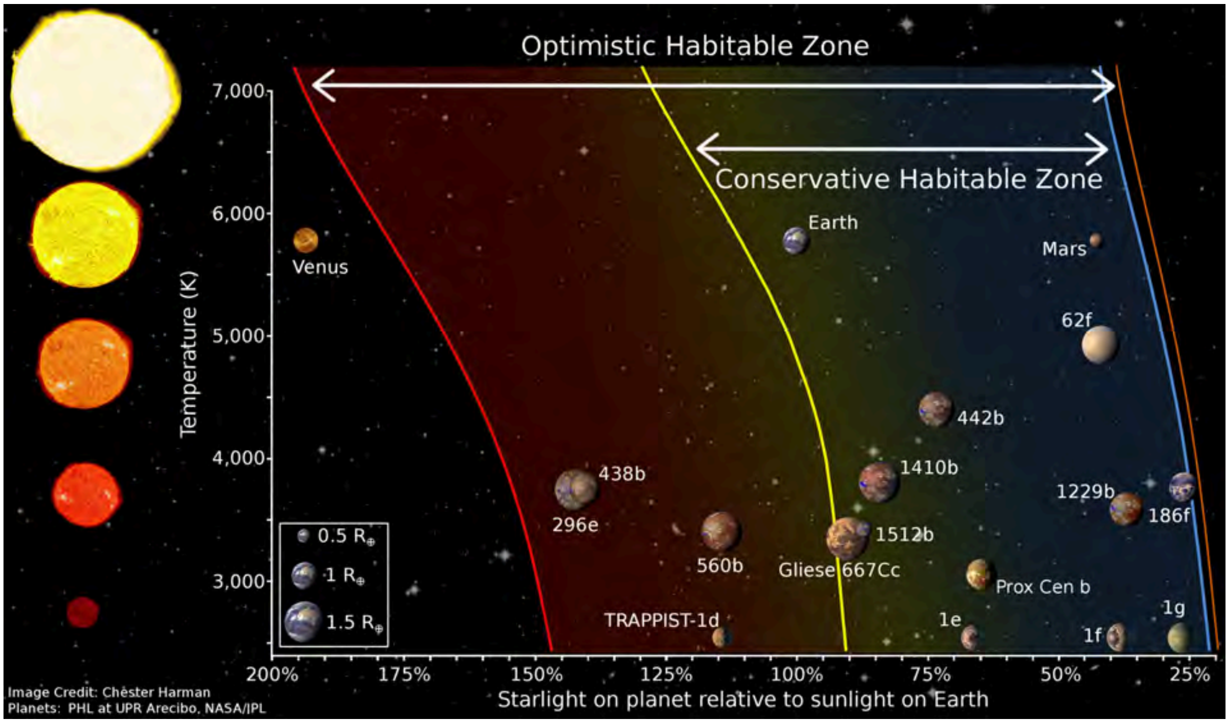

Figure 17.28: Diagram explaining the habitable zone. Shown is temperature in relation to starlight received. Important exoplanets are placed on the diagram, plus Earth, Venus, and Mars. Figure description available at the end of the chapter.

Whether surface temperatures are suitable for maintaining liquid water depends on a planet's "radiation budget"—how much starlight energy it absorbs and retains—and whether or how processes like winds and ocean circulation distribute that energy around the planet. How much stellar energy a planet receives, in turn, depends on how much and what sort of light the star emits, how far the planet is from that star, how much it reflects back to space, and how effectively the planet's atmosphere can retain heat through the greenhouse effect. All of these can vary substantially, and all matter a lot. We must consider the nature of any atmosphere as well as the distance from the star in evaluating the range of habitability.

Even when planets orbit within the habitable zone of their star, it is no guarantee that they are habitable. For example, Venus today has virtually no water, so even if it were suddenly moved to a "just right" orbit within the habitable zone, a critical requirement for life would still be lacking.

Scientists are working to understand all the factors that define the habitable zone and the habitability of planets orbiting within that zone; such an understanding will be our primary guide in targeting exoplanets on which to seek evidence of life. As technology for detecting exoplanets has advanced, so too has our potential to find Earth-size worlds within the habitable zones of their parent stars. Of the confirmed or candidate exoplanets known at the time of writing, nearly 300 are considered to be orbiting within the habitable zone and more than 10% of those are roughly Earth-size.

17.5.5 Communicating with the Stars

It seems likely that life could have developed on many planets around other stars. Even if that life is microbial, we may soon have ways to search for chemical biosignatures. This search is of fundamental importance for understanding biology, but it does not answer the question "Are we alone?" When we ask this question, many people think of other intelligent creatures, perhaps beings that have developed technology similar to our own. If any intelligent, technical civilizations have arisen, as has happened on Earth in the most recent blink of cosmic time, how could we make contact with them?

If we want to get in touch with intelligent life around other stars, we could travel or we could try to exchange messages. Because of the great distances involved, **interstellar** space travel would be very slow and prohibitively expensive. The fastest spacecraft the human species has built so far would take almost 80,000 years to get to the nearest star. While we could certainly design a faster craft, the more quickly it must travel, the greater the energy cost involved. To reach neighboring stars in less than a human life span, we would have to travel close to the **speed of light**.

Section 17.5 is adapted from OpenStax's Astronomy 2e (2022). CC BY 4.0.
It can be accessed for free at https://openstax.org/books/astronomy-2e/pages/30-thinking-ahead

While space travel by living creatures seems very difficult, robot probes can travel over long distances and over long periods of time. Five spacecraft—two Pioneers, two Voyagers, and New Horizons—are leaving the Solar System. At their coasting speeds, they will take hundreds of thousands or millions of years to get anywhere close to another star. On the other hand, they were the first products of human technology to go beyond our home system, so we wanted to put messages on board to show where they came from. Each Pioneer carries a plaque with a pictorial message engraved on a gold-anodized aluminum plate. The Voyagers, launched in 1977, have audio and video records attached, which allowed the inclusion of over 100 photographs and a selection of music from around the world.

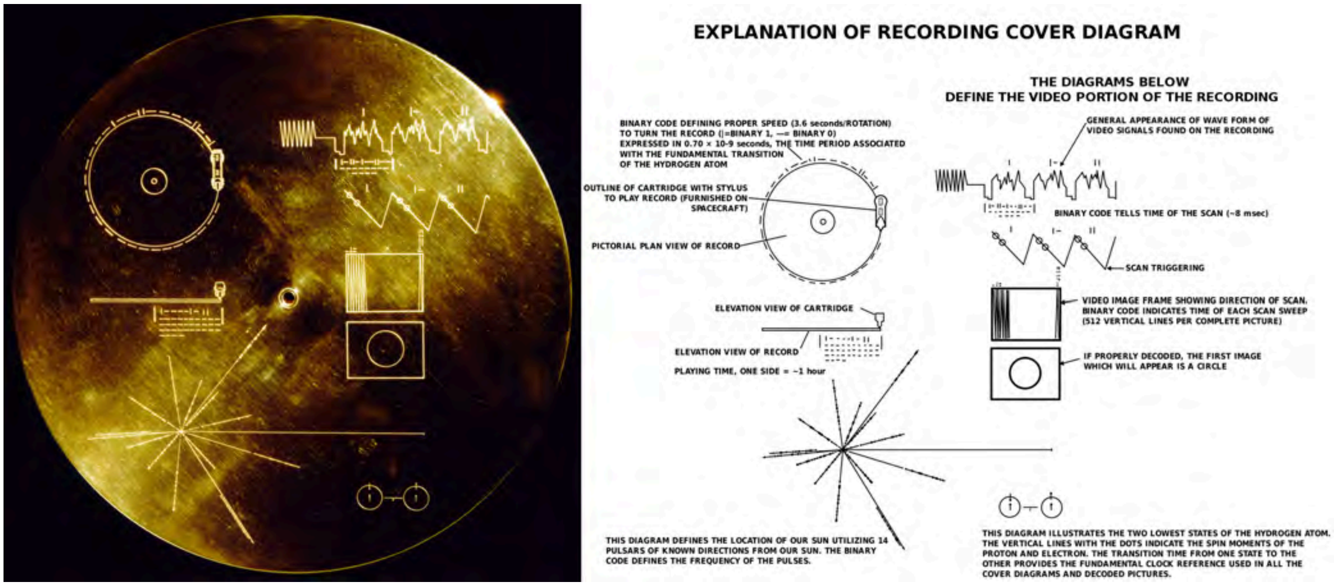

Figure 17.29: The Voyager message is carried by a phonograph record, a 12-inch gold-plated copper disk containing sounds and images selected to portray the diversity of life and culture on Earth. The Golden Record cover is shown here with its extraterrestrial instructions detailed on the right. Figure description available at the end of the chapter.

Given the enormous space between stars in our section of the galaxy, it is very unlikely that these messages will ever be received by anyone. They are more like a note in a bottle thrown into the sea by a shipwrecked sailor, with no realistic expectation of its being found soon but a slim hope that perhaps someday, somehow, someone will know of the sender's fate.

If direct visits among stars are unlikely, we must turn to the alternative for making contact: exchanging messages. Here, the news is a lot better. We already use a messenger—light or, more generally, **electromagnetic waves**—that moves through space at the fastest speed in the universe. Traveling at 300,000 kilometers per second, light reaches the nearest star in only four years and does so at a tiny fraction of the cost of sending material objects. These advantages are so clear and obvious that we assume they will occur to any other species of intelligent beings that develop technology.

However, we have access to a wide spectrum of **electromagnetic radiation**, ranging from the longest-wavelength radio waves to the shortest-wavelength gamma rays. Which would be the best for interstellar communication? It would not be smart to select a wavelength that is easily absorbed by interstellar gas and dust or one that is unlikely to penetrate the atmosphere of a planet like ours. Nor would we want to pick a wavelength that has lots of competition for attention in our neighborhood.

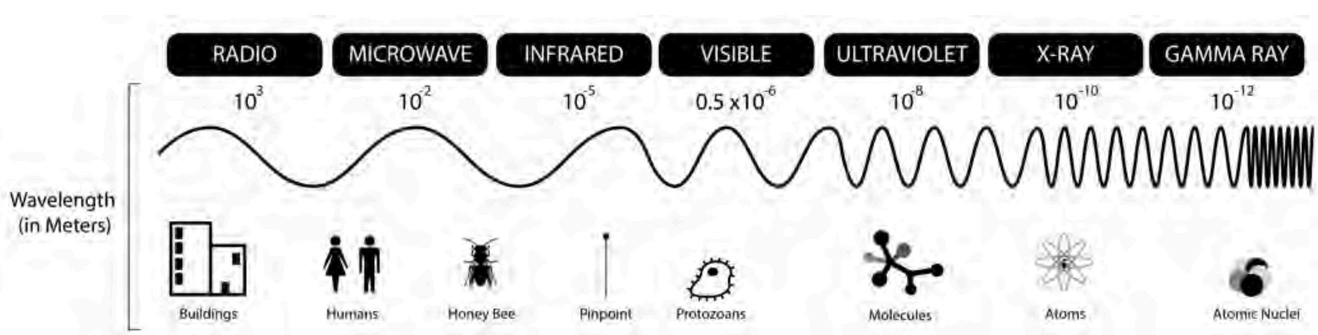

Figure 17.30: The electromagnetic (EM) spectrum. Figure description available at the end of the chapter.

Section 17.5 is adapted from OpenStax's Astronomy 2e (2022). CC BY 4.0.
It can be accessed for free at https://openstax.org/books/astronomy-2e/pages/30-thinking-ahead

One final criterion makes the selection easier; we want the radiation to be inexpensive enough to produce in large quantities. When we consider all these requirements, radio waves turn out to be the best answer. Being the lowest-frequency (and lowest-energy) band of the spectrum, they are not very expensive to produce, and we already use them extensively for communications on Earth. They are not significantly absorbed by interstellar dust and gas. With some exceptions, they easily pass through Earth's atmosphere and through the atmospheres of the other planets with which we are acquainted.

17.5.6 The Cosmic Haystack

Having made the decision that radio is the most likely means of communication among intelligent civilizations, we still have many questions and a daunting task ahead of us. Shall we send a message, or try to receive one? Obviously, if every civilization decides to receive only, then no one will be sending and everyone will be disappointed. On the other hand, it may be appropriate for us to begin by listening, since we are likely to be among the most primitive civilizations in the galaxy interested in exchanging messages.

We do not make this statement to insult the human species (of which, with certain exceptions, we are rather fond). Instead, we base it on the fact that humans have had the ability to receive (or send) a radio message across interstellar distances for only a few decades. Compared to the ages of the stars and the galaxy, this is a mere instant. If there are civilizations out there that are ahead of us in development by even a short time (in the cosmic sense), they are likely to have a technology head start of many, many years. In other words, we, who have just started, may well be the "youngest" species in the galaxy with this capability.

Just as the youngest members of a community are often told to be quiet and listen to their elders for a while before they say something foolish, so may we want to begin our exercise in extraterrestrial communication by listening. Even restricting our activities to listening, however, leaves us with an array of challenging questions. For example, if an extraterrestrial civilization's signal is too weak to be detected by our present-day radio telescopes, we will not detect them. In addition, it would be very expensive for an extraterrestrial civilization to broadcast on a huge number of channels. Most likely, they select one or a few channels for their particular message. Communicating on a narrow band of channels also helps distinguish an artificial message from the radio static that comes from natural cosmic processes. But the radio band contains an astronomically large number of possible channels. How can we know in advance which one they have selected and how they have coded their message into the signal?

Because their success depends on either guessing right about many factors or searching through all the possibilities for each factor, some scientists have compared their quest to looking for a needle in a haystack. However, this has not stopped scientists from trying. Receivers are constantly improving, and the sensitivity of search for extraterrestrial intelligence (**SETI**) programs is advancing rapidly. Equally important, modern electronics and software allow simultaneous searches on millions of frequencies (channels). If we can thus cover a broad frequency range, the cosmic haystack problem of guessing the right frequency largely goes away. One powerful telescope array (funded with an initial contribution from Microsoft founder Paul Allen) built for SETI searches is the Allen Telescope in Northern California.

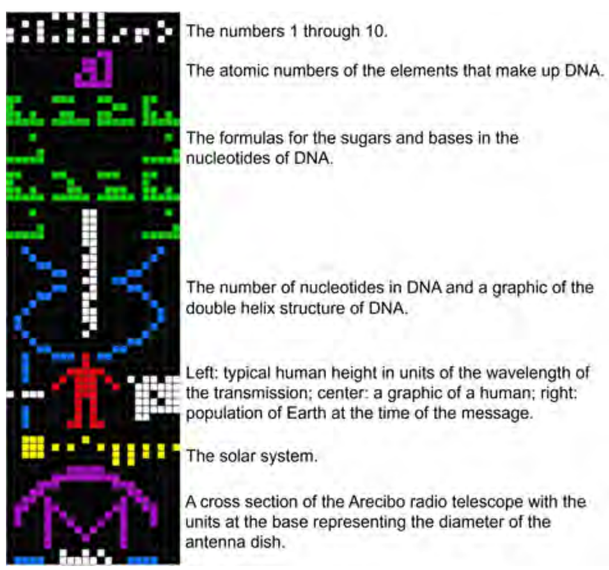

Figure 17.31: A graphical representation of the Arecibo message, as sent 1974 from the Arecibo Observatory, humanity's first attempt to use radio waves to actively communicate its existence to alien civilizations. The message consists of 1,679 bits, arranged into 73 lines of 23 characters per line (both prime numbers, which could help the aliens decode the message). The "ones" and "zeroes" were transmitted by frequency shifting at the rate of 10 bits per second. Figure description available at the end of the chapter.

Section 17.5 is adapted from OpenStax's Astronomy 2e (2022). CC BY 4.0.
It can be accessed for free at https://openstax.org/books/astronomy-2e/pages/30-thinking-ahead

Other radio telescopes being used for such searches have included the giant Arecibo radio dish in Puerto Rico (which, sadly, collapsed due to storm damage in late 2020); the recently completed, and even larger, FAST dish in China; and the Green Bank Telescope in West Virginia, which is the largest steerable radio telescope in the world.

What kind of signals do we hope to pick up? We on Earth are inadvertently sending out a flood of radio signals, dominated by military radar systems. This is a kind of leakage signal, similar to the wasted light energy that is beamed upward by poorly designed streetlights and advertising signs. Could we detect a similar leakage of radio signals from another civilization? The answer is just barely, but only for the nearest stars. For the most part, therefore, current radio SETI searches are looking for beacons, assuming that civilizations might be intentionally drawing attention to themselves or perhaps sending a message to another world or outpost that lies in our direction. Our prospects for success depend on how often civilizations arise, how long they last, and how patient they are about broadcasting their locations to the cosmos.

17.5.7 The Fermi Paradox

If the Copernican principle is applied to life, then biology may be rather common among planets. Taken to its logical limit, the Copernican principle also suggests that intelligent life like us might be common. Intelligence like ours has some very special properties, including an ability to make progress through the application of technology. Organic life around other (older) stars may have started a billion years earlier than on Earth, so they may have had a lot more time to develop advanced technology, such as sending information, probes, or even life forms between stars.

Faced with such a prospect, physicist Enrico Fermi asked a question several decades ago that is now called the **Fermi paradox**: "Where are they?" If life and intelligence are common and have such tremendous capacity for growth, why is there not a network of galactic civilizations whose presence extends even into a "latecomer" planetary system like ours?

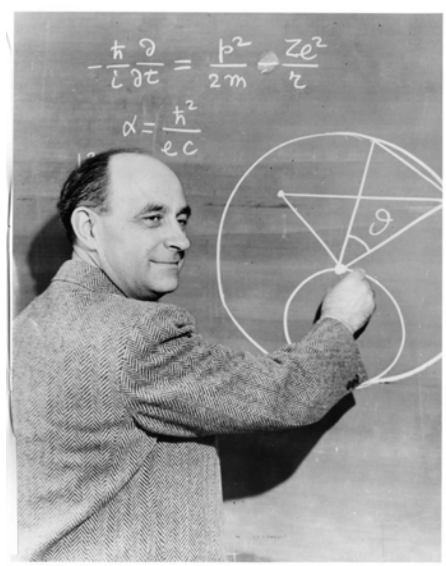

Figure 17.32: Enrico Fermi (born Sept. 29, 1901, Rome, Italy—died Nov. 28, 1954, Chicago, Illinois, US) was an Italian-born American scientist who was one of the chief architects of the Nuclear Age. Figure description available at the end of the chapter.

Several solutions have been suggested to the Fermi paradox. Perhaps life is common, but intelligence (or at least technological civilization) is rare. Perhaps such a network will come about in the future but has not yet had the time to develop. Maybe there are invisible streams of data flowing past us all the time that we are not advanced enough or sensitive enough to detect. Maybe advanced species make it a practice not to interfere with immature, developing consciousnesses such as our own. Or perhaps civilizations that reach a certain level of technology then self-destruct, meaning there are no other civilizations now existing in our galaxy. We do not yet know whether any advanced life is out there, and if it is, we don't know why we aren't aware of it.

Summary

Our Solar System currently consists of the Sun, eight planets, five dwarf planets, nearly 200 known moons, and a host of smaller objects. The planets can be divided into two groups: the inner terrestrial planets and the outer giant planets. Smaller members of the Solar System include asteroids (including the dwarf planet Ceres), which are rocky and metallic objects found mostly between Mars and Jupiter; comets, which are made mostly of frozen gases and generally orbit far from the Sun; and countless smaller grains of cosmic dust. When a meteor survives its passage through our atmosphere and falls to Earth, we call it a meteorite.

The ages of the surfaces of objects in the Solar System can be estimated by counting craters; on a given world, a more heavily cratered region will generally be older than one that is less cratered. We can also use samples of rocks with radioactive elements in them to obtain the time since the layer in which the rock formed last solidified. The half-life of a radioactive element is the time it takes for half the sample to decay; we determine how many half-lives have passed by how much of a sample remains the radioactive element and how much has become the decay product. In this way, we have estimated the age of the Moon and Earth to be roughly 4.5 billion years.

Regularities among the planets have led astronomers to hypothesize that the Sun and the planets formed together in a giant, spinning cloud of gas and dust called the solar nebula. Astronomical observations show tantalizingly similar circumstellar disks around other stars. Within the solar nebula, material first coalesced into planetesimals; many of these gathered together to make the planets and moons. The remainder can still be seen as comets and asteroids. All planetary systems have probably formed in similar ways, but many exoplanet systems have evolved along quite different paths.

Section 17.5 is adapted from OpenStax's Astronomy 2e (2022). CC BY 4.0.
It can be accessed for free at https://openstax.org/books/astronomy-2e/pages/30-thinking-ahead

Life is made up of chemical combinations of elements made by stars. The Copernican principle, which suggests that there is nothing special about our place in the universe, implies that life's development on Earth means that it should be able to develop in other places as well. The Fermi paradox asks why, if life is common, more advanced life forms have not contacted us.

The search for life beyond Earth offers several intriguing targets. Mars appears to have been more similar to Earth during its early history than it is now, with evidence for liquid water on its ancient surface and perhaps even now below ground. In the outer Solar System, the moons Europa and Enceladus likely host vast sub-ice oceans that may directly contact the underlying rocks—a good start in providing habitable conditions—while Titan offers a fascinating laboratory for understanding the sorts of **organic chemistry** that might ultimately provide materials for life. The last decade of research on exoplanets leads us to believe that there may be billions of habitable planets in the Milky Way galaxy. Study of these worlds offers the potential to find biomarkers indicating the presence of life.

Some astronomers are engaged in the search for extraterrestrial intelligent life (SETI). Because other planetary systems are so far away, traveling to the stars is either very slow or extremely expensive (in terms of energy required). Despite many UFO reports and tremendous media publicity, there is no evidence that any of these instances are related to extraterrestrial visits. Scientists have determined that the best way to communicate with any intelligent civilizations out there is by using electromagnetic waves, and radio waves seem best suited to the task. So far, they have only begun to comb the many different possible stars, frequencies, signal types, and other factors that make up what we call the cosmic haystack problem.

Take this quiz to check your comprehension of this chapter.

Access the quiz for Chapter 17 by scanning the QR code.

Text References

1. Parts of this chapter are from OpenStax's *Astronomy 2e* (2022). CC BY 4.0. Specifically, section 17.2 can be accessed for free at https://openstax.org/books/astronomy-2e/pages/7-1-overview-of-our-planetary-system, section 17.3 can be accessed for free at https://openstax.org/books/astronomy-2e/pages/7-2-composition-and-structure-of-planets, section 17.3.5 can be accessed for free at https://openstax.org/books/astronomy-2e/pages/7-3-dating-planetary-surfaces, section 17.4 can be accessed for free at https://openstax.org/books/astronomy-2e/pages/7-4-origin-of-the-solar-system, and section 17.5 can be accessed for free at https://openstax.org/books/astronomy-2e/pages/30-thinking-ahead.
2. Chapter 17 Origin of Earth and the Solar System (CC BY 4.0) by Karla Panchuk was added from Earle, S. (2019). *Physical geology, 2nd edition:* BCcampus. https://opentextbc.ca/physicalgeology2ed/chapter/22-1-starting-with-a-big-bang

Figure References

Figure 17.1: The big bang. NASA/WMAP Science Team. 2006. Public domain. https://en.wikipedia.org/wiki/File:CMB_Timeline300_no_WMAP.jpg

Figure 17.2: Cosmic microwave background (CMB) map of the sky, a baby picture of the universe. NASA/WMAP Science Team. 2012. Public domain. https://commons.wikimedia.org/wiki/File:Ilc_9yr_moll4096.png

Figure 17.3: Doppler effect. Charly Whisky. 2007. CC BY-SA 3.0. https://commons.wikimedia.org/wiki/File%3ADopplerfrequenz.gif

Figure 17.4: Red shift in light from the supercluster BAS11 compared to the Sun's light. Kindred Grey. 2022. CC BY 4.0. Includes Duck by parkjisun from Noun Project (Noun Project license).

Figure 17.5: Astronauts on the Moon. NASA Johnson Space Center; Restored by Bammesk. 1971. Public domain. https://en.wikipedia.org/wiki/File:AS15-88-11866_-_Apollo_15_flag,_rover,_LM,_Irwin_-_restoration1.jpg

Figure 17.6: Orbits of the planets. Arabik4892. 2022. CC BY-SA 4.0. https://commons.wikimedia.org/wiki/File:Planet_Orbits.jpg

Figure 17.7: Surface of Mercury. NASA/Johns Hopkins University Applied Physics Laboratory/Carnegie Institution of Washington. 2009. Public domain. https://commons.wikimedia.org/wiki/File:Mercury_Double-Ring_Impact_Basin.png

Figure 17.8: Mars Express orbiter view of Olympus Mons with its summit caldera, escarpment, and aureole. ESA/DLR/FUBerlin/AndreaLuck. March 2023. CCY BY. https://en.wikipedia.org/wiki/Olympus_Mons#/media/File:Olympus_Mons_-_ESA_Mars_Express_-_Flickr_-_Andrea_Luck.png

Figure 17.9: The four giant planets. Solar System Exploration, NASA. 2008. Public domain. https://commons.wikimedia.org/wiki/File:Gas_planet_size_comparisons.jpg

Figure 17.10: This intriguing image from the New Horizons spacecraft, taken when it flew by the dwarf planet Pluto in July 2015, shows some of its complex surface features. NASA / Johns Hopkins University Applied Physics Laboratory/Southwest Research Institute. 2015. Public domain. https://en.wikipedia.org/wiki/File:Pluto-01_Stern_03_Pluto_Color_TXT.jpg

Figure 17.11: Saturn and its A, B, and C rings in visible and (inset) infrared light. NASA/JPL-Caltech/Space Science Institute/G. Ugarkovic (ISS), NASA/JPL-Caltech/University of Arizona/CNRS/LPG-Nantes (VIMS). 2019. Public domain. https://commons.wikimedia.org/wiki/File:PIA23170-Saturn-Rings-IR-Map-20190613.jpg

Figure 17.12: Asteroid Eros. NASA/JPL/JHUAPL. 2000. Public domain. https://commons.wikimedia.org/wiki/File:Eros_-_PIA02923_(color).jpg

Figure 17.13: Comet Churyumov-Gerasimenko (67P). ESA/Rosetta/MPS for OSIRIS Team MPS/UPD/LAM/IAA/SSO/INTA/UPM/DASP/IDA. 2014. CC BY-SA 4.0. https://commons.wikimedia.org/wiki/File:Comet_67P_True_color.jpg

Figure 17.14: Generalized internal structure of terrestrial planets. Wikimedia Commons. Retrieved October 2024. Public domain. https://commons.wikimedia.org/wiki/File:Terrestial_Planets_internal_en.jpg

Figure 17.15: Jupiter with its moon Europa on the left. NASA, ESA, STScI, A. Simon (Goddard Space Flight Center), and M.H. Wong (University of California, Berkeley) and the OPAL team. 2020. Public domain. https://commons.wikimedia.org/wiki/File:Jupiter_and_Europa_2020.tiff

Figure 17.16: Jupiter's moon Ganymede. NOAA. 2009. Public domain. https://commons.wikimedia.org/wiki/File:Moon_Ganymede_by_NOAA.jpg

Figure 17.17: The present-day atmosphere of Venus. J.G. O'Rourke, C.F. Wilson, and M.E. Borrelli, et al. February 2023. CC BY-SA. https://en.wikipedia.org/wiki/Atmosphere_of_Venus#/media/File:11214_2023_956_Fig6_HTML.webp

Figure 17.18: Our cratered Moon. NASA/Goddard/Arizona State University. 2011. Public domain. https://www.nasa.gov/mission_pages/LRO/news/lro-farside.html

Figure 17.19: Radioactive decay. Andrew Fraknoi, David Morrison, and Sidney Wolff. 2015. CC BY 4.0. https://en.wikipedia.org/wiki/File:OSC_Astro_07_03_Decay_(1).jpg

Figure 17.20: Sample from NASA's lunar surface collection at Johnson Space Center's vault in Houston, Texas. Shannon Moore. 8 August 2011. CC BY. https://commons.wikimedia.org/wiki/File:Moon_rock_4,_JSC.jpg

Figure 17.21: NASA artist's conception of various planet formation processes, including exocomets and other planetesimals, around Beta Pictoris, a very young type-AV star. NASA/FUSE/Lynette Cook. 2007. Public domain. https://commons.wikimedia.org/wiki/File:NASA-ExocometsAroundBetaPictoris-ArtistView.jpg

Figure 17.22: Atlas of planetary nurseries. Credit: modification of work by NASA ESA/Hubble, L. Ricci (ESO). 2009. CC BY 4.0. https://esahubble.org/copyright/

Figure 17.23: This illustration demonstrates how a massive star (at least eight times bigger than our sun) fuses heavier and heavier elements until exploding as a supernova and spreading those elements throughout space. "Massive Stars: Engines of Creation." NASA, ESA, and L. Hustak. 2019. Public domain. https://hubblesite.org/contents/media/images/4501-Image.html

Figure 17.24: NASA's Mars Reconnaissance Orbiter used its Context Camera to capture this image of Bosporos Planum, a location on Mars. NASA/JPL-Caltech/MSSS. 2022. Public domain. https://www.nasa.gov/solar-system/nasas-mro-finds-water-flowed-on-mars-longer-than-previously-thought

Figure 17.25: The hole that NASA's Curiosity Mars rover drilled into a mudstone. NASA/JPL-Caltech/MSSS. 2013. Public domain. https://science.nasa.gov/resource/view-into-john-klein-drill-hole-in-martian-mudstone

Figure 17.26: Artist's concept of Jupiter's moon Europa. NASA/JPL-Caltech. 2013. Public domain. https://www.nasa.gov/image-article/taste-of-ocean-europas-surface

Figure 17.27: Images of Saturn's moon Titan taken in 2005 by the Huygens probe at four different altitudes. ESA/NASA/JPL/University of Arizona. 2005. Public domain. https://www.nasa.gov/image-article/ten-years-ago-huygens-probe-lands-surface-of-titan

Figure 17.28: Diagram explaining the habitable zone. Chester Harman. 2017. CC BY-SA. https://commons.wikimedia.org/wiki/File:Diagram_of_different_habitable_zone_regions_by_Chester_Harman.jpg

Figure 17.29: The Golden Record cover shown with its extraterrestrial instructions. NASA/JPL. 1977. Public Domain. https://voyager.jpl.nasa.gov/golden-record/golden-record-cover

Figure 17.30: The electromagnetic (EM) spectrum. Jonathan S Urie. 2013. CC BY-SA. https://commons.wikimedia.org/wiki/File:BW_EM_spectrum.png

Figure 17.31: A graphical representation of the Arecibo message. Laura Neser, adapted from Arne Nordmann. 2005. CC BY-SA. https://commons.wikimedia.org/wiki/File:Arecibo_message.svg

Figure 17.32: Enrico Fermi. Smithsonian Institution Archives. 1950. Public domain. https://commons.wikimedia.org/wiki/File:Enrico_Fermi_at_the_blackboard.jpg

Figure Descriptions

Figure 17.1: Big Bang Expansion began 13.77 billion years ago. From inception towards present: quantum fluctuations, inflation, afterglow light pattern (375,000 years), dark ages, first stars (400 million years), development of galaxies and planets, dark energy accelerated expansion.

Figure 17.2: An oval-shaped map of cosmic background radiation from when the universe was around 375,000 years old. The colors are artificial and show tiny temperature variations: tiny red patches have the highest temperature and the more widespread blue patches have the lowest temperature.

Figure 17.3: The ripples made in the direction the car is moving are closer together than the ripples behind the car.

Figure 17.4: Two spectrums of light stacked on top of each other: Sun on top, BAS11 on bottom. Arrows from the Sun toward BAS11 convey a slight shift of wavelength toward the longer wavelength colors. A duck swimming toward the left on rippled water is directly above the diagram, with shorter wavelength ripples in front of the duck and longer wavelength ripples behind the duck.

Figure 17.5: Photograph of Astronauts on the Moon. At center is the landing module, and to the right is the Lunar rover used by the Astronauts to travel large distances from the landing site. At left an Astronaut salutes the American flag placed near the lander. Scattered throughout the foreground are footprints in the Lunar soil.

Figure 17.6: Diagram of solar system objects orbiting the Sun. The objects plotted in the diagram moving outward from the Sun are Mercury, Venus, Earth, Mars, Asteroid belt, Jupiter, Saturn, Uranus, Neptune, and Pluto. All of the objects orbit the Sun in roughly the same plane with the exception of Pluto whose orbit is tilted with respect to the ecliptic.

Figure 17.7: Overhead view of the gray cratered surface of Mercury. Large craters, with many overlapping one upon the other, cover the surface of this 400 km wide scene.

Figure 17.8: Satellite image showing a reddish tan expanse with a large circular gently sloping volcano emerging from the surrounding lanscape.

Figure 17.9: Diagram of the four giant planets and Earth shown to scale according to size (not according to distance). Arranged from left to right are Jupiter, Saturn, Uranus, and Neptune, with Earth below the giant planets.

Figure 17.10: Enhanced-color image of the surface of Pluto. In this photograph, the smooth, white Sputnik plains are seen covering the center right of the image. Rugged, heavily cratered maroon terrain covers the lower center and left.

Figure 17.11: Image taken almost directly over one of Saturn's poles; Saturn's rings are seen nearly face-on, completely encircling the planet. Sunlight arrives from lower left as the rings cast a thin shadow on Saturn's cloud tops, while Saturn itself casts a shadow on the rings on the left. A rectangular false-color image at the right shows spectral mapping of Saturn's A, B and C rings: blue-green areas are the regions with the purest water ice and/or largest grain size (primarily the A and B rings), while the reddish color indicates increasing amounts of non-icy material and/or smaller grain sizes (primarily in the C ring and Cassini Division).

Figure 17.12: Gray asteroid that is very irregular in shape, in this case similar to a potato. The surface is pock-marked with many craters, including a 5.3- kilometer diameter crater at the top.

Figure 17.13: Gray comet that is very irregular in shape, in this case similar to a dumbbell. The surface appears powdery and pock-marked.

Figure 17.14: Mercury is a small planet and has a large core and thin mantle. Venus is a large planet and has a larger core and smaller mantle. Earth is similar to Venus, except it has a solid inner core and liquid outer core. Earth's Moon is small and might have a core, but is mostly mantle. Mars is a medium sized planet and has a smaller core and larger mantle. All of the planets have a thin crust.

Figure 17.15: Image of planet Jupiter with a tiny gray moon to its left. The planet Jupiter has multicolored white, tan, and red bands along various latitudes and there is a large red spot visible just below its equator.

Figure 17.16: Photo of a moon with a brownish gray surface and small craters scattered across the entire surface. There are a few bright white spots where recent impacts have uncovered fresh ice from underneath.

Figure 17.17: Graph with temperature on the horizontal axis increasing from 100 kelvins on the left to 800 kelvins on the right. The vertical axes have altitude increasing upward and pressure decreasing upward. There is a bold black line that starts at 0 km altitude and 750 kelvins; as it goes upward it goes to the left toward lower temperatures at higher altitude, nearly flattening into a vertical line around 90 km altitude.

Figure 17.18: View of the light gray cratered far side surface of our Moon. Craters of many sizes cover the surface, many of them overlapping. There are a few darker gray areas on the Moon in the upper left and lower portion of the image.

Figure 17.19: Graph Illustrating the Concept of Radioactive Decay. The vertical scale is labeled "Fraction of Original Sample Remaining", and increases from 0 to 1.0 in increments of 0.1. The horizontal scale is labeled "Number of Half- lives", and increases to the right from 0 to 5 in increments of 1. A curve is drawn from (0, 1.0) at upper left down to (5, 0) at lower right. A dashed line is drawn vertically upward from 1 to intersect the curve at 0.5 on the vertical scale. At this point on the curve 1/2 of the original material remains. Next, another dashed line is drawn vertically upward from 2 to intersect the curve at 0.25, where 1/4 of the original sample remains. Another dashed line is drawn upward from 3 to intersect the curve at 0.125, where 1/8 of the sample remains. Again, a dashed line is drawn upward from 4 to intersect the curve at 0.06, where 1/16 of the sample remains. Finally, the dashed line from 5 intersects the curve at 0.03, where 1/32 of the original sample remains. Above the curve are drawn six "blobs" of material, one for each data point. The blob is pink at the top of the curve representing the full radioactive sample. The blob at (1, 0.5) is about 1/2 pink and 1/2 grey representing the fact that 1/2 of the original sample remains. This illustration continues for the remaining data points so that by (5, 0.03) the blob is nearly all grey indicating that only 1/32 of the original sample remains.

Figure 17.20: Photo of a gray rock with black specks throughout it. The rock is sitting on a white sheet of paper with a metal ruler in the foreground and a black die next to it. There is a label that says 15555 in front of the rock.

Figure 17.21: Artist's conception of the view toward the young star Beta Pictoris from the outer edge of its disk. The star is surrounded by a disk of dust, gas, and rocks. A terrestrial planet gaining mass by collision with an asteroid is shown just to the right of center. Two inset panels show two possible outcomes for mature terrestrial planets around the star. The top one is a water-rich planet similar to the Earth; the bottom one is a carbon-rich planet, with a smoggy, methane-rich atmosphere similar to that of Titan, a moon of Saturn.

Figure 17.22: A Photographic Atlas of Planetary Nurseries in the Orion Nebula. These Hubble Space Telescope images show embedded circumstellar disks orbiting very young stars. Each is seen from a different angle. Some are energized to glow brightly by the light of a nearby star, while others are dark and seen in silhouette against the bright glowing gas of the Orion nebula.

Figure 17.23: Infographic showing a purple sphere with a cut-out to show the core, labeled main sequence star: the star is fueled by hydrogen-to-helium fusion in its core; stage lasts 7 million years. A dotted line connects it to a larger pink sphere with a cut-out to show the core, labeled development of multi-shelled core: after hydrogen is exhausted in the core, other elements begin to fuse; existing elements float above the denser center and form a multi-layered shell. The multi-shell core is zoomed to a larger size below and divided into four progressive stages. The first is a simple two-layered core labeled helium-to-carbon fusion; 500,000 years. To the right of that, the multi-shell core is made of three layers and labeled carbon-to-oxygen fusion; 600 years. To the right of that, the multi-shell core is made of four layers and labeled oxygen-to-silicon fusion; 6 months. To the right of that, the multi-shell core is made of five layers and labeled silicon-to-iron fusion; 1 day. Lastly, there is a purplish blob of gas following the silicon-to- iron fusion core, labeled Supernova: the iron core cannot produce energy to balance the weight of the layered gas above. In less than one second, the core collapses and the upper layers rebound outward in a dramatic explosion, populating the universe with elements, the building blocks of creation; 0.01 seconds.

Figure 17.24: Black and white aerial photograph of a generally flat area. There are channels resembling the shapes of rivers with white specks seen throughout the channels. Craters of various sizes dot the surface as well.

Figure 17.25: Closeup photograph of a hole drilled into tan fine-grained rock. There's a black scale bar labeled 2 mm to the right of the hole, showing the hole is approximately 16 mm in diameter.

Figure 17.26: Illustration showing a cross section of a moon in the foreground that has a brown crust with a thick layer of ice directly below the outer crust and a deep blue ocean beneath the ice. Multiple geysers branch vertically through the ice from the top of the ocean, causing eruptions on the surface of the moon. In the background is the planet Jupiter and a small yellow moon.

Figure 17.27: Four aerial photos getting progressively closer to the surface showing a sepia-orangeish colored landscape. The first photo shows a general orangeish haze, the second photo shows a wide landscape with branching patterns, the third photo shows the branching patterns from a lower altitude, and the final photo is closer to the ground, showing the orangeish landscape sprawling away from the camera.

Figure 17.28: A graph that has temperature in K increasing upwards on the vertical axis and starlight on planet relative to sunlight on Earth increasing toward the left on the horizontal axis. A large shaded zone covers most of the graph labeled optimistic habitable zone. Various

exoplanets are shown within the optimistic habitable zone along with Earth, Venus, and Mars, with Earth and Mars within the habitable zone and Venus outside and to the left of the habitable zone.

Figure 17.29: A photo of a golden record on the left that has various etchings visible on the surface. Including: a basic birds-eye view drawing of a music record and stylus, a side view of the flat record and stylus, graphs describing the construction of pictures from the recorded signals, a drawing of an entire picture raster, showing that there are 512 vertical lines in a complete picture, a rectangle with a circle in the center, a replica of the first picture of a birds-eye view of a record. A schematic diagram on the right shows etchings in black and white.

Figure 17.30: A black sinusoidal wave goes from the left to the right of the diagram with longer wavelengths to the left, getting progressively shorter and shorter to the right. The types of waves are labeled based on their wavelengths: from longest to shortest they are radio, microwave, infrared, visible, ultraviolet, x-ray, and gamma ray. Common things on Earth are beneath the waves for scale: from left to right they are buildings, humans, honey bee, pinpoint, protozoans, molecules, atoms, and atomic nuclei.

Figure 17.31: A colored graphical representation that consists of seven parts that encode the following from the top down in the image: the numbers one to ten in white; the atomic numbers of the elements hydrogen, carbon, nitrogen, oxygen, and phosphorus, which make up DNA in purple; the formulas for the chemical compounds that make up the nucleotides of DNA in green; the estimated number of DNA nucleotides in the human genome, and a graphic of the double helix structure of DNA in white and blue, respectively; the physical height of an average man in blue and white, a graphic figure of a human being in red, and the human population of Earth which was about 4 billion at the time in white; a graphic of the Solar System in yellow; and a graphic of the Arecibo radio telescope and the physical diameter of the transmitting antenna dish in purple, white, and blue.

Figure 17.32: Black and white photograph of a white man wearing a chevron-textured suit writing on a chalkboard with his face turned back away from the board. There are various equations and geometric shapes drawn on the chalkboard.

GLOSSARY

aa

A blocky, stubby, rubble-like lava.

absolute dating

Quantitative method of dating a geologic substance or event to a specific time in the past.

abyssal

Relating to the bottom of the ocean.

abyssal plain

Relatively flat ocean floor that accumulates very fine-grained detrital and chemical sediments.

accretionary wedge

Mix of sediments that form as a subducting plate descends, the overriding plate scrapes material, and material is added.

acid rock drainage

Toxic waters rich in heavy metals and often of low pH that come from unregulated mining districts.

active margin

A convergent boundary between continental and oceanic plates.

active solar system

A system using mechanical and electrical equipment to collect, store, or distribute solar energy for various uses.

actual preservation

Unchanged materials preserved in the fossil record, which are rare and exceedingly less likely with soft materials and older materials.

adaptation

The process by which individuals, communities, and societies adjust to new conditions or changes in their environment to maintain or improve their living standards and well-being.

adhesion

Forces that cause one substance to stick to another.

aeolian

Deposition with wind-blown sediment.

aftershocks

Earthquakes that occur after the mainshock, usually decreasing in amount and magnitude over time.

albedo

The amount of light that is reflected off of an object, measured on a scale of 0 (absorbs all light) to 1 (reflects all light).

alluvial

Depositional environments that are associated with running water.

alluvium

Loose sediment deposited from running water.

alpha decay

Radioactive decay in which two protons and two neutrons leave the isotope.

alpine glacier

A glacier that forms on a mountain.

altimeter

An instrument used to measure the altitude of an object above a fixed level.

amphibole

A group of chain silicate minerals that form needlelike or prismatic crystals; can be many colors, but the most common form, hornblende, is dark brown to black; has oblique cleavages at 54˚ and 126˚; common in many igneous rocks and some metamorphic rocks.

amplitude

Height or depth of a wave from the middle point.

andesite

General name of an intermediate igneous rock that is extrusive, usually with a gray groundmass.

angle of incidence

Angle between a light ray that hits the ground and a line perpendicular at the point of contact with the ground. If the sun is directly above a point and light rays are hitting the ground directly, then the angle of incidence is 0.

angle of repose

Slope angle where shear forces and normal forces are equal.

angular unconformity

Angular discordance between two sets of rock layers; caused when sedimentary strata are tilted and eroded, followed by new deposition of horizontal strata above.

anhedral

A mineral that shows no crystal habit, either because it is not prone to having a habit or because it was confined and could not grow with its normal habit.

anion

A negatively charged ion. In geology, this commonly includes elements and molecules like SiO4-4, S-2, SO4-4, and O-2.

anomaly

Data that is out of the ordinary and does not fit previous trends.

Anthropocene

A newly proposed time segment (an epoch) that would be representative of the time since humans began changing (and leaving evidence within) the geologic record.

anthropogenic

Made or influenced by humans.

anthropogenic climate change

Climate change caused by human activity, namely the burning of fossil fuels.

anticline

Downward-facing fold that has older rock in its core.

antidune

Similar to dunes in that they are ridges of sand that form perpendicular to flow, but internally, the sediments dip upstream; they form in the upper part of the upper flow regime.

aphanitic

Microscopic crystals within an igneous rock that are invisible to the naked eye; common in extrusive rocks.

aquiclude

A layer with so little porosity and/or permeability that fluids essentially cannot flow through it and only flow around it.

aquifer

A rock or sediment that has good permeability and porosity, which allows water to move easily, making the water accessible for human use.

aquitard

A layer with lower porosity and/or permeability, which allows only minimal and/or slow fluid flow.

arc

A chain of volcanic activity, typically in a curved pattern, rising from a subduction zone; located on the overriding plate, typically a few hundred kilometers from the trench, parallel to the trench.

Archean

Eon defined as the time between 4 billion years ago to 2.5 billion years ago, when most of the oldest rocks on Earth formed, including large portions of the continents.

arête

A ridge that is carved between two glacial valleys.

arkose

A sandstone rich in feldspar.

arroyo

Dry riverbed in an arid region.

artesian well

A well that allows pressurized water to reach the surface.

aseismic

Fault, or movement along a fault, that does not have earthquake activity.

ash

Volcanic tephra that is less than 2 mm in diameter.

assimilation

Bedrock around the magma chamber being incorporated into the magma, sometimes changing the composition of the magma.

asteroid

A small rocky body orbiting the sun.

astenosphere

A ductile physical layer of the Earth, below the lithosphere. Movement within the asthenosphere is the main driver of plate motion, pushing the overriding lithosphere.

astrobiology

The scientific study of life in the universe, including its origins, evolution, and potential existence beyond Earth.

astronomical unit (AU)

The average distance from the Earth to the Sun.

astronomy

The branch of science that deals with celestial objects, space, and the physical universe as a whole.

Atacama Desert

Driest nonpolar desert on Earth, located in west-central South America.

atmosphere

The gases that are part of the Earth, which are mainly nitrogen and oxygen.

augen

Strong crystals that do not deform as easily under ductile deformation and that form lens-shaped porphyroblasts.

aulacogen

A depression that occurs in an area that was subject to earlier rifting.

aureole

A zone of contact metamorphism that surrounds an intrusion. Since intrusions are typically somewhat round in cross section, the pattern of metamorphism is concentric about the intrusion.

authigenic mineralization

Specialized mineralization around organic material, which produces highly precise molds and casts.

axial plane

A two-dimensional line that divides the two sides of a fold.

back-arc

Area behind an arc, which can be subject to compressional forces (causing thrusted mountain belts) or extensional forces (causing back-arc basins).

back-arc basin

Depression formed by extension behind an arc, typically with seafloor spreading.

backshore

Area of the shoreline that is always entirely above normal wave action.

bajada

A group of several alluvial fans that have come together and formed a single surface.

banded iron formation

A sedimentary rock that formed long ago when free oxygen changed the solubility of iron, causing layers of iron-rich and iron-poor sediments to form in thin layers, or bands.

banding

A separation of light (felsic) and dark (mafic) minerals in higher-grade metamorphic rocks like gneiss.

bankfull stage

Largest amount of flow a river can hold before flooding.

barchan dune

Crescent-shaped dune formed by consistent wind and limited sediment.

barrier island

Ridges of sand that are made from former beach sediments and form parallel to the shoreline.

basalt

General name of a mafic rock that is extrusive, usually with a black groundmass.

base level

Elevation of the mouth of a river.

basin

A down-warped feature in the crust.

Basin and Range

The extensional tectonic province that extends east from California's Sierra Nevada Mountains to Utah's Wasatch Mountains, and south from Idaho and southern Oregon to northern Mexico; known as a wide rift, each graben (basin) is bounded by horsts (ranges).

batholith

Used to describe a large mass or chain of many plutons and intrusive rocks.

bathymetry

The measurement of depth of water in oceans, seas, or lakes.

bauxite

A highly weathered soil deposit that consists of aluminum ores.

baymouth bar

A bar formed when a spit extends outward and covers a bay.

beach face

Active area of crashing waves.

bed

A specific layer of rock with identifiable properties.

bedding

Discernible layers of rock, typically from a sedimentary rock.

bedform

A specific type of sedimentary structure (ripples, plane beds, etc.) linked to a specific flow regime.

bedload

Large, dense sediment that typically sits on the bottom of stream channels and is only moved with higher-speed flows.

bedrock

The underlying lithified rocks that make up the geologic record in an area. This term can sometimes refer to only the deeper, crystalline (nonlayered) rocks.

berm

Ridge of sand built above the beach face.

beta decay

A radioactive decay process where a neutron changes into a proton, releasing an electron.

big bang

The theory that the universe started with a expansive explosion, followed by the creation of elements (mostly hydrogen) and the formation of galaxies.

biochemical

Chemical sedimentary rocks that have a biologic component to their origin. Many limestones are biochemical.

biochemistry

The branch of science that explores the chemical processes and substances that occur within living organisms.

biofuels

Liquid fuels produced from renewable biological sources, including plants and algae.

biology

The scientific study of living organisms and their interactions with each other and their environments.

biomarker

A detectable substance or characteristic in an astronomical body's atmosphere or surface that indicates the potential presence of life.

biomass

Matter from recently living organisms, which is used for bioenergy production.

biosphere

One of Earth's interacting spheres; it is composed of all living organisms and the nonliving parts with which they interact.

biostratigraphic correlation

A type of stratigraphic correlation in which fossils are used to match different rock layers.

bioturbation

The disturbance of sedimentary layering by the movement of organisms.

black smoker

Mineral chimneys that form at hydrothermal vents.

blowout

A depression in dune sediment formed because of a lack of anchoring vegetation.

blueschist

A metamorphic facies of low-temperature, high-pressure rocks, typified by blueschist, a metamorphic rock containing a blue amphibole called glaucophane.

body wave

Seismic waves that travel through the Earth, mainly P waves and S waves.

bolide

A large extraterrestrial object, such as a meteor or asteroid, that hits the surface of the Earth.

bomb

Large volcanic tephra greater than 64 mm in diameter.

bond

Two or more atoms or ions that are connected chemically.

Bouma sequence

Predictable sequence of fining upward sediments, caused by turbidity flows.

Bowen's reaction series

A series of mineral formation temperatures that can explain the minerals that form in specific igneous rocks. For example, pyroxene will form with olivine and amphibole but not quartz.

brackish water

Water that is a mixture of sea water and fresh water.

braided channel

Channel type with many switching channels, common with large sediment volumes.

breakwater

Durable offshore structure designed to lessen wave action and reduce longshore drift.

brittle

A property of solids in which a force applied to an object causes the object to fracture, break, or snap. Most rocks are brittle at low temperatures.

brittle deformation

A style of strain in which an object suddenly breaks, fractures, or otherwise fails in a way different from ductile deformation.

burial metamorphism

Metamorphism that is caused by confining pressure and heat, both of which increase with depth.

calcite

A mineral also known as $CaCO_3$ that is clear in its pure form but can take on many different colors with impurities; it is soft, fizzes in acid, and has three cleavages that are not at 90°.

calcite compensation depth (CCD)

The point in the depths of the ocean where calcite starts to dissolve, leaving only siliceous ooze behind.

caldera

Hole left behind after a large volume of material erupts out of a volcano, which often turns into a valley or lake after the eruption is over.

calving

A process where ice from the ends of glaciers falls into the ocean.

Cambrian

The first period of the Paleozoic, 541 million years ago to 485 million years ago.

Cambrian explosion

A period of time in the early Cambrian (about 541–516 million years ago) in which a large diversification of life forms appeared in the fossil record. Many of the modern phyla of organisms evolved in this time span.

canyon

A deep, narrow valley with steep sides.

carbonate

Mineral group in which the carbonate ion (CO_3^{-2}) is the building block. This can also refer to the rocks that are made from these minerals, namely limestone and dolomite (dolostone).

carbonatite

An igneous composition or rock containing more than 50% carbonate minerals (e.g., calcite). Magma of this composition is very low temperature (500–600°C) relative to other magmas.

carbonic acid

An acid that forms from carbon dioxide and water; a large contributor to chemical weathering.

Carboniferous

The fifth (second-to-last) period in the Paleozoic, 359–299 million years ago. In North America, the Carboniferous is split into two different periods, the Mississippian (359–323 million years ago) and the Pennsylvanian (323–299 million years ago).

carbonization

A type of fossilization where only a carbon-rich film is preserved, common in plants.

cast

Material filling in a cavity left by a organism that has dissolved away.

cataclasite

A type of breccia that forms in a brittle way within fault zones.

catastrophism

The idea that large, damaging occurrences are the cause of most geologic events.

cation

A positively charged ion. In geology, this commonly includes ions of the elements Ca^{+2}, Na^{+1}, K^{+1}, $Fe^{+2,+3}$, Al^{+3}, and Mg^{+2}.

cementation

Sediment becoming "glued" together via mineralization, typically calcite and quartz from groundwater fluids.

Cenozoic

The last (and current) era of the Phanerozoic Eon, starting 66 million years ago and spanning through the present.

chalk

A limestone made of the shells of coccolithophore, a type of single-celled algae.

chemical energy

A form of potential energy stored in the bonds of chemical compounds and released during a chemical reaction.

chemical sedimentary

Sedimentary rocks that form through precipitation, from solution.

chemical weathering

Breaking down of mineral material via chemical methods, like dissolution and oxidation.

chemosynthesis

A biologic process of gaining energy from chemicals from within the Earth, similar to using the energy of the sun in photosynthesis.

chert

A fine-grained version of silica deposited with or without microfossils.

Chicxulub Crater

A 180-kilometer (110-mile) crater that exists near Chicxulub, Mexico, on the Yucatan Peninsula. Widely accepted to be the result of the asteroid that caused the K-T extinction.

Chordata

Organisms that possess vertebrae or some form of a spinal column, including humans.

chronostratigraphic correlation

A type of stratigraphic correlation that is based on similar ages.

cinder

A type of tephra that forms as blobs of magma splatter out of a volcanic vent (e.g., cinder cone) and cool and harden quickly.

cinder cone

Volcano formed from piles of cinders and tephra, containing low-viscosity lava with high-volatile content.

cirque

Glacially-carved, bowl-shaped valley.

clastic

Sedimentary rocks that are made of weathered pieces of bedrock.

claystone

A rock made primarily of clay.

cleavage

A weakness (or weaknesses) within the atomic structure of a mineral, which allows the mineral to break more easily along that plane. Cleavage can also refer to the alignment of features within metamorphic rocks., though this usage is unrelated.

climate

Long-term averages and variations within the conditions of the atmosphere.

closed basin

An internally draining watershed whose waters do not flow to the ocean.

coal

Former swamp-derived (plant) material that is part of the rock record.

coastline

The entire area related to land-sea interactions.

cohesion

Forces that hold a substance together.

collision

When two continents crash with no subduction (and thus little to no volcanism) since each continent is too buoyant. Many of the largest mountain ranges and broadest zones of seismic activity come from collisions.

comet

A celestial object consisting of a nucleus of ice and dust and, when near the Sun, a "tail" of gas and dust particles pointing away from the Sun.

compaction

Sediment being squeezed together into a coherent mass.

composition

The mineral makeup of a rock (i.e., which minerals are found within a rock).

compression

Stresses that push objects together into a smaller surface area or volume; contracting forces.

concentrator

A mechanical process that takes ore and separates it from gangue material.

conchoidal fractures

Fractures that have a circular appearance.

conduit

Pipe that connects the magma chamber to the volcanic vent.

cone of depression

Area with a lower water table due to water pumping from a well.

confining

Nondirectional pressure resulting from burial.

confining layer

A layer that has low permeability and porosity and does not allow fluid flow as easily.

conglomerate

A sedimentary rock with larger, rounded (≥ 2 mm) clasts.

connate water

Original water trapped inside a forming rock.

contact metamorphism

Metamorphism that occurs when rocks are next to a hot intrusion of magma.

continental crust

The layers of igneous, sedimentary, and metamorphic rocks that form the continents; much thicker than oceanic crust; contains higher concentrations of very light elements like K, Na, and Ca, and is the lowest density rocky layer of Earth, with an average composition similar to granite.

continental glacier

A body of ice covering large stretches of land over a continent (mainly found in Antarctica).

continental margin

The transition from land to the deep ocean, where continental crust gives way to oceanic crust.

continental shelf

Submerged part of the continental mass, with a gentle slope.

continental slope

Steep part of an ocean basin located at the transition between the continental mass and the ocean floor.

convection

The property of unevenly-heated (heated from one direction) fluids (like water, air, ductile solids) in which warmer, less dense parts within the fluid rise and cooler, denser parts sink. This typically creates convection cells: round loops of rising and sinking material.

convergent boundary

Place where two plates come together, causing subduction or collision.

Copernican principle

The Copernican principle posits that the Earth is not in a central, specially favored position in the universe.

coquina

Limestone made of shell fragments cemented together.

core

The innermost chemical layer of the Earth, made chiefly of iron and nickel, with both liquid and solid components.

correlation

Matching rocks of similar ages, types, etc.

cosmic microwave background

Radiation left over from the early stage in the development of the universe, when protons and neutrons were recombining to form atoms.

crater

A bowl-shaped depression, or hollowed-out area, produced by the impact of a meteorite, volcanic activity, or an explosion.

craton

The stable interior part of a continent, typically more than a billion years old and sometimes as much as 2.5–3 billion years old; called a shield when exposed on the surface.

creep

A slow and steady movement that can occur as part of faults, mass wasting, and grain movement.

Cretaceous

The last period of the Mesozoic, 145–66 million years ago.

Cretaceous Interior Seaway

A waterway that existed in North America around 100 million years ago, separating western and eastern North America.

crevasse

A crack that forms with glacial movement in the upper, brittle part of the glacier.

crevasse splay

Sediment that breaks through a levée and deposits in a floodplain during a flood event.

cross-bed

A sedimentary structure that forms in the lower flow regime, where ridges of sediment form perpendicular to flow direction, while within the ridges, sediment layers and dips toward flow direction; found in ripples and dunes; can be tabular, sinuous, or trough-shaped.

cross-bedding

A sedimentary structure that has inclined layers within an overall layer; forming commonly in dunes, it is larger in eolian dunes.

crust

The outermost chemical layer of the Earth, defined by its low density and higher concentrations of lighter elements. The crust has two types: continental, which is thicker, more ductile, and has lower density, and oceanic, which is thinner, more brittle, and has greater density.

cryosphere

The part of the hydrosphere (water) that is frozen, found mainly at the poles.

crystal habit

The typical form or forms a crystal takes when it grows.

crystallization

The process of liquid rock solidifying into solid rock. Because liquid rock is made of many components, the process is complex, with different components solidifying at different temperatures.

cut bank

Erosional part of a meandering channel.

dam

A barrier that stops or restricts the flow of surface water or underground streams.

daughter isotope

The atom that is made after a radioactive decay.

debris flow

A mixture of coarse material and water channeled and flowing downhill rapidly.

decay chain

A series of several radioactive decays that eventually leads to a stable isotope.

Deccan Traps

Large flood basalt province in India that occurred around the same time as the K-T extinction, 66 million years ago.

decompression melting

Melting that occurs as material is moved upward and pressure is released, typically found at divergent plate boundaries or hotspots.

deductive reasoning

Using known truths to develop new truths.

deformation

A strain that occurs in a substance in which the item changes shape due to a stress.

delta

Place where rivers enter a large body of water, forming a triangular shape as the river deposits sediment and switches course.

dendritic drainage

A common branching style of drainage pattern that resembles tree roots.

density

The mass of a substance per unit volume. Density is given in units where the density of water is 1 g/cm cubed; to get densities in units of kg/m cubed, multiply the given value by 1,000.

deposition

Sediment gathering together, typically in a topographic low point.

depositional environment

An interpretation of the rock record that describes the cause of sedimentation (ancient beach, river, swamp, etc.).

deranged pattern

Drainages that are erratic and disappearing, typically in karst environments.

desalination

The process of removing salt and other impurities from seawater or brackish water to make it suitable for drinking, irrigation, or other uses.

desert varnish

Dark mineralization that forms on rocks in desert environments.

desertification

The process that turns nondesert land into desert.

detachment fault

A style of low-angle, high-extension normal faulting.

detrital

Sedimentary rocks made of mineral grains weathered as mechanical detritus of previous rocks (sand, gravel, etc.).

Devonian

Known as the "Age of Fishes," the fourth period of the Paleozoic, about 419–359 million years ago.

dextral

Movement in a transform or strike-slip setting toward the right as viewed across the fault.

diagenesis

Changes in sedimentary rocks due to increased temperatures (though still low compared to metamorphism) and pressures. This can include deposition of new minerals (e.g., limestone converting to dolomite) or dissolution of existing minerals.

diameter

A straight line passing from side to side through the center of a body or figure, especially a circle or sphere.

diamictite

A sedimentary rock containing two distinct grain sizes, typically cobbles (or larger) mixed with mud.

diapir

A ductile material that moves toward the surface of Earth. Can be used to describe salt domes and intrusions.

differentiation

In planetary science, the process of separating the different components within a planetary body as a consequence of their physical or chemical behavior (e.g., density and chemical affinities).

dike

A narrow igneous intrusion that cuts through existing rock, not along bedding planes.

diorite

General name of intermediate rock that is intrusive and has about the same amount of felsic minerals and mafic minerals.

dip

A measure of a plane's maximum angle with respect to horizontal, where a perfectly horizontal plane has a dip of zero and a vertical plane has a dip of 90°.

dip slip

Faulting that occurs with a vertical motion.

directed stress

Stress that has a strong (unequal) directional component, typically creating elongated or flattened features.

discharge

Amount of water that leaves a system such as a river or aquifer.

disconformity

Exists when there is an erosional surface between two layered rocks that may otherwise seem conformable.

dissolution

The process in which solids (like minerals) are disassociated and the ionic components are dispersed in a liquid (usually water).

dissolved load

Amount of material dissolved in stream water.

diurnal tide

Areas that have one clear high tide and one clear low tide each tidal day.

divergent boundary

Place where two plates are moving apart, creating either a rift (continental lithosphere) or a mid-ocean ridge (oceanic lithosphere).

dome

A rock upwarping made up of symmetrical anticlines.

Doppler effect

A change in wavelength and frequency of a wave due to its source's movement relative to the observer of a wave.

drainage basin

The area within a topographic basin or drainage divide in which water collects.

drainage divide

Topographic prominence that separates drainage basins, or watersheds.

drainage pattern

The shape or form of a river and/or tributary drainage system.

drumlin

Ridge of sediment that forms under a glacier with steep uphill and gentle downhill sides in respect to the glacier.

ductile

A property of a solid, such that when a force is applied, the solid flows, stretches, or bends along with the force instead of cracking or breaking. For example, many plastics are ductile.

ductile deformation

A bending, squishing, or stretching style of deformation where an object changes shape smoothly.

dune

A large pile of sediment deposited perpendicular to flow, with internal bedding dipping toward flow direction (i.e., cross-bedding). Formed in the upper part of the lower flow regime.

dwarf planet

A small planetary-mass object that is in direct orbit of the Sun; smaller than any of the eight classical planets, but still a world in its own right.

earth flow

A fine-grained type of plastic flow.

Earth system science

The study of the interaction of the spheres within the system that is the Earth, mainly the study of the hydrosphere, atmosphere, geosphere (lithosphere), and biosphere.

eccentricity

The measure of the circular or elliptical nature of the Earth's orbit.

echo sounder

A system that applies sonar technology to measure the depth of water.

eclogite

A metamorphic rock that forms in the upper mantle as a result of high-pressure metamorphism, composed of red garnet hosted in a matrix of green pyroxene.

Ediacaran fauna

A group of relatively complex organisms that existed at the end of the Proterozoic.

elastic deformation

A type of deformation that reverses when the stress is removed.

elastic rebound

A theory concerning built-up energy that is released during an earthquake.

electromagnetic radiation

The energy emitted and propagated through space in the form of electromagnetic waves.

electromagnetic spectrum

Visible light and its related energetic waves, including X-rays, UV rays, and radio waves.

electromagnetic waves

Waves of electric and magnetic fields that propagate through space at the speed of light, encompassing a broad spectrum that includes radio waves, microwaves, infrared, visible light, ultraviolet, X-rays, and gamma rays.

electron

A stable subatomic particle with a charge of negative electricity, found in all atoms and acts as the primary carrier of electricity in solids.

electron capture

A type of radioactive decay where an electron combines with a proton, making a neutron.

element

A group of all atoms with a specific number of protons, having specific, universal, and unique properties.

emergent coastline

An exposed coastline where relative sea level is falling.

energy intensity

A measure of the energy efficiency of a nation's economy. It is calculated as the amount of energy consumed per unit of gross domestic product (GDP), with lower energy intensity indicating a more efficient use of energy in producing economic output.

entrenched channel

A channel that carves into existing bedrock, preserving its original shape and character.

eon

The largest span of time recognized by geologists, larger than an era. We are currently in the Phanerozoic Eon.

ephemeral stream

A stream or river that can be wet or dry depending on the season.

epicenter

The surface directly above the focus of an earthquake, typically associated with strong damage.

epoch

A unit of geological time recognized by geologists; smaller than a period. We are currently in the Holocene epoch.

equant

Stubby, not longer in any direction.

era

The second-largest span of time recognized by geologists; smaller than an eon, larger than a period. We are currently in the Cenozoic Era.

erg

A vast stretch of sand dunes.

erosion

The transport and movement of weathered sediments.

esker

Ridge of sediment that forms under a glacier by meltwater that has formed a river.

estuary

Lagoon with brackish water, typically with abundant biologic factors.

euhedral

A mineral that perfectly shows its true crystal habit.

eukaryote

A type of organism in with a cell or cells that contains a nucleus.

eustatic

Referring to overall global sea level change, either due to climate or seafloor spreading rate.

evaporate

Turn from liquid into vapor.

evaporite

A chemical sedimentary rock that forms as water evaporates.

evapotranspiration

A combination of evaporation and transpiration from plants, serving as a measure of water entering the atmosphere.

exfoliation

A type of mechanical weathering in which outer layers of rock fracture off, occurring approximately parallel to the surface.

exoplanet

Any planet beyond our Solar System.

experiment

A test of an idea in which new information can be gathered to either accept or reject a hypothesis.

extinct

When a species no longer exists.

extraterrestrial

Anything originating, existing, or occurring outside the Earth and its atmosphere.

extrusive

Relating to igneous rock that has formed by cooling outside of the Earth (i.e., on the surface).

facies

A specific set of features that are shared by an interpretive group of rocks. Facies can be based on mineralogy, biologic factors, fossils, rock types, etc.

failed rift arm

A section of a rift that starts to develop without fully forming. This typically occurs at 120° angles to the active rift.

fair-weather wave base

The depth reached by normal, nonstorm waves.

falsifiable

The idea that claim in science can be proved wrong with proper evidence.

fault

Planar feature where two blocks of bedrock move past each other via earthquakes.

fault scarp

Place where fault movement cuts the surface of the Earth.

feldspar

Group of minerals consisting of three end members: potassium feldspar (K-spar, KAlSi3O8), plagioclase with calcium (anorthite, CaAl2Si2O8), and plagioclase with sodium (albite, NaAlSi3O8). Commonly blocky, with two cleavages at ~90°. Plagioclase is typically dull white and gray, and K-spar is more vibrant white, orange, or red.

felsic

Can refer to a volcanic rock with higher silica composition or to the minerals that make up those rocks, namely quartz, feldspar, and muscovite mica. Felsic rocks are lighter in color and contain more minerals that are light in color. Primary felsic rocks are rhyolite (extrusive) and granite (intrusive).

Fermi paradox

The Fermi paradox highlights the contradiction between the high probability of the existence of extraterrestrial civilizations and the lack of evidence or contact with such civilizations.

fetch

Distance wind has been building a wave.

finger lake

Lake that fills a glacial valley.

firn

Snow that has been compressed and is starting to turn into ice.

fissile

Easily split along bedding planes, a characteristic of shale.

fjord

Glacial valley filled by ocean water.

flash flood

Dangerous flooding that occurs in arid regions.

flood basalt

The result of a rare, low-viscosity eruption that covers vast areas. None have been observed in human history.

floodplain

Flat area around a river channel that is filled with water during flooding events.

flow regime

A qualitative measure of the speed of a fluid flow that considers how different flows are affected by different sedimentary structures, called bedforms. Typically, it is split into upper and lower flow regimes, with upper being a more rapid flow.

flower structure

A small area along a strike-slip or transform fault with branching structures of transpression/transtension, that cause local hills or valleys.

fluvial

Deposition that has to do with rivers.

flux melting

The process in which volatiles enter the mantle wedge and the volatiles lower the melting temperature, causing volcanism.

focus

Initiation point of an earthquake or fault movement.

fold

A rock layer that has been bent in a ductile way instead of breaking (as with faulting).

foliation

A planar alignment of minerals and textures within a rock.

footwall

On a dipping fault, the part of the block that is below the fault; moves down in normal faulting, up in reverse faulting.

forearc

Area in front of the arc, between the arc and the trench. Often marked by an accretionary wedge or a forearc basin.

forearc basin

Any depression formed between the arc and the trench, commonly between the arc and the accretionary wedge.

foreshock

An earthquake that sometimes occurs before the larger mainshock.

foreshore

Area between high tide and low tide.

formation

An extensive, distinct, and mapped set of geologic layers.

fossil

Any evidence of ancient life.

fossil fuel

Energy resources (typically hydrocarbons) derived from ancient chemical energy preserved in the geologic record. Includes coal, oil, and natural gas.

fossil fuels

fossiliferous

Adjective for a rock filled with fossils, most commonly with limestones.

fracking

A process of injecting pressurized fluids into the ground to aid in hydrocarbon migration.

fracture

A break within a rock that has no relative movement between the sides; there are various causes, including cooling, pressure release, and tectonic forces.

fracture zone

Faults along mid-ocean ridges that have a transform motion but do not produce earthquakes. These faults accommodate different amounts of movement along the mid-ocean ridge.

friction

The force resisting the relative motion of solid surfaces, fluid layers, and material elements sliding against each other.

frost wedging

A process in which water freezes inside cracks in rocks, causing expansion and mechanical weathering.

fusion

A process inside stars in which smaller atoms combine and form larger atoms.

gabbro

General name of a mafic rock that is intrusive.

galaxies

A gravitationally bound system of stars and interstellar matter.

gamma ray

A penetrating form of electromagnetic radiation arising from the radioactive decay of atomic nuclei. Its electronic waves have the shortest wavelengths, typically shorter than those of X-rays.

gangue

Material found around ore that is less valuable and needs to be removed in order to obtain the ore.

geopetal structure

A feature in a rock that allows the observer to determine which direction was up in the past.

geosphere

The solid, rocky parts of the Earth, including the crust, mantle, and core. Also referred to as the lithosphere.

geothermal energy

Heat that is generated within the Earth.

geothermal gradient

The average change in temperature experienced as material moves into the Earth. Near the surface, this rate is about 25°C/km.

giant impact hypothesis

Idea that a large body struck the Earth, spraying material into space that eventually collected to form the Moon.

glacial

Deposition and erosion tied to glacier movement.

glacial budget

The net gain or loss of ice within a glacier.

glacial erratic

Large sediment (e.g., boulder) carried and then dropped by a glacier.

glacial polish

Smooth surface carved in hard rocks by glacial action.

glacial striation

Grooves scratched in rock by glacial action.

glaciation

A period of cooler temperatures on Earth in which ice sheets can grow on continents.

glacier

A body of ice that moves downhill under its own mass.

gneiss

A metamorphic rock higher in grade than schist, with separate light and dark minerals.

Goldich dissolution series

Working opposite of Bowen's reaction series, it states that minerals that are formed at conditions more dissimilar to the surface are more quickly prone to chemical weathering.

graben

A valley formed by normal faulting.

grade

A qualitative measure of the amount of metamorphism that has occurred or the amount of a resource present in an ore.

gradient

Slope of a stream channel.

grading

A sequence of layers in which the sediment changes linearly in size, getting either coarser or finer.

grain size

The average diameter of a grain of sediment, ranging from small, fine-grained (e.g., clay, silt) to large, coarse-grained (e.g., boulder).

granite

General name of a felsic rock that is intrusive.

Great Basin Desert

Desert area stretching east from California to Utah and north to Idaho/Oregon; formed due to both latitude and rain shadow.

Great Oxygenation Event

A period of the early Proterozoic (around 2.5–2 billion years ago) where atmospheric oxygen levels dramatically increased, killing many non-oxygen-breathing organisms and allowing oxygen-breathing organisms to thrive.

Great Red Spot

A reddish-colored cyclonic storm that circulates counterclockwise in the southern hemisphere of Jupiter's atmosphere. Continuously observed since the seventeenth century, the storm is so large that it could fit multiple Earths within its boundaries.

greenhouse effect

The ability for the atmosphere to absorb heat that is emitted by a planet's surface.

greywacke

A sandstone with either a significant mud component or a significant lithic fragment component.

groin

A hard stabilization structure built perpendicular to the shoreline to help control longshore drift.

gross domestic product

The total value of all goods and services produced within a country over a specific period, usually a year.

ground moraine

An accumulation of sediment that forms beneath a glacier.

groundmass

General term for the fine-grained, non-discernible part of a rock. In igneous rocks, this is the part of the rock that is not phenocrysts and can help in determining the composition of extrusive rocks. In sedimentary rocks, it typically refers to the fine-grained components, namely mud. In metamorphic rocks, it usually refers to material between porphyroblasts or a low-grade rock with only microscopic mineralization.

groundwater

Water that is below the surface.

groundwater mining

When discharge exceeds recharge and the groundwater is withdrawn at a rate that depletes groundwater storage.

gypsum

A typically clear or white evaporite mineral, $CaSo_4 \cdot 2H_2O$; has one cleavage and a hardness of 2.

gyre

Large, circular ocean currents formed by global atmospheric circulation patters.

habitable zone

The region around a star where conditions are suitable for liquid water to exist on a planet's surface, potentially allowing for life as we know it.

haboob

A dust storm that occurs in desert areas.

Hadean

Eon that represents the time from Earth's formation to four billion years ago. Noted for high levels of volcanism, impacts, and very low preservation.

Hadley cell

A part of the global circulation system that rises at the equator and sinks at 30°.

half-graben

A valley formed by normal faulting on just one side.

half-life

The calculated amount of time that half of the mass of an original (parent) radioactive isotope breaks down into a new (daughter) isotope.

halide

Minerals based on bonds to column 17 halogens, such as chlorine and fluorine.

halite

A typically clear or white mineral also known as rock salt or table salt; has 3 cleavages at 90°, a cubic crystal habit, and a hardness of 3.

hanging valley

A feature formed by a tributary glacier moving into a main glacier, forming a tributary valley floor higher in elevation than the main valley floor.

hanging wall

On a dipping fault, the side that is on top of the fault plane; moves down in normal faulting, up in reverse faulting.

hardness

The ease or difficulty in scratching a mineral, measured by the qualitative Mohs hardness scale, which ranges from soft talc (1 on the scale) to hard diamond (10 on the scale).

headwaters

The source or beginning of a river.

HMS Challenger

A former Pearl-class corvette of the Royal Navy that was picked to undertake the first global marine research expedition: the Challenger expedition.

Holocene

The most recent epoch of geologic time, from 11,700 years ago to present.

hopper crystal

Evaporites (like salt) that form cavities within rocks, mimicking the shape of the crystal.

horn

Steep spire carved by several glaciers.

hornfels

A hard, dense metamorphic rock, typically derived from contact metamorphism.

horst

Uplifted mountain block caused by normal faulting.

hotspot

Rising stationary magma, forming a succession of volcanism and appearing as islands on oceanic plates and as volcanic mountains or craters on land.

hummocky cross-stratification

A special type of cross-bedding that forms when strong storms produce mounds and divots of cross-bedded sand in deeper water.

humus

Rich organic material found in soil.

hydraulic

Relating to movement brought about by water.

hydraulic conductivity

The measure of how well a fluid flows through an object.

hydroelectric power

A renewable energy source that uses the kinetic energy of moving water to generate electricity.

hydrogen bond

A weak chemical bond that attracts hydrogen to a negative part of a molecule. Many of water's properties are due to hydrogen bonds.

hydrolysis

Water breaking into ions and replacing ions in minerals; a major type of chemical weathering in silicates.

hydropower

A renewable energy source that uses the kinetic energy of moving water to generate electricity.

hydrosphere

The part of the Earth composed of water, as a solid, liquid, or gas.

hydrothermal metamorphism

Metamorphism that occurs when hot fluids flow into rocks, altering and changing the rocks.

hypothesis

A proposed explanation for an observation that can be tested.

ice sheet

Thick glaciers that cover continents, particularly during ice ages.

igneous

Relating to molten rock.

igneous rock

Rock formed by liquid rock from volcanic processes.

imbrication

Cobbles stacked in the direction of flow.

impermeable

Referring to a material or surface that does not allow fluids, such as water, to pass through it.

inclusion

A piece of a rock that is contained inside of another rock.

index fossil

A fossil with a wide geographic reach but originating from a short geologic time span; used to match rock layers to a specific time period.

index mineral

Minerals that form at a specific range of temperatures and pressures. Studying a collection of index materials helps identify the conditions of a rock's formation.

induced seismicity

Earthquakes that occur due to human activity.

inductive reasoning

Establishing evidence (including new observations) to infer a possible truth.

infiltration

The process by which water works its way down into the subsurface.

inner core

The innermost physical layer of the Earth, which is solid.

inselberg

Isolated piece of bedrock that protrudes from an alluvial surface.

interglacial

Period of warming within a glacial or ice age cycle.

intermediate

A classification of volcanic rock with medium silica composition, equally rich in felsic minerals (e.g., feldspar) and mafic minerals (e.g., amphibole, biotite, pyroxene); grey in color, containing somewhat equal amounts of minerals that are light and dark in color. Primary intermediate rocks are andesite (extrusive) and diorite (intrusive).

interplate

Activity that occurs at the boundaries between plates.

interstadial

A very brief period of warming within a glacial or ice age cycle, even warmer than an interglacial.

interstellar

Occurring or situated between stars.

intraplate

Activity that occurs within plates, away from plate boundaries.

intrusive

Relating to igneous rock that has formed by cooling inside of the Earth (i.e., under the surface).

ion

An atom or molecule that has a charge (positive or negative) due to the loss or gain of electrons.

island arc

Place where oceanic-oceanic subduction causes volcanoes to form on an overriding oceanic plate, making a chain of active volcanoes.

isostasy

Relative balance of an object based on how it floats.

isostatic rebound

An upward movement of the lithosphere when weight is removed, such as water or ice.

isotope

An atom that has different number of neutrons but the same number of protons. While most properties are based on the number of protons in an element, there can be subtle differences in isotopes, including temperature fractionation and radioactivity.

jetty

Artificial device (typically a wall of concrete or rocks) placed to stop or slow longshore drift.

Jurassic

The middle period of the Mesozoic Era, 201–145 million years ago.

K-T extinction

The most recent mass extinction, which killed the non-avian dinosaurs and paved the way for the diversification of mammals; occurred when a bolide hit near Chicxulub, Mexico, 66 million years ago.

karst

A landscape created when carbonate rocks dissolve, leaving behind caverns and holes.

kettle

Depression formed by ice resting in sediment, then preserved after the ice melts and the sediment lithifies.

kimberlite

An ultramafic rock from deep volcanic vents that can contain diamonds.

kinetic energy

The energy an object possesses due to its motion.

Kuiper Belt

A circumstellar disc in the outer Solar System, extending from the orbit of Neptune at 30 astronomical units (AU) to approximately 50 AU from the Sun.

Kyoto Protocol

An international agreement established in 1997 in which participating industrialized countries committed to reducing their greenhouse gas emissions to help combat climate change. It set legally binding emission reduction targets for developed countries.

laccolith

Large igneous intrusion that is wedged between sedimentary layers, bulging upwards.

lacustrine deposition

Deposition in and around lakes.

Lagerstätte

An exceptionally well-preserved fossil locality, often including soft tissues.

lagoon

Interior body of ocean water, at least partially cut off from the main ocean water.

lahar

A type of volcanic mudslide in which rain or snowmelt accumulates volcanic ash on the slopes of steep volcanoes or other mountains and then wash downhill, causing damaging flooding.

laminae

Beds of rock that are thinner than 1 cm.

landslide

General term for material suddenly falling (sliding) down a slope due to gravity.

lapilli

Volcanic tephra that has a diameter between 2 mm and 64 mm. Many cinders are categorized as lapilli.

Late Heavy Bombardment

A hypothesis that states that movement of Jupiter and Saturn about four billion years ago caused a destabilization of orbits in the Asteroid and Kuiper Belts, which then caused a spike in impacts throughout our Solar System.

lateral moraine

Moraines that form at the sides of glaciers.

latitude

The measure of degrees north or south from the equator, which has a latitude of 0 degrees. The Earth's north and south poles have latitudes of 90 degrees north and south, respectively.

Laurentia

Geologic name for the craton that makes up North America.

lava

Liquid rock on the surface of the Earth.

lava dome

Volcanic feature with very steep sides formed by higher viscosity, higher-silica lava.

layered intrusion

Metallic mineral deposit consisting of mafic plutonic rocks, typically containing platinum-group elements, chromium, copper and nickel.

light years

The distance that light can travel through space in a year. One light year is 9.4607 × 10^12 km.

limestone

A chemical or biochemical rock made of mainly calcite.

linear dune

Dunes that are much longer than they are wide, forming from wind blowing in two opposite directions.

lineation

Linear alignment of minerals within a rock.

liquefaction

Process of saturated sediments becoming internally weak (like quicksand) and destabilizing foundations.

lithification

The process of turning sediment into sedimentary rock, including deposition, compaction, and cementation.

lithosphere

The outermost physical layer of the Earth, made of the entire crust and upper mantle. It is brittle and broken into a series of plates, which move in various ways (relative to one another), causing the features described by the theory of plate tectonics.

lithostratigraphic correlation

A type of stratigraphic correlation in which the physical characteristics of rocks are used to correlate.

littoral

Referring to the beach zone, also known as the shoreline, where waves crash into land.

loess

Wind-blown silt, mainly formed from glacial processes.

longitudinal profile

An illustrated topography of the base of a stream, showing zones of sediment production, transport, and deposition.

longshore current

A net movement that occurs when waves intersect the shoreline at nonperpendicular angles.

longshore drift

Sediment that moves via a longshore current.

lopolith

Large igneous intrusion that is wedged between sedimentary layers, bulging downwards.

Love waves

Surface waves that have a side-to-side motion.

luster

The shine created from light reflecting off of a mineral. This is typically divided into two main categories: metallic (metal-like shine) and nonmetallic.

mafic

Can refer to a volcanic rock with lower silica composition or to the minerals that make up those rocks, namely olivine, pyroxene, amphibole, and biotite. Mafic rocks are darker in color and contain more minerals that are dark in color, but can contain some plagioclase feldspar. Primary mafic rocks are basalt (extrusive) and gabbro (intrusive).

magma

Liquid rock within the Earth.

magma chamber

A reservoir of magma below a volcano.

magmatic differentiation

The process of changing a magma's composition, usually through assimilation or fractionation.

magnetic striping

Symmetric patterns of magnetism occurring around an ocean ridge; created by ocean floor rocks recording changes in Earth's magnetic field.

magnitude

A measure of earthquake strength. Scales include Richter and moment.

mainshock

Largest earthquake in an earthquake sequence.

mantle

Middle chemical layer of the Earth, made of mainly iron and magnesium silicates. It is generally denser than the crust (except for older oceanic crust) and less dense than the core.

mantle plume

Rising material and heat derived from the mantle. These may be responsible for hotspots.

mantle wedge

The area of the mantle where volatiles rise from the slab, causing flux melting and volcanism.

marble

A metamorphosed limestone.

marine

Referring to locations that are under ocean water at all times.

mass extinction

A pronounced increase in the extinction rate, typically caused by significant environmental change. There have been five mass extinctions in geologic history, with a sixth suggested to be currently occurring.

mass spectrometer

A device that can determine the amounts of different isotopes in a substance.

mass wasting

Any downhill movement of material caused by gravity.

massive

Referring to a geological feature with no internal structure, habit, or layering.

meander scar

Silted-in oxbow that still has a topographic expression.

meandering channel

Low-gradient channel where rivers sweep across broad flood plains.

mechanical weathering

The physical breakdown (weathering) of bedrock by processes such as pressure or ice expansion.

medial moraine

Formed by two or more glaciers merging, with lateral moraines combining to form a moraine within the glacier.

megathrust

Referring to high-magnitude faulting that occurs in subduction.

mesosphere

A solid, more brittle physical layer of the Earth, located below the asthenosphere; also called the lower mantle.

Mesozoic

Meaning "middle life," it is the middle era of the Phanerozoic, starting 252 million years ago and ending 66 million years ago. Known as the Age of Reptiles.

metal

A solid material that is typically hard, shiny, malleable, fusible, and ductile, with good electrical and thermal conductivity.

metallic

Referring to minerals that contain metals, giving them lusters similar to metals. Valuable elements like lead, zinc, copper, and tin are metallic.

metamorphic

Referring to rocks and minerals that are changed by heat and pressure within the Earth (a process known as metamorphism).

metamorphic facies

A specific set of index minerals tied to specific styles of metamorphism. The presence of these minerals allows a history of metamorphism to be determined.

metamorphic rock

Rocks formed via heat and/or pressure changing the minerals within the rock.

meteor

A small body of matter from outer space that enters the Earth's atmosphere, becoming incandescent as a result of friction and appearing as a streak of light.

meteorite

A stony and/or metallic object from our solar system that was never incorporated into a planet and has fallen onto Earth. The term "meteorite" is used to describe the rock on Earth, "meteoroid" for the object in space, and "meteor" as the object travels in the Earth's atmosphere.

meteoroid

A small rocky (or metallic) body in outer space.

meteorology

The science concerned with the Earth's atmosphere and its physical processes.

mica

$X_1A_{2-3}Z_4O_{10}(OH,F)_2$, where commonly X=K, Na, Ca; A=Al, Mg, Fe; and Z=Si, Al. A shiny silicate mineral usually occurring as a light-colored (translucent and pearly tan) muscovite or a dark-colored biotite; has one strong cleavage and is typically seen as sheets in stacks or "books"; commonly found in many igneous and metamorphic rocks; structured in two-dimensional sheets of silica tetrahedra in a hexagonal network.

micrite

Limestone made of primarily fine-grained calcite mud. Microscopic fossils are commonly present.

microbial

Relating to or involving microorganisms, such as bacteria, viruses, fungi, and other microscopic life forms.

microwave

A form of electromagnetic radiation with wavelengths shorter than other radio waves but longer than infrared waves, ranging from about one millimeter to about one meter.

mid-ocean ridge

A divergent boundary within an oceanic plate where new lithosphere and crust is created as the two plates spread apart. "Mid-ocean ridge" and "spreading center" are synonyms.

migmatite

A rock in transition between metamorphic and igneous rock, i.e., rocks so metamorphosed that they begin the process of melting.

Milankovitch cycles

A series of changes in the Earth's orbit/position in relation to the Sun, which can cause climates to fluctuate over periodicities.

mine

Place where material is extracted from the Earth for human use.

mineral

A natural substance that is typically solid and formed by inorganic processes, with a crystalline structure. Minerals are the building blocks of most rocks.

mineraloid

A mineral-like substance that does not meet all the criteria of a true mineral. Examples include glass, coal, opal, and obsidian.

Mississippi Valley-type

Metallic mineral deposit of mainly lead and zinc from groundwater movements within sedimentary rocks.

mitigation

The action of reducing the severity, seriousness, or harmful effects of something, in a general context, it involves taking steps to minimize negative impacts and manage potential risks.

mixed tide

Areas with an irregular sequence of tides over the course of a month.

modified Mercalli intensity scale

A qualitative earthquake scale of the degree of shaking in an earthquake, ranging from I to XII.

moho

Short for Mohorovičić discontinuity, it is the seismically-recognized layer within the Earth in which the crust ends and the mantle begins. The moho is easy to find since the crust is very different in composition to the mantle, with seismic waves traveling differently through the two materials.

mold

Organic material making a preserved impression in a rock.

moment magnitude

A magnitude scale based on calculation of the energy released in an earthquake.

monocline

A one-sided, fold-like structure in which layers of rock warp upwards or downwards.

moon

An object that orbits a planet or something else that is not a star (e.g., dwarf planets or large asteroids).

moraine

Accumulation of sediment at the margins of glaciers, including the base, sides, and end.

mountain

A landform that rises above its surrounding area.

mountaintop mining

A form of surface mining that involves removing the top of a mountain to expose a desired resource underneath.

mouth

The end of a river.

mud chip

Pieces of mudcracks that are incorporated into a sedimentary rock.

mudcrack

Polygonal cracking that occurs with shrinking clays. Indicative of mud submerged underwater and then exposed to air.

mudstone

A rock made of primarily mud, i.e., particles smaller than sand (≤ 0.064 mm).

mylonite

Fault-formed rock created through ductile deformation deeper within the Earth.

native element minerals

Minerals made from just a single element bonded to itself. Examples include gold, silver, copper, and diamond, which is a native version of carbon.

natural gas

Gaseous fossil fuel derived from petroleum, mostly made of methane.

natural hazard

A significant and dangerous event that is part of a natural process.

natural levee

Built-up area around a river channel that can hold river flow within a channel.

natural resources

Items that are found within Earth that are valuable and limited. Examples include coal, water, and gold.

neap tide

Lowest low tide of the month.

nearshore

Shore area between low tide and storm wave base, with the upper part dominated by fair-weather wave base and the lower dominated by storm wave base.

nebula

A cloud of gas and dust in space that can form a new star/solar system if it collapses.

negative feedback

A system that reverts back to a baseline when it deviates.

neutron

A subatomic particle without an electric charge, present in all atomic nuclei (except hydrogen).

nonconformity

Layered rocks on top of a nonlayered rock, such as crystalline basement.

nonfoliated

Referring to metamorphic textures whose minerals lack a directional component.

nonmetallic

Minerals that have a luster that is not similar to metal. Divided into subtypes based on the way light reflects (or doesn't), including glassy/vitreous, greasy, pearly, dull, etc.

nonpoint source

Pollution that does not come from one specific, known place but instead comes from a broad zone.

nonrenewable

A resource that is not able to be replaced on a human timescale.

normal fault

A dip-slip fault in which the hanging wall drops relative to the footwall, caused by extensional forces.

normal force

Component of the gravitational force that holds material on a slope.

obduction

Process in which a continental plate causes oceanic plate to rise, frequently occurring in collision zones.

objective

Referring to an observation that is completely free of bias (i.e., anyone would make the same observation).

obliquity

The angle of the Earth's axis with respect to the plane of rotation.

observation

The act of gathering new information from the senses or from a scientific instrument.

obsidian

Dark-colored volcanic glass with extremely small microscopic crystals or no crystals, typically forming from felsic volcanism.

oceanic crust

The thin, outer layer of the Earth that makes up the rocky bottom of ocean basins; much thinner (but denser) than continental crust; made of rocks similar to basalt, and as it cools, it becomes more dense.

oceanic plateau

A large, elevated, flat area on the ocean floor with steep edges, formed by extensive outpourings of basaltic lava.

oceanic-continental subduction

Process in which an ocean plate subducts beneath a continental plate, causing a volcanic arc to form.

oceanic-oceanic subduction

Process in which a dense oceanic plate subducts beneath a less dense oceanic plate, causing an island arc to form on the overriding plate.

oceanography

The scientific study of oceans.

octet rule

A rule that says the outer valence shell of electrons is complete when it contains eight electrons.

offset

Amount of movement during a faulting event.

offshore

Referring to the part of the coastline below any wave base action.

oil

A dark liquid fossil fuel derived from petroleum.

oil shale

Oil found in low-permeability, high-porosity rocks such as shale.

olivine

$(Fe,Mg)_2SiO_4$. A mineral that is typically translucent olive green and equant, with no cleavage; common in mafic igneous rocks and in the mantle, but easily weathered in surface conditions; structured as isolated silica tetrahedra; known as peridot when a gem.

ooid

Spheres of calcite that form in saline waters with slight wave agitation. A rock with these spheres is known as an oolite.

Oort cloud

A spherical layer of icy objects surrounding the Sun; likely occupies space at a distance between about 2,000 and 100,000 AU from the Sun.

open pit mine

Large surface mine with opening carved into the ground.

ophiolite

Rocks of the ocean floor, such as mid-ocean ridge rocks, that are brought to the surface.

Ordovician

The second period of the Paleozoic Era, 485–444 million years ago.

ore

Valuable material in the Earth, typically used for metallic mineral resources.

ore mineral reserve

A proven commodity of profitable material that could be mined.

ore mineral resource

Material that is potentially (but not proven to be) extractable and valuable.

organic chemistry

The branch of chemistry that studies the structure, properties, composition, reactions, and synthesis of carbon-containing compounds.

organic molecule

A molecule that contains carbon atoms bonded together, often with hydrogen, oxygen, nitrogen, and other elements, forming the basis of life on Earth.

orogeny

The process of uplifting mountains and creating mountain belts, primarily via tectonic movement. Orogenic belts are the mountain belts that result from these movements, and orogenesis is the name for the process of forming mountain belts.

outer core

The liquid outer physical layer of the core. Movement within the outer core is believed to be responsible for Earth's magnetic field and flips of the magnetic field.

outwash plain

Accumulation of fine-grained sediment formed downhill of the terminal moraine.

oversteepen

A slope, that by natural or human activity, becomes steeper than the angle of repose.

oxbow

Abandoned meanders that are cut off from the main channel.

oxidation

A process in which certain metallic elements (like iron) take in oxygen, causing reactions like rust.

oxide

Minerals in which ions are bonded to oxygen, such as hematite (Fe2O3).

P wave

The fastest seismic wave that occurs after an earthquake, compressional in nature.

pahoehoe

Rope-like, flowing basaltic lava.

Paleocene-Eocene Thermal Maximum

The warmest climate spike in recent geologic past, occurring about 55.5 million years ago. Commonly abbreviated as the PETM.

paleocurrent

Direction of flow preserved in the rock record.

paleomagnetism

As a rock cools, the iron minerals within the rock align with the current magnetic field. Since the magnetic field changes (by where you are on Earth, by flips in which "north" and "south" switch, and by migration of the magnetic north pole), scientists use the magnetic alignment within rocks to determine past movement or the magnetic field itself, along with the movement of rocks and plates via plate tectonics.

Paleozoic Era

Meaning "ancient life," the era that started 541 million years ago and ended 252 million years ago. Vertebrates (including fish, amphibians, and reptiles) and arthropods (including insects) evolved and diversified throughout the Paleozoic. Pangea formed near the era's end.

paludal

Referring to deposition that occurs in swamps.

Pangea

The most recent supercontinent, which formed over 300 million years ago and started breaking apart less than 200 million years ago. Africa and South America, as well as Europe and North America, bordered each other.

parabolic dune

Dunes that form semicircular shapes due to anchoring vegetation.

parasitic cone

Small side vent of a stratovolcano where secondary eruption can occur.

parent isotope

A radioactive atom that can and will decay.

Paris Agreement

An international accord adopted in 2015 that aims to limit global warming to well below 2°C above pre-industrial levels, with efforts to limit the increase to 1.5°C. It involves voluntary emission reduction targets from participating countries, along with financial and technological support to help them achieve their climate goals.

partial melt

The process of some material being derived from a heterogenous mixture when melting (e.g., rocks). Because all rocks are made of many different components, they have many different melting points; as they are heated, certain easy-to-melt components will be melted first.

parting lineation

Subtle ridges formed in the upper flow regime on top of plane beds in the direction of flow.

passive margin

A boundary between continental and oceanic plates that has no relative movement; despite being a place where an oceanic plate is connected to a continental plate, it is not a plate boundary.

passive solar system

An energy system that uses a building's design, materials, and placement to capture solar energy to heat and cool living spaces without relying on mechanical or electrical devices.

paternoster lake

A series of lakes between moraines within an alpine glacier basin, typically a cirque.

peer review

A process where experts in a field review and comment on a newly introduced work, typically a part of publication.

pegmatite

A rock (or texture within a rock) with unusually large crystals, minerals with rare trace element concentrations, and/or unusual minerals, typically forming in veins as the last dredges of magma crystallize.

peridotite

An intrusive ultramafic rock that is the main component of the mantle. The minerals in peridotite are typically olivine with some pyroxene.

period

A unit of the geologic timescale; smaller than an era, larger than an epoch. We are currently in the Quaternary Period.

permafrost

Soil and rock with temperatures below freezing for long periods of time.

permeability

The ability for a fluid to travel between pores, or a description of how connected the pores are within a rock or sediment.

permeable

Having interconnected spaces (pores) that allow liquids or gases to pass through.

Permian

The last period of the Paleozoic, 299–252 million years ago.

Permian Mass Extinction

The largest mass extinction in history, in which an estimated 83% of genera went extinct. The Siberian Traps are potentially related to the event causing the extinction.

permineralization

Style of fossilization in which materials are replaced by minerals in groundwater fluids.

petroleum

A liquid fossil fuel derived from shallow marine rocks; also known as crude oil.

petrology

The study of rocks, either macroscopically or microscopically; specializations within the study are typically based on the three rock types (e.g., igneous petrology).

pH scale

A logarithmic scale that measures the acidity or alkalinity of an aqueous solution. It ranges from 0 to 14, with 7 being neutral.

phaneritic

Referring to igneous rocks with large, easy-to-see crystals. This is common in intrusive rocks.

Phanerozoic

Meaning "visible life," the most recent eon in Earth's history, starting at 541 million years ago and extending through the present. Known for the diversification and evolution of life, along with the formation of Pangea.

phase diagram

Chart that shows the stability of different phases of a substance at different conditions.

phenocryst

A large crystal within an igneous rock; specifically phaneritic and porphyritic rocks.

phosphate

Minerals that are bonded with the phosphate anion, PO43-.

photovoltaic cell

An electronic device that converts the energy of light directly into electricity by means of the photovoltaic effect.

phyllite

A rock more metamorphosed than slate, to the point that microscopic (but larger) mica gives the rock a glow called a sheen. Crenulation, or small bends/folds in the foliation, can be present.

piercing point

An object that is cut by a fault, which allows the amount of movement to be determined. This is useful for studying all faults but is more commonly used in strike-slip faults.

placer

Deposit of heavy ores in stream or beach sediments.

plane bed

A specific layer of rock formed by flowing fluid, either in the lowest part of the lower flow regime or lower part of the upper flow regime.

planet

A large astronomical body that is neither a star nor a stellar remnant.

planetary system

The generic term for a group of planets and other bodies circling a star.

planetesimal

A body that could or did come together with many others under gravitation to form a planet.

plate

A solid part of the lithosphere that moves as a unit, i.e., the entire plate generally moves the same direction at the same speed.

plate boundary

Location where two plates are in contact, allowing relative motion between the two plates. Most earthquakes and volcanoes occur at plate boundaries.

plate tectonics

The theory that the outer layer of the Earth (the lithosphere) is broken into several plates that move relative to one another, causing the major topographic features of Earth (e.g., mountains, oceans) as well as most earthquakes and volcanoes.

platform

Part of a craton that is covered by mostly sedimentary rocks.

playa

A dry lake bed in a desert valley.

pluton

A coherent body of intrusive rock that formed underground and is now at (or near) the surface.

pluvial lake

Lakes that form via increased precipitation from glacial climate shifts.

point bar

Depositional portion of a meandering channel.

point source

Pollution that comes from one known source.

polar cell

Part of the global circulation pattern in which air sinks at the poles (90° latitude) and rises at 60° latitude.

polar desert

Deserts formed by descending air at the poles.

polarity

A molecule (like water) that has a positive side and a negative side.

polymorph

Minerals with matching compositions but different crystal structures. Quartz has several different polymorphs, including coesite, tridimite, and stishovite.

polymorphism

A trait in which a specific chemical composition can form different minerals at different temperatures and pressures.

pore

Empty space in a geologic material, either within sediments or within rocks. Can be filled by air, water, or hydrocarbons.

porosity

Amount of empty space within a rock or sediment, including space between grains, fractures, or voids.

porous

Having spaces or holes through which liquid or air may pass, depending on the spaces' connectivity (permeability).

porphyritic

An igneous rock with two distinctive crystal sizes.

porphyry

Large metallic mineral deposit that forms near magma bodies like plutons. Commonly contains copper, lead, zinc, molybdenum, and gold.

positive feedback

A process that exacerbates the effects of an input, amplifying the output, i.e., a one-directional loop that self-reinforces change.

potential energy

The energy stored within an object or system that has the potential to do work based on its position, configuration, or state.

potentiometric surface

The height of the water table if no confining layers or other hindrances present.

Precambrian

A term for the collective time before the Phanerozoic (pre-541 million years ago), including the Hadean, Archean, and Proterozoic. Known for a lack of easy-to-find fossils.

precession

Wobbles in the Earth's axis.

precipitation

The act of a solid coming out of solution, typically resulting from a drop in temperature or a decrease in the dissolving material.

pressure

The force applied perpendicular to the surface of an object per unit area over which that force is distributed.

principle of cross-cutting relationships

A geologic object cannot be altered until it exists, meaning that the change to the object must be younger than the object itself.

principle of faunal succession

The fossils originating from specific times are unique, and the fossils in layers of different ages have progressed and changed as time has moved forward; fossils found in newer layers have organisms that more resemble organisms that are alive today.

principle of lateral continuity

Layered rocks can be assumed to continue if interrupted within their area of deposition.

principle of original horizontality

Layered rocks generally lay down flat at their formation.

principle of superposition

In an undisturbed sequence of strata, the rocks on the bottom are older than the rocks on the top.

principle of uniformitarianism

Idea championed by James Hutton that the present is the key to the past, meaning the physical laws and processes that existed and operated in the past still exist and operate today.

proglacial lake

Lake that forms next to a glacier because of crustal loading.

prokaryote

A type of single-celled organism with no nucleus.

Proterozoic

Meaning "earlier life," the Proterozoic is the third eon of Earth's history, starting 2.5 billion years ago and ending 541 million years ago. Marked by increasing atmospheric oxygen and the supercontinent Rodinia.

protolith

The rock that existed before changes that formed a metamorphic rock, i.e., the rock that would exist if the metamorphism was reversed.

proton

A subatomic particle with a charge of positive electricity.

provenance

The study of the components of a rock, mainly sedimentary rocks, and the information that can be obtained by understanding the origins of the components.

proxy indicator

A measurement from one system that can specify a change in another system. For example, changes in climate can change the amount of certain isotopes of oxygen and carbon in sea creatures.

pseudoscience

A method of investigation that claims to be scientific but does not hold up to full scientific scrutiny. Examples include astrology, paranormal studies, young-Earth creationism, and cryptozoology (i.e., the study of creatures like Bigfoot and the Loch Ness Monster).

pumice

A low-density, highly vesiculated volcanic rock, usually white-to-tan in color and typically arising from felsic volcanism.

pycnocline

A layer in a body of water where the water density increases more rapidly with depth compared to the layers above and below.

pyroclastic

Rocks (or rock textures) that are formed from explosive volcanism.

pyroclastic flow

A mixture of rock, gas, and ash that travels down at very hot temperatures and very fast speeds, resulting from parts of the eruption column collapsing. They are the most dangerous immediate volcanic hazard.

pyroxene

XY(Al,Si)2O6, in which commonly X = Na, Ca, Mg, or Fe; Y = Mg, Fe, or Al. A mineral that is typically black to dark green, blocky, with two cleavages at ~90°; common in mafic igneous rocks and some metamorphic rocks; structured as a single chain of silica tetrahedra.

qualitative

An observation based on non-numerical data. While these types of observations are not preferred, they can still be useful.

quantitative

An observation based on numerical data. These observations are preferred because they can be used in calculations.

quartz

SiO2. A mineral that is transparent but can be any color imaginable with impurities; has no cleavage, is hard, and commonly forms equant masses; perfect crystals are hexagonal prisms topped with pyramidal shapes; structured as a three-dimensional network of silica tetrahedra, connected to each other as much as possible. One of the most common minerals, quartz is found in many different geologic settings, including the dominant component of sand on the surface of Earth.

quartzite

A metamorphosed sandstone.

Quaternary

The most recent, and current, period within the Cenozoic Era, starting 2.58 million years ago.

radar

A system for detecting the presence, direction, distance, and speed of aircraft, ships, and other objects by sending out pulses of high-frequency electromagnetic waves that are reflected off the object back to the source. It is an acronym for "radio detection and ranging."

radial drainage

Drainage pattern emanating from a high point.

radiative forcing

The difference between the incoming solar energy absorbed by the Earth and the energy radiated back to space. It is a measure of the influence that factors like greenhouse gases and aerosols have on the Earth's energy balance, typically leading to warming (positive forcing) or cooling (negative forcing) of the climate system.

radioactive

The process of atoms breaking down randomly and spontaneously.

rain shadow desert

Deserts that form as air loses moisture traveling over mountains.

raindrop impressions

Small circular pits formed by raindrops impacting soft sediments.

rainwater harvesting

The collection and storage of rainwater from rooftops, surfaces, or other catchment areas for later use in irrigation, drinking water, or other purposes.

Rayleigh wave

Surface waves that have an up and down motion.

recessional moraine

A terminal moraine that forms as a glacier melts.

recharge

Area where water infiltrates the ground and adds to the overall groundwater.

recrystallization

The process of changing a mineral without melting.

rectangular drainage

Drainage pattern in an area of low topography dominated by bedding planes, joints, and fracture patterns.

recurrence

Average time between earthquakes, calculated based on past earthquake records.

red shift

Increase in the wavelength of light resulting from the light source moving away from the observer.

redox

Reactions that are related to the availability of oxygen. Many minerals or ions change their solubility based on redox conditions.

reduction

A half-reaction in which a chemical species decreases its oxidation number, usually by gaining electrons.

reef

A topographic high found away from the beach in deeper water but still on the continental shelf, typically formed in tropical areas by organisms such as corals.

refining

Removing trace elements from desired elements.

reflection

Waves bouncing off of a boundary between mediums of different properties.

refraction

Waves changing direction due to changing speeds, typically caused by a change in density of the medium.

regional metamorphism

Metamorphism that occurs with large-scale tectonic processes, like collision zones.

regolith

Loose material that is a mixture of soil components and weathered bedrock sediments.

regression

The decrease in sea level over time.

relative dating

Determining a qualitative age of a geologic item in relation to another geologic item.

remediation

The process of cleaning up a polluted site.

renewable

A resource that is replaced on a human timescale.

reservoir (rock)

A rock that allows petroleum resources to collect or move inside it.

reservoir (water)

A body of water behind a dam, usually built to store fresh water, often doubling for hydroelectric power generation.

resonance

An amplification of earthquake waves due to buildings or other structures.

reverse fault

A dip-slip fault in which the hanging wall rises with respect to the foot wall.

revolve

To move in a circular or curving course or orbit. Not to be confused with rotate (to spin on an axis).

rhizolith

A root system preserved in rock.

rhyolite

General name of a felsic rock that is extrusive; its groundmass is usually white, tan, or pink in color.

Richter scale

A magnitude scale based on the amplitude of shaking, measured via a seismograph.

rift

Area formed when the continental lithosphere extends, forming a depression. Rifts can be narrow (focused in one place) or broad (spread out over a large area with many faults).

rip current

Currents that push seaward.

ripple

Ridges of sediment that form perpendicular to flow in the lower part of the lower flow regime.

rivers

Channels of water that flow downhill due to gravity.

rock cycle

The concept that any rock type (igneous, sedimentary, or metamorphic) can change into another rock type under the right conditions over geologic time.

rockfall

Detached rocks free-falling from very steep slopes.

Rodinia

The supercontinent that existed before Pangea, about one billion years ago. North America was positioned in the center of the landmass.

rogue wave

A wave that is large, unexpected, and dangerous.

root wedging

A process in which plants and their roots wedge into cracks in bedrock, widening them.

rotate

To spin on an axis. Not to be confused with revolve (to move in a circular or curving course or orbit).

rotational slide

Movement of regolith along a curved slip plane.

rounding

The smoothness or roughness of the edges within a sediment.

runoff

Water that flows over the surface.

S wave

Second-fastest seismic wave, which has a shear motion.

sailing stones

Rocks that move along thin ice sheets with high winds.

saltation

Silt and sand that is lifted from the bed and transported short distances.

sandstone

A rock primarily made of sand.

saturation

The point at which a solution has the maximum possible amount of the dissolved component and is unable to dissolve more.

schist

Rock more metamorphosed than phyllite, to the point that mica grains are visible. Larger porphyroblasts are sometimes present.

schistosity

Visible, coarse-grained, platy minerals in a planar fabric, typical of schists.

science denial

The act of purposely ignoring or dissenting from science for political or cultural gains.

scientific method

The idea in science that phenomena and ideas need to be scrutinized through hypothesizing, experimentation, and analysis. This can eventually result in a consensus or scientific theory.

scroll bars

Series of ridges that result from the continuous lateral migration of a meander, showing the former locations of the river channel.

seamount

A conical submarine mountain formed from an extinct volcano that rises abruptly from the ocean floor but typically does not reach the water's surface. Over geologic time, the largest seamounts may reach the sea surface, where wave action erodes the summit to form a flat surface.

sediment

Pieces of rock that have been weathered and possibly eroded.

sediment-hosted copper

Diagenetic copper deposit within sedimentary rocks.

sediment-hosted disseminated gold

Broad, low-grade deposits of microscopic gold found in sedimentary rocks with diagenetic alteration.

sedimentary

Relating to pieces of rock that have been weathered (i.e., sediment).

sedimentary basin

A local or regional depression that allows sediments to accumulate.

sedimentary rock

Rocks that are formed by sedimentary processes, such as sediment lithification and precipitation from solution.

seismic anomaly

Areas that have an unpredicted change in seismic data, indicating a change in properties.

seismic gap

Length of fault without earthquake activity, occurring due to a locked segment in the fault.

seismic wave

Energy that radiates from fault movement via earthquakes.

seismograph

Instrument used to measure seismic energy.

Seismographs

semidiurnal tide

Location with two unequal tide cycles per tidal day.

sequence stratigraphy

The study of changes in the rock record caused by changing sea level over time.

serpentinite

Rock formed from hydrothermal alteration of basalt, made of serpentine.

SETI

SETI, or the Search for Extraterrestrial Intelligence, is a scientific effort aimed at detecting signals or evidence of intelligent life beyond Earth.

shale

A very fine-grained rock with very thin layering, making it fissile.

shear

Stress within an object that causes side-to-side movement within an internal fabric or weakness.

shear force

Component of gravitational force that pushes material downslope.

shear strength

The relationship between shear force and normal force in a block of material on a slope. When shear force is greater than normal force, mass wasting can occur.

sheetwash

Planar flow of water over land surfaces.

shield

A craton that is exposed at the surface.

shield volcano

Volcano with a gentle slope, formed from low-viscosity, low-volatility, mafic, basaltic lava.

shock metamorphism

Metamorphism caused by bolide impacts.

shoreface

Part of the coastal depositional environment, located near the tidal zone but below. Lower shoreface is the part of the coastline which is only disturbed by storm waves; upper shoreface is disturbed by typical daily wave action.

shoreline

The part of the coastline that is directly related to water-land interaction, specifically the tidal zone and the range of the wave base.

Siberian Traps

One of the largest volcanic eruptions on Earth, when over three million cubic kilometers of lava erupted, based on evidence found in Siberia.

silicate

Mineral group in which the silica tetrahedra, SiO44-, is the building block.

silicon-oxygen tetrahedra

Anion structure of one silicon bonded to four oxygens in the shape of a tetrahedron, with the silicon in the center and four oxygens at the corners of the structure. It has a net charge of -4 and can bond to cations to form silicate minerals.

sill

A sheet-like igneous intrusion that has intruded parallel to bedding planes within the bedrock.

siltstone

A rock made of primarily silt.

Silurian

The third period of the Paleozoic, 444–420 million years ago.

sinistral

A strike-slip or transform motion in which the relative motion is to the left as viewed across the fault.

skarn

Carbonate rock that reacts with hot magmatic fluids, creating concentrated ore deposits, which can include copper, iron, zinc, and gold.

slab

Name given to the subducting plate, from which volatiles are driven out at depth, causing volcanism.

slate

Metamorphic rock with a strong foliation but no visible minerals, derived from mudstones or shales.

slaty cleavage

Microscopic foliation in slate, in which flat slabs and planes of rock develop.

slickenside

A rock surface that has been polished by fault movement, covered with grooves.

smelting

A process that chemically separates desired element(s) from ore minerals.

Snowball Earth hypothesis

The hypothesis that the entire ocean froze and continental glaciation covered the planet about 700 million years ago.

snowline

The line between the zone of accumulation and the zone of ablation.

soft-sediment deformation

Weak, typically saturated sediments that deform and contort before lithification.

soil

A type of non-eroded sediment mixed with organic matter, used by plants. Many essential elements for life, like nitrogen, are delivered to organisms via the soil.

soil creep

Very slow movement of soil downhill.

soil horizon

Specific layers within a soil profile, featuring specific properties.

soil profile

A hypothetical or real section cut from soil, showing the different layers (horizons) that exist within it.

solar energy

Radiation from the Sun that is capable of producing heat, causing chemical reactions, or generating electricity.

solar nebula

Rotating, flattened disk of gas and dust from which the Solar System originated.

solar system

While the generic term for a group of planets and other bodies circling a star is planetary system, our planetary system is the only one officially called "Solar System," because our Sun is sometimes called Sol.

sole mark

A series of sedimentary structures that form at the base of a flow and erode into underlying sediment. Examples include scour marks, flute casts, groove casts, and tool marks.

solid solution

Two or more elements that can easily substitute for each other due to similarities in ionic size and charge.

solution

The process of a solid dissolving into a liquid. This commonly occurs with salts and other minerals in water.

sonar

An acronym for "sound navigation and ranging," sonar uses sound waves to navigate and map surfaces. Sound waves created by an observer reflect off of surfaces and return to the observer; the amount of time it takes for the sound to return is a function of the distance the surface is from the observer. Bats use sonar to navigate through the dark, and ships use sonar to map the ocean floor.

sorting

The range of sediment sizes within a sediment or sediment within sedimentary rocks. "Well sorted" means the sediment has the same sizes, while "poorly sorted" means many different sizes are present.

source rock

A rock containing material that can be turned into petroleum resources. Organic-rich muds form good source rocks.

specific gravity

Related to density, specific gravity is the ratio of the weight of a mineral vs. the weight of an equal volume of water.

spectroscopy

The study of the details of light, which can tell you the chemical makeup of light and even the movement of a light source.

speed of light

The constant velocity at which light travels in a vacuum, approximately 299,792 kilometers per second (186,282 miles per second).

spheroidal weathering

A type of exfoliation where homogenous rocks weather into round shapes.

spit

A ridge of sediment that extends out into a body of water, formed via longshore currents.

spring

A place where pressurized groundwater flows onto the surface.

spring tide

Highest high tide of the month.

stack

An offshore rock spire that is a remnant of a rock layer.

star dune

Dunes that form from wind of many different directions.

stoping

The process of surrounding bedrock being broken up and moved upward by magma.

storm wave base

The depth that waves can reach in large storms, such as hurricanes.

straight channel

Channels that form straight, typically near headwaters.

strain

The deformation that results from application of a stress.

stratigraphic correlation

Finding matches between disconnected rock strata across long distances.

stratigraphy

The study of rock layers and their relationships to each other within a specific area.

stratovolcano

Volcano with steep sides, formed due to a combination of many types of eruption styles and from low-viscosity mafic magma, higher-viscosity felsic lava, but most commonly, intermediate andesite lava.

streak

The color(s) that a mineral produces when powdered or rubbed against a hard surface, usually a porcelain tile.

stream

A channelled body of water.

stress

Force applied to an object, typically in relation to forces within the Earth.

strike

A measure of a geologic plane's orientation in 3-D space. Used to measure beds of rocks, faults, foldhinges, and more. Using the right-hand rule, dip is perpendicular and to the right 90° of the strike.

strike-slip

Faulting that occurs with shear forces, typically on vertical fault planes as two fault blocks slide past each other.

strip mining

A surface mining technique that involves removing large strips of soil and rock to access underlying mineral deposits.

stromatolite

A fossil that forms as algal mats grow and capture sediment in mounds.

structural basin

A basin formed structurally by symmetrical synclines.

sturzstrom

Large and mysterious landslides that travel long distances.

subduction

A process where an oceanic plate descends below a less dense plate, causing the removal of the plate from the surface. Subduction causes the largest earthquakes, as the subducting plate can lock as it descends. Volcanism also occurs as the plate releases volatiles into the mantle, causing melting.

subduction zone metamorphism

Metamorphism that occurs in subduction zones, typically at a lower temperature and higher pressure.

subhedral

A mineral that only shows some characteristics of its true crystal habit and is not perfectly grown.

subjective

An observation influenced by the observer's personal bias.

submarine canyon

Canyon carved into a continental shelf.

submarine fan

Broad cone of coarse sediment deposited from a submarine flow or turbidity flow.

submergent coastline

Area of coast where relative sea level is rising.

subsidence

The act of the land surface downwarping, typically referred to when discussing sedimentation or rapid groundwater removal.

subsoil

Lower layer of the soil (B), which is a mixture of weathered bedrock, leeched materials, and organic material. Has two sublayers: the upper part, or regolith (with more organic materials), and the lower part, saprolite, which is only slightly weathered bedrock.

substratum

Lowest layer of the soil (C), which is mechanically weathered (not chemically weathered) bedrock.

sulfate

Minerals bonded via a sulfate ion, SO42-.

sulfide

Minerals bonded via a sulfur (S2-) atom.

summer berm

Lower, seaward berm that forms with lower wave energy in summer months.

supercontinent

An arrangement of many continental masses that have collided together into one larger mass. According to the Wilson cycle, this occurs every half-billion years or so.

superfund site

A federally supported pollution clean-up effort.

supergene enrichment

Oxidation occurring in sulfide deposits that can concentrate valuable elements like copper.

supernova

Large explosion when the largest stars end fusion; responsible for the formation of heavy elements in the universe, like gold and uranium.

surf zone

Shoreline area of breaking waves.

surface mining

Mining that occurs near the Earth's surface.

surface wave

Seismic waves that only move along the surface, mainly R waves and L waves.

suspended load

Bedload sediments that can be carried by higher-velocity flows.

syncline

A U-shaped, upward-facing fold with younger rocks in its core.

system

An interconnected set of parts that combine to make up a whole.

tafoni

Rounded cavities within rocks that form in various ways, including the growth of minerals (mainly salt).

talus

Loose blocks of rock that fall from steep surfaces and cover slopes.

tar sand

Sands or sandstones that contain high-viscosity petroleum.

tectonic

Relating to the movement of plates of lithosphere.

temperature

The measure of the vibrational (kinetic) energy of a substance.

tension

Stress that pulls objects apart, giving them a larger surface area or volume; stretching forces.

tephra

General term for solid but fragmented material that erupts from a volcano; divided into three subcomponents: ash (<2 mm), lapilli (2–64 mm), blocks and bombs (>64 mm).

terminal moraine

Moraine that forms at the end of a glacier.

terrace

An elevated erosional surface caused by glacial or fluvial action.

terrane

A geological province added (accreted) to a continental mass via subduction and collision.

terrestrial

Referring to depositional environments that are on land.

texture

Arrangement of minerals within a rock.

thalweg

Deepest part of a meandering channel.

theory

An accepted scientific idea that explains a process using the best available information.

thermocline

A distinct layer in a body of water where the temperature changes more rapidly with depth than it does in the layers above or below.

thermohaline circulation

A connected global ocean circulation pattern that distributes water and heat around the globe.

thick-skinned

Faulting located deep in the crust, typically involving crystalline basement rocks.

thin-skinned

Faulting that is not located deep in the crust and that typically only involves sedimentary cover, not basement rocks.

tholins

Complex organic compounds formed by the irradiation of simple carbon-containing molecules, often found on the surfaces of icy bodies in the outer Solar System.

thrust fault

A low-angle reverse fault, common in mountain building.

tidal braking

The process by which the Earth's rotation is slowed down by the friction of ocean tides.

tidal day

The amount of time the Moon takes to reappear over the same location of Earth, slightly more than 24 hours.

tidal flat

Wide and flat area of land covered by ocean water during high tide but exposed to air by low tide.

tidal force

A gravitational effect that stretches a body along the line toward and away from the center of mass of another body due to spatial variations in gravitational field strength from the other body.

tide

Movement of water (rising and falling) due to the gravity of the Moon and Sun; most often seen in marine settings.

till

General term for very poorly sorted sediment that is of glacial origin.

tillite

A rock made definitively of glacial till.

tombolo

Sand bar that connects a stack and the shore.

tomography

A process using 3-D seismic arrays to get subsurface images.

topsoil

Upper layer of soil, made mainly out of organic material.

trace fossil

Evidence of biologic activity that is preserved in the fossil record but not the organism itself. Examples include footprints and burrows. Ichnology is the study of trace fossils.

trade wind desert

Desert that forms near 30˚ latitude due to atmospheric circulation.

trade winds

Wind patterns that move from east to west near the equator due to global circulation patterns.

transform

Place where two plates slide past each other, creating strike-slip faults.

transgression

Geological event in which sea level rises over time.

translational slide

A landslide that moves along an internal plane of weakness.

transpression

A segment along a transform or strike-slip fault that has a compressional component, sometimes resulting in thrust faulting and mountains.

transtension

A place along a transform or strike-slip fault with an extensional component; sometimes includes normal faulting, basin formation, and volcanism.

trap

A geologic circumstance (such as a fold, fault, or change in lithology) that allows petroleum resources to collect.

travertine

Porous, concentric, or layered variety of carbonate that forms with often-heated water in springs and/or caves.

trellis drainage

A drainage pattern that forms between ridge lines in deformed (typically sedimentary) rocks.

trench

Deepest part of the ocean, located where a subducting plate dives below the overriding plate.

Triassic

The first period of the Mesozoic Era, from 252–201 million years ago.

tributary

A natural stream that flows into a larger river or other body of water.

trigger

An event that causes a landslide. Water is a common trigger.

triple junction

Place where three plate boundaries (typically divergent) extend from a single point at 120° angles.

truncated spur

An eroded arête that forms a triangular shape.

tsunami

A series of waves produced from a sudden movement of the floor of a ocean basin (or large lake), caused by events such as earthquakes, volcanic eruptions, landslides, and bolide impacts.

tufa

Porous variety of carbonate that forms in relatively unheated water, sometimes in the shape of towers and spires.

tuff

Rock made from pyroclastic tephra: either ash, lapilli, and/or bombs. It can be described by its tephra type (e.g., ash-fall tuff). If deposited hot, where material can fuse together while hot, the rock is then called a welded tuff.

turbidite

Rock that forms from a turbidity flow, a relatively coarse and dense sediment transported to the abyssal plain.

turbidity current

Dense flow of sediment through submarine canyons that forms submarine fans and turbidites.

turbine

A rotary mechanical device that converts the kinetic energy of fluids, such as water, steam, or air, into mechanical energy or electricity by rotating a series of blades.

ultramafic

An igneous rock with extremely low silica composition, made of almost entirely olivine and pyroxene; commonly found in the mantle. Primary ultramafic rocks are komatiite (extrusive) and peridotite (intrusive).

unconformity

Missing time in the rock record, either because of a lack of deposition and/or erosion.

underground mine

Mining that occurs within tunnels and shafts inside the Earth.

universal solvent

A chemical that can dissolve a wide range of other chemicals.

universe

All of space and time and their contents, including planets, stars, galaxies, and all other forms of matter and energy.

vadose zone

Level in which pores are filled with some water and some air, located above the water table.

valley glacier

An alpine glacier that fills a mountain valley.

varve

A type of lamination that is cyclical, perhaps seasonal or diurnal.

vent

Opening of a volcano from which lava can erupt.

ventifact

Rock with abraded surfaces formed in deserts.

vertebrate

An animal that possesses a spinal column or backbone.

vesicular

An extrusive rock filled with small bubble structures created by gases escaping from the cooling lava.

viscosity

The resistance of a fluid to flow, in which a high value means a fluid does not like to flow (like toothpaste) and a low value means a fluid flows easily (like water).

volatiles

Components of magma that dissolve until it reaches the surface, where they expand. Examples include water and carbon dioxide. Volatiles also cause flux melting in the mantle, resulting in volcanism.

volcanic arc

A chain of mountain volcanism on a continent, formed by oceanic-continental subduction.

volcanic neck

The solidified remains of a volcano's conduit and plumbing system that remains after the rest of the volcano has eroded away.

volcano

Place where lava erupts at the surface.

volcanogenic massive sulfide

Metallic mineral deposit that forms near mid-ocean ridges.

Wadati-Benioff zone

A zone of earthquakes that descend into the Earth with subducting slabs. This is commonly used as evidence for plate tectonics.

water right

A purchase or claim obtained through the state government for the legal allotment of a water source such as a spring, stream, well, or lake.

water table

The depth of the groundwater system below which its pore space is 100% filled with water.

wave base

The depth in which the movement of waves can be felt, specifically by sediments. This is approximately equal to half the wavelength. Wave bases can change based on weather (e.g., fair vs. stormy).

wave crest

Top of a wave.

wave height

The distance between the crest and trough of a wave; equal to twice the amplitude.

wave notch

Erosional notch in bedrock cut by waves.

wave period

The time between similar parts of a wave passing a fixed point.

wave train

A series of waves that form and move as a group.

wave trough

Bottommost part of a wave.

wave velocity

Speed at which a wave travels past a fixed point.

wave-cut platform

Flat erosional surface cut by wave action.

wavelength

The distance between any two repeating portions of a wave (e.g., two successive wave crests).

weather

Current conditions within the atmosphere.

weathering

Breaking rocks into small pieces by chemical or mechanical means.

westerlies

Winds that move from west to east between 30˚ and 60˚ latitude due to global circulation patterns.

Wilson cycle

The cycle of opening ocean basins with rifting and seafloor spreading then closing the basin via subduction and collision, creating a supercontinent.

wind energy

A form of renewable energy that harnesses the power of the wind to generate electricity.

winter berm

Higher, landward berm that forms with higher-wave energy in winter months.

xenolith

A piece of foreign rock that has been incorporated into a magma body, either as a different type of magma or a mantle xenolith, a rock from the mantle brought up near the surface.

yardang

Erosional rock face caused by sand abrasion.

yazoo stream

A tributary that runs parallel to a main stream within the floodplain.

yield point

The point at which the amount of strain on a substance has caused the maximum amount of elastic deformation and switches to ductile deformation.

zircon

$ZrSiO4$. A relatively chemically inert mineral with a hardness of 8.5. Common accessory mineral in igneous and metamorphic rocks, as well as detrital sediments. Uranium can substitute for zirconium, making zircon a valuable mineral in radiometric dating.

zone of accumulation

Part of a glacier that has shown a net gain of material over the course of a year.

VERSION NOTES

Most chapters in this textbook match the organization of *An Introduction to Geology* (CC BY-NC-SA) with the exception of Chapter 14 and Chapter 17. Chapter 14 was adapted from parts of Chapter 9 of *Physical Geography and Natural Disasters* (CC BY-NC-SA) and Chapter 11 of *Dynamic Planet: Exploring Geological Disasters and Environmental Change* (CC BY-NC-SA), as well as parts of Chapter 15 of *Principles of Earth Science* (CC BY-NC-SA). Chapter 17 was adapted from parts of Chapter 22 of *Physical Geology*, 2nd edition (CC BY), and parts of Chapter 7 of OpenStax *Astronomy*, 2nd edition (CC BY). Parts of Chapters 15 and 16 were adapted from *Introduction to Environmental Science*, 2nd edition (CC BY-NC-SA). Parts of Chapter 16 were also adapted from *Introduction to Environmental Sciences and Sustainability* (CC BY).

Overall Changes in the Second Edition

- Combined Chapter 13 ("Deserts") and Chapter 14 ("Glaciers") into Chapter 13 ("Deserts and Glaciers").
- Added new chapter dedicated to meteorology and severe weather, Chapter 14 ("Meteorology").
- Renamed Chapter 12 from "Coastlines" to "Earth's Coastlines and Oceans."
- New sections added to the following chapters: Chapter 12 ("Earth's Coastlines and Oceans"), Chapter 15 ("Global Climate Change"), Chapter 16 ("Energy and Mineral Resources"), and Chapter 17 ("Origin of the Universe and Our Solar System").
- Chapters and data: Updated charts and data to the most recently available.
- Replaced some figures with higher-quality images and edited some existing figure captions for clarity.
- Added new figures as well as images from textbook adapter Laura Neser's repository; specific figure numbers are listed in the following sections.
- Text: Some existing text reworded (remixed) for clarification and formatting purposes only.
- Embedded assessment questions: Updated embedded assessment questions to match the most recent data available; added new assessment questions to match newly added material.
- Glossary: Added/edited glossary terms and linked within chapter text: volcanic neck, meteorology, scroll bars, rogue wave, impermeable, desalination, rainwater harvesting, Paris Agreement, Kyoto Protocol, gross domestic product, energy intensity, radiative forcing, adaptation, mitigation, biofuels, permeable, porous, dam, reservoir (water), hydropower, hydroelectric power, potential energy, kinetic energy, turbine, wind power, biomass, active solar system, passive solar system, photovoltaic cell, geothermal energy, wind energy, solar energy, mountaintop mining, strip mining, SETI, extraterrestrial, electromagnetic radiation, electromagnetic waves, speed of light, interstellar, biology, microbial, chemical energy, pressure, organic chemistry, Fermi paradox, habitable zone, tholins, biomarker, Copernican principle, biochemistry, organic molecule, astrobiology, Great Red Spot, canyon, oceanic plateau, continental margin, altimeter, radar, echo sounder, mapping, bathymetry, HMS Challenger, pycnocline, thermocline, pH scale, oceanography, friction, tidal force, tidal braking, eclogite.
- Accessibility: Updates and expansion of alternative text (AltText) for figures are completed in the HTML/Pressbooks version of this book.

Chapter-Level Changes in the Second Edition

Chapters 1-11

- Inserted/replaced imagery for the following figures in Chapters 1-11 (numbers are as listed in the second edition):
  - 1.1, 1.18, 1.23, 1.30
  - 3.9, 3.11, 3.33, 3.41
  - 4.3, 4.31, 4.37, 4.40, 4.42, 4.44
  - 5.17, 5.25, 5.30, 5.38, 5.39, 5.42, 5.43, 5.47, 5.48, 5.53, 5.55, 5.61, 5.66
  - 6.14, 6.18, 6.25, 6.29
  - 7.36, 7.44
  - 8.18
  - 9.1
  - 11.18, 11.37

Chapter 12: Earth's Coastlines and Oceans (formerly titled "Coastlines" in first edition)

Sources: parts of OpenStax *Astronomy*, 2nd edition (CC BY), *Physical Geology*, 2nd edition (CC BY), *Physical Geography and Natural Disasters* (CC BY-NC-SA)

- Changed Introduction: Added mention of world oceans and the study of oceans.
- Inserted/remixed new text block at the end of Section 12.3.3 Tides from OpenStax *Astronomy*, 2nd edition (Section 4.6).
- Created new section, 12.4 Ocean Water Properties, by inserting and remixing text from *Physical Geology*, 2nd edition (Chapter 18) and *Physical Geography and Natural Disasters* (Chapter 7).
- Created new section, 12.5 The Ocean Floor, by inserting and remixing text from *Physical Geology*, 2nd edition (Chapter 18) and *Physical Geography and Natural Disasters* (Chapter 7).
- Removed Learning Objectives: "Explain wave behavior approaching the shoreline," "Explain how longshore currents cause the formation of spits and baymouth bars," and "Describe the relationship between the natural river of sand in the littoral zone and human attempts to alter it for human convenience."
- Added new Learning Objectives: "Summarize ocean water properties and the reasons they may vary" and "Summarize the major ocean floor properties along with the methods scientists use to observe them."
- Added new text to Summary to include ocean water properties and ocean floor features (remixed from parts of *Physical Geology*, 2nd edition (Chapter 18) and *Physical Geography and Natural Disasters* (Chapter 7)).
- Added and/or replaced imagery for the following figures (numbers are as listed in the second edition): 12.5, 12.9, 12.12, 12.25, 12.29, 12.30, 12.31, 12.32, 12.33, 12.34, 12.35, 12.36, 12.37, 12.38, 12.39, 12.40.

Chapter 13: Deserts and Glaciers (formerly Chapter 13 ("Deserts") and Chapter 14 ("Glaciers") in first edition)

Source: *Introduction to Earth Science*, 1st edition (CC BY-NC-SA)

- Renumbered sections and figures from former Chapter 14 ("Glaciers"), including references at end of chapter; added text references from that chapter to new combined chapter.
- Changed Introduction: combined/remixed "Deserts" and "Glaciers" introductions from first edition.
- Changed Summary: combined/remixed "Deserts" and "Glaciers" summary from first edition.
- Changed Learning Objective: "Explain the defining characteristic of a desert, and distinguish between the three broad categories of deserts" to "Explain the defining characteristics of a desert, and distinguish among the broad categories of deserts."
- Changed Learning Objective: "List the primary desert weathering and erosion processes" to "List the primary desert weathering and erosion processes and resulting landforms."
- Changed Learning Objective: "Identify desert landforms" to "Identify desert landforms and explain how they are formed by erosion and deposition."
- Removed Learning Objective: "Identify the main features of the Basin and Range desert (United States)."
- Removed Learning Objective: "Identify glacial erosional and depositional landforms and interpret their origin; describe glacial lakes."
- Added and/or replaced imagery for the following figures (numbers are as listed in the second edition): 13.4, 13.13, 13.25, 13.28, 13.37, 13.53.

Chapter 14: Meteorology (new chapter)

Sources: parts of *Physical Geography and Natural Disasters* (CC BY-NC-SA), *Dynamic Planet: Exploring Geological Disasters and Environmental Change* (CC BY-NC-SA), *Principles of Earth Science* (CC BY-NC-SA)

- Created Introduction by inserting and remixing text from *Physical Geography and Natural Disasters* (10.1 Climate Systems).
- Created new section, 14.1 The Atmosphere, by inserting text from *Principles of Earth Science* (15.1 The Atmosphere); remixed some text for clarification and formatting purposes; inserted additional figures throughout the section not included in the existing open-source textbooks: Figures 14.1, 14.2, 14.4, 14.6, 14.7, and 14.8.
- Created new section, 14.2 Weather Processes, by inserting text from both *Principles of Earth Science* (15.2 Weather Processes) and *Dynamic Planet: Exploring Geological Disasters and Environmental Change* (11.1 Air Masses and Weather Fronts); remixed text to combine information from both resources; inserted additional figures throughout the section not included in the existing open-source textbooks: Figures 14.11, 14.12, 14.13, 14.14, 14.15, 14.17, 14.19, and 14.20.
- Created new section, 14.3 Severe Weather, by inserting text from both *Principles of Earth Science* (15.2 Weather Processes) and *Physical Geography and Natural Disasters* (Chapter 9); remixed text to combine information from both resources; inserted additional figures throughout the section not included in the existing open-source textbooks: Figures 14.21, 14.24, 14.27, 14.28, 14.32, 14.33, 14.34, 14.35, and

14.36.

Chapter 15: Global Climate Change

Sources: parts of *Physical Geography and Natural Disasters* (CC BY-NC-SA), *Introduction to Climate Science* (CC BY-NC), *Introduction to Environmental Science*, 2nd edition (CC BY-NC-SA)

- Created new subsection, 15.4.3 Predicting Future Warming, by inserting and remixing text from *Physical Geography and Natural Disasters* (Chapter 10).
- Created new section, 15.5 Solutions, by inserting and remixing text from *Introduction to Climate Science* (Chapter 11) and *Introduction to Environmental Science*, 2nd edition (Chapter 6).
- Updated Keeling curve text, Figure 15.9, and Figure 15.10 to latest data.
- Added new Learning Objective: "Describe projected climatic changes and the various options we have for decreasing greenhouse gas emissions."
- Added new text to Summary to include addressing climate change (remixed from parts of *Introduction to Climate Science* (Chapter 11) and *Introduction to Environmental Science*, 2nd edition (Chapter 6)).
- Added and/or replaced imagery for the following figures (numbers are as listed in the second edition): 15.7, 15.26, 15.27, 15.28, 15.29, 15.30, 15.31. 15.32, 15.33, 15.34, 15.35, 15.36.

Chapter 16: Energy and Mineral Resources

Sources: parts of *Introduction to Environmental Science*, 2nd edition (CC BY-NC-SA), *Environmental and Energy Study Institute* (EESI) (CC BY), *Introduction to Environmental Sciences and Sustainability* (CC BY)

- Created new subsection, 16.4.1 Solar Energy, by inserting and remixing text from *Introduction to Environmental Science*, 2nd edition (Chapter 4) and the *Environmental and Energy Study Institute* (EESI).
- Created new subsections (16.4.2 Wind Power, 16.4.3 Hydroelectric Power, 16.4.4 Geothermal Energy, and 16.4.5 Biomass Energy) by inserting and remixing text from *Introduction to Environmental Science*, 2nd edition (Chapter 4).
- Inserted/remixed new text block at the end of Section 16.1.3 Mining Techniques from *Introduction to Environmental Sciences and Sustainability* (Chapter 11).
- Added and/or replaced imagery for the following figures (numbers are as listed in the second edition): 16.2, 16.5, 16.35, 16.37.
- Inserted additional figures throughout Section 16.4 Renewable Resources not included in the existing open-source materials: 16.40, 16.42, 16.43, 16.44, 16.45, 16.46, 16.47.

Chapter 17: Origin of the Universe and Our Solar System

Source: parts of OpenStax *Astronomy*, 2nd edition (CC BY)

- Switched order of subsections "The Giant Planets" and "The Terrestrial Planets."
- Added more detail to descriptions of the planets within our Solar System (remixed from parts of Chapters 7, 9, 10, and 11 of OpenStax *Astronomy*, 2nd edition).
- Added mention of trojan asteroids (remixed from part of Chapter 13 of OpenStax *Astronomy*, 2nd edition).
- Created new section, 17.5 The Search for Life in the Universe, by inserting and remixing text from OpenStax *Astronomy*, 2nd edition (Chapter 30).
- Changed Learning Objective: "Describe the types of small bodies in our solar system, their locations, and how they formed" to "Describe the types of bodies in our solar system, their locations, and how they formed."
- Removed Learning Objectives: "Describe the characteristics of the giant planets, terrestrial planets, and small bodies in the Solar System," "Explain why there is geological activity on some planets and not on others," and "Describe how the characteristics of extrasolar systems help us to model our own Solar System."
- Added new Learning Objectives: "Discuss the assumption underlying the Copernican principle and outline its implications for modern-day astronomers, "Identify where in the Solar System life is most likely sustainable and why," and "Understand the questions underlying the Fermi paradox."
- Added new text to Summary to include the search for life outside Earth (remixed from parts of OpenStax *Astronomy*, 2nd edition (Chapter 30)).
- Added the following figures (numbers are as listed in the second edition): 17.8, 17.14, 17.17, 17.20, 17.23, 17.24, 17.25, 17.26, 17.27, 17.28, 17.29, 17.30, 17.31, 17.32.